An Investigation of Novel Heterobimetallic μ_2-Carbido Complexes

A Thesis submitted for the degree of Doctor of Philosophy of

The Australian National University

By,

Liam Kevin Burt

Research School of Chemistry — College of Science

Canberra, Australia

April 2023

Australian National University

I acknowledge, celebrate, and pay my respects to the Ngunnawal and Ngambri people as the traditional custodians of the land upon which my studies have been conducted. I am grateful to have learned, shared, and lived on this country.

I extend this sincere respect and gratitude to the Turrbal people of Meeanjin (Brisbane), the Wurundjeri Woi Wurrung people of Naarm (Melbourne), and the Muwinina people of Nipaluna (Hobart) as custodians of lands this work has been shared upon.

I acknowledge the sovereignty was never ceded and this country always was, and always will be, Aboriginal land.

Author's Declaration

I declare that, to the best of my knowledge, the results described in this thesis are my own original work as conducted between February 2019 and April 2023 at the Research School of Chemistry and has not been presented for examination for any other degree. Previously established methodologies are acknowledging in text with due reference, where possible, to the original publications from which they are derived.

_____

Liam Kevin Burt
12th April 2023

This was a triumph. I'm making a note here: huge success. It's hard to overstate my satisfaction.
[Chemical] Science. We do what we must, because, we can. For the good of all of us.

But there's no sense crying over every mistake. You just keep on trying till you run out of cake.
And the science gets done, and you make [some] neat [bonds]
For the people who are still alive.

I'm not even angry. I'm being so, sincere, right now. Even though [palladium] broke my heart and [ruined] me.
And tore [my soul] to pieces. And threw every piece into a fire.
As they burned it hurt because I was [happy it's done].

Now these points of data make a beautiful line, and we're out of [COVID], [I'm] releasing on time.
So I'm glad I got burned, think of the things we learned, for the people who are still alive.

Go ahead and [submit] me. I think I prefer to stay inside. Maybe [I'll] find [some more, species, to make].
Maybe [bipy-carbenes]. That was a joke, ha ha, fat chance!
Anyway [our] cakes [are] great, [they're] so delicious and moist.
Look at me talking when there's science to do. When I look in [the lab] it makes me [sad] I'm not [there too].
I've got experiments to run, there is research to be done, [for] the people who are still alive.

And believe me I am still alive. I'm doing science and I'm still alive.
I feel fantastic and I'm still alive. While your [reading] I'll still be alive.

Still alive. Still alive.

[Paraphrased] lyrics to 'Still Alive' by Jonathon Coulton
for the 'Portal' Video game (Valve)

In recognition of the parallels with Chemical Research, and the influences video games have had on my attitudes.

One day, I swear, I will write 'How playing Pokémon trains you for Academia'.

Acknowledgements

The past few years have been a wild ride: bushfires, hailstorms, a global pandemic, and of course, a PhD Candidature. I have deeply enjoyed the thrill of every up and down that has occurred, and it has been the ultimate challenge I have always craved. However, no PhD is the feat of one person, and I am especially grateful to the people below for their help, expertise, and encouragement. Below is a list of, what I believe to be (and have been blessed to have), the best 'team' in the world. There are many people to thank, and I relish the chance to show how incredibly lucky I have been.

Coming to the ANU to start a PhD began with an impossible choice, but it was made simple—not through promotional material or rankings, but the small actions of everyday scholars. Dr. Mark Ellison provided me with an opportunity to develop an esteemed teaching program. Professor John Carver showed me a unique department steeped in history, talent, and diversity. Dr. Cristobal Quintana showed me an unrivalled attitude to help one another, and Dr. Harrison Barnett showed me a friendship worth moving across Australia for.

To my advisor, Tony Hill, thank you for (eventually) responding to my email those seven years ago. Your humour, support, eye for detail, sense of elegance, and love of organometallics have been a privilege to experience. I have learned a great deal from your endless knowledge of the literature and certainly an appreciation for 'molecular architecture'. I always felt I could ask you (endless) questions and your immense imagination partners perfectly with my curiosity and drive. Although we are somewhat opposite people, you have taught me to balance opposing objectives and perspectives in all my undertakings and how that is the signature of true intelligence—a valuable lesson beyond our laboratory. Tony, I have loved every minute in your group. By extension, thank you Mark Santos for being an angel and dear friend.

To Assoc. Prof. Alex Bissember, my former advisor and dear friend, thank you for being another guidance and giving superlative mentorship. This thesis has been amplified by the attitudes you instilled in me as an undergraduate and Chapter Six carries your influence. I always felt confident and motivated thanks to your encouragement, but most importantly, your belief in me has been my ultimate strength.

To the Hill Group 2016–2023, you have created the best scientific environment and I am grateful for our time together. A lab of sharing, encouragement, achievement, and endless laughs is why I arrive early in the morning, unable to contain my excitement for another day. To postdocs Dr. Ben Frogley and Dr. Richard Manzano, I thank you for your exceptional expertise and standards. I have endeavoured to absorb every word of your wisdom and my science is better from your help. You have both set an exceedingly high bar for what a postdoc should be. To the old guard (Kathy, Yong-Shen, Anders, Richard K., Kedar, and Kass) I immediately felt welcome in the group, and I am grateful for your high standards, friendship, theatre trips, and summer adventures since 2016. To the new guard (Harrison, Chee, Ryan, Steve, Lachlan, Madelaine, and Seb), thank you for being my family away from home (or you know, stuck at home for COVID-19). I treasure our time together: the singalongs in the lab, the bulk-billed coffee trips, and the sunny evenings in Prague. To Emily and Steph, my 3060 students. Thank you for your trust in my teaching, it was a real highlight to make wonderful molecules with you. Indeed, thank you to the

other 3060 students and vacation scholars from the Hill group (Angus, Andie, Antonia, Liam P., Jing, and Harrison). Thank you to the rest of the inorganic floor and the broader RSC community for the years of help and happy memories.

To the technical staff who have assisted in my experimental work, I am beyond grateful for your professionalism and flawless efforts. I thank Chris and Joe for early NMR studies, and Doug for the later help (you supercharged this thesis!). To Joe, Adam, and Anitha for their help and guidance with Mass Spectrometry, nothing was ever too hard, and I am bewildered what you managed to find! Thank you to Michael for assistance with (copious amounts) of X-Ray crystallography and a life changing synchrotron trip to ANSTO. Thank you, Rob, for your flawless, prompt IT service. Lastly, thank you to Torsten and Amelia for their work and consultancy on safety.

To Mark Ellison, thank you for the opportunity within the teaching program and your trust with the keys to the kingdom. I am so proud of all we achieved: no matter the task, no matter the odds, no matter the classroom situation. To Vance, Avis, and Bozena: thank you for all your help in a variety of ways through teaching or technical work. Most importantly, you gave me the timely reminder of why we do science in the first place. The three of you are superheroes in disguise.

Inspiration and support come from the most unlikely of places. Thank you to Clara Hill and the ANU Domestic Recruitment team for showing me another perspective of university life prior to the pandemic and trusting me to be the 'first one in'. Thank you to Prof. Inger Mewburn, Victoria Firth-Smith, and the ANU Research Training team for everything—from workshops to restoring my love of reading. I thrived in my PhD (and the pandemic thanks to you). Thank you to my friends, Dr. Adele Wilson and the Young Tassie Scientists team, for allowing me a playground to show kids the beauty of chemistry and exposing me to all areas of science.

As a kid from rural Australia, I felt I would never be in this position, but at every turn, others have had a different idea. I have used every ounce of opportunity I have been afforded. To the Royal Australian Chemical Institute (RACI), the families and trustees of the late Dr. Peter Smith and Mr. Marshall Hughes, thank you for financial support. I never would have made it to ANU without your help and encouragement.

Thanks to my friends and family for their patience. Thank you to my parents for their unconditional love and support. Your tenacity, courage, and resilience were essential tools on this journey. Thank you to my brother by blood (Nathan) and my brothers by choice (Liam, Josh, and John) for having my back. Always. I love you dearly.

Finally, to the unsung hero of this Thesis. Beth, this work is proof you catalyse my unrelenting enthusiasm into an unstoppable force.

Publications and Presentations

The following lists detail publications and presentations that have emerged from work described in this thesis, during the candidature of the Doctor of Philosophy.

Publications

5) Thiocarbonylphosphorane and arsorane ligands

L. K. Burt, A. F. Hill, and S. L. Jones
Chem. Commun., **2022**, *58*, 11091–11094.

4) Heterobimetallic μ_2-halocarbyne complexes

L. K. Burt, R. D. Dewhurst, A. F. Hill, R. Y. Kong, E. E. Nahon, C. S. Onn,
Dalton Trans., **2022**, *32*, 12080–12099. Hot Article.

3) Construction of an Iminoketenylidene

L. K. Burt and A. F. Hill
Chem. Commun., **2021**, *57*, 8480–8483.

2) Heterobimetallic μ_2-carbido complexes of platinum and tungsten

L. K. Burt and A. F. Hill,
Dalton Trans., **2020**, *56*, 5673–5676. Hot Article.[1]

1) The significance of phosphoniocarbynes in halocarbyne cross-coupling reactions

L. K. Burt, R. L. Cordiner, A. F. Hill, R. A. Manzano, J. Wagler,
Chem. Commun., **2020**, *56*, 5673–5676.

Presentations

5) A reliable synthesis of μ_2-carbido complexes and their reactivity to provide unusual ligands

An oral presentation at the 44th International Conference on Coordination Chemistry
30th July 2022, Rimini, Italy.

4) Bimetallic halocarbynes, phosphoniocarbynes and carbidos of late transition metals

An oral presentation at the 29th International Conference on Organometallic Chemistry
19th July 2022, Prague, Czech Republic.

3) μ_2-carbido complexes: General synthesis and reactivity to provide unusual ligands

An oral presentation at the 13th Australian Organometallics Meeting
12th July 2022, Cairns, Australia.

2) Midnight Blue: A vibrant family of phosphoniothioacyl complexes from phosphoniocarbynes and sulfur

A poster presentation at the 2022 Royal Australian Chemical Institute National Congress,
7th July 2022, Brisbane, Australia.
Awarded prize for best in the Inorganic Division (1 of 2).

1) Towards a general synthesis of μ_2-carbido complexes

An oral presentation at the 8th International Chemical Congress of the Pacific Basin Societies
17th December 2021, Honolulu (Virtual), USA.

[1] Hot Paper is listed for publications 'representing the top 10% of research' for the journal as indicated by reviewers.

Abstract

Complexes bearing mono-atomic carbon (μ-carbido) ligands are exceedingly rare despite origins in nature and playing a crucial role in industrial processes. The study of low-nuclearity (μ_2 and μ_3) carbido complexes is inhibited by a lack of general synthetic routes. This thesis describes the study of Class B (metallacarbyne) μ_2-carbido complexes involving disparate transition metal termini. Oxidative addition and transmetallation processes have been developed based on group 10 metals (platinum and palladium) followed by extension other transition metals allowing subsequent reactivity to be explored.

Chapter One provides an overview of low nuclearity μ_2-carbido complexes. Compound classes are introduced emphasising synthetic routes, structure and bonding and the very limited studies of reactivity to date. Specific attention is paid to metallacarbynes, the dedicated study of which provides the premise of this thesis.

Chapter Two explores the relationship between halocarbynes and metallacarbynes. A review of halocarbynes in advance provides context for the subsequent investigations into the π-coordination of $[M(\equiv C–X)(CO)_2(Tp^*)]$ (M = Mo, W; X = Cl, Br) to late transition metals (Au^I, Pt^0), to provide a series of μ_2-halocarbynes $[MAu(\mu_2\text{-}CX)Cl(CO)_2(Tp^*)]$ (X = Cl, Br) and $[MPt(\mu_2\text{-}CCl)(CO)_2(PPh_3)_2(Tp^*)]$. Species produced are interrogated by crystallographic and computational means to explore semi-bridging carbyne *vs* dimetallacyclopropene bonding descriptions. The conversion of μ_2-halocarbynes to μ_2-carbidos *via* C–halogen activation is then described, and whilst not definitive, circumstantial evidence suggests a C–halogen ionisation mechanism *cf.* a concerted metal insertion may operate.

Chapter Three expands the range of metallacarbyne complexes through ligand substitution reactions of $[WPt(\mu_2\text{-}C)Br(CO)_2(PPh_3)_2(Tp^*)]$ facilitated by the development of a multi-gram synthesis. Study of this library, which varies according to charge (neutral, anionic), donor ligand (N, S, and P), and denticity, provided a wealth of spectroscopic data from which to explore co-ligand dependent trends in Class B carbido bonding. Paramagnetic contributions to shielding are seen to dominate carbido resonance chemical shifts (δ_C) and the μ_2-carbido is seen to exert a substantial *trans* influence.

Chapter Four investigates ligand substitution of $[WPt(\mu_2\text{-}C)Br(CO)_2(PPh_3)_2(Tp^*)]$ with mildly π-acidic isocyanides, to produce $[WPt(\mu_2\text{-}C)Br(CNR)(CO)_2(PPh_3)(Tp^*)]$ and $[WPt(\mu_2\text{-}C)Br(CNR)_2(CO)_2(Tp^*)]$ (R = Xyl, Mes, and ^{t}Bu). Ligand substitution with the anionic scorpionate ligand (Bp*) revealed that isocyanide ligands are preferentially retained over PPh_3 in the reaction

with [WPt(μ_2-C)Br(CNMes)$(CO)_2(PPh_3)$(Tp*)] to afford [WPt(μ_2-C)(CNMes)$(CO)_2$(Bp*)(Tp*)]. A strong solvent dependence was observed whereby non-polar media provide the expected isocyanide/phosphine substitution species, whilst polar media afforded the first examples of μ_2-iminoketenylidene (μ_2-CCNR) ligands *via* migration of isocyanide ligands onto the μ_2-carbido forming a new C–C bond. Theoretical interrogation of free iminoketenylidenes suggest a lower energy triplet conformation (linear) rather than a singlet (bent) molecule, however as a ligand, an essentially linear C–C–N–C spine is observed.

Chapter Five explores reactions of [WPt(μ_2-C)Br$(CO)_2(PPh_3)_2$(Tp*)] with anionic, hydrocarbon-based nucleophiles. A series of species are produced, the behaviour and longevity of which is dependent on the hybridisation of carbon of the resulting σ-organyl ligand. The *trans*-isomers [WPt(μ_2-C)(R)$(CO)_2(PPh_3)_2$(Tp*)] (R = H, tolyl, C≡CSiMe_3) are isolable, whereas *cis*-intermediates undergo reductive elimination (*i.e.*, C–C bond formation with the μ_2-carbido) and are generally not sufficiently long-lived to be detected. One exception is sp^3-hybridsed carbon of *cis*-[MPt(μ_2-C)(R)$(CO)_2(PPh_3)_2$(Tp*)] (R = Me, ^{n}Bu, M = Mo, W) devoid of π-orbitals to interact with the μ_2-carbido, and series of reductive elimination rates is empirically determined as H > C≡CR ~ C≡C–C≡[W] > –C_6H_4Me-4 ≫ CH_3. The butyl-carbido *cis*-[WPt(μ_2-C)(^{n}Bu)$(CO)_2(PPh_3)_2$(Tp*)] undergoes β-hydride elimination to provide [WPt(μ_2-CH)$(CO)_2(PPh_3)_2$(Tp*)], a rare example of a μ_2-methyildyne complex, that are comprehensively reviewed. Preliminary studies on co-ligand substitution provide access to range of further examples.

Chapter Six explores cross-coupling reactions of halocarbynes akin to Sonogashira and Suzuki–Miyaura processes. Key palladium carbidos [MPd(μ_2-C)Br$(CO)_2(PPh_3)_2$(Tp*)] (M = Mo, W) are spectroscopically observable but evolve upon isolation to tetrametallic halo-bridged dimers, a process that may be diverted by installation of chelating diphosphines. The Suzuki–Miyaura cross-coupling of halocarbynes was optimised to produce functionalised carbynes *via* tandem Pd(0)/Au(I) cycles. During catalysis, phosphoniocarbynes $[M(\equiv CPR_3)(CO)_2(Tp^*)]^+$ were observed as counter-productive tangents. A range of these were shown to undergo reactions with sulfur to produce the first examples of independently unstable thiocarbonylphosphorane [M(η^2-SCPR_3)$(CO)_2$(Tp*)]PF_6 and arsorane [W(η^2-SCAsMePh_2)$(CO)_2$(Tp*)]OTf species. Computational evaluation of these complexes considers (η^2-E$CPMe_3$) (E = O, S, Se, Te) as a coupling of chalcocarbonyl (CE) and phosphine (PMe_3) ligands, where thermodynamic results suggest this is favourable for heavy chalcogens, but endothermic for CO, perhaps explaining why CO/PR_3 coupling has not been observed in the literature.

Chapter Seven develops stannylcarbyne transmetallation to yield new gold(I) and mercury(II) metallacarbynes. Synthetic optimisation of the known tetrameric species $[W(\equiv CAu)(CO)_2(Tp^*)]_4$ expedited access to mononuclear gold(I) metallacarbynes *via* disaggregation with nucleophiles such as phosphines, isocyanides and *N*-heterocyclic carbenes to scope the effect of ligand donor strength. The first gold(III) carbido complex was obtained serendipitously, while a pentameric gold aggregate was also identified $[W(\equiv CAu)(CO)_2(Tp^*)]_5$, although not representing the bulk sample used for reactions as investigated through spectroscopic and structural techniques. Mercury(II) metallacarbynes bearing aryl substituents (Hg–C bonds) form complex mixtures due to dynamic equilibria, however under careful control of stoichiometry, $[HgCl_2]$ provides interconvertible trimetallic $[W_2Hg(\mu_2\text{-}C)_2(CO)_4(Tp^*)_2]$, tetrametallic $[WHg(\mu_2\text{-}C)Cl(CO)_2(Tp^*)]_2$ or hexametallic $[W_2Hg_2(HgCl)_2(\mu_3\text{-}C)_2Cl_2(CO)_4(Tp^*)_2]$ complexes. The complexes $[W_2Hg(\mu_2\text{-}C)_2(CO)_4(Tp^*)_2]$ and $[WHg(\mu_2\text{-}C)(S_2CNMe_2)(CO)_2(Tp^*)]$ present a well-defined carbyne transfer agents, as described in the following Chapter.

Chapter Eight explores the application of $[W_2Hg(\mu_2\text{-}C)_2(CO)_4(Tp^*)_2]$ and $[WHg(\mu_2\text{-}C)(S_2CNMe_2)(CO)_2(Tp^*)]$ as reagents towards further μ-carbido species through two different processes. Firstly, an oxidative-addition/demercuration sequence employing $[WHg(\mu_2\text{-}C)(S_2CNMe_2)(CO)_2(Tp^*)]$ results in a family of heterobimetallic metallacarbynes spanning the metals Pt, Pd, Ir, Rh, and Ru, including examples that *do not* react with bromocarbyne $[W(\equiv CBr)(CO)_2(Tp^*)]$, thereby delivering the carbido ligand *via* stealth. The method is in some instance sensitive to liberation of nucleophiles (such as phosphine) which may cause symmetrisation of the heteroleptic mercury precursor to homoleptic $[Hg(S_2CNMe_2)_2]$ and $[W_2Hg(\mu_2\text{-}C)_2(CO)_4(Tp^*)_2]$. Secondly, ineffective reactions of osmium(0) reagents with the dithiocarbamate precursor is overcome *via* an alternative strategy involving hydride metathesis with $[W_2Hg(\mu_2\text{-}C)_2(CO)_4(Tp^*)_2]$ to produce the first osmium μ_2-carbido complex $[WOs(\mu_2\text{-}C)Cl(CO)_3(PPh_3)_2(Tp^*)]$, which by virtue of coordinative unsaturation is a versatile precursor to further examples.

Glossary

GENERAL

Ad, Cy, Ph	adamantly, cyclohexyl, phenyl
cat.	catalyst, catalytic amount of
CCDC	Cambridge Crystallographic Data Centre
C_n	carbon chain n-units long
DFT	Density Functional Theory
E	generalised electrophile
e.s.d	estimated standard deviation
f^-	atom-condensed Fukui function (anionic)
f^+	atom-condensed Fukui function (cationic)
hrs	hours
i-R, ^{i}R	iso-R
LUMO	Lowest Unoccupied Molecular Orbital
Me, Et, Pr, Bu	methyl, ethyl, propyl, butyl
min	minutes
ML_n	general metal fragment (M) with n ligands
MLCT (or LMCT)	metal-to-ligand charge transfer (or reverse)
NBO	natural bond orbital
n.d.	not determined
n.r.	not reported or not resolved
n-R, ^{n}R	normal-R
Nu	generalised nucleophile
OTf	trifluoromethanesulfonate, $^-SO_3CF_3$
PPN	*bis*-triphenylphosphoranylidene)iminium, $[N(PPh_3)_2]^+$
p-tolyl	*para*-tolyl, C_6H_4Me-4
py	pyridine, NC_5H_5
pz	3,5-dimethylpyrazol-1-yl
R	generalised organic group
r.t.	room temperature (25 °C)
TLC	Thin Layer Chromatography
t-R, ^{t}R	tertiary-R
w.h.h.	'width at half height' (Hz)
X	generalised halogen (or a variable)
xs.	excess (of reagent)
$\varkappa_n$	n-number of coordinated donors, denticity
μ_n	bridging n-number of metals

LIGANDS

[9]aneS_3	1,4,7-tricyclononane
Bm^{Me}	*Bis*-(*N*-methylthioimidazol-1-yl)borate
Bp	*Bis*-(pyrazol-1-yl)borate
Bp*	*Bis*-(3,5-dimethylpyrazol-1-yl)borate

Bpy	2,2'-bipyridine
CAAC	cyclicalkylamino carbene
cal4ix	calix[4]arene
COD	1,5-cyclooctadiene
Cp	η^5-cyclopentadienyl (η^5-C_5H_5)
Cp*	η^5-(pentamethyl)cyclopentadienyl (η^5-C_5Me_5)
dba	dibenzylideneacetone
dcpe	1,2-*bis*(dicyclohexylphosphino)ethane
dmpe	1,2-*bis*(dimethylphosphino)ethane
dmpm	1,2-*bis*(dimethylphosphino)methane
dppe	1,2-*bis*(diphenylphosphino)ethane
dppf	1,1'-ferrocenediyl-*bis*(diphenylphosphine)
dppm	1,2-*bis*(diphenylphosphino)methane
dtbbpy	4,4'-tertbutyl-2,2'-bipyridine
Fc	ferrocenyl
Fp^-	$[Fe(CO)_2(Cp)]^-$
Mes	mesityl (2,4,6-trimethylphenyl)
NBD	2.5-norbornadiene
nbe	2-norbornene
NHC	*N*-heterocyclic carbene
pc	phthalocyanine
Phen	2,2'-phenanthroline
pin	pinacol
PNP	P–N–P pincer ligand
TCNPP	*tetrakis*(*p*-cyanophenyl)porphyrinate
Terpy	2,2':6',2"-terpyridine
Tm^{Me}	*Tris*-(*N*-methylthioimidazol-1-yl)borate
Tp	*Tris*-pyrazolylborate
Tp*	*Tris*-(3,5-dimethyl)pyrazolylborate
TPP	tetraphenylporphyrin
Xyl	2,6-dimethylphenyl (xylyl)

REAGENTS AND SOLVENTS

CH_2Cl_2	dichloromethane (CD_2Cl_2 is deuterated)
$CHCl_3$	chloroform ($CDCl_3$ is deuterated)
HMDS	hexamethyldisilazane, *bis*-trimethylsilylamine
MeCN	Acetonitrile (solvent or N-donor ligand)
MeLi	methyllithium
MeOH	Methanol
^{n}BuLi	*n*-butyllithium
TBAF	tetrabutylammonium fluoride
THF	tetrahydrofuran
THT	tetrahydrothiophene
TMS	trimethylsilyl

SPECTROSCOPY/SPECTROMETERY

$\{^{1}H\}$	Proton decoupled NMR experiment
$\{^{31}P\}$	^{31}P decoupled NMR experiment
br, sh (in NMR)	broad, sharp
ESI-MS	Electrospray Mass Spectrometry
HMBC	heteronuclear multiple bond correlation
HOMO	Highest Occupied Molecule Orbital
IR	infrared
m/z	mass-to-charge ratio
MLCT	metal-to-ligand charge transfer
$^{n}J_{AB}$	n-bond coupling between nuclei A and B, expressed in Hz
NMR	Nuclear Magnetic Resonance
ppm	parts per million
s, d, t, m (in NMR)	singlet, doublet, triplet, multiplet
sh (in IR)	shoulder
UV-Vis	ultraviolet-visible
vs, s, m, w (in IR)	very strong, strong, medium, weak
v^{t}	virtual triplet
δ_X	chemical shift of nucleus X, expressed in ppm
θ^{T} or Θ^{T}	Tolman cone angle (phosphines)
ν^{T}	Tolman electronic parameter
ν_X	Wavenumber of functional group X

Table of Contents

1 **CHAPTER ONE Metallacarbynes: A Review of Class B μ_2-Carbido Complexes…….. 1**

1.1 Bonding and Structure of Carbido Complexes …… 2

1.1.1 High or Low Nuclearity Species 2

1.1.2 Classifying Low-Nuclearity Carbido Complexes 4

1.2 Synthesis of μ_2-Carbido Complexes……...5

1.2.1 Synthesis of Classes A, C and D 6

1.2.1.1 Classes A and C: Halocarbon Reduction 6

1.2.1.2 Class A: Thermolysis 9

1.2.1.3 Class A: Small Molecule Activation 10

1.2.1.4 Class A: Chalcogen Cleavage 11

1.2.1.5 Class C: A Ruthenium Terminal Carbido as a Metalloligand 14

1.2.1.6 Class D: Deprotonation and Cycloaddition 17

1.2.2 Class B (Metallacarbyne) Synthesis 19

1.2.2.1 Alkyne Scission 19

1.2.2.2 Substitution 20

1.2.2.3 Oxidative Addition 22

1.2.2.4 Transmetallation 24

1.2.2.5 Umpolung (Lithiocarbyne) Approach 25

1.3 Properties of Class B μ_2-Carbido Complexes……28

1.3.1 Structural Parameters 28

1.3.2 $^{13}C\{^1H\}$ NMR 30

1.3.3 Hetero-nuclear NMR and Scalar (J) Couplings 30

1.4 Reactivity of μ_2-Carbido Complexes…… 32

1.4.1 Reactivity of Classes A, C, and D 32

1.4.1.1 Class A and C: Ligand Substitutions or Transformation 32

1.4.1.2 Class A: Redox Chemistry 34

1.4.1.3 Class A: Cycloaddition with Exotic Alkyne–'Benzyne' 35

1.4.1.4 Class A and D: Formation of Thiocarbonyls 35

1.4.1.5 Class D: Carbene Coordination to provide μ_3-carbidos 36

1.4.2 Reactivity of Class B: Metallacarbynes 37

1.4.2.1 At the Carbido (Direct Reactivity) 37

1.4.2.2 Ligand Migration (Indirect Reactivity) 37

1.5 μ_2-Carbido Complexes in Catalysis……....38

1.5.1 Appearances of Classes A, C, and D 38

1.5.2 Metallacarbynes as intermediates 39

1.6 Rationale and Project Aims……....41

2 **CHAPTER TWO Heterobimetallic μ2-halocarbynes from π-coordination…… …49**

2.1 A Brief Review of Low-Nuclearity Halocarbynes…… 49

2.1.1 Terminal (η^1) Halocarbynes 49

2.1.2 μ_3-halocarbynes 54

2.1.3 μ_2-halocarbynes 55

2.2 Theoretical Properties of Terminal Halocarbynes……..59

2.3 Synthesis of Heterobimetallic μ_2-Halocarbynes……62

2.3.1 Gold(I) complexes 63

2.3.2 Platinum(0) complexes 67

2.4 Limits of Synthesis: A Trimetallic Bow-tie Structure……..75

2.5 Isomerisation of a μ2-halocarbyne: A Missing Link for Metallacarbynes……....77

2.6 Conclusions……...80

3 **CHAPTER THREE Elaboration of Platinacarbynes…… 83**
3.1 Revisiting Beck's Metallacarbyne…… ..84
3.2 Preparation of the Metallacarbyne Template Framework…….. 85
3.3 Structural and Spectroscopic Properties of the Lead Metallacarbyne **3.1b**……86
3.3.1 Experimental Properties of [WPt(μ_2-C)Br$(CO)_2(PPh_3)_2$(Tp*)] (**3.1b**) 86
3.3.2 Theoretical Properties 97
3.4 Ligand Substitution Reactions……...102
3.4.1 Halide Substitution 103
3.4.2 Chelating phosphines 105
3.4.3 Anionic, soft sulfur chelates 109
3.4.4 Incorporation of nitrogen donor ligands 114
3.4.5 Additional anionic scorpionate ligands 118
3.5 Exploring the Parameters of the New Library……...122
3.6 Conclusions…….. 127
4 **CHAPTER FOUR Isocyanide Metallacarbynes and μ_2-iminoketenylidene Ligands……129**
4.1 Basis for Isocyanide Ligands……129
4.2 Platinacarbyne Substitution with Isocyanides……132
4.3 Spectroscopic and Structural Properties of Isocyanide Metallacarbynes…….135
4.4 Unusual Reactivity in Polar Media…….150
4.5 Ligand Migration to μ_2-iminoketenylidenes…….. 152
4.6 Theoretical Studies of μ_2-iminoketenylidenes……157
4.7 Attempts Towards μ_2-ketenylidenes……..161
4.8 Conclusions…….. 162
5 **CHAPTER FIVE Reactions of a W–Pt Metallacarbyne with Non-innocent Co-ligands…...164**
5.1 Hydrocarbyl Ligands and μ_2-carbido Complexes……...164
5.2 Reactivity of [W≡C–Pt] with: Hydride Sources……167
5.3 Reactivity of [W≡C–Pt] with: Alkyllithiums…….. 172
5.4 Expanding Heterobimetallic μ_2-methylidynes……177
5.4.1 A review of μ_2-methylidynes 178
5.4.2 Producing μ_2-methylidynes *via* ligand substitution 185
5.5 Reactivity of [W≡C–Pt] with: Tolyllithium……189
5.6 Reactivity of [W≡C–Pt] with: Acetylides……... 191
5.7 Reactivity of [W≡C–Pt] with: Alkylidynes……201
5.8 Conclusions…….. 207
6 **CHAPTER SIX The Role of Metallacarbynes in Catalytic Coupling Reactions……209**
6.1 Implied μ_2-Carbidos in Catalysis……... 210
6.2 Metallacarbynes and Sonogashira Cross-Couplings……... 211
6.2.1 Palladium(II) metallacarbynes intermediates via oxidative addition……211
6.2.2 Phosphoniocarbyne complexes as off-cycle tangents…….215
6.3 Chalcocarbonylphosphoranes: A sidebar from Phosphoniocarbynes…… 222
6.3.1 Thiocarbonylphosphoranes varying electronic (ν_{CO}) and steric (Θ) parameters 226
6.3.2 Exploring heavier chalcopnitconioranes 230
6.3.3 Theoretically addressing chalcocarbonyl/phosphine coupling 230
6.4 Metallacarbynes and Suzuki-Miyaura Cross-Couplings……... 234
6.4.1 Developing a boron→gold→palladium relay 234
6.4.2 Functionalised carbynes via a boron→gold→palladium relay 238
6.5 Conclusions……...243

7 **CHAPTER SEVEN Synthesis of Group 11 and 12 Metallacarbynes……245**
7.1 Transmetallation in Alkynyl Chemistry: Significance of Tin, Copper, Gold, and Mercury. 245
7.2 Preparation of Bimetallic Gold Carbido Complexes……..... 247
7.2.1 Golden-Ring Disaggregation 248
7.2.2 Tin–Gold Transmetallation 258
7.2.3 In Search of Gold(III) Carbido Complexes 260
7.3 Revisiting Golden Rings: Species in Solution and Five-fold Symmetry……..263
7.4 Attempts Towards Bimetallic Copper Metallacarbyne Complexes…….272
7.5 Preparation of Mercury Metallacarbynes……... 276
7.5.1 A Collection from Mercury(II) Chloride 276
7.5.2 Aryls, Phenylpyridine, and Thiophene 283
7.5.3 Bidentate Dithiocarbamate 286
7.6 Catalytic Demercuration of Mercury Carbido/Organomercuriocarbyne Complexes……. 290
7.7 Conclusions…….. 292
8 **CHAPTER EIGHT Generalisable Synthesis of Metallacarbynes…… 294**
Part One: Insertion of Metals into Hg-C Bonds
8.1 Addition Reactions of Mercuriocarbynes……...294
8.2 Platinum and Palladium…….295
8.3 Iridium and Rhodium……....298
8.4 Ruthenium and Osmium……...305
Part Two: Hydride Metathesis with a *Bis*-carbido Mercurial
8.5 Preparation of the First Osmium μ_2-carbido Complex……..309
8.6 Ligand Substitution of $[WOs(\mu_2\text{-}C)Cl(CO)_3(PPh_3)_2(Tp^*)]$……. 314
8.7 Conclusions…….. 319
Conclusions and Future Directions……...321
9 **CHAPTER NINE Experimental Information…… 323**
9.1 General Considerations……... 323
9.2 Computational Methods……... 325
9.3 Crystallographic Methods……. 326
9.4 Synthetic procedures for Chapter Two compounds…….. 327
9.5 Synthetic procedures for Chapter Three compounds…… 334
9.6 Synthetic procedures for Chapter Four compounds……..347
9.7 Synthetic procedures for Chapter Five compounds……...357
9.8 Synthetic procedures for Chapter Six compounds…….374
9.9 Synthetic procedures for Chapter Seven compounds…… 391
9.10 Synthetic procedures for Chapter Eight compounds…….405
References……... 414

Chapter One

Metallacarbynes: A Review of Class B μ_2-Carbido Complexes

It should be noted that the following introduction was written as part of a larger literature review in partnership with H. J. Barnett on the entirety of μ_2-carbido chemistry. During writing, however, an exceptional and comprehensive review on the same topic was published by Reinholdt and Bendix.[1] The introduction provided here is therefore a selective overview of μ_2-carbido chemistry in general, that is specifically comprehensive for Class B examples, the subject of this thesis.

From drilling mineshafts to everyday tools, metal carbides have long been a prevalent application of organometallic chemistry. Carbides† are generally ceramic transition metal compounds containing a carbon atom inside their interstices, with carbides having been prepared for all 3d elements and groups 4–10 of the 4d and 5d elements. Carbide materials often have high melting temperatures, high conductivity/heat capacity, a characteristic hardness, and consequently, have thrust these compounds into widespread industrial use as cutting tools, hardeners and wear-resistant coatings.[2-3]

On a molecular level, a seminal report described metal carbide materials have catalytic properties similar to platinum-group metals in transformations, including but not limited to: hydrogenation, dehydrogenation and hydrogenolysis.[4] Since this early report, carbidos have been mooted as intermediates in the Fischer—Tropsch process to produce synthetic hydrocarbon fuels, splitting of CO on surfaces before entering C–C and/or C–H bond forming steps in addition to potentially being counter-productive species for this catalysis. More recently, carbidos were found at the centre of FeMo and FeV nitrogenase enzymes,[5-11] Nature's catalysts for transforming N_2 into NH_4^+, and studies have since pursued synthetic models of these cofactors.[12-13] Many reviews discuss the surface reactivity of carbides,[14-15] however, inherent challenges of solubility and ill-defined systems preclude spectroscopic interrogation that might allow deeper study and refinement of their catalytic properties. One proposed model to overcome the issues of studying heterogeneous catalysts is to think smaller: to investigate well-defined and soluble small molecule carbides that contain μ-carbido ligands yet enjoy increased exposure from fewer transition metal termini. Changing the focus to small molecules allows clearer spectroscopic and structural information relative to heterogenous environment, a variant of Muetterties 'Cluster-Surface'

† Throughout this thesis the term 'carbide' refers to the anionic species while 'carbido' refers to a single carbon atom serving as a covalent ligand, *cf.* 'chloride/hydride' anions and 'chloro/hydrido' ligands.

analogy,[16] but the problem is relatively little is known about low-nuclearity carbido complexes. Furthermore, general synthetic routes to molecular carbidos remain unknown as evident from the sporadic and serendipitous nature of their development.[17] This thesis aims to address the challenge of generalisable synthesis of a sub-class of μ-carbidos.

This Chapter will begin with an overview of molecular carbido chemistry with an emphasis of low-nuclearity‡ species. Initially the structure and bonding of carbido complexes will be discussed, exploring contrasts with conventional and heteroatom-functionalised carbyne complexes and to introduce extant classifications within the field. Secondly, molecular carbido synthesis will be discussed in general, but with particular emphasis on methods appropriate for metallcarbynes (Class B, *vide infra*). Lastly, the few demonstrations of previously established carbido reactivity will be surveyed, concluding with a commentary to contextualise of the aims of the research and further discussion that follows.

1.1 Bonding and Structure of Carbido Complexes

1.1.1 High or Low Nuclearity Species

Carbido complexes may be defined and classified by the coordination number of carbon in the first instance and the number of metals involved. A carbon atom residing between two transition metals may in principle be artificially assigned a variety of oxidation states. Strictly speaking, the formal oxidation state assignment allocates bonding electrons to the most electronegative element. The utility immediately crumbles for 4d and 5d transition metals of the later groups 6–12, on which most (indeed all encountered in the present research) molecular carbidos are based. These metals have Pauling Electronegativities in the range 2.00–2.54, resulting in a minimal difference with that of carbon (2.55) leading to substantial covalency. While atomic orbital energies of carbon are invariant, the energies and occupancies of the orbitals associated with transition metal ligand fragments to which carbon is bound may vary enormously. Accordingly, an analogy has been drawn between carbidos and the Fischer/Schrock metal-carbon multiple bonding extremes found in carbenes and carbynes.[1] If the carbido ligand is described following the Fischer paradigm, this would be consistent with deoxygenated CO and therefore a neutral *bis*-carbene C^0 ligand (:C:).[18-19] Alternatively, from a Schrock perspective, a carbido might be considered as fully deprotonated CH_4 such that an anionic ligand C^{4-} is appropriate,[20-21] without regard for Pauling's Electroneutrality Principle. In reality, carbido complexes lie on a continuum subject to electronic

‡ The arbitrary boundary between low and high nuclearity carbidos will be set at $M_3(\mu_3\text{-C})$ because as the number of metal increases to four and beyond, the carbide assumes an increasingly more interstitial and structural role, participating less directly in bond forming/breaking processes.

demands of the metal termini and bonding scenarios have been described through theoretical studies by Hoffman and Frenking as examples between extremes of Donor–Acceptor or Covalent bonding (Figure 1.1). [22-27] A similar dichotomy arises in the topical field of carbone chemistry, [28] where a zerovalent carbon atom is positioned between two neutral phosphine or *N*-heterocyclic carbene donors. Given this large electronic tuneability, carbido ligands might be expected to present rich coordination environments, bridging metal atoms in a variety of modes {μ_n: n = 2, 3, 4, 5, 6} such that for the present purposes, coordination number defines a species as high-nuclearity (μ_4–μ_6) or low-nuclearity (σ^1, μ_2 or μ_3) (Figure 1.2).

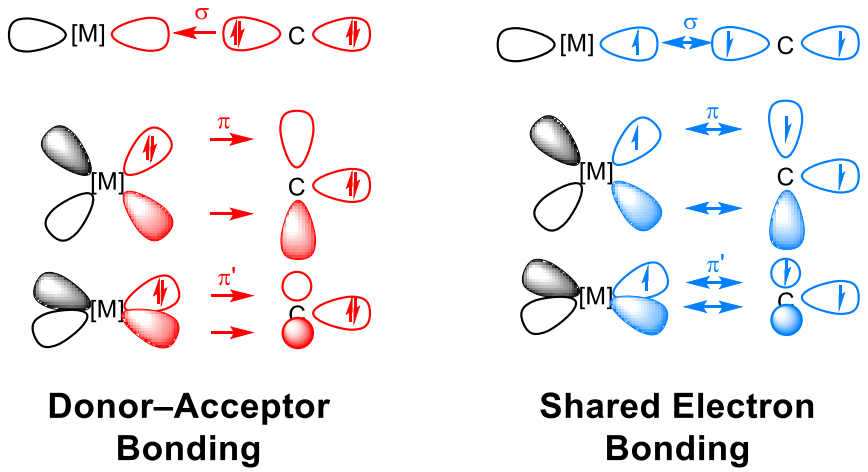

Figure 1.1: Bonding extremes for μ-carbido ligands.

High-nuclearity carbido compounds were first reported 125 years ago with Hofmann's "mercarbide" $[Hg_4(\mu_4\text{-}C)(OH)_4]$. [29] High nuclearity examples comprise the vast majority of carbido complexes with most arising from metal carbonyl cluster thermolysis in which CO is cleaved. [30] The most notable features of carbido complexes are involve high-nuclearity species such as the reduction of carbon monoxide to provide hydrocarbons (Fischer–Tropsch Process) [15, 31-34] and the reduction of dinitrogen by the FeMo nitrogenase cofactor in bacterial enzymes. [5-9] In contrast lower nuclearity carbido complexes (μ_2 and μ_3) have been far less explored. A lack of general synthetic routes means that fewer species have been discovered, however, overcoming this problem would likely lead to distinct reactivity owing to a more exposed carbon atom with unsaturated metal-carbon bonding. Furthermore, improved solubility and simpler coordination environments facilitate their study, easing spectroscopic[§] and structural analysis. For these reasons, low-nuclearity carbides have been suggested as models to study fundamental reactivity that may occur on the surface of ceramic metal carbides. [33]

[§] The vast majority of known μ_2-carbido complexes are diamagnetic and thus amenable to NMR studies.

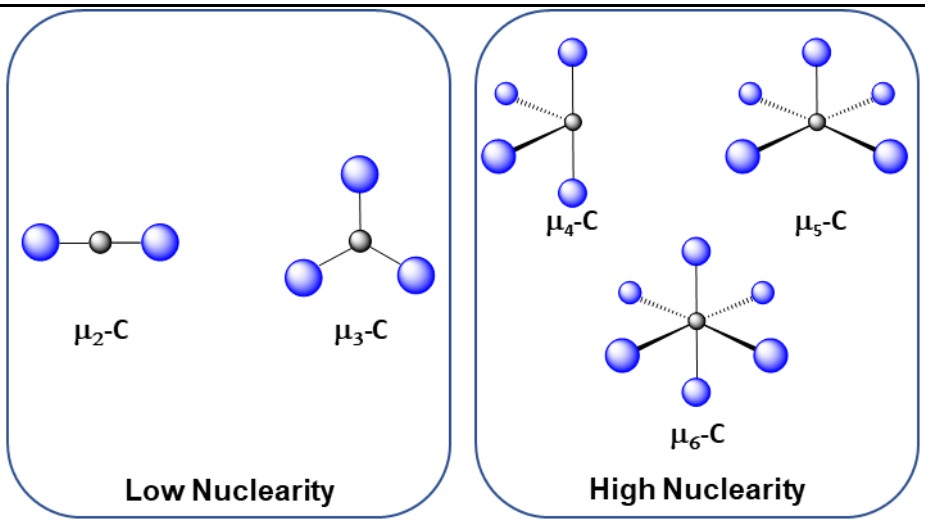

Figure 1.2: Commonly encountered geometries of μ-carbido complexes. [35-36]

1.1.2 Classifying Low-Nuclearity Carbido Complexes

For low nuclearity carbidos, the four valence electrons of carbon are available for bonding to two or three metal centres. In the case of μ_2-C species electronic accounting leads (so far) to four classes depending on the electronic distribution through the unsaturated M–C–M system. For context, the first μ_2-carbido complex ($[Fe_2(\mu_2\text{-}C)(TPP)_2]$) was reported by Mansuy in 1981, [20] the year *following* its prediction and bonding analysis by Hoffmann.[21] The broader discussion of bonding scenarios for this and other classes was not outlined until decades later in 2013. [17]

Examples of μ_2-carbido complexes can be categorised into one of four classes (Chart 1.1). Class A describes the dimetallacumulenes, featuring two formal metal-carbon double bonds and in all but two cases bear *homo*-metallic termini, resulting in a symmetric M–C–M spine. In contrast, Class B (metallacarbynes) display both a formal triple and single metal-carbon bond, in all but one case involving *hetero*-metallic termini reflecting the unsymmetrical spine. Meanwhile, Class C (Polar Covalent) contain a formal metal-carbon triple bond to one metal, such that the carbido retains a lone pair allowing it to form a dative bond to an unsaturated metal centre, akin to ligands such as CO and isocyanides. Finally, Class D (dimetallacarbenes) are the most recently identified examples, where the metal termini bend the carbido ligand such that a nucleophilic σ-donating lone pair forms, analogous to an *N*-heterocyclic carbene, containing transition metals in place of nitrogens. These classes provide the extreme bonding scenarios and the valence bond descriptions, whilst convenient for electronic book-keeping, represent significant oversimplification of what are electronically delocalised systems.

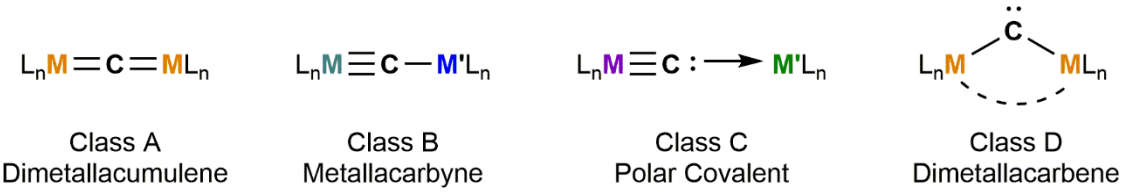

Chart 1.1: Bonding canonical forms of μ2-carbido complexes. [35-36]

The focus of this thesis surrounds the chemistry of heterobimetallic carbido complexes, specifically metallacarbynes (Class B). Other classes (A, C and D) will be mentioned where appropriate in limited discussion, or where comparison with Class B examples is instructive. By viewing Class B carbidos as metallacarbynes, it is inevitable that some comparisons with more conventional hydrocarbyl or hetero-atom functionalised carbyne complexes will be appropriate.

1.2 Synthesis of μ2-Carbido Complexes

The story of μ2-carbido systems began with controversy. In 1979, Kasai and co-workers claimed on the basis of a crystal structure determination (*sic.*) the highly implausible μ2-carbido [Re(CO)3(μ2-C)]2Sn(TPP) (TPP = tetraphenylporphyrinato)was produced from thermolysis of dichlorotetraphenylporphyrintin(IV) [Sn(TPP)Cl2] and [Re2(CO)10]. [37] Hoffman argued this was a μ2-*oxo* or methylene bridged species, given unsatisfactory electronic configuration on a theoretical basis, [22] as subsequently noted by Selegue. [33] What neither Hoffmann, nor Selegue, nor indeed the original authors seem to have appreciated is that while it is claimed that the crystal structure confirms [Re(CO)3(μ2-C)]2Sn(TPP), the terminal ligands on each rhenium in the ORTEP are mono-atomic rather than three carbonyls, which would have made the rhenium highly coordinatively unsaturated. The complex should clearly be reformulated as a *bis*(perrhenato) complex, *i.e.*, [Sn(TPP)(OReO3)2]. For these reasons, an iron-porphyrin system [Fe2(μ2-C)(TPP)2] predicted by Hoffman[22] and soon thereafter synthesised by Mansuy, [20] constitutes the original μ2-carbido species—an example of what was later described as a dimetallacumulene (Class A). Mansuy's discovery was soon followed by Selegue and co-workers disclosing the first example of a metallacarbyne [WRu(μ2-C)(O^{t}Bu)3(CO)2(Cp)] in 1987 which was also the first heterobimetallic carbido. Several years passed before a polar covalent complex Class C carbido was produced, [38] requiring prior development of what remains a rather unique terminal carbide. [39] The first isolated Class D dimetallacarbenes recently emerged from μ2-carbido templates, [40] but had been previously generated *in situ* without isolation *via* μ2-methylidyne deprotonation. [41] This section highlights selected syntheses of Class A, C and D μ2-carbido complexes, prior to a comprehensive study of producing Class B species as the primary goal of this thesis.

1.2.1 Synthesis of Classes A, C and D

1.2.1.1| Classes A and C: Halocarbon Reduction

Mansuy produced the prototypical μ_2-carbido complex from the reduction of carbon tetraiodide (CI_4) with iron powder in the presence of iron-porphyrin [FeCl(TPP)] (Figure 1.3A). [20] Reduction of a halocarbene is implied in Mansuy's synthesis, supported by the isolation of *dichloro*- and *dibromo*-carbene species, however, this was not observed for the implicit *diiodo*carbene-variant, instead furnishing the carbido complex [(TPP)Fe=C=Fe(TPP)]. The dibromocarbene [Fe(=CBr_2)(TPP)] could be reduced in the presence of further [FeCl(TPP)] to provide the same carbido complex, thereby substantiating the mechanistic proposal. Mansuy's complex was characterised by a stretching frequency consistent with a carbido bridge ($\nu_{Fe=C=Fe}$ 940 cm^{-1})** when compared to *oxo*- and *nitrido*-species ($\nu_{Fe=C=Fe}$ 940; $\nu_{Fe=N=Fe}$ 910; $\nu_{Fe=O=Fe}$ 885 cm^{-1}). The molecular structure was later elucidated by Goedken and co-workers (Figure 1.3B), revealing a highly symmetrical molecule (Fe–C 1.673 Å) with a linear Fe=C=Fe spine (180°).[42]

The porphyrin scaffold was subsequently expanded to include porphyrazines and phthalocyanines [$Fe_2(\mu_2$-C)$(pc)_2$] (pc = phthalocyanine), [43] including a ruthenium-phthalocyanine carbido. [44] Alkyl-substituted porphyrins were produced to increase solubility, [45] while mixed porphyrin/phthalocyanine species could be produced via reduction of isolated chlorocarbenes [Fe(=CCl_2)(TPP)] in the presence of [Fe(pc)]. [46] Several species were derivatised through coordination of other ligands to the axial coordination sites, as surveyed by Ercolani in a review on phthalocyanine chemistry. [47] In recent years, reduction of halocarbenes has resulted in octapropylporphyrazine derivatives on iron, [48] and one report described ruthenium phthalocyanine carbidos by thermolysis of [$Ru_3(CO)_{12}$] in which a carbonyl ligand was presumably the carbide source. The carbido ligand could also be sourced from basic chloroform, presumably via dichlorocarbene or trichloromethyl carbenoid intermediates. [49]

** A linear triatomic arrangement MCM would be expected to give rise to a symmetric (Raman active) and antisymmetric (IR-active) vibrational mode. Because of the low electronegativity difference between carbon and the transition metals for which μ_2-carbidos are known, the intensity of the IR-active mode is unlikely to be strong. Furthermore, the band is likely to occur in the fingerprint region of many co-ligands making unambiguous assignment problematic. Accordingly, rather few reports of this spectroscopic quantity have appeared.

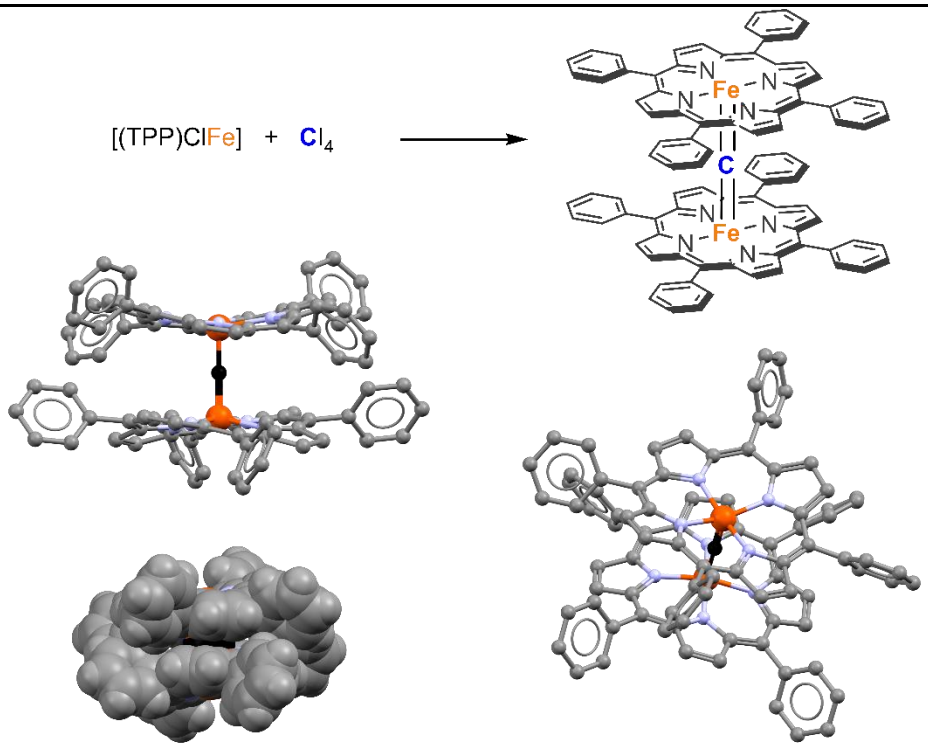

Figure 1.3: A) Original depiction of Mansuy's iron-porphyrin system.[20] B) Atomic structure later elucidated by Goedken and co-workers.[42] Inset showcasing the Fe–C–Fe linkage from the porphyrin plane accompanied by a space-filling diagram.

Dimetallacumulenes produced to this point were homobimetallic imposed by the reduction conditions. Beck and co-workers diverged from solely iron species to heterobimetallic complexes by reaction of isolated [Fe(=CCl2)(TPP)] with nucleophilic carbonyl metallates, *e.g.*, $[Re(CO)_5]^-$ to give [(TPP)Fe=C=Re(CO)$_4$Re(CO)$_5$].[50††] The vibrational frequency of the carbido ($\nu_{Fe=C=Re}$) could not be assigned and the $^{13}C\{^1H\}$ NMR spectrum exhibited a signal assigned as a μ_2-carbido (δ_C = 211.7), however, this is unlikely given a single resonance was attributed to carbonyl ligands despite three chemical environments (1:4:4). Later studies suggest carbido resonances come at much higher frequency and the effect of the porphyrin ring current magnetic anisotropy is likely to contribute to the shielding, *e.g.*, the diphenylcarbene complex [Fe(=CPh$_2$)(TPFPP)] (TPFPP = tetrakis(pentfluorophenylporphyrinato)[51] has δ_C = 358.98 while the non-haeme analogue [Fe(=CPh$_2$)(tmtaa)] (tmtaa = tetramethyldibenzotetraazaannulene)[52] has δ_C = 313.2. The elegance of this species arises in the atomic structure elucidated by X-ray diffraction (Figure 1.4), featuring an Fe–C bond length (1.61(1) Å) similar to Mansuy's complex (*ca* 1.673 Å)[20] and the Re–C bond length of (1.96(1) Å) is consistent with a typical Re–C double bond (1.959(92) Å).[‡‡] The octahedral

†† Carbido complexes are described with interchangeable line formulae [MM'(μ_2-C)L$_n$] and [L$_n$MCM'L$_n$]. This Thesis favours the former but will use the latter where ligand set is ambiguous.
‡‡ This was measured as an average of all measurements in the CCDC (*v.* 5.41)

geometry is suggestive of rhenium(0), with the implication being that a Re=C double bond must be operative to satisfy the 18-electron rule, thus being consistent with a dimetallacumulenic manifold. The many carbene complexes of the form $(OC)_5Re\text{-}(OC)_4Re(CO)=CR_2$ (*e.g.*, CR_2 = $C(OMe)SiPh_3$, Re=C = 2.09(2) Å) [53] typically have the carbene *cis* to the Re–Re bond, however it would not be sterically viable for the :C=Fe(TPP) 'carbene' to assume this position.

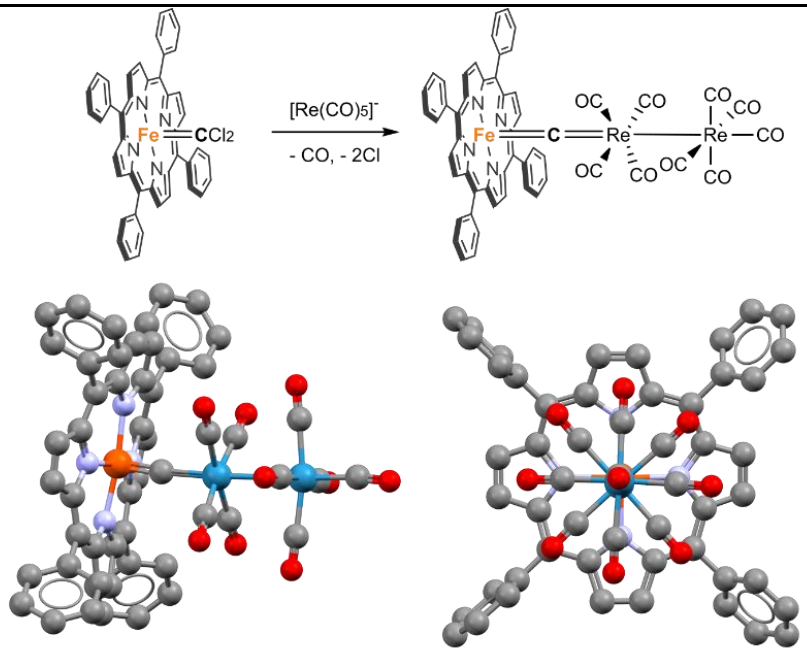

Figure 1.4: A) Synthesis of Beck's dimetallacumulenes. B) Corresponding atomic structure. [50, 54]

In later work, Beck explored other carbonyl metallates to furnish heterobimetallic species with new termini including manganese and chromium [(TCNPP)Fe=C=(ML_n)] [ML_n = $Mn(CO)_4Mn(CO)_5$ or $Cr(CO)_5$] (TCNPP = *tetrakis*(*p*-cyanophenyl)prophyrinate). [54] Although these examples were the first μ_2-carbidos to feature these elements, evidence was restricted to UV-VIS and elemental analysis due to limited solubility. In the same report, Beck returned to homometallic termini, showing this method could produce iron dimetallacumulenes with asymmetric ligand sets such as [(TPP)Fe=C=$Fe(CO)_4$] and [(TCNPP)Fe=C=$Fe(CO)_4$]. Whilst these diiron species appear plausible, their characterisation was based on infrared spectroscopy (ν_{CO}) and unsatisfactory elemental microanalysis alone. Beck concluded that nucleophilic substitution by metal carbonylates at dichlorocarbenes provides a somewhat general synthesis of heterobimetallic μ_2-carbido complexes, he noted many unsuccessful attempts, amongst which strongly nucleophilic reagents $[M(CO)_2(\eta\text{-}C_5H_5)]^-$ (M = Fe, Ru) resulted in redox processes to generate $[M_2(CO)_4(\eta\text{-}C_5H_5)_2]$.

In a further example of halocarbon reduction, Takao and Seki reported the ruthenium hydride cluster $[\{Cp^*Ru(\mu\text{-}H)\}_3(\mu_3\text{-}H)_2]$ reduces CCl_4 to provide a μ_2-chlorocarbyne $[Ru_2(\mu_2\text{-}CCl)(\mu$-

Cl)Cl_2(Cp*)$_2$] where a further reduction of the μ_2-halocarbyne with zinc and diethyl maleate (DMA) gives the Class A carbido [$Ru_2(\mu_2$-C){μ-η^1:η^2-ZnCl(DMA)}$_2$] (Scheme 1.1). A carbido species was also implied in a similar reaction with ethylene but could not be observed. The Zn–maleate supports provided an unusual ligand environment for a μ_2-carbido complex, however, structural (Ru–C: 1.84 Å) and spectroscopic data (δ_C = 458.7) still support a Class A μ_2-carbido description.

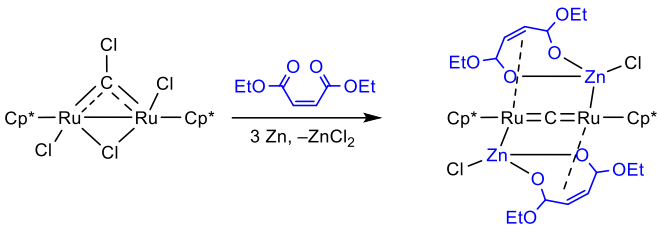

Scheme 1.1: Reduction of a μ_2-halocarbyne to a Class A dimetallacumulene.

A remarkably simple μ_2-carbido complex of chromium [$Cr_2(\mu_2$-C)Br_4(THF)$_5$] was obtained in high yield from the reduction of CBr_4, with $CrBr_2$ serving as both the metal source and the reductant (Scheme 1.2).[55] This synthetically versatile carbido complex remains the sole example of a Class C carbido not based on ruthenium, consequently arising from halocarbon reduction as opposed to a terminal carbide. This reaction is specific to CBr_4 as CCl_4 provides the μ_3-halocarbyne [$Cr_3(\mu_3$-CCl)$Cl_3(\mu$-Cl)$_3$(THF)$_6$] instead results from reduction of carbon tetrachloride (CCl_4) with [$CrCl_2$]. The derived pyridine adduct [$Cr_2(\mu_2$-C)Br_4(py)$_5$] which was structurally characterised has disparate Cr-C bond lengths (1.634(10) and 2.035(10) Å) in support of the Class C rather than dimetallacumulenic Class A description.

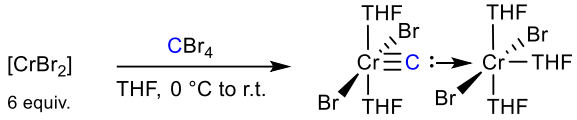

Scheme 1.2: Preparation of a chromium Class C μ_2-carbido *via* halocarbon reduction.

1.2.1.2| Class A: Thermolysis

Degradation of metal carbonyls under high temperatures is the predominant method of producing high-nuclearity carbido complexes yet also gives select μ_2-carbidos. For Class A, Sorokin and co-workers serendipitously discovered the phthalocyanine species [$Ru_2(\mu_2$-C){$(BuO)_8$pc}$_2$] during examination of monomeric sandwich precursors for catalytic activity (Scheme 1.3). They concluded the unselective thermal decomposition of the [$Ru_3(CO)_{12}$] cluster provides not only a source of ruthenium, but also the μ_2-carbido as a minor product (22% isolated yield), highlighting the lack of selectivity *via* thermolysis routes. Unfortunately, the complex was not structurally charactered, nor was the μ-carbido resonance detected by $^{13}C\{^1H\}$ NMR studies, though its

catalytic activity was explored and is mentioned in Section 1.5.1. This species is the lone example of a carbido in Classes A, C or D achieved *via* thermolysis.

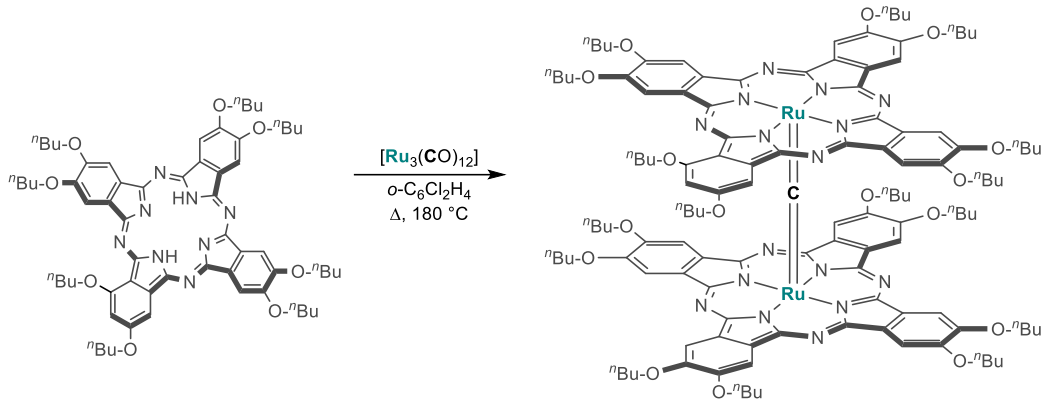

Scheme 1.3: Thermolysis of $[Ru_3(CO)_{12}]$ to give μ_2-carbido complex $[Ru_2(\mu\text{-}C)\{(^n BuO)_8pc\}_2]$.

1.2.1.3| Class A: Small Molecule Activation

Sorokin's thermolysis suggests CO is the μ_2-carbido carbon source, where evidence for this was demonstrated years early on a more discrete system. Wolczanski reported two Class A carbidos $[W_2(\mu_2\text{-}C)(=NAr)Cl_2(SiOtBu_3)_4]$ (Ar = 2,6-dimethylphenyl) and $[W_2(\mu_2\text{-}C)(=O)Cl_2(SiO^tBu_3)_4]$ that arise from cleavage of an isocyanide or carbon monoxide, respectively, across a tungsten-tungsten triple bond (Scheme 1.4).[56] Activation of CO was also demonstrated niobium calixarenes and sodium amalgam, producing two species $[Nb_2(\mu_2\text{-}C)(calix)_2]\cdot Na_n$ (n = 2 and 3) which remain the only examples of early transition metal (Groups 3–5) μ_2-carbidos (Scheme 1.5).[57] Carbon monoxide has not be activated to a μ_2-carbido since. Cleavage of CO and CNR to provide a μ_2-carbido ligand demonstrated cleavage of strong C–O and C–N bonds, respectively. Years later the analogous C–C bond cleavage from activation of acetylene was reported. Substituted alkynes reacted with the dimeric ruthenium complex $[(\eta^6\text{-}p\text{-cymene})Ru(\mu_2\text{-}Cl)_3RuCl(\eta^2\text{-}C_2H_4)(PCy_3)]$ to form vinylidenes for atom transfer radical addition reactions, however, acetylene was found to be an outlier. Acetylene reacted with the dimer to form a tetranuclear dimetallacumulene $[(p\text{-cymene})Ru(\mu_2\text{-}Cl)_3RuCl(C_2H_4)(PCy_3)]_2C$ under mild conditions, where ^{13}C isotope labelling studies confirmed acetylene as the origin of the carbido (Scheme 1.6).[58] The authors proposed a vinylidene intermediate $[(p\text{-cymene})Ru(\mu_2\text{-}Cl)_3RuCl(C{=}CH_2)(PCy_3)]$ that undergoes further transformations to form the carbide, however, this was not evidenced further. This activation of a C≡C bond remains the only example outside of Class B.

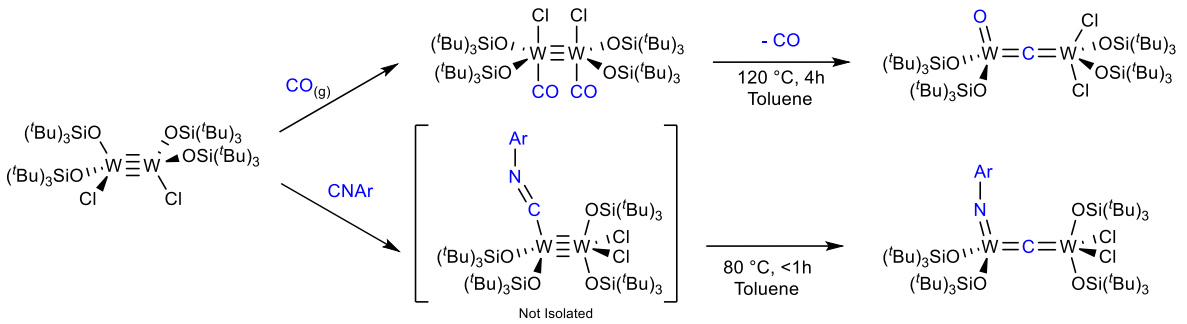

Scheme 1.4: Carbon monoxide and isocyanide dissociation across a tungsten-tungsten triple bond. [56]

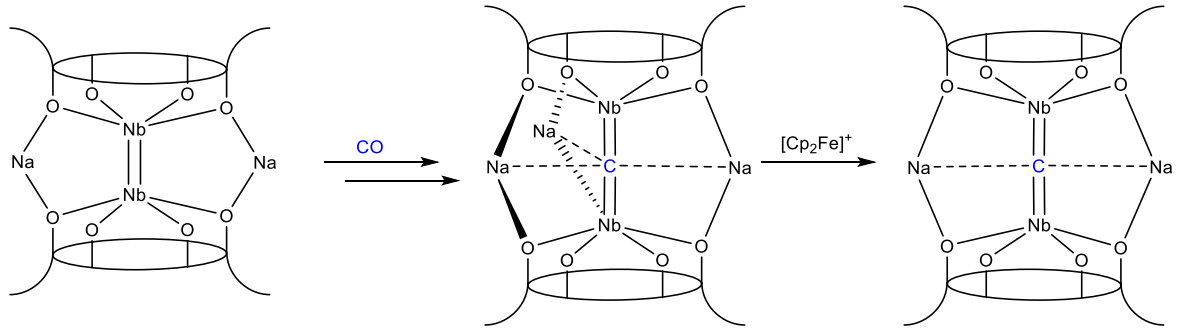

Scheme 1.5: Synthesised niobium dimetallacumulenic species. [57]

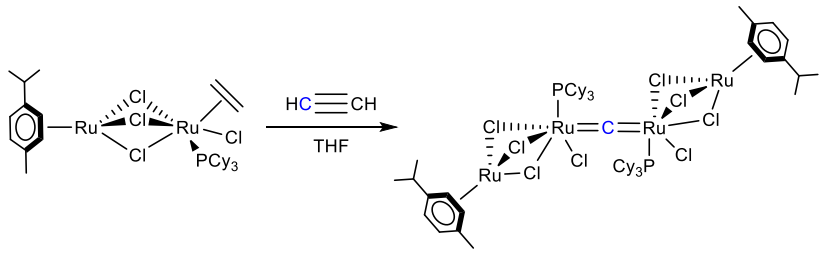

Scheme 1.6: Scission of acetylene to form a tetrametallic dimetallacumulene. [58]

1.2.1.4 | Class A: Chalcogen Cleavage

Severing carbon monoxide or acetylene is an energetically difficult route to provide a carbido ligand. A more energetically favoured alternative has since emerged through cleavage of carbon-chalcogen bonds to produce Class A and B species. The *solvento* complex [Re(THF)(CO)$_2$(Cp)]—as obtained by photolysis of [Re(CO)$_3$(Cp)] in THF—reacts with CS_2 and PPh_3 to eliminate $S{=}PPh_3$ and provide [Re(CS)(CO)$_2$(Cp)]. [59] A reinvestigation of this syntheses uncovered trace amounts of dimetallacumulene side product [Re$_2$(μ_2-C)(CO)$_4$(Cp)$_2$] (Scheme 1.7) in addition to [Re(η^2-S$_2$)(CO)$_2$(Cp)]. [60] The carbide complex could be obtained in 90% yield by treating isolated [Re(CS)(CO)$_2$(Cp)] with excess [Re(THF)(CO)$_2$(Cp)] but not PPh_3, indicating that the thiocarbonyl ligand is activated in a bimolecular process. The authors outlined the species should be assigned to Class A given the short Re–C bond lengths but recognised this may be overly simplistic, given a minimal rotation barrier around the Re=C=Re spine was identified. An accompanying

computational study supported this claim and provided first theoretical inquiry into μ-carbidos since Hoffmann's original predictions. The calculations predicted a carbido vibration ($\nu_{Re=C=Re}$ = 1004 cm^{-1}) that supported experimental observation ($\nu_{Re=C=Re}$ = 1019 cm^{-1}), providing a rare example of carbido vibrational mode observed *via* infra-red spectroscopy.

The complex $[Re(THF)(CO)_2(Cp)]$ was also found to extract selenium (as $[Re_2(\mu\text{-}Se)(CO)_4(Cp)_2]$) from selenocarbonyl ligand in $[W(CSe)(NO)(CO)(Tp^*)]$ to form $[WRe(\mu_2\text{-}C)(NO)(CO)_3(Cp)(Tp^*)]$—the first fully characterised *hetero*-bimetallic dimetallacumulene (Scheme 1.7). [61] Typical characterisation supported the formulated structure; however, the extremely deshielded carbido environment apparent in the $^{13}C\{^1H\}$ NMR is noteworthy (δ_C = 508.8), being the highest frequency carbido resonance measured to date. One example of a Class B carbide has also been observed to arise via C–Se bond activation of a selenocarbonyl ligand (*vide infra*). The reaction of $[Et_4N][Mo(CSe)(CO)_2(Tp^*)]$ with $[Ir(NCMe)(CO)(PPh_3)_2]$ was expected to provide the isoselenocarbonyl complex $[MoIr(\mu_2\text{-}CSe)(CO)_3(PPh_3)_2(Tp^*)]$ and quite possibly this is an intermediate, however iridium inserts into the C–Se bond followed by dimerization to provide as the first group 9 μ_2-carbido, a diselendiiridatetrahedrane $[Mo_2Ir_2(\mu_2\text{-}C)_2(\mu_2\text{-}Se_2)(CO)_6(PPh_3)_2(Tp^*)_2]$ spiked by by two Mo ≡C–Ir linkages. [62]

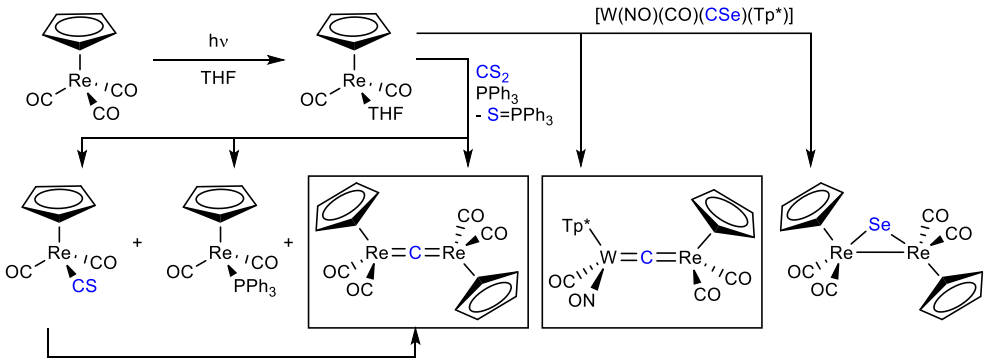

Scheme 1.7: Photolysis of a rhenium(I) carbonyl complex with subsequent chalcogen cleavage to achieve *homo*- and *hetero*-bimetallic dimetallacumulenes. Key by-products are included where verified. 60

Cleavage of chalcogens has allowed the most significant advances in Class A μ_2-carbido chemistry, particular for rhodium complexes. The boryl-rhodium(I) complex $[Rh(Bpin)(PEt_3)_3]$ (pin = pinacolato) reacts with CS_2 to afford the dimetallacumulene $[Rh_2(\mu_2\text{-}C)(SBpin)_2(PEt_3)_4]$ which can be subsequently hydrolysed to $[Rh_2(\mu_2\text{-}C)(SH)_2(PEt_3)_4]$ (Scheme 1.8). [18] The carbido resonances were challenging to detect (δ_C = 439.4 and 431.9, respectively) given extensive coupling to multiple spin active nuclei (^{103}Rh and ^{31}P 100% I = ½: $^1J_{CRh}$ = 44, 45, $^2J_{CP}$ = 11, 12 Hz), however, this could be overcome utilising labelled $^{13}CS_2$—a strength of this atom-economic synthetic

method.[§§] The authors outlined that co-ordination to rhodium weakens C=S bonds and concurrent formation of thermodynamically stable B–S bonds propels the carbido installation. The activation of CS_2 can be also performed by σ-germyl rhodium complexes with both sulfur atoms inserting into Rh–Ge bonds (Scheme 1.9) to provide $[Rh_2(\mu_2\text{-}C)(SGePh_3)_2(PEt_3)_4]$. The isolation of the intermediates $[Rh(SGePh_3)(CS)(PEt_3)_2]$ allowed the subsequent observation of the mixed species $[Rh_2(\mu_2\text{-}C)(SBpin)(SGePh_3)(PEt_3)_4]$ upon treatment with $[Rh(BPin)(PEt_3)_3]$, although this was not isolated due to subsequent ligand scrambling. While this reaction produced a mixture, discrete species were observed in solution aided by enriched ^{13}C isotopic labelling. [63]

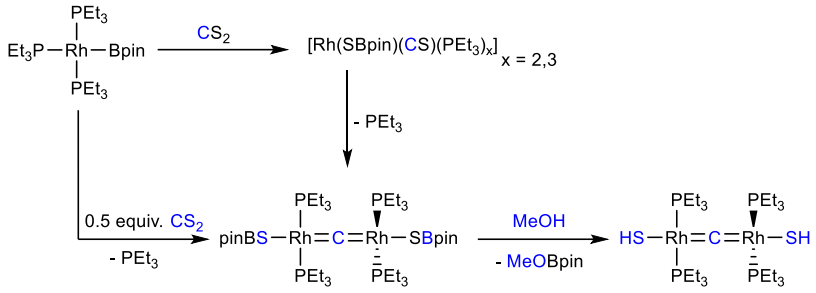

Scheme 1.8: Chalcogen cleavage of C=S bonds to provide a rhodium dimetallacumulene. [18]

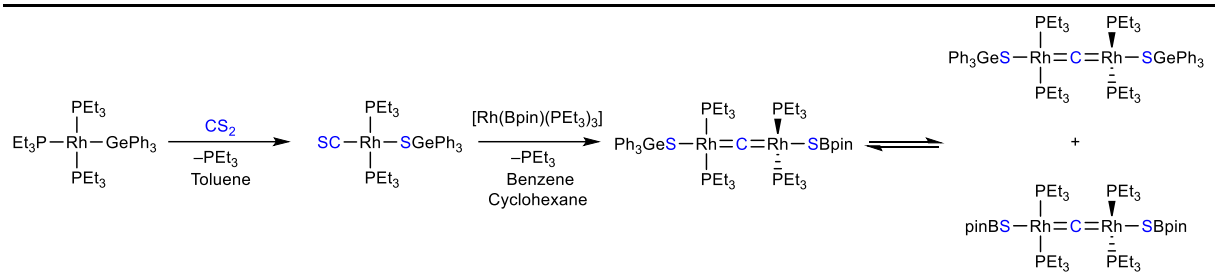

Scheme 1.9: Generation of germylthiolato-coordinated dimetallacumulenes and the equilibrium observed assisted by $^{13}C\{^1H\}$ NMR spectroscopy with ^{13}C enrichment. [63]

Cleavage of C–S bonds was subsequently found by this author[***] to also proceed with Wilkinson's archetypal thiocarbonyl complex $[RhCl(CS)(PPh_3)_2]$ when treated with catecholborane to provide the stable complex $[Rh_2(\mu_2\text{-}C)Cl_2(PPh_3)_4]$ (Scheme 1.10). [19] The rhodium species was extensively characterised, including identification of the carbido vibration ($\nu_{Rh=C=Rh}$ = 1011 cm^{-1}) with the assistance of computational modelling, and the ^{13}C carbido resonance aided by isotopic labelling (^{13}C enrichment: δ_C 424.2, $^1J_{CRh}$ = 47 Hz).[†††] Unlike those of Braun, $[Rh_2(\mu_2\text{-}C)Cl_2(PPh_3)_4]$

[§§] A simple inclusion does not correlate to an affordable option. At the time of printing, $^{13}CS_2$ is an expensive reagent [$1,520 AUD/g; Sigma–Aldrich(Merck)] although the depreciated price of rhodium [$ 440 AUD/g] from that of the all-time-high June 2020 [$1500 AUD/g] offers some consolation at time of writing. Since 80% of rhodium is used for automotive catalytic converters, the drive towards electric vehicles may see fundamental rhodium chemistry become once again viable.

[***] This work was commenced as part of an under-graduate vacation project by the author. Returning upon completion of undergraduate and honours studies, the work was further developed by a colleague Dr H. J. Barnett, during his subsequent PhD studies.

[†††] Due to the broad resonance recorded, $^2J_{CP}$ was not resolved.

contains labile chlorides and phosphines that greatly facilitated access to an extensive library of dimetallacumulenes through ligand substitutions (see Section 1.4.1.1), demonstrating a versatile species for late synthetic divergence. This versatility proved rather fortunate in that the study also included the screening of numerous other rhodium and iridium thiocarbonyls, which failed to result in carbide formation.

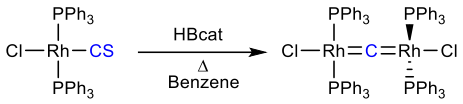

Scheme 1.10: Rhodium dimetallacumulene *via* thiocarbonyl reduction. [19]

1.2.1.5 | Class C: A Ruthenium Terminal Carbido as a Metalloligand

Class A syntheses vary greatly with multiple methods, albeit rather system-specific, to furnish μ_2-carbido complexes. Conversely, Class C μ_2-carbidos (polar covalent or 'dative') were obtained *via* a single method as the class is limited by the availability of suitable terminal (σ^1) carbido complexes (Chart 1.2).### While lithiocarbynes [M(≡CLi)(CO)$_2$(Tp*)] (M = Mo or W) [64] may be viewed as terminal carbidos in solution, they have defied isolation. Cummins *et al.*, isolated the first terminal carbido in 1997 which was based on molybdenum *viz.* [K(benzo-15-*c*-5)$_2$][Mo(≡C)(N^{t}BuC$_6$H$_3$Me$_2$)$_3$]. [65] Agapie, a contributor to the original Cummins publication, has since produced a very different trio of terminal molybdenum carbido [Mo(≡C)(CO){C$_6$H$_4$(C$_6$H$_4$P^{i}Pr$_2$-2)$_2$-1,4}]$^{n+}$ available with charges of n = –1, 0 and +1.§§§ [66-67] Both the neutral member (n = 0) and the osmium complex [Os(C)Cl$_2$(PCy$_3$)$_2$] reported by Johnson, [68] will in the future no doubt serve as precursors to a wide range of heterobimetallic Class C carbido complexes. To date, however, this approach has only been applied to the remarkably stable ruthenium complex [Ru(≡C:)Cl$_2$(PCy$_3$)$_2$] (δ_C = 471.8). Initial studies by Grubbs[36] showed that reactions with [Mo(NMe$_3$)(CO)$_5$] and [PdCl$_2$(SMe$_2$)$_2$] afforded the complexes [MoRu(μ_2-C)Cl$_2$(CO)$_5$(PCy$_3$)$_2$] (δ_C = 381.2) and [RuPd(μ_2-C)Cl$_4$(SMe$_2$)(PCy$_3$)$_2$] (δ_C = 446.3). The former is unstable in solution while the latter reacts with CO to regenerate the terminal carbido precursor (Scheme 1.11). Through the extensive studes of Reinholdt and Bendix, [69-74] this ruthenium carbido has dominated the Class C polar covalent space given the ease of synthesis relative to the other examples. The analogous osmium carbido has not yet been utilised to produce a μ_2-carbido complex, indeed osmium termini remain unknown for all μ_2-Classes (see Chapter Eight).

Terminal carbido complexes are beyond the scope of this work and only discussed when comparison is instructive. For a comprehensive discussion, see the review by Reinholdt and Bendix. [1]

§§§ Concordance: Publications from this group assign a 4– charge to the terminal carbido ligand, *i.e.*, for n = 0, this would be a d^2 complex. Assuming this formalism, [Ru(C)Cl$_2$(PCy$_3$)$_2$] would be Ru(VI) = d^2. Alternatively, these complexes may be described as Mo(0) = d^6 and Ru(II) = d^6.

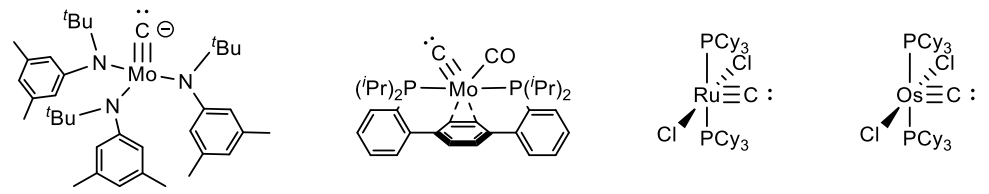

Chart 1.2: Representative terminal carbido complexes.

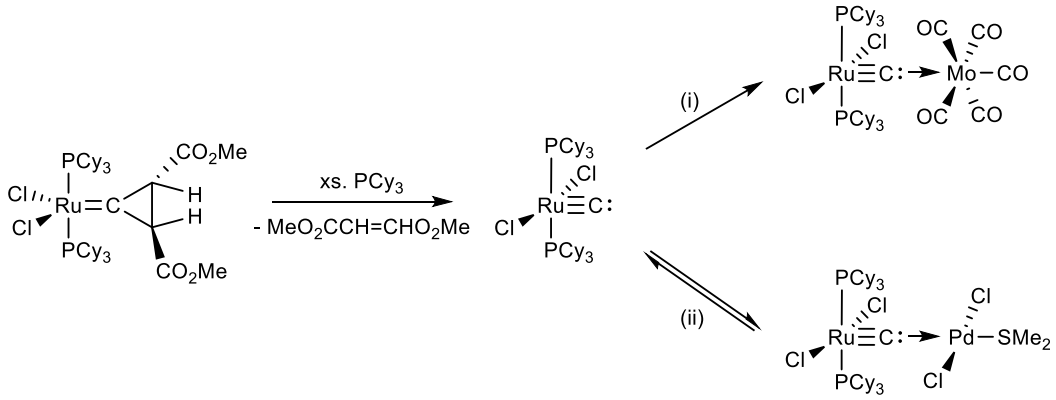

Scheme 1.11: Grubbs' archetypical synthesis of polar covalent complexes from a terminal ruthenium carbide. [38] (i) $[Mo(NMe_3)(CO)_5]$. (ii) $[PdCl_2(SMe_2)_2]$.

Reinholdt and Bendix described a further 12 Class C complexes featuring several metal termini that had previously been observed for other classes of μ_2-carbidos (M = Pd, Pt, Au, Rh[****] and Ir) in addition to silver and copper as a previously unknown termini (Scheme 1.12). [75] The resulted polar covalent family was extensive characterised, providing the most in depth study of μ_2-carbidos to date with a collection of data collected that is as impressive as the diversity of metals (Table 1.1). In addition to simple monometallic addenda, the ruthenium carbido was shown to bind to metal-sulfido cubane clusters, [76] recalling the role of metallathiocubane clusters in the nitrogenase molybdenum carbido cofactor (Chart 1.3). [5-9] Previous coordination of $[Ru(\equiv C:)Cl_2(PCy_3)_2]$ to square-planar platinum(II) provided a platform to study *trans*-influences where shifts in μ_2-carbido resonance acts as a spectroscopic reporter parameter. A family of platinum(II) complexes featuring neutral donor ligands of differing elements {CN^tBu, CNCy, PCy_3, PPh_3, $AsPh_3$, and $P(OPh)_3$} and nitrogen heterocyclic ligands were prepared as polar covalent compounds so as to correlate δ_C shifts with ligand influence. [77]

[****] Braun and co-workers released a rhodium dimetallacumulene at a similar time.

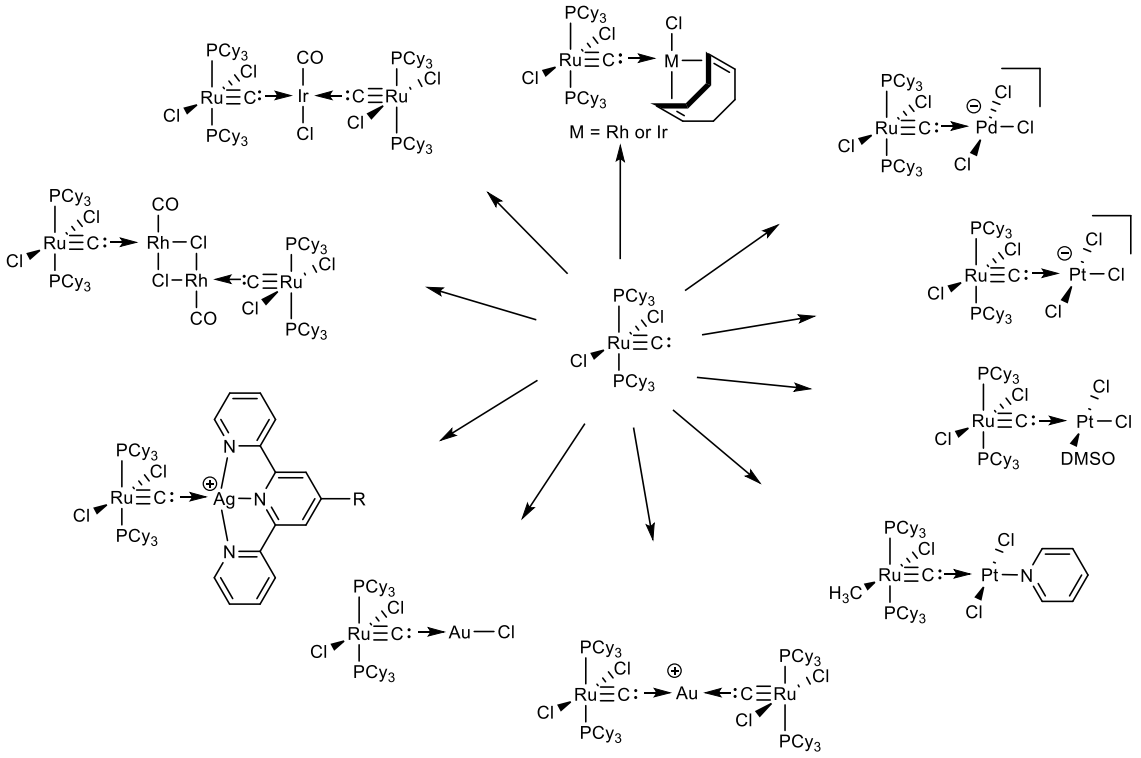

Scheme 1.12: Expansion of polar covalent complexes reported by Bendix and coworkers. [75]

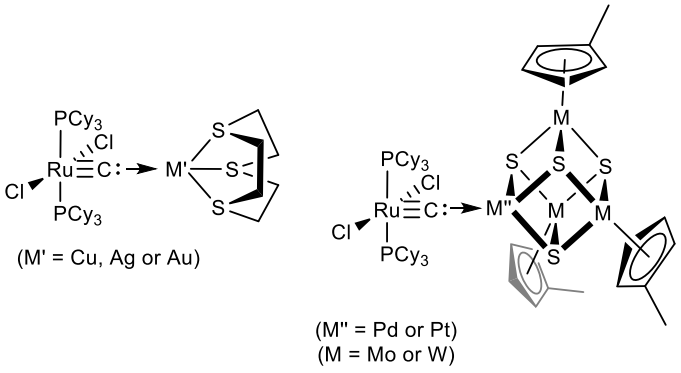

Chart 1.3: Series of polar covalent carbidos bearing metal-sulfide clusters to model the carbido geometry in nitrogenase. [76]

Table 1.1: Spectroscopic properties and atomic structural parameters of polar covalent complexes produced by Bendix and co-workers. [75]

Complex	δ_C[a] (ppm)	$^1J_{C\rightarrow M'}$ (Hz)	$r_{Ru\rightarrow C}$ (Å)	$r_{C\rightarrow M'}$ (Å)	$\angle_{Ru-C\rightarrow M'}$ (°)
$[Cl_2(PCy_3)_2Ru{\equiv}C{:}\rightarrow RhCl(COD)]$	411.7	59	1.690(2)	1.897(2)	173.4(3)
$[Cl_2(PCy_3)_2Ru{\equiv}C{:}\rightarrow IrCl(COD)]$	387.7	–	1.698(3)	1.882(3)	174.8(2)
$[PPN][Cl_2(PCy_3)_2Ru{\equiv}C{:}\rightarrow PdCl_3]$	381.1[b]	–	1.668(2)	1.892(2)	173.5(2)
$[Cl_2(PCy_3)_2Ru{\equiv}C{:}\rightarrow PtCl_3][AsPh_4]$	351.0	1396	1.691(3)	1.873(3)	174.4(4)
$[Cl_2(PCy_3)_2Ru{\equiv}C{:}\rightarrow PtCl_2(DMSO)]$	344.8	1334	1.682(2)	1.919(2)	177.6(1)
$[Cl_2(PCy_3)_2Ru{\equiv}C{:}\rightarrow PtCl_2(py)]$	350.3	1283	1.679(3)	1.881(3)	172.9(2)
$[\{Cl_2(PCy_3)_2Ru{\equiv}C{:}\rightarrow\}_2Au][BF_4]$	395.3	–	1.65(1) 1.68(1)	1.960(10)[b] 1.974(9)[b]	173.6(6)[b] 175.4(6)[b]
$[Cl_2(PCy_3)_2Ru{\equiv}C{:}\rightarrow AuCl]$	395.4	–	1.664(3)	1.921(3)	175.4(2)
$[Cl_2(PCy_3)_2Ru{\equiv}C{:}\rightarrow Ag(4'\text{-}C_6H_5\text{-terpy})][OTf]$	433.5	187	1.651(3)	2.072(3)	176.5(2)
$[\{Cl_2(PCy_3)_2Ru{\equiv}C{:}\rightarrow Rh(CO)\}_2\{\mu_2\text{-}Cl\}_2]$	397.6	60	1.688(3)	1.864(3)	176.9(1)
$[\{Cl_2(PCy_3)_2Ru{\equiv}C{:}\rightarrow\}_2IrCl(CO)]$	397.4	–	1.675(5)[c] 1.677(5)[c]	1.974(5)[c] 1.988(5)[c]	180.0[c]

Notes: [a]Measured in $CDCl_3$ unless specified otherwise. [b]Measured in CD_2Cl_2. [c] No e.s.d. as Ir lies at (½, y , ¾) on a proper *2* axis.

A later example within Class C incorporated a nitrido fragment $[Cr(\equiv N{:})(dbm)_2]$ (dbm = dibenzoylmethane) as a donor ligand on platinum(II) to provide $[(PCy_3)_2Cl_2Ru{\equiv}C{:}\rightarrow$*trans*-$PtCl_2\leftarrow{:}N{\equiv}Cr(dbm)_2]$ which contains both a μ_2-carbido and μ_2-nitrido in one molecule. Structural analysis confirmed the molecular structure, however, the chromium(V) terminus was found to have a localised unpaired electron by EPR studies, thereby making NMR spectroscopy less useful.[74]

1.2.1.6| Class D: Deprotonation and Cycloaddition

Of the four μ_2-carbido classes, dimetallacarbenes (Class D) are the most recent to emerge in 2014, understandably delayed given synthetic routes require rare μ_2-methylidynes†††† or Class A μ_2-carbidos as precursors.[78] Takemoto and co-workers generated the first dimetallacarbene *in situ via* deprotonation of $[(Cp^*Ru)_2(\mu_2\text{-}CH)(\mu_2\text{-}NPh)]^+$ with the bulky base $KN(SiMe_3)_2$ at low temperature (–78 °C). Although $[(Cp^*Ru)_2(\mu_2\text{-}C{:})(\mu_2\text{-}NPh)]$ was unable to be isolated, the complex could be spectroscopically characterised and a theoretically optimised geometry suggested a highly bent geometry at carbon, with significant carbene character akin to *N*-heterocyclic carbenes (NHCs). Takemoto's species was the first example of two metals being utilised as heteroatom substituents towards a carbene yet proved inconsistent with Mansuy's depiction of dimetallacumulenes (Class A). For these reasons, $[(Cp^*Ru)_2(\mu_2\text{-}C{:})(\mu_2\text{-}NPh)]$ pioneered (and was later classified as a) Class D μ_2-carbido (dimetallacarbenes) (Scheme 1.13).‡‡‡ The authors further demonstrated a μ_2-carbido

†††† A comprehensive review of μ_2-methylidynes is included in Chapter Five (Section 5.4).

‡‡‡ The authors of $[(Cp^*Ru)_2(\mu_2\text{-}C)(\mu_2\text{-}NPh)]$ were not responsible for coining the term 'Dimetallacarbene'; that came later in 2019 accompanied by structural authentication.

with carbene character through reactivity studies. Freshly generated [(Cp*Ru)$_2$(μ_2-C:)(μ_2-NPh)] reacted with elemental sulfur and selenium to form bridging *thio*- and *seleno*-carbonyl complexes, further supporting a new class of complexes (see Section 1.4.1.4).

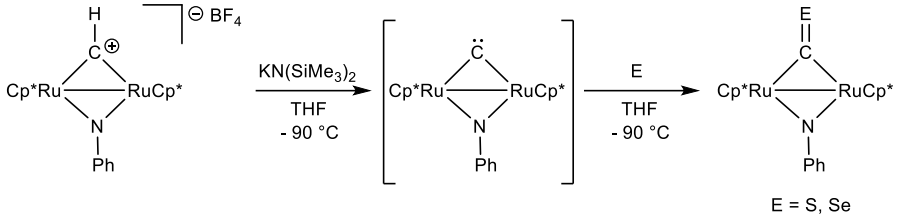

Scheme 1.13: Takemoto and co-workers *in situ* preparation of a dimetallacarbene and subsequent reactions with elemental chalcogen sources {E = S_8, Se_n}.[79]

A serendipitous discovery found the related Class A (dimetallacumulene) [Rh_2(μ_2-C)Cl_2(μ-dppm)$_2$] combined with the electrophilic alkyne DMAD (dimethyl acetylenedicarboxylate) in a formal[§§§§] [3+2]-cycloaddition to provide [Rh_2(μ_2-C)(μ_2-DMAD)Cl_2(μ-dppm)$_2$] (Scheme 1.14). The species proved robust presumably owed to the accompanying ligand bulky enveloping the carbido to give the first isolable, fully characterised dimetallacarbene, or MetallaHeterocyclic Carbene (MHC).

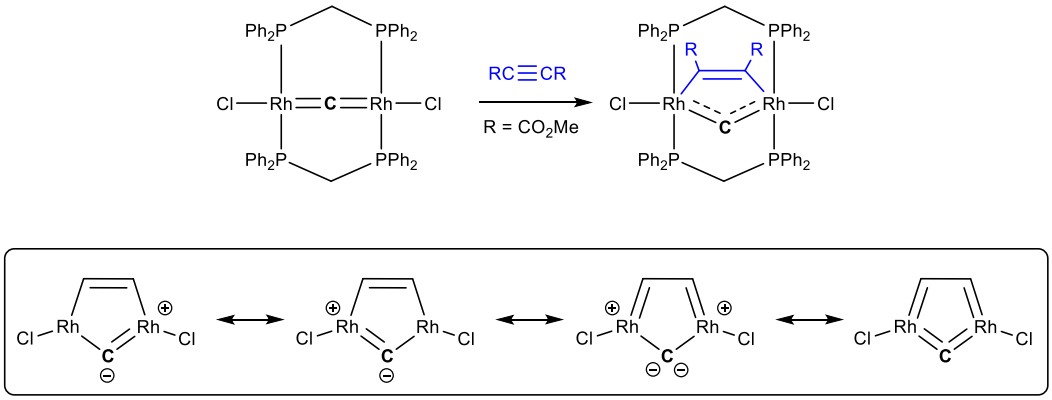

Scheme 1.14: A dimetallacarbene by Barnett *et al.*, featuring a dirhodacycle with canonical bonding descriptions.[38]

A crystallographic study confirmed the highly bent carbon (Rh1–C–Rh2: 124.2(9)°), significantly differing from the precursor (Rh1–C–Rh2: 173.4 (2)°). The inter-rhodium distance increased beyond the sum of covalent radii (Rh–Rh 3.279(2) Å; $2r_{cov}$(Rh) = 2.84 Å), thus discounting a direct Rh–Rh bond while short bond lengths indicated Rh–C multiple bonding was somewhat retained. Though absent from the original publication due to poor solubility, subsequent studies with ^{13}C enrichment revealed the carbido resonance at δ_C = 563.0 ($^1J_{RhC}$ = 30,

§§§§ Coordination of the alkyne to one rhodium centre most likely precedes metallacycle formation.

$^2J_{PC}$ = 8 Hz).[*****] The authors concluded the species might be considered as metalla-aromatic given the multiple canonical bonding descriptions. [80] The species complexed with coinage metals precursors akin to a conventional NHC to afford a range of trigonally coordinated μ_3-carbido complexes.

1.2.2 Class B (Metallacarbyne) Synthesis

Syntheses of Class A, C and D carbidos have been outlined, leaving Class B, the subject of this thesis, until last. Curiously, beyond the only recently emergent Class D, Class B μ_2-carbidos contain the fewest examples relative to other Classes, but enjoys the most numerous and diverse collection of unrelated synthetic routes. With regards to bonding and differences with Class A, when the metal termini differ, electronic differences elongate and contract bonds relative to the generally symmetrical μ_2-carbido ligand, such that a Class B description is most appropriate. Class B μ_2-carbidos will therefore be also referred to as 'metallacarbynes', drawing analogy to metal-functionalised carbyne complexes pioneered by Fischer and Schrock. [81-82] While Mansuy reported the first Class A μ_2-carbido in 1981, the first metallacarbyne was only reported six years later in 1987 by Selegue and co-workers. [33]

1.2.2.1| Alkyne Scission

The original metallacarbyne was produced from an alkyne scission reaction. The tungsten-alkylidyne $[W(\equiv CEt)(O^tBu)_3]$ undergoes metathesis with alkynyl complex $[Ru(C\equiv CMe)(CO)_2(Cp)]$, driven by elimination the volatile alkyne $[EtC\equiv CMe]$ to provide the μ_2-carbido $[WRu(\mu_2\text{-}C)(CO)_2(Cp)(O^tBu)_3]$ (Scheme 1.15). The same approach provides mixture when the iron congener $[Fe(C\equiv CMe)(CO)_2(Cp)]$ was used. The reaction also fails for terminal ethynyl complexes such as $[Pt(C\equiv CH)_2(PMe_2Ph)_2]$ due to the basicity of the tungsten alkoxide and ethynyl Brønsted acidity combining to afford W–C≡C–Pt connectivity, although the observation of $[W(\equiv CH(quin)(O^tBu)_3]$ (quin = quinuclidine) as a side product was interpreted in terms of the intermediacy of $[Pt(C\equiv CH)\{C\equiv W(O^tBu)_3\}(PMe_2Ph)_2]$ and $[Pt\{C\equiv W(O^tBu)_3\}_2(PMe_2Ph)_2]$. [83] The solubility of the μ_2-carbido allowed complete spectroscopic characterisation including the first ^{13}C NMR observation of δ_C (237.3, $^1J_{WC}$ = 290.1 Hz) for the carbido bridge. Of interest is the observation that same carbide complex is obtained from the ruthenium alkynyl and $[W_2(O^tBu)_6]$ in toluene, however of the reaction is performed in *iso*-octane, the ethyn-diyl $[Ru_2(\mu\text{-}C\equiv C)(CO)_4(Cp)_2]$ precipitates while $[WRu(\mu_2\text{-}C)(CO)_2(Cp)(O^tBu)_3]$ and $[W(\equiv CMe)(O^tBu)_3]$ remain

[*****] Several items of unpublished work (including more examples of Class D carbidos and direct detection of δ_C) are discussed in a recent PhD thesis. See H. J. Barnett: *Carbidos, Carbonyls, Carbenes and Carbynes–The Reactivity of the Bridging C_1 Ligand*, **2022**, *PhD Thesis*, Australian National University, Canberra.

in solution. A catalytic amount (3 mol%) of the ditungsten alkoxide provides predominately $[Ru_2(\mu\text{-}C{\equiv}C)(CO)_4(Cp)_2]$. [84] Like the predating dimetallacumulene, structural analysis determined a linear spine (W–C–Ru 177(2)°) devoid of steric pressure and disparate μ_2-carbido bond lengths[†††††] were recorded (W–C 1.75(2), Ru–C 2.08(2) Å) establishing the Class B bonding scenario. The authors predicted this species may model the reactivity of Fischer–Tropsch process, although no further reactivity or syntheses were reported.

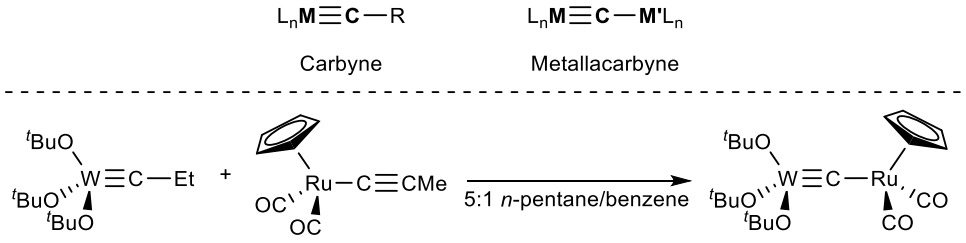

Scheme 1.15: Relationship of metallacarbynes to carbyne chemistry. [33]

1.2.2.2| Substitution

As for the preceding example, the next metallacarbyne arose from functionalisation of a prefabricated carbyne complex (Scheme 1.16). Lalor's halocarbynes[87] undergoes substitution reactions with nucleophiles, [87-96] and Templeton extended this to a single metal carbonyl anion, $K[Fe(CO)_2(Cp)]$. The chloride terminus of $[Mo(\equiv CCl)(CO)_2(Tp^*)]$ could be substituted with $[Fe(CO)_2(Cp)]^-$ akin to an S_N1 reaction to produce the metallacarbyne $[MoFe(\mu_2\text{-}C)(CO)_4(Cp)(Tp^*)]$.[97] Like the previous metallacarbyne, $^{13}C\{^1H\}$ NMR spectroscopy identified a high frequency signal consistent with a bridging carbido as a deshielded signal (δ_C = 380.9), and the authors concluded the complex featured more carbyne than cumulenic character through *X*-ray diffraction studies. The authors did not report or speculate on extension other carbonyl

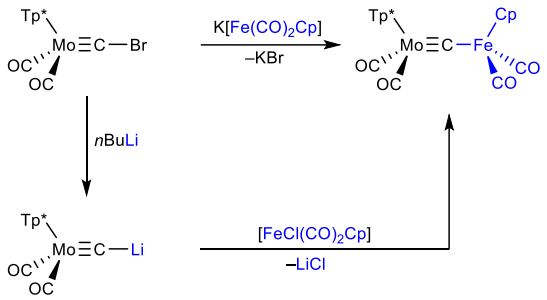

Scheme 1.16: Metallacarbyne accessed through substitution of a halocarbyne.

[†††††] Empirical covalent radii from crystallography: r_{cov}(C*sp*) = 0.69(1), r_{cov}(Ru) = 1.46(7), r_{cov}(W) = 1.62(7) Å: [85]
Theoretical covalent radii: r_{cov}(C-single) = 0.75; r_{cov}(C-triple) = 0.60, r_{cov}(Ru-single) = 1.25, r_{cov}(W) = 1.15 Å: [86]

metallates, though this would appear to be worthy of investigation. The same carbido complex could later be accessed via reaction of the lithiocarbyne [Mo(≡CLi)(CO)$_2$(Tp*)] with [FeCl(CO)$_2$(Cp)].

The majority of reactions that append a metal to the terminal carbide [Ru(≡C:)Cl$_2$(PCy$_3$)$_2$] give Class C complexes, however, one example provided a Class B species. The reaction of [Ru(≡C:)Cl$_2$(PCy$_3$)$_2$] with *trans*-[PtCl$_2$(py)$_2$] initially results in substitution of pyridine, but phosphine ejection (trapped as [PtCl$_2$(py)(PCy$_3$)]) results in chloride transfer from platinum to ruthenium with a formal single covalent bond to platinum(II) in the metallacarbyne [RuPt(μ_2-C)Cl$_4$(py)$_2$(PCy$_3$)]. [73] The metallacarbyne classification was justified by simple electron-counting and the diamagnetism of the complex which allowed a carbido resonance to be observed to lower frequency (δ_C = 354.6, $^2J_{CP}$ = 13, $^1J_{CPt}$ = 1372 Hz) in the $^{13}C\{^1H\}$ NMR spectrum *cf.* Class C relatives, in addition to structural analysis recording bond lengths (Ru–C 1.669(1), C–Pt 1.900(1) Å) consistent with the metallacarbyne canonical form.‡‡‡‡ Furthermore, a divergent Ru≡C–Pt linkage (Ru–C–Pt: 166.24(9)°) was linked as evidence of π-backdonation from a filled platinum(II) d$^{z^2}$ orbital to the π-antibonding orbital for ruthenium, only possible for bent geometries, [24, 26] further supporting a formal Pt–C single bond. The pyrazol complex was also produced, however, was not utilised further.

The ease of metallacarbyne synthesis led Bendix and co-workers to propose [RuPt(μ_2-C)Cl$_4$(py)$_2$(PCy$_3$)] as a synthon for further complexes. Subsequent reactions with bidentate phosphines (dppm and dpcm) provided more metallacarbynes, with each phosphine ligand bridging the two metal termini (Scheme 1.17). Both [RuPt(μ_2-C)Cl$_3$(μ-dppm)$_2$] and [RuPt(μ_2-C)Cl$_3$(μ-dcpm)$_2$] contain high frequency carbido resonances by $^{13}C\{^1H\}$ NMR (δ_C = δ 361.9 and 362.0, respectively) and a crystallographic study verified retention of the metallacarbyne linkage ≡Curiously, the sterically encumbering dcpm ligand imparts a bend on the spine (Ru–C–Pt: 166.2(1)°), where the less demanding dppm analogue transitions to fully linear spine (Ru–C–Pt: 180.0°) from reduced steric pressure.

Following isolation of platinum-based A-frame μ_2-carbidos, attempts to produce palladium congeners encountered low specificity, preventing isolation beyond solution-state observation *via* $^{13}C\{^1H\}$ NMR spectroscopy. The authors produced salts of a cationic metallacarbyne, [RuPt(μ_2-C)Cl$_2$(^{Ad}PNP)(py)$_2$]X (X = Cl, BPh$_4$), bearing a tridentate, meridional coordinating pincer ligand

‡‡‡‡‡ At the time, this was the first structurally characterised μ_2-platinum Class B carbido complex, however this Pt–C bond falls within the range of numerous such species reported in the interim and in subsequent Chapters in this thesis.

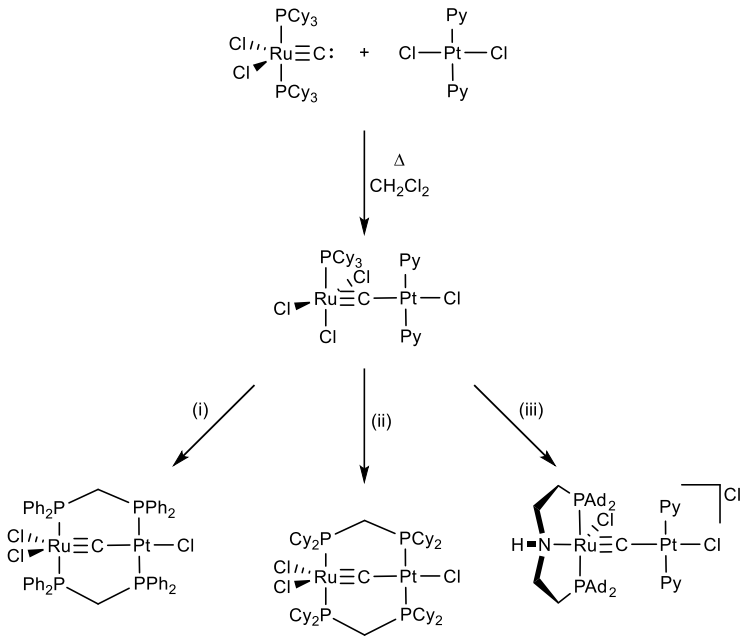

Scheme 1.17: Reaction of a terminal carbido to produce a platinum metallacarbyne and ensuing A-frame complexes. [73] (i) dppm. (ii) dcpm. (iii) ^{Ad}PNP. Ad = adamantyl.

(^{Ad}PNP: HN($CH_2CH_2PAd_2$; Ad = adamantyl) bound to ruthenium. Coordination of ^{Ad}PNP highlights an interesting point in that further addition of the pincer breaks the metallacarbyne and reforms a terminal carbide with a new ligand set [Ru(≡C:)Cl(^{Ad}PNP)]Cl indicating stability of a terminal carbido relative to a metallacarbyne and the reticence of the complex to coordinate ligands (Cl^-) *trans* to the terminal carbido.

1.2.2.3| Oxidative Addition

More than a decade passed before another metallacarbyne emerged. Grubbs§§§§§ discovered [$Ru_2(\mu_2$-C)$HCl_3\{(\eta^6$-SIMes)}(SIMes)] (SIMes = 1,3-*bis*-(2,4,6-trimethylphenyl)-4,5-dihydroimidazolidene)****** as a species that arises through decomposition of his 2nd-generation eponymous catalyst for olefin metathesis (Scheme 1.18). [98] The proposed mechanism for metallacarbyne formation mooted intramolecular oxidative addition of a parent methylidyne intermediately prior to chloride migration, although no other species were observed. Characterisation determined a high frequency signal in the $^{13}C\{^1H\}$ NMR (δ_C = 414.0) while a crystallographic study determined significantly different μ_2-carbido bond lengths (Ru1–C 1.698(4); Ru2–C 1.875(4) Å), confirming the species as a metallacarbyne despite having the same metal

§§§§§ Professor Robert H. Grubbs (1942–2021) passed away during the completion of this Thesis, and the author wishes to acknowledge the enormous contribution he made to organometallic chemistry. Prof. Grubbs was a co-recipient of the 2005 Nobel Prize for his work on olefin metathesis, the epitome of bridging organic and inorganic chemistry in harmony. A feat of great inspiration to the author.

****** The few mentions of *N*-heterocyclic carbene ligands in this Thesis will be listed as per the shorthand: "S" denotes saturated backbone, "I" denotes imidazole, "Mes" denotes the *N*-substitution mesityl. See glossary for clarification.

termini. Grubbs' complex $[Ru_2(\mu_2\text{-}C)HCl_3\{(\eta^6\text{-}SIMes)\}(SIMes)]$ represented the first example of a *homo*-metallic Class B μ_2-carbido and remains so to this day. Presumably, as this discovery was in context of undesirable catalyst breakdown, no further studies were reported.

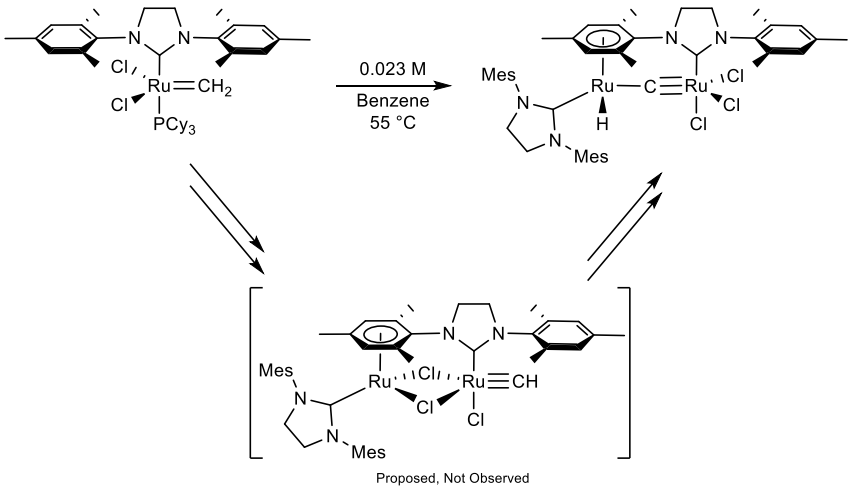

Scheme 1.18: Thermal decomposition of olefin metathesis catalyst system to provide a metallacarbyne. [98]

The breakdown of Grubbs' catalyst implied oxidative addition (C–H activation) as a synthetic route of metallacarbynes and this was later confirmed by Beck and co-workers (C–Br activation). Beck demonstrated that the low-valent complex $[Pt(\eta^2\text{-}C_2H_4)(PPh_3)_2]$ could oxidatively add the carbyne-halogen bond of Lalor's halocarbyne $[Mo(\equiv CBr)(CO)_2(Tp^*)]$ to provide the metallacarbyne $[MoPt(\mu_2\text{-}C)Br(CO)_2(PPh_3)_2(Tp^*)]$ (Scheme 1.19). The initial step of the reaction inferred π-coordination of platinum(0) across the Mo≡C bond to give the μ_2-bromocarbyne intermediate $[MoPt(\mu_2\text{-}CBr)(CO)_2(PPh_3)_2(Tp^*)]$ that could be isolated. [54] Both μ_2-carbido and μ_2-halocarbyne complexes feature an abundance of spin-active nuclei to facilitate thorough spectroscopic interrogation. A characteristic μ_2-carbido signal was identified in the $^{13}C\{^1H\}$ NMR spectrum (δ_C 339.0) with resolved coupling to *cis*-phosphorus nuclei ($^2J_{CP}$ = 9, 5 Hz), indicating inequivalent phosphine environments. This was confirmed by the $^{31}P\{^1H\}$ NMR spectrum which comprised an **AB** spin-coupled system. The authors acknowledged this inequivalence of phosphines, but did not provide a rationale for this phenomenon, a point to which we will return (Chapter Three).

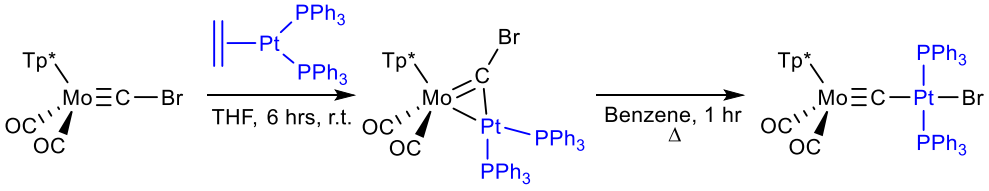

Scheme 1.19: Oxidative addition of a halocarbyne to platinum(0). [54]

1.2.2.4 | Transmetallation

The propensity for tin to transmetalate organyl groups to gold inspired a reaction between stannylcarbynes $[M(\equiv CSnMe_3)(CO)_2(Tp^*)]$ (M = Mo or W) and select prefabricated gold(I) complexes to provide μ_2-carbidos (Scheme 1.20).[99] Although the precursors are stable species, a careful match of electronics was required given the linear gold(I) species [AuCl(L)] (L = donor ligand). The molybdenum stannylcarbyne $[Mo(\equiv CSnMe_3)(CO)_2(Tp^*)]$ transmetallated with $[AuCl(PPh_3)]$ to form the metallacarbyne $[MoAu(\mu_2\text{-}C)(CO)_2(PPh_3)(Tp^*)]$, but the tungsten analogue $[W(\equiv CSnMe_3)(CO)_2(Tp^*)]$ provided a cyclic tetrameric μ_3-carbido, $[WAu(\mu_3\text{-}C)(CO)_2(Tp^*)]_4$ instead through dissociation of phosphine prior to intermolecular π-coordination. The deliberate synthesis of $[WAu(\mu_3\text{-}C)(CO)_2(Tp^*)]_4$ was achieved by the transmetallation of $[W(\equiv CSnMe_3)(CO)_2(Tp^*)]$ with the more labile $[AuCl(SMe_2)]$ or through the fleetingly observed complex $[WAu(\mu_2\text{-}C)(AsPh_3)(CO)_2(Tp^*)]$ prior to labilised arsine forming the ring. Aggregation of the golden ring could be broken by a more nucleophilic and electron donating phosphine (PEt_3) to produce $[WAu(\mu_2\text{-}C)(CO)_2(PEt_3)(Tp^*)]$ indicating another route towards metallacarbynes albeit dependent on 'masked' carbido aggregates.

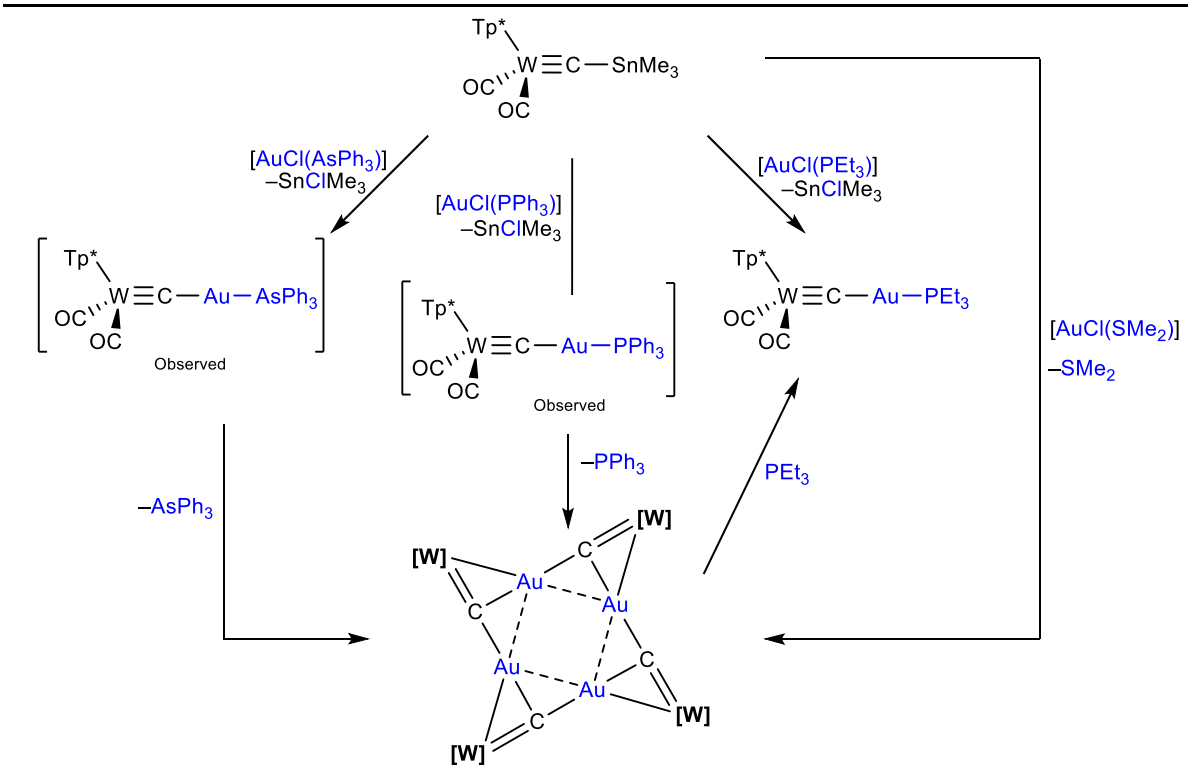

Scheme 1.20: Synthesis of gold(I) carbide complexes *via* transmetallation from tin.[99]

In the same report, transmetallation was able to produce another metallacarbyne, although not in a direct reaction. The stannylcarbyne $[W(\equiv CSnMe_3)(CO)_2(Tp^*)]$ readily transmetallates to gold(I) but not to palladium(II). However, transmetallation from tin to palladium was achieved

with a catalytic amount of gold(I) to provide the first palladium carbido complex [WPd(μ_2-C)Cl(CO)$_2$(P^{n}Bu$_3$)$_2$(Tp*)] (Figure 1.5). The acceleration of transmetallation from tin to palladium by gold additives has in the interim been developed by Espinet for enhancing the Stille reaction (Chapter Seven). [100]

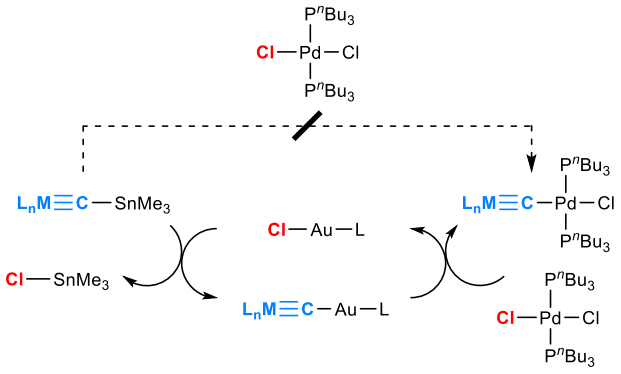

Figure 1.5: Tin→gold→palladium relay for carbido transmetallation. [99]

1.2.2.5 | Umpolung (Lithiocarbyne) Approach

Metallacarbynes discussed thus far, while varying in metal termini and synthesis are in general system specific, with caveats that may impede general synthesis of other μ_2-carbidos. A useful advance towards general synthesis involved the expedient generation of lithiocarbyne complexes [M(≡CLi)(CO)$_2$(Tp*)] (M = Mo, W) for reactions with a range of electrophiles including metal halides, [101] building from the original report by Templeton of a multi-step route to the tungsten example. [64] This method is not without caveats[102] but has demonstrated the most general route to metallacarbyne complexes to date as measured by incorporating the most diverse metal termini (Fe, Ni, Pt, Hg, Au, Sn, Pb, Bi).

Templeton originally generated the tungsten lithiocarbyne from deprotonation with alkyllithium reagents of the methylidyne [W(≡CH)(CO)$_2$(Tp*)] prepared over multiple steps.[††††††] Alternatively, Cordiner *et al.*, demonstrated lithium-halogen exchange can produce the desired lithiocarbynes directly by treating Lalor's halocarbynes [M(≡CX)(CO)$_2$(Tp*)] (M = Mo or W; X = Cl or Br) with butyllithium (^{n}BuLi) in THF to generate [M{≡CLi(THF)$_n$}(CO)$_2$(Tp*)] in solution at low temperatures. Use of lithiocarbynes is referred to, hereafter, as the 'umpolung approach' because lithiation reverses the polarity at the carbyne carbon (Scheme 1.21) relative to that of the precursor halocarbyne. The carbon in the halocarbyne precursor is electrophilic consistent with a Fischer-type carbyne complex, allowing reactions with nucleophiles. [87-96] For the lithiocarbynes, this carbon is nucleophilic and can react with a range of electrophiles, broadening the utility of the

[††††††] The same anionic carbido species is implicit in the formation of the non-classical vinylidene complex [W$_2$(μ-C=CH$_2$)(CO)$_4$(Tp*)$_2$] upon treating [W(≡CSiMe$_2$Ph)(CO)$_2$(Tp*)] with moist [^{n}Bu$_4$N]F: [305]

halocarbyne precursors to access derivatives with substituents from groups 13, [103-105] 14, [106] 15[107-110], 16[111-116], and 17[117]. Furthermore, lithiocarbynes can react with electrophilic transition metal complexes to produce metallacarbynes and these will be summarised in this sub-section.

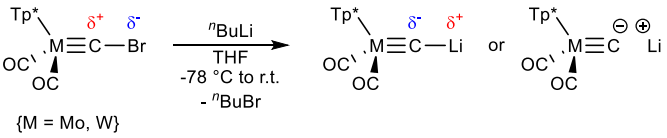

Scheme 1.21: Generation of lithiocarbynes *via* lithium/halogen exchange, the basis of the Umpolung approach to metallacarbyne synthesis. [35]

As noted above (Section 1.2.2.2), the known metallacarbyne $[MoFe(\mu_2\text{-}C)(CO)_4(Cp)(Tp^*)]$ is formed from the molybdenum lithiocarbyne and $[FeCl(CO)_2(Cp)]$ *via* simple halide metathesis. This demonstration was quickly followed by two reports of metallacarbynes produced directly or indirectly *via* lithiocarbynes with new metal termini—mercury and iridium (Scheme 1.22). The molybdenum-lithiocarbyne $[Mo(\equiv CLi)(CO)_2(Tp^*)]$ reacts with $[HgCl_2]$ to produce the *bis*-metallacarbyne $[Mo_2Hg(\mu_2\text{-}C)_2(CO)_4(Tp^*)_2]$, [118] the spectroscopic data for which included a carbido resonance (δ_C = 373.0). Extrusion of mercury occurs to give the *bis*-carbido [Mo≡C–C≡Mo(CO)$_4$(Tp*)$_2$] and this could be catalysed by $[RhCl(CO)(PPh_3)_2]$ or $[RhCl(PPh_3)_3]$ implying the intermediacy of rhodiocarbyne species although none were observed. Meanwhile, the same lithiocarbyne could be used to prepare an anionic selenocarbonyl complex $[Mo(CSe)(CO)_2(Tp^*)]^-$ which subsequently reacted with $[Ir(NCMe)(CO)(PPh_3)_2]BF_4$ to ultimately provide $[Mo_2Ir_2(\mu_2\text{-}Se_2)(\mu_2\text{-}C)_2(CO)_6(PPh_3)_2(Tp^*)_2]$, presumably *via* an isoselenocarbonyl Mo–C–Se–Ir linkage. A rearrangement to a *bis*-metallacarbyne was accompanied by formation of a diselenatetrahedrane

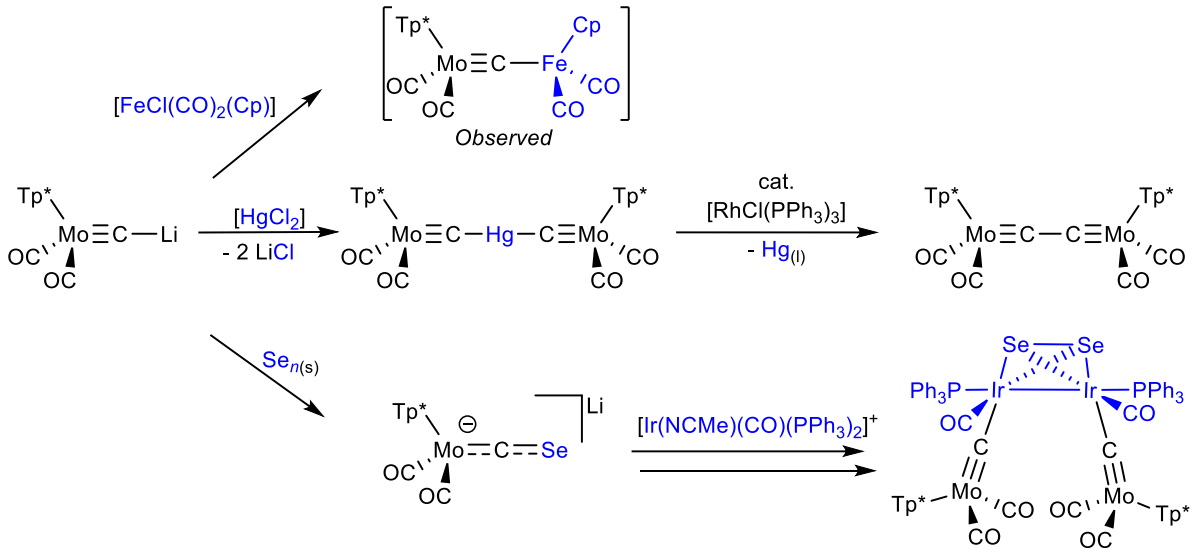

Scheme 1.22: Formation of metallacarbynes from lithiocarbyne $[Mo(\equiv CLi)(CO)_2(Tp^*)]$.[62]

motif.[62] A structural analysis demonstrated bond lengths to carbon (Mo–C: 1.840(5), 1.847(6) Å; Ir–C: 1.977(5), 1.969(6) Å) consistent with metallacarbyne bonding. While a lithiocarbyne was indirectly responsible for this metallacarbyne formation, the activation of a C–Se bond draws a parallel to chalcogen cleavage discussed for Class A μ_2-carbidos.

The reaction between [W(≡CLi)(CO)$_2$(Tp*)] and [NiCl$_2$(PEt$_3$)$_2$] provided the sole example of a nickel μ_2-carbido [WNi(μ_2-C)Cl(CO)$_2$(PEt$_3$)$_2$(Tp*)], which was structurally characterised,[119] but gradually converted to a rare heteronuclear phosphoniocarbyne [WNi(μ_2-CPEt$_3$)Cl(CO)$_2$(PEt$_3$)(Tp*)] ($t_{½}$ = 28 hours) (Scheme 1.23). Measurement by $^{13}C\{^1H\}$ NMR spectroscopy identified the metallacarbyne resonance (δ_C = 484.0), distinct from that for the bridging phosphoniocarbyne (δ_C = 280.9). Formation of the nickel metallacarbyne and subsequent conversion to a phosphoniocarbyne provided more evidence toward metallacarbyne intermediates in C–C and C–P bond forming processes (see Section 1.5.2).

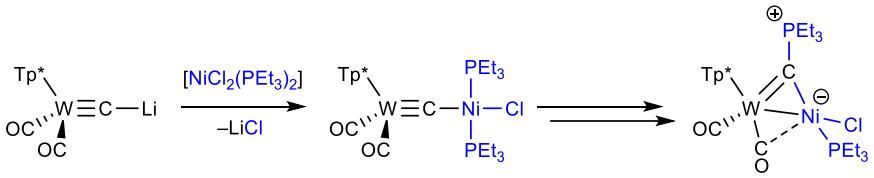

Scheme 1.23: Formation of a nickel metallacarbyne species and isomerism to a phosphinocarbyne.[119]

A combination of [W(≡CLi)(CO)$_2$(Tp*)] with the platinum(II) salt [PtCl(terpy)]PF$_6$ resulted in vividly coloured [WPt(μ_2-C)(terpy)(CO)$_2$(Tp*)]PF$_6$ (Scheme 1.24).[120] This lithiocarbyne also reacted with [PtCl$_2$(phen)] presumably forming the desired complex [WPt(μ_2-C)Cl(phen)(CO)$_2$(Tp*)] (phen = 1,10-phenanthroline) as an intermediate, however, a second nucleophilic attack occurs on the phenanthroline ligand to give [WPt(μ_2-C)Cl(phen{C≡W(CO)$_2$(Tp*)}–2)(CO)$_2$(Tp*)] likely facilitated by the Lewis acidic platinum activating phenanthroline upon coordination. Alkynyl lithium reagents do not attack free phenanthroline although more nucleophilic alkyl lithium may. The lithiocarbyne [W(≡CLi)(CO)$_2$(Tp*)] reacts with other bidentate platinum assemblies [PtCl$_2$(L$_2$)] (L$_2$ = COD, NBD), speculated to form *bis*-metallacarbyne intermediates [Pt{C≡W(CO)$_2$(Tp*)}$_2$(L$_2$)], before isomerising *via* reductive elimination to platinum(0) coordinated species [W$_2$(μ-C$_2$Pt(L$_2$)}(CO)$_4$(Tp*)] (Scheme 1.24).

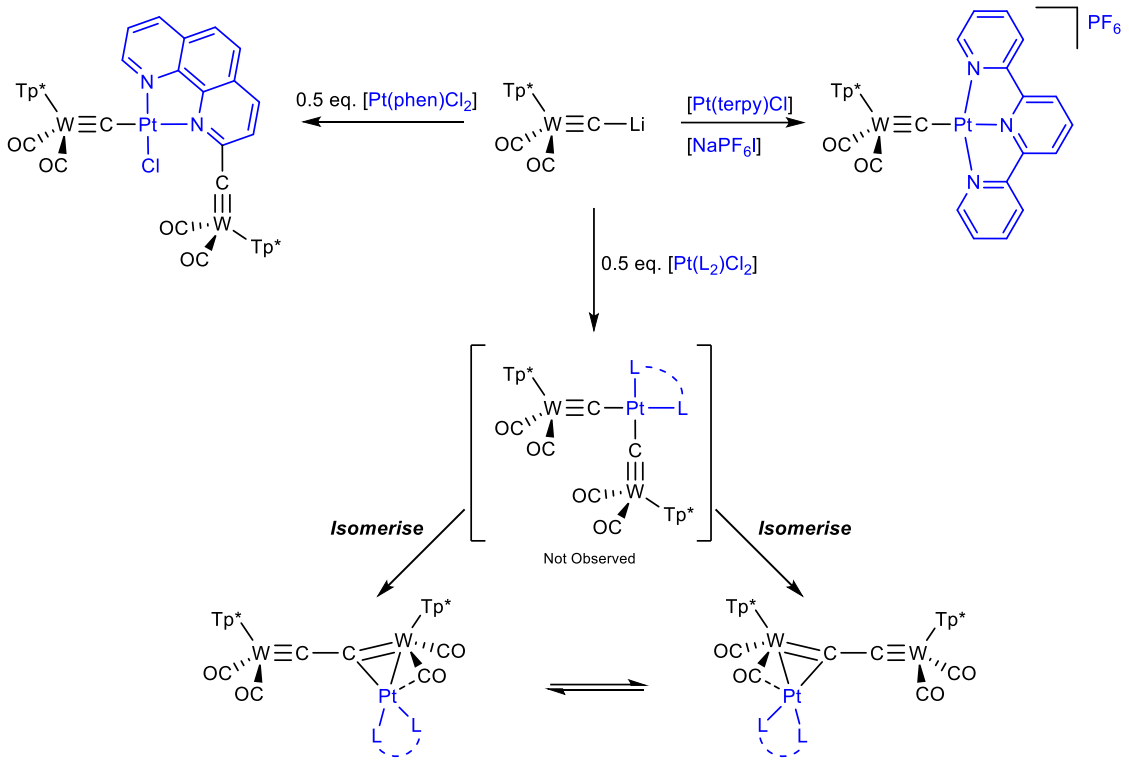

Scheme 1.24 : Production of platinum(II) metallacarbynes *via* an umpolung approach including a proposed *bis*-metallacarbyne putative intermediate. [120-121] L_2 = COD or NBD.

1.3 Properties of Class B μ2-Carbido Complexes

This section will outline the characteristic spectroscopic and structural features encountered in metallacarbyne chemistry.

1.3.1 Structural Parameters

Structural data provided the evidence necessary to describe a metallacarbyne for the first time in the same report that first measured a $^{13}C\{^1H\}$ carbide resonance. Having produced [WRu(μ2-C)(CO)2(Cp)(O^{t}Bu)3], Selegue noted the W–C distance was contracted (W–C: 1.75(2) Å) similar to alkylidyne complexes, but the Ru–C (2.09(2) Å) was consistent with single bonds to carbon ligands, albeit longer than carbonyls on ruthenium. Since this report, a majority of the metallacarbynes produced have been structurally characterised. Ruthenium forms the most common carbyne-terminus as the only example derivatised to date, with bond lengths ranging from 1.669–1.695 Å, a similar range to those of Class C complexes, which also have one σ and 2 π Ru···C bonding components. Otherwise, molybdenum is the second most common (1.820–1.847 Å), unsurprisingly given many metallacarbynes are produced from different methods from the same halocarbyne precursors. Given that these all involve 6-coordinate molybdenum while the ruthenium examples have lower coordination numbers, this contraction from group 6 to 8 is to be expected. Coordination number also plays a role in the case of the high oxidation state W≡C bond

of Selegue's WRu complex for which the bond from carbon to four-coordinate tungsten is much shorter (1.75(2) Å) compared to other Tp*-tungsten carbynes (1.835–1.867 Å) all of which have six-coordinate tungsten centres.

Metallacarbyne structure determinations include several examples of different metal termini that provide the single bond to the μ_2-carbido, though for any one metal insufficient examples exist for conclusive interpretations. The most common single-bond terminus is platinum where two examples with Tp*W termini may be compared with several based on more diversely ligated ruthenium. Curiously, the Pt–C bonds for the tungsten complexes (1.90–1.938 Å) fall within the range of the ruthenium complexes (1.842–1.951 Å). Unlike other Classes, the M≡C–M' linkage is often bent (164.3–176.5°) as a corollary of ligand influences and/or inherent asymmetry, while A-frame ligands typically accommodate linear examples [RuPt(μ_2-C)Cl$_4$(μ-dppm)$_2$] (180°) well.

For any ligand, one defining feature is the effect on bonding (*trans*-influence) and the lability (*trans*-effect) of the ligand to which it is *trans* coordinated on a metal centre. The *trans*-effect and -influence has been noted on occasion for μ_2-carbido ligands, and a reassuring method to compare changes in bonding attributable to the μ_2-carbido is through molecules that are internally referenced. Therein lies a strength of Bendix's A-frame metallacarbynes on ruthenium containing chlorides as test ligands. [73] In [RuPt(μ_2-C)Cl$_4$(μ-dppm)$_2$] the chloride bond *trans* to the μ_2-carbido is significantly longer (2.501(1) Å) than those *cis* (2.393(7) Å). Furthermore, the platinum *trans*-chloride is also elongated (2.350(1) Å) as compared to those in simpler *trans*-[PtCl$_2$(PPh$_3$)$_2$] (2.2997(11) Å). [122] It is likely the *trans*-chloride on ruthenium is elongated due to a *trans*-influence as provided by increase of π-character to form the triple bond weakening the bond. Conversely, the Pt–Cl may be elongated given the μ_2-carbido has been attributed to be a stronger σ-donor relative to carbon monoxide, [26, 69] and hence a lability could be expected.

This ruthenium example demonstrates an internal reference of μ_2-carbido (*cf.* chloro) effects for Class B. The nickel(II) complex [WNi(μ_2-C)Cl(CO)$_2$(PEt$_3$)$_2$(Tp*)] also contains an elongated Ni–Cl bond (2.2576(11) Å) as compared to *trans*-[NiCl$_2$(PPh$_3$)$_2$] (2.2075(2) Å), [123] although this is an externally referenced measurement. Otherwise, the remaining metallacarbynes structurally characterised only contain ligands that are no longer entirely *trans* to the carbido (such as *bis*-carbonyls off-axis from the carbido) or await structurally authenticated examples for comparison (no structures obtained for gold or mercury).

1.3.2 $^{13}C\{^1H\}$ NMR

Unsurprisingly, $^{13}C\{^1H\}$ NMR spectroscopy has emerged as the most obvious method of interrogating the μ_2-carbido environment assuming the complex is not paramagnetic or suffers from other unusual factors (*e.g.*, ring currents in porphyrin systems of Class A species). That said, the low natural abundance (1.1%) and sensitivity may render resonances elusive, not least because quarternary carbidos means no hydrogens are directly attached to enhance signal intensity (nuclear Overhauser effect) and some metal nuclei are quadrupolar causing signal broadening. Some metals have spin active isotopes that split signals reducing intensity, as do the donor atoms of some common ligands, *e.g.*, phosphines (^{31}P). Whilst these latter couplings compromise individual signal intensity, when sufficient signal/noise can be achieved, then further information follows from these splittings ($^1J_{MC}$, $^2J_{PC}$ *etc.*) that may respond to variations in metal-carbon bonding.

Despite the small number of carbidos and the variously populated Classes, trends are beginning to emerge with respect to the regions in which μ_2-carbido resonances appear in $^{13}C\{^1H\}$ NMR spectra. Typically, Class B carbidos often occur at lower frequency than that of other Classes. Class A carbido resonances span the widest range (δ_C = 257.0–508.8) where the lower bounds are somewhat outliers from $Na_2[Nb_2(\mu_2\text{-}C)(cal4ix)_2]$ while the majority is represented by rhodium species (*ca* δ_C: 430); several iron porphyrin-based systems are known but have not yet had carbido chemical shifts identified. Class C complexes are dominated by complexes that arise from the same $[Ru(\equiv C:)Cl_2(PCy_3)_2]$ so the range of shifts (δ_C = 341.4–446.0) may be traced specifically to the properties of the added metal. Class D complexes give rise to resonances at significantly higher frequencies than other classes (δ_C = 563.0–675.3), presumably reflecting significant paramagnetic contribution and the resonances may be difficult to detect without ^{13}C-isotopic enrichment. While many metal termini have had carbido chemical shifts measured, there are few examples of derivatives outside of the ruthenium metallacarbynes to allow a comparison of influences and is an area for further study.

1.3.3 Hetero-nuclear NMR and Scalar (*J*) Couplings

Many carbido complexes feature phosphine co-ligands with spin-active ^{31}P nuclei, the NMR characteristics of which may provide information. These phosphine ligands often, however, lie *cis*- to the μ_2-carbido spine and therefore have secondary rather than direct impact on the bonding and associated manifestations in the ^{31}P NMR spectrum (δ_P, $^2J_{PC}$).

Inclusion of spin-active metal termini provide the most direct indication of the μ_2-carbido environment, although not all have been quantified or contain inherent issues in their measurement. For example, $[Mo_2Hg(\mu_2\text{-}C)_2(CO)_4(Tp^*)_2]$ contains ^{199}Hg (I = ½; 16% abundance)

a relatively sensitive nucleus of sharp linewidth in a complex devoid of other coupling partners, however a ^{199}Hg resonance was not reported. Conversely, rhodium is entirely spin-active (^{103}Rh; I = ½) but measuring a spectrum through ^{103}Rh NMR is challenging for several reasons including: immense spectral range, low sensitivity, very low gyromagnetic ratio and long relaxation time with the Larmor frequency falling outside the majority of modern probes. This is further problematic for carbidos complexes as all rhodium carbidos are further coupled by 1–4 ^{31}P nuclei from phosphines that may not be in chemically equivalent environments.[####]

The NMR active metal common to the greatest number of carbidos is ^{195}Pt (I = ½; 33% abundance). While Bendix and Reinholdt prepared many examples of in Class C and some Class B platinum complexes, they utilised only the coupling constant ($^1J_{CPt}$) rather than direct detection of the nucleus. Similarly, Beck and co-workers utilised this coupling constant opposed to direct detection for Class B [MoPt(μ_2-C)Br(CO)$_2$(PPh$_3$)$_2$(Tp*)]. Direct detection is not always a readily accessible or routine technique; however, the chemical shift of metals is especially sensitive to the nature and bonding of ligands. At the time of writing, no published examples of metal termini in μ_2-carbido complexes had been directly measured by NMR spectroscopy.

In contrast, coupling constants provided by spin-active metal termini (*e.g.,* ^{103}Rh, ^{107}Ag, ^{109}Ag, ^{199}Hg, ^{183}W, ^{195}Pt) provide bonding information for many examples of carbido complexes. The most explored within the field is that of ^{103}Rh (I = ½) due to the 100% natural abundance and because the magnitude of scalar couplings (*e.g.*, $^1J_{RhP}$) can suggest oxidation state but more reliably the coordination number of the metal centre, such that an increase to either would be expected to reduce the coupling constants ($^1J_{CRh}$ or $^1J_{PRh}$). Rhodium has played a role in the development of each of Classes A, C and D with a range of ligand environments, coordination numbers and oxidation states, however Class B examples of rhodiocarbynes remain unknown.

While several examples of rhodium carbide complexes are known, measuring the $^1J_{RhC}$ coupling constant can be problematic since all rhodium carbidos have between one and four phosphine co-ligands, that may complicate the resonance appearance. This is not the case for ^{183}W in that no known carbidos of tungsten have phosphine co-ligands, such that coupling is commonly resolved and may be directly compared to copious data for W–C multiple bonding. The coupling to ^{183}W (I = ½; 14% abundance) of the μ_2-carbido resonance in the ^{13}C NMR spectrum is manifest as a singlet superimposed upon a doublet with relative integrated intensities of 0.86 and 0.14,

[####] ^{103}Rh resonances have recently been detected through 2D methods but remain unpublished. See H. J. Barnett: *Carbidos, Carbonyls, Carbenes and Carbynes–The Reactivity of the Bridging C_1 Ligand*, **2022**, *PhD Thesis*, Australian National University, Canberra.

respectively. By comparing two different Class B carbidos containing tungsten, a contrast in this coupling is noted. A larger coupling is noted for [WRu(μ_2-C)(CO)$_2$(Cp)(O^{t}Bu)$_3$] ($^1J_{CW}$ = 290 Hz) as compared to, *e.g.*, [WAu(μ_2-C)(CO)$_2$(PEt$_3$)(Tp*)] ($^1J_{CW}$ = 181 Hz) where the former reflects more *s*-character for the bonding to four-coordinate tungsten *cf.* six-coordinate tungsten in the latter case, and new examples to be reported in later Chapters. Wolczanski reported intermediate values for the Class A ditungstacumulenes [W$_2$(μ_2-C)(=NC$_6$H$_3$Me$_2$)Cl$_2$(OSi^{t}Bu$_3$)$_4$] (δ_C = 406.26, $^1J_{WC}$ = 194 Hz) and [W$_2$(μ_2-C)(=O)Cl$_2$(OSi^{t}Bu$_3$)$_4$] (δ_C = 379.14, $^1J_{WC}$ = 200, 187 Hz) that have the carbide bound to both 4- and 5-coordinate tungsten, but with reduced–C bond orders.§§§§§§

1.4 Reactivity of μ_2-Carbido Complexes

Despite the emergence of many carbido complexes, their novelty has meant that their isolation alone has justified publication, with little mention of subsequent reactivity studies. Those further studies that have appeared have primarily involved co-ligand substitution, as distinct from the very few that involve actual reactivity of the carbido ligand itself—a curious situation given the inevitable claims of relevance to modelling Fischer–Tropsch processes. This sub-section will describe the stoichiometric transformations of μ_2-carbido complexes of Classes A, C, and D prior to those of Class B.

1.4.1 Reactivity of Classes A, C, and D

1.4.1.1| Class A and C: Ligand Substitutions or Transformation

While not a direct substitution, the original alteration of a ligand sphere for μ_2-carbidos was shown for Class A complexes. Rossi and co-workers demonstrated methyl-imidazole (MeIm) would associate axially to the μ_2-carbido vector of [Fe$_2$(μ_2-C)(pc)$_2$] to give [Fe$_2$(μ_2-C)(MeIm)$_2$(pc)$_2$], substituting an apparent vacant coordination site on each iron terminus. [43, 124] This later included coordination of H_2O or halogens. [125]

Most ligand substitutions for Classes A and C are derived from the rhodium and ruthenium species that outnumber other species. For Class A, the hydrolysis of S–B bond in [Rh$_2$(μ_2-C)(SBpin)$_2$(PEt$_3$)$_4$] to [Rh$_2$(μ_2-C)(SH)$_2$(PEt$_3$)$_4$] initially hinted at a ligand more useful for subsequent transformations although none were reported. In the same report describing [Rh$_2$(μ_2-C)Cl$_2$(PPh$_3$)$_4$] outlined halide abstraction with silver, in addition to substitution with a range of pyrazolylborate ligands (Scheme 1.25). While ligands were altered, no change in the μ_2-carbido ligand occurs and hence the Rh=C=Rh linkage was retained. The carbido bridge deviated from linearity according

§§§§§§ Due to poor signal/noise, only one pair of satellites was observed. The corresponding value for the only other Class A tungsten carbido, [WRe(μ_2-C)(CO)$_3$(NO)(Tp*)(Cp)] (δ_C = 508.8) was similarly not provided due to weak signal intensity.[54]

to increasing steric bulk (Rh–C–Rh: 168.8(7) (Bp); 163.7(4) (Bp*); and 163.8(3)° (Tp)), suggesting the energy for spinal deformation may be comparable to those of inter and intramolecular packing effects.

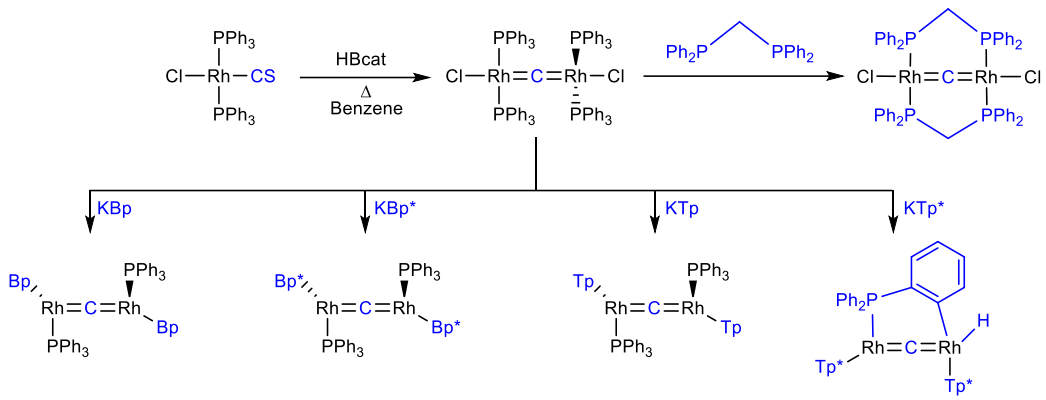

Scheme 1.25: Subsequent ligand substitution reactions from a rhodium dimetallacumulene. [19]

The same report encountered a limit where the bulkier hydro-*tris*-(3,5-dimethylpyrazolyl)borate (Tp*) instead resulted in phosphine ejection followed by *ortho*-C–H activation of the remaining phosphine to provide [$Rh_2H(\mu_2\text{-}C)(\mu\text{-}C_6H_4PPh_2\text{-}2)(Tp^*)_2$]. This was the first example of a homobimetallic dimetallacumulene with metal termini in differing oxidation states (Rh^I and Rh^{III}). Despite this clear difference in electronics, the Rh–C bond lengths were comparable (Rh–C: 1.817(6), 1.741(6) Å) and the spine angle was comparable to the previous poly(pyrazolyl) species (Rh–C–Rh: 165.9(3)°). This complex is also notable in containing both hydrido and σ-organyl ligands coordinated to a carbide ligand, with no evidence for migratory insertion processes occurring. This question will be addressed in a subsequent Chapter, where such processes are shown to operate.

The original complex [$Rh_2(\mu_2\text{-}C)Cl(PPh_3)_4$] displayed synthetic utility towards further compounds including the A-frame dimetallacumulene [$Rh_2(\mu_2\text{-}C)Cl_2(dppm)_2$] by phosphine substitution. The chloride was shown to be labile through halide abstraction by AgOTf to form [$Rh_2(\mu_2\text{-}C)(MeCN)_2(dppm)_2$]·2OTf and replacement with bromide. [126] Crystallographic studies revealed that atomic structure remained similar, however, the torsions around the Rh=C=Rh linkage are greatly reduced (P–Rh–Rh–P: 7.26(7)°) when compared to the orthogonal precursor (P–Rh–Rh–P: 83.96(2)°) due to geometric constraints of the bridging phosphine linker.

Selected examples of ligand substitution are also known in Class C (Chart 1.4). The anionic [$AsPh_4$][$Cl_2(PCy_3)_2Ru{\equiv}C{:}{\rightarrow}PtCl_3$] could be treated with pyridine, bypyridine or other nitrogen heterocycles to substitute chloride and provide complexes such as [$Cl_2(PCy_3)_2Ru{\equiv}C{:}{\rightarrow}PtCl_2(py)$]. Likewise, the halo-bridged dimer [$Cl_2(PCy_3)_2Ru{\equiv}C{\rightarrow}PtCl]_2(\mu\text{-}Cl)_2$ could be cleaved by a range of

additional donor ligands to give $[Cl_2(PCy_3)_2Ru{\equiv}C{\rightarrow}PtCl_2(L)]$ (L = $AsPh_3$, CNCy, CN^{t}Bu, PCy_3, PPh_3, $P(OPh)_3$).

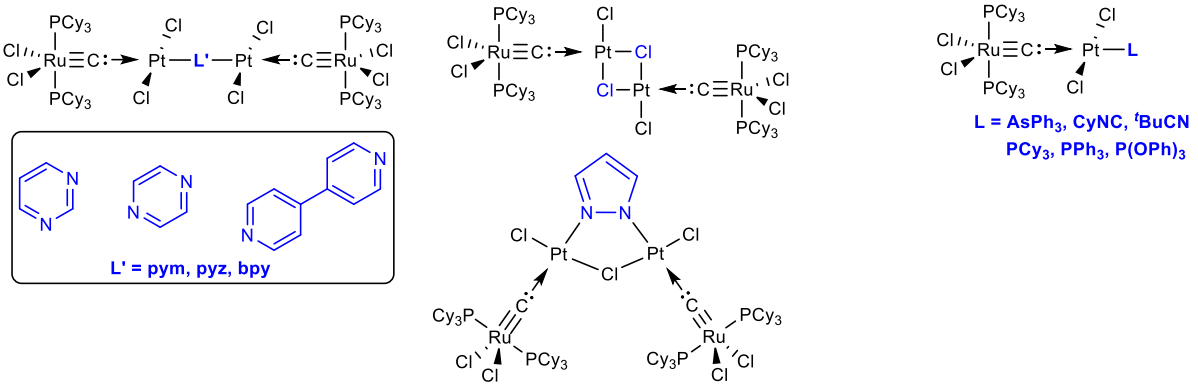

Chart 1.4: Series of polar covalents with various donor-ligands coordinated *trans* to the Ru≡C:→Pt vector to measure donor strength. [77]

1.4.1.2| Class A: Redox Chemistry

Examples of redox processes have been investigated in Class A μ2-carbido complexes. Ercolani and Rossi demonstrated partial oxidation of a phthalocyanine carbido occurs to produce $[Fe_2(\mu_2\text{-}C)(pc)_2](I_3)_{0.66}$, although oxidation was solely metal centred and the central carbido remained unchanged. [127] At a similar time, Wolczanski showed $[W_2(\mu_2\text{-}C)Cl_2(=O)(OSi^tBu_3)_4]$ can be reduced by Na/Hg amalgam under hydrogenation conditions to result in a μ2-methylidyne $[W_2(\mu_2\text{-}CH)(\mu\text{-}H)(\mu\text{-}O)(OSi^tBu_3)_4]$ as an important link to reactions proposed to occur in the Fischer—Tropsch processes (Scheme 1.26). [56] It should be noted that no mechanistic conjecture was provided, although this highlights an uncommon instance of chemical change to the μ2-carbido ligand.

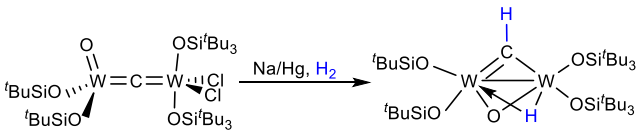

Scheme 1.26: Hydrogenation of a μ2-carbido post reduction.

Later Hill and co-workers would show oxidation of $[Rh_2(\mu_2\text{-}C)X_2(\mu\text{-}dppm)_2]$ (X = Cl/Br) did not provide the expected rhodium(III) complexes $[Rh_2(\mu_2\text{-}C)X_6(\mu\text{-}dppm)_2]$ but instead the μ2-halocarbynes $[Rh_2(\mu_2\text{-}CX)(\mu\text{-}X)X_4(\mu\text{-}dppm)_2]$; the reverse of Beck and co-workers oxidative addition in Class B synthesis. [78] Intermediate species were proposed according to both Class A and Class B μ2-carbido descriptions; however, these were not observed prior to conversion to the first examples of μ2-chlorocarbyne and μ2-bromocarbyne complexes (Scheme 1.27).

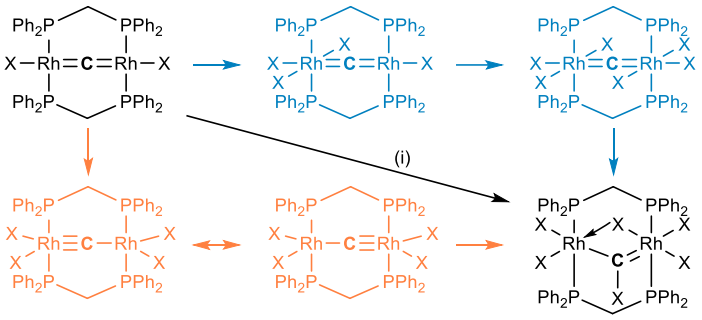

Scheme 1.27: Proposed *inter*-class conversion using an A-frame dimetallacumulene. Intermediates described by a Class A canonical form are in blue and Class B in red. Neither were observed in favour of novel halocarbyne species. [126] (i) $PhICl_2$ or $pyHBr_3$

1.4.1.3| Class A: Cycloaddition with Exotic Alkyne—'Benzyne'

Shortly following the formal [3+2]-cycloaddition of a Class A carbido to synthesise Class D species $[Rh_2(\mu_2\text{-}C\text{:})Cl_2(\mu\text{-}DMAD)(\mu\text{-}dppm)_2]$, Hill explored other cycloaddition reactions like those that underpin alkyne metathesis. Treating $[Rh_2(\mu_2\text{-}C)Cl_2(\mu\text{-}dppm)_2]$ with a benzyne precursor resulted in a formal [2+2]-cycloaddition between a Rh=C and C≡C bond to prepare two metallacycle complexes $[Rh_2(\mu_2\text{-}CC_6H_4)(\mu\text{-}Cl)(C_6H_5)Cl_2(\mu\text{-}dppm)_2]$ and $[Rh_2(\mu_2\text{-}CC_6H_4)(\mu\text{-}Cl)Cl_3(\mu\text{-}dppm)_2]$ where the latter occurs in a mixture (Scheme 1.28). [128] Again, this is a rare example of direct reactivity at a μ_2-carbido ligand.

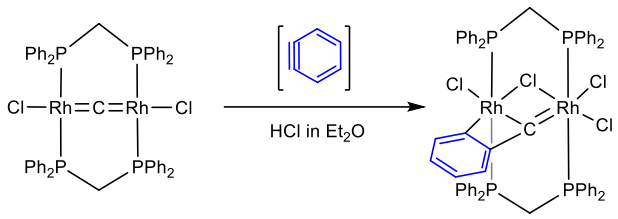

Scheme 1.28: A dimetallacumulene undergoes [2+2]-cycloaddition with benzyne.

1.4.1.4| Class A and D: Formation of Thiocarbonyls

For the Class D carbido complex $[Ru_2(\mu_2\text{-}C\text{:})(\mu\text{-}NPh)(Cp^*)_2]$, Takemoto and co-workers sought to demonstrate reactivity consistent with carbene-like character through coordination to chalcogens as observed for analogous *N*-heterocyclic carbene chemistry. A reaction occurs with elemental sulfur and grey selenium to produce μ_2-chalcocarbonyl complexes demonstrating reactivity of a Class D carbido akin to that of a singlet carbene. [129] Later reports from Hill determined the Class D $[Rh_2(\mu_2\text{-}C\text{:})Cl_2(\mu\text{-}DMAD)(\mu\text{-}dppm)_2]$ reacts similarly to produce rhodium bridging chalcocarbonyls. [130]

Having identified complexes $[Rh_2(\mu_2\text{-}CE)Cl_2(\mu\text{-}DMAD)(\mu\text{-}dppm)_2]$ (E = S, Se) that originate from the Class D carbido, Barnett *et al.* also demonstrated the related Class A carbido can form chalcocarbonyls. [130] Treating $[Rh_2(\mu_2\text{-}C)Cl_2(\mu\text{-}dppm)_2]$ with elemental sulfur or selenium provides

[$Rh_2(\mu_2\text{-}CE)Cl_2(\mu\text{-}dppm)_2$], (Scheme 1.29), subsequent treatment of which with DMAD gives the above-mentioned [$Rh_2(\mu_2\text{-}CE)Cl_2(\mu\text{-}DMAD)(\mu\text{-}dppm)_2$] (E = S, Se).

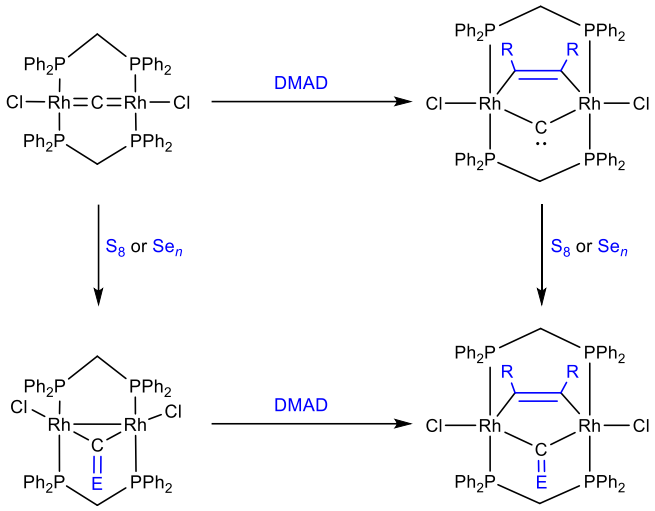

Scheme 1.29: Reactions of Class A and Class D carbidos with chalcogens.

1.4.1.5 | Class D: Carbene Coordination to provide μ3-carbidos

As an extension of the above, the nucleophilic character of Takemoto and Hill's Class D carbidos was extended to electrophilic metal reagents (Scheme 1.30). Takemoto showed a reaction of [$Ru_2(\mu_2\text{-}C\text{:})(\mu\text{-}NPh)(Cp^*)_2$] with coinage metals to give [$Ru_2M(\mu_3\text{-}C)\{N(SiMe_3)_2\}(\mu\text{-}N^tBu)(Cp^*)$] (M = Cu, Ag, Au), examples of rare μ3-carbido complexes.[41] The silver species was unable to be isolated attributed to sensitivity towards hydrolysis. Analogously, Barnett *et al.*, reported [$Rh_2(\mu_2\text{-}C\text{:})Cl_2(\mu\text{-}DMAD)(\mu\text{-}dppm)_2$] reacts with labile coinage metals [$MCl(SMe_2)$] (M = Cu and Au) to provide [$Rh_2M(\mu_3\text{-}C)Cl_3(\mu\text{-}DMAD)(\mu\text{-}dppm)_2$].[40]

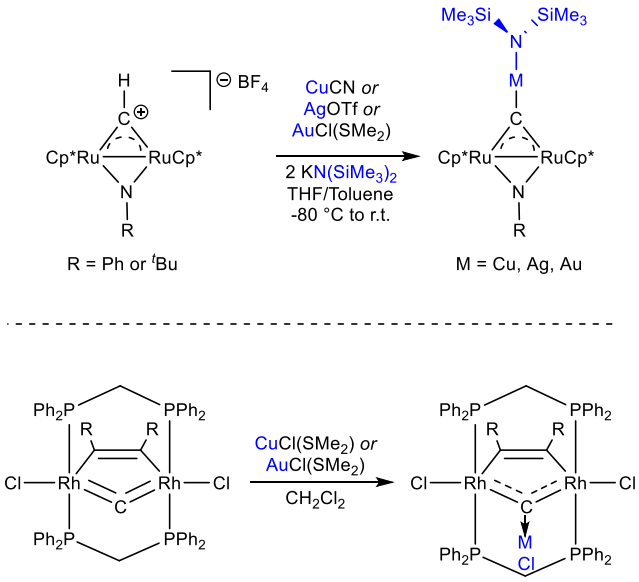

Scheme 1.30: Reactions of Class D carbidos with coinage metals to give μ3-carbidos.

1.4.2 Reactivity of Class B: Metallacarbynes

1.4.2.1| At the Carbido (Direct Reactivity)

Reactivity studies for Class B carbidos are relatively rare with many occurring within one report. Upon developing [MoFe(μ_2-C)(CO)$_4$(Cp)(Tp*)], Templeton employed a series of tests to explore reactivity at a μ_2-carbido for the first time. [97] Photolysis in the presence of CS_2 promoted insertion to give [MoFe(μ-CCS$_2$)(Cp)(CO)$_4$(Tp*)], through breaking the Fe–C bond of the carbido, suggesting a reaction at the μ_2-carbido. Photolysis in the presence of other ligands gave examples of ligand substitution [MoFe(μ_2-C)(L)$_2$(CO)$_4$(Cp)(Tp*)] (L = PMe_3, CN^{t}Bu) with substitution occurring exclusively at the iron centre. The most important result was treating [MoFe(μ_2-C)(CO)$_4$(Cp)(Tp*)] with strong acid (HBF_4) to protonate the μ_2-carbido and give a rare heterobimetallic methylidyne complex [MoFe(μ_2-CH)(CO)$_4$(Cp)(Tp*)] (Scheme 1.31). This again recalls those implicit in Fischer–Tropsch processes and is believed to occur *via* a direct protonation at the central carbon. Templeton concluded the reactions showed reactivity is possible at the metallacarbyne carbido bridge, however reluctantly, often requiring forcing conditions that further work should address.

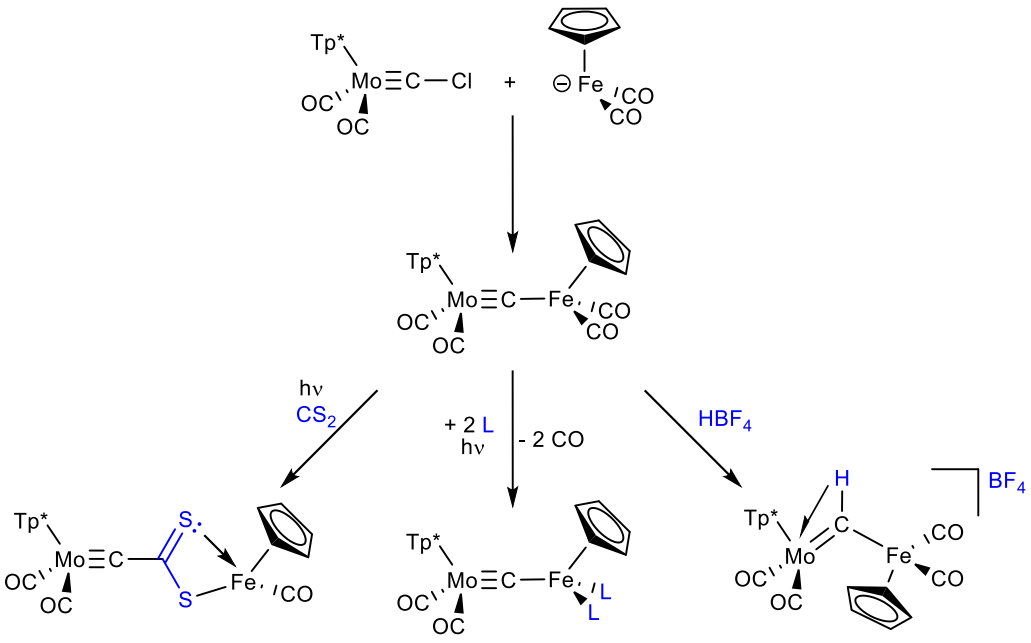

Scheme 1.31: Templeton's metallacarbyne *via* substitution of a halocarbyne and the subsequent reactivity at the μ_2-carbido. [97]

1.4.2.2| Ligand Migration (Indirect Reactivity)

Characterisation of [WNi(μ_2-C)(CO)$_2$(PEt$_3$)$_2$(Tp*)] was initially complicated by occurrence of a further reaction. [119] However, this reaction shows an example of intramolecular carbido reactivity for Class B. Formation of a μ_2-phosphoniocarbyne [WNi(μ_2-CPEt$_3$)Cl(CO)$_2$(PEt$_3$)(Tp*)] implies

that a pre-installed phosphine migrates onto the μ_2-carbido in a C–P bond forming process that is facile at ambient temperature. The μ_2-phosphoniocarbyne is an uncommon species, yet this reaction is gains significance in suggesting migration as a first step in reductive elimination processes catalysed by palladium in catalytic phosphine coupling reactions discussed below.

1.5 μ_2-Carbido Complexes in Catalysis

1.5.1 Appearances of Classes A, C, and D

Until recently, very few examples of stoichiometric reactivity at a μ_2-carbido were known as illustrated in the prior section. It is therefore unsurprising that catalytic transformations are even less well-documented. Currently no examples of catalysis have been reported from Classes C or D, whereas select examples have been observed for Classes A and B.

Sorokin's postulation of a dimetallacumulene as a catalyst akin to porphyrin μ-nitridos was explored after the unexpected production of the ruthenium phthalocyanine species [{(BuO)$_2$pc}Ru=C=Ru{pc(OBu)$_2$}].[131] The Class A carbido demonstrated catalytic activity in carbene addition to olefins and into N–H bonds of amines with turnover numbers of 580–1000 (Figure 1.6). Described by the authors as modest, this still demonstrates the first example of an isolable μ_2-carbido acting as a catalyst.

Probing catalytic potential of macrocyclic iron and ruthenium μ_2-carbido complexes has since been continued by Sorokin and co-workers in the cyclopropanation of olefins, drawing comparison to *oxo-* and *nitrido-* analogues. It was found that the *oxo*-species outperformed μ_2-carbido complex however reactivity was still observed. Such complexes have also been investigated as catalysts for natural products. Koifman and co-workers have utilised the macrocyclic complexes of iron and ruthenium as redox relays[132] to perform oxidation reactions to natural products such as pentahydroxyflavone, [133] and β-carotene. [134-135]

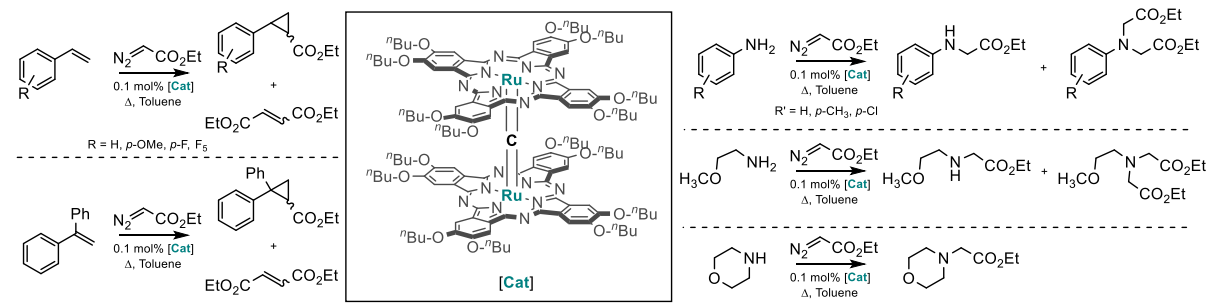

Figure 1.6: Carbene insertion to N–H bond catalysed by a dimetallacumulene. [131]

1.5.2 Metallacarbynes as intermediates

Metallacarbynes have also been inferred as intermediates in catalytic process. The initial example of a μ_2-carbido complex in catalytic processes was from Grubbs and co-workers who demonstrated the breakdown product $[Ru_2(\mu_2\text{-}C)HCl_3(\eta^1{:}\eta^6\text{-}SIMes)(SIMes)]$ was also capable of isomerising allylbenzene (Scheme 1.32),[38] though no mechanistic conjecture was provided for this reaction.

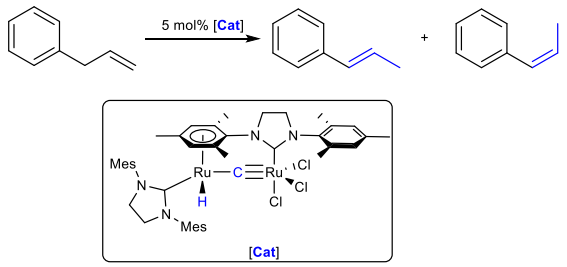

Scheme 1.32: Olefin isomerisation by Grubbs' metallacarbyne.

Bruce demonstrated cross-coupling of Lalor's halocarbyne $[Mo(\equiv CBr)(CO)_2(Tp^*)]$ with $[Co_3(\mu_3\text{-}CC{\equiv}CC{\equiv}Au(PPh_3)\}(\mu\text{-}dppm)(CO)_7]$ or $[Ru\{(C{\equiv}C)_nAu(PPh_3)\}(dppe)(Cp^*)]$ (n = 2 or 3) in the presence of catalytic $[Pd(PPh_3)_4]$ and [CuI] to give the respective poly-ynyl complexes (Scheme 1.33).[136-137] A simpler coupling also occurs without another transition metal from also from the same palladium and copper catalysts. As $[Mo(\equiv CBr)(CO)_2(Tp^*)]$ contains a C–Br bond and this is analogous to a Sonogashira cross-coupling, the likely initial step would be functionalising the C–Br *via* oxidative of palladium(0). Since this report, facile transmetallation from gold to palladium has been reported to give a palladium(II) metallacarbyne relevant to Bruces' catalytic reaction,[136-137] raising the question if the copper(I) salt is required. Furthermore, the latter of these reports describes a coupling between $[Au(C{\equiv}C\text{–}C_6F_5)(PPh_3)]$ and $[Co_3(\mu_3\text{-}CBr)(\mu\text{-}dppm)(CO)_7]$ which invites speculation to the identity of the palladium intermediate, recalling μ_4-carbidos are well established.

Cross-coupling from halocarbynes has also given rise to poly-ynylsilyl compounds which contain a utility in synthesis of extended carbyne complexes. Initially a series of propargylidynes $[W(\equiv CC{\equiv}CR)(CO)_2(Tp^*)]$ could be prepared by a Sonogashira cross-coupling bearing electron rich ($C_6H_4NH_2$), poor ($C_6H_4NO_2$), main group heteroatoms (B, Ge, Sn) and ferrocene derivatives.[138] A wealth of derivatives were produced, yet the true utility of this protocol arises from further incorporation of silyl groups. While the synthesis of $[W(\equiv CC{\equiv}CSiMe_3)(CO)_2(Tp^*)]$ from trimethylsilylacetylene cross-coupling may appear unimpressive given superior Fischer—Mayer protocols,[139] the same cross-coupling facilitated the first pentadiynylidyne $[W(\equiv CC{\equiv}CC{\equiv}CSiMe_3)(CO)_2(Tp^*)]$ from trimethylsilylbutadiyne, retaining the synthetically

versatile $SiMe_3$ terminus in a longer, analogous architecture.[140] Analogous cross-coupling has led to a series of polyl-ynyl-polyaromatic systems.[141] As these reactions arise from a palladium catalyst and cross-coupling partners to the work of Bruce, the palladium intermediate is likely common.

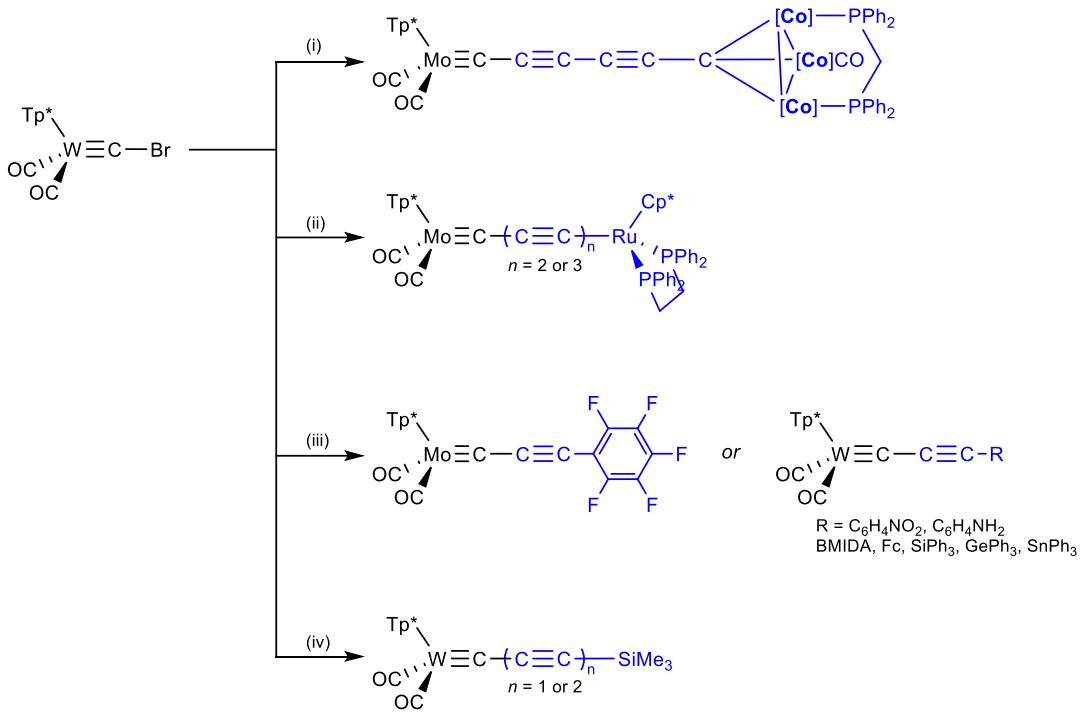

Scheme 1.33: Representative cross-couplings stipulated to have Class B carbido intermediates.

This palladium carbido intermediate is also likely the bridge between C–C and C–P bond formation processes arising from halocarbynes. A cross-coupling occurs between $[Mo(\equiv CBr)(CO)_2(Tp^*)]$ and $HP(O)(OEt)_2$ mediated by catalytic $[Pd(PPh_3)_4]$ in a basic medium (Scheme 1.34).[94] The C–P formation is proposed to occur *via* unobserved palladium metallacarbyne $[MoPd(\mu_2\text{-}C)Br(PPh_3)_2(CO)_2(Tp^*)]$ — *cf.* Beck's $[MoPt(\mu_2\text{-}C)(PPh_3)_2(CO)_2(Tp^*)]$[142]— that can be substituted by an anionic phosphorus nucleophile. Similar reactivity is recorded replacing phosphonates with secondary phosphines as PH_2R (R = Ph or Cy) which could be coupled with $[W(\equiv CBr)(CO)_2(Tp^*)]$ by palladium in basic media to give the first secondary phosphinocarbynes $[W(\equiv C\text{–}PHR)(CO)_2(Tp^*)]$.[95] Control of stoichiometry can also produce *bis*-(alkylidynyl)phosphines $[PR\{C\equiv W(CO)_2(Tp^*)\}_2]$ (R = Ph or Cy).[143]

These examples thus far represent catalytic transformations from a halocarbyne precursor, however, the reaction of reverse polarity is also known. Bromocarbynes can be converted into stannylcarbynes *via* the lithiocarbyne approach, and in the content of cross-coupling, this reverses the polarity of the coupling partner. A bromocarbyne is an electrophile synthon, while the lithiocarbyne is a nucleophilic carbyne source; the stannylcarbyne is an easier to manipulate

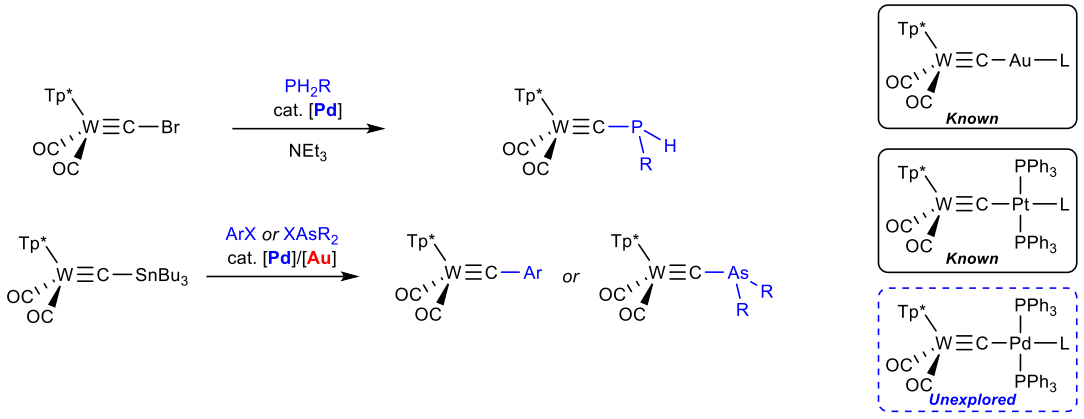

Scheme 1.34: Phosphine and aryl-cross-couplings with carbynes implicating Class B carbido complexes. Inset: Known and unexplored frameworks of the metallacarbyne intermediates.

derivative. To this end, the analogous Stille cross-coupling of carbynes was reported with arylhalides. [144] A requirement of a gold(I) co-catalyst suggests coupling of an aryl halide tostannylcarbyne proceeds *via* a gold(I) μ_2-carbido intermediate [MAu(μ_2-C)(L)$(CO)_2$(Tp*)] (L = ligand), where two isolated examples exist, [MoAu(μ_2-C)$(PPh_3)(CO)_2$(Tp*)] and [WAu(μ_2-C)$(PEt_3)(CO)_2$(Tp*)] (see Chapters One or Seven). In a similar vein, this Stille cross-coupling has extended to phenyl, pyridyl, bypyridyl, porphyrin and polycyclic aromatics, with the latter including species also pre-functionalised with more carbyne units. [145-148] A reverse in polarity afforded by the Stille cross-coupling of carbynes has also been extended to catalytic C–As bond formation. The stannylcarbyne can also transmetallate via Pd(0)/Au(I) catalysis to haloarsines such as $AsBrPh_2$, $ClAs(C_6H_4)_2NH$ and chloroarsoles to afford otherwise poorly accessible arsinocarbynes. [149] Like the phosphorus examples, the transmetallation from tin to arsenic fails without the gold(I) co-catalyst, implying a gold(I) metallacarbyne is a key catalytic intermediate.

1.6 Rationale and Project Aims

As the foregoing highlight on μ_2-carbido chemistry has shown, significant gaps become conspicuous as the field gains momentum, particularly for Class B carbidos that are yet to be systematically studied. Compared with other Classes, metallacarbynes have a relatively high number of synthetic routes that are known but have only produced a small number of examples through limited exploration. The largest issue in the field is the sporadic formation of μ_2-carbido complexes where general synthetic routes have yet to emerge, calling for investigation.

Slow development of metallacarbyne chemistry through sporadic examples has also seen only limited reactivity studies, again calling for dedicated study. For Class B specifically it is unusual that several examples of metallacarbyne intermediates are implied and catalytic manifolds employed to produce target species, but the intermediates through stoichiometric investigations are yet to be

pursued. This Thesis seeks to address these issues. Firstly, to systematically investigate the synthesis of heterobimetallic Class B carbido complexes ensuring a comprehensive characterisation to establish understanding of the M≡C–M' linkage. If successful, the desirable goal would be to identify more general method towards their synthesis to allow expansion to previously unknown metal termini (*i.e.*, diverge from known examples). Secondly, to perform exploratory stoichiometric transformations that might help to chart a reactivity profile for the μ2-carbido ligand as a reactive site itself.

Table 1.2: Spectroscopic Data for Class A μ2-carbido complexes.

Compound (Class A)	δ_C (ppm)	$\nu_{M=C=M}$ (cm^{-1})	Year	Reference
Iron				
[(TPP)Fe=C=Fe(TPP)]	-	940, 883	1981	[150]
[(1-MeIm)(pc)Fe]$_2$(μ_2-C)	-	940	1988	[43]
[F-(pc)Fe=C=Fe(pc)-F]$^{2-}$	-	917, 476	1998	[151]
[(THF)(TPP)Fe=C=Fe(pc)(THF)]	-	963	1998	[46]
[(THF)(pc)Fe=C=Fe(pc)(THF)]	-	997	1998	[46]
Niobium				
Na$_2$[(cal4ix)Nb=C=Nb(cal4ix)]	257.0[a]	-	2000	[57]
Na$_3$[(cal4ix)Nb=C=Nb(cal4ix)]	268.9[a]	-	2000	[57]
Ruthenium				
[(py)(pc)Ru=C=Ru(pc)(py)]	-	1017, 974	1997	[45]
[(cym)Ru(PCy$_3$)(μ_3-Cl)ClRu]$_2$(μ_2-C)	430.5	-	2007	[58]
[(BuOpc)Ru=C=Ru(pcOBu)]	N.D.	1013	2017	[152]
[Cl$_2$(H$_2$IMes)Ru=C=Ru(H$_2$IMes)Cl$_2$]	N.D.	N.D.	2021	[153]
Rhodium				
[(pinB)(PEt$_3$)$_2$Rh=C=Rh(PEt$_3$)$_2$(Bpin)]	439.4[b] ($^1J_{RhC}$ = 45, $^2J_{CP}$ = 11 Hz)	978	2015	[154]
[(HS)(PEt$_3$)$_2$Rh=C=Rh(PEt$_3$)$_2$(SH)]	431.9[a] ($^1J_{RhC}$ = 44, $^2J_{CP}$ = 12 Hz)	-	2015	[154]
[(Ph$_3$GeS)(PEt$_3$)$_2$Rh=C=Rh(PEt$_3$)$_2$(SGePh$_3$)]	425.8[a] ($^1J_{RhC}$ = 47, $^2J_{CP}$ = 11 Hz)	-	2017	[155]
[(Ph$_3$GeS)(PEt$_3$)$_2$Rh=C=Rh(PEt$_3$)$_2$(SBpin)]	429.3[a] ($^1J_{RhC}$ = 46, $^2J_{CP}$ = 11 Hz)	-	2017	[155]
[Cl(PPh$_3$)$_2$Rh=C=Rh(PPh$_3$)$_2$Cl]	424.4 ($^1J_{RhC}$ = 47 Hz)	1011	2018	[156]
[(Tp*)HRh(μ_2-C)(μ-C$_6$H$_4$PPh$_2$)Rh(Tp*)]	447.2 ($^1J_{RhC}$ = 50, 40 Hz)	1003	2018	[156]
[ClRh=C=RhCl(μ-dppm)$_2$]	-	999	2019	[78]
Tungsten				
[(^{t}Bu$_3$OSi)$_2$(=NAr)W=C=WCl$_2$(SiO^{t}Bu)$_2$]	406.3[a] ($^1J_{CW}$ = 194 Hz)	1120	1993	[56]
[(^{t}Bu$_3$OSi)$_2$(=O)W=C=WCl$_2$(SiO^{t}Bu)$_2$]	379.1[a] ($^1J_{CW}$ = 200, 187 Hz)	1155	1993	[56]
Rhenium				
[(TPP)Fe=C=Re(CO)$_4$Re(CO)$_5$]	211.7 (ambiguous)	-	1990	[157]
[(Cp)(CO)$_2$Re=C=Re(CO)$_2$(Cp)]	436.4[c, d]	1019	2013	[17]
[(Tp*)(CO)(NO)W=C=Re(CO)$_2$(Cp)]	508.8	-	2020	[61]

N.D. = not detected. [a]Measured in d_6-benzene. [b]Measured in d_6-cyclohexane.[c]Measured in CD_2Cl_2. [d]Identified by ^{1}H-^{13}C HMBC experiment.

Table 1.3: Spectroscopic Data for Class B μ_2-carbido complexes.

Compound (Class B)	δ_C (M≡C–M') (ppm)	δ_C (CO) (ppm)	ν_{CO} (cm^{-1})	Year	Reference
Iron					
[(Tp*)(CO)$_2$Mo≡C– Fe(CO)$_2$(Cp)]	380.9[a]	229.6, (Mo) 211.5 (Fe)	2040,1991, 1947, 1865	1991	97
[(Tp*)(CO)$_2$Mo≡C– Fe(PMe)$_2$(Cp)]	499.6	236.5	1903, 1814[d]	1991	97
[(Tp*)(CO)$_2$Mo≡C– Fe(CN^{t}Bu)$_2$(Cp)]	452.1	231.7, (δ_{CN} = 166.3)	1917, 1828	1991	97
Nickel					
[Tp*(CO)$_2$W≡C–NiCl(PEt$_3$)$_2$]	484.0[b] ($^2J_{CP}$ = 4 Hz)	237.4, 232.8[b]	1936, 1843	2012	119
Ruthenium					
[(^{t}BuO)$_3$W≡C–Ru(CO)$_2$Cp]	273.3[b] ($^1J_{CW}$ = 290.1)	201.6[b]	2030, 1980[c]	1987	33
[(H$_2$IMes)Cl$_3$Ru≡C–RuH(H$_2$IMes)]	414.0[a]	-	-	2004	158
Iridium					
[Tp*(CO)$_2$Mo≡C–]$_2$[Ir$_2$(μ-Se$_2$)(CO)$_2$(PPh$_3$)$_2$]	286.1[b] ($^2J_{CP}$ = 28 Hz)	222.8, 181.1[b] (Ir, $^2J_{CP}$ = 11 Hz)	1989, 1960, 1909[d]	2009	62
Platinum					
[Cl$_3$(PCy$_3$)Ru≡C–PtCl(py)$_2$]	354.6 ($^2J_{CP}$ = 13, $^1J_{CPt}$ = 1372 Hz)	-	-	2018	73
[Cl$_3$(PCy$_3$)Ru≡C–PtCl(pz)$_2$]	358.5 ($^2J_{CP}$ = 13, $^1J_{CPt}$ = 1285 Hz)	-	-	2018	73
[Cl$_3$Ru≡C–PtCl(μ-dppm)$_2$]	361.9 ($^2J_{CP}$ = 19, 11, $^1J_{CPt}$ = 913 Hz)	-	-	2018	73
[Cl$_3$Ru≡C–PtCl(μ-dpcm)]	362.0 ($^2J_{CP}$ = 15, 10, $^1J_{CPt}$ = 970 Hz)	-	-	2018	73
[Cl(AdPNP)Ru≡C–PtCl(py)][Cl]	353.6	-	-	2018	73
[Cl(AdPNP)Ru≡C–PtCl(py)][BPh$_4$]	353.6	-	-	2018	73
[Tp*(CO)$_2$Mo≡C–PtBr(PPh$_3$)$_2$]	339 ($^2J_{CP}$ = 9, 5 Hz)	233.7	1961, 1872	2008	142
[Tp*(CO)$_2$W≡C–Pt(phen-3-C≡W(CO)$_2$Tp*]	331.3	227.3, 226.1	1977, 1944, 1886, 1854	2019	159
[Tp*(CO)$_2$W≡C–Pt(terpy)][PF$_6$]	368.0	228.3	1954, 1858	2019	159
Gold					
[Tp*(CO)$_2$Mo≡C–Au(PPh$_3$)]	N.D.	231.4[a]	1968, 1882[d]	2013	99
[Tp*(CO)$_2$W≡C–Au(PEt$_3$)]	397.7[b] ($^1J_{CW}$ = 147 Hz)	230.0[b] ($^1J_{CW}$ = 181 Hz)	1951, 1856	2013	99
Mercury					
[Tp*(CO)$_2$Mo≡C–Hg–C≡Mo(CO)$_2$Tp*]	373.0[a]	229.6[a]	2000, 1994, 1912	2009	118

Notes: [a]Measured in CD_2Cl_2. [b]Measured in d_6-benzene. [c]Measured in *n*-pentane. [d]Measured in THF. [e]Determined by ^1H-^{13}C HMBC experiment. [f]Coupling not resolved (multiplet).

Table 1.4: Spectroscopic Data for Class C μ2-carbido complexes.

Compound (Class C)	δ_C (ppm)	$^1J_{CM'}$ (Hz)	ν_{CO} (cm^{-1})	Year	Reference
Copper					
$[Cl_2(PCy_3)_2Ru{\equiv}C{:}\rightarrow Cu([9]aneS_3)][BF_4]$	431.7	-	-	2016	[70]
Molybdenum					
$[Cl_2(PCy_3)_2Ru{\equiv}C{:}\rightarrow Mo(CO)_5]$	446.3	-	2073, 1966, 2943	2002	[38]
Rhodium					
$[Cl_2(PCy_3)_2Ru{\equiv}C{:}\rightarrow RhCl(COD)]$	411.7	59	-	2015	[69]
Trans-$[Cl_2(PCy_3)_2Ru{\equiv}C{:}\rightarrow RhCl(CO)]_2$	397.6	60	2022	2015	[69]
Palladium					
$[Cl_2(PCy_3)_2Ru{\equiv}C{:}\rightarrow PdCl_2(SMe_2)]$	381.2	-	-	2002	[38]
$[Cl_2(PCy_3)_2Ru{\equiv}C{:}\rightarrow PdCl_3]$	381.0[a]	-	-	2015	[69]
$[Cl_2(PCy_3)_2Ru{\equiv}C{:}\rightarrow PdS_3Mo_3(Cp^*)_3]$	429.8	-	-	2016	[70]
$[Cl_2(PCy_3)_2Ru{\equiv}C{:}\rightarrow PdS_3W_3(Cp^*)_3]$	421.4	-	-	2016	[70]
Silver					
$[Cl_2(PCy_3)_2Ru{\equiv}C{:}\rightarrow Ag([9]aneS_3)][BF_4]$	431.8	175	-	2016	[70]
$[Cl_2(PCy_3)_2Ru{\equiv}C{:}\rightarrow Ag(terpy)][OTf]$	433.9	187	-	2015	[69]
$[Cl_2(PCy_3)_2Ru{\equiv}C{:}\rightarrow Ag(4\text{-}Ph\text{-}terpy)][OTf]$	433.4	188	-	2015	[69]
Iridium					
$[\{Cl_2(PCy_3)_2Ru{\equiv}C{:}\rightarrow\}_2IrCl(CO)]$	397.4	-	1990	2015	[69]
$[Cl_2(PCy_3)_2Ru{\equiv}C{:}\rightarrow IrCl(COD)]$	387.7	-	-	2015	[69]
Platinum					
$[Cl_2(PCy_3)_2Ru{\equiv}C{:}\rightarrow PtCl_2(Py)]$	350.3	1283	-	2015	[69]
$[AsPh_4][Cl_2(PCy_3)_2Ru{\equiv}C{:}\rightarrow PtCl_3]$	351.0	1396	-	2015	[69]
$[Cl_2(PCy_3)_2Ru{\equiv}C{:}\rightarrow PtCl_2(dmso)]$	344.8	1334	-	2015	[69]
$[Cl_2(PCy_3)_2Ru{\equiv}C{:}\rightarrow PtS_3Mo_3(Cp^*)_3]$	385.4	2417	-	2016	[70]
$[Cl_2(PCy_3)_2Ru{\equiv}C{:}\rightarrow PtS_3W_3(Cp^*)_3]$	378.2	2600	-	2016	[70]
$[Cl_2(PCy_3)_2Ru{\equiv}C{:}\rightarrow PtCl_2(PPh_3)]$	388.8	969,	-	2017	[71]
$[Cl_2(PCy_3)_2Ru{\equiv}C{:}\rightarrow PtCl_2(PCy_3)]$	395.8	883	-	2017	[71]
$[Cl_2(PCy_3)_2Ru{\equiv}C{:}\rightarrow PtCl_2\{P(OPh_3)\}]$	387.5	952	-	2017	[71]
$[Cl_2(PCy_3)_2Ru{\equiv}C{:}\rightarrow PtCl_2(CN^tBu)]$	376.3	1103	n.r.	2017	[71]
$[Cl_2(PCy_3)_2Ru{\equiv}C{:}\rightarrow PtCl_2(CNCy)]$	376.0	1105	n.r.	2017	[71]
$[Cl_2(PCy_3)_2Ru{\equiv}C{:}\rightarrow PtCl]_2(\mu\text{-}Cl)_2$	326.2	1470	-	2017	[71]
$[Cl_2(PCy_3)_2Ru{\equiv}C{:}\rightarrow PtCl]_2(\mu\text{-}Cl)(\mu\text{-}pz)$	355.1	1169	-	2017	[71]
$[Cl_2(PCy_3)_2Ru{\equiv}C{:}\rightarrow PtCl_2]_2(\mu\text{-}pym)$	341.4	1365	-	2017	[71]
$[Cl_2(PCy_3)_2Ru{\equiv}C{:}\rightarrow PtCl_2]_2(\mu\text{-}pyz)$	342.5	1347	-	2017	[71]
$[Cl_2(PCy_3)_2Ru{\equiv}C{:}\rightarrow PtCl_2]_2(4,4'\text{-}bpy)$	348.3	1277	-	2017	[71]
$[Cl_2(PCy_3)_2Ru{\equiv}C{:}\rightarrow PtCl_2(:N{\equiv}Cr(dbm)_2]$	N/A	-	-	2019	[74]
Gold					
$[Cl_2(PCy_3)_2Ru{\equiv}C{:}\rightarrow AuCl]$	395.4	-	-	2015	[69]
$[\{Cl_2(PCy_3)_2Ru{\equiv}C{:}\rightarrow\}_2Au^+][OTf]$	395.3	-	-	2015	[69]
$[Cl_2(PCy_3)_2Ru{\equiv}C{:}\rightarrow Au([9]aneS_3)][OTf]$	414.1	-	-	2016	[70]
$[Cl_2(PCy_3)_2Ru{\equiv}C{:}\rightarrow(\mu\text{-}Au)(WCAuCl(CO)_2Tp^*]$	420.1[a]	-	1994, 1913[b]	2018	[72]

Notes: n.r. = not reported. [a]Measured in CD_2Cl_2. [b]Measured by ATR-IR.

Table 1.5: Crystallographic Data for Class A μ_2-carbido complexes.

Compound (Class A)	$r_{M=C}$ (Å)	$r_{C=M}$ (Å)]	M–C–M (°)	$r_{M-L\ (trans)}$ (Å)	Year (Reference)
Iron					
[(TPP)Fe=C=Fe(TPP)][a]	1.673	1.673	180	-	1982 [150]
	1.682	1.682	180	-	1998 [150]
[(1-MeIm)pcFe]$_2$(μ_2-C)[a]	1.689	1.689	178.4	2.100 (Fe-N)	1988 [43]
[(py)(pc)Fe=C=Fe(pc)(py)]	1.68(2)	1.70(2)	177(1)	2.18(1), 2.20(1)	1997 [45]
[(oep)Fe=C=Fe(oep)]	1.664[a]	1.664[a]	179.5[a]	-	1997 [45]
[F-(pc)Fe=C=Fe(pc)-F]	1.683(5)	1.692(5)	179.5(3)	2.013, 2.053(3) (Fe-F)	1998 [151]
[(THF)(TPP)Fe=C=Fe(pc)(THF)]	1.65(1)	1.71(1)	179.3(8)	2.233, 2.269(8) (Fe-O)	1998 [46]
[(THF)(pc)Fe=C=Fe(pc)(THF)]	1.64(2)	1.71(3)	180(1)	2.21, 2.23(1) (Fe-O)	1998 [46]
[(opp)Fe=C=Fe(opp)]	1.669(1)	1.671(1)	175.1(1)	-	2015 [48]
Niobium					
[(cal4ix)Nb=C=Nb(cal4ix)].3Na	1.918(4)	1.927(4)	173.9(2)	-	2000 [57]
Ruthenium					
[(py)(pc)Ru=C=Ru(pc)(py)]	1.77(1)	1.78(1)	177.4 (6)	2.314, 2.342 (8) (Ru-N)	1997 [45]
[(cym)Ru(PCy$_3$)(μ_3-Cl)ClRu]$_2$(μ_2-C)	1.7877(9)	1.7877(9)	178.8(9)	2.685(3) (Ru-Cl)	2007 [58]
[Cp*Ru=C=RuCp*(ZnClOR$_t$)$_2$]	1.841(2)	1.844(2)	172.1(1)	–	2021 [160]
Rhodium					
[(pinB)(PEt$_3$)$_2$Rh=C=Rh(PEt$_3$)$_2$(Bpin)]	1.776(9)	1.790(9)	176.1(5)	2.487(3) (Rh-S)	2015 [154]
[(Ph$_3$GeS)(PEt$_3$)$_2$Rh=C=Rh(PEt$_3$)$_2$(SGePh$_3$)]	1.788(4)	1.799(4)	175.6(2)	2.460, 2.490 (1) (Rh-S)	2017 [155]
[Cl(PPh$_3$)$_2$Rh=C=Rh(PPh$_3$)$_2$Cl]	1.773(2)	1.780(2)	173.4(2)	2.435, 2.422(7) (Rh-Cl)	2018 [156]
[(Bp)Rh=C=Rh(Bp)]	1.7644(11)	1.7680(11)	168.8(6)	2.189(7) (Rh-N)	2018 [156]
[(Bp*)Rh=C=Rh(Bp*)]	1.779(4)	1.779(4)	163.7(4)	2.165(4)(Rh-N)	2018 [156]
[(Tp)Rh=C=Rh(Tp)]	1.776(2)	1.776(2)	163.8(3)	2.289(3) (Rh-N)	2018 [156]
[(Tp*)HRh(μ_2-C)(μ-C$_6$H$_4$PPh$_2$)Rh(Tp*)]	1.741(6)	1.817(6)	165.92(3)	2.364(5) (Rh-N)	2018 [156]
[ClRh=C=RhCl(μ-dppm)$_2$]	1.73(1)	1.76(1)	162.6(7)	2.421, 2.418(3) (Rh-Cl)	2019 [78]
[(MeCN)Rh=C=Rh(NCMe)(μ-dppm)$_2$][OTf]$_2$	1.744(2)	1.744(2)	180.0	2.168(7) (Rh-N)	2019 [78]
[ClRh=C=RhCl(μ-dppf)$_2$]	1.766(4)	1.783(4)	168.4(3)	2.424, 2.397(1) (Rh-Cl)	2020 [161]
[Cl$_2$Rh=C=RhCl$_2$(μ-dppf)$_2$]	1.7945(3)	1.7947(3)	180	2.4240(8 (Rh-Cl)	2020 [161]

Tungsten					
$[(^tBu_3OSi)_2(=NAr)W{=}C{=}WCl_2(SiO^tBu)_2]$	1.77(2)	1.99(2)	176.0(1)	-	1993 ([56])
Rhenium					
$[(TPP)Fe{=}C{=}Re(CO)_4Re(CO)_5]$	1.61(1)	1.96(1)	173.2(8)	3.044(2) (Re-Re)	1990 ([157])
$[(Cp)(CO)_2Re{=}C{=}Re(CO)_2(Cp)]$	1.88(1)	1.88(1)	173.3(8)	-	2013 ([17])
$[(Tp^*)(CO)(NO)W{=}C{=}Re(CO)_2(Cp)]$	1.893(6)	1.966(6)	169.3(3)	-	2020 ([130])

[a]Crystallographic error values were not reported in published CIF file. [b]NMR taken in d_6-cyclohexane.[c]NMR taken in CD_2Cl_2. [d]Resonance determined by ^1H-^{13}C HMBC experiment. R_1 = –OC(OEt)CH=CHC(OEt)–.

Table 1.6: Crystallographic Data for Class B μ_2-carbido complexes.

Compound (Class B)	$r_{M\equiv C}$ (Å)	$r_{C\text{-}M'}$ (Å)	M–C–M (°)	$r_{M'\text{–}L\ (trans)}$ (Å)	Year (Reference)
Iron					
$[(Tp^*)(CO)_2Mo{\equiv}C\text{–}Fe(CO)_2(Cp)]$	1.820(8)	1.911(8)	172.1(5)	–	1991 ([97])
Nickel					
$[Tp^*(CO)_2W{\equiv}C\text{–}NiCl(PEt_3)_2]$	1.867(3)	1.808(3)	174.7(2)	2.258(1) (W-Cl)	2012 ([119])
Ruthenium					
$[(^tBuO)_3W{\equiv}C\text{–}Ru(CO)_2Cp]$	1.75(2)	2.08(2)	177(2)	–	1987 ([33])
$[(Mes_2Im)ClRu{\equiv}C\text{–}RuH(ImMes_2)]$	1.698(4)	1.875(4)	160.3(2)	–	2004 ([158])
Iridium					
$[Tp^*(CO)_2Mo{\equiv}C\text{–}Ir(CO)(PPh_3)]_2(\mu\text{-}Se)_2$	1.840(5) 1.847(6)	1.977(5) 1.969(6)	168.1(3) 171.3(3)	2.556(5) (Ir-Se) 2.557(7) (Ir-Se)	2009 ([62])
Platinum					
$[Cl_3(PCy_3)Ru{\equiv}C\text{–}PtCl(py)_2]$	1.669(1)	1.900(1)	166.24(9)	2.3411(5) (Pt-Cl)	2018 ([73])
$[Cl_3Ru{\equiv}C\text{–}PtCl(\mu\text{-}dppm)_2]$	1.693	1.852	180	2.350 (Pt-Cl)	2018 ([73])
$[Cl_3Ru{\equiv}C\text{–}PtCl(\mu\text{-}dpcm)]$	1.694(2)	1.842(2)	166.2(1)	2.352(5) (Pt-Cl)	2018 ([73])
$[Cl(AdPNP)Ru{\equiv}C\text{–}PtCl(py)][Cl]$	1.687(5)	1.923(5)	176.5(2)	2.313(1) (Pt-Cl)	2018 ([73])
$[Cl(AdPNP)Ru{\equiv}C\text{–}PtCl(py)][BPh_4]$	1.695(4)	1.921(4)	174.3(2)	2.332(1) (Pt-Cl)	2018 ([73])
$[Cl_3(PCy_3)_3Ru{\equiv}C\text{–}PtCl(pz)_2].H_2O$	1.692(3)	1.899(3)	164.3(2)	2.354(2) (Pt-Cl)	2018 ([73])
$[Tp^*(CO)_2Mo{\equiv}C\text{–}PtBr(PPh_3)_2]$	1.828(2)	1.951(2)	174.0(2)	2.5448(3) (Pt-Br)	2008 ([142])
$[Tp^*(CO)_2W{\equiv}C\text{–}Pt(phen\text{-}3\text{-}C{\equiv}W(CO)_2Tp^*]$	1.853(14)	1.890(14)	173.4(9)	2.254(12) (Pt-N)	2019 ([120])
$[Tp^*(CO)_2W{\equiv}C\text{–}Pt(terpy)][PF_6]$	1.835(6)	1.938(6)	176.3(3)	2.002(5) (Pt-N)	2019 ([120])

[a]Crystallographic error values were not reported in published CIF file. [b]NMR taken in d_6-cyclohexane.[c]NMR taken in CD_2Cl_2. [d]Resonance determined by ^1H-^{13}C HMBC experiment.

Table 1.7: Spectroscopic Data for Class C μ_2-carbido complexes.

Compound (Class C)	$r_{M=C}$ (Å)	$r_{C=M}$ (Å)	M–C–M (°)	$r_{M-L\ (trans)}$ (Å)	Year (Reference)
Chromium					
$[Br_2(py)_2Cr{\equiv}C{:}\rightarrow CrBr_2(py)_3]$	1.634(9)	2.034(9)	174.4(7)	2.209(9) (Cr-N)	2021 ([55])
Copper					
$[Cl_2(PCy_3)_2Ru{\equiv}C{:}\rightarrow Cu(^9S_3)][BF_4]$	1.653(4)	1.876(4)	177.3(2)	–	2016 ([70])
Molybdenum					
$[Cl_2(PCy_3)_2Ru{\equiv}C{:}\rightarrow Mo(CO)_5]$	–	–	–	–	2002 ([38])
Rhodium					
$[Cl_2(PCy_3)_2Ru{\equiv}C{:}\rightarrow RhCl(COD)]$	1.690(2)	1.897(2)	173.4(3)	2.315(5) (Rh-C)	2015 ([69])
Trans-$[Cl_2(PCy_3)_2Ru{\equiv}C{:}\rightarrow RhCl(CO)]_2$	1.688(3)	1.864(3)	176.9(1)	2.403(1) (Rh-C)	2015 ([69])
Palladium					
$[Cl_2(PCy_3)_2Ru{\equiv}C{:}\rightarrow PdCl_2(SMe_2)]$	1.662(2)	1.946(2)	175.1(1)	2.3556(5) (Pd-S)	2002 ([38])
$[Cl_2(PCy_3)_2Ru{\equiv}C{:}\rightarrow PdCl_3]$	1.668(2)	1.892(2)	173.5(2)	2.327(8) (Pd-Cl)	2015 ([69])
$[Cl_2(PCy_3)_2Ru{\equiv}C{:}\rightarrow Pd(S_3Mo_3)]$	1.672(3)	1.971(3)	178.3(2)	–	2016 ([70])
$[Cl_2(PCy_3)_2Ru{\equiv}C{:}\rightarrow Pd(S_3W_3)]$	1.668(5)	1.959(5)	178.1(3)	–	2016 ([70])
Silver					
$[Cl_2(PCy_3)_2Ru{\equiv}C{:}\rightarrow Ag(^9S_3)][BF_4]$	1.622(7)	2.098(7)	176.9(5)	–	2016 ([70])
$[Cl_2(PCy_3)_2Ru{\equiv}C{:}\rightarrow Ag(terpy)][OTf]$	1.642(3)	2.082(3)	177.2(2)	2.305(3) (Ag-N)	2015 ([69])
$[Cl_2(PCy_3)_2Ru{\equiv}C{:}\rightarrow Ag(4\text{-}Ph\text{-}terpy)][OTf]$	1.651(3)	2.072(3)	176.5(2)	2.317(2) (Ag-N)	2015 ([69])
Iridium					
$[Cl_2(PCy_3)_2Ru{\equiv}C{:}\rightarrow IrCl(CO)]$	1.675(5) 1.677(5)	1.974(5) 1.988(5)	180	1.677(5) (Ir-C) 1.675(5) (Ir-C)	2015 ([69])
$[Cl_2(PCy_3)_2Ru{\equiv}C{:}\rightarrow IrCl(COD)]$	1.698(3)	1.882(3)	174.8(2)	3.060(4) (Ir-C)	2015 ([69])
Platinum					
$[Cl_2(PCy_3)_2Ru{\equiv}C{:}\rightarrow PtCl_2(Py)]$	1.679(3)	1.881(3)	172.9(2)	2.096(3) (Pt-N)	2015 ([69])
$[Cl_2(PCy_3)_2Ru{\equiv}C{:}\rightarrow PtCl_3][AsPh_4]$	1.691(3)	1.873(3)	174.4(4)	2.357(1) (Pt-Cl)	2015 ([69])
$[Cl_2(PCy_3)_2Ru{\equiv}C{:}\rightarrow PtCl_2(dmso)]$	1.682(2)	1.919(2)	177.6(1)	2.333(6) (Pt-Cl)	2015 ([69])
$[Cl_2(PCy_3)_2Ru{\equiv}C{:}\rightarrow Pt(S_3Mo_3)]$	1.689(7)	1.896(7)	178.2(5)	–	2016 ([70])
$[Cl_2(PCy_3)_2Ru{\equiv}C{:}\rightarrow Pt(S_3W_3)]$	1.699(9)	1.874(9)	178.8(6)	–	2016 ([70])
$[Cl_2(PCy_3)_2Ru{\equiv}C{:}\rightarrow PtCl_2(PPh_3)]$	1.672(2)	1.983(2)	173.7(1)	2.322(6) (Pt-P)	2017 ([71])
$[Cl_2(PCy_3)_2Ru{\equiv}C{:}\rightarrow PtCl_2(PCy_3)]$	1.666(2)	1.971(2)	174.52(1)	2.333(6) (Pt-P)	2017 ([71])
$[Cl_2(PCy_3)_2Ru{\equiv}C{:}\rightarrow PtCl_2(P(OPh_3))]$	1.659(2)	2.001(2)	179.3(2)	2.242(7) (Pt-P)	2017 ([71])
$[Cl_2(PCy_3)_2Ru{\equiv}C{:}\rightarrow PtCl_2(CN^tBu)]$	1.658(5) 1.663(6)	1.967(6) 1.967(5)	174.4(3) 178.4(3)	1.983(8) (Pt-C) 1.984(7) (Pt-C)	2017 ([71])
$[Cl_2(PCy_3)_2Ru{\equiv}C{:}\rightarrow PtCl_2]_2(\mu\text{-}Cl)_2$	1.676(8)	1.871(8)	179.6(4)	2.390(2)	2017 ([71])
$[Cl_2(PCy_3)_2Ru{\equiv}C{:}\rightarrow PtCl_2]_2(pz)$	1.675(4) 1.680(3)	1.910(4) 1.908(3)	172.4(2) 167.3(2)	2.049(3) (Pt-N) 2.059(2) (Pt-N)	2017 ([71])
$[Cl_2(PCy_3)_2Ru{\equiv}C{:}\rightarrow PtCl_2]_2(pym)$	1.676(3) 1.679(2)	1.901(3) 1.885(2)	177.3(2) 174.7(2)	2.103(2) (Pt-N) 2.101(2) (Pt-N)	2017 ([71])
$[Cl_2(PCy_3)_2Ru{\equiv}C{:}\rightarrow PtCl_2]_2(pyz)$	1.669(6) 1.667(6)	1.893(6) 1.898(6)	177.8(3) 175.8(3)	2.080(5) (Pt-N) 2.090(4) (Pt-N)	2017 ([71])
$[Cl_2(PCy_3)_2Ru{\equiv}C{:}\rightarrow PtCl_2]_2(4,4'\text{-}bpy)$	1.679(3)	1.895(4)	174.0(2)	2.104(7) (Pt-N)	2017 ([71])
$[Cl_2(PCy_3)_2Ru{\equiv}C{:}\rightarrow PtCl_2(:N{\equiv}Cr(dbm)_2]$	1.676(2)	1.899(2)	174.5(1)	2.005(2) (Pt-N)	2019 ([74])

Compound (Class C) (Cont.)	$r_{M=C}$ (Å)	$r_{C=M}$ (Å)	M–C–M (°)	$r_{M-L\ (trans)}$ (Å)	Year (Reference)
Gold					
$[Cl_2(PCy_3)_2Ru{\equiv}C{:}{\rightarrow}AuCl]$	1.664(3)	1.921(3)	175.4(2)	2.263(1) (Au-Cl)	2015 ([69])
$[Cl_2(PCy_3)_2Ru{\equiv}C{:}]_2Au$	1.655(9) 1.679(10)	1.960(10) 1.974(9)	173.6(6) 175.4(6)	1.679(10) (Au-C) 1.655(9) (Au-C)	2015 ([69])
$[Cl_2(PCy_3)_2Ru{\equiv}C{:}{\rightarrow}Au(^9S_3)][BOTf]$	–	–	–	–	2016 ([70])
$[Cl_2(PCy_3)_2Ru{\equiv}C{:}{\rightarrow}(\mu\text{-}Au)(WCAuCl(CO)_2Tp^*]$	1.665(5)	1.966(5)	168.2(4)	2.091(6)	2018 ([72])

[a]Crystallographic error values were not reported in published CIF file. [b]NMR taken in d_6-cyclohexane.[c]NMR taken in CD_2Cl_2. [d]Resonance determined by ^1H-^{13}C HMBC experiment.

Table 1.8: Spectroscopic Data for Class D μ_2-carbido complexes.

Compound (Class D)	δ_C [ppm]	δ_C (CO) [ppm]	ν_{M-C-M} [cm^{-1}]	Year	Reference
[Ru–C:–Ru(μ-NPh)(Cp^*)$_2$]	675.3[a]	-	-	2014	[41]
[Rh–C:–Rh(μ-DMAD)Cl_2(μ-dppm)$_2$]	563.0	152.3	798	2020	[40]

Notes:

Table 1.9: Crystallographic Data for Class D μ_2-carbido complexes.

Compound	$r_{M=C}$ [Å]	$r_{C=M}$ [Å]	M–C–M [°]	$r_{M-L\ (trans)}$ [Å] [cm^{-1}]	τ [torsion, °]	Year (Reference)
[Rh–C:–Rh(μ-DMAD)Cl_2(μ-dppm)$_2$]	1.85(2)	1.86(2)	124.2(9)	–	4.4(1)	2020 ([40])

[a]Crystallographic error values were not reported in published CIF file. [b]NMR taken in d_6-cyclohexane.[c]NMR taken in CD_2Cl_2. [d]Resonance determined by ^1H-^{13}C HMBC experiment.

Chapter Two

Heterobimetallic μ_2-halocarbynes from π-coordination

Sporadic emergence of metallacarbyne complexes though varied (generally non-generalisable) syntheses invites systematic investigation of such species. From the preceding Chapter, one entry to metallacarbynes that offered potential for further development was provided by Beck and co-workers who demonstrated oxidative addition of Lalor's bromocarbyne $[Mo(\equiv CBr)(CO)_2(Tp^*)]$ with low-valent platinum(0). [142] At the time of publication, Beck's halocarbyne was the only isolated μ_2-halocarbyne and one of few μ-halocarbynes more generally, other than well-studied μ_3-examples. Beck's report established a connection between μ_2-halocarbynes and metallacarbynes, providing the motivation for the dedicated study this Chapter presents.

This Chapter initially surveys low-nuclearity (η^1, μ_2 and μ_3) halocarbyne chemistry given it is brief and yet to be reviewed in the literature before a section describing π-coordination of halocarbynes with labile gold(I) and platinum(0) fragments as an extension of Beck's synthesis. The spectroscopic and structural parameters of a series discussed herein provides the basis for a discussion of bonding in μ_2-halocarbynes, to explore the isoelectronic analogy between CX^+ and CO diatomics.

2.1 A Brief Review of Low-Nuclearity Halocarbynes

While few examples of halocarbyne complexes exist, known species provide sufficient insight to better understand the bonding of CX ligands and how further examples might be synthesised. Carbon's common tetravalency is manifest in halocarbyne chemistry, allowing three types of low-nuclearity halocarbynes. Terminal (η1) halocarbynes involve a formal triple bond of a carbyne with one transition metal (M≡C), where additional metal centres result in bridging to give μ_2- or μ_3-halocarbynes (Chart 2.1a). The synthesis of each class will be addressed separately (vide infra) highlighting further reactivity where relevant.

2.1.1 Terminal (η^1) Halocarbynes

While carbyne complexes have greatly advanced since Fischer's seminal work in the 1970's, [81] many examples feature carbon-based substituents driven by the pursuit of alkyne metathesis catalysts. [162] In contrast, carbyne complexes bearing heteroatoms are synthetically challenging due to the reducing

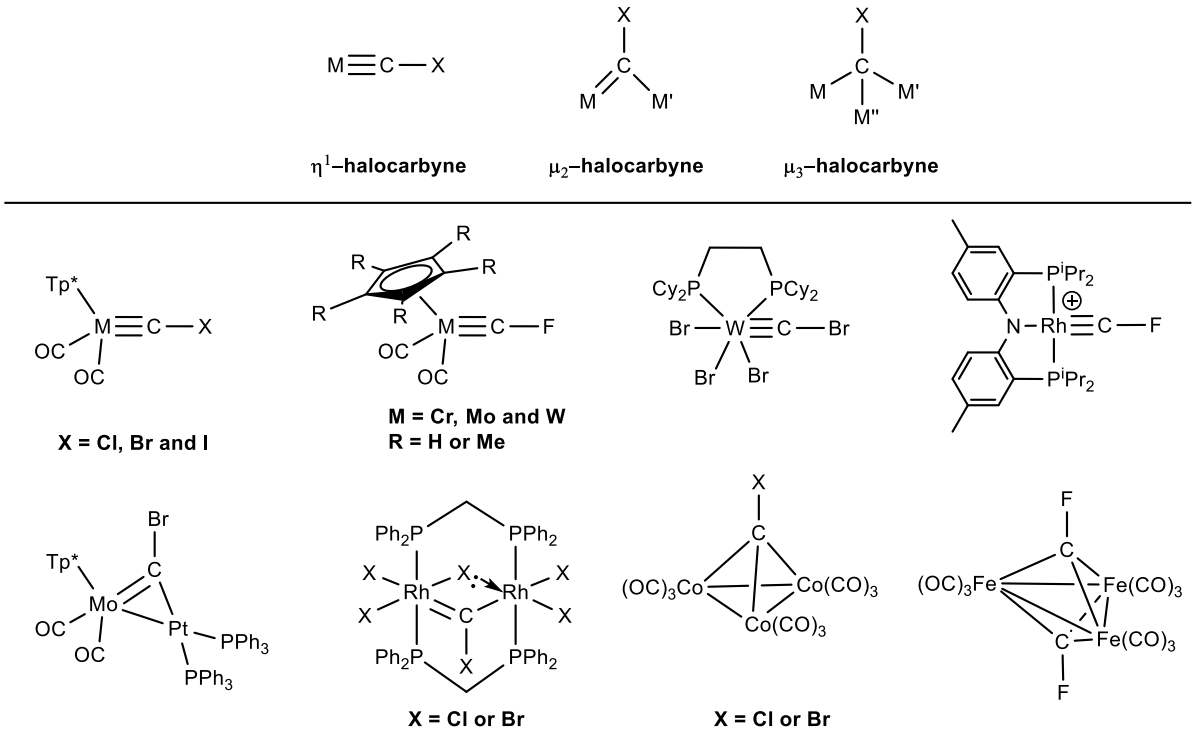

Chart 2.1: a) Bonding modes of low-nuclearity halocarbynes. b) Representative examples of low-nuclearity halocarbynes. [78, 87, 96, 142, 163-167]

nucleophilicity preventing access via the Fischer protocol. [106, 110, 168*******] Consequently, carbynes bearing halogens (group 17 substituents) did not emerge until 1983 and via a different synthesis. Lalor and co-workers reported η^1-halocarbyne complexes [M(≡CX)(CO)$_2$(Tp*)] (M = Mo, W; X = Cl, Br, I) from the reaction of [NEt$_4$][M(CO)$_3$(Tp*)] (M = Mo or W) with [PhI$_2$]$^+$ in halocarbon media (CH_2Cl_2, $CHBr_3$ or CHI_3). [87] Since Lalor's first report, the preparation of halocarbynes has undergone several refinements following extensive mechanistic investigations by Lalor. [90] With reference to [M(≡CBr)(CO)$_2$(Tp*)] (M = Mo, Br), the contemporary method is a scalable one-pot reaction from: [W(CO)$_6$], KTp*, bromoform, and the arene diazonium salt [MesN≡N]BF$_4$ which serves as a single electron oxidant. This protocol has been widely employed due to the synthetic utility of the bromocarbyne complex *via* lithium/halogen exchange. [169] The *chloro*- and *iodo*-carbynes are also available from this method when halide sources CH_2Cl_2 and CHI_3 are employed, respectively. Bromocarbynes are prepared in reduced yields (*ca* 25–30%) compared with chlorocarbyne counterparts (70–80%) owed to increased concentration of CH_2Cl_2 available for radical formation over $CHBr_3$ (expensive to utilise on large scales). However, bromocarbyne application is more prevalent given more effective lithium-halogen exchange processes for heavier halogens (See Chapter One; Section 1.2.2.5).

******* *E.g.*, thiolato or phosphido anions typically react via CO substitution; the steric bulk required to allow the generation of Yamashita's boryl anions prevents attack at coordinated CO. The only heteroatom nucleophiles employed to date in Fischer syntheses are amino, imino, or silyl anions.

As the η^1-bromocarbynes [M(≡CBr)(CO)$_2$(Tp*)] serves as the primary starting materials of this thesis, Lalor's proposed mechanism is discussed as an example, beginning from the bulky Tp* ligand {hydro-*tris*(3,5-dimethyl)pyrazol-1-ylborate} and the critical role it plays in the synthesis. Originally developed by Trofimenko, the sterically encumbering Tp* is a facially capping 'scorpionate' ligand. [170] with considerable steric bulk useful in protecting the bound metal centre from further reactions, instead directing reactivity towards the halocarbyne motif. The large Tolman cone angle of Tp* (224° *cf.* Tp 184°)[170] and tripodal geometry implicates it as an 'octahedral enforcer', which is critical for the proposed synthetic mechanism. This ligand disfavours a 7-coordinate group 6 metal, facilitating ejection of a carbonyl ligand and aiding incorporation of a dihalomethyl ligand. For this reason, the Tp* ligand is not only a helpful spectator ligand but underpins the integration of a halocarbyne in the first instance. Extensive studies by Lalor failed to extend the synthesis usefully beyond molybdenum and tungsten, or to supporting ligands other than Tp*.[90]

The original mechanism for chlorocarbyne formation was postulated by Lalor in the original report, [87] while molybdenum and tungsten bromocarbyne formation was proposed in 2008, [101] and is yet to require revision (Scheme 2.1). Furthermore, Lalor extrapolated the mechanism br*omo-* and *iodo-*counterparts. Beginning from coordination of Tp*, an outer-sphere single electron transfer to the arene-diazonium salt occurs to form two radical species: one centred on tungsten and one on the arene, which very rapidly eliminates dinitrogen. The ensuing aryl radical can abstract a halogen (in the case of bromoform) or hydrogen (in the case of CH_2Cl_2) to give and aryl bromide, or arene and a dihalomethyl radical. The [W(CO)$_3$(Tp*)]$^\bullet$ radical can be isolated when ferrocenium is used as the one-electron oxidant. [171] The radical coupling of the dihalomethyl and tungsten centres provides the 7-coordinate species [W(CHX$_2$)(CO)$_3$(Tp*)] (X = Cl, Br), where the octahedral enforcing capabilities of Tp* favour ejection of a carbonyl to give a putative six-coordinate anionic halocarbene. This halocarbene intermediate undergoes bromide dissociation to provide the final bromocarbyne as a neutral species. The steric profile of the Tp* ligand appears ideally suited for halocarbyne formation: Replacing the methyl groups on Tp* with 4-tolyl or hydrogen (Tp) in both cases results in formation of the aryldiazenido species [M(NNAr)(CO)$_2$(L)] instead.‡‡‡‡‡‡ These outcomes, which reflect covalent bond formation between electrophile and nucleophile being in competition with outer-sphere electron transfer to generate [Tp*(CO)$_3$M]$^\bullet$ and [ArNN]$^\bullet$ radicals, provides the basis for using [NNC$_6$H$_2$Me$_3$-2,4,6]BF$_4$ in the optimised syntheses. Unfortunately, the mechanism by which Lalor's η^1-halocarbynes purportedly arise inherently prevents realisation of more examples via this strategy.

‡‡‡‡‡‡ The complex [W(NNC$_6$H$_2$Me$_3$)(CO)$_2$(Tp*)] has been isolated as a very minor side product in large scale preparations. B. J. Frogley, *unpublished results*, *private communication*.

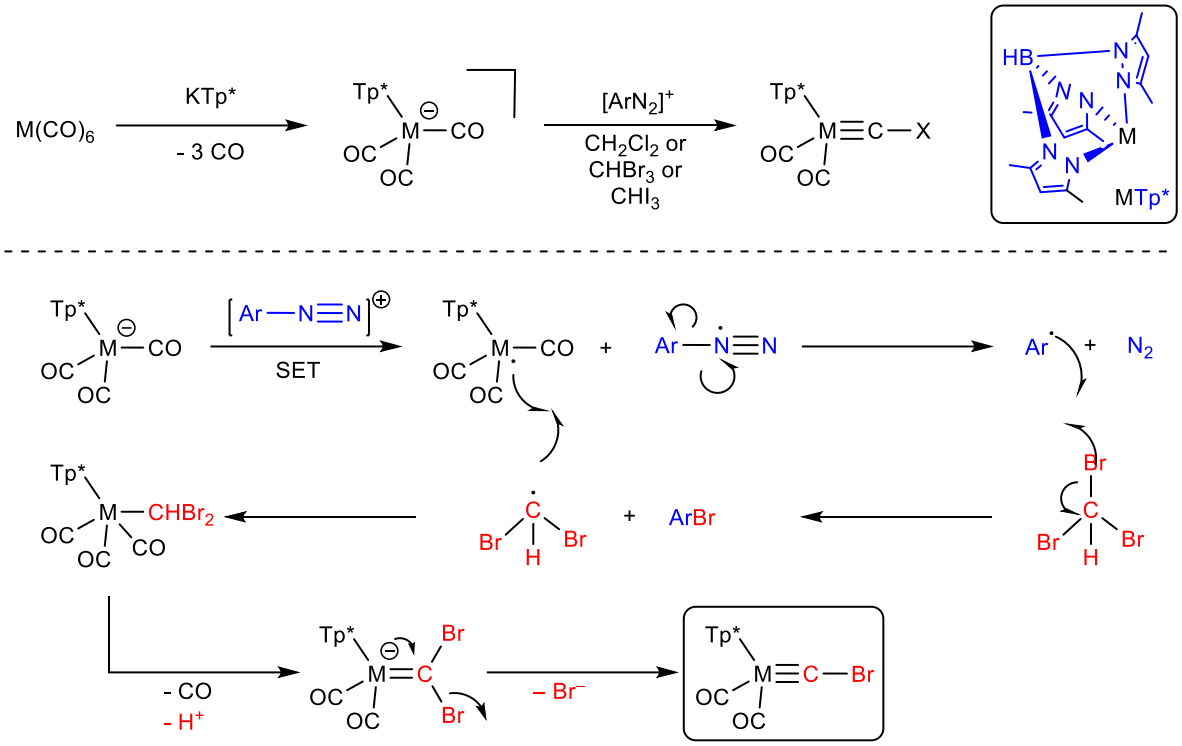

Scheme 2.1: a) Contemporary, one-pot synthesis of Lalor's halocarbynes [M(≡CX)(CO)$_2$(Tp*)] (M = Mo, W; X = Cl, Br). Inset = structure of bulky hydro-trispyrazolyl ligand, Tp*. b) Proposed synthetic mechanism of tungsten bromocarbyne [W(≡CBr)(CO)$_2$(Tp*)], representative of Lalor's other combinations.

Although the Tp* ligand remains a spectator, it serves as an informative spectroscopic reporter for ^{1}H NMR. The pzCH at the 4-position provides a useful signal between δ 5.0–6.0 and the pzCH$_3$ resonances typically lie in the range δ 1.7–3.0. Furthermore, Lalor's halocarbynes feature C_s symmetry which means that two pyrazolyl rings are chemically equivalent, such that the pzCH and pzCH$_3$ resonances manifest in 2:1 and 6:3:6:3 ratios, respectively. Departure from this pattern in derived molecules indicates that the C_s mirror plane has been lost on the NMR timescales such that the pattern provides a simple, effective indicator of species in solution. Similar patterns emerge in the ^{13}C{^{1}H} NMR with C^{3,5}(pz) signals occurring between δ_C 140–160, C^4(pz) around δ_C 105 and pzCH$_3$ between δ_C 10–20; often segregated from other signals of interest in the ^{13}C{^{1}H} spectral landscape.

The unique feature of Lalor's halocarbynes is clearly the C–X bond. Exploitation of these reactive C–X bonds has expedited the production of unusually substituted carbynes, and representative examples of substitutions are included (Scheme 2.2). Spectroscopically, the carbon resonance of the halocarbyne appears between δ 200–230 by ^{13}C{^{1}H} NMR, within the region typical of carbonyl ligands. The recent isolation of the fluorocarbynes [M(CF)(CO)$_2$(Tp*)] (M = Mo, W) completes Lalor's original series and demonstrates the effect of halogen upon the carbyne chemical shift. For conventional halocarbons, the chemical shift of carbon nuclei to which they are bound reflects a balance of both spin orbit coupling (proportional to Z^2). This causes a shift to lower frequency against paramagnetic shielding whereby mixing of virtual orbitals in a strong magnetic field is inversely proportional to the energy gap between

ground and excited states (most significantly the HOMO-LUMO gap) causing a shift to higher frequency. Given that halocarbynes give rise to resonances to low frequency of most other carbynes, it would seem that spin-orbit coupling effects are significant.

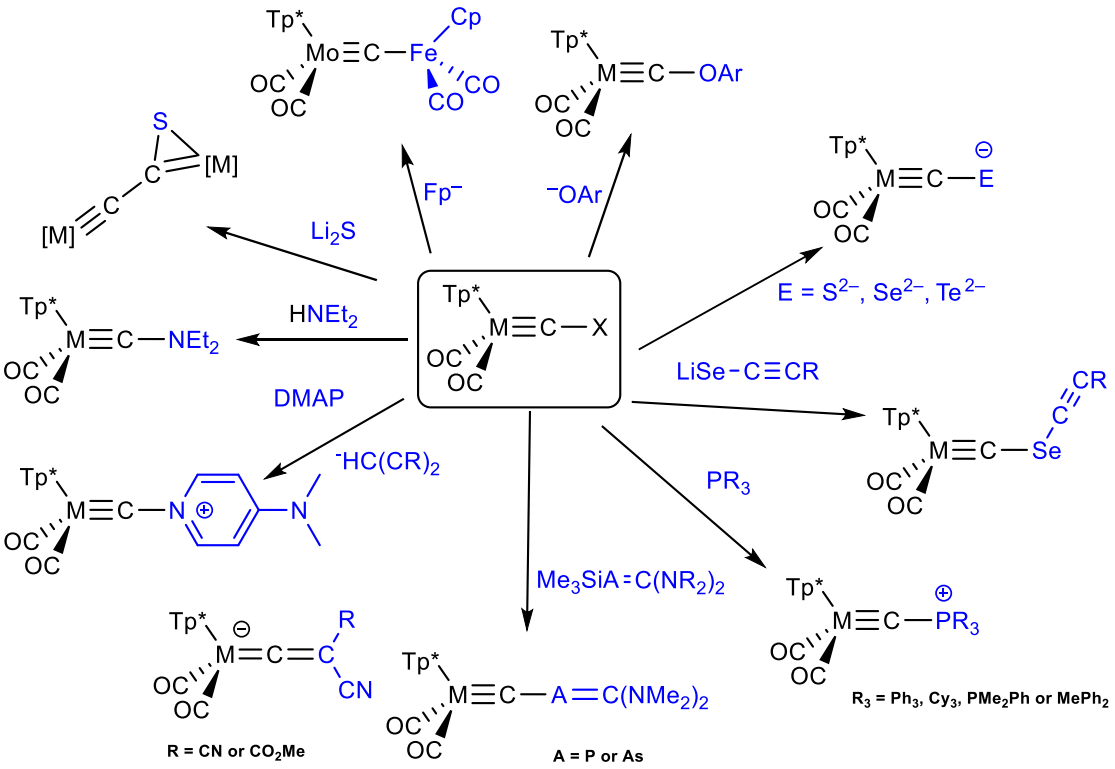

Scheme 2.2: Representative reactivity stemming from Lalor's halocarbyne complexes.

Despite the demonstrated synthetic utility of Lalor's halocarbynes, further examples only began to appear in the last decade when several η^1-fluorocarbynes arose *via* an alternate route (Scheme 2.3). Hughes and co-workers demonstrated that two-electron reduction of group 6 trifluoroalkyls $[M(CF_3)(CO)_3(L)]$ resulted in the fluorocarbynes $[M(\equiv CF)(CO)_2(L)]$ (M = Cr, Mo or W; L = Cp or Cp*), where similar treatment of group 9 complexes halts at difluorocarbenes. [165-166] In the same work, the fluorocarbynes were found to undergo metalation of the reactive π-systems to provide μ_3-halocarbynes (Section 2.1.2). Years later, Hughes and Ozerov extended fluorocarbyne synthesis to group 9, where the exotic silyl-reagents $[Et_3Si–X–SiEt_3][CHB_{11}Cl_{11}]$ (X = H or OTf) abstract fluoride from a difluorocarbene to give the cationic rhodium fluorocarbyne $[Rh(\equiv CF)(PNP)][CHB_{11}Cl_{11}]$ (PNP = diarylamido/*bis*(phosphino) ligand). [167] While this intriguing complex was thoroughly investigated experimentally and theoretically, no further examples of synthesis or reactivity have since been reported. Andrews has also investigated η^1-halocarbynes, albeit through a different lens. Laser ablation of fluoroalkyl complexes can trap various fluorocarbyne fragments, $[M(\equiv CF)X_3]$ (M = Ti, Cr, Mo, W, Rh and Th; X = halogen) in argon matrices at 10°K, supported by theoretical predictions of spectroscopic data. [172-177] Such species are yet to be isolated.

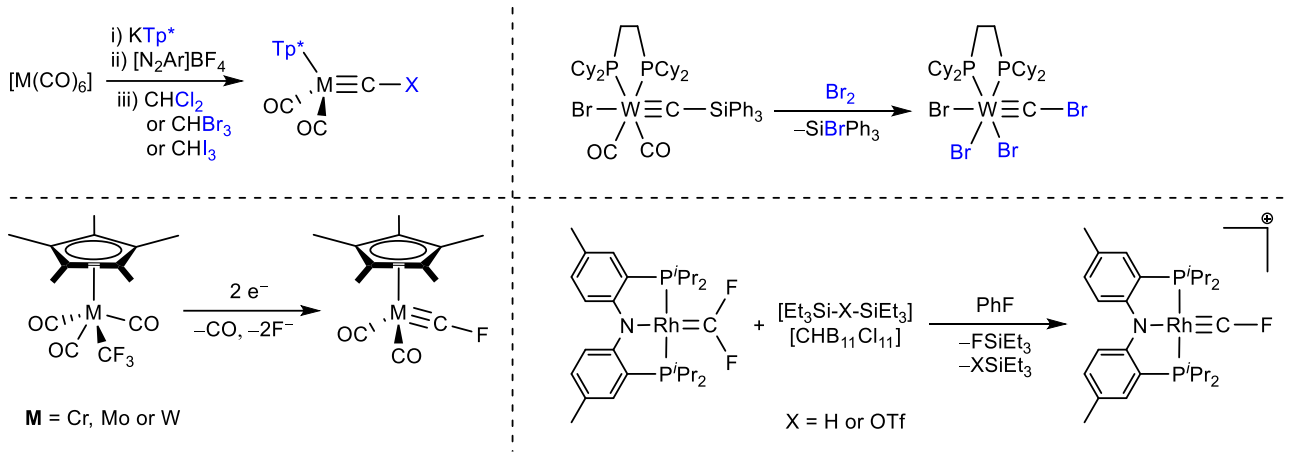

Scheme 2.3: Synthesis of η^1-halocarbynes.

More recently the silylcarbyne [W(≡CSiPh$_3$)Br(CO)$_2$(dcpe)] can be completely oxidised with elemental bromine in addition to cleaving a carbon-silicon bond to give the high-oxidation state bromocarbyne [W(≡CBr)(Br)$_2$(dcpe)] that might be viewed as a dcpe adduct of Andrews' "W(≡CF)X$_3$" species. [96] While this reaction is yet to be replicated in other systems, silylcarbyne oxidation does promise some generality compared with prior examples, limited only to the few examples of silylcarbynes. [66, 96, 178-181] It is likely that controlled desilylation to provide η^1-halocarbynes without metal oxidation will prove a challenge. These select examples alongside Lalor's seminal work round out the synthesis of η^1-halocarbynes. However, it should be noted that the chlorocarbyne [Os(≡CCl)Cl(CO)(PPh$_3$)$_2$] has been proposed as a likely intermediate in the synthesis of [Os(≡CAr)Cl(CO)(PPh$_3$)$_2$] (R = C$_6$H$_4$Me-4) [182] from the reaction of the dichlorocarbene [OsCl$_2$(=CCl$_2$)(CO)(PPh$_3$)$_2$] with *two* equivalents of ArLi. [183-184] The implication is that subsequent nucleophilic attack on the chlorocarbyne ligand by ArLi is more rapid than the reductive lithium/halogen exchange given (i) No chlorocarbyne complex could be observed with < 2 equivalents of ArLi and (ii) The chlorocarbene complex [OsCl$_2$(=CClAr)(CO)(PPh$_3$)$_2$] does not react with ArLi to afford [Os(≡CAr)Cl(CO)(PPh$_3$)$_2$].

2.1.2 μ_3-halocarbynes

The μ_3-halocarbynes are the most common halocarbynes, where three bonding electrons are shared between three metal centres, emerging from early investigations of halomethanes in cluster chemistry, and unsurprisingly, the synthetic methodology is more advanced (Scheme 2.4). The first μ_3-halocarbyne synthesis was reported by Dent and co-workers who showed halomethanes react with [Co$_2$(CO)$_8$] to give [Co$_3$(μ_3-CX)(CO)$_9$] (X = F or Br). [185-186] These initial reports were followed by a large body of work by Seyferth and Shriver employing the chlorocarbyne [Co$_3$(μ_3-CCl)(CO)$_9$]. [163] Alternatively, Keister and Horling found ruthenium and osmium μ_3-halocarbynes, [Ru$_3$(μ_3-CX)(μ_2-H)$_3$(CO)$_9$] (X = Cl or Br) and [Os$_3$(μ_3-CBr)(μ_2-H)$_3$(CO)$_9$], result from the abstraction of μ_3-alkoxides with boron trihalides. [187-188] Tricobalt halomethylidynes enjoyed something of a renaissance with the demonstration by Bruce and

Saitseva that derivatives of $[Co_3(\mu\text{-}CBr)(CO)_9]$ underwent palladium-catalysed C–C cross-coupling with organogold reagents to afford carbon-wire systems.[136-137, 189-191] Lentz and co-workers showed $[Fe_2(CO)_9]$ or $[Fe(CO)_5]$ reduce $CFBr_3$ to yield *bis*-μ_3-fluorocarbynes $[Fe_3(\mu_3\text{-}CF)_2(CO)_9]$.[164] Similarly, Seppelt demonstrated a μ_3-fluorocarbyne of molybdenum $[Mo_3(\mu_3\text{-}CF)(CO)_6(Cp)_3]$ upon photolytic acyldecarbonylaion from a fluorinated anhydride $[Cp(CO)_3MoCOCF_2COMo(CO)_3(Cp)]$.[192]

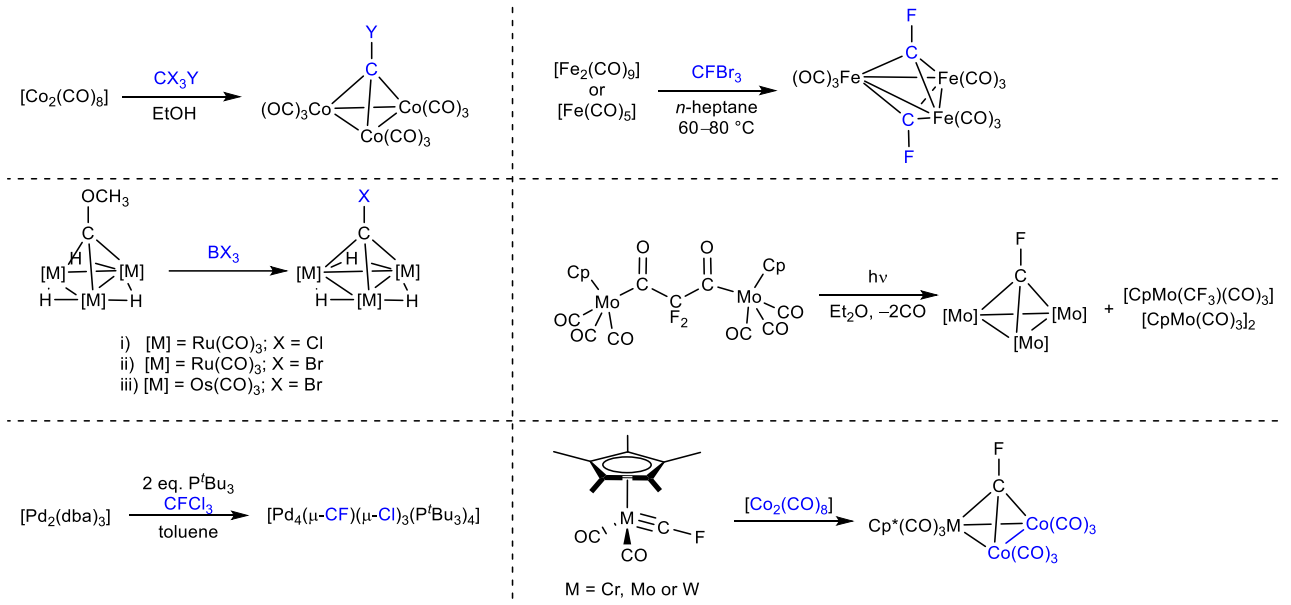

Scheme 2.4: Synthesis of μ_3-halocarbynes.

Traversing the periodic table to group 10, Mingos and co-workers reported a palladium μ_3-fluorocarbyne $[Pd_4(\mu_3\text{-}CF)(\mu_2\text{-}Br)_3(P^tBu)_4]$ produced through halocarbon reduction with $[Pd_2(dba)_3]\cdot C_6H_6$, which, intriguingly, undergoes hydrogenation to yield CFH_3—mooted as a model for fluorocarbon hydrogenation on a heterogeneous catalyst surface.[193] Recently, Kurogi and Takai have shown $[CrX_2]$ (X = Cl, Br) salts reduce halocarbons in coordinating tetrahydrofuran to give chromium clusters $[Cr_3(\mu_3\text{-}CX)(\mu_2\text{-}X)_3(X)_3(THF)_6]$ (X = Cl, isolated; Br implied), useful in further reactions as carbide transfer reagents towards aldehydes yielding vinyl-bromides.[55, 194]

Finally, Hughes showed the η^1-fluorocarbynes $[M(\equiv CF)(CO)_2(Cp^*)]$ (M = Cr, Mo, and W) react with $[Co_2(CO)_8]$ to produce the only known examples of heterometallic μ_3-halocarbynes $[MCo_2(\mu_3\text{-}CF)(CO)_8(Cp^*)]$,[165-166] as previously observed for more conventional carbynes.[195-197]

2.1.3 μ_2-halocarbynes

The rarest halocarbynes are the μ_2-bridging species, the majority of which arose serendipitously (Scheme 2.5). The first example was an unexpected discovery by Beck and Wolf, who showed elemental arsenic reduces CCl_4 in the presence of $[WCl_6]$ to return a dark compound that crystallised to $[W_2(\mu_2\text{-}CCl)Cl_7]$.[198] Although this species was not specifically isolated (crystals selected from unspecified product), the method requires halocarbon reduction, thereby linking the three classes. Recently, another

halocarbon reduction was reported, as the ruthenium-hydride cluster $[Ru_3(\mu_2\text{-}H)_6(Cp^*)_3]$ reduces CCl_4,[160] halting at the μ_2-halocabryne stage $[(Cp^*RuCl)_2(\mu_2\text{-}CCl)(\mu_2\text{-}Cl)]$ rather than higher nuclearity species akin to Keister's $[Ru_3(\mu_3\text{-}CCl)(\mu_2\text{-}H)_3(CO)_9]$.[187] It should be noted $[(Cp^*RuCl)_2(\mu_2\text{-}CCl)(\mu_2\text{-}Cl)]$ undergoes a reaction with diethyl maleate in the presence of zinc to provide a complex μ_2-carbido species (See Section 1.2.1.1); another example of halocarbynes acting as precursors to μ_2-carbido species .

Recently, evidence of the reverse reactivity of μ_2-halocarbynes arising from μ_2-carbidos emerged. Halogenation of the A-frame μ_2-carbido species $[Rh_2(\mu_2\text{-}C)X_2(\mu\text{-}dppm)_2]$ with mild oxidants such as $PhICl_2$ or $[pyH][Br_3]$, results in halocarbynes $[Rh_2(\mu_2\text{-}CX)(\mu_2\text{-}X)X_4(\mu\text{-}dppm)_2]$ (X = Cl or Br).[78] Although the mechanism remains unconfirmed, it is likely an oxidation of each rhodium(I) centre to rhodium(III), followed by halide migration to the μ-carbido to form the μ_2-CX motif,[119] although direct C-halogenation could not be excluded, given migratory insertion of bromide or chloride ligands is generally not observed. Chlorination of the μ-dppf analogue $[Rh_2(\mu\text{-}C)Cl_2(\mu\text{-}dppf)_2]$ stops at the Rh(II) μ-carbido complex $[Rh_2(\mu\text{-}C)Cl_4(\mu\text{-}dppf)_2]$, without C-halogenation.[161]

The previous examples contain homometallic (and somewhat symmetric) μ_2-halocarbyne environments, however Beck and co-workers reported the only known heterometallic example to date. Beck showed the π-system of $[Mo(\equiv CBr)(CO)_2(Tp^*)]$ replaces ethene in the low-valent complex $[Pt(\eta^2\text{-}C_2H_4)(PPh_3)_2]$ to provide $[MoPt(\mu_2\text{-}C)(CO)_2(PPh_3)_2(Tp^*)]$ before oxidative addition of the C–Br bond gives the μ_2-carbido $[MoPt(\mu_2\text{-}C)Br(CO)_2(Tp^*)]$,[142] again reflecting the behaviour of more conventional carbynes towards zerovalent platinum centres.[195] This reaction is analogous to Hughes' π-coordination to μ_3-fluorocarbynes except it utilises Lalor's framework, and is another specific link with μ_2-carbidos.

These examples provide a comprehensive survey of low-nuclearity halocarbyne complexes, while the known spectroscopic and structural properties are collected for future reference (Table 2.1). Common themes are evident from the few niche examples. First, halocarbyne reduction is the most common synthetic method that encompasses all classes. While the reactivity of C–X bonds of halocarbynes has been well-studied, the π-system of η^1-halocarbynes have been utilised to provide examples of μ_2- and μ_3-halocarbynes. It was hypothesised that Beck's precedent could be expanded with guidance from prior π-coordination of Stone's bimetallic assemblies,[199] and Hoffman's isolobal theory[200] to provide more general entry into μ_2-halocarbynes limited only by η^1-halocarbyne precursors.

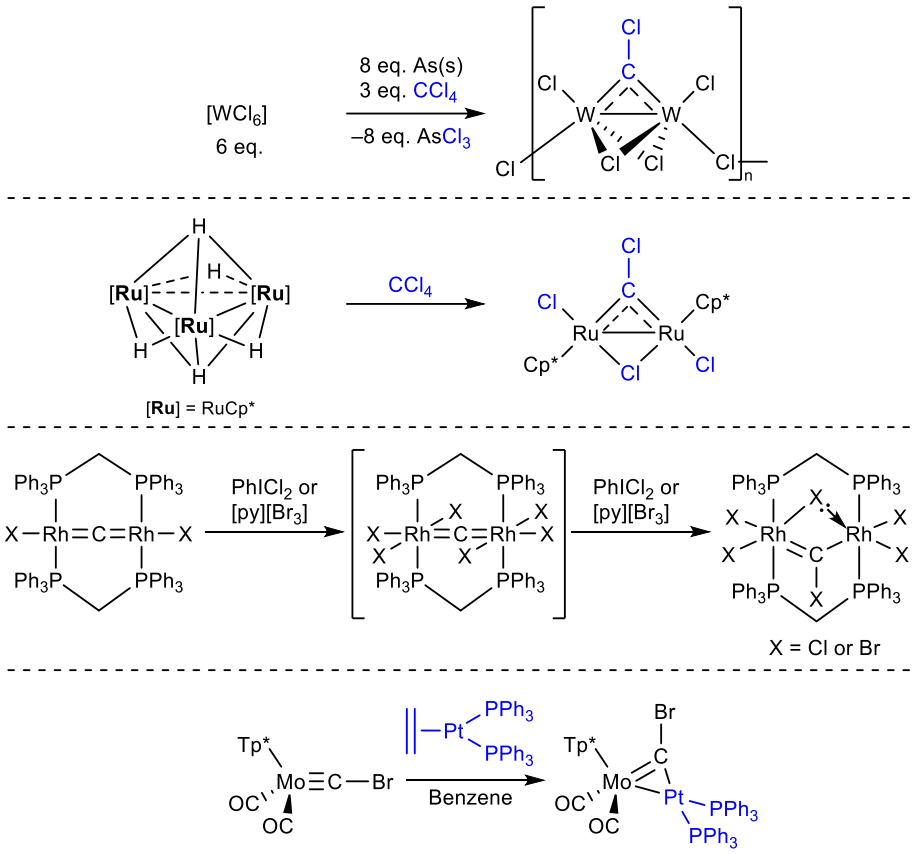

Scheme 2.5: Synthesis of μ_2-halocarbynes.

Table 2.1: Spectroscopic and structural properties of η^1 and μ_2-halocarbyne complexes.

Complex	δ_C[a] (ppm)	$^1J_{CF}$ (Hz)	δ_P (ppm)	ν_{CO}[b] (cm^{-1})	k_{CO}[c] (N cm^{-1})	r_{MC} (Å)	r_{CX} (Å)	M–C–X (°)	$r_{MM'}$ (Å)
Terminal (η^1) Halocarbynes									
[Mo(≡CCl)(CO)$_2$(Tp*)] (**2.1a**) [87]	208.7	–	–	2005, 1921[d]	15.54	–	–	–	–
[W(≡CCl)(CO)$_2$(Tp*)] (**2.1b**) [87]	205.6	–	–	1991, 1902[d]	15.29	–	–	–	–
[Mo(≡CBr)(CO)$_2$(Tp*)] (**2.1c**) [87]	202.5	–	–	2008, 1924[d]	15.59	1.910(5)[e]	1.875(5)[e]	163.7(3)[e]	–
[W(≡CBr)(CO)$_2$(Tp*)] (**2.1d**) [87]	198.0	–	–	1994, 1905[d]	15.33	1.946(12)[f]	1.901(14)[f]	169.4(5)[f]	–
[Mo(≡Cl)(CO)$_2$(Tp*)][87]	n.r.	–	–	2009, 1927[d]	15.62	–	–	–	–
[W(≡Cl)(CO)$_2$(Tp*)][87]	183.2	–	–	1992, 1907[d]	15.33	–	–	–	–
[Mo(≡CCl)(CO)$_2$({B(pz)$_4$}]	n.r.	–	–	2010, 1928[d]	15.65	1.893[i]	1.540[i]	172.0[i]	–
						1.895[i]	1.50[i]	175.0[i]	–
						1.894[i]	1553[i]	171.2[i]	–
[Mo(≡CCl)(CO)$_2${HB(pzMe$_3$)$_3$}][201]	208.2	–	–	2005, 1920[d]	15.54	1.798(5)	1.680(6)	165.7(4)	–
[Mo(≡CBr)(CO)$_2${HB(pzMe$_3$)$_3$}[201]	201.9	–	–	2007, 1923	15.58	–	–	–	–
[Cr(≡CF)(CO)$_2$(Cp*)][166]	219.7	575	–	2002, 1930	15.59	–	–	–	–
[Mo(≡CF)(CO)$_2$(Cp)] [166]	217.3	565	–	2017, 1946	15.84	–	–	–	–
[Mo(≡CF)(CO)$_2$(Cp*)][165]	219.1	556	–	2002, 1930	15.59	1.971(1)	1.15(4)	177.7(1)[h]	–
[W(≡CF)(CO)$_2$(Cp)] [166]	220.9	532	–	2020, 1935	15.78	–	–	–	–
[W(≡CF)(CO)$_2$(Cp*)][166]	223.7	538	–	1994, 1918	15.43	1.852(4)	1.300(6)	177.4(1)[h]	–
[W(≡CBr)Br$_3$(dcpe)] [96]	229.0	–	50.8[g]	–	–	1.793(6)	1.822(6)	171.5(4)	–
[Rh(≡CF)(PNP)]$^+$ [167]	n.r.	470	89.3	–	–	1.702(7)	1.257(8)	173.4(7)	–
μ_2-halocarbynes									
[W$_2$(μ_2-CCl)Cl$_7$] [198]	n.r.	–	–	–	–	1.94(1), 1.94(2)	1.67(2)	139.5(8), 137.8(9)	2.561(3)
[Rh$_2$(μ_2-CCl)(μ-Cl)Cl$_4$(dppm)$_2$] [161]	n.r.	–	3.4[g]	–	–	1.912(4), 1.947(6)	1.674(7)	125.1(3), 123.6(3)	3.1867(6)
[Rh$_2$(μ_2-CBr)(μ-Br)Cl$_4$(dppm)$_2$] [161]	n.r.	–	–5.7[g]	–	–	2.10(4), 2.10(4)	1.57(6)	130.0(13), 130.0(13)	3.221(3)
[MoPt(μ_2-CBr)(PPh$_3$)$_2$(CO)$_2$(Tp*)][142]	315.9	–	38.1, 25.8	1885, 1753	–	–	–	–	–
[Ru$_2$(μ_2-CCl)(μ-Cl)Cl$_2$(Cp*)$_2$] [160]	323.4	–	–	–	–	1.916(7), 1.929(7)	1.649(8)	135.0(4), 133.5(4)	2.740(6)

Notes: [a]Measured in C_6D_6 unless specified otherwise. [b]Measured in *n*-hexane. [c]Cotton–Kraizenhal force constant: $k_{CO} = 2.0191 \times 10^6\ \Sigma(\nu_1^2+\nu_2^2)$. [202-204] [d]Measured in cyclohexane. [e]See prior thesis[205]. [f]Work from this thesis. [g]Measured in CDCl3. [h]Halocarbyne and carbonyl ligands disordered. [i]E.S.D values not published, three crystallographically distinct molecules.

2.2 Theoretical Properties of Terminal Halocarbynes

The consequence of the limited number of halocarbyne complexes is that discussion of their bonding is incomplete. In comparison, the carbonyl ligand (CO) is arguably the most elementary ligand in organometallic chemistry: a two-electron σ-donor with accessible π* orbitals for retrodonation such that carbonyls are the primary didactic model for synergic bonding in transition complexes. However, replacing oxygen with fluorine invites comparison between the bonding of carbonyl (CO) and isoelectronic fluorocarbyne (CF^+) complexes. This comparison deconstructs the halocarbyne ligand as a σ-donor capable of π-retrodonation from transition metal d-orbitals to the two empty π*-orbitals on carbon, drawn from analogy of isoelectronic nitrosyl ligands (NO^+). However, an alternative carbyne formalism is widely employed that assigns a notional trianionic charge (CR^{3-}) to the ligand. The question remains: is the carbonyl analogy useful in halocarbyne chemistry? Several prior theoretical studies have been conducted for halocarbynes, [165-167, 172-174, 177, 206-208] including comparison to carbonyls, determining features such as localisation of μ_3-CX ligands, and to model experimental observations. To begin from a more fundamental comparison, a preliminary computational study {DFT: ωB97X-D/6-31G*} between the traditional CO/CN^- ligands and the isoelectronic CX^+ (X = F, Cl, Br and I) halocarbyne ligands was conducted in line with analogous methods that studied heavier chalcocarbonyl congeners CA (A = S, Se and Te) and trends that emerge descending group 16. [116, 209-211]

The frontier orbitals that emerge for CO, NO^+, and CX^+ (X = F, Cl, Br and I) ligands identify key similarities and differences between the isoelectronic ligands (Figure 2.1). Due to the different charges, direct comparison of orbital energies is not useful, however the similarity in orbital topologies and occupancies (*i.e.*, isolobality) is reassuring. As the currently known η^1-halocarbyne complexes involve relatively high d-occupancy metals (d^6 or d^8 assuming CX^+ formalism), the energy of the halocarbyne π* LUMO pair is of particular interest. For the diatomics' LUMOs, the most dramatic change occurs between (CF^+) and (CCl^+), as fluorine is more electronegative. However, shifting from CCl^+ through to CI^+ results in remarkably little difference in energy or morphology of the π-acceptor orbitals. This contrasts with observations made for chalcocarbonyls, where descending group 16 results in a steady and significant increase of π-acidity. The HOMO in each case serves as the σ-donor upon coordination and increases in energy progressively down group 17, suggesting improved σ-donicity for the heavier halocarbynes, though the HOMO involves a decreasing contribution from the carbon atomic orbital(s).

Experimentally the superlative π-acidity of the fluorocarbyne ligand (CF^+) is evidenced by the ν_{CO} vibrations of Hughes system $[Cr(\equiv CF)(CO)_2(Cp^*)]$ (ν_{CO}: 2002, 1930 cm^{-1}) mapping to the π-acidic nitrosyl (NO^+) complex $[Cr(NO)(CO)_2(Cp^*)]$ (ν_{CO}: 2000, 1930), [212-213] supporting the isoelectronic analogy of $CO/CF^+/NO^+$ ligands. However, absolute trends of η^1-halocarbyne ligand bonding have, until recently, been problematic to assign, given no complete set of halocarbynes exist in the one system: Hughes'

examples bear exclusively fluorine, while fluorine has only recently completed Lalor's series with the isolation of [M(≡CF)(CO)$_2$(Tp*)] (M = Mo, W). [117]

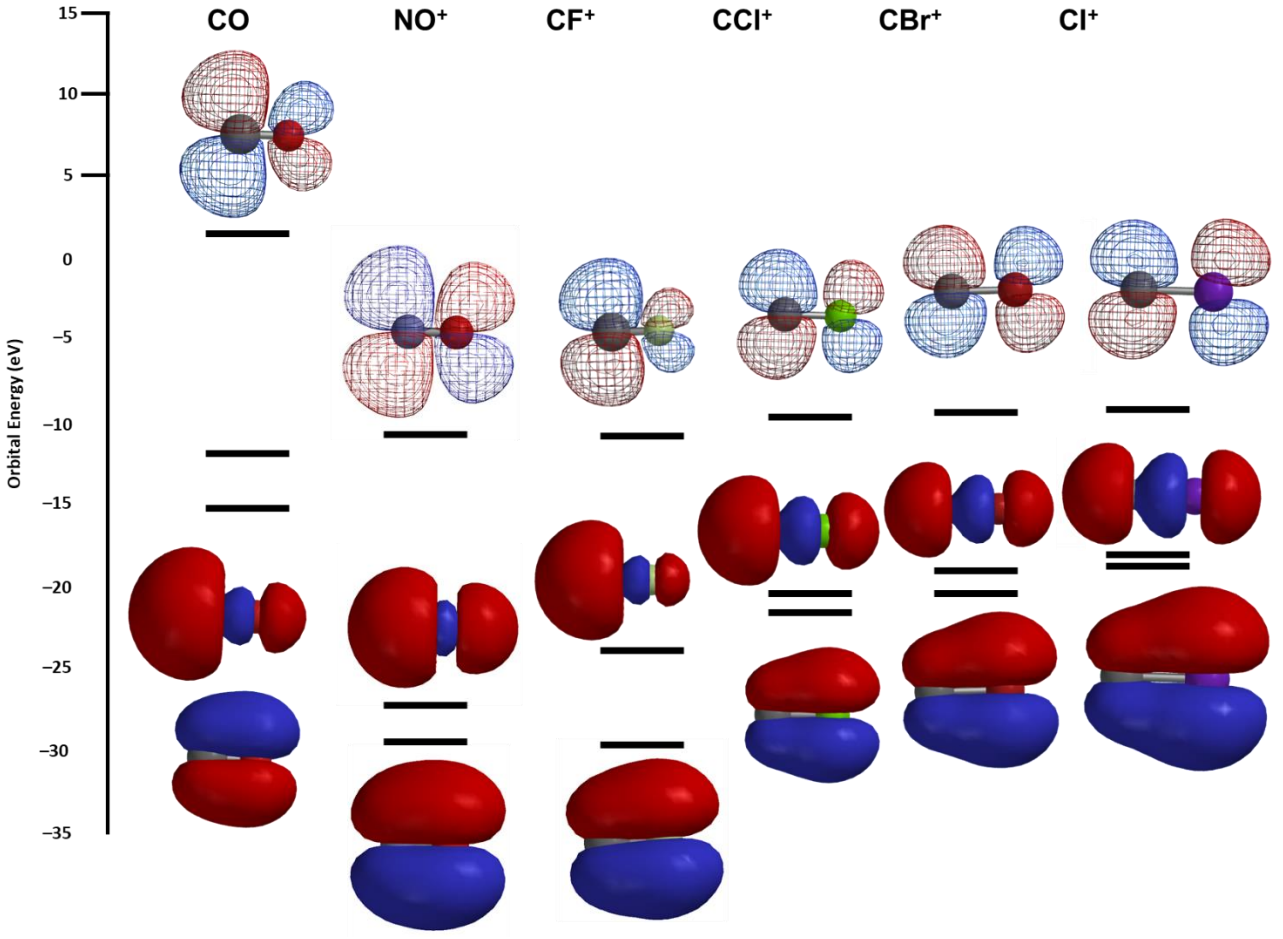

Figure 2.1: Frontier orbitals of CO, NO$^+$ and free CX$^+$ ligands (X = F, Cl, Br, or I) as calculated in *SPARTAN20* {DFT: ωB97X-D/6-31G*}. Key = occupied orbitals are colour filled, unoccupied orbitals are displayed as mesh.

To further explore halocarbyne bonding, a theoretical series bound to a pruned form of Lalor's seminal complexes [Mo(≡CX)(CO)$_2$(Tp)] (X = F, Cl, Br and I) was calculated at the same level of theory {DFT: ωB97X-D/6-31G*} (Figure 2.2). Molybdenum was chosen for the model as it features heavily later in this Chapter. The use of the reduced *tris*-pyrazolylborate ligand (Tp), as opposed to the real *tris*-(3,5-dimethylpyrazolyl)borate ligand (Tp*) was also used to reduce this cost further, justified in prior findings that it barely changes the outcome of similar calculations. [149] The primary differences to bear in mind between low-valent molybdenum and tungsten are (i) They have similar covalent radii due to the lanthanoid contraction and (ii) relativistic effects allow 5d metals to more effectively engage in multiple bonding to ligands due to the 5d orbitals becoming more diffuse as the 6s orbital contracts.

Similar to other previously computed structures of the form [M(≡CR)(CO)$_2$(Tp)] (M = Mo or W), [61, 138, 140, 149, 214-215] the HOMO of each of [Mo(≡CX)(CO)$_2$(Tp)] is associated with metal-carbonyl retrodonation and is orthogonal (of δ-symmetry) to the M–C(carbyne) vector. Consequently, little

variation in the relative HOMO energy occurs across the series. The HOMO–1 and HOMO–2 represent the mutually orthogonal π-components of the Mo≡C bond that are largely degenerate given the near degeneracy of the "t_{2g}-type" d-orbitals of molybdenum and the axially-symmetric halocarbyne ligand.‡‡‡‡‡ Meanwhile the LUMO and LUMO+1 pair consist of constructive overlap between Mo and the carbonyls, alongside the π*-orbitals of the Mo≡C bond, the latter underpinning the known proclivity towards nucleophilic substitution of Lalor's chlorocarbynes. [138, 215] [138, 215]

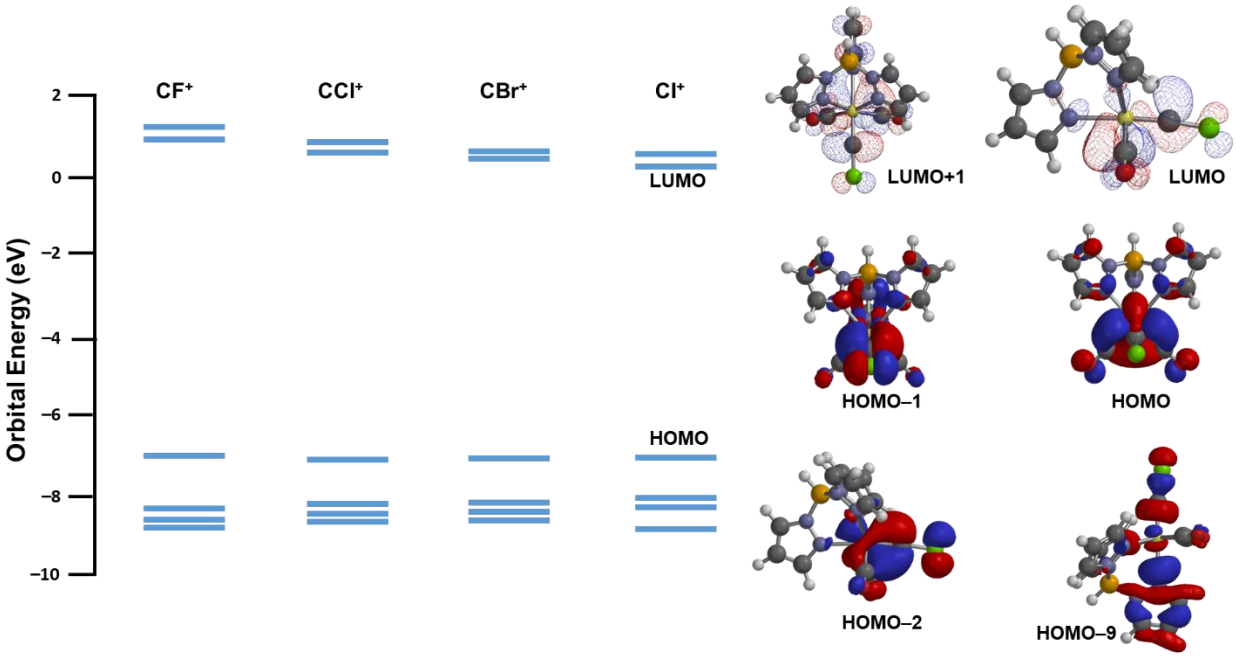

Figure 2.2: Frontier orbitals of CX^+ ligands {X = F, Cl, Br or I} coordinated to a reduced Lalor framework $[Mo(CO)_2(Tp)]^-$ as calculated in *SPARTAN*18 {DFT: ωB97X-D/6-31G*}. Key = occupied orbitals are colour filled, unoccupied orbitals are displayed as mesh.

A plethora of information was gathered through the calculation of the series $[Mo(\equiv CX)(CO)_2(Tp)]$ (Table 2.2). Additionally, the heavier tungsten congener was calculated $[W(\equiv CCl)(CO)_2(Tp)]$ to compare the group 6 termini and further substantiate emerging trends. With increasingly heavy halides, the Mo≡C bond contracts along with an increasing bond order, while the C–X bond elongates with a reduced bond order, consistent with worsening π-overlap between increasingly diffuse halogen orbitals and carbon. Overall, the shifts in bond lengths are minor and approach the limits of X-ray diffraction precision to analyse single crystals. Given the high electronegativity of fluorine it is a significant outlier when considering the natural charges for each atom along the M≡C–X spine, carrying a negative charge (–0.294), while the heavier halogens are increasingly positive down the group (+0.074 Cl to +0.251 I). Consequently, the fluorocarbyne carbon is suggested to be more electrophilic (natural charge: +0.276) with the other halocarbynes being more nucleophillic (–0.261 to –0.480), drawing analogy to the character

‡‡‡‡‡ Less symmetric carbyne substituents (aryl, amino *etc.*) break this degeneracy leading in some cases to quite different energies. [215]

of Schrock and Fischer carbynes, respectively. These factors of the halocarbyne ligand result in a molybdenum centre of increasing positive charge from X = F to Cl but is somewhat invariant descending the halogens to X =I reflected in the minor changes to ν_{CO} vibrations.

Table 2.2: Computationally derived data for complexes [M(≡CX)(CO)$_2$(Tp)] {M = Mo, W; X = F, Cl, Br, I} {DFT: ωB97X-D/6-31G*}

			Natural Charge			**Löwdin Bond Order**						
X	**M**	**L**	M	C	X	M≡C	C–X	$r_{M\equiv C}$ [Å]	$\nu_{CO}{}^a$ [cm-1]	$k_{CO}{}^b$ [N cm-1]	ν_{MC} [cm-1]	TR^c
F	Mo	CO	+0.485	+0.276	−0.294	2.410	1.395	1.810	2023, 1962 (1995, 1935)	16.04 15.60	1423	1.021
Cl	Mo	CO	+0.614	−0.261	+0.074	2.472	1.334	1.794	2027, 1969 (1999, 1941)	16.12 15.68	1153	1.003
Br	Mo	CO	+0.624	−0.351	+0.143	2.495	1.267	1.790	2029, 1972 (2001, 1944)	16.16 15.71	1110	1.037
I	Mo	CO	+0.636	−0.480	+0.251	2.545	1.194	1.786	2030, 1975 (2002, 1947)	16.20 15.75	1071	1.043
Cl	W	CO	+0.945	−0.395	+0.064	2.450	1.315	1.809	2010, 1944 (1982, 1918)	16.26 15.81	1179	1.030

Notes: [a]Uncorrected values; corrected values in parentheses. [b]Cotton–Kraihanzel force constant: $k_{CO} = 2.0191 \times 10^6\ \Sigma(\nu_1{}^2+\nu_2{}^2)$. [202-204] [c]$TR = 2r(WN_{trans})/\Sigma r(WN_{cis})$. [202-204] [c]$TR = 2r(WN_{trans})/\Sigma r(WN_{cis})$.

In comparison, vibrations of the M≡C bond ($\nu_{M\equiv C}$) are rarely identified with confidence in infra-red spectra, with few having been unambiguously reported[17, 46, 56, 152, 154, 156] for any of the classes of carbido complexes. Accordingly, computational evaluation has sometimes provided guidance in assignments. Frequency calculations of the optimised halocarbynes suggest M≡C vibrations decrease in energy from Cl ($\nu_{Mo\equiv C}$: 1153 cm^{-1}) to I ($\nu_{Mo\equiv C}$: 1071 cm^{-1}), while the value for the fluorocarbyne is unusually high. The complication in evidence here is that the M≡C bond does not oscillate 'purely' in isolation, but rather is coupled to the C–X oscillation and therefore the frequency is moderated by the mass of the halogen.

Upon computational analysis of the [Mo(C≡X)(CO)$_2$(Tp)] series, it is clear why nucleophilic substitution reactions have emerged and examination of orbital topology of the derived HOMO–1 and LUMO reveals an isolobal mapping between with those of alkynes,[200] a concept widely explored by Stone,[199] and covered in the following section.

2.3 Synthesis of Heterobimetallic μ_2-Halocarbynes

The investigation begins with labile sources of gold(I), where the halide is less important given reduced propensity of gold(I)/gold(III) oxidative addition, before proceeding to platinum(0) where selective use of Lalor's chlorocarbynes [M(≡CCl)(CO)$_2$(Tp*)] is necessary for π-coordination exclusively. It was anticipated, as is generally the case, that oxidative addition at gold(I) would be less facile than for platinum(0) thereby stabilising μ_2-halocarbynes, while simultaneously allowing further avenues of reactivity, previously unachievable with the C–F bond in Hughes' system.

2.3.1 Gold(I) complexes

The activation, often catalytic, of alkynes and alkenes *via* coordination to soft Lewis-acidic gold(I) centres has become a widely employed and versatile process in synthetic organic chemistry. [216-217] The isolobal analogy between carbon-carbon and metal-carbon multiple bonds relates the numerous examples of coordination of gold centres to metal-carbyne and carbene species. [218-219] Typically, carbyne complexes are found to react with soluble gold(I) halide complexes coordinated by a sacrificial ligand of varying lability, [AuCl(L)] (L = PPh_3 < SMe_2 ≈ THT). In accordance with the recent additions to heteroatom-functionalised alkynylselenolato-,[220-221] and phosphonio-carbyne complexes, [214] Lalor's halocarbynes were treated with [AuCl(SMe_2)], with minimum exposure to light as a precaution. The chlorocarbynes [M(≡CCl)(CO)$_2$(Tp*)](Mo = **2.1a**; W = **2.1b**) displaced the labile thioether in CH_2Cl_2 to give [MAu(μ_2-CCl)Cl(CO)$_2$(Tp*)] (Mo = **2.2a**; W = **2.2b**) within 30 minutes. Initial purification attempts *via* flash chromatography (silica gel or Al_2O_3, N_2) were unsuccessful, resulting in rapid deposition of colloidal gold and diminished yields. Employing Celite® as stationary phase for a flash chromatography prevented this deposition, allowing a sufficiently long pathlength for separation. Recrystallisation from CH_2Cl_2/*n*-hexane afforded the bimetallic chlorocarbynes as bright orange microcrystalline powders in moderate yields (75% **2.2a**, 66% **2.2b**).

Arising from investigations into the addition of 'AuCl' to alkynylselenolatocarbynes, a previous PhD Thesis from this group has described the reaction of [AuCl(SMe_2)] with [W(≡CBr)(CO)$_2$(Tp*)] (**2.1d**) to provide the structurally characterised μ_2-bromocarbyne [WAu(μ_2-CBr)Cl(CO)$_2$(Tp*)] (**2.2d**).[§§§§§§§] To now complete the series **2.2a**–**2.2d** (Scheme 2.6; Figures 2.3–2.6), the molybdenum bromocarbyne [MoAu(μ_2-CBr)Cl(CO)$_2$(Tp*)] (**2.2c**) was prepared *via* the same method.

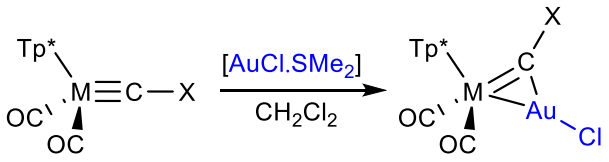

(2.1a): M = Mo; X = Cl
(2.1b): M = W; X = Cl
(2.1c): M = Mo; X = Br
(2.1d): M = W; X = Br

(2.2a): M = Mo; X = Cl
(2.2b): M = W; X = Cl
(2.2c): M = Mo; X = Br
(2.2d): M = W; X = Br

Scheme 2.6: Preparation of gold(I) μ_2-halocarbynes.

§§§§§§§ C. S. Onn, *Heteroatom Functionalised Metal Carbon Chains*, PhD Thesis, The Australian National University, 2021.

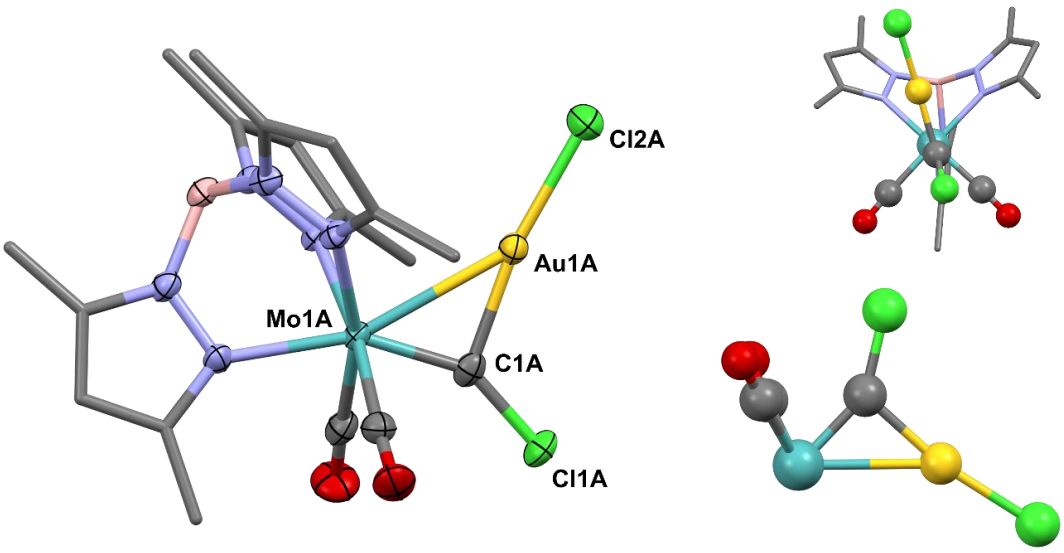

Figure 2.3: Molecular structure of [MoAu(μ_2-CCl)Cl(CO)$_2$(Tp*)] (**2.2a**) in a single crystal as determined by X-Ray diffractometry. Displacement ellipsoids are drawn at the 50% probability surface with pyrazolyl rings simplified and hydrogen atoms omitted for clarity. Insets = View along the Mo–C axis and a simplified ball and stick representation to highlight deviation of the chlorocarbyne ligand about the two metallic centres. Selected bond lengths (Å) and angles (°): Mo1A–C1A 1.878(7), C1A–Cl1A 1.698(8), Au1A–Cl2A 2.278(2), Mo1A–Au1A 2.7779(6), Au1A–C1A–Cl1A 119.7(4), Mo1A–C1A–Cl1A 149.5(4).

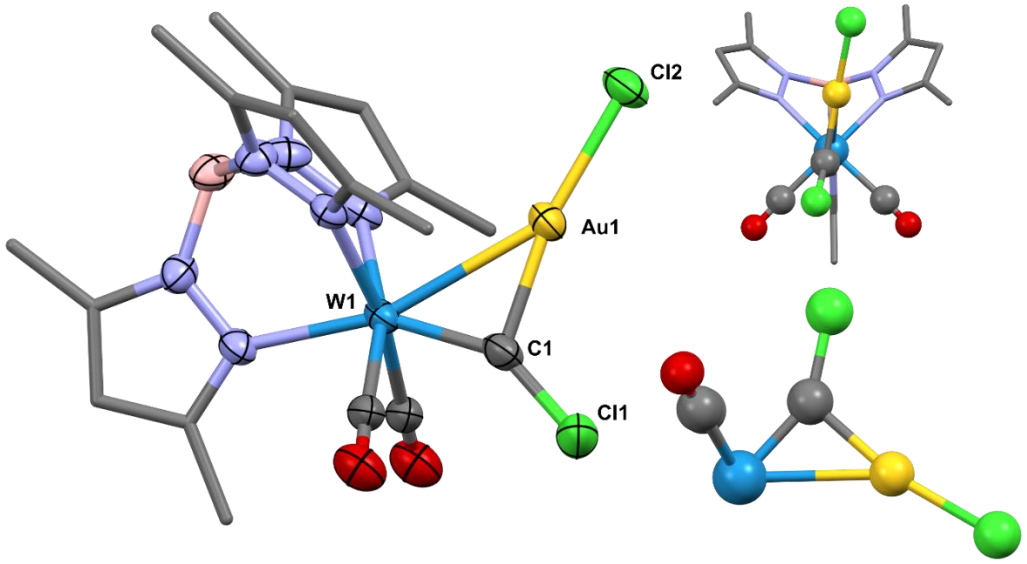

Figure 2.4: Molecular structure of [WAu(μ_2-CCl)Cl(CO)$_2$(Tp*)] (**2.2b**) in a single crystal of **2.2b**·C_6H_{12} as determined by X-Ray diffractometry. Displacement ellipsoids are drawn at the 50% probability surface with pyrazolyl rings simplified and hydrogen atoms omitted for clarity. Insets = View along the W–C axis and a simplified ball and stick representation to highlight deviation of the chlorocarbyne ligand about the two metallic centres. Selected bond lengths (Å) and angles (°): W1–C1 1.891(6), C1–Cl1 1.697(6), Au1–Cl2 2.277(2), W1–Au1 2.7926(5), C1–Au1 2.026(6), Au1–C1–Cl1 120.2(3), W1–C1–Cl 148.9(4).

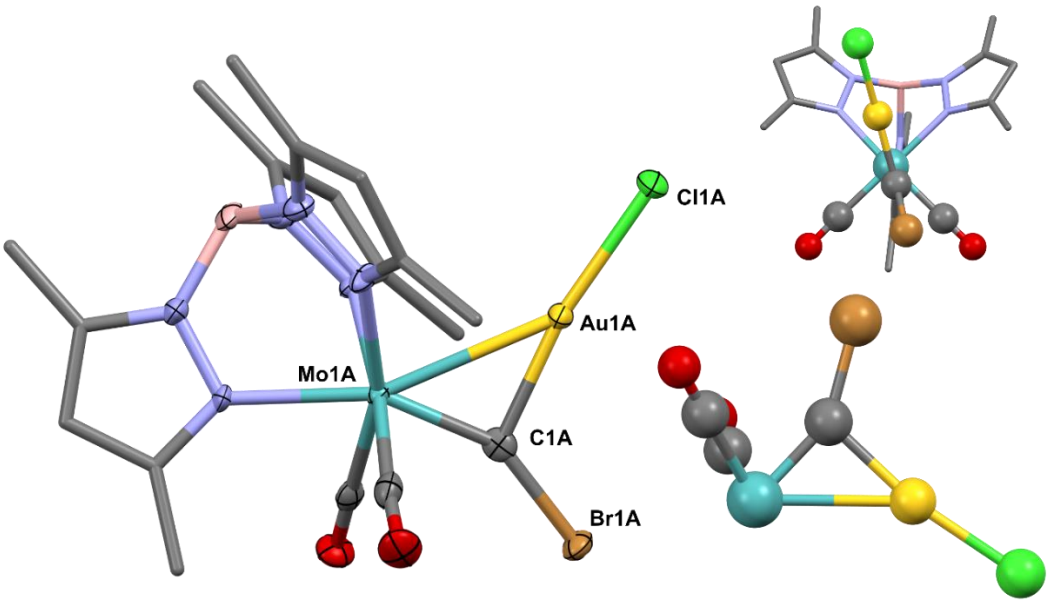

Figure 2.5: Molecular structure of [MoAu(μ_2-CBr)Cl(CO)$_2$(Tp*)] (**2.2c**) in a single crystal of 2·(**2.2c**)·CH_2Cl_2 as determined by X-Ray diffractometry. Displacement ellipsoids are drawn at the 50% probability surface with pyrazolyl rings simplified and hydrogen atoms omitted for clarity. Insets = View along the Mo–C axis and a simplified ball and stick representation to highlight deviation of the bromocarbyne ligand. Selected bond lengths (Å) and angles (°): Mo1A–C1A 1.887(9), C1A–Br1A 1.846(9), Au1A–Cl1A 2.289(2), Mo1A–Au1A 2.7830(7), C1A–Au1A 2.039(9), Au1A–C1A–Br1A 118.2(4), Mo1A–C1A–Br1A 151.5(5).

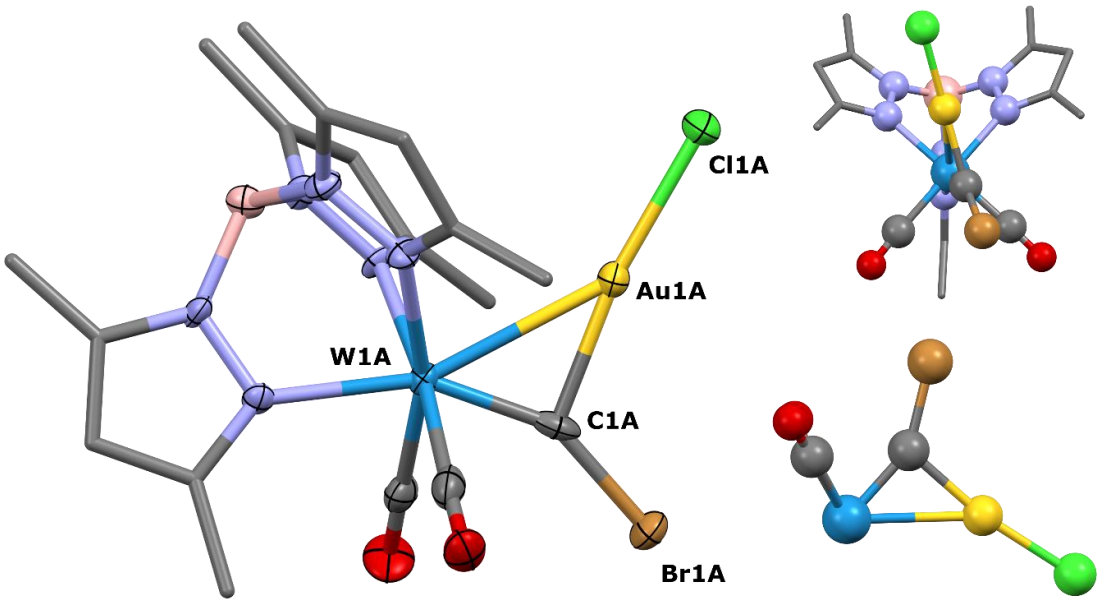

Figure 2.6: Molecular structure of [WAu(μ_2-CBr)Cl(CO)$_2$(Tp*)] (**2.2d**) in a single crystal as determined by X-Ray diffractometry. Displacement ellipsoids are drawn at the 50% probability surface with pyrazolyl rings simplified and hydrogen atoms omitted for clarity. Insets = View along the W–C axis and a simplified ball and stick representation to highlight deviation of the bromocarbyne ligand. Selected bond lengths (Å) and angles (°): W1A–C1A 1.880(9), C1A–Br1A 1.85(1), Au1A–Cl1A 2.294(2), W1A–Au1A 2.7798(6), Au1A–C1A–Br1A 118.1(5), W1A–C1A–Br1A 151.8(6).

The complete series **2.2a**–**2.2c** provides an opportunity to compare spectroscopic and structural data with respect to variations in both the metal (Mo, W) and halogen (Cl, Br, F[********]). Firstly, the Tp* ligand remains a spectator but serves as an informative reporter for both ^{1}H and ^{13}C{^{1}H} NMR spectroscopy, confirming that, at least on the ^{1}H and ^{13}C NMR timescales, the molecules have retained C_s symmetry upon addition of the 'AuCl' fragment. Assuming, as seems likely, that the spectra reflect static structures, then the AuCl unit lies in the plane bisecting two pyrazolyl groups, though its position, *syn* or *anti* to the Tp* ligand, ambiguously from spectroscopic data. The ^{13}C{^{1}H} NMR spectra reveal the characteristic shift to higher frequency for the carbyne resonances of **2.2a**–**2.2d** shift (δ_C: 212.1–230.4) relative to the mononuclear precursors (*cf.* 198.0–208.7), though this is less pronounced than what is typically found for conventional carbynes. The inferred deshielding most likely reflects increased paramagnetic contribution from the incorporation of a second metal. The infra-red spectra also include carbonyl vibrations moved to higher wavenumber (ν_{CO}) reflecting reduced π-basicity of Mo/W upon gold coordination. Otherwise, spectroscopic features of the series are unremarkable.

Incorporating gold(I) also facilitated crystallisation of complexes **2.1a**–**2.1c** to accompany the known structures of **2.2d** and [WAu(μ-CF)Cl(CO)$_2$(Tp*)] (**2.2e**). Generally, corresponding structural data for all members of the series span a remarkably narrow range despite differing metals and halogens. The obvious difference is in C–X lengths (C–Cl: 1.698(8), 1.697(6) Å) and C–Br: 1.846 (9), 1.85(1) Å), but this simply reflects the differing covalent radii sums for halogens bound to *sp*-carbon (C–F: 1.26; C–Cl: 1.72; C–Br 1.89 Å). Remarkably, the M≡C bond length barely elongates (1.879–1.893 Å) upon coordination to gold in comparison to the precursors (1.798–1.910 Å), as previously noted for carbynes of tungsten, or molybdenum, bound to gold. [220, 222-226] By applying the Dewar—Chatt—Duncanson model, this minimal elongation suggests that π-retrodonation from gold(I) to one π^* orbital of the halocarbyne is small. A small contraction of carbyne angle (M–C–X: 149.4–152.6°) is consistent with this interpretation, especially when considering the smaller angle of previous *homo*metallic and therefore symmetrical dirhodium μ_2-halocarbynes (Rh–C–X: 123.6(3)–137.8(9)°), which are much closer to the geometry of an ideal sp^2-hybridised carbon.

Stone previously discussed the unsymmetrical nature of μ_2-carbynes that bridge metal-metal bonds in which one metal is d^{10}-closed shell and most pronounced for Au(I). [227-228] These were described as 'semi-bridging' in contrast to the classical dimetallacyclopropene description that is more appropriate for less disparate metals (Chart 2.2). The gold μ_2-halocarbynes most clearly adhere to the semi-bridging description. A similar phenomenon is noted for carbonyl ligands, [229-231] as well as μ-boryl, μ-CX (X = S, Se, Te), μ-alkynyl and μ-silyl ligands where semi-bridging character arises as a terminally bound ligand is

[********] Following the completion and publication of work described in this Chapter, a synthetic route to the fluorocarbyne analogues [M(≡CF)(CO)$_2$(Tp*)] (M = Mo, W) was developed as well as the isolation of the first μ_2-fluorocarbyne complex [WAu(μ-CF)Cl(CO)$_2$(Tp*)]. Data for these compounds are included in the present discussion for completeness. [117]

able to act as a Lewis acid or form a polar-covalent interaction to a second (often electron rich) metal centre. With the empirical observation of a potentially semi-bridging halocarbyne ligand, a computational study of the reduced complex [Mo(μ_2-CBr)(CO)$_2$(Tp)] (**2.2c***) was undertaken (DFT: ωB97X-D/6–31G*/LANL2DZ) to explore the underlying bonding from the semi-bridging *vs* dimetallacyclopropene perspectives (Figure 2.7).

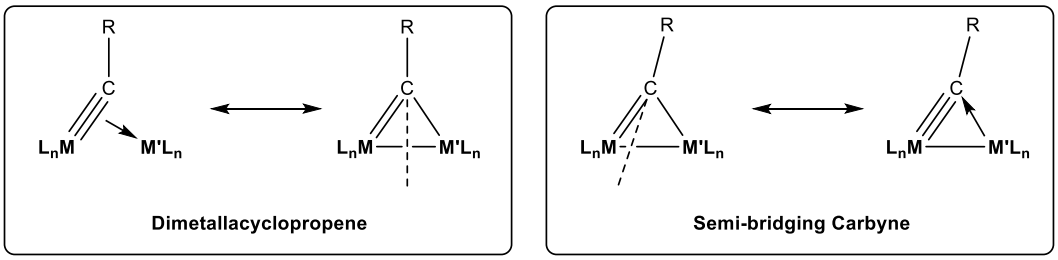

Chart 2.2: Dimetallacyclopropene *versus* semi-bridging character in μ-CX ligands as suggested by Stone.

Although the Mo≡C bond length barely decreases upon gold(I) coordination experimentally (*ca* 1.877(9) Å), a reduction in Löwden bond order was computed (1.829 *cf.* 2.495) with the reduction in bonding contribution now balanced by the formation of Mo–Au (0.659) and Au–C (0.849) bonds. Changes in natural charges indicate electron density flows from gold to the molybdenum and carbon atoms, suggesting that both descriptions of halocarbyne bonding have utility in explaining the system. Supporting these dual descriptors, no single two-centre-two-electron combination was identified in the underlying orbitals, instead returning several orbitals of different σ- and π-symmetries. For example, the HOMO–3 shows retention of *one* orthogonal π-overlap from the former Mo≡C bond, while the HOMO–16 is consistent with the Au–Mo and Au–C σ-framework. Buried in the manifold is also the HOMO–21 that involves a π-overlap of both Mo–Au and Au–C whilst HOMO–22 best resembles the proposed semi-bridging interaction. The LUMO+1 is comprised of substantial carbyne p-orbital orthogonal to the MoCAu plane suggesting a site for nucleophilic attack.

2.3.2 Platinum(0) complexes

Beck's isolation of [MoPt(μ_2-CBr)(CO)$_2$(PPh$_3$)$_2$(Tp*)] (**2.3c**) inspired the pursuit of further examples of platinum(0) halocarbynes without undergoing oxidative addition of the C–X bond. It was presumed that chlorocarbynes (**2.1a**/**2.1b**) might facilitate the arrest of oxidative addition processes of the less reactive C–Cl bonds (*ca* 350 kJmol^{-1} *cf.* 290 kJmol^{-1} for C–Br‡‡‡‡‡‡‡), to secure discrete μ_2-halocarbynes. Furthermore, to discourage polarisation of C-Cl bonds in solution (*vide infra*), the less polar THF ($\varkappa$ = 7.52) was chosen over dichloromethane ($\varkappa$ = 9.08) previously used for the gold(I) species; Beck utilised non-polar benzene ($\varkappa$ = 2.27). Stirring chlorocarbynes **2.1a**/**2.1b** with [Pt(η^2-C$_2$H$_4$)(PPh$_3$)$_2$] in THF at

‡‡‡‡‡‡‡ Though data are limited, it would appear that the enthalpy of Pt–X bond formation is less critical, *e.g.*, K$_2$[PtX$_4$] (X = Cl: 364, X = Br 330 kJmol^{-1}. [232]

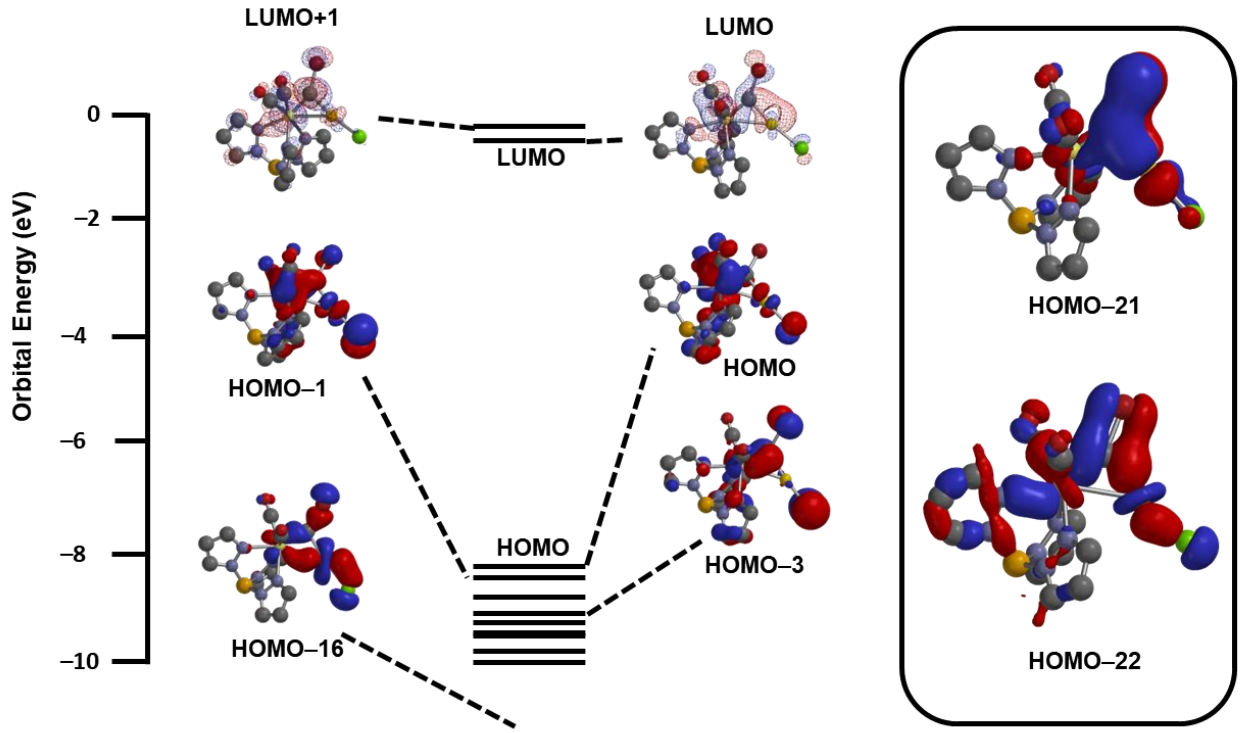

Figure 2.7: Frontier orbitals of the hypothetical μ2-halocarbyne [MoAu(μ2-CBr)Cl(CO)2(Tp)] {DFT: ωB97X-D/6-31G*/LANL2Dζ } . Key = occupied orbitals are colour filled, unoccupied orbitals are displayed as mesh.

ambient temperature resulted in a slow colour change from yellow to dark orange over several hours ($t_{½}$ ~ 3 hours) producing the bimetallic species [MPt(μ2-CCl)(CO)2(PPh3)2(Tp*)] (Mo **2.3a**; W **2.3b**) as monitored by infra-red spectroscopy (Scheme 2.7). Alternatively, the reaction was repeated by heating the THF at reflux, with completion confirmed (ν_{CO}) at 30 minutes with no evidence of oxidative addition. Later experimentation on reactivity (Section 2.5) revealed that the system could be heated at reflux in toluene or polar acetonitrile ($\varkappa$ = 37.5) without oxidative addition being observed, identifying acetonitrile as the optimal solvent as analytically pure **2.3b** precipitates from solution.

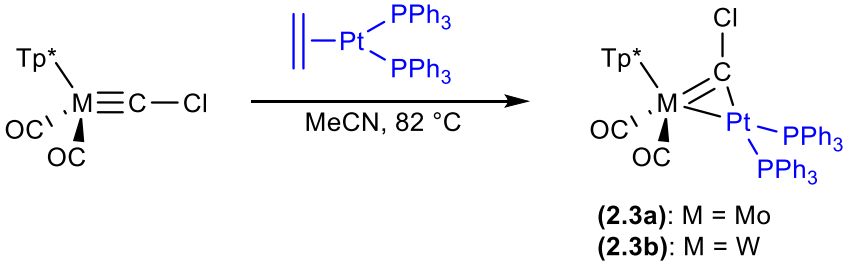

Scheme 2.7: Preparation of platinum(0) μ2-chlorocarbynes.

The $^{31}P\{^{1}H\}$ NMR spectra of crude material clearly identified formation of (**2.3a**/**2.3b**), however isolation proved non-trivial. Attempts to purify the complexes *via* flash chromatography resulted in isomerisation to another species discussed later (Section 2.5). For this reason, concentration of a THF/EtOH solution by rotary evaporation, *i.e.*, slow removal of THF, afforded olive-yellow solid

identified as pure **2.3a**/**2.3b**, analogous to Beck's original [MoPt(μ_2-CBr)(PPh_3)$_2$(CO)$_2$(Tp*)]. The main signature of **2.3a**/**2.3b** manifests in the $^{31}P\{^1H\}$ NMR spectra as a result from the coupling of multiple spin-active nuclei. With specific reference to species **2.3a** (**2.3b** is similar), two doublets arise from inequivalent phosphine ligands bearing small inter-phosphine couplings ($^2J_{PP}$ = 24 Hz) as a consequence of the *pseudo-cis*-relationship. Furthermore, the ^{195}Pt isotopomer manifests satellite peaks straddling each doublet with vastly different coupling constants ($^1J_{PPt}$ = 4398, 2761 Hz), where the former reflects phosphine lying *pseudo-trans* to Mo containing significantly higher s-character than the μ_2-CCl motif. The isolobally related symmetric complex [Pt(η^2-PhC≡CPh)(PPh_3)$_2$] has an intermediate value for $^1J_{PtP}$ of 3235 Hz. [233]

Similar spectroscopic observations are made for platinum(0) chlorocarbynes to their gold(I) counterparts. The $^{13}C\{^1H\}$ NMR spectrum contains a carbyne resonance shifted to substantially higher frequency (δ_C: 314.1 *vs* 208.7) than observed for gold(I) coordination. Because μ_2-carbyne resonances are typically found downfield of those for *both* terminal and μ_3-carbynes, the chemical shift is clearly not just the result of successive additional metal centres shielding the carbon. Because the highest frequency shifts are associated with μ_2-carbyne nuclei, it would appear that paramagnetic effects dominate for the unsaturated metallacyclopropene. As with the gold(I) species, the platinum derivatives exhibit Tp* patterns indicative of *C*s symmetry from which it may be inferred that the PtP_2 and WCPt planes align. Though not reported by Beck, ^{195}Pt NMR data are particularly responsive to geometric changes and electronic influences, [234-238] providing useful information on **2.3a**/**2.3b**. The $^{195}Pt\{^1H\}$ chemical shift is consistent with platinum(0) (δ_{Pt} = –3940) and likely a *pseudo*-trigonal planar arrangement, at lower frequency than the square-planar platinum(II) arrangement measured for Beck's carbido (*cf.* [MoPt(μ_2-C)Br(PPh_3)$_2$(CO)$_2$(Tp*)] **3.1a**; δ_{Pt}: –3810; Chapter Three). Another notable feature is that **2.3a**/**2.3b**, along with Beck's bromocarbyne analogue, confirm that Tp*-ligated carbynes can coordinate to platinum(0) with bulky PPh_3 (Θ^T = 145°)‡‡‡‡‡‡ ligands which were absent from Stone's studies which employed smaller phosphines PMe_2Ph (Θ^T = 122°), PMe_3 (Θ^T = 118°), and $P(OMe)_3$ (Θ^T = 107°).[195, 239]

Structural analysis of **2.3a**/**2.3b** was facilitated by deposition of red/orange plates surprisingly easily from various vapour diffusions, with acetonitrile proving the superior anti-solvent (Figures 2.8 and 2.9). The crystal and molecular structures of **2.3a**/**2.3b** (Figures 2.8 and 2.9) were isomorphous such that if the halocarbyne (M≡C) motif is considered a single 'ligand' the geometry is best described as a *pseudo*-trigonal planar platinum(0)—where the M≡C lies in the plane—consistent with the spectroscopic data in solution and more conventional examples from Stone. A similar platinum structure is known for the

‡‡‡‡‡‡ Θ^T =Tolman cone angle, see C. A. Tolman, *Chem. Rev.*, 1977, **77**, 313-348.

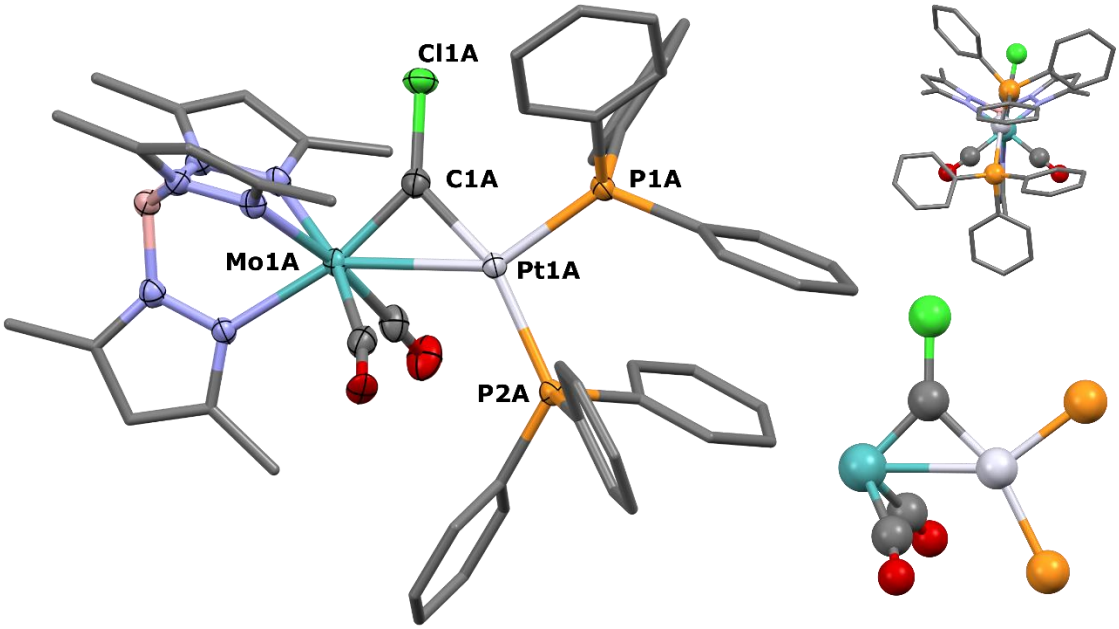

Figure 2.8: Molecular structure of **2.3a** in a single crystal of 2(**2.3a**)·2.5(C_2H_3N) as determined by X-Ray diffractometry. Displacement ellipsoids are drawn at the 50% probability surface with pyrazolyl and phenyl rings simplified and hydrogen atoms acetonitrile omitted for clarity. Insets = View along the Mo–C axis and a simplified ball and stick representation to highlight deviation of the chlorocarbyne ligand about the two metallic centres. Selected bond lengths (Å) and angles (°): Mo1A–C1A 1.934(4), C1A–Cl1A 1.719(4), Pt1A–C1A 1.986(4), Pt1A–P1A 2.269(1), Pt1A–P2A 2.359(1), Mo1A–C1A–Cl1A 135.9(3), Pt1A–C1A–Cl1A 133.3(3), P1A–Pt1A–P2A 100.60(4).

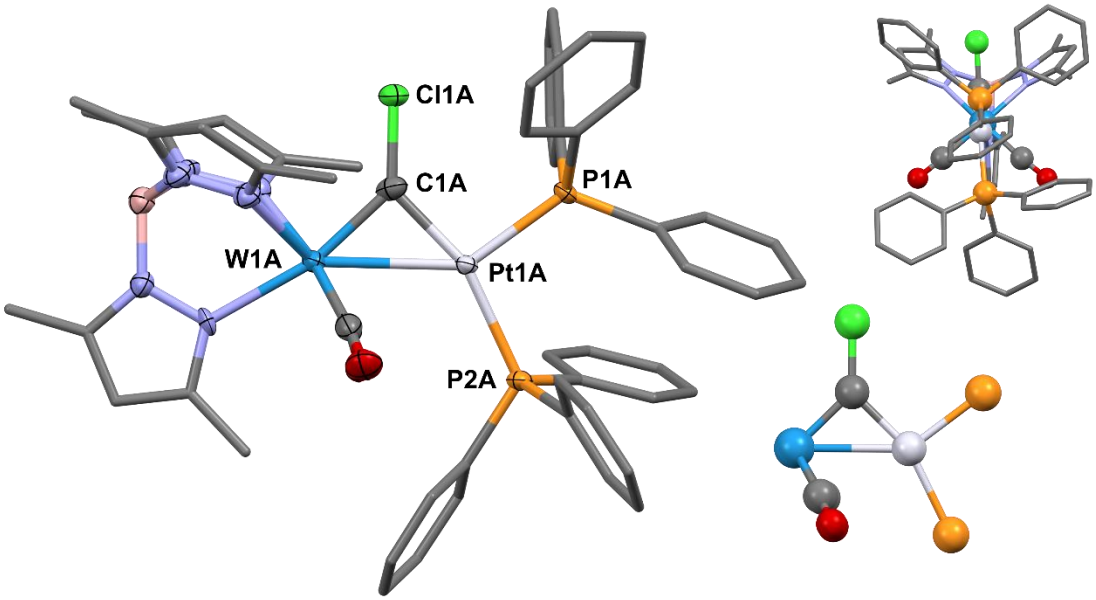

Figure 2.9: Molecular structure of **2.3b** in a single crystal of **2.3b**·3(C_2H_3N) as determined by X-Ray diffractometry. Displacement ellipsoids are drawn at the 50% probability surface with pyrazolyl and phenyl rings simplified and hydrogen atoms and acetonitriles omitted for clarity. Insets = View along the W–C axis and a simplified ball and stick representation to highlight deviation of the chlorocarbyne ligand about the two metallic centres. Selected bond lengths (Å) and angles (°): W1A–C1A 1.971(6), C1A–Cl1A 1.715(8), Pt1A–C1A 1.965(8), W1A–Pt1A 2.8076(5), Pt1A–P1A 2.268(1), Pt1A–P2A 2.352(2), W1A–C1A–Cl1A 134.3(4), Pt1A–C1A–Cl1A 134.7(4), P1A–Pt1A–P2A 100.77(6).

dichloroethyne [Pt(η^2-C_2Cl_2)(PPh_3)$_2$], which incidentally, exhibits a thermally promoted rearrangement to chloroalkynyl complex [Pt(C≡CCl)Cl(PPh_3)$_2$]. [240] Curiously for both structures, the Pt–P1A bond lengths were significantly contracted when compared to Pt–P2A distances. This may suggest that a more complicated orbital interaction *trans* to the group 6 metal may be present. Alternatively, the M≡C unit may be exerting a *trans* effect on the phosphine ligand resulting in a bond elongation which also explains the large disparity in coupling constant (*e.g.*, $^1J_{PPt}$ = 4398/2761 Hz for **2.3a**). Bond lengths and angles around the molecule were as expected, except for the angle around the chlorocarbyne motif: the most informative and desired parameter. Unlike the largely semi-bridging gold(I) counterparts (**2.2a**–**2.2d**), the platinum(0) chlorocarbyne angles are almost identical {M–C–Cl: 135.9(3)/133.3(3)° **2.3a**; 134.3(4)/134.7(4)° **2.3b**} and significantly reduced relative to gold(I) (*cf.* 148.9/120.2° **2.2b**). The angle more closely approaches the ideal for sp^2-hybridised carbon (120°) deviating only because of longer metal-carbon (Pt–C/W–C) bonds. This contracted angle likely suggests unsurprisingly that platinum(0) contributes more retrodonation as compared to gold(I), however, the caveat of two sterically large phosphines must be considered. It appears in space-filling diagrams that the phosphines fit snuggly around platinum and largely away from the chlorocarbyne ligand, which is further supported by the contracted angle (W–C–Cl: 137.9°) found in a smaller phosphine complex [WPt(μ_2-CTol)(PMe_2Ph)$_2$(CO)$_2$(Cp)]. [195, 239] This similar observation for a smaller phosphine suggests that the contracted M–C–Cl angle of the chlorocarbyne as a true response to electronic rather than steric factors.

To interrogate halocarbyne bending as an electronic response, the geometries of the hypothetical complexes [MPt(μ_2-CCl)(PMe_3)$_2$(CO)$_2$(Tp)] (M = Mo **2.3a***; W **2.3b***) were computationally optimised (Figure 2.10). Many similarities are found between metals, therefore only the optimised **2.3a*** will be discussed in comparison with real structure **2.3a**. Firstly, the optimised Mo–C–Cl angle is contracted (133.1°) despite the smaller PMe_3 ligands, further supporting the electronic effect in the real structure, while similar bond lengths (Mo–C: 1.934 Å; C–Pt 1.950 Å) reflect the small, observed reduction of bond order. Other orbitals prove similar to the gold(I) counterparts, identifying components of both the semi-bridging and dimetallacyclopropene character, such as the HOMO–1 exhibiting the intact π-component of the Mo–C bond. The optimised geometry of **2.3a*** maps well to the real structure **2.3a**, and again reflects a mixture between descriptions, but is best described as an unsymmetric dimetallacyclopropene canonical. With this behaviour elucidated, the other frontier orbitals are as expected, although the LUMO contains is π*-antibonding with respect to both C–Mo and C–Pt connections.

Co-ligand substitution of μ2-halocarbynes is yet to be established given scarce examples and many being substitution inert. The facility of ligand substitution with 2.3a was briefly explored. Stirring 2.3a with the chelating phosphine, 1,2-diphenylphosphinoethane (dppe), quickly results in the formation of [MoPt(μ-CCl)(μ-CO)(CO)(dppe)(Tp*)] (2.4) as a deep red solution (Scheme 2.8). As substantial losses

attended the initial purification of 2.3a, the optimised synthesis of 2.4 involves sequential treatment of 2.1a with [Pt(η2-C2H4)(PPh3)2] to generate 2.3a in situ prior to dppe addition to afford to 2.4 which is relatively stable toward chromatography and improves the overall yield significantly.

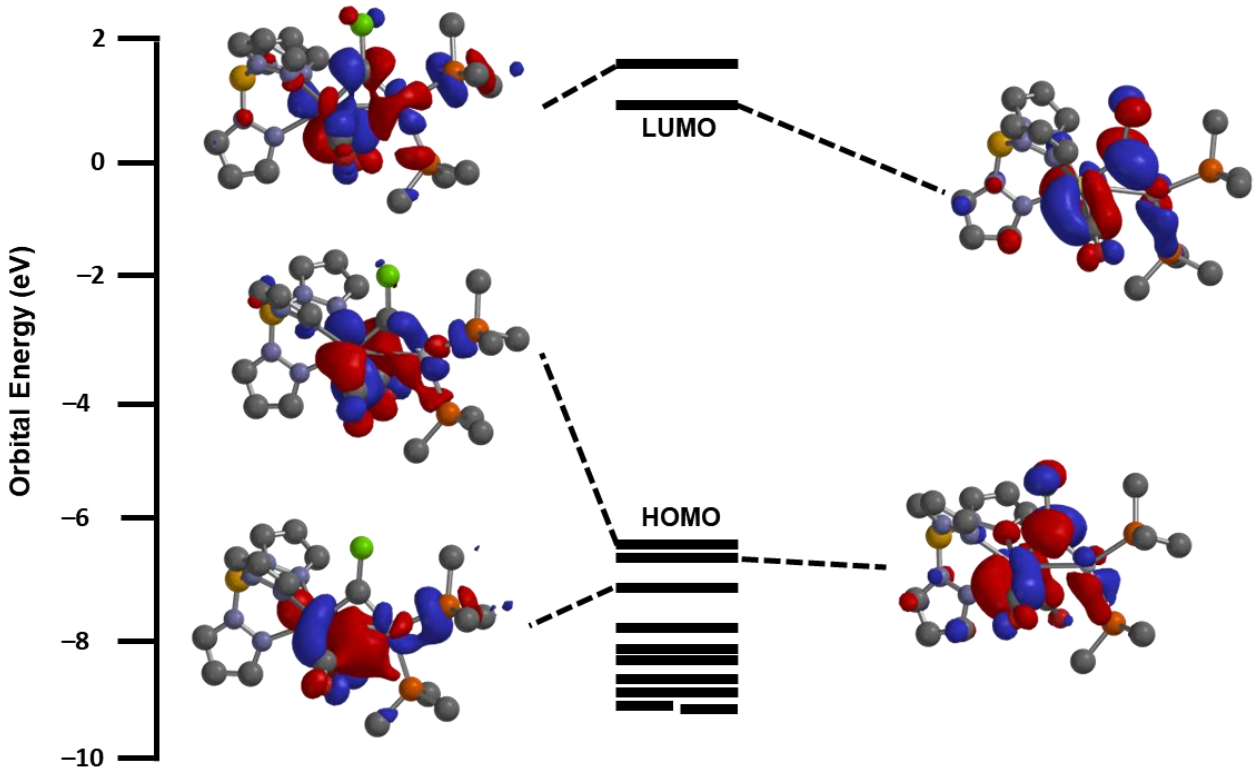

Figure 2.10: Frontier orbitals of hypothetical [MoPt(μ2-CCl)(CO)2(PMe3)2(Tp*)] (**2.3a***).

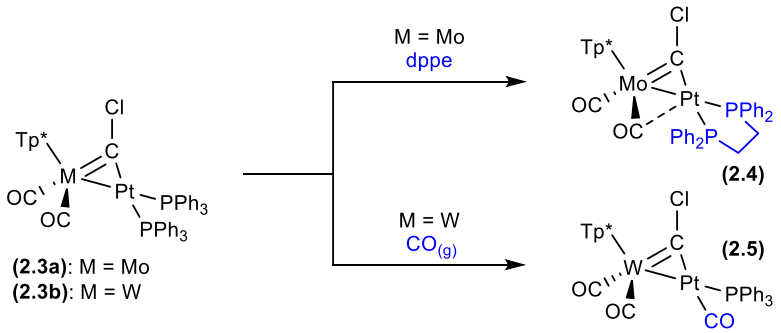

Scheme 2.8: Ligand substitution of **2.3a** with chelating phosphine dppe or CO.

Spectroscopic analysis of **2.4** proved analogous to **2.3a**. The $^{31}P\{^{1}H\}$ NMR spectrum exhibits two doublets pattern straddled by ^{195}Pt satellites, this time, with phosphines having almost identical chemical shifts (δ_P: 48.2, 47.8) yet disparate couplings ($^{1}J_{PPt}$ = 4023, 2668 Hz). The ^{195}Pt signal shifts to lower frequency (δ_{Pt}: –4203 *cf.* –3940 **2.3a**), which is likely a consequence of decreased overlap of one phosphine with molybdenum *d*-orbitals, accompanied by reduced $^{1}J_{PPt}$ coupling. It has been suggested that the value

of $^1J_{PtP}$ varies linearly with Pt–P bond length for similar complexes, *viz.* $^1J_{PtP} = 24255\times(2.421\text{-}r_{PtP})$.[241] That this approach overestimates the calculated (4172, 3230 Hz) and observed (4023, 2668 Hz) values is most likely a result of the original relationship being derived from data for d^8-square planar (sp^2d) rather than nominally d^{10} *pseudo*-trigonal planar (sp^2) complexes. The solid-state structure confirms the decreased inter-phosphine angle (P1–Pt1–P2: 86.58(3)°) from the *bis*(monodentate) precursor (*cf.* 100.60(4)° for **2.3a**) further validating the above (Figure 2.11). The solid-state structure also demonstrates a semi-bridging carbonyl (Mo–C–O: 157.0(8)°) as do both solid state and solution infra-red data ($\nu_{\mu\text{-}CO}$: 1772 cm^{-1}). The two types of carbonyls are, however, indistinguishable in the $^{13}C\{^1H\}$ NMR spectrum (δ_{CO}: 232.9), reflecting time averaged signals and the slower timescale of NMR relative to infra-red spectroscopy.

For the chlorocarbyne ligand the angle widens (Mo–C–Cl: 142.8(3)°), presumably due to the dppe chelation drawing the phosphorus donors closer together, thereby allowing a closer coordination of the Mo≡C fragment. The elongation of the phosphine *trans* to the chlorocarbyne still manifests (2.2878(9) *vs* 2.249(1) Å) indicating the *trans*-influence of the chlorocarbyne is retained by chelation drawing the phosphine away from ideal overlap. Production of **2.4** from **2.3a** confirms that ligand substitution of μ-halocarbynes is possible without cleavage of the dimetallacyclopropene core. The robust

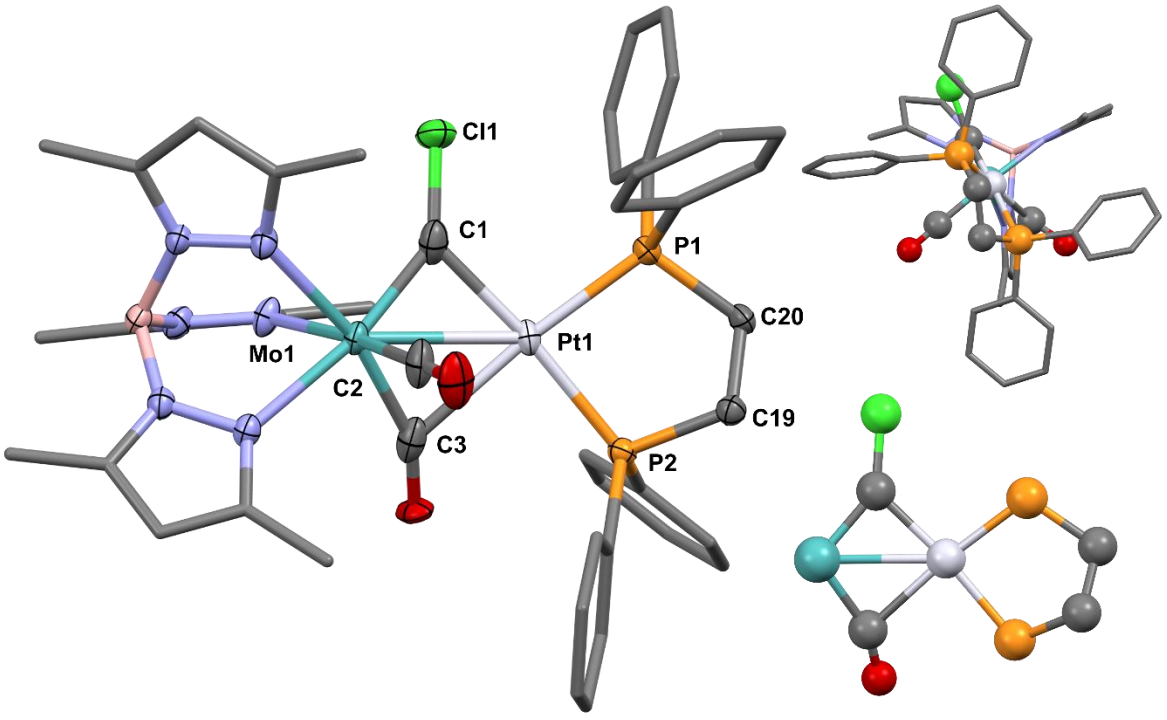

Figure 2.11: Molecular structure of [MoPt(μ_2-CCl)(μ_2-C)(dppe)(CO)(Tp*)] (**2.4**) in a single crystal as determined by X-Ray diffractometry. Displacement ellipsoids are drawn at the 50% probability surface with pyrazolyl and phenyl rings simplified and hydrogen atoms omitted for clarity. Insets = View along the Mo–C axis and a simplified ball and stick representation to highlight the chlorocarbyne ligand. Selected bond lengths (Å) and angles (°): Mo1–C1 1.937(5), C1–Cl1 1.663(5), Pt1–C1 2.087(4), Mo1–Pt1 2.7618(4), Pt1–P1 2.249(1), Pt1–P2 2.2878(9), Mo1–C1–Cl1 142.8(3), Pt1–C1–Cl1 130.0(3), P1–Pt1–P2 86.58(3).

nature of **2.4** provides a more stable platform to study reactivity of the C–Cl bond should *bis*-phosphines **2.3a**/**2.3b** prove incompatible or unstable in further reactions. A minor red species was observed during attempted chromatography of **2.3b** that was also pursued. Infra-red spectroscopic analysis of this minor species revealed an additional carbonyl vibration at higher frequency (ν_{CO} = 2027 cm^{-1}) identified as the species [WPt(μ_2-CCl)$(CO)_3(PPh_3)$(Tp*)] (**2.5**), presumably arising from scrambling CO from another unit to replace a labile phosphine. The synthesis of **2.5** was achieved deliberately through suppling an atmosphere of CO to a freshly generated solution of **2.3b**, resulting in the smooth conversion, followed by flash chromatography. Replacement of one phosphine with CO provides another example of ligand substitution of a μ_2-halocarbyne, now with a π-acidic ligand that stabilises the low oxidation state such that the complex is indefinitely stable and resistant to oxidative addition (or ionisation recognised later in Section 2.5).

Infra-red spectroscopy immediately confirmed incorporation of an additional CO ligand, however, the other carbonyl absorptions appear at higher wavenumbers than that of the *bis*-phosphine (ν_{CO}: 1917/1833 *cf.* 1895/1810 cm^{-1} **2.3b**), suggesting less semi-bridging character. The introduction of a π-acid appears sufficient to deplete electron density of platinum(0) to reduce its basicity and ability to enter into *Z*-type interactions thereby disfavouring semi-bridging carbonyl formation. This is further supported by the $^{13}C\{^1H\}$ NMR spectrum containing only terminal carbonyl resonances for tungsten (δ_C = 225.2) and platinum (δ_C = 196.8). The carbyne resonance is in a similar region (δ_C = 295.6) to that for **2.3b** which is perhaps counter-intuitive given the significant variation in the nature of the *trans* ligand (PPh_3 *vs* CO). The $^{31}P\{^1H\}$ NMR spectrum comprises a single resonance with a large coupling ($^1J_{PPt}$ = 3840 Hz) that suggests the phosphine retained in solution is *pseudo-trans* to tungsten. This may not require the initial substitution to occur at the same position since the process is most likely associative and therefore proceeds *via* tetrahedral platinum in [WPt(μ-CCl)$(CO)_3(PPh_3)_2$(Tp*)] which then dissociates phosphine to minimise steric impact. The $^{195}Pt\{^1H\}$ NMR spectrum shows the platinum resonance occurs at the highest frequency of the series at similar chemical shift to that of chelated **2.4**.

The molecular structure of **2.5** (Figure 2.12) reveals that the W–C bond (1.951(3)Å) is very similar to that in **2.3b** (1.971(6)Å), with slightly contracted Pt–C (1.950(4) Å) and W–Pt bonds (2.7732(2) Å). This is presumably a consequence of the smaller $(CO)(PPh_3)$ *vs* $(PPh_3)_2$ ligand set, allowing both tungsten and the carbyne carbon to more closely approach platinum with the μ_2-CCl ligand bridging almost symmetrically (M–C–Cl: 136.2(2)/133.2(2)°). Computational analysis of the model [WPt(μ-CCl)$(CO)_3(PMe_3)$(Tp)] (**2.5***) reproduces many of the observations made with **2.3b***, although, the LUMO is not only the halocarbyne ligand π-antibonding orbital, but it is π-bonding with platinum d-orbitals reducing the energy of the orbital overall (Figure 2.12; inset).

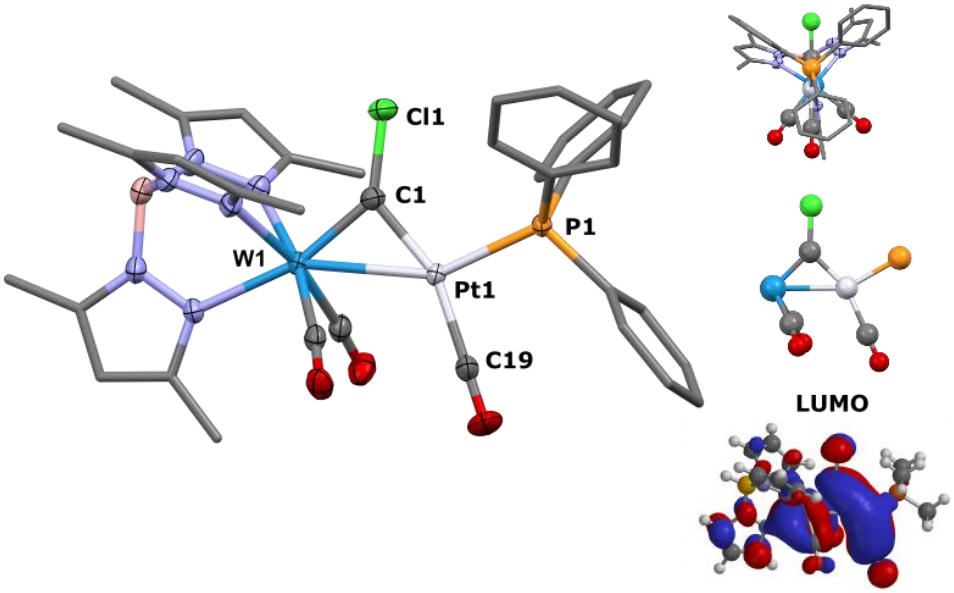

Figure 2.12: Molecular structure of [WPt(μ_2-CCl)(PPh_3)$(CO)_3$(Tp*)] (**2.5**) in a single crystal as determined by X-Ray diffractometry. Displacement ellipsoids are drawn at the 50% probability surface with pyrazolyl and phenyl rings simplified and hydrogen atoms omitted for clarity. Insets = View along the W–C axis and a simplified ball and stick representation to highlight deviation of the chlorocarbyne ligand about the two metallic centres. Selected bond lengths (Å) and angles (°): W1–C1 1.951(3), C1–Cl1 1.732(4), Pt1–C1 1.950(4), W1–Pt1 2.7733(4), Pt1–P1 2.2874(8), Pt1–C19 1.928(5), W1–C1–Cl1 136.2(2), Pt1–C1–Cl1 133.1(2), P1–Pt1–C19 95.7(1).

2.4 Limits of Synthesis: A Trimetallic Bow-tie Structure

Species **2.3a**/**2.3b** confirm two relatively large phosphines can fit around platinum(0) coordinated to the π-system of Tp* halocarbynes, but replacement with smaller $(CO)(PPh_3)$ or dppe ligand combinations confers a degree of stability. These species do raise the question, what is the size limit to the complex that can fit the M≡C bond? This becomes relevant in later Chapters where the generality of the oxidative addition pathway to μ-carbido complexes is somewhat compromised by the steric bulk of various metal-ligand combinations. Stone has previously described a plethora of trimetallic "bow-tie" structures of the form [$M_2M'(\mu_2\text{-}CR)_2(CO)_4(L)_2$] {M =Cr, Mo, W; R = Me, Ph, Tol, ½$Fe(C_5H_4)_2$; L = Cp, Cp*, Tp; M' = Ni, Pd, Pt, Cu^+, Ag^+, Au^+, $Mo(CO)_2$ and $W(CO)_2$},[195, 197, 222, 242-248] complemented by the recently isolated parent methylidyne [$W_2Pt(\mu_2\text{-}CH)_2(CO)_4$(Tp*)],[159] showing large systems are still capable of π-coordination to carbyne M≡C bonds. Therefore the challenge of adding a similar species was attractive, given examples were known for μ_3-species but *bis*-μ_2-halocarbynes were unknown.§§§§§§§§ To allow direct comparison with the known methylidyne [$W_2Pt(\mu_2\text{-}CH)_2(CO)_4$(Tp*)], **2.1b** was treated with 'ligand-free' platinum synthon [$Pt(nbe)_3$] in THF, resulting in the initially yellow mixture darkening to red through

§§§§§§§§ *Bis*-μ_3-halocarbynes have been isolated for Fe_3 [164] and King has computationally investigated *bis*-μ_2-fluorocarbynes. [207-208]

orange over 24 hours. Chromatography followed by crystallisation gave the trimetallic bow-tie halocarbyne $[W_2Pt(\mu\text{-}CCl)_2(\mu\text{-}CO)_2(CO)_2(Tp^*)_2]$ (**2.6**) as a stable, bright red powder (Scheme 2.9).

Crystallographic analysis unambiguously confirmed the gross formulation of **2.6**, but significant disorder prevented a precise structural model (Figure 2.13). Positional disorder is apparent between semi-bridging CO and CCl^+ ligands preventing analysis of perhaps the most important geometric features. Secondly, the central platinum is disordered about a special position (inversion centre ½, 0, ½). Finally in the absence of co-crystallised solvates, the periphery is dominated by Tp* ligands that falsely impose a crystallographic (almost D_{3d}) centro-symmetry on the central region of interest. Therefore, while this structural model confirms the molecular topology, it prevents further structural evaluation. This means discussion of dimetallacyclopropene and semi-bridging bonding can be extended to the instance of a trimetallic species, as observed, e.g., for $[W_2(\mu\text{-}CR)_2(\mu\text{-}CO)_2(CO)_2(Tp)_2]$. (R = Me,[249] $C_{14}H_8Br$ [148]).

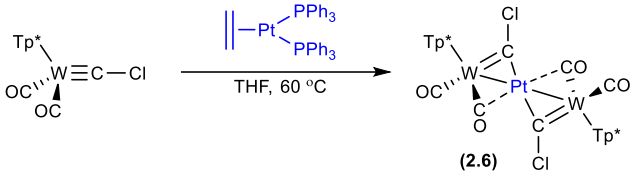

Scheme 2.9: Synthesis of a bowtie *bis*-μ_2-halocarbyne structure.

The ^{1}H NMR spectrum of **2.6** is broadened at room temperature consistent with a dynamic system—a feature also apparent in the spectra of the bow-tie species $[W_2Pt(\mu_2\text{-}CH)_2(CO)_4(Tp^*)_2]$,[159] and $[W_2Pt(\mu_2\text{-}CC_{10}H_8Br)_2(CO)_4(Tp)_2]$. Cooling to –30 °C sharpens signals in the ^{1}H spectrum, and at –40 °C, every resonance of Tp* can be distinguished, suggesting that movement is arrested and the chemical environments become chemically inequivalent, consistent with the chiral C_2-symmetric ground state. Similarly, $^{13}C\{^1H\}$ NMR spectra were measured at ambient temperature, and once cooled to –40 °C, the μ_2-chlorocarbyne ligand appears at higher frequency (δ_C: 267.9) yet slightly lower than the bimetallic species **2.3a**/**2.3b**, **2.4**, and **2.5**. As in the case of terminal halo *vs* hydrocarbyl substituted carbynes, the corresponding resonances for $[W_2Pt(\mu_2\text{-}CR)_2(CO)_4(Tp)_2]$ appear to considerably higher frequency (R = Me 310.3, C_6H_4Me-4 313.6 ppm).[249] The $^{195}Pt\{^1H\}$ NMR spectrum measured at ambient temperature (150.2 MHz, 25 °C) was comprised of a broadened resonance (w.h.h. = 216 Hz; δ_{Pt} = –2063), indicating that the fluxionality inferred from the ^{1}H NMR spectrum was also manifested in the ^{195}Pt spectrum. Infra-red spectra of **2.4** confirm a semi-bridging carbonyl, although fail to discern inequivalent carbonyls in the $^{13}C\{^1H\}$ NMR, while spectra of **2.6** exhibit carbonyls from each tungsten in a distinct environment (δ_C = 227.2), higher in frequency than the terminal carbonyl (δ_C = 219.2), indicative of a semi-bridging carbonyls in solution (*cf.* δ_C = 229.9, 224.6 for $[W_2Pt(\mu\text{-}CMe)_2(CO)_4(Tp)_2]$). No evidence of semi-bridging carbonyls was found in the infra-red spectra, but an unusually low frequency vibration ($\nu_{\mu\text{-}CO}$: 1606 cm^{-1}) was recorded, unable to be assigned.

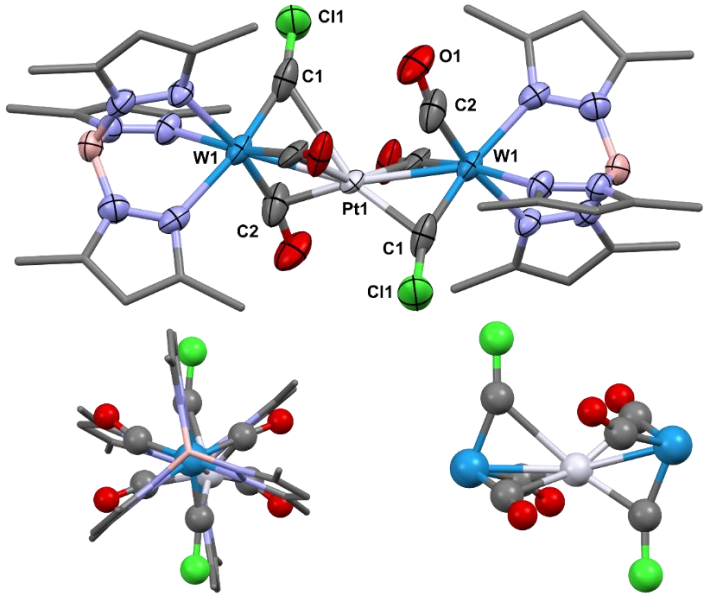

Figure 2.13: Molecular structure of **2.6** in a crystal as determined by X-Ray diffractometry. Displacement ellipsoids are drawn at the 50% probability surface with pyrazolyl rings simplified and hydrogen atoms omitted for clarity. Insets = View along the B–W–W–B axis and a simplified model to highlight the key linkage. The platinum atom is disordered about a special position (one site shown) such that caution should be exercised in over-interpreting the data beyond connectivity confirmation. Selected bond lengths (Å), angles (°) and torsions (°): W1–C1 1.97(1), C1–Cl1 1.50(1), C1–Pt1 2.745(9), C2–Pt1 2.08(2), C2'–Pt1 2.47(1), W1–Pt1 2.668(2), W1'–Pt1 2.692(1), W1–C1–Cl1 153.5(7), Cl1–W1–W1'–Cl1' 180.0.

2.5 Isomerisation of a μ_2-halocarbyne: A Missing Link for Metallacarbynes

The initial isolation of pure **2.3b** proved problematic, as a recurrent isomerism was accelerated by polar media such as flash chromatography or unpurified, commercial-grade $CDCl_3$. The initially yellow **2.3b** smoothly converts to an orange species that exhibits new ν_{CO} vibrations and $^{31}P\{^1H\}$ signals, absent from samples collected prior to chromatography. Analysis identified the isomerised product as the μ_2-carbido complex $[WPt(\mu_2\text{-}C)Cl(CO)_2(PPh_3)_2(Tp^*)]$ (**2.7**), producing spectroscopic features that match those reported for $[MoPt(\mu_2\text{-}C)Br(CO)_2(PPh_3)_2(Tp^*)]$(**3.1a**) by Beck and co-workers. Production of Beck's metallacarbyne complex arises from the oxidative addition of μ_2-bromocarbyne $[MoPt(\mu_2\text{-}CBr)(CO)_2(PPh_3)_2(Tp^*)]$ that required a benzene reflux (*ca* 80 °C, ~ 1 hr). In contrast, heating **2.3b** in d_8-toluene for 48 hours (60°C) results in no oxidative addition to form **2.7**. In contrast, a slow isomerisation ($t_{½}$ ~ 960 mins) to **2.7** occurs in purified $CDCl_3$ (distilled under argon, stored over 3Å molecular sieve and silver wire) heated to 60°C. A repeat experiment that employs 'benchtop' $CDCl_3$ as received results in accelerated isomerisation and is complete within 48 hours. To test the hypothesis of polar media, the reaction was repeated in d_3-acetonitrile, forming a suspension of **2.3b.** However, measuring the supernatant phase reveals a small amount of the **2.7** by $^{31}P\{^1H\}$ NMR spectroscopy, suggesting the minimal material that does dissolve into the polar solution likely isomerises. Incidentally, the reluctance of **2.3b** to dissolve in acetonitrile was used to optimise the synthesis of **2.3a**/**2.3b**, given the complex

could precipitate from solution once formed and therefore increase the yield by minimising purification (Section 2.3.2). Finally, heating **2.3b** in CD_2Cl_2 at reflux returned no evidence of **2.7**, yet formation was immediate upon application to a silica gel TLC plate. These observations suggest **2.7** is formed by an alternative mechanism than simple concerted oxidative addition.

It is plausible that available protons from either moist solvent or the hydroxylic surface of silica gel encourages polarisation of the μ_2-halocarbyne C–Cl bond, eventually leading to ionisation. If this is the case, then the initial plausible intermediate would be a charged, bent μ_2-carbido fragment that quickly (or even in concert with C–Cl lengthening) linearises to a cationic metallacarbyne prior to reassociation with chloride at platinum forming **2.7** (Scheme 2.10). The geometry of the μ_2-carbido intermediate is not known, although a bent geometry cannot be discounted given their recent isolation.[40] This isomerisation represents the reverse reaction, halogen migration to a μ_2-carbido, which is implied in the synthesis of μ_2-halocarbynes $[Rh_2(\mu_2\text{-}CX)(\mu_2\text{-}X)X_4(\mu\text{-dppm})]$ (X = Cl, Br),[78] therefore supplying a missing link with a plausible mechanism.

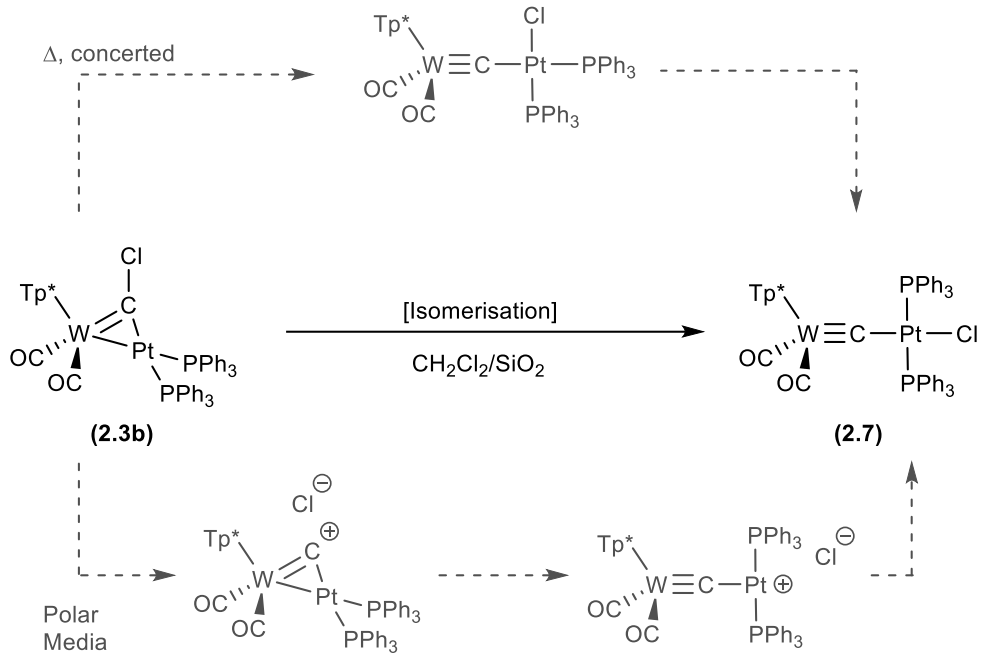

Scheme 2.10: Polar media promoted isomerisation of a μ_2-halocarbyne to give a μ_2-carbido.

Having considered the likely origin of **2.7**, a deliberate synthesis was performed by mixing **2.1a** with $[Pt(\eta^2\text{-}C_2H_4)(PPh_3)_2]$ in THF at 60 °C for 2 hours prior to flash chromatography exclusively using CH_2Cl_2 and commercial grade silica gel, where simple recrystallisation gives a pure sample. This reaction further confirms that temperature is not the determinant contributor to the formation of **2.7**, instead the polarity of silica gel stationary phase causes the rearrangement under ambient conditions.

The identity of **2.7** as a μ_2-carbido complex could be immediately confirmed through an X-ray diffraction study verifying the metallacarbyne-type bonding (W≡C–Pt) within expected bond lengths

(W–C: 1.842(4); Pt–C 1.944(4) Å) (Figure 2.14). The metallacarbyne spine is more bent than expected (W–C–Pt: 160.12(4)°), although the simpler model geometry with reduced inter-ligand interactions [WPt(μ_2-C)$(PMe_3)_2(CO)_2$(Tp)] (**3.2***) (Chapter Three, *vide infra),* is essentially linear (W–C–Pt: 174.6°). The experimental Pt–C bond was also found to be much shorter (2.413(1) Å) than that calculated for **3.2*** (2.463 Å).

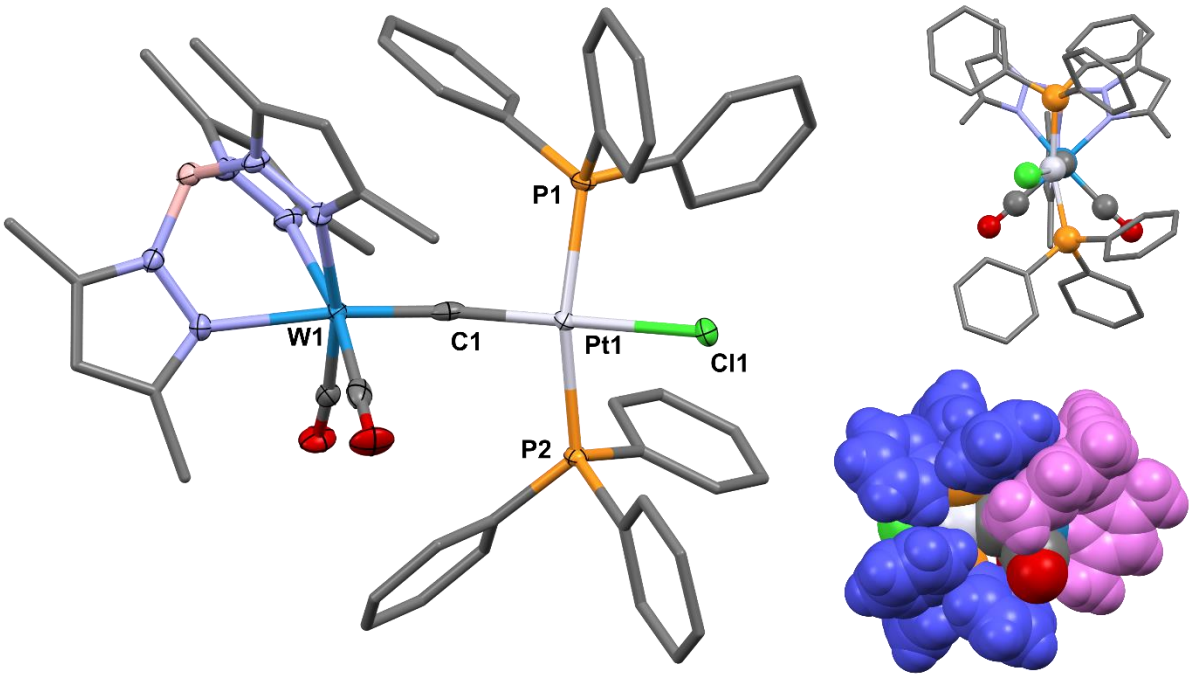

Figure 2.14: Molecular structure of **2.7** in a single crystal as determined by X-Ray diffractometry. Displacement ellipsoids are drawn at the 50% probability surface with pyrazolyl and phenyl rings simplified and hydrogen atoms omitted for clarity. Insets = View along the Mo–C axis and a simplified ball and stick representation to highlight deviation of the chlorocarbyne ligand about the two metallic centres. Insets: view along the W–C–Pt axis and a space-filling representation showing the clash of the encumbering phosphine (purple) and pyrazolylborate ligand (pink). Selected bond lengths (Å), angles (°), and torsions (°): W1–C1 1.842(4), C1–Pt1 1.944(4), Pt1–Cl1 2.413(1), Pt1–P1 2.322(1), Pt1–P2 2.323(1), W1–C1–Pt1 169.0(2), P1–Pt1–P2 160.12(4), B1–W1–Pt1–P1 7.3(1).

The $^{13}C\{^1H\}$ NMR spectrum of **2.7** displays a characteristic μ_2-carbido resonance coupled to equivalent phosphorus nuclei (δ_C = 318.8; $^2J_{CP}$ = 15 Hz), at similar chemical shift to Beck's molybdenum analogue (δ_C = 339), both to higher frequency of the μ_2-halocarbyne precursor (δ_C = 297.2; **2.3b**). The ^1H NMR spectrum indicates that **2.7** has *C*s symmetry in solution through Tp* pyrazolyl patterns, while the $^{31}P\{^1H\}$ NMR spectrum demonstrates and AB system of two chemically inequivalent phosphines (δ_P = 28.7, 23.6; $^2J_{PP}$ = 443 Hz) in accordance with Beck's analogue. The $^{195}Pt\{^1H\}$ NMR spectrum shows a triplet resonance of higher frequency than that of the **2.3b** precursor (δ_C = –3718, $^1J_{PtP}$ = 3223 Hz) consistent with a square-planar geometry. Many features echo those detailed as part of Chapter Three.

2.6 Conclusions

The π-system of Lalor's η^1-halocarbynes can coordinate gold(I) and platinum(0), leading to a series of rare bimetallic μ_2-halocarbyne complexes (Scheme 2.11). This method can extend to the trimetallic *bis*-μ_2-halocarbyne complex featuring a platinum(0) centre, encapsulated by sterically encumbering ligands and supported by semi-bridging carbonyls. Accompanied by a theoretical analysis, the underlying bonding of these complexes has identified bonding of diametallacyclopropene and semi-bridging descriptions. H*omo*-metallic examples recorded in the literature favour symmetrical ligands owed to dominant dimetallacyclopropene character, while *hetero*-metallic gold(I) complexes provide the other extreme with almost exclusively semi-bridging character resulting in asymmetric μ_2-CX ligands. The heterometallic platinum(0) species occupy a balance of bonding in between homometallic and disparate heterometallic extremes.

The phosphines coordinating the platinum(0) complex **2.3b** were found to undergo ligand substitution with chelating diphosphine or CO, to afford (in both cases) more robust bimetallics that may prove useful for further reactions involving the C–Cl bond. Furthermore, the purification of **2.3b** encountered a recurring isomerisation to the μ_2-carbido complex [WPt(μ_2-C)Cl(PPh_3)$_2$(CO)$_2$(Tp*)] clearly *not* arising *via* concerted insertion of platinum into the C–Cl bond. A series of experiments supported the possibility of ionisation of chloride in the μ_2-halocarbyne precursor as the most plausible explanation, aided by protons from moist solvent or a silica gel stationary phase prior to recombination toward the μ_2-carbido complex.

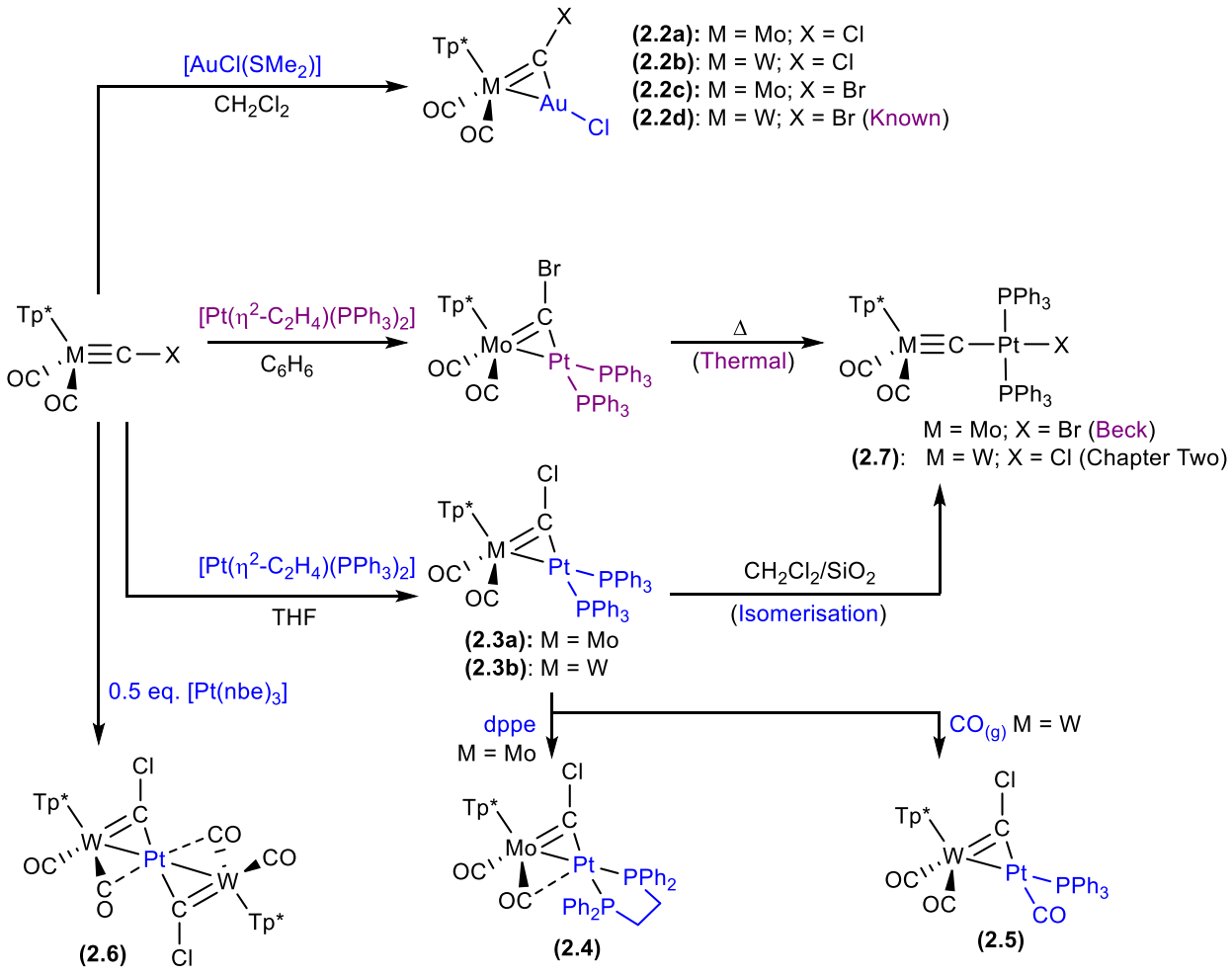

Scheme 2.11: Work presented in this chapter in literature context. Blue = work from Chapter Two; Purple = prior research.

Table 2.3: Spectroscopic and structural properties of μ2-halocarbynes including those produced in Chapter Two.

Compound	$\delta_{\equiv C}$ [ppm][c]	δ_{Pt} [ppm][c]	$^1J_{PtP}$ [Hz]	δ_P [ppm][c]	$^2J_{PP}$ [Hz]	ν_{CO} [cm^{-1}][f]	$r_{M\equiv C}$ [Å]	$r_{C-M'}$ [Å]	$r_{M-M'}$ [Å]	$\angle_{M\equiv C-X}$ [°]	$\angle_{M'\equiv C-X}$ [°]
Chapter Two μ2-halocarbynes											
[**Mo**Au(μ2-CCl)Cl] (**2.1a**)	230.4[d]	–	–	–	–	2031, 1957	1.878(7) 1.891(8)	2.022(8) 2.015(7)	2.7778(6) 2.7700(6)	149.4(5) 149.4(5)	119.7(4) 120.2(4)
[**W**Au(μ2-CCl)Cl] (**2.1b**)	222.2[d]	–	–	–	–	2018, 1934	1.891(6)	2.026(6)	2.7926(3)	148.9(4)	120.2(3)
[**Mo**Au(μ2-CBr)Cl] (**2.1c**)	224.4[d]	–	–	–	–	2032, 1960	1.894(9) 1.887(9)	2.011(9) 2.039(9)	2.038(9) 2.010(9)	149.6(5) 151.5(5)	119.6(5) 118.2(4)
[**W**Au(μ2-CBr)Cl] (**2.1d**)	212.1[d]	–	–	–	–	1989, 1896	1.908(9) 1.880(9)	2.032(8) 2.06(1)	2.057(18) 2.029(17)	151.0(5) 151.8(6)	119.5(5) 118.(5)
[**Mo**Pt(μ2-CCl)(PPh3)2] (**2.3a**)	314.8	–3940	4398, 2761	38.24 25.82	24	1906, 1823	1.934(4) 1.955(4)	1.986(4) 1.958(5)	2.7913(4) 2.7999(4)	135.9(3) 134.1(3)	133.3(4) 134.5(3)
[**W**Pt(μ2-CCl)(PPh3)2] (**2.3b**)	297.2	–3992	4316, 2760	41.89 24.39	23	1895, 1810	1.971(6) 1.952(6)	1.965(8) 1.988(6)	2.7961(4) 2.8078(4)	134.3(4) 136.3(4)	134.7(4) 133.3(4)
[**Mo**Pt(μ2-CCl)(dppe)] (**2.4**)[b]	324.2	–4203	4031, 2673	48.17 47.84	40	1911, 1808 1772	1.842(4)	1.944(4)	2.7618(3)	142.8(3)	130.0(2)
[**W**Pt(μ2-CCl)(PPh3)(CO)] (**2.5**)	295.6	–4197	3840	35.69	–	2027, 1917, 1833	1.951(4)	1.950(4)	2.7732(2)	136.2(2)	133.2(2)
[**W**2Pt(μ2-CCl)2] (**2.6**)[b]	267.9[e]	–2062	–	–	–	1967, 1865 1606	1.97(1) 1.97(1)	2.745(9) 2.118(8)	–	153.5(7) 153.5(7)	132.0(6) 123.8(6)
Literature μ2-halocarbynes											
[W2(μ2-CCl)Cl7] [198]	n.r.	–	–	–	–	–	1.94(1)	1.94(2)	2.561(3)	137.8(9)	139.5(8)
[Rh2(μ2-CCl)(μ-Cl)Cl4(dppm)2] [78]	n.r.	–	–	3.4[d]	–	–	1.912(4)	1.947(6)	3.1867(6)	123.6(3)	125.1(3)
[Rh2(μ2-CBr)(μ-Br)Cl4(dppm)2] [78]	n.r.	–	–	–5.7[d]	–	–	2.10(4)	2.10(4)	3.221(3)	130.0(13)	130.0(13)
[MoPt(μ2-CBr)(PPh3)2(CO)2(Tp*)] [142]	315.9	n.r.	4428, 2764	38.1 25.8	22	1885, 1753[g]	–	–	–	–	–
[Ru2(μ2-CCl)(μ-Cl)Cl2(Cp*)2] [160]	323.4	–	–	–	–	–	1.916(7)	1.929(7)	2.7540(6)	133.5(4)	135.0(4)

Notes: [a]**Mo** = [Mo(CO)2(Tp*)]; **W** = [W(CO)2(Tp*)]. [b]Contain μ-CO ligand.[c]Measured in C_6D_6 unless specified otherwise. [d]Measured in $CDCl_3$. [e]Measured in $CDCl_3$ at –20°C. [f]Measured in CH_2Cl_2 unless specified otherwise. [g]Measured in *n*-hexane.

Chapter Three

Elaboration of Platinacarbynes

The initial Chapter outlined the *status quo* of monoatomic carbon in low-nuclearity systems (μ_2- and μ_3-carbido ligands). Given μ_2-carbidos are classified as one of four classes based on bonding descriptions, Class B (Metallacarbynes) are the only class yet to have had a focused study undertaken, with the exception of Class D dimetallacarbenes which as a field remains in its infancy. This lack of a systematic study of metallacarbynes provides the premise of this Chapter, where a diversification of examples and investigation of their behaviour may inform methods to broaden the field more generally.

The emergence of Class B carbidos has been sporadic and the disparate species reported have origins in very different synthetic methods. The chemical processes leading to metallacarbynes so far include: (i) alkyne scission, (ii) co-ligand substitution, (iii) transmetallation, (iv) umpolung (lithiocarbyne) approach and (v) oxidative addition. In general, the novelty of the species produced has been sufficient to warrant their publication with very few examples of further reactivity having been explored. In particular, reactions that lead to variations in the coordinated co-ligands that might be expected to tune the reactivity and spectroscopic properties have not been addressed, with the exception of CO substitution in $[MoFe(\mu\text{-}C)(CO)_4(Cp)(Tp^*)]$.[97] That said, in many cases the metal centres involved are not necessarily amenable to simple co-ligand variation. Firstly, Selegue's alkyne scission approach is rather specific in that the reactivity of $[W_2(O^tBu)_6](W{\equiv}W)$ is rather unique amongst triply bonded dimetallic reagents in its ability to cleave multiple bonds, with stable dimetallatetrahedrane formation being more often the norm, *e.g.*, the reactions of $[Mo_2(CO)_4(Cp)_2]$ with alkynes.[250-251] In contrast, the well-developed use of lithium reagents for the formation of transition metal-carbon bonds in principle extends to lithiocarbynes obtained *via* lithium halogen exchange such that unsurprisingly that the umpolung (lithiocarbyne) approach has been the most generalisable route to metallacarbynes to date. Furthermore, given the versatility of lithiocarbynes and the innumerable possibilities of metal complexes featuring M–X bonds for halide metathesis, the umpolung approach will likely provide further examples of μ_2-carbidos. Curiously, despite the ubiquity of oxidative addition processes in the chemical literature, only two metallacarbynes have arisen through such a process. The first was the breakdown of Grubbs' second generation catalyst attributed oxidative addition step of a putative methylidyne intermediate,[158] and the second being an oxidative addition to platinum(0) of Lalor's halocarbyne by Beck and co-workers.[142]

This Chapter begins by revisiting the dormant work of Beck and co-workers, on the expectation that the d^8-square planar platinum centre would be versatile for the modification of the ligand set. The following section will address this challenge, providing details of synthesis, structural and spectroscopic properties, and theoretical calculations to explore the bonding present. Lastly, the lead metallacarbyne has been found to undergo several ligand substitution reactions to afford a library of metallacarbynes featuring the same core, yet with subtle perturbations through the choice of ligands, to develop a deeper understanding the behaviour of Class B μ_2-carbido complexes.

3.1 Revisiting Beck's Metallacarbyne

Beck's pioneering μ_2-carbido complex [MoPt(μ_2-C)Br(CO)$_2$(PPh$_3$)$_2$(Tp*)] (**3.1a**) is obtained from the oxidative addition of [Mo(≡CBr)(CO)$_2$(Tp*)] the zerovalent platinum reagent [Pt(η-H$_2$C=CH$_2$)(PPh$_3$)$_2$] *via* an observable heterobimetallic μ_2-halocarbyne species [MoPt(μ_2-CBr)(PPh$_3$)$_2$(CO)$_2$(Tp*)] (**2.3c**). The metallacarbyne **3.1a** could be prepared in a matter of hours with simple purification, resulting in an attractive yield of 85% (Scheme 3.1). The feature of **3.1a** that immediately captures attention is the variety of spectroscopic signatures {ν_{CO}, δ_H, δ_C, δ_P, δ_{Pt}}, available for elucidating the underlying bonding. Furthermore, the coupling between the many spin-active nuclei {$^1J_{PtP}$, $^2J_{PP}$, $^1J_{CW}$, $^2J_{CP}$} provides additional information.

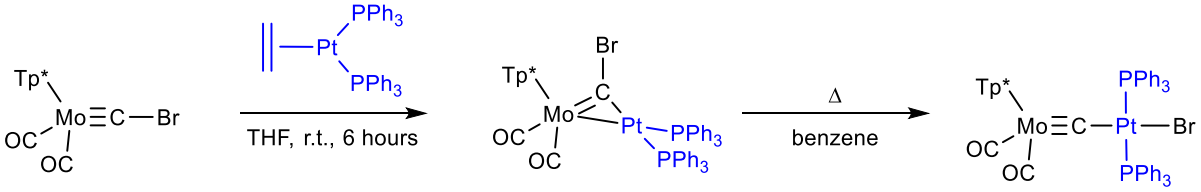

Scheme 3.1: Synthesis of a heterobimetallic class B μ_2-carbido complex by oxidative addition by Beck and co-workers.

These features are desirable, however, minor caveats of Beck's metallacarbyne were identified: (i) use of carcinogenic benzene as a solvent is now discouraged, (ii) the platinum(0) precursor, [Pt(η^2-C$_2$H$_4$)(PPh$_3$)$_2$] requires a multi-step synthesis, and (iii) the tungsten variant was considered as, unlike molybdenum, it presents a spin-active nucleus (^{183}W, I = ½, 14% abundance). Notably, tungsten is a 5d metal and descending group 6 results in stronger M–C bonding and a larger crystal field splitting energy and therefore slower reaction kinetics relative to 4d molybdenum. As with many catalytic studies, the reduction in reaction kinetics for 5d *cf.* 4d metals may provide opportunities to observe or even isolate mechanistically informative intermediates. A revised synthesis was therefore developed, taking these issues into consideration (Scheme 3.2).

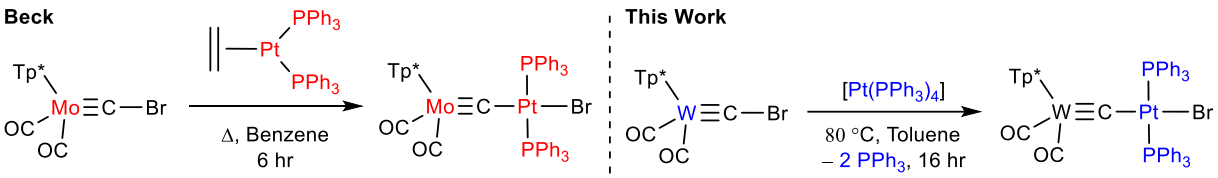

Scheme 3.2: Comparison of synthesis between Beck and co-workers with this work.

3.2 Preparation of the Metallacarbyne Template Framework

Small-scale reactions (~ 0.075 mmol in each reagent) were initially recording explored for the oxidative addition of **2.1b** and found to proceed as expected to provide the new metallacarbyne [WPt(μ_2-C)Br(CO)$_2$(PPh$_3$)$_2$(Tp*)] (**3.1b**). The originally yellow suspension of **2.1b** and [Pt(PPh$_3$)$_4$] in toluene changes to an orange solution upon heating, before a deeper orange develops over 2 hours. The reactions proceeded smoothly and could be scaled efficiently to ~3 g of **2.1b** combined with an equimolar amount [Pt(PPh$_3$)$_4$] (one step from [K$_2$PtCl$_4$]). Employing the platinum(0) source Beck originally used, [Pt(η^2-C$_2$H$_4$)(PPh$_3$)$_2$] (two steps from [K$_2$PtCl$_4$], facilitated a cleaner reaction and has been performed using up to 5 g of **2.1b**. This large-scale protocol was developed following our original publication, and the details are now included in Chapter Nine. [252-254]

The wealth of spectroscopic signatures available for **3.1b** yields dividends immediately, allowing the formation of the metallacarbyne to be monitored either through NMR or infra-red spectroscopies (δ_P or ν_{CO}) where characteristic patterns provided real-time information. Upon completion, the reaction mixture is often orange/brown in colour, with a noticeable lustre if any unreacted [Pt(PPh$_3$)$_4$] remains. Purification is simple, easily scaled, and may be performed aerobically reflecting the robust stability of **3.1b**, even in solution. Removal of solvent *via* rotary evaporation affords an orange residue which can be carefully recrystallised from CH$_2$Cl$_2$/EtOH, however, flash chromatography prior to recrystallisation increases purity with minimal extra time investment.

Oxidative addition reactions to produce **3.1b** were also performed in benzene and THF heated at reflux, to confirm that toluene was the better solvent choice. Intriguingly, each solvent has a different strength. Reactions performed in THF were often marginally faster, despite the lower temperature, at the cost of yield while benzene afforded higher yields than toluene, but like THF provided a second species—a rotational isomer of the parent as evidenced in a range of spectra. For these reasons, toluene continued to be the solvent of choice given a respectable overall yield and formation of a single isomer.

3.3 Structural and Spectroscopic Properties of the Lead Metallacarbyne 3.1b

With the metallacarbyne **3.1b** accessible on large scales, spectroscopic and structural analysis were undertaken to probe the properties of metallacarbyne complexes. As this species is the key precursor for most compounds discussed in this thesis, a detailed discussion of its properties is worthwhile. Particularly, the spectral features of [WPt(μ_2-C)Br(PPh_3)$_2$(CO)$_2$(Tp*)] provide a basis for others discussed later and hence are discussed in more detail than will be necessary for derived compounds, for which only features of note will be discussed. Experimental properties will be discussed first, later supported by findings calculated *in silico*.

3.3.1 Experimental Properties of [WPt(μ_2-C)Br(CO)$_2$(PPh_3)$_2$(Tp*)] (3.1b)

With the exception of EtOH and H_2O, **3.1b** displays remarkable solubility in common solvents. This solubility proves useful for both structural and spectroscopic studies. The molecular structure of **3.1b** as determined by single-crystal X-ray diffraction is shown below (Figure 3.1).

The molecular structure of **3.1b** immediately answers the primary query: does **3.1b** conform to the Class B (metallacarbyne) bonding canonical? Exhibiting a W–C bond length of 1.856(6) Å, the structure corresponds to common tungsten-carbon triple bond lengths previously described for six-coordinate tungsten.[255] Meanwhile the Pt–C bond measures 1.934(6) Å, and although this conforms to a platinum-*sp*-carbon single bond,[255-256] it is a short bond when compared to platinum(II) alkynyls such as the Lappert's *trans*-[PtCl(C≡CPh)(PEt_2Ph)$_2$] (Pt–C: 1.98(2) Å).[257] Comparisons to platinum alkynyls of the form *trans*-[Pt(X)(C≡CR)(PR_3)$_2$] are limited as [PtBr(C≡CMe_2OOH)(PPh_3)$_2$] is the only other bromide structure reported with a marginally longer Pt–C bond (1.990(9) Å).[258] Surveying the CCDC reveals Pt–C bonds in alkynyl complexes are shorter for *trans*-halides (1.949(45) Å) as opposed to a second alkynyl (1.999(40) Å). Platinum carbenes are considerably longer (1.973(52) Å) and highlights that **3.1b** contains significant π-bonding contribution (Figure 3.2), though the vast majority of platinum carbene complexes are of the Fischer type bearing positively mesomeric heteroatom substituents. Although the Pt–C bond length is shorter relative to platinum alkynyls, it is somewhat similar to the small but growing number of platinum metallacarbynes complexes such as [RuPt(μ_2-C)Cl$_4$(L)$_2$] (L = μ-dppm, μ-dcpm, *ca* 1.842–1.852 Å), [RuPt(μ_2-C)Cl$_4$(Py)$_2$(PCy_3)] (*ca* 1.900 Å),[73] or [WPt(μ_2-C)(terpy)(CO)$_2$(Tp*)] (1.938(5) Å) or [WPt(μ_2-C)Cl{Phen–W(CO)$_2$(Tp*)-2}(CO)$_2$(Tp*)] (1.890(14) Å).[159] The most extreme case being [RuPt(μ_2-C)Cl$_4$(μ-dcpm)$_2$] where geometric

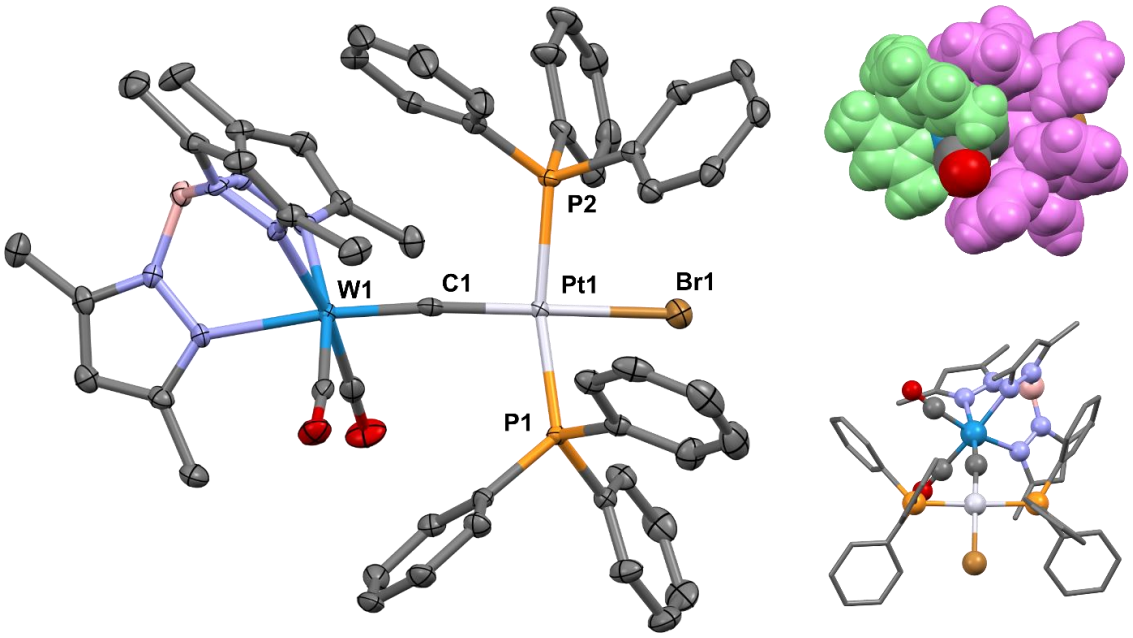

Figure 3.1: Molecular structure of [WPt(μ-C)Br(CO)$_2$(PPh$_3$)$_2$(Tp*)] (**3.1b**) in a single crystal of **3.1b** as determined by X-ray diffractometry. Displacement ellipsoids are drawn at the 50% probability surface with hydrogens omitted for clarity. Insets: a) Space-filling representation highlighting the steric clash of phenyl rings (pink) and the sterically encumbering tris(pyrazolyl)borate (green) ligand, b) Ball and stick representation as viewed down the key molecular linkage (ligands simplified for clarity). Selected bond lengths (Å) and angles (°): W1–C1 1.856(6), C1–Pt1 1.934(6), Pt1–Br1 2.5274(7), Pt1–P1 2.3265(12), Pt1–P2 2.3256(12), W1–C1–Pt1 169.2(3), C1–Pt1–Br1 169.19(15), P1–Pt1–P2 160.28(5).

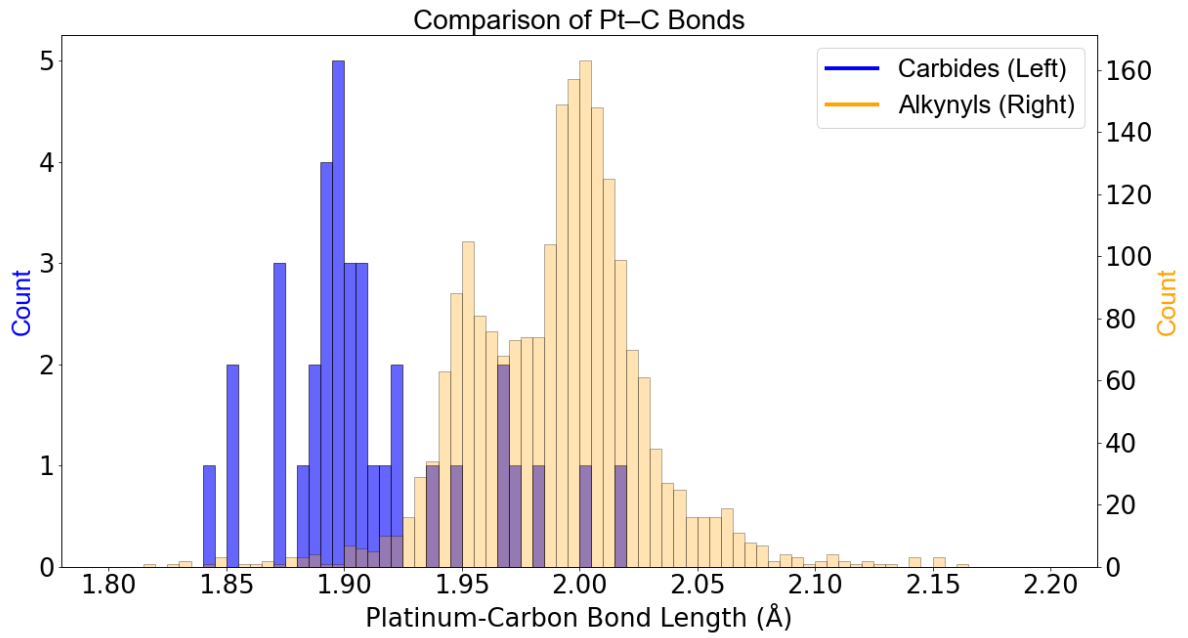

Figure 3.2: Comparison of Pt–C bond lengths between μ$_2$-carbido and alkynyl complexes as harvested from the CCDC. μ$_2$-carbidos (left-axis) are highlighted in indigo and alkynyls in peach (right-axis).

constraints imposed by the phosphine-based A-frame scaffold are likely to impact on the bond lengths. [69, 73] Although a number of ligand substitutions will be discussed subsequently, because **3.1b** contains the facially coordinating Tp* ligand access to similar tungsten-platinum A-frame species for comparison with ruthenium or rhodium species is precluded. [73, 161]

Traversing along the μ_2-carbido linkage, the Pt–Br1 bond is relatively long (2.5274(7) Å) compared with a similar platinum alkynyls such as [Pt(C≡CCMe$_2$O$_2$H)Br(PPh$_3$)$_2$] (2.478(1) Á). This suggests that the μ_2-carbido donor provides a stronger *trans*-influence compared to a regular alkynyl ligand. The platinum geometry is best described as d^8-square planar given similar Pt–P bond lengths and the somewhat bent P1–Pt–P2 angle, although this slight deviation from ideal square planar geometry is likely a response to the juxtaposition of the bulky phosphines (PPh$_3$) with the bulkier Tp* ligand. A clear steric clash is demonstrated through a space-filling representation, where the phenyl ring of P1 occupies a cleft between two pyrazolyl rings on Tp*. This clash and the residence of the phenyl ring inside the cleft as observed in the solid-state that is the likely cause of the rotational isomers in solution—one with the phenyl ring in the cleft and another where the ring remains outside. Returning to the molecular structure, the overall short W≡C–Pt linkage prompts the steric clash PPh and Tp* and likely imparts the bent W–C–Pt spine {W1–C1–Pt1 169.2(3) Å} to accommodate the ligands. Furthermore, the phenyl and pyrazolyl rings appear to be partially stacking. While [Pt(C≡CR)$_2$(L)$_2$)] systems exhibit rotational isomers on different timescales, this depends on the bulk of ligand (L) and the acetylide group (R), [259-262] so it is unsurprising that **3.2b** (a more encumbered example) exhibits two rotamers.

The formulation of Beck's metallacarbyne [MoPt(μ_2-C)Br(CO)$_2$(PPh$_3$)$_2$(Tp*)] (**3.1a**) rested on spectroscopic data alone. For comparative purposes, crystals of **3.1a** were grown and crystallographic analysis found **3.1a** exhibits many similar features to that of its tungsten counterpart **3.1b**, consistent with octahedral molybdenum and tungsten having comparable covalent radii of 1.54(5) and 1.62(7) Å, respectively (Figure 3.3). [85] The triple and single bonds confirm that Beck's species can be described as a metallacarbyne complex, while the Pt geometry is also d^8-square planar and the Pt–Br bond is elongated (2.5448(3) Å) as a consequence of the pronounced *trans* influence of the μ_2-carbido ligand. The previously reported spectroscopic data were verified in Beck's original C_6D_6 solvent system in addition to measurements in $CDCl_3$ to maintain consistency with this work. Key NMR signals remained essentially invariant between solvents the most salient being the carbido resonance which appears further downfield relative to **3.1b** (δ_C: 335.7 *cf.* 317.2 **2.3b**). The ^{195}Pt{^{1}H} resonance was identified at a similar chemical shift to the tungsten analogue (–3810 *cf.* –3821) with identical $^1J_{PtP}$ couplings (3200 Hz). Other than now

completing the full characterisation of **3.1a**, the molybdenum metallacarbyne was returned to when necessary, given the advantages of tungsten presented previously.

The convenient solubility of **3.1b** allowed strong signal-to-noise observation by NMR spectroscopy (Figures 3.4–3.7). By focusing on a single rotational isomer, the ^{1}H NMR spectra indicated that the molecule retained C_s symmetry. In contrast, ^{31}P{^{1}H} spectroscopy proved more informative: resonances of the phosphines were manifest as two second-order ($^{2}J_{PP}$ = 443 Hz, $\Delta\delta_P$ = 4.06) roofed doublets, indicative that the phosphines are chemically inequivalent in solution on the ^{31}P NMR timescale (Figure 3.6) giving rise to an **AB** system.[*********] The large coupling constant between the inequivalent phosphorus nuclei, further confirms a *trans* relationship around platinum.[†††††††] The presence of rotational isomers, each giving rise to a distinct **AB** pattern with further couplings for ^{195}Pt isotopomers (^{195}Pt, I = ½, 33% abundance), initially confounded the

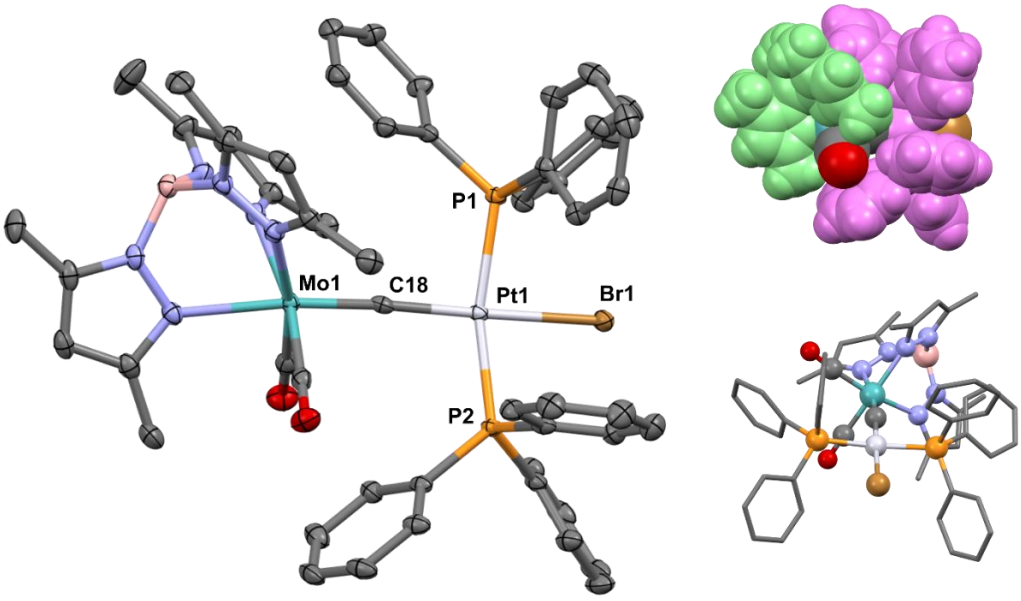

Figure 3.3: Molecular structure of [MoPt(μ-C)Br(CO)$_2$(PPh$_3$)$_2$(Tp*)] (**3.1a**) in a single crystal of **3.1a**·3(OEt$_2$) as determined by X-Ray Diffractometry. Ellipsoids are drawn at the 50% probability surface with hydrogens and Et$_2$O solvent molecules omitted for clarity. Insets: a) Space-filling diagram highlighting the steric clash of phenyl rings (pink) and the sterically encumbering *tris*-pyrazolylborate (green) ligand; b) Ball and stick representation as viewed down the key molecular linkage (ligands simplified for clarity). Selected bond lengths (Å) and angles (°): Mo1–C18 1.828(3), C1–Pt1 1.951(3), Pt1–Br1 2.5448(3), Pt1–P1 2.3267(6), Pt1–P2 2.3263(6), Mo1–C18–Pt1 173.97(15), C1–Pt1–Br1 177.09(7), P1–Pt1–P2 162.40(2).[‡‡‡‡‡‡‡‡‡]

[*********] Chemical shifts for significantly roofed resonances are quoted taking into account an appropriate weighting of the individual signals. [263]

[†††††††] *Cis*-$^{2}J_{PP}$ couplings for chemically inequivalent phosphorus nuclei in *pseudo*-square planar *cis*-[PtXY(PR$_3$)$_2$] complexes are typically of the order of 5–40 Hz. [264]

[‡‡‡‡‡‡‡] Crystal originally grown and studied by x-ray diffraction by Dr. Richard L. Cordiner (2008). Remained unpublished until coupled with this work. Credit is attributed to Dr. Cordiner for this structure and is only used for discussion purposes

identification of **3.1b** (Figure 3.8 and 3.9). Thus the obtention of a single, presumably thermodynamic, rotamer for samples prepared in refluxing toluene somewhat expedited the analysis.

Unlike the $^{31}P\{^{1}H\}$ NMR spectrum, the primary triplet resonance observed in the $^{195}Pt\{^{1}H\}$ spectrum identifies that the two phosphorus nuclei are equivalent on the ^{195}Pt timescale (or have coincidentally equal chemical shifts). This contrasts with the expected doublet of doublets if the phosphines were chemically inequivalent as was suggested by the $^{31}P\{^{1}H\}$ NMR data. Because the Lamour frequency is dependent on the gyromagnetic ratio of the nucleus under consideration (108.4 MHz.rad/T for ^{31}P, 58.0 MHz.rad/T for ^{195}Pt), each nucleus has a different frequency of observation and thus the response may differ between ^{31}P and ^{195}Pt nuclei. The observed coupling of the ^{195}Pt triplet ($^{1}J_{PtP}$ = 3187 Hz) corresponds to the two couplings derived from resonances for the diastereotopic phosphorus nuclei in the $^{31}P\{^{1}H\}$ spectrum ($^{1}J_{PtP}$ = 3178, 3200 Hz).

Finally, the μ_2-carbido resonance is the most significant, yet for practical reasons, most elusive spectral feature, given that ^{13}C-enrichment (1.1% natural abundance; 99% ^{13}CO *ca* AU$65000/mol) of the metal carbonyl precursor was considered prohibitively expensive. Fortunately, the reasonable solubility of **3.1b** allowed identification of the carbido chemical shift within hours for a somewhat concentrated sample of **3.1b** in $CDCl_3$. Pursuit of the informative spin couplings (^{183}W, ^{195}Pt, ^{31}P) however required an extended acquisition (25°C, 151 MHz, 18000 scans, ~15 hours). The primary carbido resonance is observed as an apparent triplet (δ_C: 317.2; $^{2}J_{CP}$ = 8 Hz)[§§§§§§§§§] with the true double doublet fine structure not being resolved due to the two $^{2}J_{PC}$ couplings being identical within experimental limits. Characteristic of μ_2-carbido nuclei in general, this resonance appears to remarkably high frequency compared to typical organic molecules owing to the dominant paramagnetic contribution to the shielding caused by the unsaturated MCM spine. Within the range of reported μ_2-carbido chemical shifts (*ca* 350–500 ppm),[1] however, it is towards the high field end of the range. The carbonyl resonance shifts to higher frequency of that of the terminal halocarbyne precursor (δ_C: 230.7 *cf.* 221.9 **2.1d**) though there is clear correlation between CO and infrared data (ν_{CO}: 1945, 1854 *cf.* 1994, 1905 cm^{-1} for the precursor). All other features of the $^{13}C\{^{1}H\}$ NMR spectra remain unmarkable other than to note that they reflect the C_s symmetry of resonances associated with the $HB(pzMe_2)_3W$ cage, a recurrent feature in later work.

§§§§§§§§§ Visual line-shape analysis of the signal suggests a non-binomial intensity profile that is more consistent with a non-resolved double doublet.

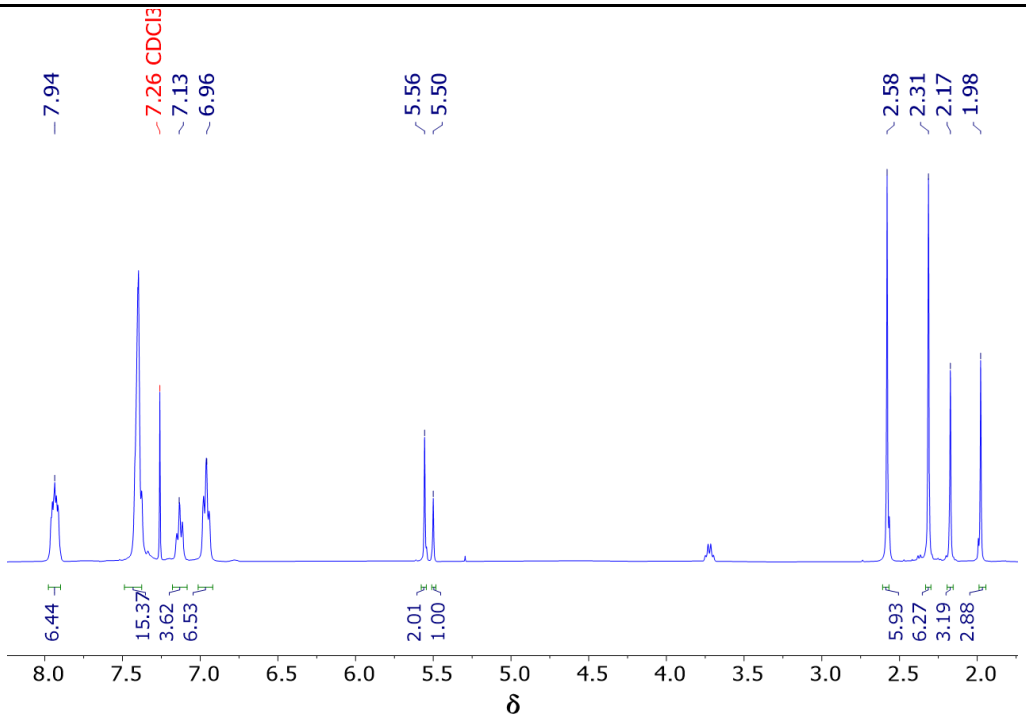

Figure 3.4: ^{1}H NMR spectrum of [WPt(μ-C)Br(PPh$_3$)$_2$(CO)$_2$(Tp*)] (**3.1b**). Note: as this species can also exist as a mixture of rotational isomers, an origin-dependent doubling of the above pattern is observed in varying ratios for different samples.

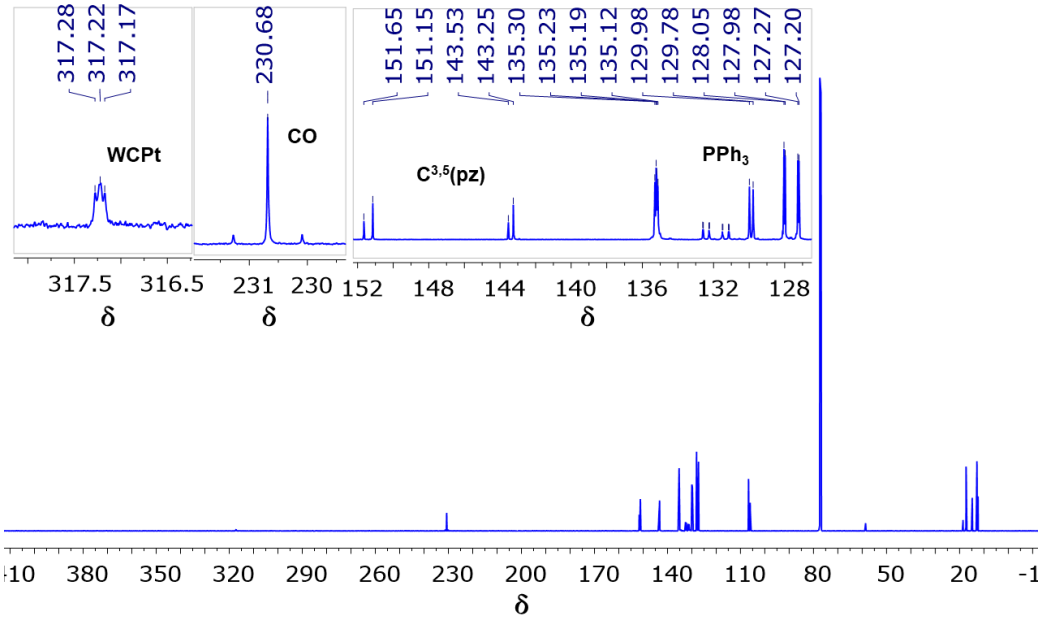

Figure 3.5: ^{13}C{^{1}H} NMR spectrum of [WPt(μ-C)Br(PPh$_3$)$_2$(CO)$_2$(Tp*)] (**3.1b**). Note: as this species can also exist as a mixture of rotational isomers, an origin-dependent doubling of the above pattern is observed in varying ratios for different samples.

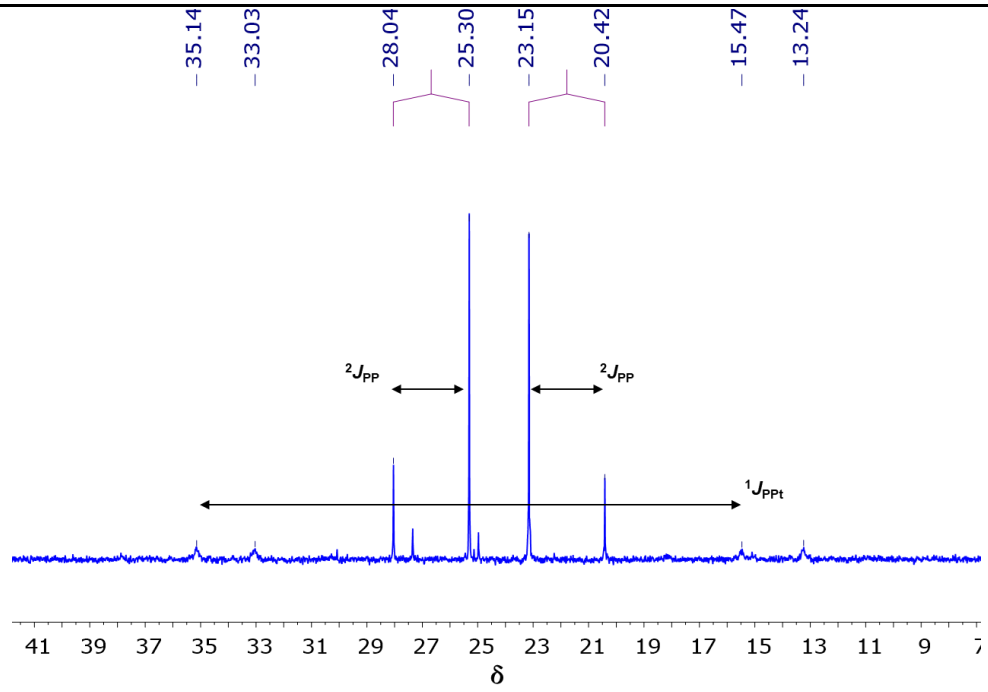

Figure 3.6: $^{31}P\{^1H\}$ NMR spectrum of $[WPt(\mu\text{-}C)Br(PPh_3)_2(CO)_2(Tp^*)]$ (**3.1b**). Signals appear as roofed doublets from second order effects. Note: as this species can also exist as a mixture of rotational isomers, a doubling up of the above pattern is observed in varying ratios.

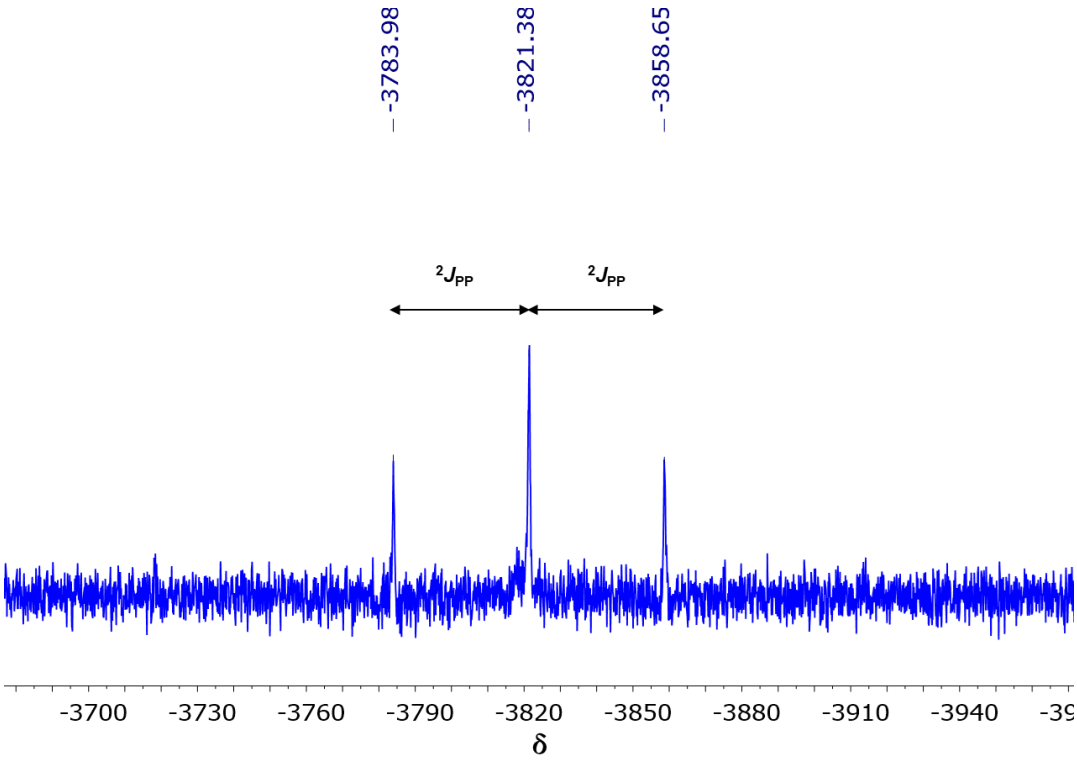

Figure 3.7: $^{195}Pt\{^1H\}$ NMR spectrum $[WPt(\mu\text{-}C)Br(PPh_3)_2(CO)_2(Tp^*)]$ (**3.1b**).

The rich array of data acquired for **3.1b** serves to exemplify those to emerge throughout this thesis, not least of which is the caveat of the repeated observation of rotational isomers about the W–C–Metal spine which complicated interpretation of data for **3.1b** (Figures 3.8 and 3.9). A close to 1:1 ratio of rotamers was observed when the synthesis of **3.1b** was performed in benzene. Repeating the reaction in other solvents with different polarities or reflux temperatures ($CHCl_3$, THF) also resulted in rotational isomers in differing ratios. These rotamers are attributed to restricted rotation about the Pt–C bond given similar spectroscopic features {^{1}H, ^{13}C, ^{31}P, ^{195}Pt and ν_{CO}} where the *trans*-phosphines of platinum(II) serve to produce a 'gearlike' plane of the phenyl ring occupying the Tp* cleft (Figure 3.3). The kinetic distribution of these two rotamers may reflect the impact of solvent polarity ($CHCl_3$, THF) on reaction coordinates to predispose product formation. This would not however account for the difference in product distribution between benzene ($\varkappa$ = 2.27) and toluene ($\varkappa$ = 2.38) and it may therefore be surmised that the elevated temperature of refluent toluene (>111 °C) allows the kinetic rotamer distribution to evolve to the thermodynamically preferred rotamer.

To study the inferred interconversion of rotational isomers, variable temperature NMR studies were conducted utilising d_8-toluene as toluene offers a wide liquid temperature range while ensuring enough material is dissolved. The sample of **3.1b** studied was prepared as a mixture of rotational isomers that arise using benzene as the solvent during synthesis. Standard ^{1}H and $^{31}P\{^{1}H\}$ NMR experiments were undertaken at intervals of 10 °C from –60 to 70 °C: the practical limit of the spectrometer in standard configuration (Figure 3.10 and 3.11). Beginning with ^{1}H, many changes in signal morphology are recorded. Lowering the temperature results in pyrazolyl methyne environments becoming equivalent while the methyl signals do not; the phenyl resonances broaden beyond useful analysis. Elevating the temperature (–20 °C) first results in resolution of several chemically inequivalent environments consistent with isomers in solution, however, resonances broaden and shift, although coalescence is not completely reached by 70 °C. It is likely even higher temperatures would achieve coalescence and hence equivalence of rotational isomers, yet the temperature would be close to boiling point of d_8-toluene and therefore endanger the spectrometer. While species **3.1b** is certainly fluxional on the ^{1}H NMR timescale, the observed changes are minor and over such a large range it is difficult to draw conclusions about the identity of species in solution. Lack of change is apparent in the $^{31}P\{^{1}H\}$ NMR spectra, a consequence of the differing timescale compared with ^{1}H. By comparing low and high temperatures against the control, relative integrations of each isomer barely change (*ca* ±10%), highlighting that species **3.1b** is not a sufficiently dynamic system over a suitable temperature range.

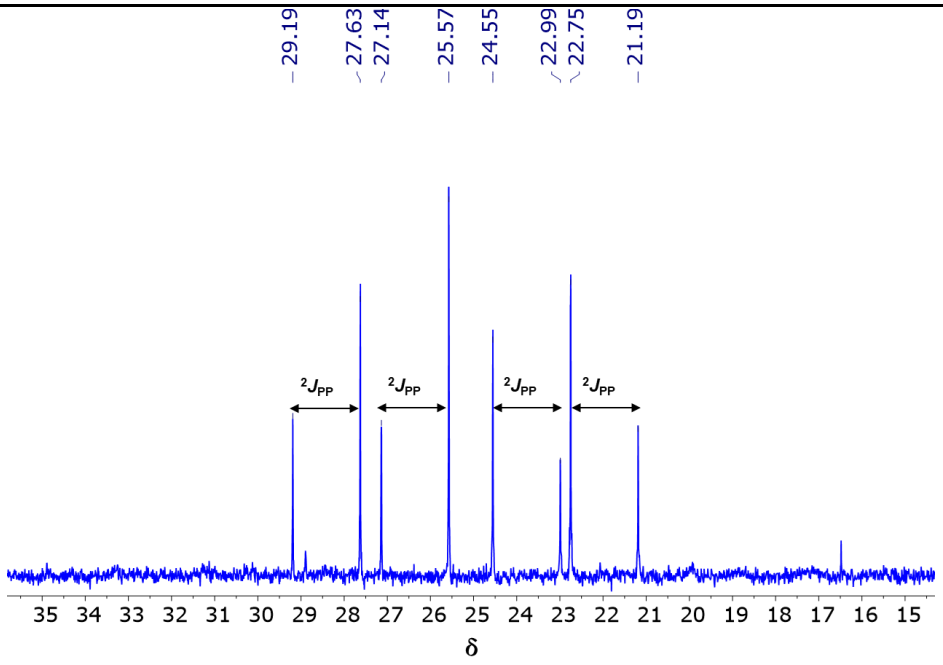

Figure 3.8: $^{31}P\{^1H\}$ NMR spectrum showing rotational isomers of $[WPt(\mu\text{-}C)Br(CO)_2(PPh_3)_2(Tp^*)]$ (**3.1b**) from a sample prepared in refluent benzene.

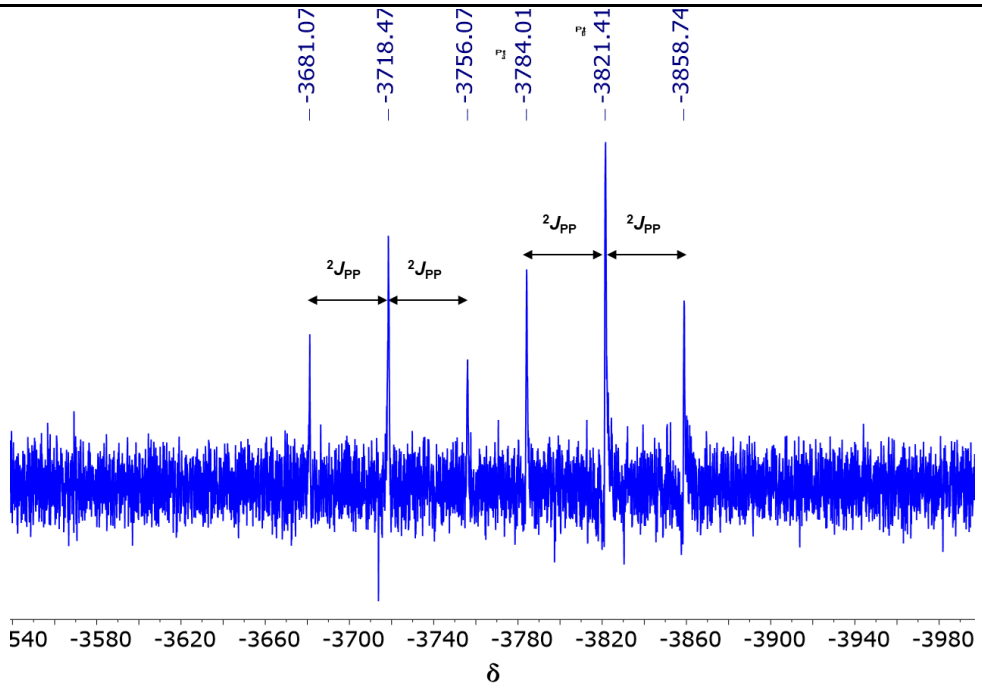

Figure 3.9: $^{195}Pt\{^1H\}$ NMR spectrum showing rotational isomers of $[WPt(\mu\text{-}C)Br(CO)_2(PPh_3)_2(Tp^*)]$ (**3.1b**) from a sample prepared in refluent benzene.

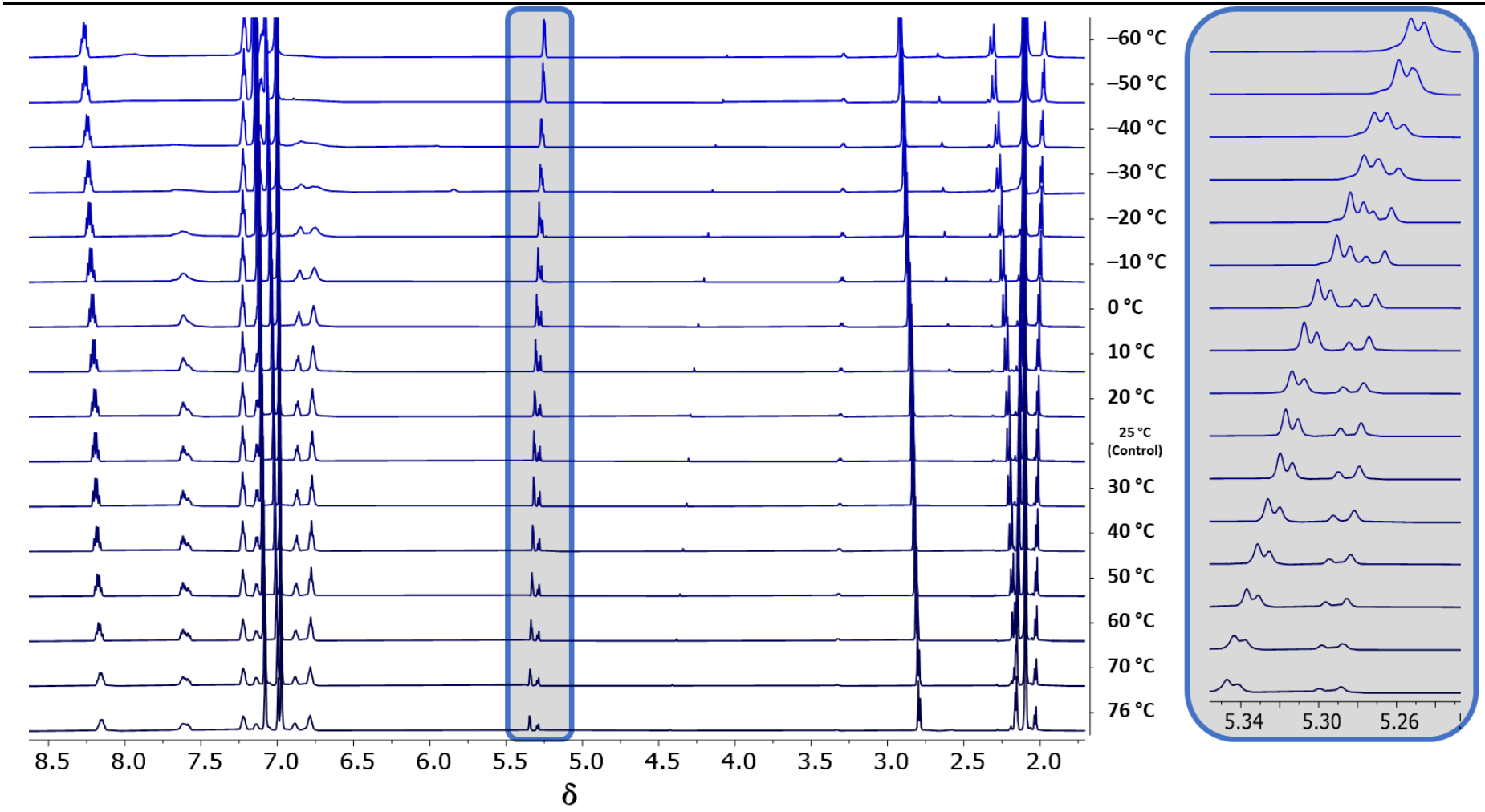

Figure 3.10: Variable temperature ^{1}H NMR spectra of a rotormeric mixture of [WPt(μ-C)Br(PPh$_3$)$_2$(CO)$_2$(Tp*)] (**3.1b**, d_8-toluene, 700 MHz). Lower temperatures (blue) result in one compound being apparent, whilst at higher temperatures (black) discreet resonances for the two rotamers are resolved on the ^{1}H NMR timescale. Inset: Focus on the pyrazolyl methine resonances merging at lower temperature .

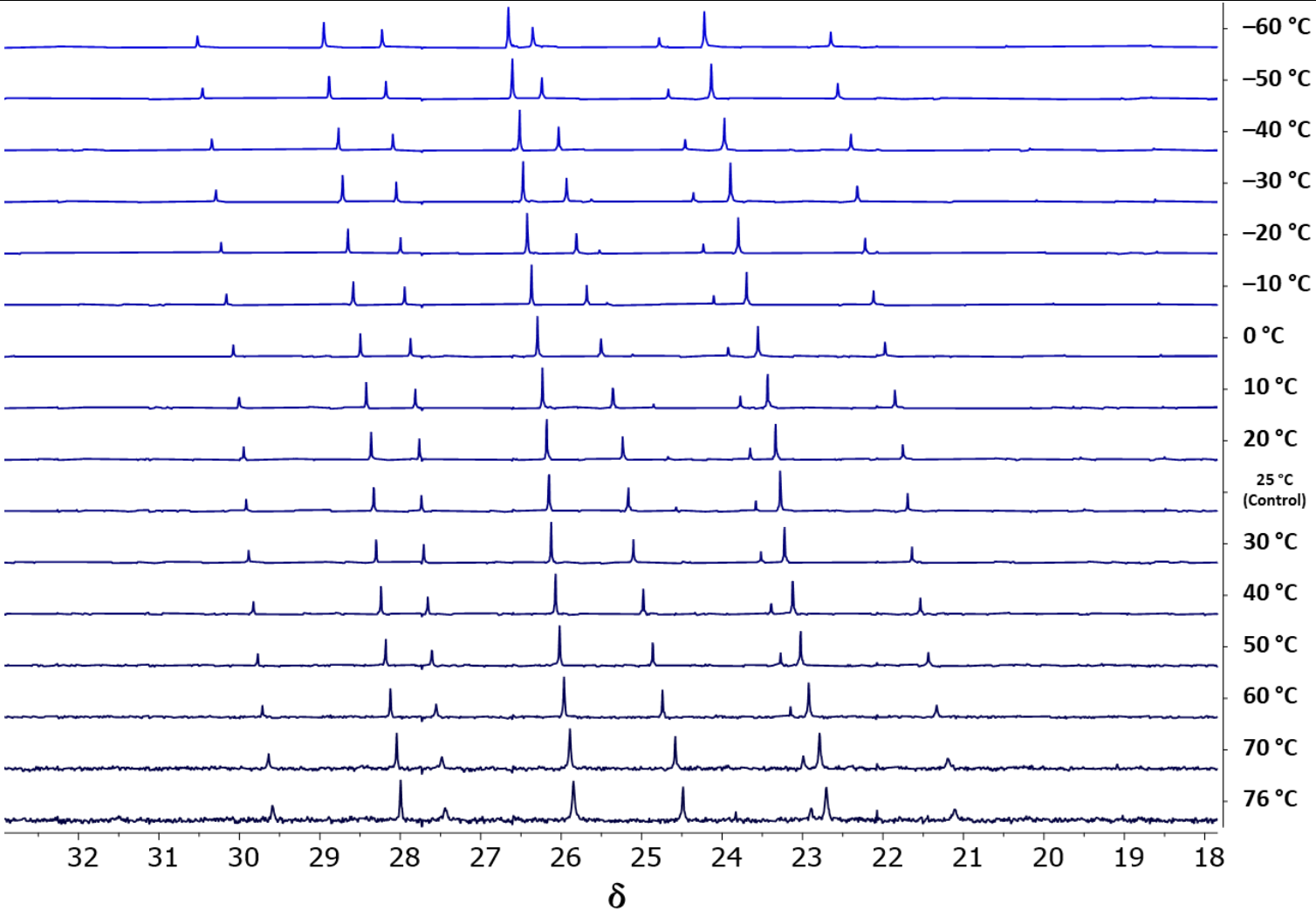

Figure 3.11: Variable temperature $^{31}P\{^{1}H\}$ NMR spectra of a rotormeric samples of [WPt(μ-C)Br$(PPh_3)_2(CO)_2$(Tp*)] (**3.1b**). Minor chemical shifts of resonances occur with temperature, however, relative ratios barely change on the ^{31}P timescale.

While the reason for isomer formation is difficult to establish, variable temperature NMR spectroscopy shows interconversion between isomers is unlikely over the temperature range used during synthesis in refluent benzene (*ca* 80 °C), chloroform (61 °C) or tetrahydrofuran (66 °C). Therefore, the production of a single isomer in toluene is likely a consequence of the formation step. Considering the solvents used, polarity is unlik3.ely the cause as both toluene and benzene are non-polar, while $CHCl_3$ ($\kappa = 4.81$) and THF ($\kappa = 7.58$) have only modest additional differences to account for varying mixtures.

The inability of the rotamers to interconvert at moderate temperatures would appear to originate from the topology of the *tris*-pyrazolylborate ligand. One of three Tp* clefts between pyrazolyl rings straddles the W≡C–Pt spine such that ligands coordinated to platinum cis to the C–Pt bond may nestle within or without the pocket. The positioning of ligand periphery in this cleft has been noted by Templeton and given the inter-ligand steric clutter in many compounds throughout this thesis this may be expected to influence further chemistry. The solvent used to produce **3.1b** was selected to be toluene purely to facilitate interpretation of spectra provided by using a single isomer.

3.3.2 Theoretical Properties

There has been very minimal discussion in the μ_2-carbido literature of theoretical calculations being performed to date, especially in class B. The first computational study of (Class A) carbido complexes actually predated their isolation.[22] Subsequently, interrogation of the Class A dirhenium complex $[Re_2(\mu\text{-}C)(CO)_4(Cp)_2]$ indicated shortcomings in the over-simplified allene analogy,[17] not least the remarkably low barrier to rotation about the Re=C=Re spine. Computational analyses have since been provided for dirhodium carbidos of Classes A,[61, 128, 161, 265-266] and D.[40-41, 129] Frenking has considered Class C carbidos leading to the conclusion that these are best considered as polar covalent donor-acceptor interactions akin to CO and isonitriles.[23-24, 26] Computational interrogation of Class B carbidos was, prior to this work, limited to the complex $[WNi(\mu\text{-}C)Cl(CO)_2(PEt_3)_2(Tp^*)]$,[119] leaving Class B carbidos, the subject of this thesis, somewhat under-studied in terms of an understanding of the bonding. This omission is now addressed.[**********]

The solid-state structure of **3.1b** provided initial atomic coordinates prior to peripheral ligand pruning in the interests of computational economy: PPh_3 was replaced PMe_3 with the appreciation that this would increase the basicity of platinum while replacing a bromide with chloride would be

[**********] Unless otherwise stated, computational analyses were generally performed at the ωB97X-D/6-31G*/LAN2Dζ (>Kr)/gas phase level of density functional theory implemented within the *SPARTAN20*® suite of programs. For details see Chapter Nine.

expected to marginally decrease this. Superficially, removing methyl groups from pyrazolyl rings in favour of hydrogens does not dramatically impact the electronic nature of the tungsten beyond slightly lifting the near degeneracy of the two retrodative orbitals directed towards the carbido due to the unequal intrusion of two 3-methyl groups on one of these. These modifications provide the hypothetical‡‡‡‡‡‡‡‡‡ complex [WPt(μ-C)Cl(PMe_3)$_2$(CO)$_2$(Tp)] (**3.1***) as a satisfactory model for cost-effective calculations with the reduction in the number of remote substituents which are not expected to contribute to the frontier orbitals of interest. [149]

Lin and Marder previously conducted a benchmark study on the influence of ligand (R) in species [*trans*-PtRCl(PMe_3)$_2$], specifically focusing on σ-boryl ligands, but also included the parent hydrocarbyls C_2H_5, $CH{=}CH_2$ and C≡CH. [267] They concluded that the σ-donor strength of the R group is, not surprisingly, the largest contributor in the determining ligand *trans*-influence as measured by Pt–Cl bond length, yet strong π-acceptor ligands also contribute to bond elongation. These results provide context for interpreting features of **3.1b** given the presumed analogy between alkynyl and alkylidynyl ligands that will be explored throughout this thesis. For consistency with the results of Lin and Marder's study, calculations were performed as per their specifications (DFT: B3LYP/6–31G*/LANL2Dζ), in addition to the preferred level of theory used in this work (DFT: ωB97X-D/6–31G*/LANL2Dζ).‡‡‡‡‡‡‡‡

Given the original coordinates obtained from the solid-state structure, the theoretical complex **3.1*** was found to optimise to a superficially similar geometry to that determined experimentally for **3.1b**. Subtle variations become apparent upon closer inspection. Firstly, both W≡C and Pt–C bonds contract in **3.1*** (1.827 and 1.921 Å *cf.* 1.856(6) and 1.934(6) Å, respectively), likely in part due to the increased σ-donor capabilities of PMe_3 but also perhaps reflecting less steric congestions due to PMe_3 being considerable smaller (θ^T = 118 °) than PPh_3 (θ^T = 145 °).[268] Nevertheless, the size reduction in pyrazolylborate and phosphine ligands surprisingly provides little alleviation of the steric clash as described in the real species, noting the methyl group of the reduced phosphine remains nestled in the pyrazolyl ring cleft. Indeed, it will become increasingly apparent throughout the thesis that this nestling of groups between two proximal pyrazolyls is most likely attractive in nature, justifying the use of a dispersion-corrected functional (ωB97X-D). It is likely for this reason that the W≡C–Pt linkage partially but not completely straightens out (174° *cf.* 169.2(3)°) to allow one methyl group to occupy the cleft. Non-linear M≡C–R geometries are commonly encountered

‡‡‡‡‡‡‡‡‡ Because Lalor's halocarbyne syntheses fail for unsubstituted pyrazolylborate ligands, this and related model complexes employed in this thesis will remain hypothetical until this hiatus is resolved.

‡‡‡‡‡‡‡‡ Head-Gordon's range-separated functional ωB97X-D is capable of capturing both short and long range interactions. This approach better accounts for long range dispersion (London forces) non-covalent effects.

in conventional carbyne chemistry and have invariably been attributed to solid-state crystal packing effects.

The intimate nature of the bonding within the W≡C–Pt spine follows from a consideration of the frontier orbitals (Figure 3.12). The HOMO is essentially irrelevant in that it is primarily tungsten-based, being orthogonal to the W···Pt vector and responsible for W–CO retrodonation. The HOMO-1 and HOMO-2, however, constitute the two π-components of the WC multiple bond and are π-antibonding with respect to the Pt–C bond. Contrasting this is the LUMO, which is substantially localised on (the 16-electron) platinum, evenly above and below the square planar geometry—a plausible place for nucleophilic attack (Fukui atom condensed index for nucleophilic attack f^-(Pt) = 0.14). An intriguing feature of this hypothetical complex is the somewhat short Pt–C 'single' bond and delving deeper into the molecular orbital manifold reveals that HOMO–6 involves continuous constructive overlap between orbitals of π-symmetry along the W≡C–Pt spine. Thus not only does HOMO–6 most likely contribute to Pt–C bond contraction, it suggests the simple σ+2π carbyne view of the W≡C multiple bond is an over-simplification. Furthermore, the calculated Löwdin bond orders between W–C (2.275) and Pt–C (1.247), suggest a degree of Pt–C multiple bonding, perhaps at the expense of W≡C bonding. This mesomeric compromise of metal-carbon multiple bonding by π-donor substituents is best-known for aminocarbynes for which zwitterionic azavinylidene canonical descriptions are often advanced. [169, 269]

Computational results for **3.1*** not only explain some intriguing phenomena observed experimentally, but also allow comparison to Lin and Marder's benchmark study of more conventional organometallic ligands (Table 3.1). The shortest Pt–C bond length is found for the theoretical metallacarbyne **3.1***, even shorted than that of the parent alkynyl ligand (1.920 Å C≡[W] *vs* 1.968 C≡CH), suggesting carbyne fragments may involve stronger π-bonding than typical alkynyls. Similarly, the Pt–Cl bond length *trans* to the carbido is longer than that of the alkynyl complex (2.517 Å C≡W *vs* 2.448 Å C≡CH), indicating a more pronounced *trans*-influence of carbidos compared with alkynyls. [267] The degree of elongation falls between that of the σ-ethenyl and σ-ethyl ligands (*ca* 2.510 Å CH=CH_2 and 2.531 Å CH_2CH_3), a notably result given these σ-donors are known for their significant *trans* influence.

The conclusion that the *trans*-influence of the carbyne fragment is greater than that of the alkynyl ligand is attended by caveats: (i) a clear steric impact is imposed on the platinum geometry of **3.1***, not present in the slender cylindrical alkynyl ligand; (ii) among σ-organyls in general, σ-alkynyls exhibit relatively weak *trans* influences which have been interpreted along with ideas from Muir and Muir, [270] as ligands entering into modest π-retrodonation thereby stabilising d^8-platinum

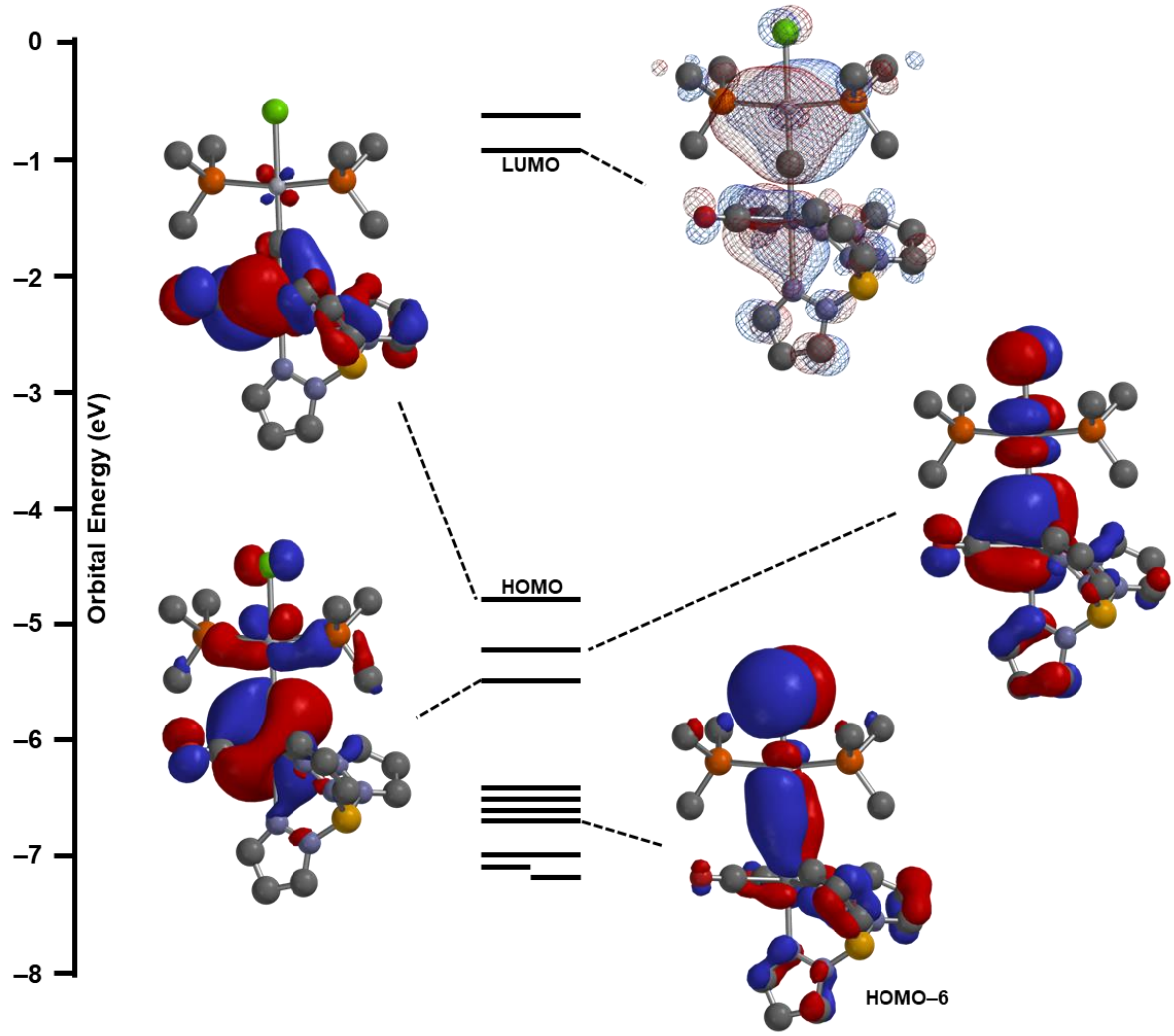

Figure 3.12: Frontier molecular orbitals of interest for theoretical complex *trans*-[WPt(μ-C)Cl(CO)$_2$(PMe$_3$)$_2$(Tp)] (**3.1***). DFT:B3LYP/6–31G*/LANL2Dζ.

Table 3.1: Calculated geometric parameters[a] for the complexes *trans*-[Pt(R)Cl(PMe$_3$)$_2$].

R	C–Pt [Å]	Pt–Cl [Å]
CH_2CH_3 [b]	2.093	2.531
$CH{=}CH_2$ [b]	2.019	2.510
C_6H_5 [b]	2.035	2.496
C≡CH [b]	1.968	2.448
C≡W(CO)$_2$(Tp) (**3.1***)	1.920	2.517

[a]DFT:B3LYP/6–31G*/LANL2Dζ. [b]Result from Lin and Marder. [267]

given the presence of a *trans*-coordinated π-donor chloride;§§§§§§§§§§ (iii) a limitation on the opportunities for tuning the energies of molybdenum or tunsten orbitals given the current synthetic protocol. As seen for more conventional carbyne complexes,[271] a continuum of π-basicity should emerge if variations in the '(Tp)$(CO)_2$W≡C' fragment were achievable.

A frequency calculation is a requisite final step to confirm validity of a model as a local energetic minimum. As **3.1*** contains carbonyl ligands, the predictions that result from a calculation frequency (ν_{CO}) provide extra information and are useful when compared with data for the experimental species (**3.1b**). Calculating the frequencies of the model **3.1*** suggest symmetric (ν_{CO}: 1930 cm^{-1}) and asymmetric (ν_{CO}: 1868 cm^{-1}) carbonyl stretches, mapping relatively close†††††††††† to those for the real **3.1b** (*ca* ν_{CO} 1945 and 1854 cm^{-1}) considering the smaller, more basic phosphines and *trans*-chloride over bromide. Furthermore, the frequency calculation predicts an asymmetric M≡C–M' stretching frequency—a measurement common for early Class A species (See Chapter One). Similar data have yet to be acquired or identified for Class B carbido complexes. Given the asymmetry of the Class B linkage compared to that of class A (M≡C–M' *vs* M=C=M), it may be expected metallacarbyne vibrations would be easier to detect, notwithstanding that the electronegativity of carbon (Pauling: 2.55) *vs* the relevant transition metals (Pauling: 2.16-2.54) means that oscillating bonds will be of low polarity and unlikely to give rise to intense absorptions.‡‡‡‡‡‡‡‡‡‡ Furthermore, these low intensity absorptions are expected to occur in an area ($\nu_{M\equiv C-M'}$ ~1000 cm^{-1}) populated by numerous and comparatively intense fingerprint modes associated with the Tp* co-ligand. A collection of similar complexes in conjunction with computational evaluation of frequencies should prove useful as such data may assist in identification and interpretation of these key vibrational modes. The geometric model for **3.1*** predicts a vibrational mode at 958 cm^{-1} ($\nu_{W\equiv C-Pt}$) while that for the computationally pruned model

§§§§§§§§§§ More superficially, simply considering the pKa values of ethane (50), ethene (45), benzene (43) and ethyne (25) provides an immediate indication of the relative σ-donor capacity that may be anticipated for various types of organyl.

†††††††††† Anharmonic corrections are applied to the raw frequencies arising from calculations. These scaling factors are empirically derived from test libraries of model compounds that rarely involve vibrational modes in the metal carbonyl region. For the ωB97X-D/6-31G* level of theory the National Institute of Standards and Technology (https://cccbdb.nist.gov/vsfx.asp) recommends 0.9485, while *SPARTAN20*® employs 0.9420 as the default scaling factor. It should be noted that a single scaling factor is in any event unlikely to be satisfactory for the full spectral range, however for interpreting trends rather than absolute quantities within a small frequency range with the same level of theory, there should be a degree of error cancellation. Throughout this thesis, reported frequencies are based on a scaling factor of 0.9420.

‡‡‡‡‡‡‡‡‡‡ Raman spectroscopy has been under-utilised for the study of bimetallic carbido complexes, being limited to a single Class D example and its Class A precursor. Given the delocalisation of electron density along MCM spines, it might be expected that vibrations would perturb the polarizability, making Raman or Resonance Raman spectroscopy particularly informative.

bromide complex **3.1*Br** has $\nu_{W\equiv C-Pt}$: 1024 (w) and 1031 (m) cm^{-1}.######### Measurement of the real **3.1b** complex reveals a weak absorption (ATR: *v*: 1094 cm^{-1}) which was therefore assigned as the metallacarbyne vibrational mode ($\nu_{W\equiv C-Pt}$) supported by computational results, being the first assigned mode for a Class B complex. In isolation this datum says little, however this vibrational data will be useful when more examples are identified, where regrettably, no other mode was unequivocally identified in this Thesis. The value provided by computations performed *in silico* in this section affirm the technique as an invaluable tool. While examples of computational enquiry in the field of μ_2-carbido complexes continues to grow, [22-24, 26, 40-41, 61, 119, 128-129, 161, 266] results described above provide a benchmark for further studies of new examples that arise in Class B (*vide infra*).

3.4 Ligand Substitution Reactions

The successful large-scale manufacture of the metallacarbynes **3.1a** and **3.1b** affords an opportunity to potentially expand the previously somewhat narrow range of metallacarbynes. Although a variety of ligand substitutions of the coordinatively unsaturated Class A complex $[Rh_2(\mu\text{-}C)Cl_2(PPh_3)_4]$ have been reported, very few examples of ligand substitution reactions of Class B carbido complexes, once formed, have been reported, being limited to two reports (Scheme 3.3). In the case of Templeton's complex, both the molybdenum and iron present thermally stable coordinatively saturated 18-electron centres such that UV irradiation is required to replace iron-bound carbonyl ligands with either PMe_3 or CN′Bu. In contrast, Reinholdt's Class B complex has both the ruthenium and platinum 16-electron centres that allow facile ligand substitution, most likely via associative pathways. The complexes **3.1** are therefore intermediate in possessing one substitution-inert centre (tungsten or molybdenum) in combination with a 16-electron platinum centre for which both associative and dissociative pathways are potentially available.§§§§§§§§§§ Both the bromide and bulky triphenylphosphine ligands are in principle replaceable, as will be shown below. This section will address the initial expansion of metallacarbynes stemming from species **3.1a** and **3.1b** with particular emphasis on **3.1b** to exploit both the spin-active ^{185}W nucleus and the slower kinetics of tungsten.

######### These vibrational modes are not entirely 'pure' $\nu_{W\equiv C-Pt}$, rather the stretching is the predominant contributor to the more complex molecular vibration.

§§§§§§§§§§ The complexes **3.1** and their palladium congeners (See Chapter Six) slowly under various conditions loose phosphine to provide halide bridged tetrametallic species $[M_2M'_2(\mu\text{-}C)_2Br_2(PPh_3)_2(Tp^*)_2]$ (M = Mo, W; M' = Pd, Pt), supporting slow phosphine dissociation may occur.

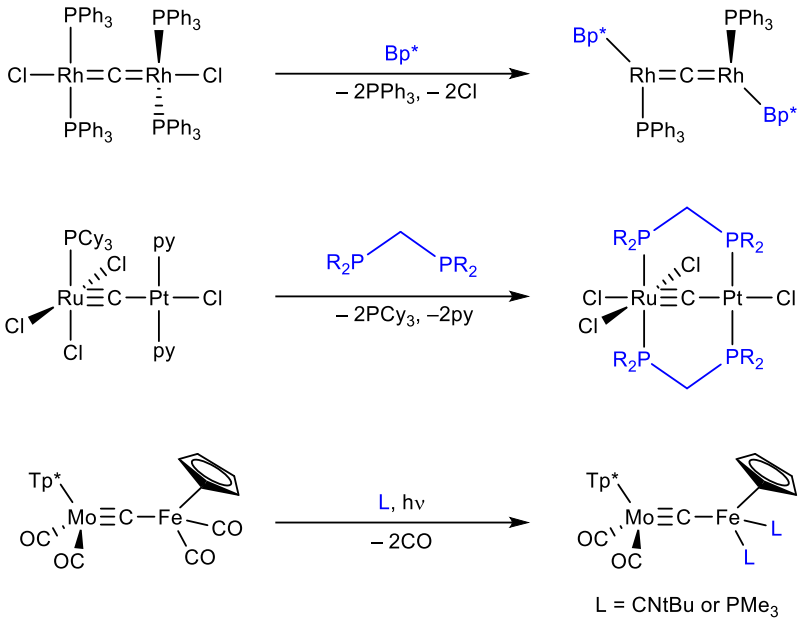

Scheme 3.3: Representative ligand substitutions of μ_2-carbido complexes.

3.4.1 Halide Substitution

It is common practice in coordination chemistry to activate metal halide complexes by abstraction of a halide. This may provide a coordinatively unsaturated metal centre, *e.g.*, $[RuCl(dppe)_2]PF_6$ obtained from $[RuCl_2(dppe)_2]$ and $NaPF_6$,[272] or a complex in which a weakly coordinating anion reversibly coordinates to the site vacated by the halogen, *e.g.*, $[Ir(OClO_3)(CO)(PPh_3)_2]$[273] obtained from Vaska's complex and $Ag[ClO_4]$. Alternatively, a weakly coordinating ligand (THF, $Me_2C{=}O$, MeCN etc) may be introduced to weakly stabilise the otherwise unsaturated metal centre. Thus the reaction of Vaska's complex $[IrCl(CO)(PPh_3)_2]$ with $Ag[ClO_4]$ in acetonitrile provides the isolable salt $[Ir(NCMe)(CO)(PPh_3)_2]ClO_4$, the nitrile of which is labile and readily substituted by a wide range of neutral and anionic ligands[274] Use of the weakly coordinating carborane anion ($CHB_{11}H_5Cl_6^-$) facilitates oxidative addition of chloroarenes that do not themselves react directly with Vaska's complex.[275] The abstraction of the bromide ligand of **3.1b** was therefore first explored.

Injecting an acetonitrile solution of **3.1b** onto silver triflate provides a white precipitate and bright orange supernatant the colour of which intensifies over time, accompanied by new set of ν_{CO} absorptions (MeCN: ν_{CO}: 1967, 1872 cm^{-1}) by infra-red spectroscopy (Scheme 3.4). NMR spectroscopic analysis of the filtered supernatant supported the formation of the salt $[WPt(\mu\text{-}C)(NCMe)(CO)_2(PPh_3)_2(Tp^*)]OTf$ (**3.2**), however, bulk isolation proved non-trivial. Recrystallisation could be achieved *via* liquid-liquid diffusion of acetonitrile/toluene mixtures over several days at –20 °C. Whilst this allowed full characterisation, it was subsequently most

conveniently generated *in situ* given spectroscopic analysis ($^{31}P\{^{1}H\}$ NMR, IR) suggests essentially quantitative conversion.

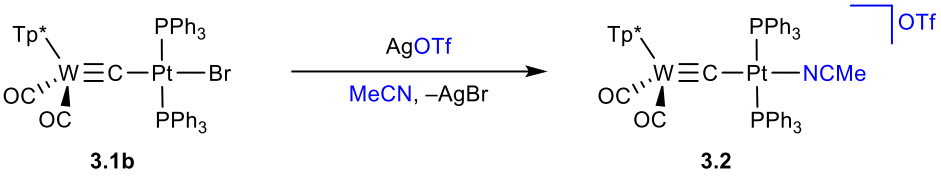

3.1b **3.2**

Scheme 3.4: Abstraction of bromide to give acetonitrile adduct **3.2**.

Single crystals suitable for X-ray diffractometry were obtained, however these were prone to significant disorder which somewhat compromised the precision of the structural model (Figure 3.13). This disorder appeared to involve 'wagging' of the coordinated acetonitrile ligand. On disorder, the oblate carbido ligand (C1) should be highlighted as an example of a common scenario throughout this thesis. As the carbon lies between two 5d metals, sometimes absorption corrections were insufficient for the ideal ellipsoid of the carbido atom to be realised in proximity to the heavy atom scatterers, including modelling movement and electron density along the spine.

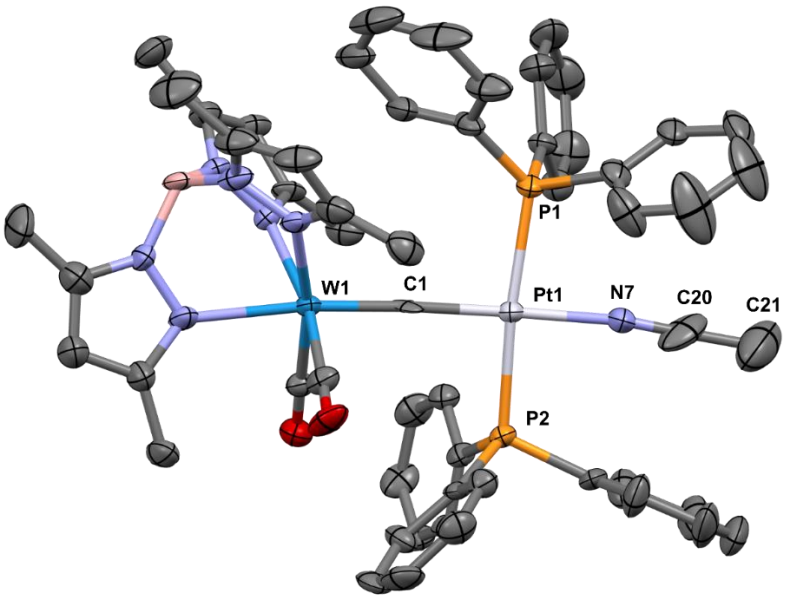

Figure 3.13: Molecular structure of $[WPt(\mu\text{-}C)(NCMe)(CO)_2(PPh_3)_2(Tp^*)]^+$ (**3.2**) in a single crystal of **3.2**·2(NCMe) as determined by X-Ray Diffractometry. Ellipsoids are drawn at the 50% probability surface with hydrogens, MeCN solvent molecules and OTf^- counter-anion omitted for clarity. Due to an imprecise structural model (R_1 = 0.064), caution should be exercised over-interpreting the data beyond connectivity confirmation. Selected bond lengths (Å), angles (°) and torsions (°): W1–C1 1.839(7), C1–Pt1 1.932(7), Pt1–N7 2.051(6), Pt1–P1 2.345(3), Pt1–P2 2.325(3), W1–C1–Pt1 177.3(3), P1–Pt1–P2 173.18(8), B1–W1–Pt1–P1 2.0(3).

The imprecise model nevertheless indicates that **3.2** conforms to the metallacarbyne bonding canonical description with metal-carbon bond lengths not dissimilar to those of its precursor **3.1a**, but with a more straightened W≡C–Pt spine (177.3(5)° *cf.* 169.2(3)°). Beyond the WCPt spine, the geometric features associated with the tungsten and platinum coordination spheres are unremarkable. The spectroscopic properties remain like those of the precursor **3.1a** noting that the blue-shifted ν_{CO} absorptions reflect the cationic platinum centre enhancing π-retrodonation from tungsten along the μ_2-carbido linkage. Furthermore, the μ_2-carbido shifts to slightly *lower* frequency in the $^{13}C\{^1H\}$ NMR spectrum (δ_C 300.1). This highlights the dangers of invoking simple inductive deshielding arguments for the interpretation of μ-carbido shifts, since conversion of the platinum from neutral to cationic might be expected to result in a more deshielded environment for the carbon nucleus. As will become increasingly clear throughout the thesis, the paramagnetic contributions to the shielding tensor appear to dominate the observed chemical shifts. In the case of **3.1b** which carries a π-donor bromide, in a strong magnetic field coupling of the bromide lone pairs with virtual empty orbitals of π-symmetry along the WCPt spine, *e.g.*, the LUMO, will significantly contribute to the paramagnetic shielding. In contrast, acetonitrile has neither filled nor vacant orbitals of π-symmetry that are energetically sufficiently accessible as to couple significantly.[**********]

3.4.2 Chelating phosphines

The stereochemistry of the thermodynamic isomers of **3.1** arrived at *via* C–Br oxidative addition involves *trans* phosphines, even though a concerted addition would traverse the kinetic *cis*-isomer. With a view to subsequently exploring carbide coupling processes with co-ligands, it was appreciated that introduction of the co-ligand of interest specifically *cis* to the carbido would be prudent. To guarantee this, it was presumed that the desired *cis* regiochemistry might best be enforced by inclusion of a chelating spectator ligand. Remaining with phosphine co-ligands, the best-known candidate is the chelating *bis*-phosphine, 1,2-*bis*(diphenylphosphino)ethane (dppe) though a multitude of variants are available. Phosphine substitution proceeds efficiently for both molybdenum (**3.1a**) and tungsten (**3.1b**) precursors to give *cis*-[MPt(μ_2-C)Br(CO)$_2$(dppe)(Tp*)] (M = Mo **3.3a**; W **3.3b**) as yellow species, distinct from the orange precursors (Scheme 3.5). Although substitution proceeds slowly at ambient temperature ($t_{½}$ = *ca* 5 hours), heating assists the slower kinetics of the tungsten variant. Simple purification and recrystallisation affords high isolated yields of **3.4a** and **3.4b** (89% and 94%, respectively).

[**********] Pope's expression for the paramagnetic contribution of two orbitals[276] is inversely proportional to the energy gap, the HOMO-LUMO gap therefore being of most, but not exclusive, interest.

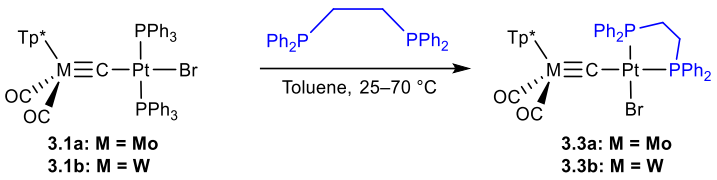

Scheme 3.5: Chelation of complexes **3.1a/b** with bidentate phosphines resulting in bromide *cis* to a carbido.

Installation of dppe significantly reduces solubility relative to precursors **3.1a**/**3.1b**, facilitating purification and the obtention of crystallographic grade crystals from mixtures of Et_2O and acetonitrile. Structurally, these complexes are almost identical in features, consistent with molybdenum (r_3 = 113 pm) and tungsten (r_3 = 115 pm) having similar covalent radii (**3.3b**; Figure 3.14).[277] Curiously, the phosphine *cis* to the carbyne is retained on the Tp* side, not the reverse where the bromide could alleviate steric pressure. This cradling of the phenyl ring by the Tp* (given ample opportunity to change) again supports a favourable interaction between the phenyl and pyrazolyl rings *vide supra*. Metallacarbyne bond lengths (W≡C and Pt–C) remain contracted indicating conjugation remains along the W≡C–Pt spine upon removal of the *trans*-bromide. Furthermore, the platinum-bromide bond significantly contracts (2.4746(9) Å *cf.* 2.5274(7) Å for **3.1b**}, no longer experiencing the strong *trans*-influence of the carbido ligand. The chelate bite angle of dppe (P1–Pt1–P2: 85.43(6)°) is only mildly contracted from the ideal (90°), easily accommodating the square planar geometry of platinum, and consistent with copious data for *cis*-platinum acetylides of the form *cis*-[Pt(C≡CR)$_2$(dppe)] (avg. 86(1) °; 67 examples).[278]

Complexes featuring dppe (**3.3a**/**3.3b**) are predicted to be spectroscopically informative though the reduced solubility somewhat compromised the acquisition of optimal signal/noise in NMR experiments such that *e.g.*, for the ^{195}Pt{^{1}H} spectrum no resonance was reliably identified within a reasonable acquisition period. For nuclei that could be measured, the ^{1}H NMR spectra remains largely similar whereas the ^{31}P{^{1}H} changes as expected in accordance with one phosphine now positioned *trans* to the carbyne (Figure 3.15). The *trans*-carbido phosphine resonance has a far larger coupling for the ^{195}Pt isotopomer ($^1J_{PPt}$ = 4059 **3.3a**; 4068 Hz **3.3b**) compared with the *cis*-phosphine (*trans* to the bromide) ($^1J_{PPt}$ = 1548 **3.3a**; 1548 Hz **3.3b**) as also observed for other σ-organyl complexes of the form *cis*-[PtBr(R)(dppe)], *e.g.*, $^1J_{PtP}$ = 4564, 1443 and $^2J_{PP}$ = 12 Hz for R = menthyl (2-isopropyl-5-methylcyclohexylyl).[279] Likewise, the carbido resonance in the ^{13}C{^{1}H} NMR spectrum has a larger coupling to the now *trans*-phosphorus ($^2J_{CP}$ = 77 **3.3a**; 74 Hz **3.3b**) while coupling to the *cis*-phosphine was not resolved (151 MHz for ^{13}C). The *trans*-phosphine contributes to significant deshielding (δ_C = 377.1 **3.3a**; 356.7 **3.3b**) relative to the π-donor bromide ligand in **3.1b**. Indeed, this is the most deshielded resonance observed in this Chapter, further

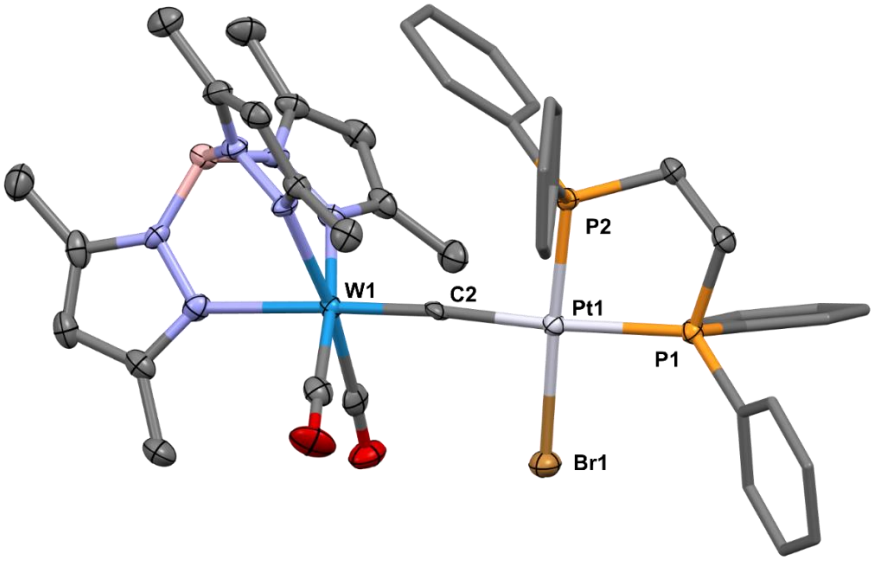

Figure 3.14: Molecular structure of [WPt(μ-C)Br(CO)$_2$(dppe)(Tp*)] (**3.3b**) in a single crystal of **3.3b**·2(NCMe) as determined by X-Ray Diffractometry. Ellipsoids are drawn at the 50% probability surface with hydrogens and MeCN solvent molecules omitted for clarity. Selected bond lengths (Å) and angles (°): W1– C1 1.833(5), C1–Pt1 1.990(6), Pt1–Br1 2.4746(9), Pt1–P1 2.331(1), Pt1–P2 2.225(2), W1–C1–Pt1 172.7(4), P1–Pt1–P2 85.43(6).

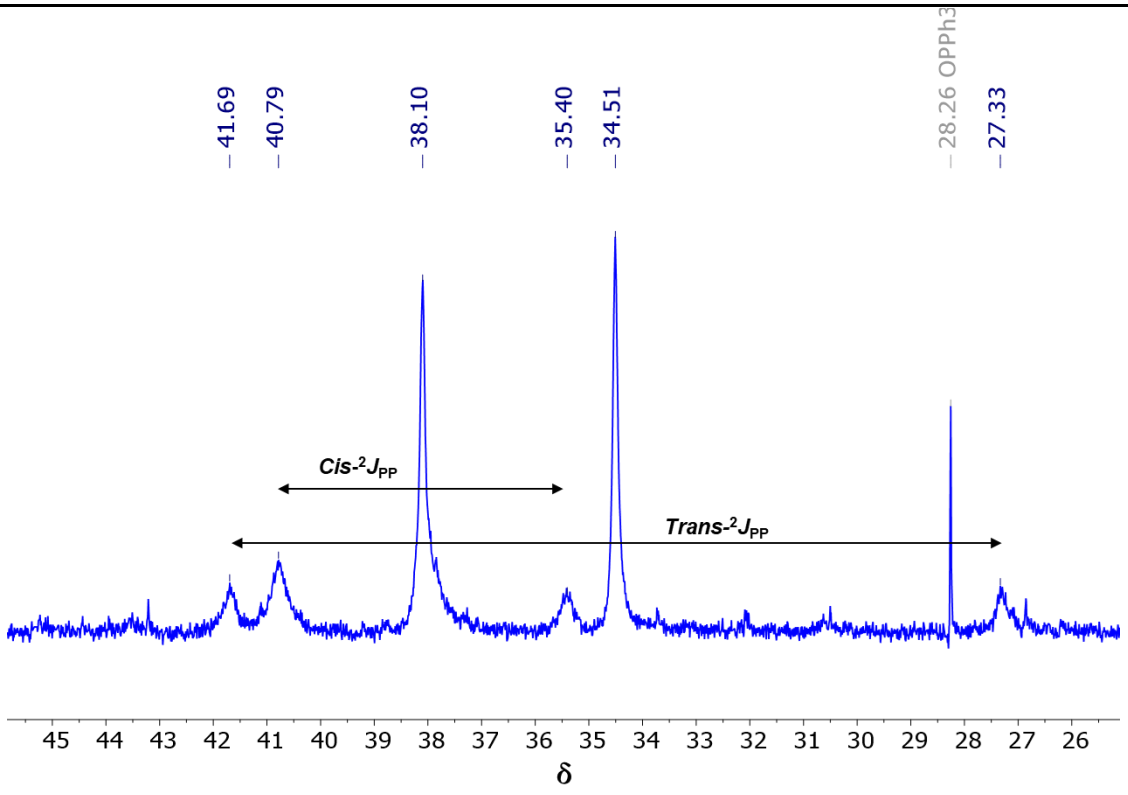

Figure 3.15: $^{31}P\{^1H\}$ NMR of dppe complex [WPt(μ-C)Br(dppe)$_2$(CO)$_2$(Tp*)] (**3.3b**) highlighting the broad resonances.

demonstrating the profound though non-trivial impact of paramagnetic contributions to the shielding tensor. It should be noted that the *cis*-Br–Pt–C geometry does not preclude contributions of bromide 'lone pair' atomic orbitals to excited states involving carbido-based orbitals.

By pruning **3.3b**, a theoretical model complex [WPt(μ_2-C)Br(dmpe)$(CO)_2$(Tp)] (**3.3***) was geometrically optimised to then visualise any changes in frontier orbitals that might attend conversion to *cis-bis*(phosphine) geometry (Figure 3.16). The frontier orbitals are surprisingly like precursor **3.1b**: the HOMO pertains to tungsten-carbonyl bonding; the HOMO–1/–2 contain the orthogonal π-bonds of the carbyne. Considering the dsp^2 square-planar hybridisation at platinum, the LUMO primarily comprises the diffuse vacant platinum p_z orbital, which having π-symmetry

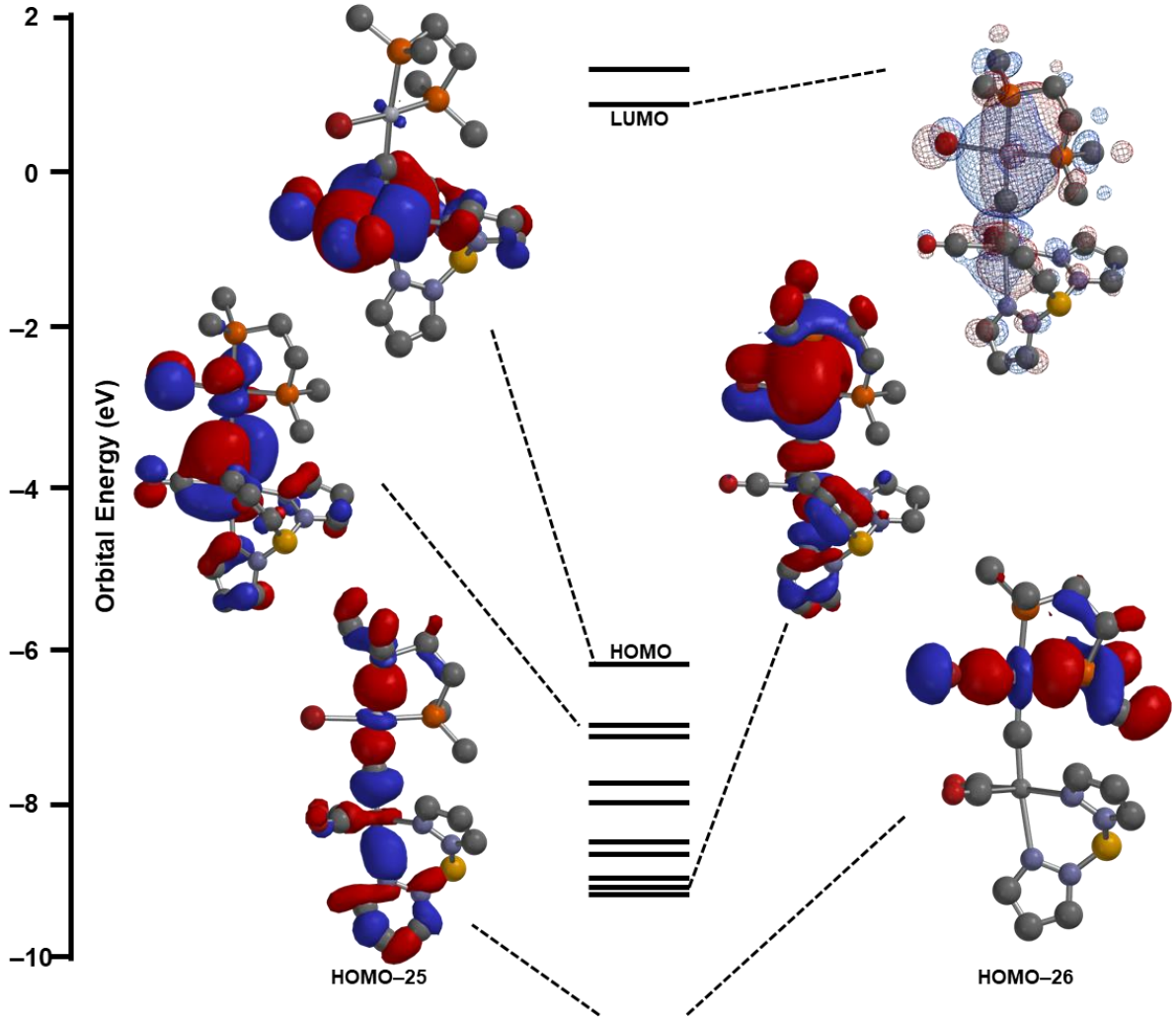

Figure 3.16: Frontier molecular orbitals of interest for the theoretical complex [WPt(μ-C)Br(dmpe)$(CO)_2$(Tp)] (**3.3***). DFT:ωB97X-D/6–31G*/LANLDζ.

with respect to the W···Pt vector overlaps in an antibonding manner with one tungsten 't_{2g}-type' orbital. The most interesting feature of **3.3*** is a low energy orbital (HOMO–25) of σ-symmetry along the entire W–C–Pt–P linkage, likely representing the orbital responsible for the *trans*-influence of the carbide, but also contributing to the large coupling between platinum and phosphorus in **3.3b** (4068 Hz). A fully bonding W–C–Pt π-conjugated orbital was unable to be identified in the 50 highest energy occupied orbitals Similarly, a σ-symmetric orbital (HOMO–26) is observed for the P-Pt-Br bonding.

3.4.3 Anionic, soft sulfur chelates

The bromide terminus can be abstracted from **3.1b** and both phosphines substituted. The complexes **3.1** are therefore set up for the introduction of anion chelates to further diversify the variety of coordination environments around platinum. A range of ionic bidentate sulfur based chelates are available, from which two were chosen: dithiocarbamates ($^{-}S_2CNR_2$) and methimazolylborates $H_nB(mt)_{4-n}$ (n = 1,2; mt = 2-mercapto-N-methylimizaolyl = methimazolyl; Bm^{Me} and Tm^{Me}) with the expectation that the bromide and a single phosphine would be substituted (Scheme 3.6).

Dithiocarbamato ligands, $^{-}S_2CNR_2$, have a rich coordination chemistry across the entire transition metal series.[280] ‡‡‡‡‡‡‡‡‡‡ In addition to being strong π-donor ligands, they have a strong propensity for bidentate coordination with electronic delocalisation around the MS_2C metallacycle. In general they serve as innocent spectator co-ligands though on occasion have been observed to fragment *via* C–S bond cleavage. The amino group NR_2 may be varied enormously, but once coordinated the ligand is planar with a degree of C–N multiple bonding and associated barrier to rotation (Chart 3.1).

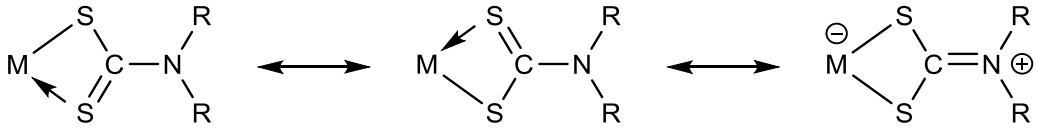

Chart 3.1: Resonance contributions for dithiocarbamato ligands $^{-}S_2CNR_2$.

Addition of the dithiocarbamate salt, $Na[S_2CNEt_2]\cdot 2H_2O$ to a stirring solution of **3.1b** in relatively polar CH_2Cl_2 resulted in an instantaneous colour change from orange to yellow, producing the desired neutral complex $[WPt(\mu_2\text{-}C)(S_2CNEt_2)(CO)_2(PPh_3)(Tp^*)]$ (**3.4**). Retention of a single phosphine (evident from ^1H NMR integration) was clear from the single resonance in the $^{31}P\{^1H\}$ NMR spectrum, straddled by ^{195}Pt satelites (δ_P = 13.7, $^1J_{PPt}$ = 3880 Hz) consistent with

‡‡‡‡‡‡‡‡‡‡ Xanthates $-S_2COR$ offer many similar features to dithiocarbamates but were not included here.

four coordinate platinum geometry. The μ_2-carbido resonance demonstrated a small coupling in the $^{13}C\{^1H\}$ NMR spectrum (δ_C = 338.4, $^2J_{CP}$ = 6 Hz) consistent with a *cis* C–Pt–P geometry. The ^1H NMR spectrum included two independent pairs of signals ethyl substituents reflecting the restricted rotation about the C–N bond characteristic of dithiocarbamato ligands with disparate *trans* ligands.

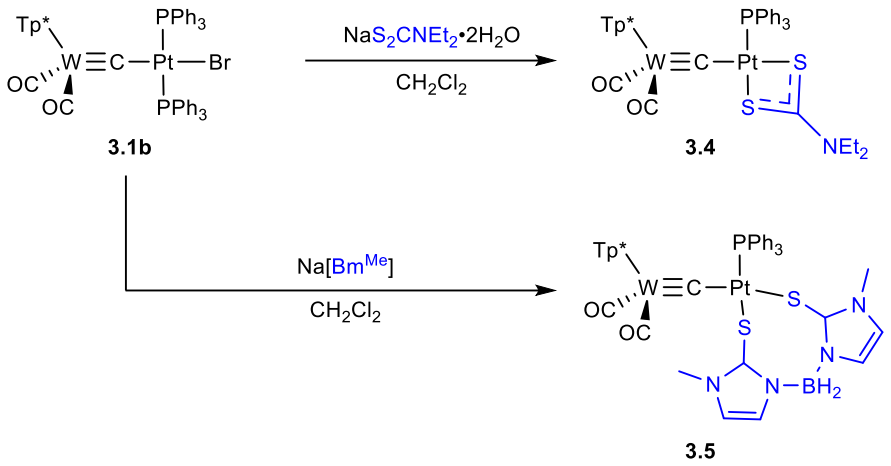

Scheme 3.6: Facile reaction between **3.1b** with a dithiocarbamato and a thioimidazolylborate ligand bearing sulfur donors.

Geometric parameters of **3.4** remain generally consistent with those of other metallacarbynes (W≡C 1.843(4), Pt–C 1.947(4) Å), featuring a bent W≡C–Pt spine {167.1(2) °} due again to the retained phosphine occupying the Tp* cleft (Chart 3.2, Figure 3.17). This confirmation again lends support to favourable phosphine-phenyl/pyrazolyl overlap as the crystal exhibits the *syn* conformer; not the *anti*-conformer as expected on steric grounds. The dithiocarbamato ligand offers a further advantage from a structural perspective in that variations I metal-sulfur ligands and deviations from collinearity of the metal-carbon and carbon-nitrogen vectors serve to report on the differential trans influences of *trans*-coordinated ligands. In the case of **3.4**, this is immediately apparent with a relative elongation of the Pt1–S1 bond (2.4166(8) Å) *trans* to the carbido relative to that *trans* to the phosphine (2.2345(1) Å) which is perhaps the opposite of what would be expected simply on the basis of steric inter-ligand repulsions. This former bond length is longer than the average of other platinum dithiocarbamato complexes (avg. 2.333(30) Å; 202 examples), many of which are symmetrical when equivalent *trans* ligands are present. The further significance of complex **3.5** will become clear in a subsequent Chapter where an alternative synthesis is described to provide a proof of concept, though the method described here remains the most expedient.

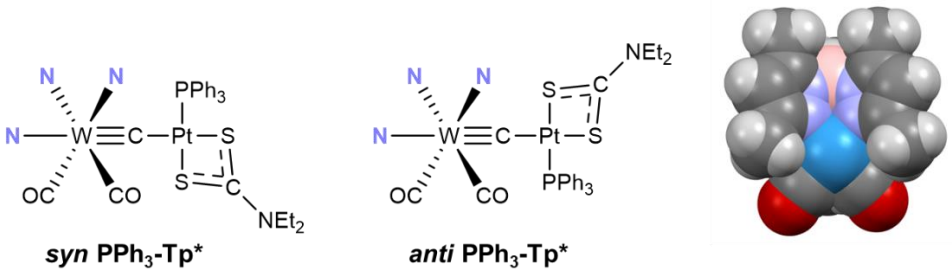

Chart 3.2: *Syn vs anti* conformations of phosphine with respect to the Tp* cleft shown right. Pyrazolyl nitrogens in lilac.

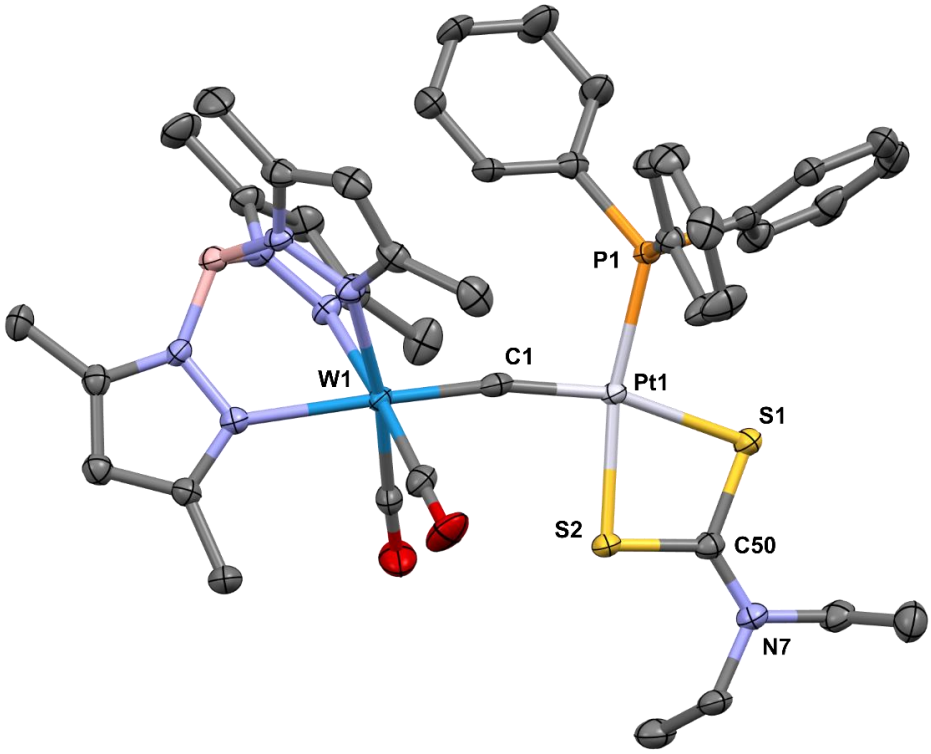

Figure 3.17: Molecular structure of [WPt(μ-C)(S_2CNEt_2)$(CO)_2$(PPh_3)(Tp*)] (**3.4**) in a single crystal of **3.4** as determined by X-Ray Diffractometry. Ellipsoids are drawn at the 50% probability surface with hydrogens omitted for clarity. Selected bond lengths (Å) and angles (°): W 1–C1 1.843(4), C1–Pt1 1.947 (4), W1–C1–Pt1 167.1(2), Pt1–P1 2.2619(9), Pt1–S1 2.4166(8), Pt1–S2 2.345(1) S1–Pt1–S2 74.05(3), S1–C50 1.735(4), S2–C50 1.723(4), S1–C50–S2 112.1(2).

Swapping to Reglinski's sulfur-based thioimidadazolyl scorpionates (Bm^{Me} and Tm^{Me}) removes the steric bulk of the heterocycles from the platinum because binding is through a single sulfur atom donor,[281] which might be expected to somewhat relieve the steric impact on the carbido. Sulfur donors also present a better soft-soft match to platinum(II) by HSAB theory verified for the dithiocarbamate ligand above. The Bm and Tm ligands, and related heterocyclic variants, have been previously employed in the chemistry of both platinum(II) and platinum(IV) [282-287] including as precursors to unusual platinaborane species. In the case of Bm, the possibility of tridentate κ^3-*H,S,S'*-coordination has also been observed.[288] It should however be noted that in unpublished

results,[289] the reaction of $[Rh_2(\mu\text{-}C)Cl_2(PPh_3)_4]$ with $Na[Bm^{Me}]$ was found to result in significant degradation of the carbido core with formation of the rhodaboratrane $[Rh\{\kappa^3\text{-}H,S,S'\text{-}H_2B(mt)_2\}\{\kappa^3\text{-}B,S,S'\text{-}HB(mt)_2\}]$ (mt = 2-mercapto-3-methylimidazolyl).

Stirring **3.1b** with $Na[Bm^{Me}]$ in CH_2Cl_2 led to decolourisation from orange to yellow, at ambient temperature with complete conversion overnight to provide $[WPt(\mu\text{-}C)(PPh_3)(CO)_2(Bm^{Me})(Tp^*)]$ (**3.5**). Likewise, the *tri*-dentate Tm^{Me} anion undergoes facile halide and phosphine substitution of **3.1b** at ambient temperature to give $[WPt(\mu\text{-}C)(PPh_3)(CO)_2(\kappa^2\text{-}Tm^{Me})(Tp^*)]$ (**3.6**), although this species defied purification and is presented only as a crystal structure to highlight connectivity (Figure 3.19). By comparing substitution of **3.1b** with *bis*-thioimidazole against *bis*-pyrazolyl (*vide infra*), the yields (77% *vs* 29% **3.11**, respectively) would seem to support the favourable soft-soft match of platinum(II) and sulfur as opposed to hard nitrogen donors.

The carbido resonances for the thioimidazolyl species **3.5** appears to lower frequency in the $^{13}C\{^1H\}$ NMR spectrum (δ_C: 328.8) compared to **3.4**, while $^1J_{PtP}$ values indicate a weaker Pt–P interaction (3994) but similar platinum chemical shifts (δ_{Pt}: –3561), indicating an increased σ/π donation from sulfur comparable to that inferred for the dithiocarbamato complex **3.4. S**olid-state structures of **3.5** and **3.6** (Figure 3.18 and 3.19, respectively) were collected albeit less precise for **3.5** due to data quality being compromised through apparent desolvation during the mounting process prior to acquisition. The bond lengths of carbido spine (W≡C and Pt–C) are unremarkable other than to note the particularly pronounced bending of the spine for **3.5** (166.9(7)°). The platinum terminus remains square-planar even with a pendant thioimidazole for Tm^{Me}, while while the flexibility of the thioimidazole ligands allows complete relaxation (S–Pt–S chelate bite angles 93.6(1)° for **3.5**, 96.03(5)° for **3.6**). It is also curious to note, the molecular structures of **3.4**, **3.5**, and **3.6** are all captured in the *syn*-conformation, with the phosphine nestled in the Tp*, although this does not necessarily reflect the species in solution and could be an effect driven by crystal packing.

In each of the molecular structures of **3.5** and **3.6**, one B–H bond lies above the platinum coordination plane however on the basis of available B–H···Pt structural data for the complexes $[PtMe_3(Bp^*)]$ (1.95 Å) $[Pt_2Me_6(Bp)_2]$ (1.88 Å),[290] $[Pt_2Me_6I(Bm)]$ (1.89 Å)[291] and $[PtMe_3(Bm)]$ (1.83 Å)[#########] for **3.5** (3.26 Å) this separation falls well outside what might be considered a bonding interaction. In a similar manner, though somewhat shorter at 2.81 Å, the approach of the B–H

[#########] I. R. Crossley, A. F. Hill and A. C. Willis, *Unpublished Results*, *Private Communication*.

group in **3.6** to platinum could only be described as incipient at best. The issue of B–H···Pt interaction is of interest because this is implicated in the formation of hydrido-platinaboratranes.

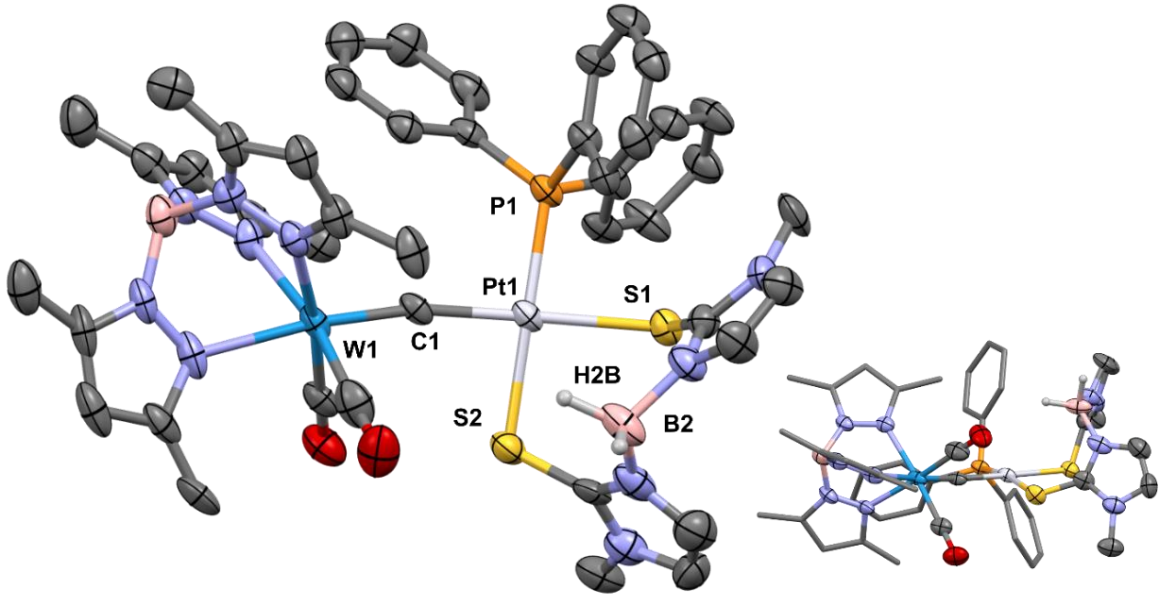

Figure 3.18: Molecular structure of [WPt(μ-C)(Bm^{Me})$(CO)_2$(PPh_3)(Tp*)] (**3.5**) in a single crystal of **3.5**·$CHCl_3$ as determined by X-Ray Diffractometry. Ellipsoids are drawn at the 50% probability surface with hydrogens and the $CHCl_3$ solvent molecule omitted for clarity. Selected bond lengths (Å) and angles (°): W1–C1 1.83(1), C1–Pt1 1.97(1), W1–C1–Pt1 166.9(7), Pt1–P1 2.250(3), Pt1–S1 2.455(2), Pt1–S2 2.346(4), S1–Pt1–S2 93.6(1), Pt1···H2b 3.3(2). Inset = View highlighting the absence of a Pt–H interaction.

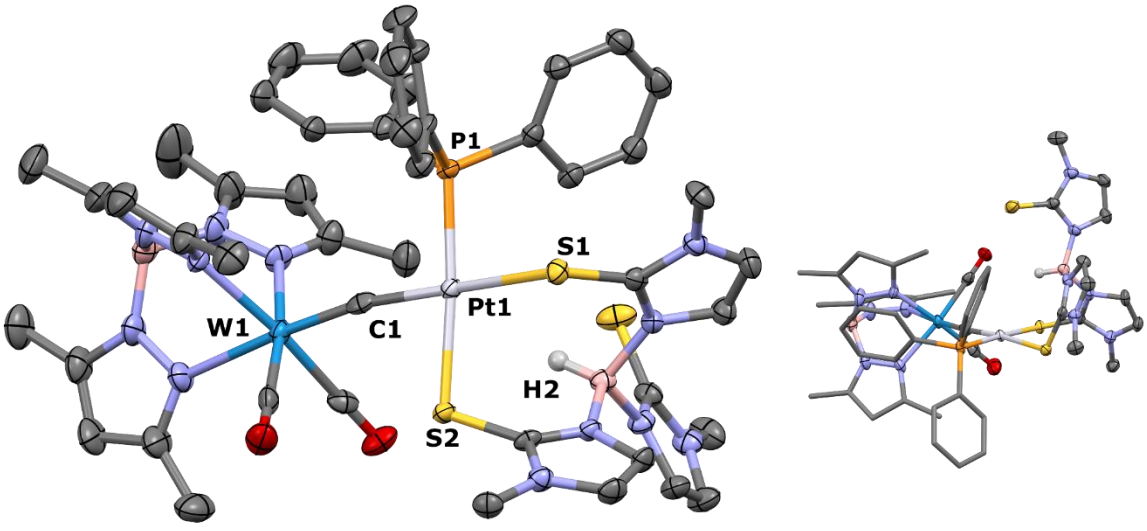

Figure 3.19: Molecular structure of [WPt(μ-C)(κ²-Tm^{Me})$(CO)_2$(PPh_3)(Tp*)] (**3.6**) in a single crystal of **3.6**·3(CH_2Cl_2) as determined by X-Ray Diffractometry. Ellipsoids are drawn at the 50% probability surface with hydrogens and the CH_2Cl_2 solvent molecules omitted for clarity. Selected bond lengths (Å) and angles (°): W1– C1 1.830(6), C1–Pt1 1.947(6), W1–C1–Pt1 170.3(3), Pt1–P1 2.259(1), Pt1–S1 2.456(1), Pt1–S2 2.360(1), S1–Pt1–S2 96.03(5), Pt1···H1 2.81. Inset: Reverse view indicating the proximal hydride and pendant thioimidazole.

3.4.4 Incorporation of nitrogen donor ligands

Prior to this work, the terpyridine framework [WPt(μ-C)(terpy)(CO)$_2$(Tp*)]PF$_6$ (**3.7**, terpy = 2,2';6',2"-terpyridine), was the lone example of a bimetallic tungsten-platinum μ$_2$-carbido complex. The complex **3.7** was obtained in 64% yield *via* reaction of the lithiocarbyne [W(≡CLi)(CO)$_2$(Tp*)] with [PtCl(terpy)]PF$_6$. A similar reaction with [PtCl$_2$(phen)] (phen = 1,10-phenathroline) afforded a more complex trimetallic μ$_2$-carbido/carbyne complex *via* subsequent nucleophilic attack by the lithiocarbyne at the coordinated phenanthroline ligand. Late installation of bidentate pyridyl-based ligands *via* reactions with **3.1b** might be expected to obviate such undesired processes, as indeed proved to be the case. To achieve the synthesis of salts such as **3.7** *via* substitution reactions commencing with neutral **3.1b**, a polar solvent media (10% *v*/*v* MeOH/CH$_2$Cl$_2$) was employed to encourage halide dissociation upon ligand substitution in the presence of the hexafluorophosphate (PF$_6$) counter anion thereby circumventing the use of silver salts noted above for **3.2**. These conditions proved effective throughout this sub-section.

Terpyridine was able to substitute all the platinum co-ligands in **3.1b** resulting in a deep purple solution after several hours. The substitution method provides **3.7** *via* a more convenient synthesis but affords inferior yields when compared to the lithiocarbyne approach (25% *vs* 65%) due to work-up issues. Unreacted terpyridine was found to drag on flash chromatography columns even when the silica retention properties are altered with dilute NEt$_3$ (a common practice for chromatography of *N*-heterocycles). [292] The lithiocarbyne route gives simpler purification as unreacted [PtCl(terpy)]$^+$ is retained on the silica baseline. While the yield of **3.7** *via* substitution is somewhat disappointing, it does serve as a proof of concept, generating **3.7** *via* an alternative approach exploiting the strategic advantage of introducing diversity from a late synthetic intermediate. A concentrated sample of **3.7** could be prepared in *d*$_3$-MeCN for ^{13}C{^{1}H} NMR measurements that allowed direct detection of the carbido resonance (δ$_C$: 368.0), where the previous report had relied on ^{1}H-^{13}C HMBC measurements. [159] The remarkable colour of the complex is not in any great part a feature of the W≡C–Pt spine itself, but rather results from the terpyridine chromophore which enters into MLCT transitions. This underpins the extensive photophysical studies of alkynyl analogues [Pt(C≡CR)(terpy)]+, for which dozens of variants on 'R' or terpyridine modification have been explored. [293-296] Time-dependent DFT calculations indicate that both LUMO and LUMO+1 are terpy ligand-based, while the first 3 HOMOs are associated with tungsten binding to CO and carbido ligands (Figure 3.20). Accordingly, the visible electronic transitions of note (λ = 456 and 553 nm) have substantial tungsten to terpy charge transfer character, accounting for their large intensities.

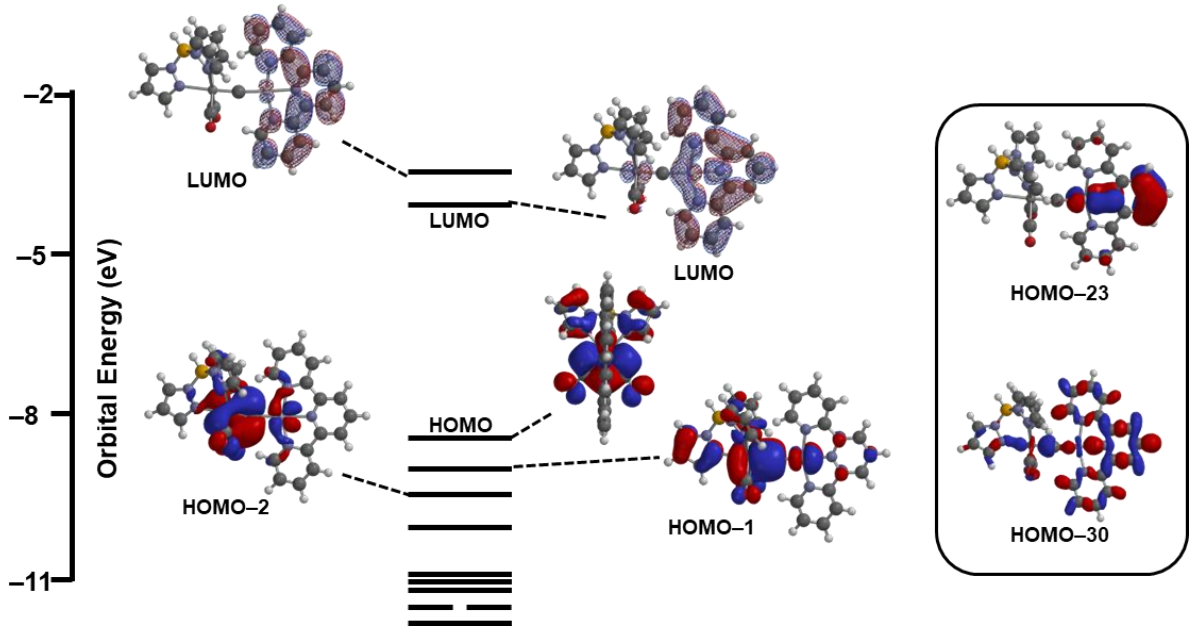

Figure 3.20: Frontier orbitals of interest for the hypothetical complex [WPt(μ$_2$-C)(terpy)(CO)$_2$(Tp)] (**3.7***).

The trio of pyridine-based ligands comprising 2,2'-bipyridine (bpy), 4,4'-ditertbutyl-2,2'-bipyridine (dtbbpy) and 1,10-phenanthroline (phen) present similar structures as chelates but with subtle differences in terms of solubility, steric bulk and backbone rigidity. As noted above attempts to prepared a 1,10-phenathroline carbido complex were confounded by reaction of excess of the lithiocarbyne nucleophile attacking the phenanthroline ligand which was activated towards nucleophilic attack as a result of coordination to platinum(II). Two outcomes were considered plausible from the reactions of **3.1b** with neutral bidentate bipyridyls (N-N) or phenanthroline, *viz.* replacement of both phosphines to provide neutral *cis*-[WPt(μ-C)Br(CO)$_2$(N-N)(Tp*)] or alternatively bromide ionisation to provide salts of the *cis*-[WPt(μ-C)(CO)$_2$(PPh$_3$)(N-N)(Tp*)]+ cations.

Despite utilising a non-polar medium such as toluene and heating **3.1b** to reflux in the presence of bpy, minimal spectroscopic changes were observed. Closer inspection of crude mixtures by ^{31}P{^{1}H} NMR spectroscopy revealed traces of another species being formed, but only when crude residues were measured in polar solvents such as CD_2Cl_2/$CDCl_3$ (but not in d_8-toluene). This suggested a facile reaction occurs in a polar media, hence the conditions optimised for terpy installation were employed for each bipyridine system. This approach proved successful with facile substitution occurring to provide three new metallacarbyne species [WPt(μ-C)(CO)$_2$(N-N)(PPh$_3$)(Tp*)]PF$_6$ (N-N = bpy **3.8**, dtbbpy **3.9**, phen **3.10**) in respectable yields (Scheme 3.7). Natural emergence of **3.8–3.10** suggests that one phosphine of **3.1b** can be easily replaced, however, the coordination of a second nitrogen opposed to phosphine is insufficient, even when influenced by the chelate effect.

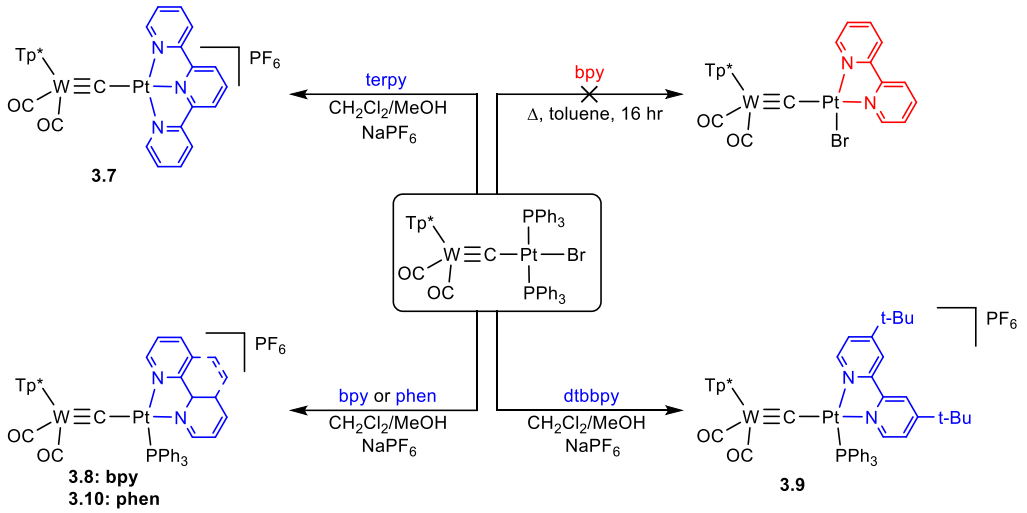

Scheme 3.7: Bi- and Tri-pyridine ligand substitution of **3.1b** in polar media to produce cationic platinum(II) complexes bearing bi- or tridentate ligands.

The molecular structures of compounds **3.8** and **3.9** were crystallographically determined with ease; however, species **3.10** proved troublesome providing crystals that rapidly desolvated and even at 150 K. The molecular structures of the cations of salts **3.8** and **3.9** are presented in Figures 3.21 and 3.22 and confirm coordination of bipyridyl ligands and retention of one phosphine. Both structures exhibited the common features already discussed: contracted Pt–C bonds, elongated Pt–N bonds *trans* to the carbido and a bent spine (164.5(4) and 168.2(2)°, respectively). However, the retained phosphine is positioned *anti* to the Tp* ligand allowing the bipyridyl to preferentially nestle between two pyrazolyl groups. This was observed for the terpyridine ligand in **3.7** but otherwise contrasts with the other structures observed thus far. It is possible that interactions between like molecules (*N*-pyrazolyl & *N*-pyridyl) are a more favourable combination than unlike molecules (*N*-pyrazolyl & *P*-phenyl) when considering occupancy of the pyrazolyl cleft, or simply that the rings are better positioned for inter-ligand interactions. In any event, the position of the bipyridyl remains the likely cause of the W≡C–Pt linkage bending. Other structural features call for little comment in that many examples of platinum alkynyls ligated by bipyridyl donors are known, though relatively few are cationic. The closest species for comparison is that of Lang and co-workers and also by Wu, who independently acquired [Pt(C≡CPh)(dmbpy)(PPh_3)]X (X = BF_4, [297] SbF_6[298]) *via* electrophilic alkynyl cleavage from [Pt($CCPh)_2$(dmbpy)] by Ag[BF_4]/PPh_3 or [Ag(NCMe)($PPh_3)_2$]SbF_6 though in neither case were spectroscopic data obtained. For the phenylethynyl structure there is no statistically significant differential *trans* influence upon the bipyridyl ligand (Pt–N: 2.068(6), 2.094(6) Å) for PPh_3 and alkynyl ligands, as is also the case for **3.8** (2.142(5), 2.104(6)Å) although for **3.9** the *trans* influence of the carbide is more clearly pronounced (2.101(3), 2.149(3) Å) due to a more precise structural model. Precision limits aside,

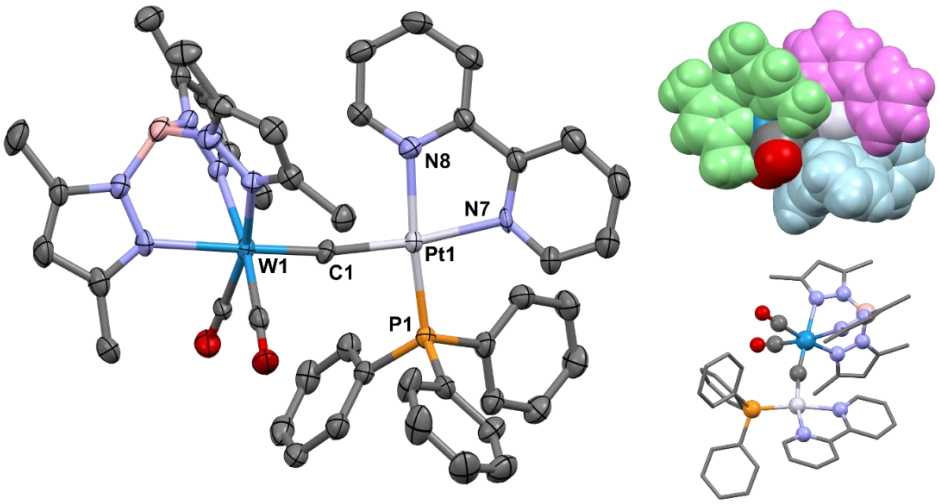

Figure 3.21: Molecular structure of [WPt(μ-C)(bpy)$(CO)_2(PPh_3)$(Tp*)]PF_6 (**3.8**) in a single crystal of **3.8**·2$(CHCl_3)$ as determined by X-Ray Diffractometry. Ellipsoids are drawn at the 50% probability surface with hydrogens, $CHCl_3$ solvent molecules and PF_6^- counter-anion omitted for clarity. Insets: a) Space-filling diagram highlighting the steric clash of phenyl rings (pink) and the sterically encumbering tris-pyrazolylborate (green) ligand, phenyl groups in turquoise; b) Ball and stick representation as viewed down the key molecular linkage (ligands simplified for clarity.Selected bond lengths (Å) and angles (°): W1–C1 1.820(5), C1– Pt1 1.960(6), W1–C1–Pt1 164.5(4), Pt1–P1 2.233(2), Pt1–N7 2.142(5), Pt1–N8 2.104(6), N7–Pt1–N8 77.2(2).

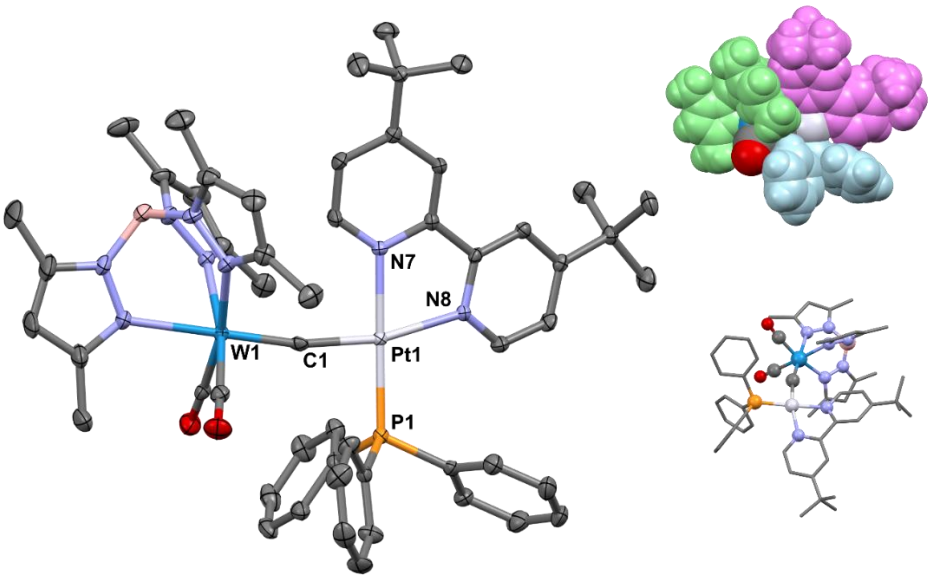

Figure 3.22: Molecular structure of [WPt(μ-C)(dtbbpy)$(CO)_2(PPh_3)$(Tp*)]$^+$ (**3.9**) in a single crystal as determined by X-Ray Diffractometry. Ellipsoids are drawn at the 50% probability surface with hydrogens and PF_6^- counter-anion omitted for clarity. Insets: a) Space-filling diagram highlighting the steric clash of phenyl rings (pink) and the sterically encumbering tris-pyrazolylborate (green) ligand, phenyl groups in turquoise; b) Ball and stick representation as viewed down the key molecular linkage (ligands simplified for clarity.Selected bond lengths (Å) and angles (°): W1–C1 1.839(5), C1–Pt1 1.945(5), W1–C1–Pt1 168.2(2), Pt1–P1 2.246(1), Pt1–N7 2.101(3), Pt1–N8 2.149(3), N7–Pt1–N8 76.1(1).

the Pt–N bond lengths are all longer in **3.8** and **3.9** than observed for the simple phenylethynyl reference complex. [297-298]

Returning to species **3.8**–**3.10**, once isolated, the initially observed phosphine signals in solution are much clearer. Resonances appear as singlet in the $^{31}P\{^{1}H\}$ NMR spectra (δ_P: 15.7–16.4), accompanied by satellites for the ^{195}Pt isotopomer, with coupling ($^{1}J_{PPt}$ ~4300 Hz) that is reproduced in the doublet resonances observed in the $^{195}Pt\{^{1}H\}$ NMR spectra. These couplings are somewhat stronger compared to the average in this Chapter, potentially due to the cationic nature of the platinum inciting a stronger phosphorus-platinum interaction. The cationic nature of the platinum is also reflected in a platinum resonance to higher frequency relative to neutral examples (δ_{Pt}: ~–3500, *cf.* –3821 **3.1b**) (Figure 3.23). The carbido resonance falls within the typical region (*e.g.*, **3.8**: δ_C = 325.8, $^{2}J_{PC}$ = 9 Hz) with no further spectroscopic features of interest.

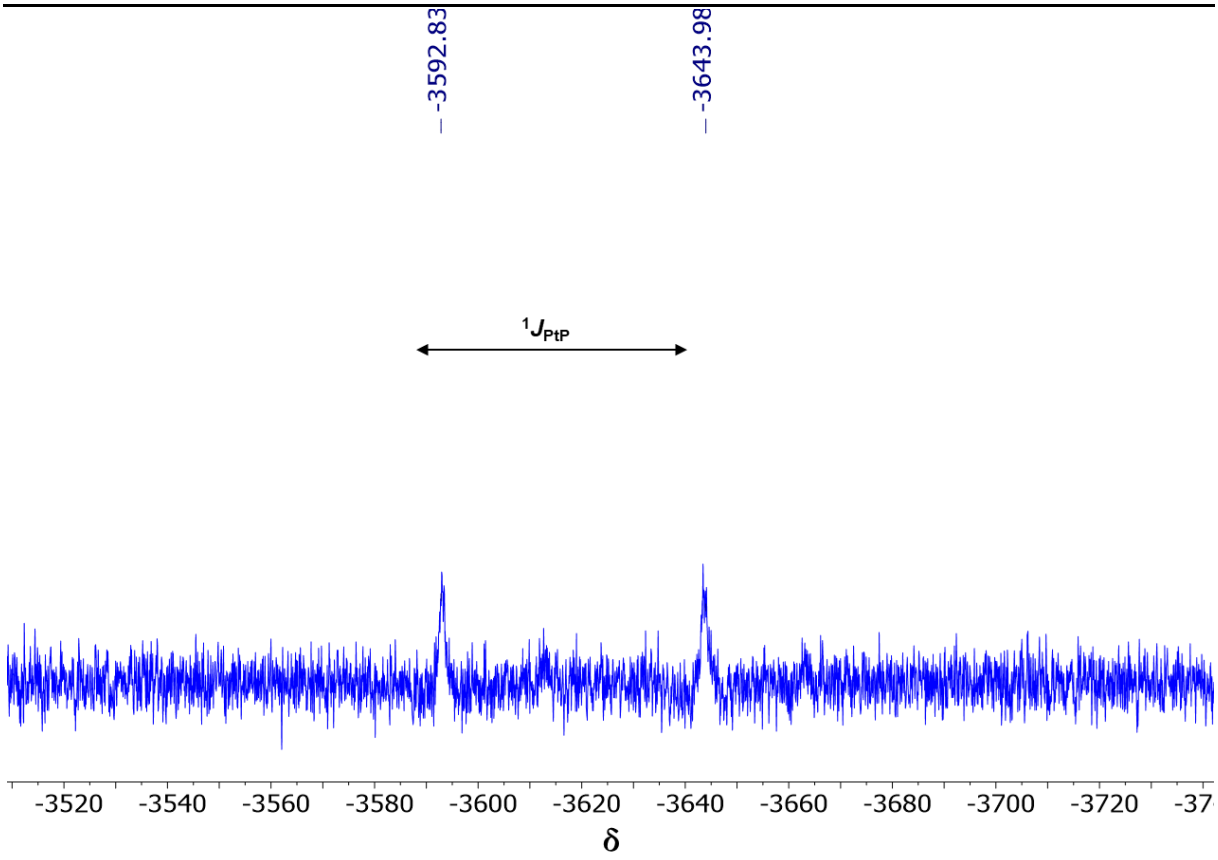

Figure 3.23: $^{195}Pt\{^{1}H\}$ NMR of aromatic complex $[WPt(\mu\text{-}C)(Phen)(CO)_2(PPh_3)(Tp^*)]PF_6$ (**3.10**).

3.4.5 Additional anionic scorpionate ligands

Contrasting with the neutral terpy, bpy and phen ligands, another set of polydentate imine donor ligands to consider are Trofimenko's anionic and sterically encumbering pyrazolyl scorpionate ligands, [299-300] upon which the very formation of the bromocarbyne starting materials

is reliant. A previous study explored this concept for homobimetallic rhodium carbidos of Class A, where scorpionate ligands (L = Bp, Bp*, and Tp) were introduced to both rhodium centres of $[Rh(\mu_2\text{-}C)Cl_2(PPh_3)_4]$ to afford $[Rh_2(\mu_2\text{-}C)(L)_2(PPh_3)_2]$, in a straightforward manner. When utilising the larger *tris*(3,5-dimethyl)pyrazolyl borate (Tp*), a more complex process operates in that presumably the steric clash of these two adjacent Tp* ligands forces phosphine dissociation on one metal followed by C–H activation of an *ortho*-proton of the remaining triphenylphosphine to provide a bridging species, $[Rh_2(\mu_2\text{-}C)H(\mu\text{-}C_6H_4PPh_2)(Tp^*)_2]$.[156] This transformation led to the first mixed valence homobimetallic carbido complex with both rhodium(I) and rhodium(III) centres in the same molecule. Although the authors described the rhodium scorpionate carbide as reluctant to react further, it was hypothesised that a tungsten-platinum species with a second, rigid pyrazolyl-scorpionate may yield interesting results, particularly involving the central carbide.

A sluggish reaction occurs between **3.1b** and K[Bp*] under reflux in dichloromethane ($t_{½}$ *ca* 8 hours) or THF ($t_{½}$ *ca* 4 hours) to give $[WPt(\mu\text{-}C)(Bp^*)(CO)_2(PPh_3)(Tp^*)]$ (**3.11**). Substitution with even larger Tp* to give $[WPt(\mu\text{-}C)(CO)_2(PPh_3)(\kappa^2\text{-}Tp^*)(\kappa^3\text{-}Tp^*)]$ (**3.12**) in poor yield occurred best in CH_2Cl_2, where more forcing conditions (solvent or temperature) failed to improve production despite multiple days of reaction time and simple purification (5% isolated yield *cf.* 29% **3.11**) (Scheme 3.8). Complex **3.12** features two coordinated pyrazolyl rings of the Tp* ligand bound to platinum while the third remains a pendant, as is commonly encountered for Tp and Tp* ligand coordinated to d^8-platinum(II)[301] for which square planar geometry predominates. However, this pendant may provide a useful if platinum(II) can be oxidised to platinum(IV) the d^6-centre of which readily accommodates κ^3-tridentate coordination.[302] Given the dismal yield of producing **3.12**, this oxidation and further reactivity studies were not pursued.

Preparation of complexes **3.11–3.12** further highlights the impact of accommodating large ligands to a μ_2-carbido already encumbered by the Tp* cage given more a more rigid ligand than Bm^{Me} (**3.5**). The constraints of this environment are clear once more from the spectroscopic and structural data. ^{1}H NMR spectra of **3.10** and **3.12** reveal 1:1 and 1:3 ratios of signals respectively, consistent with the presence of rotational isomers much like **3.1b**. The presence of rotational isomers is also suggested by NMR data for other nuclei. Complex **3.11** is observed as two approximately equal populations of isomers while one major isomer predominates (*ca* 3:1 by $^{31}P\{^1H\}$ NMR integration) for **3.12**. In each case, pairs of signature resonances for each component of are both isomers of **3.11** and **3.12** are observed to occur at similar chemical shifts. Firstly, the $^{31}P\{^1H\}$ NMR spectra reveal singlets straddled by ^{195}Pt satellites (δ_P: 3.07–7.52) significantly more upfield than those for the complexes discussed so far. The resonances display

J_{PPt} couplings ($^1J_{PPt}$: 4178–4288 Hz) comparable to those for the bipyridyl complexes, supporting the inference of 4-coordinate platinum, rather than κ^3-coordinate of the scorpionate. The higher fields where these resonances are identified in the $^{195}Pt\{^1H\}$ NMR spectra (δ_{Pt}: –3433 to –3495), most likely reflects a deshielding of platinum consistent with the prior nitrogen donors, albeit no longer cationic platinum(II). The $^{13}C\{^1H\}$ NMR spectra reveal the most downfield carbido resonances of the nitrogenous scaffolds for the major isomer of **3.10** (δ_C: 333.5), and the two isomers of **3.11** (δ_C: 332.6 and 338.3). The impacts of variation on platinum ligation on the carbide chemical shifts for **3.11** and **3.12** are not significantly transmitted to the tungsten centre as carbonyl modes fall are within instrumental resolution limits (ν_{CO}: **3.11** 1946, 1853 *cf.* **3.12** 1947, 1854 cm^{-1}), implicating an almost identical tungsten environment in solution.

Solid-state structures can also be obtained for **3.11** and **3.12**, with features largely similar to others in this Chapter (Figure 3.24 and 3.25). Of note, the rigid pyrazolyl borates slightly distort the platinum geometry (N–Pt–N chelate bite angles 81.6(3) for **3.11**, 81.39(9)° for **3.12**) but the W≡C–Pt remains relatively linear. The structure of **3.12** confirms a pendant pyrazolyl ring, and noting caveats of previous discussion, the pyrazolyl ring of the second scorpionate nestles the cleft of the original on tungsten (i.e., the *anti*-conformer).

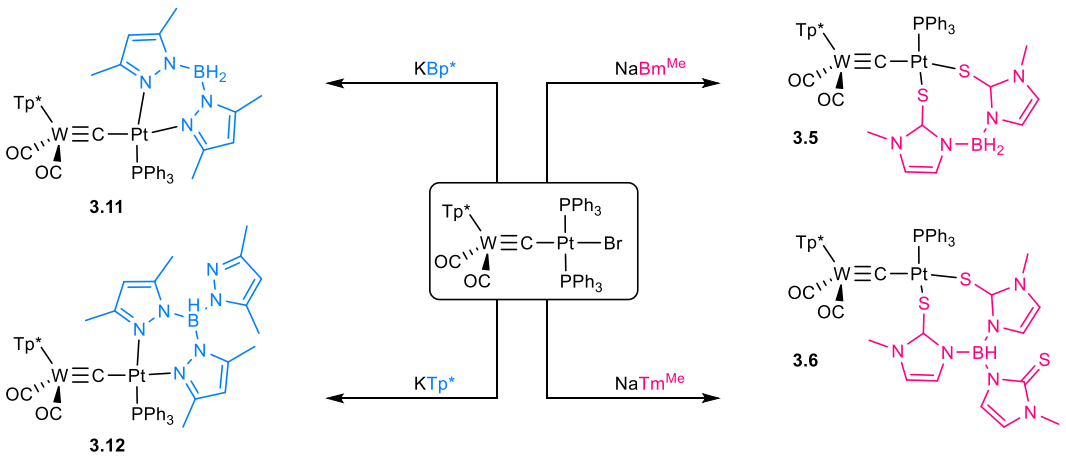

Scheme 3.8: *Bis*- and *tris*-pyrazolylborates (Bp*/Tp*) gradually substitute the platinum terminus of **3.1b**, whilst *bis*- and *tris*-thioimidazolylborates (Bm^{Me}/Tm^{Me}) undergo facile substitution owed to a more flexible ligand scaffold.

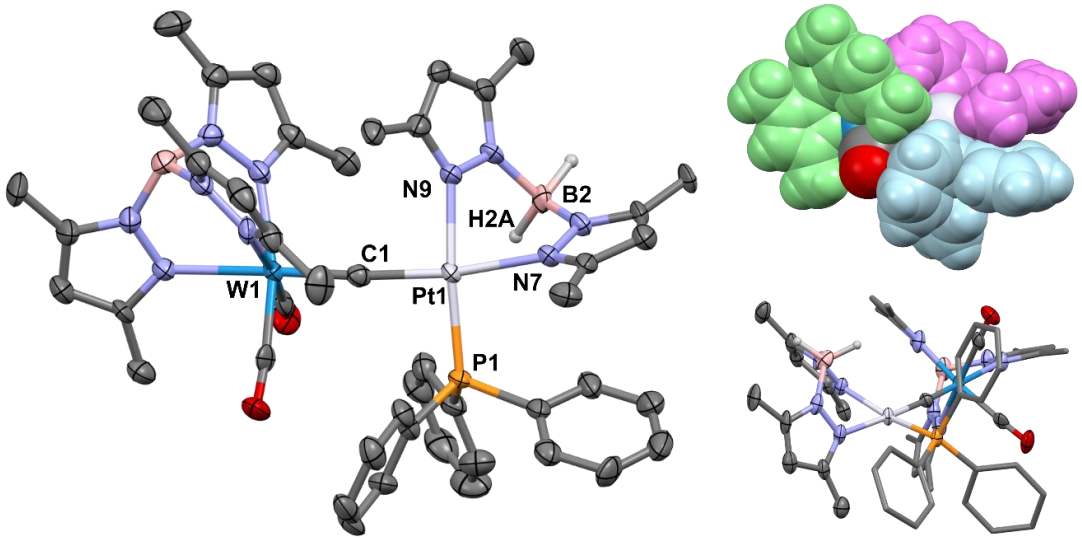

Figure 3.24: Molecular structure of [WPt(μ-C)(Bp*)(CO)$_2$(PPh$_3$)(Tp*)] (**3.11**) in a single crystal of **3.11**·CHCl$_3$ as determined by X-ray Diffraction. Ellipsoids are drawn at the 50% probability surface with hydrogens and the CHCl$_3$ solvent molecule omitted for clarity. Insets: a) Space-filling diagram highlighting the steric clash of phenyl rings (pink) and the sterically encumbering tris-pyrazolylborate (green) ligand with phenyl groups in turquoise; b) Ball and stick representation as viewed down the key molecular linkage (ligands simplified for clarity. Selected bond lengths (Å) and angles (°): W1–C1 1.835(7), C1–Pt1 1.963(7), W1–C1–Pt1 175.3(6), Pt1–P1 2.256(3), Pt1–N7 2.138(6), Pt1–N9 2.111(9), N7–Pt1–N9 81.6(3), Pt1···H2A 3.06(9).

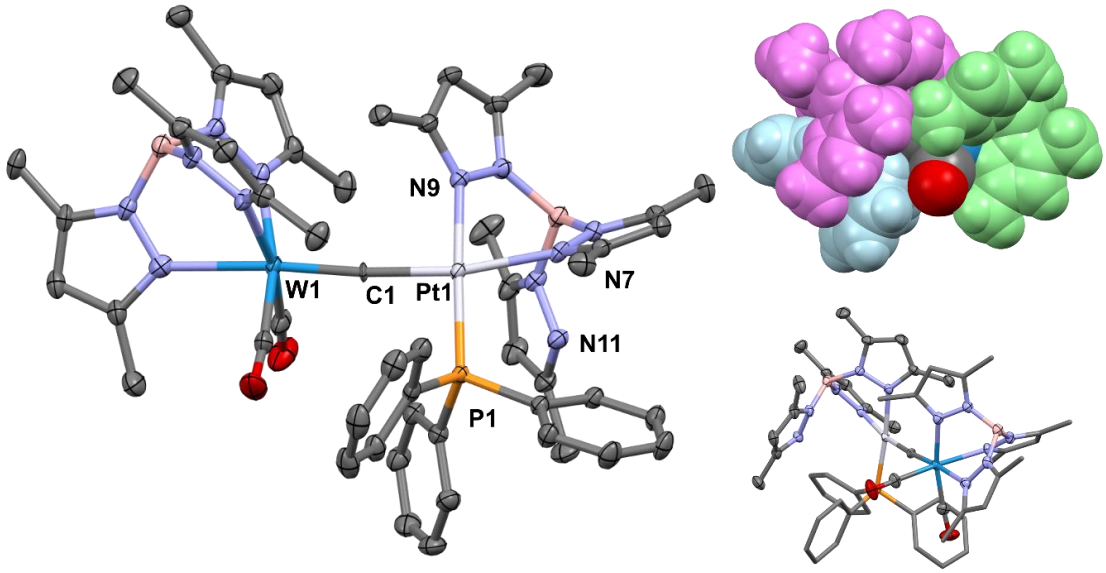

Figure 3.25: Molecular structure of [WPt(μ-C)(κ^2-Tp*)(CO)$_2$(PPh$_3$)(Tp*)] (**3.12**) in a single crystal as determined by X-Ray diffraction. Ellipsoids are drawn at the 50% probability surface with hydrogens and the CHCl$_3$ solvent molecule omitted for clarity. Insets: a) Space-filling diagram highlighting the steric clash of phenyl rings (pink) and the sterically encumbering tris-pyrazolylborate (green) ligand with phenyl groups in turquoise; b) Reverse view indicating the denticity of the second pyrazolylborate ligand. Selected bond lengths (Å) and angles (°): W1–C1 1.861(2), C1–Pt1 1.954(2), W1–C1–Pt1 175.2(1), Pt1–P1 2.2631(6), Pt1–N7 2.129(2), Pt1–N9 2.090(2), N7–Pt1–N9 81.39(9), Pt1···N11 3.525(3).

3.5 Exploring the Parameters of the New Library

The goal of this Chapter was to expand platinacarbynes to identify trends that might emerge from a controlled variation in co-ligands, given that few other systems in the literature are amenable to coordination sphere engineering. This has allowed the platinum terminus to by coordinated by a range of nitrogen, sulfur or phosphorus donors, thereby affording a wealth of spectroscopic information (Tables 3.3 and 3.4, *vide infra*). Some loose but far from definitive correlations are apparent and will now be discussed (Figure 3.26), noting the produced complexes occur of a narrow range of variation and within a margin of error. Although some molybdenum analogues were produced, only the tungsten examples will for consistency be discussed in detail, noting that tungsten is the primary metal of choice through the remaining Chapters.

The chemical shift for the carbido resonance in the $^{13}C\{^{1}H\}$ NMR spectra (δ_C) represents the datum most intimately associated with the carbide ligand itself. In the first instance, a correlation with the force constant of the carbonyl co-ligands (k_{CK})§§§§§§§§§§§§ might be anticipated given both CO and C–Pt 'ligands' involve retrodative bonding from tungsten. A plot of k_{CO} *vs* δ_C reveals no discernible correlation though the ranges for these variables are comparatively narrow (0.45 Ncm^{-1} for k_{CK} and 20 ppm for δ_C excluding the outlier **3**). Similar comparisons of δ_{Pt} *vs.* k_{CK} or W≡C bond length *vs.* k_{CK} also lack correlation, which is perhaps not surprising when considering the HOMO of the theoretical model complex **3.1*** (Section 3.3.2) is involved in the retrodonation with the carbonyls with no contribution from the carbyne fragment to which this δ-symmetry molecular orbital is orthogonal.

While no correlation was found between CO and C-Pt 'ligands' *within* the series, it is possible to order the C–Pt ligand within the wider context of carbynes in general, *viz hetero*-atomic carbynes wherein the platinum terminus is considered as an exotic, functionalised carbyne substituent. Given the now sizeable, diverse list featuring the [M(≡C–R)(CO)$_2$(Tp*)] (M = Mo, W) [116, 168, 255] framework, a collection of carbonyl vibrations can be considered for electronegative, electropositive, and metallic end groups. Carbonyl vibrations can once more be condensed to the singular Cotton-Kraihanzel force constants, [203-204, 303] and Taft's review[304] provides a series of Hammet parameters (σ_p and σ_m) to describe *para*- and *meta*- effects of more conventional organic carbyne substituents (Table 3.2).

§§§§§§§§§§§§ Two ν_{CO} values can be condensed to a Cotton-Kraihanzel force constant [$k_{CK} = 2.0191 \times 10^6 \Sigma(\nu_1^2+\nu_2^2)$] for an octahedral *bis*-carbonyl complex.

Table 3.2: Selected infrared data for carbynes complexes of the form [M(≡CR)(CO)$_2$(Tp*)].

M	R	ν_1 (CO) [cm^{-1}]	ν_2 (CO) [cm^{-1}]	k_{CK}[c] [Ncm^{-1}]	σ_m [304]	σ_p [304]
Mo	CN [90]	2026	1951	15.97	+0.56	+0.66
W	PPh_3^+ [305]	2026	1940	15.89	+0.74	+0.73
W	PEt_3^+ [306]	2020	1935	15.80	+0.74	+0.73
Mo	DMAP$^+$ [169]	2012	1929	15.66	+0.62	+0.58[e]
Mo	C(=S)NMe_2 [102]	2006	1925	15.58	+0.3	+0.34[f]
W	P(=O)Ph_2 [94, 307-308]	2004	1915	15.57	+0.38	+0.53
W	P(=S)Ph_2 [94, 307-308]	2004	1916	15.52	+0.29	+0.47
W	C(=O)Ph [64]	1999	1918	15.50	+0.34	+0.43
W	Br [88]	1994	1905	15.36	+0.39	+0.23
W	I [64]	1992	1907	15.35	+0.35	+0.18
W	H [64]	1992	1903	15.32	0.00	0.00
W	Cl [88]	1991	1902	15.32	+0.37	+0.23
W	$SnMe_3$ [99]	1979	1902	15.19	0.00	0.00[g]
W	$AsPh_2$ [110]	1983	1892	15.17	+0.03	+0.09
W	C≡CPh [138, 226]	1982	1893	15.17	+0.14	+0.16
W	$SiMePh_2$ [306]	1982	1889	15.14	+0.04	+0.07
W	PPh_2 [94, 307-308]	1982	1891	15.13	+0.11	+0.19
W	C_5H_4N-2 [144]	1981	1889	15.13	+0.33	+0.17
W	TeMe [309]	1977	1886	15.07	+0.01	0.00[h]
W	$SiMe_3$ [64]	1976	1884	15.05	–0.04	–0.07
W	CH(Ph)OH [64]	1976	1870	15.02	+0.08	–0.07[i]
W	SMe_2 [306]	1975	1880	14.99	+0.15	0.00
W	Ph [310]	1969	1876	14.93	+0.06	–0.01
W	$CH_2{}^tBu$ [311]	1969	1875	14.93	–0.05	–0.17
W	[Pt(phen)(PPh_3)]$^+$ (**3.10**)	1968	1874	14.91	––	––
W	[Pt(bpy)(PPh_3)]$^+$ (**3.8**)	1967	1875	14.91	––	––
W	[Pt(dtbbpy)(PPh_3)]$^+$ (**3.9**)	1967	1875	14.91	––	––
W	[Pt(NCMe)$(PPh_3)_2$]$^+$ (**3.2**)	1967	1872	14.89	––	––
W	OPh [305]	1967	1870	14.87	+0.25	–0.03
W	CH=CHPh [312]	1969	1867	14.87	+0.05	–0.02
W	Me [313]	1968	1867	14.86	–0.07	–0.17
Mo	Pt$Br(PPh_3)_2$ (**3.1a**)	1962	1873	14.86	––	––
W	NPh_2 [110]	1960	1859	14.73	0.00	–0.22
W	OMe [b 314]	1958	1862	14.71	+0.12	–0.27
Mo	Fe$(CO)_2$(Cp) [97]	1947	1865[d]	14.68	––	––
W	[Pt(terpy)]$^+$ (**3.7**)	1954	1858	14.68	––	––
W	$AuPEt_3$ [99]	1951	1856	14.64	––	––
W	PtBr(dppe) (**3.3b**)	1950	1856	14.63	––	––
W	Pt(Tp*)(PPh_3) (**3.12**)	1947	1854	14.59	––	––
W	Pt(Bp*)(PPh_3) (**3.11**)	1946	1853	14.58	––	––
W	Pt$Br(PPh_3)_2$ (**3.1b**)	1945	1854	14.59	––	––
W	Pt$(Bm^{Me})(PPh_3)$ (**3.5**)	1940	1848	14.49	––	––
W	$NiCl(PEt_3)_2$ [119]	1936	1843	14.42	––	––
W	Pt$(S_2CNEt_2)(PPh_3)$ (**3.4**)	1935	1843	14.42	––	––
W	NEt_2 [315-316]	1936	1833	14.35	–0.23	–0.72

[a]Unless otherwise indicated, data were measured in dichloromethane. [b]Measured in THF. [c]M $k_{CK} = (2.0191\times10^6)\Sigma(\nu\nu_1{}^2+ \nu\nu_2{}^2)$. [d]Fe$(CO)_2$: $\nu\nu_{FeCO}$ = 2040, 1991 cm^{-1}. [e]Value for 2,4,6-trimethylpyridinium. [f]Value for CSNHMe. [g]Value for $SnEt_3$. [h]Value for SeMe. [i]Value for CH(Me)OH.

Plotting the entire series of force constants (k_{CK}) for functionalised carbynes (including metallacarbynes) against each Hammett parameter returns a strong correlation with σ_p ($R^2 = 0.92$) yet less with σ_m ($R^2 = 0.72$). This is consistent with carbynes being largely influenced by mesomeric effects along the W≡C–R spine. Another feature of the σ_p regression is the lack of negatively-mesomeric carbyne substituents, and while a topic for future research, the trend suggests this void might be filled by further metallacarbynes, though metals with low d-occupancies and positive charge or oxidation state would be required to minimise the metal π-basicity. For the carbido complexes in this section the values of k_{CO} occupy a range (14.42–14.91 Ncm^{-1}) corresponding to negative values ($-0.17 > \sigma_p > -0.72$), indicating the 'R = PtL_n' fragments 'singly' bound to the carbido are positively mesomeric: retrodative and therefore π-basic, comparable to an amino substituent. This correlation of experimental carbonyl vibrations to the σ_p parameter support the partial π-delocalisation along the M≡C–Pt spine.

Calculations of **3.1*** did however show interesting interactions between carbido and the platinum terminus. The HOMO–6 revealed a π-contribution from platinum consistent with the contracted Pt–C bond length observed in the real complex **3.1b**. For this reason, δ_C was plotted against δ_{Pt}, returning a loose correlation ($R^2 = 0.89$) when two outliers are removed—the second rotational isomer of **3.1b** and the dithiocarbamate complex **3.4**. It is known that $^{195}Pt\{^1H\}$ NMR is sensitive to changes in platinum geometry which could either be provided by: (i) a rotational isomer significantly different from its counterpart such as a side-conformation; or (ii) dithiocarbamate ligands known to chelate and alter the platinum geometry through a sharper bite angle when compared with, *e.g.*, a *bis*(thioimidazolyl)borate (S1–Pt1–S2: 74.05(3) **3.4** *cf.* 93.6(1) ° **3.5**). This loose correlation also breaks down when molybdenum complexes are included though too few were considered for a meaningful comparison.

Given the loose correlation between the chemical shift of ^{195}Pt (δ_{Pt}) and ^{13}C (δ_C) carbido signals, a correlation between δ_{Pt} and the reduced Pt–C bond length (1.934(6)–1.990(6) Å) was tested. Another loose correlation ($R^2 = 0.70$) is found again by excluding dithiocarbamate **3.4** as an outlier, however, this strengthens by excluding κ^2-Tp* complex **3.12** ($R^2 = 0.80$). The dithiocarbamato ligand is sterically unassuming but a potent π-donor and so its outlier position is not unreasonable. The anomalous position of the resonance for **3.12** is more difficult to accommodate however it should be stressed that the Pt–C bond length arises from a static solid state structure while δ_{Pt} was determined in solution, wherein fluxional site exchange of free and coordinated pyrazolyl donors [317] may occur via intermediate(s) of increased coordination number at

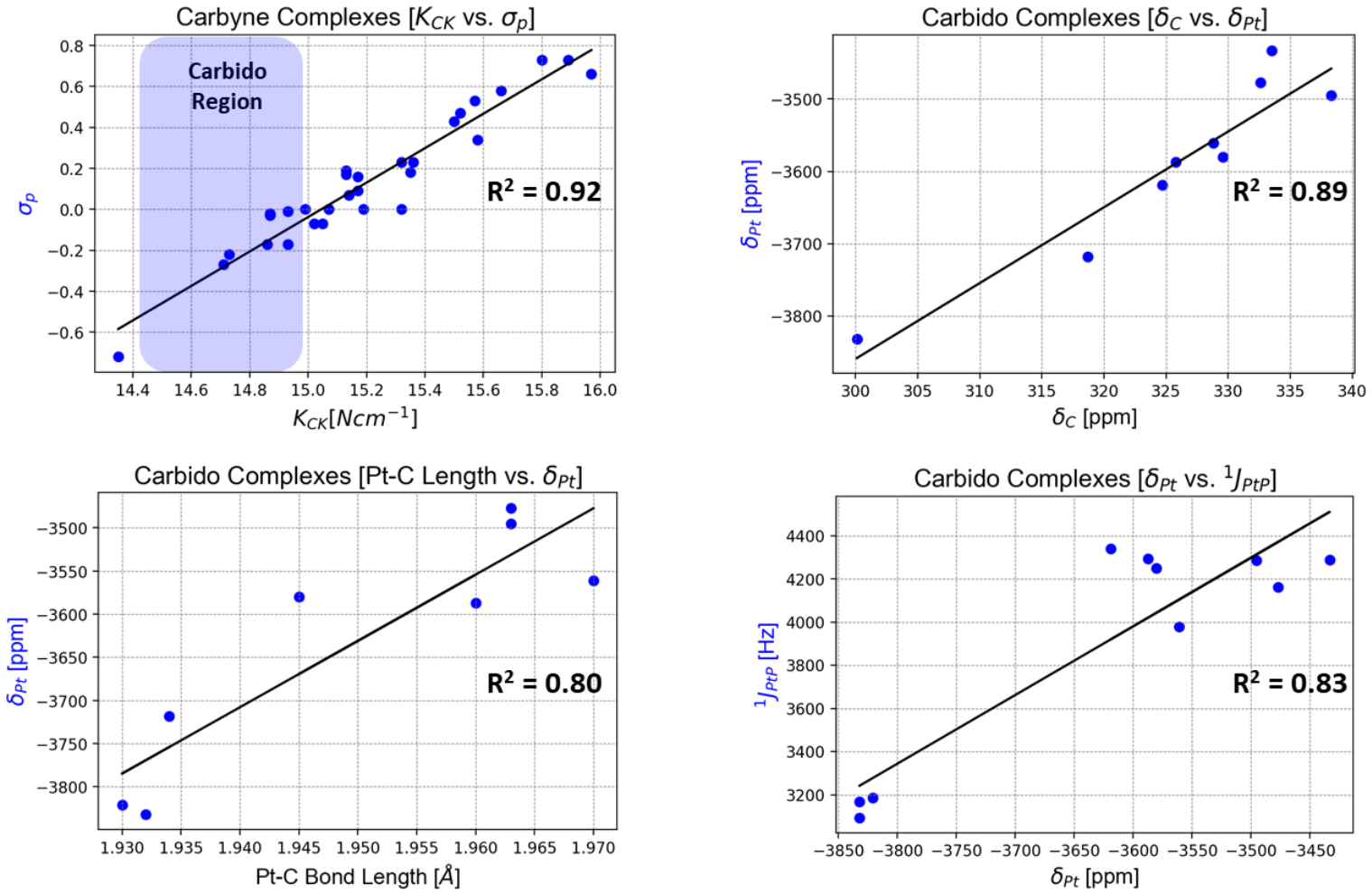

Figure 3.26: Regression analysis of metallacarbyne properties. Upper Left: Correlation between k_{CK} of carbyne complexes from Table 3.2. Upper Right: Correlation between δ_C and δ_{Pt} of tungsten-platinum metallacarbynes {excluding **3.4**}. Bottom Left: Correlation between Pt–C bond length and δ_{Pt} of tungsten-platinum metallacarbynes {excluding **3.4** and **3.12**}. Bottom Right: Correlation between δ_{Pt} and $^1J_{PtP}$ of tungsten-platinum metallacarbynes {excluding 3.4}.

Table 3.3: Spectroscopic properties of metallacarbynes and related species or precursors as discussed in this Chapter.

Compound	δ_C (ppm)[a]	J_{CP} (Hz)	δ_P (ppm)[a]	J_{PP} (Hz)	δ_{Pt} (ppm)[a]	J_{PPt} (Hz)	$\nu\nu_{CO}$ (cm^{-1})[b]
[**Mo**]≡CBr (**2.1a**)	202.5	–	–	–	–	–	2008, 1924
[**W**]≡CBr (**2.1b**)	198.0	–	–	–	–	–	1994, 1905
[**Mo**Pt(μ-C)Br(PPh_3)$_2$] (**3.1a**)	339.0 335.7	9, 5	23.76, 19.38 26.39, 21.00	– 438	– –3810	– 3200	1961, 1872 –
[**W**Pt(μ-C)Br(PPh_3)$_2$] (**3.1b**)	317.2 318.7	8	28.27, 23.91 26.21, 22.11	443 443	–3821 –3718	3187 3202	1945, 1854 1988, 1894
[**W**Pt(μ-C)(NCMe)(PPh_3)$_2$]OTf (**3.2**)	300.1	10, 4	23.29, 19.68	385	–3832	3169 3093	1967, 1872 1949, 1856
[**Mo**Pt(μ-C)Br(dppe)$_2$] (**3.3a**)[c]	377.1	77	33.60, 32.89	4059, 1548	[d]	[d]	1965, 1876
[**W**Pt(μ-C)Br(dppe)$_2$] (**3.3b**)[c]	356.7	74	38.10, 34.51	4068, 1548	[d]	[d]	1950, 1856
[**W**Pt(μ-C)(S_2CNEt_2)(PPh_3)] (**3.4**)	338.4	6	13.68	–	–3828	3880	1935, 1843
[**W**Pt(μ-C)(Bm^{Me})(PPh_3)] (**3.11**)	328.8	8	14.62	–	–3561	3979	1940, 1848
[**W**Pt(μ-C)(terpy)] (**3.5**)	368.0	–	–	–	[d]	[d]	1954, 1858
[**W**Pt(μ-C)(bpy)(PPh_3)]PF_6 (**3.6**)	325.8	9	16.37	–	–3587	4293	1967, 1835
[**W**Pt(μ-C)(dtbbpy)(PPh_3)]PF_6 (**3.7**)	329.6	[e]	16.25	–	–3580	4250	1967, 1875
[**W**Pt(μ-C)(phen)(PPh_3)]PF_6 (**3.8**)	324.7	8	15.73	–	–3619	4341	1968, 1874
[**W**Pt(μ-C)(Bp*)(PPh_3)] (**3.9**)	338.3 332.6	11 9	7.52 5.38	– –	–3495 –3477	4285 4161	1946, 1853
[**W**Pt(μ-C)(κ^2-Tp*)(PPh_3)] (**3.10**)	333.5	8	3.07	–	–3433	4288	1947, 1854

Note: Bolded metals include the common ligand set {i.e Mo = Mo(CO)$_2$(Tp*) and W = W(CO)$_2$(Tp*)}. [a]Measured in $CDCl_3$ unless specified. [b]Measured in CH_2Cl_2 unless specified. [c]Measured in CD_2Cl_2. [d]Insufficiently soluble to detect resonance. [e]Coupling was unable to be resolved, thus signals appears as a multiplet.

Table 3.4: Structural properties of metallacarbynes as discussed in this Chapter.

Compound	M≡C (Å)	M'–C (Å)	$\angle_{M\equiv C-M'}$ (°)	*Trans*–M'–L (Å)	Torsion (°)
[**Mo**Pt(μ-C)Br(PPh_3)$_2$] (**3.1a**)	1.828(3)	1.951(3)	173.97(15)	2.5448(3)	5.25(9)
[**W**Pt(μ-C)Br(PPh_3)$_2$] (**3.1b**)	1.856(6)	1.934(6)	169.2(3)	2.5274(8)	7.1(2)
[**W**Pt(μ-C)(NCMe)(PPh_3)$_2$]OTf (**3.2**)	1.839(7)	1.932(7)	177.3(5)	2.051(6)	2.0(3)
[**Mo**Pt(μ-C)Br(dppe)$_2$][c] (**3.3a**)	1.818(5)	1.981(6)	167.9(3)	2.341(1)	22.4(2)
[**W**Pt(μ-C)Br(dppe)$_2$][c] (**3.3b**)	1.833(5)	1.990(6)	172.7(4)	2.331(1)	24.7(2)
[**W**Pt(μ-C)(PPh_3)(S_2CNEt_2)] (**3.4**)	1.843(4)	1.947(4)	167.1(2)	2.4166(8)	28.6(1)
[**W**Pt(μ-C)(Bm^{Me})(PPh_3)] (**3.5**)	1.83(1)	1.97(1)	166.9(7)	2.455(2)	17.8(5)
[**W**Pt(μ-C)(Tm^{Me})(PPh_3)] (**3.6**)	1.830(6)	1.947(6)	170.3(3)	2.456(1)	1.3(2)
[**W**Pt(μ-C)(terpy)] (**3.7**)	1.835(5)	1.938(5)	176.3(3)	2.002(5)	10.9(2)
[**W**Pt(μ-C)(bpy)(PPh_3)]PF_6 (**3.8**)	1.820(5)	1.960(6)	164.5(4)	2.142(5)	172.3(2)
[**W**Pt(μ-C)(dtbbpy)(PPh_3)]PF_6 (**3.9**)	1.839(5)	1.945(5)	168.2(2)	2.149(3)	178.1(1)
[**W**Pt(μ-C)(Bp*)(PPh_3)] (**3.11**)	1.835(7)	1.963(7)	175.3(6)	2.138(6)	158.8(3)
[**W**Pt(μ-C)(κ^2-Tp*)(PPh_3)] (**3.12**)	1.861(2)	1.954(2)	175.2(1)	2.129(2)	150.97(8)

platinum that contribute to the observed (time-averaged) chemical shift which might therefore not correspond to that of the truly 4-coordinate structure.

Further consideration of the platinum terminus reveals another two loose correlations: δ_{Pt} values occupy different regions depending, as expected, on the donor ligand. Cationic complexes with nitrogen donors appear most upfield, followed by neutral counterparts, with thioimidazolylborates and lastly phosphine/halide-based species being the most downfield. A similar observation is made when comparing $^{1}J_{PtP}$ as a measurement of the bonding between platinum and the remaining phosphine, where ligand substitution and changing donors would alter the platinum environment.[264, 318-321] Indeed, plotting $^{1}J_{PtP}$ as a function of δ_{Pt} reveals a loose correlation ($R^2 = 0.83$) once more removing the outliers **3.4** one rotational isomer of **3.1b**.

3.6 Conclusions

In this Chapter, the platinacarbynes [MPt(μ_2-C)Br$(CO)_2(PPh_3)_2$(Tp*)] (M = Mo and W) have been shown to contain labile bromide and phosphine ligands useful in a series of ligand substitution reactions to elaborate the field. The series of substitution reactions varying the donor ligand to tune platinum metallacarbynes in several ways. Neutral or anionic donors for neutral or cationic platinum(II) centres, moderated by soft (P, S) donors, hard (N) donors, for a variety of π-basic and π-acidic ligands. Complexes bear ligands of various sizes and denticities from slender mono-dentate acetonitrile ligands to large, *bi*- and *tri*-dentate scorpionate ligands, such that ligands can feature pendant ligands option to preserve the square plane of platinum(II). Each new metallacarbyne is rich with spectroscopic and structural information, and while a large amount of data can be obtained no particularly strong correlations emerged between the variables, other than a loose correlation between the carbido and platinum chemical shifts (δ_C *vs* δ_{Pt}).

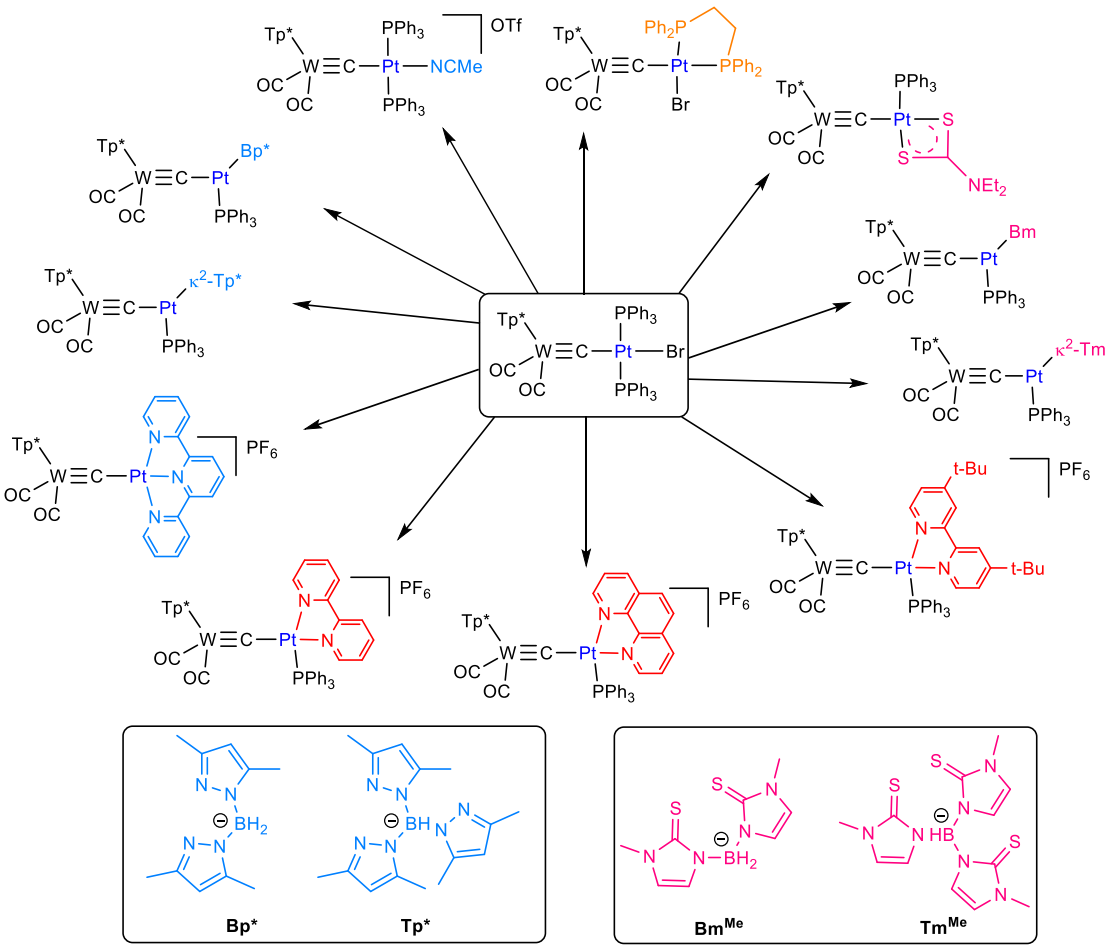

Chart 3.3: Expansion of tungsten-platinum metallacarbynes stemming from oxidative addition and subsequent ligand substitution.

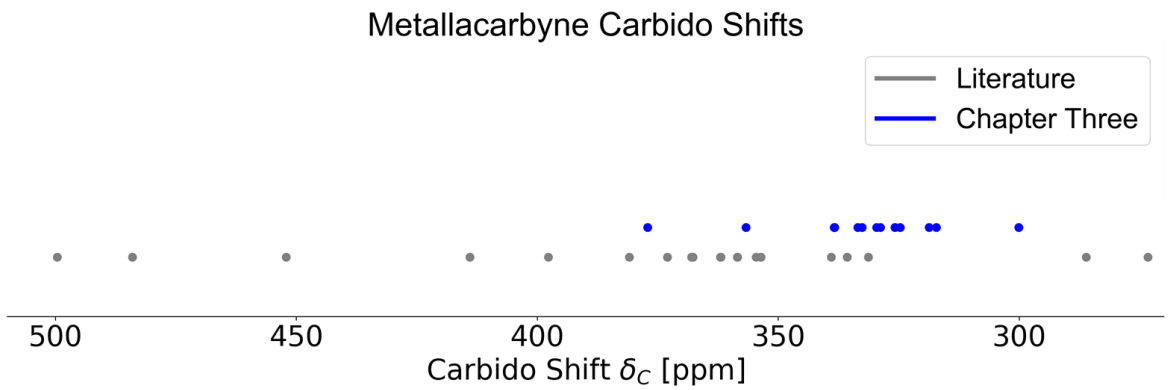

Figure 3.27: Chemical shifts of μ_2-carbido ligands from literature metallacarbynes (grey) and those contributed in this chapter (blue). Note: These values are not adjusted for solvents which may have a profound effect.

Chapter Four

Isocyanide Metallacarbynes and μ_2-iminoketenylidene Ligands

The synthetic versatility of the metallacarbyne [WPt(μ_2-C)Br(CO)$_2$(PPh$_3$)$_2$(Tp*)] (**3.1b**) with respect to ligand substitution providing a library of diverse μ_2-carbido complexes was amply demonstrated in the preceding Chapter. By choosing classical characteristically 'innocent' co-ligands, including sterically demanding variants, a wealth of spectroscopic and structural data could be acquired without risk of the carbido linkage being compromised. This Chapter, and those that follow, take a complementary approach by specifically setting out to engineer situations in which the reactivity of the carbido linkage itself may be investigated. Specifically, the installation of co-ligands with the potential for 'non-innocent' behaviour (isonitriles,[**********] hydrides, and metal-carbon bonds) sets the stage for exploring C–H and C–C bond forming processes. These are not only of interest in the context of the behaviour of surface-bound carbido centres in the heterogenous Fischer-Tropsch synthesis (C–H and C–C bond-formation), but might inform the development of catalytic cycles involving molecular carbido complexes (Chapter Six).

To address the primary goal of exploring the uncharted reactivity of Class B carbidos, smaller co-ligand sets that better expose the metal-carbon linkage would be a desirable feature. Isocyanide complexes of platinum have a long history dating back to the works of Tschugajeff in the early 20th century. [323] Their coordination to platinum involves conventional synergic σ-donor/π-acid bonding with the caveat that the poor π-basicity of platinum(II) results in activation of the isonitrile towards nucleophilic attack. Isocyanides generally bind more strongly to platinum relative to CO and are more slender than typical carbenes with a generally well-understood chemistry, especially within the coordination sphere of platinum(II). [324-329] Furthermore, whilst the size of isocyanides might open access to the μ_2-carbido, their strong σ-donor and modest π-acidity would be expected to result in a comparatively electron-rich platinum terminus.

4.1 Basis for Isocyanide Ligands

The confluence of carbide and isocyanide chemistries is previously limited to two reports (Scheme 4.1). An early dimetallacumulenic Class A carbido complex was prepared by Wolczanski *via* the activation of the C–N multiple bond of an isocyanide. [330] Subsequently, Templeton utilsed isocyanides for regioselective (Fe *vs* Mo) ligand substitution in one of the few studies of metallacarbyne reactivity,

[**********] As in the literature, the terms isonitrile and isocyanide are used interchangeably throughout. IUPAC eschews the term isonitrile, considering it to be obsolete by 1995, however it defiantly remains in current use. [322]

whereby [MoFe(μ2-C)(CN^{t}Bu)2(CO)2(Cp)(Tp*)] is obtained upon photolytic decarbonylation of [MoFe(μ2-C)(CO)4(Cp)(Tp*)].[97]

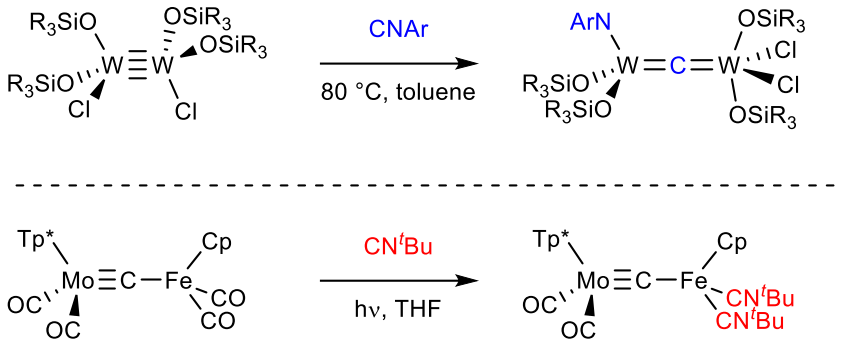

Scheme 4.1: Prior involvement of isocyanide ligands in μ2-carbido chemistry. a) capture of an isonitrile to install a μ2-carbide, b) photolysis of carbonyls in favour of isocyanide coordination.

The reported reactivity of carbido ligands (Scheme 4.2) is limited, consisting of: (i) protonation (direct);[97] (ii) migratory (indirect);[78, 119] (iii) insertion (indirect);[97] (iv) cycloaddition (direct);[40, 128] (v) redox (direct or indirect);[56, 161] (vi) class interconversion (indirect);[73] and (vii) carbene-like (direct).[40, 129-130] Furthermore, μ2-carbidos have also been used as electron relays, however, the carbido linkage is unlikely to undergo structural changes in these processes and is therefore excluded.[133-135, 266] Only one example of μ2-carbido protonation has been recorded where the *agostic* methylidyne [MoFe(μ2-CH)(CO)4(Cp)(Tp*)]BF4 is produced upon treating [MoFe(μ2-C)(CO)4(Cp)(Tp*)] with the strong acid HBF4.[97] A growing number of examples exhibiting migratory reactivity are beginning to emerge. A phosphine in [WNi(μ2-C)Cl(CO)2(PEt3)2(Tp*)] was shown to migrate to form phosphoniocarbyne [WNi(μ2-CPEt3)Cl(CO)2(PEt3)(Tp*)],[119] and recently halide migration from a proposed intermediate [Rh2(μ2-C)X6(μ-dppm)2] (X = Cl or Br) is likely the mechanism of μ2-halocarbyne [Rh2(μ2-CX)(μ-X)X4(μ-dppm)2] formation.[78] Another phosphine migration to a μ2-carbido has also since been published as a consequence of this work,[252] but is not discussed until Chapter Six. These reactivity examples are interesting, however, many occur on similar ligand frameworks; hence it is difficult to ascertain the influence of the ligand sphere on reactivity. The insertion of CS_2 into the Fe–C bond of [MoFe(μ2-C)(CO)4(Cp)(Tp*)][97] and cycloadditions of CS_2[130] or benzyne[128] to dimetallacumulenic carbidos most likely involves prior interaction of the reagent with the metal centre prior to C-element bond formation and therefore might be included as an insertion process. In contrast, the addition of selenium may occur *via* the metal centre for Class A carbidos[130] or in the case of Class D carbidos via electrophilic attack directly at the nucleophilic carbido carbon.[129-130]

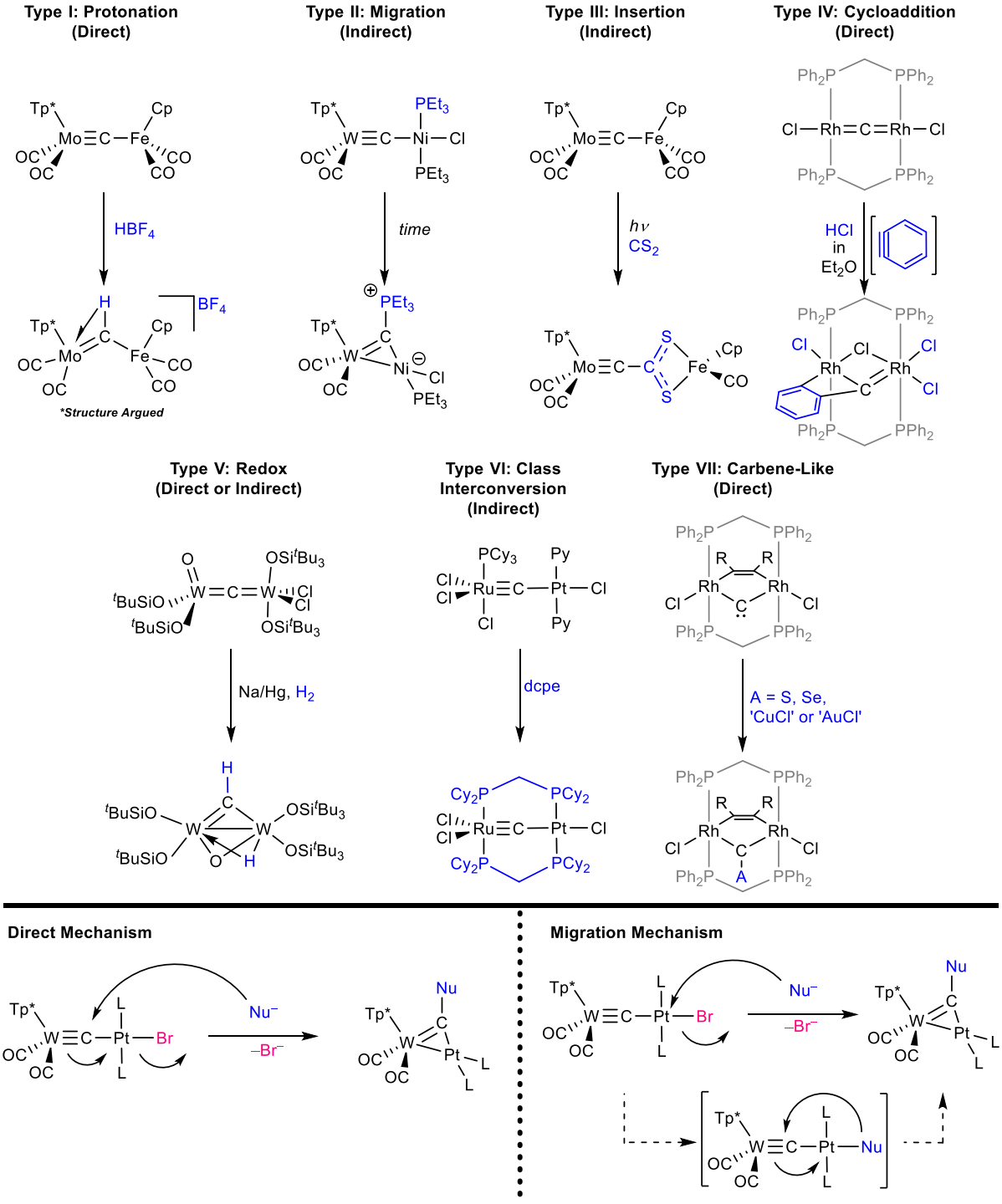

Scheme 4.2: A) Types of reactivity in μ2-carbido complexes. B) Mechanistic distinction between direct and indirect (migration) reactivity expected for tungsten-platinum metallacarbynes.

4.2 Platinacarbyne Substitution with Isocyanides

Three isocyanide variants were employed in the work to follow: 2,6-dimethylphenylisocyanide (CNXyl) as it is commercially available; 2,4,6-trimethylphenylisocyanide (CNMes) for typically favouring crystallisation; and *tert*-butylisocyanide (CN^{t}Bu, also commercially available) for stronger donor properties. Stirring a toluene solution of **3.1b** with one equivalent of isocyanide resulted in substitution of one phosphine to provide the mixed phosphine-isocyanide metallacarbynes [WPt(μ-C)Br(CNR)(CO)$_2$(PPh$_3$)(Tp*)] (R = Xyl **4.1**, Mes **4.2**; ^{t}Bu **4.3**, Scheme 4.3). The reaction progress could be monitored through either infra-red spectroscopy (ν_{CN}: ~ 2200 cm^{-1}) or ^{31}P{^{1}H} NMR spectroscopy (δ_P with $^1J_{PPt}$: ~ 3400 Hz). Formation of **4.3** is rapid owed to the more nucleophilic nature of CN^{t}Bu (*N* = 5.47) *cf.* CNXyl (*N*= 4.90)[331] where the aryls take longer. The rate dependence upon the nucleophilicity of the isocyanide points towards an associative or, given the steric congestion around platinum, possibly interchange-associative mechanisms.

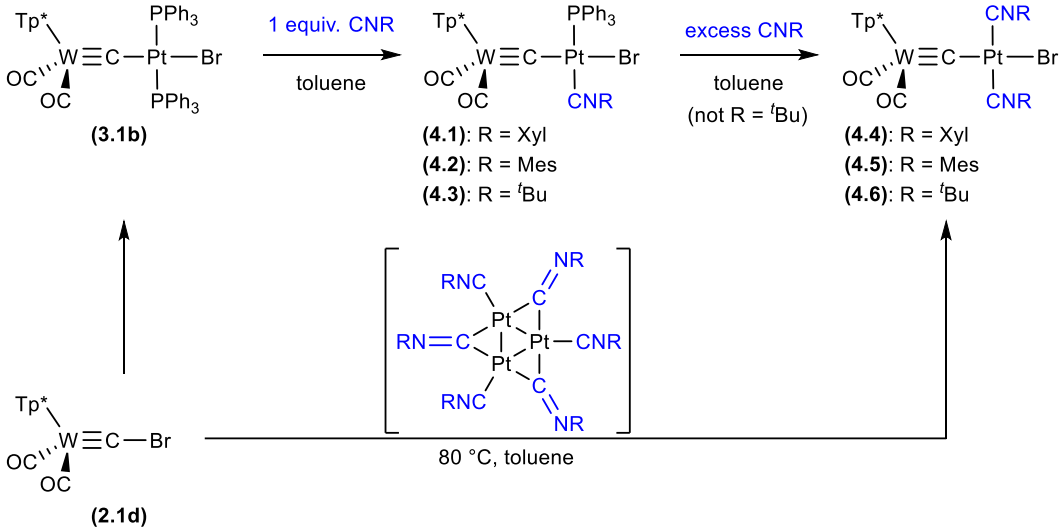

Scheme 4.3: Substitution reactions utilising isocyanides.

Substitution was also attempted with *N*-isocyanoiminotriphenylphosphorane (CNNPPh$_3$) as a more exotic isocyanide originally prepared by Fehlhammer as a form of isodiazomethane storage,[332-333] anticipating decomposition of the ligand might provide further species of interest, optimistically, delivery of C$_1$. No substitution occurred at ambient temperature whereas heating resulted in inconsistent, complex mixtures, perhaps unsurprising given the potential for fragmentation of this species.[334-339] Analytically pure samples of the new isocyanide complexes prepared via substitution were obtained through recrystallisation, as in contrast to the phosphine precursor **3.1b**, these species were not amenable to flash chromatography (see Section 4.4).

Initial investigations specifically employed one equivalent of isocyanide, however reactions of **3.1b** with bi- or tridentate ligands (discussed previously) confirm that both phosphines may, in principle, be substituted. By providing two equivalents of isocyanide (or excess) to **3.1b** (*ca* 63 mmolL^{-1}) in toluene,

the *bis*-isocyanide complexes [WPt(μ-C)Br(CNR)$_2$(CO)$_2$(Tp*)] (R = CNXyl **4.4**; CNMes **4.5**) begin to precipitate; **4.4** remains partially soluble, while **4.5** precipitates entirely. This difference in behaviour forshadows the influence a single peripheral methyl group has on solubility as **4.4** is soluble in many common organic solvents, yet **4.5** is only soluble in $CHCl_3$/$CDCl_3$ which, while convienient for NMR spectroscopy, proves challenging for further application. Meanwhile, addition of excess CN^{t}Bu to **3.1b** exclusively forms **4.3**, without replacing the second phosphine even when 10 equivalents are used and stirring continued for several days. It is likely that the strong σ-donation of CN^{t}Bu facilitates the first substitution, however a *trans*- phosphine appears to be favourable in a synergic position across platinum(II). Therefore, species **4.3** represents an energetic minimum for CN^{t}Bu addition, unable to produce [WPt(μ_2-C)Br(CN^{t}Bu)$_2$(CO)$_2$(Tp*)] (**4.6**) *via* phsophine substitution.

Opening the μ_2-carbido space (*sic.*) means the species **4.6** bearing two slender CN^{t}Bu ligands remained a desirable synthetic target. As substitution failed to produce **4.6**, an alternative pathway was sought. In addition to substitution, Chapter Three clearly demonstrated that, steric occlusion notwithstanding, oxidative addition was a viable method to produce platinum(II)-based metallacarbynes, *e.g.*, **3.1b**. Accordingly, a platinum(0) isocyanide source synthetically equivalent to 'Pt(CN^{t}Bu)$_2$' was required to possibly provide access to **4.6**. Stone previously described the preparation of low valent trimeric species [Pt$_3$(μ-CNR)$_3$(CNR)$_3$], [340] some chemistry of which is consistent with facile cleavage of the *triangulo* structure, *e.g.*, the reaction with hexafluoroacetone to afford monomeric [Pt^{II}{η^2-OC(CF$_3$)$_2$OC(CF$_3$)$_2$}(CN^{t}Bu)$_2$]. Thus by employing [Pt(η^2-nbe)$_3$] as an alternative to the 'ligand-free' source of platinum(0) [Pt(COD)$_2$] (COD = 1,5-cyclooctadiene) [197] with controlled amounts of isocyanides, the platinum clusters *triangulo*-[Pt$_3$(μ-CNR)$_3$(CNR)$_2$] (R = ^{t}Bu, Xyl, Mes) could be generated and used *in situ* without isolation. Combining these platinum trimers with bromocarbyne [W(≡CBr)(CO)$_2$(Tp*)] (**2.1d**) under various conditions provided the aforementioned *bis*-isocyanides **4.4** and **4.5**, in addition to the missing **4.6** following recrystallisation, albeit in a somewhat disappointing yield (37% isolated). This yield was not improved despite multiple attempts, thus subsequent reactivity studies focused on more readily available **4.4** and **4.5**.

Although not explored further here, zerovalent binary isonitrile complexes are known for *inter alia*, palladium, [341] iron, [342] and nickel, [343] all of which are prone to oxidative addition processes promising a degree of generality. The caveat of oxidative addition in the present case is that yields of **4.4**/**4.5** are lower compared to substitution (35/42% *vs* 74/91%, respectively) compounded by the challenging, multi-step synthesis of [Pt(η^2-nbe)$_3$]. [344-345] To further test the trimer method, the CNNPPh$_3$ ligand was treated with [Pt(η^2-nbe)$_3$] to generate the triangulo-species without purification, before addition of **2.1d** provided an even greater indeterminate mixture of products, that could not be separated to provide evidence of

[WPt(μ_2-C)Br(CNNPPh$_3$)$_2$(CO)$_2$(Tp*)]. Oxidative addition to other platinum(0) species generated *in situ* was not investigated further, although it is likely other metallacarbynes would emerge from this strategy.

Substitution preferences of the chosen isocyanides in phosphine-based **3.1b** were now clear. However, the repeated emergence of **4.3** supported by a presumably synergistic cooperation of alkyl-isocyanide and aryl-phosphine across platinum(II) invited study to determine which ligand would be retained if a further substitution reaction was attempted. Previously developed conditions to produce scorpionate [WPt(μ_2-C)(Bp*)(CO)$_2$(PPh$_3$)(Tp*)] (**3.9**) supplied an ideal system to test if an isocyanide or phosphine is lost upon addition of a bidentate ligand to a tungsten-platinum metallacarbyne framework (Scheme 4.4).

Firstly, heating the mixed isocyanide-phosphine **4.2** with KBp* in tetrahydrofuran afforded [WPt(μ_2-C)(Bp*)(CNMes)(CO)$_2$(Tp*)] (**4.7**) accompanied by minor amounts of **3.9** such that the stronger σ-donating aryl-isocyanide is retained over phosphine if supplied with both options. Heating was still required to overcome the combination of sterically clashing pyrazolyl ligands separated by a single carbon and may influence the relative amounts of **4.7** and **3.9**. The derivative **4.7** could also be produced from substitution of *bis*-isocyanide **4.5** with KBp*, or extended to tridentate KTp* to give [WPt(μ_2-C)(κ^2-Tp*)(CNMes)(CO)$_2$(Tp*)] (**4.8**) with a pendant pyrazolyl ring that does not interact with platinum or displace the isocyanide. Hence, the *bis*-arylisocyanide is likely a versatile platform for substitution and would likely perform similarly to **3.1b** in other reactions outlined in Chapter Three.

By comparing phosphine-based **3.9** with the isocyanide analogue **4.7**, the direction of substitution remained unvalidated. Stirring a tetrahydrofuran solution of **3.9** in the presence of CNMes resulted in minimal conversion to **4.7** even with heating (*ca* 60 °C). The reverse, heating **4.7** with PPh$_3$, also returned only starting material after two days heating at reflux. This suggests that the isocyanide is more strongly bound compared with the phosphine and is not reversible. Given substitution is typically associative for platinum(II), this also implies the reaction is driven by the thermodynamics of the products, or the ligand lost from a 5-coordinate intermediate. Therefore in the reaction of the mixed species, substitution of isocyanide is either unlikely or if it does occur, the liberated isocyanide would irreversibly replace the phosphine in a second step to return **4.7** anyway.

Analogous reactivity was not recorded for the alkylisocyanide CN^{t}Bu. Firstly, no substitution of **4.3** with KBp* was recorded despite multiple days at reflux, returning exclusively starting material, supporting the sturdy nature of **4.3**. Secondly, treating **3.9** with CN^{t}Bu also recorded no evidence of substitution, again after multiple days of reflux. Most curiously, if given no other choice and **4.6** is heated under reflux with KBp*, complete retention of starting material is recorded. Surprisingly this shows that **4.6** is exceptionally stable once formed *via* alternative pathways, and only certain isocyanides can substitute the phosphine of **3.9** once the scorpionate is installed on platinum, likely attributed between mutually beneficial bonding between arylisocyanides and pyrazolyl-nitrogen donors across platinum. Furthermore,

production of [WPt(μ_2-C)(CN^{t}Bu)(CO)$_2$(Bp*)(Tp*)] with an alkylisocyanide was unlikely and species **4.3** proved remarkably robust.

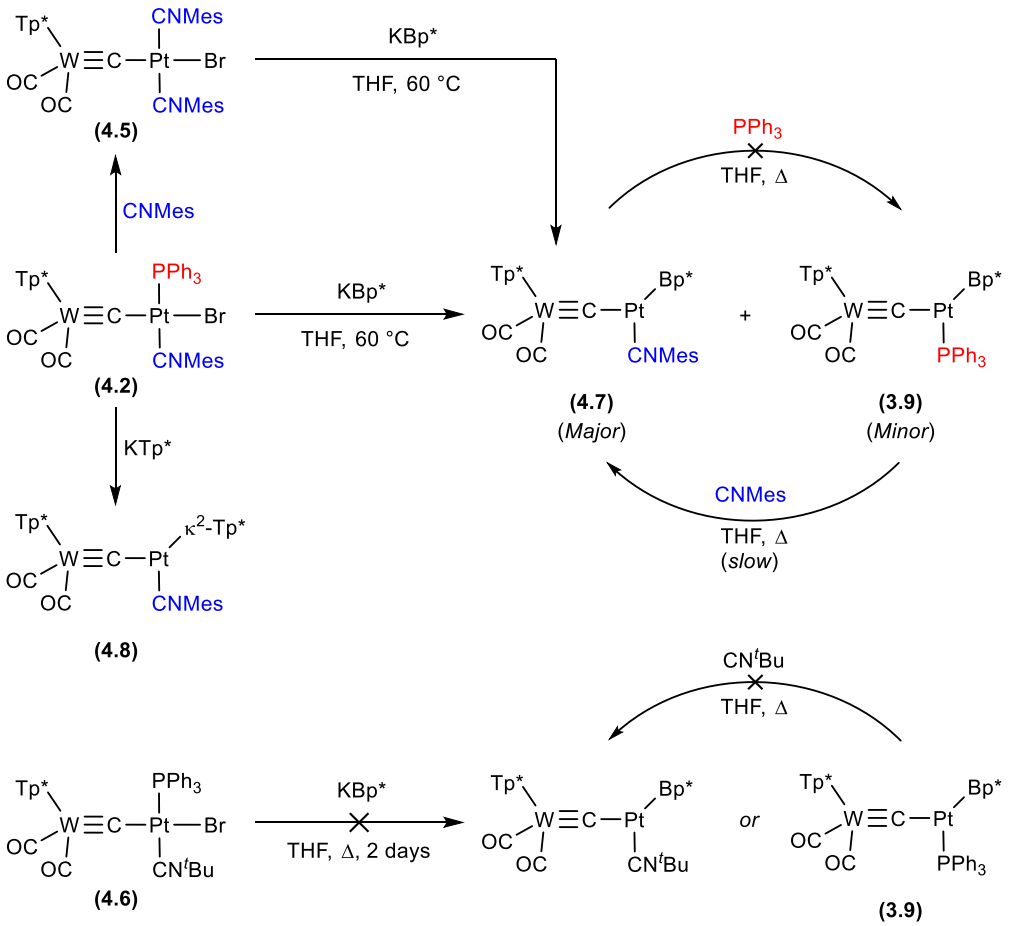

Scheme 4.4: Substitutions with scorpionate to determine relative binding strength of isocyanide compared with phosphine.

4.3 Spectroscopic and Structural Properties of Isocyanide Metallacarbynes

A collection of isocyanide metallacarbyne complexes have been produced through phosphine substitution or oxidative addition (Chart 4.1), the structural and spectroscopic data for which are summarised below (Table 4.1–4.2). Single crystal X-ray diffraction studies revealed that ligand variations gave only subtle differences to geometric parameters associated with the W≡C–Pt linkage compared to those of metallacarbynes previously reported (Figure 4.1–4.2 and 4.5–4.9).[159, 252-253] The W≡C triple bond retains similar character and the contracted Pt–C length spans a very short range (W–Pt: 1.931(6)–1.957(3) Å) such that variations are not statistically significant (≅ 6 e.s.d.). However, the shortest Pt–C length is in **4.6** (1.931(6) Å) with the smallest ligand set and the Pt–C bonds marginally shorter on average than those from Chapter Three, suggesting contraction if allowed by smaller ligands.

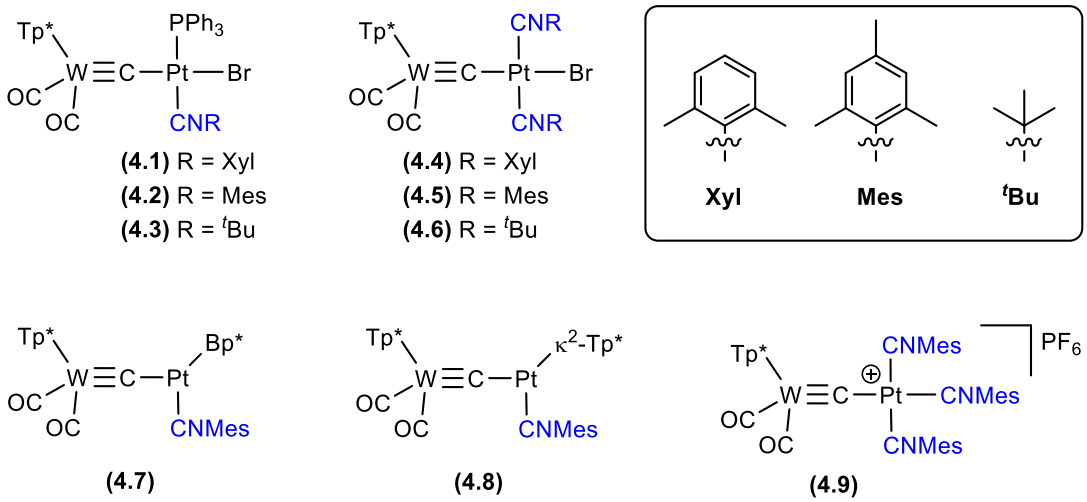

Chart 4.1: Isocyanide metallacarbynes prepared by substitution of **3.1b**.

The more interesting structural feature is the spine angle W–C–Pt (°). Several examples from Chapter Three contain bent linkages (164.5(4)–172.7(4)°) as a consequence of larger ligands, however, the isocyanide species tend to be more linear (171.2(3)–178.1(3)°). The most linear linkages are those for the *bis*-isocyanide derivatives. In contrast, the mixed isocyanide/phosphine complexes **4.1**/**4.2** both exhibit the *syn* conformation with the phosphine occupying the Tp* cleft. This requires modest bending of the spine (168.0(3) – 168.4(3) Å), extending support that phenyl-twisting owed to crystal packing.

The most pronounced change is exhibited by the scorpionates **4.7**/**4.8**, where the arylisocyanide plane is near orthogonal to the plane of platinum(II) (dihedral angles: 78.5(5)/92.5(3)°). Analysis of the crystal packing shows that the isocyanides do not stack in the solid state. The xylylisocyanide in **4.1** has no twisting and negligible π-stacking, while the *bis*-species stacks similarly but with significant twisting (40.7(4)°) (Inset, Figure 4.10). As expected, the mesitylisocyanide complexes featuring pronounced π-stacking, such that **4.2** and **4.5** undergo little to no twisting; the lattice of **4.5** stacks remarkably like sheets despite the globular Tp* group being expected to disfavour this.

Another intriguing feature of the isocyanide complexes is the 'tilting' of the isocyanides *towards* the tungsten-Tp* cleft, most evident for **4.6** containing *pseudo*-conical *tert*-butylisocyanides. For the structure of **4.6**, the angle between N7–Pt1–N8 bends away from the idealised (180°) geometry for square-planar platinum (168.0(2)°) while the bending is absent in the related **4.4**/**4.5** aryl isocyanide structures. Isocyanide ligands are certainly capable of bending at nitrogen, though only when coordinated to electron-rich π-basic metals centres,[340, 343, 346-350] however that is certainly not the case here (the C–N–C linkages are close to 180°) and this tilting most likely arises from other factors. To explore this deformation, a series of model complexes [Pt(C≡A)(L)$(CNH)_2$] {A = CH, N, P, and $W(CO)_2$(Tp)} were optimised *in silico* (DFT: ωB97X–D/6–31G*/LANL2DZ), where the ligand (L) was either a π-donor (Br)

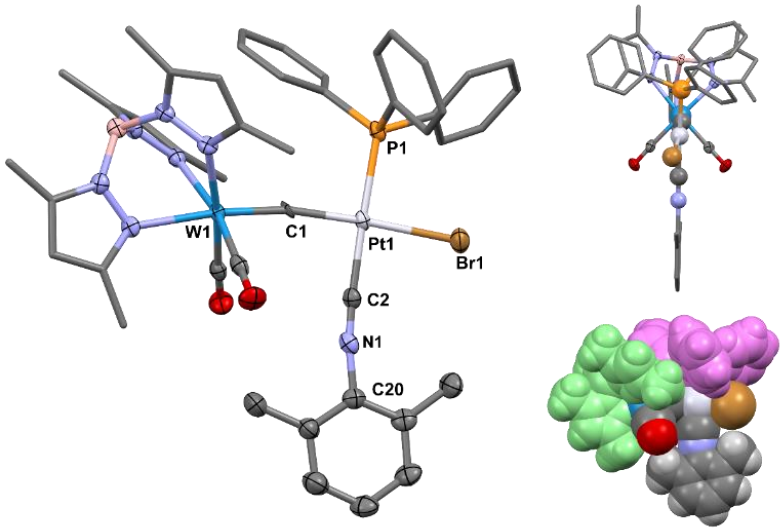

Figure 4.1: Molecular structure of [WPt(μ-C)Br(CNXyl)(PPh_3)$(CO)_2$(Tp*)] (**4.1**) in a single crystal of **4.1**·CH_2Cl_2 as determined by X-Ray Diffractometry. Ellipsoids are drawn at the 50% probability surface with phenyl and pyrazolyl rings simplified and CH_2Cl_2 solvent and hydrogens omitted for clarity. Insets: a) Ball and stick representation as viewed down the key molecular linkage, b) Space-filling representation highlighting the steric clash of phenyl rings (pink) and the sterically encumbering *tris*-pyrazolylborate (green) ligand. Selected bond lengths (Å) and angles (°): W1–C1 1.843(4), C1–Pt1 1.940(4), Pt1–Br1 2.5248(7), Pt1–P1 2.309(1), Pt1–C2 1.996(6), C2–N1 1.145(8), N1–C20 1.405(8), W1–C1–Pt1 168.4(3), C1–Pt1–Br1 174.1(1), P1–Pt1–C2 177.8(2), Pt1–C2–N1 175.7(5), C2–N1–C20 170.9(6).

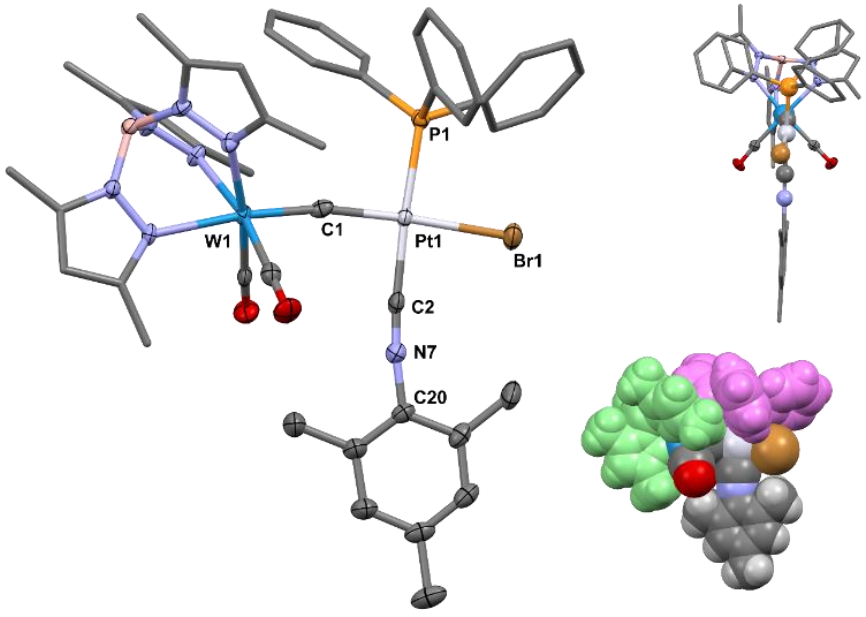

Figure 4.2: Molecular structure of [WPt(μ-C)Br(CNMes)(PPh_3)$(CO)_2$(Tp*)] (**4.2**) in a single crystal of **4.2**·$CHCl_3$ as determined by X-Ray Diffractometry. Ellipsoids are drawn at the 50% probability surface with phenyl and pyrazolyl rings simplified and $CHCl_3$ solvent and hydrogens omitted for clarity. Insets: a) Ball and stick representation as viewed down the key molecular linkage (ligands simplified for clarity), b) Space-filling representation highlighting the steric clash of phenyl rings (pink) and the sterically encumbering *tris*-pyrazolylborate (green) ligand. Selected bond lengths (Å) and angles (°): W1–C1 1.844(4), C1–Pt1 1.945(4), Pt1–Br1 2.5259(5), Pt1–P1 2.308(1), Pt1–C2 1.973(5), C2–N7 1.151(7), N7–C20 1.396(7), W1–C1–Pt1 168.0(3), C1–Pt1–Br1 173.6(1), P1–Pt1–C2 174.4(5), C2–N1–C20 172.6(5).

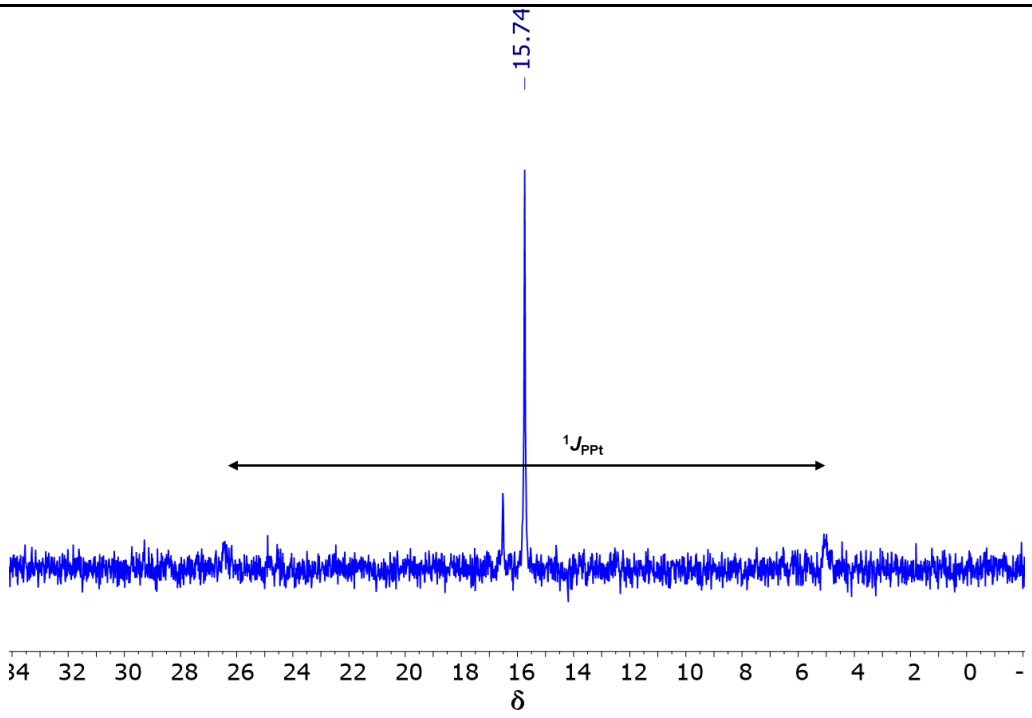

Figure 4.3: $^{31}P\{^1H\}$ NMR of [WPt(μ_2-C)Br(CNMes)(PPh_3)$(CO)_2$(Tp*)] (**4.2**, 162 MHz, 25 °C, δ_P) as a typical example for a *mono*-isocyanide metallacarbyne, displaying coupling to ^{195}Pt and exhibiting a minor isomer.

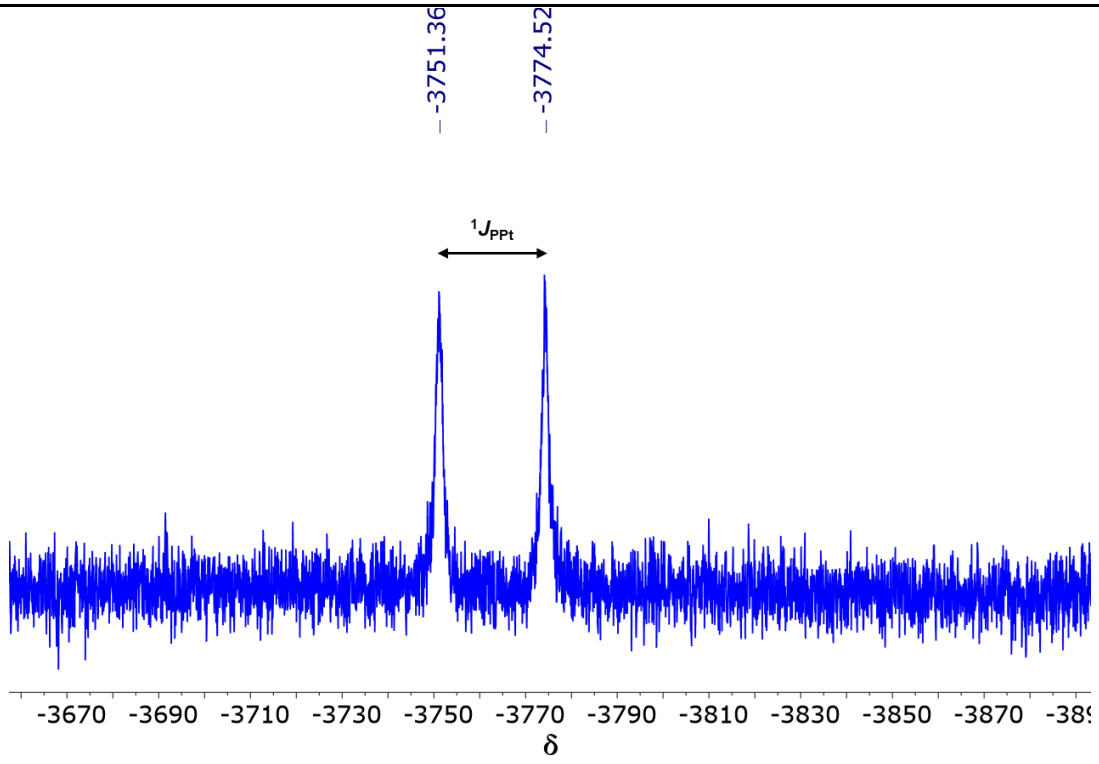

Figure 4.4: $^{195}Pt\{^1H\}$ NMR of [WPt(μ_2-C)Br(CNMes)(PPh_3)$(CO)_2$(Tp*)] (**4.2**, 150 MHz, 25 °C, δ_{Pt}) as a typical example for a *mono*-isocyanide metallacarbyne.

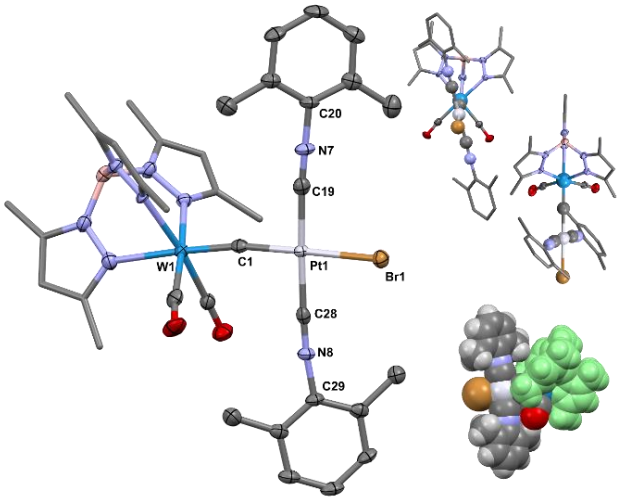

Figure 4.5: Molecular structure of [WPt(μ-C)Br(CNXyl)$_2$(CO)$_2$(Tp*)] (**4.4**) in a single crystal of **4.4**·2(CH_2Cl_2) as determined by X-Ray Diffractometry. Ellipsoids are drawn at the 50% probability surface with pyrazolyl rings simplified, and CH_2Cl_2 solvent and hydrogens omitted for clarity. Insets: a) Ball and stick representation as viewed down the key molecular linkage (ligands simplified for clarity), b) Space-filling representation highlighting the steric clash of rings and the sterically encumbering *tris*-pyrazolylborate (green) ligand. Selected bond lengths (Å) and angles (°): W1–C1 1.828(4), C1–Pt1 1.951(4), Pt1–Br1 2.5195(5), Pt1–C19 1.956(5), C19–N7 1.139(7), N7–C20 1.407(7), Pt1–C28 1.952(5), C28–N8 1.146(6), N8–C29 1.391(6), W1–C1–Pt1 171.2(3), C1–Pt1–Br1 179.0(1), C19–Pt1–C28 177.8(2), Pt1–C19–N7 175.3(4), C19–N7–C20 177.7(5), Pt1–C19–N7 177.3(4), C28–N8–C29 174.1(4).

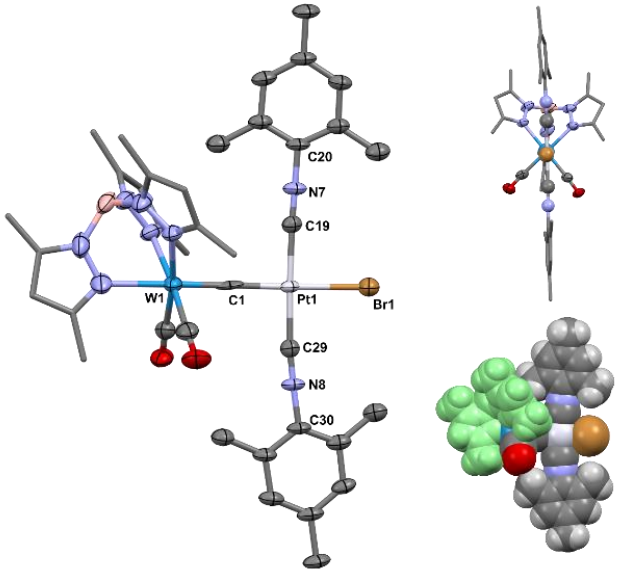

Figure 4.6: Molecular structure of [WPt(μ-C)Br(CNMes)$_2$(CO)$_2$(Tp*)] (**4.5**) in a single crystal as determined by X-Ray Diffractometry. Ellipsoids are drawn at the 50% probability surface with pyrazolyl rings simplified and hydrogens omitted for clarity. Insets: a) Ball and stick representation as viewed down the key molecular linkage (ligands simplified for clarity), b) Space-filling representation highlighting the steric clash of rings and the sterically encumbering *tris*-pyrazolylborate (green) ligand. Selected bond lengths (Å) and angles (°): W1–C1 1.833(6), C1–Pt1 1.945(6), Pt1–Br1 2.528(1), Pt1–C19 1.967(4), C19–N7 1.136(6), N7–C20 1.403(6), Pt1–C29 1.957(4), C29–N8 1.148(5), N8–C30 1.395(6), W1–C1–Pt1 178.1(3), C1–Pt1–Br1 178.5(1), C19–Pt1–C29 177.9(2), Pt1–C19–N7 177.3(4), C19–N7–C20 178.6(5), Pt1–C29–N8 175.0(4), C28–N8–C29 177.3(5).

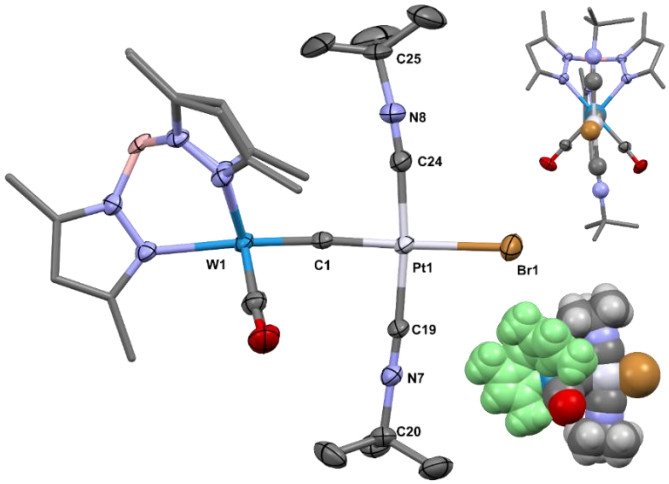

Figure 4.7: Molecular structure of [WPt(μ-C)Br(CN^{t}Bu)$_2$(CO)$_2$(Tp*)] (**4.6**) in a single crystal of **4.6**·0.5($CHCl_3$)·0.5(C_6H_{14}) as determined by X-Ray Diffractometry. Ellipsoids are drawn at the 50% probability surface with simplified pyrazolyl rings and rotational disorder about C25 and hydrogens omitted for clarity. Insets: a) Ball and stick representation as viewed down the key molecular linkage (ligands simplified for clarity), b) Space-filling representation highlighting the steric clash of ligand and the sterically encumbering *tris*-pyrazolylborate (green) ligand. Selected bond lengths (Å) and angles (°): W1–C1 1.833(5), C1–Pt1 1.932(5), Pt1–Br1 2.5180(9), Pt1–C19 1.974(6), C19–N7 1.121(7), N7–C20 1.470(8), Pt1–C24 1.957(6), C24–N8 1.138(9), N8–C25 1.48(1), W1–C1–Pt1 174.4(3), C1–Pt1–Br1 177.7(1), C19–Pt1–C24 172.7(2), Pt1–C19–N7 174.8(5), C19–N7–C20 179.6(5), Pt1–C24–N8 172.8(5), C24–N8–C25 172.6(7).

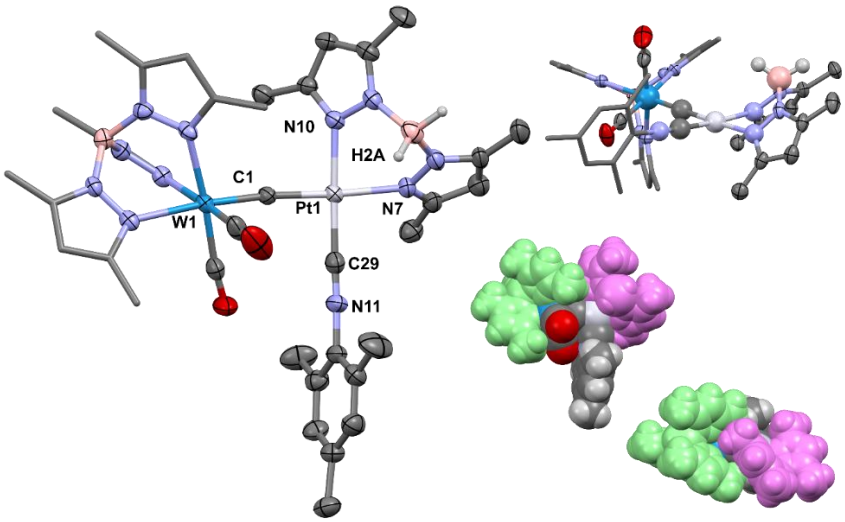

Figure 4.8: Molecular structure of [WPt(μ-C)(Bp*)(CNMes)(CO)$_2$(Tp*)] (**4.7**) in a single crystal as determined by X-Ray Diffractometry. Ellipsoids are drawn at the 50% probability surface with simplified pyrazolyl rings and hydrogens omitted for clarity. Insets: a) Ball and stick representation highlights the key molecular linkage (ligands simplified for clarity), b) Space-filling representation highlighting the steric clash of the sterically encumbering pyrazolylborate ligands (green/pink) ligands. Selected bond lengths (Å) and angles (°): W1–C1 1.833(4), C1–Pt1 1.944(4), Pt1–N7 2.107(4), Pt1–N10 2.056(4), Pt1–C29 1.916(5), C29–N11 1.145(7), Pt1···H2A 2.96(5), W1–C1–Pt1 174.0(3), C1–Pt1–N7 176.4(2), N10–Pt1–C29 176.5(2), Pt1–C29–N11 176.5(5), N7–Pt1–N10 85.3(2).

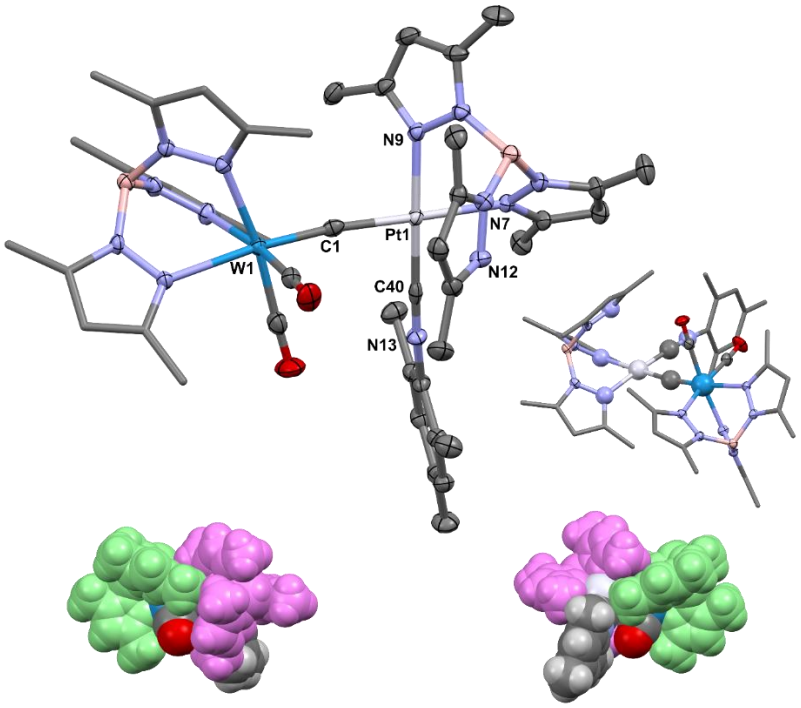

Figure 4.9: Molecular structure of [WPt(μ-C)(κ²-Tp*)(CNMes)(CO)₂(Tp*)] (**4.8**) in a single crystal of **4.8**·$CHCl_3$ as determined by X-Ray Diffractometry. Ellipsoids are drawn at the 50% probability surface with $CHCl_3$ solvent and hydrogens omitted for clarity. Insets: a) Space-filling representation highlighting the steric clash of sterically encumbering *tris*-pyrazolylborate ligands (pink/green), b) Ball and stick representation highlighting the key molecular linkage (ligands simplified for clarity). Selected bond lengths (Å) and angles (°): W1–C1 1.832(3), C1–Pt1 1.957(3), Pt1–N7 2.129(3), Pt1–N9 2.053(2), Pt1–C40 1.898(3), C40–N13 1.157(4), Pt1···N12 3.006(3), W1–C1–Pt1 173.5(2), C1–Pt1–N7 175.8(1), N9–Pt1–C40 173.5(1), Pt1–C40–N13 175.1(3).

Table 4.1: Structural parameters of isocyanide metallacarbynes and other species from Chapter Four {X = PPh_3, CNR}.

Isocyanide Metallacarbynes					
Compound	$r_{W\equiv C}$ (Å)	r_{C-Pt} (Å)	r_{Pt-CNR} (Å)	r_{C-NR} (Å)	$\angle_{W\equiv C-Pt}$ (°)
[**W**Pt(μ₂-C)Br(PPh_3)₂] (**3.1b**)	1.856(6)	1.934(6)	–	–	169.2(3)
[**W**Pt(μ₂-C)(Bp*)(PPh_3)] (**3.9**)	1.835(7)	1.963(7)	–	–	175.3(6)
[**W**Pt(μ₂-C)Br(CNXyl)(PPh_3)] (**4.1**)	1.843(4)	1.940(4)	1.996(6)	1.145(8)	168.4(3)
[**W**Pt(μ₂-C)Br(CNMes)(PPh_3)] (**4.2**)	1.844(4)	1.945(4)	1.973(5)	1.151(7)	168.0(3)
[**W**Pt(μ₂-C)Br(CN^{t}Bu)(PPh_3)] (**4.3**)	–	–	–	–	–
[**W**Pt(μ₂-C)Br(CNXyl)₂] (**4.4**)	1.827(4)	1.952(4)	1.957(5) 1.953(3)	1.138(7) 1.144(6)	171.2(3)
[**W**Pt(μ₂-C)Br(CNMes)₂] (**4.5**)	1.833(6)	1.945(6)	1.967(4) 1.957(4)	1.136(6) 1.149(5)	178.1(3)
[**W**Pt(μ₂-C)Br(CN^{t}Bu)₂] (**4.6**)	1.833(6)	1.931(6)	1.967(8) 1.966(7)	1.13(1) 1.133(9)	175.0(4)
[**W**Pt(μ₂-C)(Bp*)(CNMes)] (**4.7**)	1.835(4)	1.941(4)	1.920(6)	1.137(7)	174.0(3)
[**W**Pt(μ₂-C)(κ²-Tp*)(CNMes)] (**4.8**)	1.831(3)	1.957(3)	1.898(3)	1.157(4)	173.5(2)

Notes: W = W(CO)₂(Tp*).

Table 4.2: Spectroscopic parameters of isocyanide metallacarbynes and other species from Chapter Four.

Isocyanide Metallacarbynes						
Compound	$\delta_{\equiv C}$ [a] [ppm]	$\delta_{C\text{-}NR}$ [a] [ppm]	δ_{Pt} [a] [ppm]	δ_P [a] [ppm]	ν_{CN} [b] [cm^{-1}]	ν_{CO} [b] [cm^{-1}]
[**W**Pt(μ_2-C)Br(PPh_3)$_2$] (**3.1b**)	317.1	–	–3821	26.25 22.19	–	1994, 1905
	318.7		–3718	28.27 23.91	–	1994, 1905
[**W**Pt(μ_2-C)(Bp*)(PPh_3)] (**3.9**)	338.3 332.6	–	–3495 –3477	7.52 5.38	–	1946, 1852
[**W**Pt(μ_2-C)Br(CNXyl)(PPh_3)] (**4.1**)	308.4	126.4	–3761	16.75	2196	1943, 1852
[**W**Pt(μ_2-C)Br(CNMes)(PPh_3)] (**4.2**)	308.6	123.8	–3763	15.74	2197	1943, 1852
[**W**Pt(μ_2-C)Br(CN^{t}Bu)(PPh_3)] (**4.3**)	309.9	58.3	–3803	15.63	2228	1936, 1841
[**W**Pt(μ_2-C)Br(CNXyl)$_2$] (**4.4**)	298.7	137.2	–3658	–	2194	1951, 1860
[**W**Pt(μ_2-C)Br(CNMes)$_2$] (**4.5**)	299.3	122.8	–3656	–	2197	1943, 1852
[**W**Pt(μ_2-C)Br(CN^{t}Bu)$_2$] (**4.6**)	289.0	58.7	–3709	–	2216	1949, 1856
[**W**Pt(μ_2-C)(Bp*)(CNMes)] (**4.7**)	322.7	125.5	–3371	–	2208 2193	1965, 1875
[**W**Pt(μ_2-C)(κ^2-Tp*)(CNMes)] (**4.8**)	321.3	124.8	–3340	–	2194	1944, 1852
[**W**Pt(μ_2-C)(CNMes)$_3$]PF_6 (**4.9**)	306.5	129.6	–4177	–	2194	1946, 1853
[**Mo**Fe(μ-C)(CN^{t}Bu)(Cp)] [97]	452.1	166.3	–	–	2136 2107	1917, 1828

Notes: M = M(CO)$_2$(Tp*) (M = Mo or W). [a]Measured in CDCl3 unless specified otherwise. [b]Measured in CH_2Cl_2 unless specified otherwise.

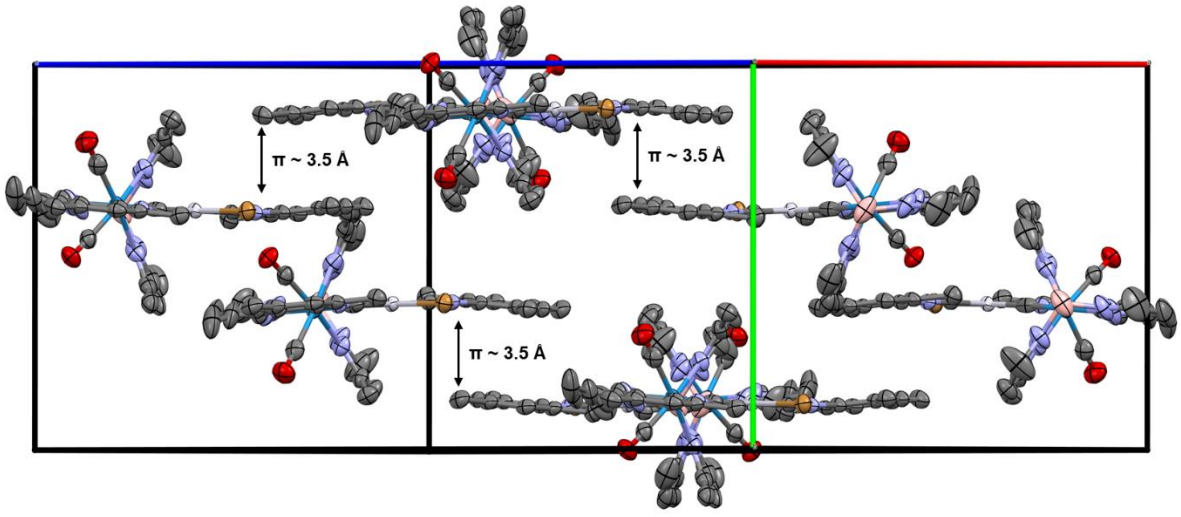

Figure 4.10: π-stacking in crystal structures of aryl-isocyanide metallacarbynes with [WPt(μ_2-C)Br(CNMes)$_2$(CO)$_2$(Tp*)] (**4.5**) shown.

or a π-acceptor (CNH). Theoretical results suggest the tilting is a recurrent feature for complexes with the π-acceptor and apparent in select cases with a π-donor (Table 4.3).

Examination of the orbital manifolds of each optimised structure in π-donor or acceptor series reveals orbitals likely responsible for the bending of the isocyanide ligands that are shared between the isonitrile and 'CA' ligands. Therefore, discussion will be limited to the orbitals of $[Pt(C{\equiv}N)(CNH)_3]^+$ and $[Pt(C{\equiv}N)Br(CNH)_2]$ as the simplest models with the clearest visual representation (Figure 4.11); all other compounds of the respective series contain similar orbital morphologies, sometimes buried deeper in the manifold (Table 4.3). The first observation between the two species is that significant variations around the bonding of the complexes are noted, especially as a modest tilting of the isocyanides is noted for the π-acceptor (169.54°) where the π-donor is essentially linear (180.51°). Several frontier orbitals of $[Pt(C{\equiv}N)(CNH)_3]^+$ comprise the π-systems of CN and CNH ligands while HOMO–9 provides the first possible origin: a constructive π-overlap *via* platinum between the *cis*-CNH ligands and the π-component of the Pt–CN linkage, but with little overlap with the π-orbitals of the unique CNH ligand and none with the π-donor bromide in $[Pt(CN)Br(CNH)_2]$. The CA ligand swells the *d*-orbital of platinum that comprises HOMO–9 and the varible ligand; the acceptor CNH is Pt–C anti-bonding while the bromide donor counteracts this effect increasing density of the platinum in the opposite direction, preventing tilting towards CA.

Comparing the π-acceptor series, if the effect originated from the *trans*-influence of the CA ligand, then bending would correlate. This *trans*-influence is evident as cyaphides are much stronger π-acceptors than cyanides, [351] such that the Pt–C bond is contracted for CA and elongated for the *trans*-CNH ligand.‡‡‡‡‡‡‡‡‡‡‡ However, few changes to the N1–Pt–N2 angle occur, even for π-donors, suggesting tilting is more complicated. For π-acceptors, the HOMO–12 and HOMO–14 indicate overlap between the π-systems of the CNH ligands interacting with the CN and *trans*-CNH ligands, where a disparity between the latter two ligands would provide an electronic influence. Although similar interactions are noted for π-donors suggesting interplay of these orbitals is more likely a corollary of the effect suggested by HOMO–9. The orbital manifolds of the π-donors remain more symmetrical in the most influential orbitals and therefore it is unsurprising the ligands are linear.

‡‡‡‡‡‡‡‡‡‡‡ A recent mini-review on cyaphides was recently reported by Müller, Grützmacher, Goicoechea and co-workers revealing revealed similar trends descending group 15, similar to pnictocarbynes[168] and chalcocarbonyls, [116] while few theoretical studies have investigated cyaphides, [352]

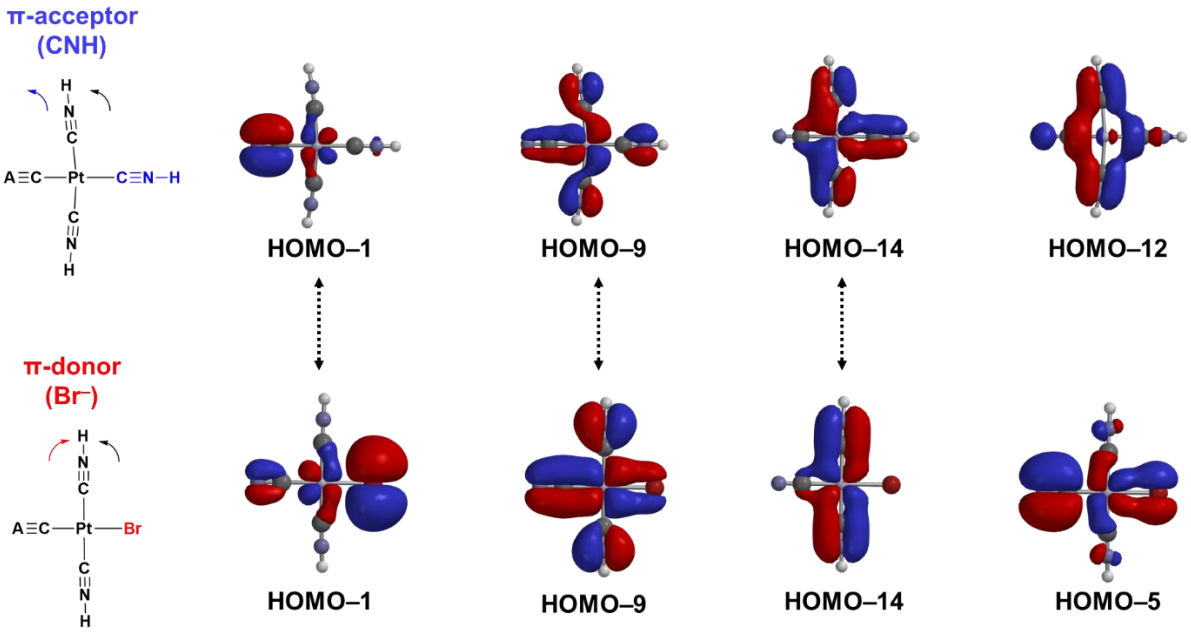

Figure 4.11: A) Computed structures of [Pt(C≡N)(CNH)$_3$] (top) and [PtBr(C≡N)(CNH)$_2$] (bottom) showing a bending deviation of isocyanide ligands. B) Orbitals likely contributing to isocyanide bending shown for [Pt(C≡A)(CNH)$_3$] but present in all cases. DFT:ωB97X–D/6–31G*/LANL2Dζ.

Simpler models for alkynyl and cyaphide ligands feature little differences between examples in the same π-donor bromide or π-acceptor *tris*(isonitrile) series. However, models behave differently when carbyne fragments are introduced. For the *tris*(isonitrile) complex, the tilting for carbynes is more pronounced, while little to no tilting is observed for the bromide example, notably absent in CA (A = CH, N, P) models. For CNH ligands, the carbyne complexes each feature tilting, thereby implicating an electronic influence of orbitals unique to the μ_2-carbido, although curiously, tilting is not pronounced for CNMe ligands. The most intriguing observation arises in [WPt(μ_2-C)Br(CNMe)$_2$(CO)$_2$(Tp)] where the CNMe *syn* to the Tp ligand tilts *towards* the pyrazolyls while the *anti* CNMe remains linear, suggesting a favourable interaction with Tp. To further pursue the potential for an attractive dispersion interaction between the *syn* isocyanide and Tp, other relevant metallacarbyne models were optimised. The pruned CN^{t}Bu complex [WPt(μ_2-C)Br(CN^{t}Bu)$_2$(CO)$_2$(Tp)] (**4.6***) exhibits tilting of both isocyanides (168.68°) in good agreement with the experimentally determined structure (X-ray diffraction, 168.0(2)°). In contrast, the model [WPt(μ_2-C)Br(CNPh)$_2$(CO)$_2$(Tp)] (**4.4***) exhibits notable tilting (170.77°) whereas the real xylyl and mesityl complexes **4.4**/**4.5** do not (184.9(1)°), instead tilting away to accommodate the 2-methyl substituent of the aryl ring within the Tp* cleft. However, including the methyl group in a theoretical model [WPt(μ_2-C)Br(CNPhMe–2)$_2$(CO)$_2$(Tp)] replicates the experimental observation and prevents tilting (178.39°).

Table 4.3: Geometric and spectroscopic parameters of: hypothetical isocyanide complexes $[Pt(C{\equiv}A)(CNH)_3]^+$ and $[Pt(C{\equiv}A)Br(CNH)_2]$ {A = N, P, CH and $W(CO)_2(Tp)$}, model metallacarbynes, and experimentally determined metallacarbynes.

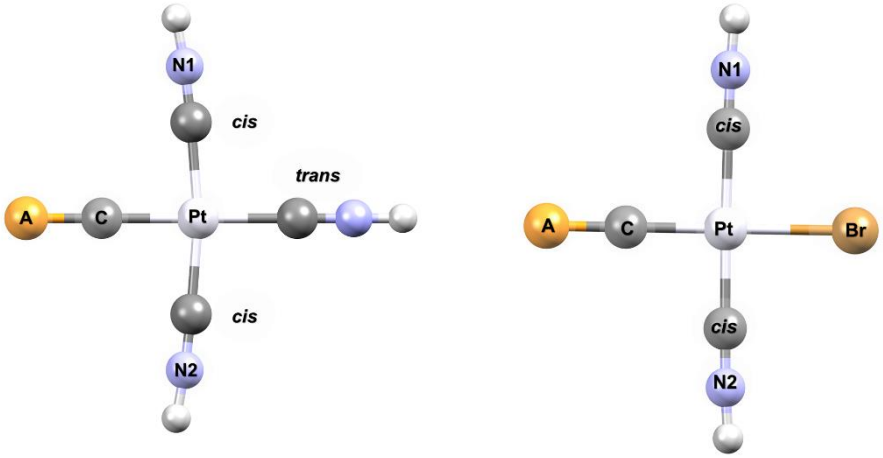

(I) Hypothetical *tris*(isocyanide) complex cations $[Pt(C{\equiv}A)(CNH)_3]^+$					
A	**$r_{Pt\text{–}cis\text{-}CNR}$ (Å)**	**$r_{Pt\text{–}trans\text{–}CNR}$ (Å)**	**$r_{Pt\text{–}C}$ (Å)**	**$\angle_{N1\text{–}Pt\text{–}N2}$ (°)**	**ν_{CN} (cm^{-1})**
CH	1.975	2.021	1.981	169.13	2132, 2151, 2184
N	1.982	2.015	1.985	169.54	2146, 2161, 2189, 2209[b]
P	1.978	2.034	1.978	169.89	2133, 2150, 2181[c]
$C{\equiv}W(CO)_2(Tp)$	1.975, 1.973	2.057	1.984	160.96	2117, 2138, 2169
$C{\equiv}W(CO)_2(Tp)$[a]	1.985, 1.975	2.060	1.977	157.98	2246, 2261, 2284
(II) Hypothetical neutral *bis*(isocyanide) complexes *trans*-$[PtBr(C{\equiv}A)(CNH)_2]$					
A	**$r_{Pt\text{–}cis\text{-}CNR}$ (Å)**	**$r_{Pt\text{–}Br}$ (Å)**	**$r_{Pt\text{–}C}$ (Å)**	**$\angle_{N1\text{–}Pt\text{–}N2}$ (°)**	**ν_{CN} (cm^{-1})**
CH	1.951	2.531	1.976	180.51	2212, 2153
N	1.956	2.518	1.973	180.51	2123, 2159, 2191[b]
P	1.956	2.539	1.957	181.72	2117, 2154
$C{\equiv}W(CO)_2(Tp)$	1.957, 1.955	2.560	1.952	176.42	2111, 2149
$C{\equiv}W(CO)_2(Tp)$[a]	1.969, 1.958	2.561	1.945	171.26	2248, 2275
(III) Theoretical metallacarbynes					
$[WPt(\mu_2\text{-}C)Br(CNtBu)_2(CO)_2(Tp)]$ (**4.6***)	1.966, 1.964	–	1.939	168.68	2224
$[WPt(\mu_2\text{-}C)Br(CNPh)_2(CO)_2(Tp)]$ (**4.4***)	1.959, 1.958	–	1.948	170.77	2206, 2237
$[WPt(\mu_2\text{-}C)Br(CNPhMe\text{-}2)_2(CO)_2(Tp)]$	1.960	–	1.943	178.39	2211, 2239
(IV) Experimentally characterised isocyanide metallacarbynes					
$[WPt(\mu_2\text{-}C)Br(CNXyl)_2(CO)_2(Tp)]$ (**4.4**)	1.957(5), 1.952(4)	–	1.952(2)	184.9(1)[d]	2194
$[WPt(\mu_2\text{-}C)Br(CNMes)_2(CO)_2(Tp)]$ (**4.5**)	1.957(4), 1.967(4)	–	1.945(6)	184.8(1)[d]	2197
$[WPt(\mu_2\text{-}C)Br(CN^tBu)_2(CO)_2(Tp)]$ (**4.6**)	1.967(8), 1.966(7)	–	1.931(6)	168.0(2)	2216

Notes: [a]CNMe instead of CNH. [b]Vibrations are coupled with CN oscillator. [c]ν_{CP} = 1404 cm^{-1}. [d]Angle beyond 180° bends away from Tp/Tp*. [e]ν_{CP} = 1387 cm^{-1}.

These theoretical results indicate isocyanide tilting is a response to both electronic and steric effects. The similar bending of isocyanides at the nitrogen position has been surmised as an electronic consequence. [343] Linear species are often observed for late transition metals (ν_{CN}: > 1900 cm^{-1}) as the isocyanide acts as a π-acceptor, although d^8 examples [Ru(CN^{t}Bu)$_5$] and [Fe(CN^{t}Bu)$_5$] feature significant bending at nitrogen (*ca* 134(2)°) accompanied by low frequency vibrations (ν_{CN}: 1815, 1830 cm^{-1}, respectively) as a consequence of significant retrodonation. [346, 348] These isocyanide examples are exceptions under electronic control, yet steric influences arise when swapping ligands, such that incorporation of a PPh_3 ligand in [Ru(CN^{t}Bu)$_4$(PPh_3)] returns a two linear (166.7, 167.9°) equatorial and one bent (145.1°) isocyanides. The less π-basic axial position of the final isonitrile favours linear coordination (174.4°).[348] In the absence of steric influence, electronic effects predominate such that isocyanides will tilt based on orbitals of π-symmetry on platinum. However, if attractive dispersion pockets exist (such as Tp*), then an additional influence such that tilting may occur where otherwise unexpected. These results suggest the experimentally determined structure of [WPt(μ_2-C)Br(CN^{t}Bu)$_2$(CO)$_2$(Tp*)] features tilting as a mixture of electronic and dispersion influences, while tilting would likely be observed for **4.4**/**4.5** if the methyl group was absent from CNXyl/CNMes ligands.

Computational interrogation of **4.4*** and **4.6*** as model complexes also provides the composition of frontier orbitals of interest, as well as indication on possible reactivity profiles. The composition is similar between species where aromatic phenyl groups of **4.4*** only complicate the bonding as compared to **4.6***. For this reason, only **4.6*** will be discussed as it represents the visually simplest model (Figure 4.12). The frontier orbitals of **4.6*** demonstrate almost identical topologies to those of [WPt(μ_2-C)Br(CO)$_2$(PMe_3)$_2$(Tp)] (**3.1*·Br**, Section 3.3.2). The HOMO comprises atomic orbitals responsible retrodonation to carbonyl ligands with a minor contribution to the carbyne (W≡C), while the platinum-centred LUMO features a larger *p* orbital (unused in sp^2d hybridisation) above and below the plane, conjugating with the CN^{t}Bu ligands' π* orbitals—an additional site for nucleophilic attack compared to **3.1***. The HOMO–1/–2 demonstrates the orthogonal π-bonding to establish the W≡C bond, while being π-antibonding to platinum. The most intriguing orbital topology of the set arises in the HOMO–5, where σ-symmetry connects the tungsten to the μ-carbido, out through platinum to a σ*(Pt–Br) antibonding interaction. This likely contributes to the significantly short C–Pt bond (*cf.* **3.1***), however, **4.6*** shows a σ-symmetric linkage down the molecular spine, whereas **3.1*** is π–π–π in symmetry. This relevance of this to migration-type reactivity of isocyanide ligands will become subsequently apparent (See Section 4.5).

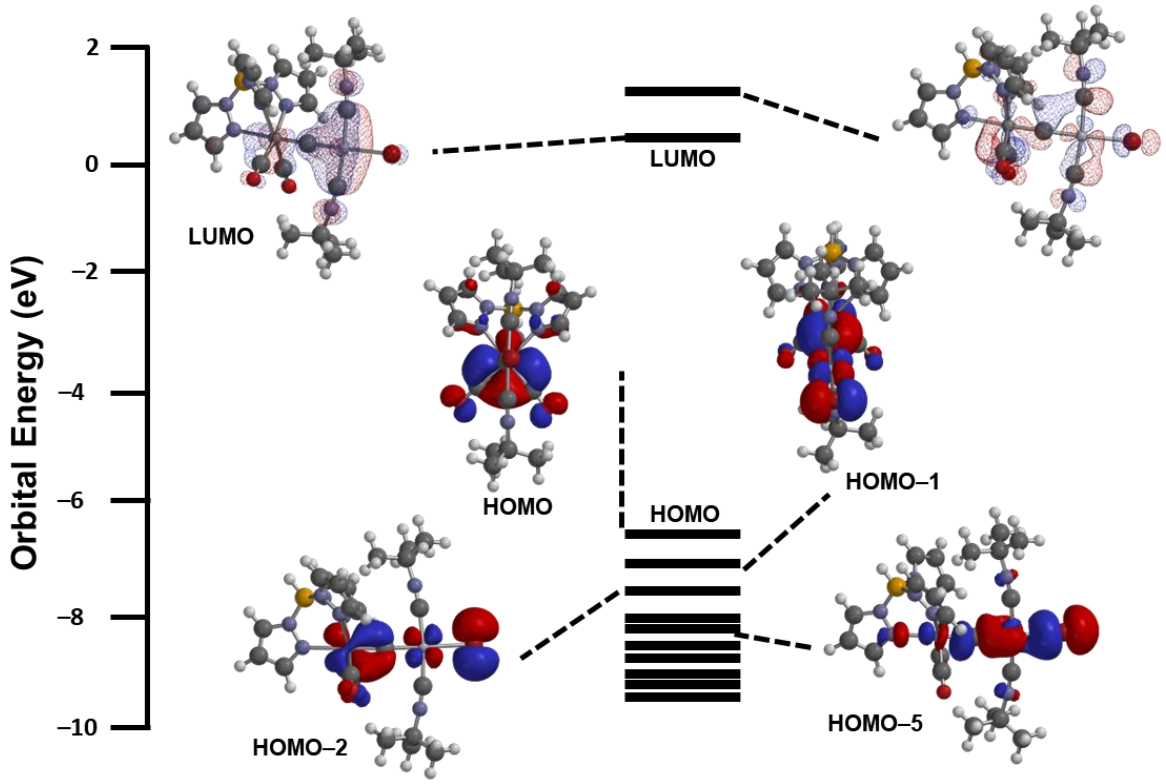

Figure 4.12: Frontier molecular orbtials of interest for hypothetical complex [WPt(μ_2-C)Br(CN^{t}Bu)$_2$(CO)$_2$(Tp)] (**4.6***). DFT: ωB97X-D/6–31G*/LANL2Dζ.

Progressively replacing phosphines with isocyanides ligands removes the useful information provided by ^{31}P{^{1}H} NMR spectroscopy,‡‡‡‡‡‡‡‡‡‡ but is rewarded by the presence of ν_{CN} vibrational modes in the infra-red spectrum with those due to aryl derivatives (CNXyl, CNMes) appearing to lower frequency (ν_{CN}: 2196–2197 cm^{-1}) than for *tert*-butyl complex (ν_{CN}: 2228 cm^{-1}). The isocyanide vibration serves as a useful assay of reaction progress being able to distinguish between coordinated and free CNR in solution. As bands for all the complexes cover an narrow range, infra-red spectroscopy is unable to reliably resolve mono- and *trans*-disubstitution.

Removal of the ^{31}P nucleus also eliminates a degree of coupling, strengthening signal intensity in both the ^{13}C{^{1}H} and ^{195}Pt{^{1}H} NMR and it was hoped (without success) that this would reveal ^{183}W coupling for the μ_2-carbido resonance, previously obscured in the phosphine system. However, the carbido resonances remained broad and the coupling was rarely resolved (except for **4.7**; Figure 4.13). Chemical shifts of the μ_2-carbido nuclei were observed to somewhat higher frequency (δ_C: 308.4–309.9) of those for the phosphine analogues **4.1**–**4.3**. A notable exception from ^{13}C{^{1}H} NMR studies was the spectrum of species **4.6**, the carbido signal of which appears as a non-binomial 1:1:1 triplet, due to coupling to quadrupolar ^{14}N nuclei (I = 1, 99.98% abundance). This arises due to chemical shift anisotropy where

‡‡‡‡‡‡‡‡‡‡ The phosphine containing species **4.1**–**4.3** give similar ^{31}P{^{1}H} and ^{195}Pt{^{1}H} spectra to those in the previous chapter.

localised magnetic fields around the axial isocyanide (symmetric environment) inhibit relaxation of ^{14}N such that coupling is resolved, where typical relaxation is efficient due to a large quadrupole moment. [238, 353] To further support this, closer inspection of broadened carbido resonance of complex **4.5** suggested unresolved fine structure. Coupling to ^{14}N was observed in the ^{195}Pt{^{1}H} NMR spectra for both **4.5** and **4.6** (pentuplet $^2J_{PtN}$ = 109 Hz, Figure 4.14), but oddly, not for **4.4**, demonstrating that subtle changes can influence the magnetic environments required to manifest these couplings. While coupling to ^{14}N presumably thwarted direct detection of the μ_2-carbido resonance in **4.6**, it could be assigned indirectly *via* a HMBC experiment (Figure 4.15, H^4(pz) correlation) as δ_C = 289.0. This chemical shift suggests a comparatively electron-rich carbido relative to published examples, *e.g.*, [Wru(μ_2-C)(CO)$_2$(Cp)(O^{t}Bu)$_3$)] (δ_C: 273.3) [33] is the closest before the *pseudo*-μ_2-carbidos (heavy *p*-block) or the calixerine-niobium carbido Na$_2$[Nb$_2$(μ_2-C)(cal4ix)$_2$] (δ_C: 257.0). [57] The ^{195}Pt{^{1}H} NMR data demonstrate chemical shifts similar to other neutral species retaining the halide terminus, which lie within the range of –3750 to –3850 ppm. The absence of clearly resolvable ^{183}W coupling is notable. It was predicted the isocyanide systems would likely exhibit this feature, therefore, as the isocyanide Pt resonances are somewhat broad, it is likely this coupling is small and enveloped beneath the linewidth. In Section 3.5, a loose correlation was determined between δ_C and δ_{Pt} but **4.1**–**4.6** fall outside this trend.

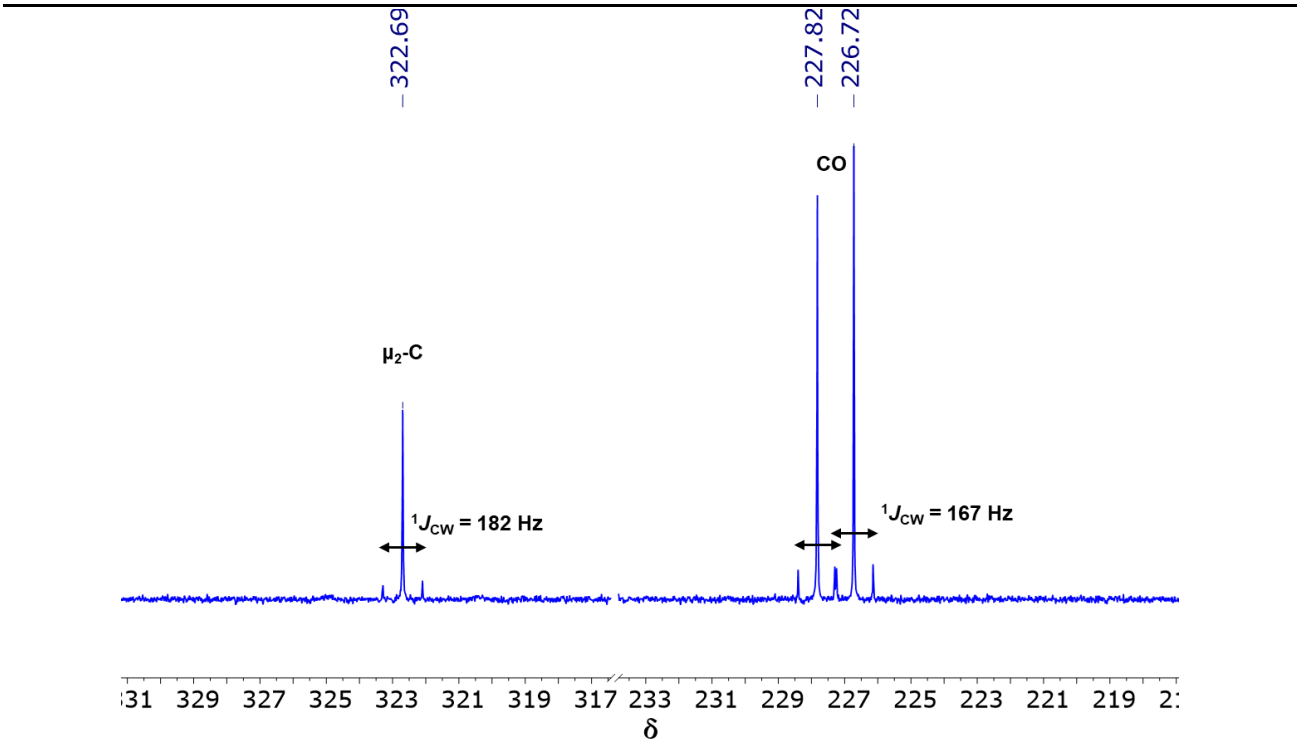

Figure 4.13: ^{13}C{^{1}H} NMR spectrum of [WPt(μ_2-C)(Bp*)(CNMes)(CO)$_2$(Tp*)] (**4.7**, 151 MHz, 25 °C, δ_C) capturing ^{183}W coupling to the μ_2-carbido and carbonyls previously precluded by phosphine coupling.

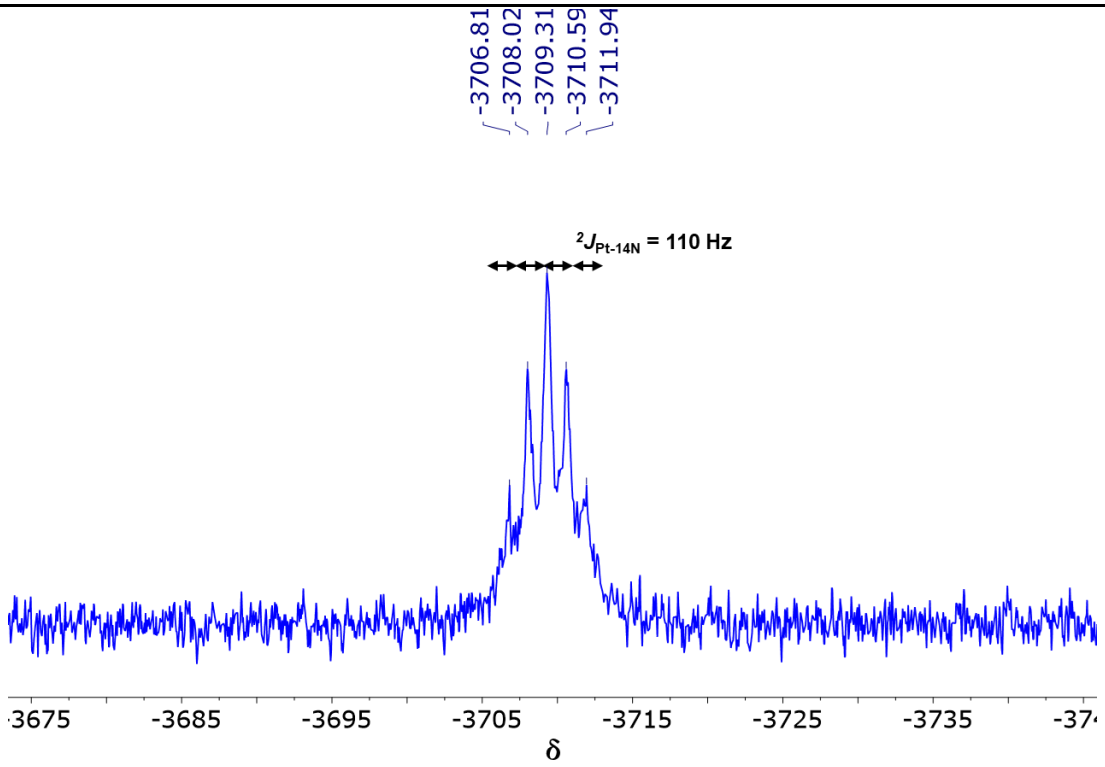

Figure 4.14: $^{195}Pt\{^1H\}$ NMR spectrum of [WPt(μ_2-C)Br($CN^tBu)_2(CO)_2$(Tp*)] (**4.6**, 86 MHz, 25 °C, δ_{Pt}) showing ^{14}N coupling.

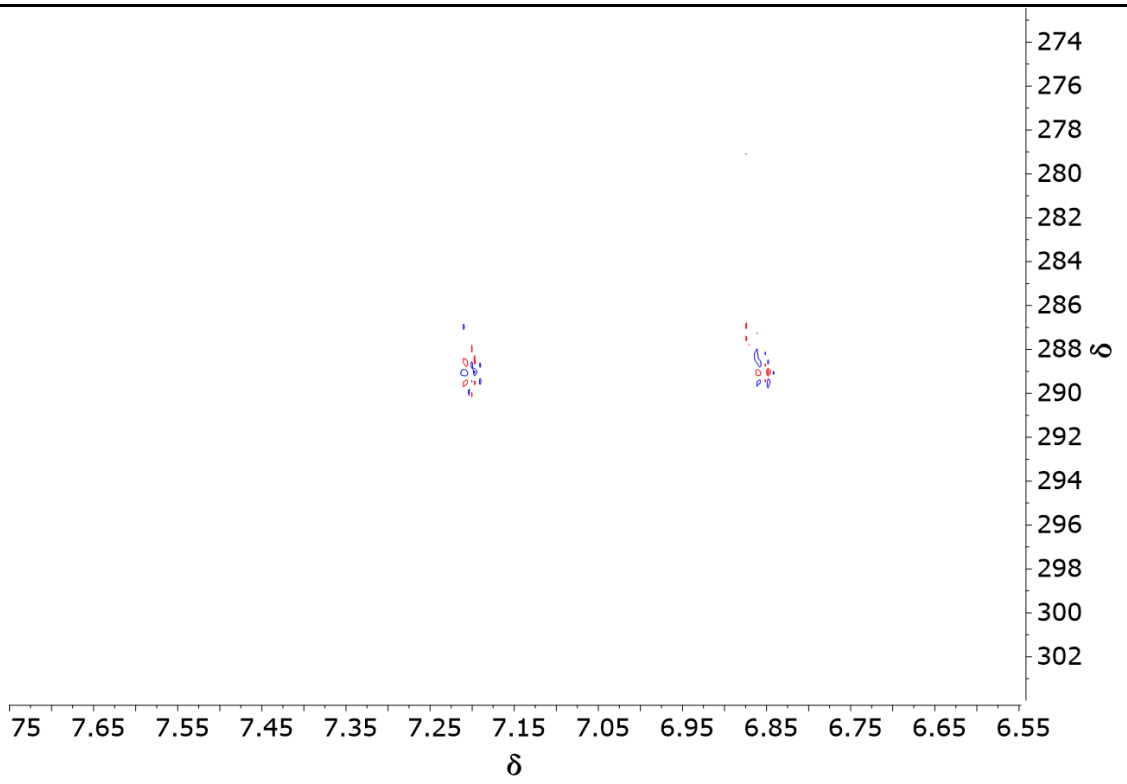

Figure 4.15: HMBC NMR spectrum of [WPt(μ_2-C)Br($CN^tBu)_2(CO)_2$(Tp*)] (**4.6,** 600/151 MHz, 25 °C, $\delta_H[H^4(pz)]$ /δ_C[WC]) allowing indirect detection of carbido.

The structural and spectroscopic properties of **4.1**–**4.6** ultimately present little variation from those of **3.1b**, yet contain a significantly more exposed platinum terminus and carbido environment. With a view to reactivity studies the LUMO of **4.6*** is as anticipated for a d^8-square-planar complex of platinum(II), for which associative ligand substitution is to be expected. Moving to isocyanide supported metallacarbynes, the C–N π*-orbitals of the isocyanide also contribute to LUMO/LUMO+1 orbitals recalling that nucleophilic attack at platinum(II) isonitriles dates some 110 years to Tschugajeff. A brief exploration of isocyanide complex reactivity towards a range of nucleophiles had lacklustre success.

Treating tetrahydrofuran solutions of **4.2**, **4.3**, **4.5** and **4.6** with lithium triethylborohydride (a hydride donor) at 0 °C or MeLi at –78 °C resulted in all cases in immediate colour changes from originally orange/yellow to brown within minutes. Thin-layer chromatography indicated formation of at least fifteen compounds for Li[Et_3BH] and greater than 10 products for MeLi. *In situ* ^1H and $^{31}P\{^1H\}$ NMR assay of crude reaction mixtures similarly indicated formation of a plethora of products and this avenue of exploration was abandoned.

4.4 Unusual Reactivity in Polar Media

Ligand substitution reactions to afford complexes **4.1**–**4.6** (Section 4.2) were performed in non-polar toluene to encourage the formation of the neutral species. However, crude product mixtures often gave bright colours when dissolved in relatively polar CH_2Cl_2 ($\varkappa$ = 8.93) prior to flash chromatography on silica gel, or $CDCl_3$ ($\varkappa$ = 4.81) for NMR spectroscopy. Pink, red, green and purple species were observed and while the red/pink species were inconsistently formed and were not successfully identified, formation of the green and purple species proved reproducible.

Reactions utilising CNMes as a ligand in polar media commonly resulted in formation of a green species (Scheme 4.5). This complex was identified as the *tris*-isocyanide cationic metallacarbyne [WPt(μ_2-C)(CNMes)$_3$(CO)$_2$(Tp*)]PF_6 (**4.9**) on the basis of two isocyanide vibrations (CH_2Cl_2: ν_{CO}: 2208, 2193 cm^{-1}) and recognition that the *trans* influence of the carbido ligand might be expected to ionise the bromide ligands in **4.5** or **4.6**. Likewise, the carbonyl vibrations are relatively higher in energy (ν_{CO}: 1965, 1875 cm^{-1}) reflecting the reduced π-basicity of tungsten upon coordination to a cationic platinum(II) centre (Figure 4.16). While the structural features of **4.9** would have been of interest, the complex proved highly reactive, often decomposing during crystallisation at low temperature with deposition to insoluble material.

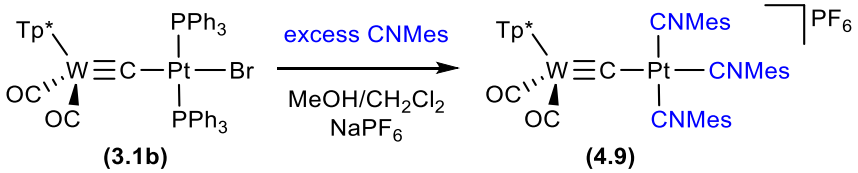

Scheme 4.5: Synthesis of a common by-product, a cationic *tris*-isocyanide salt, with bromide ionisation encouraged by polar media.

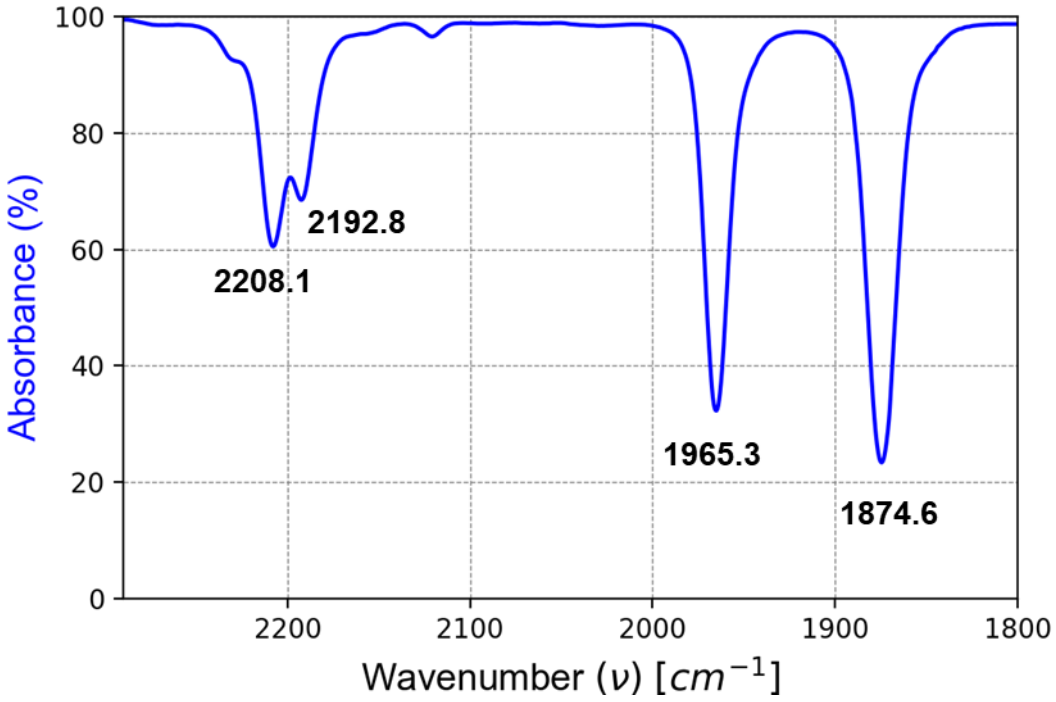

Figure 4.16: Solution-state infra-red spectrum of [WPt(μ$_2$-C)(CNMes)$_3$(CO)$_2$(Tp*)]PF$_6$ (**4.9**, CH_2Cl_2, *ν*) showing coupled ν_{CN} vibrations.

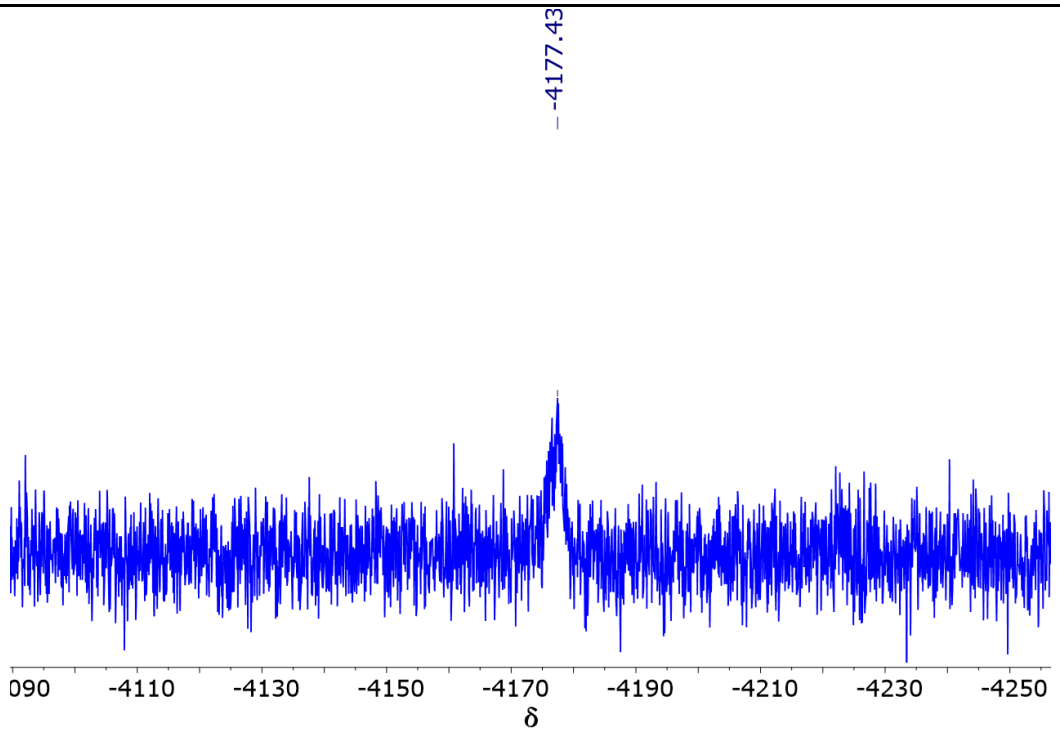

Figure 4.17: ^{195}Pt{^{1}H} NMR spectrum of [WPt(μ$_2$-C)(CNMes)$_3$(CO)$_2$(Tp*)]PF$_6$ (**4.9**, 150 MHz, 25 °C, δ_{Pt}) consistent with a cationic platinum(II) centre.

Although single crystals were obtained from CH_2Cl_2, these rapidly desolvated with loss of crystallinity. The μ_2-carbido resonance occurs at a similar chemical shift to the neutral isocyanide complexes (δ_C: 306.5) suggesting similar shielding, while the $^{195}Pt\{^1H\}$ NMR chemical shift, which is highly sensitive to the balance of σ-donor and π-acceptor ligand character, was found greatly upfield (δ_{Pt}: –4177). Though broadened, presumably by coupling to ^{14}N, this was not resolved (Figure 4.17). [238§§§§§§§§§§§§§§] A similar δ_C but different δ_{Pt} reflects the more acute sensitivity of the platinum nucleus to minor changes in shielding.

4.5 Ligand Migration to μ_2-iminoketenylidenes

As with **4.9**, the purple compound was repeatably identified during substitution of **3.1b** with CNMes: a substitution that liberates phosphine. During substitution of **3.1b** with CNXyl in non-polar toluene, the reaction proceeds as anticipated to give **4.1** and no further reaction with liberated phosphine occurs. However, if **4.1** was heated thermally, or combined with PPh_3 and PF_6^- in a polar solvent combination (Scheme 4.6), the vivid purple emerges originally suspected to be *trans*-$[WPt(\mu_2\text{-}C)(CNMes)(PPh_3)_2(CO)_2(Tp^*)]^+$ as an analogue to **4.9** and with the colour resembling $[WPt(\mu_2\text{-}C)(terpy)(CO)_2(Tp^*)]PF_6$ (**3.5**). [159]

The purple species was isolated and, with the eye of faith, several key data aligned with the proposed formulation as the salt *trans*-$[WPt(\mu_2\text{-}C)(CNXyl)(CO)_2(PPh_3)_2(Tp^*)]PF_6$, including the ESI–Mass Spectrum, infra-red data for CO and 'CNR' vibrations, and ligand signatures evident in the ^1H NMR spectra (Table 4.4). Two data conspicuously did not align. Firstly, ionisation of the Pt–Br bond should have resulted in an increased infra-red frequency for the isocyanide (ν_{CN}: 2104 *cf.* 2196 cm^{-1} for **4.1**) reflecting the reduced π-basicity of the cationic platinum(II) centre. Secondly, scanning the high-frequency region (300–500 ppm) of $^{13}C\{^1H\}$ NMR spectra failed to discern any signals in the typical carbido region. Instead, a much lower frequency double-doublet resonance was detected (δ_C: 222.8), exhibiting coupling to ^{31}P consistent with *pseudo-trans*- and *cis*-phosphines ($^2J_{CP}$ = 73, 7 Hz), although dimished signal intensity precluded observation of coupling to metal nuclei ($^{183}W/^{195}Pt$). This was taken as being suggestive of C–C coupling with an isocyanide to give a complex of a previously unknown μ_2-iminoketenylidene ligand in the complex $[WPt(\mu_2\text{-}CCNXyl)(CO)_2(PPh_3)_2(Tp^*)]^+$ (**4.10**). The molecular structure of **4.10** was confirmed *via* single crystal X-ray diffraction for both PF_6 and BPh_4 salts, where bulky BPh_4^- was used to facilitate crystallisation.

Similar treatment of **4.2** returned the μ_2-iminoketenylidene salt $[WPt(\mu_2\text{-}CCNMes)(CNMes)(PPh_3)(CO)_2(Tp^*)]PF_6$ (**4.11**), however, the mesityl derivate formed in lower yields with CNMes retained over PPh_3 *post*-CNR-carbido coupling, such that provision of additional isocyanide optimised the yield.

§§§§§§§§§§§§§§ Measuring ^{195}Pt at elevated temperatures is a valid technique to sharpen resoances broadened by ^{14}N coupling through enhancing relaxation of the quadrupolar nucleus. Such experiments were not attempted for **4.9** due to thermal decomposition (*ca* 70 °C).

While **4.11** could be formed upon treating **4.5** with PPh_3 in CH_2Cl_2/MeOH mixtures, this is less preferred synthetic strategy as **4.2** proved to be easier to manipulate and purify than **4.5**. Finally, **4.11** was not observed to be themally promoted from mixtures of either **4.2** or **4.5**; a difference to the xylyl derivative **4.10**.

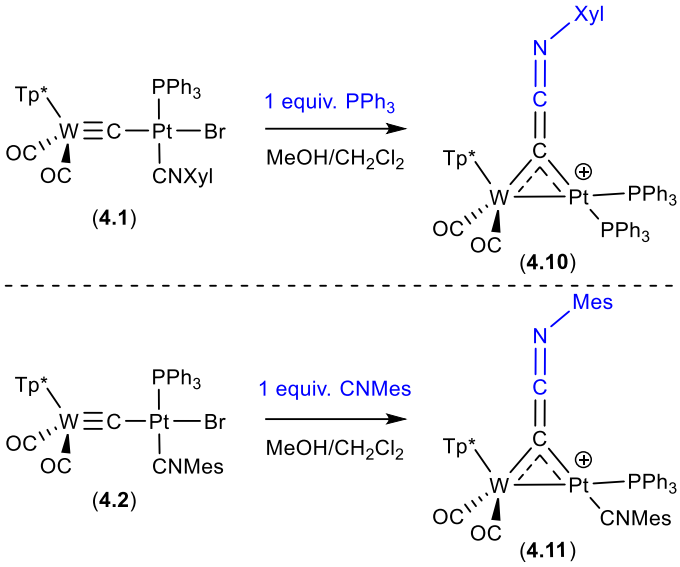

Scheme 4.6: Preparation of the novel μ_2-iminoketenylidene complexes, *via* isonitrile migration to a μ_2-carbido.

The $^{13}C\{^1H\}$ NMR spectra initially hinted toward the final structure of **4.10**/**4.11**, yet contains further interesting features. While the formerly carbido carbon resonances appear upfield (δ_C: 222.8/217.9), the precursor isocyanide carbon occupies an expected region for the carbon of aryl isocyanides (δ_C: 139.1/124.3). The shift to higher frequency points towards a structure with increased unsaturation and presumed decrease in HOMO-LUMO energy gap, impacting on paramagentic shielding, perhaps indicative of binding to more than one transition metal. The Tp* environments indicate retention of the molecular C_s symmetry in both the $^{13}C\{^1H\}$ and ^1H NMR spectra, suggesting that if the μ_2-CCNC spine bends, it does so in the mirror plane or traverses this plane on the NMR timescale *via* a C_s-symmetric conformation in solution. Closer analysis of the infra-red spectra reveals a more complicated environment about the μ_2-CCNR ligand. Complex **4.10** exhibits one ν_{CN} vibration, which is as expected but very broad, while **4.11** exhibits two ν_{CN} stretches; both are lower in energy suggestive of C–N bond weakening. The only ligands with any comparative value are a small number of iminoketenyl complexes on manganese $[Mn\{C(CNR)R'\}(CO)_2(Cp)]^+$ (R = Me, Cy, ^{t}Bu; R' = Me, Ph) which manifest intense, higher energy vibrations in the range 2212–2250 cm^{-1}.[354] The μ_2-iminoketenylidenes **4.10** and **4.11** also exhibit vibrant purple hues quantified by UV-visible spectra. Absorption maxima are found in the visible region (λ_{MAX}/nm($M^{-1}cm^{-1}$): 535(6900) **4.11**; 550(6800) **4.12**), the intensities of which point towards charge-transfer origins.

Table 4.4: Spectroscopic properties of μ2-iminoketenylidenes in comparison to their precursors.

μ2-Iminoketenylidenes						
Compound	$\delta_{\equiv C}$ [a] (ppm)	$\delta_{C\text{-}NR}$ [a] (ppm)	δ_{Pt} [a] (ppm)	δ_P [a] (ppm)	ν_{CN} [b] (cm^{-1})	ν_{CO} [b] (cm^{-1})
[WPt(μ2-CCNXyl)(PPh3)2]BPh4 (**4.10**)	222.8	139.1[c]	–4174	44.46, 25.60	2104	1944, 1853
[WPt(μ2-CCNMes)(CNMes)(PPh3)]PF6 (**4.11**)	217.9	124.3[c]	–4136	44.41	2156, 2119[d]	1943, 1862
Metallacarbyne Precursors						
[**W**Pt(μ2-C)Br(PPh3)2] (**3.1b**)	317.1	–	–3821	26.25 22.19	–	1994, 1905
	318.7		–3718	28.27 23.91	–	1994, 1905
[**W**Pt(μ2-C)Br(CNXyl)(PPh3)] (**4.1**)	308.4	126.4	–3761	16.75	2196	1943, 1852
[**W**Pt(μ2-C)Br(CNMes)(PPh3)] (**4.2**)	308.6	123.8	–3763	15.74	2197	1943, 1852
[**W**Pt(μ2-C)Br(CNXyl)2] (**4.4**)	298.7	137.2	–3658	–	2194	1951, 1860
[**W**Pt(μ2-C)Br(CNMes)2] (**4.5**)	299.3	122.8	–3656	–	2197	1943, 1852
[**W**Pt(μ2-C)(CNMes)3]PF6 (**4.9**)	306.5	129.6	–4177	–	2194	1946, 1853

Notes: [a]Measured in $CDCl_3$. [b]Measured in CH_2Cl_2. [c]Formerly isocyanide carbon (CCNR). [d]Computation and simulation suggest these oscillators are highly coupled.

The $^{31}P\{^1H\}$ NMR spectra include signals with unremarkable chemical shifts. Complex **4.10** exhibits a doublet of doublets with coupling consistent with other *cis-bis*(phosphine) systems ($^2J_{PP}$ = 20 Hz), while **4.11** displays a singlet (δ_P: 44.14), suggesting the phosphine opposite the iminoketentylidene occurs at higher chemical shift. Curiously, the phosphine-platinum coupling remains similar between precursor and iminoketentylidene ($^1J_{PPt}$ = 3440 Hz **4.10** *ca* 3466 Hz **4.1**), except for the phosphine in **4.10** that lies *pseudo-trans* to tungsten and displays a larger coupling ($^1J_{PPt}$ = 3772 Hz) (Figure 4.18). Conversely, the platinum chemical shift is different to the metallacarbyne precursors, reflecting the geometric change from true to *pseudo*-square-planar (δ_{Pt}: –4174 **4.10** *cf.* –3761 **4.1**) (Figure 4.19). Utilising **4.10** for comparison, the platinum chemical shift is further upfield to the neutral μ2-chlorocarbyne **2.3b** (δ_{Pt}: –3992), showing **4.10** is more consistent with platinum(0) character, with variation likely explained by the difference in cationic *versus* neutral metal centre. All other unmentioned spectroscopic features are within expected values.

Crystallographic studies confirmed the μ2-iminoketenylidene linkage for **4.10** (Figure 4.20), whereas crystals of **4.11** crystallographic quality were not forth-coming. As crystals of the *bis*(phosphine) iminoketenylidenes were also initially unforthcoming, several crystals emerged at once, and therefore **4.10** was measured as both the PF_6 and BPh_4 salts. The only consequence between the two structures is that **4.10.PF6** exhibits a largely co-planar scafford (W1/C1/Pt1/P1/P2: 18.1°) whereas this angle increased for **4.10.BPh4** to accommodate the bulbous counter-anion. Further discussion will focus on **4.10.PF6** as it provided superior data with fewer refined parameters. The W–C bond length is considerably elongated to that of the precursor (1.997(5) Å), consistent with π-coordinated μ2-halocarbynes (1.971(6) Å **2.3b**) or μ2-phosphoniocarbyne [WPt(μ2-CPMe2Ph)(CNMes)2(CO)2(Tp*)]+ (1.968(5) Å; alternatively, see Chapter

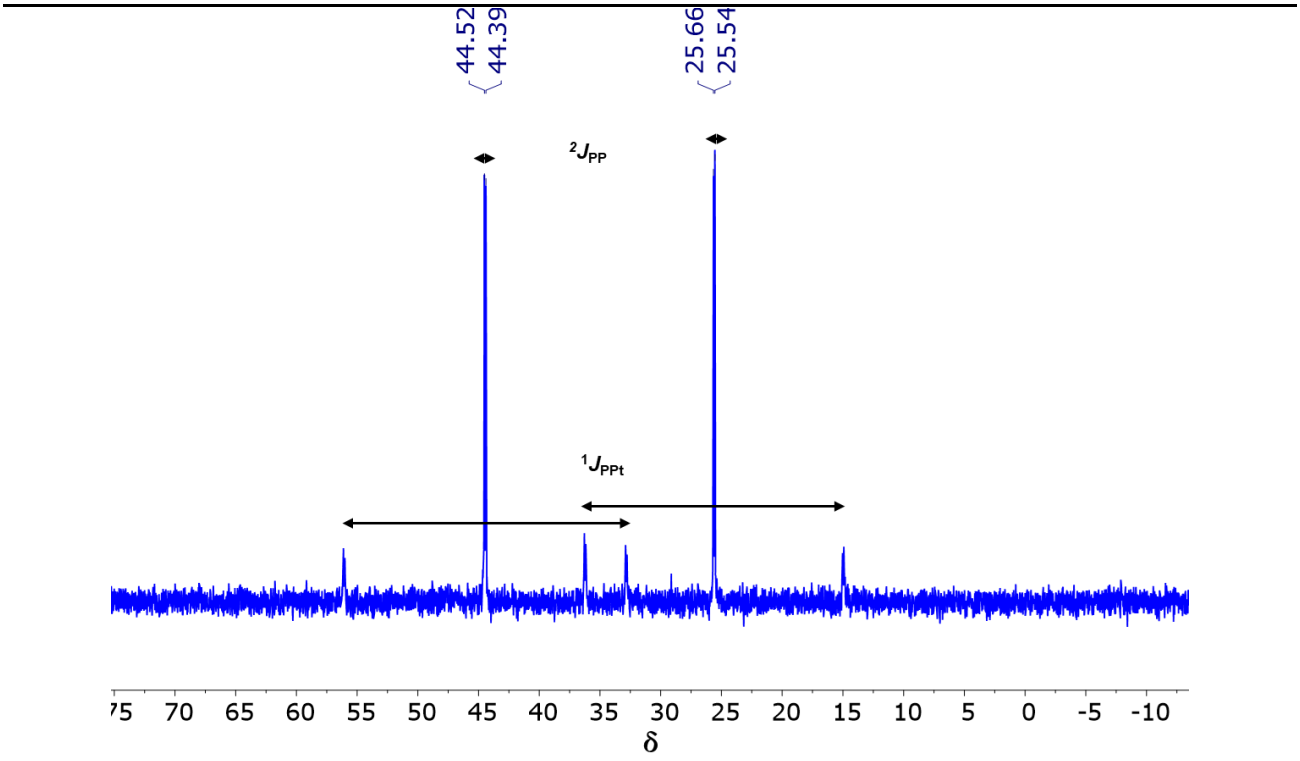

Figure 4.18: $^{31}P\{^1H\}$ NMR spectrum of the μ_2-iminoketenylidene $[WPt(\mu_2\text{-}CCNXyl)(PPh_3)_2(CO)_2(Tp^*)]PF_6$ (**4.10**, 162 MHz, 25 °C, δ_P, PF_6 resonance omitted).

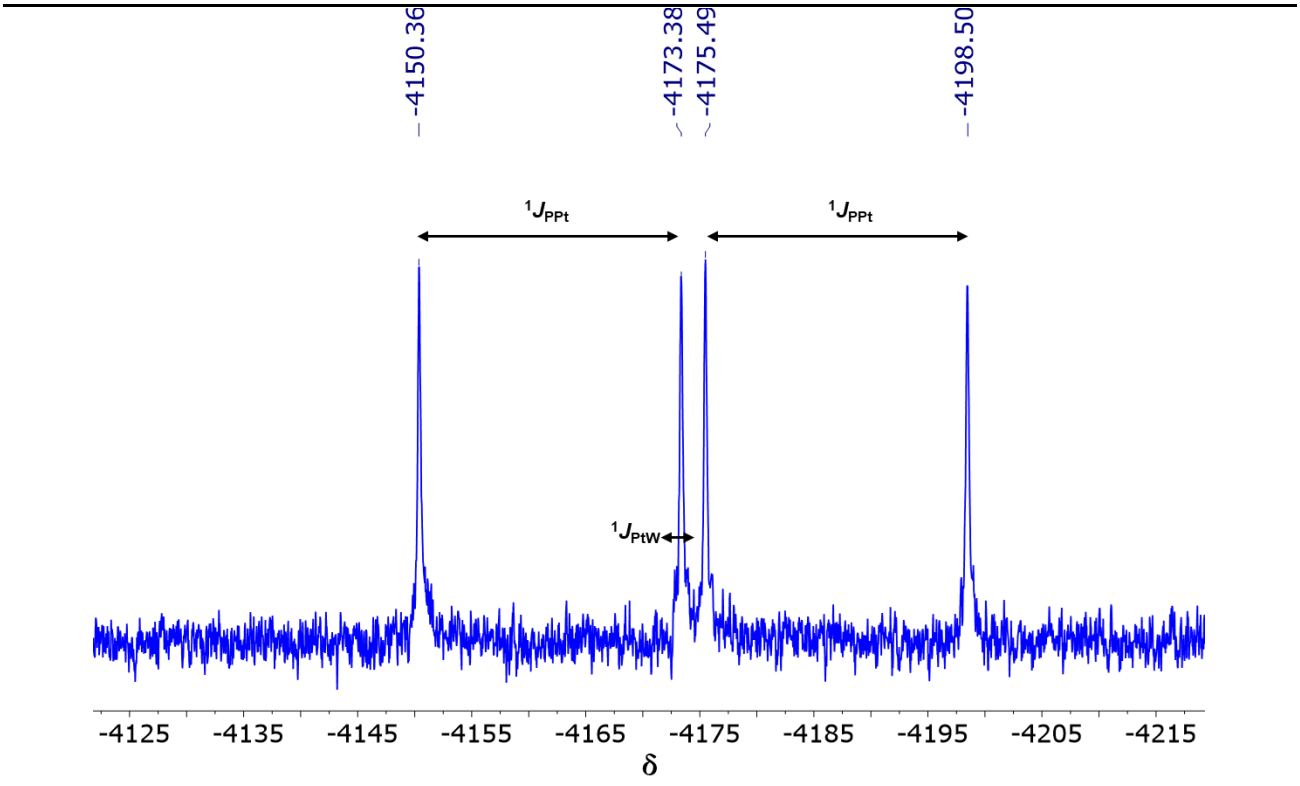

Figure 4.19: $^{195}Pt\{^1H\}$ NMR spectrum of the μ_2-iminoketenylidene $[WPt(\mu_2\text{-}CCNXyl)(PPh_3)_2(CO)_2(Tp^*)]PF_6$ (**4.10**, 150 MHz, 25 °C, δ_{Pt}).

Six),[214] reflecting a reduced bond order. Likewise, longer Pt–C lengths were determined (1.996(5) Å) consistent with a single bond.

Along the μ_2-iminoketenylidene linkage, the bonding is best described as cumulated double C=C (1.350(8) Å) and C=N (1.162(8) Å) bonds, terminating with a single N–C (1.393(8) Å) bond to incorporate the aryl substituent. Analogous μ_2-ketenylidene (μ_2-C=C=O) complexes are known (though not for tungsten and platinum),[355-357] the composition of these triatomic ligands terminating with oxygen results in a cylindrical ($C\infty$) shape, linear at each atom; μ_2-iminoketenylidenes contain nitrogen, with the additional possibility of linear or bent imine geometry. Experimentally the structure of **4.10** indicates the ligand spine (C1–C2–N1–C3) is closest to linear, although it contains a modest bend at nitrogen (C2–N1–C3: 163.8(6)°). This angle lies somewhat in between linear (180°) and bent geometries, such as μ_2-

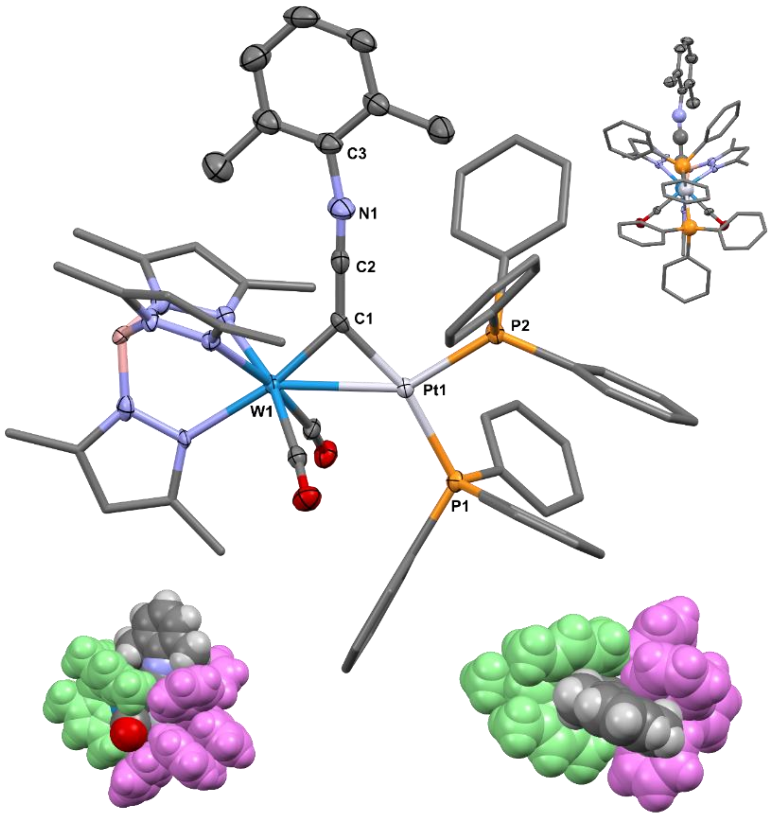

Figure 4.20: Molecular structure of [WPt(μ-CCNXyl)$(PPh_3)_2(CO)_2$(Tp*)]PF_6 (**4.10.PF_6**) in a single crystal of **4.10.PF_6**·$CHCl_3$ as determined by X-Ray Diffractometry. Ellipsoids are drawn at the 50% probability surface with pyrazoyl and phenyl rings simplified, and $CHCl_3$ solvent, PF_6^- counter-anion and hydrogens omitted for clarity. Insets: a) Ball and stick representation as viewed down the key molecular linkage (ligands simplified for clarity), b) Space-filling representation highlighting the steric clash of phenyl rings (pink) and the sterically encumbering tris-pyrazolylborate (green) ligand. Selected bond lengths (Å) and angles (°): W1–C1 1.997(5), C1–Pt1 1.996(5), W1–Pt1 2.7852(4), C1–C2 1.350(8), C2–N1 1.162(8), N1–C3 1.393(8), Pt1–P1 2.316(1), Pt1–P2 2.294(1), W1–C1–Pt1 88.5(2), W1–C1–C2 134.4(4), C1–C2–N1 178.9(7), C2–N1–C3 163.8(6), C1–Pt1–P1 164.3(1), C1–Pt1–P2 99.0(1), P1–Pt1–P2 96.26(5).

isocyanides $[W_2\{\mu\text{-}C_2Pt_2(CNMes)_3\}(CO)_4(Tp^*)_2]$ (136.4(5)°), [350] $[WPt(\mu_2\text{-}CNCF_3)(\mu\text{-dppm})(CO)_4(PPh_3)]$ (128.5(4)°), [349] or the trimeric complex $[Pt_3(CN^tBu)_6]$ (133.0(7), 132.5(9), 131.5(4)°). [347] Therefore, the CCNR angle is an inconclusive result, further compounded by lying in between a Tp* pyrazolyl cleft and two phenyl-phosphine rings that may prevent relaxation to the real conformation. As other structural features were consistent with expectations, theoretical studies were undertaken to better understand the bonding inside the μ_2-iminoketenylidene framework, and to explore what the ligand does unaccompanied by steric clutter or as a hypothetical free molecule.

4.6 Theoretical Studies of μ_2-iminoketenylidenes

The intriguing μ_2-imidoketenyldiene linkage begs a fundamental question: should it be bent or linear? Structural analysis of **4.10** suggests the ligand is closer to linear, yet the sterically encumbering environment in which the ligand resides clouds this conclusion. For this reason, theoretical models may help understand the geometry of the ligand should the environment allow the space. Firstly, analogous ketenylidene ligands can be considered simpler models, yet examples are limited to: a linear uranium complex $[(Cp')_3W\text{–}OCC\text{–}U(Cp')_3]$ (Cp' = η^5-$C_5H_4SiMe_3$), [357] the symmetrically bridged $[Zr_3(\mu_2\text{-}CCO)(\mu_3\text{-}O)(O_2CN^iPr_2)_6(Cp)_2]$ [355] and $[OsRhH(\mu\text{-}CCO)(CO)_3(dppm)_2]$, [356] and a single example of the heavy congener, the thioketenylidene $[Mo_2(\mu\text{-}CCS)(CO)_4(Tp^*)_2]$. [358] For these species, the free CCO/CCS molecules are conical ($C_{\infty v}$ symmetry) and contain doubly degenerate π and π* orbital pairs, hence a triplet configuration. Meanwhile, the π/π* orbitals of CCNR ligands may (or may not) be doubly degenerate depending on the additional N–R bond. Therefore, triplet or singlet configurations are possible resulting in a linear or bent geometry at nitrogen. [359]

For the free iminoketenylidene molecules, theoretical studies were conducted in accordance with previous calculations {DFT: 6–31G*}, now including the exchange functional {ωB97X-V} to test further long-range dispersion effects for the cumulated structure of the CCNR ligand. Furthermore, as thermodynamic properties were now of interest, frequency and thermodynamic calculations were conducted with second-order Møller Plesset methods (RI-MP2) in combination with Dunning's cc-PVTζ basis set, [360] these offering increased accuracy for thermodynamic properties. Initial experiments sought to model the hypothetical imidoketenylidenes (CCNMe **4.12Me*** and CCNPh **4.12Ph***) as free molecules in both singlet (s) and triplet states (t) (Figure 4.21). This gives an initial series of hypothetical molecules (**4.12*s*Me***, **4.12*t*Me***, **4.12*s*Ph***, and **4.13*t*Ph***) and all four combinations were calculated and summarised (Table 4.5). As antipicated, the geometry of singlet iminoketenylidenes optimise as bent molecules (CNC = 118.67–121.06°) and triplets to *pseudo*-linear molecules (CNC = 147.74–149.27°). For the smaller methyl-iminoketenylidene the triplet state lies lower in energy than the singlet state (Δ_{G0} = –4.0 kcal mol^{-1}) with a greater difference noted for the *phenyl*-iminoketenylidenes (Δ_{G0} = –9.32 kcal mol^{-1}).

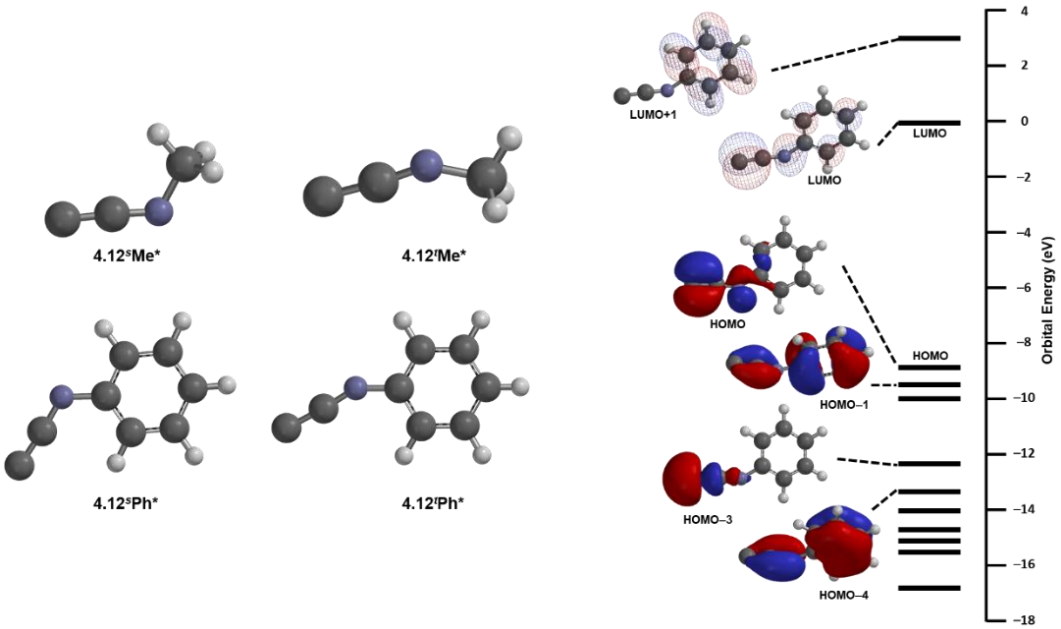

Figure 4.21: Optimised geometries of hypothetical singlet and triplet CCNR ligands (**4.12***) with frontier molecular orbitals of **4.12*t*Ph*** as the best fit to experimental μ_2-iminoketenylidene complexes. DFT: ωB97X–V/6–31G*.

Table 4.5: Calculated properties of hypothetical, free iminoketenylidene molecules in singlet and triplet states.

Species	ZPE (kJmol^{-1})	H^o (au)	S^o (Jmol^{-1}K^{-1})	G^o (au)	C_v (Jmol^{-1}K^{-1})	**G^o(triplet)–G^o(singlet) [au (kcalmol^{-1})]**
4.12^{t}Me*	124.18	–170.244791	253.24	–170.273548	100.53	–0.006359 (–4.0)
4.12^{s}Me*	129.67	–170.247660	283.96	–170.279907	57.58	
4.12^{t}Ph*	269.98	–361.514664	358.72	–361.555400	113.35	–0.01487 (–9.32)
4.12^{s}Ph*	266.41	–361.531325	342.75	–361.570247	113.21	
Species	C–N–R °))	C–C (Å)	C–N (Å)	N–R (Å)		
4.12^{t}Me*	149.27	1.344	1.211	1.430		
4.12^{s}Me*	118.67	1.316	1.246	1.459		
4.12^{t}Ph*	147.74	1.336	1.219	1.384		
4.12^{s}Ph*	121.06	1.307	1.257	1.410		
4.10 (Real)	163.8(6)	1.350(8)	1.162(8)	1.393(8)		
4.10*	164.00	1.344	1.179	1.382		

These energetic differences lend support to the linear geometry being most favourable, with delocalisation more prominent for the arene and evident from the derived bond lengths. Furthermore, the optomised triplet of **4.12.*t*Ph*** is the most comparable representation of the experimentally observed iminoketenylidene ligand in **4.10**, although it can still be contended this geometry is a geometric corollary enfored by interligand steric effects. Beyond the specific datum of interest, the calculated orbitals of triplet **4.12.*t*Ph*** are not dissimilar to the singlet state **4.12.*s*Ph***. The singlet HOMO–1 and triplet HOMO–2 present the occupied CCN π-bond at the terminal carbon, and the respective HOMO–3/HOMO–4 display the occupied two-electron σ-lobe akin to isocyanides and carbonyls. Singlet and triplet designations result in the HOMO (singlet) corresponding with the SOMO (triplet) as the coplanar

π* orbital of CCN, while the LUMO (singlet) maps with the soHOMO (triplet) as the orthogonal π* orbital. Both iminoketentylidene configurations recall similarities to the orbitals presented by isocyanides for bonding with one or more transition metals. As a ligand, the iminoketenylidene may serve as a *mono*-facial π-acceptor with an unoccupied π* orbital, but may also coordinate as a bifacial, four-π-donor ligand, especially towards transition metals with lower d-occupancies than those in **4.10** (d^6 W and $d^{8/10}$ Pt).

To build from the optimised models of free iminoketentylidenes, theoretical insight of an intact μ_2-iminoketenylidene complex was sought for comparison (Figure 4.22). Molecular pruning of **4.10** gives the hypothetical species $[WPt(\mu_2\text{-CCNXyl})(PMe_3)_2(CO)_2(Tp)]^+$ (**4.10***) and subsequent geometrical optimisation results in a similarly linear CCNR linkage (C–N–R: 164.00°). The HOMO is consistent with species encountered thus far mostly comprised of W–CO retrodonation, however, the HOMO–1 corresponds with W–C π-bonding of the μ_2-iminioketenylidene ligand (and π*-antibonding to platinum). The calculated Löwdin bond orders suggest double bond character for W–C (1.42) and a single bond for Pt–C (0.95), which is consistent with the experimental bond lengths of **4.10** (W–C 1.997(5) and Pt–C 1.9745(5) Å). The LUMO is associated with the μ_2-CCN system, that is, π-bonding for CC yet π*-antibonding for CN, accompanied by a minor π-anti- bonding with tungsten *d*-orbitals. This could be interpreted as the CCNR ligand or W–C bond presenting sites for nucleophilic attack.

Descending the calculated orbitals, the HOMO–3 reveals an interesting topology where overlap of d-orbitals from both transition metals extend continuously up the μ_2-iminoketenylidene spine and into the aromatic system in a helical manner. Such orbital topologies have previously been determined in [n]-cumulenes and described by Hoffman as Möbius co-arctate systems with remote but orthogonal orbitals of π-symmetry mix to form an extended, helical π-system. [361] The manifestation of this system in a notionally isoelectronic μ_2-iminoketenylidene compared with [n]cumulenes, remaining intact between two transition metals, is a notable result as it may suggest the topology arises from the transition metals, especially as it was noticeably absent (or very low in energy) for the calculated free molecules. Buried in the orbital manifold of **4.10***, the HOMO–15 represents the fully π-bonding orbital of the dimetallacyclopropene core. Similar to the results obtained from μ_2-halocarbynes of platinum, this bonding is consistent with (and may be deconstructed as) a π-coordination of a '$Pt(PMe_3)_2$' fragment to the hypothetical parent η^1-iminoketenylidene $[W(\text{–CCNXyl})(CO)_2(Tp)]^+$, hinting at the possibility of the complexes if the dissociation of such a platinum fragment could occur. Alternatively, by micro-reversibility, this perspective raises the challenge of preparing terminal iminoketenylidene complexes (*cf.* Hillhouse's putative $[WCl_2(CCO)(CO)(PMePh_2)_2]$ [362] as building blocks for bridge-assisted heterobimetallic bond-forming processes, perhaps *via* electrophilic *N*-alkylation of Lalor's cyanocarbynes $[M(CCN)(CO)_2(Tp^*)]$ (M = Mo, W). [363]

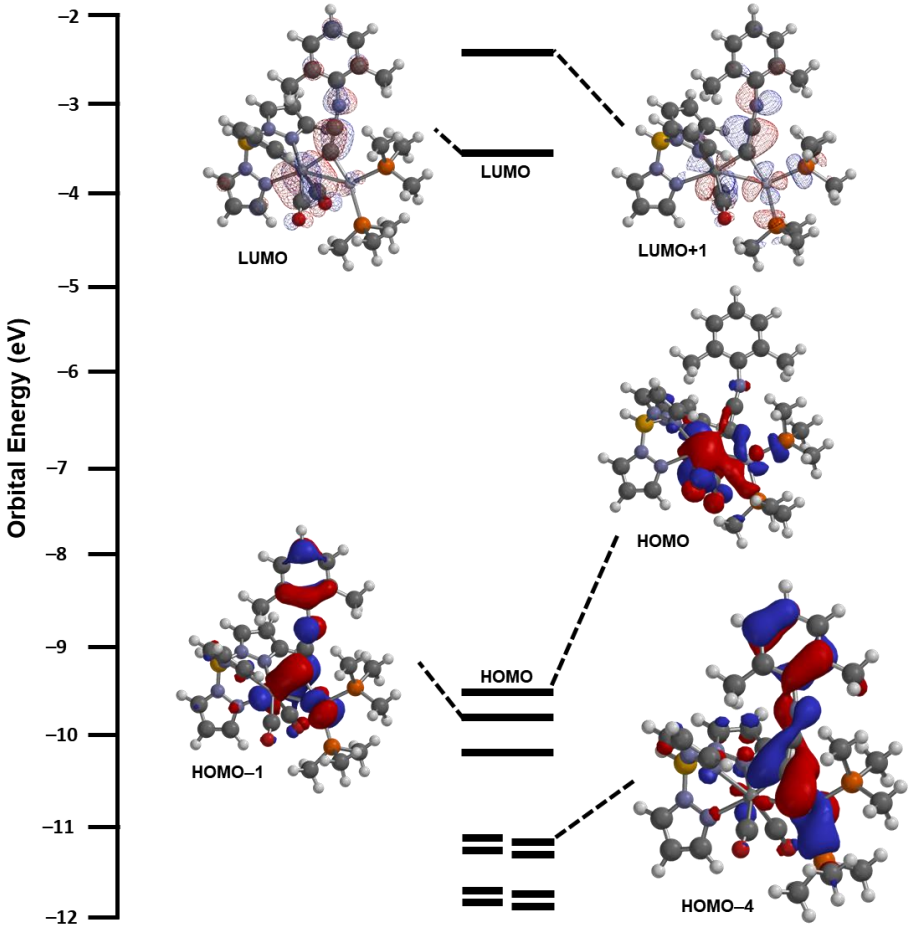

Figure 4.22: Frontier orbitals of interest for theoretical complex [WPt(μ_2-CCNXyl)(PMe_3)$_2$(CO)$_2$(Tp)] (**4.10***). DFT: ωB97X–V/6–31G*/LANLD2ζ.

Finally, the most striking feature of the iminoketenylidenes are the vibrant purple colours they exhibit, and time-dependent DFT simulations of UV-VIS spectra were calculated to assist in interpretation of the underlying reasons. Recall **4.10** exhibits an absorption in the visible region (λ_{MAX}/nm($M^{-1}cm^{-1}$): 535(6900)). Electronic transitions are predicted at 477 and 521 nm, corresponding to electronic transfer from the HOMO–1 and HOMO–2 to the LUMO respectively. As the HOMO–1 refers to W–C π bond and the HOMO–2 represents the W–CO π-bond, this suggests the colour arises from a degree of charge transfer from each of these sites through to the π-system of the μ_2-CCNR ligand (LUMO), *viz.* a Laporte-allowed and accordingly intense excitation $d_{xy}/\pi_{WC} \rightarrow \pi^*_{WC}\pi_{CCN}$.

Computational evaluation of the iminoketenylidenes, **4.10** and **4.11**, demonstrate a π-system of μ_2-CCNR ligands, which is reminiscent of previously found [n]cumulenes containing orbitals that support either a neutral π-acceptor or perhaps a four-π-donor ligand in the case of earlier transition metals. Comparisons with free hypothetical iminoketenylidenes, both in the singlet and triplet state, suggest that the ligand in **4.10**/**4.11** is most consistent with a triplet state and therefore the linear form, although caveats arising from steric impact introduce some uncertainty that may be resolved as further examples of μ_2-iminoketenylidenes arise now that they are established as viable ligands.

4.7 Attempts Towards μ2-ketenylidenes

The emergence of the μ2-iminoketenylidenes *via* isocyanide/μ2-carbido coupling, though unexpected, does represent a link between μ2-carbido complexes and their industrial relevance. Selegue first mooted the relevance of μ2-carbido complexes as intermediates in the Fischer—Tropsch process, the production of synthetic hydrocarbons from Syngas (CO/H_2) in his seminal metallacarbyne paper in 1987. [33] Many organometallic ventures have sought fundamental understanding of Fischer—Tropsch reactivity, [364-369] where a contemporary example involves CO reductions *via* magnesium(I) dimers by Jones' and co-workers (Scheme 4.7). [370-371] This reactivity was yet to be directly linked to μ2-carbidos, although Agapie and co-workers have made several advances through terminal carbido ligands on molybdenum. [66, 181, 372] Therefore, given the analogy between isocyanides (CNR) and carbon monoxide (CO), the migration of CNR onto a μ2-carbido represents an implied link for this model. For this reason, the conditions developed were explored to replace CNR with CO, anticipating a similar migration (should it occur) would yield a μ2-ketenylidene complex (μ2-CCO) and explicitly link carbidos to a C–C chain-growth event in the Fischer—Tropsch process. While these proposed migrations were not forthcoming, Takemoto concurrently reported the discrete construction of hydrocarbon motifs on the transient dimetallacarbene framework $[Ru_2(\mu_2\text{-}C{:})(\mu_2\text{-}NPh)(Cp^*)_2]$, [373] an exciting result strongly supporting this link. Our own efforts are detailed below.

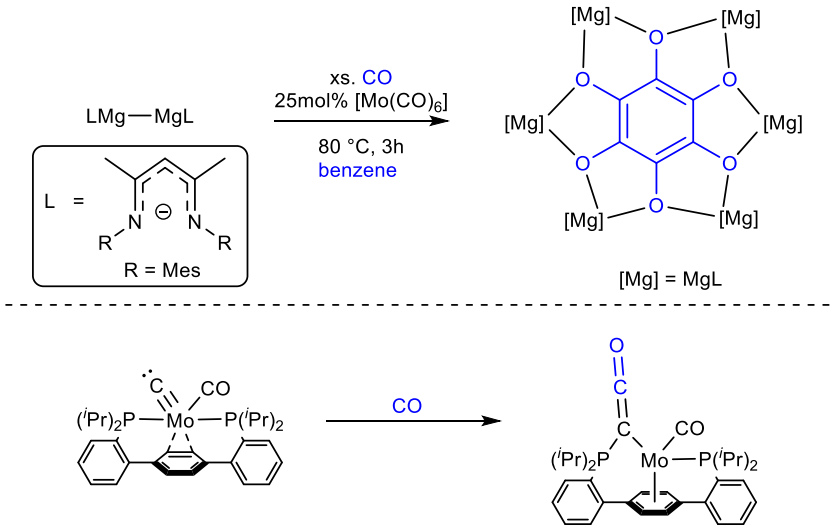

Scheme 4.7: Carbon monoxide homologation and a terminal carbide interacting with CO to form a ketenylidene.

Isocyanide migration from species **4.1** suggested a plausible framework towards an μ2-ketenylidene with the precursor already prepared (Scheme 4.8). The species $[WPt(\mu\text{-}CCl)(CO)_3(PPh_3)(Tp^*)]$ (**2.5**) was combined with phosphine in the polar 10% $MeOH/CH_2Cl_2$ medium and stirred for two days, remaining the olive/red colour of starting material. Investigation of $^{31}P\{^1H\}$ NMR spectra aided by infra-red spectroscopy confirmed that no conversion occurred.

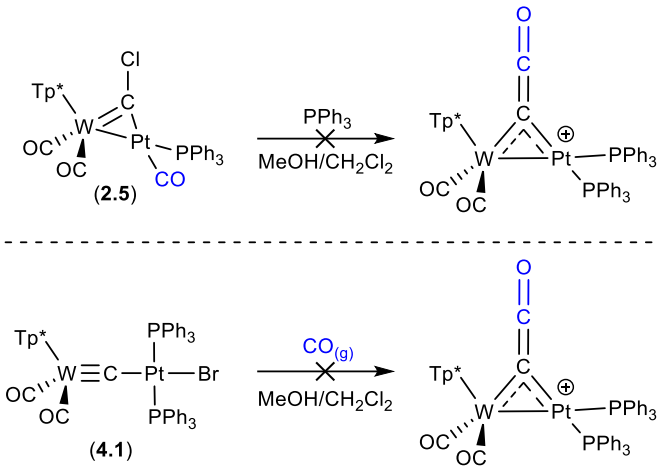

Scheme 4.8: Attempted synthesis of analogous μ_2-ketenylidene.

In one last attempt, the metallacarbyne **3.1b** was set under an atmosphere of carbon monoxide and injected with the CH_2Cl_2/MeOH solution. The mixture evolved a red colour from the orange solution, although after extended stirring returned to an orange mixture containing starting material. This reaction proved unreliable and so was no longer repeated. It could be expected the polar media would ionise the Pt–Br bond, and future work should consider utilising a silver salt to sequester the halide for a better opportunity at coordinating CO to platinum initially; a clearly unfavourable transformation. It appears the conditions that allow migration of isocyanides to form μ_2-iminoketenylidenes are insufficient for carbonyl migration toward μ_2-ketenylidenes and there is no evidence of a platinacarbyne bearing a carbonyl ligand as the initial step. Even if coordination is possible, the weaker σ-basicity of carbonyls may be insufficient to facilitate migration across the platinum centre, instead favouring phosphine retention.

Although this system currently falls short of linking μ_2-carbido complexes with carbon monoxide and μ_2-ketenylidenes, it remains an intriguing reaction of interest. Future reactions in carbido chemistry should always be attempted with carbon monoxide to produce intermediates relevant to Fischer–Tropsch processes as the concurrently published works of Takemoto and Agapie corroborate.

4.8 Conclusions

A series of tungsten-platinum metallacarbynes bearing isocyanide ligands have been produced to alleviate steric crowding around the μ-carbido ligand (Chart 4.2). Facile substitution of [WPt(μ_2-C)Br$(CO)_2(PPh_3)_2$(Tp*)] with xylyl- and mesityl-isocyanide provide *mono*-substituted or *bis*-substituted species, however, the reactions with *tert*-butylisocyanide halt at mono-addition, instead requiring an alternative oxidative addition protocol that ultimately provides access to the requisite metallacarbynes. Ligand substitution reactions identified isocyanides bind more strongly than phosphines once coordinated including examples of scorpionate derivatives.

Replacing phosphines with isocyanides progressively replaces the ^{31}P NMR nucleus with the ν_{CN} vibrational mode that complements study of isocyanide metallacarbynes, aiding confirmation that polar media gives over-substitution of isocyanide to *tris*-ligated cation $[WPt(\mu_2\text{-}C)(CNMes)_3(CO)_2(Tp^*)]PF_6$. Theoretical calculations of isocyanide complexes reveal a bonding framework similar to precursor **3.1b**, although with a W≡C–Pt linkage of σ-σ-π symmetry and a large LUMO orbital lying perpedicular to the platinum terminus plane. Calculated orbitals hinted promise for reactions with nucleophiles, yet in practice these reactions proved messy, yielding indeterminable mixtures.

Unprecedented reactivity was observed with migration of isocyanide ligands onto a μ_2-carbido promoted by polar solvents in a C–C bond forming step to yield the previously unknown μ_2-iminoketenylidene ligand (μ_2-CCNR). Two complex salts were fully characterised containing *pseudo*-linear CCNC spines as suggested by a theoretical study of free (triplet) CCNR molecules. Ultimately, formation of the μ_2-iminoketenylidene ligand represents a link to putative Fischer—Tropsch intermediates through the isoelectronic analogy of isocyanides with carbon monoxide, and although an extension to CO migration was not achieved, examples in the literature emerged concurrently to this work.

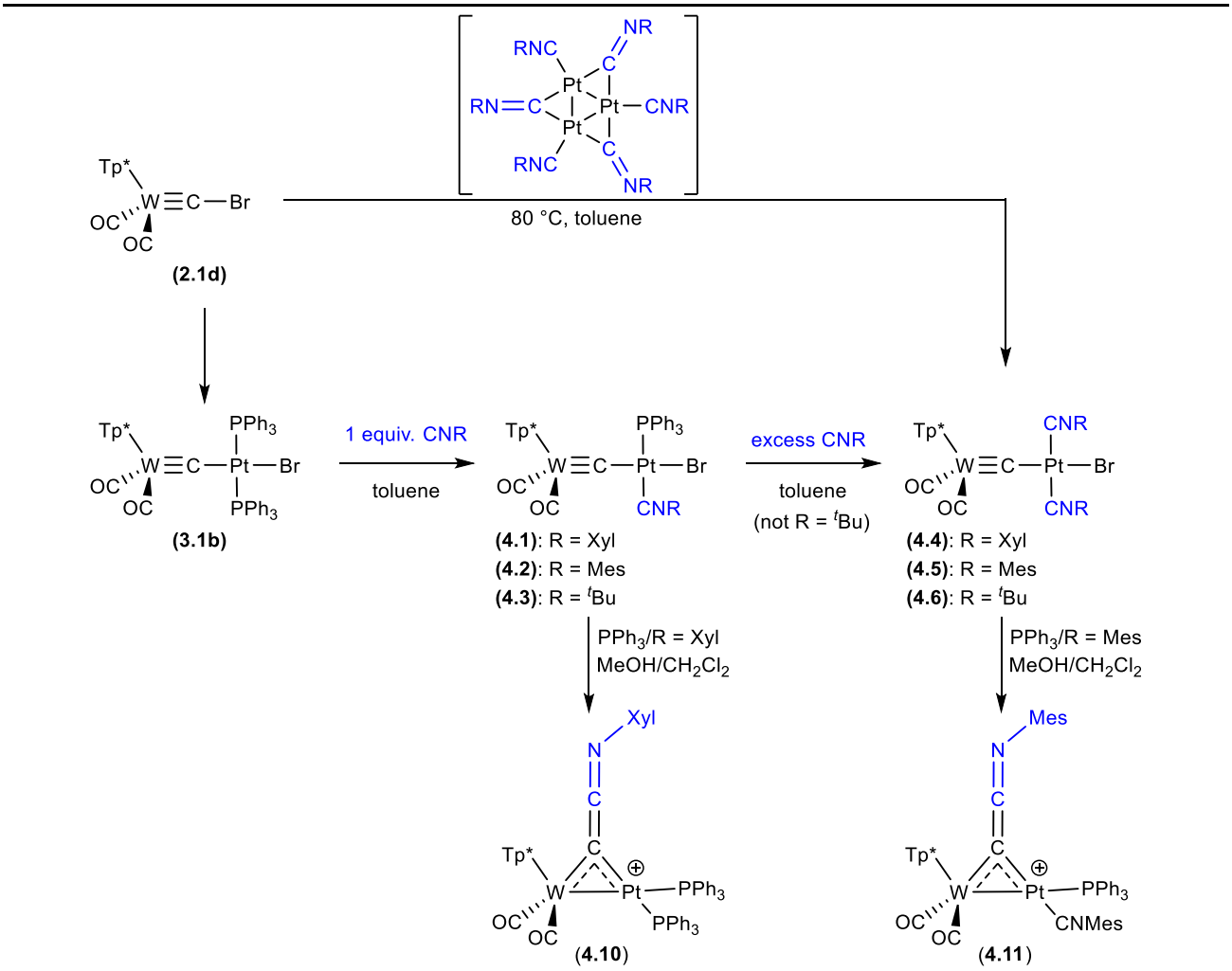

Chart 4.2: Summary of Chapter Four producing isocyanide carbido complexes and the emergence of μ_2-iminoketenylidenes .

Chapter Five

Reactions of a W–Pt Metallacarbyne with Non-innocent Co-ligands

Few instances of reactivity at the μ_2-carbido core of metallacarbynes have been reported, as ligand substitution generally only alters the periphery of the molecule. Despite carbido complexes being plausible reactive intermediates, [94, 136, 138, 141, 374-375] few systematic investigations have been reported. Beyond the development of palladium/copper/gold mediated C–C bond forming reactions described by Saitseva and Bruce for the synthesis of carbon-wire systems [136, 374] this is particularly true for carbon-based reactants that might inform understanding of, *e.g.*, the Fischer—Tropsch process, where C–C bond formation is required for hydrocarbon chain growth. Chapter Four developed isocyanide systems that ultimately underwent C–C coupling to form μ_2-iminoketenylidenes and whilst the processes are intriguing in their own right, an investigation of μ-carbido complexes bearing simpler hydrocarbyl ligands was considered worthwhile.

This Chapter therefore describes an exploration of the stoichiometric addition of carbon-based nucleophiles to **3.1b** as a controlled, spectroscopically informative system to access σ-hydrocarbyl Class B carbidos as models for subsequent C–C bond forming processes. In parallel, an analogous approach to the synthesis of carbido complexes with adjacent hydrido ligands will be described, given that C–H bond formation represents the other foundation of the Fischer-Tropsch process. Of relevance to the Fischer-Tropsch process, [1, 376-377] advances in carbido reactivity have been made for higher, [378-382] or lower[66-67] nuclearity species, while there is little intersection between μ_2-carbidos and hydride or σ-hydrocarbyl ligands.

5.1 Hydrocarbyl Ligands and μ_2-carbido Complexes

Only two examples of μ_2-carbido complexes containing a metal hydride are known (Scheme 5.1). The first, $[Ru_2(\mu_2\text{-}C)HCl_3(\mu{:}\sigma,\eta^6\text{-}H_2IMes)(H_2IMes)]$, arises from the degradation of Grubbs' second generation olefin metathesis catalyst $[Ru(=CH_2)Cl_2(H_2IMes)(PCy_3)]$ proposed to occur *via* C–H activation of a putative dimeric σ^1-methylidyne $[Ru_2(\equiv CH)(\mu_2\text{-}Cl)_2Cl(\eta^6\text{-}SIMes)(SIMes)]$. [158] This intermediate was not spectroscopically observed, being instead suggested based upon formation of $[PCy_3CH_3]Cl$ presumably from a phosphorus ylide (PCy_3CH_2). The second example $[Rh_2(\mu_2\text{-}C)H\{\mu\text{-}(C_6H_4)CPPh_2\text{–}2\}(Tp^*)_2]$ also arises from an intramolecular C–H activation. Attempted ligand substitution of $[Rh_2(\mu_2\text{-}C)Cl_2(PPh_3)_4]$ with bulky *tris*-(dimethylpyrazolyl)borate

(KTp*) results in coordination of two ligands, yet unlike examples with smaller pyrazolyl borates (Bp, Bp*, Tp), dissociation of one phosphine is followed by an *ortho*-metalation of the remaining PPh_3 ligand to give the metal hydride and σ-aryl Rh–C bond. [156] These examples demonstrate C–H activation of *sp* and sp^2 hybridised carbons in μ_2-carbido complexes, with the former invoking conversion of a σ^1-methylidyne into a μ_2-carbido.

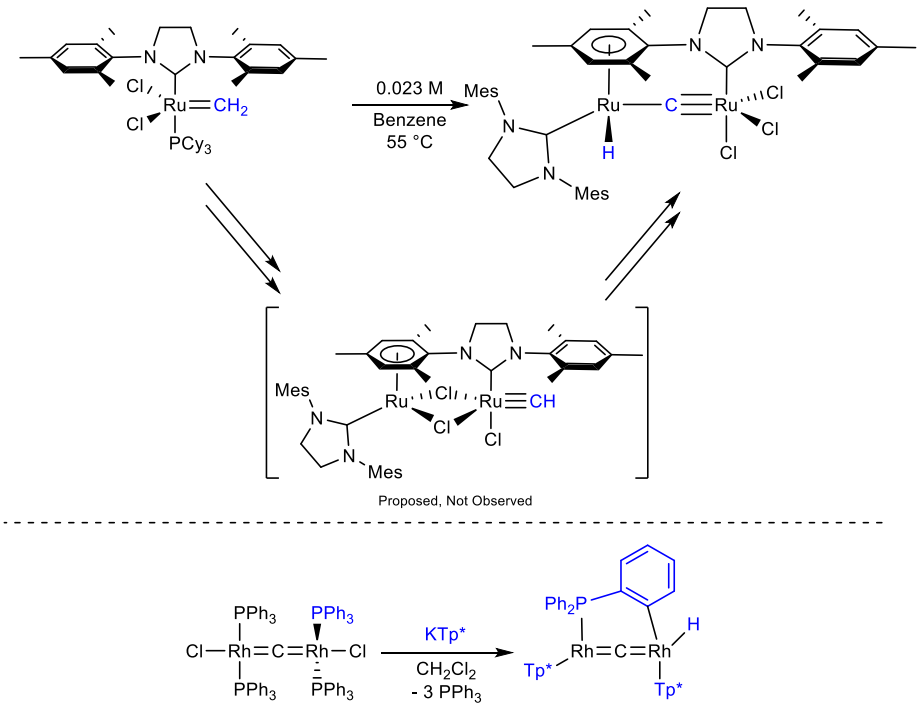

Scheme 5.1: Examples of μ_2-carbido complexes bearing hydrido ligands.

While Grubbs' demonstrated conversion of a methylidyne into a μ_2-carbido, Templeton showed the reverse reaction, as protonating the metallacarbyne [MoFe(μ_2-C)(CO)$_4$(Cp)(Tp*)] with strong acid (HBF_4) produces the μ_2-methylidyne [MoFe(μ_2-CH)(CO)$_4$(Cp)(Tp*)] (Scheme 5.2). [97] The methylidyne was formulated as involving an agostic C–H interaction based on spectroscopy given the ^{1}H NMR environment (δ_H: 1.94) to higher frequency of metal hydrides, but lower frequency of other μ_2-methylidynes (*cf.* δ_H: 20.81; [Ru_2(μ_2-CH)(μ-CO)(μ-dppm)(Cp)$_2$]BF_4). [383] Given that the HOMO of the precursor metallacarbyne is based on tungsten, initial protonation at tungsten followed by migration of the hydrido ligand to the carbido constitutes the reverse reaction to the C–H activation proposed by Grubbs. Although μ_2-methylidynes are somewhat rare, their chemistry is increasingly intertwined with that of μ_2-carbido complexes (*vide infra*).

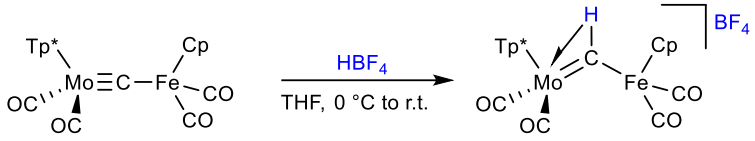

Scheme 5.2: The inverse reaction of a μ_2-carbido into a μ_2-methylidyne.

Recently, Takemoto and co-workers explicitly linked μ_2-carbido complexes to Fischer—Tropsch reactivity, showing discrete, linear hydrocarbon chain growth from a dimetallacarbene $[(Cp^*Ru)_2(\mu_2\text{-}C)(\mu\text{-}NPh)]$ generated by deprotonation of the μ_2-methylidyne $[(Cp^*Ru)_2(\mu_2\text{-}C)(\mu\text{-}NPh)]OTf$ (Scheme 5.3).[373] Treating $[(Cp^*Ru)_2(\mu_2\text{-}C)(\mu\text{-}NPh)]$ with a sulfur ylide (Ph_2SCH_2) first provides the vinylidene $[(Cp^*Ru)_2(\mu_2\text{-}CCH_2)(\mu\text{-}NPh)]$, which with a second equivalent reacts further to provide the allene $[(Cp^*Ru)_2(\mu_2\text{-}H_2C{=}C{=}CH_2)(\mu\text{-}NPh)]$. Further addition of Ph_2SCH_2 resulted in decomposition of the μ-NPh ligand, but exposure to hydrogenation conditions instead results in an alkylidene species $[(Cp^*Ru)_2\{\mu\text{-}CH(CH_2CH_3)\}(\mu\text{-}NPh)]$[384] from which hydrogen abstraction and deprotonation returns a propenylidene complex $[(Cp^*Ru)_2\{\mu_2\text{-}C{=}CH(CH_3)\}(\mu\text{-}NPh)]$; a species larger by one CH_2 unit. This propenylidene species is intriguing for two reasons. Firstly, hydrogenation liberates propane as a linear hydrocarbon accompanied by $[(Cp^*Ru)_2(\mu\text{-}H)_4]$ as the ruthenium decomposition product. More excitingly, the propenylidene can be resubjected to further sequences of successive chain growth from CH_2 units until a hexenylidene complex is isolated, $[(Cp^*Ru)_2\{\mu_2\text{-}CCH(CH_2CH_2CH_2CH_3)\}(\mu\text{-}NPh)]$, that can be hydrogenated to release *n*-hexane. Takemoto's report is not only an important result in linking μ_2-carbido complexes to hydrocarbon manufacture, but has broader implications as producing carbon chains 3-units or longer remains challenging.[385-393]

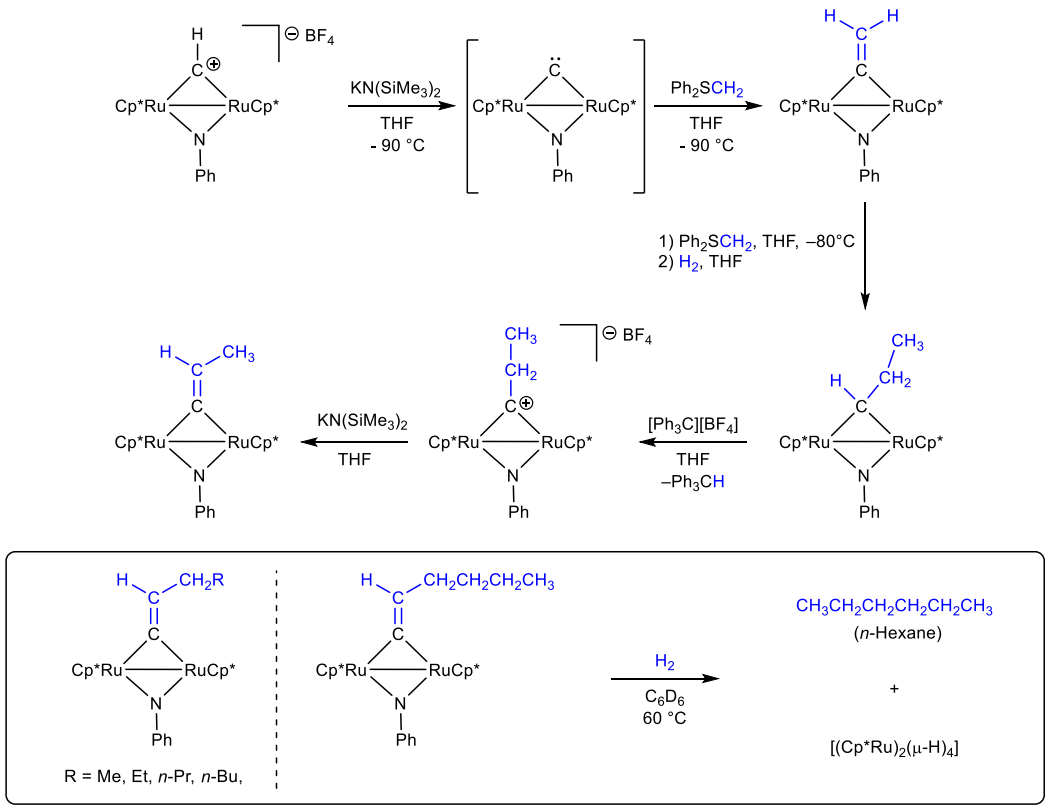

Scheme 5.3: Discrete hydrocarbon growth from a μ_2-cabrido complex and liberation of hydrocarbon.

While Takemoto's discrete chain growth is an important link, these few examples demonstrate the underexplored possibilities for μ_2-carbido complexes to take part in C–C bond forming processes. Concurrently to this work, the Class A carbido complex $[Rh_2(\mu_2\text{-}C)Cl_2(\mu\text{-}dppm)_2]$ was found to react with benzyne in a [2+2]-cycloaddition to form $[Rh_2(\mu_2\text{-}C)(\mu\text{-}Cl)(\kappa_2\text{-}C_6H_4)Cl_3(\mu\text{-}dppm)_2]$ (Scheme 5.4), indicating formation of a new Rh–C and C–C bond, encouraging a similar inquiry should investigate C–C formation in Class B carbidos. In order of increasing complexity and guided by initial computational studies of **3.1***, attempts to build carbon architectures from the defined metallacarbyne $[WPt(\mu_2\text{-}C)Br(CO)_2(PPh_3)_2(Tp^*)]$ (**3.1b**) are detailed here to elucidate direct or indirect reaction mechanisms of μ_2-carbido reactivity.

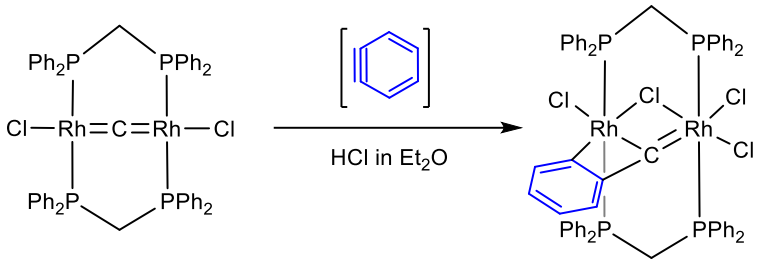

Scheme 5.4: A dimetallacumulene undergoes a [2+2]-cycloaddition with benzyne showing C–C bond formation.

5.2 Reactivity of [W≡C–Pt] with: Hydride Sources

Formates ($^-$OCOH) have provided a hydride source to metal centres for over a hundred years through a β-hydrogen,[394] particularly to platinum as a convenient source of reduction.[395] To begin our studies, **3.1b** in THF or CH_2Cl_2 was stirred with sodium formate resulting in no change even when heated at reflux for 16 hours. Repeat reactions on an NMR scale in C_6D_6 and $CHCl_3$ recorded no change or evidence of metal hydrides in the ^{1}H NMR spectrum, therefore more nucleophilic hydride sources were sought. A THF solution of **3.1b** was treated with one equivalent of $Li[HBEt_3]$[**********] where the orange of the precursor persisted, darkening slightly over five hours before infra-red and NMR spectroscopies revealed in excess of five compounds. Various spectroscopic methods suggested incomplete consumption of **3.1b** while other signals in the $^{31}P\{^1H\}$ NMR spectrum contained notable couplings but no conclusive evidence as to the identity of these species. The hydride region of the ^{1}H NMR spectrum (δ_H: –5 to –60) measured in $CDCl_3$[††††††††††] was barren, however, coupled high frequency signals emerged (δ_H = 13.0–14.0). Clearly intriguing species were forming from the reaction of borohydride solutions with **3.1b** where

[**********] Hydride is the smallest nucleophile and is conveniently available in commercial solutions such as Super–Hydride® [1M $Li[HBEt_3]$ in THF] or K–Selectride® [1M $K[HB^sBu_3]$ in THF].

[††††††††††] Measurement in $CDCl_3$ obscures the chemistry here, where similar measurement in C_6D_6 returns an important hydride resonance (see Section 5.4.2).

attempts to purify mixtures were met with unreacted **3.1b**, elemental platinum(0) (indicative of reduction), and tiny amounts of a red species consistently eluting first from flash chromatography. The red μ_2-methylidyne [WPt(μ_2-CH)(CO)$_3$(PPh$_3$)(Tp*)] (**5.1**) was the only cleanly isolated species from the mixture but represented a minor product (*ca* 5% isolated yield). Based on the previous μ_2-halocarbyne chemistry, it was possible that **5.1** was formed *via* carbonyl scavenging, potentially from a *bis*-phosphine intermediate (Scheme 5.5).

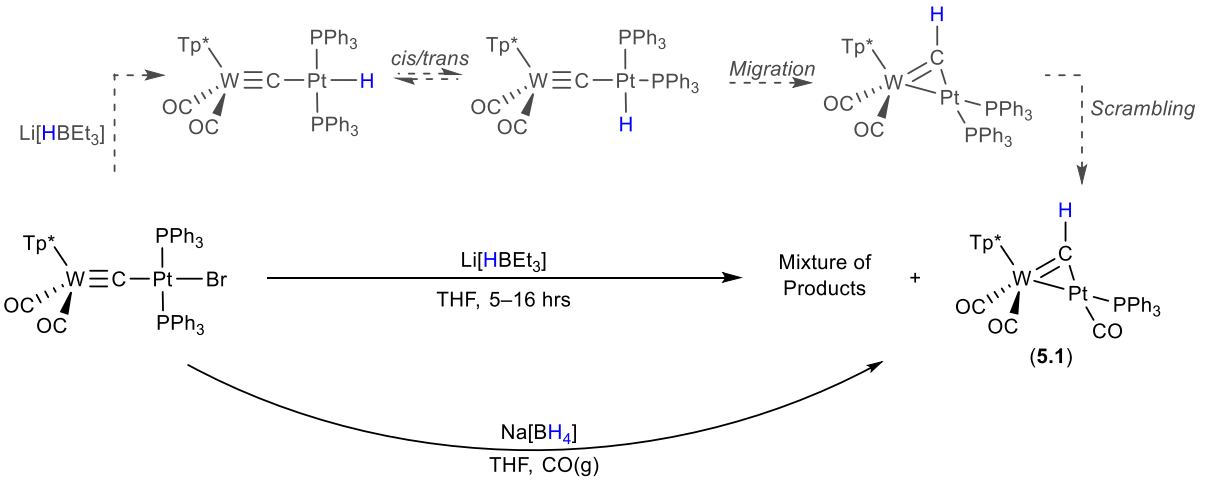

Scheme 5.5: Addition of borohydride to metallacarbyne precursor and isolation of a μ_2-methylidyne.

A deliberate synthesis of **5.1** was performed by reduction of **3.1b** with NaBH$_4$ under CO$_{(g)}$, resulting in a faster reaction and a ten-fold improvement in reaction yield (51% isolated). The ^{1}H NMR spectrum exhibits a high frequency doublet (δ_H = 13.69; $^2J_{HP}$ = 18 Hz) with ambiguous heteronuclear coupling (Figure 5.1). A decoupled ^{1}H{^{31}P} spectrum comprised a singlet with a single pair of heteronuclear satellites (J = 54 Hz) that, by integration, is more consistent with coupling to ^{195}Pt (33% abundance) than to ^{183}W (14% abundance). A platinum coupling of similar magnitude occurs for [PtMe$_3${BPh(PPh$_2$)$_3$}] ($^2J_{HPt}$ = 56 Hz) devoid of ^{183}W interference,[396] while the coupling in the *bis*-methylidyne [W$_2$Pt(μ_2-CH)$_2$(CO)$_4$(Tp*)] ($^2J_{CW}$ = 44 Hz) was assigned to ^{183}W while ^{195}Pt coupling was not resolved.[159] Therefore, it is difficult to unequivocally assign the nucleus responsible for the coupling observed in Figure 5.1, noting the ambiguity that remains in the ^{1}H{^{31}P} spectrum. The ^{31}P{^{1}H} NMR spectrum shows a coupled singlet at lower frequency than the chlorocarbyne analogue **2.5** (δ_P = 28.72 *vs* 35.69) with a reduced platinum coupling ($^1J_{PPt}$ = 3392 Hz *cf.* 3857 Hz for **2.5**) in addition to a higher frequency platinum resonance (δ_{Pt} = –4446). A higher frequency platinum signal may reflect more semi-bridging character of the W≡C–H fragment (**5.1**) as compared with W≡C–Cl (**2.5**) (see similar arguments in Chapter Two).

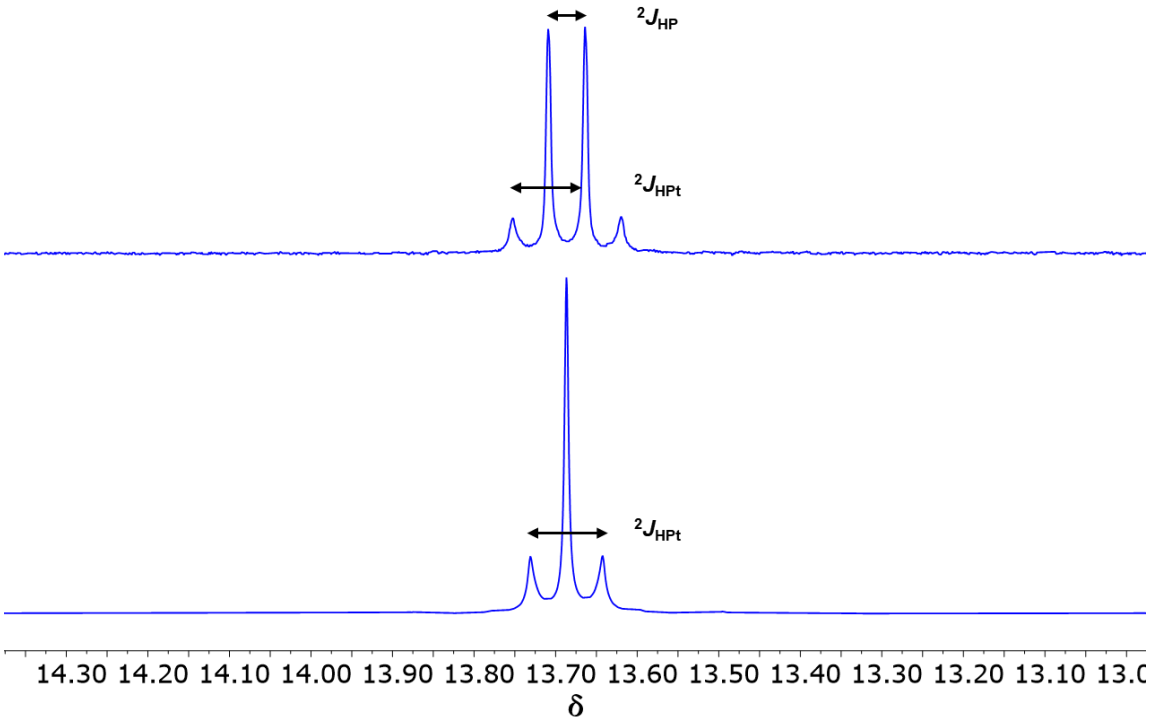

Figure 5.1: ^{1}H and ^{1}H{^{31}P} NMR spectra of [WPt(μ$_2$-CH)(μ$_2$-CO)(CO)$_2$(PPh$_3$)(Tp*)] (**5.1**) showing the methylidyne resonance with and without coupling to ^{31}P.

Structural analysis supported the formulation of **5.1** with, however, caveats associated with locating the methylidyne hydrogen in the vicinity of two heavy atoms (Pt, W). The intriguing hydrogen environment of **5.1** posits the species as a candidate for neutron diffraction, although attempts to grow single crystals of sufficient size (*ca* 0.1 mm^3) were not successful, preventing experiments of this type and precise hydrogen location. Nevertheless, the single crystal of **5.1** was strongly diffracting (I/σ = 32.2) such that a region of residual density was identified in a chemically sensible location for the methylidyne hydrogen, with no indications of disorder with the semi-bridging carbonyl. In one treatment of data, this residual density was assigned as the methylidyne hydrogen without further refinement in accordance with literature precedent (Figure 5.2). [397-398]‡‡‡‡‡‡‡‡‡‡‡‡ Care should therefore, as always, be taken when interpreting located hydrogen atom positions, and **5.1** is presented here as a consideration, not an absolute value.§§§§§§§§§§§§§

Noting these caveats, and entertaining the residual density as the methylidyne hydrogen, the C–H bond length (1.074 Å) is plausible considering organic Csp^2–H bonds derived from neutron

‡‡‡‡‡‡‡‡‡‡‡‡ Of the eight structural studies of μ$_2$-methylidyne complexes, seven are homometallic and accordingly the C–H and M–M vectors are expected to be parallel. The geometrical issues of semi-bridging do not arise and the majority of these structural models assign hydrogen atom positions through riding models.
§§§§§§§§§§§§§ The final CCDC deposited structure contains a methylidyne hydrogen riding on carbon.

diffraction (1.082(13) Å; 109 structures),[399] and an angle suggestive of semi-bridging character (M–C1–H1 = 156.4/110.56°) akin to those observed for gold(I) μ_2-halocarbynes (Chapter Two) and Stone's dicarbollide example********** $[WPt(\mu_2\text{-}CC_6H_3Me_2\text{-}2,6)(CO)_3(PEt_3)(\mu\text{:}\sigma,\eta^5\text{-}C_2B_9H_8Me_2)]$ (WCC = 160.0(8)°, W=C = 1.89(1) W–Pt 2.728(1) Å).[400] Meanwhile **5.1** exhibits contracted W–C (1.925(3) *vs* 1.951(4) Å) and elongated Pt–C (1.997(3) *vs* 1.950(4) Å) bonds compared with the analogous chlorocarbyne (**2.5**); the W–Pt bonds (2.7709(5) *vs* 2.7732(2) Å) are similar. In the solid state, the methylidyne **5.1** contains a semi-bridging carbonyl ligand whereas **2.5** does not, further evidenced by infra-red spectra in the solution state ($\nu_{\mu\text{-}CO}$ = 1786 cm^{-1}).

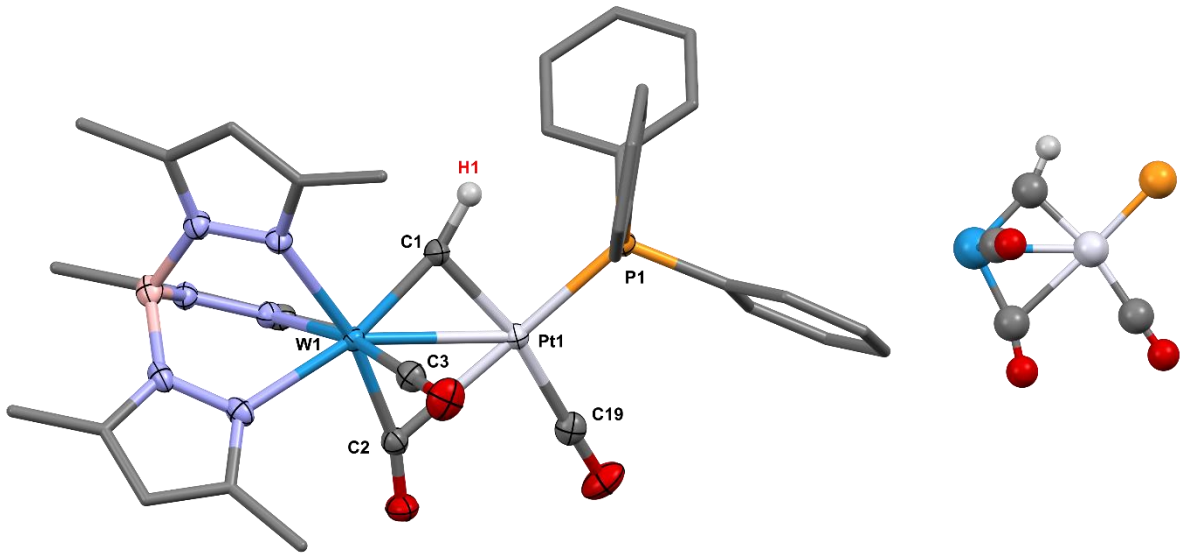

Figure 5.2: Molecular structure of $[WPt(\mu_2\text{-}CH)(\mu_2\text{-}CO)(CO)_2(PPh_3)(Tp^*)]$ (**5.1**) in a single crystal of **5.1**·2($CHCl_3$) as determined by X-Ray Diffractometry. Ellipsoids are drawn at the 50% probability surface with pyrazolyl rings simplified and hydrogens omitted for clarity. The μ-CH hydrogen (H1 denoted by red label) was located from a residual density map without refinement, whereas the finalised CIF utilises HFIX and a riding model. Inset: Ball and stick representation of the located hydrogen in the μ-CH ligand (ligands simplified for clarity). Selected bond lengths (Å) and angles (°): W1–C1 1.925(3), C1–Pt1 1.997(3), W1–Pt1 2.7709(5), W1–C2 1.982(3), C2–Pt1 2.563(3), Pt1–C19 1.905(3), Pt1–P1 2.2773(8), W1–C1–Pt1 89.9(1), W1–C2–Pt1 73.88(9), P1–Pt1–C19 101.86(9), C2–O1 1.169(4), W1–C2–O1 165.5(2), Pt1–C2–O1 120.6(2), C1–H1 1.094, W1–C1–H1 156.4 Pt1–C1–H1 110.6.

As the hydrogen location from X-ray diffractometry is uncertain, a computational inquiry was made for comparison (Figure 5.3). The geometry of the pruned species $[WPt(\mu_2\text{-}CH)(\mu\text{-}CO)(CO)_2(PMe_3)(Tp)]$ (**5.1***) was optimised commencing with atomic coordinates derived from the experimentally measured structure **5.1**. This pruning not only serves computational economy, but also reduces any impact from steric factors such that the resulting μ_2-methylidyne proton position, asymmetrically disposed between the tungsten and platinum (W–C–H: 140.2°; Pt–C–H:

********** NB: In contrast to **5.1**, this complex has a *cis* (*syn*) arrangement of carbyne and carbonyl groups about platinum.

128.3°), may be taken as a response to primarily electronic factors. This computationally-derived position is consistent with semi-bridging character and closer to the μ_2-chlorocarbynes. The variation between calculated and experimentally derived angles reinforces the caveats associated with crystallographically locating hydrogen positions without neutron diffractometry. Examining the orbital manifold reveals the LUMO is comprised of the π* component of the Pt–C1 association in conjugation with the phosphine and carbonyl ligands, while the LUMO+1 is the anti-bonding framework of the molecular core. The HOMO primarily involves tungsten retrodonation to both carbonyls while the HOMO–1 reflects orthogonal retrodonation to the semi-bridging carbonyl in the W-C-Pt plane. The HOMO–2 represents the W–C π interaction orthogonal to the "dimetallacyclopropene" plane with π* antibonding character to platinum. Deeper in the manifold, the HOMO–13 exhibits constructive W-C and C–Pt π-overlap consistent with a W–C–Pt dimetallacyclopropene description presented in Chapter Two.

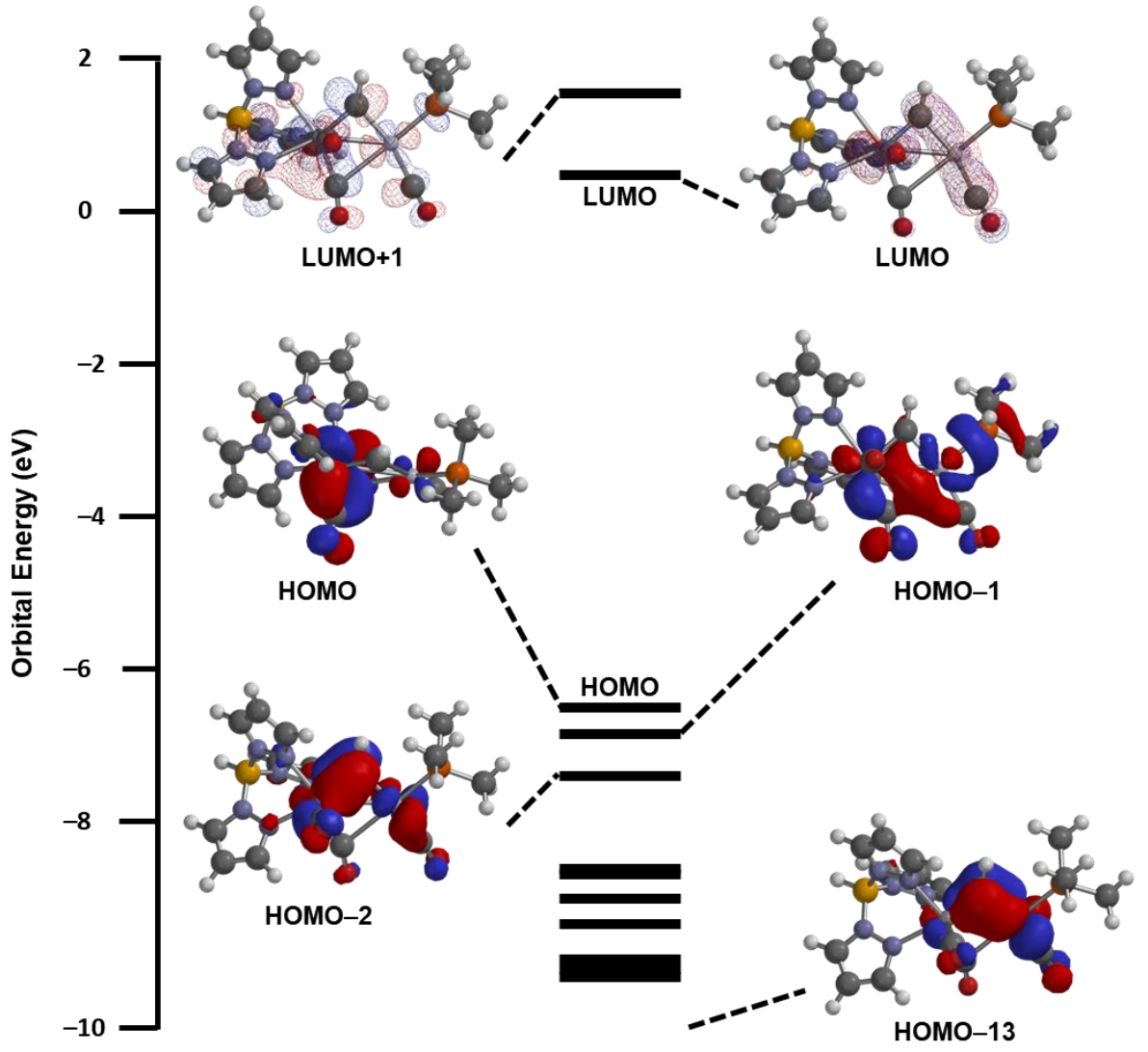

Figure 5.3: Frontier molecular orbitals of interest for [WPt(μ_2-CH)(μ-CO)$(CO)_2$$(PMe_3)$(Tp)] (**5.1***). DFT: ωB97X-D/6–31G*/LANL2Dζ.

5.3 Reactivity of [W≡C–Pt] with: Alkyllithiums

Hydride ligands are especially prone to migration and in the previous section, the putative hydrido complex [WPt(μ$_2$-C)H(CO)$_2$(PPh$_3$)$_2$(Tp*)] was not observed (see Section 5.4) presumably due to spontaneous evolution to the methylidyne [WPt(μ-CH)(CO)$_2$(PPh$_3$)$_2$(Tp*)]. Accordingly, it was also not possible to discount the possibility of direct attack by hydride at the μ-carbido ligand to provide the same ultimate product. Alternative nucleophiles with a spectrum of migratory aptitude were therefore considered in an attempt to better understand the interconversion of carbido and carbyne bridges, given that in other systems, *cis*-hydrido-carbido complexes were found to be stable. Although accessed *via* a different strategy, the structurally characterised molybdenum complex [MoPt(μ-C)(CH$_3$)(CO)$_2$(PPh$_3$)$_2$(Tp*)] was adventitiously isolated in undisclosed amounts and without further characterisational data, from the reaction of [Mo(≡CSnMe$_3$)(CO)$_2$(Tp*)] and [Pt(η^2-CH$_2$=CH$_2$)(PPh$_3$)$_2$] in toluene (60 °C, 2 days). Accordingly, it would appear that a tungsten-platinum *cis*-methyl-carbido complex might have greater longevity than the analogous hydride complex inferred above. The methyl nucleophile provides the desired size increase in addition to the opportunity for more kinetically stable Pt–C bonds as opposed to a Pt–H above.

Treating molybdenum and tungsten metallacarbynes **3.1a**/**3.1b** with MeLi (2.5M in THF) at 0 °C, immediately provided bright yellow solutions of methyl-carbido complexes *cis*-[MPt(μ$_2$-C)(CH$_3$)(CO)$_2$(PPh$_3$)$_2$(Tp*)] {M = Mo **5.2a**; W **5.2b**} (Scheme 5.6).‡‡‡‡‡‡‡‡‡‡‡‡‡ Collected ^{31}P{^{1}H} NMR spectra from either crude mixtures or isolated products confirm exclusive production of the *cis*-isomers.

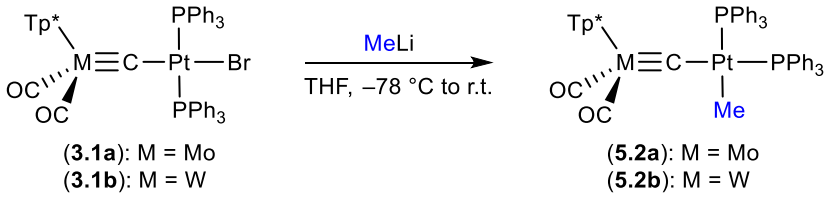

(**3.1a**): M = Mo
(**3.1b**): M = W

(**5.2a**): M = Mo
(**5.2b**): M = W

Scheme 5.6: Addition of MeLi to **3.1** to give *cis*-methyl metallacarbynes.

Spectroscopic and structural information between **5.2a**/**5.2b** prove similar and hence **5.2b** will be discussed. The ^{195}Pt NMR resonance lies at higher frequency from the precursor (δ_{Pt} = –4214 *cf.* –3718 in **3.1b**) likely reflecting an increased paramagnetic contribution from the relatively electron-rich platinum(II), being at a frequency similar to *pseudo*-trigonal planar platinum(0) species

‡‡‡‡‡‡‡‡‡‡‡‡‡ The molecular structure of **5.2a** was previously determined as a product arising in unspecified yield and without further reported characterisation from the reaction of [Mo≡CSnMe$_3$)(CO)$_2$(Tp*)] with [Pt(η^2-C$_2$H$_4$)(PPh$_3$)$_2$]. See R. Shang, *Functionalising Transition Metal Carbynes with Main Group Elements*, PhD Thesis, Australian National University, 2012.

(*cf.* –3992 **2.3b**; –4446 **5.1**). Unfortunately, insufficient signal/noise prevented the double doublet ^{195}Pt resonance for the dppe chelated complex **3.3b** being detected precluding direct comparison to an alternative *cis*-carbido complex. Curiously, the double-double-quartet ^{195}Pt signal has resolved coupling with methyl-protons ($^{2}J_{PtH}$ = 59 Hz) when acquired without ^{1}H coupling as replicated in the ^{1}H NMR spectrum, and consistent with that observed (δ_H = 0.33, $^{2}J_{PtH}$ = 68.4 Hz) for *cis*-[Pt(CH$_3$){C=O)Ph}(PPh$_3$)$_2$]. [401] Infra-red spectroscopy identified carbonyl vibrations (ν_{CO}: 1933, 1839 cm^{-1}) indicative of a more π-basic tungsten terminus, in turn reflecting the more electron rich, albeit remote, platinum centre. The μ$_2$-carbido resonance occurs at higher frequency in the ^{13}C{^{1}H} NMR spectrum (δ_C = 367.6) compared with similar metallacarbynes (δ_C = 356.7 **3.3b,** δ_C = 317.2 **3.1b**). Given the electron-rich nature of the platinum centre, this shift to high frequency for the resonance most likely reflects an increased paramagnetic contribution to the shielding rather than simple electron density at the carbido carbon.

The ^{31}P{^{1}H} NMR spectrum provides an indirect indication of μ$_2$-carbido donor strength relative to CH$_3$ ligands. Firstly, performing a ^{1}H–^{31}P HMBC experiment determines a stronger correlation of the methyl resonance with the lower frequency phosphorus resonance (δ_P = 22.27). Therefore, the higher frequency resonance (δ_P = 25.26) corresponds to the phosphine *trans* to the μ$_2$-carbido (*cis* to the CH$_3$ ligand), exhibiting a larger coupling to platinum ($^{1}J_{PPt}$ = 1963 *cf.* 1552 Hz) (Figure 5.4). Furthermore, a larger coupling to phosphorus is observed in the ^{13}C NMR spectrum of CH$_3$ compared with μ$_2$-C ($^{2}J_{CP}$ = 82 *vs* 73 Hz respectively). The solid-state structure of **5.2b** contains largely unremarkable features, but the Pt–P bond *trans* the μ$_2$-carbido is quite significantly (34 e.s.d.) elongated relative to CH$_3$ (Pt–P: 2.350(1) *vs* 2.316(1) Å), despite bowing of the W–C–Pt–P spine suggesting inter-ligand repulsions between the phosphine trans to CH$_3$ and the Tp* and remaining phosphine. Conversely, the Pt–C bond of the μ$_2$-C ligand (2.005(5) Å) is significantly shorter than that to the methyl ligand (2.119(4) Å), despite the disparate steric profiles of CH$_3$ and –CW(CO)$_2$(Tp*) 'ligands' (Figure 5.5). On the basis of Pt–Cl bond lengths calculated for the complexes *trans*-[Pt(R)Cl(PMe$_3$)$_2$], Lin and Marder concluded that the *trans* influence of σ-organyls decreases in the series R = CH$_2$CH$_3$ > CH=CH$_2$ > C$_6$H$_5$ > C≡CH. [267] In contrast, the carbido bridge for which a notional analogy with an alkynyl ligand might be entertained, appears in the present system to have a particularly strong *trans*-influence in excess of that for a methyl group, itself a ligand of renowned *trans* influence comparable to a hydride ligand. This may presumably be traced to the different nature of PPh$_3$ (σ-donor and at best weak π-acceptor) *vs* bromo (σ and π-donor) ligands with respect to their interactions with *trans* disposed ligands.

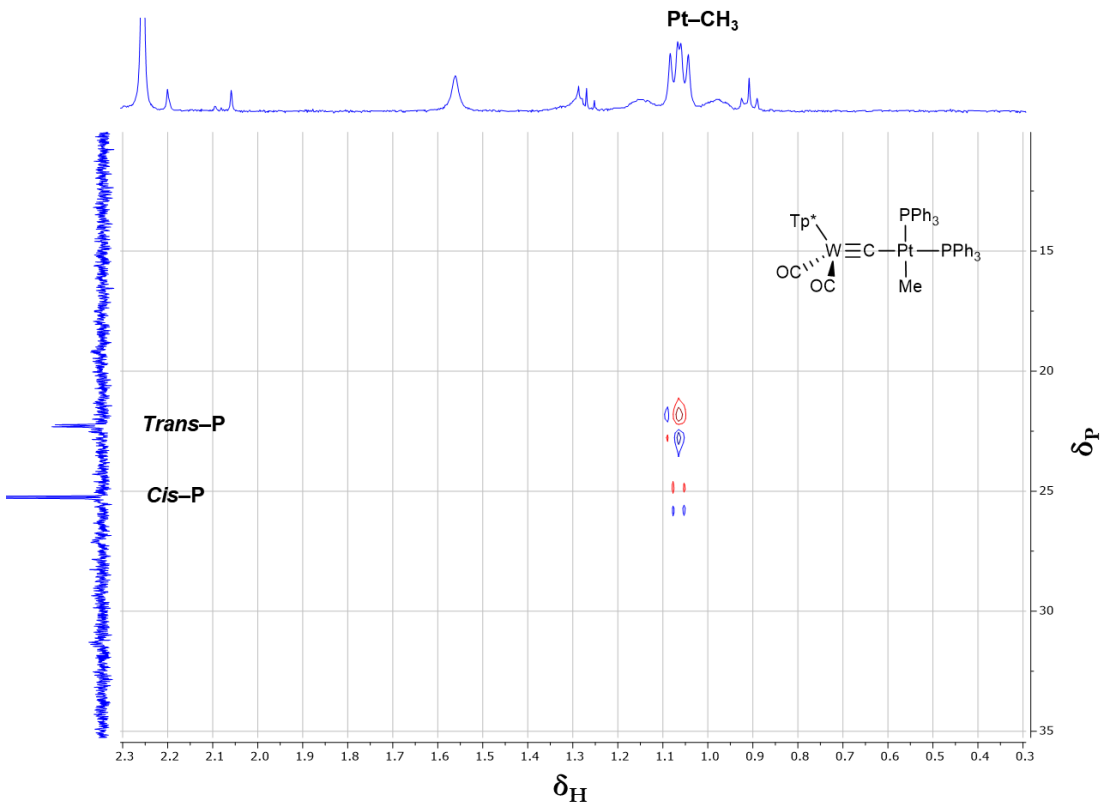

Figure 5.4: $^{1}H–^{31}P$ HMBC spectrum of [WPt(μ$_2$-C)Me(CO)$_2$(PPh$_3$)$_2$(Tp*)] (**5.3b**).

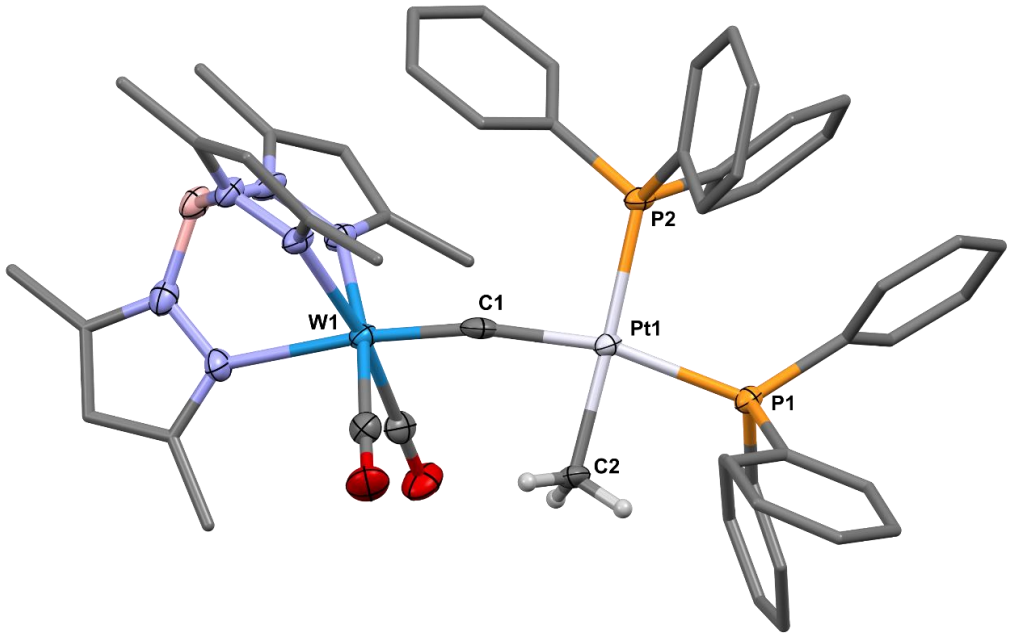

Figure 5.5: Molecular structure of [WPt(μ$_2$-C)Me(CO)$_2$(PPh$_3$)$_2$(Tp*)] (**5.2b**) in a single crystal of **5.2b**·CHCl$_3$ as determined by X-Ray Diffractometry. Ellipsoids are drawn at the 50% probability surface with pyrazolyl and phenyl rings simplified and hydrogens omitted for clarity. Selected bond lengths (Å) and angles (°): W1–C1 1.836(5), C1–Pt1 2.005(5), Pt1–C2 2.119(4), Pt1–P1 2.350(1), Pt1–P2 2.316(1), W1–C1–Pt1 166.3(3), P1–Pt1–P2 98.63(4), C2–Pt1–P2 177.3(1).

During development of **5.2a/5.2b** no evidence of μ_2-methylcarbyne complexes [MPt(μ_2-CCH_3)$(CO)_2(PPh_3)_2$(Tp*)] was observed; the product of μ_2-C/CH_3 coupling or direct nucleophilic addition to the carbido ligand. This suggests the CH_3^- exclusively reacts at the platinum terminus rather than directly at the μ_2-carbido, although it does not exclude the possibility of CH_3 migration once installed.‡‡‡‡‡‡‡‡‡‡‡‡ Heating both **5.2a/5.2b** at reflux in a range of solvents {THF, d_8-toluene and d_3-acetonitrile} returned unreacted starting material, suggesting no migration of CH_3 occurs up to 110 °C, contrasting the behaviour of hydride ligands that occur at ambient temperature (*vide supra*) or isocyanides in polar media (Chapter Four).

Having (incorrectly) anticipated migration of the methyl group onto the μ_2-carbido, the corresponding μ_2-methylcarbynes were synthesised in concert with the above investigation, permutations missing from Stones' collection (contain PMe_3 ligands). [195, 197, 243-244, 247] Combination of the ethylidyne [W(≡CCH_3)$(CO)_2$(Tp*)] with [Pt(η^2-C_2H_4)$(PPh_3)_2$] provides the analogous, but unknown heterobimetallic complex [WPt(μ_2-CCH_3)$(CO)_2(PPh_3)_2$(Tp*)] (**5.3**), where similar CO scrambling also gives the tricarbonyl derivate [WPt(μ_2-CCH_3)(μ_2-CO)$(CO)_2(PPh_3)$(Tp*)] (**5.4**), which is perhaps not unexpected given that scrambling also occurred for halocarbynes (Scheme 5.7). Both complexes were fully characterised, in addition to the trimetallic 'bow-tie' complex [W_2Pt(μ_2-CCH_3)$_2(CO)_4$(Tp*)$_2$], although X-ray diffraction studies were not pursued given the analogous [W_2Pt(μ_2-CCH_3)$_2(CO)_4$(Tp)$_2$] is known to arise from disproportionation of [WPt(μ_2-CCH_3)$(CO)_2(PMe_3)_2$(Tp)], [245] while variants with strongly π-acidic ligands such as [WPt(μ-Ctolyl)$(CO)_2${P(OMe)$_3$}$_2$(Tp)] are especially prone to formation of the corresponding trimetallic assemblies. [197, 247, 249]

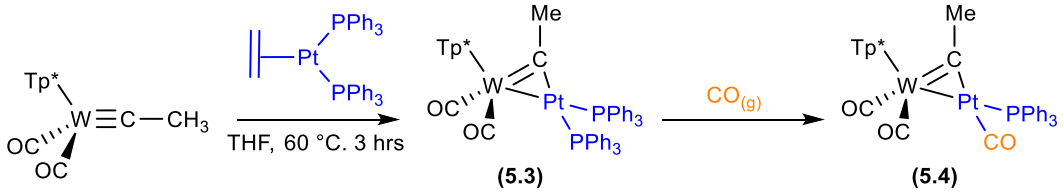

Scheme 5.7: Synthesis of μ_2-methylcarbynes *via* π-coordination.

Crystals suitable for diffractometry were able to be grown for **5.4** but not **5.3** due to facile disproportionation to [W_2Pt(μ_2-CCH_3)$_2(CO)_4$(Tp*)$_2$] in solution, for which a low quality data set was acquired that confirmed connectivity but did not provide geometrical data of sufficient

‡‡‡‡‡‡‡‡‡‡‡‡ Despite the large number of known alkyl-substituted μ_2 or μ_3-carbynes, there are no reports of the migration of an organyl group from a bridging carbyne to a metal to generate a carbido ligand.

precision for further discussion.§§§§§§§§§§§§§§§ For **5.4**, many of the key data resemble those of the analogous complexes of Stone, including a high frequency resonances for the C_1 carbon (δ_C = 338.0, $^2J_{CP}$ = 3 Hz), and as such require no further discussion. However, one notable datum appears in the $^{195}Pt\{^1H\}$ spectrum of **5.3** as the low frequency signal also exhibits coupling to ^{183}W ($^1J_{PtW}$ = 212 Hz). The solid-state structure of **5.3** provides useful information given discussion of steric pressures from pyrazolylborate and phosphine ligands. While not equal, the angles of the methylcarbyne about tungsten and platinum are relatively similar (141.2(3)/130.2(3)°) to those of the analogous chlorocarbyne (136.2(2)/133.2(2)°) and calculated for the theoretical methylidyne (**5.1***). Otherwise, the geometric features are unremarkable in isolation (Figure 5.6).

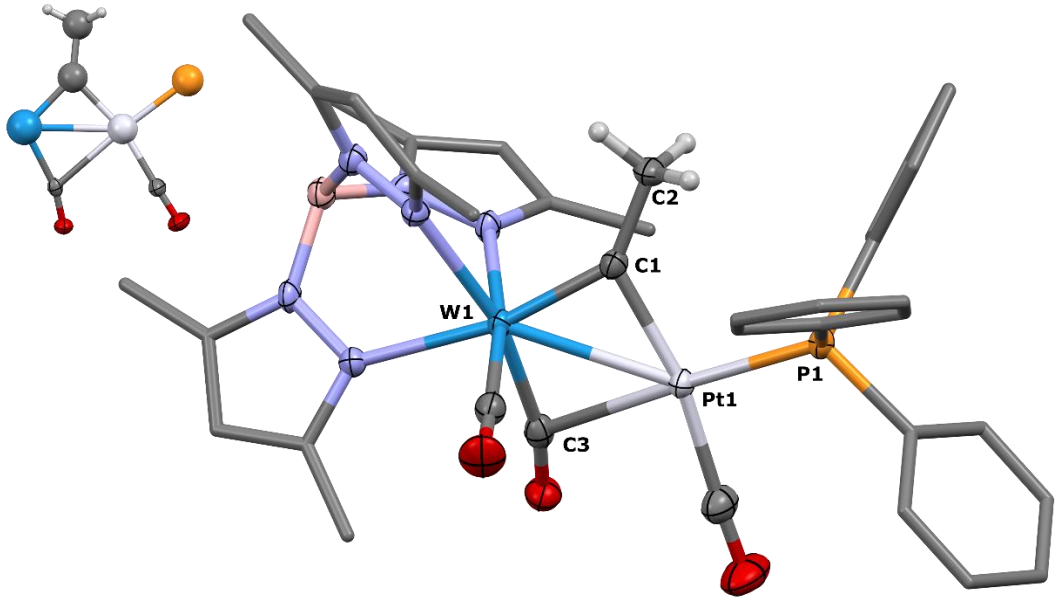

Figure 5.6: Molecular structure of [WPt(μ$_2$-CCH$_3$)(μ$_2$-CO)(CO)$_2$(PPh$_3$)(Tp*)] (**5.4**) in a single crystal as determined by X-Ray Diffractometry. Ellipsoids are drawn at the 50% probability surface with pyrazolyl and phenyl rings simplified and hydrogens omitted for clarity. Inset: Ball and stick representation showing coordination of the μ$_2$-CCH$_3$ ligand between tungsten and platinum. Selected bond lengths (Å) and angles (°): W1–C1 1.946(4), C1–Pt1 2.007(4), Pt1–W1 2.7560(5), C1–C2 1.498(6), W1–C3 1.987(4), Pt1–C3 2.554(4), Pt1–P1 2.2826(8), W1–C1–C2 141.2(3), Pt1–C1–C2 130.2(3), W1–C1–Pt1 88.4(2), W1–C3–Pt1 73.5(1).

Treatment of **3.1b** with *n*-BuLi resulted in an analogous complex *cis*-[WPt(μ$_2$-C)(*n*-Bu)(CO)$_2$(PPh$_3$)$_2$(Tp*)] (**5.5**) after an anaerobic short silica gel column and subsequent crystallisation. Once again, no evidence of *trans*-isomers or direct addition at the μ$_2$-carbido ligand was noted (*i.e.* no μ$_2$-pentylidyne). Instead, deviating from the optimal conditions results in

§§§§§§§§§§§§§§§ As with [W$_2$Pt(μ-CCl)$_2$(CO)$_4$(Tp*)$_2$], a very similar positional disorder was apparent for the bridging CO and carbyne ligands, which precluded the development of a satisfactory structural model, beyond confirmation of identity.

acceleration of the inevitable β-hydride elimination to form μ_2-methylidyne [WPt(μ_2-C)$(CO)_2(PPh_3)_2$(Tp*)] (**5.6**);[**********] no migration of a butyl group was observed (Scheme 5.8).

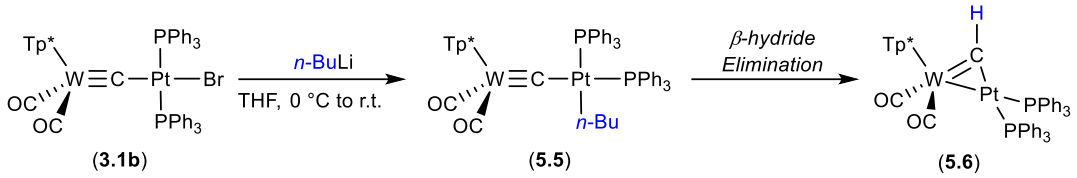

Scheme 5.8: Alkylation of **3.1b** with *n*BuLi before μ_2-methylidyne formation *via* spontaneous β-hydride elimination.

Spectroscopic interrogation of **5.5** proved challenging, firstly due to poor solubility, and secondly from better solubilising solvents accelerating inevitable β-hydride elimination to μ_2-methylidyne [WPt(μ_2-CH)$(CO)_2(PPh_3)_2$(Tp*)]. While this elimination was a desired *ultimate* outcome, it prevented deeper study of **5.5**, although select pieces of information could be acquired. Most spectroscopic features of **5.5** are analogous to those of **5.2b**. The main exception arises in the $^{31}P\{^1H\}$ NMR spectrum as the phosphine *trans* to the *n*-butyl group exhibits a reduced coupling compared with that found for CH_3 ($^1J_{PPt}$ = 1733 Hz **5.5** *cf.* 1963 Hz **5.2b**) that suggests partially improved σ-donation. Facile β-hydride elimination meant **5.5** did not survive in solution long enough to directly detect a μ_2-carbido resonance in the $^{13}C\{^1H\}$ NMR spectrum, although a ^1H–^{13}C HMBC experiment suggested a correlation (δ_{C-1} = ~345 with aryl δ_H signals) accompanied consistent with methyl-carbidos **5.2**, noting another correlation was observed (δ_C ~319 with δ_H = 5.65, 5.95) later identified as a μ_2-methylidyne (**5.6**; *vide infra*) . Likewise, the ^{195}Pt NMR spectrum contained no discernible resonance. Nevertheless, β-hydride elimination of **5.5** provides a useful entry into μ_2-methylidyne complexes from the high yield preparation of **5.6** where discussion of features is included with related species below.

5.4 Expanding Heterobimetallic μ_2-methylidynes

5.4.1 A review of μ_2-methylidynes

Repeated emergence of μ_2-methylidynes indicated further species are likely to emerge and the class should be addressed independently. Examples of μ_2-methylidyne complexes are comparatively rare, noting that inclusion of elements beyond the transition series almost doubles the population. To date, no specific review of μ_2-methylidyne (μ_2-methyne) complexes has appeared, with many examples reported in the last decade. Examples considered here omit main

[**********] The decomposition of *cis*-[Pt(^{n}Bu)$_2$(PPh$_3$)$_2$], also *via* β-Pt–H elimination, is first order in complex, with phosphine dissociation occurring before or during the rate-limiting step (Rate = (k_1 + k_2[PPh$_3$])[Pt]). [402]

group element termini (*e.g.*, Al, Ge, Si) and are presented in chronological order of synthetic method development.

Structurally authenticated μ_3-methylidyne complexes far outnumber their lower nuclearity μ_2-counterparts. Furthermore, terminal methylidynes are known for tungsten, [64, 179-180, 403-404] molybdenum, [64-65, 181] and niobium, [405-406] where the latter two are of interest in the context of coupling of carbon monoxide[181] and methylidyne transfer, [407] respectively. In contrast, μ_2-methylidyne species are less common yet are refreshingly diverse on closer inspection. The original example‡‡‡‡‡‡‡‡‡‡‡‡‡ was reported by Casey and co-workers, [410] who prepared $[Fe_2(\mu_2\text{-}CH)(\mu_2\text{-}CO)(CO)_2(Cp)_2]PF_6$ *via* trityl-mediated hydride abstraction of a methylene complex $[Fe_2(\mu_2\text{-}CH_2)(\mu_2\text{-}CO)(CO)_2(Cp)_2]$, noting that formation of isolable *cis* and *trans* isomers (Scheme 5.9). This early work immediately identified the characteristically high-frequency methylidyne resonance (δ_H = 22.8) in the ^1H NMR spectra. The same complex $[Fe_2(\mu_2\text{-}CH)(\mu_2\text{-}CO)(CO)_2(Cp)_2]^+$ could be prepared by α-methoxide abstraction from $[Fe_2\{\mu_2\text{-}CH(OCH_3)\}(\mu_2\text{-}CO)(CO)_2(Cp)_2]$ with HBF_4 or $[Ph_3C][BF_4]$. [411]

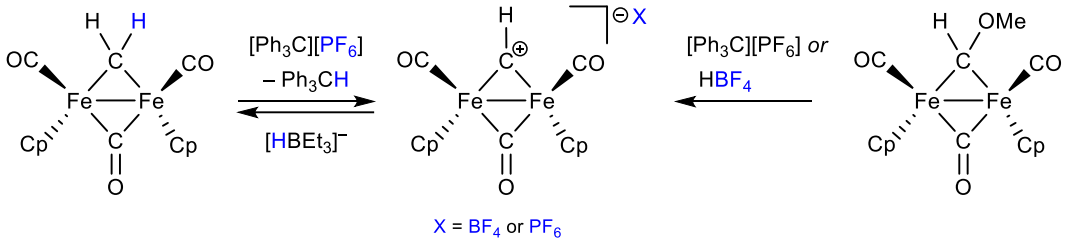

Scheme 5.9: Synthesis of diiron μ_2-methylidyne *via* hydrogen or methoxide abstraction.

The μ_2-methylidyne $[Fe_2(\mu_2\text{-}CH)(\mu_2\text{-}CO)(CO)_2(Cp)_2]PF_6$ proved to be a versatile electrophile in reactions with several reagents relevant to hydrocarbon transformations (Scheme 5.10). Addition at the μ_2-CH with carbon monoxide readily occurs to provide the parent ketenyl $[Fe_2\{\mu_2\text{-}CH(CO)\}(\mu_2\text{-}CO)(CO)_2(Cp)_2]PF_6$ which reacts with further nucleophiles toward aldehyde and carboxylic acids $[Fe_2\{\mu_2\text{-}CH(CR{=}O)\}(\mu_2\text{-}CO)(CO)_2(Cp)_2]PF_6$ (R = H or OH). [412] Addition of trimethylamine gives an ammonio complex $[Fe_2\{\mu_2\text{-}CH(NMe_3)\}(\mu_2\text{-}CO)(CO)_2(Cp)_2]PF_6$, while alkenes insert into the μ_2-methylidyne C–H bond to give a rich chemistry of substituted μ_2-alkylidyne complexes. With a cyclic alkene the 1-methylcyclohex-1-ene, a novel ring-contracted μ_2-σ,η^2-alkenyl $[Fe_2\{\sigma{:}\eta\text{-}HC{=}CHCMe(C_5H_8)\}(\mu\text{-}CO)(CO)_2(Cp)_2]$ was observed, [413] and further vinyl derivatives were later achieved from diazo reagents. [388] Reactions with alkynes provided more

‡‡‡‡‡‡‡‡‡‡‡‡‡ The complexes $[W(\equiv CH)Cl(PMe_3)_3(AlMe_2R)]$ {R = Cl or Me} by Schrock and co-workers predate Casey's complex, but are better classified as an adduct than a true μ_2-methylidyne complex, especially as TMEDA/PME_3 can abstract the aluminium to return $[W(\equiv CH)Cl(PMe_3)_4]$. [408 409]

complicated μ_2-alkylidynes arising from insertion of coordinated CO to provides η^1,η^4-vinylketene ligands. [414] Alkyllithium or enol reagents also attack the μ_2-methylidyne to give neutral μ_2-alkylidenes $[Fe_2\{\mu_2\text{-}CH(R)\}(\mu_2\text{-}CO)(CO)_2(Cp)_2]$ (R = Me, Ph *etc.*). [415]

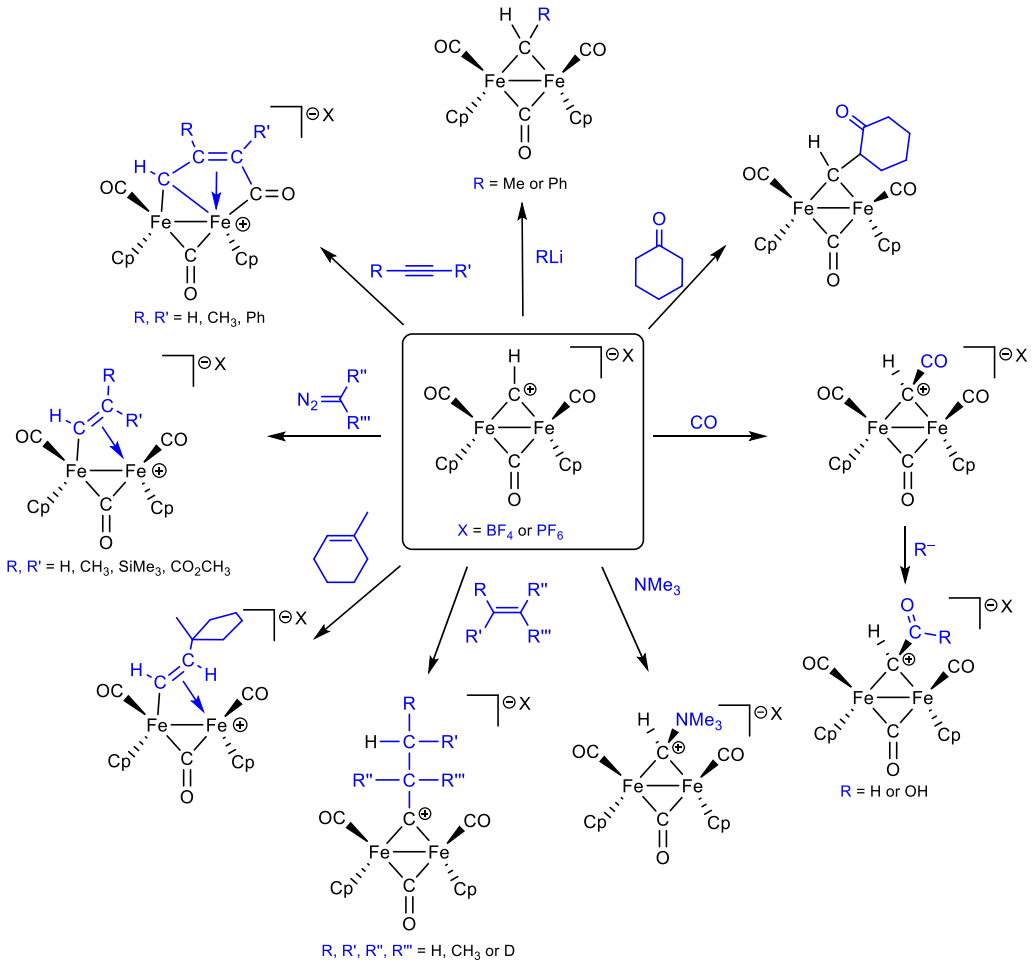

Scheme 5.10: Representative reactions of iron μ_2-methyildyne $[Fe_2(\mu_2\text{-}CH)(\mu\text{-}CO)(CO)_2(Cp)_2]^+$. [388, 410, 412-415]

A ruthenium μ_2-methylidyne was reported by Knox and co-workers in 1984 (Scheme 5.11). Photolysis of $[Ru_2(\mu_2\text{-}CH_2)(\mu\text{-}CO)(CO)_2(Cp)_2]$ with dppm results in $[Ru_2(\mu_2\text{-}CH_2)(\mu\text{-}CO)(dppm)(Cp)_2]$ before subsequent treatment with HBF_4 gives a μ_2-CH_3 complex $[Ru_2(\mu_2\text{-}CH_3)(\mu\text{-}CO)(dppm)(Cp)_2]BF_4$ that spontaneously forms the methylidyne $[Ru_2(\mu_2\text{-}CH)(\mu\text{-}CO)(\mu\text{-}dppm)(Cp)_2]BF_4$ in solution, losing an equivalent of H_2 which is proposed to occur *via* hydrogen radicals. [383] While the mechanism for this transformation remains unconfirmed, the authors outline observations that: (i) single electron oxidation of $[Ru_2(\mu_2\text{-}CH_2)(\mu\text{-}CO)(dppm)(Cp)_2]$ gives $[Ru_2(\mu_2\text{-}CH)(\mu\text{-}CO)(\mu\text{-}dppm)(Cp)_2]BF_4$; (ii) treatment of $[Ru_2(\mu_2\text{-}CH_2)(\mu\text{-}CO)(dppm)(Cp)_2]$ with trityl fails to produce the methylidyne; and (iii) $[Ru_2(\mu_2\text{-}CH)(\mu\text{-}CO)(\mu\text{-}dppm)(Cp)_2]BF_4$ does not revert to $[Ru_2(\mu_2\text{-}CH_2)(\mu\text{-}CO)(dppm)(Cp)_2]$ or $[Ru_2(\mu_2\text{-}CH_3)(\mu\text{-}CO)(dppm)(Cp)_2]BF_4]$ under an atmosphere of hydrogen.

Extensions of Casey's hydride abstraction approach have since been reported for ruthenium, niobium, and rhenium (Scheme 5.11). Analogous abstraction of a methylidene hydride from $[(Cp^*Ru)_2(\mu_2\text{-}CH_2)(\mu\text{-}NPh)]BF_4$ with trityl gives $[(Cp^*Ru)_2(\mu_2\text{-}CH)(\mu\text{-}NPh)]^+$, which is of particular significance in the context of carbide chemistry due to its subsequent deprotonation to afford a Class D μ_2-carbido (see Chapter One or Section 5.1).[416] Alternatively, Mindiola and co-workers demonstrated the niobium methylidyne $K[Nb_2(\mu_2\text{-}CH)(\mu\text{-}H)(\mu\text{-}Cl)(OAr)_4]$ (OAr = 2,6-*bis*(diphenylmethyl)-4-*tert*-butylphenoxide) is produced upon treating $[Nb_2(\mu_2\text{-}CH_2)(\mu\text{-}Cl)_2)(OAr)_4]$ with KC_8, proposed to occur *via* reduction to $K[Nb_2(\mu_2\text{-}CH_2)(\mu\text{-}Cl)(OAr)_4]$ followed by an intramolecular hydrogen transfer to the niobium centres. Furthermore, $K[Nb_2(\mu_2\text{-}CH)(\mu\text{-}H)(\mu\text{-}Cl)(OAr)_4]$ is oxidised back to $[Nb_2(\mu_2\text{-}CH_2)(\mu\text{-}Cl)_2)(OAr)_4]$ with chlorotriphenylmethane.[398] Alkyllithium reagents are also capable of deprotonating μ_2-methylene complexes. Hoffman demonstrated neopentyllithium deprotonates $[Re_2(\mu_2\text{-}CH_2)(\mu\text{-}O)(=O)_2Me_4]$ to generate $Li[Re_2(\mu_2\text{-}CH)(\mu\text{-}O)(=O)_2Me_4]$, although deuterium labelling experiments revealed this process is likely more complicated as mixed species $[Re_2(\mu_2\text{-}CHD)(\mu\text{-}O)(=O)_2Me_4]$ failed to generate any μ_2-deuteromethylidyne $Li[Re_2(\mu_2\text{-}CD)(\mu\text{-}O)(=O)_2Me_4]$.[417]

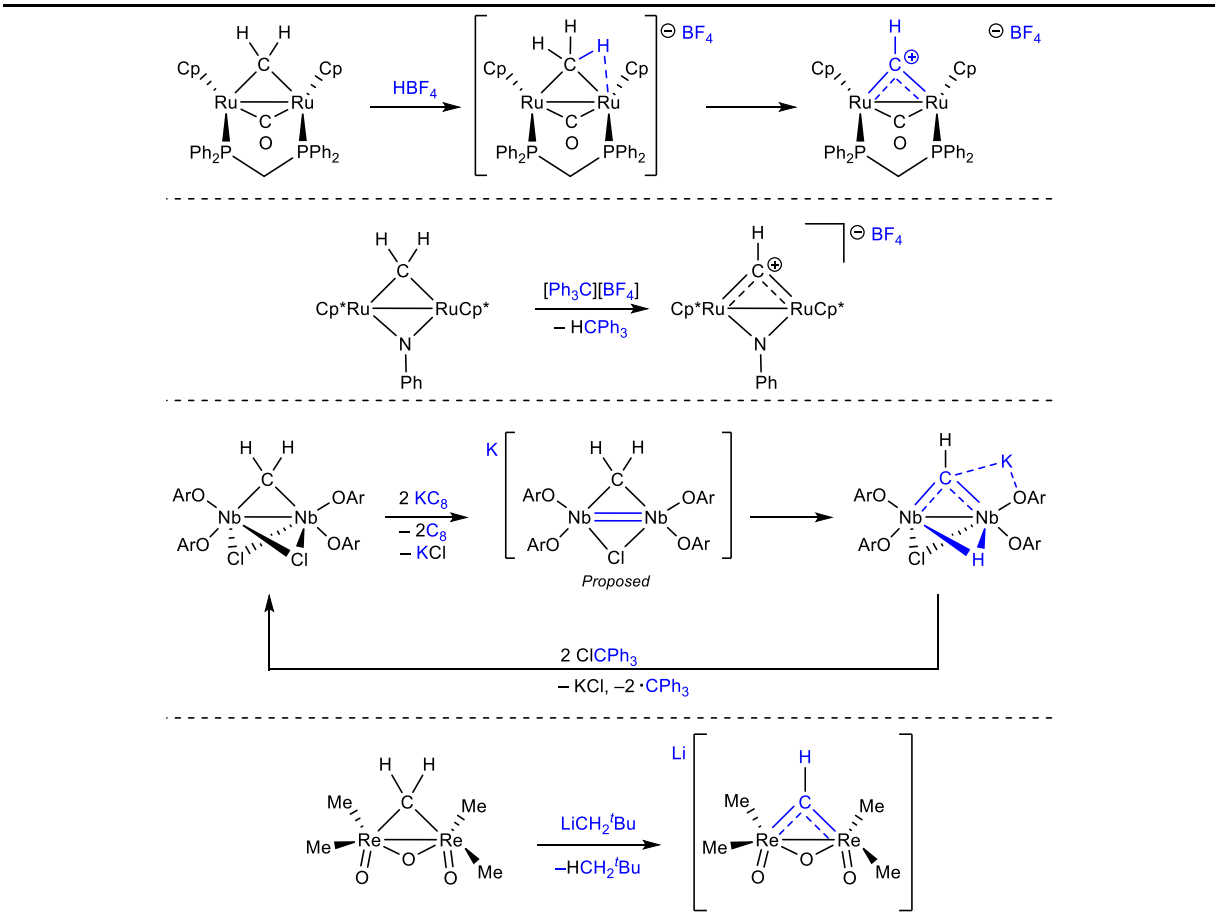

Scheme 5.11: Ruthenium, niobium, and rhenium μ_2-methylidynes from μ_2-methylidenes.

Following Casey's archetypical example, Wolczanski and Miller introduced μ_2-carbido hydrogenation as another method of μ_2-methylidyne synthesis, the first in a series of reports describing these intimately related bridging ligands (Scheme 5.12). Reduction of $[W_2(\mu_2\text{-}C)(=O)Cl_2(OSi^tBu_3)_4]$ with Na/Hg amalgam under a H_2 atmosphere results in partial hydrogenation of the Class A μ_2-carbido to the methylidyne $[W_2(\mu_2\text{-}CH)(\mu\text{-}O)(\mu\text{-}H)(OSi^tBu_3)_4]$; a link to the role of surface carbidos in Fischer-Tropsch processes. [56] Likewise, Templeton protonated the Class B μ_2-carbido $[MoFe(\mu_2\text{-}C)(CO)_4(Cp)(Tp^*)]$ with strong acid to produce μ_2-methyildyne $[MoFe(\mu_2\text{-}CH)(CO)_4(Cp)(Tp^*)]BF_4$, featuring instead an agostic C–H as identified by spectroscopy. [97] Takemoto and co-workers later demonstrated the reverse reaction—deprotonating a μ_2-methylidyne to form a μ_2-carbido—yet this has been discussed at length (See Chapter One or Section 5.1). [129]

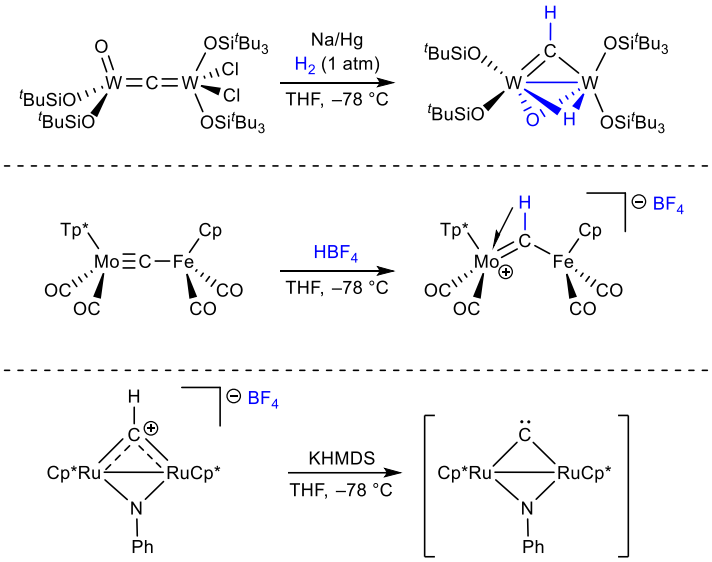

Scheme 5.12: Synthesis of a μ_2-methyildyne from a μ_2-carbido and the inverse reactivity.

The field had a seventeen-year hiatus from Wolczanski until Veige and co-workers reported the next μ_2-methylidyne (Scheme 5.13). Heating the terphenyl pincer ligand (O_2terpy; T3,3'-di-tert-butyl-1,1':3',1"-terphenyl-2,2'-diol) with $[(Me_2N)_3W{\equiv}W(NMe_2)_3]$ provides methylidyne $[W_2(\mu_2\text{-}CH)(\mu\text{-}NMe)(\mu_2\text{-}NMe_2)(O_2terpy)_2]$ accompanied by elimination of $NHMe_2$ and hydrogen. [418] This reaction proceeds by C–N bond cleavage followed by double C–H bond activation, evidenced by spectroscopic observation of a plausible μ_2-methylidyne intermediate $[W_2(\mu_2\text{-}CH)(\mu\text{-}NMe)(\mu_2\text{-}NMe_2)(NMe_2)_2(O_2terpy)]$ arising from activation of an NMe_2 amido ligand. In another case, Sitzmann and co-workers described a double C–H activation of a CH_3 ligand to form a μ_2-methylidyne $[\{C_5H(^tPr)_4Co\}_2(\mu_2\text{-}CH)(\mu\text{-}H)]$ and methane from the reaction of $[Co_2(\mu\text{-}Cl)_2(\eta^5\text{-}C_5H^tPr_4)_2]$ with MeMgCl. Intriguingly, NBO analysis found no support for invoking a direct metal-metal bond, as also found for dirhodium μ-halocarbynes $[Rh_2(\mu\text{-}CX)(\mu\text{-}X)X_4(\mu\text{-}dmpm)_2]$ (X = Cl,

Br). Ruiz and co-workers showed the μ3-methylidyne [Mo3(μ3-CH)(μ2-PCy2)(CO)9(Cp)2] when heated with trimethylphosphite liberates [Mo(CO)5{P(OMe)3}] to produce [Mo2(μ2-CH)(μ-PCy2)(μ-CO)(Cp)2], establishing a formal Mo≡Mo bond in the process. [397]

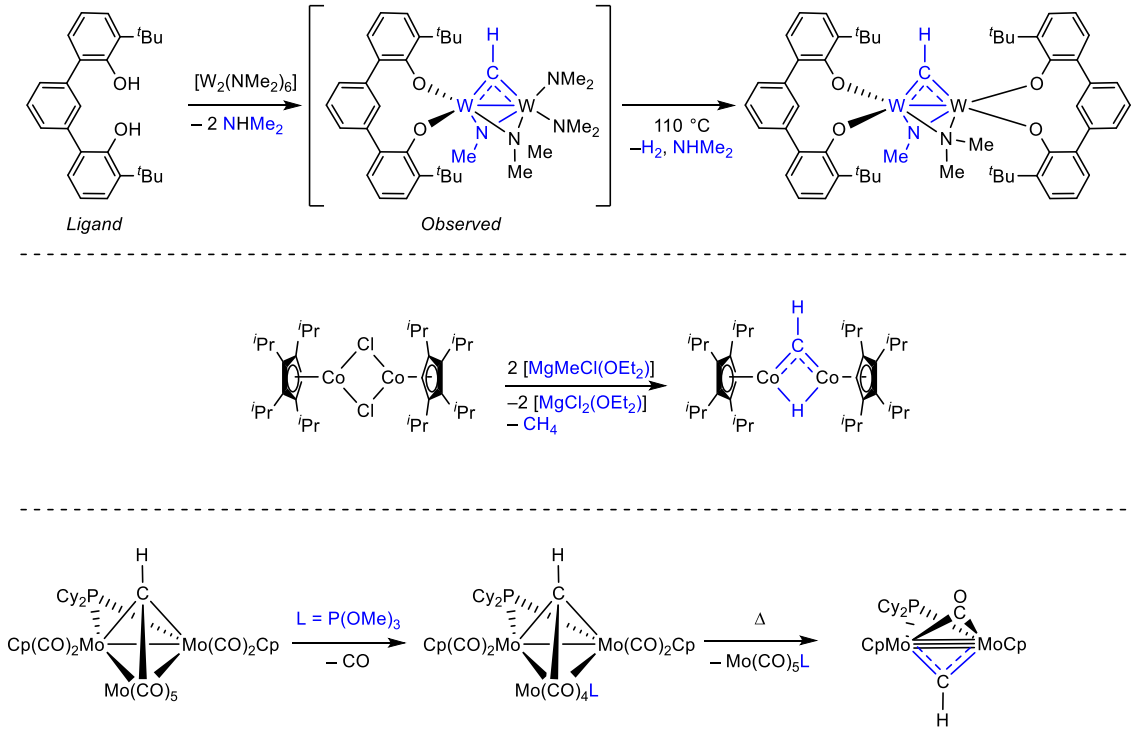

Scheme 5.13: C–H and C–N bond cleavage to μ2-methyildynes, and μ2-methylidyne synthesis accompanied by Mo≡Mo bond formation.

The most recent example of a μ2-methylidyne arises from the reaction of lithiocarbyne [W(≡CLi)(CO)2(Tp*)] with a platinum(II) cyclobutadiene complex [PtCl2(η4-C4Me4)] to produce [W2Pt(μ2-CH)2(CO)4(Tp*)2] (Scheme 5.14). [159] This species is interesting for several reasons as it: (i) is heterometallic (opposed to homometallic); (ii) contains a *bis*–methylidyne motif; and (iii) bears a d^{10} metal (opposed to d^5, d^6 or d^8). The mechanistic origin of this species is clouded, but the authors propose E_2 reductive dehydrohalogenation‡‡‡‡‡‡‡‡‡‡‡‡ from the alkylcyclobutadiene generates one equivalent of dimethyl-dimethylenecyclobutene, [420] platinum(0), and two units of methylidyne [W(≡CH)(CO)2(Tp*)] which couple to give the observed species. The same trimetallic complex could be obtained more rationally by combining authentic [W(≡CH)(CO)2(Tp*)] and [Pt(nbe)3].

‡‡‡‡‡‡‡‡‡‡‡‡ Templeton has estimated the pKa of the tungsten methylidyne [W(≡CH)(CO)2(Tp*)] to be *ca* 28.7[64] while Cummins estimates a value of *ca* 30 for the molybdenum methylidyne [Mo(°CH)(NᵗBuC6H3Me2)3], [419] *i.e.*, the E_2 requirement for a strong, sterically encumbered base would appear to be satisfied.

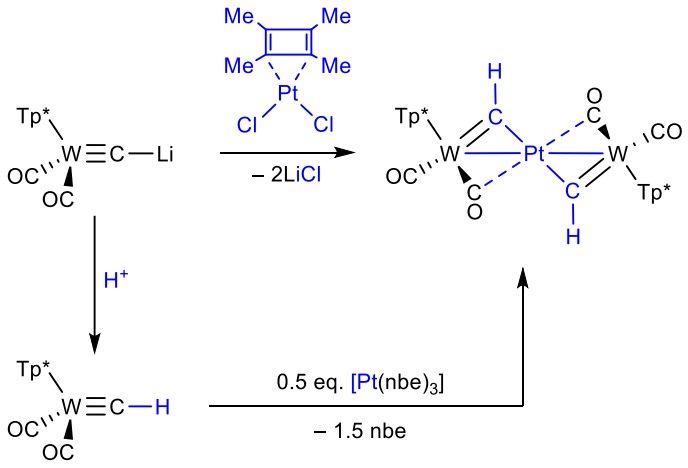

Scheme 5.14: Synthesis of a *hetero*-trimetallic *bis*-μ$_2$-methylidyne complex.

Matrix-'isolated' species and *in silico* fantasies aside, this concludes known μ$_2$-methylidyne complexes, however related species do exist (Scheme 5.15). Containing the key linkage with main group-elements, Bochkarev described group 14 functionalised carbene complexes of tungsten, [W{=CH(EPh$_3$)}Cl$_2$(O^{t}Bu)$_2$] {E = Si, Ge, Sn}, *via* protonation of carbynes [W(≡CEPh$_3$)Cl$_2$(O^{t}Bu)$_2$] with strong acid. [421] A similar reaction using phenol provides analogues [W{=CH(EPh$_3$)}(OPh)$_2$(O^{t}Bu)$_2$] {E = Si or Ge}.[422] The structures of silicon and germanium derivatives were discussed, including measurements for the methylidyne hydrogen placed and refined *via* a riding model. Subsequent reports disclosed molybdenum and tungsten derivatives for germanium although through olefin metathesis of [W(=CH^{t}Bu)(Ndipp)(OCMe$_2$CF$_3$)$_2$] (dipp = 2,6-diisopropylphenyl) with R$_3$GeHC=CH$_2$ (R = Me or Ph), consistent with the groups research interest of heavier group 14 elements in this process. [423-425]

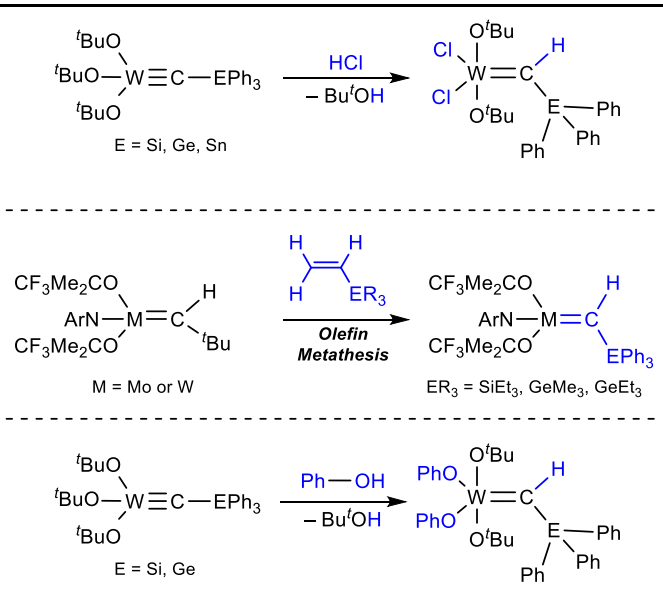

Scheme 5.15: Synthesis of heavier group 14 carbenes containing the μ$_2$-CH linkage, related to μ$_2$-methylidynes.

5.4.2 Producing μ_2-methylidynes *via* ligand substitution

Formation of methylidyne **5.6** provided a foundation for the synthesis of further μ_2-methyilidyne complexes through ligand substitution if accessible in larger amounts (Scheme 5.16). An upscaled preparation of **5.6** could be completed *via* generating **5.5** and redissolving in CH_2Cl_2 such that β-hydride elimination occurs overnight at ambient temperature ($t_{½}$ ~14 hours), promptly completed by heating at reflux for two hours. A simple recrystallisation provides analytically pure **5.6** in accessible amounts which is stable when stored as an isolated solid. Bubbling $CO_{(g)}$ through a solution of **5.6** in THF quickly evolves the scarlet colour of **5.1** but stirring overnight under $CO_{(g)}$ was required for full conversion, supporting CO scrambling as a mechanism for formation of **5.1** in the initial test reactions. Likewise, substitution of **5.6** with isocyanide CNMes occurs in a similar manner to provide [WPt(μ_2-CH)(CNMes)(μ_2-CO)(CO)(PPh_3)(Tp*)] (**5.7**) as another π-acidic analogue. Alternatively, heating a CH_2Cl_2 solution of **5.6** with the chelating phosphine dppe provides [WPt(μ_2-CH)(μ_2-CO)(CO)(dppe)(Tp*)] (**5.8**) thereby demonstrating substitution of both phosphines is possible without disrupting the dimetallacyclopropene core. Indeed, the dppe derivative, once formed, proved to be the most robust complex of the series.

Many similarities are shared between the precursor **5.6** and derivatives **5.1**/**5.7**/**5.8**. High-frequency resonances in the ^{1}H NMR spectrum corresponding to the methylidyne vary across the range δ_H = 13.56–14.92, while those in the $^{13}C\{^1H\}$ NMR spectra populate a comparatively narrow range (δ_C: 307.9–319.9). Likewise, ^{195}Pt NMR signals are also detected over a small range (δ_{Pt}: –4362 to –4530) with $^1J_{PtP}$ couplings varying with both the electronic influence of the ligand and conformation (*syn* and *anti* to the μ-CH). Perhaps the most interesting feature of the μ_2-methylidynes arises from infra-red spectroscopy as low wavenumber modes are noted in the carbonyl region both in the solution and solid-state. This suggests that semi-bridging carbonyls are evident, although single resonances were recorded in the corresponding region of the $^{13}C\{^1H\}$ NMR spectrum, consistent with exchange between carbonyls being arrested on the infra-red timescale but fast on the $^{13}C\{^1H\}$ NMR timescale. Otherwise, the methylidyne complexes exhibit similar properties to the few literature examples (summarised in Table 5.1), with further heteronuclear NMR data described in Table 5.2.

Dissolving each μ_2-methylidyne results in slow ($t_{½}$ = 16 hours for **5.6**) to no decomposition to *bis*-μ_2-methylidyne [$W_2Pt(\mu_2\text{-CH})_2(CO)_4(Tp^*)_2$] decreasing in rate as **5.6** > **5.1** ~ **5.7** ≫ **5.8**, each

Table 5.1: Spectroscopic and structural properties of μ$_2$-methylidyne complexes

Complex	δ_C[a](ppm)	δ_H[a](ppm)	ν_{CO}[b] (cm^{-1})	r_{MC} (Å)	r_{CH} (Å)[c]	M–C–X (°)[c]	$r_{MM'}$ (Å)
μ$_2$-Methylidynes (Literature)							
$[Fe_2(\mu_2\text{-}CH)(\mu\text{-}CO)(CO)_2(Cp)_2]BF_4$ [411]	n.r.	22.56	2050, 1860	–	–	–	–
$[Fe_2(\mu_2\text{-}CH)(\mu\text{-}CO)(CO)_2(Cp)_2]PF_6$ [410]	252.7	22.8	2052, 1856	–	–	–	–
$[Co_2(\mu_2\text{-}CH)(\mu\text{-}H)\{C_5H(^iPr)_4\}_2]$ [426]	392.0	20.14	–	1.758(2)	0.97(3)[d]	137.8(9)[d]	2.362(2)
$K[Nb_2(\mu_2\text{-}CH)(\mu\text{-}Cl)(\mu\text{-}H)(OAr)_4]$ [398]	335.18	13.18	–	1.977(4), 2.018(4)	0.898[e]	132.7, 138.4[e]	2.6556(5)
$[Ru_2(\mu_2\text{-}CH)(\mu\text{-}NPh)(Cp^*)_2]BF_4$ [416]	377.1[f]	18.15	–	1.870(4), 1.868(6)[g]	0.932(4)[d,g]	137.0(4), 137.1(3)[d,g]	2.5460(5)
$[Ru_2(\mu_2\text{-}CH)(\mu\text{-}NPh)(Cp^*)_2]OTf$ [416]	n.d.	18.60	–	–	–	–	–
$[Ru_2(\mu_2\text{-}CH)(\mu\text{-}NPh)(Cp^*)_2][B(C_6F_5)_4]$ [129]	379.0	18.36	–	–	–	–	–
$[Ru_2(\mu_2\text{-}CH)(\mu\text{-}CO)(\mu\text{-}dppm)(Cp)_2]BF_4$ [383]	n.r.	20.81[l]	1779	1.937(7), 2.028(6)	0.98(8)[d]	130(1)[d]	2.716(1)
$[MoFe(\mu_2\text{-}CH)(CO)_4(Cp)(Tp^*)]BF_4$ [97]	344.3[h]	1.94[h,i]	2067, 2037, 2022, 1970	–	–	–	–
$[Mo_2(\mu_2\text{-}CH)(\mu\text{-}CO)(\mu\text{-}PCy_2)(Cp)_2]$ [397]	382.7[h]	16.74[h]	1686	1.89(2), 1.92(1)	0.98[e,j]	150, 130[e,j]	2.4669(1)
$Li[Re_2(\mu_2\text{-}CH)(\mu\text{-}O)(=O)_2Me_4]$ [417]	258.4[k]	12.23[k]	–	–	–	–	–
$[W_2(\mu_2\text{-}CH)(\mu\text{-}H)(\mu\text{-}O)(OSi^tBu_3)_4]$ [56]	319.51	19.62	–	–	–	–	–
$[W_2(\mu_2\text{-}CH)(\mu\text{-}NMe)(\mu\text{-}NMe_2)(O_2terpy)_2]$ [418]	349.9[l]	19.11[l]	–	1.944(3), 1.945(3)	0.88(4)[d]	139(2), 141.2(2)[d]	2.4988(2)
$[W_2(\mu_2\text{-}CH)(\mu\text{-}NMe)(\mu\text{-}NMe_2)(NMe_2)_2(O_2terpy)]$ [418]	n.d.	16.40	–	–	–	–	–
$[W_2Pt(\mu_2\text{-}CH)_2(CO)_4(Tp^*)_2]$ [159]	293.8[l]	12.09[l]	1976, 1943, 1881	1.929(8), 1.910(8) 2.046(7), 2.001(7)	0.93(1)[d]	135.3(1), 136.7(1)[d]	2.7517(4), 2.7277(4)
Related Carbenes (Literature)							
$[Mo\{=CH(SiEt_3)\}(NDipp)(OCMe_3CF_3)_2]$ [425]	270.9	13.22		–	–	–	–
$[Mo\{=CH(GeMe_3)\}(NDipp)(OCMe_3CF_3)_2]$ [423]	275.5[m]	13.34[m]	–	1.889(2), 1.945(2)	0.93(2)[d]	105(1), 117(1)[d]	–
$[Mo\{=CH(GePh_3)\}(NDipp)(OCMe_3CF_3)_2]$ [423]	261.6[m]	13.34[m]	–	1.876(2), 1.935(2)	0.97(2)[d]	104(1), 112(1)[d]	–
$[W\{=CH(SiPh_3)\}Cl_2(O^tBu)_2]$ [421]	264.19[n]	11.83[n]	–	–	–	–	–
$[W\{=CH(GePh_3)\}Cl_2(O^tBu)_2]$ [421]	266.87[n]	11.89[n]	–	1.870(2), 1.949(2)	0.93(2)[d]	111(1), 114(1)[d]	–
$[W\{=CH(SnPh_3)\}Cl_2(O^tBu)_2]$ [421]	n.d.	12.04[n]	–	–	–	–	–
$[W\{=CH(SiPh_3)\}(OPh)_2(O^tBu)_2]$ [422]	231.8	10.27	–	–	–	–	–
$[W\{=CH(GePh_3)\}(OPh)_2(O^tBu)_2]$ [422]	235.3	10.36		1.877(2), 1.948(2), 1.878(2), 1.938(2)	0.95(2)[d]	115.9(2), 116.2(2)[d]	–
$[W\{=CH(SiEt_3)\}(NDipp)(OCMe_3CF_3)_2]$ [425]	225.9	9.30	–	–	–	–	–
$[W\{=CH(GeMe_3)\}(NDipp)(OCMe_3CF_3)_2]$ [424]	231.8	9.57	–	1.882(4), 1.927(4)	1.00(5)[d]	108(3), 114(3)[d]	–
$[W\{=CH(GeEt_3)\}(NDipp)(OCMe_3CF_3)_2]$ [425]	227.3	9.49	–	1.892(3), 1.936(3)	0.95(3)[d]	110.2(2), 110.3(2)[d]	–
μ$_2$-Methylidynes (Chapter Five)							
$[WPt(\mu_2\text{-}CH)(\mu\text{-}CO)(CO)_2(PPh_3)(Tp^*)]$ (**5.1**)	310.0[l]	13.69[l]	2016, 1924, 1786	1.924(3), 1.991(3)[d] 1.925(3), 1.997(3)[e]	0.93(4)[d] 1.094[e]	134.9(2), 135.0(2)[d] 156.4, 110.6[e]	2.7709(5)[d] 2.7709(5)[e]
$[WPt(\mu_2\text{-}CH)(CO)_2(PPh_3)_2(Tp^*)]$ (**5.6**)	317.9[l]	13.56[l]	1899, 1760	1.91(1), 2.03(1)[d]	0.95(2)[d]	134(1)[d]	2.8375(9)[d]
$[WPt(\mu_2\text{-}CH)(CNMes)(CO)_2(PPh_3)(Tp^*)]$ (**5.7**)	314.5[l]	14.14[l]	1903, 1758	1.930(5), 2.003(3)[d] 1.929(5), 2.004(3)[e]	0.97(4)[d] 1.077[e]	134.7(3)[d] 153.0, 115.6[e]	2.7951(4)[d] 2.7951(4)[e]
$[WPt(\mu_2\text{-}CH)(CO)_2(dppe)(Tp^*)]$ (**5.8**)	307.9[l]	14.92[l]	1899, 1716	–	–	–	–
$[WAu(\mu_2\text{-}CH)Cl(CO)_2(Tp^*)]$ (**5.10**)	260.8[l]	10.41[l]	2016, 1932	1.87(1), 1.99(1)[d]	0.93(2)[d]	134(1)[d]	2.799(1)[d]

Notes: OAr = 2,6-*bis*(diphenylmethyl)-4-*tert*-butylphenoxide. Dipp = 2,6-diisopropylphenyl. O_2terpy = 3,3''-*di*-*tert*-butyl-1,1':3',1''-terphenyl-2,2''-diol. [a]Measured in C_6D_6 unless specified otherwise. [b]Measured in CH_2Cl_2. [c]Refinement details located from supporting information or deposited CIF where possible. [d]Refined using a riding model. [e]Located without refinement. [f]Detected using a ^{13}C enriched sample. [g]$B(C_6F_5)_4$ counter-anion utilised for structure. [h]Measured in CD_2Cl_2. [i]Agostic hydrogen. [j]Disorder with μ-CO apparent. [k]Measured in CD_3CN. [l]Measured in $CDCl_3$. [m]Measured in d_8-toluene.

accelerated when exposed to air, most likely due to irreversible sequestration of phosphine and eliminated platinum as $O{=}PPh_3$ and $[Pt(\eta^2\text{-}O_2)(PPh_3)_2]$.§§§§§§§§§§§§§§§§ This supports the lability of both phosphines in **5.6** as anticipated but shows π-acceptors **5.1**/**5.8** spontaneously dimerise to the *bis*-μ_2-methylidyne albeit more slowly, in contrast to the μ_2-chlorocarbyne complex $[WPt(\mu_2\text{-}CCl)(CO)_3(PPh_3)(Tp^*)]$ which did not appreciably convert to the *bis*-μ_2-chlorocarbyne. The stability of $[W_2Pt(\mu_2\text{-}CH)_2(CO)_4(Tp^*)_2]$ is further supported by the observations that (i) combining the free η^1-methylidyne $[W(\equiv CH)(CO)_2(Tp^*)]$ (**5.9**) with **5.6** and **5.7** results in formation of the *bis*-μ_2-methylyidyne and (ii) The reaction of **5.9** with $[Pt(\eta^2\text{-}C_2H_4)(PPh_3)_2]$ also provides **5.6**.

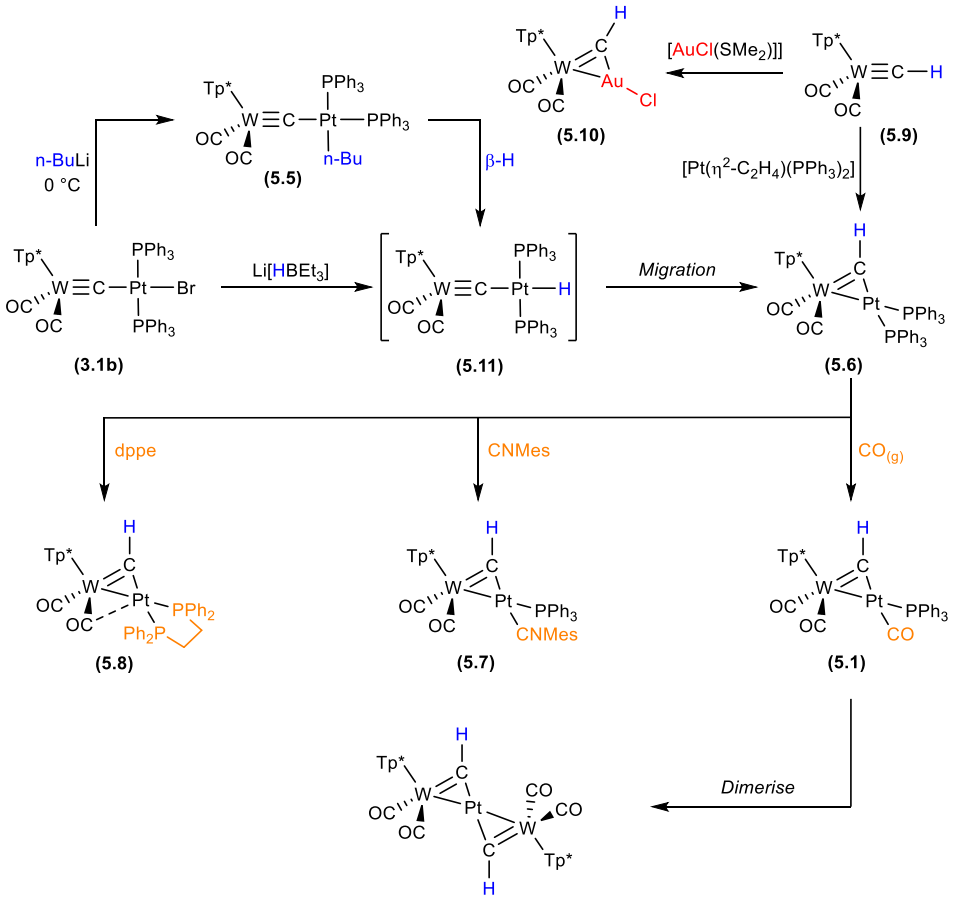

Scheme 5.16: Synthesis of heterobimetallic μ_2-methylidyne complexes and their decomposition pathways.

The reaction of $[W(\equiv CH)Br(CO)_2(dcpe)]$ with $[AuCl(SMe_2)]$ has been shown to afford a tungsten-gold μ_2-methylidyne $[WAu(\mu\text{-}CH)BrCl(CO)_2(dcpe)]$ [428] in a similar manner to the behaviour of the chlorocarbyne **2.2d** (Chapter Two, Section 2.3.1). Given the isolation of **5.1** and **5.6**–**8**, the reaction of $[W(\equiv CH)(CO)_2(Tp^*)]$[179] with $[AuCl{\cdot}SMe_2]$ was explored and resulted in the formation of $[WAu(\mu_2\text{-}CH)Cl(CO)_2(Tp^*)]$ (**5.10**, Figure 5.7), a gold(I) complex analogous to

§§§§§§§§§§§§§§§§ Observed in $CDCl_3$: $\delta_P(O{=}PPh_3)$ = 29.3 ppm; $\delta_P([Pt(\eta^2\text{-}O_2)(PPh_3)_2])$ 14.9, $^1J_{PtP}$ = 4068 Hz. [427]

2.2b/**2.2d** (Chapter Two). The ^{1}H NMR spectrum exhibits a sharp singlet at high frequency (δ_H = 10.41) although this is to significantly lower frequency than the platinum bimetallic or trimetallic examples Meanwhile the $^{13}C\{^{1}H\}$ NMR spectrum contains a signal at a lower frequency assigned to the methylidyne carbon (δ_C = 260.8) suggesting that the gold(I) complex may have a smaller paramagnetic contribution to the shielding than observed for platinum.

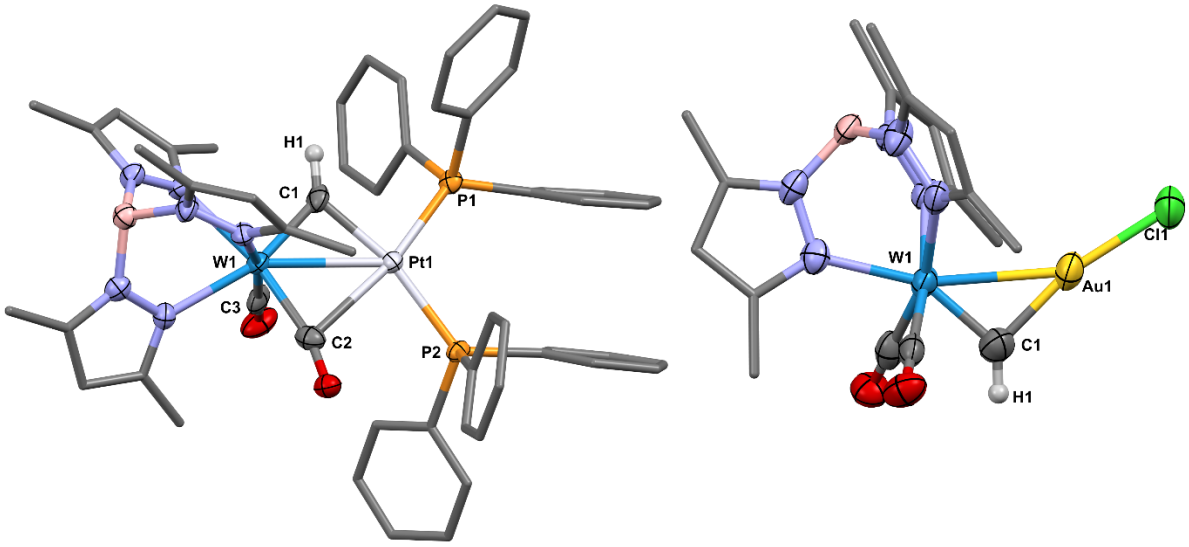

Figure 5.7: Molecular structures of [WPt(μ$_2$-CH)(CO)$_2$(PPh$_3$)$_2$(Tp*)] (**5.6**) (A) and [WAu(μ$_2$-CH)Cl(CO)$_2$(Tp*)] (**5.10**) (B) in single crystals as determined by X-Ray Diffractometry. Ellipsoids are drawn at the 50% probability surface with pyrazolyl and phenyl rings simplified and hydrogens omitted for clarity. The μ-CH hydrogens are assigned based on a riding model. (A) Selected bond lengths (Å) and angles (°): (A) W1–C1 1.91(1), C1–Pt1 2.03(1), Pt1–W1 2.8375(9), W1–C2 1.99(1), W1–C3 1.97(1), C2–Pt1 2.59(1), Pt–P1 2.269(2), Pt1–P2 2.312(3), W1–C1–Pt 92.2(5), W1–C2–Pt1 75.2(4). (B) W1–C1 1.87(1), C1–Au1 1.99(1), Au1–W1 2.799(1), Au1–Cl1 2.281(4), W1–C1–Au1 92.9(6), W1–Au1–C1 41.8(4).

These experiments suggest a rich underlying chemistry for μ$_2$-methylidyne assembly from (albeit rare) pre-isolated terminal methylidynes, but leaves the original route to **5.6** unsubstantiated. The evolution of **5.5** to **5.6** is presumed to proceed *via* β-hydride elimination, thereby implicating a hydrido-carbido complex [WPt(μ$_2$-C)H(CO)$_2$(PPh$_3$)$_2$(Tp*)] (**5.11**) as an intermediate. This hydrido species was likely not detected initially given the longer reaction times (*ca* 5 hours), halogenated solvents used to measure crude mixtures, and no measurements taken given a lack of physical change. Therefore, a sample of **3.1b** in d_6-benzene was treated with Li[Et$_3$BH], followed immediately by acquisition of ^{1}H NMR data that revealed a low-frequency triplet resonance emerging (δ_H = –9.28; $^{2}J_{HP}$ = 22 Hz) straddled by platinum ($^{1}J_{HPt}$ = 494 Hz) and tungsten satellites ($^{1}J_{HW}$ = 23 Hz), consistent with formation of **5.11**. Coupling to ^{183}W and ^{195}Pt nuclei is evident in the ^{1}H NMR spectrum but somewhat clearer in the $^{1}H\{^{31}P\}$ NMR spectrum (Figure 5.8). The

hydrido-carbido **5.11** is the first new species to accumulate in solution,[**********] followed by the μ_2-methylidyne resonance which grows in intensity following the observed hydride over 24 hours. This raises the question as to why this hydrido intermediate was not observed during the evolution of the *n*-butyl complex to the methylidyne **5.6**. The *trans* geometry of **5.11** that follows unambiguously from spectroscopic data, is the geometry that would be expected for the halide/hydride metathesis process proceeding *via* an associative or interchange-associative mechanism where the carbide exerts a stronger trans influence than does the bromide. In contrast, given that Whitesides has shown that β-elimination from *cis*-[Pt(^{n}Bu)$_2$(PPh$_3$)$_2$] proceeds *via* initial phosphine dissociation,[402] it might be assumed that similar phosphine dissociation from *cis*-**5.5** provides a 3-coordinate *n*-butyl complex that upon β-elimination provides *cis*-[WPt(μ-C)H(CO)$_2$(PPh$_3$)(L)] (L = PPh$_3$ or H$_2$C=CHEt) in which the hydride and carbido ligands adopt a mutually *cis* disposition. This would allow reductive methylidyne elimination from either the butene or phosphine complex to be more rapid than the rate-limiting β-elimination process such that these species do not accumulate in spectroscopically observable amounts.

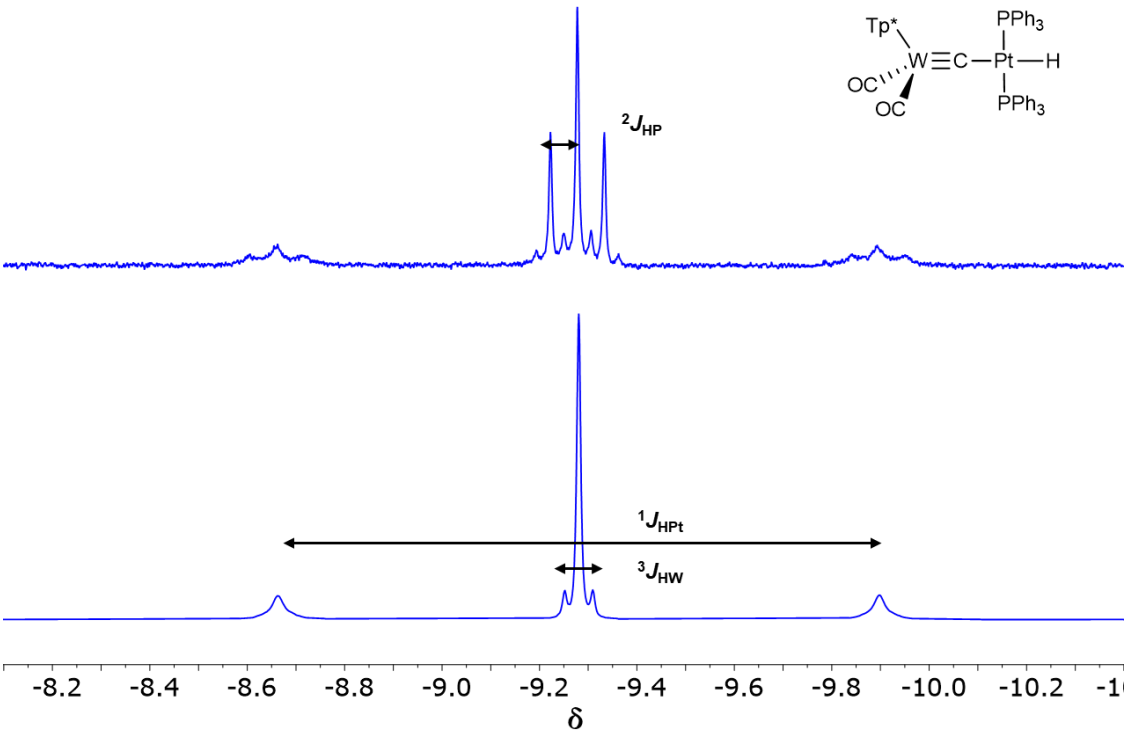

Figure 5.8: Low frequency extract of the ^{1}H and ^{1}H{^{31}P} NMR spectra of intermediate [WPt(μ$_2$-C)(H)(CO)$_2$(PPh$_3$)$_2$(Tp*)] (**5.11**) with relevant couplings shown.

[**********] Templeton observed direct attack at the methylidyne carbon of [W(≡CH)(CO)$_2$(Tp*)] by Li[Et$_3$BH] to afford the anionic methylidene Li[W(=CH$_2$)(CO)$_2$(Tp*)], in part because the tungsten centre of the precursor is coordinatively saturated. In contrast, the platinum(II) centre of **3.1b** is coordinatively unsaturated allowing direct attack by nucleophiles including Li[Et$_3$BH].

Table 5.2: Further spectroscopic properties of tungsten-platinum μ_2-methylidyne complexes.

Complex	$\delta_H{}^a$ (ppm)	$^2J_{HW}{}^a$ (Hz)	$^2J_{HPt}{}^a$ (Hz)	$^3J_{HP}{}^a$ (Hz)	$\delta_P{}^a$ (ppm)	$\delta_{Pt}{}^a$ (ppm)	$^1J_{PtP}{}^a$ (Hz)
$[WPt(\mu_2\text{-}CH)_2(CO)_4(Tp^*)_2]$	12.09	44	n.r.	–	–	–3084	n.r.
$[WPt(\mu_2\text{-}CH)(\mu\text{-}CO)(CO)_2(PPh_3)(Tp^*)]$ (**5.1**)	13.69	n.r.	54	18	28.72	–4446	3387
$[WPt(\mu_2\text{-}CH)(CO)_2(PPh_3)_2(Tp^*)]$ (**5.6**)	13.56	39	27	18, 3	32.88, 32.55	–4461	3844, 3350
$[WPt(\mu_2\text{-}CH)(CNMes)(CO)_2(PPh_3)(Tp^*)]$ (**5.7**)	14.14	–	36	17	28.78	–4362	3588
$[WPt(\mu_2\text{-}CH)(CO)_2(dppe)(Tp^*)]$ (**5.8**)	14.92	n.r.	35	14, 2	48.18, 47.41	–4530	3454, 3221

Notes: [a]Measured in $CDCl_3$ unless specified otherwise.

These observations lend strong support to exclusive, sequential production of a hydride complex before migration toward a μ_2-methylidyne species. There is no evidence of hydride directly attacking the μ_2-carbido ligand, or alternatively, the carbonyl ligands. Further attempts to characterise the hydrido-carbido were met with difficulty. Accumulation of **5.11** was clear yet still in relatively small amounts such that no resonances in the $^{31}P\{^1H\}$ NMR spectrum could be unequivocally assigned, while no additional high frequency signals were detected in the $^{13}C\{^1H\}$ NMR spectrum. Attempts to indirectly assign the carbido resonance *via* HMBC experiments failed to discern any coupling of the hydride to a high-frequency carbon resonance, somewhat disappointing given a strong *trans*-$^2J_{CH}$ coupling might be expected.

By comparing the various data between μ_2-methylidyne complexes and their corresponding μ_2-chlorocarbynes from Chapter Two, clear trends emerge to better describe the bonding of these heterobimetallic species. It would appear that μ_2-CH ligands serve as stronger σ-donors and/or weaker π-acceptors than μ_2-CCl to platinum(0). The W–C bond lengths are contracted indicating retention of W≡C character accompanied by increasingly asymmetric ligands angles (W–C–X > Pt–C–X) identified by strongly diffracting X-ray data, measurements supported by theoretically optimised structures. Furthermore, Pt–C bonds are elongated which is consistent with less π-retrodonation of platinum(0), further evidenced by ^{195}Pt and ^{13}C resonances at lower and higher frequencies, respectively. These effects are multiplied for trimetallic *bis*-μ_2-CX species, where a significantly lower frequency platinum resonance reflects the changed geometry at platinum, essentially being two coordinate rather than three coordinate in **5.6**. The trends also extend to the gold(I) analogues, noting differing properties of gold(I) and reduced paramagnetic contribution in ^{13}C NMR shifts *of cf.* the platinum examples. Due to reliance on synchrotron-derived data, the uncertainties for individual bond lengths for both **5.6** and **5.10** (e.s.d. = *ca* 0.01 Å) preclude rigorous discussion.

5.5 Reactivity of [W≡C–Pt] with: Tolyllithium

Having examined reactions of **3.1b** with hydride donors, several further carbon-based nucleophiles were considered, specifically those that might install either sp^2 or sp carbons donors.

Treating a THF solution of **3.1b** with a freshly prepared solution of tolyllithium at 0 °C returns a bright yellow solution that darkens within 15 minutes. The reaction was halted at 30 minutes as [W(≡Ctol)(CO)$_2$(Tp*)][429] was observed (TLC) to begin to form, indicating the onset of reductive elimination. At this stage, the major species by *in situ* NMR spectroscopy was formulated as *trans*-[WPt(μ$_2$-C)(tolyl)(CO)$_2$(PPh$_3$)$_2$(Tp*)] (**5.12**), which was promptly isolated *via* flash chromatography (Scheme 5.17). Closer inspection of crude NMR spectra reveal a somewhat clean reaction at 30 minutes: **5.12** is accompanied by [W(≡Ctol)(CO)$_2$(Tp*)] (130% relative to **5.12**) but no other patterns that could correspond to the *cis*-isomer. This suggests the reaction from **3.1b** occurs quickly, exclusively at the platinum terminus, as no μ$_2$-CC$_6$H$_4$Me alkylidynes were noted, and reductive elimination occurs within the timeframe of purification. In contrast to the methylidyne and halocarbyne examples, it would appear that the tolyl substituent is a 'bridge too far' in how much steric bulk can be accommodated between the adjacent Tp* and PPh$_3$ ligands.ǂǂǂǂǂǂǂǂǂǂǂǂǂǂǂ

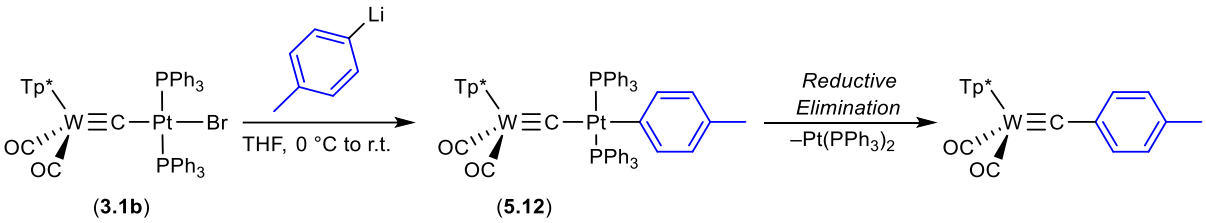

Scheme 5.17: Synthesis of *trans*-σ-aryl metallacarbyne **5.12** *via* tolyllithium and subsequent reductive elimination of [W(≡Ctol)(CO)$_2$(Tp*)].

Pure samples of **5.12** survived in solution much longer, decomposing ~5% in 24 hours indicating slow *cis-trans* isomerisation occurs in the absence of extraneous nucleophiles. The ^{1}H NMR spectrum reveals signature **AA'BB'** doublets in a region devoid of other signals (δ_H: 5.8–6.2) corresponding to the *para*-phenylene group which facilitates analysis given the 4-methyl resonance occurs alongside the pzMe$_2$-3,5 resonances. The ^{13}C{^{1}H} NMR spectrum contains a high frequency signal (δ_C = 397.2) with unresolved coupling to phosphorus, but consequently allows measurement of the coupling to ^{183}W ($^1J_{CW}$ = 162 Hz) and ^{195}Pt ($^1J_{CPt}$ = 530 Hz). The spectrum also contains a triplet signal with coupling to ^{195}Pt (δ_C = 147.2; $^2J_{CP}$ = 13 Hz, $^1J_{CPt}$ = 475 Hz) consistent with the *ipso*-carbon of the tolyl group, lending further support to the *trans* isomer as the *cis*-isomer would likely be an unresolved doublet of doublets. Inspection of the ^{31}P{^{1}H} NMR spectrum reveals resonances heavily 'roofed' doublets which occur for inequivalent phosphines ($^2J_{PP}$ = 440 Hz, $^1J_{PtP}$ = 3260 Hz), consistent with the *trans* orientation of **3.1b** but suggesting stronger second order effects in **5.12** (Figure 5.9). However, the ^{195}Pt NMR spectrum

ǂǂǂǂǂǂǂǂǂǂǂǂǂǂǂ With the smaller Tp ligand, the complexes [W$_2$Pt(μ-CMe)(CO)$_4$(Tp)$_2$] and [WPt(μ-CC$_6$H$_4$Me-4)(CO)$_2${P(OMe)$_3$}$_2$(Tp)] were stable but [W$_2$Pt(μ-CC$_6$H$_4$Me-4)(CO)$_4$(Tp)$_2$] was not.[249]

exhibits a triplet (δ_{Pt} = –4164, $^{1}J_{PtP}$ = 3266 Hz) suggesting the phosphines are equivalent or coincidentally isochronous on the platinum timescale (85.7 MHz, 25 °C), another similarity to **3.1b**. The complex **5.12** displays the highest frequency carbido resonance (δ_C) of all platinum carbido complexes reported in this thesis and the platinum resonance also occurs at much higher frequency than the typical range of platinacarbynes produced in Chapters Two and Three. Crystallographic quality crystals were not forthcoming across several solvent systems.

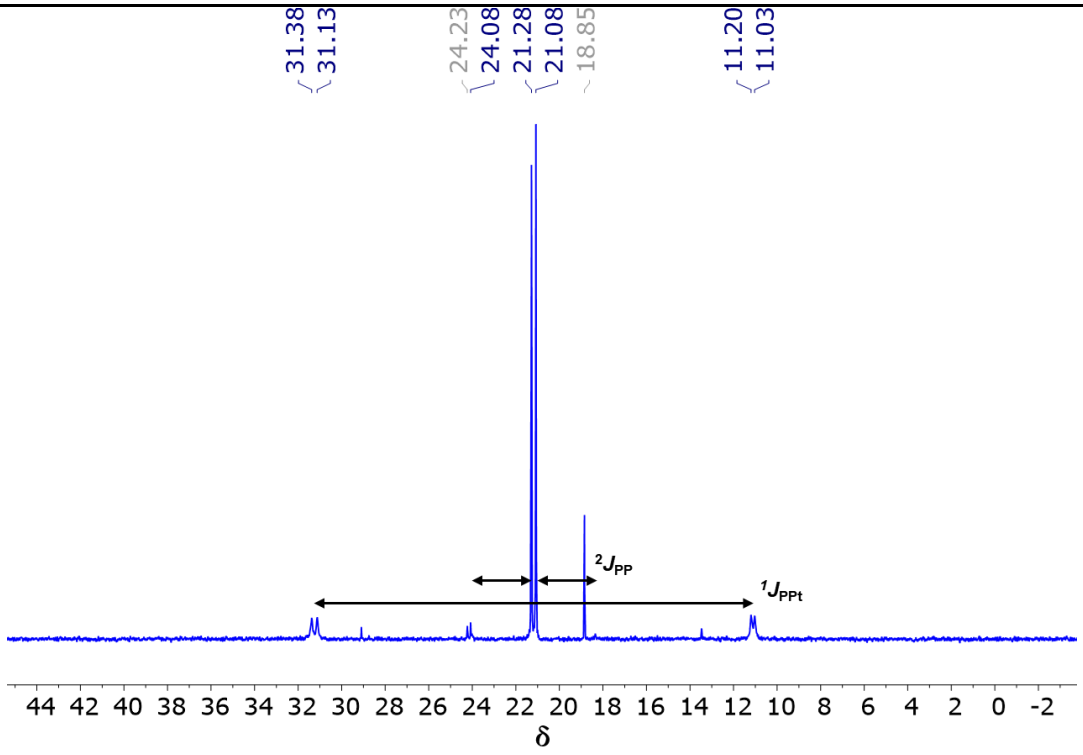

Figure 5.9: $^{31}P\{^{1}H\}$ NMR spectrum of *trans*-[WPt(μ_2-C)(tolyl)(CO)$_2$(PPh$_3$)$_2$(Tp*)] (**5.12**) showing roofed doublets of similar chemical environment. Reductive elimination impurities denoted in grey.

5.6 Reactivity of [W≡C–Pt] with: Acetylides

Platinum-based polyyne complexes and materials with unusual electro-optical properties represent an increasingly active area of interest in recent years. [262, 430-431] As a progression to *sp*-hybridised carbon, lithium trimethylsilylacetylide (LiC≡CSiMe$_3$) was added to **3.1b** in THF at 0 °C in slight excess forming a yellow solution that decomposed readily, unlike **5.12** obtained from 4-tolyllithium. Repeating the reaction and relying on crystallisation *via* liquid-liquid diffusion of *n*-pentane into THF (5:1) gave a bulk deposition of yellow plates, suitable for X-ray diffractometry. The yellow compound was identified as [WPt(μ_2-C)(C≡CSiMe$_3$)$_2${μ-η^4-Li(THF)$_2$}(CO)$_2$(PPh$_3$)(Tp*)] (**5.13**), an unexpected species where a second equivalent of acetylide substituted one phosphine. This species contained lithium as a 'tweezer' reminiscent of the work

of Walther and co-workers who obtained 'tweezer' complexes of palladium *via* analogous routes (Chart 5.1). [432]

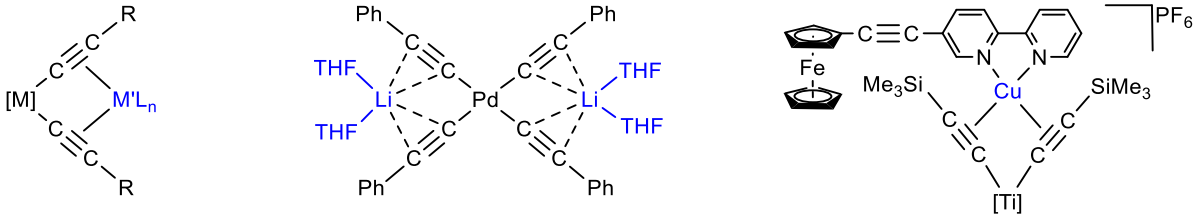

Chart 5.1: Examples of tweezer complexes: alkynyl ligands act as σ-donors to M and π-donors to M'. [432-434]

To elucidate whether **5.13** was the major product, repeat reactions were performed with precise stoichiometric addition of lithium acetylide. Equimolar LiC≡CSiMe$_3$ with **3.1b** provides a yellow solution that evaporates to an orange glass with an initially confronting crude $^{31}P\{^1H\}$ NMR spectrum that can be deconstructed with additional information (Figure 5.10). Several species decomposed during purification of these mixtures except for a pale orange species identified as the targeted *trans*-[WPt(μ$_2$-C)(C≡CSiMe$_3$)(CO)$_2$(PPh$_3$)$_2$(Tp*)] (**5.14**; δ_P = δ 24.06, 20.64; $^1J_{PtP}$ = 2998, 3005; $^2J_{PP}$ = 435 Hz) which resisted recrystallisation. A further set of doublets was detected in the $^{31}P\{^1H\}$ NMR spectrum with similar ^{31}P and ^{195}Pt coupling to the μ$_2$-methylcarbyne [WPt(μ$_2$-CCH$_3$)(CO)$_2$(PPh$_3$)$_2$(Tp*)] (**5.3**) hinting the major component was likely the reductive elimination product [WPt(μ$_2$-CCCSiMe$_3$)(CO)$_2$(PPh$_3$)$_2$(Tp*)] (**5.15**).‡‡‡‡‡‡‡‡‡‡‡‡‡ As **5.15** did not survive chromatography, it was prepared independently via the reaction of [Pt(η^2-C$_2$H$_4$)(PPh$_3$)$_2$] with the propargylidyne [W(≡C–C≡C–SiMe$_3$)(CO)$_2$(Tp*)], which resulted in exclusive coordination across the W≡C bond (*i.e.,* not the C≡C bond). This exclusive coordination is consistent with corresponding alkyne complexes [Pt(η^2-RC≡CR)(PR$_3$)$_2$] being prevalent, but unknown when R = SiMe$_3$ which have only been measured in solution. [435] The authentic sample of **5.15** unequivocally verified the identity of the major product this reaction, leaving only one species unidentified (denoted as red Figure 5.10). Although a distinct roofed **AB** pattern is observed, the lack of ^{195}Pt satellites or additional information preclude identification of this species. However, addition of CDCl$_3$ to the mixture converted the unidentified species into **5.15** which may suggest it corresponds to the species *cis*-[WPt(μ$_2$-C)(CCSiMe$_3$)(CO)$_2$(PPh$_3$)$_2$(Tp*)], yet this conjecture is unsubstantiated without further information.

Supplying excess acetylide to **3.1b** results in another species different to **5.13**. A relatively clean ^1H NMR spectrum is observed, while the $^{31}P\{^1H\}$ spectrum consisted only of liberated PPh$_3$ (δ_P

‡‡‡‡‡‡‡‡‡‡‡‡‡ Given the steric congestion, the alternative possibility that the Pt(PPh$_3$)$_2$ fragment coordinates the alkynyl triple bond (*cf.* known [Pt(η^2-PhCCPh)(PPh$_3$)$_2$] [320]) could not be discounted *a priori*.

= –5.5) suggesting the complex contains no phosphine. The species were formulated as $Li_2(THF)_n[WPt(\mu_2\text{-}C)(C{\equiv}CSiMe_3)_3(CO)_2(Tp^*)]$ (**5.16**) based on spectroscopic data and a high-resolution ESI(-ve ion) mass spectrometry fragment consistent with $[M+H-2Li-nTHF]^-$. Like **5.13**, **5.16** remains exceedingly soluble, even in *n*-pentane, likely the reason why crystals were not forthcoming. For this reason, the structure of **5.16** is presented tentatively. The persistent solubility of **5.16** also explains why reactions with excess acetylide provided pure crystalline material of **5.13**, as the *mono*-phosphine species is pentane insoluble and therefore selectively crystallises, whereas **5.14**, **5.15**, and **5.16** are pentane soluble.§§§§§§§§§§§§§§§§§

Identifying **5.16** now accounts for an additional species to those observed in the $^{31}P\{^1H\}$ NMR spectra such that a manifold for acetylide addition can be proposed (Scheme 5.18). Upon addition of acetylide to **3.1b**, most likely *via* an associative pathway would give a transient, 5-coordinate anionic intermediate, prone to Berry pseudo-rotation. Bromide elimination could provide either the *trans* or *cis* isomer of **5.14**. Once isolated, the *trans* isomer **5.14** barely decomposes (<5%) in C_6D_6 after one week suggesting *cis-trans* isomerism is significantly slower than reductive elimination and that the quantity of **5.15** produced could not have been *via* **5.16**. Except for the small amount of unidentified material in Figure 5.10, no other evidence suggests the *cis*-isomer is long-lived. Furthermore, **5.15** is the major product of the mixture and therefore suggest that if the transient 5-coordinate intermediate gave the *cis* isomer in more effective competition with the *trans* isomer, reductive elimination is almost as fast as formation of the *cis*-isomer preventing its significant accumulation.

Respective isolation and detection of **5.13** and **5.16** suggest a secondary competition occurs upon generation of the *cis*-$[WPt(\mu\text{-}C)(C{\equiv}C\text{–}SiMe_3)(CO)_2(Tp^*)]$ intermediate. A second addition of acetylide prior to reductive elimination can substitute the phosphine of *cis*-$[WPt(\mu\text{-}C)(C{\equiv}C\text{–}SiMe_3)(CO)_2(Tp^*)]$ to give **5.13******************** although the smaller amounts compared with **5.15** imply the rate of addition is also fast, but slower relative to reductive elimination. Unsurprisingly, there is no evidence of the *tris*-acetylide **5.16** in crude mixtures of a *stoichometric* addition, as the rate would be dependent on concentration of acetylide which is depleted in this scenario. Addition of a third acetylide is clearly fast, but only when an excess is supplied to outcompete the reductive elimination pathway.

§§§§§§§§§§§§§§§§§ In contrast to the well-known dianionic complexes $[Pt(CCR)_4]^{2-}$ which are typically isolated an tetra-alkylammoniun salts, the role of lithium here as 'counter-ion' requires close ion-pairing/association to achieve the observed alkane soubility.

********** It should be noted that rapid addition of LiC^oCSiMe_3 to either the *cis* or *trans* isomer would afford the same intermediate $Li[WPt(\mu\text{-}C)(C{\equiv}CSiMe_3)_2(CO)_2(PPh_3)_2(Tp^*)]$ prior to phosphine dissociation.

Considering termination of the manifold, the major species formed is **5.15** that eventually reductively eliminates to [W(≡C–C≡C–$SiMe_3$)$(CO)_2$(Tp*)] dependant on solvent. Both **5.13** and **5.16** acetylides remain in C_6D_6 for weeks ($t_{½}$ *ca* 2 weeks), while use of $CDCl_3$ results in slower reductive elimination of **5.13** (*ca* 48 hours) compared with **5.16** (*ca* 1 hour). Reductive elimination of [W(≡C–C≡C–$SiMe_3$)$(CO)_2$(Tp*)] from **5.13** gives *trans*-[$PtCl_2(PPh_3)_2$] (δ_P = 20.7) [436] and *trans*-[$Pt(C{\equiv}C{-}SiMe_3)_2(PPh_3)_2$]($\delta_P$ = 18.8) [437] presumably *via* reacting with solvent. Alternatively, subjecting **5.16** to $CDCl_3$ results in decomposition to [W(≡C–C≡C–$SiMe_3$)$(CO)_2$(Tp*)] *via* **5.13** and **5.15**, accompanied by *trans*-[$PtCl_2(PPh_3)_2$] over a period of one hour. The ^{1}H NMR spectrum of **5.16** proved inconclusive as the excess lithium acetylide reacts with chloroform to give signals consistent with authentic HC≡C$SiMe_3$ and obscures conclusive evidence of acetylide coupling to the butadiyne ($Me_3SiC{\equiv}CC{\equiv}CSiMe_3$).

Spectroscopic data collected for **5.12–5.16** are collated in Table 5.3. Several data items occur in similar regions except for large variation between μ_2-carbido (or equivalent) resonances within $^{13}C\{^1H\}$ NMR spectra. Starting material **3.1b** exhibits a relatively lower frequency carbido resonance attributed to the π-donating *trans*-bromide but swapping to a weakly π-accepting acetylide results in a shift to much higher frequency (δ_C = 378.5, **5.14**) just below that of the σ-aryl **5.12** (δ_C= 397.2). This shift further describes the significant role *trans*-influence plays on carbido resonances. Interestingly, less pronounced changes in carbido frequency also occur upon addition of further acetylides (*cis* to the carbido), appreciating the carbido and platinum nuclei of **5.16** are reasonably occluded such that significant solvent effects from C_6D_6 seem unlikely. While ^{195}Pt NMR resonances are typically less prone to electronic changes, platinum(II) acetylide species **5.13/5.14/5.16** reside in a similar region to platinum(0) like in **5.15**. Finally, the propargylidyne [W(≡C–C≡C–$SiMe_3$)$(CO)_2$(Tp*)] is well studied, [438] and it is curious that the addition of a '*trans*-$Pt(PPh_3)_2$' unit to the chain alters the δ_C and ν_{CO}, yet leaves $\delta_H(SiMe_3)$ and $\nu_{C\equiv C}$ untouched (Figure 5.11), suggesting changes only occur along the chain toward tungsten. Remaining spectroscopic features are similar to those discussed previously.

Incorporation of trimethylsilyl groups increased the solubility of many species, such that only **5.13** was obtained as crystals on bulk scale, suitable for X-ray diffraction studies (Figure 5.12). Complex **5.13** features the contracted Pt–C bond (Pt1–C1: 1.981(3) Å) expected for a metallacarbyne, although this is an interesting feature given platinum(II) is now formally anionic with a π-acidic C≡CR ligand *trans* to the carbido. One phosphine is retained in the *syn* conformation for **5.13** occupying the Tp* cleft while incorporation of lithium provides a zwitterionic complex where the Li is stabilised by coordinating THF and the acetylide π-systems. While lithium is held

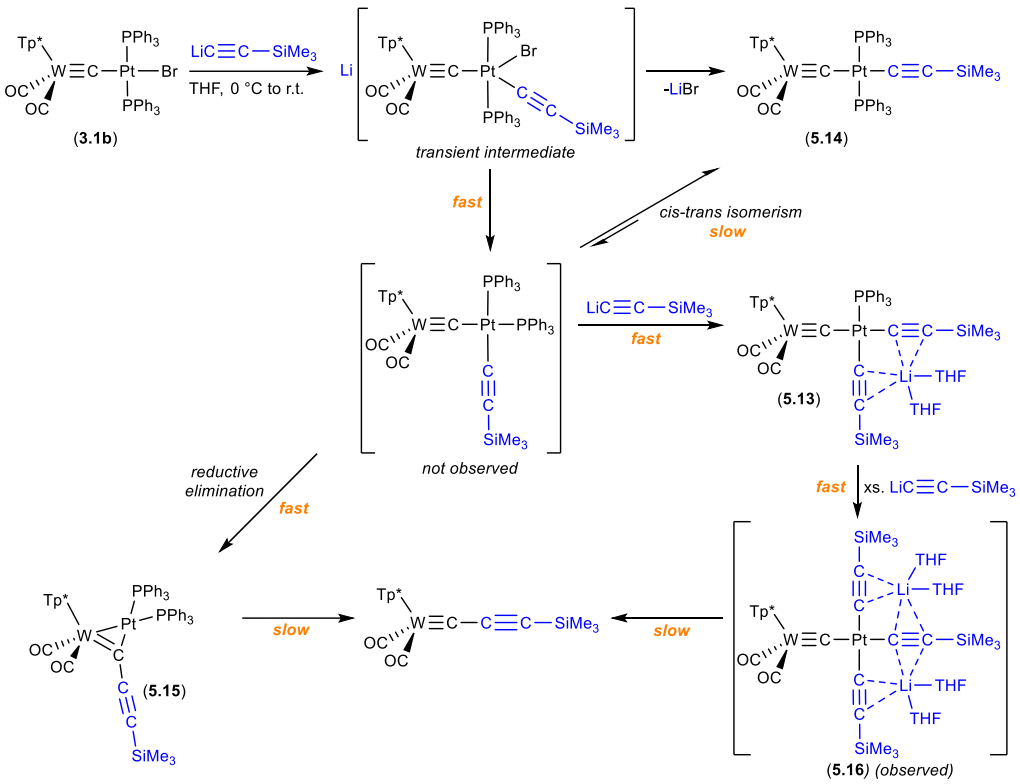

Scheme 5.18: Manifold underpinning addition of acetylide to **3.1b** show relative rates of processes in (orange).

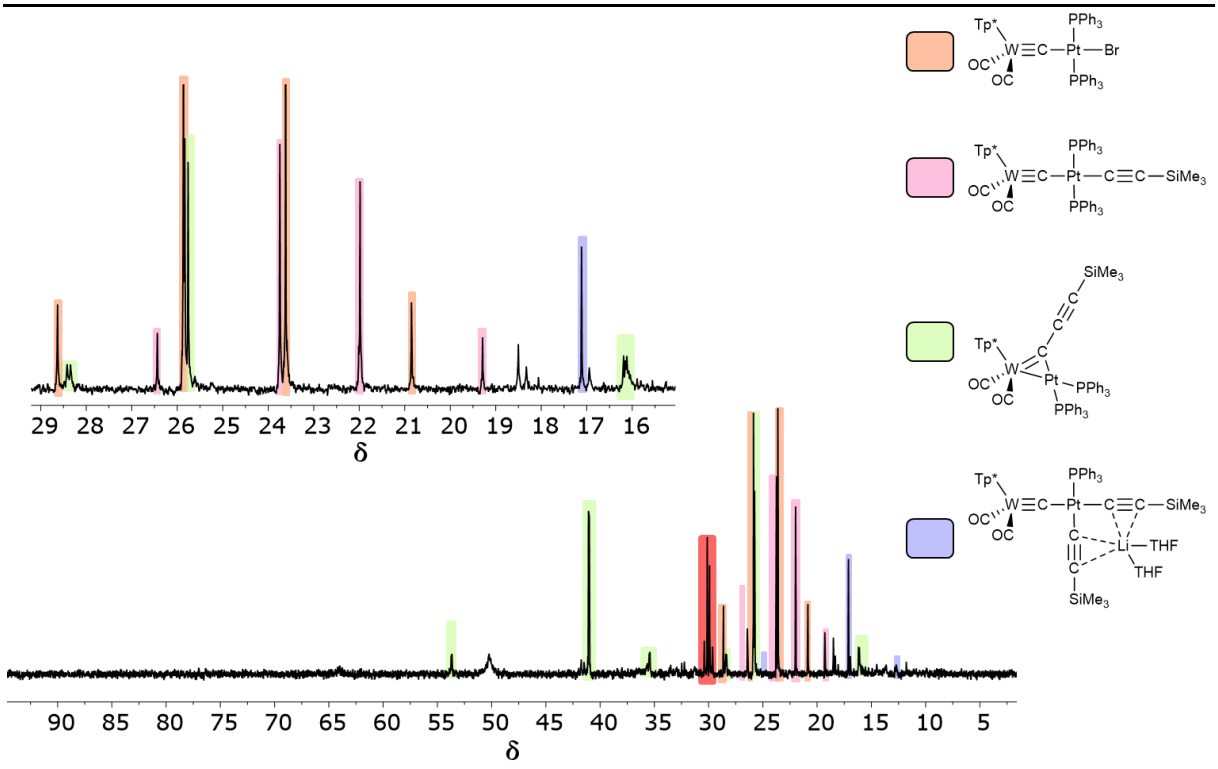

Figure 5.10: $^{31}P\{^{1}H\}$ NMR spectrum of acetylide addition to [WPt(μ_2-C)Br(CO)$_2$(PPh$_3$)$_2$(Tp*)] (**3.1b**) after 30 minutes, highlighting competition between species. Species highlighted in red remains unidentified.

Table 5.3: Spectroscopic properties of species obtain *via* lithium reagents, including those relevant to acetylide manifold.

Compound	δ_C (ppm)[a]	$\delta_{H(SiCH3)}$ (ppm)[a]	δ_P (ppm)[a]	δ_{Pt} (ppm)[a]	J_{PPt} (Hz)	ν_{CO} (cm^{-1})[b]	$\nu_{C\equiv C}$ (cm^{-1})[b]
[**W**Pt(μ-C)Br(PPh$_3$)$_2$] (**3.1b**)	317.2 318.7	–	28.27, 23.91 26.21, 22.11 ($^2J_{PP}$ = 443 Hz)	–3821 –3718	3187 3202	1945, 1854 1988, 1894	–
trans-[**W**Pt(μ-C)(tolyl)(PPh$_3$)$_2$] (**5.12**)	397.2	–	21.74, 20.62 ($^2J_{PP}$ = 440 Hz)	–4164	3266	1937 , 1843	–
trans-[**W**Pt(μ-C)(C≡CSiMe$_3$)(PPh$_3$)$_2$] (**5.14**)	378.5	0.17	24.06, 20.64 ($^2J_{PP}$ = 436 Hz)	–4193	3003	1939, 1845	2051
Li(THF)$_2$[**W**Pt(μ-C)(C≡CSiMe$_3$)$_2$(PPh$_3$)] (**5.13**)	374.6	0.26, –0.37	16.10	–4061	2675	1932, 1841	2035, 2017
Li$_2$(THF)$_4$[**W**Pt(μ-C)(C≡CSiMe$_3$)$_3$] (**5.16**)	381.2[c]	0.13, 0.11[c]	–	–3847[c]	–	1935, 1847[e]	2034, 2016[e]
[**W**Pt(μ$_2$-C–C≡CSiMe$_3$)(PPh$_3$)$_2$] (**5.15**)	294.1	–0.53	39.40, 25.29 ($^2J_{PP}$ = 11 Hz)	–4090	4091 3138	1890, 1800	2039
[W(≡C–C≡CSiMe$_3$)]	255.6	0.17	–	–	–	1985, 1895	2051

Note: Bolded metals include the common ligand set {i.e **W** = W(CO)$_2$(Tp*)}. [a]Measured in $CDCl_3$ unless specified. [b]Measured in CH_2Cl_2 unless specified. [c]Measured in C_6D_6. *d*Adjusted for roofing. [e]Measured in THF.

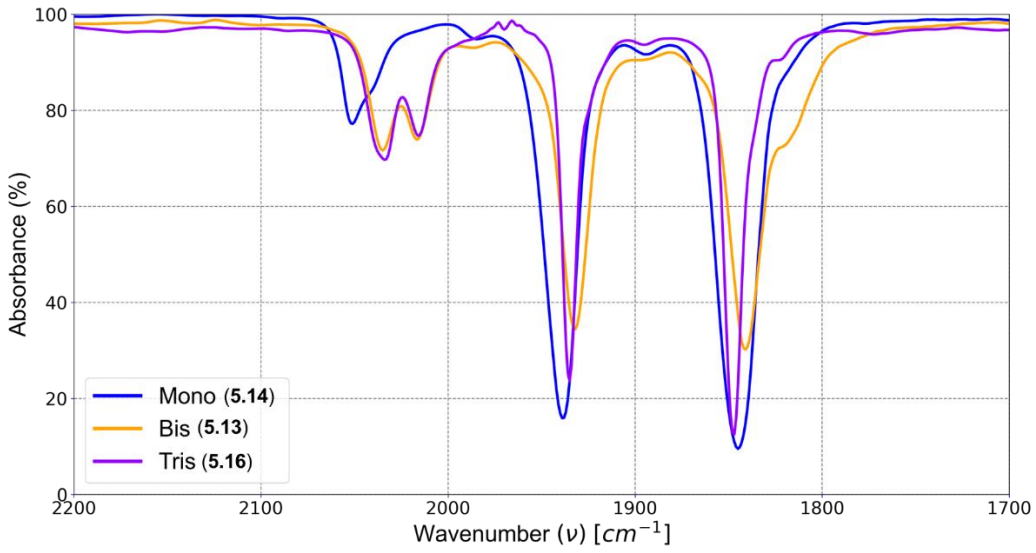

Figure 5.11: Superimposed solution-state infra-red spectra of *mono* (**5.14**), *bis* (**5.13**), and *tris*-acetylide (**5.16**) complexes.

by the acetylide π-systems, the C≡C bonds clearly retain their multiple character, with no discernible bond elongation from norms for ideal *sp*-hybridisation (*ca* ~1.21 Å). The Pt···Li distance is significantly larger (3.135(6) Å) than the sum of the covalent radii (*ca* ~2.64 Å), suggesting a primarily ionic interaction. Measuring a ^{7}Li NMR spectrum [$I = {}^{3}/_{2}$; 92% abundance] of **5.13** returns a sharp resonance devoid of coupling to ^{195}Pt ($\delta_{Li} = 0.79$) consistent with free Li^{+} in solution without Pt–Li bonding (Figure 5.13). To verify this idea, 12-crown-4 (selective for Li^{+}) was added, but this resulted in decomposition, albeit with little change in the lithium frequency. This suggests that whilst the lithium does not remain constantly coordinated, removing through sequestration the possibility for it to return to the complex leads to decomposition such that the lithium has a stabilising effect. The association of Li^{+} in the solid state specifically with the two alkynyl groups compromises the ability of **5.13** to serve as a benchmark for internally comparing the bonding and geometric features of Pt–C≡C *vs* Pt-C≡W connectivities.

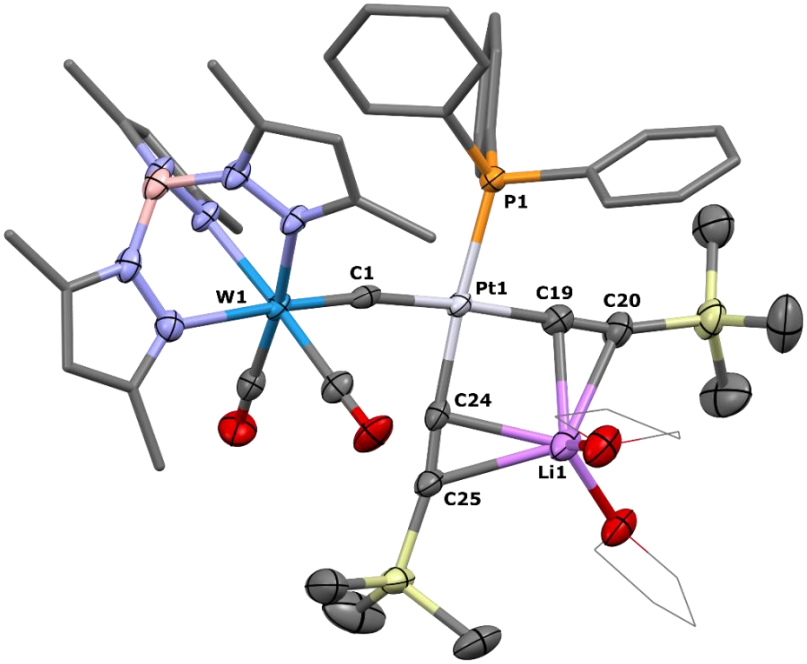

Figure 5.12: Molecular structure of $Li(THF)_2[WPt(\mu_2\text{-}C)(CCSiMe_3)_2(CO)_2(PPh_3)(Tp^*)]$ (**5.5b**) in a single crystal as determined by X-Ray Diffractometry. Ellipsoids are drawn at the 50% probability surface with pyrazolyl and phenyl rings simplified and hydrogens omitted for clarity. THF solvates presented in wireframe for clarity. Selected bond lengths (Å) and angles (°): W1–C1: 1.838(3); Pt1–C1: 1.981(3); Pt1–C19: 2.054(4); Pt1–C24: 2.000(3); Pt1–P1 2.2946(9); Pt1···Li1 3.135(6); C19–C20 1.205(5); C24–C25 1.213(5); W1–C1–Pt1 170.9(2); C19–Pt1–C24 90.1(1).

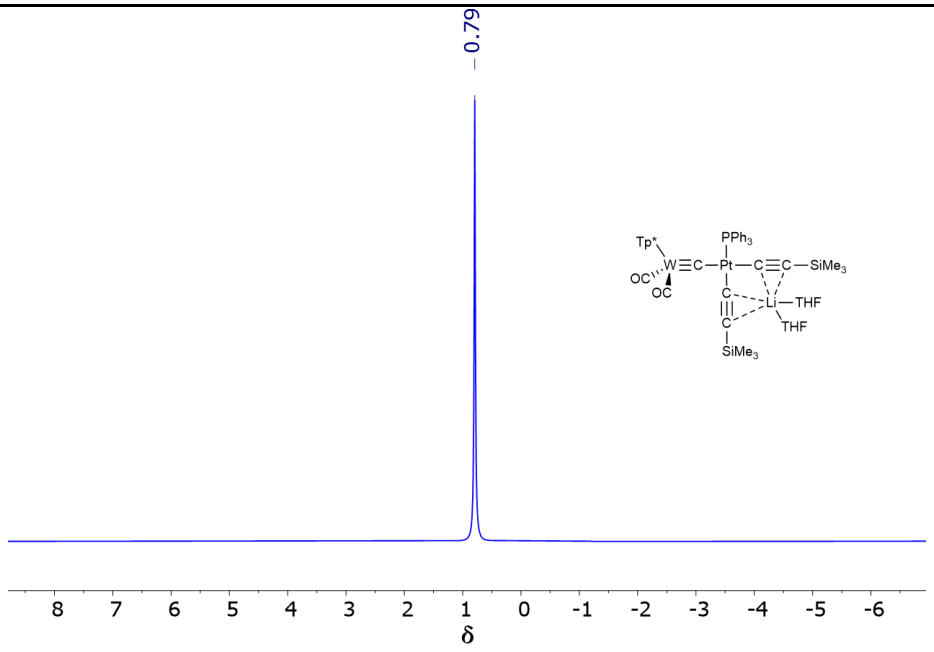

Figure 5.13: ^{7}Li NMR spectrum of Li(THF)$_2$[WPt(μ$_2$-C)(C≡CSiMe$_3$)$_2$(CO)$_2$(PPh$_3$)(Tp*)] (**5.13**) in C_6D_6 showing absence of coupling to other nuclei, ^{31}P or ^{195}Pt.

Benchmarking the μ$_2$-carbido ligand against acetylides was still desired; hence, another synthetic method was attempted. Instead of utilising **3.1b** as the metallacarbyne precursor (untethered *trans* phosphines), **3.3b** was chosen as it contains a pre-enforced *cis*-geometry as desired with chelated phosphines to prevent *trans* isomers. Initial treatment of **3.3b** with LiC≡CSiMe$_3$ resulted in mixtures with extensive reductive elimination as found for **3.1b**, and therefore was not pursued. Alternatively, transmetallation employing less nucleophilic alkynyls, *e.g.*, organocopper species provides an alternative approach to installing acetylides to platinum(II) as studied extensively by Bruce, [136, 190, 439] and Sonogashira. [440-442] This approach was therefore explored with the further variant of employing ethynylbenzene due to the solubility issues encountered with silylalkynyls.

Addition of phenylacetylene to **3.3b** suspended in THF/NEt$_3$ with copper(I) iodide results in a yellow mixture with an increasingly dark supernatant phase, with complete consumption recorded at 2 hours (TLC). Use of **3.3b** (and hence the dppe ligand) resulted in several broad resonances being observed in the ^{31}P{^{1}H} NMR spectrum, rendering the technique uninformative while the ^{1}H NMR spectrum contained no unique signals to monitor reaction progress. Measuring the reaction *via* TLC suggested a simple reaction mixture producing one red and one yellow species The red complex was identified as the terminal propargylidyne [W(≡C–C≡CPh)(CO)$_2$(Tp*)] (THF: ν_{CO} = 1979, 1893 cm^{-1}) described previously by Fischer[443] arising from reductive elimination. The yellow species was identified as [W(≡C–CC–Ph){η^2-Pt(dppe)}(CO)$_2$(Tp*)] (**5.17**); in which the propargylidyne coordinates to platinum not through the W≡C but rather the C≡C bond

(Scheme 5.19, δ_C(WC) = 266.8, δ_C(C≡C) = 145.4). No evidence of the desired complex *cis*-[WPt(μ_2-C)(C≡CPh)(dppe)$(CO)_2$(Tp*)] or the π-coordination across the W≡C bond was observed.

Isolation of **5.17** suggested reductive elimination occurred *via* a different route for phenylacetylide *vs* trimethylsilylacetylide propargylidynes (*vide supra*). To probe this mechanism further, [W(≡C–C≡CPh)$(CO)_2$(Tp*)] was treated with [Pt(η^2-C_2H_4)$(PPh_3)_2$] determining π-coordination occurs across the C≡C bond exclusively to give [W(≡C–CC–Ph){η^2-Pt$(PPh_3)_2$}$(CO)_2$(Tp*)] (**5.18**) (Scheme 5.19), in contrast to what was observed for the trimethylsilyl propargylidyne. Similar features occur for **5.17** and **5.18**, and therefore the latter will be discussed given the analogous comparator of **5.15** albeit across the W≡C π-system. As **5.15** and **5.18** contain several spin-active nuclei, the coordinated π-system is immediately determined by the chemical shift and coupling information obtained from $^{31}P\{^1H\}$ NMR spectra. For **5.18**, an **AB** pair of doublets for two nuclei of similar chemical shift and couplings to ^{195}Pt is observed (δ_P [$^1J_{PPt}$] = 28.35 [3680 Hz], 26.33 [3178 Hz]) reflecting the similar environment upon C≡C coordination. Conversely, **5.15** exhibits doublets with quite differing chemical shifts and more disparate couplings to platinum (δ_P[$^1J_{PPt}$] = 39.40[4095 Hz], 25.29[3138 Hz]) consistent with a *pseudo-trans* relationship to tungsten found previously (See complexes **2.3b** and **4.10**). Furthermore, the $^{13}C\{^1H\}$ NMR spectrum of **5.18** contains a lower frequency resonance for C_1 (δ_C = 266.6), whereas **5.15** shifts to higher frequency with evident coupling to phosphorus (δ_C = 294.1; $^2J_{CP}$ = 61 Hz). Detection of a ^{195}Pt resonance is expedited for **5.15** guided by several examples examined thus far (δ_{Pt} = –4090) but species **5.18** proved challenging. No ^{195}Pt resonance was detected for **5.17** (or **5.18**) over the range 0 to –6000 ppm, conducting experiments 1000 ppm in spectral width at 6000 scans per interval (for context, **5.15** was identified after ~300 scans). This is interesting given the analogous [Pt(η^2-PhC≡CPh)$(PPh_3)_2$] was previously measured at –208.4 ppm[320] and the alkene complex [Pt(η^2-C_2H_4)$(PPh_3)_2$] occurs at –542 ppm, [444] suggesting that **5.17**/**5.18** may lie outside these regions or the resonance is broadened into the baseline through dynamic processes.

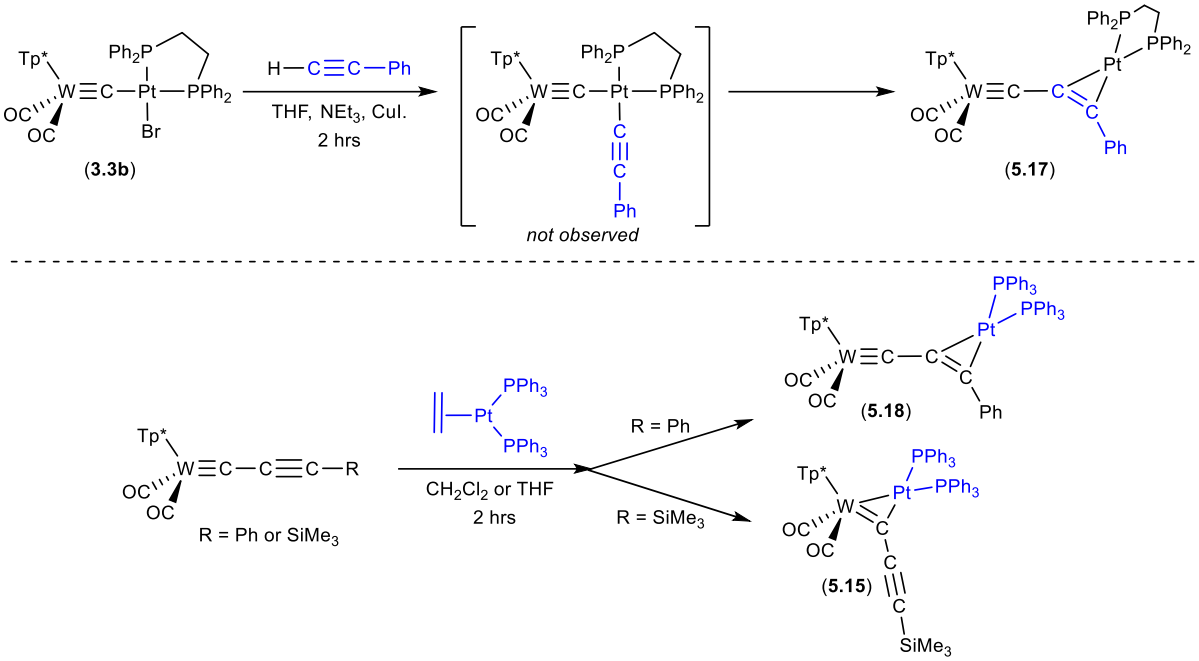

Scheme 5.19: A) Attempted synthesis of *mono*-acetylide metallacarbynes *via* transmetallation. B) Substituent-dependent regioselectivity of π-coordination to platinum(0).

Single crystals suitable for X-ray diffraction studies were obtained for **5.17** confirming reductive elimination results in coordination of the C≡C π-system (Figure 5.14). The C–C bond length is elongated by platinum coordination (C2–C3: 1.315(6) Å) relative to *sp*-hybridised carbon (*cf.* ~1.21 Å), [384] while similar to coordinated alkyne [Pt(η^2-PhC≡CPh)(dppe)] (1.30(1) Å) and butadiyne [Pt(η^2-PhC≡C–C≡CPh)(dppe)] (1.34(4) Å) analogues. [445-446] The adjacent carbon bonds are shorter for the carbyne (*sp-sp*) than for the phenyl (*sp-sp2*) group (1.455(6) *vs* 1.315(6) Å, respectively) highlighting the difference in carbon coordination number, but not discounting limited conjugation. Furthermore, the W≡C bond is consistent with literature precedent for tungsten propargylidynes (1.849(5) Å) [255] as a familiar clash of large *tris*-pyrazolylborate and dppe ligands is apparent on consideration of a space-filling representation. From a Dewar-Chatt-Duncanson perspective, the carbyne deviates more (C1–C2–C3: 150.2(5)°) than the phenyl group (C2–C3–C4: 137.2(5)°), however, this is likely a consequence of steric pressure rather than electronic influence as similar complexes feature less disparate angles (*cf.* 143(3)/139(3)° for [Pt(η^2-PhC≡C–C≡CPh)(dppe)]). [446] An asymmetric π-coordination is noted such that the Pt–C bond closest to the Tp* is significantly longer (Pt1–C2: 2.081(6) Å) than the other adjacent to phenyl (Pt1–C3: 2.000(6) Å), further highlighting the steric impact of Tp*; related Pt–C lengths lie in between these values (*ca* 2.03 Å; [Pt(η^2-PhC≡CPh)(dppe)]). [446]

Coordination of the C≡C bond could also be confirmed by infra-red spectroscopy whereas propargylidynes (and related species encountered so far) manifest weak W≡C vibrations often

obscured ($\nu_{M\equiv C}$ ~ 1000 cm^{-1}) and hence a similar analysis is prevented. The $\nu_{C\equiv C}$ vibration is a key datum for propargylidynes, (2101 cm^{-1}; [W(≡C–C≡CPh)$(CO)_2$(Tp*)])[438] such that coordination to platinum reduces the frequency of the $\nu_{C\equiv C}$ mode ($\nu_{C=C}$ = 1659 **5.17**, 1652 **5.18** cm^{-1}) indicative of reduced bond order. Likewise, ν_{CO} vibrations shift to lower wavenumber indicative of a more electron-rich tungsten centre (Figure 5.15). Production and study of **5.17**/**5.18** suggest that reductive elimination is too fast to isolate or observed acetylide ligands *cis* to a μ_2-carbido, irrespective of delivery method; however, the ultimate product of reductive elimination of propargylidynes is specific to the end group.

5.7 Reactivity of [W≡C–Pt] with: Alkylidynes

Alkynylalkylidynes (propargylidynes) $L_nM\equiv C–C\equiv C–R$ [226] were selected as the final carbon-based ligand to be supplied to a μ_2-carbido complex as a progression from alkynyls. Although not explored here, the recent isolation of chain-extended pentadiynylidynes $L_nM\equiv C– C\equiv C–C\equiv C–R$) [140] presents a future direction for investigation, guided by the results that follow. From a synthetic perspective, larger carbon chains may be expected to behave similarly; the differences arise in synthetic difficulties, analysis, properties, and applications. Many pyrazolylborato alkylidyne complexes are known with differing transition metal endcaps, [255] with [W(≡C–C≡CSiMe_3)$(CO)_2$(L)](L = Tp, Tp*)[438] having proven to be especially versatile tricarbido synthons. The Tp* complex [W(≡C–C≡CSiMe_3)$(CO)_2$(Tp*)] was selected for further studies here as it has a proven track record for tricarbido delivery through well-documented desilylation protocols, [139]†††††††††††††††† that involve *in situ* generation of the parent alkylidyne [W(≡C–C≡CH)$(CO)_2$(Tp*)] and/or its conjugate base. [448] Though neither of these have been isolated, desilylation of [W(≡C–C≡CSiMe_3)$(CO)_2$(Tp*)] can be mediated either by either alkoxide or fluoride in the presence of a range of electrophiles. Herein, fluoride was initially chosen given convenience of tetrabutylammonium fluoride (TBAF) solution (1M in THF‡‡‡‡‡‡‡‡‡‡‡‡‡‡‡‡).

With the primary objective being the isolation of a mixed *cis*-monocarbido-tricarbido complex, **3.3b** was chosen as the initial platform. Treating a suspension of **3.3b** and [W(≡C–C≡CSiMe_3)$(CO)_2$(Tp*)] in THF with TBAF rapidly formed a brown mixture from which

†††††††††††††††† Propargylidynes can also be delivered through transmetallation processes (See Bruce[136]), although this was not pursued given less expedited access in addition to favourable elimination of butadiynyl species. [447]

‡‡‡‡‡‡‡‡‡‡‡‡‡‡‡‡ The commercial reagent (Sigma-Aldrich 216143) contains 3-7% water. Attempts to completely dehydrate hydrated TBAF have been unsuccessful due to the onset of Hoffman elimination processes as the basicity of fluoride increases with decreasing hydration. Alternative anhydrous fluoride sources include TASF tris(dimethylamino)sulfonium difluorotrimethylsilicate or TBAT Tetra-n-butylammonium difluorotripehnylsilicate were not investigated here.

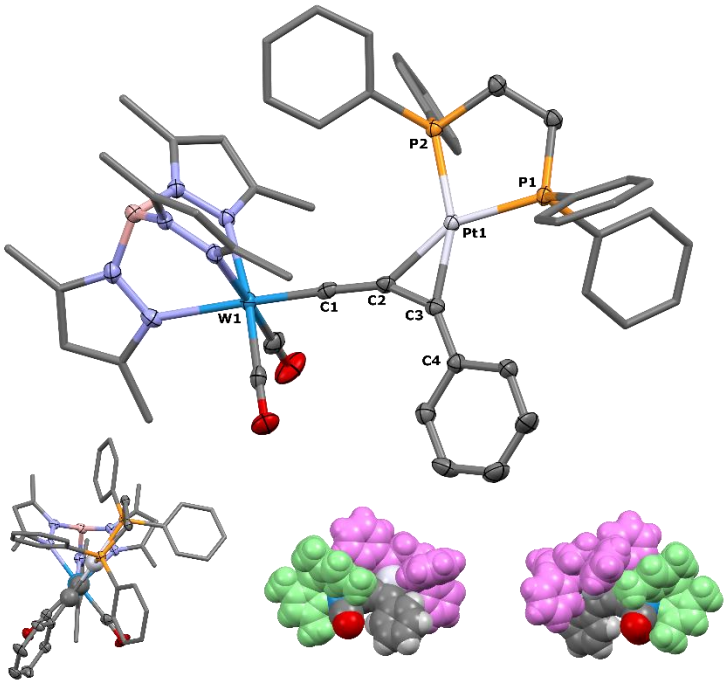

Figure 5.14: Molecular structure of [WCCC{η²-Pt(dppe)}Ph(CO)₂(Tp*)] (**5.17**) in a single crystal as determined by X-Ray Diffractometry. Ellipsoids are drawn at the 50% probability surface with pyrazolyl and phenyl rings simplified and hydrogens omitted for clarity. Insets: a) Ball and stick representation as viewed down the key molecular linkage (ligands simplified for clarity), b) Spacefill representations (front and rear view) highlighting the asymmetric interdigitation of phosphine (pink) and pyrazolyl (green) ligands about the carbon chain. Selected bond lengths (Å) and angles (°): W1–C1 1.849(5), C1–C2 1.378(7), C2–C3 1.315(6), C3–C4 1.455(6), Pt1–C2 2.081(6), Pt1–C3 2.000(6), Pt1–P1 2.236(1), Pt1–P2 2.269(1), W1–C1–C2 177.3(4), C1–C2–C3 150.2(5), C2–C3–C4 137.2(5), C2–Pt1–C3 37.5(2), P1–Pt1–P2 86.28(5).

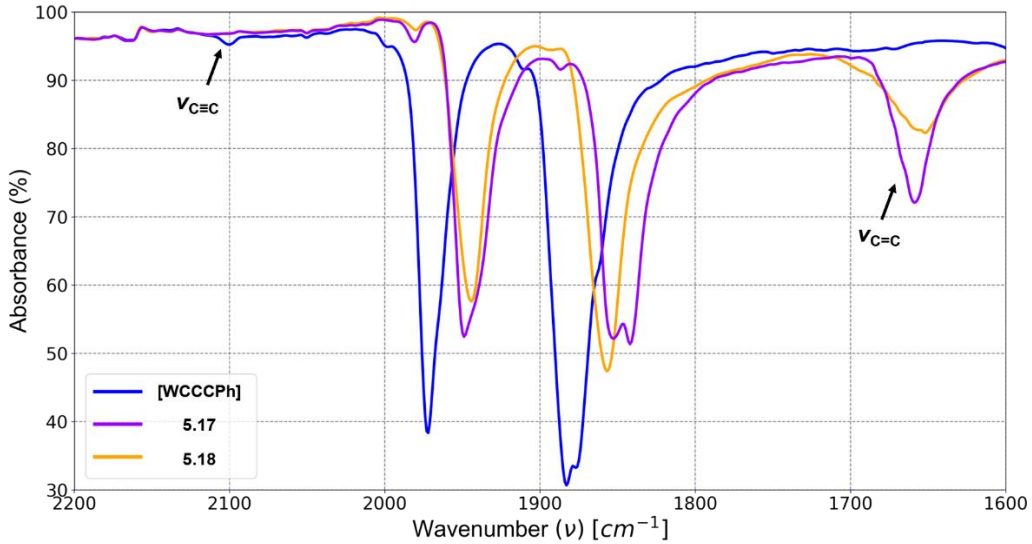

Figure 5.15: Infra-red spectra of propagyildyne [W(≡CC≡CPh)(CO)₂(Tp*)] and π-complexes **5.17**/**5.18** with impact on $\nu_{C\equiv C}$ mode.

subsequent chromatography provided [WPt{μ_2-C–C≡C–C≡W(CO)$_2$(Tp*)}(dppe)(CO)$_2$(Tp*)] (**5.19**) accompanied by the previously reported reductive elimination product [W$_2$(μ_2-C–C≡C–C)(CO)$_4$(Tp*)$_2$] (Scheme 5.20).[313] Once more, no evidence of the desired μ_2-carbido intermediate was detected, nor was the alternate symmetrical C≡C π-complex [W$_2$(μ_2-C–C=C–C){η^2-Pt(dppe)}(CO)$_4$(Tp*)$_2$] identified. The preference of platinum(0) to coordinate to W≡C rather than C≡C bonds in the hexacarbido complex [WPt{μ_2-C–(C≡C)$_2$–C≡W(CO)$_2$(Tp*)}(cod)(CO)$_2$(Tp*)] has been discussed previously,[93] however in that case the 'Pt(cod)' fragment was introduced following the prior formation and isolation of the ditungstaocatateryne (Scheme 5.21).

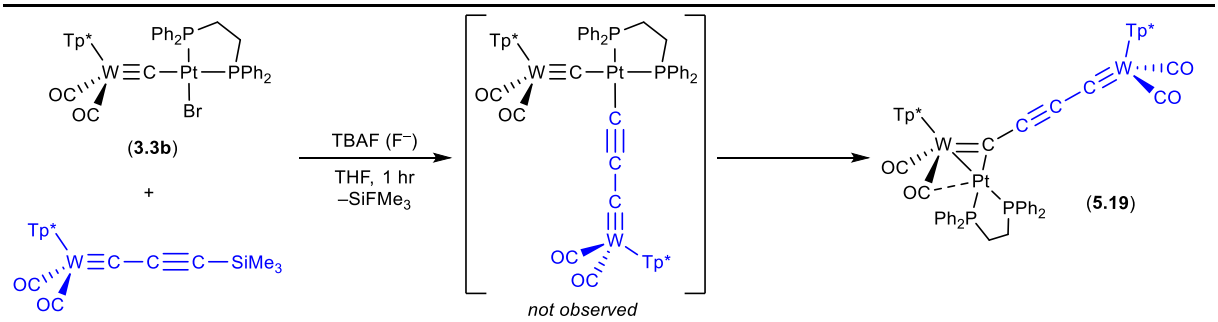

Scheme 5.20: Synthesis of alkylidyne metallacarbynes and spontaneous elimination.

Several related examples of platinum species have been explored with various carbon chain lengths (Scheme 5.21). For *bis*-μ_2-carbidos (*i.e.,* C$_1$ chains), [W(≡CLi)(CO)$_2$(Tp*)] reacts with [PtCl$_2$(L$_2$)] (L$_2$ = COD or nbd) but provides no evidence of *cis*-[W$_2$Pt(μ_2-C)$_2$(L$_2$)(CO)$_4$(Tp*)] enduring, consistent with observations made in the section. Instead, reductive elimination occurs such that the platinum(0) fragment coordinates to one W≡C bond but can 'shimmy' to the other.[350] Meanwhile for *bis*-propargylidynes (C$_3$ chains), [W$_2$Hg(≡CC≡C)$_2$(CO)$_4$(Tp*)$_2$] and [PtCl$_2$(PPh$_3$)$_2$] react to transiently provide *cis*-[W$_2$Pt(μ_2-CC≡C)$_2$(CO)$_4$(PPh$_3$)$_2$(Tp*)$_2$] prior to elimination of [W$_2$(μ-CC=CC≡CC){η^2-Pt(PPh$_3$)$_2$}(CO)$_4$(Tp*)$_2$] bearing platinum(0) bound to a C≡C bond, a process that is in competition with conversion the isomer *trans*-[W$_2$Pt{μ-CC≡C)$_2$(CO)$_4$(PPh$_3$)$_2$(Tp*)$_2$], which does not undergo reductive elimination under the conditions investigated.[449] The π-adduct is also the exclusive product from the reaction of [Pt(η^2-C$_2$H$_4$)(PPh$_3$)$_2$] with [W$_2$(μ_2-CC≡CC≡CC)(CO)$_4$(Tp*)$_2$], whereas [WPt{μ_2-C–C≡C–C≡C–C≡W(CO)$_2$(Tp*)}(L$_2$)(CO)$_2$(Tp*)] (L$_2$ = COD or NBD) are produced from [Pt(nbe)$_3$] + 'L$_2$'.[450] These results highlight the difficulty in spectroscopically observing μ_2-carbido complexes *cis* to s-organyls with available π-orbitals prior to reduction, although longer propargylidyne fragments appear longer-lived. Coupled with the formation of **5.19** which contained an asymmetric C$_1$ and C$_3$ chain, the facile reductive elimination suggests that features specific to the μ_2-carbido ligand

appear to be the dominating influence in initiating the C–C bond-forming process. Furthermore, these literature examples highlight that the regioselectivity of coordination of platinum(0) to WC_xW (W≡C *vs* C≡C bonds) is a response to a variety of factors and that the Pt(0) unit is not necessarily fixed at one site.

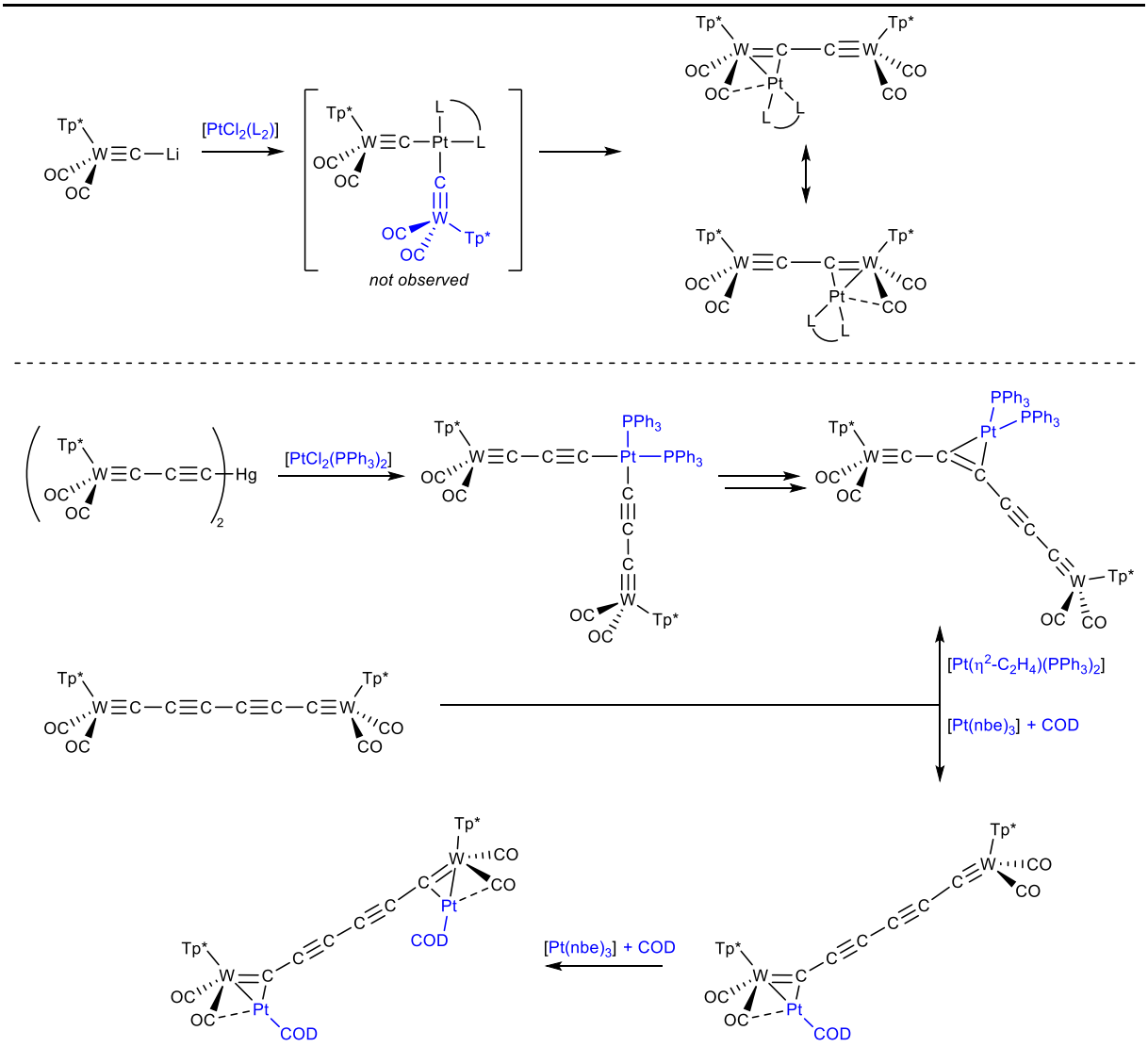

Scheme 5.21: Related platinum(0/II) species of C_1 and C_3 carbon-chains.

The complex **5.19** was spectroscopically characterised, featuring many similar values to **5.15** and other species coordinated across the W≡C bond. The $^{13}C\{^1H\}$ NMR spectrum of **5.19** exhibits a resonance (δ_C = 279.3) higher in frequency than the free carbyne signal in the same molecule (δ_C = 240.9), while $^{31}P\{^1H\}$ NMR reveals and **AB** pattern with small phosphorus couplings (δ_P = 58.24, 52.90; $^2J_{PP}$ = 6 Hz). Curiously, platinum couplings are less disparate than expected ($^1J_{PtP}$ = 3591, 3220 Hz) given the *pseudo-trans*-tungsten.§§§§§§§§§§§§§§§§§§ Meanwhile, infra-red spectroscopy

§§§§§§§§§§§§§§§§§§ It is implicit in the observation of **AB** systems in this and related compounds, that rotation of the W≡C unit with respect to the PtL_2 unit is arrested on the ^{31}P NMR timescale.

reveals a series of carbonyl vibrations (ν_{CO}: 1957, 1892, 1868 cm^{-1}) with one lower in frequency suggestive of a semi-bridging carbonyl ($\nu_{\mu\text{-}CO}$: 1745 cm^{-1}), yet the $^{13}C\{^1H\}$ NMR spectrum contained only a single resonance in the carbonyl region indicating terminal-bridging site exchange. Single crystals were not forthcoming, precluding a structural analysis of **5.19**.

Reductive elimination proved a recurrent featuring moving from sp^3 (CH_3) to sp^2 (tolyl) and sp -hybridised (alkynyl and tricarbido) carbon ligands. While the *cis*-related 'intermediate' was isolated for CH_3, no further examples in the series were observed. Hartwig has emphasised that the involvement of aryl π-systems in reductive elimination from palladium(II) cannot be discounted, [451] in addition to recognising electronic disparity in coupling partners contributes to rate beyond the approximation that electron-releasing ligands undergo faster reductive eliminate. [452] In search of underlying bonding factors that might be responsible for the couplings observed in this Chapter, the geometries of model complexes *cis*-[WPt(μ_2-C)(R)$(CO)_2(PMe_3)_2$(Tp)] {R = Me (**5.2***), Ph (**5.12***), and C≡$CSiH_3$ (**5.14***)} were optimised.

Many similarities emerge between the frontier orbitals of **5.2***, **5.12*** and **5.14*** are those of model compounds considered in prior chapters as regards their topologies, however discussion is limited to the orbitals that might be expected to play a role in reductive elimination processes (Figure 5.16). Several orbitals involve overlap between the μ_2-carbido and ligand R for **5.12*** and **5.14***, with π-systems already proximal and pre-disposed for the early stages of C–C bond formation, supporting experimental observations.********** Increased overlap is observed for acetylide **5.14*** (HOMO–15/–16/–19) relative to σ-aryl **5.12*** (HOMO–8/–16), where the HOMO–19 of the former features conjugation that traverses the length of the ligand. This improved overlap may support a faster relative rate of reductive elimination for acetylides compared with aryls. Experimentally, the methyl-carbido **5.2b** was found to not undergo reductive elimination to provide a μ_2-methylcarbyne **5.3**, and the model **5.2*** reveals a lack of overlap between orbitals of suitable morphology which may well be responsible.

Additionally, calculation of *cis* and *trans*-isomers of **5.12*** and **5.14***, reveal the *cis*-isomers are higher in energy by 6 and 11 $kcalmol^{-1}$, respectively. This suggests that while the *trans*-isomers are thermodynamically more favourable once formed, a relatively small barrier for *cis-trans* isomerism may exist and hence reductive elimination is plausible, reflecting experimental observation. These theoretical insights provide a rationale as to why *cis*-carbido species are not observed for sp^2 and

********** This treatment does not consider but acknowledges the likely possibility that reductive elimination may actually be more rapid from the 3-coordinate platinum of transient [WPt(μ_2-C)(R)$(CO)_2(PMe_3)$(Tp)], but merely serves to explore possible *inter*-ligand interactions.

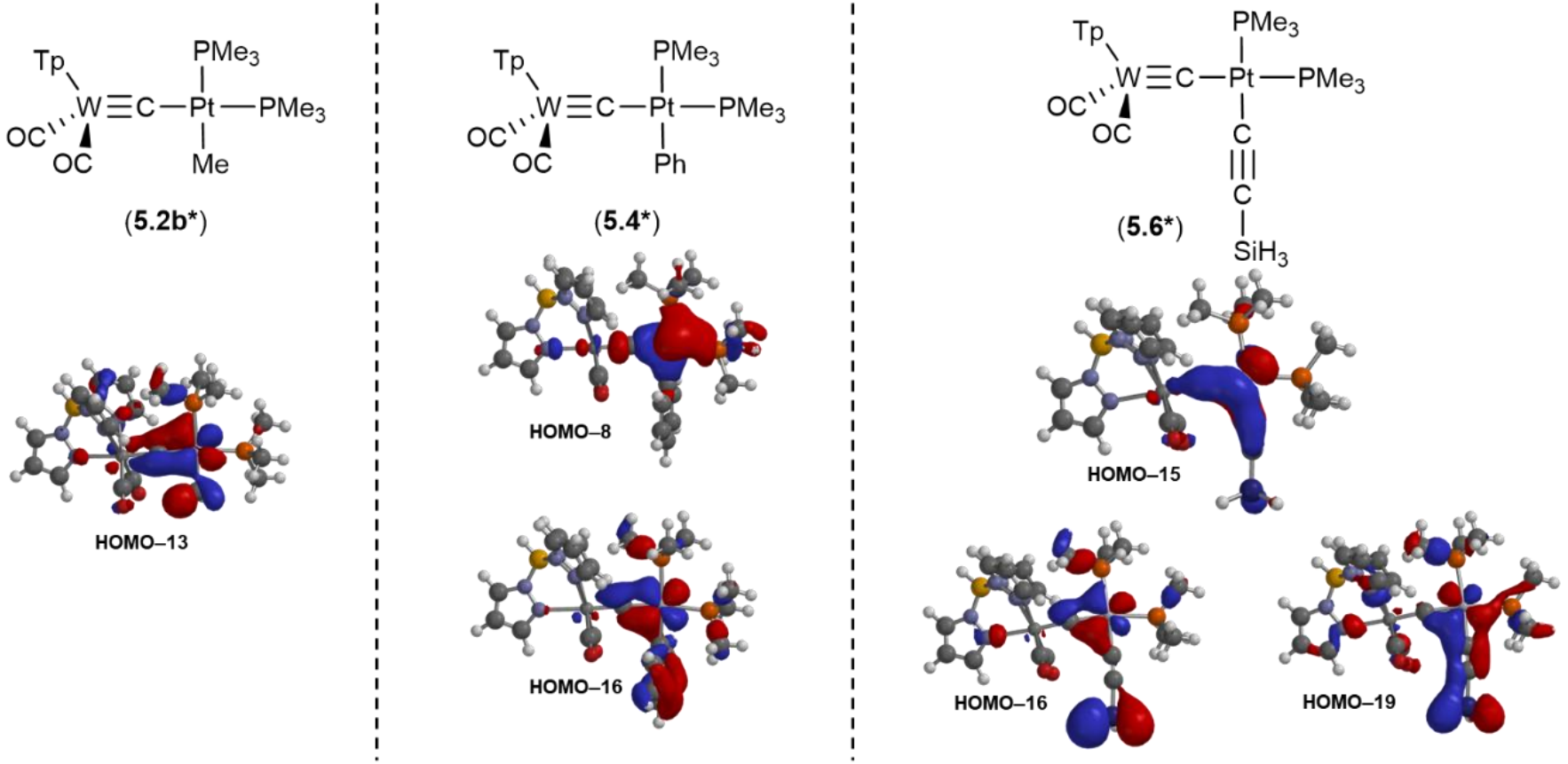

Figure 5.16: Frontier orbitals relevant to reductive elimination from models of proposed μ_2-carbido intermediates of this chapter.

sp^3-hybridised carbon, ultimately hinting alternative methods are required to benchmark the relative ligand influences as the overlap of π-systems is not easily navigated. In this context, the extensive studies of Gladysz on thermally stable poly-yn-diyl carbon chain bimetallics capped at either end by *trans*-Pt(aryl)$(PR_3)_2$ termini are of note in that the carbon chain is typically introduced last, *trans* to the pre-installed σ-aryl ligand, in synthetic sequences that avoid formation of geometries in which the σ-aryl and poly-yne-diyl chain are in a *cis*-conformation. [453-455]

5.8 Conclusions

The metallacarbyne [WPt(μ_2-C)Br$(CO)_2(PPh_3)_2$(Tp*)] (**3.1b**) undergoes bromide substitution with anionic, hydrocarbon-based nucleophiles to generate a variety of species dependent on the hybridisation of carbon of the resulting σ-organyl ligand. Initially formed complexes can adopt either be *trans*- or *cis*-geometries depending on the rates of *cis*-*trans*-isomerism (when the ligand set allows). Generally, the *trans*-[WPt(μ_2-C)(R)$(CO)_2(PPh_3)_2$(Tp*)] complexes once formed are isolable when R involves sp^2 or *sp*-hybridised carbon and are stable with respect to reductive elimination. While *cis*-isomers may be generated, these rapidly enter reductive elimination pathways in competition with rearrangement to the stable *trans* isomers such that the putative μ_2-carbido species are not observed, especially when a chelating diphosphine precludes the *cis*→*trans* isomerisation. In these cases, the resulting C–C bond-formed alkylidyne product remains within the platinum coordination sphere in the form of a μ_2-alkylidyne. However, exceptions to these observations were also observed. For a CH_3 ligand, no evidence for the formation of a *trans* isomer was observed. The complexes *cis*-[MPt(μ_2-C)$(CH_3)(CO)_2(PPh_3)_2$(Tp*)] (M = Mo, W) were isolated exclusively and shown to not convert to [WPt(μ_2-CCH_3)$(CO)_2(PPh_3)_2$(Tp*)] when heated, even though the anticipated and viable product could be accessed *via* an alternative synthetic route. The hydride *trans*-[WPt(μ_2-C)H$(CO)_2(PPh_3)_2$(Tp*)] can be spectroscopically observed although migration to the μ_2-methylidyne occurs within two days. In contrast, while *cis*-[WPt(μ_2-C)H$(CO)_2(PPh_3)_2$(Tp*)] is implicit in the evolution of *cis*-[WPt(μ_2-C)(^{n}Bu)$(CO)_2(PPh_3)_2$(Tp*)] to [WPt(μ_2-CH)$(CO)_2(PPh_3)_2$(Tp*)], it appears to be too short-lived to accumulate in sufficient quantities to be spectroscopically observed.

Reductive elimination proved the most common pathway for putative μ_2-carbido intermediates, although in the case of *sp*-C ligands (alkynyl, tricarbido) the natures of the ultimate product reflected the coordination preference of the resulting propargylidyne or tetracrabido units towards platinum(0). The more electron rich 'R = C≡CSiMe_3' and tricarbido R = C≡CC≡W$(CO)_2$(Tp*) fragments eliminate propargylidyne or tetracarbido complexes *via* μ_2-species [WPt(μ_2-CR)$(L_2)(CO)_2$(Tp*)] {L_2 = $(PPh_3)_2$ or dppe}, while in the case of the electron withdrawing 'C≡CPh' fragment [WPt(μ_2-CC≡CPh)$(L_2)(CO)_2$(Tp*)] intermediate rearranges to an isomer in which the PtL_2 fragment coordinates

to the C≡C bond of the propargylidyne [W{≡C–C=C(η^2-PtL$_2$)Ph}(CO)$_2$(Tp*)]. The competition between reductive elimination and *cis-trans* isomerism in the case of the putative *cis*-[WPt(μ_2-C)(C≡CSiMe$_3$)(CO)$_2$(PPh$_3$)$_2$(Tp*)] is further complicated by its reaction with further LiC≡CSiMe$_3$ to afford Li$_{n-1}$[WPt(μ_2-C)(C≡CSiMe$_3$)$_n$(CO)$_2$(PPh$_3$)$_{3-n}$(Tp*)] (n = 2, 3) which appear less prone to reductive elimination.

The empirically observed aptitude for σ-organyl-carbido reductive elimination to afford alkylidynes appears to be H > C≡CR ~ C≡C–C≡[W] > –C$_6$H$_4$Me ≫ CH$_3$. Whilst the mobility of the migratory aptitude of hydrido ligands is to be expected, the ordering of the remaining ligands most likely reflects the availability of organyl π-orbitals(s) for overlap with those of the carbido ligand in the early stages of C–C bond formation.

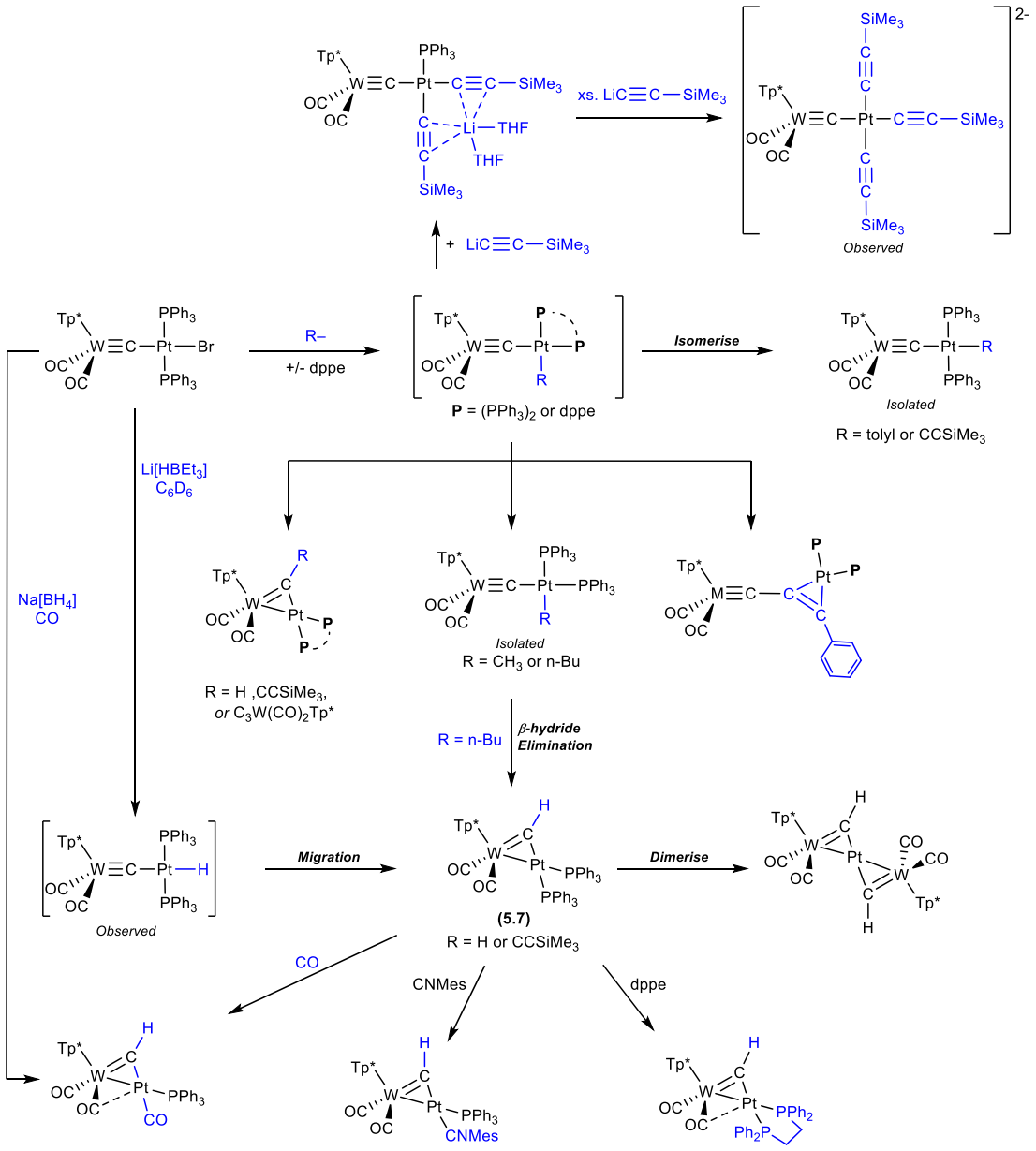

Chart 5.2: Summary of reactivity presented in Chapter Five.

Chapter Six
The Role of Metallacarbynes in Catalytic Coupling Reactions

Studying the reactivity of defined molecular carbidos is a valid method to better understand the Fischer—Tropsch process, which is hypothesised to proceed *via* surface carbides on heterogenous materials.[33] This may be seen as an extension of the 'Cluster-Surface Analogy' championed by Muetterties that "…*discreet, molecular metal clusters may be reasonable models of metal surfaces in the process of chemisorption and of catalysis.*"[16] In contrast to the obscure surfaces of metals or metal oxides/sulphides upon which heterogenous catalytic transformations occur, molecular complexes are amenable to a diverse toolbox of modern spectroscopic and crystallographic techniques and the wealth of data they provide. In a small number of instances, molecular carbidos are implicated in catalysis involving the cross-coupling of C–C,[136-138, 140-141, 144-148, 456] C–P,[94-95, 143] and C–As[149] bonds, though, buoyed by success, these studies did not explore the mechanistic details or the identities of key intermediates. The preceding Chapters contribute to understanding the discrete steps of such cross-coupling reactions: π-coordination (Chapter Two);[457] oxidative addition (Chapter Three);[253] nucleophile installation and reductive elimination (Chapters Four and Five).

As a natural progression, Chapter Six begins with an examination of catalytic reactions proposed to contain μ_2-carbido intermediates, identifying key species for further investigation. As is often the case, productive catalysis ensues at useful rates for *4d* metals while the slower kinetics typical of *5d* metals often affords the opportunity to isolate intermediates. Given the inferred parallels to platinum(II) examples, palladium(II) metallacarbynes will be discussed here in the context of Sonogashira C(*sp*)—C(*sp*) cross-coupling processes, uncovering some intricacies of solvent dependency and the formation of μ_2-phosphoniocarbynes. A brief foray into the little-explored chemistry of η^1-phosphinocarbynes, encountered novel species ultimately relevant to hypothetical coupling of chalcocarbonyl and phosphine ligands. Finally, the emerging principles have been applied to develop and optimise a Suzuki—Miyaura C(*sp*)–C(sp^2) cross-coupling of halocarbyne (electrophilic partner) and boronic acids/esters (nucleophilic partner) manifold to provide the electronic compliment of known Stille cross-coupling of stannyl carbynes (nucleophilic partner) with aryl halides (electrophilic partner).

6.1 Implied μ_2-Carbidos in Catalysis

Several bond forming processes have implied Class B μ_2-carbido intermediates of palladium (primarily), gold, and mercury (Scheme 6.1). Gold and mercury carbidos provide the focus of the subsequent Chapter, whereas prior to this work[3] only one example of a palladium metallacarbyne was known, however, no spectroscopic or structural data accompanied its disclosure. [99]

Palladium-mediated C–C cross coupling processes take many, often eponymous, forms depending on the choice of carbon nucleophilic partner employed, including Songashira (Cu), Suzuki-Miyaura (boron), Negishi (zinc) and Stille (tin) couplings (Scheme 6.2). Recent applications of Stille cross-couplings of stannyl carbyne complexes with alkylhalides and haloarsines implicate μ_2-carbido intermediates which operate through a tin→gold→palladium transmetallation relay. [144-149] Prior to this Bruce and Saitseva had demonstrated the use of gold alkynyls in combination with halocarbynes for the synthesis of carbon-wire systems mediated by a palladium/copper(I) catalyst in which the carbon nucleophilic partner most likely involves a gold→copper→palladium relay. [149] The inclusion of a gold(I) cocatalyst in the Stille-type process suggests the initial μ_2-carbido is of the form [MAu(μ_2-C)(L)(CO)$_2$(Tp*)] which have already been established. [99] Furthermore, Espinet has since explored the role of gold in accelerating more conventional Stille reactions[100] by analogy to 'the copper effect' discussed much earlier by Liebeskind. [458] In the same cross-coupling cycle, transmetallation from gold to palladium is the next step, such that [MPd(μ_2-C)(aryl)(CO)$_2$(PPh$_3$)$_2$(Tp*)] species would be involved analogous to the final step in the C–C and C–P cross-couplings from bromocarbynes (Scheme 6.1). As the heavier platinum congeners have been established, it would seem that the isolating the corresponding palladium metallacarbynes might allow an exploration of these catalytic cross-coupling reactions in more detail.

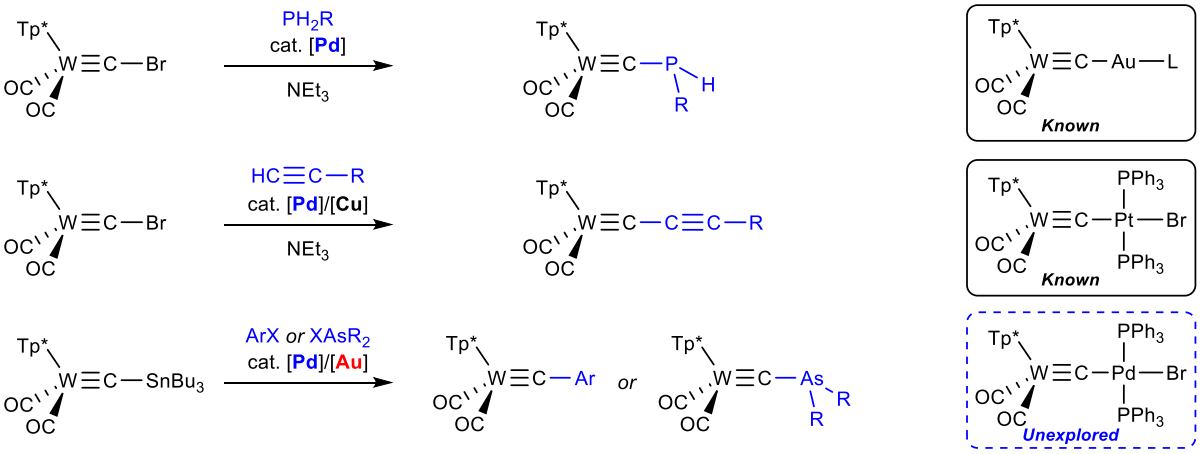

Scheme 6.1: Palladium and gold μ_2-carbido intermediates in representative carbyne cross-couplings.

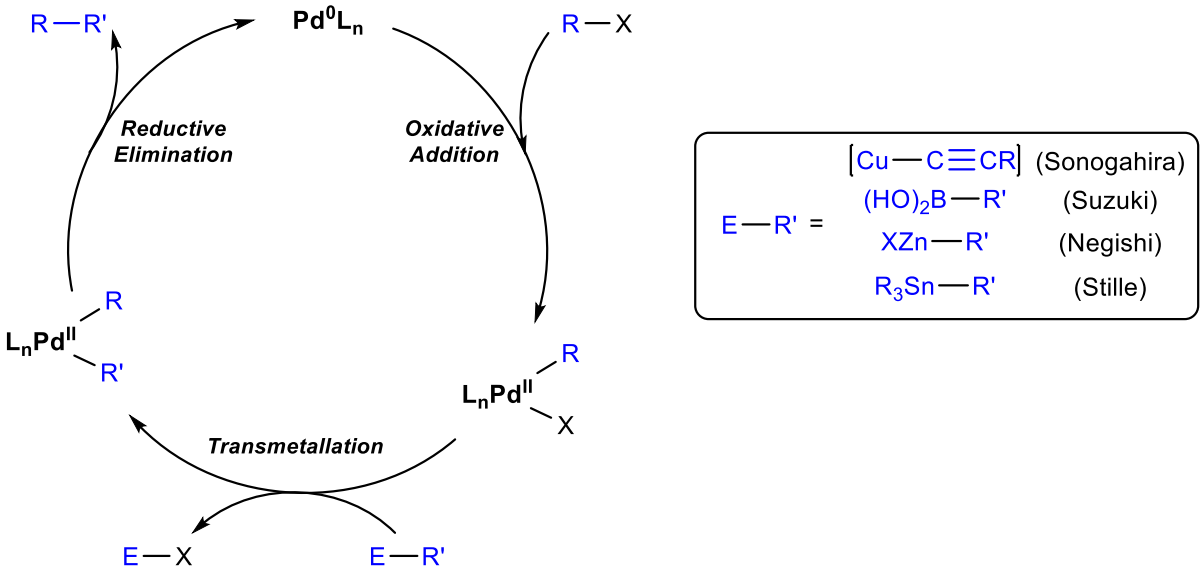

Scheme 6.2: Simplified catalytic cycle of palladium mediated C–C bond forming processes with representative nucleophilic coupling partners. R = aryl or alkyl; X = halide; E = named-coupling partner. Note: Transmetallation is often unique to each reaction but is simplified here for clarity.

6.2 Metallacarbynes and Sonogashira Cross-Couplings

From the three reactions above, coupling of [W(≡Br)(CO)$_2$(Tp*)] with ethynyltrimethylsilane (reminiscent of a Sonogashira cross-coupling)[ttttttttttttttttt] was chosen as a model system for two reasons. Firstly, the ease of manipulating starting materials and the least synthetic steps to prepare reagents was attractive and secondly, the species produced (propargylidynes) are useful building blocks for further reactions as previously discussed.

6.2.1 Palladium(II) metallacarbynes intermediates *via* oxidative addition

Oxidative addition is the initial step for the Sonogashira cross-coupling protocol analogous to the observations made previously for platinum (Chapter Three). Indeed, stirring η^1-bromocarbynes [M(≡CBr)(CO)$_2$(Tp*)] {M = Mo **2.1c**; W **2.1d**} with stoichiometric [Pd(PPh$_3$)$_4$] in C_6D_6 results in full conversion to metallacarbynes [MPd(μ$_2$-C)Br(CO)$_2$(PPh$_3$)$_2$(Tp*)] {M = Mo **6.1a**; W **6.1b**} after ~1 hour at ambient temperature; the lighter congeners of the platinum metallacarbynes [MPt(μ$_2$-C)Br(CO)$_2$(PPh$_3$)$_2$(Tp*)] {M = Mo **3.1a**; W **3.1b**}. The ^{31}P{^{1}H} NMR spectra of **6.1a**/**6.1b** contain two roofed **AB** doublets with a marginally smaller coupling between phosphines ($^2J_{PP}$ = 423–428 Hz) than for the platinum congener (443 Hz). Palladium complexes also exhibit rotational isomers but in smaller populations compared to the platinum analogues. The ^{13}C{^{1}H} NMR spectra reveal high frequency resonances (δ_C = 353.8/333.3) higher than for the platinum analogues (δ_C = 335.7/317.2) and it is unclear whether this is a reflection of greater

[ttttttttttttttttt] The corresponding C–C coupling reactions with HC≡CSiPh$_3$ and HC≡CC≡CSiMe$_3$ to afford propargylidyne and pentadiynylidyne complexes have been shown to be mediated by [Pd(PPh$_3$)$_4$]/CuI. [138, 140]

inductive shielding for the latter, or a greater paramagnetic contribution to shielding for palladium due to a decreased HOMO-LUMO separation. The group 6 metal ν_{CO} absorptions come to higher wave-number for the palladium *cf.* platinum analogues consistent with the heavier group 10 metal demonstrating greater π-basicity due in part to relativistic effects.

Attempts to isolate either palladium metallacarbyne complex encountered issues depending on the group 6 metal and solvent. For molybdenum (Scheme 6.3), attempts to crystallise **6.1a** afford the tetrametallic halo-bridged dimer $[MoPd(\mu_2\text{-}C)(CO)_2(PPh_3)_2(Tp^*)]_2(\mu_2\text{-}Br)_2$ (**6.2**) irrespective of solvent (Figure 6.1). The increased lability of phosphines bound to palladium *cf.* platinum is unsurprising, indeed this lability contributes in part to the greater activity of *4d* metal in catalysis. The Mo–C and C–Pd bond lengths confirm metallacarbyne bonding is retained upon dimerization, and the μ_2-carbido *trans*-influence elongates the bromides more significantly compared to that *trans* to the phosphine (2.5653(8) *cf.* 2.5046(8) Å). The bent Mo–C–Pd linkages (166.1(3)/166.5(3)°) are likely caused by fitting not only the large Tp* and PPh_3 ligands, but the halogen bridge that brings the two units together. The halogen-bridge planes are almost coplanar with each palladium(II) centre indicating an approximate but non-crystallographic mirror plane that includes the four metals (Mo1–Pd1–Pd2–Mo2 = 170.92(2)°). The structure is also apparently (but not crystallographically) centrosymmetric.

Complex **6.2** exhibits a partial tolerance toward organic solvents (less for halogenated or protic examples) that facilitated isolation on a bulk scale and subsequent spectroscopic evaluation. The $^{13}C\{^1H\}$ reveals a broadened resonance consistent with a μ_2-carbido to lower frequency of that for **6.1** (δ_C = 330.8 *cf.* 353.8) owing to the halogen-bridge introducing a second π-donor bromide ligand as opposed to a weakly π-accepting PPh_3. Likewise, the $^{31}P\{^1H\}$ NMR contains a somewhat broadened resonance (δ_P = 26.3; fwhm = 15 Hz) indicative of subtle liberation of the geometry in solution. When the $^{31}P\{1H\}$ NMR spectrum of samples not entirely free of PPh_3 are recorded, the resonance for the free phosphine is sharp indicating that there is no exchange with coordinated phosphine on the ^{31}P NMR timescale. Furthermore, the ^{31}P resonance of **6.2** is also apparent in the cross-coupling mixtures, when **6.1a** was employed as the (pre)catalyst. A further phosphine signal remained but was later inferred as a by-product from tungsten results (*vide infra*).

Isolation of **6.2** provided a potentially relevant species in the Sonogashira cross-coupling manifold, perhaps as a catalyst resting state. However, palladium halide bridges are typically readily cleaved and addition of the chelating phosphine (dppe) disaggregates the dimer at ambient temperature to give bimetallic $[MoPd(\mu_2\text{-}C)Br(CO)_2(dppe)(Tp^*)]$ (**6.3**), which is stable in solution

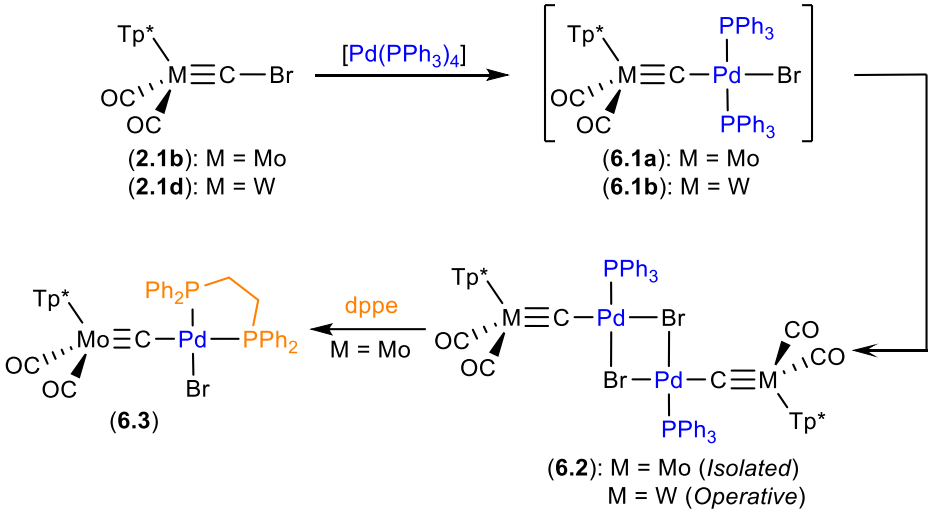

Scheme 6.3: Generation of palladium metallacarbynes in solution and isolation of a halobridged dimer.

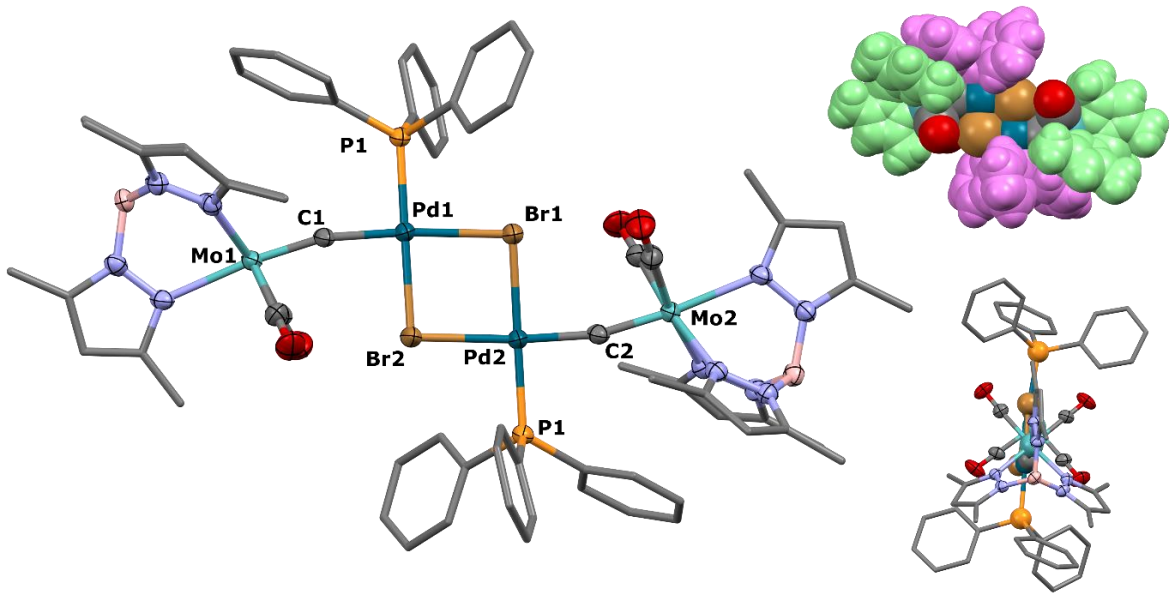

Figure 6.1: Molecular structure of $[MoPd(\mu_2\text{-}C)(CO)_2(PPh_3)_2(Tp^*)]_2(\mu_2\text{-}Br)_2$ (**6.2**) in a single crystal as determined by X-Ray Diffractometry. Ellipsoids are drawn at the 50% probability surface with pyrazolyl and phenyl rings simplified and hydrogens omitted for clarity. Insets: a) Space-filling representation highlighting a partially crowded palladium-bromide core with encumbering *tris*-pyrazolylborate (green) and phosphine (pink) ligands. b) Ball and stick representation as viewed down the key molecular linkage (ligands simplified for clarity). Selected bond lengths (Å) and angles (°): Mo1–C1 1.808(5) Mo2–C2 1.806(6), Pd1–C1 1.923(5), Pd2–C2 1.923(3), Pd1–Br1 2.5653(8), Pd2–Br2 2.5669(8), Pd1–P1 2.268(1), Pd2–P2 2.268(1), Mo1–C1–Pd1 166.1(3), Mo2–C2–Pd2 166.5(4), Pd1–Br1–Pd2 94.04(3), Pd2–Br2–Pd1 93.95(3).

including those in halogenated solvents. This implicates **6.2** as a potentially useful alternative synthetic intermediate for elaborating further palladacarbynes.

Consistent with other metallacarbynes bearing the dppe ligand, **6.3** is less soluble in most solvents, necessitating the use of CH_2Cl_2/CD_2Cl_2 for spectroscopic analysis. The $^{31}P\{^1H\}$ NMR spectrum exhibits broad **AB** doublet resonances accompanied by a second minor set of resonances consistent with the co-existence of two rotational isomers in a ratio of ~ 1:7, where the **AB** coupling is resolved ($^2J_{PP}$ = 33 Hz) unlike platinum homologue **3.3a**. A high frequency signal in the $^{13}C\{^1H\}$ is consistent with a μ_2-carbido and is shifted to higher frequency compared to **6.1a** (δ_C = 375.9 *vs* 353.8). This is attended by a reduction in coupling to the *trans* phosphorus when compared with the platinum congener ($^2J_{CP}$ = 70 *cf.* 77 Hz **3.3b**). Complex **6.3** is a robust species relative to other analogues and single crystals repeatably emerged, but these were of somewhat poor quality (R_1 = 9.6%, Figure 6.2). Caution should be exercised in their interpretation. Critically, the structure confirms metallacarbyne character of **6.3** in a *syn* conformation with unsurprising but imprecise bond lengths (Mo–C: 1.79(1); Pd–C 2.01(1) Å) and an elongated Pd–P bond *trans* to the μ_2-carbido (Pd1–P1 = 2.376(3) *vs* Pd1–P2 = 2.264(3) Å), thereby confirming the first fully characterised, bimetallic palladium metallacarbyne.

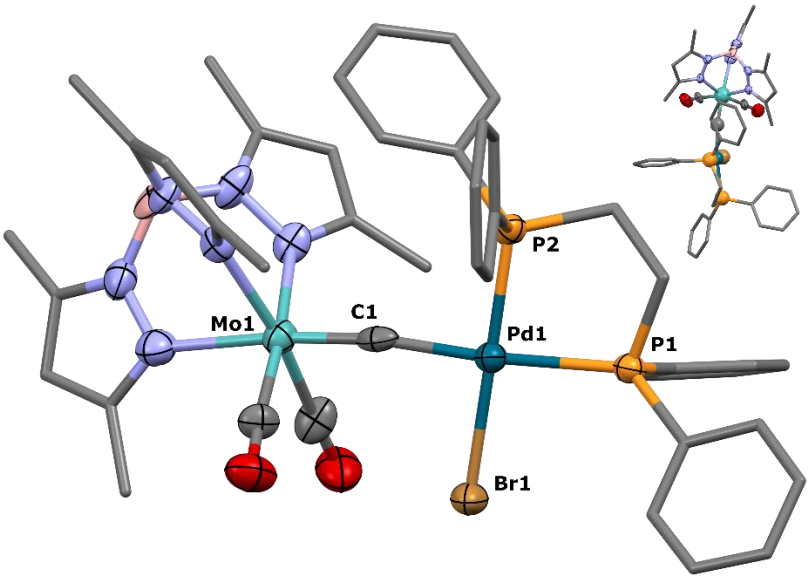

Figure 6.2: Molecular structure of [MoPd(μ_2-C)Br(CO)$_2$(dppe)(Tp*)] (**6.3**) in a single crystal of as determined by X-Ray Diffractometry. A low precision structural model followed from sub-optimal data set. Ellipsoids are drawn at the 50% probability surface with phenyl and pyrazolyl rings simplified and hydrogens omitted for clarity. Inset: Ball and stick representation as viewed down the key molecular linkage (ligands simplified for clarity), Selected bond lengths (Å) and angles (°): Mo1–C1 1.79(1), Pd1–C1 2.01(1), Pd1–P1 2.376(3), Pd1–P2 2.264(3), Pd1–Br1 2.478(2), Mo1–C1–Pd1 167.9(8), P1–Pd1–P2 85.3(1).

6.2.2 Phosphoniocarbyne complexes as off-cycle tangents

Attempts to structurally authenticate the tungsten analogue **6.1b** proved difficult yet ultimately provided more insight to the overall catalytic manifold. Single crystals of **6.1b** were not forthcoming, yet unlike molybdenum, the tungsten complex was not isolated as a halo-bridged dimer. While tungsten halo-bridged dimers cannot be excluded as operative in the catalytic manifold, no evidence for their existence was found during stoichiometric reactions. Instead, attempts at isolating **6.1b** from identical methods to molybdenum afforded the μ_2-phosphoniocarbyne complex [WPd(μ_2-CPPh$_3$)Br(CO)$_2$(PPh$_3$)(Tp*)] (**6.4**), that readily decomposes when removed from a benzene solution. Furthermore, **6.4** contains a labile palladium-bound phosphine and establishes a dynamic equilibrium with a second species [WPd(μ_2-CPPh$_3$)Br(CO)$_2$(Tp*)] (**6.5**) (Scheme 6.4).[459]‡‡‡‡‡‡‡‡‡‡‡‡‡‡‡

This equilibrium initially confounded the identification of **6.4** (Figure 6.3). For tungsten, an irreversible migration of phosphine to the μ_2-carbido established the μ_2-phosphoniocarbyne, controlled by concentration in addition to solvent polarity. Once the μ_2-CPPh$_3$ ligand is formed, a series of fractional recrystallisations is required to isolate **6.4**, but also removes adventitious phosphine such that a broad phosphine resonance (δ_P = 10.73) appears in the $^{31}P\{^1H\}$ NMR spectrum, indicative of dynamic PPh$_3$ coordination. Conversely, measuring isolated **6.4** with extraneous phosphine shifts and sharpens the ^{183}W coupling (δ_P = 13.35; $^2J_{PW}$ = 112 Hz); after which recrystallisation with *n*-hexane removes PPh$_3$ and re-establishes the original broad resonance (Figure 6.3).

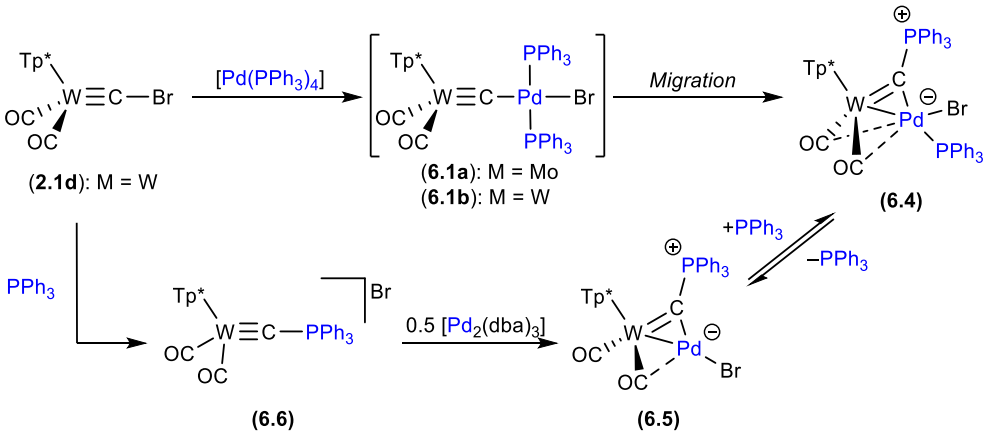

Scheme 6.4: Phosphine migration to form palladium μ_2-phosphoniocarbynes in dynamic equilibrium.

‡‡‡‡‡‡‡‡‡‡‡‡‡‡‡ Original crystallographic data kindly provided by Dr Richard A. Manzano.

To approach the equilibrium forming **6.5**, without the complication of extraneous phosphine, the salt [W(≡CPPh$_3$)(CO)$_2$(Tp*)]Br (**6.6**) was prepared§§§§§§§§§§§§§§§§§§§ and combined with [Pd$_2$(dba)$_3$]·C$_6$H$_6$ to give **6.5**. In the absence of free phosphine, the ^{31}P{^{1}H} NMR spectrum of **6.5** prepared *via* this method exhibits a sharp resonance in the ^{31}P{^{1}H} NMR spectrum (δ_P = 7.18; $^2J_{PW}$ = 119 Hz) bearing a slightly reduced coupling to ^{183}W compared with the η^1-precursor (162 Hz; **6.6**).********** Likewise, the ^{13}C{^{1}H} NMR spectrum contains a sharp signal to higher frequency (δ_C = 232.1; $^1J_{CW}$ = 178 Hz) not broadened by dynamic phosphine coordination and with a larger coupling to ^{183}W compared with the carbonyl ligands. A single environment was observed indicating rapid site exchange of terminal and semi-bridging carbonyls on the ^{13}C timescale. The carbyne signal was not detected for **6.4** owing to the broadening imposed by dynamic phosphine coordination. Addition of PPh$_3$ to a sample of **6.5** establishes the equilibrium with **6.4**, indicating an equilibrium between two species emerged after irreversible formation of

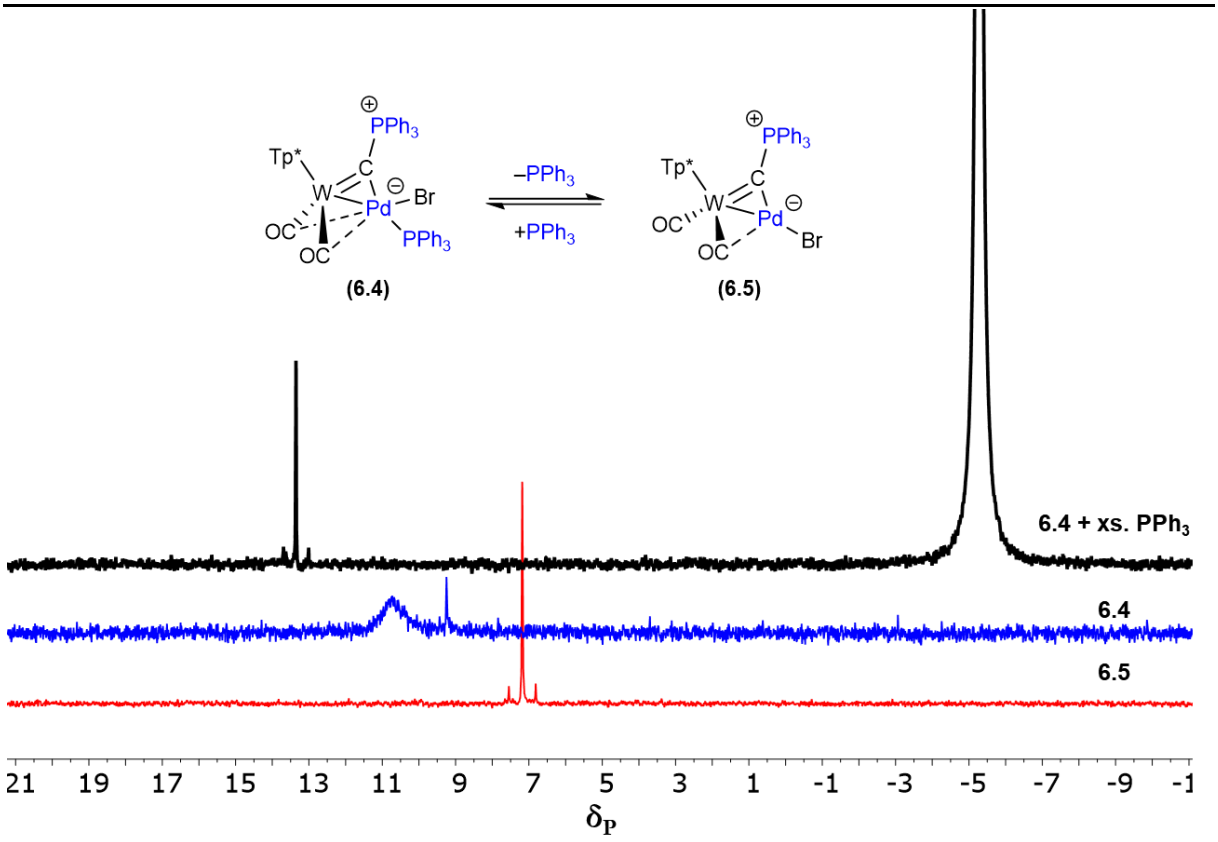

Figure 6.3: ^{31}P{^{1}H} NMR spectra of phosphoniocarbynes showcasing dynamic behaviour.

§§§§§§§§§§§§§§§§§§§[W(≡CPPh$_3$)(CO)$_2$(Tp*)]Br was prepared analogously to the reported [W(≡CPPh$_3$)(CO)$_2$(Tp*)]PF$_6$ to deliver bromide yet avoid complications of PF$_6$. Complex **6.6** is a fully characterised salt but from a well-established protocol (Chapter Nine). [305]

********** The reduction in the value of $^2J_{WP}$ is consistent with the reduction (*ca* $^2/_3$) in *s*-character in the bonding to carbon moving from linear (*sp*) to *pseudo*-trigonal (*sp*^{2}) hybridisation.

a μ_2-$CPPh_3$ species *via* phosphine migration from metallacarbyne **6.1**, potentially undermining catalysis. Furthermore, **6.6** arises from nucleophilic substitution of $[W(\equiv CBr)(CO)_2(Tp^*)]$ in polar solvents where π-coordination to this species represents another mechanism to sequester palladium(0) as a μ_2-phosphoniocarbyne. Each are important considerations for the catalytic manifold.

Aside from potential routes to catalyst deactivation, **6.4**/**6.5** contain features of fundamental interest. A small number of homometallic μ_2-phosphoniocarbynes arise from reactions of phosphorus ylides with high-valent metal centres, [460-463] while **6.4**/**6.5** accompany $[WNi(\mu_2\text{-}PEt_3)Cl(CO)_2(PEt_3)(Tp^*)]$[119] as heterobimetallic species that result from phosphine migrating onto a μ_2-carbido. Concurrent to this work, π-coordination of η^1-phosphoniocarbynes furnished examples of platinum(0) μ_2-phosphoniocarbynes,[214] through methods akin to those that produced **6.5** (Table 6.1). The molecular structure of **6.4** shares some features with $[WNi(\mu_2\text{-}PEt_3)Cl(CO)_2(PEt_3)(Tp^*)]$, however **6.5** is noteworthy given the low coordination number of palladium(0) (14 valence electrons) (Figure 6.4). Given both species can be represented by a zwitterionic description, a positive charge on phosphorus and a negative charge on palladium(0), evident by the carbonyls exhibiting semi-bridging character to compensate for high negative charge; **6.5** contains two semi-bridging carbonyls. Removal of phosphine from **6.4** to **6.5** results in contraction of the W-C bond (*ca* 0.05 Å) indicating palladium is less able to retrodonate to the carbyne. Bond contraction is accompanied by a modest straightening of the W–C–P angle (143.0(3) to 152.8(3)°) previously indicative of semi-bridging character, however, the undercoordinated palladium(0) also likely gives a more pronounced effect. Finally, as the structure of **6.4** is stabilised by two semi-bridging carbonyls, the palladium(0) plane bisects the Tp* ligand more symmetrically (B1–W1–Pd1–P1 = 8.3(6)°) than **6.5**, which deviates to one side (62.3(3)°); this solid-state phenomenon does not necessarily reflect the geometry in solution.

These experiments have isolated a series of species relevant to Sonogashira cross-coupling of halocarbynes and alkynyls. Examination of the spectra allowed assignment of each resonance observed from the stochiometric addition of $[Pd(PPh_3)_4]$ to bromocarbynes **2.1c**/**2.1d**. The only outlier occurs in the $^{31}P\{^1H\}$ spectrum of the molybdenum system (δ_P = 23.56), assigned as a μ_2-$CPPh_3$ species due to similar ^1H and infra-red data, but was not fully characterised. The final series of experiments sought to establish which of the isolated species was catalytically active when reintroduced to the cross-coupling (*i.e.* a pro-catalyst) towards production of $[M(\equiv C\text{–}C\equiv CR)(CO)_2(Tp^*)]$ {M/R = Mo/Ph **6.7a**; Mo/$SiMe_3$ **6.7b**; W/Ph **6.7c**; W/$SiMe_3$ **6.7d**}.

Table 6.1: Spectroscopic parameters of palladium metallacarbynes and phosphoniocarbynes against nickel and platinum congeners.

Complex	δ_C[a] (ppm)	J_{CP} (Hz)	ν_{CO}[b] (cm^{-1})	δ_P[a] (ppm)	J_{PP}[a] (Hz)	$r_{M\equiv C}$ [Å]	$r_{M'-C}$ [Å]	$\angle_{M-C-M'}$ [°]
μ2-carbidos								
[**W**Ni(μ2-C)Cl(PPh_3)2] [119]	484.0[c]	4[c]	1936, 1843	15.74, 8.73[c]	290	1.867(4)	1.808(4)	174.8(2)
[**Mo**Pd(μ2-C)Br(PPh_3)2] (**6.1a**)	353.8[c]	d	1971, 1888[g]	25.9, 20.7[c]	423	–	–	–
[**Mo**Pd(μ2-C)Br(dppe)] (**6.3**)	375.9[e]	d, e	1971, 1884	46.0, 35.5[e]	31	1.79(1)[f]	2.01(1)[f]	167.9(8)
[**Mo**Pd(μ2-C)(PPh_3)2]2(μ2-Br)2 (**6.2**)	330.8[c]	d	1977, 1911, 1897	26.2[c]	–	1.808(6) 1.805(6)	1.922(6) 1.923(6)	166.1(3) 166.5(3)
[**W**Pd(μ2-C)Br(PPh_3)2] (**6.1b**)	333.3[c]	d	1956, 1865[g]	28.81, 23.23	428	–	–	–
[**Mo**Pt(μ2-C)Br(PPh_3)2] (**3.1a**) [142]	339.0	6	1962, 1873	23.8, 19.4	438	1.828(3)	1.951(3)	174.0(2)
[**Mo**Pt(μ2-C)Br(dppe)] (**3.3a**)	377.1	77	1965, 1876	33.60, 32.89	–	1.818(5)	1.981(6)	167.9(3)
[**Mo**Pt(μ2-C)(PPh_3)2]2(μ2-Br)2	–	–	–	–	–	1.810(6) 1.817(6)	1.934(6) 1.926(6)	167.3(3) 166.7(3)
[**W**Pt(μ2-C)Cl(PPh_3)2] (**2.7**)	318.8	7	1945, 1852	28.32, 24.01	443	1.842(4)	1.944(4)	169.0(2)
[**W**Pt(μ2-C)Br(PPh_3)2] (**3.1b**)	318.6 317.1	8 8	1945, 1854	27.0, 21.5 23.3, 23.9	443 444	1.865(6)	1.934(6)	169.2(3)
[**W**Pt(μ2-C)Br(dppe)] (**3.3b**)	356.7	74	1950, 1856	38.10, 34.51	–	1.833(5)	1.990(6)	172.7(4)
μ2-phosphoniocarbynes								
[**W**ni(μ2-CPEt_3)Cl(Pet_3)] [119]	280.9	n.r.[d]	1881, 1767	35.8, 19.24	–	1.946(2)	1.877(3)	84.74(10)
[**W**Pd(μ2-CPPh_3)Br] (**6.5**)	232.1	–	1947, 1791	7.18	–	1.913(5)	2.014(5)	88.0(2)
[**W**Pd(μ2-CPPh_3)Br(PPh_3)] (**6.4**)	n.d.	n.d.	1940, 1809[g]	13.4,[h] 10.7[c]	–	1.962(6)	2.016(6)	86.5(3)
[**W**Pt(μ2-CPMe_2Ph)(COD)] [214]	272.8	10	2037, 1960	14.2	–	1.998(12) 1.976(10)	1.981(10) 1.998(12)	87.8(4) 86.7(4)
[**W**Pt(μ2-CPMe_2Ph)(CNMes)2] [214]	270.8	14	1941, 1853	18.7	–	1.968(5)	1.982(5)	139.6(3)
[**W**Pt(μ2-CPMe_2Ph)(CN^{t}Bu)] [214]	269.6	14	1934, 1846	17.4	–	1.970(6)	1.965(5)	138.1(3)

Notes: [a]Measured in $CDCl_3$ unless specified otherwise. [b]Measured in CH_2Cl_2 unless specified otherwise. [c]Measured in C_6D_6. [d]Coupling not resolved. [e]Measured in CD_2Cl_2. [f]Imprecise structural determination. [g]Measured in THF. [h]Excess PPh_3 present.

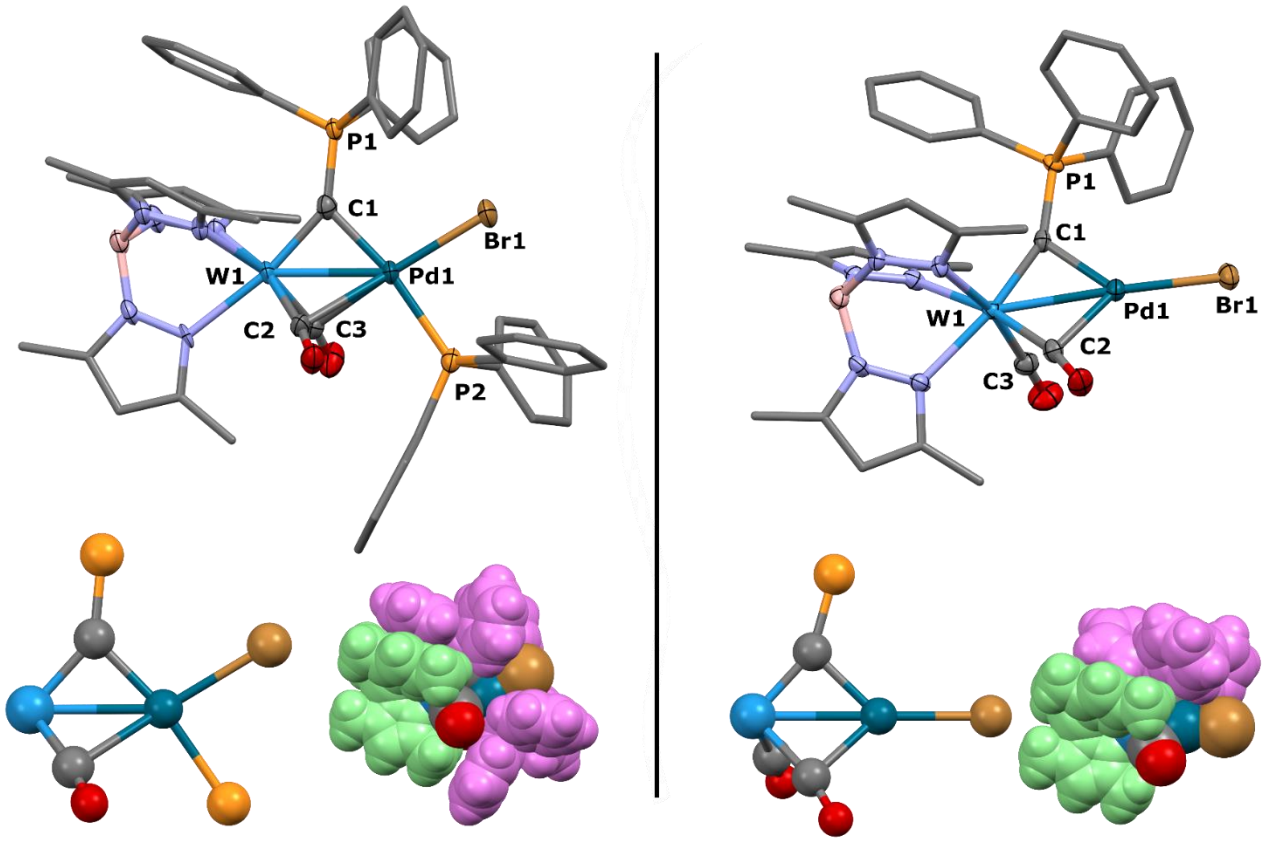

Figure 6.4: A) Molecular structures of [WPt(μ-CPPh$_3$)Br(CO)$_2$(PPh$_3$)(Tp*)] (**6.4**) and [WPt(μ-CPPh$_3$)Br(CO)$_2$(PPh$_3$)(Tp*)] (**6.5**) in single crystals of **6.4** and **6.5**·3(CHCl$_3$), respectively, as determined by X-Ray Diffractometry. Ellipsoids are drawn at the 50% probability surface with phenyl and pyrazolyl rings simplified and CHCl$_3$ solvent and hydrogens omitted for clarity. Insets: a) Ball and stick representation to highlight the coordination of the μ$_2$-CPPh$_3$ about tungsten and palladium, b) Spacefill representations highlighting the increase/decrease in bulk provided by an additional phosphine (pink) in proximity to the *tris*-pyrazolylborate (green) ligand. Selected bond lengths (Å) and angles (°) for **6.4**: W1–C1 1.962(6), Pd1–C1 2.017(7), C1–P1 1.723(7), W1–Pd1 2.7570(5), Pd1–Br1 2.5462(7), Pd1–P2 2.367(2), W1–C2 1.999(6), W1–C3 2.019(8), Pd1–C2 2.598(6), Pd1–C3 2.570(6), W1–C1–P1 143.0(4), Pd1–C1–P1 130.4(4), W1–C2–Pd1 71.4(2), W1–C3–Pd1 71.8(2). Selected bond lengths (Å) and angles (°) for **6.5**·3(CHCl$_3$): W1–C1 1.913(5), Pd1–C1 2.013(5), C1–P1 1.749(6), W1–Pd1 2.7291(4), Pd1–Br1 2.4765(6), W1–C2 2.022(5), W1–C3 2.010(6), Pd1–C2 2.164(5), W1–C1–P1 152.8(3), Pd1–C1–P1 118.4(3), W1–C2–Pd1 81.3(2).

The control reaction used the previously isolated platinum homologue (**3.1b**) where a defined metallacarbyne could be introduced to the cross-coupling system (Scheme 6.5, *vide infra*). A catalytic amount of **3.1b** (10 mol%) afforded trace‡‡‡‡‡‡‡‡‡‡‡‡‡‡‡‡‡ quantities of propargylidynes yet stochiometric addition resulted in appreciable yields (43% **6.7c**; 34% **6.7d**), suggesting platinum metallacarbyne **3.1b** can undergo the forward reaction, but conditions are insufficient to restart the cycle. This is not unexpected, given the reduced kinetics of platinum combined with the reaction being performed at ambient temperature, further implying the catalysis halts at oxidative addition. Meanwhile, this is facile for palladium, supporting **6.1** as the initial species in the cycle. Likewise, 5 mol% of **6.2** (i.e. 10 mol% of Pd) is sufficient to catalyse production of **6.7a**/**6.7b** (66 and 73%, respectively) but catalysis fails if the pro-catalyst is chelated (10 mol% **6.3** gives trace **6.7b**). Finally, complex **6.4** exhibits modest (yet inferior) activity (11% yield **6.7c**; 72% **6.7d**) but likely liberates phosphine to give **6.5**, independently verified as inactive. Alternatively, $[Pd_2(dba)_3]\cdot CHCl_3$ (10 mol% in Pd) did not catalyse propagylidyne formation indicating a phosphine is required to promote oxidative addition. Although there are reports of direct nucleophilic attack at the carbyne carbon of $[W(\equiv CPPh_3)(CO)_2(Tp^*)]^+$,[305-306] it is also inactive under these conditions, thereby representing a terminal tangent to the catalytic manifold. It is plausible that in the absence of phosphine $[Pd_2(dba)_3]\cdot CHCl_3$ provides a source of palladium(0) capable of π-coordination and formation with a trimetallic bow-tie consistent with previous studies. Thus, *e.g.*, attempts to conduct Sonogashira-type elaboration of the 10-bromoanthryl carbyne $[W(\equiv CC_{14}H_8Br\text{-}10)(CO)_2(Tp)]$ were thwarted by sequestration of palladium in the form of the catalytically inactive bow-tie complex $[W_2Pd(\mu\text{-}CC_{14}H_8Br\text{-}10)_2(CO)_4(Tp)_2]$.[148]

Oxidative addition of a bromocarbyne leads to palladium metallacarbyne intermediates that are sensitive to solvent polarity. For molybdenum, an equilibrium with a halo-bridged dimer operates, and while this is not observed for tungsten, is still plausible. For palladium metallacarbynes or the halo-bridged dimer, transmetallation is facile and therefore reductive elimination proceeds to afford propagylidynes. However, irreversible phosphine migration to a μ_2-carbido (accelerated by polar media) results in phosphoniocarbynes that represent pathways for termination of catalysis. It is for these reasons that non-polar solvents should be encouraged to maintain palladium metallacarbynes in solution, minimising phosphine migration (Scheme 6.6).

‡‡‡‡‡‡‡‡‡‡‡‡‡‡‡‡‡ During Chapter Six, 'trace' amounts of products encountered in catalytic reactions will refer to species being identified by TLC, however, not isolated through flash chromatography given milligram quantities.

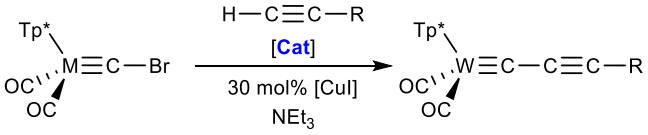

(**2.1b**): M = Mo
(**2.1d**): M = W

(**6.7a**): M = Mo; R = Ph
(**6.7b**): M = W; R = Ph
(**6.7c**): M = Mo; R = $SiMe_3$
(**6.7d**): M = W; R = $SiMe_3$

Entry	M	R	[Cat]	[Cat] mol %	Isolated Yield (%)[a]
1	W	Ph	$[Pd(PPh_3)_4]$	10	78
2	W	$SiMe_3$	$[Pd(PPh_3)_4]$	10	91
3	W	Ph	**3.1b**	10	*trace*
4	W	$SiMe_3$	**3.1b**	10	*trace*
5	W	Ph	**3.1b**	100	43
6	W	$SiMe_3$	**3.1b**	100	34
7	Mo	Ph	**6.2**	5	66
8	Mo	$SiMe_3$	**6.2**	5	73
9	Mo	$SiMe_3$	**6.3**	10	*trace*
10	W	Ph	**6.4**	10	11
11	W	$SiMe_3$	**6.4**	10	72
12	W	Ph	**6.5**	10	*trace*
13	W	$SiMe_3$	**6.5**	10	*trace*
14	W	$SiMe_3$	$[Pd_2(dba)_3]\cdot CHCl_3$	10	*trace*

Scheme 6.5: Evaluation of palladium species as pro-catalysts for production of propagylidynes.

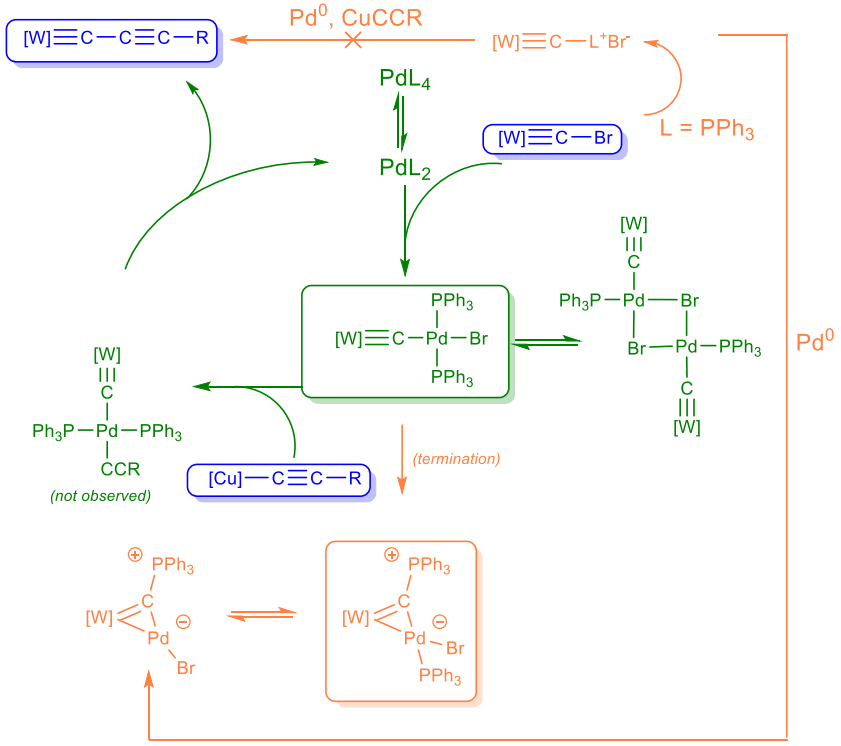

Scheme 6.6: Catalytic cycle for propagylidynes synthesis. Productive catalysis is indicated in green, termination in orange. [W] = $W(CO)_2(Tp^*)$.

6.3 Chalcocarbonylphosphoranes: A sidebar from Phosphoniocarbynes

Phosphoniocarbynes have played a role in carbido chemistry beyond the counter-productive catalysis tangents above. Treating $[W(\equiv CPPh_3)(CO)_2(Tp^*)]^+$ (**6.6**) with lithium triethylborohydride led to the isolation of the terminal methylidyne $[W(\equiv CH)(CO)_2(Tp^*)]$,[179] which could also be deprotonated to provide $[W(\equiv C)(CO)_2(Tp^*)]^-$.[179] Meanwhile, chalcogen (Se and Te) abstraction with phosphine from heavy chalcocarbonyl ligands has provided terminal (η^1) carbido complexes,[464] and while this is just beyond the scope of this work, it provides insight for potential bimetallic species (Scheme 6.7).

The chemistries of chalcocarbonyls and carbidos have also intersected in a number of instances: An additional route to synthesising $[M(\equiv C:)Cl_2(PCy_3)_2]$ (M = Ru, Os) was reported by Johnson and co-workers[15] who demonstrated the thiocarbonyls $[MCl_2(CS)(PCy_3)_2]$ could be desulfurised by the sulfur abstraction agents "$[Mo\{N(^t Pr)Ar\}_3]$" (Ar = 3,5-dimethylphenyl, M = Ru) or $[Ta(silox)_3]$ (silox = OSi^tBu_3, M = Os).[465] Chalcogen abstraction from $[Re(CS)(CO)_2(\eta\text{-}C_5H_5)]$, $[W(NO)(CSe)(CO)(Tp^*)]$ and $[RhCl(CS)(PPh_3)_2]$ afford access to the Class A carbidos $[Re_2(\mu\text{-}C)(CO)_4(\eta\text{-}C_5H_5)_2]$,[17] $[WRe(\mu\text{-}C)(NO)(CO)_3(\eta\text{-}C_5H_5)(Tp^*)]$[61] and $[Rh_2(\mu\text{-}C)Cl_2(PPh_3)_4]$[156] while $[Mo(CSe)(CO)_2(Tp^*)]^-$ provides the tetrametallic Class B carbido $[Mo_2Ir_2(\mu\text{-}C)_2(\mu\text{-}Se_2)(CO)_6(PPh_3)_2(Tp^*)_2]$.[62] Likewise, Mutoh and Ishii have shown PCy_3 can abstract selenium or tellurium from $[Ru_2Cl_2(CE)(dmap)_2(H_2IMes)]$ (E = Se or Te) to return the archetypal terminal ruthenium carbido $[Ru(\equiv C:)Cl_2(PCy_3)_2]$.[464]

Templeton's original trimethylphosphoniocarbyne $[W(\equiv CPMe_3)(CO)_2(Tp^*)]^+$ was found to equilibrate with the carbone complex $[W\{=C(PMe_3)_2\}(CO)_2(Tp^*)]^+$, an observation that raises the question as to whether phosphine dissociation from a phosphoniocarbyne might in turn reveal a cationic carbido centre. Were such an equilibrium to operate, the possibility that elemental sulfur might serve to sequester liberated phosphine was considered, with the caveat that there is considerable precedent for the *addition* of sulfur to metal-carbon multiple bonds. Carbyne complexes have been shown on a number of occasions to react with sulfur to produce either thioacyls or dithiocarboxylates. Treating the osmium carbyne $[Os(\equiv Ctolyl)Cl(CO)(PPh_3)_2]$ with chalcogens results in electrophilic addition across the Os≡C bond to give $[Os(\eta^2\text{-}ECtolyl)Cl(CO)(PPh_3)_2]$ (E = S, Se, Te[###############]) including the first examples for selenium and tellurium.[182] A thioaroyl complex is also formed as $[Ru(\equiv CPh)Cl(CO)(PPh_3)_2]$ cleaves a C–S bond of CS_2 to give the thioaroyl $[Ru(\eta^2\text{-}SCPh)Cl(CS)(PPh_3)_2]$ accompanied by carbonyl ejection and thiocarbonyl formation.[466] Electrophilic addition of chalcogens can occur more than once for group 6 species to give chalcocarboxylates such as $[W(\varkappa^2\text{-}E_2CR)(CO)_2(Cp)]$,[467] indeed double addition is difficult to prevent

[###############] For E = O, the toluoyl complex $[Os(\eta^2\text{-}OCtolyl)Cl(CO)(PPh_3)_2]$rearranges to the σ-tolyl complex $[Os(tolyl)Cl(CO)_2(PPh_3)_2]$

unless single-atom delivery agents such as propylene sulfide (SC_3H_6) and SeCNMes are used as sources of the chalcogen (Scheme 6.8D). [468-469] In select instances, inherent differences in carbyne reactivity can dictate addition of elemental chalcogens. For example, addition of elemental selenium to the phosphinocarbyne [W(≡CPPh$_2$)(CO)$_2$(Tp*)] results in oxidation to [W{≡CP(=Se)Ph$_2$}(CO)$_2$ (Tp*)], whilst addition of S_8 produces [W{≡CP(=S)Ph$_2$}(CO)$_2$(Tp*)] with [W{η^2-SCP(=S)Ph$_2$}(CO)$_2$(Tp*)] as a minor product. [470] Curiously, oxidation of the phosphine deactivates the carbyne towards further electrophilic attack.

The last reaction exemplifies two key observations for addition to analogous phosphoniocarbynes. Firstly, oxidation of phosphinocarbynes occurs given the lone pair, while this is unavailable to a phosphoniocarbyne. Secondly, the oxidised carbyne was not amenable to further electrophilic attack, hence a phosphoniocarbyne may be less likely to react at the W≡C bond, instead delivering more interesting activity, perhaps even liberating a carbonium ligand. Ultimately, this was found to not be the case, and while it forms a tangent to μ_2-carbido synthesis, the discoveries are of sufficient interest to be discussed in the context of phosphoniocarbynes *vide supra*.

Treating **6.6.PF$_6$** with elemental sulfur in THF at ambient temperature results in no appreciable reaction, however, heating at reflux provides a vibrant blue species identified as the thiophosphorane complex [W(η^2-SCPPh$_3$)(CO)$_2$(Tp*)]PF$_6$ (**6.8**). The initial formulation as a thiocarbonylphosphorane (SCPPh$_3$) as opposed to a thiocarbonyl-phosphine complex (CS/PPh$_3$) was supported by the absence of ν_{CS} vibrations (1200–1350 cm^{-1}) of the intensity that would be expected for a thicarbonyl ligand, [471] while the blue colour recalls that of thioaroyl[468, 472] and selenoaroyl[473] complexes of tungsten and molybdenum. The structure was verified through X-ray diffraction studies, thus **6.8** represents a sulfur attack at the W≡C bond and not at phosphorus as observed previously for *phosphino*-carbynes (Scheme 6.9).

Alteration of W–C bonding is clear in the $^{13}C\{^1H\}$ NMR spectrum as a relatively low frequency signal is observed for the carbyne (δ_C = 220.7) accompanied by a shifted $^{31}P\{^1H\}$ resonance with reduced coupling to ^{183}W (δ_P = 26.8; $^2J_{PW}$ = 21 Hz). Both changes in chemical shift and coupling are consistent with reduced W–C bond order and s-character accompanying ligand bending compared to precursor **6.6**. Sulfuration weakens the W–C bond evidenced through a more π-basic tungsten centre (ν_{CO}: 2006, 1919 cm^{-1}). The W–C bond is somewhat short (1.956(5) Å), which in addition to a short C–S bond (1.702(6) Å), indicates multiple bonding character in each (Figure 6.5). However, the W–S distance is relatively long (2.560(2) Å) compared with thiolato ligands bound to seven-coordinate tungsten such as [W($\varkappa^1$-S$_2$CNEt$_2$)(η^2-PhC≡CH)(CO)(Tp*)] (2.397(2) Å). [474-476] Such observations suggest the bonding of the thiocarbonylphosphorane is best described as a combination of thioacyl and metallathirene character contributing to the observed structure.

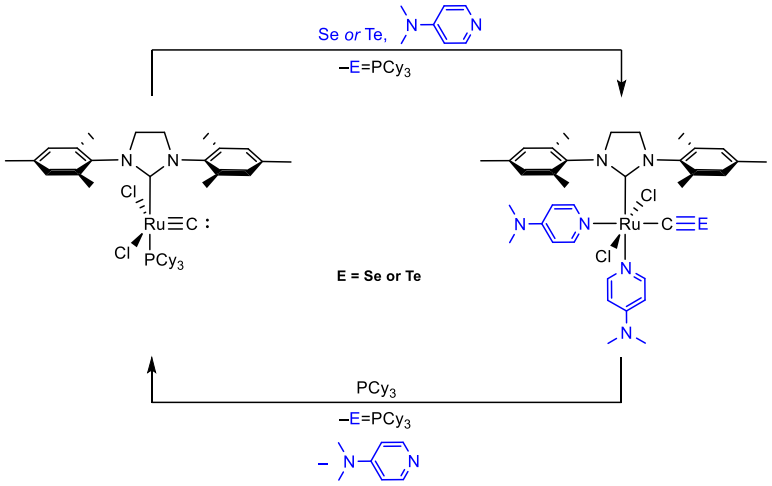

Scheme 6.7: Terminal carbido complexes *via* chalcogen/phosphine transformations.

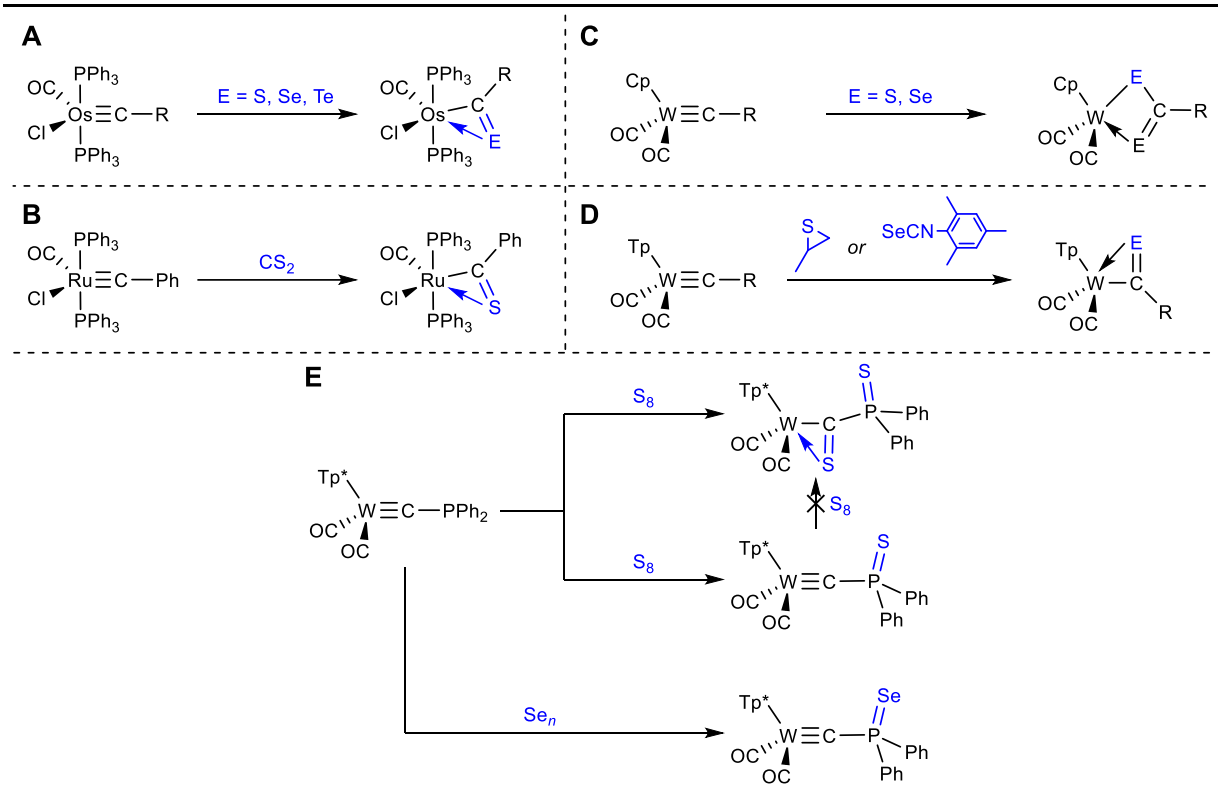

Scheme 6.8: Selected examples of chalcogen addition across carbynes. R = tolyl.

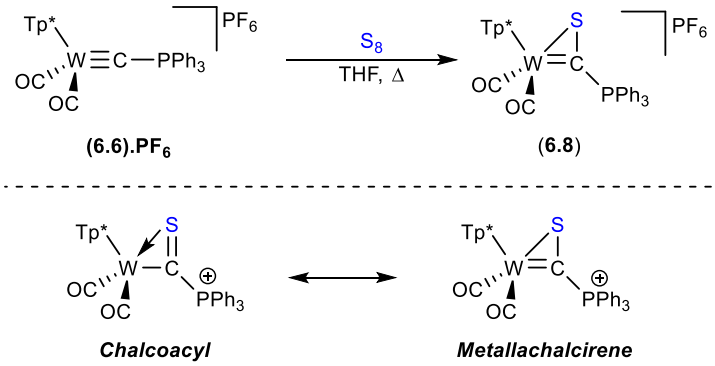

Scheme 6.9: Synthesis of a thiocarbonylphosphorane *via* a phosphoniocarbynes and sulfur.

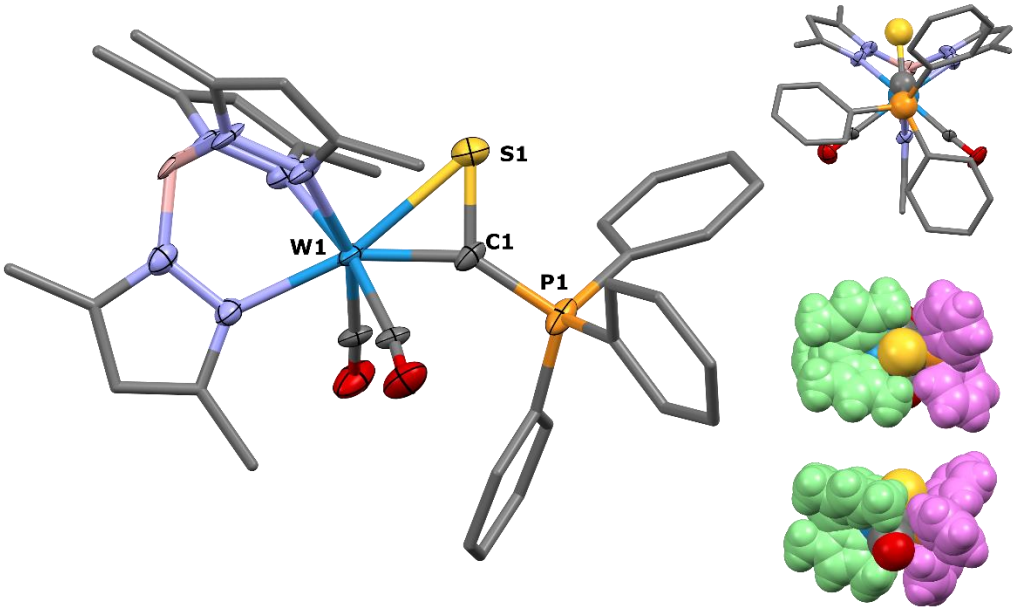

Figure 6.5: Molecular structure of [W(η²-SCPPh₃)(CO)₂(Tp*)]PF₆ (**6.8**) in a single crystal of **6.8**·C₇H₈ as determined by X-Ray Diffractometry. Ellipsoids are drawn at the 50% probability surface with phenyl and pyrazolyl rings simplified and C₇H₈ solvent, PF₆ counter-anion and hydrogens omitted for clarity. Insets: a) Ball and stick representation as viewed down the key molecular linkage, b) Spacefill representation highlighting the protruding sulfur amongst phosphine (pink) and the *tris*-pyrazolylborate (green) ligands. Selected bond lengths (Å) and angles (°): W1–C1 1.956(5), C1–S1 1.702(6), S1–W1 2.560(2), C1–P1 1.794(6), W1–C1–P1 147.6(3), W1–C1–S1 88.6(2), P1–C1–S1 123.7(3), C1–S1–W1 49.8(2).

To further explore the bonding of the thiocarbonylphosphorane, the geometry of [W(η²-SCPMe₃)(CO)₂(Tp)]⁺ (**6.8***) was optimised [DFT: ωB97X-V/6-31G*/LANL2Dζ(W)], returning Löwdin bond orders of the W–C (1.61), C–S (1.23) and W–S (1.037) bonds that agree with the empirically measured structure (Figure 6.6) and contributory canonical forms (Scheme 6.9). The HOMO comprises the W–C multiple bond that is anti-bonding relative to the sulfur 'lone pair'. At lower energy, the HOMO–9 represents the constructive π-bonding of W–C–S consistent with metallathiirine character. Moreover, the LUMO represents anti-bonding metallathiirine character at carbon, and an empty π* orbital of the C–P bond. To ascertain sites of potential reactivity, atom-condensed Fukui functions (*f*) were calculated and determine that sulfur represents the most nucleophilic site (f^- = 0.260) of **6.8***, while both carbons in the CO and SCPMe₃ ligands are electrophilic and may be susceptible to nucleophilic attack (f^+ = 0.02 and 0.14, respectively), the latter more so. Time-dependent DFT methods were used to predict a theoretical UV–Vis spectrum that helps to explain the characteristic vibrant blue colour. Excitation from the W–C multiple bond to the π* of C–P (HOMO→LUMO) is responsible for the maxima (λ_{MAX} = 627 nm). However, in addition, minor contributions of LMCT character (HOMO→LUMO+1/HOMO–1→LUMO) are also identified (calc. 452/456 nm) to moderate the observed colour.

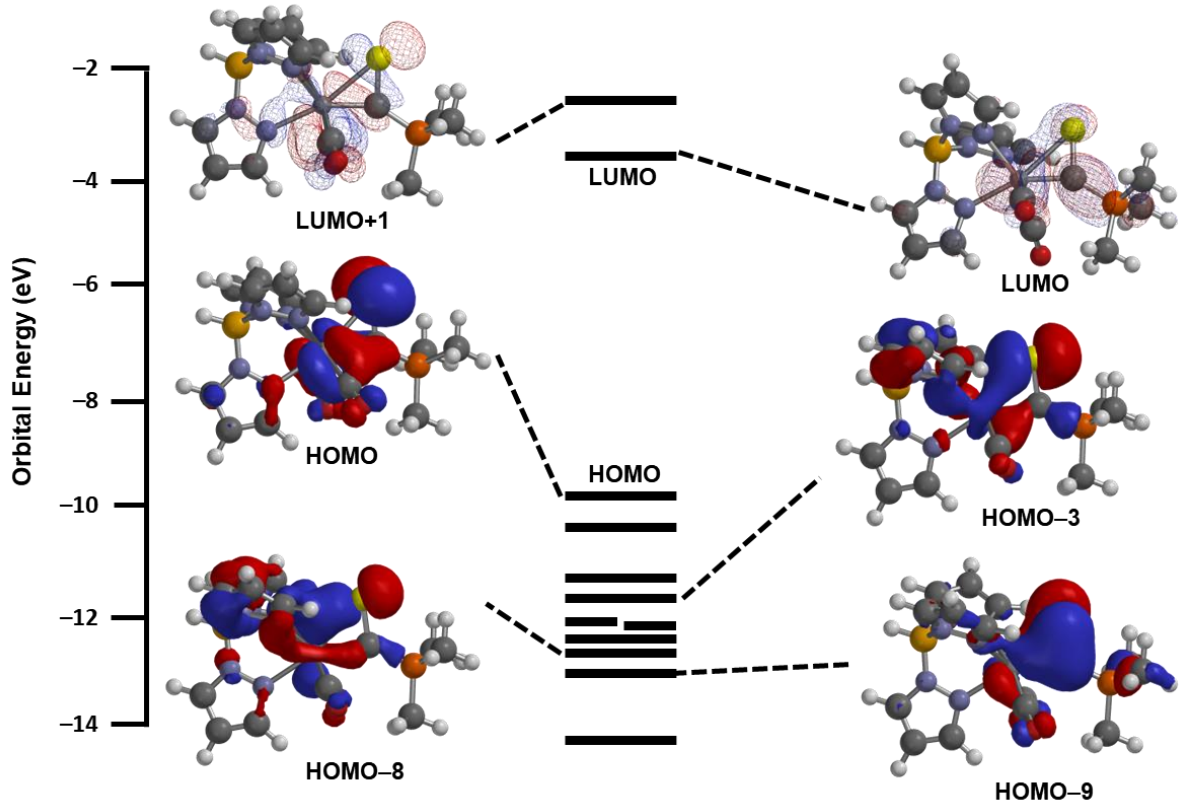

Figure 6.6: Frontier molecular orbitals of $[W(\eta^2\text{-}SCPMe_3)(CO)_2(Tp)]^+$ (**6.8***).

6.3.1 Thiocarbonylphosphoranes varying electronic (ν_{CO}) and steric (Θ) parameters

Formation of **6.8** shows that a phosphoniocarbyne serves as a precursor to the first thiocarbonylphosphorane complex. Templeton has prepared a series of phosphoniocarbynes complexes including **6.6**,[305-306] that contain phosphonio termini for which the corresponding phosphines present a range of various Tolman electronic (ν^T_{CO}) and steric (Θ) parameters,[268] that might be expected to be useful in exploring the thiocarbonylphosphorane formation (Scheme 6.10).

Heating $[Mo(\equiv CPPh_3)(CO)_2(Tp^*)]PF_6$ (**6.9**)§§§§§§§§§§§§§§§§§§§§ with elemental sulfur provides the lighter congener $[Mo(\eta^2\text{-}SCPPh_3)(CO)_2(Tp^*)]PF_6$ (**6.10**) demonstrating similar reactivity ascending group 6 (the requisite chromium precursor remains unknown). Smaller, more electron releasing phosphines were found to facilitate the reaction, producing $[W(\eta^2\text{-}SCPR_3)(CO)_2(Tp^*)]PF_6$ {R_3 = $PMePh_2$ **6.11**; PMe_2Ph **6.12**} in two hours instead of four. Likewise the electron releasing, but sterically larger $[W(\eta^2\text{-}SCPCy_3)(CO)_2(Tp^*)]PF_6$ (**6.13**) complex could be produced but required prolonged heating (*ca* 18 hours, 60 °C) to circumnavigate the large phosphine (Θ = 170°).[268] Complex **6.13** is clearly strained as storage

§§§§§§§§§§§§§§§§§§§§ Phosphoniocarbynes of molybdenum were previously unknown but **6.9** could be prepared employing Templeton's substitution conditions. Complex **6.9** is fully characterised (Chapter Nine) but return similar values not worthy of specific discussion. The phosphoniocarbynes used here were obtained from the bromo- rather than chlorocarbyne but using the same conditions.

in solution at ambient conditions results in the return of $[W(\equiv CPCy_3)(CO)_2(Tp^*)]PF_6$ ($t_{½}$ ~ 10 hours), presumably through sulfur ejection and reformation of the W≡C bond.

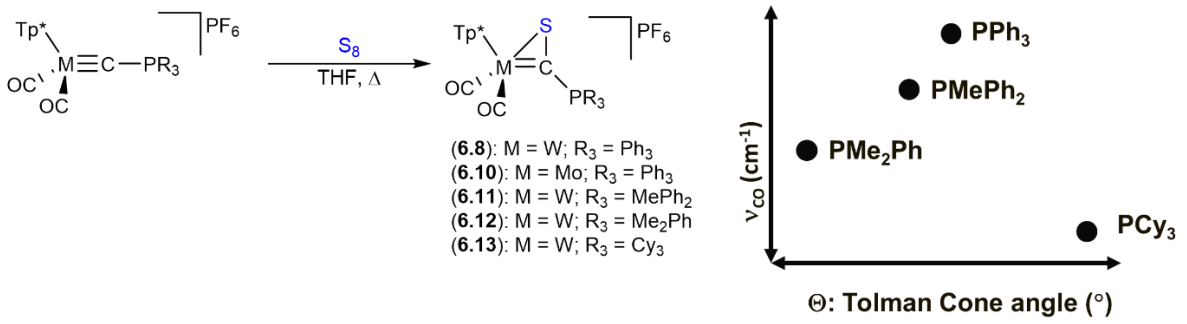

Scheme 6.10: Synthesis of thiocarbonylphosphoranes with select phosphines.

Similar spectroscopic trends emerge between phosphoniocarbynes and the resulting thiocarbonylphosphoranes. The key $^{13}C\{^1H\}$ and $^{31}P\{^1H\}$ NMR data for the acyl carbon and phosphine, respectively, are similarly rather invariant, within 5 ppm, across the series, with little variation in coupling ($^1J_{CP}$ and $^2J_{PW}$) (Figure 6.7). Infra-red spectra reveal carbonyl vibrations over a comparatively narrow range, such that despite a range of Tolman electronic parameters from PPh_3 (ν^T = 2068.9 cm^{-1}) to PCy_3 (ν^T = 2056.4 cm^{-1}),[268] this variation in basicity is not transmitted to tungsten or the thioacyl carbon, although subtle changes in apparent colour occur as quantified by electronic spectra. The most striking feature of thiocarbonylphosphoranes are the colours and subtle changes in phosphine result in changes in electronic spectra (Figure 6.8), consistent with the observations above that the primary origin of colour involves charge transfer from the metallathiirene core to an orbital that is π*-antibonding along the C–P vector. The inferred strain in the PCy_3 complex **6.13** most likely accounts for it being the greatest outlier with reduced coupling constants ($^1J_{CP}$ and $^2J_{PW}$) and δ_C/δ_P values indicative of a more strained $SCPR_3$ environment. Moreover, **6.13** co-crystallised with $[W(\equiv CPCy_3)(CO)_2(Tp^*)]PF_6$ (one crystal containing two molecules), consistent with observations of sulfur ejection, thereby preventing structural elucidation.

Growing single crystals of thiocarbonylphosphoranes proved difficult in general; no samples grew of **6.12** despite multiple conditions, while blue rods of **6.10** failed to diffract when irradiated with a synchrotron source. While spectroscopic data are analogous to **6.8**, a crystal of **6.11** was grown (Figure 6.9) containing a contracted P–C1 bond (1.767(3) *vs* 1.794(6) Å) indicative of increased basicity (ν^T_{CO}) or decreased steric obstruction for $PMePh_2$ compared with PPh_3. Conversely, the W–C (1.987(8) Å) and C–S (1.716(3) Å) bond are longer suggesting reduced metallathiairine character but with the W–S bond remaining similar.

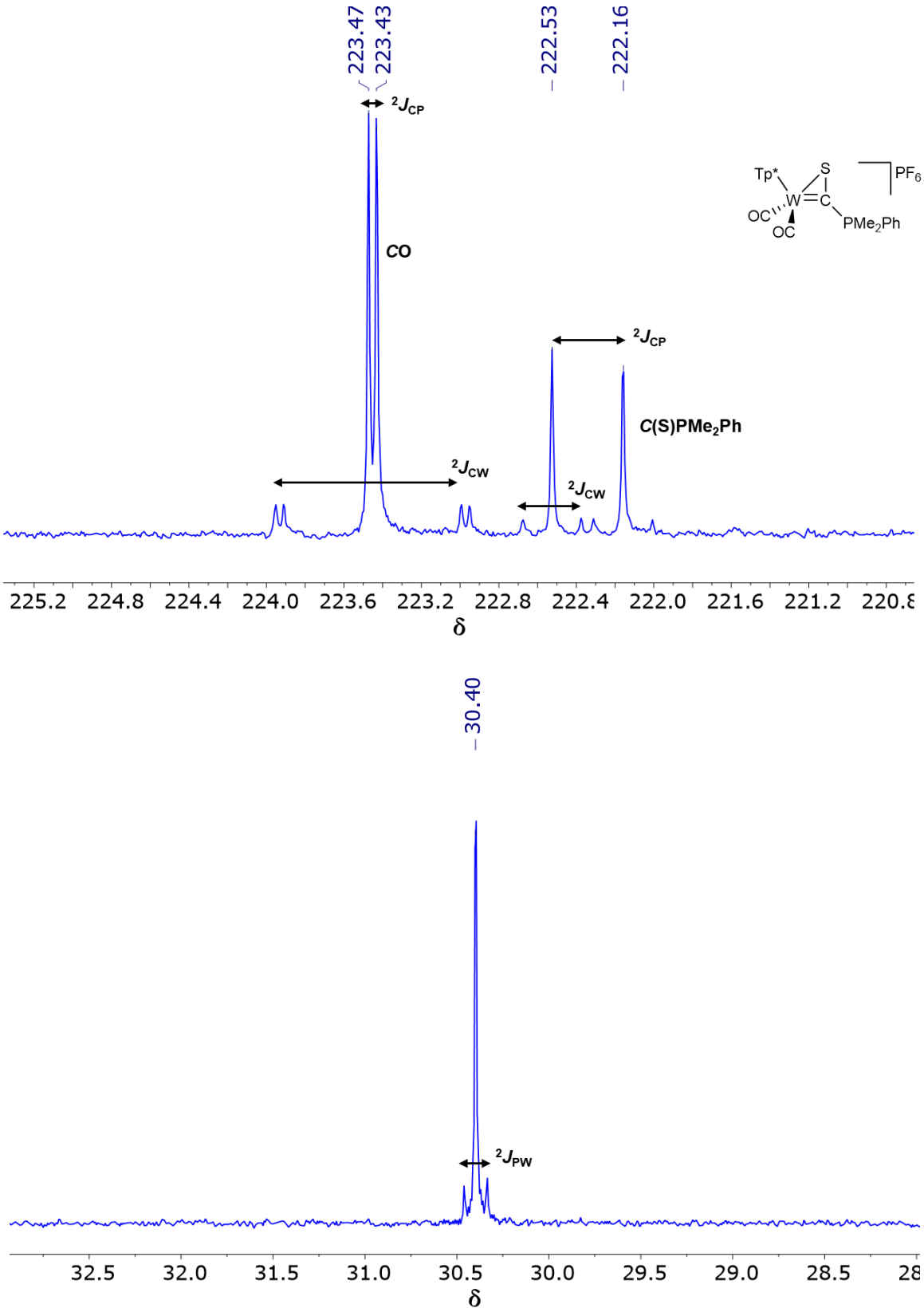

Figure 6.7: $^{13}C\{^1H\}$ and $^{31}P\{^1H\}$ resonances displaying distinctive ^{183}W coupling in thiocarbonylphosphoranes with $[W(\eta^2\text{-}SCPMe_2Ph)(CO)_2(Tp^*)]PF_6$ (**6.12**) as an example.

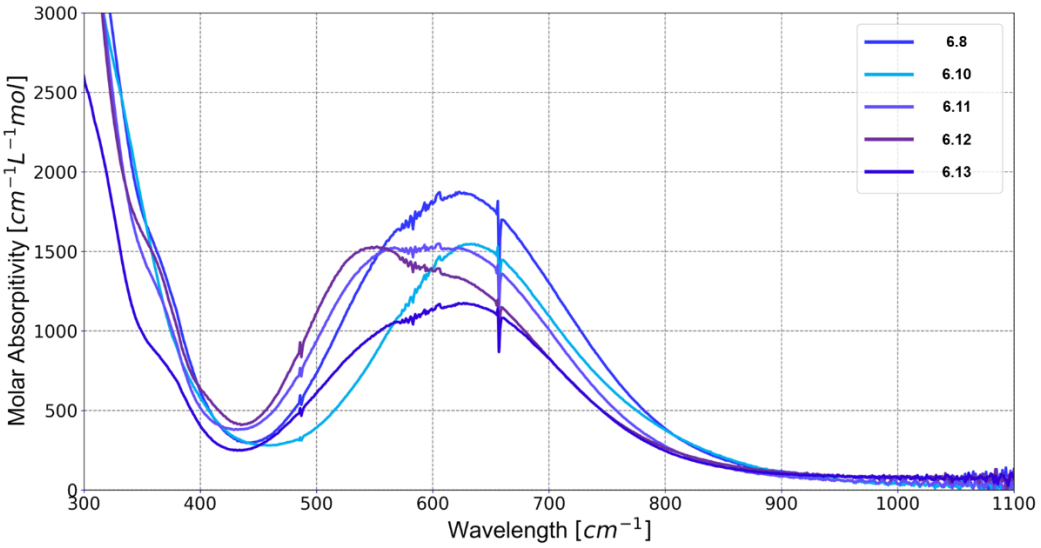

Figure 6.8: Electronic spectra of thiocarbonylphosphoranes $[M(\eta^2\text{-}SCPR_3)(CO)_2(Tp^*)]PF_6$. Line colours coordinate with observed solution colour.

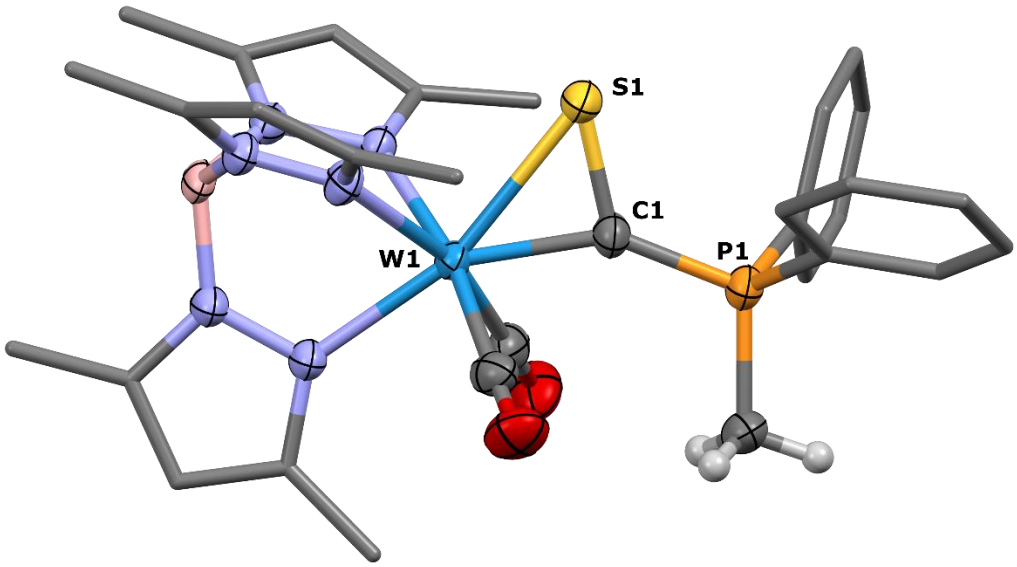

Figure 6.9: Molecular structure of $[W(\eta^2\text{-}SCPMePh_2)(CO)_2(Tp^*)]PF_6$ (**6.11**) in a single crystal of **6.11**·2(CH_3CN) as determined by X-Ray Diffractometry. Ellipsoids are drawn at the 50% probability surface with phenyl and pyrazolyl rings simplified and CH_3CN solvent, PF_6 counter-anion and hydrogens omitted for clarity. Selected bond lengths (Å) and angles (°): W1–C1 1.978(3), C1–P1 1.767(3), C1–S1 1.716(3), W1–S1 2.564(1), W1–C1–P1 147.2(2), P1–C1–S1 124.8(2), C1–S1–W1 50.4(1).

6.3.2 Exploring heavier chalcopnitconioranes

Given facile production of thiocarbonylphosphoranes, heavier congeners in either selenium or arsenic were considered (Scheme 6.11). Heating of $[W(\equiv CPMe_2Ph)(CO)_2(Tp^*)]PF_6$ with grey selenium in pursuit of a selenocarbonylphosphorane $[W(\eta^2\text{-}SeCPMe_2Ph)(CO)_2(Tp^*)]$ resulted in no conversion over 1 week, even when heated at reflux. Reduced solubility of grey selenium also plagued the synthesis of selenoaroyl complexes such as $[Mo(\eta^2\text{-}SeCC_4H_3S\text{-}2)(CO)_2(Tp)]$ [469] and $[Os(\eta^2\text{-}SeCC_6H_4Me\text{-}4)Cl(CO)(PPh_3)_2]$. [182] To combat the reduced solubility, a repeat reaction included a drop of *N*-methylimidazole (a method of activating selenium championed by Rauchfoss) [477] resulting in an intense blue species, although the compound defied isolation.

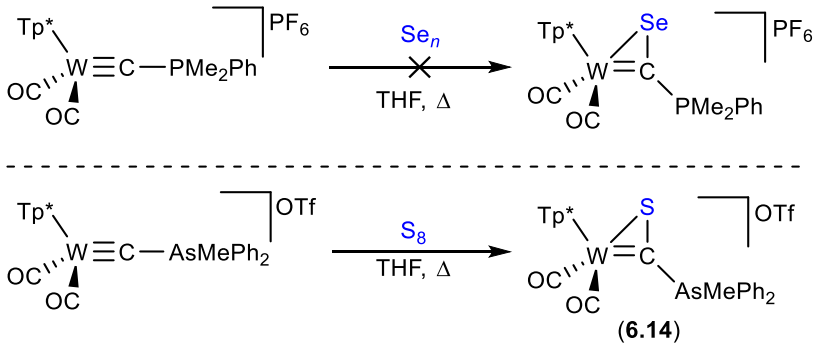

(**6.14**)

Scheme 6.11: Investigations into heavier analogues of thiocarbonylphosphoranes with selenium and arsenic.

Studies utilising selenium were not met with success but the recent emergence of an arsoniocarbyne provided an entry to a heavier pnictogen analogue. Though most likely viable, stibonio and bismuthonio carbyne remain at present unknown. Arsines are much less nucleophilic than phosphines and therefore *arsonio*-carbynes cannot be produced *via* substitution of a halocarbyne. Instead, methylation of the *arsino*-carbyne $[W(\equiv CAsPh_2)(CO)_2(Tp^*)]$ with MeOTf gives the *arsonio*-carbyne $[W(\equiv CAsMePh_2)(CO)_2(Tp^*)]OTf$. [478] Heating this salt with elemental sulfur gives the thiocarbonyl-*arsorane* $[W(\eta^2\text{-}SCAsMePh_2)(CO)_2(Tp^*)]OTf$ (**6.14**) as the heavier congener of **6.11**. Spectroscopic features of the arsorane conform to values of the analogous phosphorane, with a slightly lower frequency thioacyl-carbon resonance (δ_C = 226.0), now devoid of multiplicity. The thiocarbonylarsorane was much more sensitive and difficult to purify, owing to elimination of unidentifiable grey/brown detritus. For this reason, purification was not successfully achieved. Likewise, the apparent instability meant that single crystals were not afforded instead precipitating amorphous black and brown solids, and the lilac-coloured compound deteriorated in solution prior to quantification *via* UV-Vis electronic spectroscopy.

6.3.3 Theoretically addressing chalcocarbonyl/phosphine coupling

Formation of η^2-$SCPR_3$ ligands on a metal centre is of fundamental interest but the composition of thiocarbonylphosphoranes raises a more profound question in organometallic chemistry. Despite

thousands of structures that possess cis-disposed CO and PR_3 ligands, why is there yet to be an example of their coupling (*i.e.*, an O=C=PR_3 ligand)? Isoelectronic σ-silyl ligands (SiR_3) have been found to migrate to carbonyl,[479-480] isocyanide[481-487] and thiocarbonyl[488-489] ligands, while CO has inserted into metal *phosphido* bonds (Scheme 6.12).[490] Heteroacyls may provide a bidentate coordination geometry to satisfy electron requirements, and also match both hard (oxophillic) d^0 metal centres *via* a η^2-acyl interaction (O, N), and soft (late) centres through more contribution of a metallathiirene (S, Se, Te) canonical form. Combining CO with PR_3 would provide complexes with O=C=PR_3 ligands which remain unknown, as do the free molecules, but S=C=PR_3 species have now been constructed in the coordination sphere of group 6 metal centres (*vide supra*). Otherwise, the closest example of carbonyl and phosphine conversion is the formation of phophaketene (O=C=PR) complexes *via* coupling of CO with phosphinidenes (PR)[491] and one example of a similar phosphorylthioacyl ($SCP(S)R_2$) complex is known.[307]

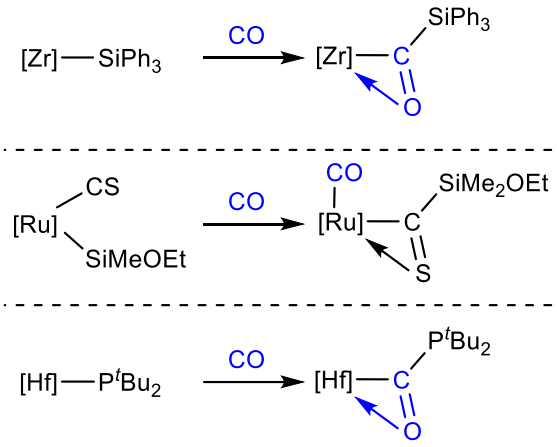

Scheme 6.12: Examples of heteroacyls related to CO migration and insertion. [Zr] = $ZrCl(Cp^*)_2$; [Ru] = $RuCl(PPh_3)_2$; [Hf] = $HfCl_2(Cp^*)_2$.

Specifically considering ligands as free molecules, the larger E=C=C=PPh_3 (E = O, S) are well-established, synthetically versatile reagents[492-493] as are, to a lesser extent bis(phosphonio)chalcocarbonyls E=C$(PPh_3)_2$,[494] but free carbonylphosphoranes or thiocarbonylphosphoranes (S=C=PR_3) remain unknown. To begin a theoretical investigation of these species as ligands, the first query is to ascertain the plausibility of each molecule, removed from the coordination sphere of a transition metal. Computational optimisation [DFT: ωB97X-V/6-31G*/LANL2Dζ(Se/Te)] of chalcophosphoranes E=C=PMe_3 (E = O, S, Se, Te) each resulted in geometries containing a shared imaginary frequency corresponding to oscillation of the carbon orthogonal to the E···P vector. Conversely, calculations of extended species E=C=C=PR_3 (E = O, S; R = H, Me) in addition to S=C$(PMe_3)_2$ at the same level of theory provided satisfactory geometries devoid of imaginary frequencies, thus suggesting E=C=PR_3 molecules with a linear E–C–P spine are unlikely to be stable in the free state. The imaginary frequency oscillates between linear and the bending at carbon found in geometries observed in thiocarbonylphosphorane complex structures (also a corollary of a Dewar-Chatt-Duncanson description

of thioketene coordination),[495-503] lending support to E=C=PR_3 acting as ligands (not free molecules), with a geometry consistent with discovery of sulfur examples. Within the chemistry of group 6 metals, the thioketene complexes [Mo{S=C=CtolylC(O)S}(=O)(Tp*)][504] and [W(S=C=CHSCH_2Ph)I(O)(Tp*)][505] have M–C–C angles of 150.0(5)° and 137.1(3)°, respectively while the C–S bond lengths (1.658(6) and 1.699(3)Å, respectively, *cf.* 1.716(3)Å for 6.11) point to a degree of multiple bond character. The suggested analogy between thioketenes and thiocarbonyl phosphoranes is not unlike current perspectives that draw parallels between phosphine and N-heterocyclic carbene (a.k.a. 'bent allenes') stabilisation of carbones,[506] *viz.* $C(NHC)_2$ *cf.* $C(PR_3)_2$.

While each species is a plausible ligand, theoretical studies were conducted to explore why chalcocarbonyl-phosphine coupling is yet to be observed (while recognising the dearth of heavier chalcocarbonyls for study).[116] Theoretical models were optimised for both precursors *cisoid*-$[W(CE)(CO)_2(PMe_3)(Tp)]^+$ {E = O, S, Se, Te and NMe} and the corresponding coupled products $[W(\eta^2\text{-}ECPMe_3)(CO)_2(Tp)]^+$. Initial calculations for $[W(CS)(CO)_2(PMe_3)(Tp)]^+$ and $[W(\eta^2\text{-}SCPMe_3)(CO)_2(Tp)]^+$ in the gas-phase suggested significantly differing dipoles (2.71 and 6.17 Debye, respectively) indicating the polarity of the surrounding media might play a role. Given that the thiocarbonylphosphoranes were found to be stable in THF, a polarisation continuum ($\varkappa$ = 7.43) was added to the models to best approximate the real-world environment so that thermodynamic properties could be calculated in search of possible trends (Figure 6.10).

For heavier chalcogens, the energies of chalcocarbonylphosphorane complexes are favoured over chalcocarbonyl-phosphine precursors, becoming more stable upon descending group 16 (–7.3 for S; –15.5 for Se; and –24.0 kcalmol^{-1}, respectively}. In contrast, the carbonylphosphorane is higher in energy (+25.6 kcalmol^{-1}) and suggested to be less stable than the carbonyl-phosphine complex. The isoelectronic isonitrilephosphorane is also disfavoured relative to the isocyanide-phosphine complex (+14.6 kcalmol^{-1}), though the difference is somewhat less pronounced than the carbonyl analogue. In search of the factor(s) that underpin this trend, it is useful to consider the Löwden bond orders of the coupled heterocarbonylphosphorane ligands (Table 6.2). Given isonitriles and the heavier chalcocarbonyls bind more strongly to transition metals than does CO, it might be expected, *a priori*, that this might discourage coupling. The factors that cause strong metal-carbon bonding for chalcocarbonyls, however, also impact on the bonding of the coupled heterocarbonylphosphorane ligands in their complexes, *i.e.*, poor C(pπ)-E(pπ) overlap causing the carbon to be more strongly π-acidic. The C–P bond order is essentially invariant down the series, leaving bonding within the metaliirene as the determining factor(s). The heavy chalcogen examples have the strongest tungsten carbon bonding and whilst there is little variation in W–E bond order, these three examples are each significantly stronger than the W–O or W–N bonding. Finally, whilst the C–A bonding would in any event be expected to decrease down the series, in the carbonyl and

isonitrile-derived ligands this remains close to double. Taken together, for the heavier chalcogens, the thermodynamic impetus for coupling would appear to originate primarily from the strong W–C and W–E bond strengths.

Table 6.2: Calculated Löwden bond orders of the coupled heterocarbonylphosphorane ligands in complexes $[W(\eta^2\text{-}ECPMe_3)(CO)_2(Tp)]^+$.

E	W–E	W–C	C–E	C–P
O	0.72	1.26	1.77	0.91
NMe	0.74	0.98	1.91	0.95
S	1.01	1.59	1.25	0.97
Se	1.01	1.63	1.15	0.99
Te	1.02	1.68	1.03	1.01

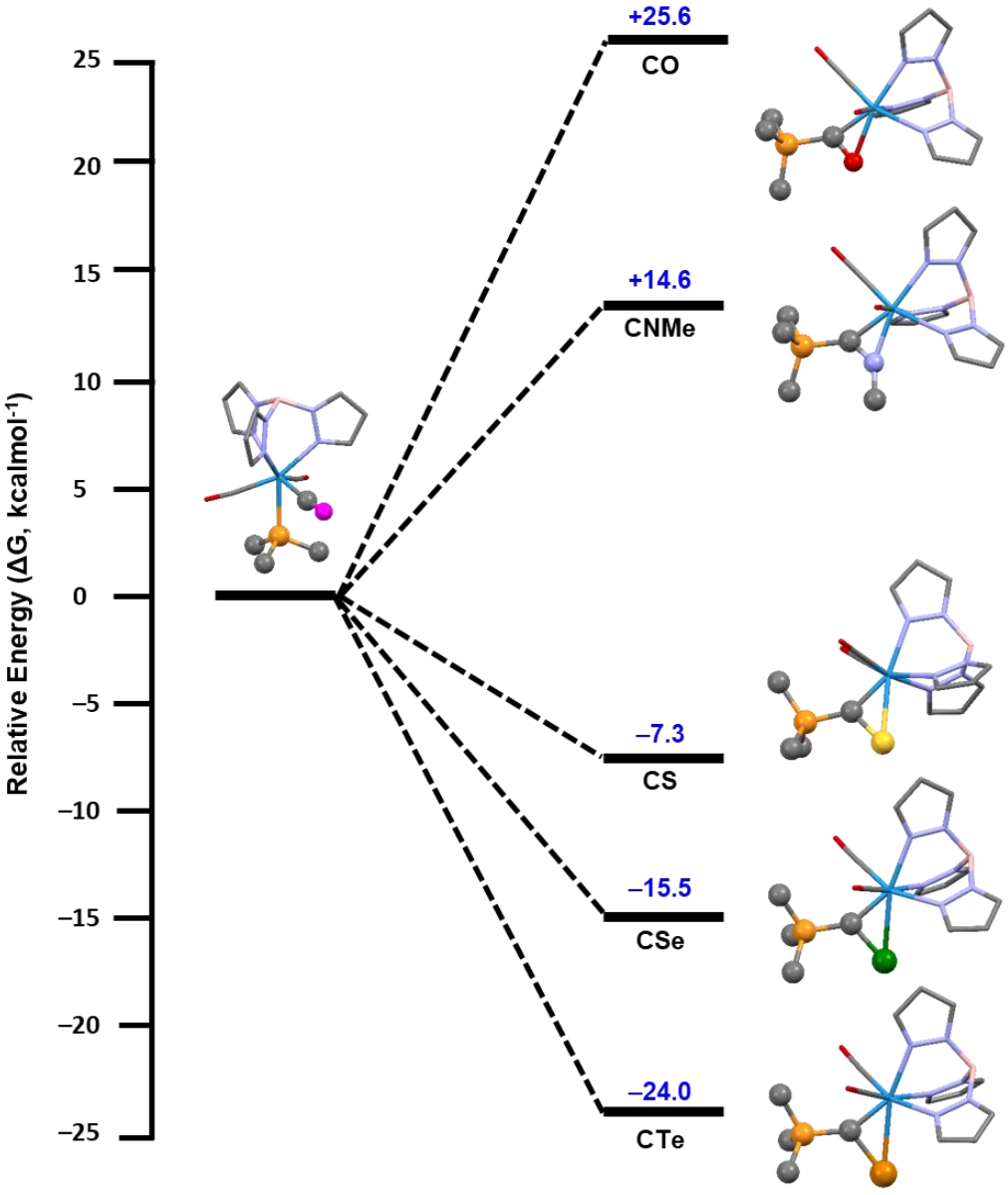

Figure 6.10: Thermodynamic energy changes upon *in silico* coupling of CE and PMe_3 ligands.

6.4 Metallacarbynes and Suzuki-Miyaura Cross-Couplings

6.4.1 Developing a boron→gold→palladium relay

The beginning of this Chapter provided insight to the μ_2-carbido complexes operative in known Sonogashira and Stille-type cross couplings. In the Sonogashira protocol the bromocarbyne serves the role of electrophilic component, but only alkynyl nucleophiles were considered. In contrast, the Stille protocol delivers the carbido as the nucleophilic partner, expedited by transmetallation first to gold *en route* to palladium. To complete the carbido synthetic toolbox, it would therefore be desirable to couple the electrophilic halocarbyne substrates with a more diverse range of nucleophilic partners.

The Suzuki—Miyaura (SM) cross-coupling and its many variants is, one of the most powerful C–C bond forming reaction,[507-510] relevant across a plethora of chemical fields from the laboratory to industrial scales. It remains the powerhouse of pharmaceutical production and its popularity can only be expected to grow due the requisite organoborates (i) becoming increasingly available through developments in catalytic borylation and hydroboration methodologies, (ii) demonstrating broad-range functional group tolerance (obviating protection/deprotection strategies) and (iii) ultimately providing environmentally benign reaction side products. Furthermore, the chemical tolerance of organoboronic acids has allowed biphasic or even fully aqueous protocols to be developed. It is yet to be utilised in the context of producing functionalised carbynes as the required coupling partners featuring a C–B bond remain rare.[**********] Lalor's complexes $[M(\equiv CX)(CO)_2(Tp^*)]$ (M = Mo, W; X = Cl, Br, I) provide the most amenable source of halocarbynes. Fluorocarbynes are less attractive, not only because they remain rare but because C–F bonds typically require electron withdrawing groups to enable palladium(0) catalysis, with little to be gained in thermodynamic terms from reactive Pd–F bond formation; [511] nickel is somewhat more promising in this respect. [512] Conversely, carbynes bearing boron groups are limited to borylcarbynes, [104] and boratocarbynes, [105] meaning the reverse of coupling partners is more difficult and hence the halocarbyne is still the clear preference for a coupling partner.

Availability of coupling partners and the niche interest mean it is unsurprising that Suzuki–Miyaura cross-coupling of carbynes has not emerged, but simultaneously, encourages development given the scope of organic reagents increasingly available to expand functionalised carbynes. Performing a Suzuki—Miyaura cross-coupling also provides a reaction of reversed polarity at the carbyne carbon from that of Stille cross-couplings (*vide supra*) and the previously established tin→gold→palladium relay.

[**********] The boratocarbyne $[Mo\{\equiv CBF_2OMe)(CO)_2(Tp^*)][K(18\text{-}c\text{-}6)]$ has been applied to an inverse protocol with p-diiodobenzene and $[Pd_2(dba)_3]/PPh_3$ to afford the iodobenzylidyne $[Mo(\equiv CC_6H_4I\text{-}4)(CO)_2(Tp^*)]$ in yields that whilst underwhelming, serve to demonstrate carbido transmetallation from boron to palladium (R. Shang, ANU, PhD Thesis 2012). The lacklustre performance of borates in this context leaves stannylcarbynes as the more effective and durable nucleophilic source of choice.

Development of a Suzuki–Miyaura manifold in carbyne chemistry would at its simplest involve a boron-palladium transmetallation. The agency of gold in kinetically enhancing the Stille-type processes does however raise the question of whether it might serve a similarly productive role. To the best of our knowledge, a boron→gold→palladium relay has not been demonstrated in palladium-mediated C–C cross coupling processes, however isolated observations collated from the literature suggest it may well be possible.

(i) Boronic acids readily transmetallate to gold(I) or gold(III) halides to provide isolable organogold species;[513-518]

(ii) Isolated organogold reagents R_3PAuAr transmetallate to palladium for use as stoichiometric C-nucleophiles for C–C cross couplings;[516]

(iii) The complex $[AuCl(SMe_2)]$ catalyses nucleophilic allylation reactions with allylboronates, implicating transetallation to generate $[Au(allyl)(SMe_2)]$. ($[AuCl(PR_3)]$ (R = Me, Ph) gave inferior performance).[519]

Combining these observations suggests that gold *might* be able to serve in a catalytic role in palladium-mediate cross-coupling reactions of boronates. To test this, the manifold of variables to optimise would include solvent, base, gold co-catalyst, and palladium catalyst (in this order) to refine the cross-coupling system.‡‡‡‡‡‡‡‡‡‡‡‡‡‡‡‡‡‡ This sub-section will discuss the optimisation of each parameter with respect to adapting the Suzuki–Miyaura reaction to *sp*-hybridised carbon (carbyne) complexes.

An enormous investment into optimisation of Suzuki–Miyaura (SM) systems has been made, resulting in an informed set of starting conditions, particularly from the literature examples presented above. Initial investigations with the bromocarbyne $[W(\equiv CBr)(CO)_2(Tp^*)]$ (**2.1d**) began with conditions optimised for Sonogashira cross-couplings, given both processes share oxidative addition as the initial step. Initially, 4-methoxyphenylboronic acid was chosen as the methoxy provides an $\boldsymbol{M^+}$ directing group to activate the *para*-position by polarising the C–B bond which is considered to facilitate the C–C coupling; it provides a useful spectroscopic handle. Tetrahydrofuran served as the initial solvent combined with K_2CO_3 as the base to provide a balanced middle ground of conditions to determine the feasibility of the reaction and establish an initial proof of concept (Table 6.3).

Employing 5 mol% $[Pd(PPh_3)_4]$ (the same loading used for Sonogashira couplings[138]) resulted in no coupling to form $[W(\equiv C\text{-}C_6H_4OMe\text{-}4)(CO)_2(Tp^*)]$ (**6.15**). This result is curious, given the ultra-low loadings commonly used in more conventional organic syntheses (*ca* 0.02 mol%).[520] Increasing this amount to 10 mol% resulted in coupling (Table 6.2, Entry 2), but the original 5 mol% palladium in the

‡‡‡‡‡‡‡‡‡‡‡‡‡‡‡‡‡‡ Typically the boronate source (acid, pinacol ester, fluoroborate salt *etc.*) would be optimised, however, this was not conducted in this study as a large scope inquiry was not the target.

presence of 5 mol% [AuCl·SMe_2] co-catalyst also provided a comparable yield (Table 6.3, Entry 4). Utilising gold(I) without palladium(0) returns no product or conversion (Table 6.3, Entry 3). This suggests that palladium(0) is likely forming the metallacarbyne **6.1b** in a facile oxidative addition, however, the transmetallation with boron is suitably slow such that deactivation through μ_2-phosphoniocarbynes is faster, hence catalysis only occurs with enough palladium. This result was repeatable and derived from reactions conducted in duplicate but remains an odd recording without a clear reason. Likewise, gold(I) forms a facile μ_2-bromocarbyne without palladium(0), incapable of turnover, however reacting isolated [WAu(μ_2-CBr)Cl$(CO)_2$(Tp*)] (**2.2d**) with PPh_3 results in [W(≡CBr)$(CO)_2$(Tp*)] and [AuCl(PPh_3)]. Likewise, a reaction of **2.2d** with [Pd$(PPh_3)_4$] provides palladium metallacarbyne **6.1b** and [AuCl(PPh_3)] by $^{31}P\{^1H\}$ NMR spectroscopy, suggesting π-coordination of gold(I) is not an issue in the presence of adventitious phosphine. This gives initial proof of SM type reactivity for carbynes.

Table 6.3: Initial proofs of Suzuki–Miyaura reactivity.

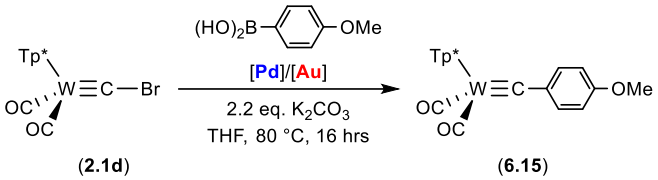

(**2.1d**) (**6.15**)

Entry	[Pd]/[Au]	Isolated Yield[a,b] (%)
1	5 mol% [Pd$(PPh_3)_4$]	0
2	10 mol% [Pd$(PPh_3)_4$]	45
3	5 mol% [AuCl·SMe_2]	0
4	5 mol% [Pd$(PPh_3)_4$] *and* [AuCl·SMe_2]	41

[a]Average of duplicates (within 10%) as measured from mass collected post-flash chromatography. [b]An isolated yield of zero means not detected by UV illumination of TLC plate (silica gel).

The importance of solvent polarity is a recurring theme for metallacarbynes and was therefore explored first, recalling that palladium metallacarbynes are sensitive to halogenated, polar and protic solvents that promote phosphine migration, which is also reflected during SM catalysis. The aprotic, medium polarity solvent THF is a functional system (Table 6.4, Entry 1), but non-polar aprotic toluene proved superior, most likely due to the increased longevity of the palladium metallacarbyne intermediate **6.1b**. One contributing factor to the utility of SM cross-coupling is solvent compatibility in synthesis which allow polar protic alcohols (^{n}PrOH) or water mixed with organic solvents to solubilise base and coupling partners. In the case of carbynes, combinations including either water or protic solvents prevent catalysis either through decomposing the metallacarbyne **6.1b**, or through nucleophilic substitution of the bromocarbyne with hydroxide/alkoxide.[305] Finally, the linear or cyclic ethers (DME/Dioxane) also resulted in no product **6.15**, contrasting the similar THF for reasons unclear, noting dioxane provided a considerable amount of homocoupling to [W_2(≡CC≡)$(CO)_4$(Tp*)], suggesting that an oxidant like oxygen enters the system and is faster than the barely existence coupling in this solvent.

Table 6.4: Suzuki–Miyaura for carbynes: Solvent optimisation.

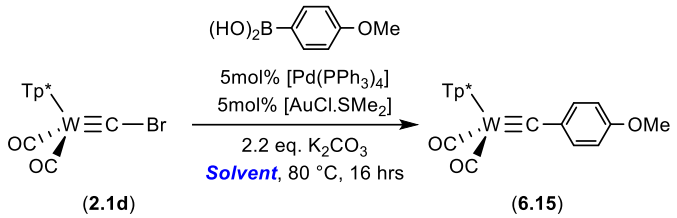

Entry	Solvent	Isolated Yield[a,b] (%)
1	THF	43
2	DME	0
3	4:1 *n*PrOH/H_2O	0
4	Toluene	41
5	Toluene/H_2O	0
6	Dioxane	0[c]

[a]Average of duplicates (within 10%) as measured from mass collected post-flash chromatography. [b]An isolated yield of zero means not detected by UV illumination of TLC plate (silica gel). [c]Significant quantities of homocoupled $[W_2(\mu_2\text{-}C_2)(CO)_4(Tp^*)_2]$ isolated.

These results narrow the options of compatible solvents, and consequently, affects the scope of useful bases. Reassuringly, the absence of base prevents catalysis, highlighting the important role of base in improving the reactivity of boron by increasing the coordination number and subsequent transmetallation to gold—already a known process.[513-514, 517] Potassium *tert*-butoxide returns a dismal yield (Table 6.5, entry 6) despite solubility in toluene, whereas NaOH is underwhelming in the absence of polar media reflecting its reduced solubility. A point of contrast arises for the liquid base NEt_3 which performs well for Sonogashira cross-coupling but poorly in SM conditions, reflecting the different role being played in each system (deprotonation of alkyne *vs* coordination to boron, respectively). The base K_3PO_4 is commonly utilised in toluene systems, improving reaction yield slightly over K_2CO_3 supporting solubility as a factor albeit confirmed by the improvement supplied by Cs_2CO_3. Caesium carbonate has the highest relative solubility of alkali carbonates in hydrocarbons; therefore the impact of base is likely a reflection of solubility rather than pK_a or interaction with boron.

Finally, the dual-catalyst combination was optimised from a series of established palladium and gold reagents. During the initial proof stage, the complex $[AuCl(PPh_3)]$ was identified as a relevant species that arises through phosphine scavenging, and when used as the gold catalyst the yield is drastically improved (Table 6.6, Entry 2). As there appeared to be no evidence of gold mirror or colloid, it is likely the preformed phosphine species ensures the maximum amount of gold(I) survives introduction to the reaction, rather than decomposition from $[AuCl{\cdot}SMe_2]$ at the beginning of the reaction. Common alternative palladium catalysts to $[Pd(PPh_3)_4]$ in organic synthesis are $[Pd_2(dba)_3]$ that introduces a phosphine-free palladium(0) centre, or $[Pd(OAc)_2]$ that can introduce an acetate as a weak base with palladium(II) reduced *in situ* without the need to manage air-reactive zerovalent palladium pre-catalysts.

Table 6.5: Suzuki–Miyaura for carbynes: base optimisation.

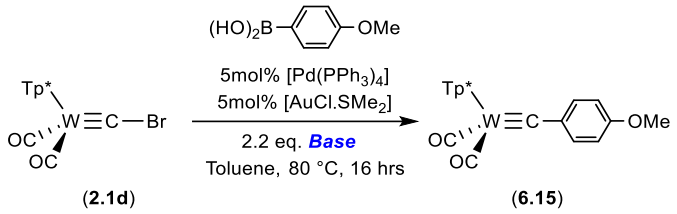

Entry	Base	Isolated Yield[a, b] (%)
1	No base	0
2	K_2CO_3	41
3	K_3PO_4	48
4	NEt_3	21
5	NaOH	36
6	KO^{t}Bu	16
7	Cs_2CO_3	60

[a]Average of duplicates (within 10%) as measured from mass collected post-flash chromatography. [b]An isolated yield of zero means not detected by UV irradiation of TLC plate (silica gel).

Using 'ligand free' [$Pd_2(dba)_3$·$CHCl_3$] provides sub-par catalysis (Table 6.6, Entry 3), however, addition of phosphine increases the yield likely suggesting yield is more reflective of the naked palladium(0) surviving rather than if the cycle is possible. The use of this reagent to prepare 'bow-tie' trimetallic clusters [$M_2Pd(\mu\text{-}CR)_2(CO)_4(L)_2$] may also account for its lacklustre performance as previously noted. [148] Meanwhile, the acetate provides a modest yield but confirms reduction *in situ*.‡‡‡‡‡‡‡‡‡‡‡‡‡‡‡‡ The increasingly popular chelated catalyst [$PdCl_2$(dppf)] also returned a low yield and this is consistent with the observation that chelate **6.3** is unable to catalyse the Sonogashira cross-coupling, implying a chelate may not be useful with metallacarbynes in catalysis. Finally, utilising [$PdCl_2(PPh_3)_2$] also provided a high yield (Table 6.6, Entry 6) that could be combined with [$AuCl(PPh_3)$] to provide the optimised catalyst system. This combination suggests adventitious phosphine may be problematic whereas enough phosphine to stabilise either metal is essential. A proposed tandem catalytic cycle derived from carbido intermediates is shown in Scheme 6.13.

6.4.2 Functionalised carbynes *via* a boron→gold→palladium relay

The purpose of developing an SM protocol for carbynes, apart from fundamental issues, was to broaden access to alternative carbyne functionalities, however, it was first useful to benchmark the system against known routes. The 'parent' benzylidyne [W(≡CPh)$(CO)_2$(Tp*)] (**6.16**) has been isolated as a side product, [310] as the analogue of [Mo(≡CPh)$(CO)_2$(Tp*)] *via* the Fischer–Mayr carbyne synthesis from phenylithium in a surprisingly low yield (18% isolated yield). [521] Curiously, this remains the most expedient

‡‡‡‡‡‡‡‡‡‡‡‡‡‡‡‡ Commencing with divalent palladium precursors requires that reduction is first achieved by two equivalents of the nucleophilic partner to form, in this case 4,4'-dianisolyl.

Table 6.6: Suzuki–Miyaura for carbynes: catalyst optimisation.

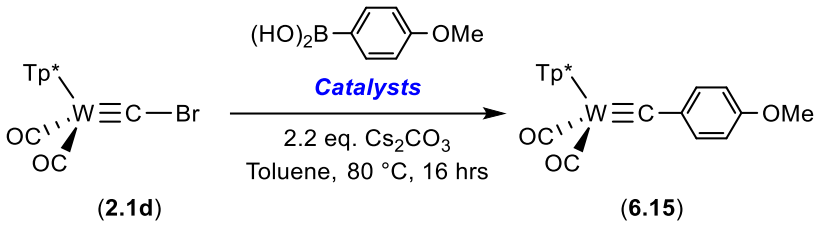

(**2.1d**) (**6.15**)

Entry	5 mol% [**Pd**]	5 mol% [**Au**]	Isolated Yield[a, b] (%)
1	$[Pd(PPh_3)_4]$	$[AuCl{\cdot}SMe_2]$	60
2	$[Pd(PPh_3)_4]$	$[AuCl(PPh_3)]$	93
3	½ $[Pd_2(dba)_3]{\cdot}CHCl_3$	$[AuCl{\cdot}SMe_2]$	20
4	½ $[Pd_2(dba)_3]{\cdot}CHCl_3$ + 5 mol% PPh_3	$[AuCl{\cdot}SMe_2]$	54
5	$[Pd(OAc)_2]$	$[AuCl{\cdot}SMe_2]$	48
6	$[PdCl_2(PPh_3)_2]$	$[AuCl{\cdot}SMe_2]$	88
7	$[PdCl_2(dppf)]$	$[AuCl{\cdot}SMe_2]$	36
8	$[PdCl_2(PPh_3)_2]$	$[AuCl(PPh_3)]$	95

[a]Average of duplicates (within 10%) as measured from mass collected post-flash chromatography. [b]An isolated yield of zero means not detected by UV illumination of TLC plate (silica gel).

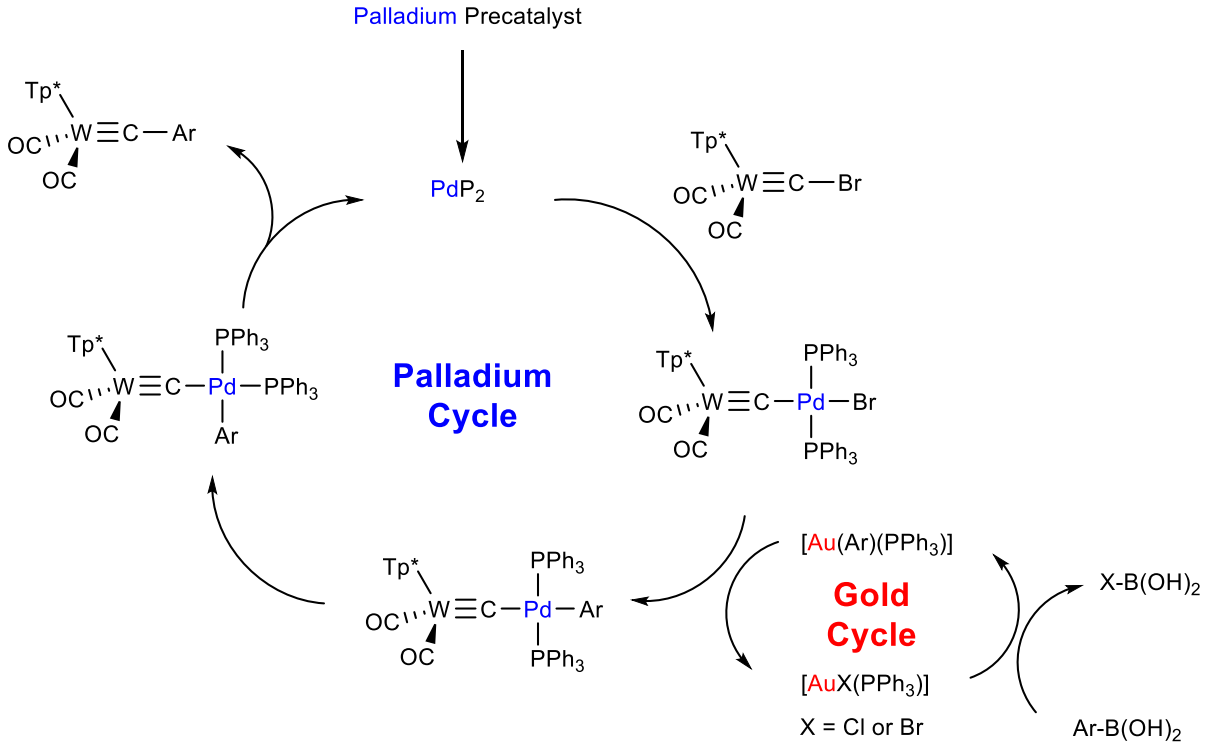

Scheme 6.13: Proposed dual-catalytic cycle for Suzuki–Miyaura cross-coupling from halocarbynes.

route reported, however this is most likely a reflection of more substitutionally sophisticated benzylidynes having been instead targeted. Alternatively, a Stille cross-coupling from [W(≡CSnBu$_3$)(CO)$_2$(Tp*)] affords the arylcarbyne [W(≡CC$_6$H$_4$Br-2)(CO)$_2$(Tp*)] in much higher amounts but retaining a bromide for further reactivity (77% isolated yield). [147] The optimised SM system employing phenylboronic acid results in [W(≡CPh)(CO)$_2$(Tp*)] in a higher yield compared with the Stille comparator with a significant reduction in catalyst and temperature.

The *meta*-pyridylcarbyne complex [W(≡CC$_5$H$_4$N-3)(CO)$_2$(Tp*)] can be produced through Stille coupling, although the *para*-isomer [W(≡CC$_5$H$_4$N-4)(CO)$_2$(Tp*)] was produced in minor amounts (*ca* 9%). This offers a point of comparison between Stille and SM manifolds. Disappointedly, employing 4-pyridylboronic acid under the optimised SM coupling results in no conversion to the pyridylcarbyne, where crude NMR is consistent with unreacted bromocarbyne **2.1d**. The lack of conversion suggests that a tangent lies early in the process while installing pyridyl groups *via* cross coupling is an ongoing issue in synthesis. [522]

Complex **6.16** arises from a neutral, non-directing phenylboronic acid in good yield although less than the electronically favoured directing group in **6.15**. Meanwhile, the unknown *para*-acetyl complex, [W(≡CC$_6$H$_4$C(O)Me-4)(CO)$_2$(Tp*)] (**6.17**) is produced in reduced yield (Table 6.7, Entry 3) consistent with an electron-withdrawing group acting to deactivate the coupling. To provide more elaborate examples, ferrocenyl carbynes are known for containing for *bis*-systems [Fe{η^5-C≡Mo(CO)$_2$(Tp*)}$_2$], [246] and SM coupling can provide the unknown *mono*-functionalised [W(≡CFc)(CO)$_2$(Tp*)] (**6.18**) (Figure 6.11). Alternatively, the larger phenylcarbozol group has been utilised for larger molecular architectures for optical applications, but no example of a carbyne or alkylidyne has been reported, now prepared as [W(≡C–C$_6$H$_4$–NC$_{12}$H$_8$)(CO)$_2$(Tp*)] (**6.19**). Finally, *bis*-thiophenes are optically relevant motifs as well as of interest in electronic communication; SM coupling can append carbynes to give [(SC$_4$H$_2$-5{C≡W(CO)$_2$(Tp*)})$_2$] (**6.20**) although in a poor yield despite the optimised conditions. The species **6.20** was clearly the major product of the reaction with no evidence of the *mono*-substituted adduct amongst the slew of unidentified compounds observed during purification. The bithienyl species highlights a possible limitation of the Suzuki–Miyaura cross-coupling for carbynes in that dilithiation of bithiophene combined with bromocarbyne **2.1d** may well be a more productive route to **6.20**, especially as dilithiobithienyl can be the precursor to the boronic acid. While subtle differences exist, spectroscopic data for the functionalised carbynes call for little comment, as they conform to the copious data previously collated for carbyne complexes [M(≡CR)(CO)$_2$(Tp*)],[255] however, values are summarised here with select relatives (Table 6.8).

The principles of Suzuki–Miyaura cross-couplings have been applied to provide an alternative C–C bond formation in carbynes. A system has been optimised from fundamental organometallic knowledge elucidated in the beginning of this chapter, to provide better methods of select carbynes previously known and extended to new species. Given the large scope of SM reactions in organic synthesis, this area is primed for a scope enquiry and future work should target carbynes with further functional groups, particularly on the remaining weakness of carbon-based substituents.

Table 6.7: Functionalised carbynes prepared by optomised Suzuki—Miyaura protocol.

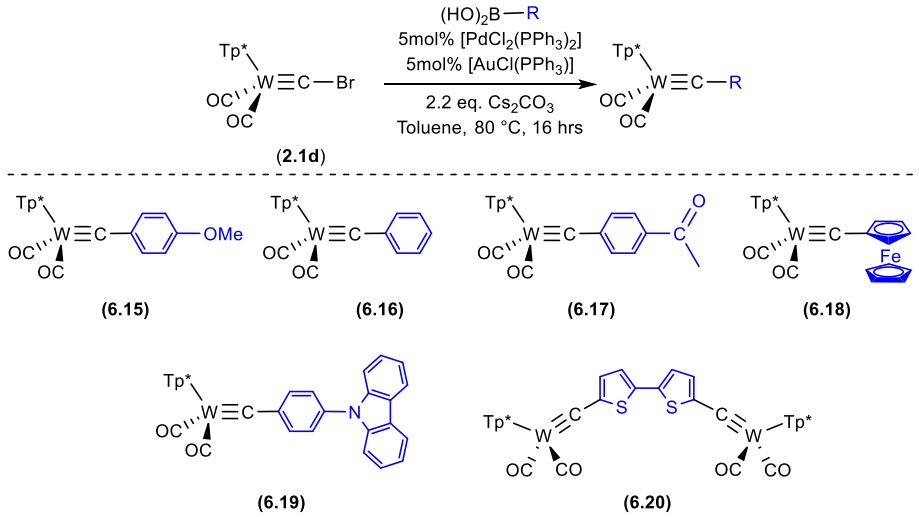

Entry	Boronic Source	Product	Isolated Yield[a] (%)
1	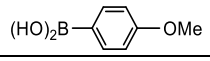	**6.15**	95
2	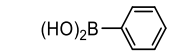	**6.16**	88
3	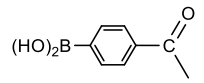	**6.17**	60
4	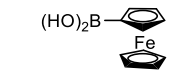	**6.18**	66
5	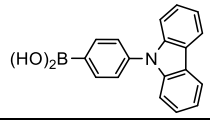	**6.19**	87
6	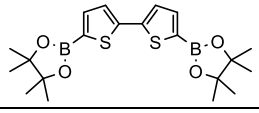	**6.20**	25

[a]Average of duplicates (within 10%) as measured from mass collected *post*-flash chromatography.

Table 6.8: Spectroscopic parameters of functionalised carbynes obtained *via* Suzuki—Miyaura cross-coupling and selected relative species.

Complex	δ_C[a] (ppm)	δ_{C1}[a] (ppm)	ν_{CO}[b] (cm^{-1})
$[W(\equiv CBr)(CO)_2(Tp^*)]$ (**2.1d**) [87, 90]	197.97	–	1994, 1905
$[W(\equiv CPh)(CO)_2(Tp^*)]$ (**6.16**) [310]	277.9	150.5	1969, 1876 [c]
$[W\{\equiv C(C_6H_4OMe\text{–}4)\}(CO)_2(Tp^*)]$ (**6.15**)	278.9	144.1	1969, 1877
$[W\{\equiv C(C_6H_4COMe\text{–}4)\}(CO)_2(Tp^*)]$ (**6.17**)	275.5	154.1	1976, 1888
$[Fe\{\eta^5\text{-}C_5H_4C\equiv W(CO)_2(Tp^*)\}(Cp)]$ (**6.18**)	280.8	95.2	1964, 1873
$[W\{\equiv C(C_6H4\text{–}NC_{12}H_8)\}(CO)_2(Tp^*)]$ (**6.19**)	276.5	149.3	1974, 1883
4,4'-$\{SC_4H_2\text{–}[C\equiv W(CO)_2(Tp^*)]\}_2$ (**6.20**)	260.8	153.7	1974, 1886
$[W\{\equiv C(SC_4H_3)\}(CO)_2(Tp^*)]$ (**7.20**) [d]	262.2	154.9	1974, 1884

Notes: [a]Measured in $CDCl_3$ unless specified otherwise. [b]Measured in CH_2Cl_2 unless specified otherwise. [c]KBr. [d]Developed in chapter Seven but relevant here.

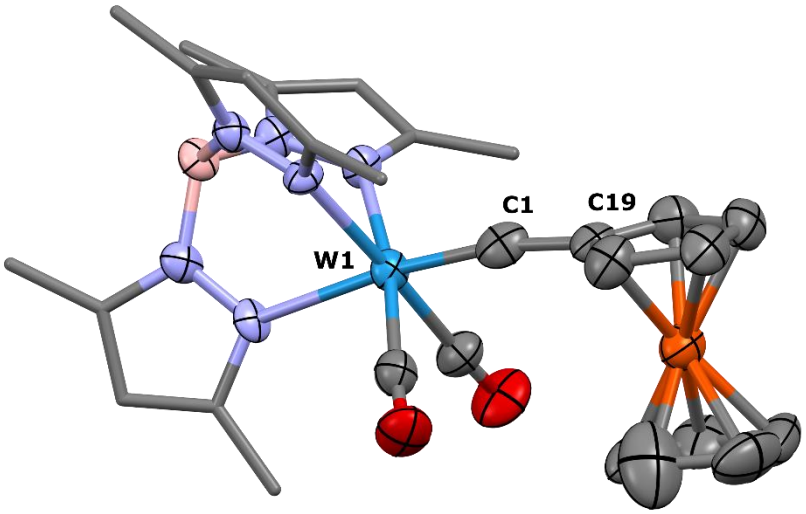

Figure 6.11: Molecular structure of $[W(\equiv CFc)(CO)_2(Tp^*)]PF_6$ (**6.18**) in a single crystal as determined by X-Ray Diffractometry. Ellipsoids are drawn at the 50% probability surface with pyrazolyl rings simplified and hydrogens omitted for clarity. Selected bond lengths (Å) and angles (°): W1–C1 1.83(1), C1–C19 1.48(1), W1–C1–C19 169.7(8).

6.5 Conclusions

Metallacarbynes have been implicated in a variety of carbyne cross-coupling reactions, but with limited mechanistic investigation prior to this work. Bromocarbyne cross-couplings were proposed to proceed *via* palladium μ_2-carbido complexes and have now been measured spectroscopically through a model Sonogashira manifold, further verified by an isolated molybdenum-palladium acting as a pro-catalyst. Meanwhile, phosphine ligands were found to be required for palladium(0) to perform oxidative addition effectively at ambient temperature, however, phosphines ultimately provide a route of termination *via* evolution to μ_2-phosphoniocarbynes in a process that, like carbido-isonitrile coupling (Chapter Four) appears to be accelerated by polar or protic media.

An exploration of carbido *cf.* phosphoniocarbyne chemistry provided tangential observations that elemental sulfur fails to cleave C–P bonds (in contrast to ylides) but instead provided the first examples of thiocarbonylphosphorane ligands, which remain unknown as free molecules. Varying the phosphine had minimal impact on spectroscopic properties and could be extended to lighter molybdenum, and heavier arsenic (thiocarbonylarsorane) analogues. Theoretical studies suggest that while coupling of heavier chalcocarbonyls with phosphine may be energetically favourable due to strong metal-carbon and metal chalcogen bonding, both of these interactions are weaker carbonylphosphoranes, perhaps accounting for the absence of observed coupling between these fundamental organometallic ligands despite thousands of structurally authenticated examples.

Knowledge of palladium intermediates developed in the Sonogashira manifold led to the adaptation of Suzuki–Miyaura cross-coupling for carbynes. This manifold was optimised to couple increasingly challenging boronic acids and produced a series of previously unknown carbyne complexes from a common late synthetic intermediate. A catalytic manifold was proposed for the dual interconnected Pd(0)/Au(I) cycles that would appear to constitute the first demonstration that gold(I) reagents [AuCl(L)] are able *catalytically* activate boronic acids to expedite the Suzuki-Miyaura cross-coupling reaction. Moving forward, a greater understanding of the role of gold in transmetallation processes would be desirable and possibly informative, an issue to be addressed in the Chapter that follows.

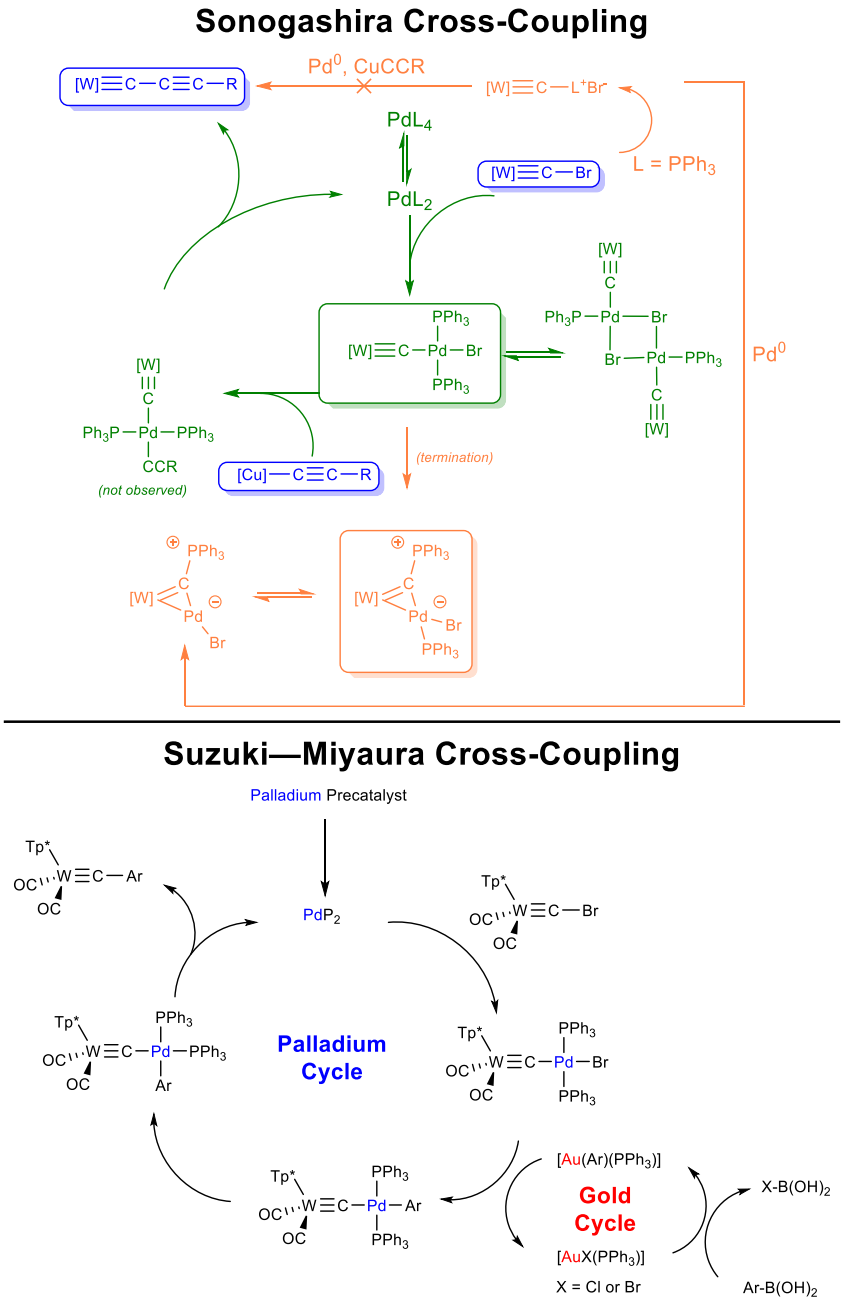

Chart 6.1: Sonogashira and Suzuki–Miyaura type reactivity with carbynes reliant on verified metallacarbyne intermediates in Chapter Six.

Chapter Seven

Synthesis of Group 11 and 12 Metallacarbynes

σ-Alkynyl complexes of gold and mercury are amongst the oldest organotransition metal species that found utility in converting organic compounds to crystalline derivatives prior to spectroscopic methods.[523-525] These σ-alkynyl species are typically hydrolytically and aerobically stable, easy to prepare, and have therefore found utility as alkynyl transfer reagents to transition metals such as insertion into a Hg–C bond of $[Hg(C{\equiv}CPh)_2]$ to give $[IrCl(C{\equiv}CPh)(HgC{\equiv}CPh)(CO)(PPh_3)_2]$.[526] The early fundamental study of these σ-alkynyls has evolved over decades from stoichiometric addition to catalytic incorporation, such as the work of Bruce and Saitseva that demonstrates C(*sp*)–C(*sp*) bond formation from gold alkynyl and polyynyls mediated by palladium catalysis.[189, 191, 439] In contrast, examples of Class B metallacarbynes are limited to two examples for gold[99] and one for mercury,[118] all acquired from transmetallation reactions from tin or lithium, respectively. Considering that the isolobal analogy with alkynes has in part inspired the exploration of carbynes,[139] this perspective raises the possible utility of gold and mercury carbidos as carbyne transfer agents, with added impetus provided by the recent application of gold(I) intermediates in mediating Stille catalysis.[144-149]

Gold(I) metallacarbynes have now been applied in carbyne transfer processes, and the catalytic demercuration of a *bis*(carbido)mercurial, which proceeds *via* transmetallation, has been demonstrated. It therefore would seem appropriate and timely to consider a systematic evaluation of the carbido chemistry of each of these elements, both from a fundamental perspective, and with a view to developing the utility of transmetallation reactions *en route* to new metallacarbynes. Accordingly, this Chapter addresses underexplored gold(I) and mercury(II) Class B carbido complexes and their relevance to transmetallation processes.

7.1 Transmetallation in Alkynyl Chemistry: Significance of Tin, Copper, Gold, and Mercury

Transmetallation reactions are ubiquitous in organometallic synthesis, though the intimate mechanistic details, *e.g.*, addition/elimination *cf.* concerted cyclic transition states, are as recently noted often overlooked.[527] For *sp*-hybridised systems such as alkynyls, the most common reagents for transmetallation are alkynyls of copper generated *in situ* (the Sonagashira protocol), or less

commonly stoichiometric alkynyls of tin, gold, and mercury, with some selected highlight examples from each element being noted (Scheme 7.1).

Long before the emergence of the Stille cross-coupling, [528-530] Lappert and co-workers charted transfer of stannylacetylenes to rhodium, iridium, and platinum, identifying four routes that underpin reactivity: (i) halide metathesis; (ii) oxidative addition; (iii) combined metathesis and oxidative addition; or (iv) oxidative cleavage. [531-532] Wrackmeyer later described further transmetallations from tin to palladium/platinum, a stoichiometric reaction that was mechanistically relevant to the catalytic Stille coupling. [533] Meanwhile transmetallation from tin to gold was shown by Gimeno and co-workers such that a stannylalkynyl ligand on iron and ruthenium afforded auroalkynyl motifs. [534] These early examples inspired the transfer a carbyne unit to gold through transmetallation of stannylcarbynes, [375] later extended to a Class C gold carbido to produce a μ_3-carbido complex after rearrangement in favour of π-coordination. [72] Transmetallation of copper reagents is epitomised by the transfer of acetylides to palladium in Sonogashira cross-couplings, prior to reductive elimination and catalyst turnover. As an extension, the 'copper effect' and 'gold effect' are known to accelerate Stille cross-couplings. [100, 458]

In scenarios when tin or copper transmetallation proves ineffective, gold may provide a potential alternative.§§§§§§§§§§§§§§§§§§§§§ Cross and co-workers demonstrated a simple σ-alkynyl species can transmetallate from gold to platinum or mercury, [535] while Bruce applied gold transfer to palladium to furnish a variety of species through cross-coupling, though it should be noted a copper co-catalyst was also included. [189, 191, 439] Inspired by this approach, Dewhurst showed tricarbidos can be produced by transmetallation from [PPN][Au{C≡CC≡W(CO)$_2$(Tp)}$_2$] to [PtCl$_2$(PPh$_3$)$_2$] to give [Pt{C≡CC≡W(CO)$_2$(Tp*)}$_2$(PPh$_3$)$_2$]. [449] The toxicity associated with organomercurials notwithstanding, [536] the aerobic stability and tolerance of alkynylmercurials toward functional groups, [523] has seen them widely utilised as transmetallation reagents to transition metals, [526, 537] lanthanides, [538-539] and main group elements. [540] So while mercury is not typically the first choice as a transmetallation reagent, it may well serve a purpose after other options have been first discarded, with appropriate care.**********

§§§§§§§§§§§§§§§§§§§§§ Gold is considerably more expensive when used stoichiometrically but for transmetallation of alkynyl fragments that otherwise fail, the metal remains relatively easy to recycle given *aqua regia* recovery.

********** In common with many heavy metal acetylides, those of mercury have been reported to be potentially explosive. In the present work, the high molecular weights of materials employed most likely accounts for no mishaps being experienced. In any event appropriate caution should be exercised in their use.

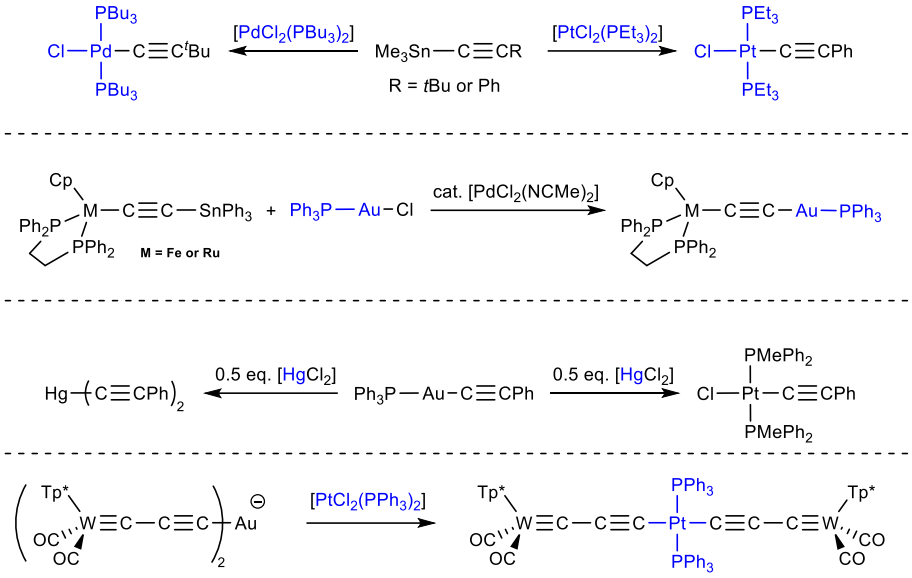

Scheme 7.1: Representative examples of transmetallation alkynyl species.

These initial examples have inspired the production of many polyynyl species of varying chain-lengths over the past two decades. Given transmetallation has shown utility in synthesis of longer carbon chain species, it was envisioned this utility might extend to carbido complexes based on these elements. The previous Chapter outlined the utility of stannylcarbynes $[M(\equiv CSnBu_3)(CO)_2(Tp^*)]$ (M = Mo, W) that were presumed to transmetallate to provide gold metallacarbynes for use in Stille type cross-coupling of carbynes, however, only three gold metallacarbynes have been reported.[99] Another gold metallacarbyne was pursued by combining stannylcarbyne $[W(\equiv CSnBu_3)(CO)_2(Tp^*)]$ with Class C carbido $[(PCy_3)_2Cl_2Ru(\equiv C:)\rightarrow AuCl]$, but rather than producing the mixed Class B/C carbido $[(PCy_3)_2Cl_2Ru(\equiv C:)\rightarrow Au–C\equiv W(CO)_2(Tp^*)]$, a rearrangement to a μ_2/μ_3-carbido $[WRuAu_2(\mu_2\text{-}C)(\mu_3\text{-}C)Cl_3(CO)_2(PCy_3)_2(Tp^*)]$ occurs.[72] Likewise, the *bis*-carbido mercurial $[Mo_2Hg(\mu_2\text{-}C)_2(CO)_4(Tp^*)_2]$ remains the only example of a carbido complex based on mercury.[118] No further chemistry of these or related species has been reported in the interim, an omission this Chapter addresses.

7.2 Preparation of Bimetallic Gold Carbido Complexes

The original report of the gold carbidos $[MoAu(\mu_2\text{-}C)(CO)_2(PPh_3)(Tp^*)]$ and $[WAu(\mu_2\text{-}C)(CO)_2(PEt_3)(Tp^*)]$[99] identified two synthetic routes: (i) Transmetallation from stannylcarbynes to gold halides and (ii) Disaggregation of the polymetallic golden ring $[W(\equiv CAu)(CO)_2(Tp^*)]_4$. The exploration and elaboration of these methods provides the premise of this section.

7.2.1 Golden-Ring Disaggregation

Of the two methods, disaggregation of the golden ring, $[W(\equiv CAu)(CO)_2(Tp^*)]_4$ (**7.1**), is the most attractive as this in principle might allow diversity from a late common synthetic intermediate. Initial findings showed PEt_3 (ν^T = 2061.7 cm^{-1})‡‡‡‡‡‡‡‡‡‡‡‡‡‡‡‡‡‡ [268] cleaves **7.1** however, PPh_3 (ν^T = 2068.9 cm^{-1}) does not, demonstrating importance of ligand nucleophilicity. [99]‡‡‡‡‡‡‡‡‡‡‡‡‡‡‡‡‡ Extending this protocol, treating a CH_2Cl_2 solution of **7.1** with more nucleophilic phosphines PCy_3 (ν^T = 2056.4 cm^{-1}) and PMe_2Ph (ν^T = 2065.3 cm^{-1}) change the initially orange solution to bright yellow to give $[WAu(\mu_2\text{-}C)(CO)_2(PR_3)(Tp^*)]$ (PR_3 = PCy_3 **7.2**; PMe_2Ph **7.3**) almost instantaneously (Scheme 7.2). Isolation through simple recrystallisation is imperative as each species deposits colloidal gold or gold mirror upon chromatography. Consistent with the original report, equimolar addition of PPh_3 to **7.1** results in a collection of broad signals during spectroscopy, however, addition of excess (5 equivalents) results in a new species being in solution consistent with $[WAu(\mu_2\text{-}C)(CO)_2(PPh_3)(Tp^*)]$ (**7.4**) that can also be isolated as a pure solid. Returning this to solution without excess phosphine results in reformation of **7.1** indicating that phosphine coordination is reversible for this ligand; the previous three phosphines coordinate irreversibly.

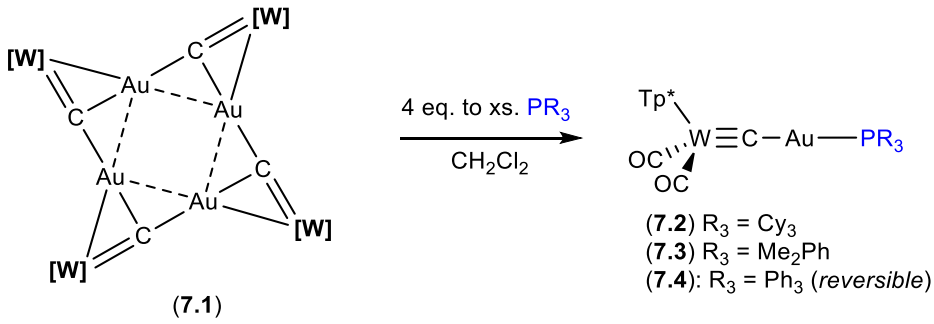

Scheme 7.2: Disaggregation of $[W(\equiv CAu)(CO)_2(Tp^*)]$ (**7.1**) with phosphines.

Solution-phase infra-red spectra exhibit carbonyl absorbances consistent with a μ_2-carbido complex (ν_{CO}: 1950/1853 cm^{-1}; **7.2**), transmitting phosphine basicity through the linear linkage and occurring at lower wavenumber than the μ_3-carbido precursor (ν_{CO}: 1990, 1900 cm^{-1}; **7.1**). Measuring **7.2** and **7.3** by $^{31}P\{^1H\}$ NMR spectroscopy reveal singlets as different chemical shifts (Solvent: δ_P = 54.97 and 14.14, respectively), whereas **7.4** in the presence of excess phosphine

‡‡‡‡‡‡‡‡‡‡‡‡‡‡‡‡‡‡ The Tolman electronic parameter (ν^T) for a ligand (L) is defined as the wavenumber of the A_1 carbonyl mode in complexes $[Ni(L)(CO)_3]$ in CH_2Cl_2. Measures are taken from Tolman's eponymous review, unless cited otherwise. Lower wavenumbers indicate a more nucleophilic ligand (L).

‡‡‡‡‡‡‡‡‡‡‡‡‡‡‡‡‡ For our purposes, the Tolman electronic parameter (a thermodynamic quantity), *i.e.*, the basicity of the phosphine, is taken as an approximate indication of nucleophilicity (a kinetic property). A broader consideration of nucleophilicity would include steric factors and bond hybridisation effects as well as temperature and solvent contributions. [541]

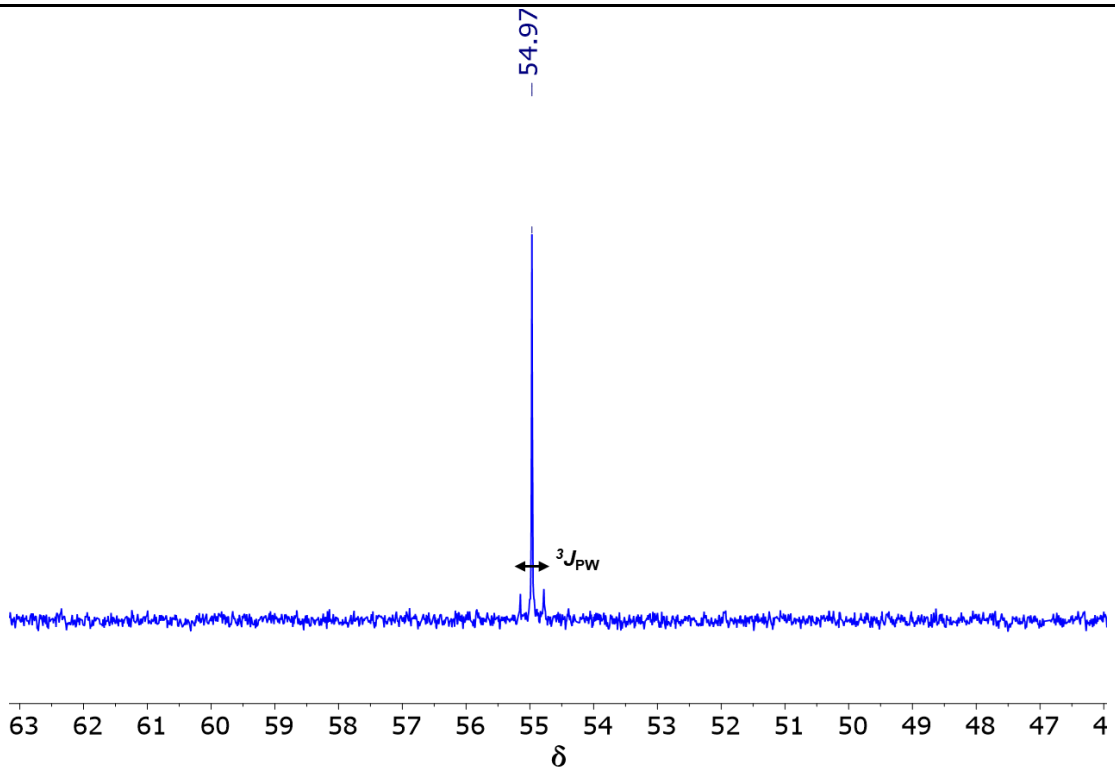

Figure 7.1 $^{31}P\{^1H\}$ NMR Spectrum of [WAu(μ$_2$-C)(CO)$_2$(PCy$_3$)(Tp*)] (**7.2**) in CD_2Cl_2 showing long range coupling to ^{183}W.

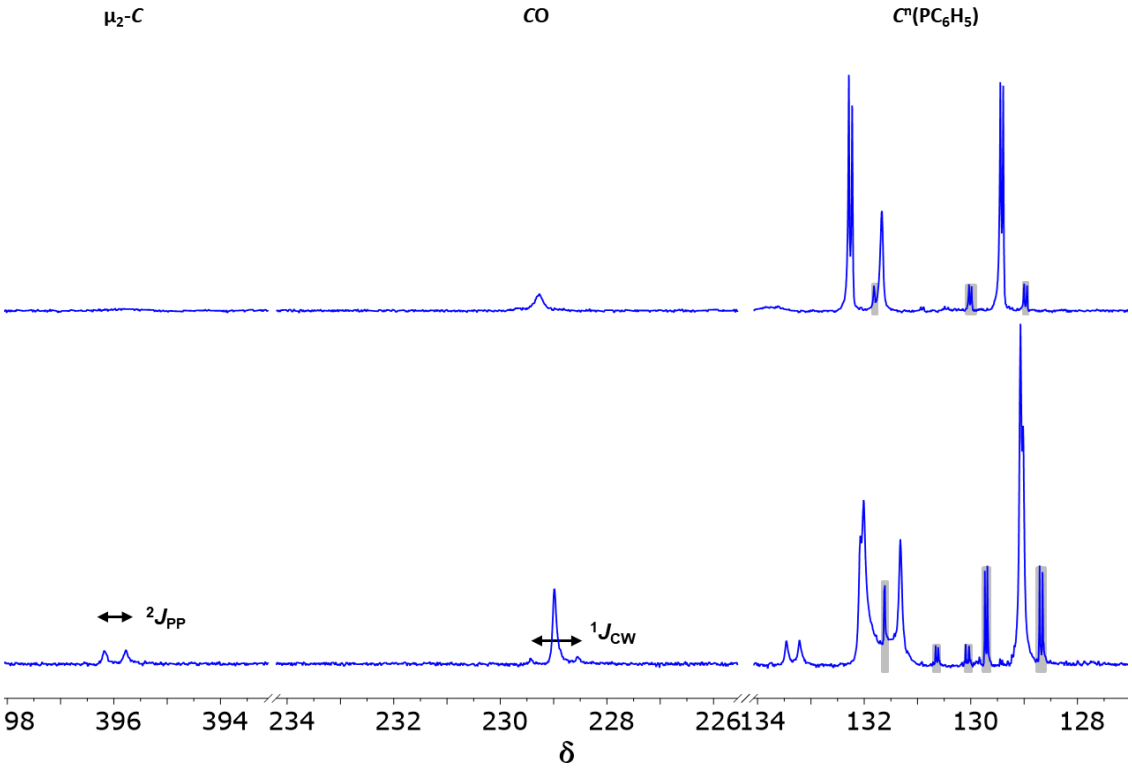

Figure 7.2: $^{13}C\{^1H\}$ NMR Spectrum of [WAu(μ$_2$-C)(CO)$_2$(PMe$_2$Ph)(Tp*)] (**7.3**) in CD_2Cl_2 at either ambient temperature or –20 °C highlighting the carbido resonance.

exhibits a broad resonance (δ_P = 1.87; fwhm = 610 Hz) lying between free PPh_3 (δ_P = –5.5) and [$AuCl(PPh_3)$] (δ_P = 33.18). Interestingly, the ^{31}P signals for **7.2** and **7.3** each show similar coupling to ^{183}W ($^3J_{PW}$ = 61 and 66 Hz, respectively) despite different chemical shifts, highlighting communication along the carbido linkage (Figure 7.1). A three-bond coupling to tungsten is often unresolved, *e.g.*, as found for the resonances for the phosphorus nuclei in chelate **3.3b**, while the coupling for gold metallacarbynes is relatively large compared with, *e.g.*, two bond couplings of phosphoniocarbyne [$WPd(\mu_2\text{-}CPPh_3)Br(CO)_2(Tp^*)$] (**6.5**) ($^2J_{PW}$ = 119 Hz) and is most likely a reflection of the high *s*-character in bonding to the *sp*-hybridised gold .

The carbido resonances in the $^{13}C\{^1H\}$ NMR spectra occur at the highest frequencies encountered thus far (δ_C = 389.9–400.5) with resolved phosphorus couplings (*ca* $^2J_{CP}$: 75–81 Hz) but devoid of ^{183}W satellites due to signal/noise being compromised by fluxional broadening that is incipient even at –20 °C (Figure 7.2). The larger PCy_3 derivative exhibits a sharp resonance while that for the smaller PMe_2Ph example is broad (fwhm = 159 Hz) indicating rotation that is inhibited, although acquiring data at low temperature (–20 °C) remedies this and a doublet is resolved. For **7.2**, a small increase in tungsten-carbonyl coupling occurs ($^1J_{CW}$ = 181 Hz) from strong σ-donation of PCy_3 along the spine, relative to **7.3** ($^1J_{CW}$ = 175 Hz). Data for the PPh_3 derivative **7.4** could only be acquired in the presence of excess PPh_3 but still results in a broad signal with unresolved coupling for the carbido (δ_C = 389.9) indicating a weak Au–P bond in solution

Satisfactory crystals of **7.3** or **7.4** were not forthcoming instead producing tiny needles that did not usefully diffract when irradiated with conventional or synchrotron radiation. Fortunately, **7.2** did provide large crystals, analysis of which confirmed the metallacarbyne linkage (W–C: 1.813(4); Au–C: 2.000(4) Å) and show a relatively short Au–C bond like the platinum(II) complexes; the first structure of a Class B gold species (Figure 7.3). This Au–C bond is longer than either [$(PCy_3)_2Cl_2Ru{\equiv}C{:}{\rightarrow}AuCl$] (1.921(3) Å) or [$\{(PCy_3)_2Cl_2Ru{\equiv}C{:}\}_2{\rightarrow}Au]BF_4$ (1.960(1)/1.974(9) Å), [69] of Class C μ_2-carbido or μ_3-species [$Rh_2(\mu_3\text{-}CAuCl)Cl_2(\mu\text{-}DMAD)(\mu\text{-}dppm)_2$] (1.979(7) Å) and [$Ru_2Au(\mu_3\text{-}C)\{N(SiMe_3)\}_2(\mu\text{-}N^tBu)(Cp^*)_2$] (1.966(4) Å) that originate from dimetallacarbenes. [40-41] The Au–C bond length falls between those for the T-shaped digoldcarbido [$WAu_2(\mu\text{-}C)Cl_3(CO)_2(PCy_3)_2(Tp^*)_2$] that has both linear W–C–Au (Au–C = 1.946(5)Å) and orthogonal W–C–Au (Au–C = 2.091(5)Å) geometries. [72] To explore the carbido/alkynyl analogy, the alkynyl complexes [$Au(C{\equiv}CMe)(PCy_3)$] and [$Au(C{\equiv}CC_6H_4NO_2\text{-}4)(PCy_3)$] have Au–C bond lengths of 2.007(8) and 2.005(7) Å, [542] *i.e.*, the bond is somewhat insensitive to variations in the mesomeric nature of substituents. Notably, the linear gold(I) positions the large distal PCy_3 furthest from the Tp* allowing a near linear W–C–Au linkage (177.6(3) °), perturbed only slightly by a proximal benzene solvate.

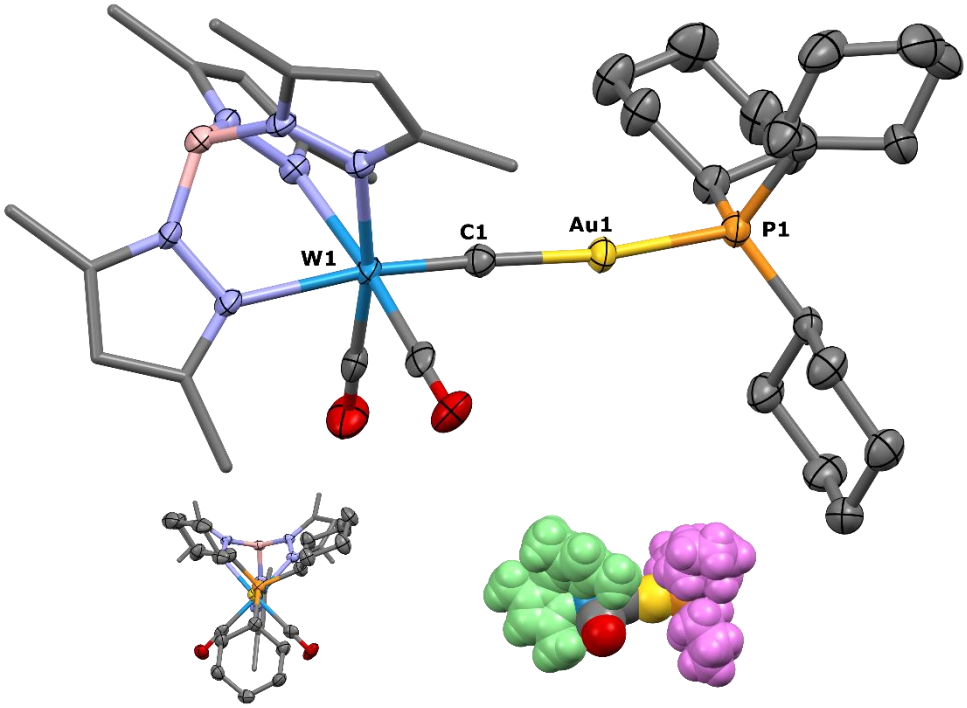

Figure 7.3: Molecular structure of [WAu(μ$_2$-C)(PCy$_3$)(CO)$_2$(Tp*)] (**7.2**) in a single crystal of **7.2**·C$_6$H$_6$ as determined by X-Ray Diffractometry. Ellipsoids are drawn at the 50% probability surface with pyrazolyl rings simplified and C$_6$H$_6$ solvent and hydrogens omitted for clarity. Insets: a) View down the key molecular linkage, b) Spacefill representation highlighting a separation of phosphine (pink) from the *tris*-pyrazolylborate (green) ligand. Selected bond lengths (Å) and angles (°): W1–C1 1.813(4), C1–Au1 2.000(4), Au1–P1 2.310(1), W1–C1–Au1 177.6(3), C1–Au1–P1 171.4(1).

Geometric optimisation of the model complex [WAu(μ$_2$-C)(CO)$_2$(PMe$_3$)(Tp)] (**7.2***) was performed (DFT: ωB97X-D/6-31G*/LANL2Dζ) to return a similar geometry to that experimentally determined for the core of **7.2** (Figure 7.4). The LUMO and LUMO+1 display empty orbitals that envelope the gold(I) centre but remain anti-bonding between the carbido and tungsten centres; a very different topology to other complexes computed thus far. The HOMO describes the retrodonation to the carbonyl ligands while the HOMO–1/–2 show the carbyne π-bond, which is anti-bonding with respect to gold(I). The HOMO–3 comprises a σ-network from the nitrogen of Tp* through tungsten and along the linear carbido linkage, and similar channels are available deeper in the manifold such as HOMO–21. This σ-bonding is quite possibly responsible for the strong transmission of coupling along the spine between ^{183}W to ^{31}P nuclei evident in the ^{31}P{^{1}H} NMR spectrum. Meanwhile, the complex contains a short Au–C bond (1.981 Å), and the HOMO–12 suggests this may in part reflect modest π-bonding to gold(I).

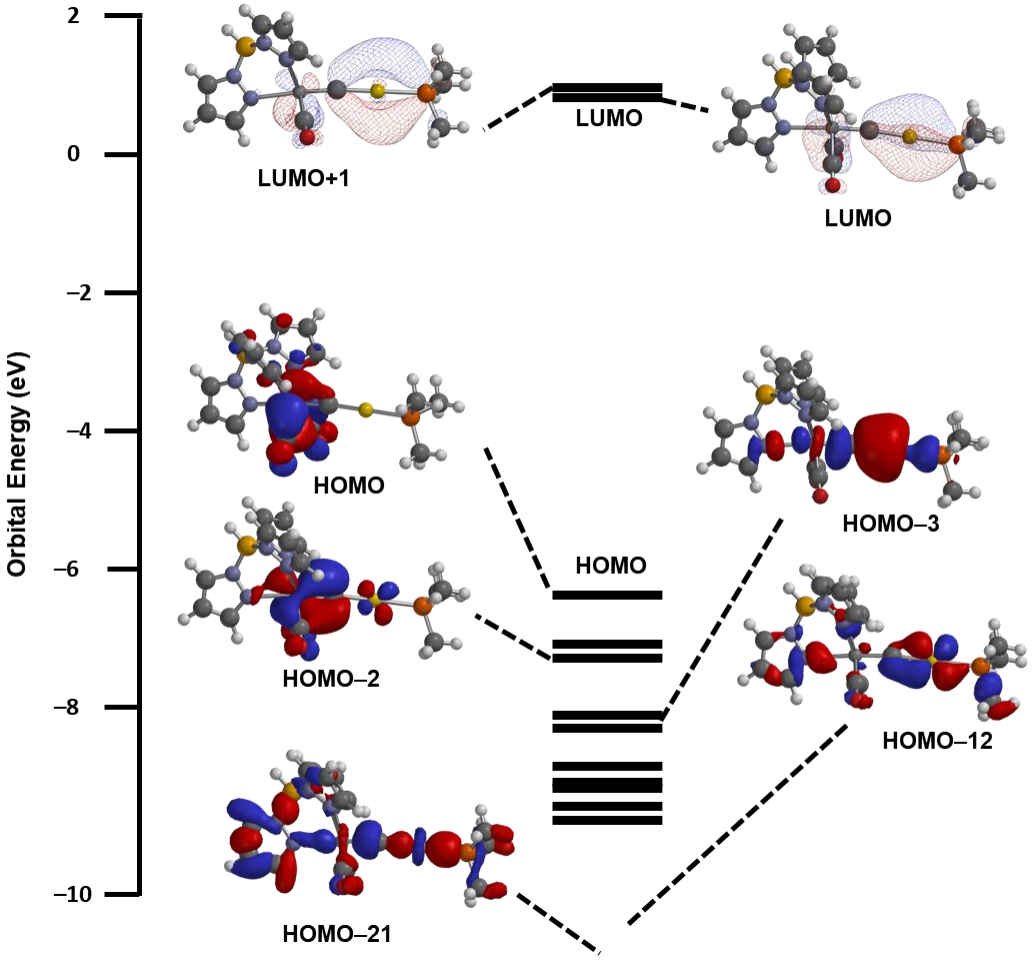

Figure 7.4: Frontier orbitals of interest for [WAu(μ$_2$-C)(CO)$_2$(PMe$_3$)(Tp)] (**7.2***).

N-heterocyclic carbenes are typically stronger σ-donors (even stronger for cyclicaminoalkane carbenes or CAAC's), [543-546] and have been deployed extensively with late transition metals as supporting ligands in catalysis, [547-549] particularly gold(I). [550-552] These ligands have also been employed for the synthesis of gold alkynyls [553-555] and as termini for carbon-wire, *e.g.*, tetracarbido, systems. [556] It therefore seemed that NHCs might serve as suitable donors for the disaggregation of **7.1**. Stirring freshly generated *N*-*N*'-dimesitylimidazolecarbene (IMes) with **7.1** in THF results in slow conversion to [WAu(μ$_2$-C)(CO)$_2$(IMes)(Tp*)] (**7.5**) as evident from infra-red spectroscopy (ν_{CO}) and a colour change to golden-yellow, however, heating overnight (60 °C) is required for full conversion (Scheme 7.3). Presumably the sluggish reaction reflects the steric obstruction of incorporating IMes, a large overhanging ligand forced to juxtapose with Tp* despite being a stronger donor (ν^T = 2050.7 cm^{-1}). [557] This is also consistent with the buried volume calculations for trivial [AuCl(L)] complexes between PMe$_2$Ph (30.5%) PCy$_3$ (38.8%) and IMes (36.5%)[558]

Alongside data already acquired for the phosphine derivatives, complex **7.5** is somewhat unremarkable spectroscopically. Lower frequency carbonyl vibrations are observed (ν_{CO}: 1945,

1850 cm^{-1}) consistent with the strong σ-basicity compared with phosphines. Likewise, the NHC causes the carbido resonance to appear in the $^{13}C\{^1H\}$ NMR spectrum at even higher frequency (δ_C = 402.1; $^1J_{CW}$ = 152 Hz (Figure 7.5). This is the most downfield resonance of any metallacarbyne bearing the Tp* framework including later discoveries (*vide infra*). Furthermore, **7.5** exhibits a carbido resonance with the best resolved coupling to ^{183}W in the ^{13}C NMR spectrum (Figure 7.5). The ^1H and $^{13}C\{^1H\}$ spectra are comprised of sharp signals indicating C_s symmetry and that the NHC-plane likely lies orthogonal to the Tp* ligand.§§§§§§§§§§§§§§§§§§§§§§

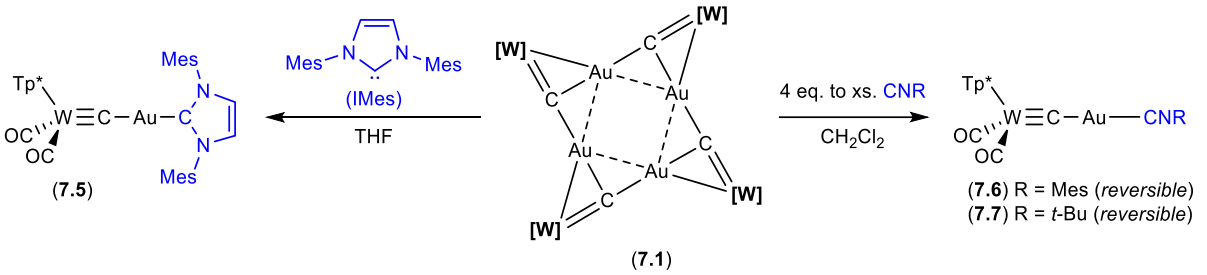

Scheme 7.3: Disaggregation of [W(≡Au)(CO)$_2$(Tp*)] **7.1** with an *N*-heterocyclic carbene or isocyanides.

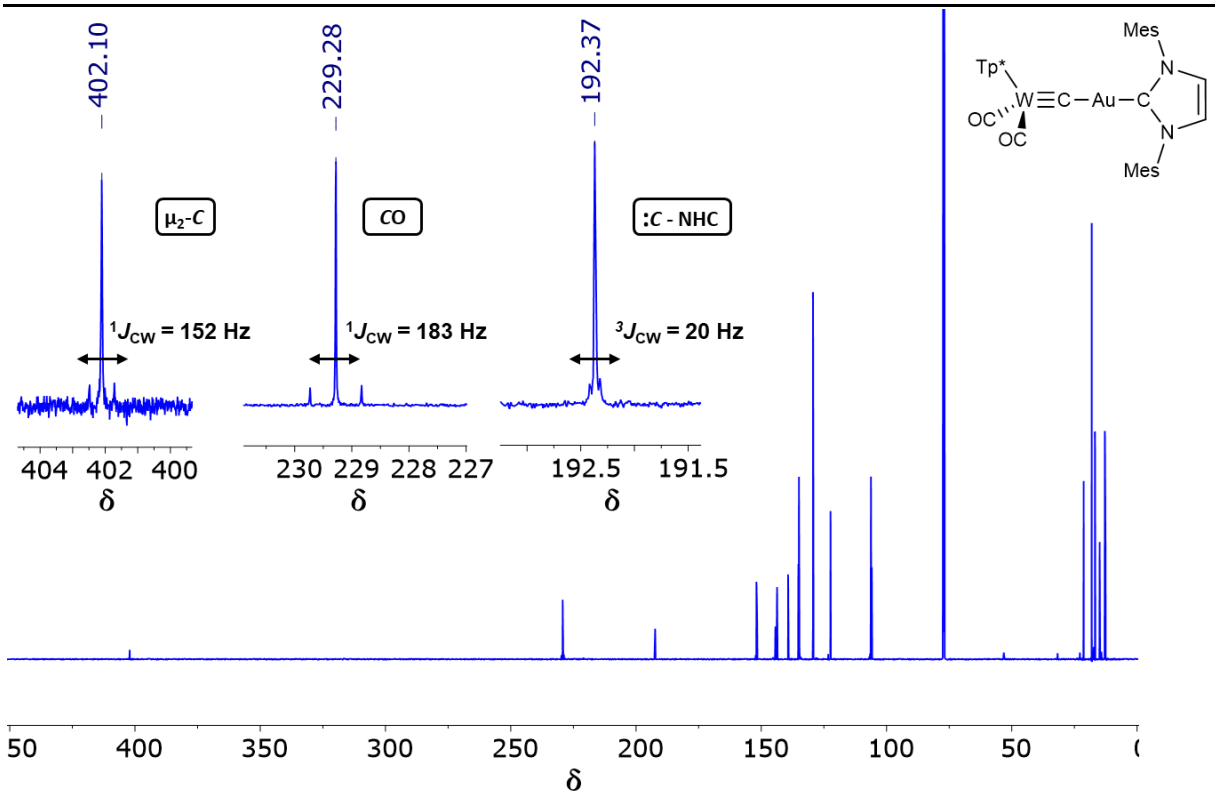

Figure 7.5: $^{13}C\{^1H\}$ NMR spectrum of [WAu(μ$_2$-C)(CO)$_2$(IMes)(Tp*)] (**7.5**).

§§§§§§§§§§§§§§§§§§§§§§ Rapid rotation about the Au–C bond could not be excluded but seems unlikely given the steric bulk of the NHC ligand directed back towards the W–C–Au spine.

Structural elucidation of a gold(I) complex bearing a carbyne and an NHC was desirable for the many comparisons that could be made. Growing single crystals was deceptively challenging with an alternative species repeatably forming (discussed in Section 7.3), while tiny needles of **7.5** only diffracted when irradiated with a synchrotron source. The consequence is that a somewhat imprecise structural model for **7.5** (R_1 = 0.0598) was developed, limiting discussion of structural parameters (Figure 7.6). The structure supports metallacarbyne bonding (W–C: 1.82(1); Au–C: 1.98(1) Å), however, the Au–C1 (carbido) is similar to that measured more precisely for **7.2**. Meanwhile, the Au–C19 (carbene) bond length of 2.04(1) Å is significantly longer despite the imprecision, suggesting (qualitatively) the μ_2-carbido is a stronger donor than a carbene to gold(I). Furthermore, the carbene bond is elongated compared with archetypical [AuCl(IMes)] [1.998(5) Å**********][560] thus the strong *trans*-influence of the μ_2-carbido most likely acts in concert with the steric clash of Tp* and IMes ligands. The NHC **7.5** is also linear along the carbido spine (W–C–Au: 174.5(6)°) in addition to the geometry of gold(I) (C1–Au–C19: 175.3(4)°), where the NHC plane is now coplanar with one pyrazolyl ring and the *trans* carbonyl; the plane no longer bisects Tp*, a phenomenon also noted for select isocyanide platinum(II) complexes (Chapter Four).

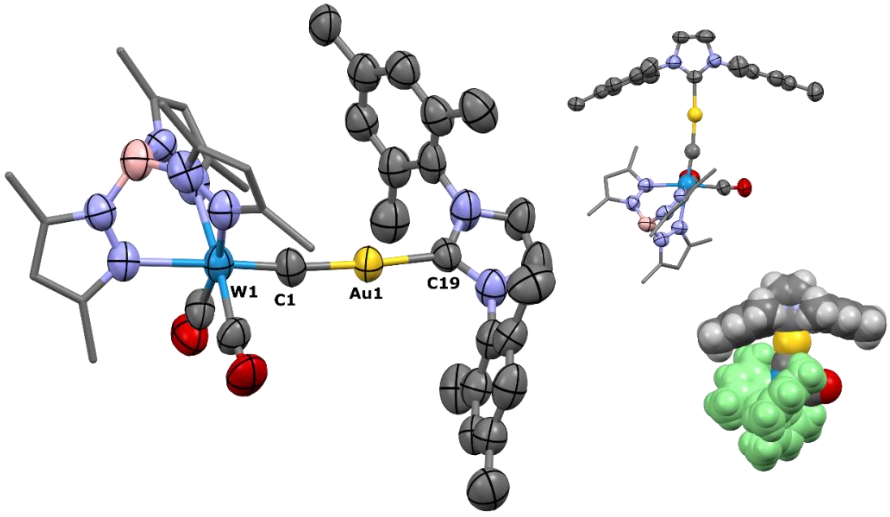

Figure 7.6: Molecular structure of [WAu(μ_2-C)(CO)$_2$(IMes)(Tp*)] (**7.5**) in a single crystal as determined by synchrotron X-Ray Diffractometry. Ellipsoids are drawn at the 50% probability surface with pyrazolyl rings simplified and hydrogens omitted for clarity. Insets: a) Ball and stick representation as viewed down the key molecular linkage and co-planar with the NHC ligand, b) Spacefill representation highlighting the proximity of NHC ligand with the *tris*-pyrazolylborate (green) ligand. Selected bond lengths (Å) and angles (°): W1–C1 1.82(1), C1–Au1 1.98(1), Au1–C19 2.04(1), W1–C1–Au1 174.5(6), C1–Au1–C19 175.3(4).

********** Several repeated structures populate the CCDC where this distance is from the structure of lowest error (R' = 1.61). Other distances exist with their corresponding R_1 values: 1.999(5) Å {R^1 = 2.9%};[559] 1.916(19) Å {R^1 = 3.42%}.[560]

Having featured earlier in this thesis, isocyanides are weakly π-accepting ligands, comparable σ-donors to phosphines but weaker net donors than NHCs. Treating **7.1** with a slight excess of aryl (CNMes) and alkyl (CN^{t}Bu) isocyanide results in a facile reaction to provide [WAu(μ$_2$-C)(CNR)(CO)$_2$(Tp*)] (R = Mes **7.6**; ^{t}Bu **7.7**) as evident in solution from infra-red spectroscopy of the newly forming product which exhibits a lone pair of carbonyl absorptions (*ca* ν_{CO}: 1956/1852 cm^{-1}) accompanied by coordinated (ν_{CN}: 2192/2219 cm^{-1}) and free (ν_{CN}: 2120/2136 cm^{-1}) isocyanide vibrations. Pure yellow solids of **7.5**/**7.6** can be obtained from concentration of these mixtures into *n*-hexane, however, returning the isolated solid into solution results in reformation of **7.1** and liberated isocyanide (Figure 7.7). This suggests **7.5**/**7.6** are only stable in the solid state or when in solution in the presence of excess isocyanide; otherwise an equilibrium ensues, indicating reversible binding of CNR ligands as observed for PPh$_3$ and in contrast to alkyl phosphines and NHCs.

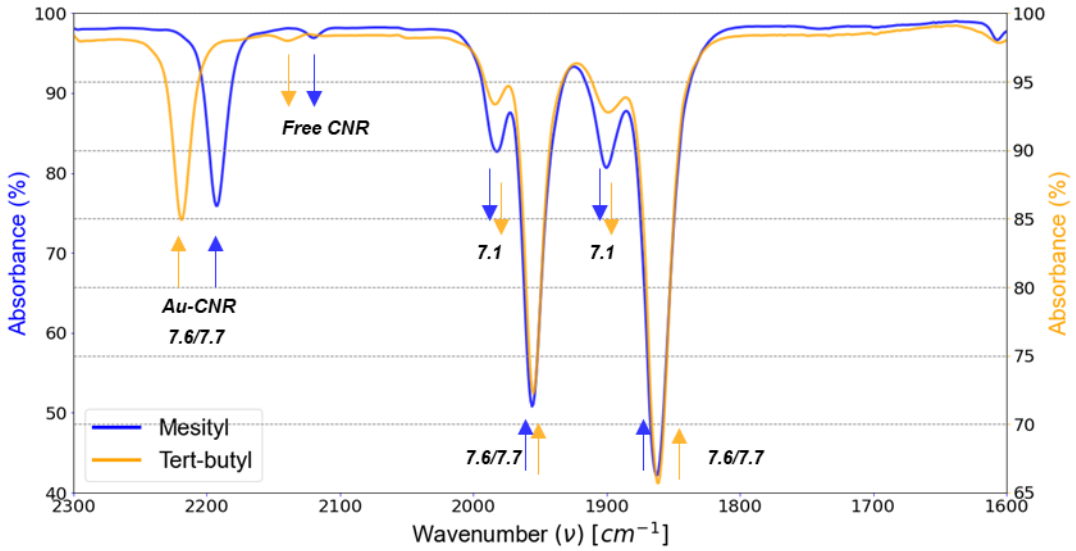

Figure 7.7: Infra-red spectra of [WAu(μ$_2$-C)(CNMes)(CO)$_2$(Tp*)] (**7.6**) and [WAu(μ$_2$-C)(CN^{t}Bu)(CO)$_2$(Tp*)] (**7.7**) when returned to solution reforming **7.1** and excess isocyanide.

This equilibrium provides a challenge for spectroscopy. Faster acquisition techniques such as IR and ^{1}H NMR spectroscopies return signals for largely one complex, however, longer ^{13}C{^{1}H} NMR acquisitions ultimately result in spectra littered with other signals consistent with **7.1** accompanying the key resonances for **7.6**/**7.7**. Nevertheless, the ^{1}H NMR spectra is unremarkable, and the carbonyl vibrations are akin to those of the phosphine adducts supporting a similarly π-basic tungsten. A change is noted in the ^{13}C{^{1}H} NMR spectra as μ$_2$-carbido signals are to lower frequency than the previous gold metallacarbynes (δ_C = 377.3/377.4), with each being too broad to discern ^{183}W coupling. Between isocyanides this suggests the weaker σ-donation of CNMes is compensated for by improved π-acidity, while the shift to lower frequency reflects the reduced,

combined donor properties of isocyanides (*ca* ν^T = 2073 cm^{-1} for related CNMe) [561] compared with phosphines and NHCs. This also explains the reversible equilibria placing isocyanide ligands at the cusp of donors sufficient to maintain disaggregation of **7.1**.

Single crystals of **7.6**/**7.7** were grown in the presence of excess isocyanide, ultimately providing needles that only diffracted *via* synchrotron irradiation for **7.6** to yield an imprecise structural model (R_1 = 8.23%) that nevertheless confirmed connectivity (Figure 7.8). Metallacarbyne bonding is clear and **7.6** contains the shortest Au–C bond of the series (1.94(1) Å) consistent with the weaker donor properties of isocyanide. Contraction of this bond agrees with the notion of isocyanide dissociation. Copious structural data are available for isocyanide complexes of gold(I) alkynyls, *e.g.*, the complex [Au(C≡CPh)(CNXyl)] has gold alkynyl and isocyanide bond lengths of 1.974(7) and 1.957(7) Å, respectively, [562] although this molecule packs as head-to-tail dimer due to a weak (3.392 Å) aurophilic interaction. These bond lengths [Au–CC (1.989(8), Au–CN 1.958(7) Å] are not varied beyond precision limits (6 e.s.d.) upon inclusion of a negatively mesomeric alkynyl substituent as, *e.g.*, in the complex [Au(C≡C$C_6H_4NO_2$-4)(CNXyl)]. [563] This insensitivity mirrors observations noted above for NCH coordinated gold(I) alkynyls. Unlike other carbido structures, **7.6** exhibits a linear gold(I) (C1–Au–C19: 174.7(6) °) but with a bent μ_2-carbido linkage (W–C–Au: 164.6(8)°), however this is clearly a consequence of crystal packing as interdigitation of each CNMes with the corresponding pyrazolyl rings results in bending of the tubular molecule. Aurophillic interactions are often exhibited in slender gold(I) complexes, [564] however the bulbous shape of Tp* prevents this interaction [Au1···Au1' = 6.606(2) Å] *via* packing of somewhat globular molecules. Similarly, to the NHC **7.5**, the mesityl plane of **7.6** is co-planar with a pyrazolyl ring and the *trans*-carbonyl, likely an electronic effect rather than a consequence of inter-ligand interactions given the long distance between rings (*ca* ~3.63(2) Å).

Geometric optimisation of the model [WAu(μ_2-C)(CN^{t}Bu)$(CO)_2$(Tp)] (**7.7***) *in silico* was successfully completed, while [WAu(μ_2-C)(CNPh)$(CO)_2$(Tp)] failed to converge. Many similar orbital morphologies are noted for **7.7*** as compared with **7.2***, such as the enveloping LUMO and contracted Au–C bond that includes a modest gold(I)-carbon π-component (Figure 7.9). The most intriguing difference is the π-retrodonation from gold(I) to the isocyanide ligand such as that exhibited in HOMO–19. Retrodonation from gold(I) to isocyanides is at best modest, accounting for their activation upon coordination towards nucleophilic attack. [565] Deep in the orbital manifold,

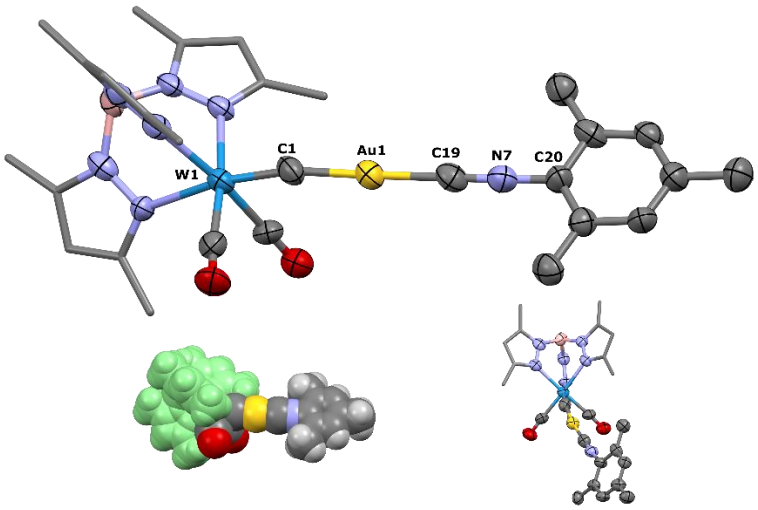

Figure 7.8: Molecular structure of [WAu(μ$_2$-C)(CNMes)(CO)$_2$(Tp*)] (**7.5**) in a single crystal of as determined by X-Ray Diffractometry. Ellipsoids are drawn at the 50% probability surface with pyrazolyl rings simplified and hydrogens omitted for clarity. Insets: a) Spacefill representation highlighting the open μ$_2$-carbido linkage protruding from the *tris*-pyrazolylborate (green) ligands, b) View down the key molecular linkage showing the deviation from linearity of the isocyanide bearing a mesityl-group. Selected bond lengths (Å) and angles (°): W1–C1 1.86(1), C1–Au1 1.94(1), Au1–C19 1.97(1), C19–N7 1.21(2), N7–C20 1.35(2), W1–C1–Au1 164.6(8), C1–Au1–C19 174.7(6), Au1–C19–N7 178(1), C19–N7–C20 177(1).

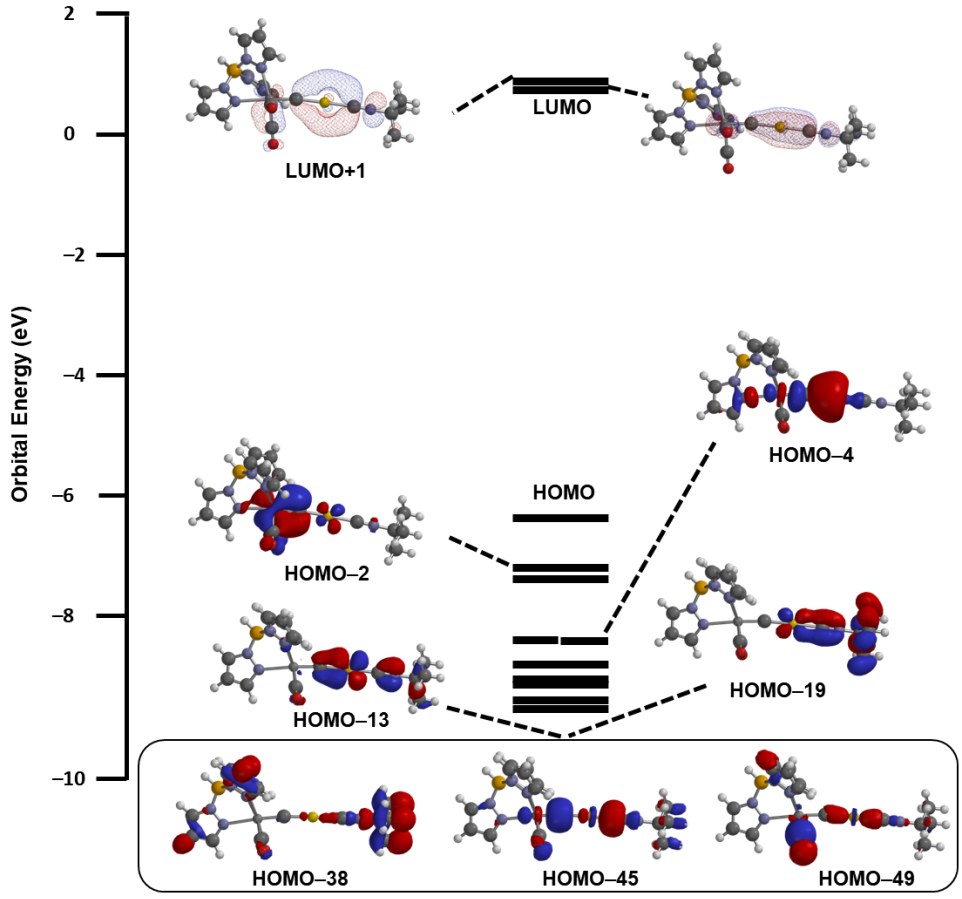

Figure 7.9: Frontier orbitals of interest for [WAu(μ$_2$-C)(CN^{t}Bu)(CO)$_2$(Tp)] (**7.7***).

a collection of σ-networks is available likely hinting intermetallic communication along this carbido spine.

This subsection demonstrates new gold(I) metallacarbynes can be prepared by disaggregation of $[WAu(\mu_2\text{-}C)(CO)_2(Tp^*)]_4$ with sufficiently nucleophilic and strong donor ligands. Although isocyanides are strong donors and readily bind to gold(I), the *trans*-influence of the μ_2-carbido is enough to labilise the *trans*-isocyanides in solution, whereas stronger donors such as alkyl phosphines (PCy_3, PMe_2Ph) and IMes (NHC) remain bound.

7.2.2 Tin–Gold Transmetallation

Disaggregation of $[W(\equiv CAu)(CO)_2(Tp^*)]_4$ provides a convenient late-stage platform to install diversity in auriocarbynes, in much the same way that oligomeric gold alkynyls $(AuC\equiv CR)_n$ have been used extensively to generate a multitude of complexes of the form [Au(C≡CR)(L)]. The alternative classical approach to such complexes involves reaction of the corresponding chloride complex [AuCl(L)] with an appropriate organometallic alkynyl nucleophile, typically Grignard reagents. Magnesio-carbidos, whilst plausible, remain unknown while the lithiocarbynes $[M(\equiv CLi)(CO)_2(Tp^*)]$ are somewhat prone to outer-sphere electron transfer in reactions with Lewis acidic metal halides, for which redox processes are facile, *e.g.*, platinum (Chapter Five), mercury(II) (*vide infra*) and gold(I).†††††††††††††††††††† The transmetallation from tin to gold has been described and has been implicated in the application of stannylcarbynes to diverse carbyne syntheses mediated by combination of $[Pd(PPh_3)_4]/[AuCl(SR_2)]$ (SR_2 = SMe_2, tetrahydrothiophene).[144-149] The synthetic utility of this approach for the isolation of auriocarbynes will now be addressed.

Previously the reaction between $[Mo(\equiv CSnMe_3)(CO)_2(Tp^*)]$ and $[AuCl(PPh_3)]$ was found to provide $[MoAu(\mu_2\text{-}C)(PPh_3)(CO)_2(Tp^*)]$ (THF: ν_{CO}: 1968, 1882 cm^{-1}), however while the tungsten analogue most likely forms similarly, it was prone to phosphine loss to provide **7.1**, which was also obtained from $[W(\equiv CSnMe_3)(CO)_2(Tp^*)]$ and $[AuCl(AsPh_3)]$ *via* the fleetingly observed $[WAu(\mu\text{-}C)(AsPh_3)(CO)_2(Tp^*)]$ (ν_{CO}: 1998, 1915 cm^{-1}). In a similar manner, stirring $[W(\equiv CSnBu_3)(CO)_2(Tp^*)]$‡‡‡‡‡‡‡‡‡‡‡‡‡‡‡‡‡‡ with $[AuCl(PPh_3)]$ initially provides carbonyl vibrations consistent with the expected phosphine complex $[WAu(\mu_2\text{-}C)(PPh_3)(CO)_2(Tp^*)]$ (**7.4**) (ν_{CO}: 1954,

†††††††††††††††††††† Similar issues are occasionally encountered in the syntheses of alkynyls of these metals in which oxidative coupling of the organometallic nucleophiles leads to 1,3-butadiynes, as productively developed in protocols such as Glaser, Eglinton or Hay couplings.

‡‡‡‡‡‡‡‡‡‡‡‡‡‡‡‡‡‡ The previous study employed trimethylstannyl carbynes, however toxicity concerns led to subsequent replacement with the tri-*n*-butyl derivative.[72]

1851 cm^{-1}, *vide supra*) before rapid emergence of **7.1** aggregating in solution. Likewise, transmetallation immediately observed *via* $^{31}P\{^{1}H\}$ NMR spectroscopy with excess [AuCl(PPh_3)] records the corresponding phosphine resonance (δ_P = 1.87) prior to reformation of golden ring **7.1** accompanied by small depositions of colloidal gold. This suggests that despite the alternative method of transmetallation, which ultimately allowed fleeting observation of the species mentioned in the literature, the donor strength of PPh_3 is too little to adequately stabilise the species once formed, consistent with the converse reaction of adding PPh_3 to the golden ring **7.1** (Figure 7.10). Notably, in his seminal paper on gold alkynyls obtained by disaggregation of the coordination polymer 'phenylethynylgold(I)', Coates developed a reactivity series that reflected a series of displacement reactions for 'L' in the complexes of the form [Au(C≡CPh)(L)], where phosphite displaced phenylisocyanide while the isocyanide with displace triethyl arsine:

$$PEt_3 > P(OPh)_3 > CNPh > AsEt_3 > SbEt_3 > NH_3 > NH_2R > NHR_2 > NR_3$$

Gratifyingly, this series then parallels observations for derivatives of **7.1**.[566]

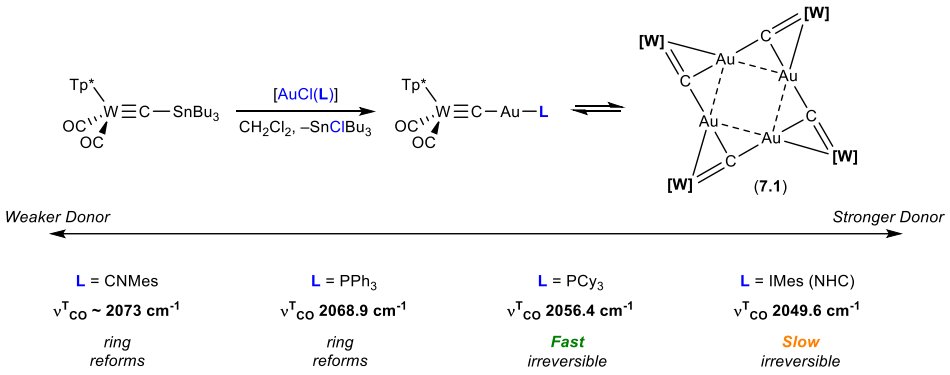

Figure 7.10: Spectroscopic observation of [WAu(μ2-C)(PPh_3)$(CO)_2$(Tp*)] (**7.4**) by infra-red analysis and $^{31}P\{^{1}H\}$ NMR with and without excess PPh_3.

Insufficient donor strength would clearly provide similar issues of auriocarbyne stability, expected to reform **7.1** irrespective of a transmetallation or disaggregation route, highlighting a consideration in species design. Having established that **7.2** is a stable bimetallic species (PCy_3 donor) once produced, a transmetallation was performed with [AuCl(PCy_3)] to compare the synthetic pathways where PCy_3 is not lost once coordinated to gold(I). Infra-red spectroscopy confirms facile transmetallation devoid of **7.1** formation on a comparable timescale to the disaggregation method yet with more by-products. Repeating the transmetallation at 0 °C with the exclusion of light somewhat alleviated the formation of by-products suggesting extrusion of gold *via* ambient light is a likely component. Similarly, transmetallation of [W(≡C$SnBu_3$)$(CO)_2$(Tp*)] with preformed carbene [AuCl(IMes)] occurs smoothly from 0 °C in the absence of light, although slower relative to PCy_3, presumably from the clash of large IMes and Tp* groups (consistent with

observations recorded from the disaggregation route). Similar treatment with [AuCl(CNMes)] also results in facile transmetallation and clear observation of **7.6**, yet as one equivalent of CNMes is delivered, then the equilibrium with **7.1** is quickly established consistent with original observations of **7.6** behaviour.

Overall, these findings support facile carbido transmetallation from tin to gold, but the stability of the ultimate metallacarbyne relative to **7.1** is dictated by donor strength. Disaggregation of **7.1** is generally the superior method for accessing diverse gold(I) metallacarbynes, however, some desired fragments (such as a terpyridine) may not behave as donors and transmetallation to a prefabricated gold(I) chloride could remedy this issue. The tetramer **7.1** involves 'ligand-free' gold and isolable aggregate formation may not be general across other elements whereas transmetallation may be more generally observed.

7.2.3 In Search of Gold(III) Carbido Complexes

In an attempt to broaden the utility of transmetallation, gold(III) metallacarbynes were sought. Unfortunately, stirring [W(≡CSnBu$_3$)(CO)$_2$(Tp*)] with [AuCl$_3$(PPh$_3$)] or [AuCl$_3$(PCy$_3$)] in each case resulted in complex mixtures of at least five species forming instantly at low temperature (–20 °C). As indicated by ^{31}P NMR spectroscopy, none of these corresponded to **7.2** or **7.4** and all resisted purification *via* chromatography. Analysis of the mixtures revealed that [W$_2$(≡C–C≡)(CO)$_4$(Tp*)$_2$] predominates accompanied colloidal gold, consistent with either outer-sphere single-electron oxidation of alternatively at least two transmetallation steps occurring prior to a reductive elimination from gold(III). To divert from this decomposition pathway, a more protected gold(III) precursor was sought, that might be less disposed to reductive elimination pathways. The cyclometallated complex [AuCl$_2$(ppy)] (ppy = phenylpyridinyl) has been used extensively as a robust core for the synthesis of numerous *bis*(alkynyl) complexes of gold(III) that do not suffer reductive elimination and provide stable materials [Au(C≡CR)$_2$(ppy)] of interest for electro-optical applications.[567] A slow transmetallation occurred over two days to provide a vivid purple complex that defied isolation despite eluting as a single species *via* chromatography. Spectroscopic measurement of crude or partially purified purple complex returned a slew of resonances, where the real structure was unable to be identified and was hence abandoned. These initial studies for gold(III) proved transmetallation is arguably more facile for gold(III) but over-addition plagues the synthesis of gold(III).

Many examples of gold(III) complexes arise from the chemical oxidation of gold(I), providing an alternative potential route to accessing gold(III) metallacarbynes. From the gold(I) metallacarbynes produced (*vide supra*), [WAu(μ$_2$-C)(PCy$_3$)(CO)$_2$(Tp*)] (**7.2**) and [WAu(μ$_2$-

C)(IMes)$(CO)_2$(Tp*)] (**7.5**) were presumed to provide the most robust scaffolds that might be the most amenable to further reactions given tris(alkynyl) complexes of gold(III) have been stabilised by trialkylphosphine[568] and NHC ligands.[569] Solutions of **7.2** and **7.5** in dichloromethane were treated with $PhICl_2$ as per a literature protocol that provides facile access to gold(III) carbenes (Scheme 7.4).[570] Each initially yellow solution changed slowly to a green colour prior to brown where infra-red spectra indicate several carbonyl species, but primarily produces [W(≡CCl)Cl_2(Tp*)][457] as an over-oxidation product, whereby $^{31}P\{^1H\}$ NMR spectroscopy verified [AuCl(PCy_3)] formation for the reaction of **7.2**. The tungsten terminus provides an alternative site of reactivity (the HOMO of **7.2*** discussed above) where oxidative decarbonylation affords the dichloro tungsten complex, as observed, *e.g.*, with the carbyne complexes [W(≡CXyl)Cl_2(Tp)].[571] W(≡CF)Cl_2(Tp*)],[117] and [W_2(μ-C_6)Cl_4(Tp*)$_2$].[450] There was no evidence for the presumed intermediates [WAu(μ-C)Cl_2(L)(Tp*)] (L = PCy_3, IMes) which must presumably enter into subsequent reaction steps that are more rapid than their formation. Increasing the amount of $PhICl_2$ had little effect on the formation of [W(≡CCl)Cl_2(Tp*)] and [W(≡C–C≡)W$(CO)_4$(Tp*)$_2$], with both species presumably arising from reductive elimination from gold(III).

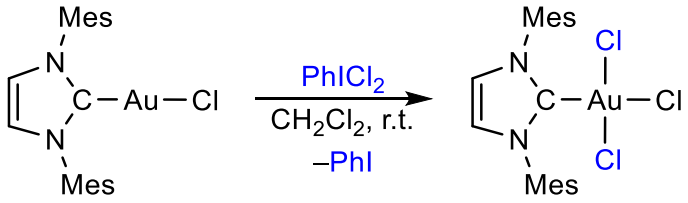

Scheme 7.4: Preparation of gold(III) carbenes *via* oxidation of gold(I).

Accessing gold(III) metallacarbynes through transmetallation or chemical oxidation proved unsuccessful. A gold(III) metallacarbyne was, however, obtained serendipitously through a reaction of platinum(II) species [WPt(μ$_2$-C)Br$(CO)_2$(PPh_3)$_2$(Tp*)] (**3.1b**) with gold(I) during attempts to coordinate a 'AuCl' fragment across the W≡C bond of a metallacarbyne to provide a μ$_3$-carbido, *cf.* [WRuAu_2(μ-C)$_2$$Cl_3$$(CO)_2$($PCy_3$)$_2$(Tp*)].[72] Supplying **3.1b** with [AuCl·SMe_2] under anaerobic conditions results in no discernible reaction. The assumed failed reaction mixture was opened to air where the orange solution rapidly changed to a deep red accompanied by colloidal gold deposition and grey metal consistent with elemental platinum, suggesting a non-trivial redox process was initiated by the air. The red compound corresponds to gold(III) metallacarbyne *cis*-[WAu(μ$_2$-C)$Cl_2$$(CO)_2$($PPh_3$)(Tp*)] (**7.8**) forming somewhat cleanly despite the reaction detritus accompanied by [AuCl(PPh_3)] as the major by-product (Scheme 7.5).

Attempted purification of **7.8** was inhibited by deposition of colloidal gold during flash chromatography, irrespective of stationary phase (silica gel or alumina). Instead, elution through

Celite® provides a clean solution of compound free of metal-containing debris, yet all attempts at recrystallisation resulted in a *ca* 1:1 mixture of **7.8** contaminated with [AuCl(PPh$_3$)]. Growth of single crystals and mechanical separation of red prisms (opposed to clear blocks) still yielded the similar compositions suggesting that larger crystals are comprised of both species co-crystallised. For this reason, spectroscopic characterisation is possible, yet each spectrum is populated with signals corresponding to [AuCl(PPh$_3$)].

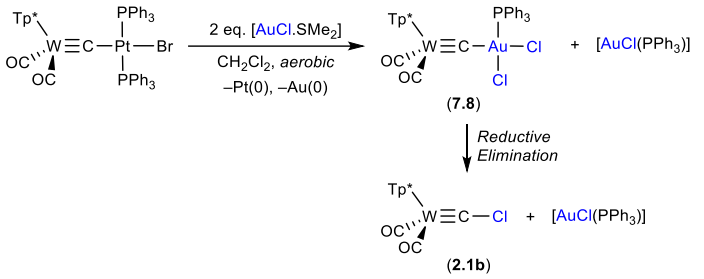

Scheme 7.5: Emergence of a gold(III) metallacarbyne from redox of gold(I) and platinum(II).

The $^{31}P\{^1H\}$ NMR spectrum shows a broad singlet for **7.8** (δ_P = 35.29; fwhm = 15 Hz) without resolvable coupling to ^{183}W indicative of the *cis*-relationship the tungsten-μ_2-carbido vector, occurring to slightly higher frequency of the co-contaminant [AuCl(PPh$_3$)] (δ_P = 33.19). Unfortunately, a $^{13}C\{^1H\}$ NMR spectrum was unable to be obtained given reductive elimination was relatively fast compared with the long acquisition time required (*ca* 16 hours), therefore, a carbido resonance was unable to be identified. This reductive elimination was verified by signals emerging that were consistent with formation of the chlorocarbyne [W(≡CCl)(CO)$_2$(Tp*)] (**2.1b,** δ_C = 205.6 and ^1H signals). A short Au–C bond is noted in the molecular structure (1.899(9) Å) (Figure 7.11) and is the shortest bond in gold metallacarbynes thus far (*ca* 1.94(1)Å **7.5**). In the solid state, a contracted Au–C bond (1.899(9) Å) is not accompanied by alteration of the W–C triple bond (1.849(9) Å) however carbonyl vibrations occur at much higher wavenumbers (ν_{CO} = 2047, 2000 cm^{-1}) indicate a relative reduction of π-basicity at tungsten as a result of the oxidised gold. With only one phosphine, interdigitation with Tp* lends support to favourable overlap between phenyl and pyrazolyl rings once more, also resulting in a bent linkage (W–C–Au: 167.7(5)°).

Access to gold(III) metallacarbynes has proved much more challenging than gold(I) species owed to over-addition, over-oxidation, or facile reductive elimination. It would however appear to be achievable through selective oxidation instead of transmetallation, where the latter is only possible in non-generalisable systems. This species represents the first examples of gold(III) carbido complexes and accompany [Rh$_2$H(μ_2-C)(μ-PPh$_2$C$_6$H$_4$-2)(Tp*)$_2$](Rh^{III}) [156] and [W$_2$(μ-

C)Cl_2(=X)(silox)$_4$](X = O, NXyl, W^{IV}) [56] as μ_2-carbidos with metal termini in elevated oxidation states.

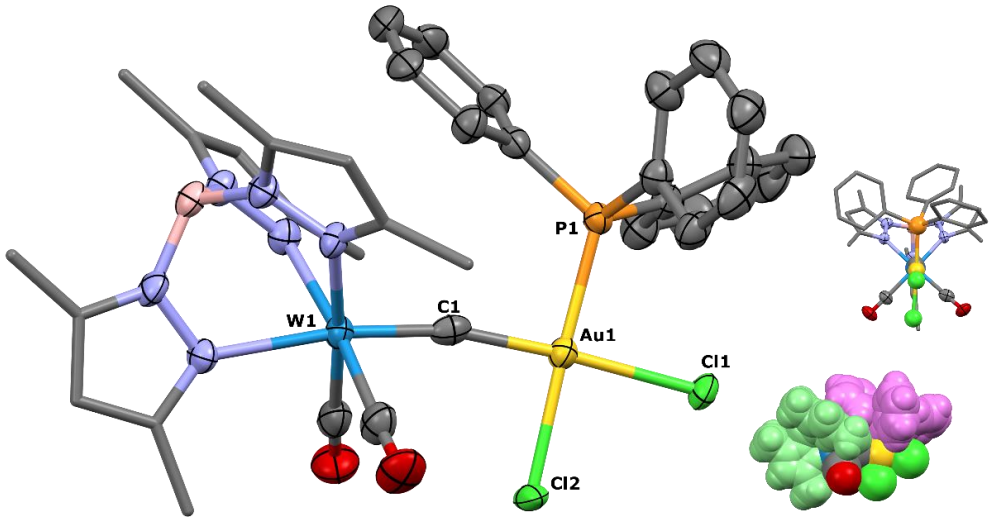

Figure 7.11: Molecular structure of [WAu(μ_2-C)Cl_2(PPh_3)$(CO)_2$(Tp*)] (**7.8**) in a single crystal of **7.8**·2($CHCl_3$) as determined by X-Ray Diffractometry. Ellipsoids are drawn at the 50% probability surface with pyrazolyl rings simplified and $CHCl_3$ solvent and hydrogens omitted for clarity. Insets: a) Ball and stick representation as viewed down the key molecular linkage, b) Space-filling representation highlighting the steric clash of phosphine (pink) with the sterically encumbering *tris*-pyrazolylborate (green) ligand. Selected bond lengths (Å) and angles (°): W1–C1 1.849(9), C1–Au1 1.899(9), Au1–Cl1 2.402(2), Au1–Cl2 2.381(2), Au1–P1 2.242(2), W1–C1–Au1 167.7(5), Cl1–Au1–Cl2 89.13(7), P1–Au1–Cl2 177.34(8).

7.3 Revisiting Golden Rings: Species in Solution and Five-fold Symmetry

Development of gold metallacarbynes has been facilitated by the availability of a tetrameric μ_3-carbido W_4Au_4 ring [W(≡CAu)$(CO)_2$(Tp*)]$_4$ (**7.1**, δ_C = 361.7; $^1J_{CW}$ = 76 Hz). The original report disclosed this aggregate that arises from transmetallation of [W(≡C$SnMe_3$)$(CO)_2$(Tp*)] to [Au$Cl(SMe_2)$], and confirmed it to be, *via* a crystal structure determination, a tetrameric, octametallic aggregation of 'W(≡CAu)$(CO)_2$(Tp*)' fragments. [375] During attempts to grow single crystals of NHC complex **7.5**, another gold aggregation was repeatably encountered across batches of yellow crystals with the molecular structure [W(≡CAu)$(CO)_2$(Tp*)]$_5$ (**7.9**)—*i.e.*, a pentameric, decametallic aggregation (Figure 7.12). These crops grown from **7.5** failed to identify crystals of the tetrameric species **7.1** in the mixture, despite collecting four datasets suggesting 7.1 was not present. This raises the issue of whether another alternative aggregations might also exist beyond the original tetramer and newly identified pentamer, cognisant that over 60 years ago, [566] Coates isolated two forms of 'AuC≡C*t*Bu', one which was soluble, yellow and tetrameric with a proposed

structure analogous to **7.1**, while the other white form was insoluble. *Both* forms reacted with PMe_3 to afford monomeric [Au(C≡C′Bu)(PMe_3)], highlighting the challenges of unravelling the structural challenges of labile, dynamic gold alkynyl chemistry. This sub-section will outline attempts into uncovering the inter-relationship of **7.9** and **7.1**.

First, it is useful to discuss the structural features of pentameric **7.9** as an independent structure compared to tetrameric **7.1**.§§§§§§§§§§§§§§§§§§§§§§§§ Pentameric **7.9** has the same space group as **7.1** ($P\bar{1}$) and hence each parameter is unique. The original report utilised mean values of structural parameters to discuss the bonding present, however, individual values should now be considered given the irregular shape of the pentamer structure (Table 7.1). The W–C and Au–C lengths are, however, largely similar with similar mean distances between tetramer and pentamer. Incorporating the extra carbyne to form a pentameric cycle does increase the angle about each pair of adjacent gold centres (113° *cf.* 104°) and this extends the inter-gold distance (Au···Au: 3.38–3.41 Å) to what might be considered as the limit defined for aurophillic interactions********** that in contrast the tetramer clearly exhibits. Given the bond strengths of aurophilic bonds are estimated to be in the range of 7-12 kcolmol^{-1}, the cumulative effect of these four aurophillic interactions (28-48 kcalmol^{-1}) presumably contributes in part to the stability of **7.1**;[564] the reduced magnitude in the pentamer likely disfavours its emergence. Specific to the pentamer are angles W–C–Au (155.6(7)/155.9°) and C–Au–C (110.2(5)/113.1(5)/113.6(5)°) altered from the tetramer (*ca.* 165 W–C–Au; 104° Au–C–Au'), which serve to connect the pentagonal core through buckling of the ring reminiscent of an open envelope conformation, whereas the octametallic core of **7.1** is essentially planar.

Structural analysis of **7.9** suggests the species is a natural extension of **7.1**, where rather modest shifts in bond lengths and angles do not hint at enthalpic ring strain disfavouring formation of more symmetric **7.1** *cf.* **7.9** other than the enhancement of circumannular aurophilic interactions. In terms of net entropy however the conversion of 5 equivalents of a tetramer to 4 equivalents of a pentamer would be expected to be thermodynamically disfavoured.

$$5 \times \mathbf{7.1} \rightarrow 4 \times \mathbf{7.9} \quad \Delta H < 0 \quad \textit{loss of aurophilic interactions}$$
$$\Delta S < 0 \quad \textit{increase in order}$$

§§§§§§§§§§§§§§§§§§§§§§§§ In this sub-section, discussion will refer to **7.1** as 'tetramer' and **7.9** and 'pentamer' as to facilitate logical progression of arguments as opposed to the standard labelling nomenclature of this thesis.

********** Schmidbaur has suggested that aurophillic interactions are broad but occupy lengths between 2.85–3.50 Å, below the sum of covalent radii (3.8 Å). [564]

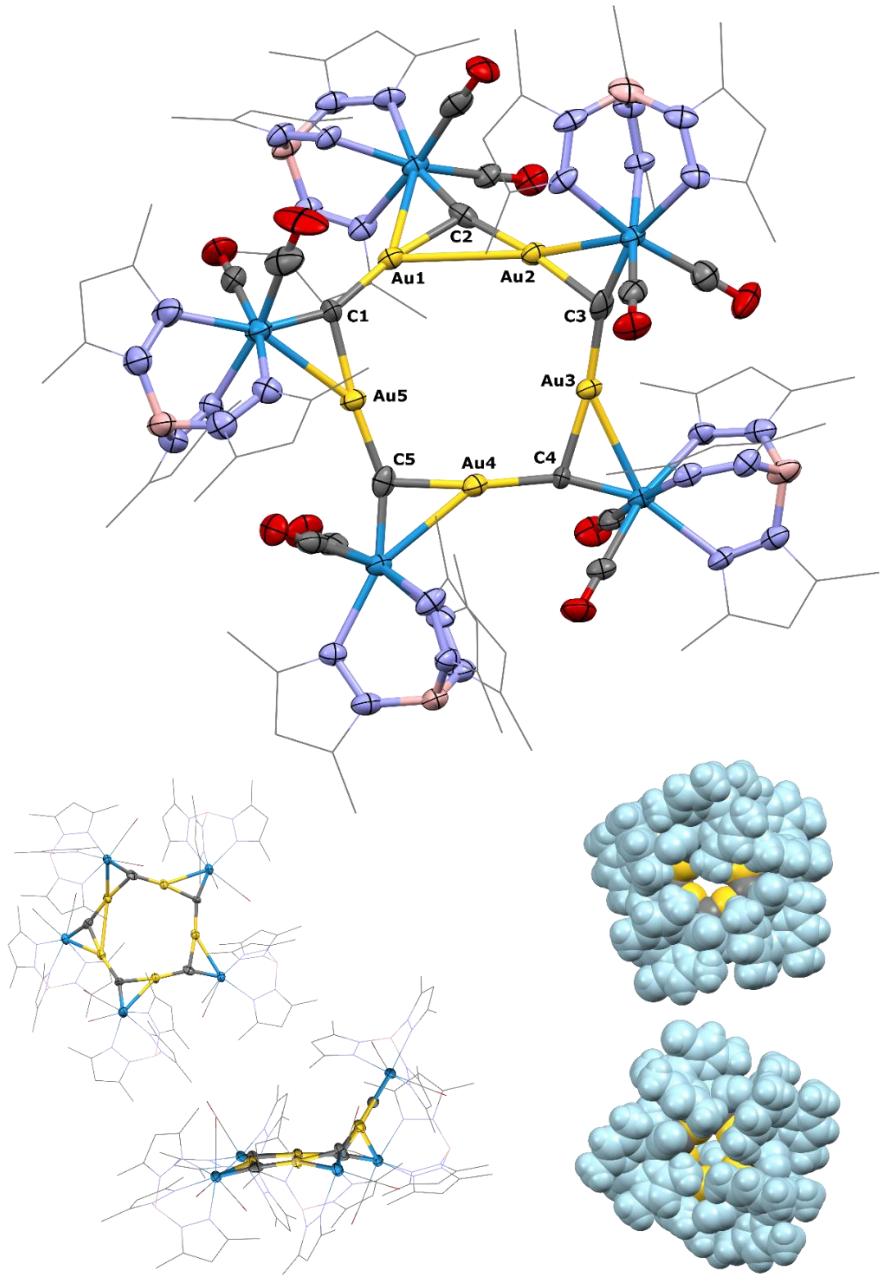

Figure 7.12: Molecular structure of $[W(\equiv CAu)(CO)_2(Tp^*)]_5$ (**7.9**) in a single crystal as determined by X-Ray Diffractometry. Ellipsoids are drawn at the 50% probability surface with pyrazolyl rings simplified and hydrogens omitted for clarity. Insets: a and b) Wireframe representations to highlight the geometry of the central ring, both facing the ring and showing the non-planarity of the structure; c and d) Space-filling representations of above and below the ring showing the encapsulating steric bulk of each tungsten ligand sphere (turquoise). For selected bond lengths (Å) and angles (°), see Table 7.1.

Table 7.1: Structural features of tetra- and pentameric Golden Rings $[W(\equiv CAu)(CO)_2(Tp^*)]_n$.

Measurement	Bond Length (Å) or Angle (°)			
	7.1 (Tetramer)	**Mean**	**7.9** (Pentamer)	**Mean**
W–C	1.85(2), 1.87(2) 1.90(2), 1.87(2)	1.873	1.879(9), 1.88(1), 1.883(9) 1.85(1), 1.86(1)	1.871
Au–C	2.03(2), 2.00(2) 1.97(2), 1.99(2)	1.998	1.98(1), 2.001(9), 1.985(9) 2.01(1), 2.00(1)	1.995
W–Au	2.822(1), 2.846(1) 2.841(1), 2.825(1)	2.834	2.8191(5), 2.8252(7), 2.8157(6) 2.8375(7), 2.8139(8)	2.822
Au···Au'	3.231(1), 3.217(1) 3.235(1), 3.236(1)	3.230	3.3880(5), 3.4198(5), 3.3849(5) 3.2338(6), 3.3090(5)	3.347
W–C–Au	165(1), 163(1) 168(1), 160(1)	164.0	160.7(6), 155.6(7), 155.9(7), 163.7(7), 163.7(7)	159.9
Au–C–Au'	103.4(9), 105.6(9) 103.2(9), 105(1)	104.3	110.2(5), 113.6(5), 113.1(5) 104.1(5), 106.6(6)	109.5

Notes: [a]Measured in $CDCl_3$ unless specified otherwise.

The key causal distinction between the structure lies with the solvent combinations that gave rise to each single crystal: **7.9** was grown from CH_2Cl_2/*n*-hexane and contained three CH_2Cl_2 solvate molecules,†††††††††††††††††††† while twinned crystals of **7.1** were reportedly grown from toluene/Et_2O but contained a region of disordered solvent that was modelled on 3 oxygen sites in addition to a solvent-accessible void (746 Å3, and 186 electrons per unit cell treated with the PLATON-SQUEEZE protocol). To determine the chemical relationship between **7.1** and **7.9** further studies were undertaken to elucidate the identify of $[W{\equiv}C–Au]_n$ used as a precursor in the prior reactions. To pre-empt the following, no definitive conclusions emerged as this is an imperfect, and it must be said frustratingly intractable, system plagued by deposition of elemental gold and loss of crystallinity through desolvation compromising measurements. Several other issues were encountered along the journey presented here as a collection of logical points.

Realising the tetrameric and pentameric crystals arose as poorly defined solvates from different solvent systems, the initial tactic was to deliberately grow crystals from the same conditions in bulk purity, noting the tetramer was presumed to contain water of solvation from adventitious moisture while the pentamer contains CH_2Cl_2 solvates and was grown in the presence of an NHC. Attempts to grow crystals all began from a solid of $[W{\equiv}C–Au]_n$ prepared as outlined in Chapter Nine, the solution NMR data for which indicate one C_s symmetric Tp* environment. From the outset it should be noted that the broad resonance observed in the $^{31}P\{^1H\}$ NMR spectrum for the PPh_3 adduct indicates that disaggregation/aggregation by nucleophiles may well operate on NMR

†††††††††††††††††††† Three molecules of CH_2Cl_2 were unable to be modelled in **7.9** and were treated with a solvent mask. However, for this section, their inclusion in discussion is paramount.

timescales such that the inference of high symmetry may in actuality reflect dynamic, time-averaged environments in a dynamic system. Attempts to selectively crystallise the tetramer failed to produce bulk material from the original toluene/Et_2O conditions, implying the reported crystals may have fortuitously arisen from evaporation, though in the present case evaporation of this mixture gave a glass. An attempt was made using a different solvent system, Acetone/Et_2O, where no single crystal emerged but deliberate evaporation resulted in an orange/brown semi-crystalline solid (Sample A). Conversely, liquid-liquid diffusion of *n*-hexane into CH_2Cl_2 provided red needles overnight at –20 °C. These crystals were noted to visibly desolvate hinting CH_2Cl_2 is incorporated into the lattice (Sample B).

Sample A clearly retained a degree of crystallinity as a powder X-ray pattern exhibited several diffractions (2θ) accompanied by an imperfect baseline implying some amorphous material was also present; understandably given the method Sample A was obtained. Curiously, the experimental data maps relatively well with the simulated pattern obtained from the single crystal of **7.1** (Figure 7.13), however no reflections were observed that corresponded to the simulation based on a single crystal of pentamer **7.9**. Despite less-than-ideal diffraction pattern, this suggests that a recrystallisation from acetone/ether provided a sample the crystalline component of which was predominantly **7.1** admixed with glassy material.

Study of Sample B proved complicated. Measuring a series of crystals from Sample B *via* single crystal X-ray diffraction revealed the sample contained a different unit cell to that of Figure 7.12. A full, high-quality dataset was collected, however, a satisfactory structural model did not emerge due in part to a non-stoichiometrically solvated channel including CH_2Cl_2, in addition to being twinned. While this precluded refinement of a final satisfactory model, the solution process could be advanced to the point of confirming that the core was consistent with the tetramer species.[################] Desolvation of these crystals was significant within 10 to 30 minutes (T = 150 K) evolving to a new unit cell but with insufficient resulting data quality for further analysis. Non-standard powder diffraction studies were conducted by sealing crystals of Sample B inside a plastic film, submerged in mother liquor to inhibit desolvation. A fast (1 minute) powder pattern was obtained prior to a full experiment (30 minutes) such that desolvation occurs over the timeframe of the experiment, evident from the data obtained (Figure 7.14).

[################] Modelling and refinement of this system was conducted by an expert crystallographer, Dr. Michael Gardiner, whose assistance is gratefully acknowledged.

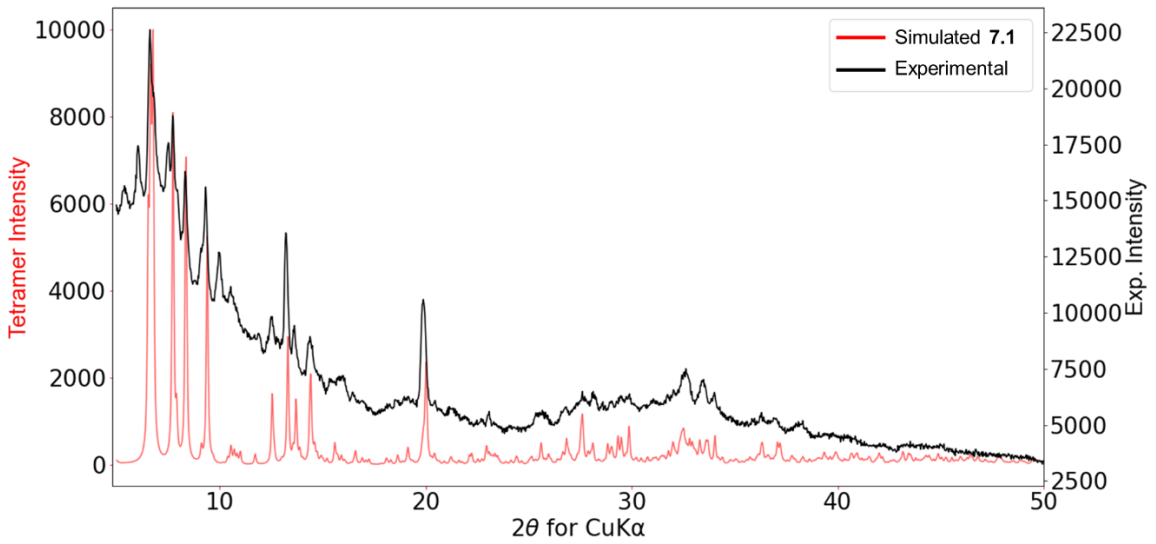

Figure 7.13: Powder diffraction patterns of Sample A (black) overlayed with a simulated powder pattern from real single crystal of **7.1**.

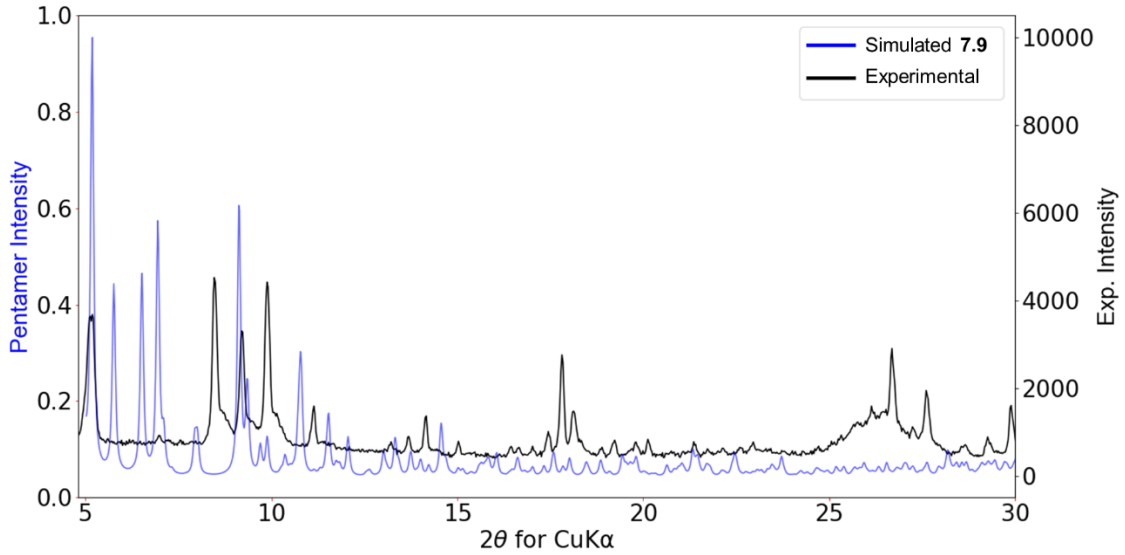

Figure 7.14: Powder diffraction patterns of Sample B (black) overlayed with a simulated powder pattern from real single crystal of **7.9**. A low angle reflection matches that is absent from the tetramer, although this is not an overall match.

The rapid data collection best aligns with the pentamer such that low angle reflections match the simulation; note that due preferred orientation effects are likely due to the non-routine acquisition, and this may explain why some diffraction peaks are missing as they do not meet the Bragg condition. This is not definitive given single crystals were determined to be the tetrameric species.

Solid-state analysis proved troubling and inconclusive, so solution state studies were conducted, with the caveats of dynamic processes noted above. Based on powder XRD results, Sample A was considered to be at least 'enriched' in the tetramer so a solution was prepared for NMR analysis. Data were rapidly acquired within 10 minutes of dissolution in CD_2Cl_2 such that two Tp* containing species were observed, the relative proportions of which varied slightly over 1 – 3 hours. This suggests Sample A slowly equilibrates from tetramer to a mixture containing a similar species in CH_2Cl_2/CD_2Cl_2 (Figure 7.16). The final integration ratio is 1:1.2 after 3 days (t_∞). A DOSY spectrum confirmed two species of similar size are present in the solution, such that the less intense signals correspond with the smaller compound. Conversely, measuring an NMR of Sample B observes a single species that does not equilibrate in CD_2Cl_2 over several days. A DOSY NMR of Sample B confirms a single species in solution (Figure 7.17), with low intensity signals present if delving toward baseline intensity. Finally, taking Sample B prepared from CH_2Cl_2 and attempting to measure in d_6-acetone—the solvent from which the sample originated—results in an orange solution post-filtering, however, orange crystals§§§§§§§§§§§§§§§§§§§§§§§§ quickly precipitate from solution to give a yellow supernatant phase. Although NMR data indicate that this solution contains only one Tp* environment, direct correlation of chemical shifts between two solvents (d_6-acetone, CD_2Cl_2) for signals with low spectral dispersion could not be determined with certainty.

The typical method to discern between species in solution as calculated by a DOSY NMR is to solve the Stokes—Einstein equation to obtain an estimate of hydrodynamic radius: the radius of an approximated molecular sphere moving through a medium at constant temperature. The experimentally determined structures of **7.1** and **7.9** reveal a shape best approximated as an oblate spheroid (Figure 7.15). If either golden ring was assumed to 'tumble' through solution as opposed to exclusively transverse diffusion, a sphere would form proportional to the largest diameter of the molecule. Therein lies the issue that the tetramer (21.78 Å) and pentamer (21.21 Å) are surprisingly similar due to the envelope fold of the latter********** and certainly

§§§§§§§§§§§§§§§§§§§§§§§§ A unit cell of these crystals was unable to be obtained given loss of crystallinity during extraction from the J. Young NMR tube prior to mounting.

********** The equatorial radii of **7.1** and **7.9** were calculated from van der Waals radii and atomic coordinates derived from the crystal structures. In the case on **7.9**, it should be assumed that the envelope fold is not static but

indistinguishable given the error margins on DOSY techniques. Meanwhile, approximating the molecules as oblate spheroids, the larger diameter may be similar, but the vertical axis is certainly smaller for the tetramer (10.77 Å) than the pentamer (15.36 Å), such that imperfect traveling through solution would result in the pentamer having a smaller diffusion constant (slower diffusion) than the tetramer. This approximation suggests that for the mixture, the relative size is not that different, hence if a tetramer is present (as powder diffraction studies suggested), it is likely accompanied by the closest larger analogue (*i.e.*, a pentamer).‡‡‡‡‡‡‡‡‡‡‡‡‡‡‡‡‡‡‡‡‡‡‡ The diffusion constant suggests the slower moving is the major species and an identical spectrum arises from Sample B produced by CH_2Cl_2/*n*-hexane, the conditions that a pentamer was grown. Therefore, Sample B is likely a sample of pentamer **7.9** in solution.

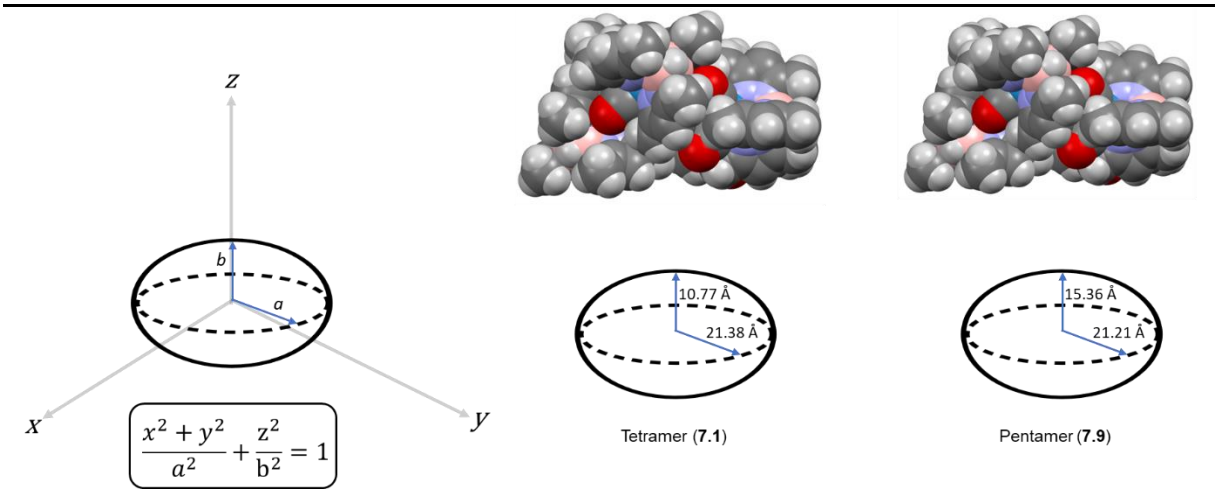

Figure 7.15: Depiction of an oblate spheroid with approximate measures of **7.1** and **7.9** showing differences in the axial direction.

Clearly approximations are made and hence little can be conclusively suggested. Other techniques were explored with little success or practical limits. For example, infra-red spectroscopy provides a faster timescale of measurement (*i.e.*, the least compromised by dynamic processes) but has insufficient resolution to determine **7.1** or **7.9** in solution, while ESI-Mass Spectrometry provided many fragmentation patterns rather than evidence a preference of aggregation. Overall, this suggests the sample used as a precursor is tetramer **7.1** in the crystalline form. However, these

flexes/inverts, such that for a time-averaged spheroidal shape this approach most likely somewhat under-estimates the equatorial radius and over-estimates the polar radius.

‡‡‡‡‡‡‡‡‡‡‡‡‡‡‡‡‡‡‡‡‡‡‡ The existence of larger (or smaller) aggregates is not considered here but it should be noted that these remain plausible, e.g., while 'AuC≡C*t*Bu' is a tetramer, 'CuC≡C*t*Bu' is an octamer!

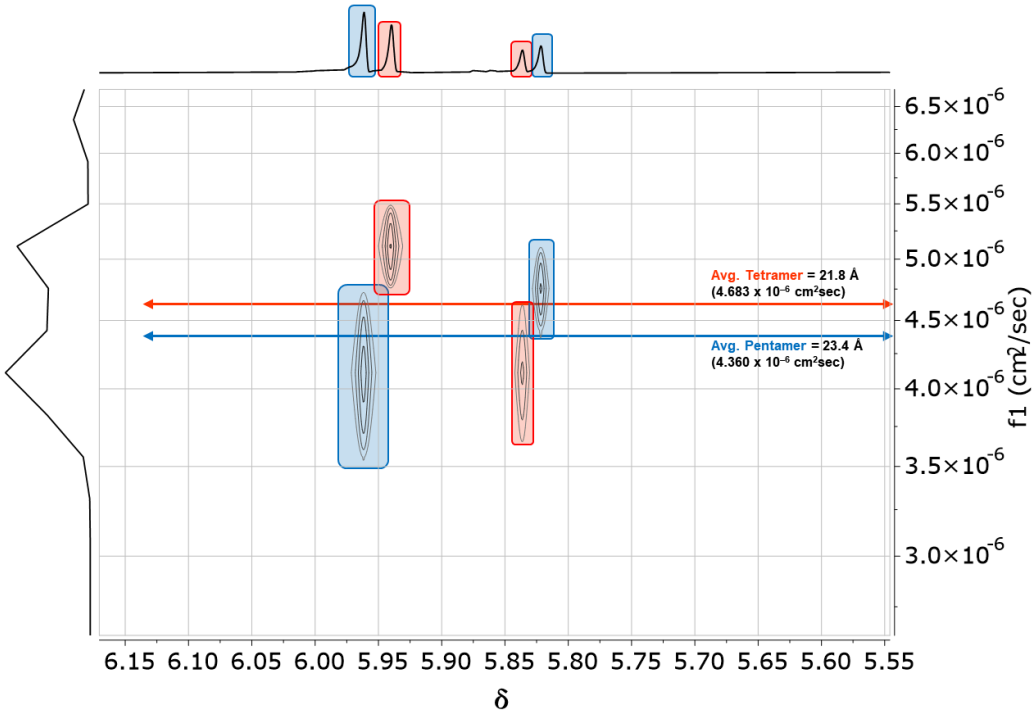

Figure 7.16: DOSY NMR spectrum of golden ring Sample A digested in CD_2Cl_2 (1 hour) suggesting two compounds in solution. These are tentatively assigned as the tetramer (7.1) and pentamer (**7.9**). Inset – Coloured lines represent average measurements from all signals per species (some are at lower frequency) with diameter calculates from the Stokes—Einstein equation.

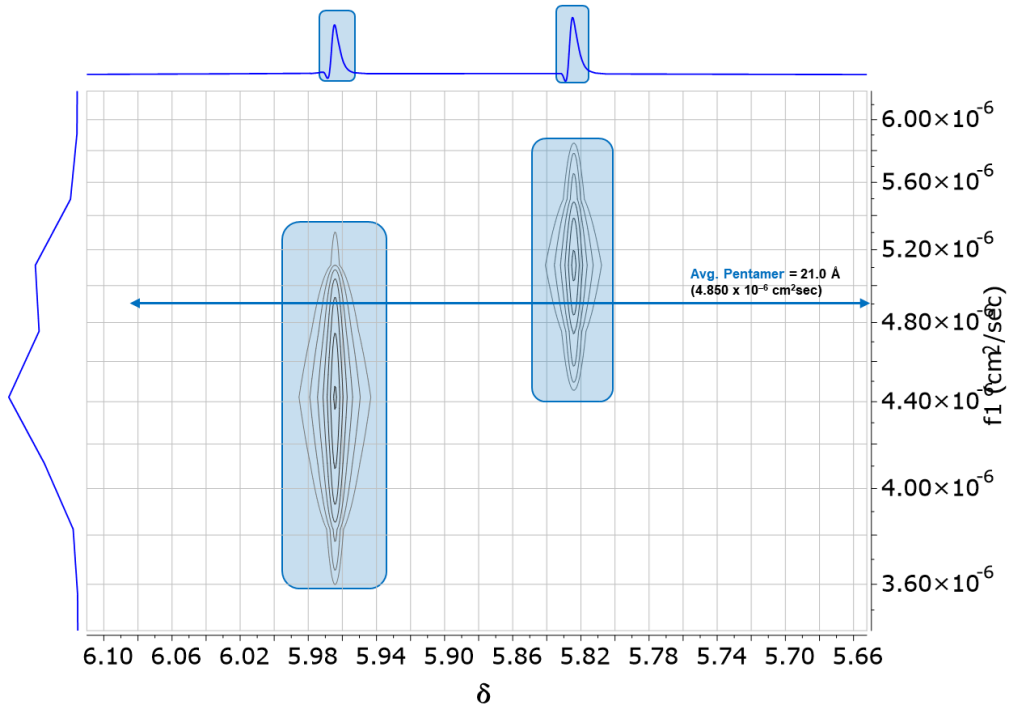

Figure 7.17: DOSY NMR spectrum of golden ring Sample B digested in CD_2Cl_2 (1 hour) suggesting one compound in solution. This is tentatively assigned as the pentamer (**7.9**). Inset – Blue line represents average measurements from all signals per species (some are at lower frequency) with diameter calculates from the Stokes—Einstein equation.

findings suggest that the pentamer may accumulate from tetramer in solution depending upon other solvents present. Finally, it is problematic to relate the kinetics and thermodynamics of crystallisation (*i.e.*, selective precipitation of tetramer) to those governing speciation in solution (tetramer redistributing to pentamer and *vice versa*). Most certainly, it must be said that the form that most readily crystallises is by no means *a priori* the form that predominates in solution. A further consideration is the impact of nucleophilic species in solution, be they specific additives such as the extraneous NHC present during formation of the first sample of **7.9**, or simply the varying donicities of the solvents employed. With impractical restrictions for measuring powder diffraction data and the errors on DOSY experiments unable to quantify the exact hydrodynamic radii of molecules, this reaches boundary of exploring the speciation of these and other oligomeric golden rings, both in solution and in the solid state.

7.4 Attempts Towards Bimetallic Copper Metallacarbyne Complexes

Transmetallation from tin to gold is now well established in μ_2-carbido chemistry, where a labile gold(I) source, [AuCl(SMe$_2$)], provides synthetically versatile golden ring aggregates (**7.1**/**7.9**). A similar labile and soluble source of copper(I) has been reported recently [CuCl·SMe$_2$],[572] and shown to add 'CuCl' units across the W≡C bond of phosphoniocarbynes,[214] raising the question could similar aggregations occur for the lighter group 11 congener? In a practical sense it should be noted that in the extensive studies of Bruce and Saitseva on the palladium-mediated C–C cross coupling reactions of gold alkynyls, a copper halide co-catalyst was invariably included, raising the possibility that copper alkynyls were actually the operative species. As noted earlier, copper halides have been long known to accelerate Stille cross-couplings, the so-called 'copper effect'. A single example of a μ_2-carbido complex with a copper terminus is known, that being a Class C complex that arises from coordination of the terminal carbido [Ru(≡C)Cl$_2$(PCy$_3$)$_2$] to "Cu([9]aneS$_3$)$^+$".[69-70] Addition of cuprous halides to Class D dimetallacarbenes has been shown to afford μ_3-species.[40-41] While copper metallacarbynes are presently unknown, their production *via* transmetallation from of either gold(I) metallacarbynes or stannylcarbynes seemed to present two possible methods for accessing such species.

As found with **7.1**, a transmetallation from [W(≡CSnBu$_3$)(CO)$_2$(Tp*)] to [CuCl·SMe$_2$] at 0 °C excluding light provided a visually similar result: facile formation of a bright orange solution. A new set of carbonyl vibrations is observed (ν_{CO}: 2003, 1919 cm^{-1}) suggestive of a π-coordinated species as exemplified in **7.1** (ν_{CO}: 1990, 1900 cm^{1}) rather than a terminal metallacarbyne species.

Surprisingly, any attempt to isolate this species was met with deposition of copper metal (Scheme 7.6). Chromatography employing a range of anaerobic stationary phases (alumina, silica gel, Celite®) decomposed the complex, with TLC suggesting $[W_2(\equiv CC\equiv)(CO)_4(Tp^*)_2]$ is the major eluent (*i.e.*, redox) accompanied by small quantities of $[W(\equiv CH)(CO)_2(Tp^*)]$ (hydrolysis). All

NMR resonances were broad with no μ-carbido or carbyne resonance being detected. It was unclear whether this broadening reflected the operation of fluxional processes or the adventitious inclusion of paramagnetic side-products. Several attempts at recrystallisation were unsuccessful in producing a pure sample of the orange species, instead providing crystals that upon returning to solution, exhibiting the same broadened spectra attended by plating of the NMR tube with black copper.

While the identify of this (likely aggregated) copper species remains unclear, a single crystal was found amongst black detritus of a THF/*n*-hexane crystallisation. A successful diffraction Diffractometry revealed identified the material as being a THF solvate of $[W_2Cu_6(\mu_4\text{-}C)_2(\mu_2\text{-}Cl)_4(THF)_2(\mu\text{-}CO)_2(CO)_2(Tp^*)_2]$, *i.e.*, $[W(CCu)(CO)_2(Tp^*)]_2(CuCl)_4(THF)_2$ (**7.10**) (Figure 7.18). While μ_4-carbidos are relatively common, this species provides clues of the copper species in solution. At first glance the cluster appears complex, however it may be deconstructed into more familiar components. Firstly, μ_3-coordination of alkynyls is commonplace in low-valent copper structural chemistry, *e.g.*, the tetrahedrane $[Cu_4(\mu_3\text{-}C\equiv CPh)_4(PPh_3)_4]$ [573] or a variety of *triangulo*-$[Cu_3(\mu_3\text{-}CCR)_n(\mu\text{-}dppm)_3]^{(3-n)+}$ (n = 1,2) salts. [574-580] The capping of a Cu_3 face by a W≡C rather than RC≡C units differs in that one copper also associates with the tungsten centre. Secondly, the T-shaped $WCCu_2$ unit recalls similar $WCAu_2$ geometries in both **7.1**/**7.9** and $[WRuAu_2(\mu_2\text{-}C)(\mu_3\text{-}C)Cl_3(CO)_2(PCy_3)_2(Tp^*)]$. Dissecting the asymmetric unit reveals a '$W(\equiv CCu)(CO)_2(Tp^*)$' fragment that is stabilised by coordination of two further 'CuCl' units: one across the W≡C bond and across the Cu–C bond to satisfy the effective electron requirements. One additional copper remains otherwise undercoordinated and is therefore stabilised by a THF ligand, while the accompanying chlorides provide halide bridges for the copper cluster core. The presence of a lone copper without chloride (indicated as blue in the intermediate; Scheme 7.6) supports transmetallation from tin, however, the ensuing species is likely unable to form a stable aggregate such as **7.1** for gold, and hence coordination of further 'CuCl' units to the W≡C bond ensues to afford a more condensed cluster framework. To understand the different behaviour of gold(I) and copper(I) the key points are: (i) Given that metallophilicity arises from correlation and relativistic effects that scale with Z^2, cuprophilicity is a far weaker[581] and less widely recognised or indeed accepted phenomenon than aurophilicity. [582] Accordingly, the circumannular Au···Au interactions

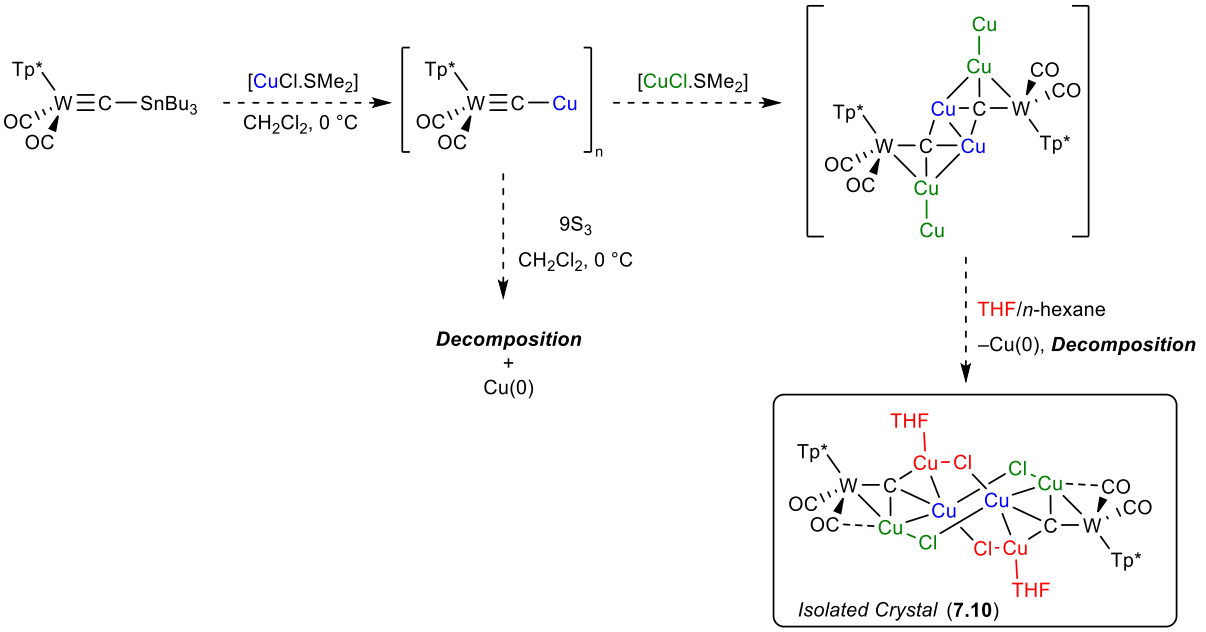

Scheme 7.6: Attempted synthesis of copper(I) metallacarbyne aggregates. Colour code is included to indicate the origins of copper fragments.

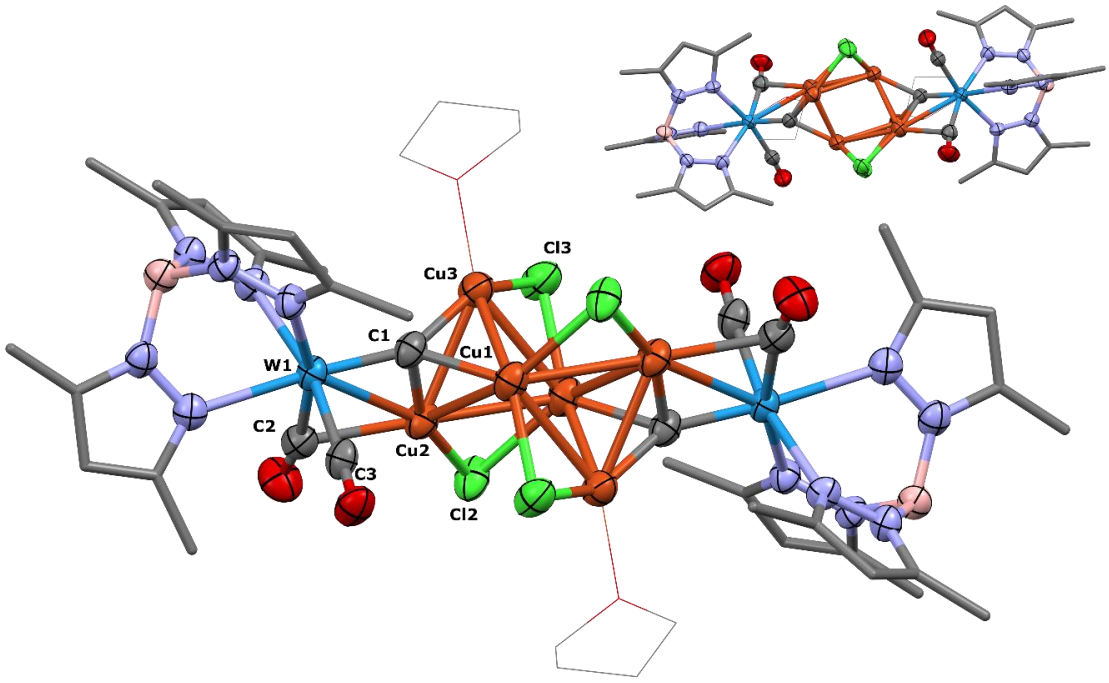

Figure 7.18: Molecular structure of $[W_2Cu_6(\mu_4\text{-}C)_2(\mu_2\text{-}Cl)_4(THF)_2(\mu\text{-}CO)_2(CO)_2(Tp^*)_2]$ (**7.10**) in a single crystal of **7.10**·(OC_4H_8) as determined by X-Ray Diffractometry. Ellipsoids are drawn at the 50% probability surface with pyrazolyl rings simplified and THF solvent omitted (or simplified) along with hydrogens for clarity. Inset: Alternative view showing the symmetry of the copper core. Selected bond lengths (Å) and angles (°): W1–C1 1.858(7), C1–Cu1 2.000(8), C1–Cu2 1.921(6), C1–Cu3 1.934(7), W1–Cu2 2.726(1), W1–Cu2 2.726(1), C2–Cu2 2.246(9), W1–C2 2.011(8), W1–C3 2.03(1), Cu1–Cu2 2.682(2), Cu1–Cu3 2.431(1), Cu2–Cu3 2.591(2), Cu2–Cl2 2.227(2), Cu3–Cl3 2.179(2).

that stabilise **7.1** will not be significant for copper analogues. (ii) The tendency towards lower coordination number on descending group 11 (again of relativistic origin) means that two-coordinate gold(I) is prevalent while copper(I) typically adopts 4-coordinate tetrahedral geometries, often by forming halide bridges, when possible. These two factors, *i.e.*, preference for increased coordination number but *not* involving cuprophilic interactions therefore accounts for the distinct nature of the aggregation seen in **7.10** *cf.* **7.1**/**7.9**. Although the hint that coordinating solvents might be utilised to stabilise copper species in solution, repeated reactions in THF or MeCN failed to provide any further species of interest. It is perhaps also of note that dimethylsulfide is liberated in the reaction when this might seem a more appropriate ligand for copper(I), from an HSAB perspective, than the observed THF coordination

The stabilisation of otherwise undercoordinated copper suggested a copper metallacarbyne might be trapped in solution with a polydentate and 'soft' ligand. Reinholdt and Bendix have previously shown that the terminal carbido complex [Ru(C)Cl2(PCy_3)$_2$] reacts with [Cu(NCMe)([9]aneS_3)]BF_4 ([9]aneS_3 = 1,4,7-trithiacyclononae) to afford the Class C μ_2-carbido salt [RuCu(μ_2-C)Cl_2(PPh_3)([9]aneS_3)]BF_4 in which the four coordinate copper is ligand in a tetrahedral geometry by the tridentate macrocyclic thioether.[70] Accordingly, 1,3,7-trithiacyclononane ($9S_3$) was add to a freshly generated sample of the intermediate copper species, again with exclusion of light. A rapid colour change to yellow from the initial brick red species was observed, however, an infra-red spectrum was inconclusive with several carbonyl vibrations detected. Alas, the yellow species could not be separated from copper debris, as similar attempts at recrystallisation or chromatography to the aforementioned copper experiment decomposed the species.

Whilst transmetallation from tin to copper was presumed to occur, purification and product stability contributed to the bottleneck. Therefore, the alternative method transmetallation to a prefabricated copper(I) complex was attempted. The iodide species [CuI([9]aneS_3)] is a known compound,[583] yet no evident transmetallation occurs with [W(≡CSnBu_3)$(CO)_2$(Tp*)] over two days at ambient temperature; heating (40 °C, 16 hours) or swapping to MeCN resulted in deposition of copper metal and formation of [W_2(≡CC≡)$(CO)_4$(Tp*)$_2$] (Scheme 7.7). As Sn–I bonds are weaker (*ca* 230 kJmol^{-1}) than Sn–Cl bonds (*ca* 410 kJmol^{-1}) it is likely the transmetallation to a copper iodide is far less favourable, hence the previously unreported chloro complex [CuCl([9]aneS_3)] was pursued, by adapting the synthetic method published for the iodo complex. Treating a CH_2Cl_2 suspension of thereby obtained [CuCl([9]aneS_3)] with [W(≡CSnBu_3)$(CO)_2$(Tp*)] returned a yellow solution with no observable reaction over two weeks as monitored by infra-red spectroscopy. The [CuCl([9]aneS_3)] solid appeared reluctant to go into solution so a repeat reaction was attempted in acetonitrile, however, decomposition to copper metal ensued over 24 hours with

no intermediate being evident, while the stannylcarbyne slowly hydrolysed to [W(≡CH)(CO)$_2$(Tp*)] when the reaction was left to stir for a week.

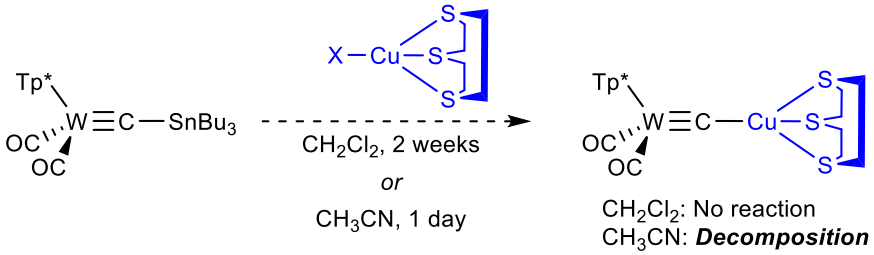

Scheme 7.7: Transmetallation to a prefabricated copper(I) complex. X = Cl or I.

Despite limited evidence of transmetallation from tin to copper in metallacarbyne chemistry, no examples of μ$_2$-carbido complexes were isolated. As cuprophillic interactions are rather weak, it is likely an aggregation analogous to **7.1** is less favourable although cuprophilic interactions are often claimed to account for the self-assembly of copper(I) aggregates.[584-591] This study did however produce a high nuclearity μ$_4$-carbido complex, implicating the key transmetallation step as suggested by retrosynthetic deconstruction of the cluster framework.

7.5 Preparation of Mercury Metallacarbynes

Having demonstrated the utility of (rather expensive) gold reagents for transmetallation, it was noted above that (rather toxic) alkynylmercurials may also serve as effective transmetallation agents. Extending this principle from alkynyls to carbidos would require suitable mercuriocarbidos, of which there is a single known example, [Mo$_2$Hg(μ$_2$-C)(CO)$_4$(Tp*)$_2$] (**7.11a**).[118] The following section therefore investigates the synthesis of mercuriocarbidos, including *via* transmetallation from stannylcarbynes to mercury(II) chlorides.

Caution: The following reactions utilise toxic organomercury reagents in conjunction with organotin by-products, each requiring the utmost care. These experiments should be conducted on a small scale, by an equipped, skilled synthetic chemist, such that all waste is contained and destroyed in an appropriate manner consistent with local statutory requirements.

See Chapter Nine for further details.

7.5.1 A Collection from Mercury(II) Chloride

The first mercurial-carbido [Mo$_2$Hg(μ$_2$-C)(CO)$_4$(Tp*)$_2$] (**7.11a**) was produced from the simple reaction of the lithiocarbyne [Mo(≡CLi)(CO)$_2$(Tp*)] with [HgCl$_2$]. An analogous reaction with the tungsten species was noted to hydrolyse to [W(≡CH)(CO)$_2$(Tp*)] during the necessary chromatography that the molybdenum analogue **7.11a** survives. In inexplicable contrast to the molybdenum example, the formation of the desired *bis*(carbido)mercurial *via* a lithiocarbyne

approach is also complicated by the formation of equilibrating mercury halide adducts.‡‡‡‡‡‡‡‡‡‡‡‡‡‡‡‡‡‡ Vinyl stannanes rapidly transmetallate to mercuric chloride[592] and it therefore stands to reason the stannylcarbyne [W(≡CSnBu$_3$)(CO)$_2$(Tp*)] may also react with [HgCl$_2$].§§§§§§§§§§§§§§§§§§§§§§§§ Adding two equivalents of [W(≡CSnBu$_3$)(CO)$_2$(Tp*)] to a dilute CH_2Cl_2 solution of [HgCl$_2$] at 0 °C protected from light provides [W$_2$Hg(μ_2-C)$_2$(CO)$_4$(Tp*)$_2$] (**7.11b**) as a vibrant orange solid upon recrystallisation (Scheme 7.8). Using a transmetallation approach requires precise stoichiometric supply of stannylcarbyne otherwise other species are detected by infra-red spectroscopy (*vide infra*), as also observed in synthetic approaches to **7.11b** based on lithiocarbyne reactions. The tungsten analogue **7.11b** was unable to be produced *via* repeating the established lithiocarbyne methodology, noting complicated mixtures *via* infra-red spectroscopy (ν_{CO}) and similar hydrolysis to [W(≡CH)(CO)$_2$(Tp*)] when attempting to purify such mixtures *via* chromatography, in accordance with previous unpublished observations.

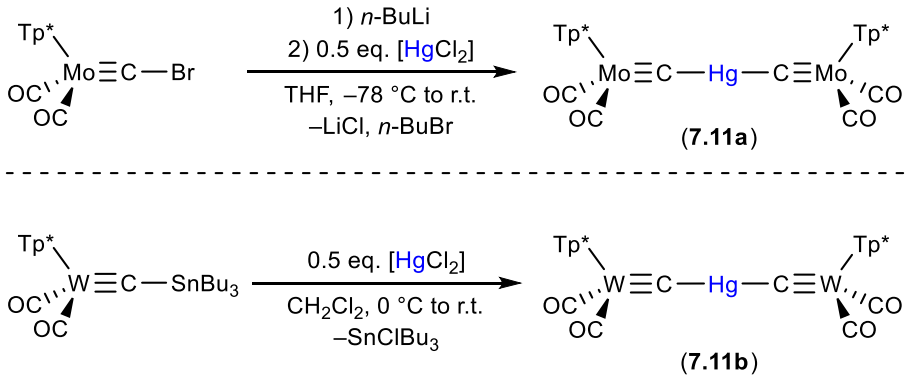

Scheme 7.8: Reactions to produce *bis*-carbido mercurial complexes.

The infra-red spectrum of **7.11b** exhibits a pattern of carbonyl vibrations that is more complex than for other metallacarbynes (ν_{CO}: 1983, 1976 and 1889 cm^{-1}), a feature that was noted for the dimolybdenum analogue **7.11a** (ν_{CO}: 2000, 1994, 1912 cm^{-1}) and ascribed to coupling of the ν_{CO} oscillators on adjacent metal centres. Mercury contains two naturally abundant spin active nuclei********** and thus ^{199}Hg{^{1}H} NMR spectroscopy can detect a resonance (δ_{Hg} = –1074) in a region similar to the *bis*(alkynyl)mercurial [Hg(C≡CSiMe$_3$)$_2$] (δ_{Hg} = –1004) [593] (Figure 7.19) but which additionally exhibits ^{183}W coupling ($^2J_{HgW}$ = 1184 Hz). Tungsten coupling was

‡‡‡‡‡‡‡‡‡‡‡‡‡‡‡‡‡‡ M. Sharma, *Unpublished Observations*, Australian National University.

§§§§§§§§§§§§§§§§§§§§§§§§ In general, halide-metathesis transmetallation typically delivers the organyl group to the more electronegative element, thereby increasing the covalent character of the metal-carbon bond but also the ionic character of the metal halide formed. This is perhaps less clear in the transmetallation from tin to mercury with similar Pauling electronegativities (Sn: 1.96, Hg 2.00) with the resulting metal halide bond strength playing a significant role. Approximate homolytic bond enthalpies ΔH_f: Sn–Cl = 406, Hg–Cl 100 kJmol^{-1}. These are thermodynamic considerations that may be subservient to actual kinetic barriers.

********** ^{199}Hg {I = ½; 16% natural abundance} and ^{201}Hg {I = 3/2; 13% natural abundance}. ^{199}Hg is the nucleus of choice for NMR studies as it yields sharp lines over a wide chemical shift range. The alternative quadrupolar ^{201}Hg isotope yields lines that are too broad to be observed with a high field instrument.

rarely detected for ^{195}Pt NMR signals previously (Chapters Three–Five) due to only one tungsten fragment and additional couplings to *e.g.*, ^{31}P. The $^{13}C\{^{1}H\}$ NMR spectra contains a high frequency resonance consistent with a μ_2-carbido (δ_C = 355.1; $^{1}J_{CW}$ = 181 Hz) but coupling to ^{199}Hg was not detected even in concentrated samples (Figure 7.20). Typical $^{1}J_{HgC}$ couplings for *bis*(alkynyl)mercurial are in the order of 2300–2550 Hz. The pattern for NMR resonances indicates that in solution **7.11b** adopts either static *anti* (C_S) or *syn* (C_{2v}) disposition for the Tp* ligands or perhaps more likely free rotation occurs about the Hg–C bonds.

Multiple attempts at crystallising **7.12b** species resulted only in amorphous powders that failed to diffract. Therefore, the geometry of $[M_2Hg(\mu\text{-}C)_2(CO)_4(Tp)_2]$ {M = Mo **7.11a*** or W **7.11b***} was optimised *via* computational methods. Unfortunately, both complexes still contain one imaginary frequency to low wavenumber suggesting this is not a local minimum,ǂǂǂǂǂǂǂǂǂǂǂǂǂǂǂǂǂǂǂǂǂǂǂǂ and while this prevents discussion of the derived thermodynamic quantities, the effect on the topologies and energies of the frontier orbitals is likely to be modest allowing discussion at a superficial level (Figure 7.21). Features are also similar between models of molybdenum and tungsten, therefore only the tungsten will be discussed. The LUMO and LUMO+1 describe an empty orbital that envelopes the mercury without significant contribution from the mercury, while being π-anti-bonding with respect to the tungsten-carbon linkage; this is akin to those described for the gold molecules **7.2*** and **7.7***. A similar HOMO describes retrodonation to carbonyl ligands while the HOMO–2/–3 constitute the W≡C π-bonding, although anti-bonding with respect to mercury such that lower energy contributions also exist such as HOMO–16. An unusual topology is observed for the HOMO–6, depicting the d_{z^2} orbital of tungsten interacting with a p-orbital of each carbido. The HOMO–12 describes a large σ-symmetry overlap along the *bis*-carbido spine like that observed for gold(I) species, implying communication along the spine that physical manifests in the magnitudes of coupling constants observed in various NMR spectra. Curiously, two orbitals lie deep in the manifold (HOMO–25, HOMO–27) that include a toroidal lobe around the mercury centre, consistent with those available for mercuriophillic interactions (much weaker than aurophillic interactions). Although such interactions were not verified crystallographically and indeed seem highly improbable given the steric sheath around the W≡C–Hg–C≡W, the aggregation of *bis*(alkynyl)mercurials due in part to inferred mercuriophilic interactions has been discussed by Nicholson for $[Hg(C{\equiv}CR)_2]$ (R = Ph, $SiMe_3$).[594]

ǂǂǂǂǂǂǂǂǂǂǂǂǂǂǂǂǂǂǂǂǂǂǂǂ The imaginary frequency for each of the complexes describes a 'breathing' mode of the molecule with slight twisting on the Hg–C bond. A similar issue is found when optimising $[Hg(C{\equiv}CPh)_2]$.

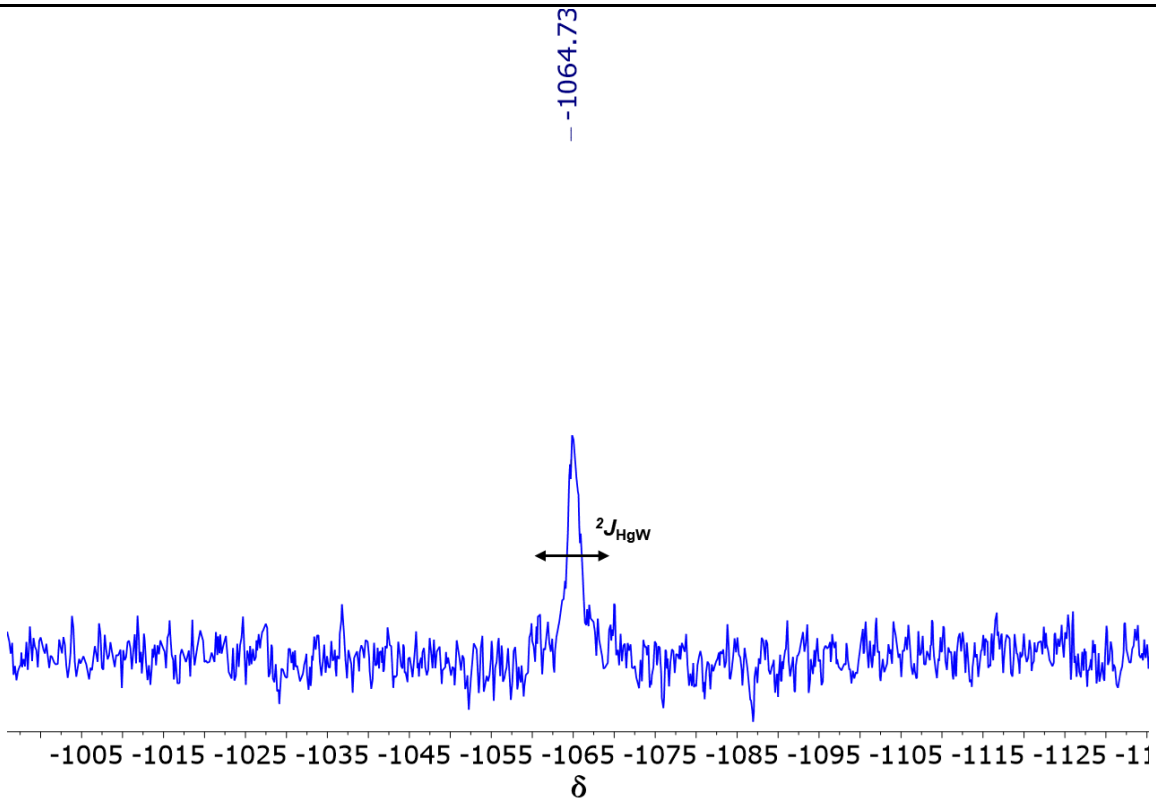

Figure 7.19: $^{199}Hg\{^1H\}$ NMR spectrum of $[W_2Hg(\mu_2\text{-}C)_2(CO)_4(Tp^*)_2]$ (**7.11b**) showing ^{183}W coupling.

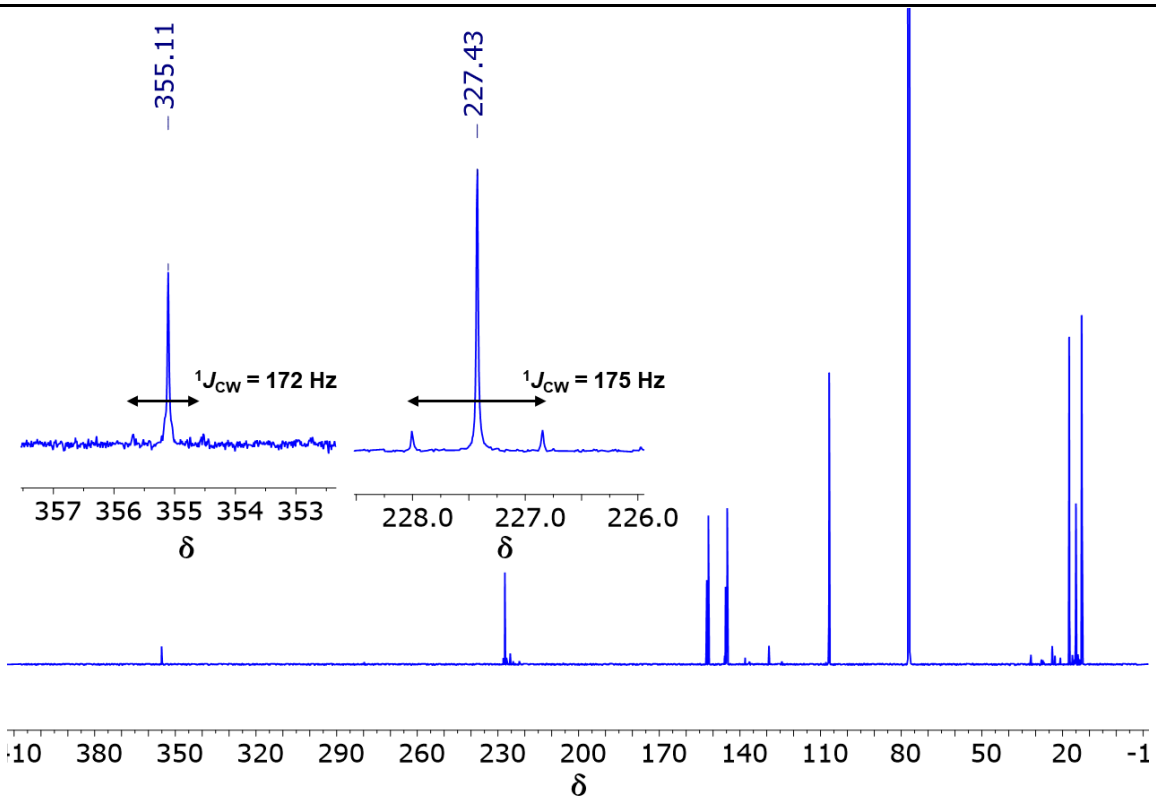

Figure 7.20: $^{13}C\{^1H\}$ NMR spectrum of $[W_2Hg(\mu_2\text{-}C)_2(CO)_4(Tp^*)_2]$ (**7.11b**) with insets showing ^{183}W coupling.

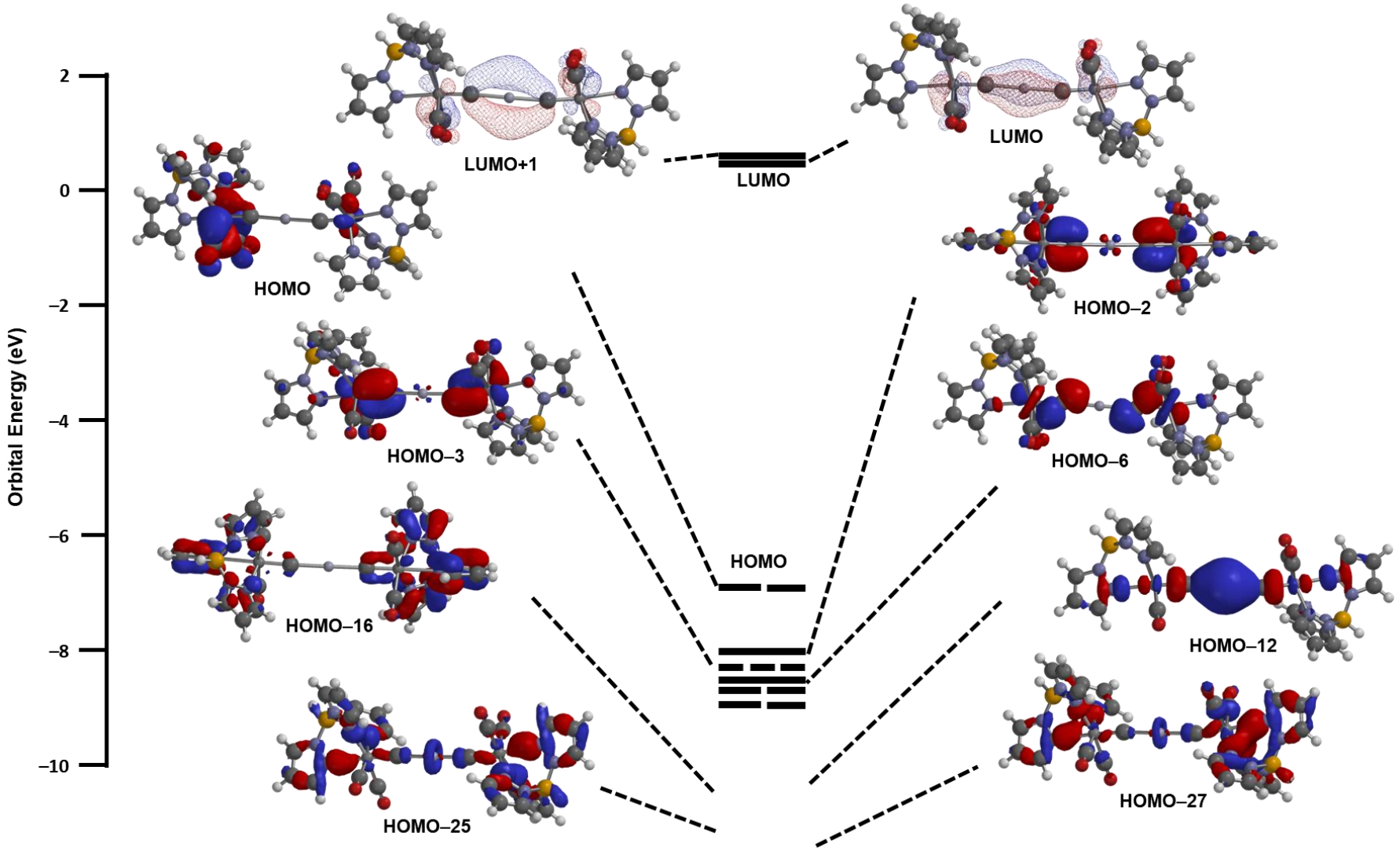

Figure 7.21: Frontier orbitals of interest for theoretical complex *anti*-[$W_2Hg(\mu_2\text{-}C)(CO)_4(Tp)$] (**7.11b***).

Preparation of **7.11b** *via* transmetallation of stannylcarbynes or directly from lithiocarbynes revealed excess [$HgCl_2$] serves to complicate the reaction, with previously unpublished structures obtained from lithiocarbyne protocols providing a guide (Figure 7.22 and 7.23). If insufficient [$W(\equiv CSnBu_3)(CO)_2(Tp^*)$] is provided and both Hg–Cl bonds are metathesised, further species arise in solution. By altering the tin to mercury stoichiometry from 2:1 to 1:1, the same reaction conditions produce [$WHg(\mu_2\text{-}C)(CO)_2(Tp^*)]_2(\mu_2\text{-}Cl)_2$ *i.e.*, [$W(\equiv CHgCl)(CO)_2(Tp^*)]_2$ (**7.12**) as a halo-bridged dimer (Scheme 7.9), Furthermore, an excess of [$HgCl_2$] provides [$WHg(\mu_3\text{-}C)(\mu\text{-}HgCl_2)(CO)_2(Tp^*)]_2(\mu_2\text{-}Cl)_2$ *i.e.*, [$W(\equiv CHgCl)(CO)_2(Tp^*)]_2(HgCl_2)_2$ (**7.13**, Figure 7.22) where a unit of $HgCl_2$ coordinates through mercury to the W≡C π-system with one chloride bridging to the first mercury. This entire "$W\{CHgCl_3\}(CO)_2(Tp^*)$" unit then dimerises *via* a Hg_2Cl_2 trapezoidal bridge to form a centrosymmetric hexametallic ensemble (Figure 7.22). The formation of **7.13** appears to be favoured by non-polar solvents (*e.g.*, toluene).‡‡‡‡‡‡‡‡‡‡‡‡‡‡‡‡‡‡‡‡ Fortunately, these two species are each distinct and recognisable by infra-red spectra for which well-resolved absorbances are observed (ν_{CO}(cm^{-1}): 1992/1900 **7.12**; 2041/1966 **7.13**) allowing monitoring and selective formation *via* additional tin or mercury precursor. Addition of [$HgCl_2$] converts **7.12** to **7.13** while the geometry of **7.13** might be seen as providing a model for intermediates in transmetallation. Conversely, addition of PPh_3 to **7.13** induces the reverse reaction by scavenging '$HgCl_2$' fragments as [$HgCl_2(PPh_3)_n$] species. [595] Finally, it should be noted that isolated samples of **7.12** and **7.13** returned to solution and monitored by ^1H, $^{199}Hg\{^1H\}$ and infra-red (ν_{CO}) spectroscopies exhibited no evidence of interconversion of equilibration over several days. These two complexes complete the deceptively tricky system underpinning transmetallation with [$HgCl_2$]; one an additional metallacarbyne, one a rare μ_3-carbido.

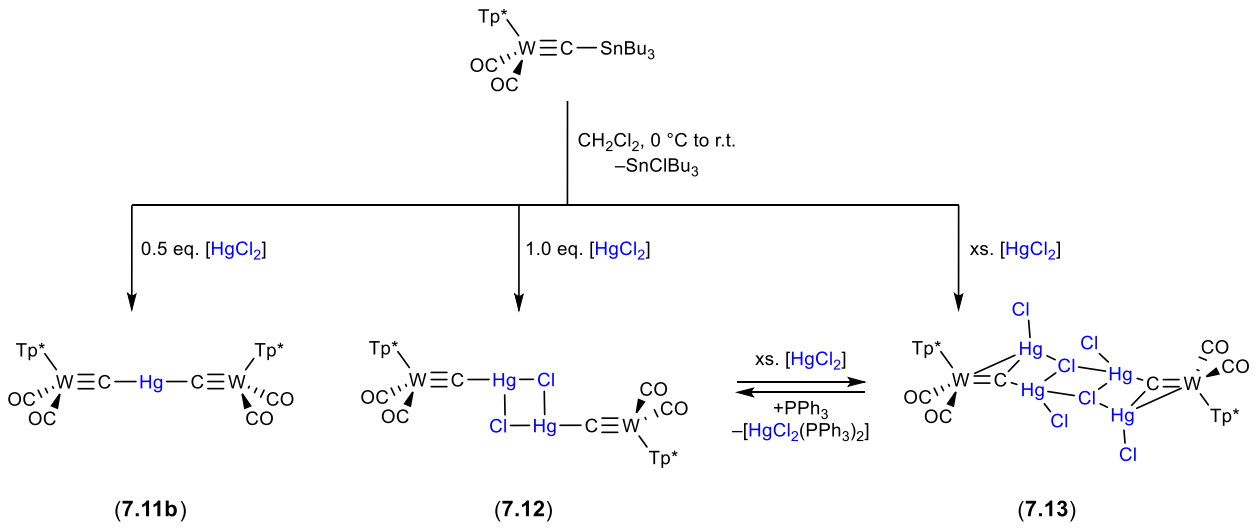

Scheme 7.9: Further mercury μ-carbido species from [$HgCl_2$] and their interconversion.

‡‡‡‡‡‡‡‡‡‡‡‡‡‡‡‡‡‡‡‡ In the related system a further solid-state combination {[$Mo(\equiv CHgCl)(CO)_2(Tp^*)]_2(HgCl_2)_2$}($HgCl_2$) was structurally identified in which two of the molybdenum analogues of **7.13** are bridged by a further $HgCl_2$ unit with a square planar geometry at mercury. M. Sharma, unpublished observations.

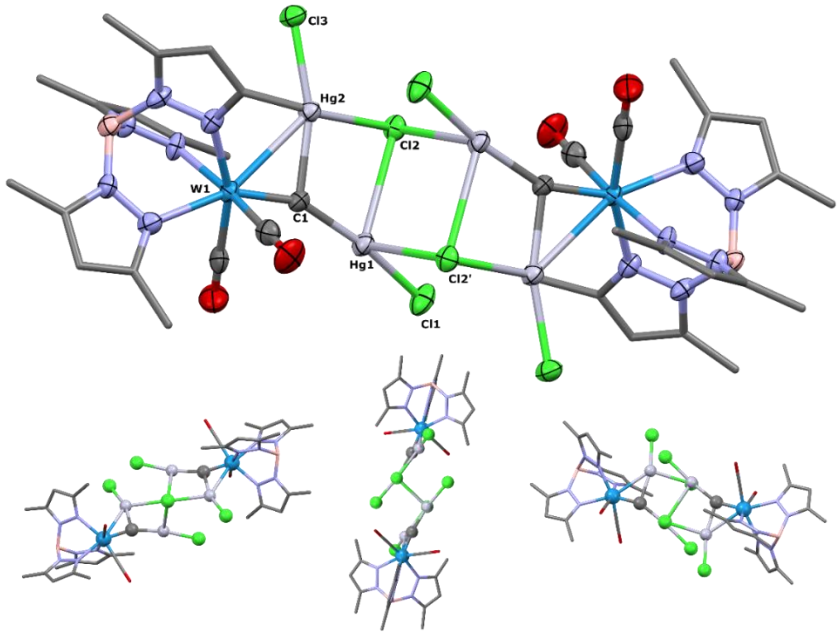

Figure 7.22: Molecular structure of $[WHg(\mu_3\text{-}C)(\mu\text{-}HgCl_2)(CO)_2(Tp^*)]_2(\mu_2\text{-}Cl)_2$ (**7.13**) in a single crystal of **7.15**·4($CHCl_3$) as determined by X-Ray Diffractometry.§§§§§§§§§§§§§§§§§§§§§§§§§§§§ Ellipsoids are drawn at the 50% probability surface with pyrazolyl rings simplified and $CHCl_3$ solvent and hydrogens omitted for clarity. Insets: Back and stick representations at different angles highlighting mercury halide bonding. Selected bond lengths (Å) and angles (°): W1–C1 1.870(9), C1–Hg1 2.065(9), Hg1–Cl1 2.311(2), Hg1–Cl2 3.060(2), Hg1–Cl2' 2.956(3), W1–Hg2 2.8873(5), Hg2–C1 2.161(8), Hg2–Cl2 2.699(2), Hg2–Cl3 2.328(2), W1–C1–Hg1 156.5(5), W1–C1–Hg2 91.2(4), C1–Hg1–Cl1 169.6(3), Cl2–Hg–Cl3 105.46(8), Hg1–C1–Hg2 111.8(4), Hg1–Cl1–Hg2 74.57(6), Cl2–Hg1–Cl2' 100.17(7).

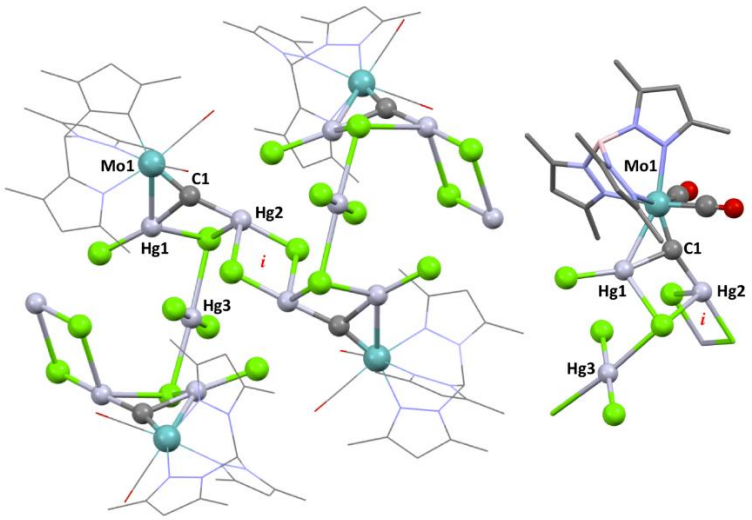

Figure 7.23: Molecular structure of centrosymmetric $\{[Mo(\equiv CHgCl)(CO)_2(Tp^*)]_2(HgCl_2)_2\}(HgCl_2)$ in a single crystal as determined by X-Ray Diffractometry. Poor data quality precluded the development of a precise structural model however connectivity was confirmed. Insets = the remarkably simple asymmetric unit from which considerable structural complexity arises due to the crystallographic symmetry elements of the space group *C2*/c (inversion, glideplanes, rotation and screw axes).

§§§§§§§§§§§§§§§§§§§§§§§§§§§§ Crystal originally grown by Dr. Manab Sharma and subsequent data analysis aided by Dr. Jas Ward. Crystal structure was finalised (for connectivity) by the author.

Complexes **7.12** and **7.13** have unremarkable spectroscopic features epitomised by almost identical ^{1}H NMR spectra to **7.11b**. Apart from carbonyl resonances, ^{199}Hg NMR spectroscopy is the most definitive identifier as the **7.12** resonance appears to marginally lower frequency (δ_{Hg} = –993) of **7.11b** (δ_{Hg} = –1004) and broadened. Otherwise, **7.13** resides in a similar region to **7.12** (δ_{Hg} = –962), although systematic attempts to locate the second μ-$HgCl_2$ resonance in **7.13** failed, presumably a signal broadened into the baseline. The μ-carbido signals in the $^{13}C\{^{1}H\}$ spectra are also sufficiently different but are challenging to detect. Additional mercury shifts the carbido resonance to higher frequency for the dimer (δ_C: 297.6 **7.12**) with the μ_3-carbido residing at a relatively high frequency (δ_C: 216.4 **7.13**) but consistent with previous π-coordination complexes albeit significantly broadened. As the species differ in units of '$HgCl_2$', high-resolution mass spectrometry managed to identify fragmentations of the species from pure isolated samples (albeit accompanied by several other fragmentations), however, elemental analysis proves far more conclusive with high consistency of composition with proposed formulae.

Crystals of **7.13** were obtained by Dr M. Sharma *via* the alternative lithiocarbyne route and the results of a crystallographic analysis are summarised in Figure 7.22. The W–C length is relatively unchanged suggesting a weak π-coordination, consistent with experimental observation that PPh_3 can extract this $HgCl_2$ unit. Curiously, the halogen bridge is established by the π-coordinated Hg–Cl unit, not the terminal unit, adopting a *trans* ladder like geometry of the molecule. A further data set was obtained for a polymeric molybdenum complex {[Mo(≡CHgCl)(CO)$_2$(Tp*)]$_2$(HgCl$_2$)$_2$}(HgCl$_2$) in which centrosymmetric cores based on molybdenum are linked to form infinite chains by a further equivalent of $HgCl_2$ (Figure 7.23).[**********]

This further illustrates the structural complexity in the solid state though these various possibilities interconvert in solution.

7.5.2 Aryls, Phenylpyridine, and Thiophene

Stannylcarbynes have been shown to transmetallate to mercury uncovering a plethora of μ-carbido species from controlled addition of [$HgCl_2$]. Arylmercury chlorides provided a logical progression to consider whether carbidos terminated with arylmercury residues might be viable, not least because this would obviate the complications arising from halide-bridge aggregation. The lipophilicity of organomercurials calls for particular attention to safety issues and for that reason alkylmercurials were specifically excluded from investigation. Arylmercury halides in contrast to notoriously neurotoxic and biologically persistent methyl mercury salts, are rapidly broken down in animals to (still toxic) inorganic Hg^{2+}.[596] Indeed, 20th century pharmacology and agrichemicals (Shirtan), saw extensive use of aryl (and some alkyl!) mercuric halides, including for direct use in humans (mercurichrome, thiomersal,

[**********] M. Sharma, *Unpublished Results*, Australian National University.

nitromersol, $PhHgNO_3$) though the general toxicity of mercury has resulted in their replacement.[ttttttttttttttttttttttt] Aryl mercuric chlorides therefore represent a prudent choice of reagent for the present work due to their crystallinity and low vapour pressures.

Combining $[HgCl(C_6H_5)]$ with $[W(\equiv CSnBu_3)(CO)_2(Tp^*)]$ in CH_2Cl_2 (dilute, 0 °C) returns an orange solution consistent with the formation of other metallacarbynes, however, the infra-red spectra contained a plethora of carbonyls, unable to be attributed but in similar regions to **7.11b** and **7.12** (Scheme 7.10). Similarly, the larger 1-napthyl $[HgCl(C_{10}H_8)]$ and smaller 2-thienyl (*vide infra*) derivatives provided the same observation, suggesting that σ-aryl mercury metallacarbynes may not be stable and hence a chelated aryl ligand was investigated. Again, the organometallic precursor [HgCl(ppy)] (ppy = 2-pyridylphenyl) returned similar results.

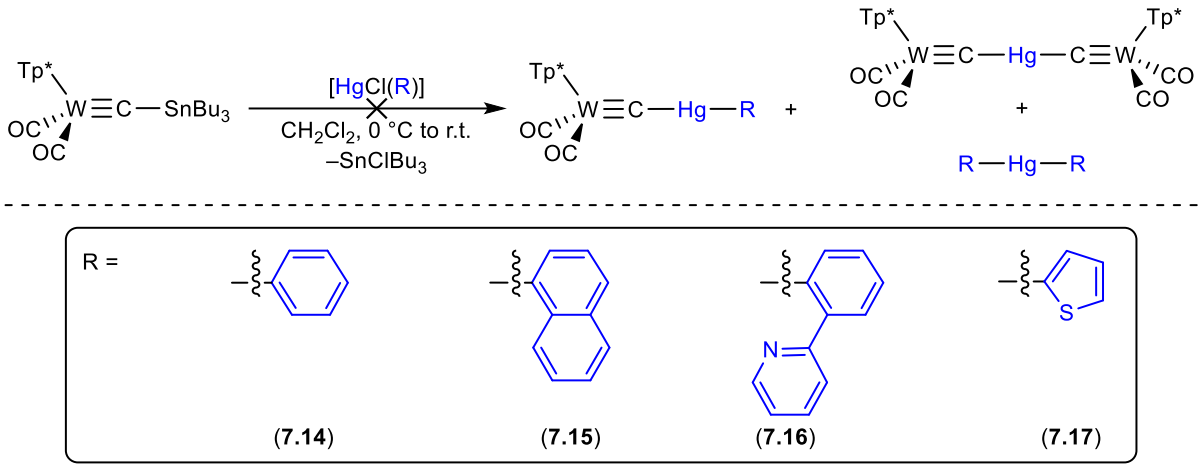

Scheme 7.10: Attempted synthesis of σ-aryl mercury metallacarbynes and their symmetrisation products identified from impure precipitated solids.

Impure solids could be obtained by concentrating CH_2Cl_2 reaction mixtures into *n*-hexane, allowing removal of unreacted stannylcarbyne and hexane soluble contaminants (*e.g.*, [W]≡CH). The $^{199}Hg\{^1H\}$ NMR spectrum of precipitated solids comprised a series of resonances that included those for **7.11b** and **7.12** consistent with symmetrisation of either the arylmercuric chloride precursor or the desired product. As mercury(II) is d^{10} closed-shell, it has no geometric preference arising from crystal field stabilisation energies, and accordingly displays a propensity for linear geometries but can increase its coordination number to allow bimolecular processes to lead to exchange of substituents and will establish equilibria in solution to achieve this. By far the most common route to symmetrical di-aryl mercurial involves the 'symmetrisation' of aryl mercuric halides (from S_EAr arene mercuration). Many factors promote mercury(II) symmetrisation including light, acids, bases, nucleophiles, electrophiles, and heat, though it

[ttttttttttttttttttttttt] See Experimental Section for details of appropriate risk management. Questions regarding mercury blood levels were repeatedly posed at International Conference proceedings presenting this work. The author wishes to disclose that routine blood tests taken at the conclusion of experimental work and immediately prior to submission did not find elevated levels of mercury, tin, or arsenic (Chapter Six).

is nucleophiles such as iodide or ammonia that are the most widely used.[523] The solids obtained from the arylmercury chlorides contain the desired metallacarbynes [WHg(μ$_2$-C)(R)(CO)$_2$(Tp*)] (R = C_6H_5 **7.14**; $C_{10}H_8$ **7.15**; ppy **7.16**; C_4H_3S **7.17**) which were only partially characterised (Table 7.2), due to being accompanied by products arising from symmetrisation (**7.11b**, **7.12**, and [Hg(R)$_2$]) (Figure 7.24).

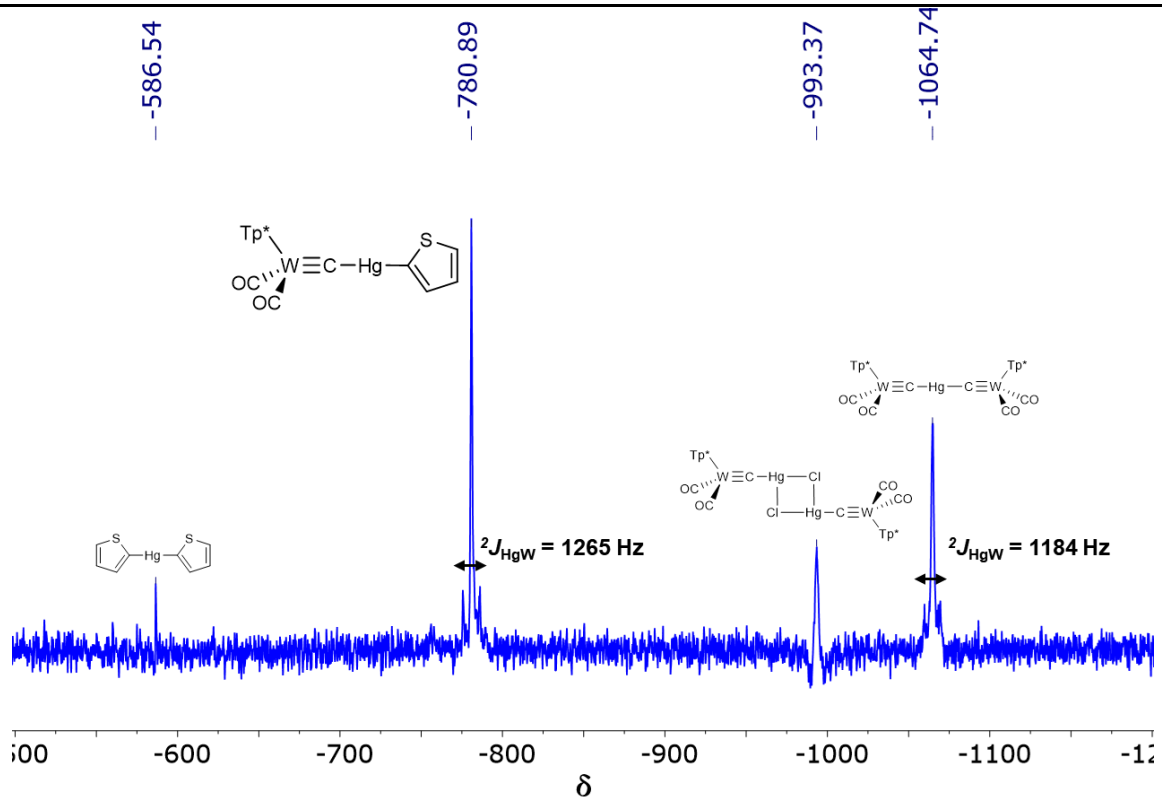

Figure 7.24: Representative ^{199}Hg{^{1}H} of isolated solid containing [WHg(μ$_2$-C)(SC$_4$H$_3$) (CO)$_2$(Tp*)] (**7.17**) with symmetrisation products assigned.

Unfortunately, attempts to isolate **7.14**–**7.17** *via* fractional crystallisation have so not met with success. The extracted spectroscopic features reflect the inductively electron-withdrawing nature of σ-aryls, recording μ$_2$-carbido resonances in the ^{13}C{^{1}H} NMR spectra to slightly higher frequency than a second μ$_2$-carbido (*ca* **7.11b**). Furthermore, the ^{199}Hg{^{1}H} NMR spectra exhibit resonances in a similar area, where a loose trend exists such that higher frequency mercury resonance coincides with a stronger coupling to tungsten ($^2J_{HgW}$). The ^{13}C{^{1}H} and ^{199}Hg{^{1}H} spectra were collected as a series of experiments (12 × 10000 scans) as opposed to a single experiment (1 × 120,000 scans) such that the relative intensities corresponding to different species do not change over the timescale of these experiments (*ca* 16 hours). This suggests that the distribution is defined during the reaction, not during isolation or dissolving the solid (*i.e.*, not an equilibrium). This is also consistent with the presence of **7.11b** which could not arise from symmetrisation of **7.17**, but rather must originate from a prior symmetrisation of [Hg(C$_4$H$_3$S-2)Cl] to afford of [Hg(C$_4$H$_3$S-2)$_2$] and [HgCl$_2$]. Control reactions of **7.11b** with [HgCl$_2$] also found no evidence

of equilibria being established over two weeks, even in the presence of $SnClBu_3$ liberated in the transmetallation mixtures.

Given the variables of the arylmercury transmetallation, a series of test reactions were conducted to elucidate whether an equilibrium is operative in complexes **7.14**–**7.17**. An authentic sample of $[Hg(SC_4H_3)_2]$ with $[HgCl_2]$ failed to produce $[HgCl(SC_4H_3)]$ after 3 days under the reaction conditions leading to **7.17**, including when repeated in the presence of $SnClBu_3$; a by-product of the transmetallation reaction. Furthermore, similar reactions of **7.11b** or the analogous alkynyl $[Hg(C{\equiv}C\text{-tolyl})_2]$ with $[HgPh_2]$ fail to symmetrise to **7.14** or [HgPh(C≡C-tolyl],### respectively, with or without adventitious $SnClBu_3$. This suggests that the symmetrisation process precedes the transmetallation reaction or are defined at the reaction event; not redistributed afterwards. Beyond this interpretation it is unclear as to the cause of the mixtures obtained.

Table 7.2: Spectroscopic parameters for observed σ-aryl mercury metallacarbynes and symmetrisation species.

Complex	δ_C[a] (ppm)	$^1J_{CW}$[a] (Hz)	δ_{Hg}[a] (ppm)	$^2J_{HgW}$[a] (Hz)	ν_{CO}[b] (cm^{-1})
$[Mo_2Hg(\mu_2\text{-}C)_2(CO)_4(Tp^*)_2]$ (**7.11a**)	373.0[c]	–	n.r.	n.r.	2000, 1994, 1912[d]
$[W_2Hg(\mu_2\text{-}C)_2(CO)_4(Tp^*)_2]$ (**7.11b**)	355.1	172	–1065	1184	1984, 1976, 1889[d]
$[WHg(\mu_2\text{-}C)Cl(CO)_2(Tp^*)]_2$ (**7.12**)	297.6	n.d.	–993.6	n.d.	1992, 1900
$[WHg(HgCl_2)(\mu_3\text{-}C)Cl(CO)_2(Tp^*)]_2$ (**7.13**)	216.4	n.d.	–961.6[e]	n.d.	2041, 1967
$[WHg(\mu_2\text{-}C)(C_6H_5)(CO)_2(Tp^*)]$ (**7.14**)[f]	360.6	n.d.	–895.4	1132	n.d.
$[WHg(\mu_2\text{-}C)(C_{10}H_8)(CO)_2(Tp^*)]$ (**7.15**)[f]	360.2	178	–815.1	1104	n.d.
$[WHg(\mu_2\text{-}C)(ppy)(CO)_2(Tp^*)]$ (**7.16**)[f]	366.3	n.d.	–813.7	1200	n.d.
$[WHg(\mu_2\text{-}C)(SC_4H_3)(CO)_2(Tp^*)]$ (**7.17**)[f]	348.5	n.d.	–780	1265	n.d.
$[WHg(\mu_2\text{-}C)(S_2CNMe_2)(CO)_2(Tp^*)]$ (**7.18**)	322.0	n.d.	–894.0	n.d.	1981, 1890
$[HgCl_2]$ [598]	–	–	–1550[g]	–	–
$[Hg(C_6H_5)_2]$ or $[HgPh_2]$ [599]	–	–	–744.8	–	–
$[Hg(C_{10}H_8)_2]$	–	–	–604.7[h]	–	–
$[Hg(ppy)_2]$ [600]	–	–	–689	–	–
$[Hg(SC_4H_3)_2]$	–	–	–586.6[h]	–	–
$[Hg(C_6H_5)(C{\equiv}CC_6H_5)]$ [597]	–	–	–773.7	–	–
$[Hg(C{\equiv}CC_6H_5)_2]$ [597]	–	–	–863.0	–	–

Notes: [a]Measured in $CDCl_3$ unless specified otherwise. [b]Measured in CH_2Cl_2 unless specified otherwise. [c]Measured in CD_2Cl_2. [d]Coupled oscillators result in split of symmetric stretch. [e]No resonance for second ^{199}Hg nucleus detected. [f]Species measured as part of a mixture. [g]Measured in D_2O. [h]Measured in this work. n.d. = not detected. n.r. = not resolved.

7.5.3 Bidentate Dithiocarbamate

Mercuriocarbynes with σ-aryl mercury substituents (and Hg–C) bonds were only observed as mixture components due to symmetrisation that occurred during or prior to Sn→Hg transmetallation. A discrete bimetallic mercury metallacarbyne was still desired to compliment the trimetallic **7.11b**, for fundamental interest and for practical reasons that will become apparent in the Chapter that follows. Strong bonds

[HgPh(C≡C-tolyl] has not been previously reported, however [HgPh(C≡CPh] has δ_{Hg} = –773.7 in CH_2Cl_2. [597]

occur between mercury and sulfur underpinning the mining of cinnabar since late neolithic times (2900–2300 B.C.) in Europe and the Yangshao period in China (4000–3500 B.C.),[601] through to the exceptional affinity for thiols, *e.g.*, cysteine complexation that underpins the potentially lethal neurotoxicity of mercury.[602-603] Given that extraneous nucleophiles promote symmetrisation of organomercurial halides and *pseudo*-halides, a mercury substituent capable of shield the mildly electrophilic mercury appeared to be a potentially desirable design feature for metallacarbynes. Therefore, the dithiocarbamato class of ligand was considered to address these issues: a strong Hg–S bond to stabilise species but also a second sulfur to chelate should electronic demands require a second donor. That said, it has also been established that even simple *bis*(dithiocarbamato) complexes of mercury can undergo facile intermetallic dithiocarbamate exchange that can be rapid on the ^{199}Hg NMR timescale.[604]

Unpublished results within this group document the reaction of [HgCl(S_2CNMe_2)] with [W(≡CLi)$(CO)_2$(Tp*)] to provide [WHg(μ_2-C)(S_2CNMe_2)$(CO)_2$(Tp*)] (**7.18**).[605] More conveniently, a transmetallation from [W(≡CSnBu_3)$(CO)_2$(Tp*)] to [HgCl(S_2CNMe_2)] was, in the present work, found to result in a bright yellow solution.§§§§§§§§§§§§§§§§§§§§§§§§§§§§ Recrystallisation is simple such that excess stannylcarbyne and halostannane by-product can be washed away to provide **7.18** as a bright yellow solid, devoid of impurities and conveniently up to 2 g quantities (Scheme 7.11).********** Unlike the aforementioned σ-aryl complexes, **7.18** appears relatively stable in solution, only decomposing slowly to [W(≡CH)$(CO)_2$(Tp*)] in the presence of moisture ($t_{1/2}$ = 10 hours). A C_6D_6 solution of **7.18** remained exposed to sunlight for four days with no appreciable change like symmetrisation. Both these observations are unusual in that Hg–C bonds are typically photo-sensitive but are stable towards air and moisture, hence the environmental persistence of biomethylated mercury and the routine synthesis of *bis*(alkynyl)mercurials in water.

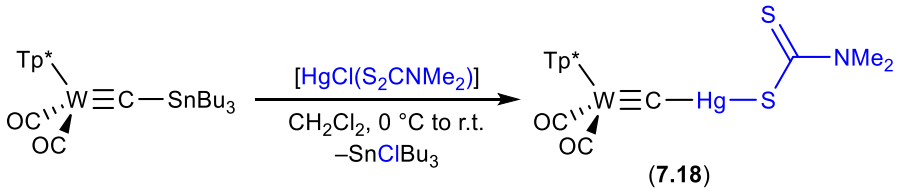

Scheme 7.11: Synthesis of a bimetallic mercury metallacarbyne [WHg(μ_2-C)(S_2CNMe_2)$(CO)_2$(Tp*)] (**7.18**) *via* stannylcarbyne transmetallation.

Isolation reaffirms the carbonyl vibrations (ν_{CO}: 1981, 1890 cm^{-1}) obscured during synthesis by stannylcarbyne absorptions, while the $^{13}C\{^1H\}$ NMR spectrum exhibits a high frequency signal consistent with a μ_2-carbido (δ_C = 322.0), consistent with the σ- and π-basic sulfur in the *trans*-position (Figure 7.25).

§§§§§§§§§§§§§§§§§§§§§§§§§§§§ The reaction progress is deceptively obscured by similar carbonyl absorptions for the product and starting material.

********** An arbitrarily agreed limit of up to ~2 g given that mercury remains a highly toxic element, even when strongly coordinated dithiocarbamate ligands are involved.

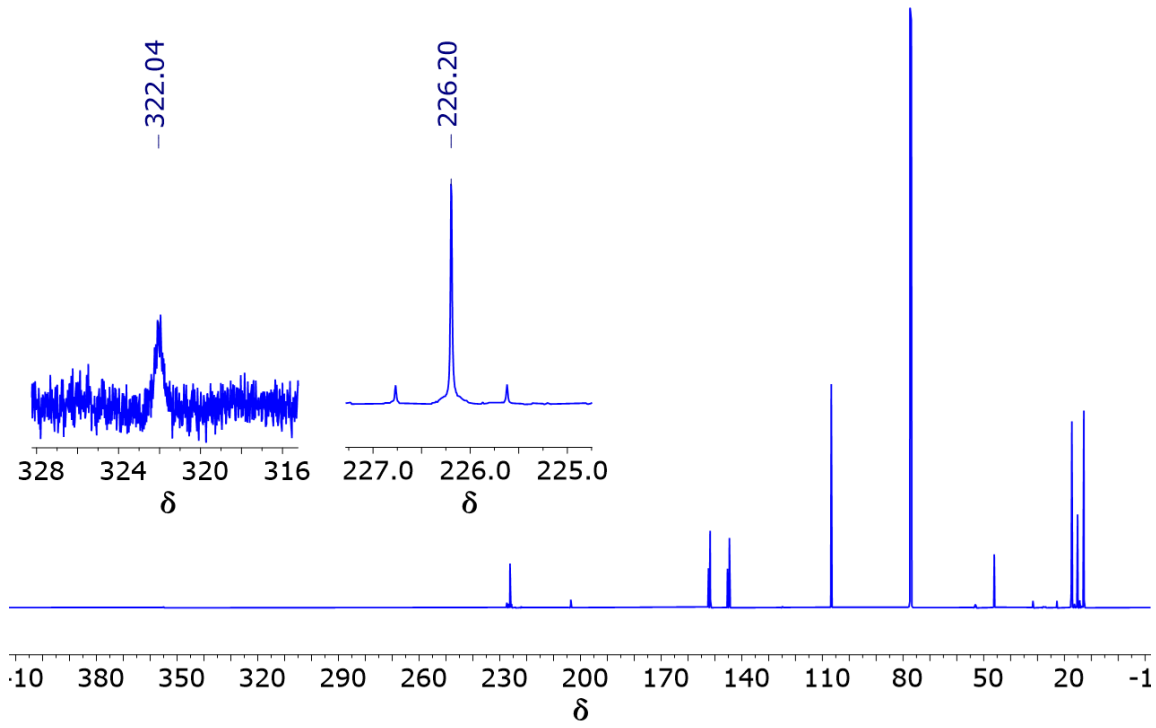

Figure 7.25: $^{13}C\{^{1}H\}$ NMR Spectrum of [WHg(μ$_2$-C)(S$_2$CNMe$_2$)(CO)$_2$(Tp*)] (**7.18**) in $CDCl_3$ highlighting the carbido resonance. Coupling to ^{199}Hg was not observed.

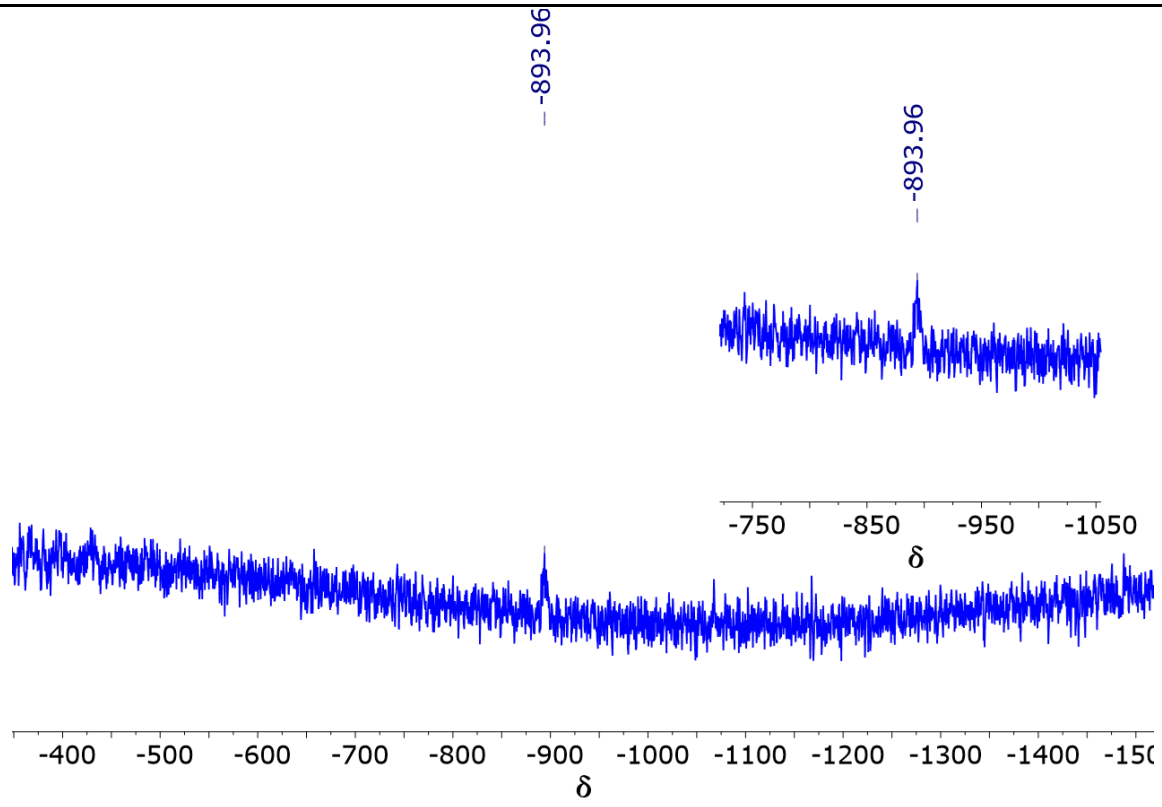

Figure 7.26: $^{199}Hg\{^{1}H\}$ NMR spectrum of [WHg(μ$_2$-C)(S$_2$CNMe$_2$)(CO)$_2$(Tp*)] (**7.18**) in $CDCl_3$ showing the broad resonance of the mercury preventing coupling to tungsten being resolved.

This μ_2-carbido signal is broad, and in the absence of further coupling partners, likely suggests that the dithiocarbamate is 'switching' between sulfur donors at a comparative rate to that of the ^{13}C timescale. Such switching is likely in the σ_h plane as all other ^{13}C and ^{1}H signals remain sharp consistent with C_s symmetry. A broad signal is also recorded for $^{199}Hg\{^{1}H\}$ NMR spectra (δ_{Hg} = –894) at a similar frequency to the σ-aryls (*ca* –895; **7.14**) (Figure 7.26). Many other spectroscopic data are unremarkable, however, a somewhat imprecise crystal structure collected of **7.18·THF** proves far more interesting as the first (and only) molecular structure of a mercury μ_2-carbido complex (Figure 7.27).ǂǂǂǂǂǂǂǂǂǂǂǂǂǂǂǂǂǂǂǂǂǂǂǂ

The bond lengths are consistent with a metallacarbyne, noting the Hg–C bond (2.02(2) Å) may be compared with Hg–C(sp^3) (2.063(12) Å) and Hg–C(sp) (2.031(12) Å) bond lengths in the elegantly internally referenced molecule [$MeHgC{\equiv}CC_6H_4C_6H_4C{\equiv}CHgCH_3$] [606] or to the Hg–C($sp^3$)/Hg–C($sp^2$) bonds in the *bis*-alkynylthiophene [$SC_4H_2(C{\equiv}CHgCH_3)_2$-2,5] (2.065(13)/2.036(13)Å), [607] however the low precision of the structural model curtails more detailed analysis. The dithiocarbamate ligand clearly binds unsymmetrically to the mercury with an essentially near linear C1–Hg–S1 angle (172.7(4)°) and short Hg1–S1 bond (2.393(4)°) while the second sulfur (S2) exhibits C=S multiple bonding character with a significantly longer Hg1···S2 bond (2.860(4) *vs* 2.393(4) Å) accompanied by a shorter C–S length (*i.e.*, C=S; 1.68(2) *vs* 1.76(2) Å). This would appear consistent with the valence bond description provided in Scheme 7.11, supplemented by a weak 'spodium' Hg···S bonding interaction. [608] Structural data are available for a large number of organomercury dithiocarbamates, though no alkynyl examples have appeared. The linear C–Hg–S motif with weak Hg···S interaction to the second sulfur is a recurring feature and this may be further supplemented by dimerization to form trapezoidal Hg_2S_2 cores, without deformation of the primary linearity of the C–Hg–S spine. In the case of **7.18**, rather than dimerising, additional spodium bonding is provided by one coordinated THF, the Hg…O separation of which (Hg···O: 2.85(1) Å) is too long to be considered a covalent bond, and is significantly longer than that of [Hg(IPr)$(OTf)_2$(THF)] (2.492(2) Å), [609] the closest structurally characterised example of a THF ligand mercury(II). The Hg–S bond in **7.18** (2.393(4)Å) is essentially similar, given the poor precision (≈ 6 e.s.d.) to those for the analogous complexes [$HgR(S_2CNMe_2)$] (R = Ph: Hg–S 2.4033(9), R = Me: Hg–S 2.418 Å). [610-611] Therefore, **7.18·THF** is indeed a mercuriocarbyne that essentially exhibits two-coordinate character at mercury (C–Hg–S = 172.7(4)°) for a linear μ-carbido complex (W–C–Hg = 172.2(9). The NMR data are therefore accommodated by the two sulfur donors swapping their roles on the NMR timescales with minimal actual reorganisation being required.

ǂǂǂǂǂǂǂǂǂǂǂǂǂǂǂǂǂǂǂǂǂǂǂǂ Dataset originally collected and solved by Dr. Manab Sharma but was reprocessed by the author.

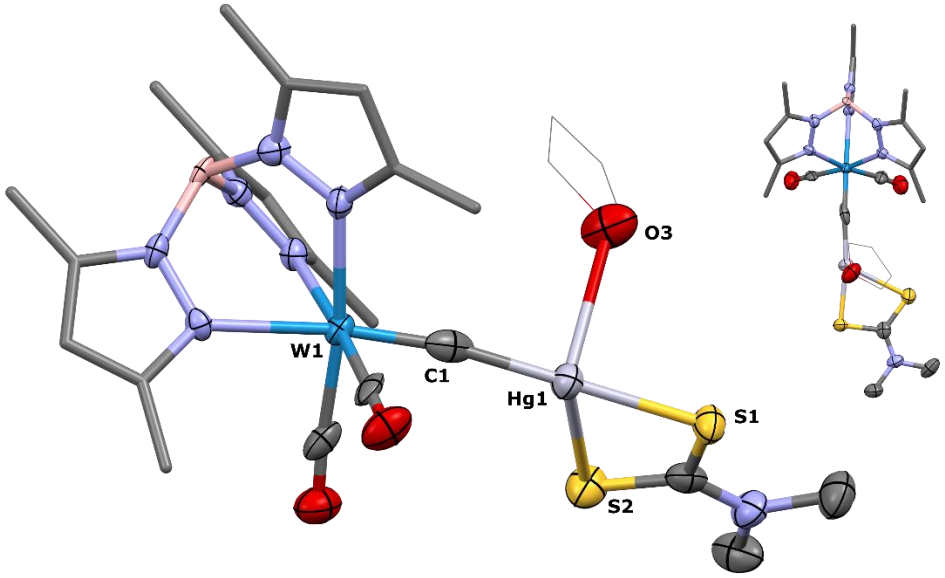

Figure 7.27: Molecular structure of [WHg(μ$_2$-C)(S$_2$CNMe$_2$)(THF)(CO)$_2$(Tp*)] (**7.18.THF**) in a single crystal as determined by X-Ray Diffractometry. Ellipsoids are drawn at the 50% probability surface with pyrazolyl rings simplified and hydrogens omitted for clarity. Inset: View normal to the dithiocarbamate plane to highlight the linear geometry of mercury and the unsymmetrical binding of the dithiocarbamato ligand. Selected bond lengths (Å) and angles (°): W1–C1 1.83(2), C1–Hg1 2.02(2), Hg1–S1 2.393(4), Hg1–S2 2.860(4), Hg1–O3 2.85(1), W1–C1–Hg1 172.2(9), C1–Hg1–S1 172.7(4), S1–Hg1–S2 68.5(1).

7.6 Catalytic Demercuration of Mercury Carbido/ Organomercuriocarbyne Complexes

Production of diynyl and related conjugated species *via* catalytic demercuration is a little method of C–C coupling.[612-617] While demercuration of organomercuriocarbynes L$_n$M≡C–Hg–R might in principle provide carbynes accessible by other routes, not least those which are now available *via* C–C cross-coupling reactions of stannylcarbynes and the processes discussed in Chapter Six. Little is known, however, about the demercuration mechanism and for this reason, an investigation into demercuration of mercury carbidos/organomercuriocarbynes was undertaken.

Catalytic demercuration of [Mo$_2$Hg(μ$_2$-C)$_2$(CO)$_4$(Tp*)$_2$] (**7.11a**) can be performed with [RhCl(CO)(PPh$_3$)$_2$] in hours at ambient temperature to produce [Mo(μ$_2$-C$_2$)(CO)$_4$(Tp*)$_2$] as an uncommon *bis*-carbyne (ethanediylidyne),[118] or alternatively a bridging 'dicarbido' with bonding that is distinct from conventional bimetallated ethyne (ethyn-diyls). The analogous reaction occurs for **7.11b** albeit more slowly ($t_{½}$ = 10 hours, 5 mol% catalyst loading) which is perhaps surprising in that the reduced kinetics of tungsten as compared with molybdenum would not be expected to impact on the general mechanism that does not involve the group 6 metal centre. The complex [W(μ$_2$-C$_2$)(CO)$_4$(Tp*)$_2$] has been reported previously, *via* an alternative synthetic route[350] For **7.11b**, an appreciable amount (*ca* 10 %) of terminal methylidyne [W(≡CH)(CO)$_2$(Tp*)] was noted *via* TLC and eluted from flash chromatography, but was apparently initially absent (or obscured) in infra-red spectra thus suggesting protons are likely abstracted

from silica gel. This suggests that other species may be active in solution (possibly unreacted **7.11b**) and react with moisture/stationary phase to produce the methylidyne, yet chromatography or spectroscopic techniques were unable to find evidence of other complexes.

The σ-arylmercurials (**7.14–7.17**) are observed in mixtures established by symmetrisation reactions, and therefore should result in a mixture of complexes *post*-demercuration. For the phenyl (**7.14**) and naphthyl (**7.15**) mixtures, the same demercuration conditions (THF, 5 mol%, 16 hours) provided the dicarbido $[W(\mu_2\text{-}C_2)(CO)_4(Tp^*)_2]$ almost exclusively with a small amount of $[W(\equiv CH)(CO)_2(Tp^*)]$, and no evidence of the corresponding carbynes $[W(\equiv CR)(CO)_2(Tp^*)]$ (R = Ph[310] or naphthyl) *via* chromatography or $^1H/^{13}C$ NMR spectroscopy (Scheme 7.12). Furthermore, the reaction mixture from **7.14** included only trace amounts (*ca* <5% mixture) of biphenyl *via* GC–MS once a silica gel plug removed metallic species,‡‡‡‡‡‡‡‡‡‡‡‡‡‡‡‡‡‡‡‡‡‡ but biphenyl or $[HgPh_2]$ was obscured in ^1H NMR mixtures. The previous report of demercuration of $[HgPh_2]$ by (more active) $[RhCl(PPh_3)_3]$[74] required heating (80 °C) for 4 hours in a range of solvents to afford yields from 4% (THF) to 100% (HMPA) of biphenyl. Amongst the variants in that study, DMF provided 36%, however it is known that Wilkinson's catalyst is converted to $[RhCl(CO)(PPh_3)_2]$ by DMF under these conditions, *i.e.*, the actual catalyst was in effect the same as used in this study at room temperature. This suggests that biphenyl quantitation is not a reliable assay of the amount of $[HgPh_2]$ present in the original mixture with **7.11b** and **7.14–7.17**. Given that the major species formed from demercuration is $[W(\mu_2\text{-}C_2)(CO)_4(Tp^*)_2]$, it would appear that symmetrisation of **7.14** is likely faster than the demercuration catalysis.

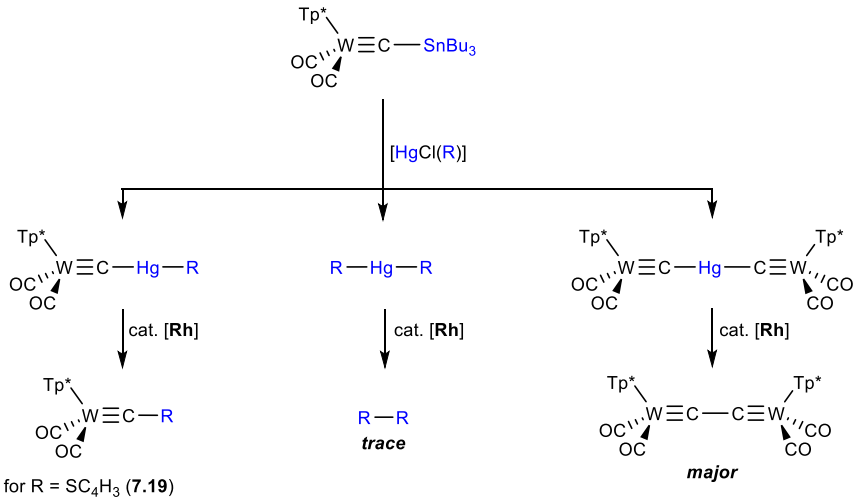

Scheme 7.12: Catalytic demercuration of *bis*-carbido mercurial and σ-aryl mixtures **7.14–7.17**.

Beginning with the 2-thienyl-derived mixture (**7.17**), more species are produced instead of $[W(\mu_2\text{-}C_2)(CO)_4(Tp^*)_2]$. While similar symmetrisation processes are likely, the demercuration conditions also

‡‡‡‡‡‡‡‡‡‡‡‡‡‡‡‡‡‡‡‡‡‡ The analogous test could not be performed for **7.15** as the likely binapthyl product has a higher boiling point (~360 °C) beyond the limit of the GC instrument (*ca* 300 °C).

return a coloured species *via* TLC identified as the carbyne [W(≡CC_4H_3S-2)$(CO)_2$(Tp*)] (**7.19**) in a relatively high isolated yield (39%). Accumulation of **7.19** suggests a slower rate of symmetrisation towards **7.11b**, or alternatively faster rates of demercuration of **7.17**; TLC identified the carbyne **7.19**, 'dicarbido' and methylidyne species, while GC–MS verified formation of 2,2-bithienyl in trace amounts (Figure 7.28). A ^{1}H NMR spectrum was measured for the demercuration of **7.17** mixtures, and while the signals of 2,2-bithienyl or [$Hg(SC_4H_3)_2$] are not obscured by PPh_3 signals, *cf.* the phenyl analogues, these were of low intensity, indicating only a trace bithienyl was formed (4% by integration against PPh_3). It should be noted that while **7.19** was a previously unknown complex, this method is unlikely to be the preferred synthesis as the molybdenum analogue can be produced almost quantitatively from lithiation of thiophene prior to a Fischer–Mayr synthesis.[468] Complex **7.19** was fully characterised including a crystal structure determination but the data call for no comment other than to note they conform to those for related carbynes.[255]

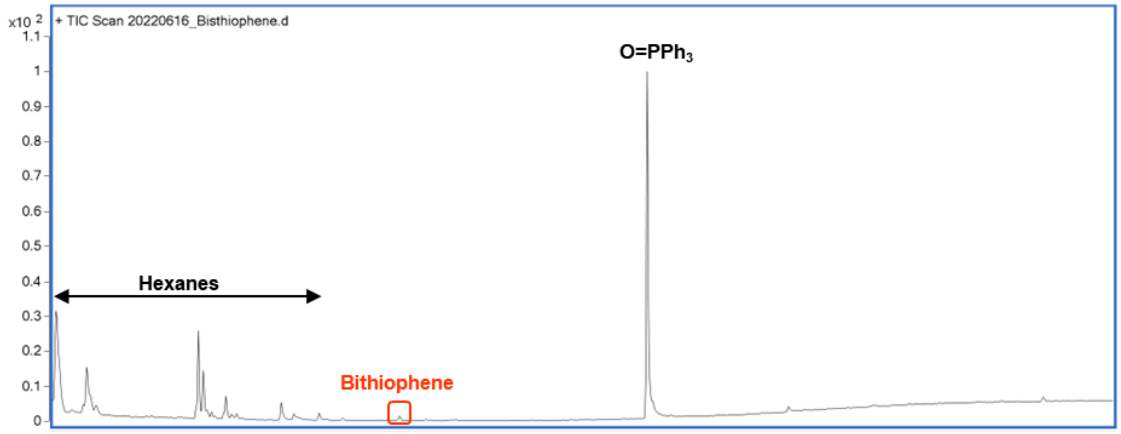

Figure 7.28: GC–MS trace with identified mass spectrum for bithenyl from demercuration reaction.

These results demonstrate the unexpected influence of mercury substituents upon the demercuration of organomercuriocarbyne complexes. It is unclear why the procedure was moderately successful for the 2-thienyl derivative alone, other than to note that the 5-membered heterocycle is marginally smaller than phenyl and especially 2-naphthyl groups, however this small variation in steric profile seems insufficient to cause a pronounced effect. The sulfur of thiophenes is very poorly nucleophilic, however a small number of σ^1-*S* coordinated (typically chelated) thiophene complexes of rhodium are known[618-621] which raises the possibility that perhaps prior weak association through the sulfur provides sufficient kinetic advantage to bring the two reagents together.

7.7 Conclusions

This Chapter has detailed the synthesis of a range of gold(I) and mercury(II) metallacarbynes by exploiting transmetallation from stannylcarbynes, where unique 'ligand-free' aggregates provides an approach specific to gold(I). While either transmetallation or disaggregation provided gold

metallacarbynes, the stability is ultimately dictated by donor strength of the ligand *trans* to the μ_2-carbido. This facilitated the benchmarking of μ_2-carbido stability against *N*-heterocyclic carbenes, isocyanides and phosphines. The first example of a gold(III) carbido complex was obtained through serendipity involving a non-trivial, non-general redox process.

An alternative pentameric gold aggregate was observed in the solid state, distinct from the previously described tetrameric ring $[W(\equiv CAu)(CO)_2(Tp^*)]_4$ which was confirmed as the bulk complex that is isolated while the pentamer was suggested to also be present in solution through a range of spectroscopic and structural techniques.

Development of tin transmetallation was extended to mercury(II) examples where supply of $[HgCl_2]$ results in *tri*-, *tetra*-, or *hexa*-metallic species where the two latter examples show conversion between μ_2 and μ_3-carbido forms. Examples of σ-arylmercuriocarbynes could be generated, but resisted isolation, and only as mixtures susceptible to symmetrisation events. Addition of $[RhCl(CO)(PPh_3)_2]$, a mediator with a successful track record in catalytic demercuration, to such mixtures revealed variation in aryl ligands influenced the rate of catalytic demercuration. Finally, a robust dithiocarbamato complex $[WHg(\mu_2\text{-}C)(S_2CNMe_2)(CO)_2(Tp^*)]$ (**7.18**) facilitated crystallographic study of the first molecular structure of a mercury carbido complex. The syntheses of $[WHg(\mu_2\text{-}C)(S_2CNMe_2)(CO)_2(Tp^*)]$ and $[W_2Hg(\mu_2\text{-}C)_2(CO)_4(Tp^*)_2]$ are scalable and both are promising reagents for exploring metallacarbynes as discussed in the following Chapter.

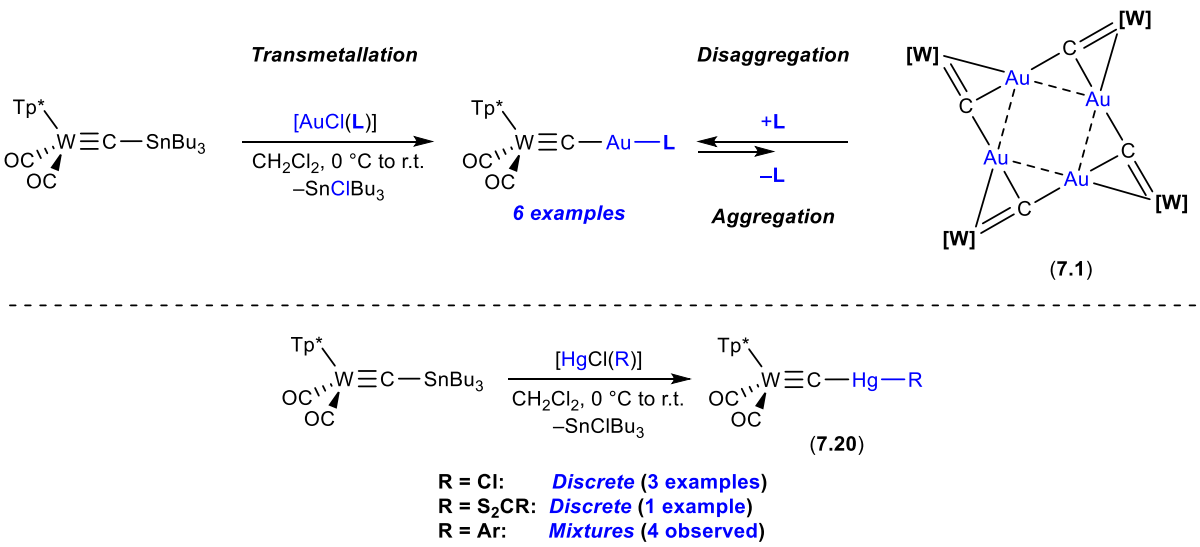

Chart 7.1: Synthesis of gold(I) and mercury(II) metallacarbynes and their peculiarities explored in Chapter Seven.

Chapter Eight

Generalisable Synthesis of Metallacarbynes

Previous Chapters progressively developed metallacarbyne chemistry with specific foci on functionalisation, reactivity of the μ_2-carbido bridge, and involvement in catalytic manifolds. These studies were limited to bimetallics involving group 6 and 10 metals and in particular those with W≡C–Pt linkages. In contrast, Chapter Seven explored the extension of carbidos to those with gold and mercury termini as compounds of fundamental interest in their own right. As will become apparent in the following Chapter, such species also serve as building blocks for the broader goal of generalisable metallacarbyne synthesis. Chapter Eight consists of two parts: Part One describes the insertion of metals into Hg–C bonds as an alternative to the bromocarbyne oxidative addition processes developed in Chapters Three and Six. Part Two considers a specific case wherein the metal reagent also includes a non-innocent hydrido ligand, resulting in an arguably distinct synthetic route to metallacarbynes. These complementary methods provide new avenues that obviate some difficulties in metallacarbyne synthesis.

Chapter Eight Part One:

Insertion of Metals into Hg–C Bonds

8.1 Addition Reactions of Mercuriocarbynes

Chapter Seven presented examples of mercury carbidos (mercuriocarbynes), the demercuration of which implicated the intermediacy of other metallacarbynes, as inferred from limited literature precedent. Demercuration of $[Mo_2Hg(\mu_2\text{-}C)_2(CO)_4(Tp^*)]$ (**7.13a**) as mediated by rhodium(I) catalysts[118] raises an important mechanistic distinction: the symmetrical *bis*-carbido only contains Hg–C bonds, therefore oxidative addition§§§§§§§§§§§§§§§§§§§§§§§§§§§§ must occur across this bond. This reaction emphasises two important points (Scheme 8.1). Firstly, when $[RhCl(CO)(PPh_3)_2]$ inserts into one Hg–C bond in **7.13**, a rhodium metallacarbyne is most plausibly formed, albeit transiently. Secondly, it follows that Hg–C bonds provide a means to synthesise rhodium metallacarbynes, which is noteworthy given $[RhCl(CO)(PPh_3)_2]$ fails to react with C–Br bonds in $[W(\equiv CBr)(CO)_2(Tp^*)]$ even when heated at reflux in toluene for one week; an otherwise facile process for palladium(0)/platinum(0).

§§§§§§§§§§§§§§§§§§§§§§§§§§§§ The term oxidative addition is used here loosely, acknowledging the caveat that the assignment of oxidation states is artificial and of limited value given that mercury is less electronegative (PE = 2.00) than the platinum group metals (PE = 2.2 – 2.28).

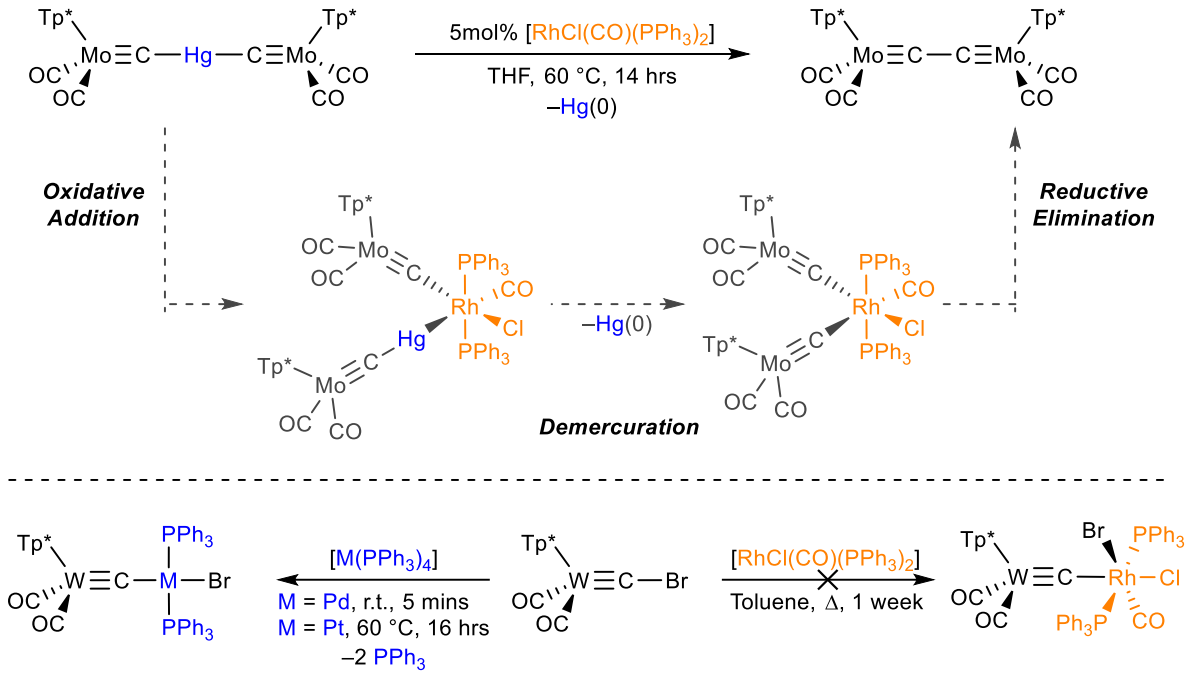

Scheme 8.1: Inferred rhodium metallacarbynes in catalytic demercuration and the failure to react with C–Br bonds.

As rhodium metallacarbyne intermediates are not observed for **7.11**, the implication is that demercuration and reductive elimination are more rapid than the initial rhodium insertion into the Hg–C bond. It therefore stands to reason that if these later steps were precluded, it might be possible to trap and isolate such species. The dithiocarbamato complex [WHg(μ_2-C)(S_2CNMe_2)$(CO)_2$(Tp*)] (**7.18**) presents an appealing precursor in that it bears a strongly chelating ligand that is not typically prone to elimination processes. This approach is unprecedented and from the outset it should be noted that there are no reports of the reactions of dithiocarbamato organomercurials R–Hg($S_2CNR'_2$) with transition metal centres. It is therefore by no means clear, *a priori*, whether the Hg–S or Hg–C bonds would prove the more reactive. In either event however, mercury extrusion should ultimately provide the same carbido-dithiocarbamato complex.

8.2 Platinum and Palladium

To first benchmark the reactivity of mercury metallacarbynes (specifically **7.18**), a target complex was selected for proof of concept, the viability of which was already established, *viz.* the complex [WPt(μ_2-C)(S_2CNEt_2)$(CO)_2$(Tp*)] (**3.4**) described in Chapter Three. Addition of [Pt(η^2-C_2H_4)$(PPh_3)_2$] to a THF solution of mercury **7.18** resulted in an immediate bright orange colouration that slowly faded to yellow over a period of 16 hours (requiring heating at 60 °C) accompanied by the deposition of elemental mercury. The reaction provides the dimethyldithiocarbamato [WPt(μ_2-C)(S_2CNMe_2)$(CO)_2$(Tp*)] (**8.1**), spectroscopic data that parallel those for the diethyl-derivative (**3.4**) obtained *via* ligand substitution in Chapter Three. Similarly, combining [Pd$(PPh_3)_4$] with **7.18** provides [WPd(μ_2-C)(S_2CNMe_2)$(CO)_2$(Tp*)] (**8.2**), which exhibits similar colour changes over a shorter time frame, but also required heating for full

conversion. The orange colour likely belongs to a species formed immediately upon oxidative addition of either the Hg–C (**A**) or Hg–S bonds (**B**) (Scheme 8.2), however, $^{31}P\{^{1}H\}$ NMR spectroscopy of the reaction mixtures failed to discern any resonances suggestive of species with a direct Pt–Hg bond.**********

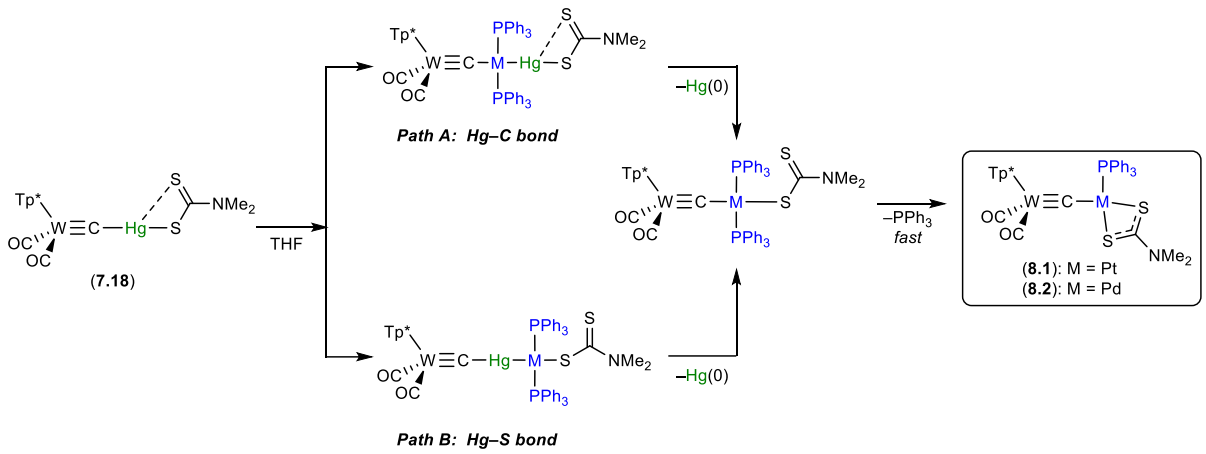

Scheme 8.2: Reactions of [WHg(S_2CNMe_2)$(CO)_2$(Tp*)] (**7.18**) with platinum(0) and palladium(0) showing alternative but convergent pathways.

Obtaining **8.1**/**8.2** *via* demercuration provides a lower yield (35%) for platinum where oxidative addition of **2.1d** is higher (*ca* 77%) and substitution with related diethyl-dithiocarbamate gives **3.4** quantitatively. A similar result is expected for palladium (*ca* 34% of isolated **8.2**); however the substitution was not tested. No other species were identified during purification of the platinum reaction to account for the lost mass. An ultra-marine species eluted from flash chromatography of palladium, devoid of Tp*, which was accordingly neither identified nor pursued. While **8.1** appears indefinitely stable, the palladium analogue **8.2** slowly decomposes to [W(≡CH)$(CO)_2$(Tp*)][64] upon exposure to moisture ($t_{½}$ ~ 8 hours). Clearly, oxidative addition of **7.18** is not the optimal route to **8.1**/**8.2**, but it serves a proof of concept that metallacarbynes can be constructed by 'stealth', employing mercury as an effective carrier.

Spectroscopic and structural data for **8.1** are almost identical to those for **3.4**, however **8.2** is only the second bimetallic palladium metallacarbyne to be isolated, allowing some comparison between palladium and platinum congeners. The $^{31}P\{^{1}H\}$ NMR spectrum of **8.2** comprises a sharp singlet with ^{183}W coupling ($^{3}J_{PW}$ = 22 Hz, Figure 8.1). The $^{13}C\{^{1}H\}$ NMR spectrum exhibits a μ_2-carbido signal (δ_C = 350.0) shifted to higher frequency of the platinum analogue (δ_C = 336.9), consistent with previous observations for dppe complexes **3.3a** and **6.3**. Crystallographic analysis of **8.2** indicates triple (W1–C1 1.830(4) Å) and single (C1–Pt1 1.966(4) Å) bonds confirming the metallacarbyne description, being once again bent (W–C–M: 168.7(2)°) due to interdigitation phenyl and pyrazolyl rings (Figure 8.2). The *trans*-influence of the

********** The natural abundance of ^{199}Hg (I = ½) is 16.9% and $^{2}J_{PHg}$ satellites would have been expected to be evident.

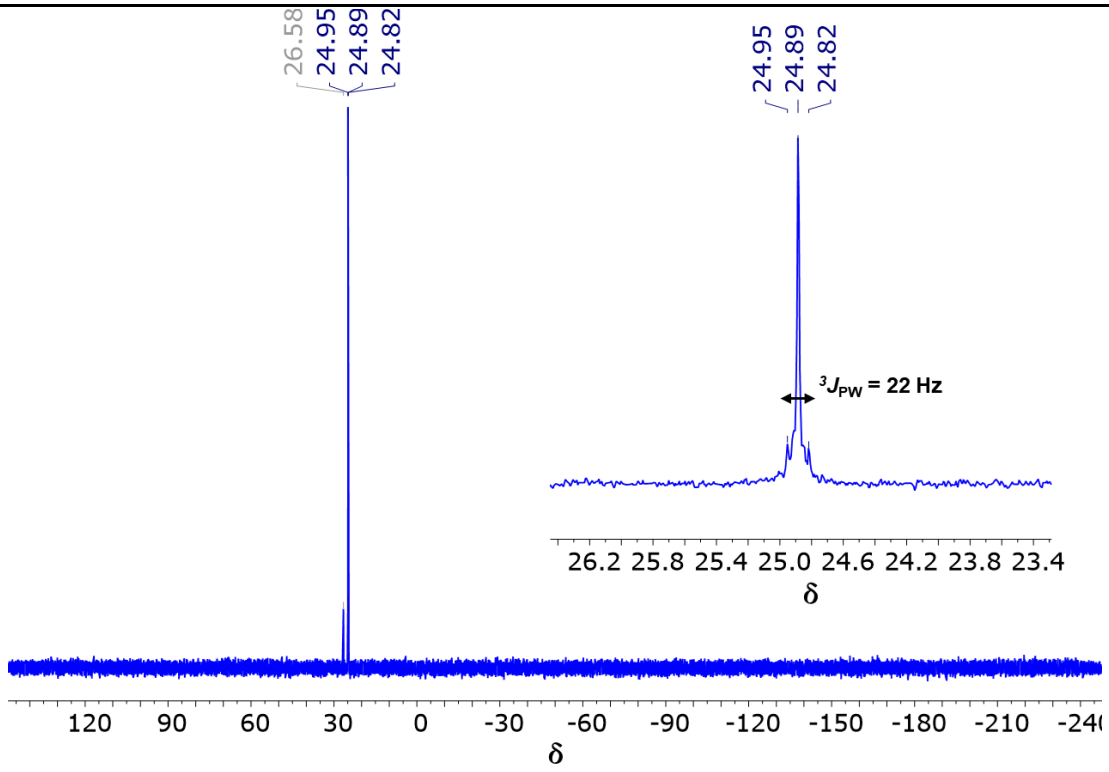

Figure 8.1: $^{31}P\{^1H\}$ NMR spectrum of [WPd(μ$_2$-C)(S$_2$CNMe$_2$)(CO)$_2$(Tp*)] (**8.2**) exhibiting coupling of ^{31}P resonance to ^{183}W.

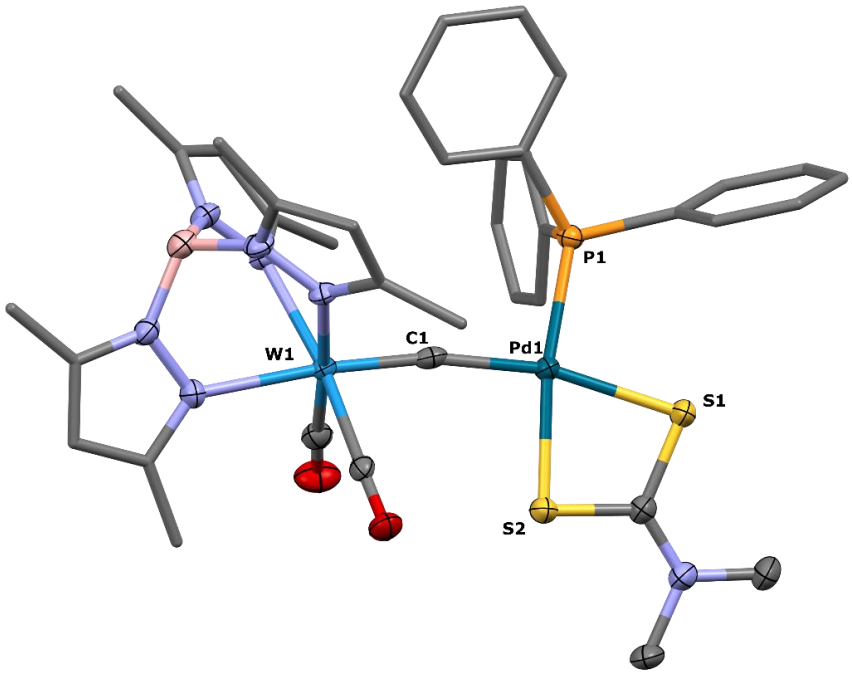

Figure 8.2: Molecular structure of [WPd(μ$_2$-C)(S$_2$CNMe$_2$)(PPh$_3$)] (**8.2**) in a single crystal of **8.2**·OC$_4$H$_{10}$ as determined by X-Ray Diffractometry. Ellipsoids are drawn at the 50% probability surface with phenyl and pyrazolyl rings simplified and OC$_4$H$_{10}$ solvent and hydrogens omitted for clarity. Selected bond lengths (Å) and angles (°): W1–C1 1.830(4), C1–Pd1 1.966(4), Pd1–S1 2.393(1), Pd1–S2 2.3525(8), Pd1–P1 2.2954(8), W1–C1–Pd1 168.7(2), S1–Pd1–S2 74.96(3), P1–Pd1–C1 97.6(1).

μ_2–carbido is manifested in the *trans* Pd–S bond elongation (2.393(1) *vs* 2.3525(8) Å). Otherwise, features of **8.1**/**8.2** conform to recurrent patterns encountered in previous Chapters.

8.3 Iridium and Rhodium

Metallacarbynes of group 9 elements are limited to a single example $[Mo_2Ir_2(\mu\text{-}C)_2(\mu\text{-}Se_2)(CO)_4(PPh_3)_2(Tp^*)_2]$ [62] and it is notable that this carbido also effectively arose *via* a stealth approach, albeit unintentionally. In this case the carbido arrives at iridium in the form of an isoselenocarbonyl linkage Mo–C–Se–Ir which extrudes selenium to form a diiridadiselenatetrahedrane ($Ir_2(\mu\text{-}Se_2)$ core. Many unsuccessful attempts to prepare group 9 metallacarbynes *via* other methods and salient observations are first noted for context. Firstly, no reaction occurs between the bromocarbyne and $[MCl(CO)(PPh_3)_2]$ (M = Rh, Ir) in C_6D_6 or d_8-toluene over seven days, even when heated at reflux. Secondly, treating $[MCl(CO)(PPh_3)_2]$ (M = Rh, Ir) with lithiocarbyne results in deep red solutions anticipated to contain $[WM(\mu_2\text{-}C)Cl(CO)_3(PPh_3)_2(Tp^*)]$, however, thermal decomposition ensues above –40 °C, precluding spectroscopic observation, although $[W(\equiv CH)(CO)_2(Tp^*)]$ eluted during chromatography suggesting hydrolysis. Finally, addition of stannylcarbyne $[W(\equiv CSn^nBu_3)(CO)_2(Tp^*)]$ to iridium(III) mercurial $[IrCl_2(HgCl)(CO)(PPh_3)_2]$ [622] resulted in formation of $[IrCl(CO)(PPh_3)_2]$ and $[W_2Hg(\mu_2\text{-}C)(CO)_4(Tp^*)_2]$ (**7.11b**) suggesting transmetallation is followed by reductive elimination of $[W(\equiv CHgCl)(CO)_2(Tp^*)]$ and subsequent symmetrisation (see Chapter Seven). The failures of each of these seemingly plausible strategies set the stage for an alternative approach based on the mercurial **7.18**.

Beginning with Vaska's complex ($[IrCl(CO)(PPh_3)_2]$)—the seminal platform for the development of oxidative addition processes[623]—the reaction with **7.18** provides an orange solution that persists for at least 6 hours but gradually proceeds to yellow upon heating accompanied by mercury deposition (Scheme 8.3). The observed colours are reminiscent of those observed above for platinum and palladium substrates. The final product isolated was identified as $[WIr(\mu_2\text{-}C)Cl(S_2CNMe_2)(CO)_3(PPh_3)(Tp^*)]$ (**8.3**) as the second iridium metallacarbyne. A similar reaction of **7.20** with the $[RhCl(CO)(PPh_3)_2]$ provided the analogous complex $[WRh(\mu_2\text{-}C)Cl(S_2CNMe_2)(CO)_3(PPh_3)(Tp^*)]$ (**8.4**) *via* a blood-red species instead of orange. In contrast to the rather modest yields obtained for **8.1** and **8.2** *via* this approach, the yields for the group 9 examples were comparatively higher (75 % for **8.3**; 46% for **8.4**). The isolation of **8.4** establishes rhodium as the first element with isolated and fully characterised examples of each of the four μ_2-carbido classes.

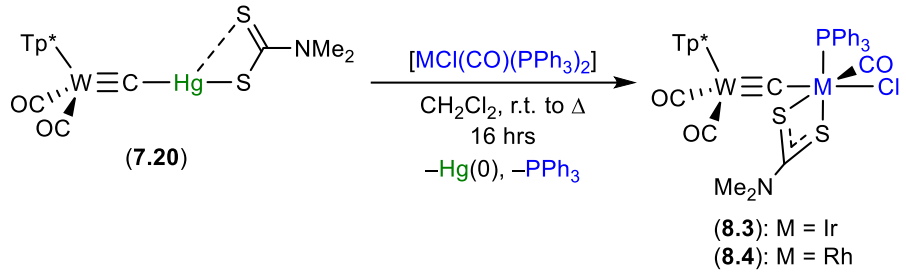

Scheme 8.3: Synthesis of iridium(III) and rhodium(III) metallacarbynes from [WHg(μ2-C)(S2CNMe2)(CO)2(Tp*)] (**7.18**).

Both **8.3** and **8.4** are stable in solution, facilitating their purification, and both contain M–Cl bonds that represent prospects for further functionalisation. The $^{31}P\{^1H\}$ NMR spectrum of iridium **8.3** exhibits a low frequency resonance (δ_P = –12.47 *cf.* δ_P = 0.70 for Vaska's complex) devoid of ^{183}W coupling suggestive of a *cis*-relationship to the carbido. Both the ^1H and $^{13}C\{^1H\}$ NMR spectra are more complicated indicating C_1 molecular symmetry due to iridium bearing five distinct ligands with one being bidentate. The $^{13}C\{^1H\}$ NMR spectrum contains a μ2-carbido signal which appears as a doublet (δ_C = 300.5; $^2J_{CP}$ = 4 Hz) to lower frequency than those of the platinum(II) complexes and with a comparatively large coupling to ^{183}W ($^1J_{CW}$ = 184 Hz). The diastereotopic CO resonances occur with unremarkable chemical shifts and couplings, but have somewhat low energy modes in the infra-red spectrum (ν_{CO} = 1943, 1851 cm^{-1}) consistent with a more π-basic tungsten despite the M(III) terminus.

The iridium stereochemistry deduced from spectroscopic data was crystallographically confirmed for a racemic crystal in the centrosymmetric $P\bar{1}$ (No. 2) space group. Structural analysis of **8.3** confirms the octahedral geometry and bond lengths consistent with the canonical metallacarbyne form (W1–C1 1.833(6); C1–Ir1 2.005(6) Å, Figure 8.3). Despite iridium having a marginally smaller covalent radius (1.22 Å) than platinum (1.23 Å), the Ir–C bond length is longer than most C–Pt bonds found in this Thesis (Chapter Three) due to the increased coordination number for d^6-iridium *cf.* four-coordinate platinum(II), but is shorter than the iridium comparators [IrH(C≡CPh)2(CO)(PPh3)2] (2.04(2) Å) [624] or [W2IrH(μ-CC≡CC≡C)2(CO)6(PPh3)2(Tp*)2] (2.053(11) Å). [140] Furthermore, it is comparable to the Ir=C bond (2.018(3) A) in [Ir{SC3H(Ph-3)(CH=CHPh-5)}HI(PPh3)2], [625] but shorter than Ir≡C (1.734(6) A) in [Ir(≡CPh)(PMe3)(η5-C5Me4Et)]+. [626] This suggests that π-retrodonation is operative for iridium, though the chelation of the dithiocarbamate (bite angle = 72.87(6)°) will perhaps allow the carbido to more closely approach the iridium centre. Conversely, the bond is longer than [MoIr(μ2-C)(CO)3(PPh3)(Tp*)]2(μ3-Se)2 (C–Ir 1.977(5) Å), [62] which is, however, built around a more compact Ir2Se2 core. The octahedral environment is likely the geometry adopted in solution with the *trans* π-donor chloride consistent with a higher frequency carbido shift (δ_C). Many recurrent features are evident: an elongated Ir–Cl bond *trans* to the carbido (2.490(2) *cf.* 2.435(2) in alkynyl [IrClI(C≡CC≡CC6H4NO2-4)(CO)(PPh3)2]), [627] a preference

for the *syn* conformation, and a phosphine nestling within the Tp* cleft producing a bent carbido linkage (W–C–Ir = 164.5(3)°).

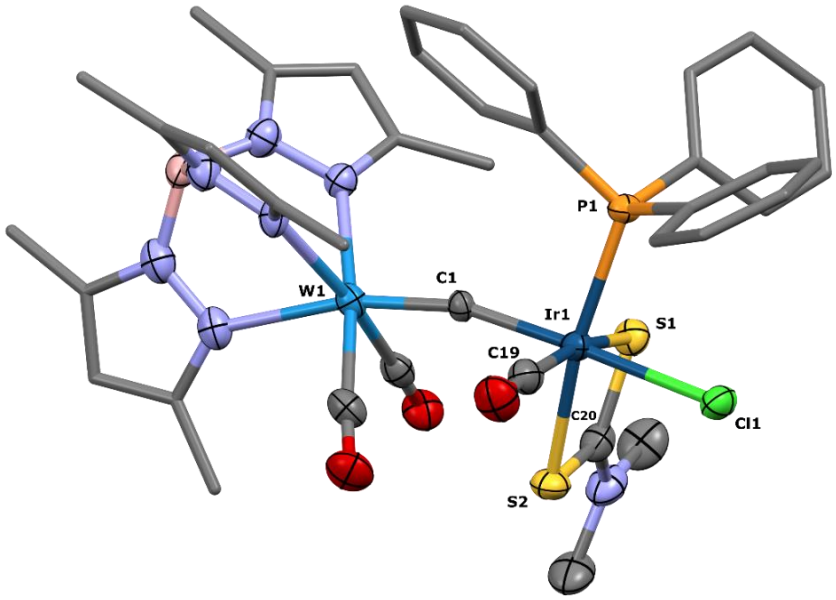

Figure 8.3: Molecular structure (one enatiomer) of [WIr(μ$_2$-C)Cl(S$_2$CNMe$_2$)(CO)$_3$(PPh$_3$)(Tp*)] (**8.3**) in a single crystal of **8.3**·2(CHCl$_3$) as determined by X-Ray Diffractometry. Ellipsoids are drawn at the 50% probability surface with phenyl and pyrazolyl rings simplified and CHCl$_3$ solvent and hydrogens omitted for clarity. Selected bond lengths (Å) and angles (°): W1–C1 1.833(6), 2.005(6), Ir1–Cl1 2.490(2), Ir1–P1 2.349(1), Ir1–S1 2.400(1), Ir1–S2 2.409(1), Ir1–C19 1.911(7), W1–C1–Ir1 164.5(3), S1–Ir1–S2 72.87(6), P1–Ir1–C1 95.8(2).

As the first rhodium metallacarbyne complex, **8.4** offers a wealth of parameters to compare all four μ$_2$-carbido complex classes. The spin-active rhodium-103 nucleus (I = ½, 100% natural abundance) provides coupling information at the cost of increasing the difficulty in direct detection of carbido resonances. It is possible to measure ^{103}Rh NMR spectra but this technique is plagued by several issues including: a broad spectral range (~12500 ppm), low sensitivity, narrow linewidths, and long relaxation times.[628-630] This is compounded by the low frequency require to detect ^{103}Rh (Ξ = 3.16 MHz), which is not accessible by many contemporary probes. Hence the ^{103}Rh resonance was not pursued for **8.4**. Coupling to ^{103}Rh gives rise to a doublet in the ^{31}P{^{1}H} NMR spectrum (δ_P = 20.20; $^1J_{PRh}$ = 112 Hz) with a coupling more similar to the rhodium(I) tricarbido complex [WRh(μ$_2$-CC≡C)(CO)$_3$(PPh$_3$)$_2$(Tp*)] ($^1J_{PRh}$ = 109 Hz) than the octahedral tricarbido [WRh(μ$_2$-CC≡C)I$_2$(CO)$_3$(PPh$_3$)$_2$(Tp*)] ($^1J_{PRh}$ = 82 Hz).[631] In comparison to other rhodium carbido complexes, the coupling is significantly less than the other rhodium(III) example [Rh$_2$(μ$_2$-C)(μ-C$_6$H$_4$PPh$_2$)H(Tp*)$_2$] (226 Hz) or rhodium(I) examples between the dimetalla-cumulene and -carbenes (Table 8.1). While rhodium-phosphine couplings are often insightful, this is not the case for **8.4**, the value for which falls between those expected for d^8 square-planar rhodium(I) and d^6 octahedral rhodium(III) species, potentially moderated by the influence of a *trans*-sulfur donor.

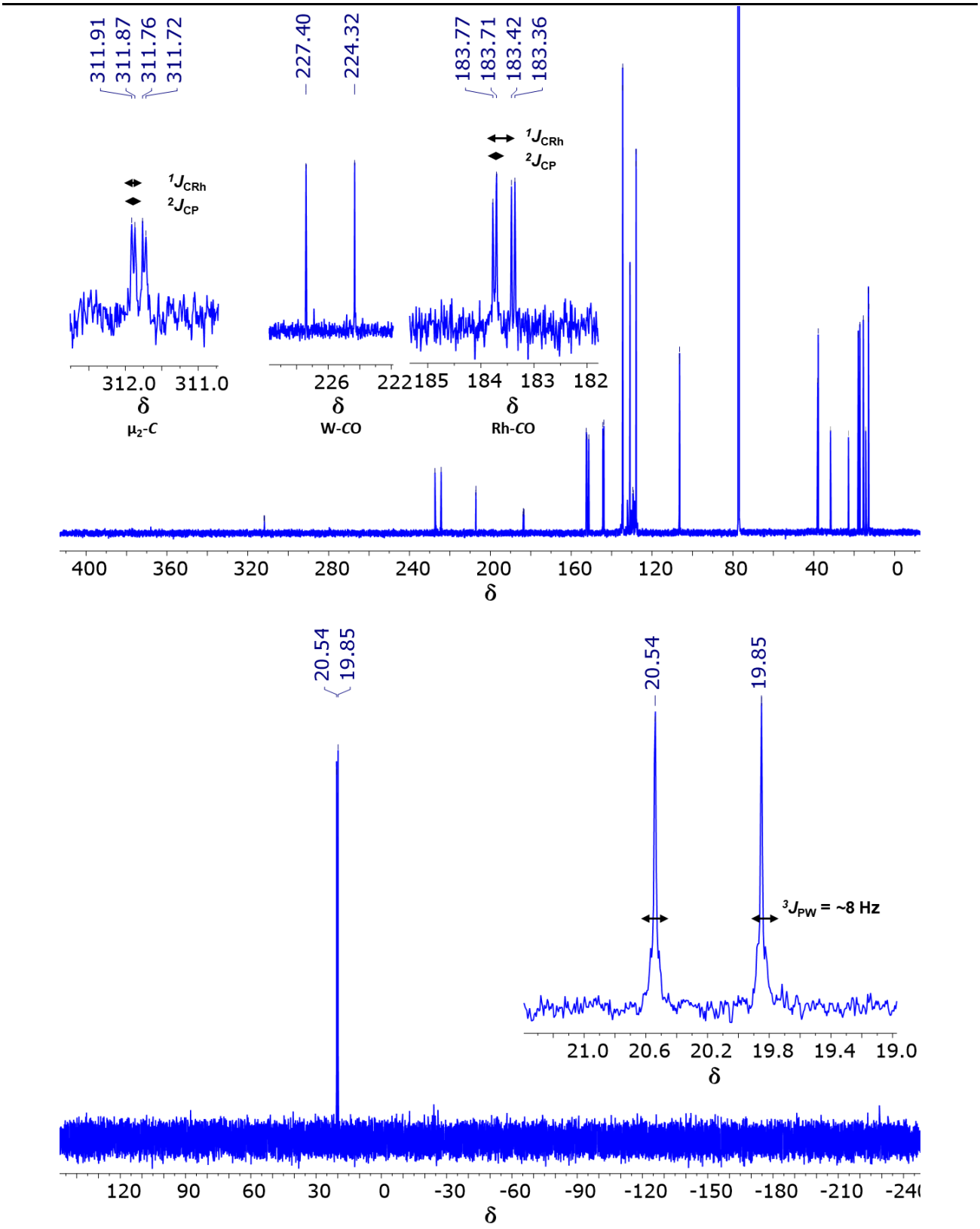

Figure 8.4: $^{13}C\{^1H\}$ and $^{31}P\{^1H\}$ spectra for [WRh(μ2-C)Cl(S2CNMe2)(CO)3(PPh3)(Tp*)] (**8.4**).

Table 8.1: Spectroscopic data of representative group 9 metallacarbynes and their related species.

Complex	δ_{C1}[a] (ppm)	δ_P[a] (ppm)	$^1J_{PRh}$ (Hz)	ν_{M-CO}[b] (cm^{-1})
$[RhCl(CO)(PPh_3)_2]$ [632]	–	30.0	127	
$[Rh_2(\mu_2\text{-}C)(SBpin)_2(PEt_3)_4]$ [154]	439.4 [c]	11.9 [d]	165 , 8	–
$[Rh_2(\mu_2\text{-}C)Cl_2(PPh_3)_4]$ [156]	424.4	21.61	180	–
$[Rh_2(\mu_2\text{-}C)Cl_2(\mu\text{-}dppm)_2]$ [78]	411.7	19.12	191, 150	–
$[Rh_2(\mu_2\text{-}C)Cl_4(\mu\text{-}dppf)_2]$ [161, 289]	418.6	18.90	191	–
$[Rh_2(\mu_2\text{-}C)(\mu\text{-}C_6H_4PPh_2)H(Tp^*)_2]$ [156]	447.2	60.70	226	–
$[\mathbf{W}Rh(\mu_2\text{-}C)Cl(S_2CNMe_2)(CO)(PPh_3)]$ (**8.4**)	311.8	20.20	112	2085
$[Ru\{\equiv C:\rightarrow RhCl(COD)\}Cl_2(PCy_3)_2]$ [69]	411.7	34.63	–	–
$[Ru\{\equiv C:\rightarrow RhCl(CO)\}Cl_2(PCy_3)_2]_2$ [69]	397.6	35.52	–	2022
$[Rh_2(\mu_2\text{-}C:)(\mu\text{-}DMAD)(\mu\text{-}dppm)]$ [40]	563.0	12.5	137	–
$[Rh_2(\mu_2\text{-}C:)\{\mu\text{-}C_2(CF_3)_2\}(\mu\text{-}dppm)_2]$ [289]	–	–0.22, 0.85, 9.27	120, 104, 136	–
$[Rh_2(\mu_2\text{-}C:)\{\mu\text{-}ETFB\}(\mu\text{-}dppm)_2]$ [289]	–	10.96, 11.54	n.r.	–
$[Rh(S_2CNEt_2)(CO)\{P(p\text{-}tol)_3\}_2]$ [633]	–	n.r.	n.r.	1960
$[\mathbf{W}Ir(\mu_2\text{-}C)Cl(S_2CNMe_2)(CO)(PPh_3)]$ (**8.3**)	300.5	–12.47	–	2057
$[\mathbf{Mo}Ir(\mu_2\text{-}C)Cl(CO)(PPh_3)]_2(\mu_2\text{-}\perp Se_2)$ [62]	286.1 [d]	28.0 [d]	–	1989 [e]
$[Ru\{\equiv C:\rightarrow IrCl(COD)\}Cl_2(PCy_3)_2]$ [69]	387.7	34.25	–	–
$[IrCl(CO)\{:C\equiv RuCl_2(PCy_3)_2\}_2]$ [69]	397.4	36.21	–	
$[Ir(S_2CNEt_2)(CO)(PPh_3)]$ [634]	–	21.61	–	1958
$[IrMeI(S_2CNEt_2)(CO)(PPh_3)]$ [634]	–	–1.17	–	2025
$[Ir(\equiv CPh)(PMe_3)(\eta^5\text{-}C_5Me_4Et)]^+$ [626]	296.9	–49.7	–	–
$[Rh(=C=C=CPh_2)(P^iPr_3)(\eta^5\text{-}C_5H_5)]$ [635]	228.6	68.5	201	

Notes: [**W**] = $W(CO)_2(Tp^*)$. [**Mo**] = $Mo(CO)_2(Tp^*)$. [a]Measured in $CDCl_3$ unless specified otherwise. [b]Measured in CH_2Cl_2 unless specified otherwise. [c] Measured in d_{12}-cyclohexane. [d]Measured in C_6D_6. [e]Measured in THF. n.r. = not resolved or recorded

Table 8.2: Structural parameters of representative rhodium-containing carbido complexes.

Compound	Rh–C (Å)	C–M (Å)	Rh–C–M (°)	Carbido Class
$[Rh_2(\mu_2\text{-}C)(SBpin)_2(PEt_3)_4]$ [154]	1.790(7)	1.776(7)	176.1(4)	A
$[Rh_2(\mu_2\text{-}C)Cl_2(PPh_3)_4]$ [156]	1.780(2)	1.773(2)	173.4(2)	A
$[Rh_2(\mu_2\text{-}C)(PPh_3)_2(Bp)_2]$ [13]	1.7680(12) 1.7644(11)	1.7652(12) 1.7596(10)	169.1(7) 168.8(6)	A
$[Rh_2(\mu_2\text{-}C)(PPh_3)_2(Tp)_2]$ [13]	1.7761(7)	1.7761(7)	163.8(3)	A
$[Rh_2(\mu_2\text{-}C)(\mu_2\text{-}C_6H_4PPh_2)H(Tp^*)_2]$ [156]	1.817(6)	1.741(6)	165.92(3)	A
$[Rh_2(\mu_2\text{-}C)Cl_2(\mu\text{-}dppm)_2]$ [78]	1.76(1)	1.73(1)	162.6(7)	A
$[Rh_2(\mu_2\text{-}C)(NCMe)_2(\mu\text{-}dppm)_2]^{2+}$ [78]	1.744(3)	1.744(3)	180.0	A
$[Rh_2(\mu_2\text{-}C)Cl_4(\mu\text{-}dppf)_2]$ [161]	1.7947(3)	1.7945(3)	180.0(2)	A
$[\mathbf{W}Rh(\mu_2\text{-}C)Cl(S_2CNMe_2)(PPh_3)(CO)]$	1.978(3)	1.841(3)	166.0(2)	B
$[Ru\{\equiv C:\rightarrow RhCl(COD)\}Cl_2(PCy_3)_2]$ [69]	1.897(2)	1.690(2)	173.41(3)	C
$[Ru\{\equiv C:\rightarrow RhCl(CO)\}Cl_2(PCy_3)_2]_2$ [69]	1.864(3)	1.688(3)	176.87(1)	C
$[Rh_2(\mu_2\text{-}C:)(\mu\text{-}DMAD)(\mu\text{-}dppm)_2]$ [40]	1.851(19)	1.860(16)	124.2(9)	D
$[Rh_2(\mu_2\text{-}C:)\{\mu\text{-}C_2(CF_3)_2\}(\mu\text{-}dppm)_2]$ [289]	1.830(7)	1.830(6)	127.4(4)	D
$[Rh_2(\mu_2\text{-}C:)\{\mu\text{-}ETFB\}(\mu\text{-}dppm)_2]$ [289]	1.818(8)	1.834(8)	128.2(4)	D

Notes: [**W**] = $W(CO)_2(Tp^*)$. DMAD = dimethyl acetylenedicarboxylate. ETFB = ethyl trifluoromethylbutynoate.

The $^{13}C\{^{1}H\}$ NMR spectrum of **8.4** exhibits a heavily coupled resonance consistent with a μ_2-carbido (δ_C = 311.8) that remains at lower frequency than the iridium analogue hinting the resonances for 4d metals occur to lower frequency of those for their 5d counterparts for groups 9 and 10 (Figure 8.4). The carbido resonance reveals a weaker coupling to ^{103}Rh ($^{1}J_{CRh}$ = 27 Hz) than the carbonyl (*ca* 61 Hz). An infra-red spectrum clearly identifies a rhodium(III) centre as a high wavenumber vibration is observed (ν_{CO}: 2085 cm^{-1}), reflecting further reduced retrodonation than iridium(III) (ν_{CO}: 2053 cm^{-1}). A peculiarity arises in the ^{1}H NMR spectrum of **8.4** such that the pzCH resonances retain a 2:1 ratio consistent with C_s symmetry, however that cannot be the case for the octahedral arrangement, hence the cause is unclear and most likely coincident isochromous chemical shifts. The corresponding carbon signals are inequivalent, but have typically narrower ^{13}C NMR line-widths and associated resolution.

An X-ray diffraction study of **8.4** revealed a molecular structure like that of iridium **8.3** such that the identical stereochemistries facilitate comparison of parameters between species. The rhodium metallacarbyne core is the most obvious unit for comparison between carbido classes, however, six-coordinate rhodium(III) is the least common oxidation state encountered to date (Figure 8.5 and Table 8.2), and therefore caution should be exercised given the variation of covalent radii with coordination number. Consistent with the single bond order implied by the Class B description, the Rh–C bond in **8.4** is the longest Rh–C bond (1.978(3) Å) found for μ_2-carbidos by a substantial margin (*ca* 0.1 Å), highlighting the lack of significant π-bonding relative to other species, for which multiple bonding is invoked. This is even longer than rhodium(III) complex $[Rh_2(\mu_2\text{-}C)(\mu_2\text{-}C_6H_4PPh_2)H(Tp^*)_2]$ (1.817(6) Å) [156] or proposed metallacarbyne contribution in the dimetallacumulene $[Rh_2(\mu_2\text{-}C)Cl_4(\mu\text{-}dppf)_2]$ (1.7947(3) Å). [161] The Rh–C bond of **8.4** is also relatively short considering a Rh=C bond such as $[Rh(=C=C=CPh_2)(P^iPr_3)(Cp)]$ (1.880(6) Å), [635] but considerably longer than a Rh≡C bond (1.702(6) A) in $[Rh(\equiv CF)(PNP)][CHB_{11}Cl_{11}]$ (PNP = diarylamido/bis(phosphino) ligand), [167] noting the caveats to this comparison such as oxidation state and coordination number.

Complex **8.4** also has a bent linkage to accommodate the juxtaposition of Tp^*/PPh_3 ligands (166.0(2)°), but is comparable to other rhodium μ_2-carbidos that also distort based on the steric profile of co-ligands or in response to solid-state packing effects (*e.g.*, μ-dppm; 162.7(6)°), [78] although far from matching the superlative bent Class D dimetallacarbenes (124.2(9)°). [40] The W≡C bond is longer than most examples listed, which seems counter-intuitive given the typically synchronous contraction and elongation along the carbido spine. This elongation serves to highlight the differences in bonding of the second metal besides rhodium like the contracted Ru≡C bond for polar covalents. [69]

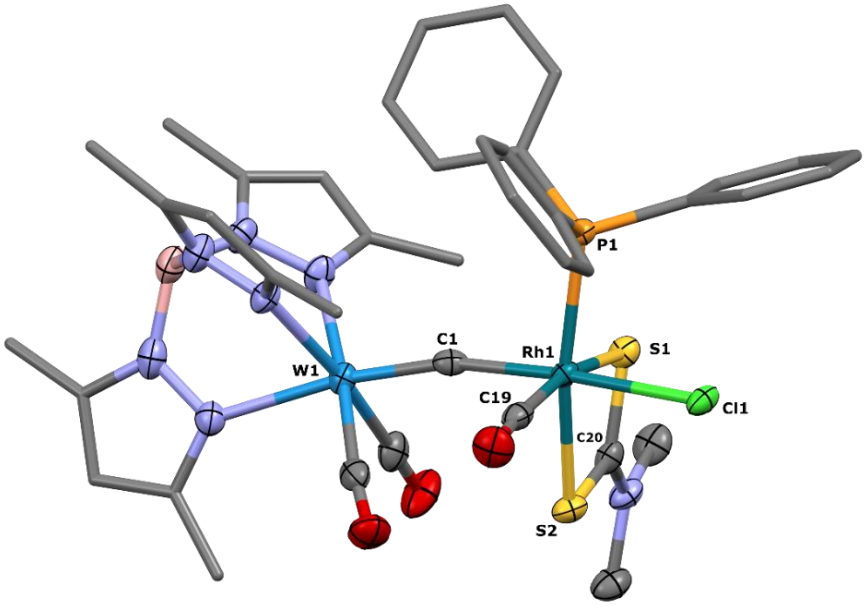

Figure 8.5: Molecular structure (one enatiomer) of [WRh(μ$_2$-C)Cl(S$_2$CNMe$_2$)(CO)$_3$(PPh$_3$)(Tp*)] (**8.4**) in a single crystal as determined by X-Ray Diffractometry. Ellipsoids are drawn at the 50% probability surface with phenyl and pyrazolyl rings simplified and hydrogens omitted for clarity. Selected bond lengths (Å) and angles (°): W1–C1 1.841(3), Rh1–C1 1.978(3), Rh1–Cl1 2.4949(6), Rh1–P1 2.3655(9), Rh1–C19 1.911(4), Rh1–S1 2.3605(9), Rh1–S2 2.3896(9), W1–C1–Rh1 166.0(2), P1–Rh1–C1 96.89(9), S1–Rh1–S2 73.99(3).

Comparing spectroscopic data for rhodium carbido complexes reveals that **8.4** gives rise to the lowest frequency carbido resonance within the collection. This likely indicates reduced paramagnetic contribution compared with other classes, since simple inductive arguments might suggest that the electronegative rhodium(III) centre would contribute to a down-field shift, albeit moderated by the π-basicity of the dithiocarbamato ligand. The phosphine resonances arising in the $^{31}P\{^1H\}$ NMR spectra vary between the classes as expected, and **8.4** contains the smallest rhodium-phosphorus coupling ($^1J_{PRh}$) consistent with it having the most highly coordinated rhodium centre with an attendant reduction in the *s*-character of metal-ligand bonding.[††††††††††††††††††††††††††] Finally, given the plethora of d^8-rhodium(I)/iridium(I) complexes that can undergo oxidative addition, an expansion of group 9 metallacarbynes akin to that of Chapter Three would seem feasible, with the caveat that while oxidative chlorination of [Rh$_2$(μ-C)Cl$_2$(dppf)$_2$] with PhICl$_2$ affords d^7,d^7-[Rh$_2$(μ-C)Cl$_4$(dppf)$_2$],[19] similar treatment of [Rh$_2$(μ-C)Cl$_2$(dppm)$_2$] results in halogenation of the carbide bridge to provide a chlorocarbyne complex [Rh$_2$(μ-CCl)(μ-Cl)Cl$_4$(dppm)$_2$].[14]

[††††††††††††††††††††††††††] To a first approximation, the amount of *s*-character will reflect the hybridisation of the metal in square-planar (sp^2d, 25%), trigonal bipyramidal (sp^3d, 20%) or octahedral (sp^3d^2, 17%) geometries.

8.4 Ruthenium and Osmium

Traversing the transition series arrives next at group 8 metals, perhaps the most variable in appearances through μ_2-carbido chemistry and the birthplace of the archetypal examples of carbidos from each of Classes A-C, *viz.* $[Fe_2(\mu\text{-}C)(TPP)_2]$,[20] $[WRu(\mu\text{-}C)(CO)_2(O^tBu)_3(\eta^5\text{-}C_5H_5)]$[33] and the many adducts of $[Ru(C)Cl_2(PCy_3)_2]$.[39] Although not isolable, this list of initial examples includes Class D carbido $[Ru_2(\mu\text{-}C)(\mu\text{-}N^tBu)(\eta^5\text{-}C_5Me_5)_2]$.[129] In contrast to the key roles played by iron and ruthenium in carbide chemistry, there is no example of a μ_2-carbido complex of osmium for any class.

Low valent ruthenium would be required to mimic the $d^8 \rightarrow d^6$ oxidative addition processes observed for Group 9 or $d^{10} \rightarrow d^8$ for Group 10 metals, a principle pioneered by Collman and Roper with zerovalent $[Ru(CO)_3(PPh_3)_2]$.[636] The tricarbonyl complex is, however, somewhat substitution-inert, leading Roper to subsequently develop the highly reactive *tris*(phosphine) complex $[Ru(CO)_2(PPh_3)_3]$, which is considered to serve as a precursor to coordinatively unsaturated '$Ru(CO)_2(PPh_3)_2$' in solution under mild conditions.‡‡‡‡‡‡‡‡‡‡‡‡‡‡‡‡‡‡‡‡‡‡‡‡ Previously, the reaction of this complex with MeHgI has been shown to proceed *via* oxidative addition and mercury extrusion to afford the methyl complex $[RuMeI(CO)_2(PPh_3)_2]$ which is in equilibrium with an acyl tautomer $[Ru(\eta^2\text{-}OCMe)I(CO)(PPh_3)_2]$.[639] Initial NMR-scale test reactions quickly established that oxidative addition of **7.18** with ruthenium(0) proceeded less cleanly than previous group 9 and 10 systems (Scheme 8.4). Spectroscopic experiments determined CD_2Cl_2 (CH_2Cl_2 on a preparative scale) provided the smoothest reaction with by-products minimised, whereas reactions using benzene or THF as solvents provided mixtures of at least 10 distinct phosphorus containing compounds. Mixing $[Ru(CO)_2(PPh_3)_3]$ with **7.18** in CH_2Cl_2 gives a yellow solution the colour of which remains unchanged when heated at reflux, with deposition of elemental mercury. From this reaction mixture the anticipated complex $[WRu(\mu_2\text{-}C)(S_2CNMe_2)(CO)_4(Tp^*)]$ (**8.5**) could be isolated after flash chromatography, albeit in a disappointing yield (11% isolated). The analogous complex $[Ru(CO)(CNMes)(PPh_3)_3]$ was also tested where the less π-acidic isocyanide ligand was anticipated to facilitate oxidative addition, but instead returned an even greater number of products, none of which predominated sufficiently to be isolated.

‡‡‡‡‡‡‡‡‡‡‡‡‡‡‡‡‡‡‡‡‡‡‡‡‡‡ It is possible to isolate complexes of the form $[Ru(CO)_2(PR_3)_2]$, however these require phosphines with considerable steric bulk such as PMe^tBu_2, which would not be expected to be compatible with the already sterically constrained Tp*W systems.[637-638]

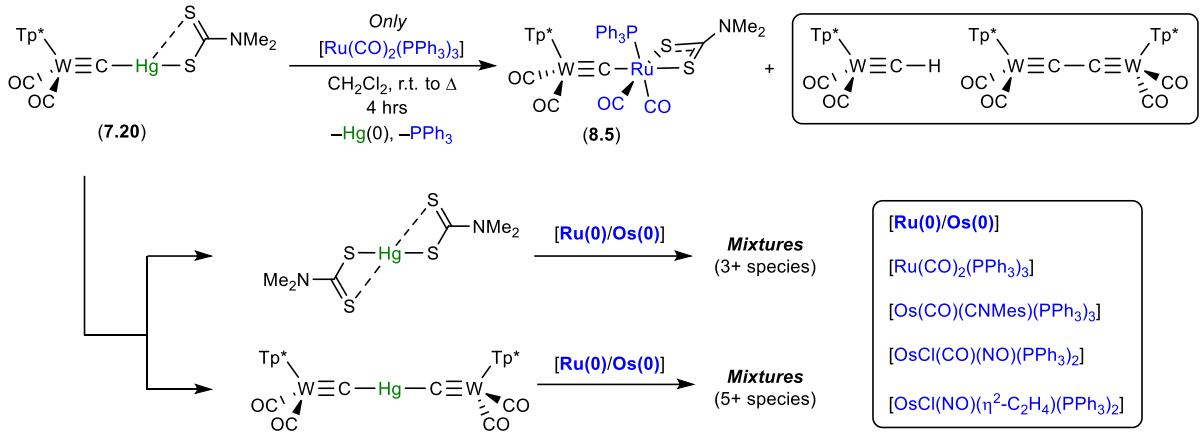

Scheme 8.4: Synthesis of ruthenium(II) metallacarbynes from [WHg(μ2-C)(S_2CNMe_2)$_2$(CO)$_2$(Tp*)] (**7.18**) and their decomposition species.

Studies were undertaken to elucidate the cause of the diminished yields of **8.5**. Unlike the reactions that produce **8.1**–**8.4**, no major compound is formed, instead producing a mixture of species that fail to converge with prolonged reaction time or heating. Thus, **8.5** exists only as a component. Furthermore, flash chromatography elutes a large amount of [W(≡CH)(CO)$_2$(Tp*)] initially absent from the ^{1}H NMR spectrum, suggesting hydrolysis occurs on the stationary phase {silica gel or alumina} indicative of weak Ru–C bonds. Another species was isolated with spectroscopic data consistent with *cis*-[Ru(S_2CNMe_2)$_2$(CO)(PPh_3)] formation.[640] This likely arises from either dithiocarbamate scavenging or symmetrisation of mercurial **7.18**, where both routes sequester ruthenium from the system and reduce yields, compounded by losses sustained during separation. Control reactions identified that **7.18** is stable when heated to reflux in either CH_2Cl_2 or benzene for several days, however, heating in the presence of PPh_3 results in a complex mixture within 30 minutes. The tungsten fragments ultimately terminate as [W$_2$(μ$_2$-≡CC≡)(CO)$_4$(Tp*)$_2$] indicating possible formation of [W$_2$Hg(μ$_2$-C)(CO)$_4$(Tp*)], later verified by ^{1}H NMR spectroscopy. Additionally, the presence of [Hg(S_2CNMe_2)$_2$] was confirmed by comparison with an authentic sample. These controls confirms that phosphine, as liberated by [Ru(CO)$_2$(PPh_3)$_3$], is sufficiently nucleophilic to symmetrise **7.18**, degrading the starting material on a competitive timescale to oxidative addition and thus limiting formation of **8.5**. Phosphines have been shown to catalyse the symmetrisation of organomercurial halides, though PPh_3 was found to be less active than alkyl-substituted phosphines.[641] Lending further support to this hypothesis, a repeat reaction of **7.18** with [Ru(CO)$_2$(PPh_3)$_3$] in THF found exclusive production of [Ru(S_2CNMe_2)$_2$(CO)(PPh_3)], implying that THF (or liberated PPh_3 in THF) is sufficiently nucleophilic to cause symmetrisation of the **7.18** and nucleophiles should be avoided when utilising **7.18**. Given that the addition of the carbido and dithiocarbamato units to a metal requires three coordination sites, and therefore loss of up to three ligands, *i.e.*, potential nucleophiles, this constitutes a limitation of the strategy.

Consistent with the group 9 examples **8.3**/**8.4**, preparation of **8.5** results in adoption of an octahedral geometry and the resulting loss of C_s symmetry is evident in the ^{1}H and $^{13}C\{^{1}H\}$ NMR spectra.§§§§§§§§§§§§§§§§§§§§§§§§§§§§§§§§ The $^{13}C\{^{1}H\}$ NMR spectrum exhibits a resonance consistent with a μ_2-carbido (δ_C = 367.9), to higher frequency than observed for the isoelectronic d^6 rhodium(III) example (δ_C = 311.8; **8.4**). The $^{13}C\{^{1}H\}$ NMR spectrum includes two ruthenium-carbonyl resonances that appear as doublets, coupling to *cis*- (δ_C = 210.2; $^{2}J_{CP}$ = 14 Hz) and *trans*-phosphines (δ_C = 197.4; $^{2}J_{CP}$ = 108 Hz) to lower frequency of resonances for the diastereotopic tungsten carbonyls (δ_C = 226.1, 226.4) and dithiocarbamato carbon (δ_C = 208.5). The symmetric and antisymmetric pairs of vibrational modes for each metal dicarbonyl unit can be identified in the infra-red spectrum, reflecting a less π-basic ruthenium(II) centre ($\nu_{CO\text{-}Ru}$ = 2058, 1929 cm^{-1}) as compared with tungsten(0) ($\nu_{CO\text{-}W}$ = 1986, 1840 cm^{-1}), though some degree of coupling between the pairs of oscillators is to be expected. This is a relatively π-acidic tungsten environment for similar carbidos.

Crystallographic analysis of single crystals of racemic **8.5** ($P\bar{1}$) confirmed a geometry with the dithiocarbamato *trans* to the carbido and one carbonyl, with the phosphine assuming the usual position between two pyrazolyl rings and *trans* to the second carbonyl (Figure 8.6). The long Ru–C bond (Ru–C: 2.029(7) Å) conforms to the metallacarbyne description and, consistent with ruthenium being the largest platinum group metal (r_{cov} = 1.46(7) Å), is significantly longer than other platinum group metals thus far (M–C: 1.93(2) Pt; 1.966(4) Pd; 2.005(6) Ir; 1.978(3) Rh Å). This is similar to the first ruthenium metallacarbyne [WRu(μ$_2$-C)(CO)$_2$(Cp)(O^{t}Bu)$_3$] (2.09(2) Å) [33] while much longer than [Ru$_2$(μ$_2$-C)HCl$_3${η^6-Mes(SIMes)}SIMes)] (1.875(5) Å), however the latter is possibly an outlier due to the geometric constraints imposed by the unusual μ:σ-η^6 NHC coordination. [158] The dithiocarbamate is strongly bound to ruthenium where very similar C–S distances indicate a symmetrical chelate. The phosphine nestles the Tp* linkage to give the *syn*-conformation and a bent W≡C–Ru (167.7(3) °) linkage though this is not as pronounced as in [Ru$_2$(μ$_2$-C)HCl$_3${η^6-Mes(SIMes)}(SIMes)] (160.3(2) °) wherein η^6-mesityl coordination needs to be accommodated.

Ruthenium(0) can perform oxidative addition of the mercury carbido complex and give metallacarbynes, but is inhibited symmetrisation of the mercurial and hydrolysis of the product upon the necessary chromatography. Previous Chapters highlight metallacarbynes bearing 5d metals are often more stable, or at least have slower kinetics, than their lighter 4d counterparts, which is unsurprising as M–C bond strength increases down the group. Therefore, reactions with osmium(0) were expected to provide more durable metallacarbynes for group 8 albeit *via* longer reaction times. An analogous

§§§§§§§§§§§§§§§§§§§§§§§§§§§§§§§§ The loss of symmetry is a useful indicator to monitor reaction progress given the simplistic $^{31}P\{^{1}H\}$ spectrum; a singlet devoid of coupling ([Ru(CO)$_2$(PPh$_3$)$_3$]: δ_P(CD$_2$Cl$_2$) = 20.34).

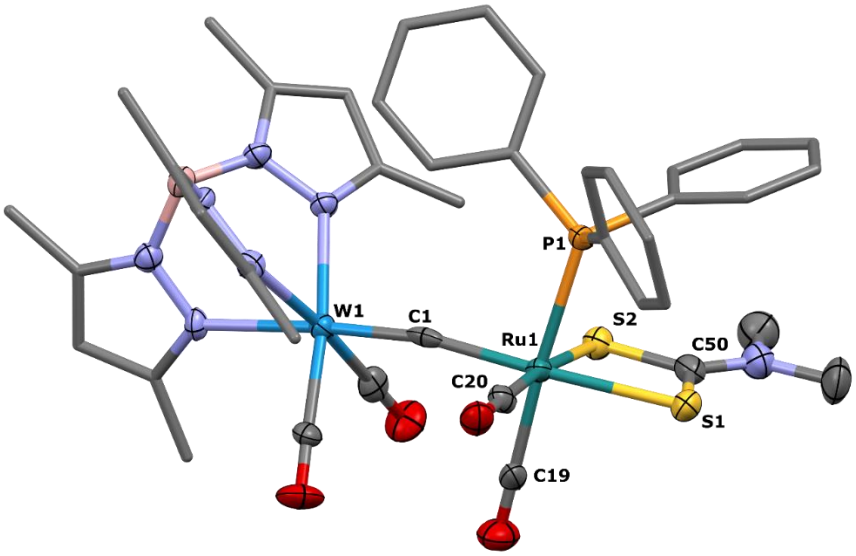

Figure 8.6: Molecular structure of [WRu(μ$_2$-C)(S$_2$CNMe$_2$)(CO)$_4$(PPh$_3$)(Tp*)] (**8.5**) in a single crystal of **8.5**·C$_6$H$_6$ as determined by X-Ray Diffractometry. Ellipsoids are drawn at the 50% probability surface with phenyl and pyrazolyl rings simplified and C$_6$H$_6$ solvent and hydrogens omitted for clarity. Selected bond lengths (Å) and angles (°): W1–C1 1.847(7), Ru1–C1 2.031(7), Ru1–S1 2.522(2), Ru1–S2 2.462(2), Ru1–P1 2.461(1), Ru1–C19 1.970(6), Ru1–C20 1.872(5), W1–C1–Ru1 167.7(3), S1–Ru1–S2 70.61(5).

reaction was conducted with [Os(CO)(CNMes)(PPh$_3$)$_3$],********** where prolonged heating in either CH_2Cl_2 or benzene return a yellow mixture with mercury deposition. No species of interest could be isolated *via* chromatography noting only [W(≡CH)(CO)$_2$(Tp*)] and signals consistent with [Os(S$_2$CNMe$_2$)$_2$(CO)(PPh$_3$)] although this was not obtained in sufficient amounts for characterisation due to the small-scale reactions (*ca* 50 mg). A nitrosyl derivative, [OsCl(NO)(CO)(PPh$_3$)$_2$], [643-644] which is known to oxidatively add $HgCl_2$, [645] was combined with **7.18** to return similar evidence of [W(≡CH)(CO)$_2$(Tp*)] [Os(S$_2$CNMe$_2$)$_2$(CO)(PPh$_3$)]. This suggested that either no metallacarbyne was forming or was unstable under the reaction conditions. Finally, combining [Os(η^2-C$_2$H$_4$)Cl(NO)(PPh$_3$)$_2$] [646] with **7.18** was anticipated to provide a cleaner reaction, as the ethene ligand is more labile than the carbonyl in the previous reagent. The osmium(0) intermediate [OsCl(NO)(PPh$_3$)$_2$] is formally isoelectronic with Vaskas' complex (OsNO = IrCO) which had proven successful in such reactions described above. Again, the reaction produced a messy $^{31}P\{^1H\}$ NMR spectrum at ambient temperature and no major species were isolated *via* chromatography.

Studies to elucidate the issues were conducted for osmium by monitoring reactions with ^1H and $^{31}P\{^1H\}$ NMR spectroscopy. The initial species [Os(CO)(CNMes)(PPh$_3$)$_3$] and [OsCl(NO)(CO)(PPh$_3$)$_2$] give reactions that are reluctant to begin unless heated at reflux (*ca* 110 °C, toluene), and upon reacting, the $^{31}P\{^1H\}$ spectra reveal multiple species in solution devoid of informative couplings. Phosphine

********** [Os(CO)(CNMes)(PPh$_3$)$_3$] is a new analogue of the known complex [Os(CO)(CN-4-tolyl)(PPh$_3$)$_3$], prepared using the same multi-step procedure. [642]

dissociation occurs below this temperature and mixture arises due to symmetrisation of mercurial **7.18.** Likewise, long acquisition $^{13}C\{^1H\}$ NMR spectra of crude mixtures from $[Os(CNMes)(CO)(PPh_3)_3]$ and $[OsCl(NO)(CO)(PPh_3)_2]$ fail to identify high frequency signals consistent with a μ_2-carbido with the exception of **7.11b** as a product of symmetrisation. However, a similar $^{13}C\{^1H\}$ NMR spectrum from $[Os(\eta^2\text{-}C_2H_4)Cl(NO)(PPh_3)_2]$ identified an addition high frequency signal (δ_C = 304.3) consistent with the desired μ_2-carbido albeit in miniscule amounts (<5% total material) and no species was isolated from subsequent chromatography. This suggests no metallacarbynes substantially formed in the first two instances given release of several phosphines and symmetrisation, evidence by large amounts of $[W_2(\equiv CC\equiv)(CO)_4(Tp^*)_2]$ noted in each experiment.†††††††††††††††††††††††††††† Meanwhile, reactions with $[Os(\eta^2\text{-}C_2H_4)Cl(NO)(PPh_3)_2]$ release less phosphine hence formation may be possible, but there is no conclusive evidence besides a lone ^{13}C NMR resonance of such low intensity making pursuit impractical. Given the reluctance of osmium to provide a metallacarbyne or the instability of such carbidos under the thermally forcing conditions required for their formation, an alternative route would have to be designed. The shortfall at osmium should not cast doubt on the generalisability of the oxidative addition method, as the reaction clearly occurs, but more careful ligand design away from dithiocarbamate or other *pseudo*-halides so as to obviate symmetrisation pathways.

Chapter Eight Part Two:

Hydride Metathesis with a *Bis*-carbido Mercurial

Symmetrisation of **7.18** to $[W_2Hg(\mu_2\text{-}C)_2(CO)_4(Tp^*)_2]$ (**7.11b**) was repeatably encountered, complicating successful synthesis. It should be noted that **7.11b** is not necessarily a dead end in that the corresponding molybdenum analogue is readily and catalytically demercurated by $[RhCl(CO)(PPh_3)_2]$ in a reaction sequence that must involve it serving as a carbido transfer agent. [118] Embracing the energetic well that is **7.11b** would be an elegant solution as that would inherently eliminate symmetrisation as an issue. Alternative methods to utilise **7.11b** for carbido delivery to osmium were therefore explored, leading to a new method of metallacarbyne synthesis.

8.5 Preparation of the First Osmium μ_2-carbido Complex

The coordinatively unsaturated σ-aryl complexes $[M(C_6H_4R\text{-}4)Cl(CO)(PPh_3)_2]$ (M = Ru, Os; R = H, Me) are formed *via* hydride metathesis of $[MHCl(CO)(PPh_3)_3]$ (M= Ru, Os) with $[Hg(C_6H_4R\text{-}4)_2]$ with elimination of elemental mercury and arene as byproducts (Scheme 8.5). [648] A similar process is implicit in the reactions of these hydrido complexes with *bis*(alkynyl)mercurials $[Hg(C\equiv CR)_2]$ to afford putative

†††††††††††††††††††††††††††† It should be noted that while *bis*(alkynyl)mercurials $Hg(C\equiv CR)_2$ react with $[M(CO)_2(PPh_3)_3]$ to afford *bis*(alkynyl) complexes, the mercury centre of $Hg\{C\equiv W(CO)_2(Tp^*)\}_2$ is likely to be difficult to access given the steric congestion of two Tp* ligands. [647]

alkynyl complexes [M(C≡CR)Cl(CO)$(PPh_3)_n$] (n = 2,3) however these then react with the equivalent of alkyne to provide ene-yn-yl complexes [M{C(CCR)=CHR}Cl(CO)$(PPh_3)_2$] which are stable in the case of ruthenium but for osmium, [613, 649] β-Os-H elimination ensues to regenerate the starting hydrido complex and 1,3-diyne RC≡CC≡CR in a catalytic manner. [614] Building on these observations it was anticipated that supplying **7.11b** to [OsHCl(CO)$(PPh_3)_3$] might result in hydride metathesis to provide an osmium metallacarbyne, eliminate elemental mercury, and give [W(≡CH)$(CO)_2$(Tp*)] as a petroleum soluble by-product. It was also hoped that unlike liberated terminal alkyne, the methylidyne would be too sterically encumbered to enter into subsequent reactions. An ideal reaction, in terms of atom economy, would use [WHg(μ_2-C)$(C_6H_5)(CO)_2$(Tp*)] (**7.14**) to eliminate benzene only, however **7.14** was unable to be isolated as a single species (see Chapter Seven) and therefore is not yet feasible.

Heating **7.11b** with [OsHCl(CO)$(PPh_3)_3$] in toluene at reflux results in a slow reaction that required multiple hours to complete in contrast, to the reactions with aryl mercurial which are complete in 15 minutes (Scheme 8.5). The initially orange mixture darkens within 10 minutes to a maroon colour that intensifies with time, clearly limited by poor solubility of **7.11b** in toluene as orange solid remains suspended. A repeat reaction determined chlorobenzene better dissolves **7.11b** allowing reaction completion within five hours, thus proving to be the superior solvent. Anaerobic filtration through diatomaceous earth removes elemental mercury prior to fractional crystallisation which reveals the maroon colour of the mixture is comprised of purple and yellow products, where the latter is a mixture of [$W_2(\mu_2\text{-}C_2H_2)(CO)_4$(Tp*)$_2$] and [W(≡CH)$(CO)_2$(Tp*)]H$(CO)_2$(Tp*)] which is readily washed away during filtration. The purple complex gives rise to somewhat broad resonances in the ^{1}H NMR spectrum, initially confounding identification, although a molecular structure unambiguously confirms the complex as osmium μ$_2$-carbido [WOs(μ_2-C)Cl$(CO)_3(PPh_3)_2$(Tp*)] (**8.6**)—the missing link of the μ$_2$-carbido field.

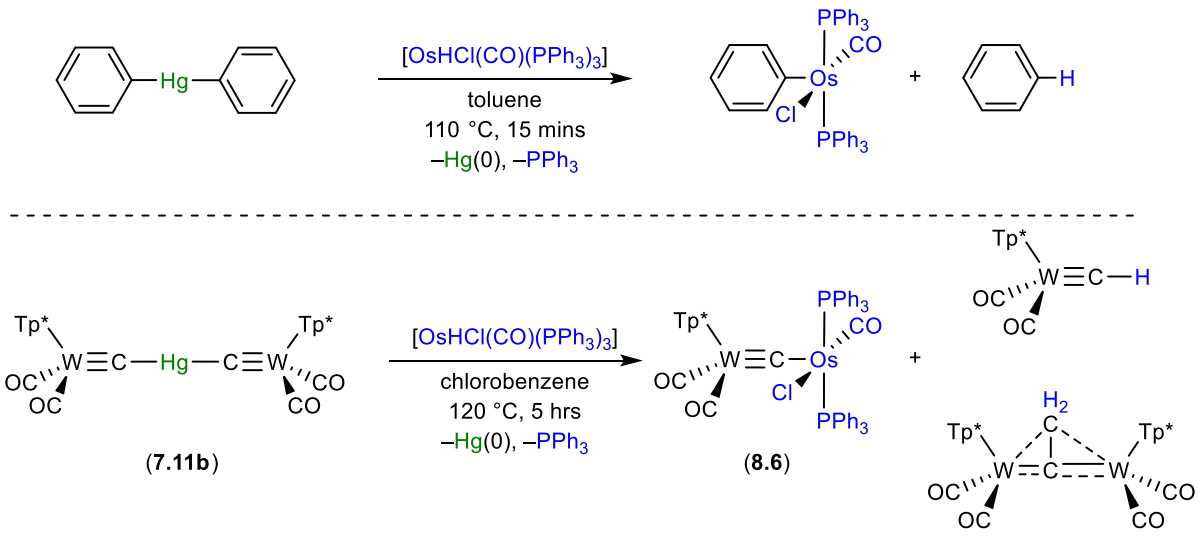

Scheme 8.5: Hydride metathesis with [OsHCl(CO)$(PPh_3)_3$] and production of an osmium μ$_2$-carbido complex.

The molecular structure reveals a coordinatively unsaturated, distorted square pyramidal geometry for osmium(II),‡‡‡‡‡‡‡‡‡‡‡‡‡‡‡‡‡‡‡‡‡‡‡‡‡‡ a configuration yet to be observed in Class B μ_2-carbidos (Figure 8.7). The complex has approximate (non-crystallographic) C_S symmetry with a vertical mirror plane bisecting the Tp* and *trans*-phosphines with a chloride and carbonyl on either side containing minor positional disorder, as is often encountered for a *trans* Cl–M–C–O arrangement in *trans-bis*$(PPh_3)_2$ structures. The phosphines have comparable bond lengths (Os–P = ~ 2.387(1) Å) and lie *pseudo-trans* (P1–Os–P2: 158.09(3)°) as the phosphine proximity to Tp* distorts the square- pyramidal geometry. Furthermore, a phenyl ring nestles the Tp* cleft as expected, however, is unable to bend the μ_2-carbido linkage (W–C–Os = 177.7(2)°) as a second phosphine provides opposing steric pressure. As with similar square-pyramidal osmium complexes,[648] one phenyl hydrogen occupies the space of the vacant coordination site with an empty orbital (Os···H: 2.8444 Å): a weak proximity-induced interaction, which on the basis of broad ^{1}H NMR signals does not persist appreciably in solution. The W≡C bond is the longest of the metallacarbynes (1.881(3) Å) where other examples are shorter (*ca* 1.83–1.86 Å)—perhaps indicating a degree of cumulenic character, noting that Os(II) is the most π-basic of the metals so far explored herein. Despite osmium having a comparatively large covalent radius (r_{cov}(Os) = 1.44(4) Å) relative to other platinum group metals, the contracted Os–C bond (1.926(3) Å) gives evidence of π-retrodonation, being the shortest for the metallacarbynes in this thesis, contracted further than the Pt–C bond (1.934(6) Å) in [WPt(μ_2-C)Br$(CO)_2(PPh_3)_2$(Tp*)] (**3.1b**) known to contain significant π-retrodonation. This Os–C bond is also shorter than comparable osmium acetylides such as [Os(C≡CMe)H(CO)(CS)$(PPh_3)_2$] (2.097(4) and 2.089(5) Å),[650] or [Os_2(μ-C≡CC≡CC≡C)$(PPh_3)_4(Cp)_2$] (2.013(3) and 1.97(1) Å),[651] where the closest comparator is the 5-coordinate acetylide-carbene complex [Os(C≡CPh)Cl(=CHPh)(IPr){P(^{i}Pr)$_3$}] (1.975(12) Å)[652] that exhibits a short bond likely influenced through a π-donor *trans*-chloride and reduced coordination number for the metal. Osmium is also capable of forming η^1-cumulenylidenes with short Os–C multiple bonds (*ca* 1.898(4) Å in [Os(=C=C=CPh_2)Cl_2(CO)$(PPh_3)_2$])[653] while five coordinate σ-aryl complexes, *e.g.*, [OsCl(C_6H_4Br–2)(CO)$(PPh_3)_2$] (Os–C: 2.038(7) Å) are elongated in comparison.[654] These observations suggest the contracted Os–C length in **8.6** is likely a corollary of retrodonation along the metallacarbyne linkage possibly with cumulenic character.

The distorted square-pyramidal geometry also complicates the spectroscopic interrogation of **8.6** as a dynamic process, perhaps Berry *pseudo*-rotation is responsible for broadening several resonances. This meant that the ^{1}H NMR spectrum is broad at ambient temperature and could not be definitively assigned, while low-temperature data acquisition (*ca* –20 °C) resolves each signal by reducing fluxionality. The

‡‡‡‡‡‡‡‡‡‡‡‡‡‡‡‡‡‡‡‡‡‡‡‡‡‡ The preferred geometry for d^6-5-coordinate metal centres is typically square pyramidal with a vacant site opposite the ligand with the strongest *trans* influence, steric factors notwithstanding.

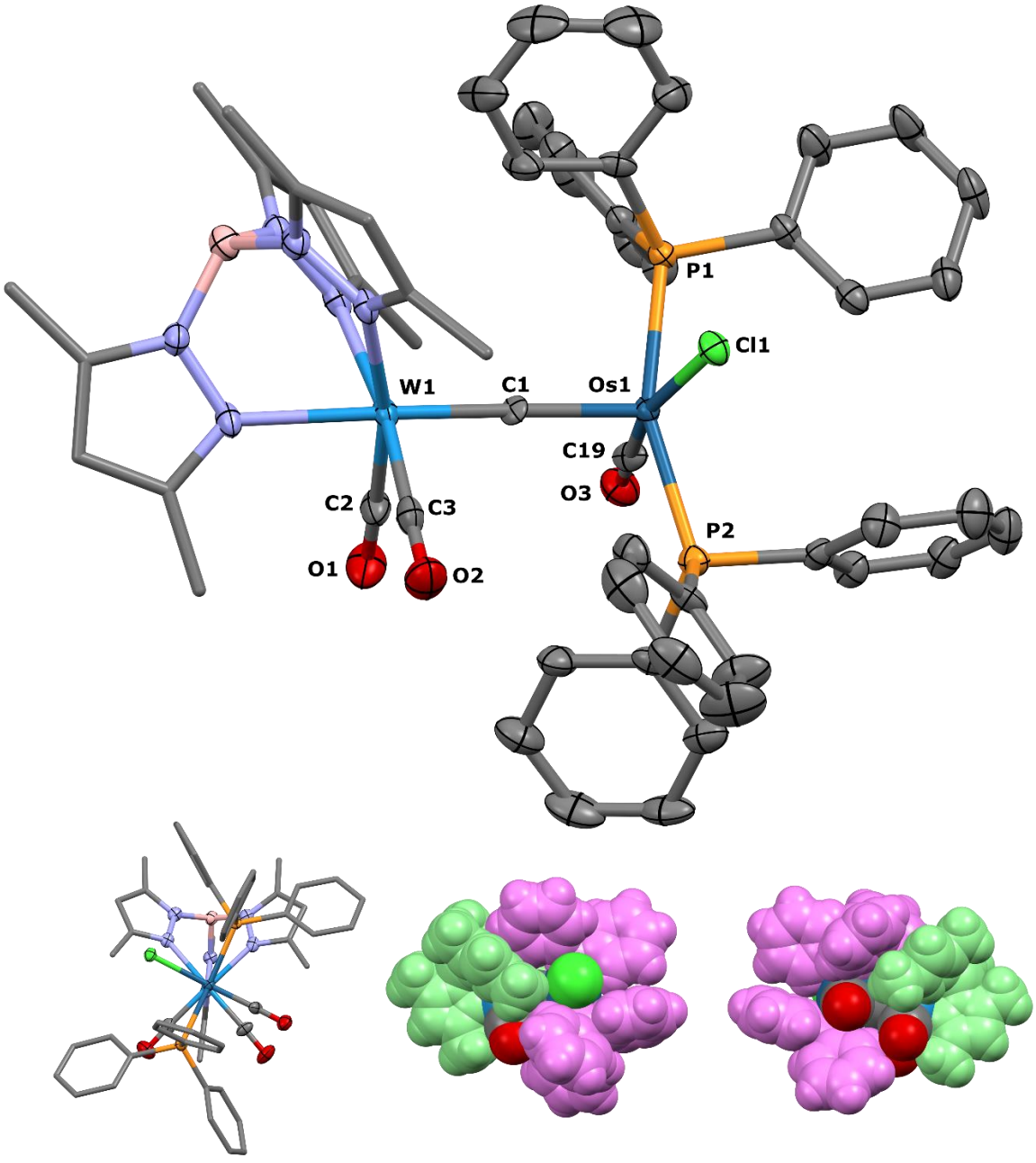

Figure 8.7: Molecular structure of [WOs(μ$_2$-C)Cl(CO)$_3$(PPh$_3$)$_2$(Tp*)] (**8.6**) in a single crystal as determined by X-Ray Diffractometry. Ellipsoids are drawn at the 50% probability surface with pyrazolyl rings simplified and disorder component and hydrogens omitted for clarity. Insets: a) View down the key molecular linkage highlighting the phosphine plane no longer bisects the Tp* ligand, b) Space-filling representations (front and rear view) highlighting the steric clash of phenyl rings (pink) and the sterically encumbering *tris*-pyrazolylborate (green) ligand. Selected bond lengths (Å) and angles (°): W1–C1 1.878(3), Os–C1 1.928(3), Os1–Cl1 2.421(3), Os1–C19 1.821(9), Os1–P1 2.387(1), Os1–P2 2.386(1), C19–O3 1.14(1), W1–C3 1.962(4), W–C2 1.965(5), C3–O2 1.153(6), C2–O1 1.165(6), W1–C1–Os1 177.5(2), C19–Os1–Cl1 164.0(3), P1–Os1–P2 158.07(4).

resolved ^{1}H NMR spectrum demonstrates C_S symmetry but is otherwise unremarkable. More importantly, the $^{13}C\{^{1}H\}$ NMR spectrum reveals a high frequency signal consistent with a μ_2-carbido (δ_C = 316.6) without resolved coupling to phosphorus and at a remarkably similar chemical shift to d^8 **3.1b** as another *bis*-phosphine (δ_C = 317.2; $^{2}J_{CP}$ = 8 Hz) (Figure 8.8). As phosphorus coupling is unresolved, the improved signal intensity allows measurement of tungsten coupling to the carbido ($^{1}J_{CW}$ = 187 Hz) which is a relatively high value compared with previous examples (*ca* 152 Hz in **7.5**; 148 Hz in **8.2**; 187 Hz in **8.3**) supporting an increase in *s*-character of the W≡C bond. Signals for the tungsten carbonyls are unresolved,§§§§§§§§§§§§§§§§§§§§§§§§§§§§§§§§ broadening into the baseline at ambient temperature but emerge at lower temperature (δ_C = 229.6/227.5), while the osmium carbonyl is a persistent triplet (δ_C = 179.9; $^{2}J_{CP}$ = 8 Hz). Infra-red spectroscopy shows carbonyl vibrations at lower wavenumber for both tungsten ($\nu_{CO\text{-}W}$: 1952, 1833 cm^{-1}) and osmium ($\nu_{CO\text{-}Os}$ = 1912 cm^{-1}), the latter being comparable to that observed for the corresponding σ-aryl complex [Os(C_6H_4Me-4)Cl(CO)(PPh_3)$_2$] (Nujol: ν_{CO} = 1906 cm^{-1}) [655] highlighting the π-basicity of both metal termini. The $^{31}P\{^{1}H\}$ NMR spectrum comprises a single singlet resonance (δ_P = 11.29) demonstrating phosphine equivalence on the ^{31}P NMR timescale. However, swapping from d_8-toluene to $CDCl_3$ results in what appears to be a broad doublet being observed but is more likely the inner resonances of a strongly roofed **AB** system approaching coalescence (δ_P = 10.21, 10.60) suggesting the coalescence temperature is solvent-dependent.

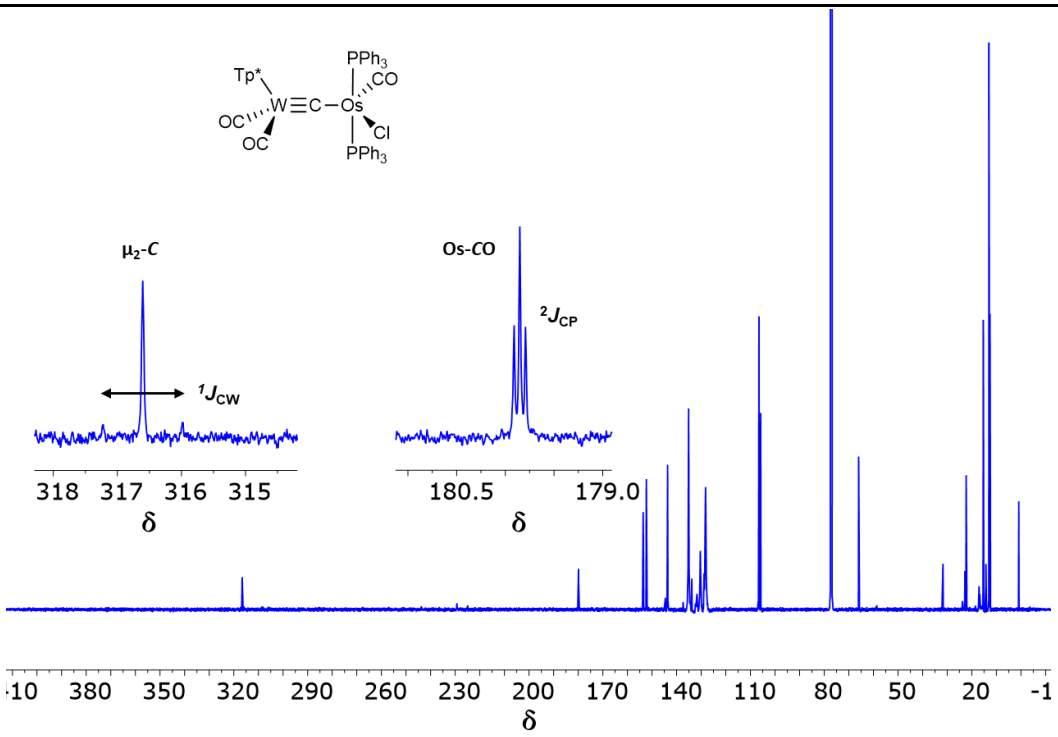

Figure 8.8: Key $^{13}C\{^{1}H\}$ NMR spectrum resonances of [WOs(μ$_2$-C)Cl (CO)$_3$(PPh$_3$)$_2$(Tp*)] (**8.6**).

§§§§§§§§§§§§§§§§§§§§§§§§§§§§§§§§ In contrast to the tungsten carbonyl ligands in the previous ruthenium, rhodium and iridium complexes which are diastereotopic, rotation about the Os–CW bond would traverse a geometry with C_s-symmetry in which the CO ligands were chemically equivalent.

The square-pyramidal geometry and vacant coordination site implicate **8.6** as a 16-electron d^6 complex of osmium (II), which also carries a potentially labile chloride ligand. The σ-aryl complexes [M(C_6H_4R-4)Cl(CO)(PPh_3)$_2$] have been shown to serve as versatile precursors for a host of ligand addition/substitution reactions, and by analogy, this synthetic potential should extend to osmium metallacarbynes if useful amounts of **8.6** can be obtained. This osmium metallacarbyne can be prepared on gram-scale in relatively high yield (80%), however, a specific order of purification is crucial. Any deviation from the method results in immediate decomposition. Recrystallisation in the first instance must be performed with CH_2Cl_2/EtOH to isolate the purple compound whereas MeOH causes decomposition and solids obtained from *n*-hexane are impure. Other solvent combinations facilitate dissociation of one labile phosphine, returning orange solids that are an indeterminable mixture of species while exposing solutions to air results in the formation of $OPPh_3$ and orange compounds.

8.6 Ligand Substitution of [WOs(μ$_2$-C)Cl(CO)$_3$(PPh_3)$_2$(Tp*)]

When a sample of **8.6** in $CDCl_3$ is exposed to air, decomposition occurs to produce a series of species, including small quantities of [WOs(μ$_2$-C)Cl(CO)$_4$(PPh_3)$_2$(Tp*)] (**8.7**) (amongst other unidentified species), presumably occurring *via* CO scrambling to fill the vacant coordination site and form an 18-electron octahedral osmium species. Alternatively, $CO_{(g)}$ immediately discolours the vivid purple solution of **8.6** in CH_2Cl_2 to afford the bright yellow of **8.7**, with quantitative conversion within 10 minutes (Scheme 8.6). Given **8.7** is an octahedral 18-electron species, it might be expected to be stable, *cf.* [Os(C_6H_4Me-4)Cl(CO)$_2$(PPh_3)$_2$] (Nujol: ν_{CO} = 2025, 1935 cm^{-1}) [655] however, single crystals were not forthcoming, repeatably giving [WOs(μ$_2$-C)Cl(CO)$_5$(PPh_3)(Tp*)] (**8.8**) *via* phosphine dissociation and sequestration by carbon monoxide within 16 hours. Attempts were made to deliberately prepare **8.8** through stirring **8.7** for one week under a $CO_{(g)}$ atmosphere in CH_2Cl_2, providing a mixture that required chromatography, ultimately resulting in **8.8** contaminated with *ca* 57% [OsHCl(CO)$_2$(PPh_3)$_2$],* presumably due to coelution (TLC suggests single compound across several polarities). Furthermore, repeating the reaction in 10% MeOH/CH_2Cl_2 fails to increase the relative rate of formation, suggesting ionisation of the chloride may not be a reliable cause of **8.8** formation. Once formed, **8.8** appears stable with no further decomposition being noted.

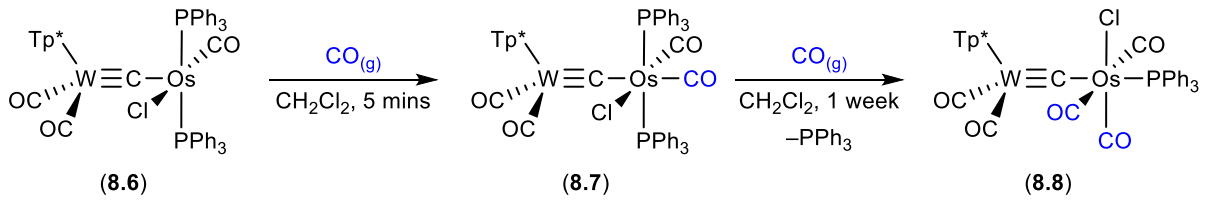

Scheme 8.6: Reactions of [WOs(μ$_2$-C)Cl(CO)$_3$(PPh_3)$_2$(Tp*)] (**8.6**) with carbon monoxide.

* δ_H = –3.63, $^2J_{PH}$ = 20 Hz, δ_P = 8.33; ν_{CO} (KBr) = 2035, 1975 cm^{-1}. [656-657]

Spectroscopic data collected for **8.7** and **8.8** represent trends of sequential increase of CO and decrease of phosphine, although crystallographic grade crystals of **8.7** were not obtained. A contraction in W–C bonds occurs for **8.8** (1.815(7) Å) relative to other tungsten carbynes, accompanied by gradual increase of the Os–C bond elongating **8.8** (2.100(8) Å) with increased coordination number, although this may be influenced by the *trans*-phosphine. The influence of the μ_2-carbido in **8.8** can be measured by the *trans*-phosphine bond length ($Os–P_{trans}$ = 2.461(2) Å), significantly elongated compared with those in **8.7** (*ca* 2.386 Å). Containing three carbonyls, the osmium terminus of **8.8** has an array of bond lengths (Os–C: 1.93(1), 1.991(8), 2.046(8) Å) and an expectedly complicated infra-red spectrum of osmium ($\nu_{CO\text{-}Os}$ = 2109, 2045, 2008 cm^{-1}) and tungsten ($\nu_{CO\text{-}W}$ = 1948, 1856 cm^{-1}) vibrations, all different than those of **8.7** (2028, 1965, 1948, 1856 cm^{-1}).

The $^{13}C\{^1H\}$ NMR spectra exhibit resonances indicative of μ_2-carbidos where **8.7** is curiously to higher frequency (δ_C = 371.9) of that for **8.8** (δ_C = 337.9). Furthermore, the signal for **8.8** is a doublet ($^2J_{CP}$ = 10 Hz) with a conspicuously small coupling which indicates a phosphine lies *cis* to the μ_2-carbido, a different configuration in solution than the solid-state (Figure 8.9). This is further substantiated by the appearance of *three* Os–CO resonances which is inconsistent with a *mer*-$Os(CO)_3$ arrangement. Two of these resonances are doublets with magnitude of $^2J_{PC}$ (9, 8 Hz) being as expected for *cis*-P–Os–CO couplings, while the third (δ_C = 167.8) has a substantially larger coupling ($^2J_{PC}$ = 101 Hz) indicating a *trans*-P–Os–CO arrangement. Finally, the tungsten carbonyl ligands are chemically inequivalent ([$\delta_C(^1J_{WC})$ = 226.5(181 Hz) and 225.3(176 Hz)], as would be expected for a *fac*-$Os(CO)_3$ geometry that renders the chiral osmium stereogenic. The *mer*-$Os(CO)_3$ geometry that is indicated in the solid-state crystal structure would allow the osmium carbonyl ligands to become chemically equivalent with free rotation about the W≡C–Os spine. It may therefore be concluded that the *mer*-$Os(CO)_3$ geometry found in the solid state is *not* that adopted by the bulk material in solution.

While the $^{31}P\{^1H\}$ NMR spectrum of **8.6** in toluene is a simple singlet (Figure 8.10). The spectrum of **8.7** comprises an **AB** system (δ_P = –12.55, –15.05) at a lower frequency than precursor **8.6**, now sharp given the octahedral geometry prevents broadening, possibly through the Berry *pseudo*-rotation mechanism. These signals exist as roofed doublets due to the coupling ($^2J_{PP}$ = 288 Hz) being of a comparable magnitude to the chemical shift difference (405 Hz), yet with weaker coupling than inequivalent *trans*-phosphorus nuclei of platinum(II) **3.1b** ($^2J_{PP}$ =443 Hz). For **8.8**, a low frequency signal is returned which is indicative of a *cis*-phosphine-carbido geometry in solution, by virtue of no ^{183}W coupling being discerned as compared with the unambiguous *trans* geometry found in *trans* [$WAu(\mu_2\text{-}C)(PCy_3)(CO)_2(Tp^*)$] (**7.2**) ($^3J_{PW}$ = 61 Hz).

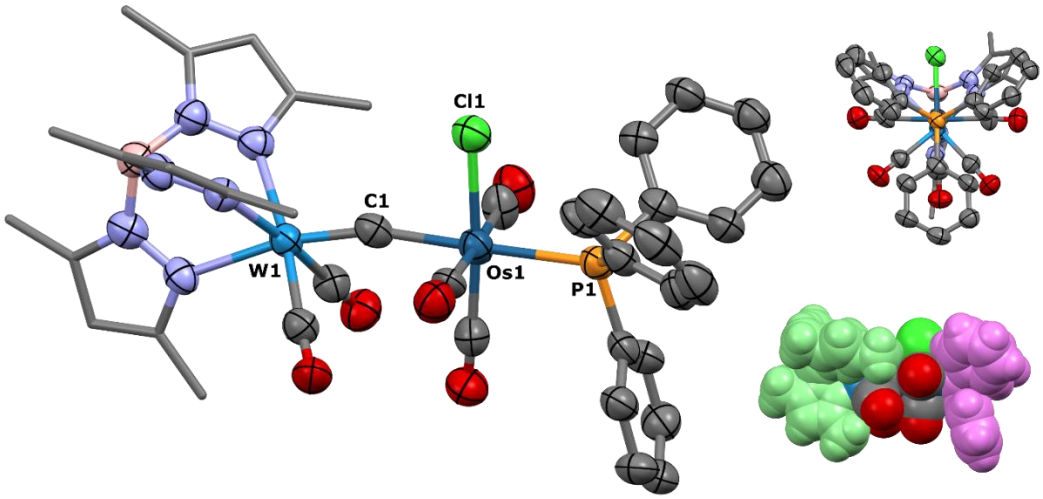

Figure 8.9: Molecular structure of *trans*-[WOs(μ$_2$-C)Cl(CO)$_5$(PPh$_3$)(Tp*)] (**8.8**) in a single crystal as determined by X-Ray Diffractometry. Ellipsoids are drawn at the 50% probability surface with pyrazolyl rings simplified and hydrogens omitted for clarity. Insets: a) View down the key molecular linkage, b) Spacefill representation highlighting the steric clash of phenyl rings (pink) and the sterically encumbering *tris*-pyrazolylborate (green) ligand. Selected bond lengths (Å) and angles (°): W1–C1 1.815(7), C1–Os1 2.100(8), Os1–Cl1 2.422(2), Os1–P1 2.461(2), W1–C1–Os1 164.6(5).

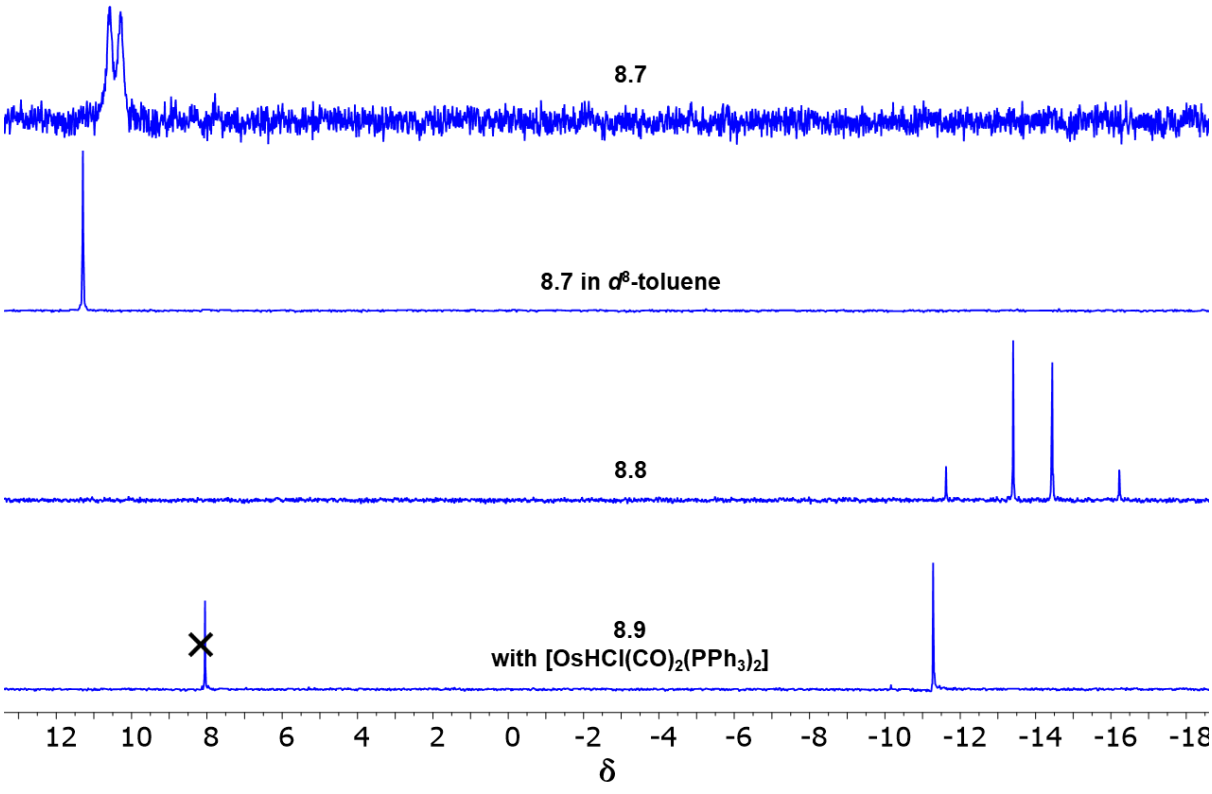

Figure 8.10: $^{31}P\{^1H\}$ NMR spectra of osmium metallacarbynes **8.7**–**8.9** showing changes in signal morphology. Measured in $CDCl_3$ unless specified otherwise; **8.9** spectrum contains ~ 0.5 eq. [OsHCl(CO)$_2$(PPh$_3$)$_2$] co-contaminant (δ_P = 8.03).

Each osmium metallacarbyne contains a very different coordination environment, perhaps the most variation for a single metal terminus other than rhodium. For this reason, theoretical models were explored to understand the orbital manifolds of geometrically optimised species from prior Chapters. Consequently, following standard conditions for consistency (DFT: ωB97X-D/6–31G*/LAND2Dζ) the geometry of simplified complexes [WOs(μ_2-C)Cl(CO)$_3$(PMe$_3$)$_2$(Tp)] (**8.6***), [WOs(μ_2-C)Cl(CO)$_4$(PMe$_3$)$_2$(Tp)] (**8.7***), and [WOs(μ_2-C)Cl(CO)$_5$(PMe$_3$)(Tp)] (**8.8***) were optimised and verified as energetic minima *via* frequency calculations. It should be borne in mind that replacement of PPh$_3$ by PMe$_3$ will increase the basicity of osmium, while replacing Tp* with Tp will reduce the basicity of tungsten. However, these perturbations are expected to be modest, and duplicated in results for other complexes discussed previously. Both modifications will reduce the impact of steric factors. A collection of parameters is obtained for comparison with experimental results (Table 8.3). One germane question is understanding why **8.8** is *trans* in the solid state but *syn* in solution since the disparity in donor/acceptor properties of the *trans* carbonyl or phosphine ligand would be expected to impact on bonding in the W≡C–Os spine. Computational results indicate that the *syn* conformer is lower in energy by 9.7 kcalmol^{-1}, a significant difference which implies the *trans* isomer may well crystallise preferentially due to packing effects in the solid state only and is unlikely to accumulate in sufficient quantities to be spectroscopically observed in solution.[†]

The frontier orbitals for **8.7*** and **8.8*** are like the many metallacarbynes investigated before so only superficial discussion of specific features is required. The main observation of each system concerns a reduced involvement of π-orbitals around the Os–C bond, consistent with the progressively elongated bond lengths in both computational and experimental studies. The most insightful results arise with **8.6*** as an unsaturated five-coordinate complex with a unique geometry for Class B carbidos (Figure 8.11),[‡] where minimal computational studies have been conducted on five coordinate ruthenium, [658] and osmium[659] species of the form [M(R)Cl(CO)(PR'$_3$)$_2$] in the wider literature. The LUMO of **8.6*** contains a large σ*-lobe *trans* to the carbido linkage– effectively the Lewis-acidic vacant coordination site, while the LUMO+1 pertains to a π-anti-bonding sequence along the W≡C–Os linkage. Like many of the other computed tungsten complexes, the HOMO–1/–2 describes the carbyne π-orbitals, but now comprises bonding interactions with the carbonyls whilst being anti-bonding to osmium; a new feature in these systems. What the computational study does clarify is the origins of the short Os–C bond in **8.6**. Delving

[†] Throughout this work, a recurring observation is the significant structural *trans* influence of the carbido ligand, which would be expected to also be manifest as a *trans* effect. Thus, both *fac* and *mer* isomers have the phosphine *trans* to a strongly *trans*-directing ligand. Accordingly, while unimolecular rearrangements (*e.g.*, Bailar twist or Ray-Dutt mechanisms) of octahedral complexes are typically high energy, dissociation of the phosphine to afford a stereochemically, non-rigid, 5-coordinate osmium centre seems likely to afford a low energy isomerism pathway.

[‡] Grubbs' diruthenium carbido also have a 5-coordinate 16-electron ruthenium centre, however it is the one with a Ru ≡C rather than Ru–C bond.

into the orbital manifold reveals a significant number of π-symmetric orbitals encompassing constructive overlap of osmium and the μ_2-carbido orbitals, that would result in a contracted bond, for which a Löwdin bond order of 1.48 is derived. Consistent with the reduced steric pressures from ligand pruning, the optimised geometry predicts more contracted bonds between carbon and both osmium (1.908 Å) and tungsten (1.842 Å, Löwden bond order = 2.15). These computations further hint at partial cumulenic (Class A) character along the W≡C–Os linkage specific to **8.6***, likely a consequence of being five-coordinate, but this raises an interesting notion of delocalisation in metallacarbynes and more broadly, evidence of inter-class contributions. A cumulenic description would, in valence bond terms, call for zwitterionic canonical forms and it is worth noting in this respect that the natural charges calculated for tungsten (0.796) and osmium (0.879) perhaps reflect this.

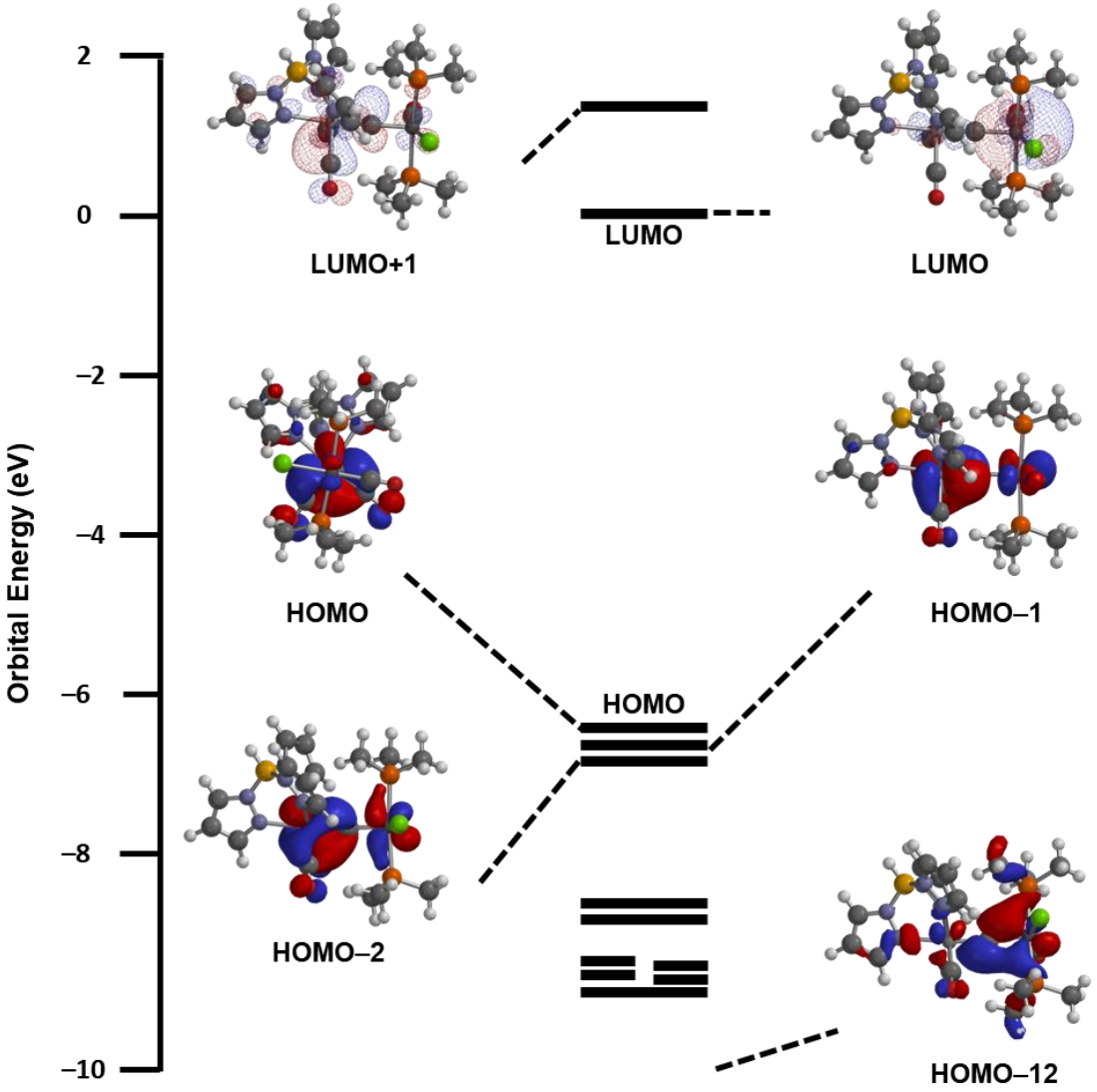

Figure 8.11: Frontier orbitals of interest for theoretical osmium metallacarbyne [WOs(μ_2-C)Cl(PMe_3)$_2$(CO)$_3$(Tp)] (**8.6***). DFT: ωB97X-D/6–31G*/LANL2Dζ.

Table 8.3: Parameters for theoretically and experimentally derived osmium metallacarbynes.

Complex	δ_C[a] (ppm)	δ_P[a] (ppm)	$^2J_{PP}$ (Hz)	$\nu_{Os\text{-}CO}$[b] (cm^{-1})	$\nu_{W\text{-}CO}$[b] (cm^{-1})	$r_{M\equiv C}$ (Å)	$r_{C\text{-}M'}$ (Å)[c]	M–C–M' (°)[c]
Experimental Species								
[**W**Os(μ2-C)Cl(CO)(PPh3)2]	317.2	11.29	–	1952	1912, 1833	1.878(3)	1.928(3)	177.5(2)
[**W**Os(μ2-C)Cl(CO)2(PPh3)2]	371.9	–12.55 –15.05	288	2028, 1965	1947, 1856	–	–	–
syn-[**W**Os(μ2-C)Cl(CO)3(PPh3)]	337.9	–11.28	–	2109, 2045 2008	1948, 1856	–	–	–
trans-[**W**Os(μ2-C)Cl(CO)3(PPh3)]	–	–	–	–	–	1.815(7)	2.100(8)	164.6(5)
Theoretical Species								
[**W'**Os(μ2-C)Cl(CO)(PMe3)2]	–	–	–	1967	1935, 1875	1.842	1.908	171.2
[**W'**Os(μ2-C)Cl(CO)2(PMe3)2]	–	–	–	2025, 1975	1957, 1890	1.818	2.063	176.7
syn-[**W'**Os(μ2-C)Cl(CO)3(PMe3)]	–	–	–	2105, 2033, 2028	1970, 1907	1.809	2.063	174.07
trans-[**W'**Os(μ2-C)Cl(CO)3(PMe3)]	–	–	–	2096, 2038, 2013	1984, 1919	1.807	2.067	178.12

Notes: W = $W(CO)_2(Tp^*)$; **W'** = $W(CO)_2(Tp)$. [a]Measured in $CDCl_3$ unless specified otherwise. [b]Measured in CH_2Cl_2 unless specified otherwise. Calculations at the wB97X-D/6-31G*/LANL2Dz level of DFT.

8.7 Conclusions

This Chapter has outlined two potentially general syntheses of Class B μ2-carbido complexes that complement oxidative addition or halide metathesis processes described in previous Chapters. The initial approach exploited the reactivity of the Hg–C or Hg–S bonds of [WHg(μ2-C)(S_2CNMe_2)$(CO)_2(Tp^*)$] (**7.20**) towards insertion of low valent, d^8 or d^{10} late transition metal reagents to produce metallacarbynes with Pt^{II}, Pd^{II}, Ir^{III}, Rh^{III} and Ru^{II} termini providing potentially useful entry points into the μ2-carbido chemistry of these elements. In many cases, the metal reagents did not react with the corresponding halocarbynes, most likely due to steric encumbrance and so this approach delivers the carbido by stealth. Initial bond formation occurs one atom removed from the carbon of interest to afford an intermediate which then extrudes mercury to finally install the W≡C–M' linkage. Yields of these complexes vary between metal reagents, in part due to competitive formation of a mercury *bis*-dithiocarbamato complex which in turn counter-productively provide metal dithiocarbamato complexes of little interest. While an osmium(II) metallacarbyne was not isolated *via* this method, room exists for process optimisation that may yet yield such species in useful amounts. Nevertheless, with the proof of concept in hand, oxidative addition of C–Hg bonds is therefore a promising advance for many transition metals left untested.

The second approach, hydride metathesis was found to provide an entry into previously unknown μ2-carbidos of osmium and once again, the possibility of extending this approach to other metal hydrido complexes has considerable broad potential.

The approaches of this Chapter are not without limitations. The use of mercury (and the alkyltin reagents necessary to acquire them) present issues of toxicity that are however easily manageable for small-scale preparation. The most useful aspect of the mercury (or stannyl) transmetallation approach is

therefore providing access to establish the viability of target carbido complexes in advances of developing more scalable routes. Future work should build upon the fundamental processes discussed but aim to design less toxic species capable of similar reactivity (*e.g.*, environmentally benign boron or bismuth).

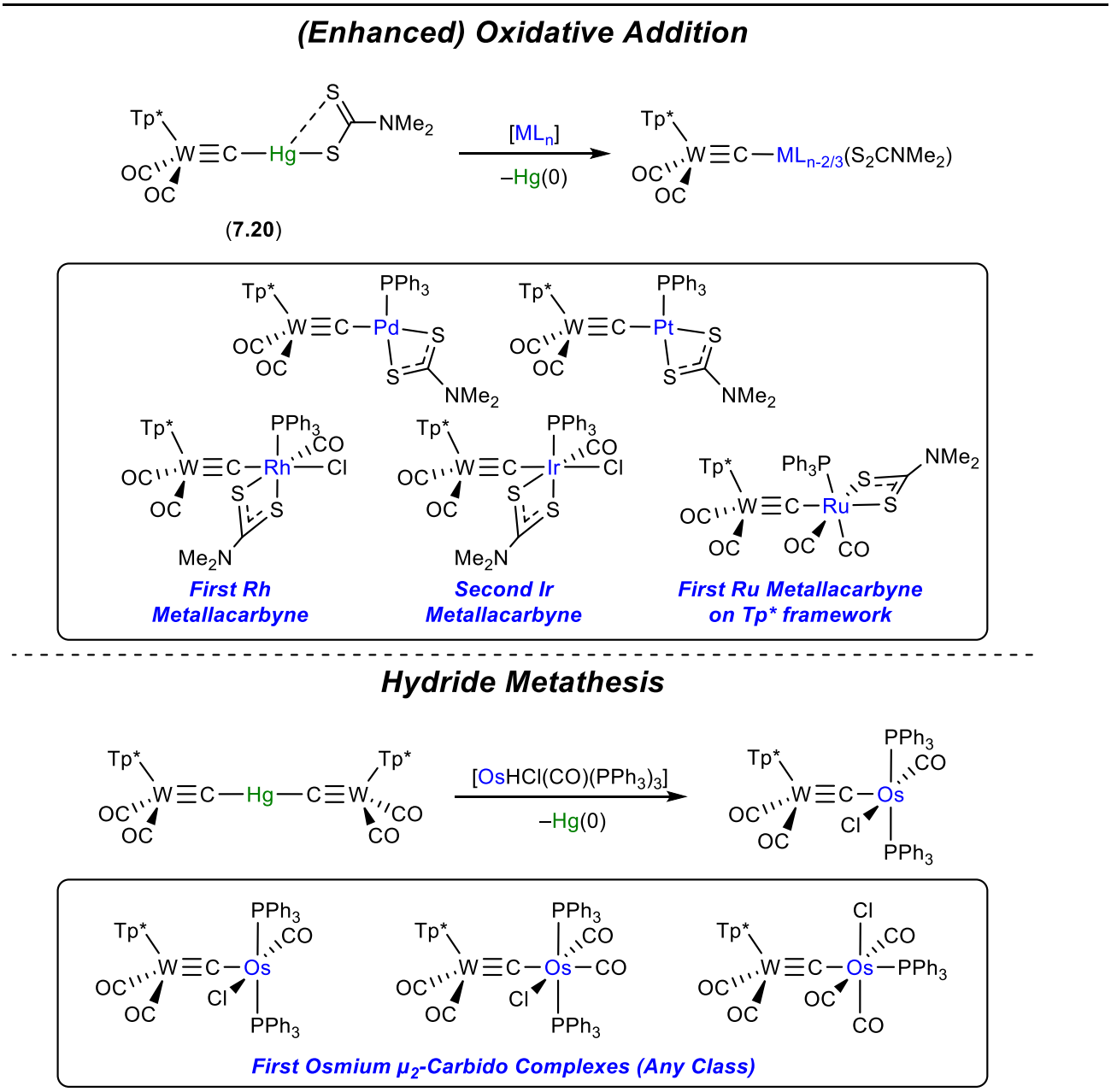

Chart 8.1: Two potentially generalisable syntheses of metallacarbynes developed in Chapter Eight.

Conclusions and Future Directions

A vast library of heterobimetallic μ_2-carbido complexes (metallacarbynes) and their derivatives have been prepared *via* fundamental organometallic processes. A review of the low-nuclearity μ_2-carbido complexes provided an informed entry into metallacarbyne chemistry *via* oxidative addition to provide a tungsten-platinum framework $[WPt(\mu_2\text{-}C)Br(CO)_2(PPh_3)_2(Tp^*)]$ (analogous to a prior species on molybdenum) that can be prepared on multi-gram scales in high yield. This complex facilitated significant diversification of metallacarbynes to identify the underlying structural, bonding and potential reactivity characteristics of metallacarbynes.

The inter-relationship of metallacarbynes to other heterobimetallic species were explored either as precursors (μ_2-halocarbynes), or products from stoichiometric reactions to give μ_2-methylidynes (CH), μ_2-methyl-carbynes (CCH_3), μ_2-iminoketenylidenes (CCNR), propargylidynes (CCCR), and tricarbidos (CCC[W]) and tetracarbidos ([W]CCCC[W]). Amongst the stoichiometric reactions explored, reductive elimination informed a study of μ_2-carbido complexes in cross-coupling reactions, identifying $[WPd(\mu_2\text{-}C)Br(CO)_2(PPh_3)_2(Tp^*)]$ as the immediate oxidative addition product, followed by Sonogashira and Suzuki–Miyaura nucleophile installation protocols. The later was shown to be enhanced by inclusion of a B→Au→Pd transmetallation relay employing a gold(I) co-catalyst.

Recognising the significance of gold(I) metallacarbynes in such syntheses, disaggregation of the golden ring $[W(\equiv CAu)(CO)_2(Tp^*)]_4$ with nucleophilic ligands allowed a diversification of gold metallacarbynes for further study. The stability of gold(I) bimetallics is dictated by the donor strength of a ligand *trans* to the μ_2-carbido, where labile examples reform $[W(\equiv CAu)(CO)_2(Tp^*)]_4$, and pentameric $[W(\equiv CAu)(CO)_2(Tp^*)]_5$ perhaps suggesting the plausibility of other gold aggregates in solution. Carbido transmetallation from tin could also be extended to a rich, albeit complex chemistry of mercury(II). These mercuriocarbynes aggregate with Hg–Cl bonds, while Hg–C bonds are prone to symmetrisation. Two leading species, $[W_2Hg(\mu_2\text{-}C)_2(CO)_4(Tp^*)_2]$ and $[WHg(\mu_2\text{-}C)(S_2CNMe_2)(CO)_2(Tp^*)]$, present isolable sources of reactive Hg–C bonds for transmetallation to recalcitrant metal centres that resist halocarbyne oxidative addition processes.

Thus, insertion of electron rich transition metal reagents into the Hg–C or Hg–S bonds of $[WHg(\mu_2\text{-}C)(S_2CNMe_2)(CO)_2(Tp^*)]$ followed by mercury extrusion results in a series of metallacarbynes of palladium, platinum, rhodium, iridium and ruthenium, promising a somewhat generalisable synthesis. Lack of success in extending this protocol to osmium(II) was overcome by developing and alternative hydride metathesis approach with $[W_2Hg(\mu_2\text{-}C)_2(CO)_4(Tp^*)_2]$

efficiently installing an osmiocarbyne linkage in synthetically versatile [WOs(μ_2-C)Cl$(CO)_3(PPh_3)_2$(Tp*)]. This new method in principle promises many more opportunities given the multitude of potential hydrido complexes.

One consideration is that future work should seek species that mimic reactivity of the mercuriocarbynes and stannylcarbynes, without the associated toxicity, before extending the chemistry to the first-row elements, for which μ_2-carbidos remain scarce. This line of research ultimately provides a framework for much broader study of heterobimetallic μ_2-carbido complexes, whilst unambiguously confirming their reactive nature.

Chapter Nine:
Experimental Information

9.1 General Considerations

Unless otherwise stated, all manipulations were carried under an anhydrous and anaerobic nitrogen or argon atmosphere using standard Schlenk line and glove-box techniques with dried and degassed solvents at ambient temperature (25 °C). Solvents were purified by distillation from an appropriate drying agent {ethers and paraffins over sodium with a benzophenone-ketyl as indicator; halocarbons and acetonitrile from CaH_2; alcohols over magnesium turnings aided by iodine}. Otherwise, solvents were collected from a solvent purification system, degassed with nitrogen or argon, and stored over appropriate molecular sieves. Triethylamine was distilled over KOH. The term petroleum ether refers to the fraction of petroleum with the boiling range 60–80 °C. Unless specified below, all other reagents were used as obtained from commercial suppliers without further purification.

The following compounds were prepared according to published procedures: [AuCl(IMes)],[660] [AuCl(SMe_2)],[661] [CuCl(SMe_2)],[572] [HgCl(ppy)]$_n$,[662] [HgCl(SC_4H_3)],[523] [IrCl(CO)(PPh_3)$_2$],[663] [OsHCl(CO)(PPh_3)$_3$],[664] [Pd(PPh_3)$_4$],[665] [Pd_2(dba)$_3$]·$CHCl_3$,[666] [$PdCl_2$(dppf)],[667] [Pt(PPh_3)$_4$],[668] [Pt(η^2-C_2H_4)(PPh_3)$_2$],[669] [RhCl(CO)(PPh_3)$_2$],[670] [Ru(CO)$_2$(PPh_3)$_2$],[671] 1,3-dimesitylimidazolium chloride,[672] KBp*,[299-300] and KTp*.[299-300] [AuCl(PCy_3)] and [AuCl(PPh_3)] were prepared from addition of one equivalent of phosphine to [AuCl(SMe_2)]. [HgCl(S_2CNMe_2)] was prepared by a modified procedure,[673] using a dilute solution of [$HgCl_2$]. [HgCl($C_{10}H_7$)] was prepared from a modified lithiation procedure and 2-bromonaphthalene.[148] [W(≡CAu)(CO)$_2$(Tp*)] was prepared from the literature procedure, although purified from CH_2Cl_2/n-hexane recrystallisation as opposed to cryostatic flash chromatography.[99] [W(≡CH)(CO)$_2$(Tp*)][179] was prepared *via* a H_2O quench of lithiocarbyne [W{≡CLi(THF)$_n$}(CO)$_2$(Tp*)]. Syntheses of following compounds have previously been described: [M(≡CX)(CO)$_2$(Tp*)] {M = Mo or W; X = Cl or Br}[87-88, 90, 101], [W(≡CAsMePh$_2$)(CO)$_2$(Tp*)]OTf,[478] [W(≡CC≡CSiMe$_3$)(CO)$_2$(Tp*)],[443] [W(≡CPR_3)(CO)$_2$(Tp*)] (PR_3 = PPh_3, $PMePh_2$, PMe_2Ph, PCy_3),[305] and [W(≡CSnBu_3)(CO)$_2$(Tp*)].[99, 674] The following were used as inherited from fellow group members, prepared as per literature procedures: [Pt(nbe)$_3$][344-345] was prepared by Dr Cheeseng Onn; CNMes[675] by Dr Lorraine M. Caldwell, and Na[Bm^{Me}] or

$Na[Tm^{Me}]$ [676] by Steven S. Welsh. All other chemicals were obtained from commercial suppliers and purified as required.

NMR spectra were obtained at 25 °C (unless specified otherwise) on a Bruker Avance 400 Bruker Avance 400 (^{1}H at 400.1 MHz, ^{13}C at 100.6 MHz, ^{19}F at 376.5 MHz, ^{31}P at 162.0 MHz, ^{195}Pt at 86.0 MHz, ^{199}Hg at 71.7 MHz), a Bruker Avance 600 (^{1}H at 600.0 MHz, ^{13}C at 150.9 MHz), a Bruker Avance 700 (^{1}H at 700.0 MHz, ^{7}Li at 291.5 MHz, ^{13}C at 176.1 MHz, ^{31}P at 283.4 MHz, ^{195}Pt at 150.5 MHz, ^{199}Hg at 125.4 MHz), or a Bruker Avance 800 (^{1}H at 150.5 MHz, ^{13}C at 201.2 MHz) spectrometer. Chemical shifts (δ) for ^{1}H and ^{13}C spectra are reported in ppm relative to the residual solvent signal, where other nuclei are relative to an external reference {LiBr in D_2O for ^{7}Li; $CFCl_3$ for ^{19}F; 85% H_3PO_4 for ^{31}P; 1.2M Na_2PtCl_6 for ^{195}Pt; $[HgPh_2]$ for ^{199}Hg} with coupling constants given in Hz. All ^{1}H DOSY NMR spectra were obtained using the convection compensated dstebpgp2s[677-678]pulse sequence within TopSpin®. The spectra in CD_2Cl_2 or d6-acetone were obtained with delta = 2.0 ms,[§] Δ = 100 ms, and g = 2–60%. The multiplicities of NMR resonances are denoted by the abbreviations: s (singlet), d (doublet), t (triplet), m (multiplet), br (broad) and combinations thereof for more highly coupled systems. Where applicable, the stated multiplicity refers to that of the primary resonance exclusive of heteronuclear ^{183}W or ^{195}Pt satellites. Complexes involving a *trans*-$M(PR_3)_2$ geometry typically give rise to virtual coupling in the $^{13}C\{^1H\}$ NMR spectrum, in which case the signal multiplicities are given as t^v (virtual triplet), accompanied by apparent J_{PC} coupling constants. Phosphorus-31 chemical shifts are reported having, where appropriate, been corrected for roofing effects in AB spin systems. [263] Some compounds contain variable, non-negligible ratios of rotamers, hence absolute assignment of all signals is sometimes not possible.

In some cases, distinct peaks were observed in the ^{1}H and $^{13}C\{1H\}$ NMR spectra, but to the level of accuracy that is reportable (*i.e.,* 2 decimal places for ^{1}H NMR, 1 decimal place for ^{13}C NMR) they are reported as having the same chemical shift. The abbreviation 'pz' is used to refer to the pyrazolyl rings on the hydro-*tris*(3,5-dimethylpyrazol-1-yl)borate (Tp*) ligand. The abbreviations 'im', 'Xyl' and 'Mes' stands for imidazole, xylyl (2,6-dimethylphenyl) and mesityl (2,4,6-trimethylphenyl) rings, respectively.

Spectra provided in the electronic supporting information generally correspond to samples obtained directly from chromatography and may contain residual solvent as recrystallised samples often displayed reduced solubility. The B*H* protons give rise to very broad signals around 4–5 ppm in the 1H NMR spectra due to coupling to the quadrupolar boron nuclei. These are not listed in

[§] p30×2 = 2 ms

the experimental NMR data in all cases as their chemical shifts and associated integrals are not determined accurately. The *BH* unit, being remote from the metal centre of interest is not particularly responsive to variations and accordingly the typically broad $^{11}B\{^{1}H\}$ NMR spectra were not recorded.

Infrared spectra were obtained using a Perkin-Elmer Spectrum One FT-IR spectrometer. The strengths of IR absorptions are denoted by the abbreviations vs (very strong), s (strong), m (medium), w (weak), sh (shoulder) and br (broad). Elemental microanalytical data were provided by London Metropolitan University or Macquarie University, Sydney. Solvates evident from data were confirmed where possible by NMR spectroscopy to support elemental microanalytical data. High resolution electrospray ionisation mass spectrometry (ESI-MS) was performed by the ANU Research School of Chemistry mass spectrometry service with acetonitrile, methanol, tetrahydrofuran or dichloromethane as the matrix. For salts, [M]+ refers to the cationic complex. UV-Vis data was collected as solutions in 1 cm quartz cells using a PerkinElmer lambda 950 spectrophotometer.

For experiments involving alkyltin and organomercurial reagents, additional protection and controls were used to manage risk. All reactions were strictly performed in a well-ventilated fumehood, utilising a double-glove protocol (nitrile inner; latex outer), and all wastes collected separately. Glassware was washed with dilute nitric acid (3%) prior to standard base and acid bath methods. Upon reaction completion, a handwash was completed with D-Lead® hand soap from CAGroup.[**] Routine tests of the author after completion of experimental work and prior to submission found no elevated levels of tin, mercury or arsenic in the blood.

9.2 Computational Methods

Computational studies were performed by using the *SPARTAN20*® suite of programs. [679] Geometry optimisation (gas phase) was performed at the DFT level of theory using the exchange functionals ωB97X-D of Head-Gordon. [680-681] The Los Alamos effective core potential type basis set (LANL2DZ) of Hay and Wadt[682-684] was used for elements >Kr while people 6-31G* basis sets[685] were used for all other atoms. Frequency calculations were performed for all compounds to confirm that each optimised structure was a local minimum and also to identify vibrational models of interest. Atomic coordinates are available from the author on request.

[**] Specific hand soap available from CAGroup: https://www.cagroup.com.au/hand-soap/

9.3 Crystallographic Methods

Data for X-ray crystallography were collected with an Agilent Xcalibur CCD diffractometer using Mo-Kα radiation (λ = 0.71073 A) or an Agilent SuperNova CCD diffractometer using Cu-Kα radiation (λ = 1.54184 A) using the CrysAlis PRO-CCD and -RED software, with gaussian absorption corrections being applied. [686] Data for complexes **5.6**, **5.10**, **7.5**, **7.6**, **7.10**, **8.1**, and **8.8** were collected at the Australian Synchrotron using the MX2 beamline using silicon double crystal monochromated synchrotron radiation at 100 K and the Australian Cancer Research Foundation Eiger 16M detector. [687] These data were collected or assisted by Dr Michael Gardiner or Dr Nicholas White who are gratefully acknowledged. Raw frame data were collected using BluIce[688] and data reduction, interframe scaling, unit cell refinement and absorption corrections were processed using XDS. [689] The structures were solved by direct or Patterson methods and refined by full-matrix least-squares on F^2 using the SHELXL programs[690-691] and Olex2 suite of programs. [692] Hydrogen atoms were located geometrically and refined using a riding model. Diagrams were produced using the CCDC visualisation program Mercury. [693] Following interrogation by the CheckCif portal, the Crystallographic Information Files (CIF) were archived with the Cambridge Crystallographic Data Centre (CCDC) and are available using the CCDC numbers provided.

9.4 Synthetic procedures for Chapter Two compounds

Synthesis of [MoAuCl(μ-CCl)(CO)$_2$(Tp*)] (2.2a).

Under reduced light conditions, samples of halocarbyne [Mo(≡CCl)(CO)$_2$(Tp*)] (200 mg, 0.403 mmol) and [AuCl· SMe$_2$] (0.120 g, 0.407 mmol) were dissolved is CH_2Cl_2 (10 mL) initially giving a yellow solution yet changing to orange within 1 minute. The subsequent reaction was monitored by infra-red spectroscopic methods, identifying reaction completion around 90 minutes. During the reaction the flask was covered with aluminium foil to largely exclude light, thus preventing formation of colloidal gold. Upon completion, the solution was exposure to air and eluted through celite with more CH_2Cl_2 prior to layering with *n*-hexane and concentrating by rotary evaporation. This gave a bright orange powder which could be collected *via* vacuum filtration while washing with *n*-hexane (2 x 10 mL) and *n*-pentane (1 x 10 mL) before drying in air over 2 hours. This afforded the title compound as a fine orange powder (0.220 g, 0.302 mmol, 75% isolated yield). Crystals suitable for x-ray diffraction studies were grown from the vapour diffusion of *n*-hexane into a $CHCl_3$ solution of the title compound at 5 °C. IR (CH_2Cl_2, cm^{-1}): 2031 vs ν_{CO}, 1957 vs ν_{CO}. IR (ATR, cm^{-1}): 2556 w ν_{BH}, 2020 vs ν_{CO}, 1962 vs ν_{CO}. ^{1}H NMR (700 MHz, $CDCl_3$, 25 ºC, δ): 5.90 [s, 3H, pzCH], 2.45 [s, 6H, pzCH_3], 2.43 [s, 3H, pzCH_3], 2.38 [s, 6H, pzCH_3], 2.35 [s, 3H, pzCH_3]. ^{13}C{^{1}H} NMR (176 MHz, $CDCl_3$, 25ºC, δ): 230.4 [MoAu(=CCl)], 218.2 [CO], 152.6 151.9 [C^5(pz)],

146.3 145.9 [C^3(pz)], 108.1 107.7 [C^4(pz)], 16.9 15.4 13.2 12.9 [pzCH_3]. MS (ESI, *m/z*): Found: 731.0084. Calcd for $C_{18}H_{23}{}^{11}BN_6O_2{}^{35}Cl_2{}^{98}Mo{}^{197}Au$ $[M+H]^+$: 731.0072. Anal. Found: C, 29.68; H, 3.17; N, 10.92%. Calcd for $C_{18}H_{22}AuBCl_2MoN_6O_2$: C, 29.66; H, 3.04; N, 11.53%. *Crystal data for* 2($C_{18}H_{22}AuBCl_2MoN_6O_2$), M = 1458.06, monoclinic, $P2_1/c$, a = 25.4253 (3) Å, b = 10.9689 (1) Å, c = 19.7589 (2) Å, β = 108.022 (1)°, V = 5240.15 (10) Å^3, Z = 4, ρ_{calc} = 1.848 Mgm^{-3}, μ(Cu $K\alpha$) = 16.38 mm^{-1}, T = 150(0) K, plate, 0.16 × 0.12 × 0.05 mm {clear light orange}, 10256 independent measured reflections (θ = 73.9), R_1 = 0.042, wR_2 = 0.102 for 9646 reflections [$I > 2\sigma(I)$], 565 parameters, 0 restraints. CDCC 2173043.

Synthesis of [WAuCl(μ-CCl)(CO)$_2$(Tp*)] (2.2b).

Under reduced light conditions, samples of halocarbyne [W(≡CCl)(CO)$_2$(Tp*)] (200 mg, 0.342 mmol) and [AuCl·SMe$_2$] (0.100 g, 0.340 mmol) were dissolved is CH_2Cl_2 (10 mL) initially giving a yellow solution yet changing to orange within 1 minute. The subsequent reaction was monitored by infra-red spectroscopic methods, identifying reaction completion around 90 minutes. During the reaction the flask was covered with aluminium foil to largely exclude light, thus preventing formation of colloidal gold. Upon completion, the solution was exposure to air and eluted through celite with more CH_2Cl_2 prior to layering with *n*-hexane and concentrating by rotary evaporation. This gave a bright orange powder which could be collected *via* vacuum filtration while washing with *n*-hexane (2 x 10 mL) and *n*-pentane (1 x 10 mL) before drying in air over 2 hours. This afforded the title compound as a fine orange powder (0.184 g, 0.225 mmol, 66% isolated yield). Crystals suitable for x-ray diffraction studies were grown from the vapour diffusion of cyclohexane into a $CHCl_3$ solution of the title compound at 5 °C. IR (CH_2Cl_2, cm^{-1}): 2018 vs ν_{CO}, 1934 vs ν_{CO}. IR (ATR, cm^{-1}): 2559 w ν_{BH}, 2008 vs ν_{CO}, 1943 vs ν_{CO}, 1933 vs ν_{CO}. ^{1}H NMR (700 MHz, $CDCl_3$, 25 °C, δ): 5.95 [s, 2H, pzCH], 5.93 [s, 1H, pzCH], 2.48 [s, 9H, pzCH_3], 2.38 [s, 6H, pzCH_3], 2.34 [s, pzCH_3]. ^{13}C{^{1}H} NMR (176 MHz, $CDCl_3$, 25°C, δ): 222.2 [$^1J_{CW}$ = 125 Hz, WAu(=CCl)], 213.8 [152 Hz, CO], 153.7 152.8 [C^5(pz)], 146.2 145.9 [C^3(pz)], 108.4 108.0 [C^4(pz)], 17.6 16.0 13.2 12.8 [pzCH_3]. MS (ESI, *m/z*): Found: 839.0344. Calcd for $C_{18}H_{22}{}^{11}BN_6O_2{}^{23}Na{}^{35}Cl_2{}^{184}W{}^{197}Au$ $[M]^+$: 839.0347. Anal. Found: C, 28.01; H, 3.03; N, 10.12%. Calcd for $C_{18}H_{22}AuBCl_2N_6O_2W$: C, 26.46; H, 2.71; N, 10.29%. The unsatisfactory elemental microanalytical data is attributed to, without evidence, partial desolvation of cyclohexane during extended drying under vacuum, noting that Calcd for $C_{18}H22AuBCl_2N_6O_2W{\cdot}0.25(C_6H_{12})$: C, 27.95; H, 3.01; N, 10.03%. *Crystal data for* $C_{18}H_{22}AuBCl_2N_6O_2W{\cdot}C_3H_6$, M = 859.02, monoclinic, $P2_1/n$, a = 13.3472 (2) Å, b = 10.4746 (1) Å, c = 19.2527 (3) Å, β = 102.807 (1)°, V = 2624.69 (6) Å^3, Z = 4, ρ_{calc} = 2.174 Mgm^{-3}, μ(Cu $K\alpha$) = 20.46 mm^{-1}, T = 150 (0) K, plate, 0.15 × 0.06 × 0.04 mm {clear light orange},

5126 independent measured reflections (θ = 73.5°), R_1 = 0.032, wR_2 = 0.087 for 4570 reflections [$I > 2\sigma(I)$], 301 parameters, 0 restraints. CDCC 2173040.

Synthesis of [MoAu(μ$_2$-CBr)Cl(CO)$_2$(Tp*)] (2.2c).

Samples of [Mo(≡CCl)(CO)$_2$(Tp*)] (94 mg, 0.173 mmol) and [AuCl·SMe$_2$] (50 mg, 0.170 mmol) were set dissolved in CH_2Cl_2 (10 mL) and wrapped in aluminum foil to exclude light. Beginning as a bright yellow solution, within 10 minutes this darkened to a bright orange. The ensuing reaction was monitored by infra-spectroscopic analysis, determining reaction completion at ~90 minutes. At this point, the reaction mixture was eluted through a flash column {celite, neat CH_2Cl_2} removing colloidal gold and providing a bright orange solution. This solution was layered with *n*-hexane and concentrated by rotary evaporation to recrystallise an orange solid. Following sonication for 5 minutes, the orange solid was collected via vacuum filtration, washing with *n*-hexane (2 x 10 mL) and *n*-pentane (1 x 10 mL) before drying *in vacuo* for 4 hours, to give the title compound (110 mg, 0.142 mmol, 84% yield). Crystals suitable for single crystal x-ray diffraction studies were grown from the vapour diffusion of *n*-hexane into a CH_2Cl_2 solution of compound at 5 °C overnight. IR (CH_2Cl_2, cm^{-1}): 2032 vs ν_{CO}, 1960 vs ν_{CO}. IR (ATR, cm^{-1}): 2562 w ν_{BH}, 2024 vs ν_{CO}, 1957 vs ν_{CO}, 1946 vs ν_{CO}. ^{1}H NMR (600 MHz, $CDCl_3$, 25 °C, δ): 5.92 [s, pzCH, 3H], 2.48 [s, pzCH$_3$, 6H], 2.45 [s, pzCH$_3$, 3H], 2.40 [s, pzCH$_3$, 6H], 2.37 [s, pzCH$_3$, 3H]. ^{13}C{^{1}H} NMR (151 MHz, $CDCl_3$, 25°C, δ): 224.4 [MoAu(=CCl)], 218.5 [CO], 152.5 151.9 [C^5(pz)], 146.4 145.9 [C^3(pz)], 108.1 107.7 [C^4(pz)], 16.9 15.4 13.3 12.9 [pzCH$_3$]. MS (ESI, *m/z*): Found: 740.9482. Calcd for $C_{16}H_{22}{}^{11}BN_6{}^{23}Na{}^{35}Cl{}^{79}Br{}^{98}Mo{}^{197}Au$ [M–2CO+Na]$^+$: 740.9488. Anal. Found: C, 27.92; H, 2.88; N, 10.62%. Calcd for $C_{18}H_{22}AuBBrClMoN_6O_2$: C, 27.95; H, 2.87; N, 10.87%. *Crystal data for* 2($C_{18}H_{22}AuBBrClMoN_6O_2$)·$CH_2Cl_2$, M = 1631.91, orthorhombic, *Pca*2$_1$, a = 19.9121 (1) Å, b = 10.8854 (1) Å, c = 23.8615 (1) Å, V = 5172.01 (6) Å^3, Z = 4, ρ_{calc} = 2.096 Mgm^{-3}, μ(Cu $K\alpha$) = 18.43 mm^{-1}, T = 150(0) K, block 0.37 × 0.25 × 0.09 mm {clear light orange}, 10173 independent measured reflections (θ = 73.7), R_1 = 0.032, wR_2 = 0.080 for 10151 reflections [$I > 2\sigma(I)$], 587 parameters, 16 restraints. CDCC 2173050.

Synthesis of [MoPt(μ$_2$-CCl)(PPh$_3$)$_2$(CO)$_2$(Tp*)] (2.3a).

Samples of halocarbyne [Mo(≡CCl)(CO)$_2$(Tp*)] (0.098 g, 0.197 mmol) and [Pt(η^2-C_2H_4)(PPh$_3$)$_2$] (0.161 g, 0.215 mmol) were dissolved in toluene (10 mL) to give a yellow solution. A small amount of gas was steadily liberated. The solution darkened around 90 minutes with hints of orange and reaction was completed as identified by infra-red spectroscopic methods. Upon completion the solvent was removed under reduced pressure before opening to air and recrystallizing the residue

from concentration of THF into EtOH affording an yellow powder identified as the title compound (0.190 g, 0.156 mmol, 79% isolated yield). Crystals suitable for x-ray diffraction studies were prepared by the vapour diffusion of *n*-hexane into a THF solution of compound at 5 °C overnight. IR (CH_2Cl_2, cm^{-1}): 1906 vs ν_{CO}, 1823 vs ν_{CO}. Note: other bands at 1960/1870 arise from the isomerisation as the title compound enters a sufficiently polar medium such as CH_2Cl_2. IR (ATR, cm^{-1}): 2518 w ν_{BH}, 1898 vs ν_{CO}, 1830 vs ν_{CO}, 1816 vs ν_{CO}. ^{1}H NMR (700 MHz, C_6D_6, 25 ºC, δ): 7.96 [m, 6H, PPh], 7.50 [m, 6H, PPh], 6.99 [m, 9H, PPh], 6.87 [m, 9H, PPh], 5.66 [s, 2H, pzCH], 5.52 [s, 1H, PPh], 2.53 [s, 6H, $pzCH_3$], 2.25 [s, 3H, $pzCH_3$], 2.19 [s, 6H, $pzCH_3$], 2.16 [s, 3H, $pzCH_3$]. ^{13}C{^{1}H} NMR (176 MHz, C_6D_6, 25ºC, δ): 314.8 [dd, $^2J_{CP}$ = 75, 6 Hz, WPt(=CCl)], 228.5 [m, $^2J_{CP}$ = 70 Hz, CO], 153.1 150.5 [C^5(pz)], 144.1 143.2 [C^3(pz)], 136.6 [d, $^1J_{CP}$ = 38 Hz, $C^1(C_6H_5)$], 135.6 [d, $^2J_{CP}$ = 13 Hz, $C^{2,6}(C_6H_5)$], 135.1 [d, $^2J_{CP}$ = 12 Hz, $C^{2,6}(C_6H_5)$], 134.3 [d, $^1J_{CP}$ = 46 Hz, $C^1(C_6H_5)$], 129.5 [d, $^3J_{CP}$ = 10 Hz, $C^{3,5}(C_6H_5)$], 128.4 [$C^4(C_6H_5)$], 127.6 [d, $^3J_{CP}$ = 10 Hz, $C^{3,5}(C_6H_5)$], 106.7 106.5 [C^4(pz)], 16.1 15.8 13.0 12.7 [$pzCH_3$]. ^{31}P{^{1}H} NMR (162 MHz, C_6D_6, 25 ºC, δ): 38.24 [d, $^2J_{PP}$ = 24 Hz, $^1J_{PPt}$ = 4391 Hz], 25.82 [d, $^2J_{PP}$ = 24 Hz, $^1J_{PPt}$ = 2758 Hz]. ^{195}Pt{^{1}H} NMR (150 MHz, C_6D_6, 25ºC, δ): –3940 [dd, $^1J_{PtP}$ = 4398, 2761 Hz]. MS (ESI, *m/z*): Found: 1217.2092. Calcd for $C_{54}H_{52}{}^{11}BN_6O_2P_2{}^{35}Cl^{98}Mo^{195}Pt$ $[M]^+$: 1217.2110. Anal. Found: C, 53.34; H, 4.29; N, 6.67%. Calcd for $C_{54}H_{52}BClMoN_6O_2P_2Pt$: C, 53.33; H, 4.31; N, 6.91%. *Crystal data for* $2(C_{54}H_{52}BClMoN_6O_2P_2Pt)\cdot2.5(C_2H_3N)$, M = 2535.12, triclinic, $P\bar{1}$, a = 11.5634 (2) Å, b = 21.0076 (4) Å, c = 24.0458 (5) Å, α = 71.105 (2)°, β = 80.456 (2)°, γ = 78.496 (2)°, V = 5383.22 (19) Å^3, Z = 2, ρ_{calc} = 1.564 Mgm^{-3}, μ(Cu $K\alpha$) = 8.10 mm^{-1}, T = 150 (0) K, block, 0.20 × 0.09 × 0.05 mm {clear light orange}, 20974 independent measured reflections (θ = 73.7), R_1 = 0.037, wR_2 = 0.087 for 19434 reflections [$I > 2\sigma(I)$], 1303 parameters, 15 restraints. CDCC 2173043.

Synthesis of [WPt(μ-CCl)(PPh$_3$)$_2$(CO)$_2$(Tp*)] (2.3b).

Samples of [W(≡CCl)(CO)$_2$(Tp*)] (0.115 g, 0.197 mmol) and [Pt(η^2-C_2H_4)(PPh_3)$_2$] (0.165 g, 0.221 mmol) were dissolved in THF (10 mL) and stirred at reflux for 30 minutes and cooled for 30 minutes. During this time, the initially yellow solution transitioned to an orange colour with reaction completion measured by infra-red spectroscopic analysis. Solvent was removed under reduced pressure to give an orange solid, which could be recrystallised from THF and EtOH and collected *via* vacuum filtration. The collected sample was dried *in vacuo* for 4 hours to give a yellow powder confirmed as the title compound (0.108 g, 0.083 mmol, 42% isolated yield). Crystals suitable for single-crystal x-ray diffraction studies were grown from the vapour diffusion of MeCN into a THF solution of the compound at ambient temperature over 4 nights. IR (CH_2Cl_2, cm^{-1}):

1895 vs ν_{CO}, 1810 vs ν_{CO}. IR (ATR, cm^{-1}): 2529 w ν_{BH}, 1897 sh ν_{CO}, 1888 vs ν_{CO}, 1818 vs ν_{CO}, 1806 vs ν_{CO}. ^1H NMR (700 MHz, C_6D_6, 25 ºC, δ): 8.00 [m, 6H, PPh], 7.53 [m, 6H, PPh], 7.00 [m, 10H, PPh], 6.89 [m, 8H, PPh], 5.64 [s, 2H, pzCH], 5.46 [s, 1H, pzCH], 2.65 [s, 6H, $pzCH_3$], 2.27 [s, 3H, $pzCH_3$], 2.13 [s, 6H, $pzCH_3$], 2.09 [s, 3H, $pzCH_3$]. $^{13}C\{^1H\}$ NMR (151 MHz, C_6D_6, 25ºC, δ): 297.2 [dd, $^2J_{CP}$ = 76, 5 Hz, W(CCl)Pt], 223.2 [d, $^3J_{CP}$ = 5 Hz, $^1J_{CW}$ = 67 Hz, CO], 153.6 151.0 [C^5(pz)], 143.8 142.7 [C^3(pz)], 136.5 [d, $^1J_{CP}$ = 37 Hz, $C^1(C_6H_5)$], 135.3 [d, $^2J_{CP}$ = 13 Hz, $C^{2,6}(C_6H_5)$], 134.7 [d, $^2J_{CP}$ = 12 Hz, $C^{2,6}(C_6H_5)$], 134.3 [d, $^1J_{CP}$ = 45 Hz, $C^1(C_6H_5)$], 128.9 [d, $^3J_{CP}$ = 12 Hz, $C^{3,5}(C_6H_5)$], 128.0 [$C^4(C_6H_5)$], 127.1 [d, $^3J_{CP}$ = 12 Hz, $C^{3,5}(C_6H_5)$], 106.6 106.4 [C^4(pz)], 16.4 15.9 12.4 12.2 [$pzCH_3$]. $^{31}P\{^1H\}$ NMR (162 MHz, C_6D_6, 25 ºC, δ): 41.89 [d, $^2J_{PP}$ = 23 Hz, $^1J_{PPt}$ = 4312 Hz], 24.39 [d, $^2J_{PP}$ = 23 Hz, $^1J_{PPt}$ = 2762 Hz]. $^{195}Pt\{^1H\}$ NMR (85.7 MHz, $CDCl_3$, 25ºC, δ): –3992 [dd, $^1J_{PtP}$ = 4316, 2760 Hz, $^1J_{PtW}$ = 345 Hz]. MS (ESI, *m/z*): Found: 1303.2570. Calcd for $C_{54}H_{52}{}^{11}BN_6O_2P_2{}^{35}Cl^{195}Pt^{184}W$ $[M]^+$: 1303.2566. Anal. Found: C, 49.73; H, 4.16; N, 7.08%. Calcd for $C_{54}H_{52}BClN_6O_2P_2PtW$: C, 49.73; H, 4.02; N, 6.44%. *Crystal data for* $2(C_{54}H_{52}BClN_6O_2P_2PtW)\cdot 2(C_2H_3N)$, M = 2690.41, triclinic, $P\bar{1}$, a = 11.5580 (2) Å, b = 21.0234 (3) Å, c = 24.0391 (5) Å, α = 71.013 (2)°, β = 80.492 (2)°, γ = 78.102 (1)°, V = 5374.29 (18) $Å^3$, Z = 2, ρ_{calc} = 1.663 Mgm^{-3}, μ(Cu $K\alpha$) = 10.10 mm^{-1}, T = 150(0) K, block 0.09 × 0.05 × 0.05 mm {clear light red}, 21031 independent measured reflections (θ = 73.7), R_1 = 0.044, wR_2 = 0.100 for 18930 reflections [$I > 2\sigma(I)$], 1357 parameters, 22 restraints. CDCC 2173046.

Synthesis of [MoPt(μ$_2$-CCl)(μ-CO)(dppe)(CO)(Tp*)] (2.4).

A yellow solution containing [Mo(≡CCl)$(CO)_2$(Tp*)] (0.100 g, 0.201 mmol) and [Pt(η^2-C_2H_4)$(PPh_3)_2$] (0.165 g, 0.221 mmol) was refluxed in THF (10 mL) for 30 minutes. The subsequent orange solution was cooled before a solution of dppe (0.094 g, 0.235 mmol) in THF (5 mL) was add, changing the orange solution to red over several hours. The reaction continued stirring at ambient temperature for 16 hours. Solvent was removed via rotary evaporation to give an orange/red residue that could be recrystallised from CH_2Cl_2/EtOH to give a red solid. The solid was collected via vacuum filtration, washed with EtOH (1 x 10 mL) and *n*-hexane (2 x 10 mL) before drying *in vacuo* for 4 hours to provide the title compound (0.136 g, 0.125 mmol, 62% isolated yield). Crystals suitable for single-crystal x-ray diffraction studies were grown from the vapour diffusion of *n*-hexane into a THF solution of the compound at ambient temperature over 4 nights. IR (CH_2Cl_2, cm^{-1}): 1911 vs ν_{CO}, 1808 sh ν_{CO}, 1772 s $\nu_{\mu\text{-}CO}$. IR (ATR, cm^{-1}): 2544 w ν_{BH}, 2526 w ν_{BH}, 1885 vs ν_{CO}, 1786 s $\nu_{\mu\text{-}CO}$, 1767 vs $\nu_{\mu\text{-}CO}$. ^1H NMR (700 MHz, C_6D_6, 25 ºC, δ): 7.73 [m, 4H, PPh], 7.51 [m, 4H, PPh], 6.96 [m, 3H, PPh], 6.92 [m, 3H, PPh], 6.83 [m, 3H, PPh], 6.79 [m, 3H, PPh],

5.40 [s, 2H, pzCH], 5.26 [s, 1H, pzCH], 2.53 [s, 3H, pzCH_3], 2.16 [s, 6H, pzCH_3], 1.96 [s, 6H, pzCH_3], 1.90 [s, 3H, pzCH_3], 1.84 [m, 4H, dppe-CH_2]. $^{13}C\{^1H\}$ NMR (151 MHz, C_6D_6, 25ºC, δ): 324.2 [d, $^2J_{CP}$ = 73 Hz, MoPt(CCl)], 232.9 [CO], 152.7 150.3 [C^5(pz)], 144.0 143.1 [C^3(pz)], 134.5 [d, $^2J_{CP}$ = 12 Hz, $C^{2,6}(C_6H_5)$], 133.5 [d, $^2J_{CP}$ = 12 Hz, $C^{2,6}(C_6H_5)$], 132.7 [dd, $^1J_{CP}$ = 36; $^2J_{CP}$ = 5 Hz, $C^1(C_6H_5)$], 130.5 [$C^4(C_6H_5)$], 130.3 [$C^4(C_6H_5)$], 128.6 [m, $C^{3,5}(C_6H_5)$], 107.1 106.6 [C^4(pz)], 31.09 [dt, $^1J_{CP}$ = 34; $^2J_{CP}$ = 14 Hz, PCH_2], 16.1 15.0 12.9 12.7 [pzCH_3]. $^{31}P\{^1H\}$ NMR (162 MHz, C_6D_6, 25 ºC, δ): 48.17 [d, $^2J_{PP}$ = 40 Hz, $^1J_{PPt}$ = 2675 Hz], 47.84 [d, $^2J_{PP}$ = 40 Hz, $^1J_{PPt}$ = 4031 Hz]. $^{195}Pt\{^1H\}$ NMR (85.7 MHz, C_6D_6, 25ºC, δ): –4203 [dd, $^1J_{PtP}$ = 4031, 2673 Hz]. MS (ESI, *m/z*): Found: 1035.1771. Calcd for $C_{42}H_{46}{}^{11}BN_6P_2{}^{35}Cl^{98}Mo^{195}Pt$ $[M–2CO]^+$: 1035.1743. Anal. Found: C, 48.46; H, 4.57; N, 7.54%. Calcd for $C_{44}H_{46}BClMoN_6O_2P_2Pt$: C, 48.48; H, 4.25; N, 7.71%. *Crystal data for* $C_{44}H_{46}BClMoN_6O_2P_2Pt$, M = 1090.10, triclinic, $P\bar{1}$, a = 10.6762 (2) Å, b = 13.5205 (4) Å, c = 15.4074 (4) Å, α = 83.317 (2)°, β = 89.918 (2)°, γ = 87.946 (2)°, V = 2207.48 (10) $Å^3$, Z = 2, ρ_{calc} = 1.640 Mgm^{-3}, μ(Cu $K\alpha$) = 9.76 mm^{-1}, T = 150(0) K, block 0.21 × 0.19 × 0.14 mm {clear light red}, 8625 independent measured reflections (θ = 73.6), R_1 = 0.029, wR_2 = 0.067 for 8509 reflections [$I > 2\sigma(I)$], 548 parameters, 7 restraints. CDCC 2173047.

Synthesis of [WPt(μ$_2$-CCl)(CO)$_3$(PPh$_3$)(Tp*)] (2.5).

A yellow solution of [W(≡CCl)(CO)$_2$(Tp*)] (0.203 g, 0.347 mmol) and [Pt(η^2-C_2H_4)(PPh$_3$)$_2$] (0.257 g, 0.344 mmol) was stirred in THF (36 mL) for 2 hours at 60 ºC. The solution darkened gradually to orange with red hues. Upon cooling to ambient temperature, carbon monoxide (CO) was bubbled through the mixture, immediately changing the colour from orange to a dark red. After one hour, excess CO was purged from the flask with N_2 and evaporated via a rotary evaporator to give a yellow/red solid that could be purified by flash column chromatography {silica gel, N_2, petroleum ether/CH_2Cl_2 gradient}. After eluting a yellow band of unreacted [W(≡CCl)(CO)$_2$(Tp*)], 20% CH_2Cl_2/petroleum ether eluted a deep red coloured band that could be recrystallised by concentration on a rotary evaporator. The resulting olive coloured solid was collected via vacuum filtration, washing with *n*-hexane (3 × 10 mL) before drying in vacuo for 16 hours. The olive-coloured solid was confirmed as the title compound (0.126 g, 0.118 mmol, 34% isolated yield), noting the deep red colour returns when redissolved. Furthermore, the yield of this reaction is reduced as heat also provides the μ$_2$-carbido complex [WPt(μ$_2$-C)Cl(PPh$_3$)$_2$(CO)$_2$(Tp*)] and incomplete consumption retains μ$_2$-halocarbyne [WPt(μ$_2$-CCl)(PPh$_3$)$_2$(CO)$_2$(Tp*)]. Crystals suitable for x-ray diffraction were grown from the vapour diffusion of *n*-hexane into a THF solution of compound at 0 °C. IR (CH_2Cl_2, cm^{-1}): 2027 vs ν_{CO}, 1917 vs ν_{CO}, 1833 vs ν_{CO}. IR (ATR, cm^{-1}): 2545 w ν_{BH}, 2040 vs ν_{CO}, 1917 vs ν_{CO}, 1843 vs ν_{CO}. Despite flash column chromatography,

minor amounts of bis-phosphine [WPt(μ-CCl)(PPh_3)$(CO)_2$(Tp*)] remain given similar retention properties. The corresponding signals in the following spectra are denoted by grey text. ^{1}H NMR (600 MHz, $CDCl_3$, 25 ºC, δ): 7.56 [m, 6H, PPh], 7.39 [m, 9H, PPh], 5.83 [s, 1H, pzCH], 5.77 [s, 2H, pzCH], 2.74 [s, 3H, pzCH_3], 2.41 [s, 6H, pzCH_3], 2.34 [s, 3H, pzCH_3], 2.06 [s, 6H, pzCH_3]. ^{13}C{^{1}H} NMR (151 MHz, $CDCl_3$, 25ºC, δ): 295.6 [d, $^2J_{CP}$ = 6; $^1J_{CW}$ = 151; $^1J_{CPt}$ = 885 Hz, WPt(=CCl)], 225.2 [d, $^1J_{CW}$ = 152 Hz, W-CO], 196.8 [$^1J_{CPt}$ = 1381 Hz], 154.0 151.0 [C^5(pz)], 145.1 143.5 [C^3(pz)], 134.1 [d, $^2J_{CP}$ = 12 Hz, $C^{2,6}(C_6H_5)$], 132.8 [d, $^1J_{CP}$ = 50 Hz, $C^1(C_6H_5)$], 130.5 [d, $^4J_{CP}$ = 3 Hz, $C^4(C_6H_5)$], 128.4 [d, $^3J_{CP}$ = 11 Hz, $C^{3,5}(C_6H_5)$], 107.5 106.6 [C^4(pz)], 16.7 15.6 12.9 [pz*C*H_3]. ^{31}P{^{1}H} NMR (283 MHz, $CDCl_3$, 25 ºC, δ): 35.69 [d, $^1J_{PPt}$ = 3857 Hz]. ^{195}Pt{^{1}H} NMR (150 MHz, $CDCl_3$, 25ºC, δ): –4197 [d, $^1J_{PtP}$ = 3840; $^1J_{PtW}$ = 295 Hz]. MS (ESI, *m/z*): Found: 1041.1670. Calcd for $C_{36}H_{37}{}^{11}BN_6O_2P^{35}Cl^{184}W^{195}Pt[M–CO]^+$:1041.1654. Anal. Found: C, 41.50; H, 3.60; N, 7.64%. Calc. for $C_{37}H_{37}BClN_6O_3PPtW$: C, 41.54; H, 3.49; N, 7.86%. *Crystal data for* $C_{37}H_{37}BClN_6O_3PPtW$, *M* = 1069.89, monoclinic, *P*$2_1/n$, *a* = 15.0798 (1) Å, *b* = 16.5138 (1) Å, *c* = 15.4322 (3) Å, β = 93.404 (1)º, *V* = 3836.22 (4) Å^3, *Z* = 4, ρ_{calc} = 1.852 Mgm^{-3}, μ(Cu *K*α) = 13.57 mm^{-1}, *T* = 150(0) K, prizm 0.18 × 0.10 × 0.08 {clear light pink}, 7008 independent measured reflections (θ = 73.7), R_1 = 0.024, wR_2 = 0.058 for 6747 reflections [$I > 2\sigma(I)$], 466 parameters. CDCC 2173048.

Synthesis of [$W_2Pt(\mu_2\text{-}CCl)_2(\mu_2\text{-}CO)_2(CO)_2(Tp^*)_2$] (2.6).

A yellow solution containing [(Tp*)W(≡CBr)$(CO)_2$] (0.050 g, 0.085 mmol) and [Pt(nbe)$_3$] (0.025 g, .052 mmol) was stirred in THF (20 mL) for 5 days at ambient temperature. The reaction was observed to darken to orange in several hours however by 24 hours appeared as a deep-red colour. It was at this time that solvent was removed via rotary evaporation to give a red residue which could be purified via flash column chromatography {silica gel, N_2, neat petroleum ether then 1:1 CH_2Cl_2/petroleum ether 60–80}. This step provided a red solution that could be recrystallised from the concentration of CH_2Cl_2 into *n*-hexane to give a maroon powder. The ensuing solid could be collected via vacuum filtration upon washing with *n*-hexane (3 x 10 mL) to give the title compound prior to drying *in vacuo* overnight (0.031 g, 0.023 mmol, 46% isolated yield). Crystals suitable for x-ray diffraction were grown from the slow evaporation of Et_2O at 0 °C. IR (CH_2Cl_2, cm^{-1}): 2555 w ν_{BH}, 1967 vs ν_{CO}, 1865 vs ν_{CO}, 1606 s $\nu_{\mu-CO}$. IR (ATR, cm^{-1}): 2542 w ν_{BH}, 1963 vs ν_{CO}, 1852 vs ν_{CO}, 1606 s $\nu_{\mu-CO}$. ^{1}H NMR (700 MHz, $CDCl_3$, 25 ºC, δ): 5.92 [br, 2H, pzCH], 5.85 [s, 2H, pzCH], 5.81 [s, pzCH], 2.66 [s, 6H, pzCH_3], 2.43 [br, 12H, pzCH_3], 2.36 [m, 12H, pzCH_3], 2.30 [br, 6H, pzCH_3]. ^{1}H NMR (700 MHz, $CDCl_3$, –40 ºC, δ): 5.94 5.87 5.81 [s, 2H, pzCH], 2.65 2.43

2.40 2.34 2.33 2.24 [s, 6H, pzCH_3]. $^{13}C\{^1H\}$ NMR (151 MHz, $CDCl_3$, –40 °C, δ): 267.9 [WPt(=*C*Cl)], 227.2 219.2 [CO], 153.4 153.1 152.5 [C^5(pz)], 145.6 144.1 143.9 [C^3(pz)], 107.5 107.2 106.8 [C^4(pz)], 17.3 15.6 15.5 [pzCH_3], 13.07 13.05 13.02 [overlapping singlets, pzCH_3]. $^{195}Pt\{^1H\}$ NMR (150 MHz, $CDCl_3$, –40 °C, δ): –2062 [*Pt*$(CCl)_2W_2$]. MS (ESI, *m/z*): Found: 1363.1827. Calcd for $C_{36}H_{44}{}^{11}B_2{}^{35}Cl^{37}ClN_{12}O_4{}^{195}Pt^{183}W_2$ $[M]^+$: 1363.1827. Anal. Found: C, 31.78; H, 3.28; N, 12.14%. Calcd for $C_{36}H_{44}B_2Cl_2N_{12}O_4PtW_2$: C, 31.70; H, 3.25; N, 12.32%. All single crystals suffered from rotational disorder of CO and CCl ligands in addition to multiple sites for the central platinum atom. For this reason this crystal is reported as a confirmation of connectivity but does not return metrical parameters of sufficient precision for detailed analysis. *Crystal data for* $C_{25.96}H_{44}B_2Cl_2N_{12}O_4Pt_{0.8}W_2{\cdot}0.19(Pt)$, M = 1361.59, triclinic, $P\bar{1}$, a = 10.4275 (7) Å, b = 10.6735 (7) Å, c = 11.3340 (9) Å, α = 73.274 (6), β = 64.083 (7)°, γ = 83.109 (5), V = 1086.56 (15) $Å^3$, Z = 1, ρ_{calc} = 2.081 Mgm^{-3}, μ(Cu *K*α) = 16.98 mm^{-1}, T = 150(0) K, plate, 0.10 × 0.06 × 0.04 mm {clear dark red}, 4291 independent measured reflections (θ = 73.4), R_1 = 0.037, wR_2 = 0.088 for 3579 reflections [$I > 2\sigma(I)$], 324 parameters. CCDC: 2173039.

Synthesis of [WPt(μ$_2$-C)Cl(CO)$_2$(PPh$_3$)$_2$(Tp*)] (2.7).

A yellow solution containing [(Tp*)W(≡CCl)$(CO)_2$] (0.204 g, 0.349 mmol) and [Pt$(PPh_3)_4$] (0.431 g, 0.346 mmol) was stirred in THF (20 mL) heated at reflux for 2 days. The subsequent orange solution had solvent removed via rotary evaporation to give an orange residue. Crude NMR found the title compound was in competition with bridging halocarbyne [WPt(=CCl)$(PPh_3)_2(CO)_2$(Tp*)] in a 1:4 ratio measured by $^{31}P\{^1H\}$ NMR spectroscopy. Attempts to isolate the halocarbyne compound included purification by flash column chromatography {silica gel, N_2, neat petroleum ether then neat CH_2Cl_2} eluting a major orange compound before removing solvent under reduced pressure. This was identified as pure title compound, [WPt(μ$_2$-C)Cl$(CO)_2(PPh_3)_2$(Tp*)], suggesting the sorbent of the flash column was sufficiently polar to initiate an isomerisation from the halocarbyne to the μ-carbido complex. A recrystallization from the evaporation of CH_2Cl_2 into EtOH by rotary evaporation gave a yellow solid which could be collected *via* vacuum filtration. The solid was washed with EtOH (2 x 10 mL) and n-hexane (10 mL) before drying in vacuo for 3 hours to afford compound **2.7** as a fine orange powder (0.124 g, 0.0951 mmol, 27% isolated yield). Crystals suitable for x-ray diffraction were grown from the vapour diffusion of *n*-hexane into a $CHCL_3$ solution of the title compound at 5 °C overnight. IR (CH_2Cl_2, cm^{-1}): 1945 vs ν_{CO}, 1852 vs ν_{CO}. IR (ATR, cm^{-1}): 2548 w ν_{BH}, 2539 w ν_{BH}, 1933 vs ν_{CO}, 1836 vs ν_{CO}. ^1H NMR (400 MHz, $CDCl_3$, 25 °C, δ): 7.96 – 7.90 [m, 6H, PPh], 7.43 – 7.40 [m, 9H, PPh], 7.39 – 7.34 [m, 6H, PPh], 7.14 [m, 3H, PPh], 6.96 [m, 6H, PPh], 5.55 [s, 2H, pzC*H*], 5.51 [s, 1H,

pzC*H*], 2.57 [s, 6H, pzCH_3], 2.32 [s, 6H, pzCH_3], 2.19 [s, 3H, pzCH_3], 2.00 [s, 3H, pzCH_3]. $^{13}C\{^1H\}$ NMR (151 MHz, $CDCl_3$, 25ºC, δ): 318.8 [t, $^2J_{CP}$ = 7 Hz, W≡C–Pt], 230.7 [$^1J_{CW}$ = 179 Hz, CO], 151.7 151.1 [C^5(pz)], 143.6 143.2 [C^3(pz)], 135.2 135.2 [overlapping doublets, $^2J_{CP}$ =11 Hz, $C^{2,6}(C_6H_5)$], 132.4 [dd, $^1J_{CP}$ = 53 Hz, $^3J_{CP}$ = 5 Hz, PPh], 131.7 130.7 [dd, $^1J_{CP}$ = 53 Hz, $^3J_{CP}$ = 5 Hz, $C^1(C_6H_5)$], 130.0 129.8 [$C^4(C_6H_5)$], 128.0 [d, $^2J_{CP}$ = 11 Hz, $C^{3,5}(C_6H_5)$], 127.2 [d, $^2J_{CP}$ = 10 Hz, $C^{3,5}(C_6H_5)$], 106.7 106.0 [C^4(pz)], 17.2 14.8 12.9 12.4 [pz*C*H_3]. $^{31}P\{^1H\}$ NMR (162 MHz, $CDCl_3$, 25 ºC, δ): 28.32 [d, $^2J_{PP}$ = 443 Hz, $^1J_{PPt}$ = 3200 Hz], 24.01 [d, $^2J_{PP}$ = 443 Hz, $^1J_{PPt}$ = 3223 Hz]. $^{195}Pt\{^1H\}$ NMR (85.7 MHz, $CDCl_3$, 25ºC, δ): –3718 [t, $^1J_{PtP}$ = 3223 Hz]. MS (ESI, *m*/*z*): Found: 1268.2902. Calcd for $C_{54}H_{52}BN_6O_2P_2PtW$ $[M–Cl]^+$: 1268.2877. Anal. Found: C, 49.82; H, 4.08; N, 6.47%. Calcd for $C_{54}H_{52}BClN_6O_2P_2PtW$: C, 49.73; H, 4.02; N, 6.44%. *Crystal data for* $C_{54}H_{52}BClN_6O_2P_2PtW$, *M* = 1304.15, monoclinic, $P2_1/n$, *a* = 9.5614 (1) Å, *b* = 22.6311 (2) Å, *c* = 23.3107 (3) Å, β = 98.430 (1)º, *V* = 4989.59(9) Å^3, *Z* = 4, ρ_{calc} = 1.736 Mgm^{-3}, μ(Cu *K*α) = 10.21 mm^{-1}, 85, *T* = 150(0) K, plate, 0.1 × 0.06 × 0.05 mm {clear light yellow}, 9939 independent measured reflections (θ = 73.6), R_1 = 0.032, wR_2 = 0.086 for 8797 reflections [$I > 2\sigma(I)$], 623 parameters. CDCC 2173042.

9.5 Synthetic procedures for Chapter Three compounds

Synthesis of [MoPt(μ$_2$-C)Br(CO)$_2$(PPh$_3$)$_2$(Tp*)] (3.1a).

This compound was prepared by a modified synthesis from literature precedent.[142] A mixture of [Mo(≡CBr)(CO)$_2$(Tp*)] (229 mg, 0.423 mmol) and [Pt(PPh$_3$)$_4$] (408 mg, 0.328 mmol) was stirred in toluene (20 mL) for 16 hours at 60 ºC. Originally a yellow solution, this quickly darkened and concluded as a brown solution. Solvent was removed via rotary evaporation to give a crude orange solid (854 mg).†† Flash column chromatography {silica gel, N_2, neat petroleum ether then neat CH_2Cl_2} was performed eluting a major yellow compound before removing solvent under reduced pressure. Recrystallisation from concentration of CH_2Cl_2 into *n*-hexane afforded an orange powder. This was collected via vacuum filtration and dried *in vacuo* for 1 hour to afford the title compound (232 mg, 0.184 mmol, 56% yield). IR (CH_2Cl_2, cm^{-1}): 1962 vs ν_{CO}. 1873 vs ν_{CO}. ^1H NMR (400 MHz, $CDCl_3$, 25 ºC, δ): 7.91 – 7.98 [m, 6H, PPh], 7.48 – 7.38 [m, 14H, PPh], 7.21 – 7.12 [m, 4H, PPh], 7.00 [dt, $^1J_{HH}$ = 8 Hz, $^2J_{HH}$ = 4 Hz, PPh], 5.54 [s, 2H, pzCH], 5.49 [s, 1H, pzCH], 2.58 [s, 6H, pzCH$_3$], 2.34 [s, 6H, pzCH$_3$], 2.20 [s, 3H, pzCH$_3$], 1.96 [s, 3H, pzCH$_3$]. $^{13}C\{^1H\}$ NMR (151 MHz, $CDCl_3$, 25ºC, δ): 335.7 [m, Mo≡*C*–Pt], 232.8 [CO], 150.7 150.4 [C^5(pz)], 143.5 143.3 [C^3(pz)], 135.3 [d, $^2J_{CP}$ = 11 Hz, $C^{2,6}(C_6H_5)$], 135.2 [d, $^2J_{CP}$ = 10 Hz, $C^{2,6}(C_6H_5)$], 132.2 [dd, $^1J_{CP}$ = 53 Hz, $^3J_{CP}$

†† Immediate recrystallisation proved unsuccessful due to the presence of minor products.

= 5 Hz, $C^1(C_6H_5)$], 131.0 (dd, $^1J_{CP}$ = 53 Hz, $^3J_{CP}$ = 5 Hz, $C^1(C_6H_5)$], 130.2 129.9 [$C^4(C_6H_5)$], 129.0 [d, $^2J_{CP}$ = 10 Hz, $C^{3,5}(C_6H_5)$], 127.3 [d, $^2J_{CP}$ = 11 Hz, $C^{3,5}(C_6H_5)$], 106.4 105.7 [C^4(pz)], 16.7 14.3 13.0 12.5 [pzCH_3]. ^{31}P NMR (162 MHz, $CDCl_3$, 25 ºC, δ): 23.76 [d, $^2J_{PP}$ = 438 Hz, PPh], 19.38 [d, $^2J_{PP}$ = 438 Hz, PPh]. ^{195}Pt NMR (85.7 MHz, $CDCl_3$, 25ºC, δ): –3810 [t, $^1J_{PtP}$ = 3200 Hz]. MS (ESI, *m/z*): calcd for $C_{54}H_{53}BBrMoN_6O_2P_2Pt$ $[M+H]^+$: 1262.16823. Found: 1262.16794. Anal. Calcd for $C_{54}H_{52}BBrN_6O_2P_2Pt$: C, 51.45; H, 4.16; N, 6.67 %. Found: C, 51.33; H, 4.00; N, 6.66 %. CCDC 1988587.

Synthesis of [WPt(μ$_2$-C)Br(CO)$_2$(PPh$_3$)$_2$(Tp*)] (3.1b) – Single Rotamer.

Note: This compound exists as a single rotomer.

A yellow solution containing [(Tp*)W(≡CBr)(CO)$_2$] (5.000 g, 7.949 mmol) and [Pt(η^2-C_2H_4)(PPh_3)$_4$] (5.944 g, 7.949 mmol) was stirred in toluene (100 mL) for four days at 60 ºC. The subsequent orange solution had solvent removed *via* rotary evaporation to give a crude residue. Flash column chromatography {silica gel, N_2, neat petroleum ether then neat CH_2Cl_2} was performed eluting a major orange compound before removing solvent under reduced pressure. A recrystallization from the evaporation of CH_2Cl_2 into EtOH by rotary evaporation gave an orange solid which could be collected via vacuum filtration. The solid was washed with EtOH (2 x 10 mL) and n-hexane (10 mL) before drying in vacuo for 3 hours to afford compound **3.1b** as a fine orange powder (8.394 g, 6.224 mmol, 78% yield). Crystals suitable for x-ray diffraction were grown from the slow evaporation of Et_2O at 0 °C. IR (CH_2Cl_2, cm^{-1}): 1945 vs ν_{CO}, 1854 vs ν_{CO}. IR (ATR, cm^{-1}): 1935 vs ν_{CO}, 1838 vs ν_{CO}, 1094 w ν_{WCPt}. ^{1}H NMR (400 MHz, $CDCl_3$, 25 ºC, δ): 7.94 [m, 6H, PPh], 7.48 – 7.37 [m, 15H, PPh], 7.13 [m, 3H, PPh], 6.96 [m, 6H, PPh], 5.56 [s, 2H, pzCH], 5.50 [s, 1H, pzCH], 2.58 [s, 6H, pzCH_3], 2.31 [s, 6H, pzCH_3], 2.17 [s, 3H, pzCH_3], 1.98 [s, 3H, pzCH_3]. ^{13}C{^{1}H} NMR (151 MHz, $CDCl_3$, 25ºC, δ): 317.2 [t, $^2J_{CP}$ = 8 Hz, W≡*C*–Pt], 230.7 [$^1J_{CW}$ = 179 Hz, CO], 151.7 151.2 [C^5(pz)], 143.5 143.3 [C^5(pz)], 135.3 [d, $^2J_{CP}$ =11 Hz, $C^{2,6}(C_6H_5)$], 135.2 [d, $^2J_{CP}$ =11 Hz, $C^{2,6}(C_6H_5)$], 132.4 [dd, $^1J_{CP}$ = 53 Hz, $^3J_{CP}$ = 5 Hz, $C^1(C_6H_5)$], 131.3 [dd, $^1J_{CP}$ = 53 Hz, $^3J_{CP}$ = 5 Hz, $C^1(C_6H_5)$], 130.0 129.8 [$C^4(C_6H_5)$], 128.0 [d, $^3J_{CP}$ = 11 Hz, $C^{3,5}(C_6H_5)$], 127.2 [d, $^3J_{CP}$ = 11 Hz, $C^{3,5}(C_6H_5)$], 106.7 106.0 [C^4(pz)], 17.4 14.8 12.9 12.4 [pzCH_3)]. ^{31}P{^{1}H} NMR (162 MHz, $CDCl_3$, 25 ºC, δ): 26.25 [d, $^2J_{PP}$ = 443 Hz, $^1J_{PPt}$ = 3178 Hz], 22.19 [d, $^2J_{PP}$ = 443 Hz, $^1J_{PPt}$ = 3200 Hz]. ^{195}Pt NMR (85.7 MHz, $CDCl_3$, 25ºC, δ): –3821 [t, $^1J_{PtP}$ = 3200 Hz]. MS (ESI, *m/z*): Found: 1347.20589. Calcd for $C_{54}H_{52}BBrN_6O_2P_2PtW$ $[M]^+$: 1347.20534. Anal. Found: C, 48.91; H, 3.80; N, 6.26%. Calcd for $C_{54}H_{52}BBrN_6O_2P_2PtW$: C, 48.09; H, 3.89; N, 6.23%. *Crystal data for* $C_{54}H_{52}BBrN_6O_2P_2PtW$, M = 1648.61, monoclinic, $P2_1/n$, a = 9.5923 (1) Å, b = 22.6404 (4) Å, c = 23.4154 (3) Å, β = 98.636 (1)º, V = 5027.55(12) Å^3, Z = 4, ρ_{calc} = 1.782 Mgm^{-3}, μ(Cu

*K*α) = 11.21 mm^{-1}, *T* = 150(0) K, plate {clear light orange}, 9886 independent measured reflections (θ = 73.8), R_1 = 0.037, wR_2 = 0.098 for 8545 reflections [$I > 2\sigma(I)$], 619 parameters. CDCC 1988588.

Synthesis of [WPt(μ$_2$-C)Br(CO)$_2$(PPh$_3$)$_2$(Tp*)] (3.1b) – Rotormeric Mixture.

Note: This compound exists as a pair of inseparable rotational isomers.

A yellow solution containing [W(≡CBr)(CO)$_2$(Tp*)] (0.783 g, 1.24 mmol) and [Pt(PPh$_3$)$_4$] (1.480 g, 1.190 mmol) was stirred in benzene (36 mL) for 16 hours at 60 ºC. The resulting orange solution was evaporated under reduced pressure to give a crude residue solid. Now exposed to air, a subsequent recrystallization from the evaporation of CH_2Cl_2 into EtOH by rotary evaporation gave an orange solid which could be collected via vacuum filtration. The solid was washed with EtOH (2 x 10 mL) and n-hexane (10 mL) before drying in vacuo for 4 hours to afford compound the listed compound as a fine orange powder (1.23 g, 0.920 mmol, 77% yield). Crystals suitable for single crystal X-ray diffraction were grown from the slow evaporation of Et_2O at 0 ºC. IR (CH_2Cl_2, cm^{-1}): 1988 vs ν_{CO}, 1948 vs ν_{CO}, 1894 vs ν_{CO}, 1854 vs ν_{CO}. ^{1}H NMR (600 MHz, $CDCl_3$, 25 ºC, δ): 7.98 – 7.91 [m, 12H, PPh], 7.43–7.39 [m, 27H, PPh], 7.16–7.11 [m, 6H, PPh], 7.00–6.95 [m, 11H, PPh], 5.56 [s, 2H, pzCH], 5.55 [s, 2H, pzCH], 5.51 [s, 1H, pzCH], 5.50 [s, 1H, pzCH], 2.58 [s, 6H, pzCH$_3$], 2.57 [s, 6H, pzCH$_3$], 2.33 [s, 6H, pzCH$_3$], 2.32 [s, 6H, pzCH$_3$], 2.19 [s, 3H, pzCH$_3$], 2.18 [s, 3H, pzC*H*$_3$], 2.00 [s, 3H, pzCH$_3$], 1.99 [s, 3H, pzCH$_3$]. ^{13}C{^{1}H} NMR (151 MHz, $CDCl_3$, 25ºC, δ): 318.7 317.1 [W≡*C*–Pt], 230.7 [$^1J_{CW}$ = 178 Hz, CO], 151.6 151.5 151.0 [C^5(pz)], 143.4 143.3 143.1 143.0 [C^3(pz)], 135.2–134.8 [m, PPh], 131.8 [dd, $^1J_{CP}$ = 53, $^3J_{CP}$ = 5 Hz; C^1(C_6H_5)], 130.0 129.8 [C^4(C_6H_5)], 128.0 [t, $^3J_{CP}$ = 11 Hz, C^{3,5}(C_6H_5)], 127.3 [t, $^3J_{CP}$ = 11 Hz, C^{3,5}(C_6H_5)], phenyl resonances from the corresponding single isomer are omitted for clarity, 106.5 105.8 [C^4(pz)], 17.2 17.0 14.7 12.7 12.2 [pzCH$_3$]. ^{31}P{^{1}H} NMR (162 MHz, $CDCl_3$, 25 ºC, δ): 28.27 [d, $^2J_{PP}$ = 443 Hz], 26.21 [d, $^2J_{PP}$ = 443 Hz], 23.91 [d, $^2J_{PP}$ = 443 Hz], 22.11 [d, $^2J_{PP}$ = 443 Hz]. ^{195}Pt NMR (85.7 MHz, $CDCl_3$, 25ºC, δ): –3718 [t, $^1J_{PtP}$ = 3214 Hz], –3821 [t, $^1J_{PtP}$ = 3202 Hz]. MS (ESI, *m*/*z*): calcd for $C_{54}H_{52}BN_6O_2P_2PtW$ [M–Br]$^+$: 1268.2890. Found: 1268.2884. Anal. Calcd for $C_{54}H_{52}BBrN_6O_2P_2PtW$: C, 48.09; H, 3.89; N, 6.23%. Found: C, 48.10; H, 4.04; N, 6.19%.

Synthesis of [WPt(μ$_2$-C)(NCMe)(CO)$_2$(PPh$_3$)$_2$(Tp*)]OTf (3.2).

A solution of [WPt(μ$_2$-C)Br(CO)$_2$(PPh$_3$)$_2$(Tp*)] (**3.1b**; 94 mg, 70 μmol) and AgOTf (29 mg, 113 μmol) was stirred in acetonitrile (10 mL). The reaction was concluded after 2 hours as identified by ^{31}P NMR spectroscopic analysis to present a grey precipitate and a bright orange supernatant phase. The supernatant was collected *via* filter cannula and solvent removed under reduced

pressure to provide a crude mass of 95 mg as an orange semi-crystalline solid. The solid was sonicated in Et_2O (3 x 10 mL) decanting each time, allowing for orange solid. Recrystallisation from MeCN/Et_2O afforded red crystals identified as the title compound. (34 mg, 23 μmol, 33% yield). These crystals were also suitable for x-ray diffraction. IR (CH_2Cl_2, cm^{-1}): 1967 vs ν_{CO}, 1949 vs ν_{CO}, 1872 vs ν_{CO}, 1856 vs ν_{CO}. ^{1}H NMR (400 MHz, $CDCl_3$, 25 ºC, δ): 7.94 – 7.81 [m, 5H, PPh], 7.48 [bs, 8H, PPh], 7.40–7.31 [m, 3H, PPh], 7.29–7.15 [m, 11H, PPh], 7.14–7.02 [m, 7H, PPh], 6.92–6.73 [m, 2H, PPh], 5.50 [s, 1H, pzCH], 5.42 [s, 1H, pzCH], 5.22 [s, 1H, pzCH], 2.31 [s, 5H, $pzCH_3$], 2.27 [s, 5H, $pzCH_3$], 2.10 [s, 3H, $pzCH_3$], 1.92 [s, 3H, $pzCH_3$], 1.84 [s, 2H, $pzCH_3$], 1.03 [s, 3H, $NCCH_3$]. ^{13}C{^{1}H} NMR (150 Hz, $CDCl_3$, 25 ºC, δ): 300.1 [dd, $^2J_{CP}$ = 10, $^2J_{CP}$ = 4 Hz, W≡C–Pt], 229.2 [$^1J_{CW}$ = 174 Hz, CO], 151.9 150.9 [C^5(pz)], 144.2 143.9 [C^3(pz)], 134.7 134.4 [d, $^3J_{CP}$ = 11 Hz, $C^{3,5}(C_6H_5)$], 131.8 131.6 [d, $^4J_{CP}$ = 3 Hz, $C^4(C_6H_5)$] 129.2 128.6 [d, $^2J_{CP}$ = 11 Hz, $C^{2,6}(C_6H_5)$], 116.5 (Pt–N*C*Me), 106.9 106.4 [C^4(pz)], 17.2 14.7 12.9 12.5 [$pzCH_3$], 2.01 [$NCCH_3$]. ^{19}F{^{1}H} NMR (377 MHz, $CDCl_3$, 25 ºC, δ): –78.0 [1F, $^-$OTf]. ^{31}P{^{1}H} NMR (161 MHz, $CDCl_3$, 25 ºC, δ): 23.29 [d, $^2J_{PP}$ = 385, $^1J_{PPt}$ = 3169 Hz, PPh], 19.68 [d, $^2J_{PP}$ = 385, $^1J_{PPt}$ = 3093 Hz, PPh_3]. These second order spin-coupled doublets are weighted according to literature procedure. ^{195}Pt NMR (85.7 MHz, $CDCl_3$, 25ºC, δ): –3832 [t, $^1J_{PtP}$ = 3132 Hz]. MS (ESI, *m/z*): calcd for $C_{57}H_{55}BF_3N_7O_5P_2PtSW$ $[M\text{-}MeCN\text{-}H]^+$: 1268.2883. Found: 1268.2900. Anal. Calcd for $C_{57}H_{55}BF_3N_7O_5P_2PtSW$: C, 46.86; H, 3.81; N, 6.73%. Found: C, 46.84; H, 3.80; N, 6.79%. *Crystal data for* $C_{54}H_{52}BBrN_6O_2P_2PtW$, *M* = 1614.43, monoclinic, $P2_1/c$, *a* = 24.2079 (16) Å, *b* = 10.5921 (5) Å, *c* = 26.1839 (17) Å, β = 116.111 (8)º, *V* = 6028.7 (7) Å^3, *Z* = 4, ρ_{calc} = 1.779 Mgm^{-3}, μ(Cu *K*α) = 5.27 mm^{-1}, *T* = 150(0) K, block {clear light orange}, 15101 independent measured reflections (θ = 79.3), R_1 = 0.064, wR_2 = 0.157 for 11224 reflections [$I > 2\sigma(I)$], 766 parameters, 0 restraints. Due to low precision, the .cif file was not deposited with the CCDC. Available from author on request.

Synthesis of [MoPt(μ$_2$-C)Br(CO)$_2$(dppe)(Tp*)] (3.3a).

The compounds [Mo(≡CBr)(CO)$_2$(Tp*)] (92 mg, 73 μmol) and dppe (37 mg, 93 μmol) were dissolved in toluene (10 mL) to afford an yellow solution. Stirring for 16 hours allowed for a yellow suspension. Solvent was removed via rotary evaporation to give a yellow solid. This was purified via flash column chromatography {silica gel, N_2, gradient elution}. A bright yellow band was eluted with neat CH_2Cl_2 and was subsequently recrystallised from CH_2Cl_2/*n*-hexane to give a yellow powder. This was collected *via* vacuum filtration, washed with *n*-pentane and dried *in vacuo* for 4 hours to give the title compound (74 mg, 65 μmol, 89% yield). IR (CH_2Cl_2, cm^{-1}): 1965 vs ν_{CO}, 1876 vs ν_{CO}. ^{1}H NMR (400 MHz, $CDCl_3$, 25 ºC, δ): 7.82 [m, 5H, PPh], 7.67 [m, 5H, PPh], 7.44 [m, 5H,

PPh], 7.11 [m, 5H, PPh], 5.62 [s, 2H, pzCH], 5.58 [s, 1H, pzCH], 2.47 [bs, 6H, $pzCH_3$], 2.35 [s, 6H, $pzCH_3$], 2.28 [s, 3H, $pzCH_3$], 2.23 [m, 3H, $pzCH_3$], 1.97 [m, 4H, PCH_2]. $^{13}C\{^1H\}$ NMR (151 MHz, CD_2Cl_2, 25 ºC, δ): 377.1 [bd, $^2J_{CP}$ = 77 Hz, Mo≡*C*–Pt], 231.5 [CO], 151.5 151.3 [C^5(pz)], 145.1 144.3 [C^3(pz)], 134.3 [d, $^2J_{CP}$ = 11 Hz, $C^{2,6}(C_6H_5)$], 134.1 [d, $^2J_{CP}$ = 11 Hz, $C^{2,6}(C_6H_5)$], 132.0 131.7 [$C^4(C_6H_5)$], 130.6 [d, $^2J_{CP}$ = 46 Hz, PPh], 129.3 [d, $^3J_{CP}$ =10 Hz, $C^{3,5}(C_6H_5)$], 128.7 [d, $^3J_{CP}$ =10 Hz, $C^{3,5}(C_6H_5)$], 106.4 106.0 [C^4(pz)], 30.8 [m, P*C*H_2], 24.9 [dd, $^1J_{CP}$ = 31 Hz, $^2J_{CP}$ = 7 Hz, P*C*H_2], 16.6 14.6 13.1 12.7 [$pzCH_3$]. $^{31}P\{^1H\}$ NMR (161 MHz, $CDCl_3$, 25 ºC, δ): 33.60 [bs, $^1J_{PPt}$ = 1548 Hz, *cis*-PPh_2], 32.89 [bs, $^1J_{PPt}$ = 4053 Hz, *trans*-PPh_2]. ^{195}Pt NMR could not be detected irrespective of solvent or temperature (–60–50 ºC), this is predicted to be caused by coupling and broadening. MS (ESI, *m/z*): calcd for $C_{44}H_{46}B^{81}BrMoN_6O_2P^{195}Pt$ $[M]^+$: 1135.11396. Found: 1135.11401. Anal. Calcd for $C_{44}H_{46}BBrMoN_6O_2P_2Pt$: C, 46.58; H, 4.09; N, 7.41%. Found: C, 46.37; H, 3.95; N, 7.34%. *Crystal data for* $C_{44}H_{46}BBrMoN_6O_2P_2Pt$, *M* = 1293.18, monoclinic, *C*2/*c*, *a* = 42.7794 (12) Å, *b* = 10.3970 (3) Å, *c* = 20.4764 (7) Å, β = 94.581 (3)º, *V* = 9078.3 (5) Å^3, *Z* = 7, ρ_{calc} = 1.656 Mg m^{-3}, μ(Cu *K*α) = 4.35 mm^{-1}, *T* = 150(0) K, plate {clear light yellow}, 9240 independent measured reflections (θ = 26.4 º), R_1 = 0.040, wR_2 = 0.089 for 7954 reflections [$I > 2\sigma(I)$], 529 parameters, 0 restraints. CDCC 1997713.

Synthesis of [WPt(μ$_2$-C)Br(CO)$_2$(PPh$_3$)$_2$(Tp*)] (3.3b).

A solution of [WPt(μ$_2$-C)Br(CO)$_2$(PPh$_3$)$_2$(Tp*)] (608 mg, 0.450 mmol) and dppe (178 mg, 0.446 mmol) was stirred in toluene (20 mL) for 4 hours at 70 ºC. Beginning as an orange solution, the reaction colour lessened and a yellow solid precipitated. Solvent was removed *via* rotary evaporation before recrystallisation from the concentration of CH_2Cl_2 into *n*-hexane gave a yellow solid. This solid was collected *via* vacuum filtration and washed with *n*-hexane (10 mL) before drying *in vacuo* for 4 hours to give the listed compound as a yellow powder (508 mg, 0.416 mmol, 94% yield). Crystals suitable for x-ray diffraction were grown from the vapour diffusion of Et_2O into a solution of **3.3b** in acetonitrile. IR (CH_2Cl_2, cm^{-1}): 1950 vs ν_{CO}, 1856 vs ν_{CO}. ^1H NMR (400 MHz, $CDCl_3$, 25 ºC, δ): 7.86–7.78 [m, 5H, PPh], 7.71–7.64 [m, 5H, PPh], 7.46–7.42 [m, 5H, PPh], 7.39 [s, 4H, PPh], 7.17–7.05 [m, 5H, PPh], 5.62 [s, 2H, pzCH], 5.58 [s, 1H, pzCH], 2.47 and 2.45 [overlapping s, 6H, $pzCH_3$], 2.35 [s, 6H, $pzCH_3$], 2.28 [s, 3H, $pzCH_3$], 2.23 [s, 3H, $pzCH_3$], 2.03–1.93 [m, 4H, PCH_2]. $^{13}C\{^1H\}$ NMR (151 MHz, CD_2Cl_2, 25 ºC, δ): 356.7 [bd, $^2J_{CP}$ = 74 Hz, W≡C–Pt], 229.4 [$^1J_{CW}$ = 177 Hz, CO], 152.4 152.0 [C^5(pz)] 145.2 144.3 [C^3(pz)], 134.3 134.1 [d, $^3J_{CP}$ = 11 Hz, $C^{3,5}(C_6H_5)$], 131.9 131.6 [$C^4(C_6H_5)$], 130.8 [d, $^1J_{CP}$ = 45 Hz, $C^1(C_6H_5)$], 129.2 [d, $^2J_{CP}$ = 11 Hz, $C^{2,6}(C_6H_5)$], 128.7 [d, $^2J_{CP}$ = 11 Hz, $C^{2,6}(C_6H_5)$], 106.6 106.3 [C^4(pz)], 31.3 [bs, PCH_2], 25.0 [d, $^1J_{CP}$ = 31 Hz, PCH_2], 17.4 15.2 13.1 12.7 [$pzCH_3$]. $^{31}P\{^1H\}$ NMR (162 MHz, $CDCl_3$, 25 ºC, δ): 38.10

[bs, $^{1}J_{PPt}$ = 1526 Hz, *cis*-*P*Ph$_3$], 34.51 [bs, $^{1}J_{PPt}$ = 4068 Hz, *trans*-*P*Ph]. ^{195}Pt NMR could not be detected irrespective of solvent or temperature (–60–50 ºC), this is predicted to be caused by coupling and broadening. MS (ESI, *m*/*z*): calcd for $C_{44}H_{46}B^{81}BrN_6O_2P_2{}^{195}Pt^{184}W$ $[M+H]^+$: 1222.1665. Found: 1222.1672. Anal. Calcd for $C_{44}H_{46}BBrN_6O_2P_2PtW$: C, 46.13; H, 4.69; N, 6.38%. Found: C, 46.05; H, 4.74; N, 6.28%. *Crystal data for* $C_{44}H_{46}BBrN_6O_2P_2PtW{\cdot}2(C_2H_3N)$, *M* = 1304.57, monoclinic, *P*2$_1$, *a* = 12.1891 (1) Å, *b* = 10.5285 (1) Å, *c* = 19.6792 (1) Å, β = 108.011 (1)º, *V* = 2401.73 (4) Å^3, *Z* = 2, ρ_{calc} = 1.804 Mg m^{-3}, μ(Cu *K*α) = 11.71 mm^{-1}, *T* = 150(0) K, needle 0.24 × 0.11 × 0.04 mm {clear light orange}, 9573 independent measured reflections (θ = 73.9 º), R_1 = 0.027, wR_2 = 0.073 for 9520 reflections [$I > 2\sigma(I)$], 585 parameters, 1 restraint. CDCC 1997712.

Synthesis of [WPt(μ$_2$-C)(S$_2$CNEt$_2$)(CO)$_2$(PPh$_3$)(Tp*)] (3.4).

A solution containing [WPt(μ$_2$-C)Br(CO)$_2$(PPh$_3$)$_2$(Tp*)] (156 mg, 116 mmol) and sodium *N*-diethyldithiocarbamate dihydrate (25 mg, 140 μmol) in toluene (20 mL) was heated at reflux for 4 hours. The resulting yellow solution was filtered through celite and evaporated under reduced pressure producing a yellow powder. This powder was be recrystallised from CH_2Cl_2/*n*-hexane to give a yellow microcrystalline powder that was collected by vacuum filtration, washed with *n*-hexane and dried *in vacuo* affording the title compound (125 mg, 108 μmol, 93% isolated yield). IR (CH_2Cl_2, cm^{-1}): 1935 vs ν_{CO}, 1843 vs ν_{CO} cm^{-1}. ^{1}H NMR (700 MHz, $CDCl_3$, 25 ºC, δ): 7.45 [t, $^{1}J_{HH}$ = 9 Hz, 3H, PPh], 7.22 [br, 3H, PPh], 2.02 [br, 6H, PPh], 5.63 [s, 1H, pzCH], 5.59 [s, 2H, pzCH], 3.78 [d, $^{1}J_{HH}$ = 8 Hz, 2H, C^1(NEt)], 3.56 [d, $^{1}J_{HH}$ = 8 Hz, 2H, C^1(NEt)], 2.38 [s, 15H, pzCH$_3$], 2.26 [s, 3H, pzCH$_3$], 21.35 [t, $^{1}J_{CP}$ = 7 Hz, 3H, C^2(NEt)], 1.17 [t, $^{1}J_{CP}$ = 7 Hz, 3H, C^2(NEt)]. ^{13}C{^{1}H} NMR (176 MHz, $CDCl_3$, 25ºC, δ): 338.4 [d, $^{2}J_{CP}$ = 6 Hz, W≡C–Pt], 227.0 [$^{1}J_{CW}$ = 177 Hz, CO], 208.3 [S$_2$C], 152.2 151.7 [C^5(pz)], 144.1 143.0 [C^3(pz)], 134.4 [d, $^{2}J_{CP}$ = 11 Hz, C^{2,6}(C$_6$H$_5$)], 130.5 [C^4(C$_6$H$_5$)], 130.3 [d, $^{1}J_{CP}$ = 57 Hz, C^1(C$_6$H$_5$)], 127.8 [d, $^{3}J_{CP}$ = 11 Hz, C^{3,5}(C$_6$H$_5$)], 106.2 105.9 [C^4(pz)], 44.8 43.8 [C^1(NEt)], 16.5 15.4 12.8 12.6 [pzCH$_3$], 12.7 12.5 [C^2(NEt)]. ^{31}P{^{1}H} NMR (162 MHz, $CDCl_3$, 25 ºC, δ): 13.68 [s, $^{1}J_{PPt}$ = 3880 Hz]. ^{195}Pt{^{1}H} NMR (85.7 MHz, $CDCl_3$, 25ºC, δ): –3828 [d, $^{1}J_{PtP}$ = 3889 Hz]. MS (ESI, *m*/*z*): Found 1154.22514. Calcd for $C_{41}H_{47}BN_7NaO_2PPtS_2W$ $[M+Na]^+$: 1154.22876. Anal. Found: C, 40.30; H, 3.35; N, 7.55%. Calcd for $C_{41}H_{47}BN_7O_2PPtS_2W{\cdot}CH_2Cl_2$: C, 40.69; H, 2.98; N, 7.91%. *Crystal data for* $C_{41}H_{47}BN_7O_2PPtS_2$, *M* = 1154.69, triclinic, $P\bar{1}$, *a* = 12.5263 (2) Å, *b* = 12.9390 (2) Å, *c* = 13.8769 (2) Å, α = 76.435 (1)°, β = 89.141 (1)º γ = 82.519 (1)°, *V* = 2167.50 (6) Å^3, *Z* = 2, ρ_{calc} = 1.769 Mgm^{-3}, μ(Cu *K*α) = 12.37 mm^{-1}, *T* = 150(0) K, plate 0.13 × 0.05 × 0.03 mm {clear light orange}, 8662 independent measured

reflections (θ = 73.6), R_1 = 0.027, wR_2 = 0.071 for 7905 reflections [$I > 2\sigma(I)$], 513 parameters. CDCC 1997714.

Synthesis of [WPt(μ$_2$-C)(Bm^{Me})(CO)$_2$(PPh$_3$)(Tp*)] (3.5).

Upon stirring [WPt(μ$_2$-C)Br(CO)$_2$(PPh$_3$)$_2$(Tp*)] (99 mg, 73 μmol) with NaBm^{Me} (24 mg, 92 μmol) in CH_2Cl_2 (10 mL), the orange solution quickly transitioned to a yellow colour. This was further stirred for 16 hours remaining yellow. Solvent was removed *via* rotary evaporation to give an orange glass. Flash column chromatography {silica gel, N_2, isocratic elution, neat CH_2Cl_2 then 8% THF/CH_2Cl_2} was performed allowing for a yellow eluate to be collected. The solvent was removed before recrystallisation by concentration of CH_2Cl_2 into *n*-hexane under reduced pressure afforded a yellow microcrystalline powder. This was collected by vacuum filtration, washed with *n*-pentane (10 mL) before drying *in vacuo* for 2 hours. This was identified to be the title compound (70 mg, 56 μmol, 77% yield). Fluxional processes operate when this molecule is in solution. It is for this reason that not all signals can be completely assigned. IR (CH_2Cl_2, cm^{-1}): 1940 vs ν_{CO}, 1848 vs ν_{CO}. ^{1}H NMR (400 MHz, $CDCl_3$, 25 ºC, δ): 7.45–7.32 [m, 4H, PPh], 7.28 [s, 1H overlapping $CDCl_3$, PPh], 7.24 [s, 2H overlapping $CDCl_3$, PPh], 7.19–7.16 [m, 5H, PPh], 7.06 [bs, 3H, PPh], 6.82 [s, 2H, Bm^{Me}CH], 6.68 [s, 2H, Bm^{Me}CH], 5.60 [s, 1H, pzCH], 5.56 [s, 2H, pzCH], 4.47 [bs, 2H, BH], 3.80 [s, 3H, Bm^{Me}CH$_3$], 3.64 [s, 3H, Bm^{Me}CH$_3$], 2.38 [s, 3H, pzCH$_3$], 2.36 [s, 6H, pzCH$_3$], 2.34 [s, 6H, pzCH$_3$], 2.22 [s, 3H, pzCH$_3$]. ^{13}C{^{1}H} NMR (151 MHz, $CDCl_3$, 25 ºC, δ): 328.8 [d, $^2J_{CP}$ = 8, $^1J_{CPt}$ = 793 Hz, W≡C–Pt], 227.9 [$^1J_{CW}$ = 178 Hz, CO], 158.3 154.3 [C^1(im)], 152.1 151.6 [C^5(pz)], 143.7 142.8 [C^3(pz)], 138.0 [C_6H_5], 134.4 [d, $^2J_{CP}$ = 11 Hz, C^{2,6}(C_6H_5)], 130.9 [d, $^1J_{CP}$ = 57 Hz, C^1(C_6H_5)], 129.5 [C^4(C_6H_5)], 127.1 [d, $^3J_{CP}$ = 11 Hz, C^{3,5}(C_6H_5)], 123.8 123.7 [C^4(im)], 119.1 117.9 [C^3(im)], 106.3 105.8 [C^4(pz)], 35.7 34.2 [imCH$_3$], 16.9 15.4 12.8 12.6 [pzCH$_3$]. ^{31}P{^{1}H} NMR (162 MHz, $CDCl_3$, 25 ºC, δ): 14.62 [s, $^1J_{PPt}$ = 3979 Hz]. ^{195}Pt{^{1}H} NMR (85.7 MHz, $CDCl_3$, 25ºC, δ): –3561 [d, $^1J_{PtP}$ = 3994 Hz]. MS (ESI, *m/z*): calcd for $C_{44}H_{50}{}^{11}B_2N_{10}O_2P^{195}Pt^{32}S_2{}^{184}W$ [M+H]$^+$: 1245.2640. Found: 1245.2608. Anal. Calcd for $C_{44}H_{49}B_2N_{10}O_2PPtS_2W$: C, 42.43; H, 3.97; N, 11.25%. Found: C, 42.48; H, 4.19; N, 11.37%. Rapid solvent loss prevented a crystal of suitable quality. The example presented here is the best obtained from several attempts, to be used for connectivity purposes only. *Crystal data for* $C_{44}H_{49}B_2N_{10}O_2PPtS_2W{\cdot}2(CHCl_3)$, M = 1450.02, triclinic, $P\bar{1}$, a = 11.8256 (10) Å, b = 12.6412 (5) Å, c = 18.1304 (7) Å, α = 74.246 (3)°, β = 82.640 (5)°, γ = 76.424 (5)°, V = 2529.6 (3) Å^3, Z = 2, ρ_{calc} = 1.904 Mg m^{-3}, μ(Cu $K\alpha$) = 12.21 mm^{-1}, T = 150(0) K, needle 0.20 × 0.06 × 0.03 mm {clear light orange}, 9945 independent measured reflections (θ = 73.7 º), R_1 = 0.068, wR_2 = 0.188 for 6618 reflections [$I > 2\sigma(I)$], 606 parameters, 0 restraints. CDCC 1997719.

Partial synthesis of [WPt(μ$_2$-C)(κ-Tm^{Me})(CO)$_2$(PPh$_3$)(Tp*)] (3.6).

Note: This compound was only partially synthesised, unable to be purified despite eluting as a single band during chromatography. Therefore, the preparation is included accompanied by a molecular structure measured by X-ray diffraction studies only. A yellow solution containing [WPt(μ$_2$-C)Br(CO)$_2$(PPh$_3$)$_2$(Tp*)] (99 mg, 73 μmol) was stirred with NaTm^{Me} (33 mg, 88 μmol) in CH_2Cl_2 (10 mL), changing from orange solution to yellow suspension over 16 hours. Solvent was removed via rotary evaporation to give a yellow solid (110 mg crude). Flash column chromatography {silica gel, N_2, isocratic elution, neat CH_2Cl_2 then 2% THF/CH_2Cl_2} was performed allowing for an orange fraction to be collected. Solvent was removed before recrystallisation by concentration of CH_2Cl_2 into *n*-hexane under reduced pressure afforded a yellow microcrystalline powder. This was collected by vacuum filtration, washed with *n*-pentane (10 mL) before drying *in vacuo* for 2 hours. This was identified to be the title compound although as an impure mixture that defined further purification (67 mg). Crystal suitable for X-ray diffraction studies were grown from the liquid-liquid diffusion of *n*-hexane into a CH_2Cl_2 solution of **3.12** at ambient temperature. *Crystal data for* $C_{48}H_{53}B_2N_{12}O_2PPtS_3W{\cdot}2(CH_2Cl_2)$, M = 1527.58, monoclinic, $P2_1/c$, a = 19.0405 (1) Å, b = 19.3138 (2) Å, c = 17.0988 (3) Å, β = 94.333 (1)°, V = 6270.01 (14) Å^3, Z = 4, ρ_{calc} = 1.618 Mgm^{-3}, μ(Cu $K\alpha$) = 10.57 mm^{-1}, T = 150(0) K, 0.20 × 0.11 × 0.07 mm plate{clear light yellow}, 12514 independent measured reflections (θ = 73.7), R_1 = 0.045, wR_2 = 0.124 for 10387 reflections [$I > 2\sigma(I)$], 721 parameters. Crystal structure has not been uploaded to the CDCC.

Synthesis of [WPt(μ$_2$-C)(CO)$_2$(terpy)(Tp*)]PF$_6$ (3.7).

Compound prepared via a modified literature procedure. [120] A sample of [WPt(μ$_2$-C)Br(CO)$_2$(PPh$_3$)$_2$(Tp*)] (100 mg, 76 μmol) and 2,2':6',2"-terpyridine (14 mg, 60 μmol) was dissolved in CH_2Cl_2 (10 mL) to give an orange solution. A solution of $NaPF_6$ (14 mg, 83 μmol) in MeOH (2 mL) was injected and then left to stir for 16 hours in which time the solution had drastically changed to a deep purple/orange colour. The solvent was removed via rotary evaporation to afford an orange/pink residue. This was then purified by flash column chromatography (neutral alumina, N_2, CH_2Cl_2/MeCN gradient), where neat CH_2Cl_2 eluted excess **3.1b** as an orange band, and neat MeCN eluted a purple band. A subsequent recrystallisation of the purple mixture from concentration of MeCN into toluene afforded a purple solid. This could be collected via vacuum filtration washing with toluene (2 x 10 mL) and Et_2O (2 x 10 mL) before drying in vacuo overnight, resulting in the listed species (16 mg, 14 μmol, 25% isolated yield). Spectroscopic data matches those of the reported compound, however, a previously imprecisely

identified (HMBC) resonance was also directly recorded. $^{13}C\{^1H\}$ NMR (151 MHz, CD_3CN, 25 ºC, δ): 367.7 [W≡C–Pt].

Synthesis of [WPt(μ$_2$-C)(bpy)(CO)$_2$(PPh$_3$)(Tp*)]PF$_6$ (3.8).

A sample of [WPt(μ$_2$-C)Br(CO)$_2$(PPh$_3$)$_2$(Tp*)] (103 mg, 76 μmol) and 2,2'-bipyridine (34 mg, 218 μmol) was dissolved in CH_2Cl_2 (10 mL) to give an orange solution. A solution of $NaPF_6$ (24 mg, 143 μmol) in MeOH (2 mL) was injected and then left to stir for 4 hours in which time the solution had darkened to an orange/brown colour. The solvent was removed via rotary evaporation to afford a brown residue. This was then purified by flash column chromatography (silica gel, N_2, gradient elution), where neat THF eluted a brown band (78 mg). A subsequent recrystallisation from concentration of CH_2Cl_2 into EtOH afforded the listed species as a brown solid (42 mg, 42 μmol, 55% isolated yield). Crystals suitable for x-ray diffraction were obtained by the vapour diffusion of *n*-hexane into a solution of **3.6** in $CHCl_3$ at 5 °C. IR (CH_2Cl_2, cm^{-1}): 1967 vs ν_{CO}, 1953 sh ν_{CO}, 1875 vs ν_{CO}, 1863 sh ν_{CO}. ^1H NMR (400 MHz, $CDCl_3$, 25 ºC, δ): 8.87 [bs, 1H, bpyCH], 8.50 [d, $^1J_{HH}$ = 7 Hz, 2H, bpyCH], 8.07 [m, 2H, bpyCH], 7.91 [dd, $^1J_{HH}$ = 12 Hz, $^2J_{HH}$ = 8 Hz, 5H, PPh], 7.59 [m, 3H, PPh], 7.52 [m, 6H, PPh], 7.29 [d, $^1J_{HH}$ = 6 Hz, 1H, bpyCH], 7.10 [bs, 1H, PPh], 6.85 [t, $^1J_{HH}$ = 7 Hz, 1H, bpyCH], 6.36 [t, $^1J_{HH}$ = 7 Hz, 1H, bpyCH], 5.83 [s, 2H, pzCH], 5.64 [s, 2H, pzCH], 2.67 [s, 6H, $pzCH_3$], 2.46 [s, 6H, $pzCH_3$], 2.30 [s, 3H, $pzCH_3$], 2.06 [s, 3H, $pzCH_3$]. $^{13}C\{^1H\}$ NMR (151 MHz, $CDCl_3$, 25 ºC, δ): 325.8 [d, $^2J_{CP}$ = 9 Hz, W≡C–Pt], 228.6 [CO], 155.9 155.1 [C^2(bpy)], 152.2 151.9 [C^5(pz)], 151.1 150.7 [C^5(bpy)], 145.4 144.7 [C^3(pz)], 141.5 141.4 [C^4(bpy)], 135.2 [d, $^3J_{CP}$ = 11 Hz, $C^{3,5}(C_6H_5)$], 132.3 [$C^4(C_6H_5)$], 129.4 [d, $^2J_{CP}$ = 11 Hz, $C^{2,6}(C_6H_5)$], 128.8 [d, $^1J_{CP}$ = 64 Hz, $C^1(C_6H_5)$], 126.4 125.3 124.8 124.5 [$C^{3,5}$(bpy)], 107.2 106.5 [C^4(pz)], 17.2 14.9 12.7 [$pzCH_3$]. $^{19}F\{^1H\}$ NMR (377 MHz, $CDCl_3$, 25 ºC, δ): –73.47 [d, $^1J_{FP}$ = 712 Hz, PF_6]. ^{31}P NMR (162 MHz, $CDCl_3$, 25 ºC, δ): 16.37 [s, $^1J_{PPt}$ = 4293 Hz, PPh], –144.28 [septet, $^1J_{PF}$ = 709 Hz, PF_6]. $^{195}Pt\{^1H\}$ NMR (85.7 MHz, $CDCl_3$, 25ºC, δ): –3587 [d, $^1J_{PtP}$ = 4265 Hz]. MS (ESI, *m/z*): calcd for $C_{46}H_{45}BN_8O_2P^{195}Pt^{184}W$ $[M]^+$: 1162.26642. Found: 1162.26672. Anal. Calcd for $C_{46}H_{45}BF_6N_8O_2P_2PtW$: C, 42.25; H, 3.47; N, 8.57 %. Found: C, 42.10; H, 3.39; N, 8.36 %. *Crystal data for* $C_{46}H_{45}BN_8O_2PPtW{\cdot}2(CHCl_3){\cdot}PF_6$, M = 1546.32, triclinic, $P\bar{1}$, a = 9.5287 (2) Å, b = 16.3575 (4) Å, c = 18.2918 (2) Å, α = 84.892 (2)º, β = 78.583 (2)º, γ = 85.769 (2)º, V = 2778.94 (10) Å^3, Z = 2, ρ_{calc} = 1.848 Mg m^{-3}, μ(Cu $K\alpha$) = 12.18 mm^{-1}, T = 150(0) K, plate 0.19 × 0.05 × 0.04 mm {clear light orange}, 10934 independent measured reflections (θ = 73.3 º), R_1 = 0.045, wR_2 = 0.125 for 9217 reflections [$I > 2\sigma(I)$], 682 parameters, 0 restraints. CDCC 1997715.

Synthesis of [WPt(μ$_2$-C)(dtbbpy)(CO)$_2$(PPh$_3$)(Tp*)]PF$_6$ (3.9).

Note: This compound exists as a mixture of inseparable isomers in a ratio of ~1:5. This has been attributed to the orientation of bipyridine either free or occupying the cleft of the Tp* ligand. A sample of [WPt(μ_2-C)Br(CO)$_2$(PPh$_3$)$_2$(Tp*)] (102 mg, 76 μmol) and 4,4'-ditertbutyl-2,2'-bipyridine (26 mg, 97 μmol) was dissolved in CH_2Cl_2 (10 mL) to give an orange solution. A solution of $NaPF_6$ (24 mg, 143 μmol) in MeOH (2 mL) was injected and then left to stir for 16 hours in which time the solution had darkened to a yellow/brown colour. The solvent was removed via rotary evaporation to afford a brown residue. This was then purified by flash column chromatography (silica gel, N_2, CH_2Cl_2/THF gradient), which eluted a dark yellow band. Solvent was evaporated to give a dark yellow solid which could not be recrystallised from typical CH_2Cl_2/*n*-hexane combination. Ultrasonication in Et_2O allowed to emergence of a brick red solid and yellow supernatant phase. The red solid was collected via vacuum filtration washing with Et_2O (2 x 10 mL) before drying in vacuo to give the title compound as a red powder (80 mg, 71 μmol, 94% isolated yield). Crystals suitable for x-ray diffraction were grown by the vapour diffusion of *n*-hexane into a solution of **3.7** in $CHCl_3$ at 5 °C. IR (CH_2Cl_2, cm^{-1}): 1967 vs ν_{CO}, 1951 m ν_{CO}, 1875 vs ν_{CO}, 1860 m ν_{CO}. IR (ATR, cm^{-1}): 2560 w ν_{BH}, 1964 vs ν_{CO}, 1871 vs ν_{CO}. Rotational isomers present in a 1:3 mixture. Data reported here corresponds to the major isomer however due to this unavoidable mixture absolute assignments may not have been possible. ^{1}H NMR (400 MHz, $CDCl_3$, 25 ºC, δ): 8.62 [dd, $^1J_{HH}$ = 6 Hz, $^2J_{HH}$ = 4 Hz, 1H, bpyCH], 8.17 [m, 2H, PPh], 7.89 [m, 6H, PPh], 7.58 [m, 2H, PPh], 7.52 [m, 5H, PPh], 7.19 [d, $^1J_{HH}$ = 6 Hz, 1H, bpyCH], 7.10 [m, 2H, bpyCH], 6.81 [dd, $^1J_{HH}$ = 6 Hz, $^2J_{HH}$ = 2 Hz, 1H bpyCH], 6.20 [d, $^1J_{HH}$ = 5 Hz, 1H, bpyCH], 5.81 [s, 2H, pzCH], 5.64 [s, 1H, pzCH], 2.69 [s, 6H, pzCH$_3$], 2.47 [s, 6H, pzCH$_3$], 2.30 [s, 3H, pzCH$_3$], 2.07 [s, 3H, pzCH$_3$], 1.33 1.30 [s, 9H, bpyC(CH$_3$)$_3$]. ^{13}C{^{1}H} NMR (176 MHz, $CDCl_3$, 25 ºC, δ): 329.6 [m, W≡C–Pt], 228.7 [CO], 166.1 165.8 [C^4(dtbbpy)], 155.8 155.0 [C^2(dtbbpy)], 152.2 152.1 [C^5(pz)], 150.6 150.5 [C^6(dtbbpy)], 145.4 144.4 [C^3(pz)], 135.2 [d, $^3J_{CP}$ = 12 Hz, C^{3,5}(C$_6$H$_5$)], 132.2 [C^4(C$_6$H$_5$)], 129.3 [d, $^2J_{CP}$ = 11 Hz, C^{2,6}(C$_6$H$_5$)], 128.9 [d, $^1J_{CP}$ = 63 Hz, C^1(C$_6$H$_5$)], 123.6 122.0 120.9 120.4 [C^{3,5}(dtbbpy)], 107.1 106.4 [C^4(pz)], 36.0 35.8 [bpyCMe$_3$], 30.0 [bpyC(*C*H$_3$)$_3$], 17.2 15.4 14.9 12.8 12.7 [pzCH$_3$]. ^{19}F{^{1}H} NMR (377 MHz, $CDCl_3$, 25 ºC, δ): –73.08 [d, $^1J_{FP}$ = 713 Hz, PF_6]. ^{31}P{^{1}H} NMR (162 MHz, $CDCl_3$, 25 ºC, δ): 16.25 [s, $^1J_{PPt}$ = 4250 Hz, PPh], –144.39 [septet, $^1J_{PF}$ = 711 Hz, PF_6]. ^{195}Pt{^{1}H} NMR (85.7 MHz, $CDCl_3$, 25ºC, δ): –3580 [d, $^1J_{PtP}$ = 4287 Hz]. No plausible mass fragment could be identified for this compound. Anal. Found: C, 45.84; H, 4.42; N, 7.77%. Calcd for $C_{54}H_{61}BF_6N_8O_2P_2PtW$: C, 45.68; H, 4.33; N, 7.89%. *Crystal data for* $C_{54}H_{61}BN_8O_2PPtW{\cdot}PF_6$, M = 1416.77, *Triclinic*, $P\bar{1}$, a = 11.6701 (3) Å, b = 11.7291 (4) Å, c = 21.3711 (7) Å, α = 79.857 (3)º, β = 86.505 (2)º, γ = 75.021 (2)º, V = 2781.34 (15) Å^3, Z = 2, ρ_{calc}

= 1.692 Mg m^{-3}, μ(Cu *K*α) = 4.70 mm^{-1}, *T* = 150(0) K, block 0.31 × 0.22 × 0.13 mm {lustrous dark red}, 12835 independent measured reflections (θ = 29.9º), R_1 = 0.031, wR_2 = 0.066 for 11077 reflections [$I > 2\sigma(I)$], 688 parameters, 0 restraints. CDCC 1997716.

Synthesis of [WPt(μ$_2$-C)(phen)(CO)$_2$(PPh$_3$)(Tp*)]PF$_6$ (3.10).

Note: This compound exists as a mixture of inseparable isomers in a ratio of ~1:5. This has been attributed to the orientation of phenanthroline either free or occupying the cleft of the Tp* ligand. A sample of [WPt(μ$_2$-C)Br(CO)$_2$(PPh$_3$)$_2$(Tp*)] (**3.1b**; 101 mg, 75 μmol) and 1,10-phenthroline (10 mg, 55 μmol) was dissolved in CH_2Cl_2 (10 mL) to give an orange solution. A solution of $NaPF_6$ (24 mg, 84 μmol) in MeOH (2 mL) was injected and then left to stir for 16 hours in which time the solution had darkened to an orange/brown colour. The solvent was removed via rotary evaporation to afford a brown residue. This was then purified by flash column chromatography (silica gel, N_2, gradient elution), where CH_2Cl_2 eluted excess **3.1b** and neat THF eluted a brown band (72 mg). A subsequent recrystallisation of the brown band from the concentration of CH_2Cl_2 into EtOH afforded a brown solid which was collected via vacuum filtration washing with toluene (2 × 10 mL) and Et_2O (2 × 10mL). Drying in vacuo for 2 hours provided the listed compound (56 mg, 42 μmol, 76% isolated yield). Rotational isomers present in a 1:5 mixture. Data reported here corresponds to the major isomer however due to this unavoidable mixture, absolute assignments may have not been possible. IR (CH_2Cl_2, cm^{-1}): 1968 vs ν_{CO}, 1874 vs ν_{CO}. ^{1}H NMR (400 MHz, $CDCl_3$, 25 ºC, δ): 9.05 [m, 1H, phenCH], 8.62 [t, $^1J_{HH}$ = 9 Hz, 2H, phenCH], 8.14 [m, 3H, phenCH], 7.95 [dd, $^1J_{HH}$ = 12, $^2J_{HH}$ = 8 Hz, 6H, PPh], 7.60 [m, 3H, PPh], 6.53 [m, 6H, PPh], 7.11 [bs, 1H, phenCH], 6.77 [t, $^1J_{HH}$ = 7 Hz, 1H, phenCH], 5.81 [s, 2H, pzCH], 5.67 [s, 1H, pzCH], 2.67 [s, 5H, pzCH_3], 2.51 [s, 5H, pzCH_3], 2.46 [s, 2H, pzCH_3], 2.38 [s, 1H, pzCH_3], 2.32 [s, 3H, pzCH_3], 2.09 [s, 2H, pzCH_3]. ^{13}C{^{1}H} NMR (151 MHz, $CDCl_3$, 25 ºC, δ): 324.7 [d, $^2J_{CP}$ = 8 Hz, W≡C–Pt], 228.7 [$^1J_{CW}$ = 174 Hz, CO], 153.7 152.5 [C^6(phen)], 152.2 151.9 [C^5(pz)], 146.5 [C^2(phen)], 145.9[C$^{2'}$(phen)], 145.4 145.0 [C^3(pz)], 140.6 140.5 [C^4(phen)], 135.3 [d, $^3J_{CP}$ = 12 Hz, C^{3,5}(C_6H_5)], 132.4 [C^4(C_6H_5)], 131.1 [C^5(phen)], 129.4 [d, $^2J_{CP}$ = 12 Hz, [C^{2,6}(C_6H_5)], 128.7 [d, $^1J_{CP}$ = 64 Hz, C^1(C_6H_5)], 125.4 [C^{13,14}(phen)], 107.3 106.5 [C^4(pz)], 17.2 15.0 13.0 12.7 [pz*C*H$_3$]. ^{19}F{^{1}H} NMR (376 MHz, $CDCl_3$, 25 °C, δ): –73.28 [d, $^1J_{FP}$ = 713 Hz, PF_6]. ^{31}P{^{1}H} NMR (162 MHz, $CDCl_3$, 25 ºC, δ): 15.73 [s, $^1J_{PPt}$ = 4341 Hz, PPh], –144.33 [septet, $^1J_{PF}$ = 712 Hz, PF_6]. ^{195}Pt{^{1}H} NMR (85.7 MHz, $CDCl_3$, 25ºC, δ): –3619 [d, $^1J_{PtP}$ = 4428 Hz]. MS (ESI, *m/z*): calcd for $C_{48}H_{45}BN_8O_2P^{195}Pt^{184}W$ $[M]^+$: 1186.26645. Found: 1186.26721. Anal. Calcd for $C_{48}H_{45}BF_6N_8O_2P_2PtW$: C, 43.30; H, 3.41; N, 8.42 %. Found: C, C, 43.18; H, 3.31; N, 8.23 %. No

crystal was obtained as each single crystal was soft and malleable, failing to retain shape even in the cryostream.

Synthesis of [WPt(μ_2-C)(Bp*)(CO)$_2$(PPh$_3$)(Tp*)] (3.11).

Note: This compound exists as a 1:1 mixture of rotomers.

A sample of [WPt(μ_2-C)Br(CO)$_2$(PPh$_3$)$_2$(Tp*)] (**3.1b**; 102 mg, 75.6 μmol) and KBp* (43 mg, 178 μmol) was refluxed in CH_2Cl_2 (10 mL) for 16 hours. Beginning as an orange solution, a clear colour transition to yellow was recorded. Solvent was removed via rotary evaporation to give a crude mass of 165 mg as an orange solid. Flash column chromatography {silica gel, N_2, 67 % CH_2Cl_2/Petroleum Ether, isocratic} was performed on the orange residue affording elution of a major orange component. Solvent removal was performed prior to subjecting to an ultrasonic bath in *n*-hexane (10 mL) afforded a yellow solid and a red supernatant phase. The supernatant phase was decanted and the solid was further titriated with *n*-hexane (2 x 10 mL). The yellow solid was dried *in vacuo* for 2 h to provide the title compound (22 mg, 22 μmol, 29 % yield). Crystal suitable for x-ray diffraction were grown from the vapour diffusion of *n*-hexane into a solution of **3.9** in $CHCl_3$. Rotational isomers are present in a 1:1 mixture. Data collected was not able to elucidate a dominant species, hence signals reported are of both species consistent with their relative assignments. Integrals are relative to the isomer present and hence have been normalised. It is for this reason that absolute assignments could not be assigned in some cases. IR (CH_2Cl_2, cm^{-1}): 1946 vs ν_{CO}, 1853 vs ν_{CO}. ^{1}H NMR (600 MHz, $CDCl_3$, 25 ºC, δ): 7.48–7.36 [m, 4H, PPh], 7.23–6.98 [m, 10H, PPh], 5.85 [s, 1H, pzCH], 5.79 [s, 1H, pzCH], 5.68 [s, 1H, pzCH], 5.59 [s, 1H, pzCH], 5.58 [s, 1H, pzCH], 5.53 [s, 1H, pzCH], 5.50 [s, 1H, pzCH], 5.25 [s, 1H, pzCH], 5.11 [s, 1H, pzCH], 5.02 [s, 1H, pzCH], 2.84 [s, 3H, pzCH$_3$], 2.80 [s, 3H pzCH$_3$], 2.72 [s, 3H pzCH$_3$], 2.39 [s, 3H pzCH$_3$], 2.34 [s, 6H pzCH$_3$], 2.32 [s, 3H pzCH$_3$], 2.30 [overlapping s, 8H pzCH$_3$], 2.27 [s, 3H pzCH$_3$], 2.22 [s, 9H pzCH$_3$], 2.17 [s, 3H pzCH$_3$], 2.08 [s, 3H pzCH$_3$], 1.96 [s, 3H pzCH$_3$], 1.55 [s, 3H pzCH$_3$], 1.33 [s, 3H pzCH$_3$], 1.30 [s, 3H pzCH$_3$]. ^{13}C{^{1}H} NMR (151 MHz, $CDCl_3$, 25 ºC, δ): 338.3 [d, $^2J_{CP}$ = 9 Hz, W≡C–Pt], 332.6 [d, $^2J_{CP}$ = 11 Hz, W≡C–Pt], 233.4 [$^1J_{CW}$ = 176 Hz, CO], 231.5 [$^1J_{CW}$ = 178 Hz, CO], 228.5 [$^1J_{CW}$ = 176 Hz, CO], 225.0 [$^1J_{CW}$ = 181 Hz, CO], 153.6 152.5 151.9 151.7 151.6 [C^5(W-pz)], 148.48 148.45 147.91 147.88 [C^5(Pt-pz)], 147.4 147.2 [C^3(Pt-pz)], 144.8 144.7 144.6 144.0 143.8 143.6 143.0 142.5 [C^3(W-pz)], 135.8–134.1 [br, C^{2,6}(C_6H_5)], 130.6–130.0 [m, C^{3,5}(C_6H_5)], 129.3 [bd, $^1J_{CP}$ = 61 Hz, C^1(C_6H_5)], 128.1 127.3 [bs, PPh], 106.6 105.9 [C^4(W-pz)], 105.8 105.2 105.02 104.99 104.8 104.63 104.60 [C^4(Pt-pz)], 18.7 17.9 16.0 15.3 14.9 14.8 14.1 13.1 13.0 12.9 12.8 12.7 12.64 12.59 12.55 12.2 [pzCH$_3$]. ^{31}P{^{1}H} NMR (162 MHz, $CDCl_3$, 25 ºC, δ): 7.52 [s, $^1J_{PPt}$ = 4285 Hz], 5.38 [s, $^1J_{PPt}$ = 4161 Hz]. ^{195}Pt{^{1}H} NMR (85.7 MHz, $CDCl_3$, 25ºC, δ): –

3495 [d, $^{1}J_{PtP}$ = 4178 Hz], –3477 [d, $^{1}J_{PtP}$ = 4297 Hz]. MS (ESI, *m/z*): calcd for $C_{46}H_{53}B_2N_{10}O_2PPtW$ $[M]^+$: 1209.3459. Found: 1209.3442. Anal. Calcd for $C_{46}H_{53}B_2N_{10}O_2PPtW$: C, 44.43; H, 4.50; N, 10.50%. Found: C, 44.49; H, 4.48; N, 10.51%. *Crystal data for* $C_{46}H_{53}B_2N_{10}O_2PPtW\cdot(CHCl_3)$, M = 1328.88, triclinic, $P\bar{1}$, a = 10.1322 (6) Å, b = 14.7017 (8) Å, c = 19.3416 (7) Å, α = 103.794 (4)°, β = 102.422 (4)°, γ = 106.487 (5)°, V = 2556.3 (2) Å^3, Z = 2, ρ_{calc} = 1.726 Mg m^{-3}, μ(Cu *K*α) = 11.27 mm^{-1}, T = 150(0) K, plate 0.09 × 0.05 × 0.04 mm {clear light yellow}, 9298 independent measured reflections (θ = 68.3 º), R_1 = 0.048, wR_2 = 0.127 for 6912 reflections [$I > 2\sigma(I)$], 622 parameters, 0 restraints. CDCC 1997717.

Synthesis of [WPt(μ$_2$-C)(κ$_2$-Tp*)(CO)$_2$(PPh$_3$)(Tp*)] (3.12).

Note: This compound exists a mixture of ~1:3 rotational isomers. A mixture of [WPt(μ$_2$-C)Br(CO)$_2$(PPh$_3$)$_2$(Tp*)] (152 mg, 113 μmol) and KTp* (76 mg, 226 μmol) was heated at reflux in CH_2Cl_2 (10 mL) for 16 hours. Beginning as an orange solution, a clear colour transition to red was recorded. Solvent was removed via rotary evaporation to give an orange solid. Flash column chromatography {silica gel, N_2, neat CH_2Cl_2, isocratic} was performed on the orange residue affording elution of a major red compound. Solvent removal was performed prior to subjecting to an ultrasonic bath in *n*-hexane (10 mL) to give a red solid. The supernatant phase was decanted and the solid was dried *in vacuo* for 2 h to provide the listed compound (8 mg, 6 μmol, 5% yield). Crystals suitable for x-ray diffraction were grown from the vapour diffusion of *n*-hexane into a solution of **3.10** in $CHCl_3$. Note: This compound exists a mixture of ~1:3 rotational isomers. It is for this reason that absolute assignments may not be appropriate on some occasions. The signals reported are for the dominant species. IR (CH_2Cl_2, cm^{-1}): 1947 vs ν_{CO}, 1854 vs ν_{CO}. ^{1}H NMR (400 MHz, $CDCl_3$, 25 ºC, δ): 8.11 [dd, $^{1}J_{HH}$ = 12, $^{2}J_{HH}$ = 7 Hz, 2H, PPh], 7.90 [dd, $^{1}J_{HH}$ = 13, $^{2}J_{HH}$ = 7 Hz, 2H, PPh], 7.54 [d, $^{1}J_{HH}$ = 8 Hz, 2H, PPh], 7.47–7.30 [m, 6H, PPh], 7.12 [t, $^{1}J_{HH}$ = 8 Hz, 1H, PPh], 6.92 [t, $^{1}J_{HH}$ = 7 Hz, 2H, PPh], 5.78 [s, 2H, pzCH], 5.60 [s, 1H, pzCH], 5.53 [s, 1H, pzCH], 5.45 [s, 1H, pzCH], 5.27 [s, 1H, pzCH], 2.51 [s, 3H, pzCH$_3$], 2.39 [s, 3H, pzCH$_3$], 2.37 [s, 3H, pzCH$_3$], 2.34 [s, 2H, pzCH$_3$], 2.32 [s, 3H, pzCH$_3$], 2.24 [s, 3H, pzCH$_3$], 2.20 [s, 3H, pzCH$_3$], 2.15 [s, 3H, pzCH$_3$], 2.08 [s, 3H, pzCH$_3$], 1.72 [s, 3H, pzCH$_3$], 1.60 [s, 3H, pzCH$_3$], 1.51 [s, 3H, pzCH$_3$]. ^{13}C{^{1}H} NMR (151 MHz, $CDCl_3$, 25 ºC, δ): 333.5 [d, $^{2}J_{CP}$ = 8, $^{1}J_{CW}$ = 179 Hz, W≡C–Pt], 230.7 229.5 [$^{1}J_{CW}$ = 179 Hz, $^{3}J_{CPt}$ = 1360 Hz, CO], 153.7 151.7 151.5 150.4 [C^5(W-pz)], 149.2 147.6 [C^5(Pt-pz)], 146.9 146.5 [C^3(Pt-pz)], 143.9 143.7 143.5 142.7 [C^3(W-pz)], 136.7 [d, $^{2}J_{CP}$ = 12 Hz, C^{2,6}(C_6H_5)], 136.2 [d, $^{2}J_{CP}$ = 12 Hz, C^{2,6}(C_6H_5)], 133.9 [d, $^{2}J_{CP}$ = 12 Hz, C^{2,6}(C_6H_5)], 133.4 [d, $^{1}J_{CP}$ = 58 Hz, C^1(C_6H_5)], 131.0 130.3 129.3 [C^4(C_6H_5)], 128.3 128.2 127.1 [d, $^{3}J_{CP}$ = 12 Hz, C^{3,5}(C_6H_5)], 129.5 [d, $^{1}J_{CP}$ = 60 Hz, C^1(C_6H_5)], 129.2 [d, $^{1}J_{CP}$ = 65 Hz, C^1(C_6H_5)], 106.2 106.0 105.7 105.6 105.5

[C^4(pz)], 18.8 16.2 15.6 14.8 14.2 14.1 13.7 13.3 13.3 13.0 12.6 [pzCH_3]. $^{31}P\{^1H\}$ NMR (162 MHz, $CDCl_3$, 25 ºC, δ): 3.07 [s, $^1J_{PPt}$ = 4288 Hz]. $^{195}Pt\{^1H\}$ NMR (85.7 MHz, $CDCl_3$, 25ºC, δ): –3433 [d, $^1J_{PtP}$ = 4305 Hz]. MS (ESI, *m/z*): Calcd for $C_{51}H_{59}B_2N_{12}O_2P^{195}Pt^{184}W$ $[M]^+$: 1303.4053. Found: 1303.4037. Anal. Calcd for $C_{51}H_{59}B_2N_{12}O_2PPtW$: C, 46.74; H, 4.50; N, 12.70%. Found: C, 46.82; H, 4.56; N, 12.73%. *Crystal data for* $C_{51}H_{59}B_2N_{12}O_2PPtW$, M = 1303.63, triclinic, $P\bar{1}$, a = 10.8902 (2) Å, b = 15.0338 (4) Å, c = 17.0497 (4) Å, α = 71.254 (2)°, β = 79.943 (2)°, γ = 82.947 (2)°, V = 2596.04 (11) $Å^3$, Z = 2, ρ_{calc} = 1.668 Mg m^{-3}, μ(Cu $K\alpha$) = 9.71 mm^{-1}, T = 150(0) K, block 0.18 × 0.13 × 0.06 mm {clear light yellow}, 10286 independent measured reflections (θ = 73.8 º), R_1 = 0.022, wR_2 = 0.059 for 9765 reflections [$I > 2\sigma(I)$], 643 parameters, 17 restraints. CDCC 1997718.

9.6 Synthetic procedures for Chapter Four compounds

Synthesis of [WPt(μ$_2$-C)Br(CNXyl)(CO)$_2$(PPh$_3$)(Tp*)] (4.1).

A sample of [WPt(μ$_2$-C)Br(CO)$_2$(PPh$_3$)$_2$(Tp*)] (0.631 g, 0.462 mmol) and 2,6-dimethylphenylisonitrile (CNXyl) (0.066 g, 0.50 mmol) was stirred in toluene (30 mL) for 16 hours. The ensuing orange solution had solvent removed *via* rotary evaporation where the residue was sonicated in *n*-hexane (5 × 10 mL), decanted each time to remove excess phosphine. Now free of excess phosphine, flash column chromatography {silica gel, N_2, dry loaded, isocratic elution, 75% CH_2Cl_2/petroleum ether 60–80} first eluting the target as an orange band, followed by a minor band returning starting material and [WPt(μ$_2$-C)Br(CNXyl)$_2$(CO)$_2$(Tp*)] (**4.4**). The target eluate was recrystallised from the evaporation of CH_2Cl_2 into EtOH by rotary evaporation to give an orange solid which could be collected *via* vacuum filtration. The solid was washed with EtOH (2 × 5 mL) and *n*-hexane (10 mL) before drying *in vacuo* for 16 hours to afford compound **4.1** as a pale, yellow powder (0.220 g, 0.181 mmol, 40% yield). Crystals suitable for x-ray diffraction were grown from the slow vapour diffusion of *n*-hexane into a CH_2Cl_2 solution of **4.1** at 5 °C. Note: spectra hint at a related isomer in a 1:4 ratio. The following describes the major component. IR (CH_2Cl_2, cm^{-1}): 2196 s ν_{CN}, 1943 vs ν_{CO}, 1852 vs ν_{CO}. IR (ATR, cm^{-1}): 2552 2532 w ν_{BH}, 2184 s ν_{CN}, 1939 vs ν_{CO}, 1846 vs ν_{CO}. ^1H NMR (400 MHz, $CDCl_3$, 25 ºC, δ): 7.49 [br, 6H, PPh], 7.25–7.17 [m, 4H, PPh], 7.12 [d, $^1J_{HH}$ = 8 Hz, XylCH], 7.03 [br, 5H, PPh], 5.64 [s, 1H, pzCH], 5.62 [s, 2H, pzCH], 2.71 [s, 6H, XylCH_3], 2.40 [s, 6H, pzCH_3], 2.37 [s, 6H, pzCH_3], 2.31 [s, 3H, pzCH_3], 2.25 [s, 3H, pzCH_3]. $^{13}C\{^1H\}$ NMR (151 MHz, $CDCl_3$, 25ºC, δ): 308.4 [d, $^2J_{CP}$ = 10 Hz, W≡C–Pt], 227.5 [$^1J_{CW}$ = 175 Hz, CO], 152.0 151.3 [C^5(pz)], 144.3 143.3 [C^3(pz)], 136.9 [$C^{2,5}$(Xyl)], 135.1 [d, $^2J_{CP}$ = 11 Hz, $C^{2,6}(C_6H_5)$], 130.6 [$C^4(C_6H_5)$], 129.4 [C^4(Xyl)], 129.2 [d, $^1J_{CP}$ = 59 Hz, $C^1(C_6H_5)$], 128.1 [$C^{3,5}$(Xyl)], 127.7 [d, $^2J_{CP}$ = 11 Hz, $C^{3,5}(C_6H_5)$], 126.4 [C*C*NXyl], 106.6 106.2 [C^4(pz)], 19.8 [XylCH_3], 16.7 15.2 12.8 12.6 [pzCH_3]. $^{31}P\{^1H\}$ NMR (162 MHz, $CDCl_3$, 25 ºC, δ): 16.75 [s, $^1J_{PPt}$ = 3466 Hz]. $^{195}Pt\{^1H\}$

NMR (85.7 MHz, $CDCl_3$, 25ºC, δ): –3761 [br.d, $^1J_{PtP}$ = 3489 Hz]. MS (ESI, *m/z*): Found: 1216.1874. Calcd for $C_{45}H_{46}{}^{11}B^{79}BrN_7O_2P^{195}Pt^{184}W$ $[M]^+$: 1347.20534. Anal. Found: C, 44.36; H, 3.87; N, 8.00%. Calcd for $C_{45}H_{46}BBrN_7O_2PPtW$: C, 44.39; H, 3.81; N, 8.05%. *Crystal data for* $C_{45}H_{46}BBrN_7O_2PPtW{\cdot}CH_2Cl_2$, M = 1302.44, triclinic, $P\bar{1}$, a = 9.4191 (2) Å, b = 15.8501 (2) Å, c = 16.1962 (4) Å, α = 88.182 (2)°, β = 77.516 (2)°, γ = 82.340 (2)°, V = 2339.74 (10) Å^3, Z = 2, ρ_{calc} = 1.849 Mgm^{-3}, μ(Cu $K\alpha$) = 12.73 mm^{-1}, T = 150(0) K, plate, 0.18 × 0.06 × 0.04 mm {clear light orange}, 8849 independent measured reflections (θ = 73.7), R_1 = 0.042, wR_2 = 0.112 for 7651 reflections [$I > 2\sigma(I)$], 571 parameters, 9 restraints. CDCC 2084969.

Synthesis of [WPt(μ$_2$-C)Br(CNMes)(CO)$_2$(PPh$_3$)(Tp*)] (4.2).

A sample of [WPt(μ$_2$-C)Br(CO)$_2$(PPh$_3$)$_2$(Tp*)] (**3.1b**; 0.181 g, 0.134 mmol) and 2,4,6-trimethylphenylisonitrile (CNMes) (0.029 g, 0.199 mmol) was stirred in toluene (10 mL) for 16 hours. The subsequent orange solution had solvent removed *via* rotary evaporation where the residue was sonicated in *n*-hexane (5 × 10 mL), decanted each time to remove excess phosphine. Now free of excess phosphine, flash column chromatography {silica gel, N_2, dry loaded, isocratic elution, 75% CH_2Cl_2/petroleum ether 60–80} first eluting the target as an orange band, followed by a minor band of **3.1b** and [WPt(μ$_2$-C)Br(CNMes)$_2$(CO)$_2$(Tp*)] (**4.5**). The target eluate was recrystallised from the evaporation of CH_2Cl_2 into EtOH by rotary evaporation to give an orange solid which could be collected *via* vacuum filtration. The solid was washed with EtOH (2 x 5 mL) and *n*-hexane (10 mL) before drying in vacuo for 16 hours to afford compound **4.2** as a pale orange powder (0.077 g, 0.063 mmol, 47% yield). Crystals suitable for x-ray diffraction were grown from the vapour diffusion of *n*-hexane into a $CHCl_3$ solution of the compound, overnight at 5 °C. Note: Following spectra shows another isomer in a ratio of 1:6 with the major isomer. IR (CH_2Cl_2, cm^{-1}): 2197 s ν_{CN}, 1943 vs $\nu_{CO,}$ 1852 vs ν_{CO}. IR (ATR, cm^{-1}): 2544 2529 w ν_{BH}, 2180 s ν_{CN}, 1931 vs $\nu_{CO,}$ 1835 vs ν_{CO}. ^{1}H NMR (400 MHz, $CDCl_3$, 25 ºC, δ): 7.49 [br.m, 6H, PPh], 7.19 [br.m, 3H, PPh], 7.02 [br.m, 6H, PPh], 6.92 [s, 2H, MesCH], 5.63 [s, 1H, pzCH], 5.61 [s, 2H, pzCH], 2.65 [s, 6H, *o*-MesCH$_3$], 2.40 [s, 6H, pzCH$_3$], 2.36 [s, 6H, pzCH$_3$], 2.30 [overlapping singlets, 3H and 3H, *p*-MesCH$_3$ and pzCH$_3$], 2.24 [s, 3H, pzCH$_3$]. ^{13}C{^{1}H} NMR (176 MHz, $CDCl_3$, 25ºC, δ): 308.6 [m, W≡C–Pt], 227.4 [$^1J_{CW}$ = 175 Hz, CO], 152.0 151.3 [C^5(pz)], 144.3 143.3 [C^3(pz)], 140.1 [C^4(Mes)], 136.6 [C^{2,6}(Mes)], 135.1 [d, $^2J_{CP}$ = 11 Hz, C^{2,6}(C_6H_5)], 130.6 [C^4(C_6H_5)], 129.2 [d, $^1J_{CP}$ = 55 Hz, C^1(C_6H_5)], 128.9 [C^{3,5}(Mes)], 127.6 [d, $^3J_{CP}$ = 12 Hz, C^{3,5}(C_6H_5)], 123.8 [Pt–*C*CNMes], 106.6 106.2 [C^4(pz)], 21.5 19.7 [MesCH$_3$], 16.7 15.3 12.8 12.6 [pzCH$_3$]. ^{31}P{^{1}H} NMR (162 MHz, $CDCl_3$, 25 ºC, δ): 15.74 [s, $^1J_{PPt}$ = 3477 Hz]. This spectrum also hints at another isomer in a ratio of 1:6 with

the major isomer. ^{195}Pt{^{1}H} NMR (150 MHz, $CDCl_3$, 25ºC, δ): –3763 [d, $^{1}J_{PtP}$ = 3473 Hz]. MS (ESI, *m/z*): Found: 1232.2062. calcd for $C_{46}H_{48}{}^{11}B^{81}BrN_7O_2P_1{}^{195}Pt^{184}W$ $[M]^+$: 1232.2020. Anal. Found: C, 44.87; H, 4.00; N, 7.86%. Calcd for $C_{46}H_{48}BBrN_7O_2PPtW$: C, 44.86; H, 3.93; N, 7.96%. *Crystal data for* $C_{46}H_{48}BBrN_7O_2PPtW{\cdot}CHCl_3$, M = 1350.91, triclinic, $P\bar{1}$, a = 9.5314 (3) Å, b = 16.2298 (5) Å, c = 16.3030 (5) Å, α = 91.074 (2)°, β = 103.031 (2)°, γ = 93.835 (2), V = 2450.02 (13) Å^3, Z = 2, ρ_{calc} = 1.831 Mgm^{-3}, μ(Cu $K\alpha$) = 12.67 mm^{-1}, T = 150(0) K, plate {0.10 × 0.06 × 0.04 mm, clear light yellow}, 9597 independent measured reflections (θ = 73.5), R_1 = 0.033, wR_2 = 0.088 for 8386 reflections [$I > 2\sigma(I)$], 590 parameters, 0 restraints. CDCC 2084966.

Synthesis of [WPt(μ$_2$-C)Br(CN^{t}Bu)(CO)$_2$(PPh$_3$)(Tp*)] (4.3).

An orange solution of [WPt(μ$_2$-C)Br(CO)$_2$(PPh$_3$)$_2$(Tp*)] (202 mg, 150 μmol) in benzene (10 mL) was treated with *tert*-butylisocyanide (0.040 mL, 360 μmol), rapidly changing to a yellow colour. The reaction was stirred for 2 hours until completion identified *via* thin layer chromatography. The solvent was removed under reduced pressure to give an orange solid. Sonication in Et_2O (10 mL) allowed for a very fine pale orange powder to form and bright yellow supernatant phase. The supernatant phase was extracted *via* a filtered canula and recrystallised from concentration of CH_2Cl_2 into *n*-hexane to give a bright yellow solid. Now open to air, the yellow solid was collected *via* vacuum filtration, washed with *n*-hexane (3 × 10 mL) and 20% Et_2O/*n*-hexane (10 mL) and dried *in vacuo* for 2 hours to afford the title compound (63 mg, 54 μmol, 36 % yield). Crystals were unable to be grown for single crystal x-ray diffraction, despite multiple attempts and solvent systems. IR (CH_2Cl_2, cm^{-1}): 2228 vs ν_{CN}, 1941 vs ν_{CO}, 1850 vs ν_{CO}. IR (ATR, cm^{-1}): 2539 w ν_{BH}, 2233 sh ν_{CN}, 2222 vs ν_{CN}, 1936 vs ν_{CO}, 1841 vs ν_{CO}. ^{1}H NMR (400 MHz, $CDCl_3$, 25 ºC, δ): 7.44 [m, 6H, PPh], 7.18 [m, 3H, PPh], 7.00 [m, 6H, PPh], 5.65 [s, 1H, pzCH], 5.61 [s, 2H, pzCH], 2.36 [s, 6H, $pzCH_3$], 2.34 [s, 3H, $pzCH_3$], 2.33 [s, 6H, $pzCH_3$], 2.25 [s, 3H, $pzCH_3$], 1.68 [s, 9H, ^{t}BuCH$_3$]. ^{13}C{^{1}H} NMR (151 MHz, $CDCl_3$, 25 ºC, δ): 309.9 [d, $^{2}J_{CP}$ = 9 Hz, W≡C–Pt], 227.1 [$^{1}J_{CP}$ = 175 Hz, CO], 151.9 151.2 [C^5(pz)], 144.2 143.2 [C^3(pz)], 134.9 [d, $^{2}J_{CP}$ = 11 Hz, C^{2,6}(C_6H_5)], 130.4 [C^4(C_6H_5)], 129.1 [d, $^{1}J_{CP}$ = 59 Hz, C^1(C_6H_5)], 127.5 [d, $^{2}J_{CP}$ = 11 Hz, C^{3,5}(C_6H_5)], 106.4 106.1 [C^4(pz)], 58.3 [*C*N^{t}Bu], 29.9 [CNC*C*H$_3$], 16.4 15.0 12.6 12.5 [pz*C*H$_3$]. ^{31}P{^{1}H} NMR (162 MHz, $CDCl_3$, 25 ºC, δ): 15.63 [s, $^{1}J_{PPt}$ = 3436 Hz, PPh]. ^{195}Pt{^{1}H} NMR (85.7 MHz, $CDCl_3$, 25ºC, δ): –3803 [dt, $^{1}J_{PtP}$ = 3451 Hz, $^{2}J_{Pt-14N}$ = 110 Hz]. MS (ESI, *m/z*): Found: 1169.19563. Calcd for $C_{41}H_{47}{}^{11}BBrN_7O_2P^{195}Pt^{184}W$ $[M+H]^+$: 1169.19018. Anal. Found: C, 42.24; H, 3.86; N, 8.27 %. Calcd for $C_{41}H_{46}BBrN_7O_2PPtW$: C, 42.11; H, 3.96; N, 8.38 %.

Synthesis of [WPt(μ$_2$-C)Br(CNXyl)$_2$(CO)$_2$(Tp*)] (4.4).

Note: This compound readily isomerises in polar media in the presence of phosphine. A sample of [WPt(μ$_2$-C)Br(CO)$_2$(PPh$_3$)$_2$(Tp*)] (**3.1b**; 0.402 g, 0.295 mmol) and 2,6-dimethylphenylisonitrile (CNXyl) (0.164 g, 1.25 mmol) was stirred in toluene (20 mL) for 16 hours at 40 ºC.# The subsequent orange solution was removed of solvent *via* rotary evaporation to give a crude residue prior to sonication in *n*-hexane (5 × 10 mL), decanting the clear supernatant each time to remove excess phosphine. With phosphine essentially removed, the residue was dissolved in CH_2Cl_2 and flash column chromatography performed {silica gel, N_2, neat petroleum ether then neat CH_2Cl_2} obtaining a major orange eluent. If CH_2Cl_2 is added to the crude residue without removing phosphine, colour changes from orange to red, green, or purple, consistent with isomerisation occurred. The orange band was recrystallised from evaporation of CH_2Cl_2 into EtOH by rotary evaporation gave an orange solid which could be collected via vacuum filtration. The solid was washed with EtOH (2 × 10 mL) and *n*-hexane (10 mL) before drying in vacuo for 16 hours to afford compound **4.4** as a fine orange powder (0.238 g, 0.219 mmol, 74% isolated yield). Crystals suitable for x-ray diffraction were grown from the vapour diffusion of *n*-hexane into CH_2Cl_2 solution of the title compound at 5 °C overnight. IR (CH_2Cl_2, cm^{-1}): 2194 s ν_{CN}, 1951 vs ν_{CO}, 1860 vs ν_{CO}. IR (ATR, cm^{-1}): 2542 2523 w ν_{BH}, 2191 s ν_{CN}, 1943 vs ν_{CO}, 1848 vs ν_{CO}. ^{1}H NMR (400 MHz, $CDCl_3$, 25 ºC, δ): 7.22 [t, 2H, $^1J_{HH}$ = 8 Hz, C^{3,5}H(Xyl)], 7.05 [d, 4H, $^1J_{HH}$ = 8 Hz, C^{4}H(Xyl)], 5.75 [s, 2H, pzCH], 5.70 [s, 1H, pzCH], 2.82 [s, 6H, pzCH$_3$], 2.35 [s, 6H, pzCH$_3$], 2.34 [s, 3H, pzCH$_3$], 2.29 [s, 3H, pzCH$_3$], 2.22 [s, 12H, pzCH$_3$]. ^{13}C{^{1}H} NMR (151 MHz, $CDCl_3$, 25ºC, δ): 298.7 [$^1J_{CPt}$ = 578 Hz, W≡C–Pt], 269.7 [$^1J_{CW}$ = 175 Hz, CO], 152.1 151.7 [C^5(pz)], 144.8 143.7 [C^3(pz)], 137.2 [br, Pt–*C*NXyl], 136.8 [C^{2,6}(Xyl)], 130.2 [C^4(Xyl)], 128.1 [C^{3,5}(Xyl)], 125.4 [C^1(Xyl)], 106.3 106.2 [C^4(pz)], 18.3 [XylCH$_3$], 17.1 15.3 12.8 12.7 [pzCH$_3$]. ^{195}Pt NMR (86 Hz, $CDCl_3$, 25 °C, δ): –3658 [br.m]. MS (ESI, *m*/*z*): Found: 1085.1716. Calcd for $C_{36}H_{40}{}^{11}B^{79}BrN_8O_2{}^{195}Pt^{184}W$ [M]$^+$: 1085.1708. Anal. Found: C, 39.83; H, 3.67; N, 10.17%. Calcd for $C_{36}H_{40}BBrN_8O_2PtW$: C, 39.80; H, 3.71; N, 10.31%. *Crystal data for* $C_{36}H_{40}BBrN_8O_2PtW{\cdot}2(CH_2Cl_2)$, M = 1256.27, triclinic, $P\bar{1}$, a = 10.8184 (3) Å, b = 13.9334 (3) Å, c = 16.8609 (4) Å, α = 73.948 (2)°, β = 88.154 (2)°, γ = 67.363 (2)°, V = 2246.40 (10) Å^3, Z = 2, ρ_{calc} = 1.857 Mgm^{-3}, μ(Cu $K\alpha$) = 13.97 mm^{-1}, T = 150(0) K, plate, 0.29 × 0.07 × 0.05 mm {clear light orange}, 8833 independent measured reflections (θ = 73.6), R_1 = 0.031, wR_2 = 0.081 for 8217 reflections [$I > 2\sigma(I)$], 515 parameters, 0 restraints. CDCC 2251817.

Heating higher than 50 °C causes isomerisation to the iminoketeylidene [WPt(μ$_2$-CCNXyl)(CO)$_2$(PPh$_3$)$_2$(Tp*)]$^+$ (**4.10**).

Synthesis of [WPt(μ$_2$-C)Br(CNMes)$_2$(CO)$_2$(Tp*)] (4.5).

A mixture of [WPt(μ$_2$-C)(CO)$_2$(PPh$_3$)$_2$(Tp*)] (**3.1b**; 502 mg, 0.372 mmol) with 2,4,6-trimethylphenylisocyanide (CNMes) (148 mg, 1.02 mmol) was dissolved in benzene (30 mL) and stirred for 4 hours. Upon solvent injection an orange suspension was noted. The reaction was stirred for 16 hours at 60 ºC until precipitation of an orange solid and a clear supernatant phase was recorded. The solvent was removed via rotary evaporation to give a pale orange solid. Flash column chromatography (silica gel, N_2, CH_2Cl_2/THF/$CHCl_3$ gradient) was employed for purification, eluting a major orange band and evaporated to an orange solid. Sonication in Et_2O (10 mL) allowed for a very fine particulate orange powder to form. This was collected on a Hirsch funnel equipped with fine filter paper and washed with *n*-hexane (3 × 10 mL) and *n*-pentane (3 × 10 mL) and dried *in vacuo* for 1 hour to afford the title compound (376 mg, 0.337 mmol, 91% isolated yield). Crystal suitable for x-ray diffraction were obtained by the slow evaporation of $CDCl_3$ at ambient temperature. IR (CH_2Cl_2, cm^{-1}): 2194 vs ν_{CN}, 1951 vs ν_{CO}, 1859 vs ν_{CO}. IR (ATR, cm^{-1}): 2536 w ν_{BH}, 2190 vs ν_{CN}, 1940 vs ν_{CO}, 1850 vs ν_{CO}. ^{1}H NMR (400 MHz, $CDCl_3$, 25 ºC, δ): 7.36 [s, 2H, MesCH], 6.85 [s, 4H, MesCH], 5.76 [s, 2H, pzCH], 5.69 [s, 1H, pzCH], 2.81 [s, 6H, *p*-CH_3Mes], 2.35 [s, 6H, pzCH_3], 2.33 [s, 3H, pzCH_3], 2.29 [s, 3H, pzCH_3], 2.28 [s, 6H, pzCH_3], 2.15 [s, 12H, *o*-CH_3Mes]. ^{13}C{^{1}H} NMR (151 MHz, $CDCl_3$, 25 ºC, δ): 299.3 [W≡C–Pt], 226.7 [$^1J_{CW}$ = 174 Hz, CO], 152.1 151.7 [C^5(pz)], 144.8 143.7 [C^3(pz)], 140.7 [C^4(Mes)], 136.5 [C^{2,6}(Mes)], 128.8 [C^{3,5}(Mes)], 128.5 [C^1(Mes)], 122.8 [Pt-*C*NMes], 106.3 106.2 [C^4(pz)], 21.5 18.1 [MesCH_3], 17.1 15.3 12.8 12.7 [pzCH_3]. ^{195}Pt{^{1}H} NMR (85.7 MHz, $CDCl_3$, 25ºC, δ): –3656 [bs]. MS (ESI, *m*/*z*): Found: 1114.20745. Calcd for $C_{38}H_{45}{}^{11}B^{79}BrN_8O_2{}^{195}Pt^{184}W$ [M+H]$^+$: 1114.20883. Anal. Found: C, 41.00; H, 3.82; N, 9.94%. Calcd for $C_{38}H_{44}BBrN_8O_2PtW$: C, 40.95; H, 3.98; N, 10.05%. *Crystal data for* $C_{38}H_{45}BBrN_8O_2PtW$, *M* = 1258.87, monoclinic, *I*2/*a*, *a* = 20.9197 (3) Å, *b* = 13.80583 (17) Å, *c* = 34.4091 (6) Å, β = 90.7607 (14)º, *V* = 9936.9 (4) Å^3, *Z* = 8, ρ_{calc} = 1.683 Mg m^{-3}, μ(Mo *K*α) = 12.15 mm^{-1}, *T* = 150(0) K, block {clear light orange}, 9812 independent measured reflections (θ = 73.0 º), R_1 = 0.034, *w*R_2 = 0.087 for 8154 reflections [*I* >2σ(*I*)], 481 parameters, 0 restraints. CDCC 2084968. Assistance in solving the crystal structure was provided by Dr. Michael Gardiner who the author gratefully acknowledges in dealing with a modulated structure.

Synthesis of [WPt(μ$_2$-C)Br(CN^{t}Bu)$_2$(CO)$_2$(Tp*)] (4.6).

A sample of [Pt(nbe)$_3$] (26 mg, 55 μmol) was dissolved in benzene (3 mL) to give a clear off-white solution. Injection of *tert*-butylisocyanide (0.02 mL, 180 μmol) immediately changed to a red solution and stirred for 30 minutes before the addition of a benzene solution (2 mL) containing

[W(≡CBr)(CO)$_2$(Tp*)] (35 mg, 56 μmol). This mixture transformed to a bright yellow solution within 30 minutes and was left to stir for 16 hours. Solvent was removed under reduced pressure before sonication in *n*-hexane (10 mL) liberated a pale yellow solid. The resulting solid was collected *via* vacuum filtration and washed with *n*-hexane (2 × 10 mL) and 20% Et_2O/*n*-hexane (10 mL) to afford the title compound as a yellow powder (19 mg, 19 μmol, 37% isolated yield). Crystals suitable for single crystal x-ray diffraction were grown from the vapour diffusion of *n*-hexane into a $CHCl_3$ solution of **4.6** at 5 °C. IR (CH_2Cl_2, cm^{-1}): 2216 vs ν_{CN}, 1949 vs ν_{CO}, 1856 vs ν_{CO}. IR (ATR, cm^{-1}): 2541 w ν_{BH}, 2211 vs ν_{CN}, 1943 vs ν_{CO}, 1849 vs ν_{CO}. ^{1}H NMR (400 MHz, $CDCl_3$, 25 ºC, δ): 5.60 [s, 2H, pzCH], 5.44 [s, 1H, pzCH], 3.08 [s, 6H, pzCH_3], 2.55 [s, 3H, pzCH_3], 2.11 [s, 6H, pzCH_3], 2.10 [s, 3H, pzCH_3], 0.75 [s, 18H, CNCCH_3]. ^{13}C{^{1}H} NMR (151 MHz, $CDCl_3$, 25 ºC, δ): 226.4 [t, $^1J_{C–14N}$ = 36 Hz, CO], 152.0 151.7 [t, $^1J_{C–14N}$ = 36 Hz, C^5(pz)], 144.8 143.7 [t, $^1J_{C–14N}$ = 36 Hz, C^3(pz)], 107.3 106.1 [t, $^1J_{C–14N}$ = 36 Hz, C^4(pz)], 58.7 [t, $^1J_{C–14N}$ = 36 Hz, *C*N^{t}Bu], 29.6 [t, $^1J_{C–14N}$ = 36 Hz, CNC*C*H$_3$], 17.1 15.2 12.7 12.6 [t, $^1J_{C–14N}$ = 36 Hz, pzCH_3]. The μ$_2$-carbido ligand was unable to be directly detected from ^{13}C{^{1}H} NMR analysis due to splitting of signals, however, W≡*C*–Pt is tentatively assigned to 289.0 ppm due to a ^{1}H-^{13}C HMBC experiment. ^{195}Pt{^{1}H} NMR (85.7 MHz, $CDCl_3$, 25ºC, δ): –3709 [pentet, $^2J_{Pt–14N}$ = 116 Hz]. MS (ESI, *m*/*z*): Found: 990.17545. Calcd for $C_{28}H_{41}{}^{11}B^{79}BrN_8O_2{}^{195}Pt^{184}W$ $[M+H]^+$: 990.17812. Anal. Found: C, 33.82; H, 3.90; N, 11.12%. Calcd for $C_{28}H_{40}BBrN_8O_2PtW$: C, 33.96; H, 4.07; N, 11.32%. *Crystal data for* $C_{28}H_{40}BBrN_8O_2PtW{\cdot}CHCl_3{\cdot}0.5(C_6H_{14})$, M = 1152.79, monoclinic, $P2_1/n$, a = 10.2377 (2) Å, b = 32.8680 (6) Å, c = 14.4482 (3) Å, β = 100.020 (2)º, V = 4787.56 (16) Å^3, Z = 4, ρ_{calc} = 1.599 Mg m^{-3}, μ(Mo $K\alpha$) = 6.36 mm^{-1}, T = 150(0) K, block 0.42 × 0.17 × 0.17 mm {clear light yellow}, 12380 independent measured reflections (θ = 29.8 º), R_1 = 0.045, wR_2 = 0.109 for 10737 reflections [$I > 2\sigma(I)$], 498 parameters, 45 restraints. CDCC 2251819.

Synthesis of [WPt(μ$_2$-C)(Bp*)(CNMes)(CO)$_2$(Tp*)] (4.7).

An orange suspension of [WPt(μ$_2$-C)Br(CNMes)$_2$(CO)$_2$(Tp*)] (**4.5**; 105 mg, 0.094 mmol) and KBp* (28 mg, 0.116 mmol) in CH_2Cl_2 was stirred for 16 hours resulting in a red/orange solution. Solvent was removed *via* rotary evaporation to give an orange residue before purification by flash column chromatography {silica gel, N_2, petroleum ether/CH_2Cl_2 gradient elution}. A yellow band eluted first before recovering leftover **4.5** and a red compound refusing to elute off the column despite polar eluents. The yellow fraction was concentrated from CH_2Cl_2/*n*-hexane mixture which dried to a yellow powder, as the species was soluble in a variety of solvents. This yellow powder was dried *in vacuo* for several hours before mechanical retrieval gave the listed compound as a yellow powder (28 mg, 0.026 mmol, 28% isolated yield). Crystals suitable for x-ray diffraction

studies were grown from the vapour diffusion of EtOH into a $CHCl_3$ solution of compound at 5 °C overnight. IR (CH_2Cl_2, cm^{-1}): 2194 s ν_{CNR}, 1944 vs ν_{CO}, 1852 vs ν_{CO}. IR (ATR, cm^{-1}): 2524 w ν_{BH}, 2185 vs ν_{CN}, 1941 vs ν_{CO}, 1840 vs ν_{CO}. ^{1}H NMR (400 MHz, $CDCl_3$, 25 ºC, δ): 6.90 [s, 2H, MesCH], 5.88 5.68 5.63 5.57 5.52 [s, 1H, pzCH], 3.05 [s, 3H, $pzCH_3$], 2.41 [s, 6H, $MesCH_3$], 2.38 [s, 3H, $MesCH_3$], 2.32 2.31 [overlapping singlets, 3H each, $pzCH_3$], 2.29 [s, 3H, $pzCH_3$], 2.28 [s, 6H, $pzCH_3$], 2.26 [overlapping singlets, 3H each, $pzCH_3$], 2.19 [s, 3H, $pzCH_3$], 1.88 [s, 3H, $pzCH_3$]. ^{13}C{^{1}H} NMR (151 MHz, $CDCl_3$, 25ºC, δ): 322.7 [$^1J_{CW}$ = 182 Hz, $^1J_{CPt}$ = 690 Hz, W≡C–Pt], 227.8 226.7 [$^1J_{CW}$ = 167 Hz, CO], 152.8 152.0 151.6 149.7 148.5 [C^5(pz)], 145.0 144.5 144.2 143.5 143.3 [C^3(pz)], 139.6 [C^4(Mes)], 135.6 [$C^{2,6}$(Mes)], 128.7 [$C^{3,5}$(Mes)], 125.5 [$^1J_{CPt}$ = 1800 Hz, *C*NMes], 124.5 [C^1(Mes)], 106.2 106.0 105.7 105.5 105.2 [C^4(pz)], 21.4 18.6 [$MesCH_3$], 17.2 15.3 15.0 14.7 13.7 13.0 12.88 12.85 12.8 12.7 [$pzCH_3$]. ^{195}Pt{^{1}H} NMR (150.0 MHz, $CDCl_3$, 25°C, δ): –3371 [br.s]. MS (ESI, *m/z*): Found: 1092.3448. Calcd for $C_{38}H_{49}{}^{11}B_2N_{11}O_2{}^{195}Pt^{184}W$ $[M]^+$: 1092.3482. Anal. Found: C, 41.75; H, 4.47; N, 13.45%. Calcd for $C_{38}H_{49}B_2N_{11}O_2PtW$: C, 41.78; H, 4.52; N, 14.10%. Satisfactory microanalytical elemental analysis results were unable to be achieved despite multiple attempts. The best result is recorded. *Crystal data for* $C_{38}H_{49}B_2N_{11}O_2PtW$, M = 1092.44, monoclinic, $P2_1/n$, a = 7.9965 (1) Å, b = 24.0347 (3) Å, c = 21.9700 (2) Å, β = 97.630 (1)°, V = 4185.11 (8) Å^3, Z = 4, ρ_{calc} = 1.734 Mgm^{-3}, μ(Cu $K\alpha$) = 11.54 mm^{-1}, T = 150(0) K, plate 0.43 × 0.08 × 0.05 mm {clear light yellow}, 8341 independent reflections (θ = 73.6), R_1 = 0.034, wR_2 = 0.134 for 7756 reflections [$I > 2\sigma(I)$], 513 parameters, 7 restraints. CDCC 2251816.

Synthesis of [WPt(μ$_2$-C)(κ$_2$-Tp*)(CNMes)(CO)$_2$(Tp*)] (4.8).

A sample of [WPt(μ$_2$-C)Br(CNMes)$_2$(CO)$_2$(Tp*)] (**4.5**; 0.090 g, 0.081 mmol) was combined with KTp* (0.054, g, 0.16 mmol) and dissolved in ample CH_2Cl_2 (30 mL) and heated to reflux for 2 days. The solution began as an orange and did not change during the course of the reaction. Solvent was removed *via* rotary evaporation to give a orange residue that could be purified by flash column chromatography {silica gel, N_2, CH_2Cl_2/THF gradient}. Neat CH_2Cl_2 eluted an initial orange band as unreacted **4.5** (0.022 g, 0.020 mmol) before 2% THF/CH_2Cl_2 eluted a bright yellow band of the title compound. Some material remained on the baseline despite polar solvents. Once the elute of compound was evaporated, the compound could be recrystallised from concentration of a CH_2Cl_2/*n*-hexane solution to give a yellow solid that could be collected via vacuum filtration, washing with *n*-hexane (3 × 10 mL) before drying in vacuo for 16 hours. This provided the title compound as a yellow microcrystalline solid (0.030 g, 0.026 mmol, 32% isolated yield). Crystals

suitable for x-ray diffraction were grown from the vapour diffusion of *n*-hexane into a $CHCl_3$ solution of compound at 5 °C. IR (CH_2Cl_2, cm^{-1}): 2194 vs ν_{CN}, 1946 vs ν_{CO}, 1853 vs ν_{CO}. IR (ATR cm^{-1}): 2529 w ν_{BH}, 2187 br.s ν_{CN}, 1940 br.vs ν_{CO}, 1848 br.vs ν_{CO}. ^{1}H NMR (600 MHz, $CDCl_3$, 25 ºC, δ): 6.93 [s, 2H, MesCH], 5.77 [s, 2H, pzCH], 5.73 [s, 3H, pzCH], 5.60 [s, 1H, pzCH], 2.61–2.53 [br.m, $pzCH_3$], 2.51 [s, 6H, $MesCH_3$], 2.34 [s, 6H, $pzCH_3$], 2.32 [s, 3H, $MesCH_3$], 2.25 [s, 3H, $pzCH_3$], 2.24 [s, 3H, $pzCH_3$], 2.19 [br.s, 6H, $pzCH_3$], 2.15–2.03 [br.m, 6H, $pzCH_3$]. ^{13}C{^{1}H} NMR (151 MHz, $CDCl_3$, 25ºC, δ): 321.3 [$^1J_{CW}$ = 179 Hz, W≡C–Pt], 227.2 [$^1J_{CW}$ = 173 Hz, CO], 152.3 [br.s, C^5(pz)], 152.0 [C^5(pz)], 149.6 [br.s, C^5(pz)], 145.0 [br.s, C^3(pz)], 144.4 143.4 [C^3(pz)], 139.6 [C^1(Mes)], 135.6 [$C^{2,6}$(Mes)], 128.8 [$C^{3,5}$(Mes)], 124.8 [br, Pt–*C*NMes], 124.6 [C^4(Mes)], 106.3 106.0 105.9 [C^4(pz)], 21.4 18.8 [$MesCH_3$], 16.6 15.2 [$pzCH_3$], 14.5 13.1 [br.s, $pzCH_3$], 12.9 12.6 [$pzCH_3$]. ^{195}Pt{^{1}H} NMR (150.0 MHz, $CDCl_3$, 25ºC, δ): –3340 [br.s]. MS (ESI, *m/z*): Found: 1186.4026. Calcd for $C_{43}H_{56}{}^{11}B_2N_{13}O_2{}^{195}Pt^{183}W$ $[M+H]^+$: 1186.4016. Samples of sufficient purity were unable to be obtained for elemental analsysis. The best data obtained is shown here. Anal. Found: C, 43.65; H, 4.67; N, 15.35%. Calcd for $C_{43}H_{55}B_2N_{13}O_2PtW$: C, 43.51; H, 5.20; N, 16.47%. *Crystal data for* $C_{43}H_{55}B_2N_{13}O_2PtW{\cdot}CHCl_3$, M = 1305.92, monoclinic, $P2_1/c$, a = 17.7971 (1) Å, b = 16.8739 (1) Å, c = 17.0568 (1) Å, β = 97.849 (1)º, V = 5074.28 (5) Å^3, Z = 4, ρ_{calc} = 1.709 Mgm^{-3}, μ(Cu *K*α) = 11.06 mm^{-1}, T = 150(0) K, block 0.33 × 0.27 × 0.05 mm {clear light yellow}, 10115 independent measured reflections (θ = 73.6), R_1 = 0.028, wR_2 = 0.074 for 9677 reflections [$I > 2\sigma(I)$], 610 parameters, 0 restraints. CDCC 2251818.

Synthesis of $[WPt(\mu_2\text{-}C)(CNMes)_3(CO)_2(Tp^*)]PF_6$ (4.9).

A mixture of solid $[WPt(\mu_2\text{-}C)Br(CNMes)_2(CO)_2(Tp^*)]$ (**4.5**; 77 mg, 0.069 mmol), 2,4,6-methylphenylisocyanide (CNMes) (18 mg, 0.12 mmol) and $NaPF_6$ (36 mg, 0.21 mmol) were set under inert atmosphere of argon. Injection of CH_2Cl_2 (10 mL) changed the orange solid to a dark yellow mixture prior to the injection of MeOH (2 mL) giving a dark green solution. This was stirred for 10 minutes before solvent was removed under reduced pressure. The ensuing residue was recrystallised from concentration of CH_2Cl_2/*n*-hexane to give a pale green powder and further washed with *n*-hexane (3 × 10 mL). The resulting powder was determined to pure except for 1:2 ratio of product to MeOH solvent molecules retained despite drying *in vacuo* for 4 hours (85 mg, 0.064 mmol, 88% yield). The solid was stored under argon at 5°C in the Schlenk flask it was originally crystallised; air exposure or elevated temperature results in deposition of platinum black. IR (CH_2Cl_2, cm^{-1}): 2208 s ν_{CN}, 2193 s ν_{CN}, 1965 vs ν_{CN}, 1875 vs ν_{CN}. IR (ATR, cm^{-1}): 2552 w ν_{BH}, 2206 s ν_{CN}, 2189 s ν_{CN}, 1958 vs ν_{CO}, 1864 vs ν_{CO}. ^{1}H NMR (600 MHz, CD_2Cl_2, 25 ºC, δ): 7.04 [s, MesCH, 2H], 6.96 [s, MesCH, 4H], 5.82 [s, pzCH, 2H], 5.77 [s, pzCH, 1H], 3.42

[s, C*H*$_3$OH, 6H], 2.74 [s, MesCH$_3$, 6H], 2.40 [overlapping singlets, MesCH$_3$, 6H], 2.35 [s, pzCH$_3$, 3H], 2.33 [overlapping singlet, pzCH$_3$, 6H], 2.32 [overlapping singlet, pzCH$_3$, 6H], 2.30 [s, pzCH$_3$, 3H], 2.16 [br, MesCH$_3$, 9H]. ^{13}C{^{1}H} NMR (151 MHz, CD_2Cl_2, 25°C, δ): 306.5 [W≡C–Pt], 227.6 [$^1J_{CW}$ = 171 Hz, CO], 152.9 151.7 [C^5(pz)], 146.4 146.3 [C^3(pz)], 143.2 [C^1(Mes)], 136.8 [br, C^4(Mes)], 136.3 [C^{2,6}(Mes)], 129.9 [C^{3,5}(Mes)], 129.6 [*C*NMes, $^1J_{CPt}$ = 1076 Hz], 107.0 106.9 [C^3(pz)], 21.8 19.0 [Mes*C*H$_3$], 18.3 [br, MesCH$_3$], 17.5 15.4 12.93 12.87 [pz*C*H$_3$]. ^{195}Pt NMR (150 MHz, CD_2Cl_2, 25°C, δ): –4177 [br, W≡C–Pt]. MS (ESI, *m/z*): Found: 1179.37299. Calcd for $C_{48}H_{55}BN_9O_2PtW$ [M]$^+$: 1179.37269. A sample of suitable purity for elemental analysis was unable to be obtained due to the reactivity of the compound. The best data is described here despite being a significant deviation. Anal. Found: C, 32.07; H, 2.92; N, 6.72%. Calcd for $C_{48}H_{55}BF_6N_9O_2PPtW$: C, 43.52; H, 4.19; N, 9.52%. *Crystal data for* this compound was unable to be collected due to the rapid desolvation; shattering the crystals grown from a range of solvent systems. This issue was compounded by consistent formation in thin needle form.

Synthesis of [WPt(μ$_2$-CCNXyl)(CO)$_2$(PPh$_3$)$_2$(Tp*)]BPh$_4$ (4.10).

A solvent mixture of 1:5 MeOH/CH_2Cl_2 (15 mL) was injected to a flask charged with solid [WPt(μ$_2$-C)Br(CNXyl)(PPh$_3$)(CO)$_2$(Tp*)] (**4.1**; 0.102 g, 0.0838 mmol), triphenylphosphine (0.026 g, 0.099 mmol) and $NaBPh_4$ (0.032 g, 0.094 mmol). With rapid stirring, this mixture transitioned immediately from an orange solution to a pink/maroon colour before stirring for 20 hours gave a vivid purple colour, initially evident by ~ 5 hours. The solvent was removed *via* rotary evaporation and the resulting purple residue was eluted through a short column {silica gel, neat CH_2Cl_2} to remove excess $NaBPh_4$ and then be purified by flash column chromatography {silica gel, N_2, isocratic elution, neat CH_2Cl_2} eluting a major purple band, where 5 fractions (40 mL) were sampled across the band. Samples of each fraction were tested by ^{1}H NMR spectroscopy determining that fraction 1 was pure, fractions 2–4 could be purified by recrystallisation and fraction 5 was an unidentified compound of similar colour and polarity. Recrystallisation on relevant fractions was performed by the concentration of CH_2Cl_2 into EtOH by rotary evaporation. When solids began emerging, the flash was sonicated to encourage more precipitation before concentrating further. This resulting precipitate was collected via vacuum filtration to give a pastel purple powder and a pink/red supernatant after careful washing with EtOH (2 x 5 mL) and *n*-hexane (2 x 10 mL). The powders were dried *in vacuo* for 16 hours to afford compound **4.10** as a purple powder (0.080 g total, 0.047 mmol total, 56% isolated yield). Crystals suitable for x-ray diffraction were grown from the vapour diffusion of *n*-hexane into a solution of the title compound in $CHCl_3$ at 5 °C overnight. IR (CH_2Cl_2, cm^{-1}): 2104 s $\nu_{\mu\text{-CCN}}$, 1944 vs ν_{CO}, 1853 vs ν_{CO}.

IR (ATR, cm^{-1}): 2556 w ν_{BH}, 2094 s $\nu_{\mu\text{-}CCN}$, 1936 vs ν_{CO}, 1855 vs ν_{CO}. UV-Vis[$1.95(2)\times10^{-5}$ $molL^{-1}$, nm(ϵ), CH_2Cl_2]: 268 (36100), 276 (36000), 292 (36200), 365 (14000), 535 (6900). ^{1}H NMR (400 MHz, $CDCl_3$, 25 ºC, δ): 7.73 [m, 5H, PhCH], 7.49 [m, 8H, PhCH], 7.42 [m, 4H, PhCH], 7.30 [m, 8H, PhCH], 7.21 [m, 9H, PhCH], 7.07 [m, 14H, PhCH], 6.92 [m, 4H, PhCH], 6.78 6.76 [d, $^1J_{HH}$ = 7 Hz, 2H, $C^{3,5}$H(Xyl)], 5.87 [s, 2H, pzCH], 5.81 [s, 1H, pzCH], 2.51 [s, 6H, $pzCH_3$], 2.37 [s, 3H, $pzCH_3$], 2.24 [s, 6H, $pzCH_3$], 1.76 [s, 3H, $pzCH_3$], 0.95 [s, 6H, $XylCH_3$]. $^{13}C\{^1H\}$ NMR (151 MHz, $CDCl_3$, 25ºC, δ): 226.5 [d, $^2J_{CP}$ = 6, $^2J_{CPt}$ = 48, $^2J_{CW}$ = 158 Hz, CO], 222.8 [dd, $^2J_{CP}$ = 73, 7 Hz, W(μ-C)Pt], 164.5 [quart + hept., $^1J_{C\text{-}11B}$ = 50, $^1J_{C\text{-}10B}$ = 17 Hz, $C^1(BC_6H_5)$], 156.1 151.2 [C^5(pz)], 147.3 145.2 [C^3(pz)], 139.1 [t, $^3J_{CP}$ = 9, $^2J_{CPt}$ = 111 Hz, WPt(μ-C*C*NXyl)], 136.5 [$C^{2,6}(BC_6H_5)$], 135.1 134.5 [d, $^2J_{CP}$ = 12 Hz, $C^{2,6}(C_6H_5)$], 133.3 [d, $^1J_{CP}$ = 49 Hz, $C^1(C_6H_5)$], 132.9 [C^2(Xyl)], 132.3 [d, $^1J_{CP}$ = 50 Hz, $C^1(C_6H_5)$], 131.0 130.8 [$C^4(C_6H_5)$], 129.7 [C^4(Xyl)], 128.5 [d, $^3J_{CP}$ = 10 Hz, $C^{3,5}(C_6H_5)$], 128.4 [$C^{3,5}$(Xyl)], 128.2 [d, ^3J = 10 Hz, $C^{3,5}(C_6H_5)$], 127.2 [C^1(Xyl)], 125.6 [m, $C^{3,5}(BC_6H_5)$], 121.6 [$C^4(BC_6H_5)$], 108.6 107.7 [C^4(pz)], 17.4 [$pzCH_3$], 17.0 [$XylCH_3$], 16.0 13.2 12.7 [$pzCH_3$]. $^{31}P\{^1H\}$ NMR (162 MHz, $CDCl_3$, 25 ºC, δ): 44.46 [d, $^2J_{PP}$ = 20, $^1J_{PPt}$ = 3772 Hz, PPh_3], 25.60 [d, $^2J_{PP}$ = 20, $^1J_{PPt}$ = 3440 Hz, PPh_3]. $^{195}Pt\{^1H\}$ NMR (149.9 MHz, $CDCl_3$, 25ºC, δ): –4174 [dd, $^1J_{PtP}$ = 3766, 3448 Hz]. MS (ESI, *m/z*): Found: 1399.3612. Calcd for $C_{63}H_{61}{}^{11}BN_7O_2P_2{}^{195}Pt{}^{184}W$ $[M]^+$: 1399.3612. Anal. Found: C, 60.77; H, 4.63; N, 5.73%. Calcd for $C_{87}H_{81}B_2N_7O_2P_2PtW$: C, 60.78; H, 4.75; N, 5.70%. *Crystal data for* $C_{63}H_{61}BN_7O_2P_2PtW.2(CHCl_3).C_{24}H_{20}B$, M = 1957.82, monoclinic, $P2_1/c$, a = 20.9875 (3) Å, b = 15.7357 (2) Å, c = 26.1799 (5) Å, β = 105.436 (2)º, V = 8334.1 (2) $Å^3$, Z = 4, ρ_{calc} = 1.560 Mgm^{-3}, μ(Cu $K\alpha$) = 8.15 mm^{-1}, T = 150(0) K, plate, 0.11 × 0.04 × 0.03 mm {clear light red}, 16087 independent measured reflections (θ = 72.8), R_1 = 0.047, wR_2 = 0.128 for 12305 reflections [$I > 2\sigma(I)$], 1003 parameters. CDCC 2084967. Compound also crystallised with PF_6 counter-anion. *Crystal data for* $C_{63}H_{61}BN_7O_2P_2PtW\cdot(CHCl_3)\cdot PF_6$, M = 1664.21, triclinic, $P\bar{1}$, a = 11.8143 (3) Å, b = 14.7029 (4) Å, c = 22.6429 (8) Å, α = 100.170 (3)°, β = 103.965 (3)º, γ = 107.433 (2)°, V = 3507.58 (19) $Å^3$, Z = 2, ρ_{calc} = 1.576 Mgm^{-3}, μ(Mo $K\alpha$) = 3.88 mm^{-1}, T = 150(0) K, block, 0.23 × 0.13 × 0.04 mm {clear dark purple}, 19658 independent measured reflections (θ = 32.2), R_1 = 0.044, wR_2 = 0.103 for 15114 reflections [$I > 2\sigma(I)$], 805 parameters, 0 restraints. CDCC 2085626.

Synthesis of $[(Tp^*)(CO)_2W(\mu\text{–}CCNMes)Pt(CNMes)(PPh_3)].PF_6$ (4.11).

A mixture of solid $[WPt(\mu_2\text{-}C)Br(CNMes)_2(CO)_2(PPh_3)_2(Tp^*)]$ (**4.5**; 178 mg, 0.159 mmol), PPh_3 (56 mg, 0.21 mmol) and $NaPF_6$ (46 mg, 0.274 mmol) were dissolved in a mixture of

MeOH/CH_2Cl_2 (15 mL, 1:5 *v*/*v*), immediately changing from orange to green and slowly transition to deep purple colour over 16 hours. The solvent was removed to give a dark solid that was purified by flash column chromatography {silica gel, N_2, isocratic elution, 2% THF/CH_2Cl_2} on to collect a major purple eluate. The residue was dissolved in benzene (10 mL) and layered with *n*-hexane (25 mL) before sitting at −20 °C for 3 days, resulting in fine purple crystalline solid. This solid could be collcted *via* vacuum filtration, washing with cold benzene (2 × 3 mL) and *n*-hexane (3 × 10 mL) before drying *in vacuo* to give the title compound as a deep purple powder (77 mg, 0.053 mmol, 34% isolated yield). Single crystals were not achieved for X-ray crystallographic analysis. IR (CH_2Cl_2, cm^{-1}): 2558 w ν_{BH}, 2156 vs ν_{CN}, 2115 vs ν_{CN}, 1943 vs ν_{CO}, 1862 vs ν_{CO}. IR (ATR): 2553 w ν_{BH}, 2119 br vs ν_{CN}, 1933 vs ν_{CO}, 1844 vs ν_{CO}. UV-Vis [$2.11(6)\times10^{-5}$ $molL^{-1}$, nm(ϵ), CH_2Cl_2]: 263 (35000), 320 (30300), 347 sh (17700), 550 (6800). ^{1}H NMR (400 MHz, $CDCl_3$, 25 ºC, δ): 7.58 [m, 6H, PPh], 7.36 [m, 9H, PPh], 7.17 [m, 2H, PPh], 6.90 [s, 2H, MesCH], 6.67 [s, 2H, μ-CCNMesC*H*], 5.95 [s, 1H, pzCH], 5.91 [s, 2H, pzCH], 2.62 [s, 3H, $pzCH_3$], 2.55 [s, 6H, $pzCH_3$], 2.41 [s, 3H, $pzCH_3$], 2.33 [s, 3H, $MesCH_3$], 2.15 [s, 6H, μ-CCNMesCH_3], 2.11 [s, 3H, $MesCH_3$], 1.02 [s, 6H, μ-CCNMesCH_3]. ^{13}C{^{1}H} NMR (151 MHz, $CDCl_3$, 25ºC, δ): 229.0 228.9 [overlapping singlets, CO], 217.9 [d, $^2J_{CP}$ = 6 Hz, μ-*C*CNMes], 156.2 151.2 [C^5(pz)], 147.4 145.4 [C^3(pz)], 141.3 [C^1(Mes)], 139.7 [C^1(μ-CCN*Mes*)], 134.8 [C^4(μ-CCN*Mes*)], 134.0 [d, $^2J_{CP}$ = 12 Hz, $C^{2,6}(C_6H_5)$], 133.8 [C^4(Mes)], 132.3 [d, $^1J_{CP}$ = 53 Hz, $C^1(C_6H_5)$], 131.7 [$C^4(C_6H_5)$], 129.0 [d, $^3J_{CP}$ = 11 Hz, $C^{3,5}(C_6H_5)$], 129.5 [$C^{3,5}$(Mes)], 128.8 [$C^{3,5}$(μ-CCN*Mes*)], 124.7 [Pt-CNMes], 124.3 [μ-C*C*NMes], 125.4 [C^1(μ-CCNMes)], 124.6 [Pt−*C*NMes], 124.2 [C^1(Pt-CNMes)], 109.3 107.8 [C^4(pz)], 21.6 21.4 [$MesCH_3$], 18.5 17.8 [$MesCH_3$], 16.9 16.1 13.2 12.7 [$pzCH_3$]. ^{31}P{^{1}H} NMR (162 MHz, $CDCl_3$, 25 ºC, δ): 44.14 [s, $^1J_{PPt}$ = 3575 Hz]. ^{195}Pt{^{1}H} NMR (150 MHz, $CDCl_3$, 25ºC, δ): –4136 [d, $^1J_{PtP}$ = 3587 Hz]. MS (ESI, *m*/*z*): Found: 1296.3772. Calcd for $C_{56}H_{59}{}^{11}BN_8O_2P^{195}Pt^{184}W$ $[M]^+$: 1296.3749. Anal. Found: C, 47.62; H, 4.26; N, 7.34%. Calcd for $C_{59}H_{67}BF_6N_8O_2P_2PtW$: C, 47.69; H, 4.55; N, 7.54%.

9.7 Synthetic procedures for Chapter Five compounds

Synthesis of [WPt(μ$_2$-CH)(μ$_2$-CO)(CO)$_2$(PPh$_3$)(Tp*)] (5.1).

Note: This compound slowly decomposes to [W_2Pt(μ$_2$-CH)$_2$(μ$_2$-CO)$_2$(CO)$_2$(Tp*)$_2$] if exposed to moisture.

Method 1 (Borohydride Reduction)—Preferred: A solution of [WPt(μ$_2$-C)Br(CO)$_2$(PPh$_3$)$_2$(Tp*)] (**3.1b**; 111 mg, 0.0813 mmol) was stirred with $NaBH_4$ (11 mg, 0.29 mmol) in THF (10 mL) under at atmosphere of carbon monoxide for 20 hours. Commencing as an orange solution, the mixture darkened to deep red, while suspended pieces of $NaBH_4$ decreased in size.

The resulting solution was evaporated under reduced pressure affording an red residue. Now open to air, the residue was dissolved in CH_2Cl_2 and purified *via* flash column chromatography {silica gel, N_2, isocratic elution 1:1 CH_2Cl_2/petroleum ether 60–80}. This eluted the title compound as a red band which had solvent removed by rotary evaporation and dried *in vacuo* for 4 hours to give the title compound as a maroon powder (43 mg, 0.041 mmol, 51% isolated yield). Single crystals suitable for x-ray diffraction analysis were grown over several weeks from the slow evaporation of the compound dissolved in 1:1 CH_2Cl_2/*n*-hexane at −20 °C.

Method 2 (Ligand Substitution): A sample of [WPt(μ_2-CH)(μ_2-CO)(CO)(PPh_3)$_2$(Tp*)] (**5.6**; 0.080 g, 0.063 mmol) in THF (5 mL) was bubbled with carbon monoxide for 5 minutes. The originally red/orange solution brightens slightly to a magenta colour. After the bubbling is concluded the reaction vessel is sealed under a CO(g) atmosphere and left to stir for 16 hours. The ensuing red/pink solution is eluted through celite and recrystallised from concentration of CH_2Cl_2 into *n*-hexane aided by rotary evaporation, prior to collection via vacuum filtration and washing with minimal cold MeOH (0 °C, 2 × 1 mL) to control losses given partial solubility. The collected solid can be dried *in vacuo* for 16 hours to give the title compound as a bright red microcrystalline powder (0.040 g, 0.039 mmol, 62% isolated yield). IR (CH_2Cl_2, cm^{-1}): 2016 vs ν_{Pt-CO}, 1924 vs ν_{W-CO}, 1786 m $\nu\mu$-$_{CO}$. IR (ATR, cm^{-1}): 2551 w ν_{BH}, 2378 m $\nu\mu$-$_{CH}$, 2008 vs ν_{Pt-CO}, 1906 vs ν_{W-CO}, 1774 s $\nu\mu$-$_{CO}$.. ^{1}H NMR (600 MHz, $CDCl_3$, 25 ºC, δ): 13.69 [d, $^3J_{HP}$ = 18, $^2J_{HPt}$ = 54 Hz, 1H, μ_2-CH], 7.59 [m, 3H, PPh], 7.53 [m, 2H, PPh], 7.46 [m, 6H, PPh], 7.37 [m, 10H, overlaps with $H_3B{\rightarrow}PPh_3$ impurity], 5.81 [s, 1H, pzCH], 5.77 [s, 2H, pzCH], 2.64 [s, 3H, $pzCH_3$], 2.39 [s, 6H, $pzCH_3$], 2.34 [s, 3H, $pzCH_3$], 2.12 [s, 6H, $pzCH_3$]. ^{13}C{^{1}H} NMR (151 MHz, $CDCl_3$, 25ºC, δ): 310.0 [m, $^1J_{CPt}$ = 590 Hz, μ-CH], 231.7 [d, $^3J_{CH}$ = 48 Hz, $^1J_{CW}$ = 156 Hz, CO], 198.5 [d, $^2J_{CP}$ = 48 Hz, $^1J_{CPPt}$ = 477 Hz, μ_2-CO], 153.3 152.2 [C^5(pz)], 144.6 144.1 [C^3(pz)], 134.5 [d, $^1J_{CP}$ = 48 Hz, $C^1(C_6H_5)$], 133.8 [d, $^2J_{CP}$ = 13 Hz, $C^{2,6}(C_6H_5)$], 133.3 [d, $^2J_{CP}$ = 10 Hz, $C^{2,6}(C_6H_5)$], 131.4 [d, $^4J_{CP}$ = 3 Hz, $C^4(C_6H_5)$], 130.3 [d, $^4J_{CP}$ = 3 Hz, $C^4(C_6H_5)$], 129.4 [d, $^1J_{CP}$ = 58 Hz, $C^1(C_6H_5)$], 128.9 [d, $^3J_{CP}$ = 10 Hz, $C^{3,5}(C_6H_5)$], 128.5 [d, $^3J_{CP}$ = 48 Hz, $C^{3,5}(C_6H_5)$], 107.3 107.1 [C^4(pz)], 18.1 15.3 12.9 12.8 [$pzCH_3$]. ^{31}P{^{1}H} NMR (162 MHz, $CDCl_3$, 25 ºC, δ): 28.72 [s, $^1J_{PPt}$ = 3392 Hz, PPh]. ^{195}Pt{^{1}H} NMR (85.7 MHz, $CDCl_3$, 25ºC, δ): −4446 (d, $^1J_{PtP}$ = 3387 Hz). MS (ESI, *m*/*z*): Found: 1036.2065. Calcd for $C_{37}H_{39}{}^{11}BN_6O_3P^{184}W^{195}Pt$ $[M+H]^+$: 1036.2071. Anal. Found: C, 42.56; H, 3.77; N, 8.27%. Calcd for $C_{37}H_{38}BN_6O_3PPtW$: C, 42.92; H, 3.70; N, 8.12%. *Crystal data for* $C_{37}H_{38}BN_6O_3PPtW{\cdot}2(CHCl_3)$, M = 1274.19, monoclinic, $P2_1/c$, a = 17.9165 (4) Å, b = 14.4174 (3) Å, c = 17.9375 (4) Å, β = 106.849 (2)º, V = 4434.52 (17) Å^3, Z = 4, ρ_{calc} = 1.909 Mgm^{-3}, μ(Mo $K\alpha$) = 6.19 mm^{-1}, T = 150(0) K, block 0.29 × 0.25 × 0.22 mm {lustrous dark red}, 14573 independent measured reflections (θ

= 32.5), R_1 = 0.027, wR_2 = 0.053 for 12367 reflections [$I > 2\sigma(I)$], 557 parameters. CDCC 2251836. Methylidyne hydrogen models riding on carbon.

Synthesis of [MoPt(μ$_2$-C)Me(CO)$_2$(PPh$_3$)$_2$(Tp*)] (5.2a).

An orange solution containing [MoPt(μ$_2$-C)Br(CO)$_2$(PPh$_3$)$_2$(Tp*)] (**3.1a**; 0.123 mmol) in THF (10 mL) was cooled to –78 ºC and treated with methyllithium (0.25 mL, 1.6M in diethyl ether, 0.40 mmol). An instantaneous colour change occurred from orange to bright yellow. This mixture was stirred at low temperature for 90 minutes before slowly returning to room temperature such that the yellow colour persisted. Once warmed, small quantities of isopropanol were added to the mixture and stirred to quench methyllithium. Solvent was removed *via* rotary evaporation to give a bright yellow powder prior to recrystallisation from the concentration of CH_2Cl_2 into *n*-hexane. The resulting solid was collected *via* vacuum filtration and washed thoroughly with *n*-hexane (4 × 10 mL) and *n*-pentane (2 × 10 mL) to and dried *in vacuo* for 4 hours to afford the title compound (0.063 g, 0.053 mmol, 43% isolated yield). Crystals suitable for single crystal X-ray diffraction were grown from the vapour diffusion of *n*-hexane into a $CHCl_3$ solution of the compound over several days at 5 ºC. IR (CH_2Cl_2, cm^{-1}): 1948 vs ν_{CO}, 1859 vs ν_{CO}. IR (ATR, cm^{-1}): 2521 w ν_{BH}, 1941 vs ν_{CO}, 1852 vs ν_{CO}. ^{1}H NMR (600 MHz, CD_2Cl_2, 25 ºC, δ): 7.25 [m, 15H, PPh], 7.14 [m, 7H, PPh], 7.01 [br.m, 3H], 6.78 [br.m, 5H], 5.63 [s, 1H, pzCH], 5.59 [s, 2H, pzCH], 2.60 [s, 6H, pzCH$_3$], 2.35 [s, 6H, pzCH$_3$], 2.32 [s, 3H, pzCH$_3$], 2.25 [s, 3H, pzCH$_3$], 0.95 [m, overlaps with *n*-hexane, $^2J_{HPt}$ = 64 Hz, Pt–CH$_3$]. ^{13}C{^{1}H} NMR (151 MHz, CD_2Cl_2, 25ºC, δ): 390.7 [dd, $^2J_{CP}$ = 70 hz, $^2J_{CH}$ = 6 as outside decoupler range, Mo≡C–Pt], 232.0 [CO], 151.5 151.0 [C^5(pz)], 135.3 [d, $^2J_{CP}$ = 11 Hz, C^{2,6}(C$_6$H$_5$)], 134.7 [d, $^2J_{CP}$ = 12 Hz, C^{2,6}(C$_6$H$_5$)], 133.6 [d, $^1J_{CP}$ = 45 Hz, C^1(C$_6$H$_5$)], 133.3 [d, $^1J_{CP}$ = 42 Hz, C^1(C$_6$H$_5$)], 130.1 129.9 [C^4(C$_6$H$_5$)], 128.3 127.8 [d, $^3J_{CP}$ = 10 Hz, C^{3,5}(C$_6$H$_5$)], 106.5 105.9 [C^4(pz)], 16.6 14.6 13.1 12.7 [pzCH$_3$], 10.1 [dd, $^2J_{CP}$ = 81, 8 Hz, $^1J_{CPt}$ = 587 Hz, Pt–CH$_3$]. ^{31}P{^{1}H} NMR (162 MHz, $CDCl_3$, 25 ºC, δ): 24.42 [d, $^2J_{PP}$ = 13 Hz, $^1J_{PPt}$ = 1991 Hz], 17.68 [d, $^2J_{PP}$ = 14 Hz. $^1J_{PPt}$ = 1580]. ^{195}Pt{^{1}H} NMR (150 MHz, $CDCl_3$, 25ºC, δ): –4301 [ddd, $^1J_{PtP}$ = 2007, 1561 Hz, $^2J_{PtH}$ = 68 Hz]. MS (ESI, *m*/*z*): Found: 1197.2709. Calcd for $C_{55}H_{55}{}^{11}B^{98}MoN_6O_2P_2{}^{195}Pt$ [M]$^+$: 1197.2657. Anal. Found: C, 55.52; H, 4.89; N, 6.79%. Calcd for $C_{55}H_{55}BMoN_6O_2P_2Pt$: C, 55.52; H, 4.64; N, 7.03%. *Crystal data for* $C_{55}H_{55}BMoN_6O_2P_2Pt{\cdot}CHCl_3$, M = 1315.19, triclinic, $P\bar{1}$, a = 11.0486 (3) Å, b = 16.2224 (4) Å, c = 17.2241 (4) Å, α = 91.427 (2)º, β = 107.900 (2)º, γ = 108.323 (2)º, V = 2763.43 (13) Å^3, Z = 2, ρ_{calc} = 1.581 Mgm^{-3}, μ(Cu $K\alpha$) = 8.78 mm^{-1}, T = 150(0) K, plate, 0.09 × 0.06 × 0.02 mm {clear light yellow}, 10924 independent measured reflections (θ = 73.6), R_1 = 0.044, wR_2 = 0.123 for 9765 reflections [$I > 2\sigma(I)$], 660 parameters. CDCC 2251837.

Synthesis of [WPt(μ$_2$-C)Me(CO)$_2$(PPh$_3$)$_2$(Tp*)] (5.2b).

An orange solution containing [WPt(μ$_2$-C)Br(CO)$_2$(PPh$_3$)$_2$(Tp*)] (**3.1b**; 0.156 g, 0.114 mmol) was cooled to –78 °C beginning to precipitate starting material. The mixture was treated with a methyllithium (0.10 mL, 0.16 mmol, 1.6M in THF), immediately changing colour to bright yellow, completely dissolving the precipitate. Stirring was continued at –78 °C for 30 minutes prior to slowly warming to ambient temperature with no further colour changes observed. Drops of isopropanol were added and stirred to quench excess methyllithium and stirred for a further 10 minutes, prior to solvent removal *via* rotary evaporation to give a bright yellow solid. Subsequent recrystallisation from concentration of a CH_2Cl_2 solution into EtOH gave a birght yellow microcrystalline powder that was collected *via* vacuum filtration and washed with EtOH (2 × 10 mL), *n*-hexane (2 × 10 mL) and *n*-pentane (2 × 10 mL). Drying the compound *in vacuo* for 16 hours afforded the title compound as a bright yellow powder (140 mg, 0.109 mmol, 96% isolated yield). Crystals suitable for X-ray diffraction studies were grown overnight from the vapour diffusion of *n*-hexane into a $CHCl_3$ solution of the title compound. IR (CH_2Cl_2, cm^{-1}): 1933 vs ν_{CO}, 1839 vs ν_{CO}. IR (ATR, cm^{-1}): 2539 w ν_{BH}, 1936 vs ν_{CO}, 1841 vs ν_{CO}. ^{1}H NMR (700 MHz, $CDCl_3$, 25 ºC, δ): 7.24 [m, 16H, PPh], 7.11 [t, $^1J_{HH}$ = 8 Hz, PPh], 6.97 [m, 3H, PPh], 6.75 [m, PPh], 5.61 [s, 1H, pzCH], 5.58 [s, 2H, pzCH], 2.62 [s, 6H, pzCH$_3$], 2.39 [s, 3H, pzCH$_3$], 2.34 [s, 6H, pzCH$_3$], 2.24 [s, 3H, pzCH$_3$], 1.05 [m, 3H, $^2J_{HPt}$ = 58 Hz, PtCH$_3$]. ^{13}C{^{1}H} NMR (151 MHz, $CDCl_3$, 25ºC, δ): 367.6 [dd, $^2J_{CP}$ = 73, 6 Hz, W≡C–Pt], 229.3 [s, $^1J_{CW}$ = 178 Hz, CO], 152.1 151.2 [C^5(pz)], 143.7 142.8 [C^3(pz)], 135.0 [d, $^2J_{CP}$ = 11 Hz, C^{2,6}(C$_6$H$_5$)], 134.3 [d, $^2J_{CP}$ = 13 Hz, C^{2,6}(C$_6$H$_5$)], 133.3 [virtual t, $^1J_{CP}$ = 42 Hz, C^1(C$_6$H$_5$)], 129.4 129.2 [C^4(C$_6$H$_5$)], 127.8 [d, $^3J_{CP}$ = 10 Hz, C^{3,5}(C$_6$H$_5$)], 127.2 [d, $^3J_{CP}$ = 10 Hz, C^{3,5}(C$_6$H$_5$)], 106.3 105.8 [C^4(pz)], 17.1 15.2 12.8 12.5 [pzCH$_3$], 11.4 [dd, $^2J_{CP}$ = 82, 7 Hz; $^1J_{CPt}$ = 580 Hz, Pt–CH$_3$]. ^{31}P{^{1}H} NMR (162 MHz, $CDCl_3$, 25 ºC, δ): 25.26 [d, $^2J_{PP}$ = 14 Hz, $^1J_{PPt}$ = 1963 Hz, *trans*–PPtCW], 22.27 [d, $^2J_{PP}$ = 13 Hz, $^2J_{PC}$ = 68 Hz, $^1J_{PPt}$ = 1552 Hz, *cis*–PPtCW]. ^{195}Pt NMR (150 MHz, $CDCl_3$, 25ºC, δ): –4214 [ddd, $^1J_{PtP}$ = 1966, 1547 Hz, $^2J_{PtH}$ = 59 Hz]. MS (ESI, *m*/*z*): Found: 1283.3140. Calcd for $C_{55}H_{55}{}^{11}BN_6O_2P_2{}^{195}Pt{}^{184}W$ [M]$^+$: 1283.3112. Anal. Found: C, 51.44; H, 4.24; N, 6.61%. Calcd for $C_{55}H_{55}BN_6O_2P_2PtW$: C, 51.46; H, 4.32; N, 6.55%. *Crystal data for* $C_{55}H_{55}BN_6O_2P_2PtW{\cdot}CHCl_3$, M = 1403.10, triclinic, $P\bar{1}$, a = 11.0523 (2) Å, b = 16.2307 (4) Å, c = 17.1827 (3) Å, α = 91.505 (2)º, β = 107.938 (2)º, γ = 108.411 (2)º, V = 2756.27 (11) Å^3, Z = 2, ρ_{calc} = 1.691 Mgm^{-3}, μ(Cu $K\alpha$) = 10.74 mm^{-1}, T = 150(0) K, plate, 0.17 × 0.06 × 0.03 {clear light yellow}, 10911 independent measured reflections (θ = 73.7), R_1 = 0.031, wR_2 = 0.081 for 9598 reflections [$I > 2\sigma(I)$], 660 parameters, 0 restraints. CDCC 2251838.

Synthesis of [WPt(μ$_2$-CCH$_3$)(CO)$_2$(PPh$_3$)$_2$(Tp*)] (5.3).

A yellow solution containing [W(≡CCH$_3$)(CO)$_2$(Tp*)] (0.125 g, 0.222 mmol) and [Pt(η^2-C$_2$H$_4$)(PPh$_3$)$_2$] (0.166 g, 0.222 mmol) in THF (10 mL) was heated for an hour at 60 ºC, darkening to orange/red. Once cooled the solvent was removed under reduced pressure to return an orange residue that could be recrystalised from hot *n*-hexane (15 mL). A paste orange solid precipitated from solution and was left at –20 °C for 2 days to ensure all material was collected. This orange solid was collected *via* vacuum filtration and washed with *n*-pentane (3 × 10 mL) before drying *in vacuo* for 16 hours to give the title compound (0.192 g, 0.149 mmol, 67% yield). No crystals suitable for x-ray diffraction were grown. IR (CH_2Cl_2, cm^{-1}): 1881 vs ν_{CO}, 1794 vs ν_{CO}. IR (ATR, cm^{-1}): 2524 w ν_{BH}, 1879 vs ν_{CO}, 1798 vs ν_{CO}. Isolated pure residues hold onto THF solvent molecules in a ratio of 3:2 title molecules. They appear in the following spectra and are integrated as such. ^{1}H NMR (400 MHz, C_6D_6, 25 ºC, δ): 8.03 [m, 6H, PPh], 7.50 [m, 7H, PPh], 7.09–6.99 [m, 10H, PPh], 6.96 [m, 3H, PPh], 6.88 [m, 10H, PPh], 5.63 [s, 2H, pzCH], 5.48 [s, 1H, pzCH], 2.58 [s, 6H, pzCH$_3$], 2.39 [s, 3H, pzCH$_3$], 2.28 [dd, $^3J_{HP}$ = 9, 4 Hz, 3H, CCH$_3$], 2.19 [s, 6H, pzCH$_3$], 2.14 [s, 3H, pzCH$_3$]. ^{13}C{^{1}H} NMR (151 MHz, C_6D_6, 25ºC, δ): 341.4 [unresolved dd, $^2J_{CP}$ = 55 Hz, WPt(μ-*C*CH$_3$)], 224.5 [t, $^3J_{CP}$ = 5 Hz, $^2J_{CPt}$ = 52 Hz, CO], 154.0 151.1 [C^5(pz)], 143.9 143.1 [C^3(pz)], 137.7 [d, $^1J_{CP}$ = 35 Hz, C^1(C$_6$H$_5$)], 135.7 134.9 [d, $^2J_{CP}$ = 13 Hz, C^{2,6}(C$_6$H$_5$)], 129.1 128.9 [C^4(C$_6$H$_5$)], 127.6 [d, $^3J_{CP}$ = 10 Hz, C^{3,5}(C$_6$H$_5$)], 106.9 106.7 [C^4(pz)], 41.0 [dd; $^3J_{CP}$ = 7, 4 Hz; $^2J_{CPt}$ = 48 Hz, (μ$_2$-C*C*H$_3$)], 16.8 16.3 12.8 12.6 [pzCH$_3$]. ^{31}P{^{1}H} NMR (162 MHz, C_6D_6, 25 ºC, δ): 38.98 [d, $^2J_{PP}$ = 30 Hz, $^1J_{PPt}$ = 4309 Hz], 26.30 [d, $^2J_{PP}$ = 30 Hz, $^1J_{PPt}$ = 2712 Hz]. ^{195}Pt{^{1}H} NMR (150 MHz, C_6D_6, 25ºC, δ): –4066 [dd, $^1J_{PtP}$ = 4310, 2706 Hz]. MS (ESI, *m/z*): Found: 1284.3151. Calcd for C$_{55}$H$_{56}$^{11}BN$_6$O$_2$P$_2$^{195}Pt^{184}W [M+H]$^+$: 1284.3190. Anal. Found: C, 51.41; H, 4.438; N, 6.28%. Calcd for $C_{55}H_{55}BN_6O_2P_2PtW$: C, 51.46; H, 4.32; N, 6.55%.

Synthesis of [WPt(μ$_2$-CCH$_3$)(CO)$_3$(PPh$_3$)(Tp*)] (5.4).

Samples of [W(≡CMe)(CO)$_2$(Tp*)] (100 mg, 0.177 mmol) and [Pt(η^2-C$_2$H$_4$)(PPh$_3$)$_2$] (130 mg, 0.173 mmol) were dissolved in THF and heated at 60 °C for 3 hours. During this time the initially yellow solution changed to orange and then through to red/orange. While stirring, CO (g) was bubbled through the solution for 2 hours before stopping gas flow and stirring for 16 hours to give a red solution. The solvent was removed *via* rotary evaporation resulting in a red residue which could be purified by flash column chromatography {silica gel, Ar, 20–50% CH_2C_2/petroleum ether gradient}. Excess [W(≡CMe)(CO)$_2$(Tp*)] eluted first as a yellow band prior to the title compound as a red eluate. This red eluate could be recrystallized from CH_2Cl_2/*n*-hexane to give a red powder and subsequently collected *via* vacuum filtration with washing from *n*-hexane (3 x 10 mL). This was dried *in vacuo* to give the title compound as a brick red powder (40 mg, 0.038 mmol, 22%

Isolated yield). Crystals suitable for x-ray diffraction were grown from vapour diffusion of *n*-hexane into a THF solution of compound at 5 °C. IR (CH_2Cl_2, cm^{-1}): 2013 vs ν_{Pt-CO}, 1903 vs ν_{W-CO}, 1717 m.br $\nu_{\mu-CO}$. IR (ATR, cm^{-1}): 2549 2532 w ν_{BH}, 1999 vs ν_{Pt-CO}, 1898 vs ν_{W-CO}, 1808 s $\nu_{\mu-CO}$, 1784 sh $\nu_{\mu-CO}$. ^{1}H NMR (700 MHz, C_6D_6, 25 ºC, δ): 7.54 [m, 6H, PPh_3], 6.98 [m, 10H, PPh_3], 5.62 [s, 2H, pzCH], 5.44 [s, 1H, pzCH], 2.99 [s, 3H, $pzCH_3$], 2.41 [d, $^2J_{HP}$ = 3 Hz, 3H, $=CCH_3$], 2.27 [s, 6H, $pzCH_3$], 2.20 [s, 6H, $pzCH_3$], 2.10 [s, 3H, $pzCH_3$]. ^{13}C{^{1}H} NMR (176 MHz, C_6D_6, 25ºC, δ): 338.0 [d, $^2J_{CP}$ = 3 Hz, $=\mathit{C}CH_3$], 227.0 [d, $^3J_{CP}$ = 7 Hz, CO], 199.8 [d, $^3J_{CP}$ = 4 Hz, $=C\mathit{C}H_3$], 154.4 151.0 [C^5(pz)], 144.5 143.4 [C^3(pz)], 134.3 [overlapping d, $^1J_{CP}$ = 46 Hz, $C^1(C_6H_5)$], 134.2 [overlapping d, $^2J_{CP}$ = 13 Hz, $C^{2,6}(C_6H_5)$], 130.3 [$C^4(C_6H_5)$], 128.5 [$C^{3,5}(C_6H_5)$], 107.7 107.0 [C^4(pz)], 32.0 [$=C\mathit{C}H_3$], 23.1 17.1 14.4 12.8 [$pzCH_3$]. ^{31}P{^{1}H} NMR (162 MHz, C_6D_6, 25 ºC, δ): 33.98 [s, $^1J_{PPt}$ = 3759 Hz, PPh_3]. ^{195}Pt{^{1}H} NMR (86 MHz, C_6D_6, 25ºC, δ): –4230 [d, $^1J_{PtP}$ = 3758, $^1J_{PtW}$ = 212 Hz]. MS (ESI, *m/z*): Found: 1021.2231. Calcd for $C_{37}H_{40}{}^{11}BN_6O_2P^{195}Pt^{184}W$ $[M-CO]^+$: 1021.2200. Anal. Found: C, 43.55; H, 4.226; N, 7.67%. Calcd for $C_{38}H_{40}BN_6O_3PPtW$: C, 43.49; H, 3.84; N, 8.01%. *Crystal data for* $C_{38}H_{40}BN_6O_3PPtW{\cdot}C_4H_7O$, M = 1120.57, triclinic, $P\bar{1}$, a = 10.6787(4) Å, b = 11.2738(4) Å, c = 18.6023(7) Å, α = 78.618(3)°, β = 87.291(3)°, γ =69.499(3), V = 2055.85(14) Å^3, Z = 2, ρ_{calc} = 1.810 Mgm^{-3}, μ(Cu $K\alpha$) = 12.13 mm^{-1}, T = 150(0) K, prism 0.07 × 0.06 × 0.04 mm {clear dark pink}, 7430 independent measured reflections (θ = 70.8), R_1 = 0.025, wR_2 = 0.055 for 6528 reflections [$I > 2\sigma(I)$], 513 parameters, 7 restraints. CDCC 2251832.

Synthesis of [WPt(μ$_2$-C)(^{n}Bu)(CO)$_2$(PPh$_3$)$_2$(Tp*)] (5.5).

Note: This compound readily undergoes β-hydride elimination to produce the μ$_2$-methylidyne [WPt(μ$_2$-CH)(CO)$_2$(PPh$_3$)$_2$(Tp*)] (**5.6**) and the process is accelerated in polar media. A sample of [WPt(μ$_2$-C)Br(CO)$_2$(PPh$_3$)$_2$(Tp*)] (**3.1b**; 203 mg, 0.150 mmol) was dissolved in THF (10 mL) and cooled to –78 °C, precipitating orange solid. The suspension was treated dropwise with *n*-butylithium (0.07 mL, 2.5 M in hexanes, 0.2 mmol) where the solid dissipated and changed to yellow over 30 minutes. This was stirred at low temperature for 2 hours and then slowly warmed to ambient temperature for a further 2 hours. Solvent was removed under reduced pressure to obtain a yellow residue that was then purified by flash chromatography {silica gel, Ar, 20–100% CH_2Cl_2/*n*-hexane gradient}. A single yellow band eluted during this eluent concentration which had solvent removed under reduced pressure to recrystallise a yellow solid that could be collected by vacuum filtration. The solid was washed with *n*-hexane (10 mL) before drying *in vacuo* for 3 hours to afford compound **5.5** as a fine yellow powder (32 mg, 0.88 mmol, 77% yield). Crystals for C-ray diffraction were grown from the slow evaporation of Et_2O at 0 °C, however, were found

to be so disordered that a structure could not be solved even to highlight connectivity. Spectra were measured with atypical variation in solvent for differing reasons, therefore, methylidyne [WPt(μ$_2$-CH)(CO)$_2$(PPh$_3$)$_2$(Tp*)] was often present. This has been labelled in gray as appropriate. IR (CH_2Cl_2, cm^{-1}): 1932 vs ν_{CO}, 1840 vs ν_{CO}. IR (ATR, cm^{-1}): 2566 2532 w ν_{BH}, 1933 vs ν_{CO}, 1838 vs ν_{CO}. ^{1}H NMR (700 MHz, C_6D_6, 25 ºC, δ): 7.49 [m, 8H, PPh], 7.44 [m, 6H, PPh], 6.90 [m, 7H, PPh], 6.77 [m, 3H, PPh], 6.64 [m, 6H, PPh], 5.40 [s, 2H, pzCH], 5.34 [s, 1H, pzCH], 2.93 [s, 6H, pzCH_3], 2.66 [s, 3H, pzCH_3], 2.31 [br, 2H, Pt–CH_2CH$_2$CH$_2$CH$_3$], 2.19 [s, 6H, pzCH_3], 2.08 [s, 3H, pzCH_3], 1.85 [br, 2H, Pt–CH$_2$CH_2CH$_2$CH$_3$], 1.29 [br, 2H, Pt–CH$_2$CH$_2$CH_2CH$_3$], 0.97 [br, 3H, Pt–CH$_2$CH$_2$CH$_2$CH_3]. Isomerisation was unavoidable in C_6D_6 so although CD_2Cl_2 accelerates isomerisation, enough compound was soluble to measure the ^{13}C{^{1}H} NMR including the highly coupled μ$_2$-carbido resonance. The consequence was the spectrum contains prominent methylidyne signals (indicated as grey). ^{13}C{^{1}H} (151 MHz, CD_2Cl_2, 25ºC, δ): 318.4 [dd; $^2J_{CP}$ = 44, 10 Hz; W≡C–Pt], 234.2 [$^1J_{CW}$ = 160 Hz, CO], 153.4 152.5 [C^5(pz)], 145.2 144.7 [C^3(pz)], 135.3 [d, $^2J_{CP}$ = 13 Hz, C^{2,6}(C_6H_5)], 134.4 [d, $^2J_{CP}$ = 11 Hz, C^{2,6}(C_6H_5)], 134.1 [d, $^1J_{CP}$ = 42 Hz, C^1(C_6H_5)], 132.4 [d, $^1J_{CP}$ = 41 Hz, C^1(C_6H_5)], 129.7 129.3 [C^4(C_6H_5)], 128.2 [d, $^3J_{CP}$ = 10 Hz, C^{3,5}(C_6H_5)], 127.9 [d, $^3J_{CP}$ = 9 Hz, C^{3,5}(C_6H_5)], 107.2 106.9 [C^4(pz)], 34.4 [Pt–*C*H$_2$CH$_2$CH$_2$CH$_3$], 30.5 [dd; $^3J_{CP}$ = 79, 6 Hz; Pt–CH$_2$*C*H$_2$CH$_2$CH$_3$], 27.5 [d, $^4J_{CP}$ = 11 Hz, Pt–CH$_2$CH$_2$*C*H$_2$CH$_3$], 17.9 15.41 [pzCH_3], 14.5 [Pt–CH$_2$CH$_2$CH$_2$*C*H$_3$], 13.09 13.03 [pzCH_3]. ^{31}P{^{1}H} NMR (162 MHz, $CDCl_3$, 25 ºC, δ): 23.74 [d, $^2J_{PP}$ = 11 Hz, $^1J_{PPt}$ = 1733, P *trans*-μ$_2$-C], 20.06 [d, $^2J_{PP}$ = 11 Hz, $^1J_{PPt}$ = 1593 Hz, *cis*-μ$_2$-C]. No platinum resonance was detected on the timescale of ^{195}Pt{^{1}H} NMR, presumably from strong coupling to spin active ^{31}P not uncommon in these systems. MS (ESI, *m/z*): Found: 1325.3623. Calcd for $C_{58}H_{61}{}^{11}BN_6O_2P_2{}^{184}W^{195}Pt$ [M]$^+$: 1325.3581. Anal. Found: C, 52.49; H, 4.90; N, 6.56%. Calcd for $C_{58}H_{61}BN_6O_2P_2PtW$: C, 52.54; H, 4.64; N, 6.34%.

Synthesis of [WPt(μ$_2$-CH)(CO)$_2$(PPh$_3$)$_2$(Tp*)] (5.6).

Note: This compound decomposes to [WPt(μ-CH)(μ$_2$-CO)(CO)$_2$(PPh$_3$)(Tp*)] (**5.1**) and [W$_2$Pt(μ$_2$-CH)$_2$(μ$_2$-CO)$_2$(CO)$_2$(Tp*)$_2$] if returned to solution once isolated, even under rigorous exclusion of air and moisture. A sample of [WPt(μ$_2$-C)(*n*Bu)(CO)$_2$(PPh$_3$)$_2$(Tp*)] (**5.5**; 0.300 g, 0.226 mmol) in CH_2Cl_2 (20 mL) was heated at reflux changing from a yellow to red solution, where infra-red spectroscopy revealed the reaction is clean but slow and 16 hours is required for complete conversion. The mixture was filtered through celite and concentrated into *n*-hexane aided by rotary evaporation to provide a red microcrystalline solid that could be collected *via* vacuum filtration, washed with *n*-pentane (3 × 10 mL) and dried *in vacuo* for 16 hours. The red powder was identified as the title compound (0.244 g, 0.192 mmol, 85% isolated yield. Crystals suitable for x-ray diffraction were grown from vapour diffusion of *n*-hexane into a THF solution of **5.6** at ambient

temperature. IR (CH_2Cl_2, cm^{-1}): 1899 vs ν_{CO}, 1760 s $\nu_{\mu\text{-}CO}$. IR (ATR, cm^{-1}): 2547 w ν_{BH}, 1895 vs ν_{CO}, 1765 vs $\nu_{\mu\text{-}CO}$. ^{1}H NMR (400 MHz, $CDCl_3$, 25 ºC, δ): 13.56 [dd, $^3J_{HP}$ = 18, 3 Hz; $^2J_{HPt}$ obscured, 1H, WPt(μ$_2$-CH)], 7.52 [m, 6H, PPh], 7.28 [m, 6H, PPh], 7.19 [m, 6H, PPh], 7.1 [m, 12H, PPh], 5.69 [s, pzCH, 2H], 5.66 [s, pzCH, 1H], 2.34 [s, pzCH_3, 6H], 2.28 [s, pzCH_3, 3H], 2.21 [s, pzCH_3, 3H], 2.11 [s, pzCH_3, 6H]. A spectrum is also included in CD_2Cl_2 as the β-hydride elimination of [(Tp*)(CO)$_2$W≡C–Pt(*n*-Bu)(PPh$_3$)$_2$] providing evidence of butene and is labelled in grey with grey shaded boxes. ^{1}H{^{31}P} NMR (400 MHz, $CDCl_3$, 25 ºC, δ): 13.55 [s, $^2J_{HW}$ = 39 Hz; $^2J_{HPt}$ = 27 Hz, 1H, WPt(μ$_2$-CH)], 7.51 [d, $^1J_{HH}$ = 7 Hz, 6H, PPh], 7.28 [d, $^1J_{HH}$ = 8 Hz, 6H, PPh], 7.19 [m, 6H, PPh], 7.11 [m, 12H, PPh], 5.69 [s, 2H, pzCH], 5.65 [s, 1H, pzCH], 2.33 [s, 6H, pzCH_3], 2.27 [s, 3H, pzCH_3], 2.20 [s, 3H, pzCH_3], 2.11 [s, 6H, pzCH_3]. ^{13}C{^{1}H} NMR (151 MHz, $CDCl_3$, 25ºC, δ): 317.9 [dd, $^2J_{CP}$ = 43, 6 Hz, WPt(μ$_2$-CH)], 233.5 [$^1J_{CW}$ = 163 Hz; $^2J_{CPt}$ = 20 Hz, CO], 153.0 152.0 [C^5(pz)], 143.8 143.5 [C^3(pz)], 135.9 [overlapping dd, $^1J_{CP}$ = 38 Hz; $^3J_{CP}$ = 4 Hz, C^1(C_6H_5)], 135.7 [overlapping dd, $^1J_{CP}$ = 38 Hz; $^3J_{CP}$ = 4 Hz, C^1(C_6H_5)], 135.0 [d, $^2J_{CP}$ = 12 Hz, C^{2,6}(C_6H_5)], 134.0 [d, $^2J_{CP}$ = 12 Hz, C^{2,6}(C_6H_5)], 129.1 [C^4(C_6H_5)], 128.7 [C^4(C_6H_5)], 127.7 [d, $^3J_{CP}$ = 10 Hz, C^{3,5}(C_6H_5)], 127.4 [d, $^2J_{CP}$ = 9 Hz, C^{3,5}(C_6H_5)], 106.8 106.5 [C^4(pz)], 17.7 15.2 13.0 12.7 [pzCH_3]. ^{31}P{^{1}H} NMR (162 MHz, $CDCl_3$, 25 ºC, δ): 32.88 [d, $^2J_{PP}$ = 28 Hz; $^1J_{PPt}$ = 3535 Hz, PPh_3]. 32.55 [d, $^2J_{PP}$ = 28 , $^1J_{PPt}$ = 3647 Hz, PPh_3]. ^{195}Pt{^{1}H} NMR (150 MHz, CD_2Cl_2, 25ºC, δ): –4461 [ddd, $^1J_{PtP}$ = 3844, 3350, $^2J_{PtH}$ = 22, $^1J_{PtW}$ = 225 Hz]. MS (ESI, *m/z*): Found: 1269.2992. Calcd for $C_{54}H_{53}{}^{11}BN_6O_2P_2{}^{184}W^{195}Pt$ [M]$^+$: 1269.2955. Anal. Found: C, 51.35; H, 4.37; N, 6.73%. Calcd for $C_{54}H_{53}BN_6O_2P_2PtW$: C, 51.08; H, 4.21; N, 6.62%. *Crystal data for* $C_{54}H_{53}BN_6O_2P_2PtW$, *M* = 1269.71, triclinic, $P\bar{1}$, *a* = 11.560 (2) Å, *b* = 11.722 (2) Å, *c* = 20.686 (4) Å, α = 82.06 (3)°, β = 85.92 (3)º, γ = 64.19 (3)°, *V* = 2499.0 (10) Å^3, *Z* = 2, ρ_{calc} = 1.684 Mgm^{-3}, μ(Synchrotron, λ = 0.71073 Å) = 5.21 mm^{-1}, *T* = 100(0) K, plate 0.02 × 0.02 × 0.01 mm {orange}, 8449 independent measured reflections (θ = 25.4°), R_1 = 0.093, wR_2 = 0.253 for 7410 reflections [$I > 2\sigma(I)$], 610 parameters. CDCC 2251833. Methylidyne proton was modelled riding on carbon.

Synthesis of [WPt(μ-CH)(μ-CO)(CNMes)(CO)(PPh$_3$)(Tp*)] (5.7).

A sample of [WPt(μ$_2$-CH)(μ$_2$-CO)(CO)(PPh$_3$)$_2$(Tp*)] (**5.6**; 0.080 g, 0.063 mmol) in THF (5 mL) was treated with CNMes (0.011 g, 0.075 mmol), resulting in the red/orange solution becoming pinker in colour. The mixture was stirred for 16 hours as infra-red spectroscopy (ν_{CO}/ν_{CN}) revealed incomplete conversion at 3 hours. The solution was eluted through celite and concentrated into *n*-hexane aided by rotary evaporation, prior to collection *via* vacuum filtration, washing with MeOH (3 × 10 mL) and drying *in vacuo* for 16 hours. The resulting red microcrystalline powder was confirmed as the title compound (0.055 g, 0.048 mmol, 77% isolated yield). Crystal suitable for

single crystal x-ray diffraction studied were grown from evaporation of an acetone solution at ambient temperature. IR(CH_2Cl_2, cm^{-1}): 2114 vs ν_{CN}, 1903 vs ν_{CO}, 1758 vs $\nu_{\mu\text{-}CO}$. IR (ATR, cm^{-1}): 2534 w ν_{BH}, 2112 vs ν_{CN}, 1901 vs ν_{CO}, 1762 vs $\nu_{\mu\text{-}CO}$. ^{1}H NMR (400 MHz, $CDCl_3$, 25 ºC, δ): 14.14 [d, $^3J_{HP}$ = 17 Hz, $^2J_{HPt}$ = 53 Hz, 1H, WPt(μ$_2$-CH)], 7.67 [m, 1H, PPh], 7.49 [m, 6H, PPh], 7.30 [m, 9H, PPh], 6.79 [s, 2H, MesCH], 5.78 [s, 1H, pzCH], 5.74 [s, 2H, pzCH], 2.64 [s, 3H, MEsCH$_3$], 2.37 [s, 6H, MesCH$_3$], 2.33 [s, 3H, pzCH$_3$], 2.23 [s, 3H, pzCH$_3$], 2.22 [s, 6H, pzCH$_3$], 2.11 [s, 6H, pzCH$_3$]. ^{1}H{^{31}P} NMR (400 MHz, $CDCl_3$, 25 ºC, δ): 14.14 [s, $^2J_{HPt}$ = 36 Hz, 1H, WPt(μ$_2$-CH)], 7.49 [m, 6H, PPh], 7.30 [m, 9H, PPh], 6.79 [s, 2H, MesCH], 5.78 [s, 1H, pzCH], 5.74 [s, 2H, pzCH], 2.64 [s, 3H, MesCH$_3$], 2.37 [s, 6H, MesCH$_3$], 2.33 [s, 3H, pzCH$_3$], 2.23 [s, 3H, pzCH$_3$], 2.22 [s, 6H, pzCH$_3$], 2.11 [s, 6H, pzCH$_3$]. ^{13}C{^{1}H} NMR (151 MHz, $CDCl_3$, 25ºC, δ): 314.5 [d, $^1J_{CH}$ = 4 Hz, coupling observed from resonance outside decoupler bounds, WPt(μ$_2$-CH)], 234.5 [d, $^3J_{CP}$ = 4 Hz, $^1J_{CW}$ = 155 Hz, CO], 166.2 [C^1(Mes)], 153.0 152.2 [C^5(pz)], 144.1 143.7 [C^3(pz)], 137.2 [C^4(Mes)], 135.8 [d, $^1J_{CP}$ = 45 Hz, C^1(C_6H_5)], 134.3 [C^{2,6}(Mes)], 134.0 [d, $^3J_{CP}$ = 13 Hz, C^{3,5}(C_6H_5)], 129.7 [C^4(C_6H_5)], 129.1 128.4 [C^{3,5}(Mes)], 128.1 [d, $^2J_{CP}$ = 10 Hz, C^{2,6}(C_6H_5)], 107.0 106.9 [C^4(pz)], 21.3 21.1 [MesCH$_3$], 18.7 18.0 [pzCH$_3$], 15.2 [MesCH$_3$], 13.0 12.8 [pzCH$_3$]. ^{31}P{^{1}H} NMR (162 MHz, $CDCl_3$, 25 ºC, δ): 28.78 (s, $^1J_{PPt}$ = 3568, $^2J_{PW}$ = 23 Hz). ^{195}Pt{^{1}H} NMR (150 MHz, $CDCl_3$, 25ºC, δ): −4362 [d, $^1J_{PtP}$ = 3588 Hz]. MS (ESI, *m/z*): Found: 1152.2980. Calcd for $C_{46}H_{49}{}^{11}BN_7O_2P^{184}W^{195}Pt$ $[M]^+$: 1152.2935. Anal. Found: C, 47.80; H, 4.35; N, 6.37%. Calcd for $C_{46}H_{49}BN_7O_2PPtW$: C, 47.93; H, 4.21; N, 6.62%. *Crystal data for* $C_{46}H_{49}BN_7O_2PPtW$, M = 1152.64, triclinic, $P\bar{1}$, a = 10.9436 (2) Å, b = 12.4463 (3) Å, c = 17.6151 (5) Å, α = 71.910 (2)°, β = 79.617 (2)°, γ =74.814 (2)°, V = 2188.24 (10) Å^3, Z = 2, ρ_{calc} = 1.749 Mgm^{-3}, μ(Cu $K\alpha$) = 11.39 mm^{-1}, T = 150(0) K, plate 0.14 × 0.05 × 0.03 mm {clear light orange}, 8484 independent measured reflections (θ = 73.0), R_1 = 0.027, wR_2 = 0.070 for 7523 reflections [$I > 2\sigma(I)$], 549 parameters. CDCC 2251835.

Synthesis of [WPt(μ$_2$-CH)(CO)$_2$(dppe)(Tp*)] (5.8).

A sample of [WPt(μ$_2$-CH)(CO)$_2$(PPh_3)$_2$(Tp*)] (**5.6**; 0.300 g, 0.236 mmol) with dppe (0.100 g, 0.250 mmol) was dissolved in CH_2Cl_2 (10 mL) and stirred for 16 hours to give an orange/red solution. The ensuing solution was eluted through diatomaceous earth with CH_2Cl_2 and MeOH (10 mL) added prior to concentration by rotary evaporator that resulted in a red microcrystalline powder. Vacuum filtration was used to collect the powder, washing with MeOH (3 × 10 mL) and *n*-hexane (2 × 10 mL) before drying *in vacuo* for 16 hours gave the title compound as a red microcrystalline powder (0.191 g, 0.167 mmol, 71% isolated yield). Crystals suitable for x-ray diffraction were unable to be grown. IR (CH_2Cl_2, cm^{-1}): 1899 vs ν_{CO}, 1716 br.m $\nu\mu\text{-}_{CO}$. IR (ATR,

cm^{-1}): 2550 2532 w ν_{BH}, 1881 vs ν_{CO}, 1723 s $\nu\mu$-$_{CO}$. ^{1}H NMR (400 MHz, $CDCl_3$, 25 ºC, δ): 14.92 [dd, $^{3}J_{HP}$ = 14, 2 Hz; $^{2}J_{HPt}$ = 35 Hz, 1H, μ_2-CH], 7.87 [m, 4H, PPh], 7.59 [m, 4H, PPh], 7.38 [m, 6H, PPh], 7.34 [m, 6H, PPh], 5.73 [s, 1H, pzCH], 5.71 [s, 2H, pzCH], 2.58 [s, 3H, $pzCH_3$], 2.52 [m, 2H, P–CH_2], 2.39 [m, 2H, P–CH_2], 2.34 [s, 6H, $pzCH_3$], 2.30 [s, 3H, $pzCH_3$], 2.11 [s, 6H, $pzCH_3$]. ^{1}H{^{31}P} NMR (400 MHz, $CDCl_3$, 25 ºC, δ): 14.92 [s, $^{2}J_{HPt}$ = 35 Hz, 1H, μ_2-CH], 7.85 [m, 4H, PPh], 7.59 [m, 4H, PPh], 7.38 [m, 6H, PPh], 7.34 [m, 6H, PPh], 5.73 [s, 1H, pzCH], 5.70 [s, 2H, pzCH], 2.58 [s, 3H, $pzCH_3$], 2.55 [zm, 2H, P–CH_2], 2.40 [m, 2H, P–CH_2], 2.34 [s, 6H, $pzCH_3$], 2.29 [s, 3H, $pzCH_3$], 2.11 [s, 6H, $pzCH_3$]. ^{13}C{^{1}H} NMR (201 MHz, $CDCl_3$, 25ºC, δ): 307.9 [dd, $^{2}J_{CP}$ = 56, 46 Hz; W≡C–Pt], 237.6 [$^{1}J_{CW}$ = 158 Hz, CO], 152.9 152.0 [C^5(pz)], 143.9 143.6 [C^3(pz)], 134.1 132.9 [d, $^{2}J_{CP}$ = 12 Hz, $C^{2,6}(C_6H_5)$], 132.3 132.2 [overlapping d, $^{1}J_{CP}$ = 38 Hz, $C^1(C_6H_5)$], 130.0 129.9 [$C^4(C_6H_5)$], 128.5 128.2 [d, $^{3}J_{CP}$ = 10 Hz, $C^{3,5}(C_6H_5)$], 107.0 106.8 [C^4(pz)], 31.9 [dd, $^{1}J_{CP}$ = 34 Hz; $^{2}J_{CP}$ = 16 Hz, P–CH_2], 31.3 [dd, $^{1}J_{CP}$ = 36 Hz; $^{2}J_{CP}$ = 16 Hz, P–CH_2], 17.9 14.8 12.9 12.7 [pz*C*H_3]. ^{31}P{^{1}H} NMR (162 MHz, $CDCl_3$, 25 ºC, δ): 48.18 [roofed d, $^{2}J_{PP}$ = 40 Hz; $^{2}J_{PW}$ = 23 Hz; $^{1}J_{PPt}$ = 3460 Hz, *pseudo-trans*-W], 47.41 [roofed d, $^{2}J_{PP}$ = 42 Hz, $^{1}J_{PPt}$ = 3200 Hz]. ^{195}Pt{^{1}H} NMR (85.7 MHz, $CDCl_3$, 25ºC, δ): –4530 [dd, $^{1}J_{PtP}$ = 3454, 3221 Hz]. MS (ESI, *m/z*): Found: 1144.2543. Calcd for $C_{44}H_{48}{}^{11}BN_6O_2P_2{}^{195}Pt{}^{184}W$ $[M+H]^+$: 1144.2564. Anal. Found: C, 46.21; H, 4.353; N, 7.05%. Calcd for $C_{44}H_{47}BN_6O_2P_2PtW$: C, 46.21; H, 4.14; N, 7.35%.

Synthesis of [WAu(μ_2-C)Cl(CO)$_2$(Tp*)] (5.10).

Samples of [W(≡CH)(CO)$_2$(Tp*)] (**5.9**; 0.050 g, 0.091 mmol) and [AuCl·SMe_2] (0.027 g, 0.092 mmol) were injected with CH_2Cl_2 (10 mL) with stirring. The initially yellow solution immediately changed to an olive colour and stirring was continued in the absence of light for 30 minutes with no further colour changes noted. Infra-red spectroscopy confirmed reaction completion hence the olive solution was filtered through dry diatomaceous earth to give a bright yellow eluate. *N*-hexane was added to the eluate before concentration *via* rotary evaporation resulted in a yellow solid emerging that could be collected *via* vacuum filtration and washed with *n*-hexane (3 × 5 mL) and dried *in vacuo* for 16 hours. The yellow microcrystalline solid was confirmed as the title compound (0.040 g, 0.051 mmol, 56% isolated yield). Crystal suitable for single crystal x-ray diffraction could be grown from the vapour diffusion of n-hexane into a CH_2Cl_2 solution of **5.10** at ambient temperature. IR (CH_2Cl_2, cm^{-1}): 2016 vs ν_{CO}, 1932 vs ν_{CO}. IR (ATR, cm^{-1}): 2570 w ν_{BH}, 2004 vs ν_{CO}, 1928 vs ν_{CO}, 1910 vs ν_{CO}. ^{1}H NMR (600 MHz, $CDCl_3$, 25 ºC, δ): 10.41 [s, $^{2}J_{HW}$ = 63 Hz, WAu(μ-CH)], 5.95 [s, 2H, pzCH], 5.93 [s, 1H, pzCH], 2.51 [s, 3H, $pzCH_3$], 2.48 [s, 6H, $pzCH_3$], 2.38 [s, 6H, $pzCH_3$], 2.35 [s, 3H, $pzCH_3$]. ^{13}C{^{1}H} NMR (151 MHz, $CDCl_3$, 25ºC, δ): 260.8 [$^{1}J_{CW}$ = 85 Hz, WAu(μ_2-CH)],

215.4 [$^{1}J_{CW}$ = 157 Hz, CO], 153.6 152.1 [C^{5}(pz)], 146.4 145.8 [C^{3}(pz)], 108.4 107.9 [C^{4}(pz)], 17.7 15.8 13.2 12.8 [pzCH_3]. A suitable match was not obtained through high-resolution mass spectrometry with many unidentifiable fragments detected. This likely suggests the gold fragment is lost from the carbyne in mass spec and forms other cluster species before detection. Anal. Found: C, 27.87; H, 3.10; N, 10.94%. Calcd for $C_{18}H_{23}BN_6O_2ClWAu$: C, 27.63; H, 2.96; N, 10.74%. *Crystal data for* $C_{18}H_{23}AuBClN_6O_2W$, M = 782.50, monoclinic, $P2_1/c$, a = 10.213(2) Å, b = 21.629(4) Å, c = 10.395(2) Å, β = 104.31(3)°, V = 2225.0(8) Å^3, Z = 4, ρ_{calc} = 2.336 Mgm^{-3}, μ(Synchrotron; λ = 0.710753 Å) = 11.90 mm^{-1}, T = 100(0) K, plate, 0.05 × 0.03 × 0.01 mm {yellow}, 4075 independent measured reflections (θ = 25.4°), R_1 = 0.069, wR_2 = 0.192 for 3713 reflections [$I > 2\sigma(I)$], 277 parameters. CCDC 2251831.

Spectroscopic observation of [WPt(μ$_2$-C)H(CO)$_2$(PPh$_3$)$_2$(Tp*)] (5.11).

A d_6-benzene (0.5 mL) solution of [WPt(μ$_2$-C)Br(CO)$_2$(PPh$_3$)$_2$(Tp*)] (**3.1b**; 0.050 g, 0.037 mmol) inside a J. Young NMR tube was treated with Li[HBEt$_3$] (0.05 mL, 0.05 mmol, 1M solution in THF) to give an orange solution. The sample was investigated by NMR spectroscopic analysis from 15 minutes over 48 hours, during which time the title compound could be observed, before the solution transitions to red forming [WPt(μ$_2$-CH)(CO)$_2$(PPh$_3$)$_2$(Tp*)] (**5.6**) ($t_{½}$ = 3 hours). Attempts to measure infra-red spectra only identified starting material and formation of μ$_2$-methylidyne (**5.6**). NB: due to the complicated mixture, no signals could be unequivocally identified beyond the hydride resonance and hence only this signal will be listed. ^{1}H NMR (400 MHz, C_6D_6, 25 ºC, δ): –9.24 [t, $^{2}J_{HP}$ = 22 Hz; $^{1}J_{HPt}$ = 495 Hz; $^{3}J_{HW}$ = 23 Hz, 1H, Pt–H]. ^{1}H{^{31}P} NMR (400 MHz, C_6D_6, 25 ºC, δ): –9.28 [s, $^{1}J_{HPt}$ = 495 Hz; $^{3}J_{HW}$ = 23 Hz, 1H, Pt–H]. Both ^{13}C{^{1}H} NMR and HMBC experiments failed to discern any μ$_2$-carbido resonance. Furthermore, ^{31}P{^{1}H} NMR spectroscopy was unable to detect any unaccounted resonances with appropriate coupling for the title compound, nor was a resonance detected by ^{195}Pt{^{1}H} NMR, suggesting the title species forms in insufficient quantities for sensitive measurements beyond ^{1}H NMR.

Synthesis of *trans*-[WPt(μ$_2$-C)(tolyl)(CO)$_2$(PPh$_3$)$_2$(Tp*)] (5.12).

Note: This compound undergoes reductive elimination to form orange [W(≡Ctolyl)(CO)$_2$(Tp*)].[429]

A fresh sample of tolyllithium (0.090 M) was prepared from treating 4-bromotoluene (0.300 g, 1.75 mmol) in THF (20 mL) with *n*-butyllithium (0.7 mL, 1.8 mmol, 2.5M in hexanes) at –78 °C and stirring for 15 minutes. The clear organolithium solution was warmed to 0 °C, where a solution of [WPt(μ$_2$-C)Br(CO)$_2$(PPh$_3$)$_2$(Tp*)] (**3.1b**; 0.200 g, 0.148 mmol) in THF (5 mL) was added dropwise with stirring to give a bright yellow solution. Maintained at 0 °C, the solution remained

yellow for 10 minutes before darkening to orange at 20 minutes and brown by 30 minutes, where TLC confirmed consumption of the μ_2-carbido precursor. Solvent was removed to give a yellow/brown residue which could be purified *via* flash column chromatography {silica gel, N_2, CH_2Cl_2/petroleum ether 60–80 gradient}: 20% CH_2Cl_2/petroleum ether eluted an orange band as [W(≡Ctolyl)$(CO)_2$(Tp*)] (150 mg) before 50% CH_2Cl_2/petroleum ether eluted a bright yellow compound which could be evaporated *via* rotary evaporator. The yellow species defied recrystallisation, remaining soluble in a range of organic solvents and therefore was evaporated under high vacuum to give a pale-yellow powder as the title compound (0.026 g, 0.019 mmol, 13% yield). Crystals suitable for x-ray diffraction were unable to be grown. IR (CH_2Cl_2, cm^{-1}): 1937 vs ν_{CO}, 1843 vs ν_{CO}. ^{1}H NMR (400 MHz, $CDCl_3$, 25 ºC, δ): 7.73 [br.m, 6H, PPh], 7.45 [br.m, 6H, PPh], 7.29 [m, 8H, PPh], 7.06 [m, 4H, PPh], 6.83 [br.m, 6H, PPh], 6.14 [d, $^1J_{HH}$ = 8 Hz, tolylCH], 5.82 [d, $^1J_{HH}$ = 8 Hz, 2H, tolylCH], 5.58 [s, 2H, pzCH], 5.49 [s, 1H, pzCH], 2.49 [s, 6H, pzCH_3], 2.33 [s, 6H, pzCH_3], 2.18 [s, 3H, pzCH_3], 2.04 [s, 3H, pzCH_3], 1.82 [s, 3H, tolylCH_3]. ^{13}C{^{1}H} NMR (201 MHz, $CDCl_3$, 25ºC, δ): 397.2 [br.m, $^1J_{CW}$ = 162 Hz; $^1J_{CPt}$ = 530 Hz, W≡C–Pt], 232.0 [$^1J_{CW}$ = 183 Hz, CO], 151.5 151.3 [C^5(pz)], 147.2 [t, $^2J_{CP}$ = 13 Hz; $^1J_{CPt}$ = 475 Hz, Pt–C^1(tolyl)], 143.4 143.1 [C^3(pz)], 136.1 [C^4(tolyl)], 134.9 134.8 [d, $^2J_{CP}$ = 9 Hz, $C^{2,6}(C_6H_5)$], 134.6 [m, $C^{2,6}$(tolyl)], 132.55 132.50 [overlapping d, $^1J_{CP}$ = 43 Hz, $C^1(C_6H_5)$], 129.3 129.1 [$C^4(C_6H_5)$], 127.7 [$C^{3,5}(C_6H_5)$], 127.5 [m, $C^{3,5}$(tolyl)], 127.1 [$C^{3,5}(C_6H_5)$], 106.1 105.7 [C^4(pz)], 20.3 [tolylCH_3], 17.8 14.6 13.0 12.4 [pz*C*H_3]. ^{31}P{^{1}H} NMR (162 MHz, $CDCl_3$, 25 ºC, δ): 21.74 [roofed d, $^2J_{PP}$ = 440 Hz, $^1J_{PPt}$ = 3260 Hz], 20.62 [roofed d, $^2J_{PP}$ = 440 Hz, $^1J_{PPt}$ = 3260 Hz]. ^{195}Pt{^{1}H} NMR (85.7 MHz, $CDCl_3$, 25ºC, δ): –4164 [t, $^1J_{PtP}$ = 3266 Hz]. MS (ESI, *m/z*): Found: 1360.3496. Calcd for $C_{61}H_{60}{}^{11}BN_6O_2P_2{}^{195}Pt{}^{184}W$ $[M]^+$: 1360.3503. A satisfactory sample for elemental analysis could not be obtained.

Synthesis of [Li(THF)$_2$][WPt(μ$_2$-C)(–C≡C–SiMe$_3$)$_2$(CO)$_2$(PPh$_3$)(Tp*)] (5.13).

Note: This compound undergoes reductive elimination to [W(≡C–C≡C–SiMe$_3$)$(CO)_2$(Tp*) A suspension of [WPt(μ$_2$-C)Br$(CO)_2(PPh_3)_2$(Tp*)] (**3.1b**; 0.200 g, 0.148 mmol) in THF (5 mL) was treated with lithium trimethylsilylacetylide (10 mL, 0.3 mmol, 0.03 M in THF) at –78 °C to give an orange/yellow solution. The solution was stirred for 2 hours at –78 °C and 1 hour at ambient temperature changing to bright yellow. The mixture was concentrated (*ca* 3 mL) under reduced pressure and layered with *n*-pentane (12 mL) and stored in the freezer for 1 week where bright yellow plates deposited, accompanied by a clear supernatant phase. The plates were filtered and washed with *n*-pentane (5 × 5 mL) and dried *in vacuo* for 3 hours before collection inside an argon glovebox. The title compound was obtained as a yellow crystalline solid (0.122 g, 0.090 mmol, 61% isolated yield). The crystals obtained from liquid-liquid diffusion of *n*-pentane into THF at –20 °C

were suitable for single crystal x-ray diffraction. IR (CH_2Cl_2, cm^{-1}): 2035 m $\nu_{C\equiv C}$, 2017 m $\nu_{C\equiv C}$, 1932 vs ν_{CO}, 1841 vs ν_{CO}. IR (ATR, cm^{-1}): 2521 w ν_{BH} 2041 m $\nu_{C\equiv C}$, 2017 m $\nu_{C\equiv C}$, 1929 vs ν_{CO}, 1841 vs ν_{CO}. ^{1}H NMR (700 MHz, $CDCl_3$, 25 ºC, δ): 7.41 [br.m, 6H, PPh], 7.11 [br.m, 3H, PPh], 6.90 [br.m, 6H], 5.61 [s, 1H, pzCH], 5.55 [s, 2H, pzCH], 3.92 [m, 8H, THF], 2.38 [overlapping s, 6H, $pzCH_3$], 2.38 [overlapping s, 3H, $pzCH_3$], 2.36 [s, 6H, $pzCH_3$], 2.25 [s, 3H, $pzCH_3$], 1.92 [m, 8H, THF-CH_2], 0.26 [s, 9H, $Si(CH_3)_3$], –0.37 [s, 9H, $Si(CH_3)_3$]. ^{7}Li NMR (272 MHz, $CDCl_3$, 25 °C, δ): 0.79 [s, Li^+]. NB: $^{13}C\{^1H\}$ NMR experiment was conducted at –20 °C to maximise longevity of species in solution, the consequence being, some aryl carbons are unable to be unequivocally assigned. Furthermore, HMBC experiments suggest the C≡*C*–$SiMe_3$ signals are obscured by broad phenyl resonances. $^{13}C\{^1H\}$ NMR (201 MHz, $CDCl_3$, –20ºC, δ): 374.6 [m, $^1J_{CW}$ = 168 Hz], 228.3 [$^1J_{CW}$ = 185 Hz, CO], 152.1 151.1 [C^5(pz)], 143.9 142.7 [C^3(pz)], 134.9 [br.m, $C(C_6H_5)$], 129.6 [br.m, $C(C_6H_5)$], 127.2 [br.m, $C(C_6H_5)$], 119.5 [*trans*-Pt–*C*≡C], 108.8 [d, $^2J_{CP}$ = 28 Hz, *cis*-Pt–*C*≡C], 106.1 105.7 [C^4(pz)], 68.5 [$C^{2,5}(OC_4H_8)$], 25.7 [$C^{3,4}(OC_4H_8)$], 16.5 15.3 13.0 12.8 [$pzCH_3$], 1.4 0.6 [$Si(CH_3)_3$]. $^{31}P\{^1H\}$ NMR (283 MHz, $CDCl_3$, 25 ºC, δ): 16.10 [s, $^1J_{PPt}$ = 2670 Hz]. $^{195}Pt\{^1H\}$ NMR (149.9 MHz, $CDCl_3$, 25ºC, δ): –4061 [d, $^1J_{PtP}$ = 2675 Hz; $^2J_{PtW}$ = 420 Hz]. MS (ESI, *m/z*): Found: 1200.2927. Calcd for $C_{46}H_{55}{}^{11}BN_6O_2Si_2P^{195}Pt^{184}W$ $[M–Li–2(C_4H_8O)]^-$: 1200.2913. Anal. Found: C, 47.96; H, 5.460; N, 6.07%. Calcd for $C_{54}H_{69}BLiN_6O_4PPtSi_2W$: C, 48.04; H, 5.15; N, 6.23%. *Crystal data for* $C_{54}H_{71}BLiN_6O_4PPtSi_2W$, M = 1352.00, monoclinic, $P2_1/c$, a = 11.6600 (1) Å, b = 20.3999 (1) Å, c = 26.8469 (2) Å, β = 92.522 (1)º, V = 6379.69 (8) $Å^3$, Z = 4, ρ_{calc} = 1.408 Mgm^{-3}, μ(Cu *K*α) = 8.26 mm^{-1}, T = 150(0) K, 0.24 × 0.21 × 0.06 mm plate{clear light yellow}, 12540 independent measured reflections (θ = 72.1), R_1 = 0.029, wR_2 = 0.077 for 11694 reflections [$I > 2\sigma(I)$], 653 parameters. CDCC 2251839.

Synthesis of [WPt(μ$_2$-C)(–C≡C–SiMe$_3$)(CO)$_2$(PPh$_3$)$_2$(Tp*)] (5.14).

Note: This compound forms in competition with other species. A solution of [WPt(μ$_2$-C)Br(CO)$_2$(PPh$_3$)$_2$(Tp*)] (**3.1b**; 0.100 g, 0.0741 mmol) in THF (10 mL) was treated with lithium trimethylsilylacetylide (0.15 mL, 0.075 mmol, 0.5M in THF) at 0 °C with stirring. Maintaining the temperature at 0 °C, the solution remained orange if not slightly more yellow where TLC confirmed reaction completion after 30 minutes. Solvent was removed aided by rotary evaporation before prompt purification *via* flash column chromatography {silica gel, N_2, CH_2Cl_2/petroleum ether gradient}. First, 20% CH_2Cl_2/petroleum ether eluted a pink band corresponding to [W(≡C–C≡C–$SiMe_3$)(CO)$_2$(Tp*)] (12 mg) before 50% CH_2Cl_2/petroleum ether elutes a yellow/orange band corresponding to the title compound. The solvent of this eluate was removed, and the compound defied recrystallisation from a variety of organic solvents. The resulting orange/yellow

glass was dried under high vacuum for 16 hours and measured without further purification (0.014 g, 0.010 mmol, 14% yield). No crystal suitable for X-ray diffraction were grown. IR (CH_2Cl_2, cm^{-1}): 2051 m $\nu_{C\equiv C}$, 1939 vs ν_{CO}, 1845 vs ν_{CO}. ^1H NMR (600 MHz, $CDCl_3$, 25 °C, δ): 7.92 [m, 6H, PPh], 7.39 [m, 10H, PPh], 7.35 [m, 6H, PPh], 7.11 [m, 3H, PPh], 6.91 [m, 6H, PPh], 5.53 [s, 2H, pzCH], 5.51 [s, 1H, pzCH], 2.52 [s, 6H, $pzCH_3$], 2.32 [s, 6H, $pzCH_3$], 2.19 [s, 3H, $pzCH_3$], 2.04 [s, 3H, $pzCH_3$], –0.76 [s, 9H, $Si(CH_3)_3$]. $^{13}C\{^1H\}$ NMR (151 MHz, $CDCl_3$, 25°C, δ): 378.5 [t, $^2J_{CP}$ = 7 Hz; $^1J_{CW}$ = 175 Hz; $^1J_{CPt}$ = 606 Hz, W≡C–Pt], 232.1 [$^1J_{CW}$ = 180 Hz, CO], 151.6 151.2 [C^5(pz)], 143.5 143.0 [C^3(pz)], 135.2 [unresolved d, $^2J_{CP}$ = 10 Hz, $C^{2,6}(C_6H_5)$], 135.1 [unresolved d, $^2J_{CP}$ = 10 Hz, $C^{2,6}(C_6H_5)$], 133.1 [d, $^1J_{CP}$ = 52 Hz; $^3J_{CP}$ = 7 Hz, $C^1(C_6H_5)$], 131.9 [d, $^1J_{CP}$ = 52 Hz; $^3J_{CP}$ = 7 Hz, $C^1(C_6H_5)$], 129.7 129.5 [$C^4(C_6H_5)$], 128.4 [m, Pt–*C*≡C–$SiMe_3$], 127.8 [d, $^3J_{CP}$ = 11 Hz, $C^{3,5}(C_6H_5)$], 127.0 [d, $^3J_{CP}$ = 10 Hz, $C^{3,5}(C_6H_5)$], 123.7 [Pt–C≡*C*–$SiMe_3$], 106.5 105.8 [C^4(pz)], 17.2 14.7 12.9 12.4 [pz*C*H_3], 0.17 [$Si(CH_3)_3$]. $^{31}P\{^1H\}$ NMR (162 MHz, $CDCl_3$, 25 °C, δ): 24.06 [roofed d, $^2J_{PP}$ = 435 Hz, $^1J_{PPt}$ = 2998 Hz], 20.64 [roofed d, $^2J_{PP}$ = 435 Hz, $^1J_{PPt}$ = 3005 Hz]. $^{195}Pt\{^1H\}$ NMR (149.8 MHz, $CDCl_3$, 25°C, δ): –4193 [t, $^1J_{PtP}$ = 3003 Hz]. MS (ESI, *m/z*): Found: 1365.3330. Calcd for $C_{59}H_{61}{}^{11}BN_6O_2{}^{28}SiP_2{}^{195}Pt{}^{184}W$ $[M]^+$: 1365.3351. A sample satisfactory for elemental analysis was unable to be obtained.

Synthesis of [WPt(μ$_2$-C–C≡C–$SiMe_3$)(CO)$_2$(PPh_3)$_2$(Tp*)] (5.15).

Note: This compound undergoes reductive elimination to [W(≡C–C≡C–$SiMe_3$)(CO)$_2$(Tp*)] as an impurity evident in spectra (denoted in grey). Samples of [W(≡C–C≡C–$SiMe_3$)(CO)$_2$(Tp*)] (0.200 g, 0.309 mmol) and [Pt(η^2-C_2H_4)(PPh_3)$_2$] (0.218 g, 0.308 mmol) were dissolved in CH_2Cl_2 (20 mL), immediately dissipating the pink colour of the starting material in favour of a yellow/orange. The solution was stirred at ambient temperature for two hours before 60 °C for 15 minutes to ensure consumption of platinum(0) reagent; no further changes were observed. The mixture was concentrated (*ca* 10 mL) under reduced pressure before addition of *n*-hexane (30 mL) and concentration once more to afford a bright orange precipitate and pink supernatant phase. Sonication of the mixture aided liberation of solid which was subsequently collected *via* vacuum filtration washing with *n*-hexane (2 × 10 mL) and *n*-pentane (2 × 10 mL) until washings were colourless. The solid was dried *in vacuo* for 16 hours to afford the title compound as an orange powder (0.326 g, 0.239 mmol, 78% isolated yield). Crystals suitable for x-ray diffraction were unable to be grown. NB: spectra contain traces of propagylidyne [W(≡C–C≡C–$SiMe_3$)(CO)$_2$(Tp*)] and are denoted in grey. IR (CH_2Cl_2, cm^{-1}): 2039 m $\nu_{C\equiv C}$, 1890 vs ν_{CO}, 1800 s ν_{CO}. IR (ATR, cm^{-1}): 2041 m $\nu_{C\equiv C}$, 1892 vs ν_{CO}, 1814 vs ν_{CO}. ^1H NMR (700 MHz, $CDCl_3$, 25 °C, δ): 7.70 [m, 6H, PPh], 7.25 [overlapping m, 3H, PPh], 7.21 [m, 6H, PPh], 7.18 [m, 6H, PPh], 7.12 [m, 3H, PPh], 6.98 [m,

6H, PPh], 5.67 [s, 2H, pzCH], 5.64 [s, 1H, pzCH], 2.37 [s, 6H, pzCH$_3$], 2.29 [s, 3H, pzCH$_3$], 2.10 [s, 6H, pzCH$_3$], 1.97 [s, 3H, pzCH$_3$], –0.53 [s, 9H, Si(CH$_3$)$_3$]. ^{13}C{^{1}H} NMR (201 MHz, CDCl$_3$, 25ºC, δ): 294.1 [d, $^2J_{CP}$ = 61 Hz, WPt(μ$_2$-*C*CCSiMe$_3$)], 226.1 [m, CO], 153.7 151.3 [C^5(pz)], 144.7 142.5 [C^3(pz)], 136.3 [d, $^1J_{CP}$ = 39 Hz, C^1(C$_6$H$_5$)], 135.2 [d, $^2J_{CP}$ = 13 Hz, C^{2,6}(C$_6$H$_5$)], 134.9 [d, $^2J_{CP}$ = 12 Hz, C^{2,6}(C$_6$H$_5$)], 134.2 [d, $^1J_{CP}$ = 45 Hz, C^1(C$_6$H$_5$)], 129.0 128.7 [C^4(C$_6$H$_5$)], 127.7 [d, $^3J_{CP}$ = 9 Hz, C^{3,5}(C$_6$H$_5$)], 126.9 [d, $^3J_{CP}$ = 10 Hz, C^{3,5}(C$_6$H$_5$)], 121.1 [d, $^3J_{CP}$ = 6 Hz; $^2J_{CPt}$ = 68 Hz, WPt(μ$_2$-C*C*CSiMe$_3$)], 120.6 [WPt(μ$_2$-CC*C*SiMe$_3$)], 106.7 106.3 [C^4(pz)], 16.7 15.8 12.9 12.7 [pzCH$_3$], –0.81 [SiCH$_3$]. ^{31}P{^{1}H} NMR (162 MHz, CDCl$_3$, 25 ºC, δ): 39.40 [d, $^2J_{PP}$ = 11 Hz; $^1J_{PPt}$ = 4095 Hz], 25.29 [d, $^2J_{PP}$ = 11 Hz; $^1J_{PPt}$ = 3145 Hz]. ^{195}Pt{^{1}H} NMR (149.8 MHz, CDCl$_3$, 25ºC, δ): –4090 [dd, $^1J_{PtP}$ = 4091, 3138 Hz; $^2J_{PtW}$ = 240 Hz]. MS (ESI, *m/z*): Found: 1366.3398. Calcd for $C_{59}H_{62}{}^{11}BN_6O_2{}^{28}SiP_2{}^{195}Pt{}^{184}W$ [M+H]$^+$: 1366.3429. Anal. Found: C, 51.90; H, 4.814; N, 6.16%. Calcd for $C_{59}H_{61}BN_6O_2P_2PtSiW$: C, 51.88; H, 4.50; N, 6.15%.

Spectroscopic observation of [Li(THF)$_2$]$_2$[WPt(μ$_2$-C)(–C≡C–SiMe$_3$)$_3$(CO)$_2$(Tp*)] (5.16).

An orange solution of [WPt(μ$_2$-C)Br(CO)$_2$(PPh$_3$)$_2$(Tp*)] (**3.1b**; 0.200 g, 0.148 mmol) in THF (20 mL) was treated with excess lithium trimethylsilylacetylide (1.5 mL, 0.8 mmol, 0.5M solution in THF) at 0 °C. A bright yellow colour quickly emerges and remains after 30 minutes. The mixture was evaporated under reduced pressure to give a yellow glass where a sample was prepared for NMR spectroscopic analysis without further purification as the sample defies purification. No crystal suitable for X-ray diffraction studies emerged despite multiple attempts. IR (CH$_2$Cl$_2$, cm^{-1}): 2034 vs ν$_{CO}$, 2016 vs ν$_{CO}$, 1935 vs ν$_{CO}$, 1847 vs ν$_{CO}$. Spectra contain resoances associated with liberated phosphine, reductive elimination and products and unreacted acetylide; these are denoted as grey. ^{1}H NMR (700 MHz, C$_6$D$_6$, 25 ºC, δ): 5.64 [s, 2H, pzCH], 5.35 [s, 1H, pzCH], 3.11 [s, 6H, pzCH$_3$], 2.58 [s, 3H, pzCH$_3$], 2.14 [s, 6H, pzCH$_3$], 2.06 [s, 3H, pzCH$_3$], 0.03 [s, 9H, *trans*-CCSiCH$_3$], 0.00 [s, *cis*-CCSiCH$_3$]. ^{13}C{^{1}H} NMR (201 MHz, C$_6$D$_6$, 25ºC, δ): 381.2 [m, W≡C–Pt], 229.3 [$^1J_{CW}$ = 181 Hz, CO], 152.1 151.9 [C^5(pz)], 143.4 142.7 [C^3(pz)], 114.2 [*trans*-Pt*C*CSiMe$_3$], 108.6 [$^1J_{CPt}$ = 271 Hz, *cis*-Pt*C*CSiMe$_3$], 106.1 105.9 [C^4(pz)], 94.1 [PtC*C*SiMe$_3$], 17.4 15.6 12.8 12.5 [pzCH$_3$], –0.03 [SiCH$_3$]. ^{195}Pt{^{1}H} NMR (150 MHz, C$_6$D$_6$, 25ºC, δ): –3847 [br.s]. MS (ESI, *m/z*): Found: 1036.2554. Calcd for $C_{33}H_{50}{}^{11}BN_6O_2Si_3{}^{195}Pt{}^{184}W$ [M+H]$^-$: 1036.2553.

Synthesis of [Pt{η^2-Ph–C≡C–C≡W(CO)$_2$(Tp*)}(dppe)] (5.17).

Samples of [WPt(μ$_2$-C)Br(CO)$_2$(dppe)(Tp*)] (**3.3b**; 0.150 g, 0.123 mmol) and [CuI] (0.018 g, 0.094 mmol) were suspended in THF (15 mL) before the reaction was initiated by injection of phenylacetylene (0.02 mL, 0.2 mmol) and NEt$_3$ (1 mL). The yellow suspension was stirred for 2

hours before TLC confirmed consumption of carbido precursor and the solvent was removed by rotary evaporation to give a yellow/brown solid. This solid was purified by flash chromatography {silica gel, N_2, CH_2Cl_2/petroleum spirit gradient} where 50% CH_2Cl_2/petroleum spirit gave a yellow eluate that could be evaporated and recrystallised from concentration of *n*-hexane into CH_2Cl_2 to give a yellow powder. The yellow solid was collected *via* vacuum filtration washing with *n*-hexane (3 × 10 mL) and dried *in vacuo* for 16 hours to give the title compound as a yellow powder (0.026 g, 0.021 mmol, 17% isolated yield). Crystals suitable for x-ray diffraction were grown from the vapour diffusion of *n*-hexane into a CH_2Cl_2 solution of compound at 5 °C over three days. IR (CH_2Cl_2, cm^{-1}): 1947 vs ν_{CO}, 1859 vs ν_{CO}. IR (ATR, cm^{-1}): 2527 w ν_{BH}, 1949 vs ν_{CO}, 1853 vs ν_{CO}, 1842 vs ν_{CO}, 1659 br.m $\nu_{C=C}$. ^{1}H NMR (700 MHz, $CDCl_3$, 25 ºC, δ): 7.80 [m, 6H, PPh and Ph], 7.75 [m, 4H, PPh], 7.36 [m, 6H, PPh], 7.17 [m, 2H, Ph], 7.15 [m, 3H, PPh], 6.90 [m, 4H, PPh], 5.75 [s, 1H, pzCH], 5.52 [s, 2H, pzCH], 2.48 [s, 3H, $pzCH_3$], 2.39 [s, 6H, $pzCH_3$], 2.35 [s, 3H, $pzCH_3$], 2.32 [m, 2H, P–CH_2], 2.24 [m, 2H, P–CH_2], 2.19 [s, 6H, $pzCH_3$]. $^{13}C\{^1H\}$ NMR (201 MHz, $CDCl_3$, 25ºC, δ): 266.8 [br.d, $^3J_{CP}$ = 9 Hz, W≡C], 228.5 [$^1J_{CW}$ = 169 Hz, CO], 152.8 152.6 [C^5(pz)], 145.4 [dd, $^2J_{CP}$ = 61, 6 Hz; W≡C–*C*=C], 144.7 143.5 [C^3(pz)], 137.4 [dd, $^2J_{CP}$ = 80, 6 Hz; $^1J_{CPt}$ = 390 Hz, W≡C–C=*C*], 135.0 [t, $^3J_{CP}$ = 6 Hz, C^1(Ph)], 134.2 [m, $C^1(C_6H_5)$], 133.6 133.2 [d, $^2J_{CP}$ = 14 Hz, $C^{2,6}(C_6H_5)$], 132.2 [d, $^4J_{CP}$ = 6 Hz, $C^{2,6}$(Ph)], 130.4 129.8 [$C^4(C_6H_5)$], 128.7 [d, $^3J_{CP}$ = 10 Hz, $C^{3,5}(C_6H_5)$], 128.6 [$C^{3,5}$(Ph)], 128.1 [d, $^3J_{CP}$ = 10 Hz, $C^{3,5}(C_6H_5)$], 126.8 [C^4(Ph)], 106.5 106.2 [C^4(pz)], 30.3 [dd, $^1J_{CP}$ = 35 Hz; $^3J_{CP}$ = 16 Hz, P–*C*H_2], 29.5 [dd, $^1J_{CP}$ = 34 Hz; $^3J_{CP}$ = 14 Hz, P–*C*H_2], 16.7 15.6 12.7 [$pzCH_3$]. $^{31}P\{^1H\}$ NMR (283 MHz, $CDCl_3$, 25 ºC, δ): 49.41 [roofed d, $^2J_{PP}$ = 50 Hz, $^1J_{PPt}$ = 3100 Hz], 48.02 [roofed d, $^2J_{PP}$ = 50 Hz, $^1J_{PPt}$ = 3443 Hz]. $^{195}Pt\{^1H\}$ NMR spectroscopy failed to detect a resonance in a series of experiments of {1000 ppm spectral width, 6000 scans, +1000 to –6000 ppm}. MS (ESI, *m*/*z*): Found: 1244.2860. Calcd for $C_{52}H_{52}{}^{11}BN_6O_2P_2{}^{195}Pt^{184}W$ $[M+H]^+$: 1244.2877. Anal. Found: C, 50.21; H, 3.995; N, 6.80%. Calcd for $C_{52}H_{51}BN_6O_2P_2PtW$: C, 50.22; H, 4.13; N, 6.76%. *Crystal data for* $C_{52}H_{51}BN_6O_2P_2PtW{\cdot}CH_2Cl_2$, *M* = 1328.60, triclinic, $P\bar{1}$, *a* = 13.3447 (4) Å, *b* = 13.7733 (5) Å, *c* = 15.3696 (4) Å, α = 105.973 (3)°, β = 92.478 (2)°, γ = 107.722 (3)°, *V* = 2561.99 (15) $Å^3$, *Z* = 2, ρ_{calc} = 1.722 Mgm^{-3}, μ(Mo *K*α) = 5.18 mm^{-1}, *T* = 150(0) K, block 0.13 × 0.07 × 0.06 mm {clear dark yellow}, 9369 independent measured reflections (θ = 25.4°), R_1 = 0.030, wR_2 = 0.058 for 7644 reflections [$I > 2\sigma(I)$], 619 parameters. CDCC 2251834.

Synthesis of [Pt{η²-Ph–C≡C–C≡W(CO)₂(Tp*)}(PPh₃)₂] (5.18).

Samples of [W(≡C–C≡C–Ph)(CO)$_2$(Tp*)] (0.100 g, 0.154 mmol) and [Pt(η²-C_2H_4)(PPh_3)$_2$] (0.110 g, 0.155 mmol) were dissolved in CH_2Cl_2 (10 mL) instantly changing from maroon to golden

brown. The mixture was stirred for 2 hours with no further changes recorded. *N*-hexane (20 mL) was added and the solution concentrated (*ca* 5 mL) to precipitate of a brown solid with yellow supernatant, aided by sonication. The solid was collected *via* vacuum filtration and washed with *n*-hexane (5 mL) and *n*-pentane (2 × 5 mL) where losses were sustained as the title compound is sparingly soluble in pentane. The solid was dried *in vacuo* for 16 hours to give the title compound as a brick red powder (0.126 g, 0.092 mmol, 60% isolated yield). Crystals suitable for X-ray diffraction were unable to be grown. IR (CH_2Cl_2, cm^{-1}): 1947 vs ν_{CO}, 1861 vs ν_{CO}. IR (ATR, cm^{-1}): 2521 w ν_{BH}, 1944 vs ν_{CO}, 1857 vs ν_{CO}, 1652 br.m $\nu_{C=C}$. ^{1}H NMR (700 MHz, $CDCl_3$, 25 ºC, δ): 7.31 [m, 7H, PPh], 7.25 [overlapping m, 7H, PPh and Ph], 7.15 [m, 3H, PPh], 7.05 [m, 6H, PPh], 6.98 [m, 3H, PPh], 6.90 [m, 1H, Ph], 6.80 [m, 2H, Ph], 6.72 [m, 6H, PPh], 5.73 [s, 1H, pzCH], 5.69 [s, 2H, pzCH], 2.46 [s, 3H, $pzCH_3$], 2.39 [s, 6H, $pzCH_3$], 2.33 [s, 3H, $pzCH_3$], 2.21 [s, 6H, $pzCH_3$]. $^{13}C\{^1H\}$ NMR (201 MHz, $CDCl_3$, 25ºC, δ): 266.6 [m, W≡C], 228.3 [$^1J_{CW}$ = 169 Hz, CO], 152.6 152.4 [C^5(pz)], 144.5 143.5 [C^3(pz)], 136.2 [d, $^1J_{CP}$ = 42 Hz, $C^1(C_6H_5)$], 135.4 [d, $^1J_{CP}$ = 43 Hz, $C^1(C_6H_5)$], 134.4 134.2 [d, $^2J_{CP}$ = 13 Hz, $C^{2,6}(C_6H_5)$], 130.3 [d, $^3J_{CP}$ = 5 Hz; $^2J_{CW}$ = 30 Hz, *C*≡*C*], 129.3 128.9 [$C^4(C_6H_5)$], 127.7 127.5 [d, $^3J_{CP}$ = 10 Hz, $C^{3,5}(C_6H_5)$], 127.4 [$C^{3,5}(C_6H_5)$], 127.0 [d, $^3J_{CP}$ = 10 Hz, $C^1(C_6H_5)$], 126.1 [$C^4(C_6H_5)$], 106.43 106.41 [C^4(pz)], 16.7 15.6 12.8 12.7 [$pzCH_3$]. $^{31}P\{^1H\}$ NMR (283 MHz, $CDCl_3$, 25 ºC, δ): 28.35 [d, $^2J_{PP}$ = 32 Hz, $^1J_{PPt}$ = 3178 Hz], 26.33 [d, $^2J_{PP}$ = 33 Hz, $^1J_{PPt}$ = 3680 Hz]. $^{195}Pt\{^1H\}$ NMR spectroscopy failed to detect a resonance in a series of experiments of {1000 ppm spectral width, 6000 scans, 0 to –6000 ppm}. MS (ESI, *m*/*z*): Found: 1370.3322. Calcd for $C_{62}H_{58}{}^{11}BN_6O_2P_2{}^{195}Pt^{184}W$ $[M+H]^+$: 1370.3347. Anal. Found: C, 54.34; H, 4.384; N, 6.32%. Calcd for $C_{62}H_{57}BN_6O_2P_2PtW$: C, 54.36; H, 4.19; N, 6.14%.

Synthesis of [WPt{μ$_2$-C–C≡C–C≡W(CO)$_2$(Tp*)}(dppe)(CO)$_2$(Tp*)] (5.19).

A solution of [WPt(μ$_2$-C)Br(CO)$_2$(dppe)(Tp*)] (**3.3b**; 0.125 g, 0.102 mmol) and [W(≡C–C≡C–$SiMe_3$)(CO)$_2$(Tp*)] (0.060 g, 0.093 mmol) in THF (15 mL) is treated dropwise with TBAF (0.24 mL, 0.20 mmol, 1.0 M solution in THF) rapidly changing from maroon to brown. This mixture was stirred for an hour before TLC confirmed reaction completion, and solvent evaporated to a brown residue. The residue was purified *via* flash column chromatography {silica gel, N_2, CH_2Cl_2/petroleum spirit gradient} where 60% CH_2Cl_2/petroleum spirit gave an orange/brown eluate that was evaporated to a dark brown microcrystalline solid without further purification to give the title compound after drying in vacuo for 16 hours (0.064 g, 0.037 mmol, 40% isolated yield). No crystals suitable for X-ray diffraction were grown. IR (CH_2Cl_2, cm^{-1}): 1957 vs ν_{CO}, 1892 br.vs ν_{CO}, 1868 br.vs ν_{CO}, 1745 br.m $\nu_{\mu\text{-}CO}$. IR (ATR, cm^{-1}): 2521 w ν_{BH}, 1950 vs ν_{CO}, 1879 sh ν_{CO}, 1856 vs ν_{CO}, 1756 m $\nu_{\mu\text{-}CO}$. ^{1}H NMR (400 MHz, $CDCl_3$, 25 ºC, δ): 7.84 [m, 4H, PPh], 7.69 [m, 4H,

PPh], 7.43 [m, 6H, PPh], 7.33 [m, 6H, PPh], 5.76 [s, 2H, pzCH], 5.70 [s, 2H, $pzCH_3$], 5.67 [s, 2H, pzCH], 2.62–2.37 [m, 14H, $pzCH_3$], 2.34 [s, 6H, $pzCH_3$], 2.30 [s, 6H, $pzCH_3$], 2.27 [s, 3H, $pzCH_3$], 2.18–2.04 [m, 5H, $pzCH_3$ and P–CH_2], 2.02 [s, 6H, $pzCH_3$]. $^{13}C\{^1H\}$ NMR (201 MHz, $CDCl_3$, 25°C, δ): 279.3 [d, $^2J_{CP}$ = 59 Hz, WPt(μ$_2$-C)], 240.9 [W≡C], 234.6 [br.s, $^1J_{CW}$ = 158 Hz, PtW–CO], 229.2 [$^1J_{CW}$ = 165 Hz, W–CO], 156.5 [d, $^3J_{CP}$ = 8 Hz, WPt(μ$_2$-C–*C*)], 153.3 152.3 152.0 151.1 [C^5(pz)], 144.8 144.1 143.6 142.8 [C^3(pz)], 134.3 133.3 [d, $^2J_{CP}$ = 12 Hz, $C^{2,6}(C_6H_5)$], 132.0 [overlapping d, $^1J_{CP}$ = 41 Hz, $C^1(C_6H_5)$], 131.8 [overlapping d, $^1J_{CP}$ = 46 Hz, $C^1(C_6H_5)$], 130.2 130.0 [$C^4(C_6H_5)$], 128.3 [d, $^3J_{CP}$ = 10 Hz, $C^{3,5}(C_6H_5)$], 128.2 [d, $^3J_{CP}$ = 9 Hz, $C^{3,5}(C_6H_5)$], 107.2 106.8 106.3 106.1 [C^4(pz)], 86.6 [W≡C–*C*], 31.4 [m, P–CH_2], 16.7 16.3 15.3 15.0 12.7 12.6 [$pzCH_3$]. $^{31}P\{^1H\}$ NMR (283 MHz, $CDCl_3$, 25 °C, δ): 58.24 [d, $^2J_{PP}$ = 6 Hz, $^1J_{PPt}$ = 3578 Hz], 52.90 [d, $^2J_{PP}$ = 6 Hz, $^{1z}J_{PPt}$ = 3210 Hz]. $^{195}Pt\{^1H\}$ NMR (85.7 MHz, $CDCl_3$, 25°C, δ): –4294 [dd, $^1J_{PtP}$ = 3591, 3220 Hz]. MS (ESI, *m/z*): Found: 1716.3862. Calcd for $C_{64}H_{69}{}^{11}B_2N_{12}O_4P_2{}^{195}Pt^{184}W$ $[M+H]^+$: 1716.3892. Anal. Found: C, 44.79; H, 4.013; N, 9.69%. Calcd for $C_{64}H_{68}B_2N_{12}O_4P_2PtW_2$: C, 44.81; H, 4.00; N, 9.80%.

9.8 Synthetic procedures for Chapter Six compounds

Spectroscopic Observation of [MoPd(μ$_2$-C)Br(CO)$_2$(PPh$_3$)$_2$(Tp*)] (6.1a).

An NMR sample of [Mo(≡CBr)(CO)$_2$(Tp*)] (35 mg, 0.065 mmol) and [Pd(PPh_3)$_4$] (80 mg, 0.069 mmol) in C_6D_6 (0.5 mL) was prepared under argon. Upon combination, the solution colour rapid changed from yellow to a bright red. The sample was subjected to NMR spectroscopic analysis after 1 hour to measure the title compound in solution. IR (CH_2Cl_2, cm^{-1}): 1974 vs ν_{CO}, 1886 vs ν_{CO}. IR (THF, cm^{-1}): 1971 vs ν_{CO}, 1888 vs ν_{CO}. IR ($CHCl_3$, cm^{-1}): 1974 vs ν_{CO}, 1889 vs ν_{CO}. IR (benzene, cm^{-1}): 1973 vs ν_{CO}, 1891 vs ν_{CO}. ^1H NMR (400 MHz, C_6D_6, 25 °C, δ): 8.33 [t, $^1J_{HH}$ = 9 Hz, 3H, PPh], 7.82 [m, 4H, PPh], 7.53 [m, 16H, PPh], 7.02 [m, 3H, PPh], 6.92 [m, 4H, PPh], 5.64 [s, 1H, pzCH], 5.48 [s, 2H, pzCH], 2.65 [s, 3H, $pzCH_3$], 2.29 [s, 3H, $pzCH_3$], 2.28 [s, 6H, $pzCH_3$], 2.22 [s, 3H, $pzCH_3$], 2.16 [s, 3H, $pzCH_3$]. ^{13}C NMR (176 MHz, C_6D_6, 25 °C, δ): 353.8 [m, Mo≡*C*–Pd], 224.7 [CO], 151.7 151.5 [C^5(pz)], 145.0 144.3 [C^3(pz)], 132.4 [d, $^2J_{CP}$ = 9 Hz, $C^{2,6}(C_6H_5)$], 129.9 [d, $^1J_{CP}$ = 37 Hz, $C^1(C_6H_5)$], some aryl resonances obscured by PPh_3, 107.0 106.6 [C^4(pz)], 15.7 14.8 12.6 12.5 [$pzCH_3$]. ^{31}P NMR (162 MHz, C_6D_6, 25 °C, δ): 25.90 [d, $^1J_{PP}$ = 423 Hz, PPh_3], 20.72 [d, $^1J_{PP}$ = 421 Hz, PPh_3].

Spectroscopic Observation of [WPd(μ$_2$-C)Br(CO)$_2$(PPh$_3$)$_2$(Tp*)] (6.1b).

An NMR sample of [W(≡CBr)(CO)$_2$(Tp*)] (27 mg, 43 μmol) and [Pd(PPh_3)$_4$] (50 mg, 43 μmol) in d_6-benzene (0.5 mL) was prepared under argon. Upon combination, the solution colour rapidly

changed from yellow to a bright red. The sample was subjected to NMR spectroscopic analysis after 1 hour to measure the title compound **6.1b** in solution. IR(THF, cm^{-1}): 1962 sh ν_{CO}, 1956 vs ν_{CO}, 1872 sh ν_{CO}, 1865 vs ν_{CO}. IR(CH_2Cl_2, cm^{-1}): 1957 br ν_{CO}, 1865 br ν_{CO}. IR($CHCl_3$, cm^{-1}): 1960 br ν_{CO}, 1866 br ν_{CO}. IR(NaCl, benzene): 1957 s ν_{CO}, 1872 s ν_{CO}, 1864 s ν_{CO}. ^{1}H NMR (400 MHz, C_6D_6, 25 ºC, δ): 8.36 [t, $^1J_{HH}$ = 9 Hz, 6H, PPh], 7.79 [t, $^1J_{HH}$ = 9 Hz, 8H, PPh], 7.34 [t, $^1J_{HH}$ = 8 Hz, 6H, PPh], 7.04–6.97 [m, 4H, PPh], 6.94–6.87 [m, 6H, PPh], 5.54 [s, 2H, pzCH], 5.40 [s, 1H, pzCH], 2.35 [s, 3H, $pzCH_3$], 2.23 [s, 6H, $pzCH_3$], 2.17 [s, 6H, $pzCH_3$], 2.11 [s, 3H, $pzCH_3$]. $^{13}C\{^1H\}$ NMR (151 MHz, C_6D_6, 25 ºC, δ): 333.7 [m, W≡C–Pd], 231.1 [$^1J_{CW}$ = 179 Hz, CO], 151.9 151.4 [C^5(pz)], 143.6 143.3 [C^3(pz)], 132.9 [dd, $^1J_{CP}$ = 42 Hz, $^2J_{CP}$ = 4 Hz, $C^1(C_6H_5)$], 129.8 129.7 [$C^4(C_6H_5)$], 107.3 107.1 [C^4(pz)], 18.1 15.1 12.7 12.3 [$pzCH_3$]; some aryl resonances cannot be unequivocally assigned, obscured by C_6D_6 and excess PPh_3 signals. $^{31}P\{^1H\}$ NMR (162 MHz, C_6D_6, 25 ºC, δ): 28.81 [d, $^1J_{PP}$ = 428 Hz, PPh_3], 23.23 [d, $^1J_{PP}$ = 428 Hz, PPh_3].

Synthesis of $[MoPd(\mu_2\text{-}C)(CO)_2(PPh_3)(Tp^*)]_2(\mu_2\text{-}Br)_2$ (6.2).

A sample of $[Mo(\equiv CBr)(CO)_2(Tp^*)]$ (480 mg, 0.881 mmol) was stirred with $[Pd(PPh_3)_4]$ (1.001 g, 0.866 mmol) in benzene (20 mL) at room temperature for 3 hours darkening to red. Complete conversion of starting material was recognised *via* infra-red spectroscopic analysis and solvent was removed under reduced pressure to afford a red residue. This mixture was subjected to an ultrasonic bath in *n*-hexane (10 mL) for several minutes until an orange powder was liberated. The powder was recrystallised from concentration of THF into *n*-hexane before collection by vacuum filtration, washing with *n*-hexane (3 × 10 mL) and *n*-pentane (10 mL), before drying *in vacuo* for 5 hours gave the title compound (768 mg, 0.422 mmol, 97% yield). Crystals suitable for X-ray diffraction were obtained by the vapour diffusion of *n*-hexane into a solution of **6.2** in benzene at 5 °C. IR (THF, cm^{-1}): 1986 w ν_{CO}, 1977 vs ν_{CO}, 1911 m ν_{CO}, 1897 vs ν_{CO}. IR (ATR, cm^{-1}): 2524 w ν_{BH}, 1970 vs ν_{CO}, 1888 vs ν_{CO}. ^{1}H NMR (400 MHz, C_6D_6, 25 ºC, δ): 7.91 [m, 1H, PPh], 7.77–7.73 [m, 2H, PPh], 7.71–7.60 [m, 8H, PPh], 7.08–6.97 [m, 5H, PPh], 6.95–6.88 [m, 4H, PPh], 6.87–6.83 [m, 2H, PPh], 6.78–6.63 [m, 8H, PPh], 5.34 [s, 2H, pzCH], 5.30 [s, 1H, pzCH], 2.54 [s, 6H, $pzCH_3$], 2.29 [s, 3H, $pzCH_3$], 2.16 [s, 6H, $pzCH_3$], 2.04 [s, 3H, $pzCH_3$]. $^{13}C\{^1H\}$ NMR (151 MHz, C_6D_6, 25 ºC, δ): 330.8 [bs, Mo≡C–Pd], 230.0 [CO], 150.9 [C^5(pz)], 143.7 143.0 [C^3(pz)], 135.7 134.5 [C_6H_5], 132.5 [d, $^2J_{CP}$ = 10 Hz, $C^{2,6}(C_6H_5)$], 131.6 130.6 130.4 [C_6H_5], 128.5 [d, $^1J_{CP}$ = 12 Hz, $C^{3,5}(C_6H_5)$], 106.5 106.1 [C^4(pz)], 16.7 14.8 12.7 12.5 [$pzCH_3$]. MS (ESI, *m/z*): Found: 1843.00201. Calcd for $C_{72}H_{74}B_2Br_2Mo_2N_{12}O_4P_2Pd_2Na$ $[M+Na]^+$: 1843.00915. Samples of sufficient purity for microanalytical analysis were unable to be achieved despite multiple attempts, potentially

due to decomposition initialised by breakdown of the fragile, halogen bridge. *Crystal data for* $C_{72}H_{74}B_2Br_2Mo_2N_{12}O_4P_2Pd_2$, M = 2005.73, monoclinic, $P2_1/n$, a = 27.0575 (4) Å, b = 11.7128 (2) Å, c = 29.6534 (3) Å, β = 104.965 (1)°, V = 9079.0 (2) Å^3, Z = 4, ρ_{calc} = 1.437 Mg m^{-3}, μ(Cu $K\alpha$) = 7.17 mm^{-1}, T = 150(0) K, block 0.25 × 0.11 × 0.05 mm {clear light orange}, 17953 independent measured reflections (θ = 73.8 °), R_1 = 0.057, wR_2 = 0.137 for 14248 reflections [$I > 2\sigma(I)$], 895 parameters, 0 restraints. CDCC 1988590.

Synthesis of [MoPd(μ$_2$-C)Br(CO)$_2$(dppe)(Tp*)] (6.3).

A solution of [MoPd(μ$_2$-C)(CO)$_2$(PPh$_3$)(Tp*)]$_2$(μ$_2$-Br)$_2$ (**6.2**; 101 mg, 0.056 mmol) and dppe (84 mg, 0.211 mmol) in THF (10 mL) was stirred for 16 hours, resulting in an orange solution that was evaporated under reduced pressure to give an orange solid. The resulting solid was recrystallised from concentration of CH_2Cl_2 into *n*-hexane to give an orange powder, that was collected *via* vacuum filtration and washed with EtOH (3 × 10 mL) and Et_2O (3 × 10 mL) before drying *in vacuo* to give the title compound as a pale orange powder (65 mg, 0.062 mmol, 55% isolated yield). Crystals suitable for X-ray diffraction studies were obtained by the slow evaporation of a $CHCl_3$ solution of **6.3** at ambient temperature. IR (CH_2Cl_2, cm^{-1}): 1971 vs ν_{CO}, 1884 vs ν_{CO}. IR (ATR, cm^{-1}): 2527 w ν_{BH}, 1969 vs ν_{CO}, 1887 vs ν_{CO}. NMR resonances are broadened due to limited solubility of compound. ^{1}H NMR (600 MHz, CD_2Cl_2, 25 °C, δ): 7.80 [m, 4H, PPh], 7.59 [m, 4H, PPh], 7.49 [m, 6H, PPh], 7.30 [m, 2H, PPh], 7.07 [br, 4H, PPh], 5.61 [s, 3H, pzCH], 2.36 [s, 12H, pzCH_3], 2.23 [s, 6H, pzCH_3], 2.00 [m, 4H, PCH_2]. ^{13}C{^{1}H} NMR (151 MHz, CD_2Cl_2, 25°C, δ): 375.9 [br d, $^2J_{CP}$ = 70 Hz, Mo≡C–Pd], 231.1 [CO], 151.4 151.0 [C^5(pz)], 145.0 144.2 [C^3(pz)], 134.0 [d × 2, $^2J_{CP}$ = 11 Hz, C^{2,6}(C_6H_5)], 131.8 131.4 [C^4(C_6H_5)], 130.7 [d, 1C, $^1J_{CP}$ = 36 Hz, C^1(C_6H_5)], 129.2 [d, $^3J_{CP}$ = 10 Hz, C^{3,5}(C_6H_5)] 129.1 [d, 1C, $^1J_{CP}$ = 36 Hz, C^1(C_6H_5)], 128.7 [d, $^2J_{CP}$ = 11 Hz, C^{3,5}(C_6H_5)], 106.2 105.9 [C^4(pz)], 23.5 23.3 [d × 2, $^1J_{CP}$ = 12 Hz, PCH_2], 16.6 14.4 12.9 12.6 [pzCH_3]. ^{31}P{^{1}H} NMR (162 MHz, CD_2Cl_2, 25 °C, δ): Two rotamers are apparent on this ^{31}P timescale in a ratio of 1:7. Major rotamer: 45.96 [d, $^2J_{PP}$ = 29 Hz], 35.50 [d, $^2J_{PP}$ = 32 Hz]; Minor Rotamer: 46.48 34.36 [d × 2, $^2J_{PP}$ = 33 Hz]. MS (ESI, *m/z*): Found: 966.1305. Calcd for $C_{44}H_{46}BMoN_6O_2P_2Pd$ [M–Br]$^+$: 966.1365. Sufficiently pure material by microanalytical analysis was unable to be achieved despite multiple attempts. The reason in this scenario is unclear. *Crystal data for* $C_{44}H_{46}BBrMoN_6O_2P_2Pd$, M = 1045.87, monoclinic, $C2/c$, a = 42.971 (3) Å, b = 10.4460 (5) Å, c = 20.5602 (10) Å, β = 94.607 (6)°, V = 9199.1 (9) Å^3, Z = 8, ρ_{calc} = 1.510 Mgm^{-3}, μ(Cu $K\alpha$) = 7.40 mm^{-1}, T = 150(0) K, plate 0.08 × 0.04 × 0.03 mm {clear light orange}, 9109 independent measured reflections (θ = 72.6), R_1 = 0.096, wR_2 = 0.321 for 4590 reflections [$I > 2\sigma(I)$], 529

parameters. CDCC 1588592. Despite multiple attempts, crystals of sufficient precision for rigorous discussion were unable to be achieved. While the refinement returned reasonable geometric parameters, these should be considered with appropriate caution.

Synthesis of [WPd(=CPPh$_3$)Br(PPh$_3$)(CO)$_2$(Tp*)](6.4).

A mixture of [W(≡CBr)(CO)$_2$(Tp*)] (152 mg, 0.242 mmol) and [Pd(PPh$_3$)$_4$] (294 mg, 0.254 mmol) in benzene (10 mL) was stirred for 20 hours transitioning yellow to a bright red colour. The solvent was removed under reduced pressure before recrystallisation by the addition of *n*-hexane into benzene at 60 ºC, prior to cooling to ambient temperature, and then storage at 5 ºC. This was performed twice, discarding the pale orange supernatant phase both times. The ensuing red solid was collected *via* vacuum filtration in an argon charged glove-box and washed with *n*-pentane (2 × 10 mL). This afforded the title compound as a red solid (193 mg, 0.153 mmol, 63% isolated yield). Crystals suitable for X-ray diffraction were grown from the vapour diffusion of *n*-hexane into a solution of **6.4** in benzene under a strictly argon-charged atmosphere at ambient temperature. IR(THF, cm^{-1}): 1940 vs ν_{CO}, 1910 br ν_{CO}, 1809 sh ν_{CO}, 1797 br ν_{CO}. ^{1}H NMR (700 MHz, C_6D_6, 50 ºC, δ): 8.00 [m, 5H, PPh], 7.75 [m, 5H, PPh], 7.18 [m, overlapping solvent, 7H, PPh], 7.12 [t, $^1J_{HH}$ = 7 Hz, 3H, PPh], 7.01 [t, $^1J_{HH}$ = 7 Hz, 4H, PPh], 6.93 [m, 6H, PPh], 5.33 [s, 1H, pzCH], 5.11 [s, 2H, pzCH], 2.42 [s, 3H, pzCH_3], 2.17 [s, 6H, pzCH_3], 2.01 [s, 9H, pzCH_3]. ^{13}C{^{1}H} NMR (176 MHz, C_6D_6, 50 ºC, δ): Very poor solubility so only limited data could be acquired, 153.0 152.5 [C^5(pz)], 144.5 143.9 [C^3(pz)], 135.5 [m,C_6H_5], 135.4 [t, $^2J_{CP}$ = 6 Hz, C_6H_5], 134.9 [m, C_6H_5], 133.9 [d, $^1J_{CP}$ = 19 Hz, C_6H_5], 132.6 [t, $^1J_{CP}$ = 23 Hz, C_6H_5], 131.8 [m, C_6H_5], 129.9 128.9 128.6 128.4 [C_6H_5], 107.3 107.0 [C^4(pz)], 17.8 16.9 15.9 12.5 [pzCH_3]. Some aryl signals cannot be unequivocally assigned due to presence of C6D6 and excess PPh$_3$ compounded by low solubility compromising signal quality. ^{31}P{^{1}H} NMR (162 MHz, C_6D_6, 50 ºC, δ): 10.73 [bs, C*P*Ph]. ^{31}P{^{1}H} NMR (162 MHz, C_6D_6 + PPh$_3$, 25 ºC, δ): 13.35 [$^2J_{CP}$ =112 Hz, C*P*Ph), –5.28 [s.br, PPh$_3$]. MS (ESI, *m*/*z*): Found: 1179.2261. Calcd for $C_{54}H_{52}BN_6O_2P_2PdW$ [M–Br]$^+$: 1179.2256. Despite multiple attempts, a suitable sample could not be obtained for elemental analysis. While retaining its colour in air, this compound rapidly decomposes in the absence of excess to PPh$_3$ to **6.5** in the following solvents $CHCl_3$, CH_2Cl_2, MeOH, EtOH, Et_2O, MeCN, and deuterated variants. *Crystal data for* $C_{54}H_{52}B\,BrN_6O_2P_2PdW$, *M* = 1259.92, monoclinic, $P2_1/n$, *a* = 21.7995 (4) Å, *b* = 12.8236 (1) Å, *c* = 22.8740 (4) Å, β = 111.409 (2)º, *V* = 5953.16 (19) Å^3, *Z* = 4, ρ_{calc} = 1.406 Mg m^{-3}, μ(Cu *K*α) = 7.57 mm^{-1}, *T* = 150(0) K, plate 0.17 × 0.13 × 0.04 mm {clear light red}, 10888 independent measured reflections (θ = 68.3 º), R_1 = 0.056, wR_2 = 0.166 for 10888 reflections [$I > 2\sigma(I)$], 619 parameters. CDCC 1988593.

Synthesis of [WPd(μ_2-CPPh$_3$)Br(μ-CO)(CO)(Tp*)] (6.5).

A flask charged with [W(≡CPPh$_3$)(CO)$_2$(Tp*)]Br (**6.6**; 101 mg, 125 μmol) and [Pd$_2$(dba)$_3$]·CHCl$_3$ (63 mg, 69 μmol) was injected with THF (5 mL) to give a purple solution that quickly transitioned to an orange brown mixture. This was stirred for 90 minutes before solvent was removed *via* rotary evaporation to afford a brown residue. The prepared residue was purified *via* flash chromatography {silica gel, N_2, 1–10 % THF/CH_2Cl_2 gradient elution} eluting a brown compound at 5% eluent strength. This eluate was the major component and was removed of solvent before recrystallization from concentration of CH_2Cl_2 into *n*-hexane. An orange powder was obtained and subsequently collected *via* vacuum filtration, washing with *n*-hexane (3 × 10 mL) and *n*-pentane (5 mL) before drying *in vacuo* for 2 hours to give the title compound (36 mg, 36 μmol, 29% isolated yield). IR (CH_2Cl_2, cm^{-1}): 1947 s ν_{CO}, 1791 s $\nu_{\mu\text{-}CO}$. IR (ATR, cm^{-1}): 1932 s ν_{CO}, 1774 s $\nu_{\mu\text{-}CO}$. ^{1}H NMR (600 MHz, $CDCl_3$, 25 ºC, δ): 7.62–7.51 [m, 9H, PPh], 7.39–7.31 [m, PPh], 5.73 [s, 1H, pzCH], 5.49 [s, 2H, pzCH], 2.45 [overlapping singlets, 6H and 3H, pzCH$_3$], 2.27 [s, 3H, pzCH$_3$], 1.71 [s, 6H, pzCH$_3$]. ^{13}C{^{1}H} NMR (151 MHz, $CDCl_3$, 25ºC, δ): 238.7 [$^1J_{CW}$ = 147 Hz, CO], 232.1 [$^1J_{CW}$ = 178 Hz, CPPh], 153.0 152.7 [C^5(pz)], 145.4 144.5 [C^3(pz)], 134.1 [d, $^2J_{CP}$ =10 Hz, C^{2,6}(C_6H_5)], 133.0 [C^4(C_6H_5)], 129.1 [d, $^3J_{CP}$ = 12 Hz, C^{3,5}(C_6H_5)], 123.1 [d, $^1J_{CP}$ = 88 Hz, C^1(C_6H_5)], 107.4 107.3 [C^4(pz)], 17.5 15.3 12.8 [pzCH$_3$]. ^{31}P{^{1}H} NMR (162 MHz, $CDCl_3$, 25 ºC, δ): 7.18 [s, $^2J_{PW}$ = 119 Hz, PPh]. MS (ESI, *m/z*): Found: 917.1373. Calcd for $C_{36}H_{37}BN_6O_2PPdW$ [M–Br]$^+$: 917.1371. A sample of sufficient purity to satisfy microanalytical analysis criteria was unable to be obtained; the closest result is included. Anal. Found: C, 45.85; H, 3.72; N, 8.30%. Calcd for $C_{36}H_{37}BBrN_6O_2PPdW$: C, 43.34; H, 3.74; N, 8.42%. §§*Crystal data for* $C_{36}H_{37}BBrN_6O_2PPdW{\cdot}3(CHCl_3)$, *M* = 1355.76, triclinic, $P\bar{1}$, *a* = 11.4100 (4) Å, *b* = 13.4275 (5) Å, *c* = 17.2454 (5) Å, α = 85.274 (3)º , β = 87.055 (2)º, γ = 70.722 (3)º, *V* = 2485.43 (15) Å^3, *Z* = 2, ρ_{calc} = 1.812 Mg m^{-3}, μ(Cu *K*α) = 4.03 mm^{-1}, *T* = 150(0) K, block 0.24 × 0.11 × 0.04 mm {clear dark red}, 10177 independent measured reflections (θ = 26.4 º), R_1 = 0.040, wR_2 = 0.089 for 8724 reflections [$I > 2\sigma(I)$], 556 parameters. CDCC 1988594.

Synthesis of [W(≡C–PPh$_3$)(CO)$_2$(Tp*)]Br (6.6).

A solution of [W(≡CBr)(CO)$_2$(Tp*)] (1.021 g, 1.620 mmol) and triphenylphosphine (1.773 g, 6.76 mmol) in acetonitrile (40 mL) was stirred at 40 °C for 20 hours. The resulting purple solution

§§ Data for this crystal structure was obtained and analysed by Dr. Richard A. Manzano, and is reprinted, with permission, for comparison and completeness.

was evaporated under reduced pressure affording a purple oil. The residue was purified *via* flash column chromatography {silica gel, N_2} initially eluting with neat CH_2Cl_2 before eluting with 5% THF/CH_2Cl_2. A purple band was collected, and solvent removed under reduced pressure to provide a purple oil. As recrystallization attempts resulted in more oils, ultra-sonication in *n*-hexane (10 mL) with mechanical agitation eventually resulted in a purple powder. This could be collected *via* vacuum filtration washing with *n*-hexane (3 × 10 mL) and *n*-pentane (3 × 10 mL) before drying *in vacuo* for 16 hours to provide the title compound (784 mg, 0.88 mmol, 55% isolated yield). IR (CH_2Cl_2, cm^{-1}): 2025 vs ν_{CO}, 1940 vs ν_{CO}. ^1H NMR (400 MHz, $CDCl_3$, 25 ºC, δ): 7.84 [m, 3H, PPh], 7.70 [m, 6H, PPh], 7.63–7.56 [m, 6H, PPh], 5.97 [s, 2H, pzCH], 5.81 [s, 1H, pzCH], 2.41 [s, 6H, $pzCH_3$], 2.31 [s, 3H, $pzCH_3$], 2.30 [s, 3H, $pzCH_3$], 1.99 [s, 6H, $pzCH_3$]. $^{13}C\{^1H\}$ NMR (100 MHz, $CDCl_3$, 25ºC, δ): 241.6 [$^1J_{CP}$ not resolved, W≡C–P], 224.0 [$^1J_{CW}$ = 158 Hz, CO], 153.1 151.5 [C^5(pz)], 147.1 146.4 [C^3(pz)], 135.2 [d, $^4J_{CP}$ = 3 Hz, $C^4(C_6H_5)$], 133.3 [d, $^3J_{CP}$ = 11 Hz, $C^{3,5}(C_6H_5)$], 130.6 [d, $^2J_{CP}$ = 13 Hz, $C^{2,6}(C_6H_5)$], 120.5 [d, $^1J_{CP}$ = 90 Hz, $C^1(C_6H_5)$], 108.2 107.7 [C^4(pz)], 16.7 15.4 12.89 12.85 [$pzCH_3$]. $^{31}P\{^1H\}$ NMR (162 MHz, $CDCl_3$, 25 ºC, δ): 10.2 [s, $^1J_{PW}$ = 162 Hz]. Data associated with the cation [**6.6**]$^+$ correspond to those reported by Templeton for [**6.6**]PF_6.

General Procedure – Alkyne-Bromocarbyne Cross-Coupling

Cuprous iodide (10 mg, 53 μmol), [M(≡CBr)$(CO)_2$(Tp*)] (192 μmol) and the mediator complex under investigation (5–10 mol%) were combined under argon. To this was sequentially added, with stirring, triethylamine (10 mL) and the alkyne of choice (210 μmol). The reaction was monitored by thin layer chromatography utilising 1:1 CH_2Cl_2/petroleum ether as eluent. Upon completion, the mixture was freed of volatiles and the residue subjected to anaerobic flash column chromatography (silica gel, CH_2Cl_2/petroleum ether gradient} followed by solvent removal. Recrystallisation by concentration of CH_2Cl_2 into EtOH provided propargylidyne complexes as microcrystalline powders that were collected by vacuum filtration and dried *in vacuo*.

Synthesis of [Mo(≡C–C≡CPh)$(CO)_2$(Tp*)] (6.7a).

Prepared as per the general procedure above employing [MoPd(μ_2-C)$(CO)_2(PPh_3)$(Tp*)]$_2$(μ-Br)$_2$ (**6.2**: 5 mol%) as a catalyst to a mixture of [Mo(≡CBr)$(CO)_2$(Tp*)] and ethynylbenzene. The title compound was obtained as a purple powder (68 mg, 121 μmol, 66% isolated yield). IR (CH_2Cl_2, cm^{-1}): 2095 w $\nu_{C\equiv C}$, 1997 vs ν_{CO}, 1915 vs ν_{CO}. ^1H NMR (600 MHz, $CHCl_3$, 25 °C, δ) 7.50 [d, 2 H, $^1J_{HH}$ = 7 Hz, C_6H_5], 7.36 [t, 1 H, $^1J_{HH}$ = 8 Hz, C_6H_5], 7.29 [t, 2 H, $^1J_{HH}$ = 7 Hz, C_6H_5], 5.86 [s, 2 H, pzCH], 5.72 [s, 1 H, pzCH], 2.59 [s, 6 H, $pzCH_3$], 2.37 [s, 6 H, $pzCH_3$], 2.35 [s, 3 H, $pzCH_3$], 2.33

[s, 3 H, pzCH$_3$]. ^{13}C{^{1}H} NMR (151 MHz, CDCl$_3$, 25 °C, δ) 253.5 [Cα], 227.8 [CO], 151.5, 151.4 [C^5(pz)], 145.2 144.6 [C^3(pz)], 133.2 [C^{2,6}(C$_6$H$_5$)], 129.2 [C^4(C$_6$H$_5$)], 128.6 [C^{3,5}(C$_6$H$_5$)], 121.4 [C^1(C$_6$H$_5$)], 106.5 [C^4(pz)], 100.6 (Cβ), 65.9 (Cγ), 16.0 14.7 12.8 [pzCH$_3$]. MS (ESI, *m/z*): Found: 565.1416. Calcd for $C_{26}H_{28}BMoN_6O_2$ $[M+H]^+$: 565.1416. Data correspond to those previously published.[13]

Synthesis of [Mo(≡C–C≡CSiMe$_3$)(CO)$_2$(Tp*)] (6.7b)

Proof of concept reaction where the title compound has been prepared previously *via* an alternative route. [136] Prepared by general procedure employing [MoPd(μ$_2$-C)(CO)$_2$(PPh$_3$)(Tp*)]$_2$(μ-Br)$_2$ (**6.2**: 5 mol%) as a catalyst to a mixture of [Mo(≡CBr)(CO)$_2$(Tp*)] and ethynyltrimethylsilane. The title compound was obtained as a pink powder (78 mg, 140 μmol, 75% isolated yield). IR (THF, cm^{-1}): 2046 w ν$_{C≡C}$, 1997 vs ν$_{CO}$, 1916 vs ν$_{CO}$. ^{1}H NMR (400 MHz, CDCl$_3$, 25 °C, δ) 5.85 [s, 2 H, pzCH], 5.70 [s, 1 H, pzCH], 2.54 [s, 6 H, pzCH$_3$], 2.36 [s, 6 H, pzCH$_3$], 2.32 [s, 3 H, pzCH$_3$], 2.31 [s, 3 H, pzCH$_3$], 0.18 [s, 9 H, SiCH$_3$]. ^{13}C{^{1}H} NMR (101 MHz, CDCl$_3$, 25 °C, δ) 255.6 [Cα], 227.5 [CO], 151.6, 151.3 [C^5(pz)], 145.2, 144.5 [C^3(pz)], 113.4 (Cβ), 106.44 106.42 [C^4(pz)], 75.2 [Cγ], 15.8 14.7 12.8 [pzCH$_3$], –0.2 [SiCH$_3$]. Data correspond to those previously published.[13]

Synthesis of W(≡C–C≡CPh)(CO)$_2$(Tp*)] (6.7c).

Proof of concept reaction where the title compound has been prepared previously via an alternative route. [438] Prepared as per the general procedure above employing a mixture of [WPt(μ-C)Br(CO)$_2$(PPh$_3$)$_2$(Tp*)] (**3.1b**: 100 mol%) and ethynylbenzene for 16 hours. The title compound was obtained as a maroon powder (21 mg, 32 μmol, 43% isolated yield). The only other spectroscopically observable organometallic species present was the precursor **3.1b** such that isolated yields approximate to % conversion. IR (CH$_2$Cl$_2$, cm^{-1}): 2100 w ν$_{C≡C}$, 1982 vs ν$_{CO}$, 1893 vs ν$_{C≡C}$. ^{1}H NMR (400 MHz, CDCl$_3$, 25 °C, δ): 7.48 [d, $^1J_{HH}$ = 7 Hz, PhCH], 7.35 [t, $^1J_{HH}$ = 7 Hz, PhCH], 7.28 [d, $^1J_{HH}$ = 8 Hz, PhCH], 5.91 [s, 2H, pzCH], 5.75 [s, 1H, pzCH], 2.62 [s, 6H, pzCH$_3$], 2.39 [s, 3H, pzCH$_3$], 2.38 [s, 6H, pzCH$_3$], 2.32 [s, 3H, pzCH$_3$]. ^{13}C{^{1}H} NMR (101 MHz, CDCl$_3$, 25°C, δ): 246.4 [*C*α], 226.2 [CO], 152.3 152.3 [C^5(pz)], 145.2 144.4 [C^3(pz)], 132.5 128.4 122.1 [C$_6$H$_5$], 107.0 [*C*β], 106.7 106.6 [overlapping singlets, C^4(pz)], 70.2 [*C*$_γ$], 16.6 15.2 12.7 12.6 [pzCH$_3$]. Data were consistent with those previously published.[13]

[W(≡C–C≡CSiMe$_3$)(CO)$_2$(Tp*)] (6.7d).

Proof of concept reaction where the title compound has been prepared previously. [438] Prepared as per general procedure employing a mixture of [WPt(μ-C)Br(CO)$_2$(PPh$_3$)$_2$(Tp*)] (**3.1b**; 100 mol%) and ethynyltrimethylsilane. The title compound was obtained as a pink powder (17 mg, 26

μmol, 34% isolated yield). The only other spectroscopically observable organometallic species present was the precursor **3.1b** such that isolated yields approximate to % conversion. IR (CH_2Cl_2, cm^{-1}): 2051 w $\nu_{C\equiv C}$, 1985 vs ν_{CO}, 1895 vs ν_{CO}. ^{1}H NMR (400 MHz, $CDCl_3$, 25 °C, δ): 5.90 [s, 2 H, pzCH], 5.73 [s, 1 H, pzCH], 2.57 [s, 6 H, $pzCH_3$], 2.36 [s, 9 H, $pzCH_3$], 2.31 [s, 3 H, $pzCH_3$], 0.17 [s, 9 H, $SiCH_3$]. ^{13}C{^{1}H} NMR (101 MHz, $CDCl_3$, 25 °C, δ): 255.6 [Cα], 227.6 [CO], 151.6 151.3 [C^5(pz)], 145.2 144.5 [C^3(pz)], 113.5 [Cβ], 106.44 106.42 [overlapping singlets, C^4(pz)], 75.2 [Cγ], 15.8 14.7 12.8 [$pzCH_3$], –0.2 [$SiCH_3$]. Data correspond to those previously published.[13]

Synthesis of $[W(SCPPh_3)(CO)_2(Tp^*)]PF_6{\cdot}2(C_4H_4O)$ (6.8).

A sample of $[W(CPPh_3)(CO)_2(Tp^*)]PF_6$ (202 mg, 0.211 mmol) and excess elemental sulfur in THF (10 mL) were heated at reflux over 4 hours. The initially pink solution darkened steadily to a deep purple colour, with this transformation clearly visible 2 hours into the reaction. Completion was identified *via* infra-red spectroscopic techniques such that heating was ceased and cooled to ambient temperature. Solvent was removed to give a crude purple solid. This was recrystallized from concentration of CH_2Cl_2 into toluene, resulting in a dark purple crystalline solid and a pink supernatant phase. This was collected *via* vacuum filtration, washing with toluene (4 × 10 mL) and *n*-hexane (4 × 10 mL) before drying *in vacuo* for 10 hours. This gave the title compound as a blue crystalline powder, where THF is retained in the lattice. Isolated yield [·2(THF) solvate, 162 mg, 0.144 mmol, 68% isolated yield]. Crystals suitable for single crystal x-ray diffraction were grown from the slow evaporation of a CH_2Cl_2 solution of title compound layered with toluene, left at 5 °C overnight. IR (CH_2Cl_2, cm^{-1}): 2006 vs ν_{CO}, 1919 vs ν_{CO}. IR (ATR, cm^{-1}): 2574 w ν_{BH}, 1992 vs ν_{CO}, 1908 vs ν_{CO}, 839 vs ν_{PF6}. UV-Vis[$2.420(2)\times10^{-5}$ $molL^{-1}$, nm(ϵ, $LMol^{-1}cm^{-1}$), CH_2Cl_2]: λ_{max} = 269 (21820), 562 sh (15760), 627 (2222). ^{1}H NMR (400 MHz, CD_2Cl_2, 25 ºC, δ): 7.89 [m, PPh], 7.76 [m, PPh], 5.99 [s, pzCH], 3.68 [m, 4H, THF], 2.45 [s, 6H, $pzCH_3$], 2.36 [s, 3H, $pzCH_3$], 2.30 [s, 3H, $pzCH_3$], 2.20 [s, 6H, $pzCH_3$], 1.82 [m, 4H, THF]. ^{13}C{^{1}H} NMR (151 MHz, CD_2Cl_2, 25ºC, δ): 223.4 [d, $^3J_{CP}$ = 7 Hz, $^1J_{CW}$ = 145 Hz, CO], 220.7 [d, $^1J_{CP}$ = 54 Hz, $^1J_{CW}$ = 46 Hz, W–$CSPPh_3$], 153.9 152.8 [C^5(pz)], 147.4 146.5 [C^3(pz)], 136.3 [d, $^4J_{CP}$ = 3 Hz, $C^4(C_6H_5)$], 134.8 [d, $^2J_{CP}$ = 11 Hz, $C^{2,6}(C_6H_5)$], 131.0 [d, $^3J_{CP}$ = 13 Hz, $C^{3,5}(C_6H_5)$], 119.2 [d, $^1J_{CP}$ = 91 Hz, $C^1(C_6H_5)$], 109.3 108.3 [C^4(pz)], 68.3 [THF], 26.2 [THF], 16.4 14.7 13.5 12.9 [$pzCH_3$]. ^{31}P{^{1}H} NMR (162 MHz, $CDCl_3$, 25 ºC, δ): 26.84 [s, $^2J_{PW}$ = 91 Hz], –144.9 [sept, $^1J_{PF}$ = 706 Hz, PF_6]. MS (ESI, *m/z*): Found: 843.2034. Calcd for $C_{36}H_{37}{}^{11}BN_6O_2P^{32}S^{184}W$ $[M]^+$: 843.20332. Anal. Found: C, 41.66; H, 3.829; N, 7.43; S, 6.15%. Calcd for $C_{36}H_{37}BF_6N_6O_2P_2SW$ [M–2(OC_4H_8)]: C, 43.75; H, 3.77; N, 8.50; S, 2.85%. Closest match for elemental analysis given multiple submissions. *Crystal data for* $C_{36}H_{37}BN_6O_2PSW{\cdot}PF_6{\cdot}C_7H_8$, M = 1080.46, monoclinic, $I2/a$, a = 25.2847 (5) Å, b =

13.3933 (3) Å, c = 28.4487 (5) Å, β = 92.090 (2)°, V = 9627.6 (3) Å^3, Z = 8, ρ_{calc} = 1.491 Mgm^{-3}, μ(Cu $K\alpha$) = 6.03 mm^{-1}, T = 150(0) K, plate, 0.30 × 0.10 × 0.07 mm {clear dark blue}, 8711 independent measured reflections (θ = 73.3), R_1 = 0.064, wR_2 = 0.173 for 7942 reflections [$I > 2\sigma(I)$], 596 parameters, 0 restraints. CDCC 2180154.

Synthesis of [Mo(CPPh$_3$)(CO)$_2$(Tp*)]PF$_6$ (6.9).

Samples of [Mo(≡CBr)(CO)$_2$(Tp*)] (0.999 g, 1.85 mmol), PPh$_3$ (0.537 g, 2.05 mmol) and NaPF$_6$ (0.360 g, 2.14 mmol) were heated at reflux in THF for 16 hours. The initially yellow solution darkened quickly to an orange colour, with this transformation clearly visible 1 hour into the reaction. The resulting red/pink mixture was cooled and solvent was removed *via* rotary evaporatory to give a crude orange residue. The residue was purified by flash column chromatography {silica gel, N_2, CH_2Cl_2/THF gradient elution} where a bright pink band was eluted in 2% THF/CH_2Cl_2. Concentration of this pink band by rotary evaporation resulted in a pink foam which could be liberated by sonication with *n*-pentane. The crystalline solid, which was collected *via* vacuum filtration, washing with *n*-pentane (3 × 10 mL) before drying in vacuo for 16 hours. The title compound was obtained as a pink crystalline powder. Isolated yield [1.260 g, 1.450 mmol, 78% isolated yield]. Crystals suitable for single crystal x-ray diffraction were grown from the liquid-liquid diffusion of *n*-hexane into a THF solution of compound at ambient temperature inside an argon glovebox for two weeks. IR (CH_2Cl_2, cm^{-1}): 2039 vs ν_{CO}, 1965 vs ν_{CO}. IR (ATR, cm^{-1}): 2561 w ν_{BH}, 2026 vs ν_{CO}, 1944 vs ν_{CO}, 832 vs ν_{PF6}. UV-Vis [2.851(3)×10^{-4} molL^{-1}, nm(ϵ), CH_2Cl_2]: 267 (25820), λ_{MAX} 525 (379). ^{1}H NMR (400 MHz, $CDCl_3$, 25 °C, δ): 7.86 [m, 3H, PPh], 7.71 [m, 12H, PPh], 5.92 [s, 2H, pzCH], 5.78 [s, 1H, pzCH], 2.42 [s, 6H, pzCH_3], 2.32 [s, 3H, pzCH_3], 2.28 [s, 3H, pzCH_3], 2.00 [s, 6H, pzCH_3]. ^{13}C{^{1}H} NMR (176 MHz, $CDCl_3$, 25°C, δ): 251.0 [d, $^1J_{CP}$ = 21 Hz, Mo(≡CP)], 225.5 [d, $^2J_{CP}$ = 4 Hz, CO], 152.0 150.7 [C^5(pz)], 146.8 146.3 [C^3(pz)], 135.5 [d, $^4J_{CP}$ = 3 Hz, C^4(C_6H_5)], 133.7 [d, $^2J_{CP}$ = 11 Hz, C^{2,6}(C_6H_5)], 135.5 [d, $^3J_{CP}$ = 14 Hz, C^{3,5}(C_6H_5)], 119.9 [d, $^1J_{CP}$ = 90 Hz, C^1(C_6H_5)], 107.8 107.4 [C^4(pz)], 16.1 14.9 13.0 12.9 [pzCH_3]. ^{31}P{^{1}H} NMR (162 MHz, $CDCl_3$, 25 °C, δ): –0.88 [s, PPh_3], –144.4 [sept, $^1J_{PF}$ = 706 Hz, PF_6]. MS (ESI, m/z): Found: 725.1859. Calcd for $C_{36}H_{36}{}^{11}B^{98}MoN_6O_2P$ [M]$^+$: 725.18573. Anal. Found: C, 49.79; H, 4.37; N, 9.68%. Calcd for $C_{36}H_{37}BF_6MoN_6O_2P_2$: C, 49.79; H, 4.29; N, 9.68%. *Crystal data for* $C_{36}H_{37}BMoN_6O_2P{\cdot}F_6P{\cdot}C_4H_8O$, M = 940.51, monoclinic, $P2_1/n$, a = 9.2673 (1) Å, b = 18.2717 (2) Å, c = 25.4905 (2) Å, β = 91.331 (1)°, V = 4315.12 (7) Å^3, Z = 4, ρ_{calc} = 1.448 Mgm^{-3}, μ(Cu $K\alpha$) = 3.08 mm^{-1}, T = 150(0) K, needle, 0.28 × 0.11 × 0.04 mm {clear light

pink}, 8599 independent measured reflections (θ = 73.9), R_1 = 0.031, wR_2 = 0.081 for 7762 reflections [$I > 2\sigma(I)$], 542 parameters, 261 restraints. CDCC 2180156.

Synthesis of [Mo(η²-SCPPh₃)(CO)₂(Tp*)]PF₆ (6.10).

A sample of [Mo(CPPh$_3$)(CO)$_2$(Tp*)]PF$_6$ (**6.9**; 0.100 g, 0.115 mmol) and elemental sulfur (0.037 g, 1.2 mmol, 10/8 equiv. S_8) were heated in THF at 60 °C over 4 hours. The initially pink solution darkened quickly to a deep blue colour, with this transformation clearly visible 30 minutes into the reaction. The reaction mixture was cooled and solvent was removed *via* rotary evaporation to give a crude blue residue. The residue was dissolved in minimal $CHCl_3$ (~2 mL), prior to precipitation from Et_2O assisted by sonication. Collection of the dark solid resulted in a dark filtrate prior to washing with minimal cold $CHCl_3$ (0.5 mL). A wash with cold 40% $CHCl_3$/Et_2O provided a bright blue solid which was further washed with Et_2O (2 × 10 mL) before drying *in vacuo* for 16 hours to give the title compound as a blue powder (0.031 g, 0.034 mmol, 30% isolated yield). IR (CH_2Cl_2, cm^{-1}): 2016 vs ν_{CO}, 1936 vs ν_{CO}. IR (ATR, cm^{-1}): 2569 w ν_{BH}, 2002 vs ν_{CO}, 1926 vs ν_{CO}, 845 vs ν_{PF6}. UV-Vis[2.731(3)×10^{-5} $molL^{-1}$, nm(ϵ, $Lmol^{-1}cm^{-1}$), CH_2Cl_2]: λ_{max} = 261 (17160), 630 (1550). ^{1}H NMR (600 MHz, CD_2Cl_2, 25 ºC, δ): 7.95 [m, 3H, PPh], 7.87 [m, 6H, PPh], 7.77 [m, 6H, PPh], 5.95 [s, 1H, pzCH], 5.92 [s, 2H, pzCH], 2.42 [s, 6H, pzCH_3], 2.38 [s, 3H, pzCH_3], 2.25 [s, 3H, pzCH_3], 2.12 [s, 6H, pzCH_3]. ^{13}C{^{1}H} NMR (151 MHz, CD_2Cl_2, 25ºC, δ): 235.5 [d, $^1J_{CP}$ = 45 Hz, Mo–SCPPh$_3$], 227.0 [d, $^3J_{CP}$ = 7 Hz, CO], 153.1 151.9 [C^5(pz)], 147.3 146.4 [C^3(pz)], 136.4 [d, $^4J_{CP}$ = 3 Hz, C^4(C_6H_5)], 134.7 [d, $^2J_{CP}$ = 10 Hz, C^{2,6}(C_6H_5)], 131.0 [d, $^3J_{CP}$ = 14 Hz, C^{3,5}(C_6H_5)], 118.6 [d, $^1J_{CP}$ = 90 Hz, C^1(C_6H_5)], 108.6 107.8 [C^4(pz)], 15.8 14.3 13.4 12.8 [pzCH_3]. ^{31}P{^{1}H} NMR (162 MHz, CD_2Cl_2, 25 ºC, δ): 20.95 [s, PPh_3], –144.5 [sept, $^1J_{PF}$ = 706 Hz, PF_6]. MS (ESI, *m/z*): Found: 757.1589. Calcd for $C_{36}H_{37}{}^{11}B^{98}MoN_6O_2P^{32}S$ [M]$^+$: 757.15780.

Synthesis of [W(η²-SCPMePh₂)(CO)₂(Tp*)]PF₆ (6.11).

A sample of [W(CPMePh$_2$)(CO)$_2$(Tp*)]PF$_6$ (0.101 g, 0.113 mmol) and elemental sulfur (S_8; 0.018 g, 0.070 mmol) were heated at reflux in THF over 6 hours. The initially pink solution darkened quickly to a deep blue colour, with this transformation clearly visible 2 hours into the reaction. The reaction mixture was cooled and solvent was removed via reduced pressure before being dissolved in CH_2Cl_2 (~2 mL) and precipitated a dark blue solid with Et_2O (20 mL) in addition to a pale pink supernatant phase. The deep blye solid was collected *via* vacuum filtration, washing with Et_2O (2 × 10 mL) and *n*-pentane (3 × 10 mL) before drying *in vacuo* for 16 hours. The title compound was obtainined as a blue crystalline powder (0.080 g, 0.086 mmol, 76% isolated yield). Crystals suitable for single crystal X-ray diffraction were grown from the liquid-liquid diffusion of Et_2O layered on a MeCN solution of compound at –20 °C under an argon atmosphere over a

week. IR (CH_2Cl_2, cm^{-1}): 1998 vs ν_{CO}, 1914 vs ν_{CO}. IR (ATR, cm^{-1}): 2563 w ν_{BH}, 1998 vs ν_{CO}, 1902 vs ν_{CO}, 836 vs ν_{PF6}. UV-Vis[$2.610(3)\times10^{-5}$ $molL^{-1}$, nm(ϵ, $Lmol^{-1}cm^{-1}$), CH_2Cl_2]: λ_{max} 266 sh (19520, 569 (1517), 622 (1520). ^{1}H NMR (700 MHz, CD_2Cl_2, 25 ºC, δ): 7.89 [m, 6H, PPh], 7.73 [m, 4H, PPh], 6.02 [s, 1H, pzCH], 5.95 [s, 2H, pzCH], 2.85 [d, $^2J_{HP}$ = 13 Hz, 3H, PCH_3], 2.44 [overlapping s, 3H, $pzCH_3$], 2.43 [overlapping s, 6H, $pzCH_3$], 2.37 [s, 3H, $pzCH_3$], 1.96 [s, 6H, $pzCH_3$]. $^{13}C\{^1H\}$ NMR (151 MHz, CD_2Cl_2, 25ºC, δj): 223.4 [d, $^3J_{CP}$ = 7 Hz, $^1J_{CW}$ = 145c Hz, CO], 219.0 [d, $^1J_{CP}$ = 56 Hz, $^1J_{CW}$ not detected, W–CSPMePh$_2$], 153.9 152.7 [C^5(pz)], 147.3 146.3 [C^3(pz)], 135.9 [d, $^4J_{CP}$ = 4 Hz, $C^4(C_6H_5)$], 133.1 [d, $^2J_{CP}$ = 10 Hz, $C^{2,6}(C_6H_5)$], 130.8 [d, $^3J_{CP}$ = 13 Hz, $C^{3,5}(C_6H_5)$], 119.6 [d, $^1J_{CP}$ = 90 Hz, $C^1(C_6H_5)$], 109.1 108.2 [C^4(pz)], 16.4 14.0 13.4 12.7 [$pzCH_3$], 9.9 [d, $^1J_{CP}$ = 59 Hz, PCH_3]. $^{31}P\{^1H\}$ NMR (283 MHz, CD_2Cl_2, 25 ºC, δ): 26.39 [s, $^2J_{PW}$ = 21 Hz], –144.5 [sept, $^1J_{PF}$ = 706 Hz, PF_6]. MS (ESI, *m/z*): Found: 781.1900. Calcd for $C_{31}H_{35}{}^{11}BN_6O_2PS^{184}W$ $[M]^+$: 781.1882. Anal. Found: C, 40.20; H, 3.769; N, 9.07; S, 20.843%. Calcd for $C_{31}H_{35}BF_6N_6O_2P_2SW$: C, 40.20; H, 3.81; N, 9.07; S, 3.46%. *Crystal data for* $C_{31}H_{35}BN_6O_2PSW{\cdot}PF_6{\cdot}2(C_2H_3N)$, M = 1008.42, monoclinic, $P2_1/c$, a = 14.1710 (2) Å, b = 13.2958 (1) Å, c = 22.8330 (3) Å, β = 103.452 (1)º, V = 4184.05 (9) $Å^3$, Z = 4, ρ_{calc} = 1.601 Mgm^{-3}, μ(Cu $K\alpha$) = 6.91 mm^{-1}, T = 150(0) K, plate, 0.14 × 0.09 × 0.03 mm {clear dark blue}, 7935 independent measured reflections (θ = 73.6), R_1 = 0.027, wR_2 = 0.065 for 7020 reflections [$I > 2\sigma(I)$], 514 parameters, 0 restraints. CDCC 2180155.

Synthesis of [W(η^2-SCPMe$_2$Ph)(CO)$_2$(Tp*)]PF$_6$ (6.12).

A sample of [W(CPMe$_2$Ph)(CO)$_2$(Tp*)].PF$_6$ (0.099 g, 0.119 mmol) and elemental sulfur (S_8; 0.038 g, 0.148 mmol) were heated at reflux in THF over 6 hours. The initially peach-coloured solution darkened quickly to a deep blue colour by 1 hour and transitioned to the final indigo colour by 2 hours. The reaction mixture was cooled and solvent removed under reduced pressure before dissolving in minimal CH_2Cl_2 (~2 mL). Et_2O (20 mL) was added to precipitate an indigo coloured solid and a pale orange supernatant phase; vacuum filtration acquired the solid material that was subsequently washed with Et_2O (3 × 10 mL) and *n*-pentane (3 × 5 mL) before drying *in vacuo* for 16 hours. The title compound was obtained as an indigo crystalline powder (0.090 g, 0.104 mmol, 87% isolated yield). IR (CH_2Cl_2, cm^{-1}): 1999 vs ν_{CO}, 1912 vs ν_{CO}. IR (ATR, cm^{-1}): 2557 w ν_{BH}, 2001 vs ν_{CO}, 1884 vs ν_{CO}, 836 vs ν_{PF6}. UV-Vis[$2.498(3)\times10^{-5}$ $molL^{-1}$, nm(ϵ, $Lmol^{-1}cm^{-1}$), CH_2Cl_2]: λ_{max} 267 (18520), 552 (1531), 627 (1324). ^{1}H NMR (600 MHz, CD_2Cl_2, 25 ºC, δ): 7.95 [dd, J_{HH} = 13, 8 Hz, 2H, PPh], 7.85 [t, J_{HH} = 8 Hz, 1H, PPh], 7.74 [m, 2H, PPh], 6.01 [s, 1H, pzCH], 5.93 [s, 2H, pzCH], 2.55 [d, $^2J_{HP}$ = 13 Hz, 6H, PCH_3], 2.45 [s, 3H, $pzCH_3$], 2.42 [s, 6H, $pzCH_3$], 2.37 [s,

3H, pzCH$_3$], 1.94 [s, 6H, pzCH$_3$]. ^{13}C{^{1}H} NMR (151 MHz, CD_2Cl_2, 25ºC, δ): 223.5 [d, $^3J_{CP}$ = 6 Hz, $^1J_{CW}$ = 144 Hz, CO], 222.3 [d, $^1J_{CP}$ = 56 Hz, $^1J_{CP}$ = 55 Hz, W(S*C*PMe$_2$Ph)], 154.0 153.0 [C^5(pz)], 147.4 146.3 [C^3(pz)], 136.0 [d, $^4J_{CP}$ = 3 Hz, C^4(C$_6$H$_5$)], 131.9 [d, $^2J_{CP}$ = 10 Hz, C^{2,6}(C$_6$H$_5$)], 130.8 [d, $^3J_{CP}$ = 13 Hz, C^{3,5}(C$_6$H$_5$)], 119.5 [d, $^1J_{CP}$ = 88 Hz, C^1(C$_6$H$_5$)], 109.1 108.3 [C^4(pz)], 16.6 14.2 13.6 12.8 [pzCH$_3$], 9.3 [d, $^1J_{CP}$ = 59 Hz, PCH$_3$]. ^{31}P{^{1}H} NMR (162 MHz, CD_3CN, 25 ºC, δ): 30.40 [s, $^2J_{PW}$ = 20 Hz], –144.6 [sept, $^1J_{PF}$ = 706 Hz, PF_6]. MS (ESI, *m/z*): Found: 719.1733. Calcd for $C_{26}H_{33}{}^{11}BN_6O_2PS^{184}W$ [M]$^+$: 719.1726. Anal. Found: C, 36.08; H, 3.825; N, 9.74; S, 3.989%. Calcd for $C_{26}H_{33}BF_6N_6O_2P_2SW$: C, 36.13; H, 3.85; N, 9.72; S, 3.71%.

Synthesis of [W(η^2-SCPCy$_3$)(CO)$_2$(Tp*)]PF$_6$ (6.13).

A sample of [W(≡CPCy$_3$)(CO)$_2$(Tp*)]PF$_6$ (0.200 g, 0.205 mmol) and elemental sulfur (S_8, 0.070 g, 0.272 mmol) were heated at reflux in THF over 16 hours. The initially orange suspension changed slowly due to poor solubility, although a deep blue colour emerged overnight. TLC identified the prolonged heated resulted in several unidentified sulfur decomposition species, hence the reaction mixture was purified by short column chromatography {silica gel, N_2, CH_2Cl_2/THF gradient elution}. Neat CH_2Cl_2 elution resulted in a black, pungent fraction where species could not be identified by spectroscopic analysis, whereas 2% THF/CH_2Cl_2 eluted a deep blue band. This blue band was evaporated to dryness with a rotary evaporator and dissolved minimal $CHCl_3$ (~2 mL) before precipitation of a dark blue solid with Et_2O (20 mL). The ensuing solid was collected *via* vacuum filtration, washing with cold 50% $CHCl_3$/Et_2O until washing was clear and somewhat pale blue (yield sacrificed for purity) and Et_2O (3 × 10 mL) before drying *in vacuo* for 16 hours. The title compound was obtained as a blue crystalline powder, although repeatably contained parent phosphoniocarbyne that resisted removal during purification without decomposition of the title species. Isolated yield (0.166 g, 0.165 mmol, 80% yield at ~90% purity]. Crystals suitable for single-crystal x-ray diffraction were grown from the slow evaporation of a CH_2Cl_2 solution of title compound layered with toluene, left at 5 °C overnight. Crystals formed, however, no sufficient structure could be analysed or extracted from data given multiple compounds per unit cell of *P*1 symmetry in addition to weak diffraction. Synchrotron radiation source did not improve the collected dataset. IR (CH_2Cl_2, cm^{-1}): 1996 vs ν_{CO}, 1911 vs ν_{CO}. IR (ATR, cm^{-1}): 2571 w ν_{BH}, 1981 vs ν_{CO}, 1894 vs ν_{CO}, 840 vs ν_{PF6}. UV-Vis [3.922(4)×10^{-5} molL^{-1}, nm(ϵ), CH_2Cl_2]: 255 (18440), 281 sh (13220), λ_{MAX} 627 (1175). Spectra contain traces of [W(CPCy$_3$)(CO)$_2$(Tp*)].PF$_6$ that were unable to be removed without decomposing the title species, these are denoted in grey on figures, but not listed herein. ^{1}H NMR (400 MHz, CD_2Cl_2, 25 ºC, δ): 6.09 [s, 1H, pzCH], 6.02 [s, 2H, pzCH], 2.51 [s, 3H, pzCH$_3$], 2.49 [s, 6H, pzCH$_3$], 2.43 [s, 3H,

$pzCH_3$], 2.25 [s, 6H, $pzCH_3$], 2.04 [br.m, 10H, PCH_2], 1.86 [m, 10H, PCH_2], 1.44 [m, 10H, PCH_2]. Cyclohexyl 1H resonances overlap with that of the impurity and therefore were not able to be assigned for certain even with 2D correlation spectra. $^{13}C\{^1H\}$ NMR (151 MHz, CD_2Cl_2, 25ºC, δ): 226.8 [d, $^3J_{CP}$ = 4; $^1J_{CW}$ = 149 Hz, CO], 222.7 [d, $^1J_{CP}$ = 30; $^1J_{CW}$ = 45 Hz, W–$SCPCy_3$], 153.5 152.4 [C^5(pz)], 147.2 146.2 [C^3(pz)], 109.3 108.2 [C^4(pz)], 35.3 [d, $^1J_{CP}$ = 39 Hz, $C^1(C_6H_{10})$], 28.3 [d, $^3J_{CP}$ = 4 Hz, $C^{3,5}(C_6H_{10})$], 27.2 [d, $^2J_{CP}$ = 12 Hz, $C^{2,6}(C_6H_{10})$], 25.8 [$C^4(C_6H_{10})$], 16.1 14.8 13.4 12.8 [$pzCH_3$]. $^{31}P\{^1H\}$ NMR (162 MHz, CD_2Cl_2, 25 ºC, δ): 41.95 [s, $^1J_{PW}$ too small for detection], –144. [sept, $^1J_{PF}$ = 706 Hz, PF_6]. MS (ESI, *m/z*): Found: 861.3465. Calcd for $C_{36}H_{55}{}^{11}BN_6O_2P^{32}S^{184}W$ $[M]^+$: 861.34417.

Synthesis of [W(η²-SCAsMePh₂)(CO)₂(Tp*)]OTf (6.14).

A sample of [W(CAsMePh₂)(CO)₂(Tp*)]OTf (0.090 g, 0.096 mmol) and elemental sulfur (0.040 g, 1.25 mmol S) were heated at reflux in THF over 16 hours. The initially orange solution darkened slowly, eventually to give a dark purple/black coloured solution overnight. TLC monitoring identified that much of the reaction mixture reacts to a series of dark coloured sulfur decomposition species that were unable to be identified by ^1H NMR spectroscopy, whereas a reaction overnight at least ensured complete consumption of the arsoniocarbyne precursor. The mixture was concentrated under reduced pressure (~ 2 mL) before Et_2O was injected to precipitate a dark solid from a black supernatant phase. The supernatant phase was removed *via* filter cannula and thoroughly washed with Et_2O (3 × 15 mL). The remaining dark solid was dried *in vacuo* before being redissolved in minimal CH_2Cl_2 (~2 mL). Precipitation from CH_2Cl_2 with Et_2O (20 mL) resulted in a purple solid being formed that could be liberated from the flask periphery aided with by ultrasonication. The solid was collected *via* vacuum filtration, washing with cold 50% $CHCl_3/Et_2O$ until washings were colourless, before Et_2O (2 × 10 mL) and drying *in vacuo* for 16 hours. This afforded the title compound as a deep purple solid (0.012 g, 0.012 mmol, 13% isolated yield), although some impurities remain; the main being [W(≡CAsMePh₂)(CO)₂(Tp*)] although this may be present as a consequence of sulfur loss, suspected to occur. Further attempts at purification resulted in the decomposition of the already diminished, minimal yield. Sample used for spectroscopic analysis contains [W(≡CAsMePh₂)(CO)₂(Tp*)].OTf that resisted purification and is present as a minor impurity in spectra according to literature precedent. IR (CH_2Cl_2, cm^{-1}): 1995 vs ν_{CO}, 1909 vs ν_{CO}. IR (ATR, cm^{-1}): 2561 w ν_{BH}, 1987 vs ν_{CO}, 1897 vs ν_{CO}, 863 vs ν_{OTf}. ^1H NMR (800 MHz, CD_2Cl_2, 25 ºC, δ): 7.84 [m, 6H, $AsPh_2$], 7.74 [m, 4H, $AsPh_2$], 6.00 [s, 1H, pzCH], 5.95 [s, 2H, pzCH], 2.84 [s, 3H, $AsCH_3$], 2.42 [s, 6H, $pzCH_3$], 2.36 [s, 6H, $pzCH_3$], 2.04 [s, 6H, $pzCH_3$]. $^{13}C\{^1H\}$ NMR (200 MHz, CD_2Cl_2, 25ºC, δ): 226.0 [$^1J_{CW}$ = 41 Hz, W(SCAsMePh₂)], 223.4

[$^{1}J_{CW}$ = 145 Hz, CO], 153.8 152.7 [C^{5}(pz)], 147.2 146.2 [C^{3}(pz)], 135.1 [$C^{4}(C_6H_5)$], 132.4 [$C^{2,6}(C_6H_5)$], 131.4 [$C^{3,5}(C_6H_5)$], 128.9 [$C^{1}(C_6H_5)$], 108.9 108.1 [C^{4}(pz)], 16.2 14.1 13.4 12.7 [pzCH_3], 8.8 [AsCH_3]. MS (ESI, *m/z*): Found: 825.1347. Calcd for $C_{31}H_{35}{}^{11}BN_6O_2{}^{75}As{}^{32}S{}^{184}W$ $[M]^+$: 825.1361. Insufficient material was obtained for the acquisition of elemental microanalytical data.

General Procedure – Suzuki-Miyaura Carbyne Cross-Coupling

[M(≡CBr)$(CO)_2$(Tp*)] (1 equiv.), boronic acid (1.2 equiv.), base (2.2 equiv.) and catalyst (0–10 mol% Pd and/or Au) were suspended in solvent (5 mL). The mixture was heated at 80 °C for 16 hours. After completion, mixture were evaporated *via* rotary evaporation and purified by flash column chromatography {silica gel, N_2, CH_2Cl_2/petroleum ether gradient} and eluates recrystallised accordingly. Microcrystalline powders were collected via vacuum filtration and dried in vacuo for 16 hours. Note: for reactions of tabulated data, each reaction was performed in duplicate and an average yield taken from isolated yields. A percentage difference of +10% between duplicates deemed the reaction as invalid and was repeated until this criterion was satisfied.

Synthesis of [W(≡C–C_6H_4OMe–4)$(CO)_2$(Tp*)] (6.15).

As per the general conditions, [W(≡CBr)$(CO)_2$(Tp*)] (0.100 g, 0.159 mmol), 4-methoxyphenylboronic acid (0.031 g, 0.189 mmol), Cs_2CO_3 (0.104 g, 0.319 mmol) are suspended in toluene (5 mL) with [$PdCl_2(PPh_3)_2$] (0.006 g, 0.008 mmol, 5 mol%) and [AuCl·SMe_2] (0.002 g, 0.008 mmol, 5 mol%) add as co-catalysts. The mixture is heated at 80 °C for 16 hours beginning as yellow but changing to orange within 10 minutes. The next day, an orange solution was noted absent of palladium(0)/gold(0) deposition. Solvent was removed to give an orange solid that could be purified by flash chromatography {silica gel, N_2, CH_2Cl_2/petroleum spirit} such that 50% CH_2Cl_2/petroleum spirit gave an orange eluate that could be evaporated to give a orange residue. The residue could be recrystallised from CH_2Cl_2 and *n*-hexane to give an orange powder that was collected *via* vacuum filtration and washed with *n*-hexane (2 × 5 mL) and *n*-pentane (5 mL) before drying *in vacuo* for 16 hours to give the title compound as an orange microcrystalline solid (0.096 g, 0.146 mmol, 92% isolated yield). IR (CH_2Cl_2, cm^{-1}): 1969 vs ν_{CO}, 1877 vs ν_{CO}. IR (ATR, cm^{-1}): 2550, w ν_{BH}, 1956 vs ν_{CO}, 1860 vs ν_{CO}. ^{1}H NMR (600 MHz, $CDCl_3$, 25 ºC, δ): 7.42 [d, $^{1}J_{HH}$ = 9 Hz, 2H, PhH], 6.80 [d, $^{1}J_{HH}$ = 9 Hz, 2H, PhH], 5.88 [s, 2H, pzCH], 5.78 [s, 1H, pzCH], 3.81 [s, 3H, OCH_3], 2.52 [s, 6H, pzCH_3], 2.46 [s, 3H, pzCH_3], 2.37 [s, 6H, pzCH_3], 2.34 [s, 3H, pzCH_3]. $^{13}C\{^{1}H\}$ NMR (151 MHz, $CDCl_3$, 25ºC, δ): 278.9 [$^{1}J_{CP}$ = 187 Hz, W≡C], 224.1 [$^{1}J_{CP}$ = 168 Hz, CO], 159.1 [$C^{4}(C_6H_4)$], 152.4 152.1 [C^{5}(pz)], 145.1 144.5 [C^{3}(pz)], 144.1 [$^{2}J_{CW}$ = 43 Hz, $C^{1}(C_6H_4)$], 131.0 [$C^{2,6}(C_6H_4)$], 113.6 [$C^{3,5}(C_6H_4)$], 106.7 106.5 [C^{4}(pz)], 55.4 [OCH_3], 16.7 15.4 12.8 12.7 [pzCH_3]. MS

(ESI, *m/z*): Found: 657.19798. Calcd for $C_{25}H_{30}{}^{11}BN_6O_3{}^{184}W$ $[M+H]^+$: 657.19873. Anal. %. Found: C, 45.80; H, 4.386; N, 12.64%. Calcd for $C_{25}H_{29}BN_6O_3W$: C, 45.76; H, 4.45; N, 12.81%.

Synthesis of [W(≡C–C_6H_5)$(CO)_2$(Tp*)] (6.16).

As per the general conditions, [W(≡CBr)$(CO)_2$(Tp*)] (0.100 g, 0.159 mmol), phenylboronic acid (0.023 g, 0.189 mmol), Cs_2CO_3 (0.104 g, 0.319 mmol) are suspended in toluene (5 mL) with [$PdCl_2(PPh_3)_2$] (0.006 g, 0.008 mmol, 5 mol%) and [AuCl(PPh_3)] (0.004 g, 0.008 mmol, 5 mol%) add as co-catalysts. The mixture is heated at 80 °C for 16 hours beginning as yellow but changing to orange within 10 minutes. The next day, an orange solution was noted absent of palladium(0)/gold(0) deposition. Solvent was removed to give an orange solid that could be purified by flash chromatography {silica gel, N_2, CH_2Cl_2/petroleum spirit} such that 50% CH_2Cl_2/petroleum spirit gave an orange eluate that could be evaporated to give a orange residue. The residue could be recrystallised from CH_2Cl_2 and n-hexane to give an orange powder that was collected via vacuum filtration and washed with *n*-hexane (2 × 5 mL) and *n*-pentane (5 mL) before drying in vacuo for 16 hours to give the title compound as an orange microcrystalline solid (0.088 g, 0.141 mmol, 88% isolated yield). Spectroscopic data were consistent with literature precedent.[310]

Synthesis of [W(≡C–C_6H_4Ac-4)$(CO)_2$(Tp*)] (6.17).

As per the general conditions, [W(≡CBr$(CO)_2$(Tp*)] (0.100 g, 0.159 mmol), 4-acetylphenylboronic acid (0.031 g, 0.189 mmol), Cs_2CO_3 (0.104 g, 0.319 mmol) were suspended in toluene (5 mL) with [$PdCl_2(PPh_3)_2$] (0.006 g, 0.008 mmol, 5mol %) and [AuCl(PPh_3)] (0.004 g, 0.008 mmol, 5mol%) add as co-catalysts. The mixture is heated at 80 °C for 16 hours beginning as yellow but changing to orange within 3 minutes and black/brown in 10 minutes. The next day, palladium(0) was visible accompanied by a gold mirror. Solvent was removed to give a brown residue that could be purified by flash chromatography {silica gel, N_2, CH_2Cl_2/petroleum spirit} such that 50% CH_2Cl_2/petroleum spirit gave a purple eluate that could be evaporated to give a purple residue. The species resisted recrystallisation and was dried under high vacuum for 16 hours and the ensuing pink solid measured as the title compound (0.064 g, 0.096 mmol, 60% yield). IR (CH_2Cl_2, cm^{-1}): 1976 vs ν_{CO}, 1888 vs ν_{CO}. IR (ATR, cm^{-1}): 2547 w ν_{BH}, 1967 vs ν_{CO}, 1870 vs ν_{CO}, 1683 vs ν_{CO}. ^{1}H NMR (400 MHz, $CDCl_3$, 25 ºC, δ): 7.88 [d, $^1J_{HH}$ = 9 Hz, PhH], 7.47 [d, $^1J_{HH}$ = 8 Hz, PhH], 5.91 [s, 2H, pzCH], 5.80 [s, 1H, pzCH], 2.57 [s, 3H, COMe], 2.47 [s, 6H, $pzCH_3$], 2.45 [s, 3H, $pzCH_3$], 2.39 [s, 6H, $pzCH_3$], 2.35 [s, 3H, $pzCH_3$]. $^{13}C\{^1H\}$ NMR (151 MHz, $CDCl_3$, 25ºC,

δ): 275.5 [$^{1}J_{CW}$ = 188 Hz, W≡C], 224.1 [$^{1}J_{CW}$ = 164 Hz, CO], 197.6 [C(O)Me], 154.1 [$^{2}J_{CW}$ = 43 Hz, $C^{1}(C_6H_4)$], 152.6 152.0 [C^{5}(pz)], 145.4 144.8 [C^{3}(pz)], 134.9 [$C^{4}(C_6H_4)$], 129.3 [$C^{2,6}(C_6H_4)$], 128.4 [$C^{3,5}(C_6H_4)$], 106.9 106.7 [C^{4}(pz)], 26.8 [CO*C*H$_3$], 16.7 15.4 12.81 12.79 [pzCH_3]. MS (ESI, *m/z*): Found: 669.1979. Calcd for $C_{26}H_{30}{}^{11}BN_6O_3{}^{184}W$ $[M+H]^+$: 669.1982. Anal. Found: C, 46.78; H, 4.258; N, 12.46%. Calcd for $C_{26}H_{29}BN_6O_3W$: C, 46.73; H, 4.37; N, 12.46%.

Synthesis of [W(≡C–Fc)(CO)$_2$(Tp*)] (6.18).

As per the general conditions, [W(≡CBr(CO)$_2$(Tp*)] (0.100 g, 0.159 mmol), 4-ferrocenylboronic acid (0.044 g, 0.191 mmol), Cs_2CO_3 (0.104 g, 0.319 mmol) were suspended in toluene (5 mL) with [$PdCl_2(PPh_3)_2$] (0.006 g, 0.008 mmol, 5mol %) and [AuCl(PPh_3)] (0.004 g, 0.008 mmol, 5mol%) add as co-catalysts. The mixture is heated at 80 °C for 16 hours beginning as yellow but changing to red within 3 minutes with no further colour changes. Solvent was removed to give a red solid that could be purified by flash chromatography {silica gel, N_2, CH_2Cl_2/petroleum spirit} such that 50% CH_2Cl_2/petroleum spirit gave a red eluate that could be evaporated to give a microcrystalline red powder that was collected *via* vacuum filtration, washed with *n*-hexane (3 × 10 mL) and dried *in vacuo* for 16 hours to give the title compound (0.078 g, 0.106 mmol, 67% yield). IR (CH_2Cl_2, cm^{-1}): 1964 vs ν_{CO}, 1873 vs ν_{CO}. ^{1}H NMR (400 MHz, $CDCl_3$, 25 ºC, δ): 5.87 [s, 2H, pzCH], 5.77 [s, 1H, pzCH], 4.58 [t, $^{1}J_{HH}$ = 2 Hz, 2H, FcCH], 4.41 [s, 5H, FcCH], 4.20 [t, $^{1}J_{HH}$ = 2 Hz, 2H, FcCH], 2.62 [s, 6H, pzCH_3], 2.47 [s, 3H, pzCH_3], 2.35 [s, 6H, pzCH_3], 2.33 [s, 3H, pzCH_3]. ^{13}C{^{1}H} NMR (151 MHz, $CDCl_3$, 25ºC, δ): 280.8 [$^{1}J_{CW}$ = 189 Hz, W≡C–C_5H_4), 225.3 [$^{1}J_{CW}$ = 167 Hz, CO], 152.4 151.9 [C^{5}(pz)], 145.0 144.4 [C^{3}(pz)], 106.6 106.5 [C^{4}(pz)], 95.2 [*ipso-C*$_5$H$_4$], 70.0 69.4 68.5 [FeCH], 16.9 15.5 12.8 12.7 [pzCH_3]. MS (ESI, *m/z*): Found: 735.15444. Calcd for $C_{28}H_{32}BFeN_6O_2W$ $[M+H]^+$: 735.15371. Anal. Found: C, 45.77; H, 4.217; N, 11.65%. Calcd for $C_{28}H_{31}BFeN_6O_2W$: C, 45.81; H, 4.26; N, 11.45%. *Crystal data for* $C_{28}H_{31}BFeN_6O_2W$, M = 734.10, triclinic, $P\bar{1}$, a = 10.4904 (5) Å, b = 11.0007 (7) Å, c = 14.1803 (5) Å, α = 93.089 (4)°, β = 103.186 (4)°, γ = 116.530 (5)°, V = 1402.53 (14) Å^3, Z = 2, ρ_{calc} = 1.738 Mgm^{-3}, μ(Cu *K*α) = 11.91 mm^{-1}, T = 150(0) K, plate 0.14 × 0.08 × 0.05 mm {clear light orange}, 5131 independent measured reflections (θ = 73.4), R_1 = 0.059, wR_2 = 0.159 for 4725 reflections [$I > 2\sigma(I)$], 358 parameters, 163 restraints. CDCC 2251841.

Synthesis of [W(≡C–C$_6$H$_4$-NC$_{12}$H$_8$)(CO)$_2$(Tp*)] (6.19).

As per the general conditions, [W(≡CBr)(CO)$_2$(Tp*)] (0.100 g, 0.159 mmol), (4-(9H-carbazol-9-yl)phenyl)boronic acid (0.055 g, 0.192 mmol), Cs_2CO_3 (0.104 g, 0.319 mmol) are suspened in

toluene (5 mL) with [$PdCl_2(PPh_3)_2$] (0.006 g, 0.008 mmol, 5mol %) and [$AuCl(PPh_3)$] (0.004 g, 0.008 mmol, 5mol%) add as co-catalysts. The mixture is heated at 80 °C for 16 hours beginning as yellow but changing to orange within 3 minutes and red/pink by 10 minutes. The next day, no palladium(0) or gold mirror was visible. Solvent was removed to give a red residue that could be purified by flash chromatography {silica gel, N_2, CH_2Cl_2/petroleum spirit} such that 50% CH_2Cl_2/petroleum spirit gave a pink eluate that could be evaporated to give a pink residue. The residue could be recrystallised from CH_2Cl_2 and *n*-hexane to give a pastel pink solid that was collected *via* vacuum filtration washing with *n*-hexane (3 × 5 mL) before drying *in vacuo* for 16 hours to give the title compound as a pale pink powder (0.109 g, 0.137 mmol, 87% isolated yield). IR (CH_2Cl_2, cm^{-1}): 1974 vs ν_{CO}, 1883 vs ν_{CO}. IR (ATR, cm^{-1}): 2547 w ν_{BH}, 1966 vs ν_{CO}, 1877 vs ν_{CO}. UV-Vis [$2.460(2)\times10^{-5}$ $molL^{-1}$, nm (ϵ, $Lmol^{-1}cm^{-1}$), CH_2Cl_2]: λ_{max} = 293 (17080), 344 (13460), 510 (390). ^{1}H NMR (400 MHz, $CDCl_3$, 25 ºC, δ): 8.14 [m, 2H, carbCH], 7.65 [m, 2H, carbCH], 7.49 [m, 4H, PhCH], 7.42 [m, 2H, carbCH], 7.29 [m, 2H, carbCH], 5.93 [s, 2H, pzCH], 5.81 [s, 1H, pzCH], 2.60 [s, 6H, $pzCH_3$], 2.49 [s, 3H, $pzCH_3$], 2.40 [s, 6H, $pzCH_3$], 2.36 [s, 3H, $pzCH_3$]. $^{13}C\{^1H\}$ NMR (201 MHz, $CDCl_3$, 25ºC, δ): 276.5 [W≡C], 224.1 [$^1J_{CW}$ = 165 Hz, CO], 152.6 152.1 [C^5(pz)], 149.3 [$C^1(C_6H_4)$], 145.3 144.7 [C^3(pz)], 140.6 [$C^{1,12}$(carb)], 136.6 [$C^4(C_6H_4)$], 130.7 [$C^{2,6}(C_6H_4)$], 126.5 [$C^{3,5}(C_6H_4)$], 126.1 [$C^{3,10}$(carb)], 123.7 [$C^{6,7}$(carb)], 120.4 [$C^{5,8}$(carb)], 120.3 [$C^{4,9}$(carb)], 110.2 [$C^{2,11}$(carb)], 106.9 106.7 [C^4(pz)], 16.9 15.4 12.9 12.8 [$pzCH_3$]. MS (ESI, *m/z*): Found: 792.2451. Calcd for $C_{36}H_{35}{}^{11}BN_7O_2{}^{184}W$ $[M+H]^+$: 792.2455. Anal. Found: C, 54.62; H, 4.192; N, 12.10%. Calcd for $C_{36}H_{34}BN_7O_2W$: C, 54.64; H, 4.33; N, 12.39%.

Synthesis of [{SC_4H_2–C≡W(CO)$_2$(Tp*)}$_2$] (6.20).

As per the general conditions, [W(≡CBr(CO)$_2$(Tp*)] (0.200 g, 0.318 mmol), 2,2'-bithiophene-5,5'diboronic acid *bis*(pinacol) ester (0.080 g, 0.191 mmol), Cs_2CO_3 (0.208 g, 0.638 mmol) are suspened in toluene (5 mL) with [$PdCl_2(PPh_3)_2$] (0.011 g, 0.016 mmol, 5mol %) and [$AuCl(PPh_3)$] (0.008 g, 0.016 mmol, 5mol%) add as co-catalysts. The mixture is heated at 80 °C for 16 hours beginning as yellow but changing to vibrant orange within 3 minutes. The next day, an vibrant orange solution was recorded with limited palladium(0) or gold mirror. Solvent was removed to give an orange/red residue that could be purified by flash chromatography {silica gel, N_2, CH_2Cl_2/petroleum spirit} such that 50% CH_2Cl_2/petroleum spirit gave a bright orange eluate that could be evaporated to give an orange solid. The solid was recrystallised from CH_2Cl_2 and *n*-hexane to give a brick red solid that was collected *via* vacuum filtration washing with *n*-hexane (3 × 5 mL) before drying *in vacuo* for 16 hours to give the title compound as a brick red microcrystalline solid (0.050 g, 0.040 mmol, 25% isolated yield). IR (CH_2Cl_2, cm^{-1}): 1974 vs ν_{CO}, 1886 vs ν_{CO}. IR (ATR,

cm^{-1}): 2550 w ν_{BH}, 1961 vs ν_{CO}, 1870 vs ν_{CO}. UV-Vis [1.445(2)×10^{-5} $molL^{-1}$, nm (ϵ, $Lmol^{-1}cm^{-1}$), CH_2Cl_2]: λ_{max} = 307 sh (10650), 464 (25650), 486 sh (21360). ^{1}H NMR (400 MHz, $CDCl_3$, 25 ºC, δ): 7.05 [d, $^1J_{HH}$ = 4 Hz, 2H, thiopheneCH], 6.97 [d, $^1J_{HH}$ = 4 Hz, 2H, thiopheneCH], 5.90 [s, 4H, pzCH], 5.78 [s, 2H, pzCH], 2.56 [s, 12H, $pzCH_3$], 2.42 [s, 6H, $pzCH_3$], 2.37 [s, 12H, $pzCH_3$], 2.34 [s, 6H, $pzCH_3$]. $^{13}C\{^1H\}$ NMR (201 MHz, $CDCl_3$, 25ºC, δ): 260.8 [W≡C], 224.1 [$^1J_{CW}$ = 165 Hz, CO], 153.7 [$^2J_{CW}$ = 50 Hz, $C^{5,5'}(SC_4H_2)$], 152.4 152.1 [C^5(pz)], 145.2 144.5 [C^3(pz)], 136.9 [$C^{2,2'}(SC_4H_2)$], 130.2 [$C^{4,4'}(SC_4H_2)$], 123.4 [$C^{3,3'}(SC_4H_2)$], 106.7 106.5 [C^4(pz)], 16.7 15.3 12.6 [$pzCH_3$]. MS (ESI, *m/z*): Found: 1263.2659. Calcd for $C_{44}H_{49}{}^{11}B_2N_{12}O_4S_2{}^{184}W_2$ $[M+1]^+$: 1263.2646. A sample that satisfied ±0.4% element was not achieved with N% being marginally low. The closest match is included. Anal. Found: C, 41.92; H, 3.741; N, 12.84%. Calcd for $C_{44}H_{48}B_2N_{12}O_4S_2W_2$: C, 41.86; H, 3.83; N, 13.31%.

9.9 Synthetic procedures for Chapter Seven compounds

Synthesis of [WAu(μ$_2$-C)(CO)$_2$(PCy$_3$)(Tp*)] (7.2).

A sample of $[W(\equiv CAu)(CO)_2(Tp^*)]_4$ (**7.1**; 0.300 g, 0.100 mmol) and PCy_3 (0.124 g, 0.442 mmol) was dissolved in CH_2Cl_2 (10 mL), quickly changing from orange to a bright yellow. Infrared spectroscopic analysis confirmed reaction completion after 30 minutes. The compound could be recrystallised by addition of *n*-hexane (10 mL) before concentration under reduced pressure to precipitate a bright yellow solid. The solid was collected *via* vacuum filtration, washing with *n*-hexane (10 mL) and *n*-pentane (2 × 5 mL) before drying *in vacuo* for 4 hours. The title compound was produced as a bright yellow microcrystalline powder (0.323 g, 0.315 mmol, 79% isolated yield). Crystals suitable for X-ray diffraction were grown from the vapour diffusion of benzene into a CH_2Cl_2 solution of compound at ambient temperature inside an argon glovebox. IR (CH_2Cl_2, cm^{-1}): 1950 vs ν_{CO}, 1856 vs ν_{CO}. IR (ATR, cm^{-1}): 2532 vs ν_{CO}, 1939 vs ν_{CO}, 1844 vs ν_{CO}. ^{1}H NMR (400 MHz, $CDCl_3$, 25 ºC, δ): 5.86 [s, 2H, pzCH], 5.68 [s, 1H, pzCH], 2.83 [s, 6H, $pzCH_3$], 2.38 [s, 3H, $pzCH_3$], 2.32 [s, 6H, $pzCH_3$], 2.28 [s, 3H, $pzCH_3$], 1.91 [m, 8H, PCy], 1.82 [m, 6H, PCy], 1.72 [m, 2H, PCy], 1.58 [m, 1H, PCy], 1.39 [m, 6H, PCy], 1.30 [m, 7H, PCy]. $^{13}C\{^1H\}$ NMR (151 MHz, $CDCl_3$, 25ºC, δ): 400.5 [d, $^2J_{CP}$ = 75 Hz, W≡C–Au], 229.5 [$^1J_{CW}$ = 180 Hz, CO], 151.84 151.81 [C^5(pz)], 144.6 144.0 [C^3(pz)], 106.4 106.1 [C^4(pz)], 33.2 [d, $^1J_{CP}$ = 24 Hz, $C^1(C_6H_{11})$], 30.8 [$C^{3,5}(C_6H_{11})$], 27.4 [d, $^2J_{CP}$ = 12 Hz, $C^{2,6}(C_6H_{11})$], 26.2 [$C^4(C_6H_{11})$], 17.3 15.0 12.9 12.7 [$pzCH_3$]. $^{31}P\{^1H\}$ NMR (162 MHz, $CDCl_3$, 25 ºC, δ): 54.97 [s, $^2J_{PW}$ = 61 Hz]. MS (ESI, *m/z*): Found: 1027.3484. Calcd for $C_{36}H_{56}{}^{197}Au^{11}BN_6O_2P^{184}W$ $[M]^+$: 1027.3470. A sample of sufficient purity was not obtained to satisfy elemental analysis criteria. The closest match is included. Anal. Found: C, 42.76; H, 5.51; N, 8.27%. Calcd for $C_{36}H_{55}BN_6O_2PWAu$: C, 42.12; H, 5.40; N, 8.19%. *Crystal data*

for $C_{36}H_{55}AuBN_6O_2PW{\cdot}C_6H_6$, M = 1104.56, monoclinic, $P2_1/c$, a = 17.7842 (2) Å, b = 13.1359 (1) Å, c = 18.5100 (2) Å, β = 95.667 (1)°, V = 4303.01 (8) Å^3, Z = 4, ρ_{calc} = 1.705 Mgm^{-3}, μ(Cu $K\alpha$) = 11.86 mm^{-1}, T = 150(0) K, plate 0.10 × 0.07 × 0.02 mm {clear light yellow}, 7833 independent measured reflections (θ = 73.1), R_1 = 0.027, wR_2 = 0.074 for 6787 reflections [$I > 2\sigma(I)$], 493 parameters, 0 restraints. CDCC 2251849.

Synthesis of [(Tp*)(CO)$_2$W≡C–Au(PMe$_2$Ph)] (7.3).

Note: This compound slowly dissociates PMe_2Ph in solution and is best crystallised in presence of excess phosphine. An orange solution of [W(≡CAu)(CO)$_2$(Tp*)]$_4$ (**7.1**; 0.310 g, 0.104 mmol) in CH_2Cl_2 (10 mL) was cooled to 0 °C and treated dropwise with neat PMe_2Ph (0.06 mL, 0.4 mmol), instantly changing the solution bright yellow. The yellow solution was stirred for 1 hour, slowly returning to ambient temperature where infra-red spectroscopy (ν_{CO}) verified full conversion. The bright yellow solution was injected with *n*-hexane (10 mL) and concentrated under reduced pressure to precipitate a yellow solid that proved to be waxy even when exposed to an ultrasonic bath. The precipitate was mechanically manipulated multiple times (3 cycles) under an argon counterflow to break the solid prior to further sonication, eventually liberating a fine yellow solid. The ensuing solid could then be collected *via* vacuum filtration, washing with ample *n*-hexane (5 × 20 mL) and *n*-pentane (3 × 10 mL) before drying *in vacuo* for 16 hours to provide the title compound as a bright yellow solid (0.286 g, 0.373 mmol, 81% isolated yield). Despite many tested conditions, single crystals were only obtained from the vapour diffusion of *n*-hexane into a CH_2Cl_2 solution of compound at ambient temperature. Regrettably, these tiny needles (*ca* 5 × 2 × 1 μm) did not diffract, even on the MX2 beamline at the Australian Synchrotron. IR (CH_2Cl_2, cm^{-1}): 1953 vs ν_{CO}, 1859 vs ν_{CO}. IR (ATR, cm^{-1}): 2548 w ν_{BH}, 1950 vs ν_{CO}, 1852 vs ν_{CO}. The ligand PMe_2Ph slowly dissociates from the gold in solution, therefore prolonged exposure to solution results in accumulation of free ligand and hence the oxide. These impurities are noticeable in spectra and are inherent to the system, unable to be removed as chromatography further cleaves the Au–P bond. ^{1}H NMR (700 MHz, CD_2Cl_2, 25 °C, δ): 7.75 [m, 2H, PPh], 7.53 [m, 3H, PPh], 5.97 [s, 2H, pzCH], 5.78 [s, 1H, pzCH], 2.84 [s, 6H, pzCH$_3$], 2.40 [s, 6H, pzCH$_3$], 2.39 [s, 3H, pzCH$_3$], 2.34 [s, 3H, pzCH$_3$], 1.59 [br.s, 6H, P(CH$_3$)]. ^{1}H NMR (700 MHz, CD_2Cl_2, –60 °C, δ): 7.72 [m, 2H, PPh], 7.51 [m, 3H, PPh], 5.97 [s, 2H, pzCH], 5.79 [s, 1H, pzCH], 2.78 [s, 6H, pzCH$_3$], 2.35 [s, 6H, pzCH$_3$], 2.34 [s, 3H, pzCH$_3$], 2.29 [s, 3H, pzCH$_3$], 1.69 [d, $^1J_{HP}$ = 9 Hz, 6H, P(CH$_3$)]. ^{13}C{^{1}H} NMR (201 MHz, CD_2Cl_2, 25°C, δ): 395.9 [br.s, W≡C–Au], 229.3 [br.s, CO], 152.3 152.1 [C^5(pz)], 145.7 145.0 [C^3(pz)], 133.6 [br.s, C^1(C$_6$H$_5$)], 132.3 [d, $^2J_{CP}$ = 13 Hz, C^{2,6}(C$_6$H$_5$)], 131.7 [C^4(C$_6$H$_5$)], 129.4 [d, $^3J_{CP}$ = 11 Hz, C^{3,5}(C$_6$H$_5$)], 106.6 106.4 [C^4(pz)], 17.3 [pzCH$_3$], 15.5 [d, $^1J_{CP}$ = 33 Hz, PCH$_3$], 14.9 12.9

12.6 [pzCH$_3$]. ^{13}C{^{1}H} NMR (201 MHz, CD_2Cl_2, –20 ºC, δ): 396.0 [br.d, $^2J_{CP}$ = 81 Hz, W≡C–Au], 229.0 [br.s, $^1J_{CW}$ = 175 Hz, CO], 151.9 [br.s, C^5(pz)], 151.6 [C^5(pz)], 145.6 144.8 [br.s, C^3(pz)], 133.3 [br.d, $^1J_{CP}$ = 50 Hz, C^1(C_6H_5)], 132.0 [br.d, $^2J_{CP}$ = 12 Hz, C^{2,6}(C_6H_5)], 131.3 [br.s, C^4(C_6H_5)], 129.0 [br.d, $^3J_{CP}$ = 10 Hz, C^{3,5}(C_6H_5)], 106.2 106.1 [C^4(pz)], 17.1 [br.s, pzCH$_3$], 15.0 [br.d, $^1J_{CP}$ = 32 Hz, P(CH$_3$)], 14.7 [br.s, pzCH$_3$], 12.7 [pzCH$_3$], 12.5 [br.s, pzCH$_3$]. ^{31}P{^{1}H} NMR (162 MHz, CD_2Cl_2, 25 ºC, δ): 13.38 [br.s]. ^{31}P{^{1}H} NMR (162 MHz, CD_2Cl_2, –60 ºC, δ): 14.14 [s, $^3J_{PW}$ = 66 Hz, W≡C–Au–P]. MS (ESI, *m/z*): Found: 883.1746. Calcd for $C_{26}H_{34}{}^{197}Au^{11}BN_6O_2P^{182}W$ [M+H]$^+$: 883.17160. Anal. Found: C, 35.28; H, 3.91; N, 9.60%. Calcd for $C_{26}H_{33}BN_6O_2PWAu$: C, 35.32; H, 3.76; N, 9.51%.

Synthesis of [WAu(μ$_2$-C)(CO)$_2$(PPh$_3$)(Tp*)] (7.4).

Note: This compound is stable as an isolated solid, however, reforms the golden ring tetramer **7.1** in the absence of excess phosphine. Samples of [W(≡CAu)(CO)$_2$(Tp*)]$_4$ (**7.1**; 0.100 g, 0.036 mmol) and PPh$_3$ (0.160 g, 0.610 mmol; 5 equiv. per Au atom) were dissolved in CH_2Cl_2 (10 mL), initially returning an orange solution that changed to yellow within 5 minutes. The solution was stirred for 1 hour with no further changes observed (including precipitation, or colloidal gold). *N*-hexane (20 mL) was add and subsequent concentration (*ca* 5 mL) resulted in a bright precipitate that was washed with ample *n*-hexane (5 × 10 mL) discarding the clear supernatant phase each time. Finally, the yellow powder was collected *via* vacuum filtration, washing with *n*-hexane (2 × 10 mL) before drying *in vacuo* for 16 hours gave the title compound as a bright yellow powder (0.080 g, 0.080 mmol, 56% isolated yield). Solution-state spectra are taken in the presence of 5-fold excess of PPh$_3$ and therefore some signals are unable to be unequivocally assigned. IR (CH_2Cl_2, cm^{-1}): 1954 vs ν_{CO}, 1861 vs ν_{CO}. NB: reformed tetramer [W(≡CAu)(CO)$_2$(Tp*)]$_4$ (**7.1**) evident in spectrum [ν_{CO}: 1987, 1892 cm^{-1}]. IR (ATR, cm^{-1}): 2550 w ν_{BH}, 1947 vs ν_{CO}, 1851 vs ν_{CO}. ^{1}H NMR (400 MHz, $CDCl_3$, 25 ºC, δ): 5.92 [s, 2H, pzCH], 5.72 [s, 1H, pzCH], 2.93 [s, 6H, pzCH$_3$], 2.44 [s, 3H, pzCH$_3$], 2.38 [s, 6H, pzCH$_3$], 2.33 [s, 3H, pzCH$_3$]. No independent phenyl protons were identified beneath signals corresponding to excess phosphine. ^{13}C{^{1}H} NMR (101 MHz, $CDCl_3$, 25ºC, δ): 389.9 [br.s, W≡C–Au], 229.2 [$^1J_{CW}$ = 178 Hz, CO], 151.9 151.8 [C^5(pz)], 144.7 144.1 [C^3(pz)], no independent phenyl carbon resonances were identified beneath the signals of excess phosphine, 106.5 106.2 [C^4(pz)], 17.4 15.0 12.8 12.7 [pzCH$_3$]. ^{31}P{^{1}H} NMR (162 MHz, $CDCl_3$, 25 ºC, δ): 1.87 [br, average of Au–P and PPh$_3$]. Broad resonance between free PPh$_3$ and expected values for gold metallacarbynes supports dynamic equilibria. MS (ESI, *m/z*): Found: 1009.2088. Calcd for $C_{36}H_{37}{}^{11}BN_6O_2P^{184}W^{197}Au$ [M+H]$^+$: 1009.2062. A sample that satisfies ±0.4% elemental analysis was not found, unsurprising given labile ligand and oxidation. The closest match

is included with a marginally lower (–1% N). Anal. Found: C, 42.84; H, 3.504; N, 6.99%. Calcd for $C_{36}H_{37}AuBN_6O_2PW$: C, 42.88; H, 3.70; N, 8.33%.

Synthesis of [WAu(μ_2-C)(CO)$_2$(IMes)(Tp*)] (7.5).

A clear solution of 1,3-dimesitylimidazolium chloride (0.102 g, 0.299 mmol) in THF (10 mL) was treated dropwise with a solution of KHMDS (0.068 g, 0.341 mmol) in THF (10 mL) at –78 °C. This mixture was allowed to stir at low temperature for 30 minutes prior to warming to ambient temperature over 3 hours with no observable changes. The mixture was cooled to 0 °C once more, before dropwise addition of $[W(\equiv CAu)(CO)_2(Tp^*)]_4$ (**7.1**; 0.219 g, 0.0734 mmol) in THF (5 mL) resulted in a yellow solution that was left to stir for 1 hour at ambient temperature. Monitoring the reaction via infra-red spectroscopy (ν_{CO}) revealed slow conversion to the major product over 16 hours. The mixture was then heated at 60 °C for 2 days to give a birght yellow solution with a small amount of reaction detritus with full consumption of **7.1**. The yellow reaction mixture was filtered through diatomaceous earth and evaporated to a bright yellow solid that could be recrystallised from concentration of CH_2Cl_2 into *n*-hexane under reduced pressure. The yellow solid was collected *via* vacuum filtration and washed with *n*-pentane (3 × 10 mL) to give the title compound (0.171 g, crop 1). The filtrate remained bright yellow and concentration *via* rotary evaporator gave a second amount of compound collected analogously (0.070 g, crop 2). Both fractions revealed to be of the same purity giving the title compound as a bright yellow microcrystalline solid (0.241 g, 0.229 mmol, 78% isolated yield). Crystals suitable for X-ray diffraction were grown from liquid-liquid diffusion of *n*-hexane into a CH_2Cl_2 solution of **7.5** at 5 °C. IR (CH_2Cl_2, cm^{-1}): 1945 vs ν_{CO}, 1850 vs ν_{CO}. IR (ATR, cm^{-1}): 2524 w ν_{BH}, 1937 vs ν_{CO}, 1842 vs ν_{CO}. ^{1}H NMR (400 MHz, $CDCl_3$, 25 °C, δ): 7.02 [s, 2H, MesCH], 6.99 [s, 4H MesCH], 5.77 [s, 2H, pzCH], 5.61 [s, 1H, pzCH], 2.48 [s, 6H, $pzCH_3$], 2.37 [s, 6H, $MesCH_3$], 2.30 [s 3H, $pzCH_3$], 2.27 [s, 6H, $pzCH_3$], 2.23 [s, 3H, $pzCH_3$], 2.09 [s, 12H, $MesCH_3$]. $^{13}C\{^1H\}$ NMR (201 MHz, $CDCl_3$, 25°C, δ): 402.1 [$^1J_{CW}$ = 152 Hz, W≡C–Au], 229.3 [$^1J_{CW}$ = 183 Hz, CO], 192.4 [$^3J_{CW}$ = 20 Hz, C^1(Im)], 151.9 151.7 [C^5(pz)], 144.4 143.7 [C^3(pz)], 139.3 [C^1(Mes)], 135.2 [C^4(Mes)], 135.0 [$C^{2,6}$(Mes)], 129.3 [$C^{3,5}$(Mes)], 122.3 [$C^{3,4}$(Im)], 106.2 105.9 [C^4(pz)], 21.3 18.1 [$MesCH_3$], 16.8 14.9 12.8 12.6 [$pzCH_3$]. MS (ESI, *m/z*): Found: 1051.3088. Calcd for $C_{39}H_{47}{}^{11}BN_8O_2{}^{184}W^{197}Au$ $[M+H]^+$: 1058.3090. Anal. Found: C, 44.70; H, 4.39; N, 10.61%. Calcd for $C_{39}H_{46}AuBN_8O_2W$: C, 44.59; H, 4.41; N, 10.67%. *Crystal data for* $C_{39}H_{46}AuBN_8O_2W$, M = 1050.46, orthorhombic, *Pbca*, a = 19.272 (4) Å, b = 15.534 (3) Å, c = 29.865 (6) Å, V = 8941 (3) Å^3, Z = 8, ρ_{calc} = 1.561 Mgm^{-3}, μ(Synchrotron; λ = 0.71073 Å) = 5.89 mm^{-1}, T = 100(0) K, plate 0.02 × 0.01 × 0.01 mm {yellow}, 8173

independent measured reflections (θ = 25.4°), R_1 = 0.060, wR_2 = 0.169 for 6191 reflections [$I > 2\sigma(I)$], 481 parameters. CDCC 2251853.

Synthesis of [WAu(μ$_2$-C)(CNMes)(CO)$_2$(Tp*)] (7.6).

Note: This compound loses CNMes in solution to form the golden ring aggregate [WAu(μ-C)(CO)$_2$(Tp*)]$_4$ (**7.1**). A solution of [W(≡CAu)(CO)$_2$(Tp*)]$_4$ (**7.1**; 0.300 g, 0.100 mmol) in CH_2Cl_2 (5 mL) is treated with a CH_2Cl_2 solution containing excess CNMes (0.120 g, 0.826 mmol, 5 mL) at 0 °C. No initial colour change from the vibrant orange solution is noted and the reaction is warmed to ambient temperature before stirring for 1 hour. The reaction is monitored by infra-red spectroscopy (ν_{CO}/ν_{CN}) given an equilibrium exists, ensuring that excess isocyanide is in solution to maximise formation of the title compound and minimal starting material is recorded (**7.1**; ν_{CO}: 1990, 1900 cm^{-1}). After conversion is maximised, *n*-hexane (20 mL) is added and the mixture concentrated under reduced pressure to precipitate a fine yellow powder. Subsequent vacuum filtration collects the solid, washing with *n*-hexane (5 × 20 mL) and *n*-pentane (5 × 10 mL) before drying *in vacuo* overnight to give the title compound as a microcrystalline yellow powder (0.225 g, 0.252 mmol, 63% isolated yield). Recrystallisation only works in the presence of excess isocyanide. This hypothesis was further supported as single crystals could be obtained from the liquid-liquid diffusion of *n*-hexane into a CH_2Cl_2 of compound with excess CNMes. Due to the loss of CNMes in solution, signals corresponding to the ligand and [W(≡CAu)(CO)$_2$(Tp*)]$_4$ (**7.1**) are highlighted in grey. It is not possible to get a pure sample of **7.6** for analysis upon returning to solution without excess isocyanide. IR (CH_2Cl_2, cm^{-1}): 2193 vs ν_{CN}, 1956 vs ν_{CO}, 1862 vs ν_{CO}. IR (ATR, cm^{-1}): 2527 w ν_{BH}, 2194 m ν_{CN}, 1944 vs ν_{CO}, 1855 vs ν_{CO}. ^{1}H NMR (400 MHz, $CDCl_3$, 25 ºC, δ): 6.93 [s, 2H, MesCH], 5.88 [s, 2H, pzCH], 5.69 [s, 1H, pzCH], 2.82 [br.s, 6H, MesCH$_3$], 2.40 [s, 3H, pzCH$_3$], 2.36 [s, 6H, pzCH$_3$], 2.34 [s, 6H, pzCH$_3$], 2.31 [br.s, 3H, MesCH$_3$], 2.29 [s, 3H, pzCH$_3$]. ^{1}H NMR (700 MHz, $CDCl_3$, –20 ºC, δ): 6.93 [s, 2H, MesCH], 5.89 [s, 2H, pzCH], 5.70 [s, 1H, pzCH], 2.81 [s, 6H, MesCH$_3$], 2.38 [s, 3H, pzCH$_3$], 2.35 [s, 6H, pzCH$_3$], 2.32 [s, 6H, pzCH$_3$], 2.31 [s, 3H, MesCH$_3$], 2.27 [s, 3H, pzCH$_3$]. ^{13}C{^{1}H} NMR (151 MHz, $CDCl_3$, 25ºC, δ): 377.3 [br.s, W≡C–Au], 228.7 [br.s, CO], 162.6 [br.s, Au–CNMes] 152.0 151.8 [C^5(pz)], 144.8 144.1 [C^3(pz)], 141.3 [br.s, C^{2,6}(Mes)], 139.1 [br.s, C^4(Mes)], 128.7 [C^{3,5}(Mes)], 124.3 [br.s, C^1(Mes)], 106.4 106.3 [br.s, C^4(pz)], 21.5 18.8 [br.s, MesCH$_3$], 15.1, 14.9, 13.1, 12.7 [br.s, pzCH$_3$]. MS (ESI, *m/z*): Found: 892.2054. Calcd for $C_{28}H_{34}{}^{197}Au^{11}BN_7O_2{}^{184}W$ [M+Na]$^+$: 892.2040. Anal. Found: C, 37.74; H, 3.738; N, 10.80%. Calcd for $C_{21}H_{28}BHgN7O_2S_2W$: C, 37.74; H, 3.73; N, 11.00%. *Crystal data for* $C_{28}H_{33}AuBN_7O_2W$, M = 891.24, triclinic, $P\bar{1}$, a = 8.1040(16) Å, b = 11.364(2) Å, c =

16.471(3) Å, V = 1485.5(5) Å^3, Z = 2, ρ_{calc} = 1.993 Mgm^{-3}, μ(Synchrotron; λ = 0.71073 Å) = 8.84 mm^{-1}, T = 100(0) K, shard, 0.01 × 0.002 × 0.001 mm {yellow}, 5052 independent measured reflections (θ = 25.4°), R_1 = 0.082, wR_2 = 0.232 for 4214 reflections [$I > 2\sigma(I)$], 370 parameters, 3 restraints. CCDC 2251850.

Synthesis of [WAu(μ$_2$-C)(CN^{t}Bu)(CO)$_2$(Tp*)] (7.7).

Note: This compound loses CN^{t}Bu in solution to aggregate as the golden ring [WAu(μ-C)(CO)$_2$(Tp*)]$_4$ (**7.1**). An orange solution of [W(≡CAu)(CO)$_2$(Tp*)]$_4$ (**7.1**; 0.101 g, 0.0338 mmol) in CH_2Cl_2 (10 mL) was treated with excess CN^{t}Bu (0.02 mL, 0.177 mmol), quickly changing to a bright yellow colour. No further change was observed and the mixture stirred for 30 minutes before infra-red spectroscopy (ν_{CO}/ν_{CN}) confirmed complete conversion. To obtain the product, *n*-hexane (10 mL) was added to the solution before concentration under reduced pressure resulted in a bright yellow precipitate that was subsequently collected *via* vacuum filtration washing with *n*-pentane (5 × 5 mL). After drying *in vacuo* for 16 hours to provide the title compound as a microcrystalline yellow solid (0.088 g, 0.106 mmol, 78% isolated yield). Despite multiple attempts, single crystals for X-ray diffraction could only be grown from the liquid-liquid diffusion of *n*-hexane into a CH_2Cl_2 solution of compound containing excess isocyanide. The tiny crystals (*ca* 5 × 2 × 1 μm) were found to diffract weakly on the MX2 beamline at the Australian Synchrotron, often destroyed in the beamline during collection, so no suitable structure could be obtained. Due to the loss of CN^{t}Bu in solution, features of the ligand and [W(≡CAu)(CO)$_2$(Tp*)]$_4$ (**7.1**) are highlighted as impurities in grey. It is not possible to get a pure sample upon returning to solution without excess isocyanide. IR (CH_2Cl_2, cm^{-1}): 2219 s ν_{CN}, 1955 vs ν_{CO}, 1861 vs ν_{CO}. IR (ATR, cm^{-1}): 2524 w ν_{BH}, 2218 m ν_{CN}, 1939 vs ν_{CO}, 1850 vs ν_{CO}. ^{1}H NMR (700 MHz, $CDCl_3$, 25 ºC, δ): 5.87 [s, 2H, pzCH], 5.68 [s, 1H, pzCH], 2.78 [s, 6H, pzCH_3], 2.38 [s, 3H, pzCH_3], 2.33 [s, 3H, pzCH_3], 2.28 [s, 6H, pzCH_3], 1.51 [s, 9H, CNC(CH_3)]. ^{13}C{^{1}H} NMR (151 MHz, $CDCl_3$, 25ºC, δ): 377.4 [br.s, W≡C–Au], 228.6 [br.s, $^1J_{CW}$ = 179 Hz, CO], 152.0 151.7 [C^5(pz)], 150.1 [br.s, Au–*C*N^{t}Bu], 144.7 144.1 [C^3(pz)], 106.4 106.2 [C^4(pz)], 58.3 [CN*C*(CH$_3$)], 30.8 30.0 [br.s, [CNC(*C*H$_3$)], 17.3 15.0 12.8 12.7 [pzCH_3]. MS (ESI, *m/z*): Found: 830.1883. Calcd for $C_{23}H_{32}{}^{11}BN_7O_2{}^{184}W^{197}Au$ [M]$^+$: 830.1882. Anal. Found: C, 33.29; H, 3.63; N, 11.70%. Calcd for $C_{23}H_{31}AuBN_7O_2W$: C, 33.32; H, 3.77; N, 11.83%.

Synthesis of *cis*-[WAu(μ$_2$-C)Cl$_2$(CO)$_2$(PPh$_3$)(Tp*)] (7.8).

Note: Species readily decomposes in solution, developing [W(≡CCl)(CO)$_2$(Tp*)] and [AuCl(PPh$_3$)] accompanied by colloidal gold and/or mirror. Samples of [WPt(μ$_2$-C)Br(CO)$_2$(PPh$_3$)$_2$(Tp*)] (0.150 g, 0.111 mmol) and [AuCl·SMe$_2$] (0.060 g, 0.204 mmol) were

dissolved in CH_2Cl_2 (10 mL) immediately changing from orange to a deep red. The evolution of the red solution was accompanied by a coating of colloidal gold(0), gold(0) mirror, and a grey precipitate consistent with platinum(0). The reaction was stirred for 30 minutes in the absence of light where infra-red spectroscopy confirmed the presence of a single set of ν_{CO} vibrations. The red solution was anaerobically filtered through dry celite and EtOH (10 mL) added before concentration resulted in a red powder. The red powder was collected *via* vacuum filtration washing with EtOH (2 × 5 mL) and Et_2O (2 × 2 mL) before drying *in vacuo* for 16 hours. The red powder was identified as a mixture of the title compound with [$AuCl(PPh_3)$] (~1:1) where all attempts to separate the compounds failed, resulting in decomposition of the title species. Mechanical separations of single crystals on a bulk scale also resulted in similar NMR spectra. As compound was isolated as an inseparable mixture, impurities are denoted in grey. Furthermore, the species readily decomposes in solution, especially *via* reductive elimination to [$W(\equiv CCl)(CO)_2(Tp^*)$] and [$AuCl(PPh_3)$. IR ($CH_2Cl_2$, cm^{-1}): 2049 vs ν_{CO}, 2000 vs ν_{CO}. Not every resonance can be assigned unequivocally with confidence by ^1H NMR and impurities are denoted in grey. ^1H NMR (400 MHz, $CDCl_3$, 25 °C, δ): aromatic PhH unable to be assigned, 5.89 [s, 2H, $pzCH_3$], 5.82 [s, 1H, $pzCH_3$], 2.38 [overlapping s, 3H, $pzCH_3$], 2.38 [overlapping s, 6H, $pzCH_3$], 2.25 [overlapping s, 6H, $pzCH_3$], 2.24 [overlapping s, 3H, $pzCH_3$]. Reductive elimination occurred over 16 hours required to perform $^{13}C\{^1H\}$ NMR experiment and therefore cannot be assigned. No μ_2-carbido resonance could be identified, however [$W(\equiv CCl)(CO)_2(Tp^*)$] could be identified supported by TLC. $^{31}P\{^1H\}$ NMR (162 MHz, $CDCl_3$, 25 °C, δ): 35.28. No fragmentation pattern alighed with the title compound, suggesting the species does not survive the electrospray ionisation of the mass spectrometer. Given isolation as a mixture, no sample was submit for elemental analysis. *Crystal data for* $C_{36}H_{37}AuBCl_2N_6O_2PW \cdot 2(CHCl_3)$, M = 1317.95, monoclinic, $P2_1/n$, a = 17.6143 (5) Å, b = 14.4960 (2) Å, c = 19.5170 (5) Å, β = 112.839 (3)°, V = 4592.7 (2) $Å^3$, Z = 4, ρ_{calc} = 1.906 Mgm^{-3}, μ(Cu $K\alpha$) = 15.43 mm^{-1}, T = 150(0) K, plate 0.08 × 0.05 × 0.03 mm {clear light red}, 8416 independent measured reflections (θ = 73.8), R_1 = 0.041, wR_2 = 0.114 for 6531 reflections [$I > 2\sigma(I)$], 566 parameters, 84 restraints. CDCC 2251852.

Preparation of $[WAu(\mu\text{-}C)(CO)_2(Tp^*)]_5$ (7.9) crystals.

A yellow solution of [$WAu(\mu_2\text{-}C)(IMes)(CO)_2(Tp^*)$] (*ca* 5 mg) was dissolved in CH_2Cl_2 (0.3 mL) and layered with n-hexane (1 mL), left to evaporate over 4 days exposed to air. A series of bright yellow blocks were deposited and upon measuring via single crystal X-ray diffraction were found

to be the title compound. Screening runs determined that each yellow block (12 crystals) each had the same unit cell. Insufficient material was grown to measure the spectroscopic properties and attempts to produce bulk quantities from "Golden Ring" solids were inconclusive. A series of ^{1}H and DOSY NMR experiments were conducted for golden ring mixtures, however, these proved in conclusive. Spectra are included in the supporting information, but are left unassigned given the uncertainty. *Crystal data for* $C_{90}H_{110}Au_5BN_{30}O_{10}W_5$, M = 3730.17, triclinic, $P\bar{1}$, a = 18.0908 (2) Å, b = 18.3521 (3) Å, c = 20.0421 (3) Å, α = 84.8329 (14)°, β = 71.0271 (13)°, γ = 84.6686 (12)°, V = 3252.68 (16) Å^3, Z = 2, ρ_{calc} = 1.981 Mgm^{-3}, μ(Cu Kα) = 19.42 mm^{-1}, T = 150(1) K, block 0.47 × 0.15 × 0.10 mm {clear light orange}, 22870 independent measured reflections (θ = 68.3), R_1 = 0.055, wR_2 = 0.150 for 19615 reflections [I >2σ(I)], 1336 parameters. CDCC 2251854.

Preparation of [WCu(μ$_4$-C)(CuCl){CuCl(THF)$_2$}]$_2$ (7.10) crystals.

A solution of [CuCl(SMe$_2$)] (0.038 g, 0.238 mmol) in CH_2Cl_2 (20 mL) was treated with a yellow solution of [W(≡SnBu$_3$)(CO)$_2$(Tp*)] (0.200 g, 0.238 mmol) in CH_2Cl_2 (5 mL) at 0 °C. The yellow solution quickly changed to a bright orange colour and was stirred for 4 hours with the exclusion of light. The ensuing solution was filtered through celite and *N*-hexane (10 mL) was add prior to concentration under reduced pressure to afford a brick red microcrystalline solid. The solid was collected *via* vacuum filtration, washing with *n*-pentane (2 × 5 mL) and dried *in vacuo* for 16 hours. The solid was not pure by various spectroscopic techniques, repeatably depositing copper metal and copper black, however, a vapour diffusion of *n*-hexane into a THF solution of the solid resulted in 5 single crystals of **7.10**. *Crystal data for* $C_{22}H_{30}BCl_2Cu_3N_6O_3W$, M = 882.70, monoclinic, $P2_1/n$, a = 11.229 (2) Å, b = 20.872 (4) Å, c = 14.556 (3) Å, β = 102.76 (3)°, V = 3327.3 (12) Å^3, Z = 4, ρ_{calc} = 1.762 Mgm^{-3}, μ(Synchrotron, Mo Kα) = 5.53 mm^{-1}, T = 100(1) K, needle 0.03 × 0.01 × 0.01 mm {clear light orange}, 6088 independent measured reflections (θ = 23.6), R_1 = 0.061, wR_2 = 0.184 for 5369 reflections [I >2σ(I)], 350 parameters. CDCC 2251851.

Synthesis of [W$_2$Hg(μ$_2$-C)$_2$(CO)$_4$(Tp*)$_2$] (7.11b).

A cold (0 °C) solution of [$HgCl_2$] (0.324 g, 1.19 mmol) in CH_2Cl_2 (80 mL) was treated dropwise with [W(≡CSnBu$_3$)(CO)$_2$(Tp*)] (2.210 g, 2.634 mmol) in CH_2Cl_2 (15 mL). It is important to note that slow delivery and adequate dilution are required for control of this reaction. The yellow solution quickly changed to a vivid orange during addition and the mixture was allowed to slowly warm to ambient temperature over 90 minutes where infra-red spectroscopy identified

completion. If more than one set of ν_{CO} bands are recorded, then add extra [W(≡CSnBu$_3$)(CO)$_2$(Tp*)]. The ensuing orange solution was layered with *n*-hexane (20 mL) and concentrated under reduced pressure to afford a vivid orange solid and pale-yellow supernatant phase, aided by sonication. The solid was collected *via* vacuum filtration, washed with cold *n*-hexane (10 mL) and *n*-pentane (2 × 10 mL) before drying *in vacuo* overnight to afford the title compound as an orange microcrystalline powder (1.540 g, 1.189 mmol, 99% isolated yield). Crystals suitable for X-ray diffraction were not forthcoming despite various attempts utilising a variety of solvent combinations and temperatures. Clear white crystals continuously emerged, validated as mercury(II) chloride. IR (CH_2Cl_2, cm^{-1}): 1984 vs ν_{CO}, 1976 vs ν_{CO}, 1889 vs ν_{CO}. IR (ATR, cm^{-1}): 2542 w ν_{BH}, 1965 vs ν_{CO}, 1865 vs ν_{CO}. Slowly reacts with solvent to form [W(≡CH)(CO)$_2$(Tp*)]. ^{1}H NMR (600 MHz, $CDCl_3$, 25 ºC, δ): 5.92 [s, 2H, pzCH], 5.72 [s, 1H, pzCH], 2.66 [s, 6H, pzCH$_3$], 2.37 [s, 3H, pzCH$_3$], 2.35 [s, 6H, pzCH$_3$], 2.29 [s, 3H, pzCH$_3$]. ^{13}C{^{1}H} NMR (151 MHz, $CDCl_3$, 25ºC, δ): 355.1 [$^1J_{CW}$ = 172; W≡C–Hg], 227.4 [$^1J_{CW}$ = 175 Hz, CO], 152.3 151.7 [C^5(pz)], 145.3 144.7 [C^3(pz)], 106.8 106.7 [C^4(pz)], 17.5 15.0 12.8 12.7 [pzCH$_3$]. ^{199}Hg{^{1}H} NMR (125 MHz, $CDCl_3$, 25ºC, δ): –1065 [$^2J_{HgW}$ = 1184 Hz, WC–Hg]. MS (ESI, *m*/*z*): Found: 1301.2652. Calcd for $C_{36}H_{45}{}^{11}B_2N_{12}O_4{}^{184}W_2{}^{202}Hg$ $[M+H]^+$: 1301.2618. Anal. Found: C, 33.33; H, 3.54; N, 12.68%. Calcd for $C_{36}H_{44}BHgN_{12}O_4W_2$: C, 33.29; H, 3.42; N, 12.94%.

Synthesis of [WHg(μ$_2$-C)(CO)$_2$(Tp*)]$_2$(μ$_2$-Cl)$_2$ (7.12).

A cold (0 °C) solution of [$HgCl_2$] (0.324 g, 1.193 mmol) in CH_2Cl_2 (80 mL) was treated with a cold solution of [W(≡CSnBu$_3$)(CO)$_2$(Tp*)] (1.001 g, 1.314 mmol) in CH_2Cl_2 (15 mL) dropwise. It is important to note that slow delivery and adequate dilution are required to control this reaction. The yellow solution changed to an orange/yellow colour during addition, and the mixture was allowed to slowly warm to ambient temperature over 3 hours where infra-red identified completion. Additional [W(≡CSnBu$_3$)(CO)$_2$(Tp*)] (0.102 g, 0.124 mmol) was introduced as a solid, reacting the accompanying over-mercurated **7.13** into the target compound was in solution confirmed by infra-red spectroscopy. The ensuing orange solution was layered with *n*-hexane (20 mL) and concentrated under reduced pressure to afford an orange solid and pale-yellow supernatant phase, aided by sonication. The solid was collected *via* vacuum filtration washing with cold *n*-hexane (10 mL) and *n*-pentane (2 × 10 mL) before drying *in vacuo* overnight to afford the title compound as an orange/yellow powder (0.928 g, 0.591 mmol, 99% isolated yield). Crystals suitable for X-ray diffraction studies were not forthcoming despite multiple attempts and various solvent combinations. IR (CH_2Cl_2: cm^{-1}): 1992 vs ν_{CO}, 1900 vs ν_{CO}. IR (ATR, cm^{-1}): 2551 w ν_{BH}, 2030 m ν_{CO}, 1976 vs ν_{CO}, 1952 m ν_{CO}, 1881 vs ν_{CO}. ^{1}H NMR (400 MHz, $CDCl_3$, 25 ºC, δ): 5.95 [s,

2H, pzCH], 5.77 [s, 1H, pzCH], 2.58 [s, 6H, $pzCH_3$], 2.40 [s, 3H, $pzCH_3$], 2.37 [s, 6H, $pzCH_3$], 2.31 [s, 3H, $pzCH_3$]. $^{13}C\{^1H\}$ NMR (151 MHz, $CDCl_3$, 25ºC, δ): 297.6 [br, W≡C–Hg], 224.7 [br, $^1J_{CW}$ = 170 Hz, CO], 152.7 151.6 [C^5(pz)], 145.8 145.2 [C^3(pz)], 107.2 107.0 [C^4(pz)], 17.4 15.2 [$pzCH_3$], 12.82 12.80 [overlapping s, $pzCH_3$]. $^{199}Hg\{^1H\}$ NMR (72 MHz, $CDCl_3$, 25ºC, δ): –993.6 [br]. MS (ESI, *m/z*): Found: 1535.1893. Calcd for $C_{36}H_{44}{}^{11}B^{35}ClN_{12}O_4{}^{184}W_2{}^{200}Hg^{202}Hg$ $[M–Cl]^+$: 1535.1899. Anal. Found: C, 27.55; H, 2.678; N, 10.33%. Calcd for $C_{36}H_{44}B_2ClN_{12}O_4W_2Hg_2$: C, 27.54; H, 2.82; N, 10.70%.

Synthesis of $[WHgCl(HgCl_2)(\mu_3\text{-}C)(CO)_2(Tp^*)]_2$ (7.13).

Samples of $[W(\equiv CSnBu_3)(CO)_2(Tp^*)]$ (0.360 g, 0.429 mmol) and $[HgCl_2]$ (0.201 g, 0.740 mmol) were suspended in toluene (20 mL) and heated at 80 °C for 4 hours in which time an orange solid precipitated from solution. Once cooled, the orange solid was collected via vacuum filtration washing with toluene (2 × 10 mL) and *n*-hexane (5 × 10 mL) before drying in vacuo for 16 hours gave the title compound as a microcrystalline orange solid (0.340 g, 0.161 mmol, 44% isolated yield). IR (CH_2Cl_2, cm^{-1}): 2041 vs ν_{CO}, 1967 vs ν_{CO}. When dissolved in polar CH_2Cl_2, $HgCl_2$ dissociates to give rise to vibrational modes consistent with $[(Tp^*)(CO)_2WCHgCl]_2$ {ν_{CO} 1990, 1900 cm^{-1}}. IR (ATR, cm^{-1}): 2562 w ν_{BH}, 2035 vs ν_{CO}, 1953 vs ν_{CO}, 1887 m ν_{CO}. ^1H NMR (400 MHz, $CDCl_3$, 25 ºC, δ): 6.05 [s, 2H, pzCH], 5.92 [s, 1H, pzCH], 2.53 [s, 6H, $pzCH_3$], 2.48 [s, 3H, $pzCH_3$], 2.40 [s, 6H, $pzCH_3$], 2.32 [s, 3H, $pzCH_3$]. $^{13}C\{^1H\}$ NMR (151 MHz, $CDCl_3$, 25ºC, δ): 216.4 [br.s, $WHg_2(\mu_3\text{-}C)$], 207.0 [CO], 153.4 152.7 [C^5(pz)], 147.1 146.9 [br.s, C^3(pz)], 108.5 108.3 [br.s, C^4(pz)], 31.1 17.7 15.7 13.2 12.9 [$pzCH_3$]. $^{199}Hg\{^1H\}$ NMR (125 MHz, $CDCl_3$, 25ºC, δ): –962 [br, W≡C–*Hg*]. No resonance was detected for η^2-$HgCl_2$ despite long acquisition (ca 6000 scans) across +1000 to –2000 ppm (spectra width 1000 ppm). It is likely this resonance is broadened into the baseline. MS (ESI, *m/z*): Found: 1535.1960. Consistent with $[M–HgCl_3]$ but is indistinguishable from what is detected from the species $[(Tp^*)(CO)_2WCHgCl]_2$. Therefore, the title compound was not discretely detected. Anal. Found: C, 20.49; H, 2.110; N, 7.67%. Calcd for $C_{36}H_{44}B_2Cl_6Hg_4N_{12}O_4W_2$: C, 20.46; H, 2.10; N, 7.95%. *Crystal data for* $C_{36}H_{44}B_2Cl_6Hg_4N_{12}O_4W_2{\cdot}4(CHCl_3)$, M = 2590.68, triclinic, $P\bar{1}$, a = 11.8328 (3) Å, b = 12.4896 (3) Å, c = 12.5771 (3) Å, α = 105.454 (2)°, β = 92.418 (2)°, γ = 97.180 (1)°, V = 1771.93 (8) $Å^3$, Z = 1, ρ_{calc} = 2.428 Mgm^{-3}, μ(Mo *K*α) = 12.59 mm^{-1}, T = 150(0) K, block 0.1 × 0.1 × 0.1 {clear light orange}, 10409 independent measured reflections (θ = 30.0), R_1 = 0.066, wR_2 = 0.192 for 7628 reflections [$I > 2\sigma(I)$], 376 parameters and 42 restraints. Crystal is to highlight connectivity only and contains issues of residual density around the

many heavy elements, where absorption correction provided ineffective. Subsequently this was not uploaded to the CDCC but is available from the author.

Synthesis of [WHg(μ$_2$-C)(Ph)(CO)$_2$(Tp*)] (Mixture) (7.14).

A solution of [W(≡CSnBu$_3$)(CO)$_2$(Tp*)] (0.203 g, 0.242 mmol) in CH_2Cl_2 (15 mL) was added dropwise to a dilute solution of [HgCl(Ph)] (0.075 g, 0.24 mmol) in CH_2Cl_2 (30 mL) at 0 °C. The resulting yellow/orange solution was stirred at 0 °C (2 hours) before a warming to ambient temperature (2 hours), with no additional colour change observed. The yellow solution was injected with *n*-hexane (20 mL) and concentrated under reduced pressure to precipitate an orange powder leaving a yellow supernatant phase. The orange solid was collected *via* vacuum filtration and washed with *n*-hexane (3 × 10 mL) before drying *in vacuo* overnight to afford a mixture of mercurial species (0.108 g impure material). No crystals suitable for X-ray diffraction were grown despite multiple attempts and a variety of solvent combinations. The obtained orange solid is a combined mixture of the target compound and products of symmetrisation about mercury: [W$_2$Hg(μ$_2$-C)(CO)$_4$(Tp*)$_2$] and [HgPh$_2$]. Signals are recorded only when unequivocally identified. Solution and solid-state infra-red analysis revealed carbonyl stretches that were clean but matched [W$_2$Hg(μ$_2$-C)$_2$(CO)$_4$(Tp*)$_2$] with no second set that may belong to this compound. ^{1}H NMR of the solid shows signals of identical chemical shift to analytically pure [W$_2$Hg(μ$_2$-C)(CO)$_4$(Tp*)$_2$]. ^{13}C{^{1}H} NMR revealed a previously unrecorded carbido resonance at δ_C = 360.2 [$^1J_{CW}$ = 177 Hz] and ^{199}Hg{^{1}H} NMR demonstrated a signal at δ_{Hg} = –895.4 [$^2J_{HgW}$ = 1153 Hz]. Furthermore, sequential ^{13}C{^{1}H} and ^{199}Hg{^{1}H} NMR experiments over 16 hours reveal relative ratios of key resonances remain the same suggesting that symmetrisation occurs prior to isolation. MS (ESI, *m*/*z*): Found: 829.1613. Calcd for $C_{24}H_{28}{}^{11}BN_6O_2{}^{184}W^{202}Hg$ [M+H]$^+$: 829.1582. GC–MS identified a positive match for [($C_{12}H_{10}$)] when the species was demercurated with 5mol% [RhCl(CO)(PPh$_3$)$_2$]. Elemental analysis of this compound was not appropriate given the isolated solid is certainly a mixture.

Synthesis of [WHg(μ$_2$-C)($C_{10}H_7$)(CO)$_2$(Tp*)] (Mixture) (7.15).

Note: This species was not isolated cleanly as symmetrisation occurs during the reaction. Therefore, key signals are reported with the attempted method, however, this compound could not be produced alone. A sample of [W(≡CSnBu$_3$)(CO)$_2$(Tp*)] (0.204 g, 0.243 mmol) in CH_2Cl_2 (15 mL) was added dropwise to CH_2Cl_2 (30 mL) solution of [HgCl($C_{10}H_7$)] (0.083 g, 0.227 mmol) at 0 °C. The resulting yellow/orange solution was stirred at 0 °C (2 hours) before a further warming to ambient temperature (2 hours) with no additional colour change observed. The yellow solution

was injected with *n*-hexane (20 mL) and concentrated under reduced pressure to precipitate a yellow powder, leaving a yellow supernatant phase. This solid was collected *via* vacuum filtration and washed with *n*-hexane (3 × 10 mL) before drying *in vacuo* for 3 hours to afford a mixture of species including $[W_2Hg(\mu_2\text{-}C)_2(CO)_4(Tp^*)_2]$ and compound **7.15** (161 mg impure material). No crystals suitable for x-ray diffraction were grown despite multiple attempts and a variety of solvent combinations. The obtained orange solid is a mixture of the target compound and products of symmetrisation about mercury: $[W_2Hg(\mu_2\text{-}C)(CO)_4(Tp^*)_2]$ and $[HgPh_2]$. Signals are recorded only when unequivocally identified. Solution and solid-state infra-red analysis revealed carbonyl stretches that were clean but matched $[W_2Hg(\mu_2\text{-}C)_2(CO)_4(Tp^*)_2]$ with no second set that may belong to this compound. ^{1}H NMR of the solid shows signals of identical chemical shift to analytically pure $[W_2Hg(\mu_2\text{-}C)(CO)_4(Tp^*)_2]$ and despite multiple aromatic signal, none could be assigned with confidence to the title compound. This compound is in a relatively clean mixture and hence $^{13}C\{^1H\}$ NMR signals can be tentatively assigned. $^{13}C\{^1H\}$ NMR (176 MHz, $CDCl_3$, 25 °C, δ): 360.2 [$^1J_{CW}$ = 178 Hz, W≡C–Hg], 227.6 [$^1J_{CW}$ = 175 Hz, CO], 166.4 [$^3J_{CW}$ = 23 Hz, C^1(naph)], 152.3 151.6 [C^5(pz)], 145.3 144.7 [C^3(pz)], 140.6 [C^{10}(naph)], 135.1 [C^2(naph)], 134.7 [C^5(naph)], 130.4 129.0 128.1 [$C^{4,6,9}$(naph)], 126.0 [$C^{3,7,8}$(naph)], 106.8 106.7 [C^4(pz)], 17.6 15.0 12.9 12.8 [pzCH_3]. $^{199}Hg\{^1H\}$ NMR demonstrated a signal at δ_{Hg} = –815.1 [$^2J_{HgW}$ = 1104 Hz]. Furthermore, sequential $^{13}C\{^1H\}$ and $^{199}Hg\{^1H\}$ NMR experiments over 16 hours reveal relative ratios of key resonances remain the same suggesting that symmetrisation occurs prior to isolation. MS (ESI, *m/z*): Found: 879.1762. Calcd for $C_{28}H_{29}{}^{11}B^{202}HgN_6O_2{}^{184}W^{202}Hg$ $[M]^+$: 835.1170. MS spectrum is littered with signals consistent of mercurial dimer. GC–MS identified a positive match for $[(C_{10}H_9)_2]$ when the species was demercurated with 5mol% $[RhCl(CO)(PPh_3)_2]$. Elemental analysis of this compound was not appropriate given the isolated solid is certainly a mixture.

Synthesis of $[WHg(\mu_2\text{-}C)(ppy)(CO)_2(Tp^*)]$ (Mixture) (7.16).

A mixture of $[W(\equiv CSnBu_3)(CO)_2(Tp^*)]$ (0.198 g, 0.236 mmol) and $[HgCl(ppy)]_n$ (0.103 g, 0.263 mmol) was heated in toluene at 80 °C for 6 hours where the initially yellow solution changed to orange before precipitation gave an orange solid. The orange solid was collected *via* vacuum filtration leaving a yellow supernatant phase, washed with toluene (2 × 10 ml) and *n*-hexane (5 × 10 mL) before drying in vacuo for 16 hours. This provided an orange powder containing the title compound as a mixture; this defied further purification and was measured as a mixture of symmetrisation products. While the mixture was analysed by several spectroscopic techniques, many signals measured were unable to be unequivocally assigned, hence only some are listed. IR spectra in the solution and solid-state mirror those of $[W_2Hg(\mu_2\text{-}C)(CO)_4(Tp^*)_2]$ (**7.11b**) know to be present (included in ESI). ^{1}H NMR spectra contain a wealth of signals provided by the

phenylpyridine ring but are unable to be assigned. $^{13}C\{^{1}H\}$ NMR (176 MHz, d_8-toluene, 25ºC, δ): 366.1 [W≡C–Hg]. $^{199}Hg\{^{1}H\}$ NMR (125 MHz, CD_2Cl_2, 25ºC, δ): –813 [t, $^{2}J_{HgW}$ = 1199 Hz]. MS (ESI, *m/z*): Found: 906.1841. Calcd for $C_{29}H_{31}{}^{11}BN_7O_2{}^{184}W^{202}Hg$ $[M+H]^+$: 906.1848.

Attempted synthesis of [WHg(μ$_2$-C)(SC$_4$H$_3$)(CO)$_2$(Tp*)] (Mixture) (7.17).

Note: This species was not isolated as symmetrisation occurs during the reaction. Therefore, key signals are reported with the attempted method, however, this compound is accompanied by symmeterisation products. A sample of [W(≡CSnBu$_3$)(CO)$_2$(Tp*)] (0.202 g, 0.250 mmol) in CH_2Cl_2 (15 mL) was added dropwise to CH_2Cl_2 (30 mL) solution of [HgCl(SC$_4$H$_3$)] (0.075 g, 0.235 mmol) at 0 °C. The resulting yellow/orange solution was stirred at 0 °C (2 hours) before warming to ambient temperature (2 hours) with no additional colour change observed. The yellow solution was injected with *n*-hexane (20 mL) and concentrated under reduced pressure to precipitate a yellow powder leaving a yellow supernatant phase. This solid was collected *via* vacuum filtration and washed with *n*-hexane (3 × 10 mL) before drying *in vacuo* for 3 hours to afford a mixture of species including [W$_2$Hg(μ$_2$-C)$_2$(CO)$_4$(Tp*)$_2$], [Hg(SC$_4$H$_3$)$_2$] and compound **7.17** (140 mg impure material). No crystals suitable for x-ray diffraction were grown despite multiple attempts and a variety of solvent combinations. The species defied further purification with chromatography causing demercuration or decomposition, while fractional crystallisation returned similar mixtures. The obtained yellow solid is a mixture of the target compound and products of symmetrisation about mercury: [W$_2$Hg(μ$_2$-C)(CO)$_4$(Tp*)$_2$] and [Hg(SC$_4$H$_3$)$_2$]. Solution and solid-state infra-red analysis revealed carbonyl stretches that were clean but matched the *bis*-carbido-mercurial [W$_2$Hg(μ$_2$-C)$_2$(CO)$_4$(Tp*)$_2$] yet could not distinguish a second set that may belong to this compound. This compound is in a relatively clean mixture compared with those prior, and subtraction of species allows tentative assignment of NMR signals. ^{1}H NMR (400 MHz, $CDCl_3$, 25 °C, δ): 7.74 [d, $^{1}J_{HH}$ = 5 Hz, 1H, thiopheneCH], 7.44 [m, 1H, thiopheneCH], 7.12 [d, $^{1}J_{HH}$ = 3 Hz, 1H, thiopheneCH], 5.94 [s, 2H, pzCH], 5.74 [s, 1H, pzCH], 2.71 [s, 6H, pzCH$_3$], 2.59 [s, 3H, pzCH$_3$], 2.40 [s, 3H, pzCH$_3$], 2.31 [s, 6H, pzCH$_3$]. $^{13}C\{^{1}H\}$ NMR (600 MHz, $CDCl_3$, 25 °C, δ): 348.5 [W≡C–Hg], 227.2 [$^{1}J_{CW}$ = 173 Hz, CO], 162.4 [$^{3}J_{CW}$ = 27 Hz, C^1(SC$_4$H$_3$)], 152.4 151.6 [C^5(pz)], 145.4 144.8 [C^3(pz)], 135.7 [C^2(SC$_2$H$_3$)], 130.0 [C^4(SC$_4$H$_3$)], 127.6 [C^3(SC$_4$H$_3$)], 106.8 106.7 [C^4(pz)], 17.5 15.4 15.0 12.7 [pzCH$_3$]. $^{199}Hg\{^{1}H\}$ NMR (125 MHz, $CDCl_3$, 25 °C, δ): –780 [$^{2}J_{CW}$ = 1265 Hz]. Sequential $^{13}C\{^{1}H\}$ and $^{199}Hg\{^{1}H\}$ NMR experiments reveal relative ratios of key resonances remain the same, thus suggesting that symmetrisation occurs prior to isolation. MS (ESI, *m/z*): Found: 835.114111. Calcd for $C_{22}H_{26}{}^{11}B^{202}HgN_6O_2{}^{32}S^{184}W$ $[M+H]^+$: 835.1170. MS spectrum is also filled with signals consistent of mercury halo bridged dimer. GC–MS identified a

positive match for [$(SC_4H_3)_2$] when the species was demercurated with 5mol% [$RhCl(CO)(PPh_3)_2$]. Elemental analysis of this compound was not appropriate given the isolated solid is certainly a mixture.

Synthesis of [$WHg(\mu_2\text{-}C)(S_2CNMe_2)(CO)_2(Tp^*)$] (7.18).

Samples of [$W(\equiv CSnBu_3)(CO)_2(Tp^*)$] (1.079g, 1.286 mmol) and [$HgCl(S_2CNMe_2)$] (420 mg, 1.17 mmol) were dissolved in CH_2Cl_2 (30 mL) and stirred for 16 hours such that the initially yellow solution changed to a bright orange colour. After the reaction conclusion, the solvent was eluted through a thin pad of celite such that elemental mercury was not present in the orange filtrate. This filtrate was combined with *n*-hexane (10 mL) concentration on a rotary evaporator to give a yellow powder subsequently collected *via* vacuum filtration, washed with *n*-hexane (2 × 10 mL) and *n*-pentane (10 mL) before drying *in vacuo* for 2 hours to give the title compound as a fine yellow powder (741 mg, 0.850 mmol, 73% isolated yield). Crystals suitable for X-ray diffraction were grown from the slow diffusion of Et_2O into a THF solution of the compound at 0 °C. IR (CH_2Cl_2): 1981 vs ν_{CO}, 1890 vs ν_{CO} cm^{-1}. IR (ATR): 2589 w ν_{BH}, 2527 w ν_{BH}, 1966 vs ν_{CO}, 1868 vs ν_{CO}. ^1H NMR (600 MHz, $CDCl_3$, 25 ºC, δ): 5.91 (s, 2H, pzCH), 5.74 (s, 1H, pzCH), 3.43 (s, 6H, S_2CNCH_3), 2.66 (s, 6H, $pzCH_3$), 2.40 (s, 3H, $pzCH_3$), 2.36 (s, 6H, $pzCH_3$), 2.30 (s, 3H, $pzCH_3$). $^{13}C\{^1H\}$ NMR (151 MHz, $CDCl_3$, 25ºC, δ): 322.0 [br, W≡C–Hg], 226.2 [$^1J_{CW}$ = 173 Hz, CO], 203.6 [S_2CNCH_3], 152.4 151.8 [C^5(pz)], 145.3 144.6 [C^3(pz)], 106.7 [C^4(pz)], 46.1 [S_2CNCH_3], 17.2 15.1 12.8 12.7 [$pzCH_3$]. Two carbido resonances were detected in the $^{13}C\{^1H\}$ NMR: one is sharp from linear dithiocarbamate coordination to mercury and the other is broadened as a consequence of the mercury shuttling between sulfur donors. $^{199}Hg\{^1H\}$ NMR (71.6 MHz, $CDCl_3$, 25ºC, δ): –894.1 [br]. MS (ESI, *m/z*): Found: 894.0930. Calcd for $C_{21}H_{28}{}^{11}BN_7O_2{}^{23}NaS_2{}^{184}W^{202}Hg$ $[M+H+Na]^+$: 894.0952. Anal. Found: C, 29.16; H, 3.259; N, 11.11%. Calcd for $C_{21}H_{28}BHgN7O_2S_2W$: C, 29.00; H, 3.240; N, 11.27%. An imprecise dataset was able to be collected however the structure should only illustrate connectivity.*** *Crystal data for* $C_{21}H_{28}BHgN_7O_2S_2W{\cdot}C_4H_4O$, M = 937.94, orthorhombic, $Pca2_1$, a = 19.4509(2) Å, b = 10.2865(1) Å, c = 15.9024(2) Å, V = 3181.78(6) $Å^3$, Z = 4, ρ_{calc} = 1.958 Mgm^{-3}, μ(Cu $K\alpha$) = 16.65 mm^{-1}, T = 150(0) K, needle, 0.08 × 0.03 × 0.02 mm {clear light yellow}, 5004 independent measured reflections (θ = 62.6), R_1 = 0.047, wR_2 = 0.088 for 4847 reflections [$I > 2\sigma(I)$], 369 parameters. Imprecise structure was not uploaded to CCDC.

Synthesis of [$W(\equiv C\text{–}SC_4H_3)(CO)_2(Tp^*)$] (7.19).

*** Data originally collected by Dr. Manab Sharma but was processed and modelled by the author.

Samples of [W(≡CSnBu$_3$)(CO)$_2$(Tp*)] (0.200 g, 0.238 mmol) and [HgCl(SC$_4$H$_3$)] (0.078 g, 0.244 mmol) were dissolved in CH_2Cl_2 (10 mL) and stirred for 3 hours beginning as yellow and changing to orange by 30 minutes. Next, [RhCl(CO)(PPh$_3$)$_2$] (0.009 g, 0.013 mmol, 5 mol%) was added resulted in precipitation of black solid over 16 hours yet retaining the orange solution. The solution was filtered through celite removing amorphous mercury and purified by flash column chromatography {silica gel, N_2, 20% CH_2Cl_2/petroleum spirit, isocratic} where the second eluate was orange and evaporated to an orange powder. The powder resisted recrystallisation from a variety of organic solvents and instead was dried *in vacuo* for 16 hours to give the title compound as a pink/orange powder (0.058 g, 0.092 mmol, 39% isolated yield). Crystals suitable for X-ray diffraction studies were not forthcoming despite multiple attempts and solvent combinations. IR (CH_2Cl_2, cm^{-1}): 1974 vs ν_{CO}, 1884 vs ν_{CO}. IR (ATR, cm^{-1}): 2545 w ν_{BH}, 1963 vs ν_{CO}, 1873 vs ν_{CO}. ^{1}H NMR (600 MHz, $CDCl_3$, 25 ºC, δ): 7.18 [m, 2H, thiopheneCH], 6.91 [m, 1H, thiopheneCH], 5.89 [s, 2H, pzCH], 5.78 [s, 1H, pzCH], 2.56 [s, 6H, pzCH$_3$], 2.43 [s, 3H, pzCH$_3$], 2.37 [s, 6H, pzCH$_3$], 2.34 [s, 3H, pzCH$_3$]. ^{13}C{^{1}H} NMR (151 MHz, $CDCl_3$, 25ºC, δ): 262.2 [W≡C], 224.1 [$^1J_{CW}$ = 165 Hz, CO], 154.9 [$^2J_{CW}$ = 49 Hz, C^2(SC$_4$H$_3$)], 152.5 [C^5(pz)], 145.3 144.6 [C^3(pz)], 129.1 [C^2(SC$_4$H$_3$)], 126.5 [C^4(SC$_4$H$_3$)], 125.9 [C^3(SC$_4$H$_3$)], 106.8 106.7 [C^4(pz)], 16.8 15.4 12.8 [pzCH$_3$]. MS (ESI, *m/z*): Found: 633.1431. Calcd for $C_{22}H_{26}{}^{11}BN_6O_2{}^{32}S^{184}W$ [M+Na]$^+$: 633.14348. Anal. Found: C, 41.84; H, 3.97; N, 13.34; S, 5.00%. Calcd for $C_{22}H_{25}BN_6O_2SW$: C, 41.80; H, 3.99; N, 13.29; S, 5.07%.

9.10 Synthetic procedures for Chapter Eight compounds

Synthesis of [WPt(μ$_2$-C)(S$_2$CNMe$_2$)(CO)$_2$(PPh$_3$)(Tp*)] (8.1).

A sample of [WHg(μ$_2$-C)(S$_2$CNMe$_2$)(CO)$_2$(Tp*)] (**7.18**; 102 mg, 0.117 mmol) and [Pt(η^2-C$_2$H$_4$)(PPh$_3$)$_2$] (87 mg, 0.12 mmol) were dissolved in THF (10 mL) and heated at 60 °C with stirring for 16 hours, noting elemental mercury was extruded during the reaction. The mixture was initially eluted through celite to remove elemental mercury, before evaporating the filtrate by rotary evaporation. The ensuing residue was purified by flash column chromatography {silica gel, N_2, THF/CH_2Cl_2 gradient} eluting a major yellow compound with 2% THF/CH_2Cl_2 as eluent. A recrystallisation from the evaporation of CH_2Cl_2 into *n*-hexane by rotary evaporation gave a yellow solid which was collected *via* vacuum filtration and washed with *n*-hexane (2 × 10 mL) and *n*-pentane (10 mL) before drying *in vacuo* for 3 hours to afford compound **8.1** as a fine yellow powder (46 mg, 0.041 mmol, 35% isolated yield). Crystals suitable for X-ray diffraction studies were grown from the vapour diffusion of methanol into a $CHCl_3$ solution of compound at 5 °C. IR (CH_2Cl_2, cm^{-1}): 1935 vs ν_{CO}, 1843 vs ν_{CO}. IR (ATR): 2524 w ν_{BH}, 1930 vs ν_{CO}, 1833 vs ν_{CO} cm^{-1}. ^{1}H NMR (400 MHz, $CDCl_3$, 25 ºC, δ): 7.44 [m, $^1J_{HH}$ = 12, 8 Hz, 6H, PPh], 7.21 [t, $^1J_{HH}$ = 8 Hz, 3H, PPh], 7.01

[m, 6H, PPh], 5.62 [s, 1H, pzCH], 5.58 [s, 2H, pzCH], 3.34 [s, 3H, S_2CNCH_3], 3.13 [s, 3H, S_2CNCH_3], 2.37 [s, 15H, $pzCH_3$], 2.25 [s, 3H, $pzCH_3$]. $^{13}C\{^1H\}$ NMR (151 MHz, $CDCl_3$, 25ºC, δ): 336.9 [m, W≡C–Pt], 227.0 [$^1J_{CW}$ = 175 Hz, CO], 209.8 [S_2CNMe_2], 152.2 151.7 [C^5(pz)], 144.1 143.1 [C^3(pz)], 134.4 [d, $^2J_{CP}$ = 12 Hz, $C^{2,6}(C_6H_5)$], 130.6 [$C^4(C_6H_5)$], 130.2 [d, $^1J_{CP}$ = 58 Hz, $C^1(C_6H_5)$], 127.8 [d, $^3J_{CP}$ = 12 Hz, $C^{3,5}(C_6H_5)$], 106.3 105.9 [C^4(pz)], 39.8 39.0 [$S_2CN(CH_3)$], 16.5 15.4 12.8 12.6 [$pzCH_3$]. $^{31}P\{^1H\}$ NMR (162 MHz, $CDCl_3$, 25 ºC, δ): 13.34 [s, $^1J_{PPt}$ = 3920 Hz]. $^{195}Pt\{^1H\}$ NMR (85.7 MHz, $CDCl_3$, 25ºC, δ): –3853 [d, $^1J_{PtP}$ = 3923 Hz]. MS (ESI, *m/z*): Found: 1127.1940. Calcd for $C_{39}H_{44}{}^{11}BN_7O_2P^{195}Pt^{32}S_2{}^{184}W$ $[M+H]^+$: 1127.1918. Anal. Found: C, 41.47; H, 3.693; N, 8.74; S, 5.639 %. Calcd for $C_{39}H_{43}BN_7O_2PPtS_2W$: C, 41.58; H, 3.85; N, 8.70; S, 5.69 %. *Crystal data for* $C_{39}H_{43}BN_7O_2PPtS_2W$, M = 1126.64, triclinic, $P\bar{1}$, a = 11.853 (2) Å, b = 16.968 (3) Å, c = 20.973 (4) Å, α = 84.89 (3)°, β = 89.85 (3)°, γ = 82.98 (3)°, V = 4169.8 (15) $Å^3$, Z = 4, ρ_{calc} = 1.795 Mgm^{-3}, μ(Synchrotron; λ =0.71073 Å) = 6.29 mm^{-1}, T = 100(0) K, needle 0.10 × 0.05 × 0.02 mm {clear light yellow}, 13432 independent measured reflections (θ = 25.4°), R_1 = 0.126, wR_2 = 0.334 for 10930 reflections [$I > 2\sigma(I)$], 990 parameters, 2 restraints. CDCC 2251874.

Synthesis of [WPd(μ$_2$-C)(S_2CNMe_2)(CO)$_2$(PPh_3)(Tp*)] (8.2).

A sample of [WHg(μ$_2$-C)(S_2CNMe_2)(CO)$_2$(Tp*)] (**7.18**; 0.100 g, 0.115 mmol) and [Pd(PPh_3)$_4$] (0.146 g, 0.126 mmol) was stirred in THF (10 mL) for 16 hours at 60 ºC. The mixture began with a rapid colour change to orange and lightened while depositing elemental mercury. Upon cooling, the removal of solvent under reduced pressure gave an orange/brown residue that could be purified by anaerobic flash column chromatography {silica gel, N_2, *n*-hexane/CH_2Cl_2 gradient}. Initially eluting a blue/green band at 50% CH_2Cl_2/*n*-hexane, a bright yellow band trailed in 80% CH_2Cl_2/*n*-hexane, which could be concentrated under reduced pressure to give a pastel yellow solid. This solid was collect *via* vacuum filtration and washed with *n*-hexane (3 × 10 mL) before drying *in vacuo* for 16 hours to afford compound **8.2** as a fine yellow powder (0.040 g, 0.039 mmol, 34% isolated yield). Crystals suitable for X-ray diffraction were grown from the slow vapour diffusion of Et_2O into a $CHCl_3$ solution of **8.2** at 0 °C over two nights. IR (CH_2Cl_2, cm^{-1}): 1944 vs ν_{CO}, 1852 vs ν_{CO}. IR (ATR, cm^{-1}): 2527 w ν_{BH}, 1934 vs ν_{CO}, 1842 vs ν_{CO}. ^1H NMR (600 MHz, $CDCl_3$, 25 ºC, δ): 7.43 [dd; J_{HH} = 12, 8 Hz; 6H, PPh], 7.22 [t, J_{HH} = 8 Hz, 3H, PPh], 7.02 [t, J_{HH} = 8 Hz, 6H, PPh], 5.63 [s, 1H, pzCH], 5.59 [s, 2H, pzCH], 3.41 [s, 3H, S_2CNCH_3], 3.19 [s, 3H, S_2CNCH_3], 2.37 [overlapping s, 6H, $pzCH_3$], 2.37 [overlapping s, 3H, $pzCH_3$], 2.35 [s, 6H, $pzCH_3$], 2.25 [s, 3H, $pzCH_3$]. $^{13}C\{^1H\}$ NMR (151 MHz, $CDCl_3$, 25ºC, δ): 350.0 [d, $^2J_{CP}$ = 15 Hz, $^1J_{CW}$ = 148 Hz, W≡C–Pd], 226.9 [$^1J_{CW}$ = 177 Hz, CO], 210.0 [S_2CNMe_2], 152.3 151.6 [C^5(pz)], 144.3 143.2 [C^3(pz)], 134.5

[d, $^{2}J_{CP}$ =12 Hz, $C^{2,6}(C_6H_5)$], 130.9 [d, $^{1}J_{CP}$ = 45 Hz, $C^{1}(C_6H_5)$], 130.4 [d, $^{4}J_{CP}$ = 3 Hz, $C^{4}(C_6H_5)$], 128.0 [d, $^{3}J_{CP}$ = 11 Hz, $C^{3,5}(C_6H_5)$], 106.3 106.0 [C^{4}(pz)], 39.8 39.2 [S_2CNCH_3], 16.8 15.4 12.8 12.7 [$pzCH_3$]. $^{31}P\{^{1}H\}$ NMR (162 MHz, $CDCl_3$, 25 ºC, δ): 24.89 [s, $^{1}J_{PW}$ = 22 Hz]. MS (ESI, *m/z*): Found: 1038.1352. Calcd for $C_{39}H_{44}{}^{11}BN_7O_2P^{106}Pd^{32}S_2{}^{184}W$ $[M+H]^+$: 1038.1345. Anal. Found: C, 45.16; H, 4.101; N, 9.20; S, 6.292 %. Calcd for $C_{39}H_{543}BN_7O_2PPdS_2W$: C, 45.13; H, 4.18; N, 9.45; S, 6.18 %. *Crystal data for* $C_{39}H_{43}BN_7O_2PPdS_2W{\cdot}C_4H_{10}O$, M = 1112.07, Triclinc, $P\bar{1}$, a = 10.0841 (3) Å, b = 16.0178 (4) Å, c = 16.3326 (5) Å, α = 112.969 (2)°, β = 107.083 (2)°, γ = 92.631 (2)°, V = 2282.84 (12) Å^3, Z = 2, ρ_{calc} = 1.618 Mgm^{-3}, μ(Cu *K*α) = 9.32 mm^{-1}, T = 150 (0) K, plate 0.59 × 0.22 × 0.06 mm {clear light yellow}, 8915 independent measured reflections (θ = 73.6), R_1 = 0.035, wR_2 = 0.095 for 8559 reflections [$I > 2\sigma(I)$], 536 parameters. CDCC 2251869.

Synthesis of [WIr(μ$_2$-C)Cl(S_2CNMe_2)(CO)$_2$(PPh_3)(Tp*)] (8.3).

A sample of [WHg(μ$_2$-C)(S_2CNMe_2)(CO)$_2$(Tp*)] (**7.18**; 120 mg, 0.135 mmol) and [IrCl(CO)(PPh_3)$_2$] (103 mg, 0.132 mmol) was suspended in toluene (15 mL) to give a yellow/orange mixture. This was stirred with heating at 80 °C for 16 hours, in which the colour darkened to orange (~2 hours) before transitioning back to yellow (~8 hours). After reaction completion, a yellow mixture ensued accompanied by elemental mercury deposits. The solvent was removed under reduced pressure to give a yellow/orange residue that could be purified by flash column chromatography {silica gel, N_2, CH_2Cl_2/petroleum ether gradient}. Neat CH_2Cl_2 eluted a bright yellow band that could be recrystallised from concentration of CH_2Cl_2 into *n*-hexane by rotary evaporation to give a yellow powder. This powder was collected *via* vacuum filtration and washed with *n*-hexane (3 × 10 mL) before drying *in vacuo* for 16 hours to afford the title complex as a yellow microcrystalline powder (118 mg, 0.0990 mmol, 75% isolated yield. Crystals suitable for X-ray diffraction studies were grown from the slow vapour diffusion of *n*-hexane into a $CHCl_3$ solution of the compound at 0 °C. IR (CH_2Cl_2, cm^{-1}): 2057 vs ν_{CO}, 1943 vs ν_{CO}, 1851 vs ν_{CO}. IR (ATR, cm^{-1}): 2548 w ν_{BH}, 2532 w ν_{BH}, 2058 vs ν_{CO}, 1937 vs ν_{CO}, 1847 vs ν_{CO}. ^{1}H NMR (600 MHz, $CDCl_3$, 25 ºC, δ): 7.51 [m, 6H, PPh], 7.23 [t, $^{1}J_{HH}$ = 8 Hz, 3H, PPh], 7.02 [m, 6H, PPh], 5.76 [s, 1H, pzCH], 5.66 [s, 1H, pzCH], 5.63 [s, 1H, pzCH], 3.21 [s, 3H, S_2CNCH_3], 3.12 [s, 3H, S_2CNCH_3], 2.43 [s, 3H, $pzCH_3$], 2.42 [s, 3H $pzCH_3$], 2.40 [s, 3H, $pzCH_3$], 2.27 [s, 6H, $pzCH_3$], 2.13 [s, 3H, $pzCH_3$]. $^{13}C\{^{1}H\}$ NMR (151 MHz, $CDCl_3$, 25ºC, δ): 300.5 [d; $^{2}J_{CP}$ = 4 , $^{1}J_{CW}$ = 184 Hz; W≡C–Ir], 227.6 [s, $^{1}J_{CW}$ = 177 Hz, W–CO], 223.9 [s, $^{1}J_{CW}$ = 179 Hz, W–CO], 208.3 [$S_2CN(CH_3)_2$], 163.2 [d, $^{2}J_{CP}$ = 8 Hz, Ir–CO], 152.5 151.9 151.3 [C^{5}(pz)], 144.2 143.9 143.7 [C^{3}(pz)], 134.5 [d, $^{2}J_{CP}$ = 10 Hz, $C^{2,6}(C_6H_5)$], 131.1 [d, $^{4}J_{CP}$ = 3 Hz, $C^{4}(C_6H_5)$], 128.5 [d, $^{1}J_{CP}$ = 57 Hz, $C^{1}(C_6H_5)$], 127.9 [d,

$^{3}J_{CP}$ = 11 Hz, $C^{3,5}(C_6H_5)$], 106.4 106.3 [C^4(pz)], 38.2 37.8 [$S_2CN(CH_3)_2$], 18.2 16.8 15.5 13.0 12.9 12.7 [pzCH_3]. $^{31}P\{^1H\}$ NMR (162 MHz, $CDCl_3$, 25 °C, δ): –12.47 [s, Ir–P]. MS (ESI, *m/z*): Found: 1152.1864. Calcd for $C_{40}H_{43}{}^{11}B^{193}IrN_7O_3P^{32}S_2{}^{184}W$ $[M–Cl]^+$: 1152.1838. Anal. Found: C, 40.47; H, 3.599; N, 8.31; S, 5.042 %. Calcd for $C_{40}H_{43}BClIrN_7O_3PS_2W$: C, 40.47; H, 3.65; N, 8.26; S, 5.40 %. *Crystal data for* $C_{40}H_{43}BClIrN_7O_3PS_2W{\cdot}2(CHCl_3)$, M = 1425.95, monoclinic, $P2_1/n$, a = 17.9871(6) Å, b = 18.4128(4) Å, c = 18.2601(6) Å, β = 118.531(4)°, V = 5313.2(2) Å^3, Z = 4, ρ_{calc} = 1.783 Mgm^{-3}, μ(Cu $K\alpha$) = 13.34 mm^{-1}, T = 150(0) K, plate, 0.08 × 0.08 × 0.03 mm {clear light yellow}, 9718 independent measured reflections (θ = 73.7), R_1 = 0.040, wR_2 = 0.105 for 8498 reflections [$I > 2\sigma(I)$], 594 parameters. CDCC 2251873.

Synthesis of [WRh(μ$_2$-C)Cl(S_2CNMe_2)$(CO)_3(PPh_3)$(Tp*)] (8.4).

A sample of [WHg(μ$_2$-C)(S_2CNMe_2)$(CO)_2$(Tp*)] (**7.18**; 263 mg, 0.296 mmol) and [RhCl(CO)$(PPh_3)_2$] (208 mg, 0.301 mmol) was dissolved in CH_2Cl_2 (10 mL) to give a yellow solution that quickly darkened to yellow/orange.[†††] Stirring was continued for 16 hours at to return a light orange solution accompanied by deposition of elemental mercury. The solvent was removed under reduced pressure to give an orange residue which could be purified by flash column chromatography {silica gel, N_2, neat CH_2Cl_2 then 2% THF/CH_2Cl_2}, eluting a major orange compound before solvent was removed under reduced pressure. A recrystallisation from the evaporation of CH_2Cl_2 into EtOH by rotary evaporation gave an orange solid which could be collected *via* vacuum filtration, washed with EtOH (2 × 10 mL) and *n*-hexane (10 mL), before drying *in vacuo* for 3 hours to afford compound **8.4** as a fine orange powder (150 mg, 0.137 mmol, 46% yield). Crystals suitable for X-ray diffraction were grown from the slow vapour diffusion of *n*-hexane into a $CHCl_3$ solution of the compound at 0 °C. IR (CH_2Cl_2, cm^{-1}): 2085 vs ν_{CO}, 1949 vs ν_{CO}, 1858 vs ν_{CO}. IR (ATR, cm^{-1}): 2534 w ν_{BH}, 2085 vs ν_{CO}, 1943 vs ν_{CO}, 1855 vs ν_{CO}. ^{1}H NMR (700 MHz, $CDCl_3$, 25 °C, δ): 7.55 [m, 6H, PPh], 7.24 [s, 3H, PPh], 7.01 [m, 6H, PPh], 5.74 [s, 1H, pzCH], 5.66 [s, 2H, pzCH], 3.27 [s, 3H, S_2CNCH_3], 3.20 [s, 3H, S_2CNCH_3], 2.42 [s, 6H, pzCH_3], 2.40 [s, 3H, pzCH_3], 2.26 [s, 3H, pzCH_3], 2.19 [s, 3H, pzCH_3], 2.12 [s, 3H, pzCH_3]. $^{13}C\{^1H\}$ NMR (176 MHz, $CDCl_3$, 25°C, δ): 311.8 [dd, $^1J_{CRh}$ = 27; $^2J_{CP}$ = 8 Hz, W≡C–Rh], 227.4 [$^1J_{CW}$ = 171 Hz, W–CO], 224.3 [$^1J_{CW}$ = 175 Hz, W–CO], 207.1 [d, $^2J_{CRh}$ = 4 Hz, S_2CNCH_3], 183.6 [dd, $^1J_{CRh}$ = 61; $^2J_{CP}$ = 12 Hz, Rh–CO], 152.5 152.3 151.3 [C^5(pz)], 144.4 143.9 143.8 [C^3(pz)], 134.5 [d, $^2J_{CP}$ = 9 Hz, $C^{2,6}(C_6H_5)$], 130.9 [d, $^4J_{CP}$ = 2 Hz, $C^4(C_6H_5)$], 129.4 [d, $^1J_{CP}$ = 48 Hz, $C^1(C_6H_5)$], 127.9 [d, $^3J_{CP}$ = 11 Hz, $C^{3,5}(C_6H_5)$], 106.5 106.43 106.37 [C^4(pz)], 38.0 37.8 [S_2CNCH_3], 18.0 17.1 15.5 12.94 12.93

[†††] Note that concentrated NMR test experiments result in a colour change to a deep red colour, highlighting an intermediate.

12.69 [pzCH_3]. $^{31}P\{^1H\}$ NMR (162 MHz, $CDCl_3$, 25 ºC, δ): 20.20 [d, $^1J_{PRh}$ = 112 Hz]. MS (ESI, *m/z*): Found: 1062.1270. Calcd for $C_{40}H_{43}{}^{11}BN_7O_3PS_2{}^{103}Rh{}^{183}W$ $[M–Cl]^+$: 1062.1264. Anal. Found: C, 43.83; H, 4.075; N, 8.60%. Calcd for $C_{40}H_{43}BClN_7O_3PRhS_2W$: C, 43.76; H, 3.95; N, 8.93%. *Crystal data for* $C_{40}H_{43}BClN_7O_3PRhS_2W$, M = 1097.92, triclinic, $P\bar{1}$, a = 10.8974(3) Å, b = 13.1501(3) Å, c = 19.2395(4) Å, α = 98.907(2)°, β = 13.1501(2)°, γ = 93.982(2), V = 2658.11(11) Å^3, Z = 2, ρ_{calc} = 1.372 Mgm^{-3}, μ(Cu $K\alpha$) = 8.24 mm^{-1}, T = 150(0) K, plate, 0.11 × 0.07 ×0.04 mm {clear light orange}, 9988 independent measured reflections (θ = 73.4), R_1 = 0.0287, wR_2 = 0.071 for 8817 reflections [$I > 2\sigma(I)$], 523 parameters. CDCC 2251871.

Synthesis of [WRu(μ$_2$-C)(S_2CNMe_2)$(CO)_4(PPh_3)$(Tp*)] (8.5).

A sample of [WHg(μ$_2$-C)(S_2CNMe_2)$(CO)_2$(Tp*)] (**7.18**; 0.190 g, 0.218 mmol) and [Ru$(CO)_2(PPh_3)_3$] (0.210 g, 0.222 mmol) was refluxed in CH_2Cl_2 (30 mL) for 4 hours. The yellow solution darkened to orange within 30 minutes and amorphous mercury solids deposited after 1 hour. The orange solution was concentrated (*ca* 3 mL) and loaded onto a flash column anaerobically. Flash chromatography {silica gel, N_2, neat CH_2Cl_2 then 2% THF/CH_2Cl_2} was performed, eluting a major yellow compound {2% THF/CH_2Cl_2} before removing solvent under reduced pressure. A recrystallisation from the concentration of CH_2Cl_2 into *n*-hexane under reduced pressure gave a yellow solid which could be collected *via* anaerobic vacuum filtration. The solid was washed with *n*-hexane (3 × 10 mL) before drying *in vacuo* for 3 hours to afford compound **8.5** as a fine yellow powder (0.027 g, 0.025 mmol, 11% yield). Crystals suitable for x-ray diffraction were grown from the slow evaporation of a benzene solution at ambient temperature. IR (CH_2Cl_2, cm^{-1}): 2058 vs ν_{CO}, 1986 vs ν_{CO}, 1929 vs ν_{CO}, 1840 vs ν_{CO}. IR (ATR, cm^{-1}): 2532 w ν_{BH}, 2049 vs ν_{CO}, 1923 vs ν_{CO}, 1836 vs ν_{CO}. ^1H NMR (600 MHz, $CDCl_3$, 25 ºC, δ): 7.54 [m, 6H, PPh], 7.20 [m, 3H, PPh], 6.94 [m, 6H, PPh], 5.82 [s, 1H, pzCH], 5.67 [s, 1H, pzCH], 5.55 [s, 1H, pzCH], 2.93 [s, 3H, S_2CNCH_3], 2.73 [s, 3H, S_2CNCH_3], 2.57 [s, 3H, pzCH_3], 2.47 [s, 3H, pzCH_3], 2.43 [s, 3H, pzCH_3], 2.37 [s, 3H, pzCH_3], 2.30 [s, 3H, pzCH_3], 2.27 [s, 3H, pzCH_3]. $^{13}C\{^1H\}$ NMR (151 MHz, $CDCl_3$, 25ºC, δ): 367.9 [d, $^2J_{CP}$ = 8 Hz, W≡C–Ru], 226.4 226.1 [W–CO], 210.2 [Ru–CO], 208.5 [S_2CNMe_2], 197.4 [d, $^2J_{CP}$ = 14 Hz, Ru–CO], 191.5 [d, $^2J_{CP}$ = 109 Hz, Ru–CO], 152.5 151.6 150.9 [C^5(pz)], 144.2 143.7 143.7 143.3 [C^3(pz)], 134.9 [d, $^2J_{CP}$ = 10 Hz, $C^{2,6}(C_6H_5)$], 130.5 [d, $^1J_{CP}$ = 41 Hz, $C^1(C_6H_5)$], 130.0 [$C^4(C_6H_5)$], 127.1 [d, $^3J_{CP}$ = 10 Hz, $C^{3,5}(C_6H_5)$], 106.2 106.1 105.7 [C^4(pz)], 39.4 38.8 [$S_2CN(CH_3)$], 18.0 17.1 15.6 13.0 12.8 12.7 [pzCH_3]. Some impurities are visible in this spectrum as it was measured directly from the eluent of a column. $^{31}P\{^1H\}$ NMR (162 MHz, $CDCl_3$, 25 ºC, δ): 20.34 [s, PPh_3]. MS (ESI, *m/z*): Found: 1090.1260. Calcd for $C_{41}H_{44}{}^{11}BN_7O_4P{}^{102}Ru{}^{32}S_2{}^{184}W$

$[M+H]^+$: 1090.1280. Anal. Found: C, 45.37; H, 4.14; N, 8.93; S, 5.12%. Calcd for $C_{41}H_{43}BN_7O_4PRuS_2W$: C, 45.23; H, 3.98; N, 9.01; S, 5.88%. *Crystal data for* $C_{41}H_{43}BN_7O_4PRuS_2W{\cdot}C_6H_6$, M = 1166.75, triclinic, $P\bar{1}$, a = 12.4812 (3) Å, b = 13.3721 (3) Å, c = 17.0334 (6) Å, α = 98.855 (2)°, β = 98.636 (1)°, γ = 115.722 (2)°, V = 2494.20 (13) Å^3, Z = 2, ρ_{calc} = 1.554 Mgm^{-3}, μ(Cu $K\alpha$) = 8.13 mm^{-1}, T = 150(0) K, plate 0.15 × 0.10 × 0.03 mm {clear light yellow}, 9096 independent measured reflections (θ = 68.3°), R_1 = 0.041, wR_2 = 0.093 for 7602 reflections [$I > 2\sigma(I)$], 585 parameters. CDCC 2251872.

Synthesis of [WOs(μ$_2$-C)Cl(CO)$_3$(PPh$_3$)$_2$(Tp*)] (8.6).

A sample of [W$_2$Hg(μ$_2$-C)(CO)$_4$(Tp*)$_2$] (**7.11b**; 0.500 g, 0.385 mmol) and [OsHCl(CO)(PPh$_3$)$_3$] (0.400, 0.384 mmol) were suspended in chlorobenzene (25 mL) and heated at 120 °C for 8 hours, where the orange solid slowly went into solution to form a dark maroon supernatant phase with the deposition of elemental mercury. The mixture was cooled and evaporated under reduced pressure, requiring heating (50 °C) for efficient removal of chlorobenzene, eventually returning maroon residue. The residue was dissolved in CH_2Cl_2 (10 mL) and filtered through celite before EtOH (5 mL) was added and concentrated under reduced pressure (*ca* 8 mL) to give a marron solid and yellow supernatant phase. Ultrasonication assisted in liberating more precipitate that adhered to the surface and in solution. *Note the following order of solvent used for washing; deviation results in gross decomposition and poor yields.* The maroon solid was collected *via* vacuum filtration and washed with minimal EtOH (3 × 5 mL), MeOH (3 × 5 mL), cold EtOH (2 × 5 mL), and finally, cold Et_2O (2 × 5 mL). This method obtained a purple powder that was subsequently dried *in vacuo* for 16 hours to give the title compound as a vivid purple microcrystalline solid (0.814 g, 0.613 mmol, 80% isolated yield). Crystals suitable for X-ray diffraction were grown from the vapour diffusion of *n*-hexane into a solution of toluene solution of compound in the presence of excess PPh_3 over three days 5 °C. IR (CH_2Cl_2, cm^{-1}): 1952 vs $\nu_{W\text{-}CO}$, 1912 vs $\nu_{Os\text{-}CO}$, 1833 vs $\nu_{W\text{-}CO}$. IR (ATR, cm^{-1}): 2533 w ν_{BH}, 1945 vs $\nu_{W\text{–}CO}$, 1906 vs $\nu_{Os\text{–}CO}$, 1824 vs $\nu_{W\text{–}CO}$. ^{1}H NMR (700 MHz, $CDCl_3$, 25 ºC, δ): 8.09–7.64 [br, 6H, PPh], 7.48–7.29 [br, 12H, PPh], 7.20–6.93 [br, 12H, PPh], 5.62 [br.s, 2H, pzCH], 5.54 [s, 1H, pzCH], 2.45 [s, 9H, pzCH$_3$], 2.26 [s, 3H, pzCH$_3$], 2.24 [s, 6H, pzCH$_3$]. ^{1}H NMR (700 MHz, $CDCl_3$, –20 ºC, δ): 8.14 [br.m, 4H, PPh], 7.47 [m, 14H, PPh], 7.07 [br.m, 6H, PPh], 6.96 [br.m, 6H, PPh], 5.71 [s, 1H, pzCH], 5.55 [s, 2H, pzCH], 2.47 [s, 3H, pzCH$_3$], 2.41 [s, 3H, pzCH$_3$], 2.32 [s, 3H, pzCH$_3$], 2.26 [s, 3H, pzCH$_3$], 2.23 [s, 3H, pzCH$_3$], 1.69 [s, 3H, pzCH$_3$]. ^{1}H NMR (400 MHz, d_8-toluene, 25ºC, δ): 8.39–7.23 [br.m, 15H, PPh], 7.21–7.00 [br.m, 15H, PPh], 5.53 [br.s, 2H, pzCH], 5.26 [s, 1H, pzCH], 2.46 [s, 3H, pzCH$_3$], 2.36 [s, 6H, pzCH$_3$], 2.10 [s, overlaps solvent, 6H, pzCH$_3$], 1.98 [s, 3H, pzCH$_3$]. ^{13}C{^{1}H} NMR (151 MHz, $CDCl_3$, 25ºC, δ): 316.6 [$^1J_{CW}$ = 187 Hz,

W≡C–Os], 229.4 [br, W–CO], 179.9 [t^{v}, J_{CP} = 9 Hz, Os–CO], 153.6 152.3 [C^5(pz)], 143.7 [br.s, C^3(pz)], 135.1 131.7 130.4 128.2 [br, C_6H_5], aryl resonances cannot be unequivocally assigned due to broadening, 106.5 105.8 [C^4(pz)], 22.3 15.4 13.1 12.6 [pzCH_3]. $^{13}C\{^1H\}$ NMR (201 MHz, $CDCl_3$, –20ºC, δ): 317.0 [br.m, W≡C–Os], 229.6 227.5 [W–CO], 179.7 [br.m, Os–CO], 153.3 152.2 [C^5(pz)], 143.9 143.7 143.3 [C^3(pz)], 136.2 134.7 134.3 131.8 130.9 130.0 128.8 127.8 [br.m, C_6H_5], aryl resonances cannot be unequivocally assigned due to broadening, 106.4 106.3 105.7 [C^4(pz)], 22.14 17.0 15.5 15.4 13.2 12.8 [pzCH_3]. $^{31}P\{^1H\}$ NMR (162 MHz, $CDCl_3$, 25 ºC, δ): 10.44 [br.m, PPh]. $^{31}P\{^1H\}$ NMR (162 MHz, d_8-toluene, 25 ºC, δ): 11.29 [s, Os–PPh_3]. MS (ESI, *m*/*z*): Found: 1293.2822. Calcd for $C_{55}H_{52}{}^{11}BN_6O_3P_2{}^{184}W^{192}Os$ $[M–Cl]^+$: 1293.2793. Anal. Found: C, 49.64; H, 4.02; N, 6.61%. Calcd for $C_{55}H_{52}BClN_6O_3OsP_2W$: C, 49.77; H, 3.95; N, 6.33%. *Crystal data for* $C_{55}H_{52}BClN_6O_3OsP_2W$, M = 1327.27, triclinic, $P\bar{1}$, a = 11.2461 (3) Å, b = 16.0018 (4) Å, c = 19.7315 (5) Å, α = 89.137 (2)°, β = 74.816 (2)°, γ = 77.623 (2)°, V = 3344.05 (15) Å^3, Z = 2, ρ_{calc} = 1.318 Mgm^{-3}, μ(Mo *K*α) = 3.74 mm^{-1}, T = 150(0) K, prism 0.24 × 0.13 × 0.09 mm {clear dark purple}, 12190 independent measured reflections (θ = 25.4), R_1 = 0.030, wR_2 = 0.079 for 10234 reflections [$I > 2\sigma(I)$], 658 parameters, 8 restraints. CDCC 2251875.

Synthesis of [WOs(μ$_2$-C)Cl(CO)$_4$(PPh$_3$)$_2$(Tp*)] (8.7).

A purple solution containing [WOs(μ$_2$-C)Cl(CO)$_3$(PPh$_3$)$_2$(Tp*)] (**8.6**; 0.050 g, 0.038 mmol) in CH_2Cl_2 (5 mL) was treated with excess carbon monoxide (bubble) for 5 minutes, rapidly changing from purple to a bright yellow colour. The resulting mixture was sealed ander a $CO_{(g)}$ atmosphere and stirred for a further 10 minutes before infra-red spectroscopy (ν_{CO}) verified complete conversion. The $CO_{(g)}$ was purged from the vessel and the solution filtered through diatomous earth before concentrating into *n*-hexane aided by rotary evaporation. This gave a yellow solid that could be collected *via* vacuum filtration and washed with *n*-pentane (2 × 5 mL) before drying *in vacuo* for 16 hours. The solid was confirmed as the title compound (0.045 g, 0.033 mmol, 87% Isolated yield). Attempts to grow single crystals resulted in crystals of the following species **8.8**, even in the presence of excess PPh_3. IR (CH_2Cl_2, cm^{-1}): 2028 vs $\nu_{Os\text{-}CO}$, 1964 vs $\nu_{W–CO}$, 1947 vs $\nu_{Os\text{-}CO}$, 1856 vs $\nu_{W–CO}$. IR (ATR, cm^{-1}): 2547 w ν_{BH}, 2024 vs $\nu_{Os\text{-}CO}$, 1962 vs $\nu_{W\text{-}CO}$, 1940 vs $\nu_{Os\text{-}CO}$, 1854 vs $\nu_{W\text{-}CO}$. ^1H NMR (400 MHz, $CDCl_3$, 25 ºC, δ): 8.04 [m, 6H, PPh], 7.49 [t, $^1J_{HH}$ = 9 Hz, 6H, PPh], 7.41–7.38 [m, 10H, PPh], 7.24 [m, 3H, PPh], 7.00 [br.m, 5H, PPh], 5.75 [s, 1H, pzCH], 5.54 [s, 1H, pzCH], 5.51 [s, 1H, pzCH], 2.54 [s, 3H, pzCH_3], 2.43 [s, 3H, pzCH_3], 2.36 [s, 3H, pzCH_3], 2.20 [s, 3H, pzCH_3], 2.11 [s, 3H, pzCH_3], 1.77 [s, 3zH, pzCH_3]. $^{13}C\{^1H\}$ NMR (201 MHz, $CDCl_3$, 25ºC, δ): 371.9 [m, W≡C–Os], 234.1 [$^1J_{CW}$ = 187, W–CO], 228.6 [$^1J_{CW}$ = 180 Hz, W–CO], 180.7

[t, $^{2}J_{CP}$ = 8 Hz, Os–CO], 175.6 [t, $^{2}J_{CP}$ = 7 Hz, Os–CO], 153.1 152.6 151.7 [C^{5}(pz)], 144.3 143.8 143.6 [C^{3}(pz)], 135.1 [d, $^{2}J_{CP}$ = 10 Hz, $C^{2,6}(C_6H_5)$], 135.0 [d, $^{2}J_{CP}$ = 9 Hz, $C^{2,6}(C_6H_5)$], 133.5 133.4 [overlapping doublets, $^{1}J_{CP}$ = 48 Hz, $C^{1}(C_6H_5)$], 130.4 130.3 [$C^{4}(C_6H_5)$], 128.0 127.7 [d, $^{3}J_{CP}$ = 10 Hz, $C^{3,5}(C_6H_5)$], 106.6 106.2 106.0 [C^{4}(pz)], 18.4 16.5 14.6 13.14 13.08 12.6 [pzCH_3]. $^{31}P\{^{1}H\}$ NMR (162 MHz, $CDCl_3$, 25 °C, δ): –12.55 [d, $^{2}J_{PP}$ = 288 Hz], –15.05 [d, $^{2}J_{PP}$ = 288 Hz]. MS (ESI, *m*/*z*): Found: 1362.2996. Calcd for $C_{58}H_{55}{}^{11}BN_7O_4{}^{192}OsP_2{}^{184}W$ $[M–Cl+MeCN]^+$: 1362.3008. Anal. Found: C, 49.50; H, 4.00; N, 6.35%. Calcd for $C_{56}H_{52}BClN_6O_4OsP_2W$: C, 49.63; H, 3.87; N, 6.20%.

Synthesis of [WOs(μ$_2$-C)(CO)$_5$(PPh$_3$)(Tp*)] (Mixture) (8.8).

A purple solution containing [WOs(μ$_2$-C)Cl(CO)$_3$(PPh$_3$)$_2$(Tp*)] (**8.6**; 0.050 g, 0.038 mmol) in CH_2Cl_2 (5 mL) was treated with excess carbon monoxide (bubble) for 5 minutes, rapidly changing from purple to a bright yellow colour. The resulting mixture was sealed under a $CO_{(g)}$ atmosphere and stirred for a further 7 days remaining the same yellow colour, slowly precipitating small amounts of dark green reaction detritus. The $CO_{(g)}$ was purged from the vessel and the solution filtered through diatomaceous earth prior to solvent removal aided by rotary evaporation to give a yellow residue. The ensuing residue containing several species by TLC and NMR necessitating purification via flash column chromatography {silica gel, N2, CH_2Cl_2/petroleum ether gradient} where 50% Ch_2Cl_2 obtained a yellow eluate. The eluate was evaporated and recrystallised from CH_2Cl_2/*n*-hexane to give a yellow solid that could be collected *via* vacuum filtration and washed with *n*-pentane (2 × 5 mL) before drying *in vacuo* for 16 hours. The solid was confirmed as a mixture of the title compound with [OsHCl(CO)$_2$(PPh$_3$)$_2$] in a 1:0.5 ratio (0.045 g) that defied further purification. This likely reflects hydrolysis from the stationary phase, although it is apparent **8.8** and the osmium by-product have similar retention properties. Single crystals were obtained (as a different isomer) from the vapour diffusion of MeOH into a CH_2Cl_2 solution of **8.7**, suggesting MeOH was responsible for chemical change. A series of experiments determined this is unlikely as incorporation of methanol as solvent in the above procedure did not affect formation of **8.8** against **8.7**. Spectra are contaminated with signals corresponding to [OsHCl(CO)$_2$(PPh$_3$)$_2$] and are denoted in grey. IR (CH_2Cl_2, cm^{-1}): 2109 vs $\nu_{Os\text{-}CO}$, 2045 vs $\nu_{Os\text{-}CO}$, 2007 vs $\nu_{Os\text{-}CO}$, 1948 vs $\nu_{W\text{-}CO}$, 1856 vs $\nu_{W\text{-}CO}$. IR (ATR, cm^{-1}): 2098 vs $\nu_{Os\text{-}CO}$, 2037 vs $\nu_{Os\text{-}CO}$, 1997 vs $\nu_{Os\text{-}CO}$, 1943 vs $\nu_{W\text{-}CO}$, 1850 vs $\nu_{W\text{-}CO}$. ^{1}H NMR (400 MHz, $CDCl_3$, 25 °C, δ): 7.50 [m, 6H, PPh], 7.33 [m, 3H, PPh], 7.10 [m, 6H, PPh], 5.75 [s, 1H, pzCH], 5.71 [s, 1H, pzCH], 5.67 [s, 1H, pzCH], 2.43 [s, 3H, pzCH_3, 2.41 [s, 6H, pzCH_3], 2.26 [s, 3H, pzCH_3], 2.10 [s, 3H, pzCH_3], 1.99 [s, 3H, pzCH_3]. $^{13}C\{^{1}H\}$ NMR (201 MHz, $CDCl_3$, 25°C, δ): 337.9 [d, $^{2}J_{CP}$ = 11 Hz, W≡C–Os], 226.6 225.4 [$^{1}J_{CW}$ = 177 Hz, W–CO], 174.3 [d, $^{2}J_{CP}$ = 9 Hz, Os–CO], 169.5 [d, $^{2}J_{CP}$ = 8 Hz, Os–CO], 167.9 [d, $^{2}J_{CP}$ = 100 Hz, Os–CO], 153.1 152.4 151.1 [C^{5}(pz)], 144.4 144.1 143.9 [C^{3}(pz)], 134.6 [d, $^{2}J_{CP}$ = 10 Hz, $C^{2,6}(C_6H_5)$], 130.4

[$C^4(C_6H_5)$], 129.3 [d, $^1J_{CP}$ = 53 Hz, $C^1(C_6H_5)$], 128.3 [d, $^3J_{CP}$ = 10 Hz, $C^{3,5}(C_6H_5)$], 106.5 106.3 106.2 [C^4(pz)], 18.0 16.5 15.4 13.04 13.00 12.64 [pzCH_3]. $^{31}P\{^1H\}$ NMR (162 MHz, $CDCl_3$, 25 ºC, δ): –11.28 [s, Os-P]. MS (ESI, *m/z*): Found: 1123.1541. Calcd for $C_{39}H_{38}{}^{11}B^{35}ClN_6O_5{}^{192}Os^{31}P^{184}W$ $[M+H]^+$: 1123.1547. A sample was not submit for elemental analysis given the measured species is a mixture. *Crystal data for* $C_{39}H_{37}BClN_6O_5OsPW$, M = 1121.02, triclinic, $P\bar{1}$, a = 10.493 (2) Å, b = 14.433 (3) Å, c = 16.082 (3) Å, α = 72.45 (3)°, β = 78.73 (3)°, γ = 70.21 (3)°, V = 2173.2 (9) $Å^3$, Z = 2, ρ_{calc} = 1.713 Mgm^{-3}, μ(Synchrotron; λ = 0.71073 Å) = 5.71 mm^{-1}, T = 100(0) K, plate 0.02 × 0.01 × 0.01 mm {yellow}, 7413 independent measured reflections (θ = 25.4°), R_1 = 0.054, wR_2 = 0.155 for 7413 reflections [$I > 2\sigma(I)$], 502 parameters. CDCC 2251870.

References

1. A. Reinholdt, J. Bendix, *Chem. Rev.,* **2022**, *122*, 830.
2. H. O. Pierson, *Handbook of Refractory Carbides and Nitrides*. William Andrew Publishing: **1996**.
3. A. T. Santhanam, Application of transition metal carbides and nitrides in industrial tools. In *The Chemistry of Transition Metal Carbides and Nitrides*; S. T. Oyama, Ed. Springer Netherlands: Dordrecht, **1996**; pp 28.
4. R. B. Levy, M. Boudart, *Science,* **1973**, *181*, 547.
5. K. M. Lancaster, M. Roemelt, P. Ettenhuber, Y. Hu, M. W. Ribbe, F. Neese, U. Bergmann, S. DeBeer, *Science,* **2011**, *334*, 974.
6. T. Spatzal, M. Aksoyoglu, L. Zhang, S. L. Andrade, E. Schleicher, S. Weber, D. C. Rees, O. Einsle, *Science,* **2011**, *334*, 940.
7. J. A. Wiig, Y. Hu, C. Chung Lee, M. W. Ribbe, *Science,* **2012**, *337*, 1672.
8. K. M. Lancaster, Y. Hu, U. Bergmann, M. W. Ribbe, S. DeBeer, *J. Am. Chem. Soc.,* **2013**, *135*, 610.
9. J. A. Wiig, C. C. Lee, Y. Hu, M. W. Ribbe, *J. Am. Chem. Soc.,* **2013**, *135*, 4982.
10. J. A. Rees, R. Bjornsson, J. Schlesier, D. Sippel, O. Einsle, S. DeBeer, *Angew. Chem., Int. Ed.,* **2015**, *54*, 13249.
11. D. Sippel, O. Einsle, *Nat. Chem. Biol.,* **2017**, *13*, 956.
12. I. Čorić, P. L. Holland, *J. Am. Chem. Soc.,* **2016**, *138*, 7200.
13. C. Joseph, J. P. Shupp, C. R. Cobb, M. J. Rose, *Catalysts,* **2020**, *10*, 1317.
14. J. G. Chen, B. Frühberger, J. Eng, B. E. Bent, *J. Mol. Catal. A: Chem.,* **1998**, *131*, 285.
15. A. L. Stottlemyer, T. G. Kelly, Q. Meng, J. G. Chen, *Surf. Sci. Rep.,* **2012**, *67*, 201.
16. E. L. Muetterties, T. N. Rhodin, E. Band, C. F. Brucker, W. R. Pretzer, *Chem. Rev.,* **1979**, *79*, 91.
17. R. D. Young, A. F. Hill, G. E. Cavigliasso, R. Stranger, *Angew. Chem., Int. Ed.,* **2013**, *52*, 3699.
18. S. I. Kalläne, T. Braun, M. Teltewskoi, B. Braun, R. Herrmann, R. Laubenstein, *Chem. Commun.,* **2015**, *51*, 14613.
19. H. J. Barnett, L. K. Burt, A. F. Hill, *Dalton Trans.,* **2018**, *47*, 9570.
20. D. Mansuy, J. P. Lecomte, J. C. Chottard, J. F. Bartoli, *Inorg. Chem.,* **1981**, *20*, 3119.
21. E. N. Bakshi, C. D. Delfs, K. S. Murray, B. Peters, H. Homborg, *Inorg. Chem.,* **1988**, *27*, 4318.
22. K. Tatsumi, R. Hoffmann, M.-H. Whangbo, *J. Chem. Soc., Chem. Commun.,* **1980**, 509.
23. Y. Chen, W. Petz, G. Frenking, *Organometallics,* **2000**, *19*, 2698.
24. A. Krapp, K. K. Pandey, G. Frenking, *J. Am. Chem. Soc.,* **2007**, *129*, 7596.
25. J. B. Gary, C. Buda, M. J. A. Johnson, B. D. Dunietz, *Organometallics,* **2008**, *27*, 814.
26. A. Krapp, G. Frenking, *J. Am. Chem. Soc.,* **2008**, *130*, 16646.
27. D. J. Harding, C. Kerpal, G. Meijer, A. Fielicke, *J. Phys. Chem. Lett.,* **2013**, *4*, 892.
28. L. Zhao, C. Chai, W. Petz, G. Frenking, *Molecules,* **2020**, *25*, 4943.
29. K. A. Hofmann, *Ber. Dtsch. Chem. Ges.,* **1898**, *31*, 1904.
30. J. S. Bradley, *The Chemistry of Carbidocarbonyl Clusters.* In *Adv. Organomet. Chem.*, F. G. A. Stone; R. West, Eds.; Academic Press: **1983**; Vol. 22, pp 1.
31. F. Fischer, H. Tropsch, *Ber. Dtsch. Chem. Ges.,* **1926**, *59*, 830.
32. F. Fischer, H. Tropsch, *Ber. Dtsch. Chem. Ges.,* **1926**, *59*, 832.
33. S. L. Latesky, J. P. Selegue, *J. Am. Chem. Soc.,* **1987**, *109*, 4731.
34. S. R. Caskey, M. H. Stewart, J. E. Kivela, J. R. Sootsman, M. J. Johnson, J. W. Kampf, *J. Am. Chem. Soc.,* **2005**, *127*, 16750.
35. R. L. Cordiner, A. F. Hill, J. Wagler, *Organometallics,* **2008**, *27*, 5177.

36. H. J. Barnett, A. F. Hill, *Angew. Chem., Int. Ed.*, **2020**, *59*, 4274.
37. I. Noda, S. Kato, M. Mizuta, N. Yasuoka, N. Kasai, *Angew. Chem., Int. Ed.,* **1979**, *18*, 83.
38. A. Hejl, T. M. Trnka, M. W. Day, R. H. Grubbs, *Chem. Commun.,* **2002**, 2524.
39. R. G. Carlson, M. A. Gile, J. A. Heppert, M. H. Mason, D. R. Powell, D. V. Velde, J. M. Vilain, *J. Am. Chem. Soc.,* **2002**, *124*, 1580.
40. H. J. Barnett, A. F. Hill, *Angew. Chem., Int. Ed.,* **2020,** *59*, 4274.
41. S. Takemoto, M. Tsujita, H. Matsuzaka, *Organometallics,* **2017**, *36*, 3686.
42. V. L. Goedken, M. R. Deakin, L. A. Bottomley, *J. Chem. Soc., Chem. Commun.,* **1982**, 607.
43. G. Rossi, V. L. Goedken, C. Ercolani, *J. Chem. Soc., Chem. Commun.,* **1988**, 46.
44. A. Kienast, C. Bruhn, H. Homborg, *Z. Anorg. Allg. Chem.,* **1997**, *623*, 967.
45. A. Kienast, L. Galich, K. S. Murray, B. Moubaraki, G. Lazarev, J. D. Cashion, H. Homborg, *J. Porphyrins Phthalocyanines,* **1997**, *1*, 141.
46. L. Galich, A. Kienast, H. Hückstädt, H. Homborg, *Z. Anorg. Allg. Chem.,* **1998**, *624*, 1235.
47. B. Floris, M. P. Donzello, C. Ercolani, *Single-Atom Bridged Dinuclear Metal Complexes with Emphasis on Phthalocyanine Systems*. In *The Porphyrin Handbook*, K. M. Kadish; K. M. Smith; R. Guilard, Eds; Academic Press: Amsterdam, **2003**; pp 1.
48. C. Colomban, E. V. Kudrik, D. V. Tyurin, F. Albrieux, S. E. Nefedov, P. Afanasiev, A. B. Sorokin, *Dalton Trans.,* **2015**, *44*, 2240.
49. A. P. Kroitor, A. G. Martynov, Y. G. Gorbunova, A. Y. Tsivadze, A. B. Sorokin, *Eur. J. Inorg. Chem.,* **2019**, *2019*, 1923.
50. W. Beck, W. Knauer, C. Robl, *Angew. Chem., Int. Ed.,* **1990**, *29*, 318.
51. Y. Li, J.-S. Huang, Z.-Y. Zhou, C.-M. Che, X.-Z. You, *J. Am. Chem. Soc.,* **2002**, *124*, 13185.
52. A. Klose, E. Solari, C. Floriani, N. Re, A. Chiesi-Villa, C. Rizzoli, *Chem. Commun.,* **1997**, 2297.
53. U. Schubert, K. Ackermann, P. Rustemeyer, *J. Organomet. Chem.,* **1982**, *231*, 323.
54. W. Knauer, W. Beck, *Z. Anorg. Allg. Chem.,* **2008**, *634*, 2241.
55. T. Kurogi, K. Irifune, K. Takai, *Chem. Sci.,* **2021**, *12*, 14281.
56. R. L. Miller, P. T. Wolczanski, A. L. Rheingold, *J. Am. Chem. Soc.,* **1993**, *115*, 10422.
57. A. Caselli, E. Solari, R. Scopelliti, C. Floriani, *J. Am. Chem. Soc.,* **2000**, *122*, 538.
58. E. Solari, S. Antonijevic, S. Gauthier, R. Scopelliti, K. Severin, *Eur. J. Inorg. Chem.,* **2007**, *2007*, 367.
59. I. S. Butler, N. J. Coville, D. Cozak, *J. Organomet. Chem.,* **1977**, *133*, 59.
60. R. D. Young, A. F. Hill, G. E. Cavigliasso, R. Stranger, *Angew. Chem., Int. Ed.,* **2013**, *52*, 3699.
61. A. F. Hill, L. J. Watson, *Chem. Commun.,* **2020**, *56*, 2356.
62. I. A. Cade, A. F. Hill, C. M. A. McQueen, *Organometallics,* **2009**, *28*, 6639.
63. T. Ahrens, B. Schmiedecke, T. Braun, R. Herrmann, R. Laubenstein, *Eur. J. Inorg. Chem.,* **2017**, *2017*, 713.
64. A. E. Enriquez, P. S. White, J. L. Templeton, *J. Am. Chem. Soc.,* **2001**, *123*, 4992.
65. J. C. Peters, A. L. Odom, C. C. Cummins, *Chem. Commun.,* **1997**, 1995.
66. J. A. Buss, T. Agapie, *Nature,* **2016**, *529*, 72.
67. J. A. Buss, T. Agapie, *J. Am. Chem. Soc.,* **2016**, *138*, 16466.
68. M. H. Stewart, M. J. A. Johnson, J. W. Kampf, *Organometallics,* **2007**, *26*, 5102.
69. A. Reinholdt, J. E. Vibenholt, T. J. Morsing, M. Schau-Magnussen, N. E. A. Reeler, J. Bendix, *Chem. Sci.,* **2015**, *6*, 5815.
70. A. Reinholdt, K. Herbst, J. Bendix, *Chem. Commun.,* **2016**, *52*, 2015.
71. A. Reinholdt, J. Bendix, *Inorg. Chem.,* **2017**, *56*, 12492.
72. A. Reinholdt, J. Bendix, A. F. Hill, R. A. Manzano, *Dalton Trans.,* **2018**, *47*, 14893.
73. A. Reinholdt, A. F. Hill, J. Bendix, *Chem. Commun.,* **2018**, *54*, 5708.
74. A. Reinholdt, J. Bendix, *Chem. Commun.,* **2019**, *55*, 8270.

75. A. Reinholdt, J. E. Vibenholt, T. J. Morsing, M. Schau-Magnussen, N. E. A. Reeler, J. Bendix, *Chem. Sci.,* **2015**, *6*, 5815.
76. A. Reinholdt, K. Herbst, J. Bendix, *Chem. Commun.,* **2016**, *52*, 2015.
77. A. Reinholdt, J. Bendix, *Inorg. Chem.,* **2017**, *56*, 12492.
78. H. J. Barnett, A. F. Hill, *Chem. Commun.,* **2019**, *55*, 1734.
79. A. Reinholdt, J. Bendix, A. F. Hill, R. A. Manzano, *Dalton Tran.,* **2018**, *47*, 14893.
80. B. J. Frogley, L. J. Wright, *Chemistry,* **2018**, *24*, 2025.
81. E. O. Fischer, G. Kreis, C. G. Kreiter, J. Müller, G. Huttner, H. Lorenz, *Angew. Chem., Int. Ed.,* **1973**, *12*, 564.
82. M. L. Listemann, R. R. Schrock, *Organometallics,* **2002**, *4*, 74.
83. R. J. Blau, M. H. Chisholm, K. Folting, R. J. Wang, *J. Chem. Soc., Chem. Commun.,* **1985**, 1582.
84. G. A. Koutsantonis, J. P. Selegue, *J. Am. Chem. Soc.,* **1991**, *113*, 2316.
85. B. Cordero, V. Gómez, A. E. Platero-Prats, M. Revés, J. Echeverría, E. Cremades, F. Barragán, S. Alvarez, *Dalton Trans.,* **2008**, 2832.
86. P. Pyykkö, S. Riedel, M. Patzschke, *Chem. Eur. J.,* **2005**, *11*, 3511.
87. T. Desmond, F. J. Lalor, G. Ferguson, M. Parvez, *J. Chem. Soc., Chem. Commun.,* **1983**, 457.
88. T. Desmond, F. J. Lalor, G. Ferguson, M. Parvez, *J. Chem. Soc., Chem. Commun.,* **1984**, 75.
89. S. Chaona, F. J. Lalor, G. Ferguson, M. M. Hunt, *J. Chem. Soc., Chem. Commun.,* **1988**, 1606.
90. F. J. Lalor, T. J. Desmond, G. M. Cotter, C. A. Shanahan, G. Ferguson, M. Parvez, B. Ruhl, *J. Chem. Soc., Dalton Trans.,* **1995**, 1709.
91. L. Weber, G. Dembeck, R. Boese, D. Bläser, *Chem. Ber.,* **1997**, *130*, 1305.
92. L. Weber, G. Dembeck, R. Boese, D. Bläser, *Organometallics,* **1999**, *18*, 4603.
93. F. J. Lalor, S. A. O'Neill, *J. Organomet. Chem.,* **2003**, *684*, 249.
94. R. L. Cordiner, P. A. Gugger, A. F. Hill, A. C. Willis, *Organometallics,* **2009**, *28*, 6632.
95. A. L. Colebatch, A. F. Hill, *J. Am. Chem. Soc.,* **2014**, *136*, 17442.
96. A. F. Hill, R. Y. Kong, *Chem. Commun.,* **2017**, *53*, 759.
97. M. Etienne, P. S. White, J. L. Templeton, *J. Am. Chem. Soc.,* **1991**, *113*, 2324.
98. S. H. Hong, M. W. Day, R. H. Grubbs, *J. Am. Chem. Soc.,* **2004**, *126*, 7414.
99. E. S. Borren, A. F. Hill, R. Shang, M. Sharma, A. C. Willis, *J. Am. Chem. Soc.,* **2013**, *135*, 4942.
100. J. delPozo, D. Carrasco, M. H. Perez-Temprano, M. Garcia-Melchor, R. Alvarez, J. A. Casares, P. Espinet, *Angew. Chem., Int. Ed.,* **2013**, *52*, 2189.
101. R. L. Cordiner, A. F. Hill, J. r. Wagler, *Organometallics,* **2008**, *27*, 5177.
102. A. L. Colebatch, A. F. Hill, R. Shang, A. C. Willis, *Organometallics,* **2010**, *29*, 6482.
103. E. F. Van Der Eide, W. E. Piers, P. E. Romero, M. Parvez, R. McDonald, *Organometallics,* **2004**, *23*, 314.
104. A. F. Hill, R. Shang, A. C. Willis, *Organometallics,* **2011**, *30*, 3237.
105. A. F. Hill, R. Shang, *Organometallics,* **2012**, *31*, 4635.
106. R. L. Cordiner, A. F. Hill, R. Shang, A. C. Willis, *Organometallics,* **2011**, *30*, 139.
107. A. L. Colebatch, A. F. Hill, *Organometallics,* **2016**, *35*, 2249.
108. B. J. Frogley, A. F. Hill, *Chem. Commun.,* **2018**, *54*, 7649.
109. B. J. Frogley, A. F. Hill, *Chem. Commun.,* **2018**, *54*, 12373.
110. B. J. Frogley, A. F. Hill, *Chem. Commun.,* **2018**, *54*, 2126.
111. W. W. Greaves, R. J. Angelici, B. J. Helland, R. Klima, R. A. Jacobson, *J. Am. Chem. Soc.,* **1979**, *101*, 7618.
112. T. Desmond, F. J. Lalor, G. Ferguson, M. Parvez, *J. Chem. Soc., Chem. Commun.,* **1984**, 75.
113. R. A. Doyle, R. J. Angelici, *J. Am. Chem. Soc.,* **1990**, *112*, 194.
114. A. R. Johnson, W. M. Davis, C. C. Cummins, S. Serron, S. P. Nolan, D. G. Musaev, K. Morokuma, *J. Am. Chem. Soc.,* **1998**, *120*, 2071.
115. I. A. Cade, A. F. Hill, C. M. A. McQueen, *Dalton Trans.,* **2019**, *48*, 2000.

116. B. J. Frogley, A. F. Hill, L. J. Watson, *Chem. Eur. J.,* **2020**, *26*, 12706.
117. A. Hill, R. Manzano, *Chem. Sci.,* **2023**, *14*, 3776.
118. A. L. Colebatch, R. L. Cordiner, A. F. Hill, K. T. H. D. Nguyen, R. Shang, A. C. Willis, *Organometallics,* **2009**, *28*, 4394.
119. A. F. Hill, M. Sharma, A. C. Willis, *Organometallics,* **2012**, *31*, 2538.
120. B. J. Frogley, A. F. Hill, *Chem. Commun.,* **2019**, *55*, 12400.
121. B. J. Frogley, A. F. Hill, *Angew. Chem., Int. Ed.,* **2019**, *58*, 8044.
122. M. H. Johansson, S. Otto, *Acta Crystallogr. Sec. C,* **2000**, *56*, e12.
123. L. Brammer, E. D. Stevens, *Acta Crystallogr. Sec. C,* **1989**, *45*, 400.
124. C. Ercolani, M. Gardini, V. L. Goedken, G. Pennesi, G. Rossi, U. Russo, P. Zanonato, *Inorg. Chem.,* **1989**, *28*, 3097.
125. A. Kienast, H. Homborg, *Z. Anorg. Allg. Chem.,* **1998**, *624*, 107.
126. H. J. Barnett, A. F. Hill, *Chem. Commun.,* **2019**, *55*, 1734.
127. A. M. Paoletti, G. Pennesi, G. Rossi, C. Ercolani, *Inorg. Chem.,* **1995**, *34*, 4780.
128. H. J. Barnett, A. F. Hill, *Dalton Trans.,* **2021**, *50*, 9383.
129. S. Takemoto, J. Ohata, K. Umetani, M. Yamaguchi, H. Matsuzaka, *J. Am. Chem. Soc.,* **2014**, *136*, 15889.
130. H. J. Barnett, A. F. Hill, *Chem. Commun.,* **2020**, *56*, 12593.
131. A. P. Kroitor, L. P. Cailler, A. G. Martynov, Y. G. Gorbunova, A. Y. Tsivadze, A. B. Sorokin, *Dalton Trans.,* **2017**, *46*, 15651.
132. O. R. Simonova, S. V. Zaitseva, S. A. Zdanovich, O. I. Koifman, *Macroheterocycles,* **2018**, *11*, 29.
133. D. V. Tyurin, S. V. Zaitseva, E. V. Kudrik, *Russ. J. Phys. Chem. A,* **2018**, *92*, 870.
134. S. V. Zaitseva, E. Y. Tyulyaeva, S. A. Zdanovich, O. I. Koifman, *J. Mol. Liq.,* **2019**, *287*, 111023.
135. S. V. Zaitseva, E. Y. Tyulyaeva, D. V. Tyurin, S. A. Zdanovich, O. I. Koifman, *J. Organomet. Chem.,* **2020**, *912*, 121164.
136. M. I. Bruce, M. L. Cole, M. Gaudio, B. W. Skelton, A. H. White, *J. Organomet. Chem.,* **2006**, *691*, 4601.
137. D. J. Armitt, M. I. Bruce, M. Gaudio, N. N. Zaitseva, B. W. Skelton, A. H. White, B. Le Guennic, J.-F. Halet, M. A. Fox, R. L. Roberts, F. Hartl, P. J. Low, *Dalton Trans.,* **2008**, 6763.
138. A. F. Hill, R. A. Manzano, *Dalton Trans.,* **2019**, *48*, 6596.
139. R. A. Manzano, A. F. Hill, *Adv. Organomet. Chem.*, **2019**, *72*, 103.
140. A. F. Hill, R. A. Manzano, *Angew. Chem., Int. Ed.,* **2019**, *58*, 7357.
141. B. J. Frogley, A. F. Hill, *Chem. Eur. J.,* **2020**, *26*, 12125.
142. W. Knauer, W. Beck, *Z. Anorg. Allg. Chem.,* **2008**, *634*, 2241.
143. A. L. Colebatch, Y. S. Han, A. F. Hill, M. Sharma, R. Shang, J. S. Ward, *Chem. Commun.,* **2017**, *53*, 1832.
144. B. J. Frogley, A. F. Hill, *Chem. Commun.,* **2019**, *55*, 15077.
145. B. J. Frogley, A. F. Hill, *Dalton Trans.,* **2020**, *49*, 12390.
146. B. J. Frogley, A. F. Hill, *Dalton Trans.,* **2020**, *49*, 3272.
147. B. J. Frogley, A. F. Hill, A. Seitz, *Chem. Commun.,* **2020**, *56*, 3265.
148. A. Hill, B. Frogley, S. S. Welsh, *Dalton Trans.,* **2021**, *50*, 15502.
149. B. J. Frogley, A. F. Hill, R. M. Kirk, *Chem. Commun.,* **2021**, *57*, 8770.
150. V. L. Goedken, M. R. Deakin, L. A. Bottomley, *J. Chem. Soc., Chem. Commun.,* **1982**, *0*, 607.
151. A. Kienast, H. Homborg, *Z. Anorg. Allg. Chem.,* **1998**, *624*, 107.
152. A. P. Kroitor, L. P. Cailler, A. G. Martynov, Y. G. Gorbunova, A. Y. Tsivadze, A. B. Sorokin, *Dalton Trans.,* **2017**, *46*, 15651.
153. S. A. Gonsales, Z. C. Mueller, F. Zhao, P. H. S. Paioti, L. Karmazin, J. Wan, F. Liu, K. N. Houk, A. H. Hoveyda, *J. Am. Chem. Soc.,* **2021**, *143*, 20640.

154. S. I. Kallane, T. Braun, M. Teltewskoi, B. Braun, R. Herrmann, R. Laubenstein, *Chem. Commun.,* **2015**, *51*, 14613.
155. T. Ahrens, B. Schmiedecke, T. Braun, R. Herrmann, R. Laubenstein, *Eur. J. Inorg. Chem.,* **2017**, *2017*, 713.
156. H. J. Barnett, L. K. Burt, A. F. Hill, *Dalton Trans.,* **2018**, *47*, 9570.
157. W. Beck, W. Knauer, C. Robl, *Angew. Chem., Int. Ed.,* **1990**, *29*, 318.
158. S. H. Hong, M. W. Day, R. H. Grubbs, *J. Am. Chem. Soc.,* **2004**, *126*, 7414.
159. B. J. Frogley, A. F. Hill, *Chem. Commun.,* **2019**, *55*, 12400.
160. T. Takao, K. Seki, *Organometallics,* **2021**, *40*, 467.
161. H. J. Barnett, A. F. Hill, *Chem. Commun.,* **2020**, *56*, 7738.
162. R. R. Schrock, *Chem. Rev.,* **2002**, *102*, 145.
163. D. Seyferth, J. E. Hallgren, P. L. K. Hung, *J. Organomet. Chem.,* **1973**, *50*, 265.
164. D. Lentz, I. Brüdgam, H. Hartl, *Angew. Chem., Int. Ed.,* **1985**, *24*, 119.
165. H. Huang, R. P. Hughes, C. R. Landis, A. L. Rheingold, *J. Am. Chem. Soc.,* **2006**, *128*, 7454.
166. H. Huang, R. P. Hughes, A. L. Rheingold, *Dalton Trans.,* **2011**, *40*, 47.
167. C. J. Pell, Y. Zhu, R. Huacuja, D. E. Herbert, R. P. Hughes, O. V. Ozerov, *Chem. Sci.,* **2017**, *8*, 3178.
168. A. L. Colebatch, B. J. Frogley, A. F. Hill, C. S. Onn, *Chem. Eur. J.,* **2021**, *27*, 5322.
169. R. L. Cordiner, A. F. Hill, J. Wagler, *Organometallics,* **2008**, *27*, 4532.
170. S. Trofimenko, J. C. Calabrese, J. S. Thompson, *Inorg. Chem.,* **1987**, *26*, 1507.
171. C. C. Philipp, P. S. White, J. L. Templeton, *Inorg. Chem.,* **1992**, *31*, 3825.
172. J. T. Lyon, L. Andrews, *Inorg. Chem.,* **2006**, *45*, 9858.
173. J. T. Lyon, H.-G. Cho, L. Andrews, *Organometallics,* **2007**, *26*, 6373.
174. J. T. Lyon, H.-G. Cho, L. Andrews, H.-S. Hu, J. Li, *Inorg. Chem.,* **2007**, *46*, 8728.
175. H. G. Cho, L. Andrews, *Eur. J. Inorg. Chem.,* **2008**, *2008*, 2537.
176. J. T. Lyon, L. Andrews, *Eur. J. Inorg. Chem.,* **2008**, *2008*, 995.
177. H.-G. Cho, L. Andrews, *Dalton Trans.,* **2009**, 5858.
178. E. O. Fischer, P. Rustemeyer, K. Ackermann, *Chem. Ber.,* **1982**, *115*, 3851.
179. G. M. Jamison, A. E. Bruce, P. S. White, J. L. Templeton, *J. Am. Chem. Soc.,* **1991**, *113*, 5057.
180. A. F. Hill, J. S. Ward, Y. Xiong, *Organometallics,* **2015**, *34*, 5057.
181. J. A. Buss, G. A. Bailey, J. Oppenheim, D. G. VanderVelde, W. A. Goddard, 3rd, T. Agapie, *J. Am. Chem. Soc.,* **2019**, *141*, 15664.
182. G. R. Clark, K. Marsden, W. R. Roper, L. J. Wright, *J. Am. Chem. Soc.,* **1980**, *102*, 6570.
183. M. A. Gallop, W. R. Roper, Carbene and Carbyne Complexes of Ruthenium, Osmium, and Iridium. In *Adv. Organomet. Chem.*, F. G. A. Stone; R. West, Eds.; Academic Press: **1986**; *Vol. 25*, pp 121.
184. W. R. Roper, *J. Organomet. Chem.,* **1986**, *300*, 167.
185. G. Bor, B. Marko, L. Marko, *Acta Chem. Acad. Sci. Hung.,* **1961**, *27*, 395.
186. W. T. Dent, L. A. G. Duncanson, R. G., H. W. B. Reed, B. L. Shaw, *Proc. Chem. Soc.,* **1961**, 153.
187. J. B. Keister, T. L. Horling, *Inorg. Chem.,* **1980**, *19*, 2304.
188. N. J. Zhu, C. Lecomte, P. Coppens, J. B. Keister, *Acta. Crystallogr. B. Struct. Sci. Cryst. Eng. Mater.,* **1982**, *38*, 1286.
189. M. I. Bruce, M. E. Smith, N. N. Zaitseva, B. W. Skelton, A. H. White, *J. Organomet. Chem.,* **2003**, *670*, 170.
190. A. B. Antonova, M. I. Bruce, B. G. Ellis, M. Gaudio, P. A. Humphrey, M. Jevric, G. Melino, B. K. Nicholson, G. J. Perkins, B. W. Skelton, B. Stapleton, A. H. White, N. N. Zaitseva, *Chem. Commun.,* **2004**, 960.
191. M. I. Bruce, P. A. Humphrey, G. Melino, B. W. Skelton, A. H. White, N. N. Zaitseva, *Inorg. Chim. Acta,* **2005**, *358*, 1453.

192. W. Schulze, H. Hartl, K. Seppelt, *J. Organomet. Chem.,* **1987**, *319*, 77.
193. R. Vilar, S. E. Lawrence, D. M. P. Mingos, D. J. Williams, *Chem. Commun.,* **1997**, 285.
194. T. Kurogi, K. Irifune, T. Enoki, K. Takai, *Chem. Commun.,* **2021**, *57*, 5199.
195. T. V. Ashworth, J. A. K. Howard, F. G. A. Stone, *J. Chem. Soc., Chem. Commun.,* **1979**, 42.
196. T. V. Ashworth, J. A. K. Howard, F. G. A. Stone, *J. Chem. Soc., Dalton Trans.,* **1980**, 1609.
197. T. V. Ashworth, M. J. Chetcuti, J. A. K. Howard, F. G. A. Stone, S. J. Wisbey, P. Woodward, *J. Chem. Soc., Dalton Trans.,* **1981**, 763.
198. J. Beck, F. Wolf, *Z. Anorg. Allg. Chem.,* **2002**, *628*, 1453.
199. F. G. A. Stone, *Angew. Chem., Int. Ed.,* **1984**, *23*, 89.
200. R. Hoffmann, *Angew. Chem., Int. Ed.,* **1982**, *21*, 711.
201. T. J. Desmond, F. J. Lalor, G. Ferguson, M. Parvez, T. Wieckowski, *Acta Crystallogr. Sec. C,* **1990**, *46*, 59.
202. F. A. Cotton, C. S. Kraihanzel, *J. Am. Chem. Soc.,* **1962**, *84*, 4432.
203. C. S. Kraihanzel, F. A. Cotton, *Inorg. Chem.,* **1963**, *2*, 533.
204. J. A. Timney, *Inorg. Chem.,* **1979**, *18*, 2502.
205. R. Shang. *Functionalising transition metal carbynes with main group elements*. PhD Thesis. Australian National University, Canberra, Australia, **2012**.
206. L. J. Farrugia, C. Evans, *C. R. Chim.,* **2005**, *8*, 1566.
207. X.-M. Liu, C.-Y. Wang, Q.-S. Li, Y. Xie, R. B. King, H. F. Schaefer, *Chem. Eur. J.,* **2009**, *15*, 5520.
208. X. Gong, X. Zhang, Q.-S. Li, Y. Xie, R. B. King, H. F. Schaefer Iii, *Dalton Trans.,* **2010**, *39*, 5242.
209. Z. Zhang, Q.-s. Li, Y. Xie, R. B. King, *Inorg. Chim. Acta,* **2011**, *375*, 193.
210. Z. Zhang, L. Pu, Q.-S. Li, R. B. King, *New J. Chem.,* **2014**, *38*, 4282.
211. H. Gong, Q. Luo, Q.-S. Li, Y. Xie, R. B. King, H. F. Schaefer, *Inorg. Chem.,* **2015**, *54*, 132.
212. R. B. King, A. Efraty, W. M. Douglas, *J. Organomet. Chem.,* **1973**, *60*, 125.
213. J. T. Malito, R. Shakir, J. L. Atwood, *J. Chem. Soc., Dalton Trans.,* **1980**, 1253.
214. C. S. Onn, A. F. Hill, A. Olding, *Dalton Trans.,* **2020**, *49*, 12731.
215. B. J. Frogley, A. F. Hill, S. S. Welsh, *Chem. Commun.,* **2021**, *57*, 13353.
216. E. Jiménez-Núñez, A. M. Echavarren, *Chem. Rev.,* **2008**, *108*, 3326.
217. R. Dorel, A. M. Echavarren, *Chem. Rev.,* **2015**, *115*, 9028.
218. G. R. Clark, C. M. Cochrane, W. R. Roper, L. J. Wright, *J. Organomet. Chem.,* **1980**, *199*, C35.
219. A. F. Hill, W. R. Roper, J. M. Waters, A. H. Wright, *J. Am. Chem. Soc.,* **1983**, *105*, 5939.
220. B. J. Frogley, A. F. Hill, C. S. Onn, *Dalton Trans.,* **2019**, *48*, 11715.
221. B. J. Frogley, A. F. Hill, C. S. Onn, L. J. Watson, *Angew. Chem.,* **2019**, *131*, 15493.
222. G. A. Carriedo, J. C. Jeffery, F. G. A. Stone, *J. Chem. Soc., Dalton Trans.,* **1984**, 1597.
223. C. E. Strasser, S. Cronje, H. G. Raubenheimer, *New J. Chem.,* **2010**, *34*, 458.
224. A. L. Colebatch, A. F. Hill, *Dalton Trans.,* **2017**, *46*, 4355.
225. B. J. Frogley, A. F. Hill, L. J. Watson, *Chem. Commun.,* **2019**, *55*, 14450.
226. R. A. Manzano, A. F. Hill, *Chapter Three - Propargylidyne and tricarbido complexes*. In *Adv. Organomet. Chem.*, P. J. Pérez, Ed. Academic Press: **2019**; *Vol. 72*, pp 103.
227. M. Green, J. A. K. Howard, A. P. James, C. M. Nunn, F. G. A. Stone, *J. Chem. Soc., Chem. Commun.,* **1984**, 1113.
228. M. Green, J. A. K. Howard, A. P. James, C. M. Nunn, F. G. A. Stone, *J. Chem. Soc., Dalton Trans.,* **1987**, 61.
229. R. H. Crabtree, M. Lavin, *Inorg. Chem.,* **1986**, *25*, 805.
230. P. Macchi, L. Garlaschelli, A. Sironi, *J. Am. Chem. Soc.,* **2002**, *124*, 14173.
231. S. R. Parmelee, N. P. Mankad, *Dalton Trans.,* **2015**, *44*, 17007.
232. F. R. Hartley, *Nat. Phys. Sci.,* **1972**, *236*, 75.
233. N. M. Boag, M. Green, J. A. K. Howard, J. L. Spencer, R. F. D. Stansfield, M. D. O. Thomas, F. G. A. Stone, P. Woodward, *J. Chem. Soc., Dalton Trans.,* **1980**, 2182.

234. R. Benn, R.-D. Reinhardt, A. Rufińska, *J. Organomet. Chem.,* **1985**, *282*, 291.
235. M. A. Bennett, T. Dirnberger, D. C. R. Hockless, E. Wenger, A. C. Willis, *J. Chem. Soc., Dalton Trans.,* **1998**, 271.
236. H. C. Clark, A. M. de P. Nicholas, *Magn. Reson. Chem.,* **1990**, *28*, 99.
237. A. Moor, P. S. Pregosin, L. M. Venanzi, *Inorg. Chim. Acta,* **1982**, *61*, 135.
238. B. M. Still, P. G. Kumar, J. R. Aldrich-Wright, W. S. Price, *Chem. Soc. Rev.,* **2007**, *36*, 665.
239. T. V. Ashworth, J. A. K. Howard, F. G. A. Stone, *J. Chem. Soc., Dalton Trans.,* **1980**, 1609.
240. K. Suenkel, U. Birk, C. Robl, *Organometallics,* **1994**, *13*, 1679.
241. P. G. Waddell, A. M. Z. Slawin, J. D. Woollins, *Dalton Trans.,* **2010**, *39*, 8620.
242. J. A. Abad, L. W. Bateman, J. C. Jeffery, K. A. Mead, H. Razay, F. G. A. Stone, P. Woodward, *J. Chem. Soc., Dalton Trans.,* **1983**, 2075.
243. M. R. Awang, J. C. Jeffery, F. G. A. Stone, *J. Chem. Soc., Dalton Trans.,* **1983**, 2091.
244. M. R. Awang, J. C. Jeffery, F. G. A. Stone, *J. Chem. Soc., Chem. Commun.,* **1983**, 1426.
245. M. D. Bermúdez, E. Delgado, G. P. Elliott, N. H. Tran-Huy, F. Mayor-Real, F. G. A. Stone, M. J. Winter, *J. Chem. Soc., Dalton Trans.,* **1987**, 1235.
246. S. J. Davies, A. F. Hill, M. U. Pilotti, F. G. A. Stone, *Polyhedron,* **1989**, *8*, 2265.
247. S. J. Davies, F. G. A. Stone, *J. Chem. Soc., Dalton Trans.,* **1989**, 785.
248. S. J. Dossett, A. F. Hill, J. A. K. Howard, B. A. Nasir, T. P. Spaniol, P. Sherwood, F. G. A. Stone, *J. Chem. Soc., Dalton Trans.,* **1989**, 1871.
249. S. H. F. Becke, M. D. Bermúdez, N. H. Tran-Huy, J. A. K. Howard, O. Johnson, F. G. A. Stone, *J. Chem. Soc., Dalton Trans.,* **1987**, 1229.
250. J. A. Beck, S. A. R. Knox, R. F. D. Stansfield, F. G. A. Stone, M. J. Winter, P. Woodward, *J. Chem. Soc., Dalton Trans.,* **1982**, 195.
251. W. I. Bailey, Jr., M. H. Chisholm, F. A. Cotton, L. A. Rankel, *J. Am. Chem. Soc.,* **1978**, *100*, 5764.
252. L. K. Burt, R. L. Cordiner, A. F. Hill, R. A. Manzano, J. Wagler, *Chem. Commun.,* **2020**, *56*, 5673.
253. L. K. Burt, A. F. Hill, *Dalton Trans.,* **2020**, *49*, 8143.
254. L. K. Burt, A. F. Hill, *Chem. Commun.,* **2021**, *57*, 8480.
255. L. M. Caldwell, *Alkylidyne Complexes Ligated by Poly(pyrazolyl)borates*. In *The Organotransition Metal Chemistry of Poly(pyrazolyl)borates. Part 1*, R. West; A. F. Hill; M. J. Fink, Eds. Academic Press: **2008**; *Vol. 56*, pp 1.
256. J. M. A. Wouters, K. Vrieze, C. J. Elsevier, M. C. Zoutberg, K. Goubitz, *Organometallics,* **2002**, *13*, 1510.
257. C. J. Cardin, D. J. Cardin, M. F. Lappert, K. W. Muir, *J. Chem. Soc., Dalton Trans.,* **1978**, 46.
258. J. M. A. Wouters, K. Vrieze, C. J. Elsevier, M. C. Zoutberg, K. Goubitz, *Organometallics,* **1994**, *13*, 1510.
259. H. D. Empsall, B. L. Shaw, A. J. Stringer, *J. Organomet. Chem.,* **1975**, *96*, 461.
260. X. Wang, D. Fortin, G. Brisard, P. D. Harvey, *Macromol. Rapid Commun.,* **2014**, *35*, 992.
261. J. D. Bullock, S. R. Valandro, A. N. Sulicz, C. J. Zeman, K. A. Abboud, K. S. Schanze, *J. Phys. Chem. A,* **2019**, *123*, 9069.
262. T. Maganti, K. Venkatesan, *ChemPlusChem,* **2022**, *87*.
263. H. J. Reich AX and AB Spectra. https://www.chem.wisc.edu/areas/reich/nmr/05-hmr-10-axab.htm (accessed 4/3/2020).
264. J. G. Verkade, *Coord. Chem. Rev.,* **1972**, *9*, 1.
265. C. Colomban, E. V. Kudrik, V. Briois, J. C. Shwarbrick, A. B. Sorokin, P. Afanasiev, *Inorg. Chem.,* **2014**, *53*, 11517.
266. L. P. Cailler, M. Clemancey, J. Barilone, P. Maldivi, J. M. Latour, A. B. Sorokin, *Inorg. Chem.,* **2020**, *59*, 1104.
267. J. Zhu, Z. Lin, T. B. Marder, *Inorg. Chem.,* **2005**, *44*, 9384.
268. C. A. Tolman, *Chem. Rev.,* **1977**, *77*, 313.

269. A. J. L. Pombeiro, M. F. C. Guedes da Silva, R. A. Michelin, *Coord. Chem. Rev.,* **2001**, *218*, 43.
270. L. J. Manojlovic-Muir, K. W. Muir, *Inorg. Chim. Acta,* **1974**, *10*, 47.
271. M. R. S. J. Foreman, A. F. Hill, A. J. P. White, D. J. Williams, *Organometallics,* **2003**, *22*, 3831.
272. M. A. Fox, J. E. Harris, S. Heider, V. Pérez-Gregorio, M. E. Zakrzewska, J. D. Farmer, D. S. Yufit, J. A. K. Howard, P. J. Low, *J. Organomet. Chem.,* **2009**, *694*, 2350.
273. J. Peone, L. Vaska, *Angew. Chem., Int. Ed.,* **1971**, *10*, 511.
274. C. A. Read, W. R. Roper, *J. Chem. Soc., Dalton Trans.,* **1973**, 1370.
275. C. Douvris, C. A. Reed, *Organometallics,* **2008**, *27*, 807.
276. J. A. Pople, *Mol. Phys.,* **1964**, *7*, 301.
277. P. Pyykkö, *J. Phys. Chem. A,* **2015**, *119*, 2326.
278. Cambridge Crystallographic Data Centre (CCDC). Cambridge, UK, 2023; Vol. CSD Version 5.42.
279. A. A. Zuzek, S. C. Reynolds, D. S. Glueck, J. A. Golen, A. L. Rheingold, *Organometallics,* **2011**, *30*, 1812.
280. G. Hogarth, *Transition Metal Dithiocarbamates: 1978–2003*. In *Prog. Inorg. Chem.*, **2005**; pp 71.
281. J. Reglinski, M. Garner, I. D. Cassidy, P. A. Slavin, M. D. Spicer, D. R. Armstrong, *J. Chem. Soc., Dalton Trans.,* **1999**, 2119.
282. A. F. Hill, G. R. Owen, A. J. P. White, D. J. Williams, *Angew. Chem., Int. Ed.,* **1999**, *38*, 2759.
283. I. R. Crossley, A. F. Hill, *Organometallics,* **2004**, *23*, 5656.
284. I. R. Crossley, A. F. Hill, *Dalton Trans.,* **2008**, 201.
285. I. R. Crossley, A. F. Hill, A. C. Willis, *Organometallics,* **2008**, *27*, 312.
286. G. R. Owen, P. H. Gould, A. Hamilton, N. Tsoureas, *Dalton Trans.,* **2010**, *39*, 49.
287. A. Neshat, H. R. Shahsavari, P. Mastrorilli, S. Todisco, M. G. Haghighi, B. Notash, *Inorg. Chem.,* **2018**, *57*, 1398.
288. R. J. Abernethy, F. H. Anthony, H. Neumann, A. C. Willis, *Inorg. Chim. Acta,* **2005**, *358*, 1605.
289. H. J. Barnett. *Carbidos, Carbonyls, Carbynes and Carbenes: Reactivity of the Bridging C1 Ligand*. PhD Thesis. Australian National University, Canberra, Australia, **2022**.
290. S. Pal, M. W. Drover, B. O. Patrick, J. A. Love, *Eur. J. Inorg. Chem.,* **2016**, *2016*, 2403.
291. I. R. Crossley, A. F. Hill, A. C. Willis, *Organometallics,* **2005**, *24*, 4889.
292. M. R. Patil, N. P. Dedhia, A. R. Kapdi, A. V. Kumar, *J. Org. Chem.,* **2018**, *83*, 4477.
293. V. Phillips, K. J. Willard, J. A. Golen, C. J. Moore, A. L. Rheingold, L. H. Doerrer, *Inorg. Chem.,* **2010**, *49*, 9265.
294. Z. Chen, K. M.-C. Wong, E. C.-H. Kwok, N. Zhu, Y. Zu, V. W.-W. Yam, *Inorg. Chem.,* **2011**, *50*, 2125.
295. C. Y.-S. Chung, S. P.-Y. Li, K. K.-W. Lo, V. W.-W. Yam, *Inorg. Chem.,* **2016**, *55*, 4650.
296. V. W.-W. Yam, *Nat. Synth.,* **2023**, *2*, 94.
297. H. Lang, A. del Villar, B. Walfort, G. Rheinwald, *J. Organomet. Chem.,* **2003**, *682*, 155.
298. M.-M. Wu, L.-Y. Zhang, Y.-H. Qin, Z.-N. Chen, *Acta Crystallogr. Sec. E,* **2003**, *59*, m210.
299. S. Trofimenko, *Scorpionates – The Coordination Chemistry of Polypyrazolylborate Ligands*. Imperial College Press: London, **1999**.
300. C. Pettinari, *Scorpionates II: Chelating Borate Ligands*. Imperial College Press: London, **2008**.
301. P. K. Byers, A. J. Canty, R. T. Honeyman, *Organometallic Chemistry of Palladium and Platinum with Poly(pyrazol-1-yl)alkanes and Poly(pyrazol-1-yl)borates*. In *Adv. Organomet. Chem.*, F. G. A. Stone; R. West, Eds. Academic Press: **1992**; *Vol. 34*, pp 1.
302. I. R. Crossley, *Chapter 2 - The Organometallic Chemistry of Group 10 Poly(pyrazolyl)borate Complexes*. In *Adv. Organomet. Chem.*, A. F. Hill; M. J. Fink, Eds. Academic Press: **2010**; *Vol. 58*, pp 109.

303. F. A. Cotton, C. S. Kraihanzel, *J. Am. Chem. Soc.,* **1962**, *84*, 4432.
304. C. Hansch, A. Leo, R. W. Taft, *Chem. Rev.,* **1991**, *91*, 165.
305. G. M. Jamison, P. S. White, J. L. Templeton, *Organometallics,* **1991**, *10*, 1954.
306. A. E. Bruce, A. S. Gamble, T. L. Tonker, J. L. Templeton, *Organometallics,* **1987**, *6*, 1350.
307. A. L. Colebatch, A. F. Hill, M. Sharma, *Organometallics,* **2015**, *34*, 2165.
308. A. L. Colebatch, A. F. Hill, *Dalton Trans,* **2017**, *46*, 4355.
309. B. J. Frogley, A. F. Hill, R. A. Manzano, M. Sharma, *Chem. Commun.,* **2018**, *54*, 1702.
310. K. C. Stone, G. M. Jamison, P. S. White, J. L. Templeton, *Inorg. Chim. Acta,* **2002**, *330*, 161.
311. D. S. Frohnapfel, P. S. White, J. L. Templeton, *Organometallics,* **2000**, *19*, 1497.
312. B. E. Woodworth, D. S. Frohnapfel, P. S. White, J. L. Templeton, *Organometallics,* **1998**, *17*, 1655.
313. B. E. Woodworth, P. S. White, J. L. Templeton, *J. Am. Chem. Soc.,* **1997**, *119*, 828.
314. K. C. Stone, P. S. White, J. L. Templeton, *J. Organomet. Chem.,* **2003**, *684*, 13.
315. A. C. Filippou, C. Wagner, E. O. Fischer, C. Völkl, *J. Organomet. Chem.,* **1992**, *438*, C15.
316. A. C. Filippou, P. Hofmann, P. Kiprof, H. R. Schmid, C. Wagner, *J. Organomet. Chem.,* **1993**, *459*, 233.
317. O. Masayoshi, S. Koji, H. Katsuma, *Bull. Chem. Soc. Jpn.,* **1978**, *51*, 3209.
318. S. O. Grim, R. L. Keiter, W. McFarlane, *Inorg. Chem.,* **1967**, *6*, 1133.
319. P. S. Pregosin, R. Kunz, *Helv. Chim. Acta,* **1975**, *58*, 423.
320. Y. Koie, S. Shinoda, Y. Saito, *J. Chem. Soc., Dalton Trans.,* **1981**, 1082.
321. B. A. Chalmers, P. S. Nejman, A. V. Llewellyn, A. M. Felaar, B. L. Griffiths, E. I. Portman, E.-J. L. Gordon, K. J. H. Fan, J. D. Woollins, M. Bühl, O. L. Malkina, D. B. Cordes, A. M. Z. Slawin, P. Kilian, *Inorg. Chem.,* **2018**, *57*, 3387.
322. G. P. Moss, P. A. S. Smith, D. Tavernier, *Pure Appl. Chem.,* **1995**, *67*, 1307.
323. L. Tschgajeff, M. J. Skanawy-Grigorjewa, *Russ. Chem. Ges.,* **1915**, *47*, 776.
324. W. P. Fehlhammer, M. Fritz, *Chem. Rev.,* **1993**, *93*, 1243.
325. F. E. Hahn, *Angew. Chem., Int. Ed.,* **1993**, *32*, 650.
326. M. V. Barybin, J. J. Meyers Jr, B. M. Neal, *Renaissance of Isocyanoarenes as Ligands in Low-Valent Organometallics*. In *Isocyanide Chemistry*, **2012**; pp 493.
327. B. Altundas, J.-P. R. Marrazzo, F. F. Fleming, *Org. Biomol. Chem.,* **2020**, *18*, 6467.
328. M. Knorn, E. Lutsker, O. Reiser, *Chem. Soc. Rev.,* **2020**, *49*, 7730.
329. S. Mukhopadhyay, A. G. Patro, R. S. Vadavi, S. Nembenna, *Eur. J. Inorg. Chem.,* **2022**, *2022*.
330. R. L. Miller, P. T. Wolczanski, A. L. Rheingold, *J. Am. Chem. Soc.,* **2002**, *115*, 10422.
331. V. V. Tumanov, A. A. Tishkov, H. Mayr, *Angew. Chem., Int. Ed.,* **2007**, *46*, 3563.
332. B. Weinberger, W. P. Fehlhammer, *Angew. Chem., Int. Ed.,* **1980**, *19*, 480.
333. H. Stolzenberg, B. Weinberger, W. P. Fehlhammer, F. G. Pühlhofer, R. Weiss, *Eur. J. Inorg. Chem.,* **2005**, *2005*, 4263.
334. A. E, M. P., L. Á., *Synlett,* **2000**, *2000*, 526.
335. T.-W. Chiu, Y.-H. Liu, K.-M. Chi, Y.-S. Wen, K.-L. Lu, *Inorg. Chem.,* **2005**, *44*, 6425.
336. A. Ramazani, A. Rezaei, *Organic Letters,* **2010**, *12*, 2852.
337. G. M. Ojeda-Carralero, L. G. Ceballos, J. Coro, D. G. Rivera, *ACS Comb. Sci.,* **2020**, *22*, 475.
338. Y. Wang, C. Zhang, *ChemistrySelect,* **2020**, *5*, 171.
339. D. Matheau-Raven, D. J. Dixon, *J. Org. Chem.,* **2022**, *87*, 12498.
340. M. Green, J. A. Howard, J. L. Spencer, F. G. A. Stone, *J. Chem. Soc., Chem. Commun.,* **1975**, 3.
341. C. G. Francis, S. I. Khan, P. R. Morton, *Inorg. Chem.,* **1984**, *23*, 3680.
342. J.-M. Bassett, M. Green, J. A. K. Howard, F. G. A. Stone, *J. Chem. Soc., Chem. Commun.,* **1978**, 1000.
343. Y. Yamamoto, *Coord. Chem. Rev.,* **1980**, *32*, 193.

344. L. E. Crascall, J. L. Spencer, R. A. Doyle, R. J. Angelici, *Olefin Complexes of Platinum*. In *Inorg. Synth.*, **1990**; pp 126.
345. T. F. Vaughan, D. J. Koedyk, J. L. Spencer, *Organometallics,* **2011**, *30*, 5170.
346. J.-M. Bassett, M. Green, J. A. K. Howard, F. G. A. Stone, *J. Chem. Soc., Chem. Commun.,* **1977**, 853.
347. M. Green, J. A. K. Howard, M. Murray, J. L. Spencer, F. G. A. Stone, *J. Chem. Soc., Dalton Trans.,* **1977**, 1509.
348. J.-M. Bassett, D. E. Berry, G. K. Barker, M. Green, J. A. K. Howard, F. G. A. Stone, *J. Chem. Soc., Dalton Trans.,* **1979**, 1003.
349. M. Knorr, I. Jourdain, D. Lentz, S. Willemsen, C. Strohmann, *J. Organomet. Chem.,* **2003**, *684*, 216.
350. B. J. Frogley, A. F. Hill, *Angew. Chem., Int. Ed.,* **2019**, *58*, 8044.
351. T. Görlich, P. Coburger, E. Yang, J. Goicoechea, H. Grützmacher, C. Müller, *Angew. Chem., Int. Ed.,* **2023**, *Accepted Manuscript*, doi:10.1002/anie.202217749.
352. P. Pyykkö, Y. Zhao, *Mol. Phys.,* **1990**, *70*, 701.
353. D. Knol, N. J. Koole, M. J. A. De Bie, *Org. Magn. Reson.,* **1976**, *8*, 213.
354. E. O. Fischer, W. Schambeck, *J. Organomet. Chem.,* **1980**, *201*, 311.
355. F. Calderazzo, U. Englert, A. Guarini, F. Marchetti, G. Pampaloni, A. Segre, G. Tripepi, *Chem. Eur. J.,* **1996**, *2*, 412.
356. K. D. Wells, R. McDonald, M. J. Ferguson, M. Cowie, *Inorg. Chem.,* **2011**, *50*, 3523.
357. N. Tsoureas, F. G. N. Cloke, *Chem. Commun.,* **2018**, *54*, 8830.
358. L. M. Caldwell, A. F. Hill, R. Stranger, R. N. L. Terrett, K. M. von Nessi, J. S. Ward, A. C. Willis, *Organometallics,* **2015**, *34*, 328.
359. M. Z. Kassaee, M. Ghambarian, S. M. Musavi, *Heteroat. Chem,* **2008**, *19*, 377.
360. R. A. Kendall, T. H. D. Jr., R. J. Harrison, *J. Chem. Phys.,* **1992**, *96*, 6796.
361. M. H. Garner, R. Hoffmann, S. Rettrup, G. C. Solomon, *ACS Cent. Sci.,* **2018**, *4*, 688.
362. A. K. List, G. L. Hillhouse, A. L. Rheingold, *J. Am. Chem. Soc.,* **1988**, *110*, 4855.
363. F. J. Lalor, S. A. O'Neill, *J. Organomet. Chem.,* **2003**, *684*, 249.
364. W. A. Herrmann, *Angew. Chem., Int. Ed.,* **1982**, *21*, 117.
365. M. J. Overett, R. O. Hill, J. R. Moss, *Coord. Chem. Rev.,* **2000**, *206-207*, 581.
366. H.-Y. Jang, M. J. Krische, *Acc. Chem. Res.,* **2004**, *37*, 653.
367. P. M. Maitlis, *J. Organomet. Chem.,* **2004**, *689*, 4366.
368. O. O. James, B. Chowdhury, M. A. Mesubi, S. Maity, *RSC Adv.,* **2012**, *2*, 7347.
369. M. K. Samantaray, V. D'Elia, E. Pump, L. Falivene, M. Harb, S. Ould Chikh, L. Cavallo, J.-M. Basset, *Chem. Rev.,* **2020**, *120*, 734.
370. K. Yuvaraj, I. Douair, A. Paparo, L. Maron, C. Jones, *J. Am. Chem. Soc.,* **2019**, *141*, 8764.
371. A. Paparo, K. Yuvaraj, A. J. R. Matthews, I. Douair, L. Maron, C. Jones, *Angew. Chem., Int. Ed.,* **2021**, *60*, 630.
372. G. A. Bailey, J. A. Buss, P. H. Oyala, T. Agapie, *J. Am. Chem. Soc.,* **2021**, *143*, 13091.
373. J. Ohata, A. Teramoto, H. Fujita, S. Takemoto, H. Matsuzaka, *J. Am. Chem. Soc.,* **2021**, *143*, 16105.
374. D. J. Armitt, M. I. Bruce, M. Gaudio, N. N. Zaitseva, B. W. Skelton, A. H. White, B. Le Guennic, J.-F. Halet, M. A. Fox, R. L. Roberts, F. Hartl, P. J. Low, *Dalton Trans.,* **2008**, 6763.
375. E. S. Borren, A. F. Hill, R. Shang, M. Sharma, A. C. Willis, *J Am Chem Soc,* **2013**, *135*, 4942.
376. C. K. Rofer-Depoorter, *Chem. Rev.,* **1981**, *81*, 447.
377. N. M. West, A. J. M. Miller, J. A. Labinger, J. E. Bercaw, *Coord. Chem. Rev.,* **2011**, *255*, 881.
378. J. S. Bradley, G. B. Ansell, E. W. Hill, *J. Am. Chem. Soc.,* **1979**, *101*, 7417.
379. M. Tachikawa, E. L. Muetterties, *J. Am. Chem. Soc.,* **1980**, *102*, 4541.
380. J. S. Bradley, G. B. Ansell, M. E. Leonowicz, E. W. Hill, *J. Am. Chem. Soc.,* **1981**, *103*, 4968.

381. J. H. Davis, M. A. Beno, J. M. Williams, J. Zimmie, M. Tachikawa, E. L. Muetterties, *Proc. Natl. Acad. Sci.,* **1981**, *78*, 668.
382. P. L. Bogdan, M. Sabat, S. A. Sunshine, C. Woodcock, D. F. Shriver, *Inorg. Chem.,* **1988**, *27*, 1904.
383. D. L. Davies, B. P. Gracey, V. Guerchais, S. A. R. Knox, A. G. Orpen, *J. Chem. Soc., Chem. Commun.,* **1984**, 841.
384. F. H. Allen, O. Kennard, D. G. Watson, L. Brammer, A. G. Orpen, R. Taylor, *J. Chem. Soc., Perkin Trans. 2,* **1987**, S1.
385. A. Nutton, A. V. de Miguel, K. Isobe, P. M. Maitlis, *J. Chem. Soc., Chem. Commun.,* **1983**, 166.
386. E. L. Hoel, G. B. Ansell, S. Leta, *Organometallics,* **1984**, *3*, 1633.
387. E. L. Hoel, G. B. Ansell, S. Leta, *Organometallics,* **1986**, *5*, 585.
388. C. P. Casey, E. A. Austin, A. L. Rheingold, *Organometallics,* **1987**, *6*, 2157.
389. I. M. Saez, D. G. Andrews, P. M. Maitlis, *Polyhedron,* **1988**, *7*, 827.
390. J. M. Martinez, H. Adams, N. A. Bailey, P. M. Maitlis, *J. Chem. Soc., Chem. Commun.,* **1989**, 286.
391. V. C. Gibson, G. Parkin, J. E. Bercaw, *Organometallics,* **1991**, *10*, 220.
392. S. J. Trepanier, J. N. L. Dennett, B. T. Sterenberg, R. McDonald, M. Cowie, *J. Am. Chem. Soc.,* **2004**, *126*, 8046.
393. A. I. O. Suarez, M. P. del Río, K. Remerie, J. N. H. Reek, B. de Bruin, *ACS Catal.,* **2012**, *2*, 2046.
394. B. Sjollema, *J. Chem. Soc., Abstr.,* **1898**, *74*, B307.
395. H. G. Julsing, R. I. McCrindle, *J. Chem. Technol. Biotechnol.,* **2001**, *76*, 349.
396. J. C. Thomas, J. C. Peters, *Polyhedron,* **2004**, *23*, 489.
397. M. A. Alvarez, M. E. García, D. García-Vivó, M. E. Martínez, M. A. Ruiz, *Organometallics,* **2011**, *30*, 2189.
398. K. Searles, K. T. Smith, T. Kurogi, C. H. Chen, P. J. Carroll, D. J. Mindiola, *Angewandte Chemie,* **2016**, *128*, 6754.
399. F. H. Allen, I. J. Bruno, *Acta Crystallogr. B.,* **2010**, *66*, 380.
400. D. D. Devore, J. A. K. Howard, J. C. Jeffery, M. U. Pilotti, F. G. A. Stone, *J. Chem. Soc., Dalton Trans.,* **1989**, 303.
401. J. T. Chen, T. M. Huang, M. C. Cheng, Y. Wang, *Organometallics,* **1990**, *9*, 539.
402. G. M. Whitesides, J. F. Gaasch, E. R. Stedronsky, *J. Am. Chem. Soc.,* **1972**, *94*, 5258.
403. S. J. Holmes, D. N. Clark, H. W. Turner, R. R. Schrock, *J. Am. Chem. Soc.,* **1982**, *104*, 6322.
404. A. F. Hill, R. Y. Kong, *Chem. Commun.,* **2017**, *53*, 2032.
405. T. Kurogi, P. J. Carroll, D. J. Mindiola, *J. Am. Chem. Soc.,* **2016**, *138*, 4306.
406. T. Kurogi, B. Pinter, D. J. Mindiola, *Organometallics,* **2018**, *37*, 3385.
407. T. Kurogi, D. J. Mindiola, *Organometallics,* **2020**, *39*, 4474.
408. P. R. Sharp, S. J. Holmes, R. R. Schrock, M. R. Churchill, H. J. Wasserman, *J. Am. Chem. Soc.,* **1981**, *103*, 965.
409. M. R. Churchill, A. L. Rheingold, H. J. Wasserman, *Inorg. Chem.,* **1981**, *20*, 3392.
410. C. P. Casey, P. J. Fagan, W. H. Miles, *J. Am. Chem. Soc.,* **1982**, *104*, 1134.
411. S. C. Kao, P. P. Y. Lu, R. Pettit, *Organometallics,* **1982**, *1*, 911.
412. C. P. Casey, P. J. Fagan, V. W. Day, *J. Am. Chem. Soc.,* **1982**, *104*, 7360.
413. C. P. Casey, P. J. Fagan, *J. Am. Chem. Soc.,* **1982**, *104*, 4950.
414. C. P. Casey, L. K. Woo, P. J. Fagan, R. E. Palermo, B. R. Adams, *Organometallics,* **1987**, *6*, 447.
415. C. P. Casey, M. Crocker, P. C. Vosejpka, P. J. Fagan, S. R. Marder, M. A. Gohdes, *Organometallics,* **1988**, *7*, 670.
416. S. Takemoto, T. Kobayashi, T. Ito, A. Inui, K. Karitani, S. Katagiri, Y. Masuhara, H. Matsuzaka, *Organometallics,* **2011**, *30*, 2160.

417. D. M. Hoffman, D. A. Wierda, *J. Am. Chem. Soc.,* **1990**, *112*, 7056.
418. S. Sarkar, J. A. Culver, A. J. Peloquin, I. Ghiviriga, K. A. Abboud, A. S. Veige, *Angew. Chem., Int. Ed.,* **2010**, *49*, 9711.
419. J. B. Greco, J. C. Peters, T. A. Baker, W. M. Davis, C. C. Cummins, G. Wu, *J. Am. Chem. Soc.,* **2001**, *123*, 5003.
420. R. Criegee, *Angew. Chem., Int. Ed.,* **1962**, *1*, 519.
421. A. V. Safronova, L. N. Bochkarev, N. E. Stolyarova, I. K. Grigorieva, I. P. Malysheva, G. V. Basova, G. K. Fukin, Y. A. Kurskii, S. Y. Khorshev, G. A. Abakumov, *J. Organomet. Chem.,* **2004**, *689*, 1127.
422. A. V. Safronova, L. N. Bochkarev, G. K. Fukin, E. V. Baranov, Y. A. Kurskii, G. A. Abakumov, *Russ. J. Gen. Chem.,* **2009**, *79*, 1825.
423. L. N. Bochkarev, A. V. Nikitinskii, Y. E. Begantsova, V. I. Shcherbakov, N. E. Stolyarova, I. K. Grigorieva, I. P. Malysheva, G. V. Basova, G. K. Fukin, E. V. Baranov, Y. A. Kurskii, G. A. Abakumov, *J. Organomet. Chem.,* **2005**, *690*, 3212.
424. L. N. Bochkarev, Y. E. Begantsova, A. L. Bochkarev, N. E. Stolyarova, I. K. Grigorieva, I. P. Malysheva, G. V. Basova, E. O. Platonova, G. K. Fukin, E. V. Baranov, Y. A. Kurskii, G. A. Abakumov, *J. Organomet. Chem.,* **2006**, *691*, 5240.
425. Y. P. Barinova, A. L. Bochkarev, Y. E. Begantsova, L. N. Bochkarev, Y. A. Kurskii, G. K. Fukin, A. V. Cherkasov, G. A. Abakumov, *Russ. J. Gen. Chem.,* **2010**, *80*, 1945.
426. G. Y. Vollmer, M. W. Wallasch, D. Saurenz, T. R. Eger, H. Bauer, G. Wolmershäuser, M. H. Prosenc, H. Sitzmann, *Organometallics,* **2015**, *34*, 644.
427. R. Meij, D. J. Stufkens, K. Vrieze, E. Roosendaal, H. Schenk, *J. Organomet. Chem.,* **1978**, *155*, 323.
428. R. Y. Kong. *Reactivity of a Terminal Methylidyne*. Honours Thesis. Australian National University, Canberra, Australia, **2016**.
429. J. C. Jeffery, F. Gordon, A. Stone, G. K. Williams, *Polyhedron,* **1991**, *10*, 215.
430. A. Haque, R. A. Al-Balushi, I. J. Al-Busaidi, M. S. Khan, P. R. Raithby, *Chem. Rev.,* **2018**, *118*, 8474.
431. R. He, R. A. Domingues, S. Valandro, K. S. Schanze, *Macromolecules,* **2021**, *54*, 9888.
432. D. Walther, K. Lamm, H. Görls, *Z. Anorg. Allg. Chem.,* **2009**, *635*, 1187.
433. H. Lang, R. Packheiser, B. Walfort, *Organometallics,* **2006**, *25*, 1836.
434. R. Packheiser, B. Walfort, H. Lang, *Organometallics,* **2006**, *25*, 4579.
435. G. Butler, C. Eaborn, A. Pidcock, *J. Organomet. Chem.,* **1981**, *210*, 403.
436. L. Rigamonti, C. Manassero, M. Rusconi, M. Manassero, A. Pasini, *Dalton Trans.,* **2009**, 1206.
437. T. B. Peters, Q. Zheng, J. Stahl, J. C. Bohling, A. M. Arif, F. Hampel, J. A. Gladysz, *J. Organomet. Chem.,* **2002**, *641*, 53.
438. B. Schwenzer, J. Schleu, N. Burzlaff, C. Karl, H. Fischer, *J. Organomet. Chem.,* **2002**, *641*, 134.
439. M. I. Bruce, B. W. Skelton, A. H. White, N. N. Zaitseva, *J. Organomet. Chem.,* **2003**, *683*, 398.
440. K. Sonogashira, S. Takahashi, N. Hagihara, *Macromolecules,* **1977**, *10*, 879.
441. K. Sonogashira, Y. Fujikura, T. Yatake, N. Toyoshima, S. Takahashi, N. Hagihara, *J. Organomet. Chem.,* **1978**, *145*, 101.
442. K. Sonogashira, S. Kataoka, S. Takahashi, N. Hagihara, *J. Organomet. Chem.,* **1978**, *160*, 319.
443. B. Schwenzer, J. Schleu, N. Burzlaff, C. Karl, H. Fischer, *J. Organomet. Chem.,* **2002**, *641*, 134.
444. F. Asaro, M. Lenarda, G. Pellizer, L. Storaro, *Spectrochimica Acta Part A,* **2000**, *56*, 2167.
445. S. Yamazaki, Z. Taira, T. Yonemura, A. J. Deeming, *Organometallics,* **2005**, *24*, 20.
446. Y. Nakajima, M. Nakatani, K. Hayashi, Y. Shiraishi, R. Takita, M. Okazaki, F. Ozawa, *New J. Chem.,* **2010,** *34*, 1713.

447. D. S. Frohnapfel, B. E. Woodworth, H. H. Thorp, J. L. Templeton, *J. Phys. Chem. A,* **1998**, *102*, 5665.
448. R. D. Dewhurst, A. F. Hill, M. K. Smith, *Angew. Chem., Int. Ed.,* **2004**, *43*, 476.
449. R. D. Dewhurst, A. F. Hill, A. C. Willis, *Organometallics,* **2009**, *28*, 4735.
450. A. R. Delaney, B. J. Frogley, A. F. Hill, *Dalton Trans.,* **2019**, *48*, 13674.
451. J. F. Hartwig, *Inorg. Chem.,* **2007**, *46*, 1936.
452. S. Shekhar, J. F. Hartwig, *J. Am. Chem. Soc.,* **2004**, *126*, 13016.
453. Q. Zheng, J. C. Bohling, T. B. Peters, A. C. Frisch, F. Hampel, J. A. Gladysz, *Chem. Eur. J.,* **2006**, *12*, 6486.
454. G. R. Owen, J. Stahl, F. Hampel, J. A. Gladysz, *Chem. Eur. J.,* **2008**, *14*, 73.
455. S. Dey, T. Zhang, N. Bhuvanesh, J. A. Gladysz, *J. Organomet. Chem.,* **2017**, *849-850*, 237.
456. A. F. Hill, R. A. Manzano, *Angew. Chem., Int. Ed.,* **2019**, *58*, 15354.
457. L. K. Burt, R. D. Dewhurst, A. F. Hill, R. Y. Kong, E. E. Nahon, C. S. Onn, *Dalton Trans.,* **2022**, *51*, 12080.
458. V. Farina, S. Kapadia, B. Krishnan, C. Wang, L. S. Liebeskind, *J. Org. Chem.,* **1994**, *59*, 5905.
459. R. A. Manzano. *The Odd Nature of Main Group Organometallic Polyyne Complexes*. PhD Thesis. Australian National University, Canberra, Australia, **2019**.
460. G. W. Rice, G. B. Ansell, M. A. Modrick, S. Zentz, *Organometallics,* **1983**, *2*, 154.
461. H. Schmidbaur, R. Pichl, G. Müller, *Angew. Chem., Int. Ed.,* **1986**, *25*, 574.
462. K. A. Hughes, P. G. Dopico, M. Sabat, M. G. Finn, *Angew. Chem., Int. Ed.,* **1993**, *32*, 554.
463. F. G. Schröder, C. Lichtenberg, M. Elfferding, J. Sundermeyer, *Organometallics,* **2013**, *32*, 5082.
464. Y. Mutoh, N. Kozono, M. Araki, N. Tsuchida, K. Takano, Y. Ishii, *Organometallics,* **2010**, *29*, 519.
465. Y.-C. Tsai, M. J. A. Johnson, D. J. Mindiola, C. C. Cummins, W. T. Klooster, T. F. Koetzle, *J. Am. Chem. Soc.,* **1999**, *121*, 10426.
466. R. B. Bedford, A. F. Hill, A. J. P. White, D. J. Williams, *Angew. Chem., Int. Ed.,* **1996**, *35*, 95.
467. F. R. Kreissl, N. Ullrich, *J. Organomet. Chem.,* **1989**, *361*, C30.
468. D. J. Cook, A. F. Hill, *Organometallics,* **2003**, *22*, 3502.
469. L. M. Caldwell, A. F. Hill, A. C. Willis, *Chem. Commun.,* **2005**, 2615.
470. A. L. Colebatch, A. F. Hill, M. Sharma, *Organometallics,* **2014**, *34*, 2165.
471. W. Petz, *Coord. Chem. Rev.,* **2008**, *252*, 1689.
472. J. C. Green, A. L. Hector, A. F. Hill, S. Lin, J. D. E. T. Wilton-Ely, *Organometallics,* **2008**, *27*, 5548.
473. L. M. Caldwell, A. F. Hill, A. C. Willis, *Chem. Commun.,* **2005**, 2615.
474. P. J. Lim, D. A. Slizys, J. M. White, C. G. Young, E. R. T. Tiekink, *Organometallics,* **2003**, *22*, 4853.
475. C. J. Adams, A. Baber, S. Boonyuen, N. G. Connelly, B. E. Diosdado, A. Kantacha, A. G. Orpen, E. Patrón, *Dalton Trans.,* **2009**, 9746.
476. S. Ludwig, K. Helmdach, M. Hüttenschmidt, E. Oberem, J. Rabeah, A. Villinger, R. Ludwig, W. W. Seidel, *Chem. Eur. J.,* **2020**, *26*, 16811.
477. T. B. Rauchfuss, *Inorg. Chem.,* **2004**, *43*, 14.
478. B. J. Frogley, A. F. Hill, *Dalton Trans.,* **2022**, *51*, 1907.
479. T. D. Tilley, *J. Am. Chem. Soc.,* **1985**, *107*, 4084.
480. H. G. Woo, W. P. Freeman, T. D. Tilley, *Organometallics,* **1992**, *11*, 2198.
481. F. H. Elsner, T. D. Tilley, A. L. Rheingold, S. J. Geib, *J. Organomet. Chem.,* **1988**, *358*, 169.
482. Z. Wu, L. H. McAlexander, J. B. Diminnie, Z. Xue, *Organometallics,* **1998**, *17*, 4853.
483. Z. Wu, J. B. Diminnie, Z. Xue, *Organometallics,* **1999**, *18*, 1002.
484. D. Frank, J. Baumgartner, C. Marschner, *Chem. Commun.,* **2002**, 1190.

485. R. Fischer, D. Frank, W. Gaderbauer, C. Kayser, C. Mechtler, J. Baumgartner, C. Marschner, *Organometallics,* **2003**, *22*, 3723.
486. M. J. Sgro, W. E. Piers, *Inorg. Chim. Acta,* **2014**, *422*, 243.
487. R. Fischer, C. Marschner, *Mendeleev Commun.,* **2022**, *32*, 52.
488. C. E. F. Rickard, W. R. Roper, D. M. Salter, L. J. Wright, *Organometallics,* **1992**, *11*, 3931.
489. M. T. Attar-Bashi, C. E. F. Rickard, W. R. Roper, L. J. Wright, S. D. Woodgate, *Organometallics,* **1998**, *17*, 504.
490. D. M. Roddick, B. D. Santarsiero, J. E. Bercaw, *J. Am. Chem. Soc.,* **1985**, *107*, 4670.
491. A. Grundmann, M. B. Sárosi, P. Lönnecke, E. Hey-Hawkins, *Eur. J. Inorg. Chem.,* **2014**, *2014*, 2997.
492. C. N. Matthews, G. H. Birum, *Acc. Chem. Res.,* **1969**, *2*, 373.
493. U. Belluco, R. A. Michelin, M. Mozzon, R. Bertani, G. Facchin, L. Zanotto, L. Pandolfo, *J. Organomet. Chem.,* **1998**, *557*, 37.
494. H. Schmidbaur, C. E. Zybill, D. Neugebauer, *Angew. Chem., Int. Ed.,* **1982**, *21*, 310.
495. D. Wormsbächer, F. Edelmann, U. Behrens, *Chem. Ber.,* **1981**, *114*, 153.
496. H. Werner, J. Wolf, R. Zolk, U. Schubert, *Angew. Chem., Int. Ed.,* **1983**, *22*, 981.
497. R. Drews, D. Wormsbächer, U. Behrens, *J. Organomet. Chem.,* **1984**, *272*, C40.
498. K. Seitz, U. Behrens, *J. Organomet. Chem.,* **1985**, *288*, c47.
499. H. Werner, O. Kolb, U. Schubert, K. Ackermann, *Chem. Ber.,* **1985**, *118*, 873.
500. J. Benecke, R. Drews, U. Behrens, F. Edelmann, K. Keller, H. W. Roesky, *J. Organomet. Chem.,* **1987**, *320*, C31.
501. K. Seitz, U. Behrens, *J. Organomet. Chem.,* **1988**, *345*, 351.
502. J. Wolf, R. Zolk, U. Schubert, H. Werner, *J. Organomet. Chem.,* **1988**, *340*, 161.
503. Y.-J. Kim, S.-C. Lee, M. H. Cho, S.-W. Lee, *J. Organomet. Chem.,* **1999**, *588*, 268.
504. A. F. Hill, J. M. Malget, A. J. P. White, D. J. Williams, *Inorg. Chem.,* **1998**, *37*, 598.
505. K. Helmdach, A. Villinger, W. W. Seidel, *Z. Anorg. Allg. Chem.,* **2015**, *641*, 2300.
506. C. A. Dyker, V. Lavallo, B. Donnadieu, G. Bertrand, *Angew. Chem., Int. Ed.,* **2008**, *47*, 3206.
507. N. Miyaura, A. Suzuki, *J. Chem. Soc., Chem. Commun.,* **1979**, 866.
508. N. Miyaura, K. Yamada, A. Suzuki, *Tetrahedron Letters,* **1979**, *20*, 3437.
509. A. J. J. Lennox, G. C. Lloyd-Jones, *Chem. Soc. Rev.,* **2014**, *43*, 412.
510. J. P. G. Rygus, C. M. Crudden, *J. Am. Chem. Soc.,* **2017**, *139*, 18124.
511. Y. M. Kim, S. Yu, *J. Am. Chem. Soc.,* **2003**, *125*, 1696.
512. M. Tobisu, T. Xu, T. Shimasaki, N. Chatani, *J. Am. Chem. Soc.,* **2011**, *133*, 19505.
513. D. V. Partyka, M. Zeller, A. D. Hunter, T. G. Gray, *Angew. Chem., Int. Ed.,* **2006**, *45*, 8188.
514. A. S. K. Hashmi, T. D. Ramamurthi, F. Rominger, *J. Organomet. Chem.,* **2009**, *694*, 592.
515. M. A. Peay, J. E. Heckler, N. Deligonul, T. G. Gray, *Organometallics,* **2011**, *30*, 5071.
516. M. Peña-López, L. A. Sarandeses, J. Pérez Sestelo, *Eur. J. Org. Chem.,* **2013**, *2013*, 2545.
517. M. Hofer, E. Gomez-Bengoa, C. Nevado, *Organometallics,* **2014**, *33*, 1328.
518. D. V. Partyka, M. Zeller, A. D. Hunter, T. G. Gray, *Inorg. Chem.,* **2012**, *51*, 8394.
519. L. O'Brien, S. P. Argent, K. Ermanis, H. W. Lam, *Angew. Chem., Int. Ed.,* **2022**, *61*, doi: 10.1002/anie.202202305.
520. M.-Q. Yan, J. Yuan, F. Lan, S.-H. Zeng, M.-Y. Gao, S.-H. Liu, J. Chen, G.-A. Yu, *Org. Biomol. Chem.,* **2017**, *15*, 3924.
521. D. C. Brower, M. Stoll, J. L. Templeton, *Organometallics,* **1989**, *8*, 2786.
522. X. A. F. Cook, A. Gombert, J. McKnight, L. R. E. Pantaine, M. C. Willis, *Angew. Chem., Int. Ed.,* **2021**, *60*, 11068.
523. L. G. Makarova, A. N. Nesmeyanov, *The Organic Compounds of Mercury*. Noth-Holland Publishing Company: Amsterdam, **1967**; *Vol. 4*, p 518.
524. H. Schmidbaur, A. Schier, *2.05 - Gold Organometallics*. In *Comprehensive Organometallic Chemistry III*, D. M. P. Mingos; R. H. Crabtree, Eds. Elsevier: Oxford, **2007**; pp 251.

525. H. Schmidbaur, *Gold: Progress in Chemistry, Biochemistry, and Technology*. John Wiley & Sons: New York, **1999**; p 894.
526. J. P. Collman, J. W. Kang, *J. Am. Chem. Soc.,* **1967**, *89*, 844.
527. M. N. Peñas-Defrutos, C. Bartolomé, M. García-Melchor, P. Espinet, *Angew. Chem., Int. Ed.,* **2019**, *58*, 3501.
528. K. Masanori, S. Kazuo, S. Yutaka, M. Toshihiko, *Chem. Lett.,* **1977**, *6*, 301.
529. D. Milstein, J. K. Stille, *J. Am. Chem. Soc.,* **1978**, *100*, 3636.
530. C. Cordovilla, C. Bartolomé, J. M. Martínez-Ilarduya, P. Espinet, *ACS Catal.,* **2015**, *5*, 3040.
531. B. Cetinkaya, M. F. Lappert, J. McMeeking, D. Palmer, *J. Organomet. Chem.,* **1972**, *34*, C37.
532. B. Cetinkaya, M. F. Lappert, J. McMeeking, D. E. Palmer, *J. Chem. Soc., Dalton Trans.,* **1973**, 1202.
533. A. Sebald, C. Stader, B. Wrackmeyer, W. Bensch, *J. Organomet. Chem.,* **1986**, *311*, 233.
534. M. P. Gamasa, J. Gimeno, I. Godefroy, E. Lastra, B. M. Martín-Vaca, S. García-Granda, A. Gutierrez-Rodriguez, *J. Chem. Soc., Dalton Trans.,* **1995**, 1901.
535. R. J. Cross, M. F. Davidson, *J. Chem. Soc., Dalton Trans.,* **1986**, 411.
536. D. W. Nierenberg, R. E. Nordgren, M. B. Chang, R. W. Siegler, M. B. Blayney, F. Hochberg, T. Y. Toribara, E. Cernichiari, T. Clarkson, *N. Engl. J. Med.,* **1998**, *338*, 1672.
537. B. F. G. Johnson, J. Lewis, P. R. Raithby, D. A. Wilkinson, *J. Organomet. Chem.,* **1991**, *408*, C9.
538. G. B. Deacon, D. L. Wilkinson, *Inorg. Chim. Acta,* **1988**, *142*, 155.
539. G. Lin, R. McDonald, J. Takats, *Organometallics,* **2000**, *19*, 1814.
540. D. J. Cook, A. F. Hill, D. J. Wilson, *J. Chem. Soc., Dalton Trans.,* **1998**, 1171.
541. W. A. Henderson, S. A. Buckler, *J. Am. Chem. Soc.,* **1960**, *82*, 5794.
542. W. Lu, N. Zhu, C.-M. Che, *J. Am. Chem. Soc.,* **2003**, *125*, 16081.
543. V. Lavallo, Y. Canac, C. Präsang, B. Donnadieu, G. Bertrand, *Angew. Chem., Int. Ed.,* **2005**, *44*, 5705.
544. M. Soleilhavoup, G. Bertrand, *Acc. Chem. Res.,* **2015**, *48*, 256.
545. S. Roy, K. C. Mondal, H. W. Roesky, *Acc. Chem. Res.,* **2016**, *49*, 357.
546. M. Melaimi, R. Jazzar, M. Soleilhavoup, G. Bertrand, *Angew. Chem., Int. Ed.,* **2017**, *56*, 10046.
547. W. A. Herrmann, *Angew. Chem., Int. Ed.,* **2002**, *41*, 1290.
548. F. E. Hahn, M. C. Jahnke, *Angew. Chem., Int. Ed.,* **2008**, *47*, 3122.
549. S. Díez-González, N. Marion, S. P. Nolan, *Chem. Rev.,* **2009**, *109*, 3612.
550. N. Marion, S. P. Nolan, *Chemical Society Reviews,* **2008,** *37*, 1776.
551. S. P. Nolan, *Acc. Chem. Res.,* **2011**, *44*, 91.
552. A. Collado, D. J. Nelson, S. P. Nolan, *Chem. Rev.,* **2021**, *121*, 8559.
553. L. Canovese, C. Levi, F. Visentin, C. Santo, V. Bertolasi, *Inorg. Chim. Acta,* **2013**, *404*, 105.
554. M. C. Jahnke, T. Pape, F. E. Hahn, *Z. Naturforsch., B,* **2013**, *68*, 467.
555. A. A. Penney, G. L. Starova, E. V. Grachova, V. V. Sizov, M. A. Kinzhalov, S. P. Tunik, *Inorg. Chem.,* **2017**, *56*, 14771.
556. Y. Tanaka, Y. Kato, T. Tada, S. Fujii, M. Kiguchi, M. Akita, *J. Am. Chem. Soc.,* **2018**, *140*, 10080.
557. D. G. Gusev, *Organometallics,* **2009**, *28*, 6458.
558. H. Clavier, S. P. Nolan, *Chem. Commun.,* **2010**, *46*, 841.
559. M. V. Baker, P. J. Barnard, S. J. Berners-Price, S. K. Brayshaw, J. L. Hickey, B. W. Skelton, A. H. White, *J. Organomet. Chem.,* **2005**, *690*, 5625.
560. P. De Frémont, N. M. Scott, E. D. Stevens, S. P. Nolan, *Organometallics,* **2005**, *24*, 2411.
561. T. Ziegler, A. Rauk, *Inorg. Chem.,* **1979**, *18*, 1755.
562. H. Xiao, K.-K. Cheung, C.-M. Che, *J. Chem. Soc., Dalton Trans.,* **1996**, 3699.
563. M. J. Irwin, J. J. Vittal, R. J. Puddephatt, *Organometallics,* **1997**, *16*, 3541.
564. H. Schmidbaur, A. Schier, *Chem. Soc. Rev.,* **2012**, *41*, 370.

565. A. S. K. Hashmi, Y. Yu, F. Rominger, *Organometallics,* **2012**, *31*, 895.
566. G. E. Coates, C. Parkin, *J. Chem. Soc.,* **1962**, 3220.
567. R. Malmberg, K. Venkatesan, *Coord. Chem. Rev.,* **2021**, *449*, 214182.
568. O. Schuster, H. Schmidbaur, *Organometallics,* **2005**, *24*, 2289.
569. G. Starova, A. Penny, *CSD Communication,* **2018**, CCDC: 1584574.
570. S. Gaillard, A. M. Z. Slawin, A. T. Bonura, E. D. Stevens, S. P. Nolan, *Organometallics,* **2010**, *29*, 394.
571. S. Anderson, D. J. Cook, A. F. Hill, J. M. Malget, A. J. P. White, D. J. Williams, *Organometallics,* **2004**, *23*, 2552.
572. E. A. Doud, M. S. Inkpen, G. Lovat, E. Montes, D. W. Paley, M. L. Steigerwald, H. Vázquez, L. Venkataraman, X. Roy, *J. Am. Chem. Soc.,* **2018**, *140*, 8944.
573. L. Naldini, F. Demartin, M. Manassero, M. Sansoni, G. Rassu, M. A. Zoroddu, *J. Organomet. Chem.,* **1985**, *279*, c42.
574. M. P. Gamasa, J. Gimeno, E. Lastra, A. Aguirre, S. García-Granda, *J. Organomet. Chem.,* **1989**, *378*, C11.
575. V. Wing-Wah Yam, W. Kit-Mai Fung, K.-K. Cheung, *Chem. Commun.,* **1997**, 963.
576. V. W.-W. Yam, W. K.-M. Fung, K.-K. Cheung, *Organometallics,* **1998**, *17*, 3293.
577. J. H. K. Yip, J. Wu, K.-Y. Wong, K.-W. Yeung, J. J. Vittal, *Organometallics,* **2002**, *21*, 1612.
578. W.-Y. Lo, C.-H. Lam, V. W.-W. Yam, N. Zhu, K.-K. Cheung, S. Fathallah, S. Messaoudi, B. Le Guennic, S. Kahlal, J.-F. Halet, *J. Am. Chem. Soc.,* **2004**, *126*, 7300.
579. M. Zhang, B.-C. Su, C.-L. Li, Y. Shen, C.-K. Lam, X.-L. Feng, H.-Y. Chao, *J. Organomet. Chem.,* **2011**, *696*, 2654.
580. M. I. Bruce, B. G. Ellis, J.-F. Halet, B. Le Guennic, B. K. Nicholson, H. Sahnoune, N. Scoleri, B. W. Skelton, A. N. Sobolev, C. J. Sumby, A. H. White, N. N. Zaitseva, *Inorg. Chim. Acta,* **2016**, *453*, 654.
581. C. L. Collins, K. G. Dyall, H. F. Schaefer, *J. Chem. Phys.,* **1995**, *102*, 2024.
582. N. V. S. Harisomayajula, B.-H. Wu, D.-Y. Lu, T.-S. Kuo, I. C. Chen, Y.-C. Tsai, *Angew. Chem., Int. Ed.,* **2018**, *57*, 9925.
583. H.-J. Küppers, K. Wieghardt, Y.-H. Tsay, C. Krüger, B. Nuber, J. Weiss, *Angew. Chem., Int. Ed.,* **1987**, *26*, 575.
584. K. Singh, J. R. Long, P. Stavropoulos, *J. Am. Chem. Soc.,* **1997**, *119*, 2942.
585. X.-M. Zhang, M.-L. Tong, M.-L. Gong, H.-K. Lee, L. Luo, K.-F. Li, Y.-X. Tong, X.-M. Chen, *Chem. Eur. J.,* **2002**, *8*, 3187.
586. R. D. Köhn, G. Seifert, Z. Pan, M. F. Mahon, G. Kociok-Köhn, *Angew. Chem., Int. Ed.,* **2003**, *42*, 793.
587. G. Margraf, J. W. Bats, M. Bolte, H.-W. Lerner, M. Wagner, *Chem. Commun.,* **2003**, 956.
588. M. A. Carvajal, S. Alvarez, J. J. Novoa, *Chem. Eur. J.,* **2004**, *10*, 2117.
589. A. Sundararaman, L. N. Zakharov, A. L. Rheingold, F. Jäkle, *Chem. Commun.,* **2005**, 1708.
590. S.-L. Zheng, M. Messerschmidt, P. Coppens, *Angew. Chem., Int. Ed.,* **2005**, *44*, 4614.
591. G. M. Chiarella, D. Y. Melgarejo, A. Rozanski, P. Hempte, L. M. Perez, C. Reber, J. P. Fackler Jr, *Chem. Commun.,* **2010**, *46*, 136.
592. T. N. Mitchell, B. Kowall, *J. Organomet. Chem.,* **1994**, *471*, 39.
593. A. Sebald, B. Wrackmeyer, *Spectrochim. Acta, Part A,* **1986**, *42*, 1107.
594. S. J. Faville, W. Henderson, T. J. Mathieson, B. K. Nicholson, *J. Organomet. Chem.,* **1999**, *580*, 363.
595. H. B. Buergi, R. W. Kunz, P. S. Pregosin, *Inorg. Chem.,* **1980**, *19*, 3707.
596. L. W. Chang, *Toxicology of Metals*. Lewis Publishers: Boca Raton, FL, **1996**.
597. A. Sebald, B. Wrackmeyer, *J. Magn. Reson.,* **1985**, *63*, 397.
598. G. Klose, F. Volke, G. Peinel, G. Knobloch, *Magn. Reson. Chem.,* **1993**, *31*, 548.
599. K. E. Rowland, R. D. Thomas, *Magn. Reson. Chem.,* **1985**, *23*, 916.
600. D. Black, G. Deacon, G. Edwards, B. Gatehouse, *Aust. J. Chem.,* **1993**, *46*, 1323.

601. S. D. Emslie, A. M. Silva, A. Valera, E. Vijande Vila, L. Melo, F. Curate, D. Fidalgo, N. Inácio, M. Molina Moreno, O. Cambra-Moo, A. González Martín, R. Barroso-Bermejo, R. Montero Artús, L. García Sanjuán, *Int. J. Osteoarchaeol.,* **2022**, *32*, 202.
602. L. Yang, Y. Zhang, F. Wang, Z. Luo, S. Guo, U. Strähle, *Chemosphere,* **2020**, *245*, 125586.
603. G. Guzzi, A. Ronchi, P. Pigatto, *Chemosphere,* **2021**, *263*, 127990.
604. A. M. Bond, R. Colton, M. L. Dillon, J. E. Moir, D. R. Page, *Inorg. Chem.,* **1984**, *23*, 2883.
605. M. Sharma, *Unpublished Results*, *Private Communication*, Australian National University, Canberra, **2012**.
606. L. Liu, S.-Y. Poon, W.-Y. Wong, *J. Organomet. Chem.,* **2005**, *690*, 5036.
607. W.-Y. Wong, K.-H. Choi, G.-L. Lu, Z. Lin, *Organometallics,* **2002**, *21*, 4475.
608. A. Bauzá, I. Alkorta, J. Elguero, T. J. Mooibroek, A. Frontera, *Angew. Chem., Int. Ed.,* **2020**, *59*, 17482.
609. M. M. D. Roy, M. J. Ferguson, R. McDonald, E. Rivard, *Chem. Eur. J.,* **2016**, *22*, 18236.
610. C. Chieh, L. P. C. Leung, *Can. J. Chem.,* **1976**, *54*, 3077.
611. C. S. Lai, E. R. T. Tiekink, *Appl. Organomet. Chem.,* **2003**, *17*, 194.
612. T. Kentaro, H. Naomi, O. Tadashi, S. Yasumasa, O. Shinzaburo, *Bull. Chem. Soc. Jpn.,* **1977**, *50*, 2741.
613. A. F. Hill, M. C. J. Harris, R. P. Melling, *Polyhedron,* **1992**, *11*, 781.
614. R. B. Bedford, A. F. Hill, A. R. Thompsett, A. J. P. White, D. J. Williams, *Chem. Commun.,* **1996**, 1059.
615. A. F. Hill, J. D. E. T. Wilton-Ely, *Organometallics,* **1997**, *16*, 4517.
616. R. D. Dewhurst, A. F. Hill, A. D. Rae, A. C. Willis, *Organometallics,* **2005**, *24*, 4703.
617. L. Apostolico, H. Braunschweig, A. G. Crawford, T. Herbst, D. Rais, *Chem. Commun.,* **2008**, 497.
618. M. Alvarez, N. Lugan, R. Mathieu, *Inorg. Chem.,* **1993**, *32*, 5652.
619. S. P. Tunik, I. O. Koshevoy, A. J. Poë, D. H. Farrar, E. Nordlander, M. Haukka, T. A. Pakkanen, *Dalton Trans.,* **2003**, 2457.
620. M. M. Tomashevskaya, S. P. Tunik, I. S. Podkorytov, B. T. Heaton, J. A. Iggo, M. Haukka, T. A. Pakkanen, P. L. Pirilä, J. Pursiainen, *J. Organomet. Chem.,* **2007**, *692*, 2911.
621. J. Lloret, F. Estevan, P. Lahuerta, P. Hirva, J. Pérez-Prieto, M. Sanaú, *Chem. Eur. J.,* **2009**, *15*, 7706.
622. R. S. Nyholm, K. Vrieze, *J. Chem. Soc.,* **1965**, *0*, 5337.
623. J. P. Collman, W. R. Roper, *Oxidative-Addition Reactions of d* ^{8} *Complexes*. In *Adv. Organomet. Chem.*, F. G. A. Stone; R. West, Eds. Academic Press: **1969**; *Vol. 7*, pp 53.
624. K. Osakada, M. Kimura, J.-C. Choi, *J. Organomet. Chem.,* **2000**, *602*, 144.
625. G.-L. Lu, W. R. Roper, L. J. Wright, G. R. Clark, *J. Organomet. Chem.,* **2005**, *690*, 972.
626. H. F. Luecke, R. G. Bergman, *J. Am. Chem. Soc.,* **1998**, *120*, 11008.
627. B. Pigulski, A. Jarszak, S. Szafert, *Dalton Trans.,* **2018**, *47*, 17046.
628. B. R. Bender, M. Koller, D. Nanz, W. Von Philipsborn, *J. Am. Chem. Soc.,* **1993**, *115*, 5889.
629. R. Fornika, H. Görls, B. Seemann, W. Leitner, *J. Chem. Soc., Chem. Commun.,* **1995**, 1479.
630. L. Carlton, *Chapter 3 - Rhodium-103 NMR*. In *Annual Reports on NMR Spectroscopy*, G. A. Webb, Ed. Academic Press: **2008**; **Vol. 63**, pp 49.
631. R. D. Dewhurst, A. F. Hill, A. C. Willis, *Organometallics,* **2004**, *23*, 5903.
632. D. S. Tsang, S. Yang, F.-A. Alphonse, A. K. Yudin, *Chem. – Eur. J.,* **2008**, *14*, 886.
633. J. V. Heras, E. Pinilla, P. Ovejero, *J. Organomet. Chem.,* **1984**, *269*, 277.
634. G. Suardi, B. P. Cleary, S. B. Duckett, C. Sleigh, M. Rau, E. W. Reed, J. A. B. Lohman, R. Eisenberg, *J. Am. Chem. Soc.,* **1997**, *119*, 7716.
635. H. Werner, R. Wiedemann, M. Laubender, B. Windmüller, P. Steinert, O. Gevert, J. Wolf, *J. Am. Chem. Soc.,* **2002**, *124*, 6966.
636. J. P. Collman, W. R. Roper, *J. Am. Chem. Soc.,* **1965**, *87*, 4008.

637. M. Ogasawara, S. A. Macgregor, W. E. Streib, K. Folting, O. Eisenstein, K. G. Caulton, *J. Am. Chem. Soc.,* **1995**, *117*, 8869.
638. M. Ogasawara, S. A. Macgregor, W. E. Streib, K. Folting, O. Eisenstein, K. G. Caulton, *J. Am. Chem. Soc.,* **1996**, *118*, 10189.
639. W. R. Roper, G. E. Taylor, J. M. Waters, L. J. Wright, *J. Organomet. Chem.,* **1979,** *182*, C46.
640. P. B. Critchlow, S. D. Robinson, *Inorg. Chem.,* **1978**, *17*, 1902.
641. K. Stanley, J. Martin, J. Schnittker, R. Smith, M. C. Baird, *Inorg. Chim. Acta,* **1978**, *27*, L111.
642. T. J. Collins, K. R. Grundy, W. R. Roper, *J. Organomet. Chem.,* **1982**, *231*, 161.
643. K. R. Laing, W. R. Roper, *Chem. Commun.,* **1968**, 1556.
644. R. D. Wilson, J. A. Ibers, *Inorg. Chem.,* **1979**, *18*, 336.
645. G. A. Bentley, K. R. Laing, W. R. Roper, J. M. Waters, *J. Chem. Soc., Chem. Commun.,* **1970**, 998.
646. A. H. Wright. PhD Thesis. University of Auckland, **1983**.
647. A. F. Hill, A. D. Rae, M. Schultz, A. C. Willis, *Organometallics,* **2007**, *26*, 1325.
648. C. E. F. Rickard, W. R. Roper, G. E. Taylor, J. M. Waters, L. J. Wright, *J. Organomet. Chem.,* **1990**, *389*, 375.
649. A. F. Hill, R. P. Melling, *J. Organomet. Chem.,* **1990**, *396*, C22.
650. C. E. F. Rickard, W. R. Roper, S. D. Woodgate, L. J. Wright, *J. Organomet. Chem.,* **2001**, *623*, 109.
651. M. I. Bruce, K. A. Kramarczuk, B. W. Skelton, A. H. White, *J. Organomet. Chem.,* **2010**, *695*, 469.
652. M. L. Buil, J. J. F. Cardo, M. A. Esteruelas, E. Oñate, *J. Am. Chem. Soc.,* **2016**, *138*, 9720.
653. T. B. Wen, Z. Y. Zhou, M. F. Lo, I. D. Williams, G. Jia, *Organometallics,* **2003**, *22*, 5217.
654. C. E. F. Rickard, W. R. Roper, S. D. Woodgate, L. J. Wright, *J. Organomet. Chem.,* **2000**, *607*, 27.
655. W. R. Roper, L. J. Wright, *J. Organomet. Chem.,* **1977**, *142*, C1.
656. K. R. Laing, W. R. Roper, *J. Chem. Soc. A,* **1969**, 1889.
657. G. V. Goeden, B. L. Haymore, *Inorg. Chim. Acta,* **1983**, *71*, 239.
658. J. Maurer, M. Linseis, B. Sarkar, B. Schwederski, M. Niemeyer, W. Kaim, S. Záliš, C. Anson, M. Zabel, R. F. Winter, *J. Am. Chem. Soc.,* **2008**, *130*, 259.
659. R. Bosque, E. Clot, S. Fantacci, F. Maseras, O. Eisenstein, R. N. Perutz, K. B. Renkema, K. G. Caulton, *J. Am. Chem. Soc.,* **1998**, *120*, 12634.
660. P. de Frémont, N. M. Scott, E. D. Stevens, S. P. Nolan, *Organometallics,* **2005**, *24*, 2411.
661. A. K. Al-Sa'Ady, C. A. McAuliffe, R. V. Parish, J. A. Sandbank, R. A. Potts, W. F. Schneider, *A General Synthesis for Gold(I) Complexes*. In *Inorg. Synth.*, **1985**; pp 191.
662. D. S. Black, G. B. Deacon, G. L. Edwards, B. M. Gatehouse, *Aust. J. Chem.,* **1993**, *46*, 1323.
663. L. Vaska, J. W. DiLuzio, *J. Am. Chem. Soc.,* **1961**, *83*, 2784.
664. L. Vaska, *J. Am. Chem. Soc.,* **1964**, *86*, 1943.
665. D. R. Coulson, L. C. Satek, S. O. Grim, *Tetrakis(Triphenylphosphine)Palladium(0)*. In *Inorg. Synth.*, **1990**; pp 107.
666. S. S. Zalesskiy, V. P. Ananikov, *Organometallics,* **2012**, *31*, 2302.
667. B. Corain, B. Longato, G. Favero, D. Ajò, G. Pilloni, U. Russo, F. R. Kreissl, *Inorg. Chim. Acta,* **1989**, *157*, 259.
668. R. Ugo, F. Cariati, G. L. Monica, J. J. Mrowca, *Tris- and Tetrakis(Triphenylphosphine)-Platinum(0)*. In *Inorg. Synth.*, **1990**; pp 123.
669. U. Nagel, *Chem. Ber.,* **1982**, *115*, 1998.
670. D. Evans, J. A. Osborn, G. Wilkinson, R. P. Jr, R. W. Parry, *trans-Carbonylchlorobis(Triphenyl-Phosphine)Rhodium and Related Complexes*. In *Inorg. Synth.*, **1990**; pp 79.
671. A. F. Hill, D. A. Tocher, A. J. P. White, D. J. Williams, J. D. E. T. Wilton-Ely, *Organometallics,* **2005**, *24*, 5342.

672. A. J. Arduengo, R. Krafczyk, R. Schmutzler, H. A. Craig, J. R. Goerlich, W. J. Marshall, M. Unverzagt, *Tetrahedron,* **1999**, *55*, 14523.
673. M. Hrubaru, D. C. Onwudiwe, E. Hosten, *J. Sulfur Chem.,* **2016**, *37*, 37.
674. B. J. Frogley, A. F. Hill, R. Shang, M. Sharma, A. C. Willis, *Chem. Eur. J.,* **2020**, *26*, 8819.
675. L. M. Caldwell. *Organotransition Metal Chemistry of Isoselenocyanate and Alkynyl Chalcoethers*. PhD Thesis, Australian National University, Canberra, Australia, **2006**.
676. M. R. S. J. Foreman, A. F. Hill, N. Tshabang, A. J. P. White, D. J. Williams, *Organometallics,* **2003**, *22*, 5593.
677. A. Jerschow, N. Müller, *J. Magn. Reson., Ser A,* **1996**, *123*, 222.
678. A. Jerschow, N. Müller, *J. Magn. Reson.,* **1997**, *125*, 372.
679. Wavefunction. Inc., *SPARTAN'20*®. 18401 Von Karmen Ave. Suite 370, Irvine CA, 92612 U.S.A., 2020.
680. J. D. Chai, M. Head-Gordon, *J. Chem. Phys.,* **2008**, *128*, 084106.
681. J. D. Chai, M. Head-Gordon, *Phys. Chem., Chem. Phys.,* **2008**, *10*, 6615.
682. P. J. Hay, W. R. Wadt, *J. Chem. Phys.,* **1985**, *82*, 270.
683. P. J. Hay, W. R. Wadt, *J. Chem. Phys.,* **1985**, *82*, 299.
684. W. R. Wadt, P. J. Hay, *J. Chem. Phys.,* **1985**, *82*, 284.
685. W. J. Hehre, R. Ditchfeld, J. A. Pople, *J. Chem. Phys.,* **1972**, *56*, 2257.
686. CrysalisPRO, *Oxford Diffraction, , Agilent Technologies UK Ltd*, England.
687. D. Aragão, J. Aishima, H. Cherukuvada, R. Clarken, M. Clift, N. P. Cowieson, D. J. Ericsson, C. L. Gee, S. Macedo, N. Mudie, S. Panjikar, J. R. Price, A. Riboldi-Tunnicliffe, R. Rostan, R. Williamson, T. T. Caradoc-Davies, *J. Synchrotron Radiat.,* **2018**, *25*, 885.
688. T. M. McPhillips, S. E. McPhillips, H.-J. Chiu, A. E. Cohen, A. M. Deacon, P. J. Ellis, E. Garman, A. Gonzalez, N. K. Sauter, R. P. Phizackerley, S. M. Soltis, P. Kuhn, *J. Synchrotron Radiat.,* **2002**, *9*, 401.
689. W. Kabsch, *J. Appl. Crystallogr.,* **1993**, *26*, 795.
690. G. M. Sheldrick, *Acta Crystallogr. A.,* **2008**, *64*, 112.
691. G. M. Sheldrick, *Acta Crystallogr. A.,* **2015**, *71*, 3.
692. O. V. Dolomanov, L. J. Bourhis, R. J. Gildea, J. A. K. Howard, H. Puschmann, *J. Appl. Crystallogr.,* **2009**, *42*, 339.
693. C. F. Macrae, I. J. Bruno, J. A. Chisholm, P. R. Edgington, P. McCabe, E. Pidcock, L. Rodriguez-Monge, R. Taylor, J. van de Streek, P. A. Wood, *J. Appl. Crystallogr.,* **2008**, *41*, 466.

Dear Tino,

A promise 11 years in the making.

A promise I never forgot for a second.

A promise, kept.